Thermal Conductivity

Proceedings of the Seventh Conference

United States Department of Commerce
National Bureau of Standards
Special Publication 302

UNITED STATES DEPARTMENT OF COMMERCE
C. R. Smith, *Secretary*
NATIONAL BUREAU OF STANDARDS • A. V. Astin, *Director*

Thermal Conductivity

Proceedings of the Seventh Conference

Held at the National Bureau of Standards, Gaithersburg, Maryland November 13–16, 1967

Edited by
Daniel R. Flynn and Bradley A. Peavy, Jr.
Institute for Applied Technology
National Bureau of Standards
Washington, D.C. 20234

 National Bureau of Standards, Special Publication 302
Issued September 1968

For sale by the Superintendent of Documents, U.S. Government Printing Office
Washington, D.C. 20402 - Price $6.25

Library of Congress Catalog Card Number: 68-61552

FOREWORD

The determination of the thermal and physical properties of materials and the development of methods of making such determinations are continuing responsibilities of the National Bureau of Standards. The Bureau carries out these responsibilities through its own research program, by providing services that support and stimulate research in other laboratories, and by encouraging and promoting the dissemination of relevant information.

To provide a forum for exchange of information and ideas among specialists in the field of heat conduction, the Bureau sponsored the "Seventh Conference on Thermal Conductivity", held November 13 - 16, 1967 in the new NBS Laboratories at Gaithersburg, Maryland. Over 180 scientists and engineers, representing industry, government, and university laboratories in the United States and ten other countries, participated.

This volume contains the text or abstracts of the ninety papers contributed at this Conference.

A. V. ASTIN, DIRECTOR
NATIONAL BUREAU OF STANDARDS

Abstract

The Seventh Conference on Thermal Conductivity was held at the National Bureau of Standards on November 13 - 16, 1967. This volume contains the texts of the papers presented. Topics covered include surveys of the present state of knowledge regarding the thermal conductivity of different materials, descriptions of different apparatuses for measuring thermal conductivity, new experimental data on the thermal conductivity or diffusivity of a variety of materials, and correlations between experimental results and theoretical predictions.

Key Words: Conductance, conductivity, contact conductance, contact resistance, electrical conductivity, electrical resistivity, heat transfer, Lorenz function, resistivity, temperature, thermal conductivity, thermal diffusivity, thermal resistivity, thermophysical properties.

Preface

This conference was the seventh in a series of annual conferences which began in 1961. The first conference stemmed from an informal discussion of thermal conductivity measurement methods by Messrs. D. L. McElroy, Oak Ridge National Laboratory, C. F. Lucks and H. W. Deem, Battelle Memorial Institute, D. R. Flynn, National Bureau of Standards, and A. I. Dahl, General Electrical Company, while attending the Symposium on Temperature, Its Measurement and Control in Science and Industry, in Columbus, Ohio. This group believed it would be very worthwhile to expand the exchange of ideas and experiences to an informal conference on thermal conductivity measurement methods applicable to solid materials at elevated temperatures. Battelle Memorial Institute agreed to develop and sponsor such a conference. During the first conference, which was held in October, 1961, M. J. Laubitz of the National Research Council of Canada agreed to sponsor a second conference the following year. Each subsequent year a different laboratory has volunteered to host the next conference. The sponsor and time of each of these conferences are listed below:

Sponsoring Organization	Chairman	Date
Battelle Memorial Institute	C. F. Lucks	October, 1961
National Research Council (Canada)	M. J. Laubitz	October, 1962
Oak Ridge National Laboratory	D. L. McElroy	October, 1963
U.S. Naval Radiological Defense Laboratory	R. L. Rudkin	October, 1964
University of Denver	J. D. Plunkett	October, 1965
Air Force Materials Laboratory	M. L. Minges and G. L. Denman	October, 1966
National Bureau of Standards	D. R. Flynn and B. A. Peavy	November, 1967

The keen interest in and active enthusiasm for these conferences is evidenced by the fact that they have grown larger in attendance and scope, and moreover, have been self-perpetuating in that there has been no single sponsoring organization or society pressing for their continuance.

The first six thermal conductivity conferences were informal in the sense that the proceedings of these conferences were not formally published. A limited number of copies of the proceedings were printed for distribution to active workers in the field. These previous proceedings were not supposed to be referenced in the open literature. The informal proceedings of these first six conferences contained approximately 200 technical papers plus a number of shorter progress reports; these proceedings occupy over 1 foot of shelf space and weigh almost 28 pounds. Many of the papers in these

proceedings have never been published formally. These considerations led us to the conclusion that a great deal of valuable information was not reaching the open literature and led us to the decision that the proceedings of the Seventh Conference on Thermal Conductivity would be published formally.

The Eighth Conference on Thermal Conductivity will be held in October, 1968, under the sponsorship of the Thermophysical Properties Research Center and the chairmanship of C. Y. Ho and R. E. Taylor.

DANIEL R. FLYNN
BRADLEY A. PEAVY, JR.

April 1, 1968

Introduction

The last two decades have witnessed a very large growth in the amount of activity in the various fields of thermophysical property measurement. Thermal conductivity is no exception. Engineering data on thermal conductivity are needed for a wide variety of heat transfer applications in such diverse industries as nuclear, aerospace, housing, cryogenics, electronics, and food processing. Since the thermal conductivity of many materials is extremely sensitive to trace impurities or small imperfections, the measurement of thermal conductivity has also become a useful tool for the study of other properties of matter.

This book represents the formal proceedings of the Seventh Conference on Thermal Conductivity, which was held at the new site of the National Bureau of Standards in Gaithersburg, Maryland, from November 13 through November 16, 1967.

This Conference brought together over 180 leading authorities, both from the United States and abroad, in the fields which are concerned with conductive heat transport in solids, liquids, gases, and phase mixtures. In this book are included the text or abstract of nearly all of the papers which were orally presented at the conference. In addition, a few papers are included which were not presented orally because of travel problems.

We thank the session chairmen for an excellent job of conducting their sessions and for their assistance in reviewing and editing the manuscripts. Particular thanks go to W. L. Carroll for his able assistance in handling much of the pre-conference arrangements and correspondence and in editing the manuscripts. The NBS Office of Technical Information and Publications, under the direction of W. R. Tilley, gave invaluable assistance in different areas ranging from the excellent handling of the logistics of the Conference by R. T. Cook, G. T. Leighty, and coworkers to the final publication of this book under the direction of J. E. Carpenter and his coworkers.

DANIEL R. FLYNN
BRADLEY A. PEAVY, JR.

April 1, 1968

Contents

METALS: VERY LOW TEMPERATURES
Chairman: R. L. Powell
National Bureau of Standards
Boulder, Colorado

METALS: INTERMEDIATE TEMPERATURES
Chairman: R. W. Powell
Thermophysical Properties Research Center
Purdue, University
West Lafayette, Indiana

METALS: INTERMEDIATE AND HIGH TEMPERATURES
Chairman: M. L. Minges
Air Force Materials Laboratory
Wright-Patterson Air Force Base
Dayton, Ohio

NON-METALLICS AND GRAPHITES
Chairman: J. Kaspar
Aerospace Corporation
Los Angeles, California

The State of Knowledge Regarding the Thermal Conductivity of the Metallic Elements

R. W. Powell and C. Y. Ho[1]

Thermophysical Properties Research Center, Purdue University
West Lafayette, Indiana 47906

The program of the Thermophysical Properties Research Center has since its inception included the extraction, evaluation, and publication of all thermal conductivity data that have been combed from a major portion of the world literature. The values so derived for many metallic elements have now been critically assessed. Some examples are presented which indicate the problems involved in arriving at probable thermal conductivity values from the limited information. Much more work is still required, and the elements and temperature ranges are clearly indicated for which the investigation shows the need for additional measurements, indeed for 19 metals a first measurement has yet to be reported. The provisional recommendations are presented as logarithmic plots of thermal conductivity against temperature.

Key Words: Conductivity, critical evaluation, elements, heat conductivity, liquid metals, metallic elements, metals, most probable values, provisional recommendations, solids, state of knowledge, thermal conductivity.

1. Introduction[2]

In many fields of scientific investigation information centers have been established and at these centers groups of workers are engaged in combing and storing the ever-increasing output of literature relating to certain specified topics so that others may readily receive answers to relevant aspects of their current problems without making costly independent searches. The Thermophysical Properties Research Center (TPRC) was one of the earliest of such centers, and, for rather more than a decade, thermal conductivity, the property that forms the subject of this Conference, has been one of several properties investigated by that Center.

A more recent development has been the work promoted by the National Standard Reference Data System which seeks to make readily available the quantitative data of physical science after it has been critically evaluated. The National Bureau of Standards has the responsibility for administering this effort, and, on their behalf, the TPRC is endeavouring to assess critically the available data for the thermal conductivity of certain substances. Not only does the progress of this work relate closely to the programme of this Conference, but there is a more important reason why the authors welcome this opportunity to present these papers at this time. They seek your help and that of others who will read these Proceedings. This help may be of the immediate or short-term type that could lend support to a tentative suggested value, or, what is more important, could disagree with it so convincingly as to lead to revision and a more satisfactory final set of data. Maybe relevant information has been overlooked or new values are known to be in course of publication. Or the help may be long term. TPRC would like to receive reprints of subsequent publications in this field.

---

[1] Senior Researcher and Head of Reference Data Tables Division, respectively.

[2] Much of this Introduction also applies to the accompanying paper by C. Y. Ho and R. W. Powell and to that of P. E. Liley.

The following outlines the position reached at the time of writing. The report [1][3] for the first years' work dealt with the thermal conductivity of the metallic elements, aluminum, copper, gold, iron (also Armco iron), mercury, platinum, silver and tungsten, the oxides of aluminum, beryllium, magnesium, silicon, thorium and titanium, two alloys, diamond, two glasses, liquid and gaseous argon, helium, nitrogen, carbon tetrachloride, toluene, diphenyl and water and of two other liquids. The report for the second year [2] dealt with the metallic elements, cadmium, chromium, lead, magnesium, molybdenum, nickel, niobium, tantalum, tin, titanium, zinc and zirconium, several grades of graphite and gaseous acetone, ammonia and methane.

In the case of gases and liquids (not liquid metals) most probable values are tabulated usually at 10 deg intervals and departure plots of the percent difference between available and recommended values are included.

For each of the other materials each report contains complete updated specification tables of the type used in the TPRC data sheets[3](An example is included later in Table 1) and graphical plots, on linear thermal conductivity and temperature scales. These include all of the existing data. The number assigned to each curve is included in the accompanying specification table and serves to indicate the authorship, year, method used and reference. This last relates to the number as listed in the relevant TPRC Data Book. On the basis of this available information, recommended curves have been inserted in each figure and tables of the recommended values are included.

This assessment of available data is proving a formidable task, possibly an unenviable one; it is clearly an essential service, but its value depends on its reliability. In order to give a greater degree of confidence to the recommendations made, the first drafts of these two reports have been internationally distributed to fifty or so workers who are active in this field, for comment and criticism. The response has proved most helpful and many changes have been made in the published versions, for which, it should be noted, the authors assume complete responsibility.

Work is currently on hand on the rest of the elements for which thermal conductivity information is available, and early in 1968 it is proposed to issue a first draft, covering not less than 59 additional elements, for similar reviewing. The new data now presented should therefore be regarded as provisional. It is hoped subsequently to prepare for publication by the NBS-NSRDS a book on the thermal conductivity of the elements. Hence, information on those elements for which no or incomplete values are given, and constructive comments bearing on the sections already published will also be welcomed to assist in the final updating and revision.

In the present account graphs are used to illustrate the amount and range of the information available, the data for some specific elements and the final recommended values. Tables of recommended values will become available in the final report to NSRDS.

One of the primary purposes of this presentation is to direct attention to the areas in which further work would be helpful.

2. Existing Information

In connection with this investigation the many specification tables that had been prepared and published [3] have been carefully checked against the original papers and, in many cases expanded by the inclusion of pertinent information regarding the electrical resistivity, or conductivity of a specimen. A typical example of such an updated table is reproduced as table 1. This relates to zirconium for which the corresponding linear and logarithmic plots of thermal conductivity against temperature appear as figures 1 and 2.

So far, experimental thermal conductivity information is available for 62 of the 81 metallic elements, and, since each of these elements cannot be treated in detail in a paper of the present type, the number of available measurements for each element is shown in figure 3 whilst figure 4 indicates the temperature or temperature range covered by these measurements.

Figure 4 brings to light a few surprises. Among the 19 metals listed in Table 2 for which no experimental information has been found are the three related metals calcium, strontium and barium. That no information is available for calcium is truly surprising since calcium rates third after iron and magnesium in the scale of abundance

[3] Figures in brackets indicate the literature references at the end of this paper.

Table 1. Specifications of the Specimens of Zirconium

Cur. No.	Ref. No.*	Author(s)	Year	Met'd Used	Temp. Range (K)	Name and Specimen Designation	Composition (weight percent), Specifications, and Remarks
1	83	Kemp, W.R.G., Klemens, P.G., and White, G.K.	1956	L	2.2-91	Zr 1a	99.99 Zr; spectroanalysis shows Fe (all sensitive lines), Hf and Ni (all sensitive lines faintly), Si and Ti (some sensitive lines), and Al, Cr, Cu, and Mg (faintly visible); JM 5000 from Johnson, Matthey and Co.; 3 mm dia rod annealed at 950 C for 5 hrs in vacuum; electrical resistivity 48 μohm cm at 293 K, residual electrical resistivity 1.98 μohm cm; mounted in the cryostat with a push fit into copper fitting; measured with the current lead (for the measurements of electrical resistivity) attached.
2	83	Kemp, W.R.G., Klemens, P.G., and White, G.K.	1956	L	3.3-90	Zr 1b	The above specimen measured with the current lead removed.
3	83	Kemp, W.R.G., Klemens, P.G., and White, G.K.	1956	L	14-90	Zr 1c	The above specimen unintentionally strained by drilling and tapping to insert the connectors for re-mounting.
4	292	Danielson, G.C.	1954	P	298, 873		Preliminary results.
5	27	Deem, H.W.	1953	C	323-673	2682 A	Pure; low Hf, arc-melted from WAPD grade 1 crystal bar.
6	27	Deem, H.W.	1953	C	323-673	498	Pure; low Hf; arc-melted from Bureau of Mines sponge Zr.
7	101	Moss, M.	1955	L	336-950		Nominally pure; cylindrical specimen 7.938 in. long, 0.787 in. in dia; obtained from Westinghouse; prepared from Foote Grade I crystal-bar ingot; the ingot being melted in tungsten arc furnace; forged in Argon to size 10 x 1 x 1 in. at 845 C; annealed in vacuum for 0.5 hr at 1000 C; machined to final shape.
8	555	Smith, K.F. and Chiswik, H.H.	1956	C	373.2		Hafnium-containing crystal bar.
9	614	Fieldhouse, I.B. and Lang, J.I.	1961	R	484-1925		99.95 Zr; 0.029 Fe, 0.017 C, 0.0045 Hf and all other elements < 0.031; specimen composed of 5 one-in. disks.
10	194	Vianey, L.R.	1951	L	402-639	D-151	Assumed to be pure; crystal bar; lot No. D-151.
11	441	Mikryukov, V.E.	1957		331-917	Iodide Zirconium	99.9 pure; annealed in vacuum for 8 hrs at 700 C; electrical resistivity at 58.0, 124.1, 239.8, 321.0, 415.6, 490.6, 558.8, and 644.0 C being respectively, 361.1, 47.6, 66.6, 75.8, 87.0, 94.4, 100.0, and 106 μohm cm; Lorenz numbers reported at these temperatures were 3.38, 3.33, 3.18, 3.11, 3.08, 3.04, 3.03, and 2.92 x 10^{-8} V^2K^{-2}, respectively.
12	441	Mikryukov, V.E.	1957		332-879		99.78 Zr; 0.14 Hf, 0.08 C; electrical resistivity reported as 53.76, 64.93, 78.74, 87.71, 95.23, 105.26, 111.11, 120.48, and 125.00 μohm cm at 59.0, 117.0, 202.0, 262.0, 318.0, 402.0, 456.0, 548.0, and 606.0 C, respectively; Lorenz numbers reported at these temperatures were 3.46, 3.44, 3.54, 3.36, 3.37, 3.34, 3.37, 3.28 and 3.29 x $10^{-8}V^2K^{-2}$, respectively.
13	295	McCreight, L.R.	1952	R	473-823		Pure; 98-100% of theoretical density.
14	401	White, G.K. and Woods, S.B.	1959	L	2.0-121	Zr 4	99.95 pure; annealed in vacuum.
15	401	White, G.K. and Woods, S.B.	1959	L	4.4-89	Zr 4a	99.95 pure; annealed in vacuum.
16	442	Bing, G., Fink, F.W., and Thompson, H.B.	1951	C	323-573	Zr 1	0.001 Sn, 0.007 Ti, 0.04 Hf, 0.001 Al, 0.04 Fe, 0.02 Ni, Westinghouse ingot D-216 forged at 1250 F, and machined; electrical resistivity reported as 44.1 and 81.3 μohm cm at 298 and 533 K, respectively.

*For references see TPRC Data Book Vol. 1, Chapter 1 [3]

Cur. No.	Ref. No.*	Author(s)	Year	Met'd Used	Temp. Range (K)	Name and Specimen Designation	Composition (weight percent), Specifications, and Remarks
17	442	Bing, G., Fink, F.W., and Thompson, H.B.	1951	C	323-573	Zr 7	0.07 Ta, 0.07 C, 0.0055 N, 0.007 Ti, 0.02 Al, 0.1 Fe; obtained from ANL, identified as SA 1568; annealed; electrical resistivity reported as 50.5, 68.2, and 85.1 μohm cm at 298, 415, and 533 K, respectively.
18	442	Bing, G., Fink, F.W., and Thompson, H.B.	1951	C	323-573	Zr 8	0.16 Ta, 0.002 C, 0.015 N, 0.005 Ti, 0.06 Al, 0.1 Fe; obtained from ANL, identified as SA 1576; annealed; electrical resistivity reported as 52.4, 70.1, and 86.6 μ ohm cm at 298, 415, and 533 K, respectively.
19	715	Powell, R.W. and Tye, R.P.	1961	L,C	323,423	050	99.827 Zr (by difference), 0.11 O, 0.045 Fe, 0.01 C, 0.008 N; as-extruded rod 10 cm long, 1.27 cm in dia; arc-melted; electrical resistivity reported as 59.5 and 75 μohm cm at 323 and 423 K, respectively; Armco iron used as a reference standard, energy flow also measured calorimetrically.
20	715	Powell, R.W. and Tye, R.P.	1961	L,C	323-823		0.3-0.6 O (analysis made after completion of tests), 0.016 C, 0.016 H, 0.012 Fe, and 0.0025 N; specimen 0.435 cm in dia and 9.7 cm long, cold swaged from a bar of about 0.5 cm dia that had been prepared by the Van Arkel method; the bar was polycrystalline and consisted almost entirely of hexagonal crystals with their c-axis parallel to the axis of the bar, and considerable preferred orientation present in the specimen; density of the bar 6.57 g cm^{-3}; electrical resistivity reported as 49.2, 65.6, 82.1, 97.8, 111.2, and 119.7 μohm cm at 323, 423, 523, 623, 723, and 823 K, respectively, at these temperatures the Lorenz function being, respectively, 3.03, 2.96, 2.92, 2.87, 2.85, and 2.80 x $10^{-8} V^2K^{-2}$; Armco iron used as a reference standard; energy flow also measured calorimetrically.
21	715	Powell, R.W. and Tye, R.P.	1962	L,C	323-1023	Sample 715	0.1-0.6 O (analysis made after completion of tests), 0.043 C, 0.018 Fe, 0.0075 N, 0.007 Al, 0.007 Nb, and 0.0025 H; specimen 1.27 cm in dia and 10 cm long; in the as-extruded condition, melted in graphite before extrusion; electrical resistivity reported as 53.5, 70.0, 85.0, 98, 110, 119, 127, and 133 μohm cm at 323, 423, 523, 623, 723, 823, 923, and 1023 K, respectively, at these temperatures the Lorenz function being, respectively, 3.10, 3.06, 2.98, 2.88, 2.80, 2.69, 2.60, and 2.55 x 10^{-8} V^2K^{-2}; Armco iron used as a reference standard; energy flow also measured calorimetrically.
22	741	Timrot, D.L. and Peletskii, V.E.	1965	L	1160-2000	Iodide Zirconium	99.5+ pure; 14 mm dia x 65 mm long; vacuum annealed; density 6.45 g cm^{-3} at room temperature.

*For references see TPRC Data Book Vol. 1, Chapter 1 [3]

of the elements now under consideration. A value of 0.3 cal cm^{-1} s^{-1} deg^{-1} (125.5 W m^{-1} deg^{-1}) at 20C has been listed for calcium in several editions of the ASM "Metals Handbook" [6] but the source of this value has not been traced, furthermore, this value would appear to be low since with ρ_{295K} as 3.6×10^{-8} ohm m [7] the Lorenz function has the low value of $1.53 \times 10^{-8} V^2 K^{-2}$. Cobalt has not been measured above 430K and such high melting point metals as iridium, ruthenium, rhodium and palladium have not been measured above 493 to 592K or only for about one quarter of the temperature range for which they are solid. These stand out as definite gaps in knowledge, and several others will appear as the attempt is made to assess the available data.

Table 2. Metallic Elements that Lack Experimental Thermal Conductivity Values

Name	Atomic No.	Name	Atomic No.	Name	Atomic No.
Actinium	89	Einsteinium	99	Nobelium	102
Americium	95	Europium(a)	63	Polonium	84
Barium	56	Fermium	100	Promethium(b)	61
Berkelium	97	Francium	87	Protactinium	91
Calcium	20	Lawrencium	103	Radium	88
Californium	98	Mendelevium	101	Strontium	38
Curium	96				

(a) For estimated value at 291K see [4].
(b) For estimated values range 300-2250K see [5]. This paper also contains estimated values for neodymium up to its melting point.

3. Assessment of Information - Some Guides

Earlier analytical work at the TPRC [8,9,10] has shown that the low-temperature thermal conductivities of many metals can be correlated to a single curve given by

$$\lambda^* = \left[1/3\ (T^*)^2 + \frac{2}{3T^*}\right]^{-1} \qquad (1)$$

where $\lambda^* = \frac{\lambda}{\lambda_m}$ and $T^* = \frac{T}{T_m}$, λ^* being the ratio of thermal conductivity λ at temperature T to the maximum conductivity λ_m at temperature T_m.

It was further shown that in the low temperature region below $1.5T_m$, λ could be derived from the equation

$$\lambda = \left[\alpha' T^n + \beta T^{-1}\right]^{-1} \qquad (2)$$

where $$\alpha' = \alpha'' \left(\frac{\beta}{n\alpha''}\right)^{\frac{a}{m+1}}$$

In this equation a, m, n and α'' are constants for a metal whereas α' and β depend on the purity and perfection of the particular sample. Theoretically,

$$\beta = \rho_o L_o^{-1} \qquad (3)$$

where L_o is the theoretical Lorenz function and ρ_o is the residual electrical resistivity and this parameter, as derived through equation (2) or (3) gives a measure of the purity and/or perfection of the sample. For those metals which conform to this equation its use enables the full curve to be derived up to $1.5\ T_m$ even if only a few observations are available. This course has usually been adopted to complete the curve through the highest points and thus to obtain a more complete curve for the sample of highest apparent purity. If ρ_o is known, use of the equation

$$\lambda = L_o T \rho_o^{-1} = 2.443 \times 10^{-8} T \rho_o^{-1} \qquad (4)$$

also serves to give the lower end of the curve, or can serve as a check in this region.

The low-temperature thermal conductivity values to which equation (2) applies depend most strongly on the sample characteristics of a particular metal. At higher temperatures, whilst the purest sample usually has the highest thermal conductivity, the differences tend to be smaller. Furthermore, for any particular metal, even

although the Wiedemann-Franz-Lorenz law does not always hold, a sample with a higher electrical conductivity should generally have a higher thermal conductivity. Liquid metals appear to conform reasonably well with the WFL correlation [11], although for some metals the Lorenz function has been found to be lower than the theoretical value by as much as 15 per cent.

The foregoing are the main guidelines in considering this group of elements. They are seen to rely strongly on parallel electrical conductivity information being available for the same sample. This fact is now well recognized and it is mainly for older determinations that the corresponding electrical measurements are found to be lacking.

4. Some Typical Sets of Data

In this section it is proposed to present and discuss the thermal conductivity data that are available for the four metals zirconium, zinc, tungsten and lithium. Tungsten is included because of its potential use as a thermal conductivity standard at high temperatures and the others as illustrating behaviour or problems of particular interest.

4.1 Zirconium

Table 1 lists the experimental investigations into the thermal conductivity of zirconium and contains details of each specimen and of the range covered. The letters L,C,R and T in the column headed 'method used' are the initial letters of methods of the following types: longitudinal, comparative, radial and thermoelectrical. The corresponding thermal conductivity values are plotted against temperature in figures 1 and 2.

Using the β-value calculated from data due to White and Woods [12] the low-temperature section of the proposed curve was derived to about 20K and this continues smoothly to pass through their values near 90K. Above 90K uncertainties enter. From 94 to 297K only one measured value is available. This is the 121K limiting point of White and Woods which may be uncertain due to increased radiation transfer. From 298K to about 900K a $\pm$ 20 per cent band of values are available with minima of from 17 to 24.5 $W\,m^{-1}deg^{-1}$ at around 600K. The highest curve is by Mikryukov [13] for a 99.9 per cent sample of iodide zirconium. Zirconium readily combines with oxygen and it seems likely that differences in the pre-treatment and test conditions could help to account for some of the observed differences in thermal conductivity. Treco [14] had made a study of the influence of oxygen content on the electrical resistivity of oxygen-free high-purity zirconium at 273K, the value increasing to 0.577 μ ohm m for 2.5 atomic per cent of oxygen. In view of these measurements it is surprising to note that Mikryukov gives 0.361 μ ohm m as the resistivity of his higher conductivity sample at 331K, which would probably extrapolate to about 0.26 μohm m at 273K. This seems to be an excessive difference if both samples are polycrystalline zirconium. But α-zirconium has a hexagonal crystal structure so varying degrees of preferred orientation may be another factor associated with the observed differences in conductivity. No documented information is available regarding the anisotropy of zirconium for either heat or electrical conduction.

When attention is directed to the reported mean values for the Lorenz function in this temperature range it is seen that the values for Mikryukov's two samples decrease from $3.42 \times 10^{-8} V^2K^{-2}$ at 323K to $3.11 \times 10^{-8} V^2K^{-2}$ at 833K; those of Powell and Tye [15] from $3.10 \times 10^{-8} V^2K^{-2}$ for three samples at 323K to $2.73 \times 10^{-8} V^2K^{-2}$ for two samples at 823K whilst those of Bing et al. [16] for three samples decrease from $3.14 \times 10^{-8} V^2K^{-2}$ at 323K to $2.84 \times 10^{-8} V^2K^{-2}$ at 523K.

On the basis of these data an extrapolated average Lorenz function at 273K has been obtained, and used with Treco's electrical resistivity value to give a thermal conductivity of 22.9 $W\,m^{-1}\,deg^{-1}$ at 273K. This value is 3 per cent above the value obtained by Moss[17] for nominally high purity zirconium. The curve now proposed for the thermal conductivity of pure zirconium continues smoothly from 35.0 $W\,m^{-1}\,deg^{-1}$ at 90K to 22.9 $W\,m^{-1}\,deg^{-1}$ at 273K, runs about 3 percent above Moss's curve, to cross the curve of Fieldhouse and Lang [18] and to continue some 3 percent below this curve to its upper temperature limit of 1925K. The other data of Timrot and Peletskii [19] in this high temperature region which cross the recommended curve yield a Lorenz function of only about $2 \times 10^{-8} V^2K^{-2}$ at its lower end, which seems unduly low for this element, despite there being a phase transformation at 1135K. A drop of about 14 per

cent in the electrical resistivity has been reported in this region. The thermal conductivity measurements of Fieldhouse and Lang are the only ones to span the transition region and these indicate no corresponding change. Hence, the proposed curve has been drawn with no discontinuity.

Clearly zirconium is a metal to which much more attention should be given. Once single crystals become available, information on their anisotropy is certainly required for both thermal and electrical conductivities. The phase transition region requires study, and, pending the production of the further required high temperature thermal conductivity values, it would be useful to extend electrical resistivity determinations above their present limit of 1280K, even into the liquid phase. The effects of high temperature working conditions on the samples might also be investigated through a preliminary series of electrical resistivity measurements. Thermal conductivity data are also required for the 100 to 300K region.

4.2 Zinc

Zinc has been included so as to be able to mention a difficulty that had not appeared previously. Zinc has a hexagonal crystal structure and both thermal and electrical conductivities show definite anisotropy. The unusual feature is that the low-temperature curves for $\lambda_{\perp}$ and $\lambda_{//}$ appear to cross both above and below T_m. In figure 5, curves 22 and 23, both due to Mendelssohn and Rosenberg[20] behave in this way and their findings agree above T_m with some earlier data due to Goens and Grüneisen[21] and below T_m with subsequent data of λ by Zavaritskii[22]. Incidentally, electrical resistivity data of Goens and Grüneisen showed no corresponding cross over, $\rho_{\perp}$ exceeding $\rho_{//}$ at 21.2, 83.2 and 293.2K, which suggests that the explanation might require a markedly different temperature dependence of the anisotropy of the lattice component of the thermal conductivity. The subject is clearly one that calls for further investigation.

The type of thermal conductivity behaviour shown by the above three sets of data is quite incompatible with the usual treatment of Cezairliyan and Touloukian[8][9][10], which has formed the basis of the evaluation of thermal conductivity values in this low temperature region, since different values of β yield a family of non-intersecting curves. It has also been thought undesirable to give recommended curves that cross over in this way at the present time, and so the recommendations given for zinc relate only to the polycrystalline form.

The highest low-temperature value is a single observation of $\lambda_{\perp}$ by Zavaritskii[22] at 0.825K. The corresponding λ (polycrystal) is derived through his ratio $\lambda_{\perp}/\lambda_{//}$ for two other samples at this temperature. This has then been used to evaluate β and to derive the curve for polycrystalline zinc in the normal (non-superconducting) state up to about 8K. It is then continued through the 83K value for polycrystalline zinc and about 2 per cent below the 293K value, both being derived from the single crystal data of Goens and Grüneisen. The available data at higher temperatures are shown more clearly in figure 6. There have been no measurements reported on zinc at normal temperatures and above within the past twenty years, with the exception of a single low value of Parker, Jenkins, Butler and Abbott [23]. Such early measurements as those of Shelton and Swanger[24] were probably reliable but to allow for the possible reduced purity of these specimens the proposed curve lies about mid-way between that of Shelton and Swanger and the most recent determinations, those reported by Mikryukov and Rabotnov[25] in 1944.

Clearly the high purity melting-point zinc now available should be used for new measurements on polycrystalline and on single crystal samples.

There is also a strong case for the new determinations to be extended into the liquid phase. The two early measurements by Konno[26] and Bidwell[27] happen to agree well, but they yield a solid/liquid ratio λ_s/λ_l, of 1.67 whereas Roll and Motz[28] report 2.2 for the ratio ρ_l/ρ_s. Also both Konno and Bidwell obtain a negative temperature coefficient where consideration of the Lorenz function would give a strong positive coefficient, at least near the melting point. Dutchak and Panasyuk [29] have recently reported a positive coefficient but their values seem too high as they would yield a ratio of 1.72 for λ_s/λ_l. The recommended curve has accordingly been drawn in a lower position. Of course it may be that the proposed value of λ_s is too low.

Zinc certainly calls for some new determinations just above and below the melting point and well into the liquid phase.

4.3 Tungsten

The thermal conductivity data available for tungsten to high temperatures is shown in a linear plot against temperature in figure 7. Somewidely-scattered values are evident but the recommended curve lies within about 5 per cent of several recent determinations and is thought to be satisfactory to within about these limits. The corresponding Lorenz functions are approaching 20 per cent above the theoretical value.

4.4 Lithium

The experimental data for lithium are shown in figures 8 and 9. The recommended curve has a maximum value of 743 $W\,m^{-1}deg^{-1}$ at about 16.5K and above 60K it follows an intermediate course between the values of Rosenberg[30] and of MacDonald, White and Woods[31]. These last stop at 121K and from this temperature to the melting point(453.7K) further information is required. Rather tentatively the proposed curve is shown to continue with a gradual decrease to the melting point passing close to Bidwell's values[32] for the solid near this region.

Much more attention has been given to the liquid state and at about 500K the five available sets of experimental thermal conductivity measurements lie within about 10 per cent of 43 $W\,m^{-1}deg^{-1}$. These measurements,however, show serious differences regarding the variation of thermal conductivity with temperature. Two[33,34] indicate liquid lithium to have a large initial negative coefficient, one a small positive coefficient[35] and two indicate large positive coefficients[36,37]. These last receive support from estimates based on the Lorenz function and knowledge of the electrical resistivity. Noteworthy among such estimates is that of Grosse[38], who includes lithium among the several metals for which he has made thermal conductivity predictions from the melting point to the critical point. He does admit that more uncertainty is associated with his estimate of 4150K for the critical temperature of lithium; it also seems that the empirical method used to extrapolate the essential electrical resistivity data to the critical point is less certain for lithium than for some of the other liquid metals that he has treated in this way.

Mercury is the only metal for which the electrical conductivity,σ, has been determined to the critical point[39]. From these results and others covering less complete temperature ranges, Grosse[40] has derived for molten metals an equation of the form:

$$(\sigma^* + b)(T^+ + b) = a \qquad (5)$$

where $\sigma^* = \sigma_T/\sigma_f$ and $T^+ = (T - T_f)/(T_c - T_f)$

and σ_T is the electrical conductivity of a molten metal at a temperature, T, between the melting point, T_f , and the critical point, T_c, and σ_f is the corresponding electrical conductivity at the melting point. The quantities a and b are constants. At T_c both σ and λ are assumed to be zero.

For lithium Grosse has chosen to use the electrical conductivity data of Freedman and Robertson[41] which extend only to 830K, to determine the constants of equation (5). He comments that the more recent measurements of Rigney, Kapelner and Cleary[42], although extending to the much higher temperature of 1703K could not be fitted to the equation. The differences are quite significant, Grosse's estimated resistivity at 1700K exceeding the observed value by about 45 per cent.

Another parameter which introduces rather smaller uncertainties is the Lorenz function. Both Grosse and Tepper, Zelenak, Rochlich and May[43] selected to use the theoretical value, so any difference in their thermal conductivity curves must be attributed to the electrical resistivity values used. Kapelner[44] chose 2.16×10^{-8} V^2K^{-2}, in agreement with some unpublished measurements by C. T. Ewing for temperatures of 556.5, 636.0 and 796.0K; whilst Rigney, Kapelner and Cleary chose $2.29 \times 10^{-8} V^2K^{-2}$. This last was the average value given by their own electrical resistivity values and the thermal conductivity determinations of Cooke.[36] It should, however, be noted that the smooth curve fitted by Cooke to his admittedly more scattered high temperature results, together with their resistivity value at 1073K, yields a Lorenz function of $2.46 \times 10^{-8} V^2K^{-2}$.

Cooke's thermal conductivity measurements extended to 1105K and he predicted that at higher temperatures the thermal conductivity of lithium would have a maximum

value of about 78W $m^{-1}deg^{-1}$ at about 1973K. This prediction was made on the assumption of an apparently low value of 2966K for the critical temperature[45].

Of interest in this connection are the subsequent thermal conductivity values derived by Rudnev, Lyashenko and Abramovich[37] who determined the thermal diffusivity of a 99 per cent sample of lithium for the range 623 to 1273K by means of a method of the Angstrom type. The thermal conductivity values which they obtained using literature values of the density and specific heat, are included in figure 9. They are still increasing at 1150K and would indicate that any maximum should occur at well above Grosse's estimated temperature of 1150K.

The curve drawn in figure 9 as the most probable lies between the experimental data of Cooke and of Rudnev el al. and a little below the derived curve of Tepper et al. At 1700K it passes through a value derived from the electrical resistivity measurements of Rigney et al. but using the theoretical Lorenz function rather than $2.29 \times 10^{-8} v^2 K^{-2}$.

Above this temperature the course of the curve is very conjectural. It is shown with a maximum at about 1800K and an increasing rate of fall to merge at 4150K the critical temperature as estimated by Grosse, with the probable lithium vapor value of about 0.2 W m^{-1} deg^{-1} [36]. Curve 17 of figure 9 indicates the temperature range of calculated values for lithium vapor [46].

Lithium is another instance for which electrical resistivity determinations to the highest possible temperature would be most helpful. For mercury the predicated curve is of similar form, and as the maximum in the thermal conductivity curve occurs at a little below 800K, experimental confirmation should present less difficulty.

5. Provisional Recommendations

Figures 10 to 17 are logarithmic plots of the provisional recommendations for the temperature dependence of the thermal conductivity of each of the 64 metallic elements for which either experimental or estimated values have been found in the literature. Each curve has been derived in the manner indicated in the foregoing sections and the curves are presented according to the periodic-table grouping but with two groups combined in many of the figures. The solid circles and continuous curves represent a temperature or temperature range for which experimental information is available, whilst an open circle or broken curve indicates that the corresponding data is only estimated.

Some changes will be noticed from the earlier reports [1,2]. The curve for platinum has been revised, the range for mercury has been extended to include the solid phase (although no data exists for the temperature range 4.4 to 80K) and the estimated values due to Grosse [38,47] for the liquid state are now included.

The new recommendations for platinum are greater by 4 and 7.5 per cent at 900 and 1250K respectively and the curve now fits to within about $\pm$ 3 per cent with several recent determinations [48,49,50,51]. This curve has been smoothly extrapolated to higher temperatures.

For mercury and some other metals of low or moderate melting point, the estimates by Grosse for the thermal conductivity in the liquid state agree well with experimental values, but, of the higher melting point metals now included, experimental data are only available for copper[52,53,54], and are all lower than the predicted values by some 13 to nearly 40 per cent. The evidence is fairly strong that liquid potassium has a Lorenz function that is some 14 per cent less than the theoretical value[55,56] but, the experimental uncertainties are likely to increase with temperature, and there is need for further careful investigation before copper can be accepted as another metal having an exceptionally low Lorenz function.

Scandium can be mentioned as a metal for which large differences were evident at the other end of the temperature scale. At 4.2K the measurements of Arajs and Colvin [57] give a Lorenz function of the order of $7 \times 10^{-8} v^2 K^{-2}$ whereas those of Aliyev and Volkenshteyn [58] yield a value only about 20 per cent above the theoretical value. These last have been accepted as more likely to be correct, and again at room temperature, an independent check measurement seems desirable where the single observation of Jolliffe et al. [4] has been preferred to the much higher series of values due to Arajs and Colvin. Scandium, with a melting point of 1812K, is indeed a metal for which thermal conductivity measurements are required for the full range of temperatures since no determinations have yet been made above 300K. These measurements should in-

clude single crystal samples since scandium has a hexagonal crystal structure.

Another metal calling for comment and further check measurements is sodium. This time however the measurements are required in the immediate sub-normal temperature range, so as to confirm the undulatory character of the curve which seems to give the best fit to the data so far available.

It would be possible to continue with similar comments for many more metals, but these will need to be reserved for a more detailed account. In order to make the present account as complete as possible, it does however seem desirable to include estimated values for three metals for which electrical conductivity values only are available. This is done in the next section.

6. Estimated Thermal Conductivity Values for Barium, Calcium and Strontium

Using the recently assembled electrical resistivity ρ data of Meaden[7] and the theoretical Lorenz function, L_o, the thermal conductivity values, λ, given in table 3 have been obtained for barium, calcium and strontium.

Table 3. Barium, Calcium and Strontium: Electrical Resistivity and Derived Thermal Conductivity

Metal	Temperature (^oK)	Electrical Resistivity (10^{-8} ohm m)	Thermal Conductivity (W $m^{-1}deg^{-1}$)	
	T	ρ	$L_oT\rho^{-1}$	$L_oT(\rho-\rho_o)^{-1}$
Barium	4	$0.25(\rho_o)$	39	--
	200	25.25	19.4	19.6
	273	36.25	18.4	18.5
	295	39.25	18.4	18.5
Calcium	295	3.6 ± 0.03	200	200
Strontium	4	$2.0(\rho_o)$	4.9	--
	200	16.1	30.4	34.7
	273	21.8	30.6	33.7
	295	23.5	30.7	33.6

Meaden considers that electrical resistivity values have not yet been obtained for these metals in a pure state. For calcium he only tabulates the one room temperature value, for which he thinks the residual resistivity, ρ_o, was probably quite small. It had been large for earlier reported measurements on calcium and is clearly large for the samples on which the tabulated barium and strontium data are based. The derived thermal conductivity values given in the last column should apply to fairly pure samples, for the approximate range 200 to 300 K, provided these metals satisfy the Wiedemann-Franz-Lorenz law.

7. Suggestions for Future Work

In this section it is proposed to bring together the various suggestions for further work that have been interspersed in the foregoing account.

The extent of existing knowledge is shown in figures 3 and 4, and these should be helpful in indicating the metals and temperature ranges for which measurements or estimated values are required. Of the metals for which thermal conductivity measurements have yet to be reported, barium, calcium and strontium stand out as the three for which suitable samples could be obtained most readily.

Unfortunately, figures 3 and 4 do not reveal the only areas where there is a need for further experimental investigation. More detailed examination of the available information reveals many regions of uncertainty, of which the few following have received mention:

Lithium: Measurements are required to confirm the thermal conductivity temperature dependence from about 80 K to the melting point. Electrical resistivity determinations for the liquid phase are required to the highest possible temperature in connection with Grosse's predictions. It would be of interest also if the thermal conductivity measurements could extend beyond the suggested maximum.

Mercury: Thermal conductivity measurements on single crystals are required in the range 4 K to the melting point. Possibility of a thermal conductivity maximum in the region 700 to 1000 K should be investigated.

Scandium: Single crystal and polycrystalline samples should be studied over the full temperature range.

Sodium: Thermal conductivity measurements are required from about 50 K to the melting point, to confirm if the curve has a minimum and a maximum in this region.

Zinc: High purity single and polycrystalline samples should be studied; also liquid zinc.

Zirconium: First measurements for the approximate range 100 to 300 K are required and further measurements from 300 K upwards. Single crystals should be included and particular attention given to any possible discontinuity associated with the $\alpha \rightarrow \beta$ phase transformation. (Similar suggestions hold for titanium.)

In planning any future work it is important to include electrical resistivity determinations whenever possible. Indeed, within the liquid helium temperature range and at high temperatures, particularly for the liquid phase of a metallic conductor, such measurements can often provide a basis for the estimation of thermal conductivity values.

8. References

[1] Powell, R.W., Ho., C.Y., and Liley, P.E., Thermal Conductivity of Selected Materials, National Standard Reference Data System, NSRDS-NBS 8 (Nov. 1966).

[2] Ho, C.Y., Powell, R.W., and Liley, P.E., Thermal Conductivity of Selected Materials, Part 2, National Standard Reference Data System, NSRDS-NBS-16, in press.

[3] Touloukian, Y.S., Thermophysical Properties Research Center Data Book, Volume 1, Metallic Elements and Their Alloys(In Solid, Liquid or Gaseous State), Chapter 1, Thermal Conductivity, 849 pages in Chapter 1 as of December 1966.

[4] Jolliffe, B.W., Tye, R.P., and Powell, R. W., The thermal and electrical conductivities of scandium, yttrium, and manganese and twelve rare-earth metals, at normal temperatures, J. Less-Common Metals 11, 388-394 (1966).

[5] Williams, R.K. and McElroy, D.L., Estimated Thermal Conductivity Values for Solid and Liquid Promethium, ORNL-TM-1424 (March 1966).

[6] Metals Handbook, 8th Edition, Editor T. Lyman, Published by American Society for Metals, Vol. 1, p. 48 (1961).

[7] Meaden, G.T., Electrical Resistance of Metals , Plenum Press, New York, p. 75 (1965).

[8] Cezairliyan, A., Prediction of Thermal Conductivity of Metallic Elements and Their Dilute Alloys at Cryogenic Temperatures, Purdue University, Thermophysical Properties Research Center, TPRC Rept. 14, 1-140 (1962).

[9] Cezairliyan, A., and Touloukian, Y.S., Generalization and calculation of the thermal conductivity of metals by means of the law of corresponding states, High Temperature 3, 63-75 (1965); A translation of Teplofizika Vysokikh Temperatur 3, 75-85 (1965).

[10] Cezairliyan, A. and Touloukian, Y.S., Correlation and prediction of thermal conductivity of metals through the application of the principle of corresponding states, in Advances in Thermophysical Properties at Extreme Temperatures and Pressures, 3rd Symposium on Thermophysical Properties, A.S.M.E., 301-303 (1965).

[11] Powell, R.W., Correlation of metallic thermal and electrical conductivities for both solid and liquid phases, Intnl. J. Heat Mass Trans. 8, 1033-1045 (1965).

[12] White, G.K. and Woods, S.B., Electrical and thermal resistivity of the transition elements at low temperature, Phil. Trans. Roy. Soc. A251 (995), 273-302 (1959).

[13] Mikryukov, V.E., Temperature dependence of the heat conductivity and electrical resistance of titanium, zirconium and of zirconium alloys, Vest. Moskov Univ., Ser. Mat.Mekh. Astron. Fiz. Khim. 12(5), 73-80 (1957).

[14] Treco, R.M., Some properties of high purity zirconium and dilute alloys with oxygen, Trans. Amer. Soc. Metals 45, 872-892 (1953).

[15] Powell, R.W. and Tye, R.P., The thermal and electrical conductivities of zirconium and of some zirconium alloys, J. Less-Common Metals 3, 202-215 (1961).

[16] Bing, G., Fink, F.W., and Thompson, H.B., The Thermal and Electrical Conductivities of Zirconium and Its Alloys, USAEC Rept. BMI-65, 1-19 (1951).

[17] Moss, M., An apparatus for measuring the thermal conductivity of metals in vacuum at high temperatures, Rev. Sci. Instrum. 26, 276-280 (1955).

[18] Fieldhouse, I.B. and Lang, J.I., Measurement of Thermal Properties, WADD TR 60-904, 1-119 (1961). [AD268304]

[19] Timrot, D.L. and Peletskii, V.E., The thermal conductivity and integral blackness of zirconium, High Temperature 3 (2), 199-202 (1965); Translation of Teplofiz Vysokikh Temperatur 3(2), 223-227 (1965).

[20] Mendelssohn, K. and Rosenberg, H.M., The thermal conductivity of metals at low temperatures, I: The elements of groups 1,2, and 3, II: The transition elements, Proc. Phys. Soc. (London) A65, 385-394 (1952).

[21] Goens, E. and Grüneisen, E., Electrical and thermal conductivities of single crystals of zinc and cadmium, Ann. Physik 14, 164-180 (1932).

[22] Zavaritskii, N.V., Measurement of heat conductive anisotropy of zinc and cadmium in the superconducting state, Zhur. Eksptl. i Teoret. Fiz. 39, 1193-7 (1960); Soviet Phys. JETP 12(5), 831-3 (1961).

[23] Parker, W.J., Jenkins, R.J., Butler, C.P., and Abbott, G.L., Flash method of determining thermal diffusivity, heat capacity, and thermal conductivity, J. Appl. Phys. 32(9), 1679-84 (1961).

[24] Shelton, S.M. and Swanger, W.H., Thermal conductivities of irons and steels and some other metals in the temperature range 0-600°, Trans. Amer. Soc. Steel Treating 21, 1061-77 (1933).

[25] Mikryukov, V.E. and Rabotnov, S.N., Thermal and electrical conductivities of mono-and polycrystalline substances from 100 degrees to the melting point, Uchenye Zapiski Moskov Ordena Lenina Gosudarst Univ. M.V. Lomonosova Fizika 74, 167-79 (1944).

[26] Konno, S., On the variation of thermal conductivity during the fusion of metals, Sci. Repts. Tôhoku Imp. Univ. 8, 169-79 (1919).

[27] Bidwell, C.C., A precise method of measuring thermal conductivity applicable to either molten or solid metals. Thermal conductivity of zinc, Phys. Rev. 56, 594-598 (1939).

[28] Roll, A. and Motz, H., The electrical resistance of metals, I. Measuring method and electrical resistance of molten pure metals, Z. Metallkunde 48(5), 272-80 (1957).

[29] Dutchak, Ya.I. and Panasyuk, P.V., Investigation of the heat conductivity of certain metals on transition from the solid to the liquid state, Fiz. Tverdogo Tela 8(9), 2805-2808 (1966); for Transl. see Soviet Phys.-Solid State 8(9), 2244-2246 (1967).

[30] Rosenberg, H.M., The thermal and electrical conductivity of lithium at low temperatures, Phil. Mag. (Eighth Ser.) 1, 738-746 (1956).

[31] MacDonald, D.K.C., White, G.K., and Woods, S.B., Thermal and electrical conductivities of the alkali metals at low temperatures, Proc. Roy. Soc. (London) A235, 358-374 (1956).

[32] Bidwell, C.C., Thermal conductivity of lithium and sodium by a modification of the Forbes bar method, Phys. Rev. 28, 584-597 (1926).

[33] Yaggee, F.L. and Untermyer, A., The Relative Thermal Conductivities of Liquid Lithium, Sodium and Eutectic NaK, and the Specific Heat of Liquid Lithium, USAEC Rept. ANL-4458, 1-27 (1950).

[34] Webber, H.A., Goldstein, D., and Fellinger, R.C., Determination of the thermal conductivity of molten lithium, Trans. Amer. Soc. Mech. Engrs. 77, 97-102 (1955).

[35] Nickol'skii, N.A., Kalakutskaya,N.A., Pchelkin,I.M., Klassen, T.V., and Vel'tishcheva, V.A., Thermophysical properties of some metals and alloys in the molten state, Voprosy Teploobmena, Akad. Nauk S.S.S.R., Energet. Inst. im. G.M. Krzhizharovoskogo, 11-45 (1959).

[36] Cooke, J.W., Experimental determination of the thermal conductivity of molten lithium from 320° to 830°C, J. Chem. Phys. 40(7), 1902-1909(1964).

[37] Rudnev, I.I., Lyashenko, V.S., and Abramovich, M.D., Diffusivity of sodium and lithium, At. Energy (USSR) 11(3), 230-232(1961); for English trans. see At. Energy (USSR) 11(3), 877-880 (1962).

[38] Grosse, A.V., Electrical and thermal conductivities of metals over their entire liquid range, Rev. Hautes Temper et Réfract. 3, 115-146 (1966)(in English).

[39] Birch, F., The electrical resistance and the critical point of mercury, Phys. Rev. 41, 641-648 (1932).

[40] Grosse, A.V., An empirical relationship between the electrical conductivity of mercury and temperature over its entire liquid range also its thermal conductivity and the latter's regular behaviour, J. Inorg. Nucl. Chem. 28, 803-811 (1966).

[41] Freedman, J.F. and Robertson, W.D., Electrical resistivity of liquid sodium, liquid lithium, and dilute liquid sodium solutions, J. Chem. Phys. 34, 769-780 (1961).

[42] Rigney, D.V., Kapelner, S.M., and Cleary, R.E., The Electrical Resistivity of Lithium and Columbium (Niobium)-1 Zirconium Alloy to 1430° Pratt and Whitney Aircraft-Canel, Middletown, Conn., USAEC Rept. TIM-854, 1-14(1965).

[43] Tepper, F., Zelenak, J., Rochlich, F., and May, V., Thermophysical and Transport Properties of Liquid Metals, AFML-TR-65-99, 1-103(1965). [AD 464138; X65-18506]

[44] Kapelner, S.M., The Electrical Resistivity of Lithium and Sodium-Potassium Alloy, Pratt and Whitney Aircraft Division, USAEC Rept. PWAC -349, 1-33 (1961).

[45] Gates, D.S. and Thodos, G., The critical constants of the elements, A.I. Ch.E.J. 6(1), 50-54 (1960).

[46] Weatherford, W.D.,Jr., Tyler, J.C., and Ku, P.M., Properties of Inorganic Energy-Conversion and Heat-Transfer Fluids for Space Applications, Southwest Research Inst., San Antonio, Texas, WADD TR-61-96, 1-470 (1961).[AD 267 541]

[47] Grosse, A.V., Thermal Conductivity of Liquid Metals over Their Entire Liquid Range, i.e., from Melting Point to Critical Point, in Relation to Their Electrical Conductivities, and the Fallacy of Dividing Metals into "Normal" and "Abnormal" Thermal Conducting Ones, (Temple University Philadelphia, Pa.,Research Institute) TID-21737, 1-76 (Dec. 7, 1964).

[48] Flynn D. R. and O'Hagan, M. E., Measurements of the thermal conductivity and electrical resistivity of platinum from 100 to 900 °C, J. Research NBS 71C, 255 - 284 (1967).

[49] Flynn, D. R. and O'Hagan, M. E., Measurements of the thermal conductivity and electrical resistivity of platinum from 100 to 900 °C, Engelhard Tech. Bull. (March, 1968).

[50] Martin, J.J., Sidles, P.H., and Danielson, G.C., Thermal diffusivity of platinum from 300 to 1200K, J. Appl. Phys. 38 (8), 3075-3078 (1967).

[51] Laubitz, M.J. and van der Meer, M.P., The thermal conductivity of platinum between 300 and 1000K, Canadian J. Phys. 44(12), 3173-3184 (1966).

[52] Fieldhouse, I.B., Hedge, J.C., Lang, J.I., and Waterman, T.E., Measurements of Thermal Properties, WADC-TR-55-495 Part II, 1-18 (1956). [AD110 510]

[53] McClelland, J.D.,Rasor,N.S., Dahleen, R.C., and Zehms, E.H., Thermal Conductivity of Liquid Copper, WADC-TR-56-400 Part II,1-6 (1957). [AD 118243]

[54] Lucks, C.F. and Deem, H.W.,Thermal properties of Thirteen Metals, American Society for Testing and Materials, Special Technical Publication No.227, 1-29(1958).

[55] Ewing, C.T., Grand, J.A., and Miller, R.R., Thermal conductivity of liquid sodium and potassium, J. Am. Chem. Soc. 74,11-14(1952).

[56] Deem, H.W. and Matolich, J.,Jr., The Thermal Conductivity and Electrical Resistivity of Liquid Potassium and the Alloy Niobium-1 Zirconium, NASA Rept. BATT-4673-T6, 1-26 (1963).

[57] Arajs, S. and Colvin, R.V.,Thermal conductivity of scandium between 5 and 320°K, in 4th Rare Earth Research Conference, Phoenix, Ariz., Conf.-405-23, 1-10 (1964).

[58] Aliyev, N.G. and Volkenshteyn, N.V., Low-temperature thermal conductivity of scandium and yttrium, Fiz.Metal. i Metalloved 19(5),793 (1965); English Translation: Phys. Metals Metallog. 19(5),141 (1965).

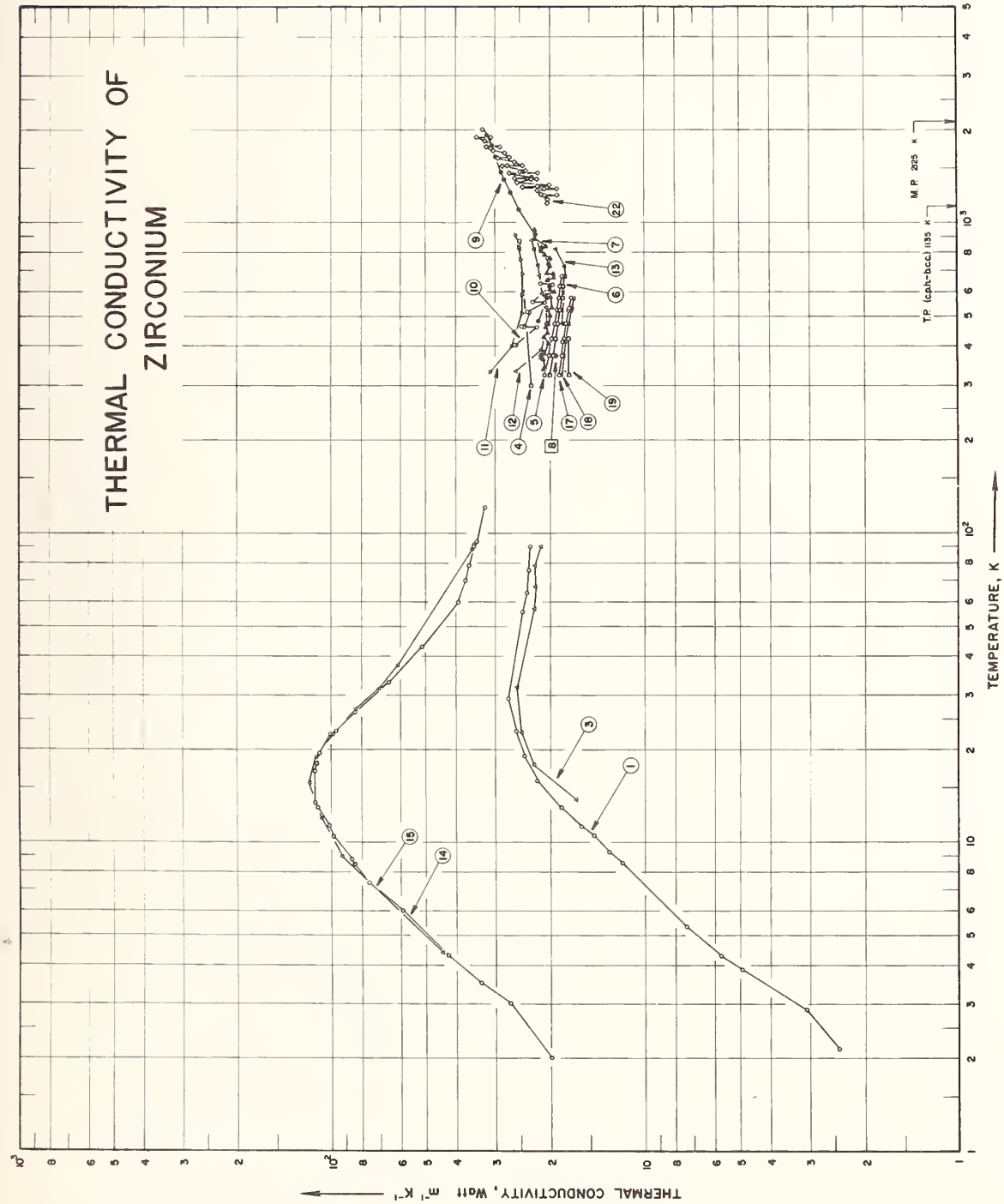

Figure 1. Thermal Conductivity of Zirconium (Logarithmic Scales)

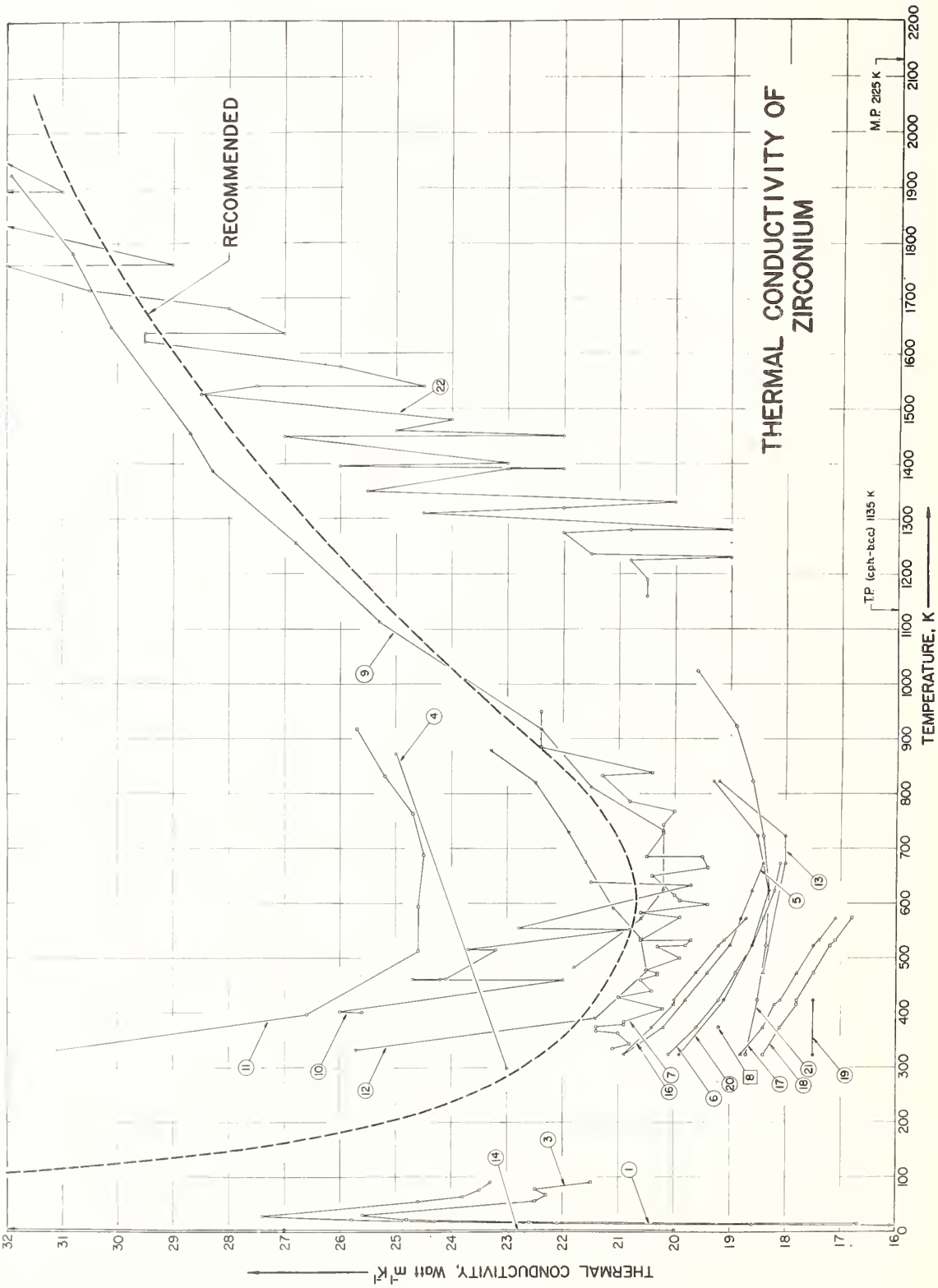

Figure 2. Thermal Conductivity of Zirconium (Linear Scales)

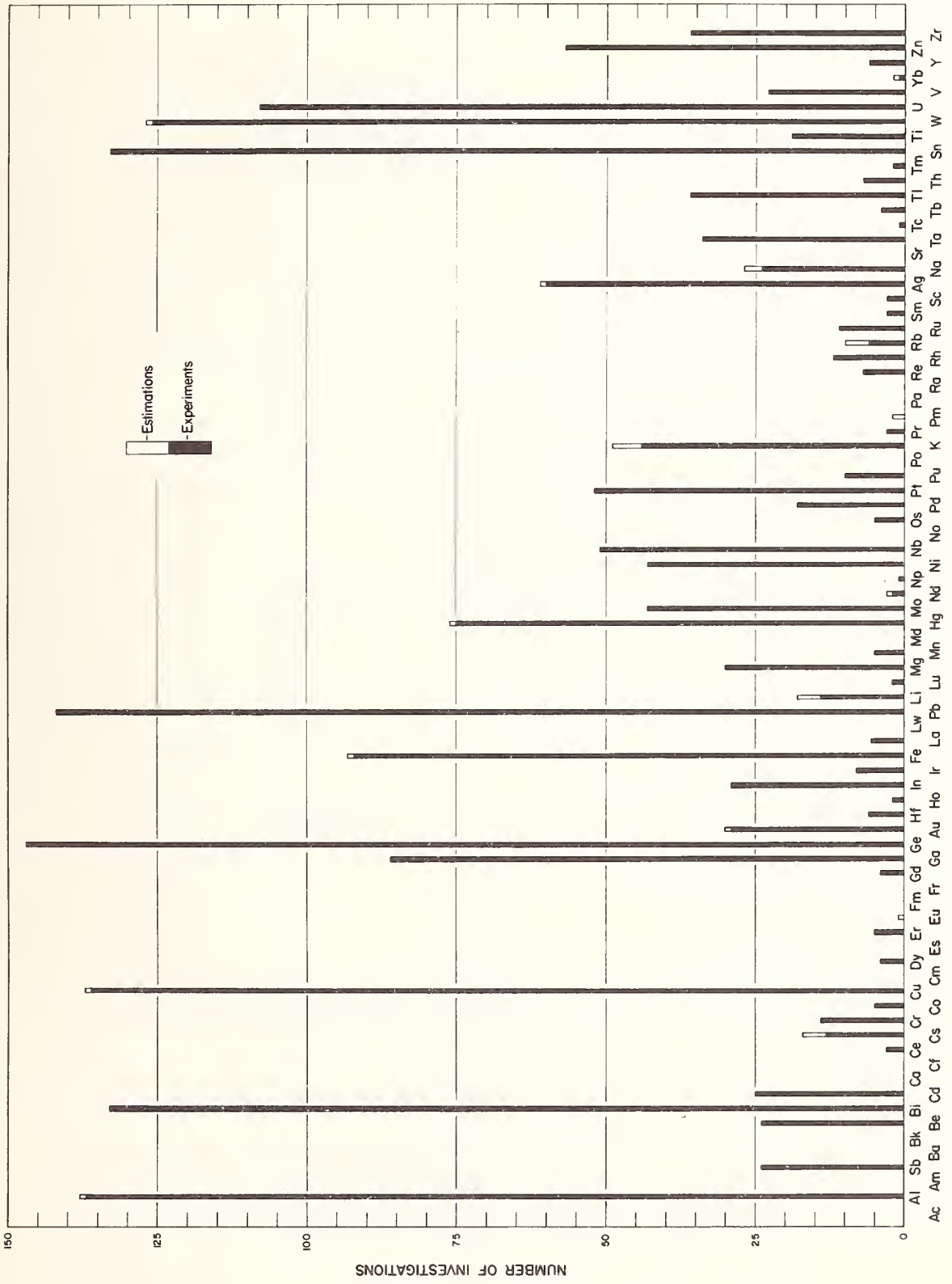

Figure 3. Number of Investigations on the Thermal Conductivity of Metallic Elements

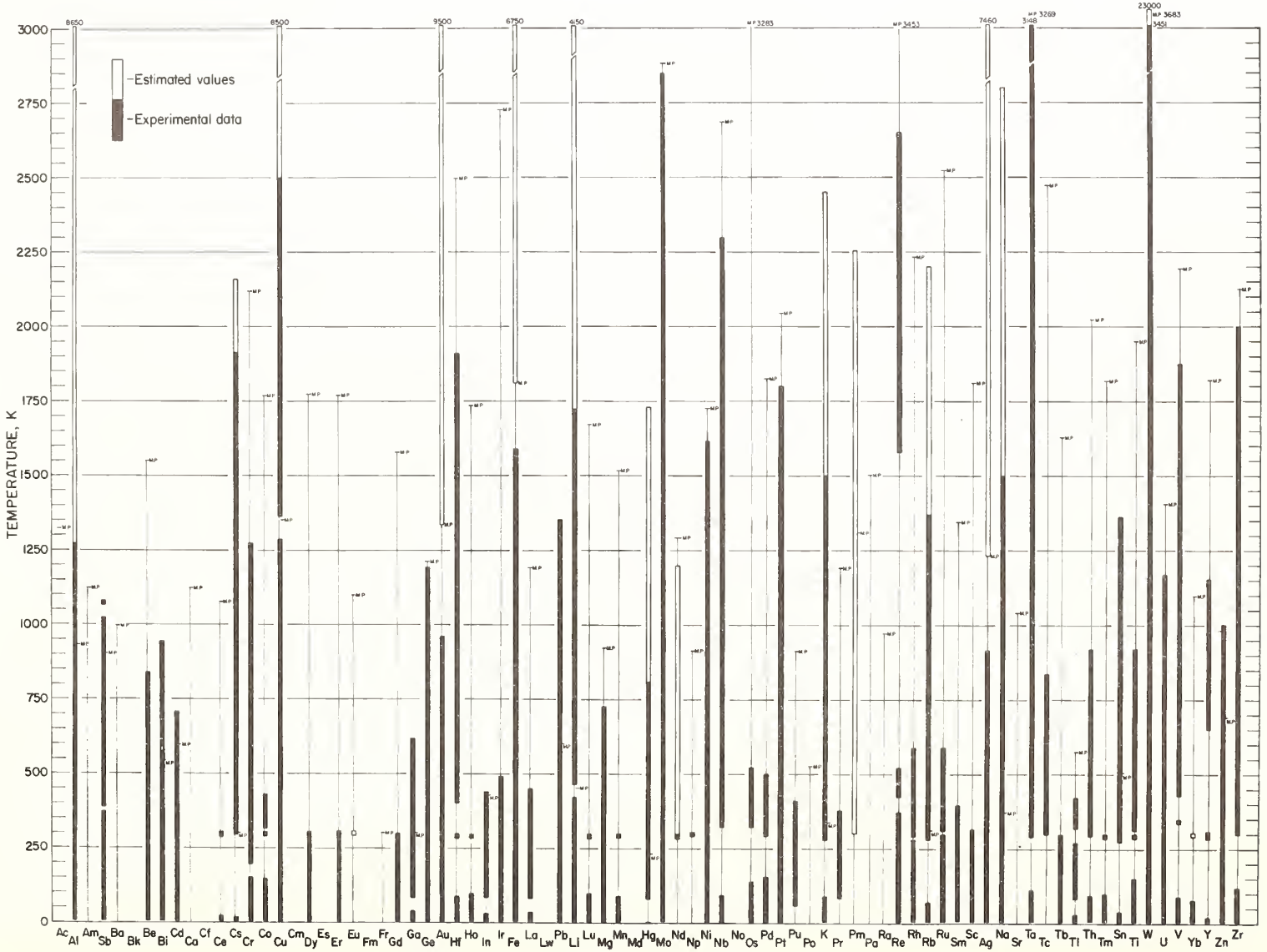

Figure 4. Temperature Ranges of Available Thermal Conductivity Data for the Metallic Elements

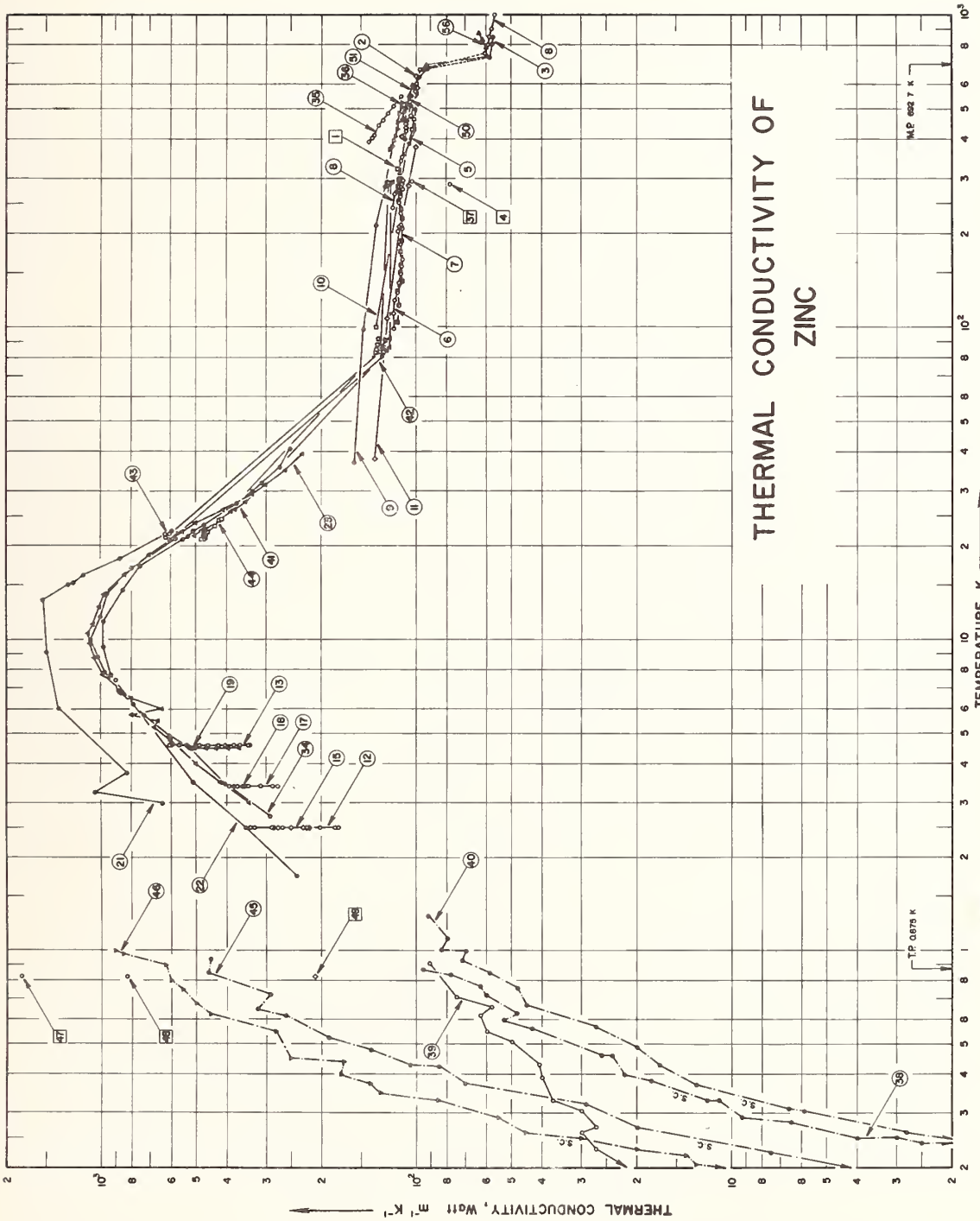

Figure 5. Thermal Conductivity of Zinc (Logarithmic Scales)

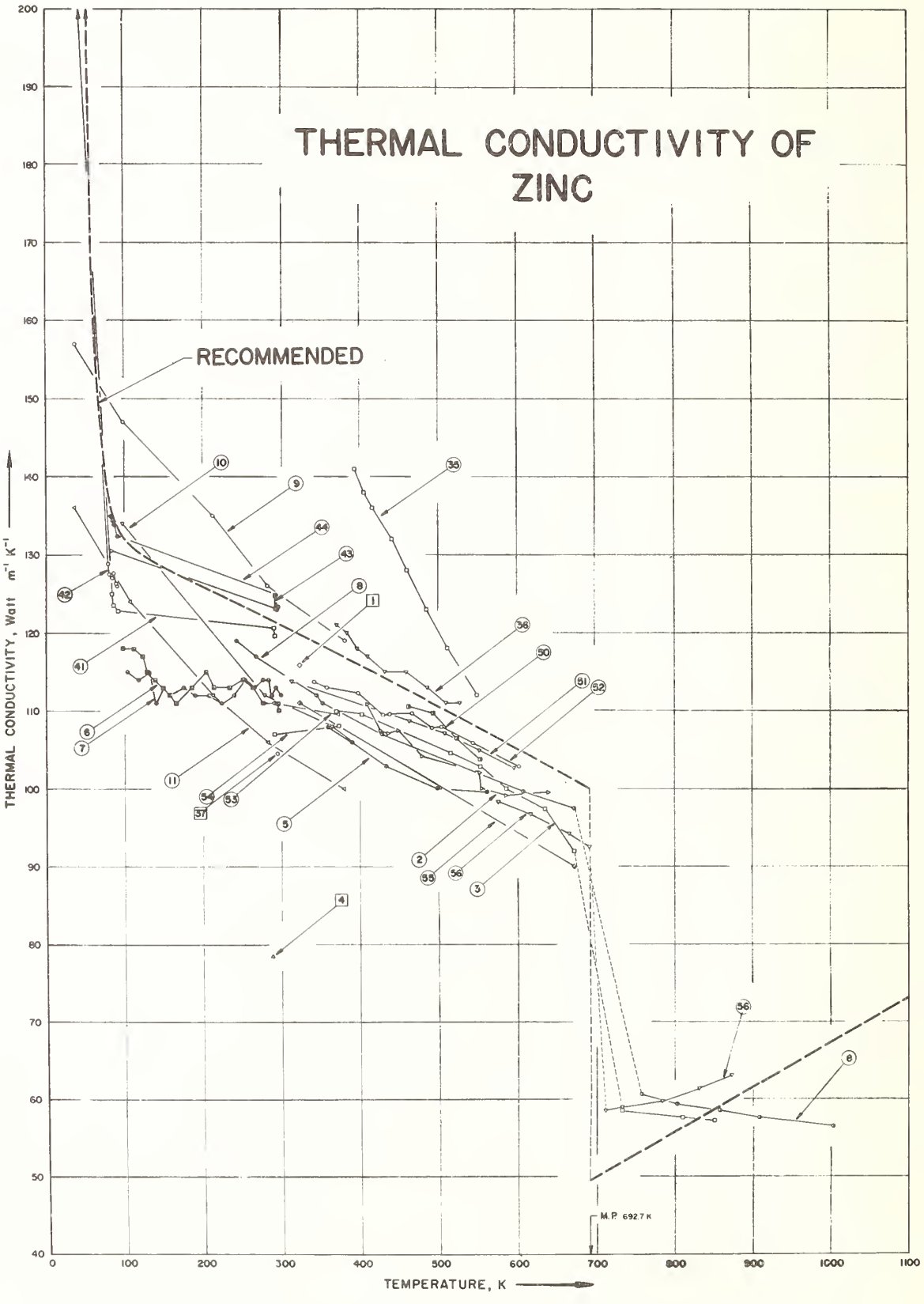

Figure 6. Thermal Conductivity of Zinc (Linear Scales)

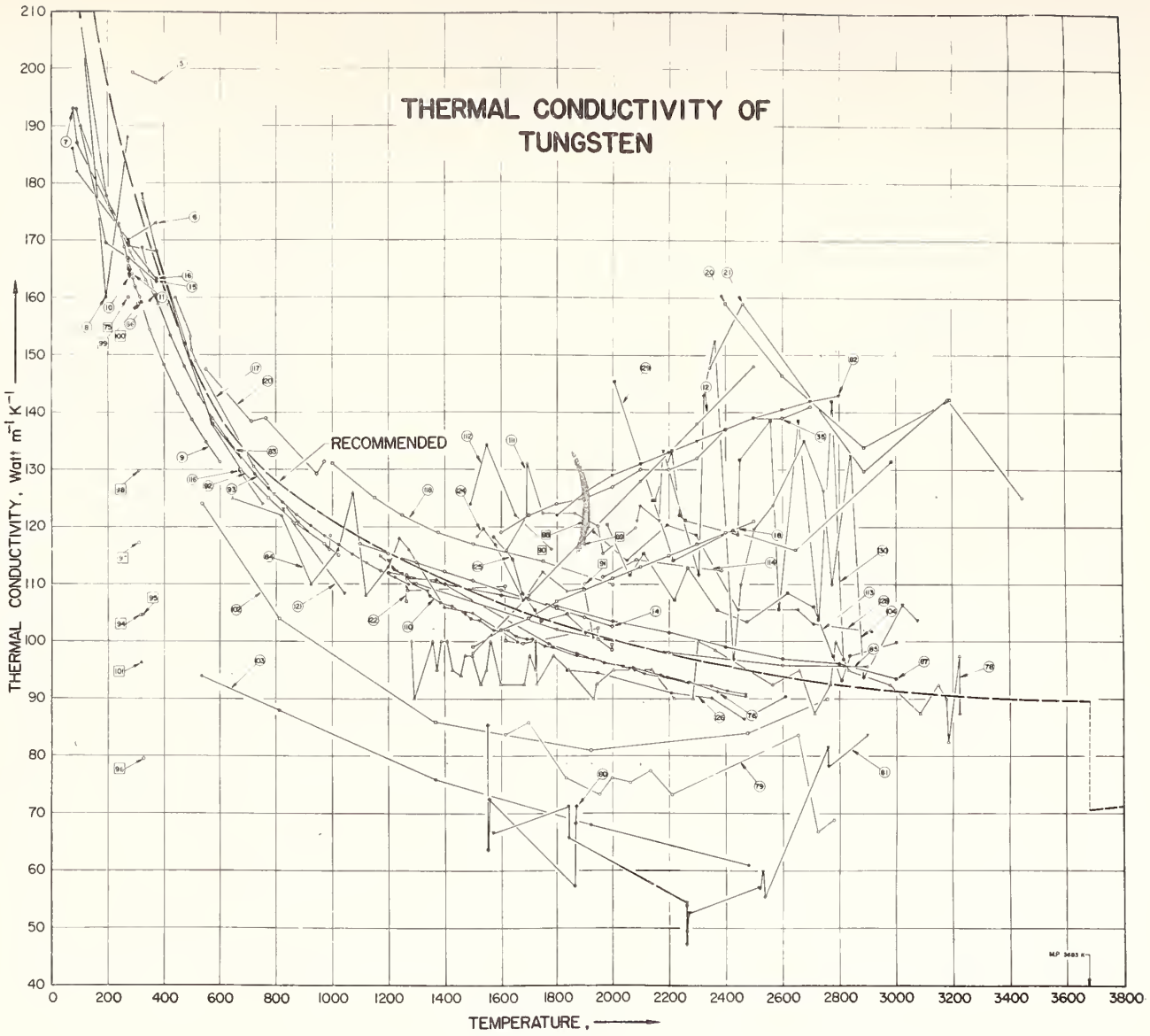

Figure 7. Thermal Conductivity of Tungsten (Linear Scales)

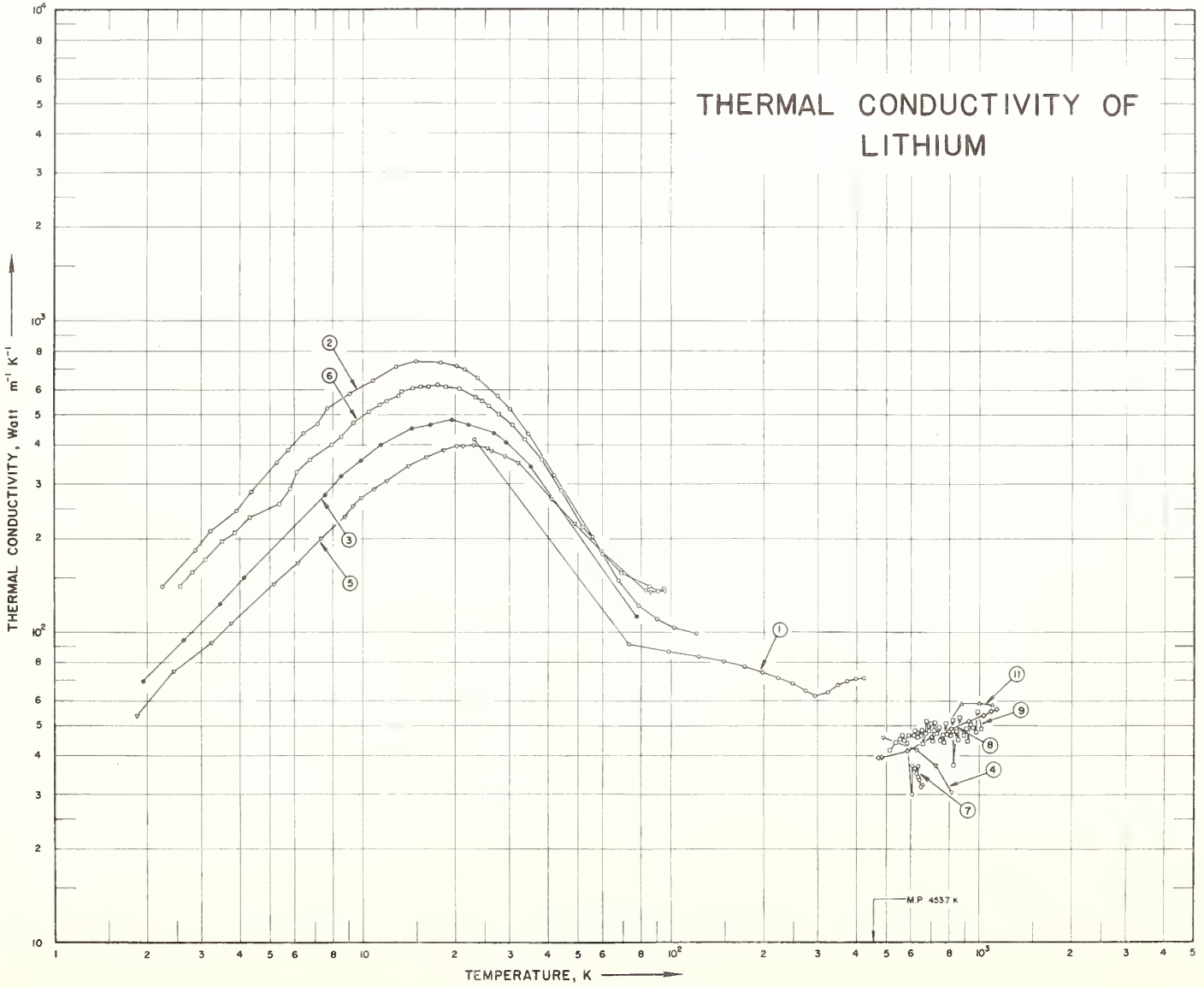

Figure 8. Thermal Conductivity of Lithium (Logarithmic Scales)

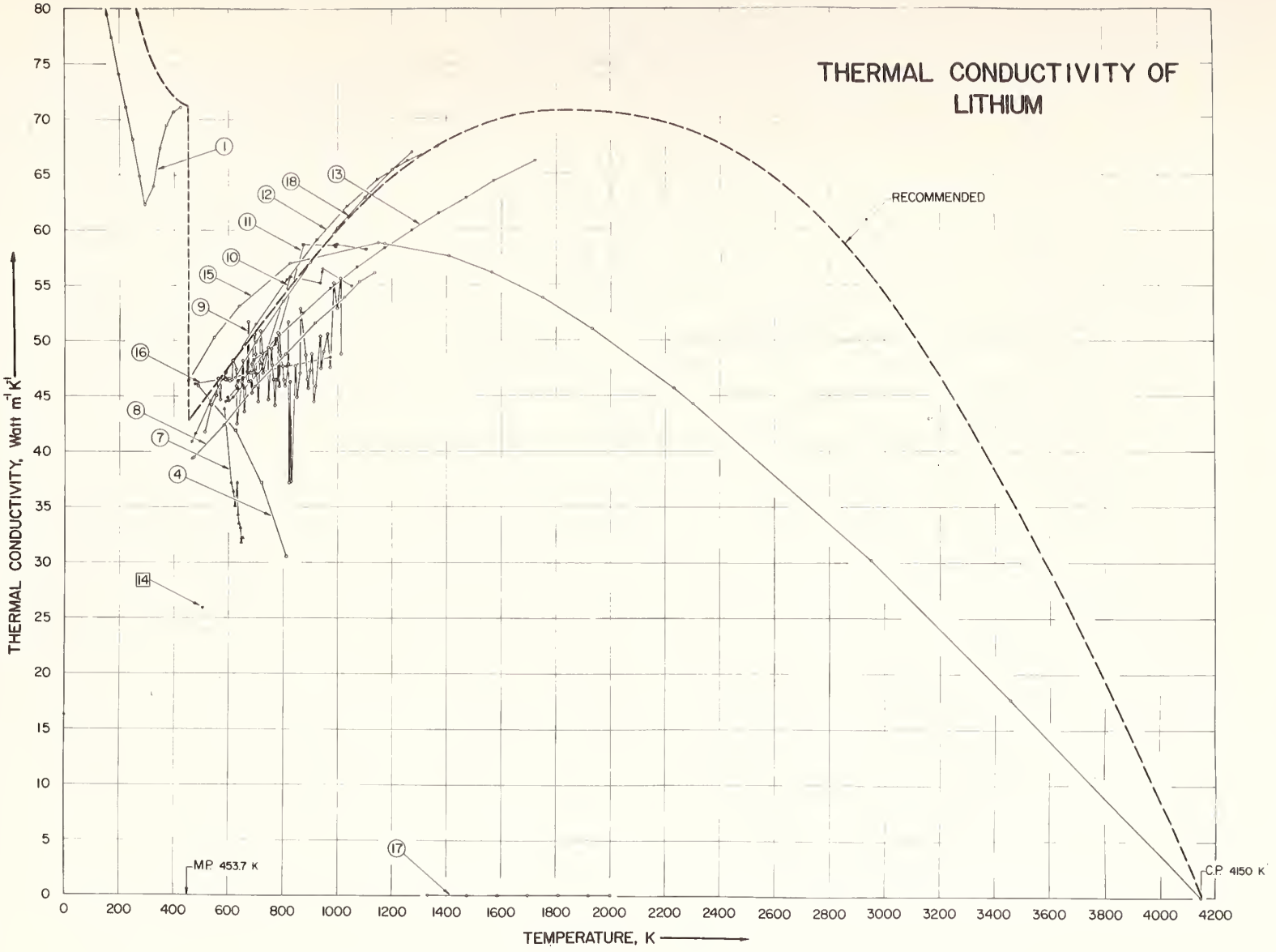

Figure 9. Thermal Conductivity of Lithium (Linear Scales)

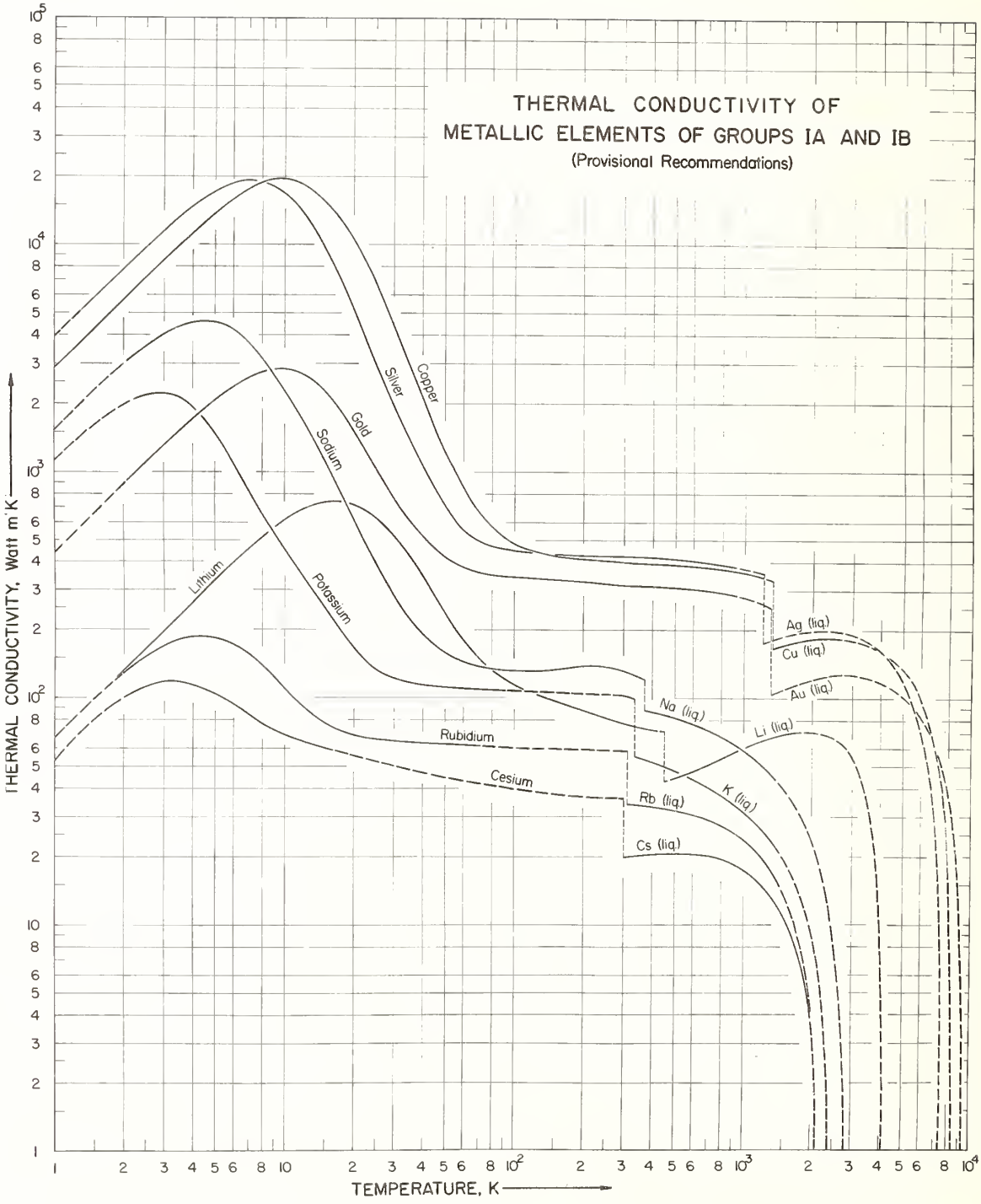

Figure 10. Thermal Conductivity of Metallic Elements of Groups 1A and 1B (Provisional Recommendations)

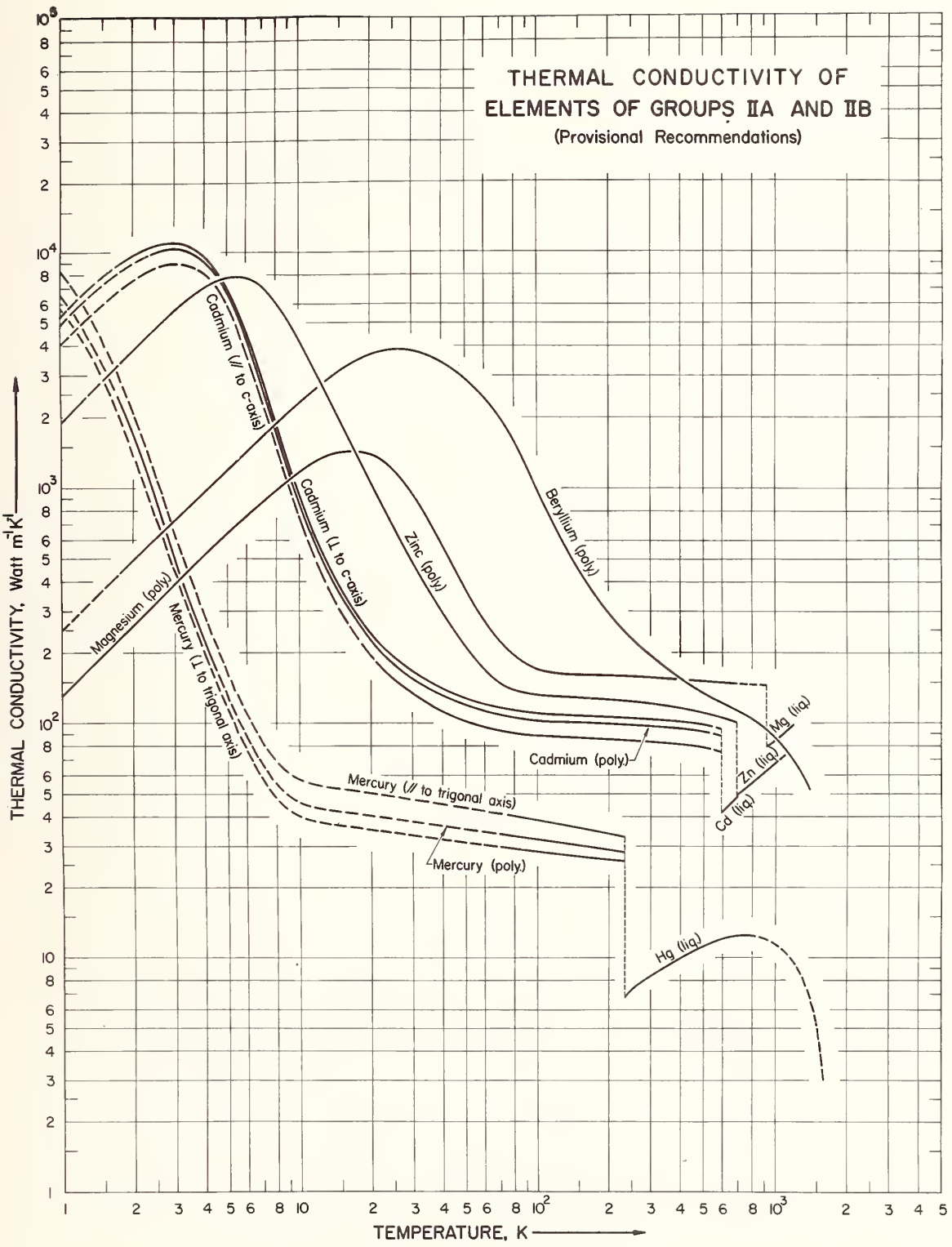

Figure 11. Thermal Conductivity of Elements of Groups IIA and IIB(Provisional Recommendations)

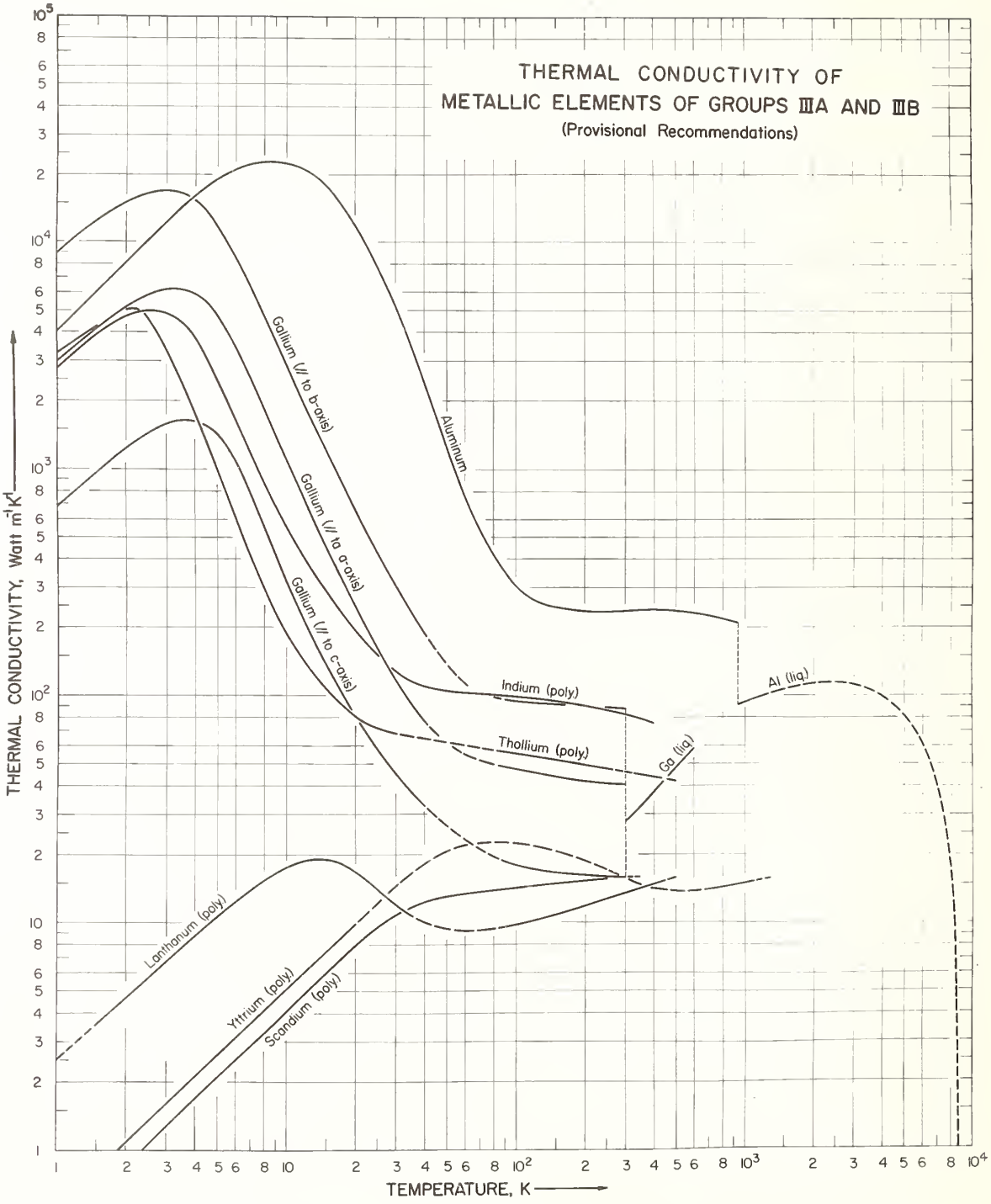

Figure 12. Thermal Conductivity of Metallic Elements of Groups IIIA and IIIB (Provisional Recommendations)

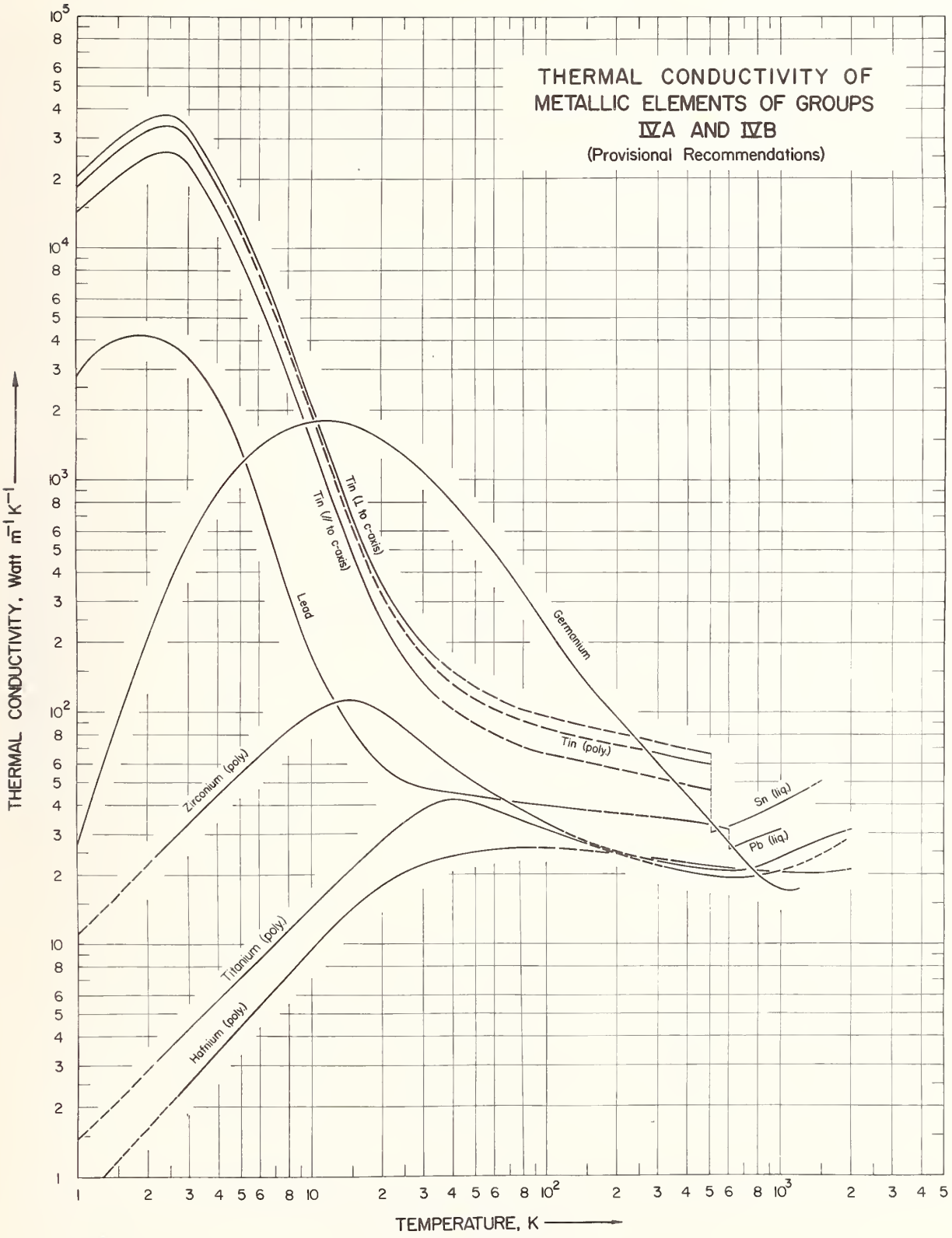

Figure 13. Thermal Conductivity of Metallic Elements of Groups IVA and IVB (Provisional Recommendations)

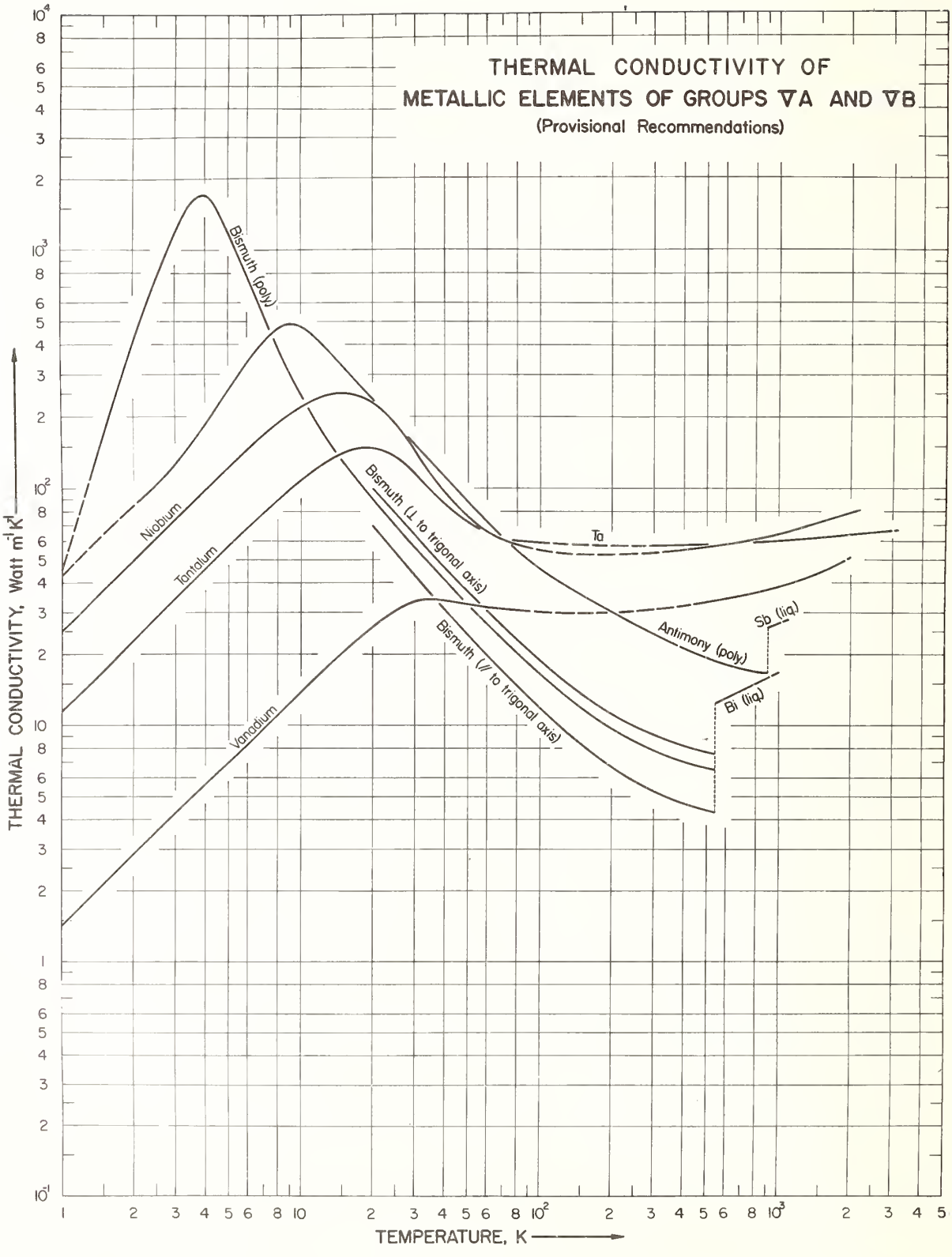

Figure 14. Thermal Conductivity of Metallic Elements of Groups VA and VB (Provisional Recommendations)

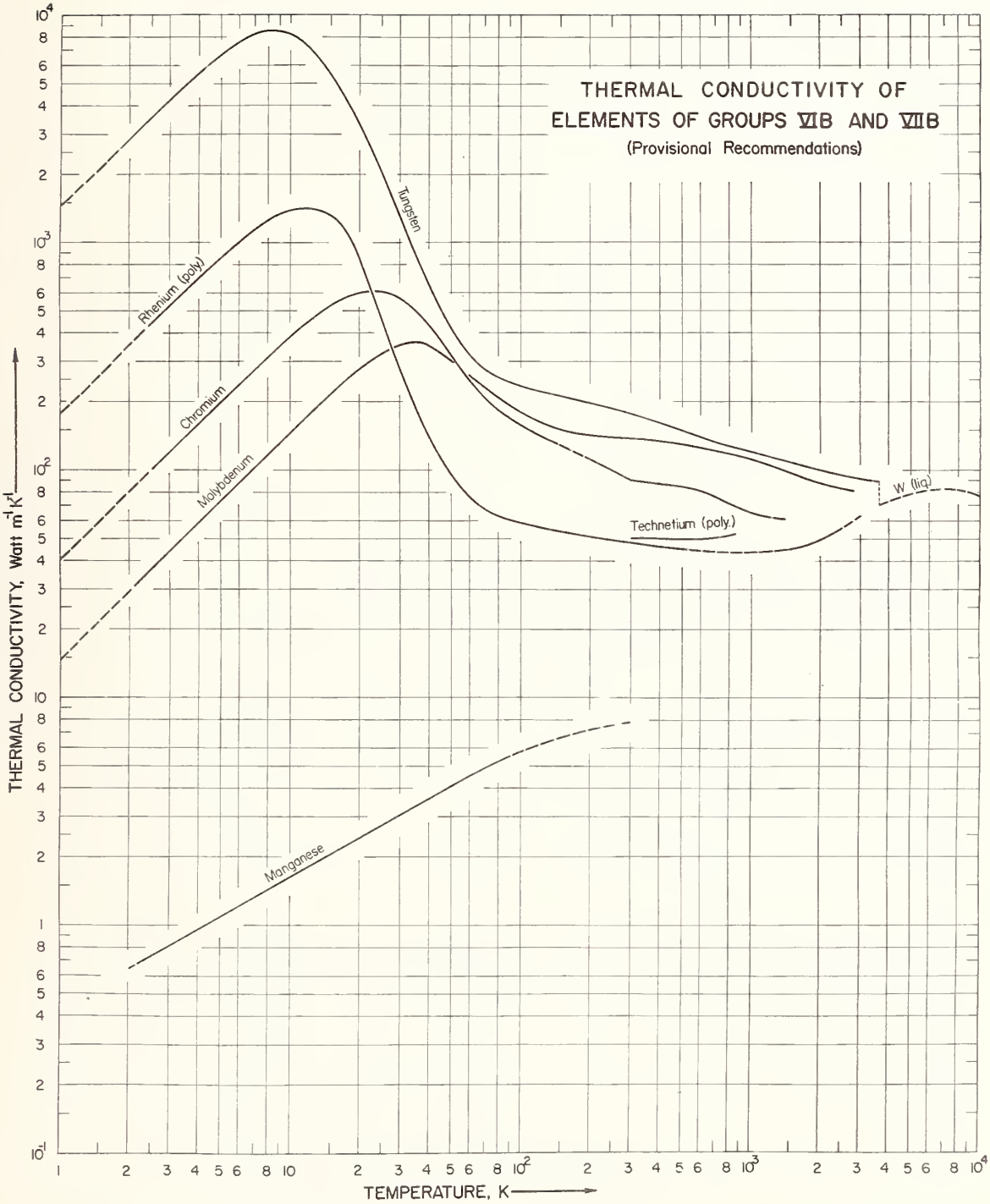

Figure 15. Thermal Conductivity of Elements of Groups VIB and VIIB (Provisional Recommendations)

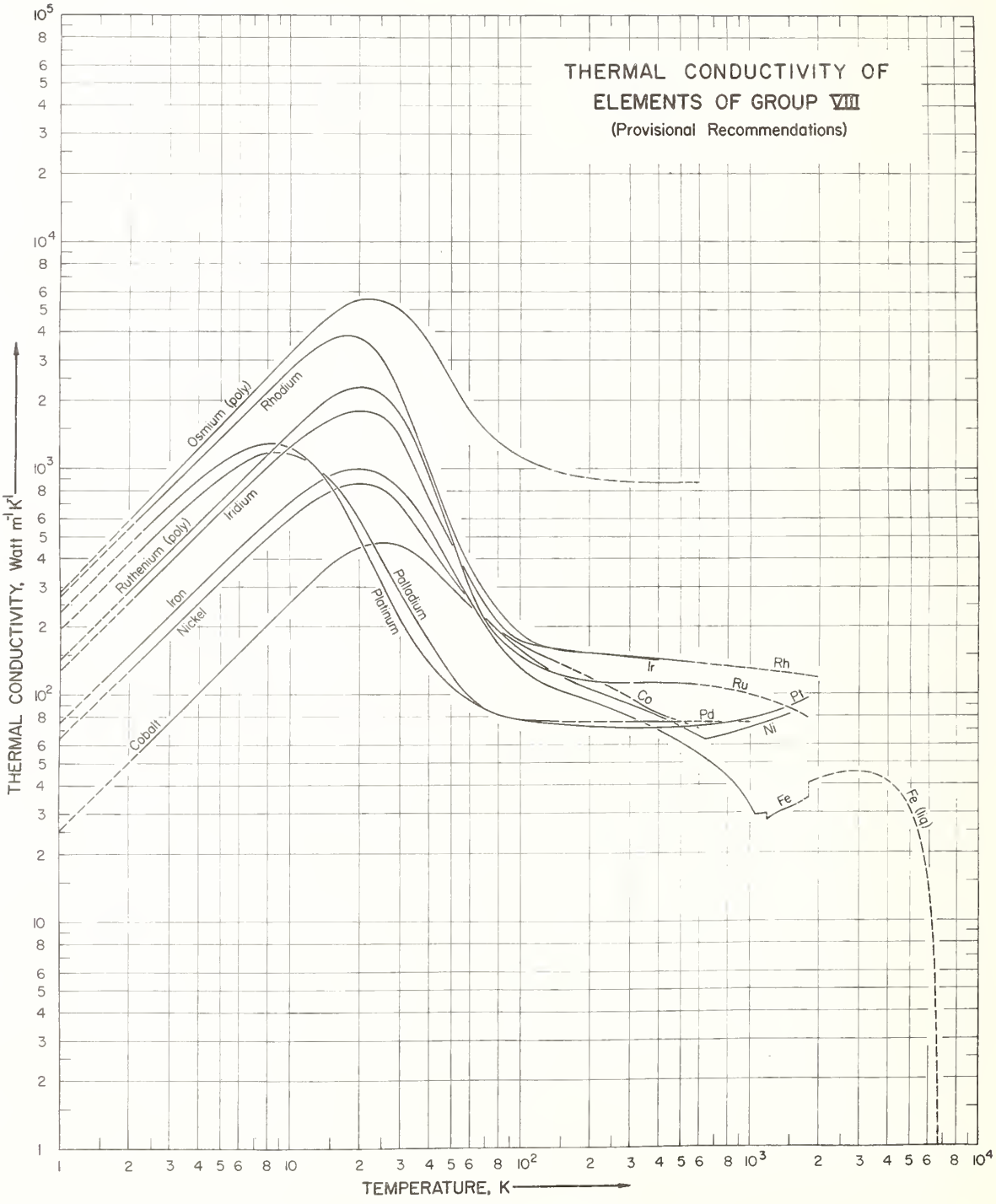

Figure 16. Thermal Conductivity of Elements of Group VIII (Provisional Recommendations)

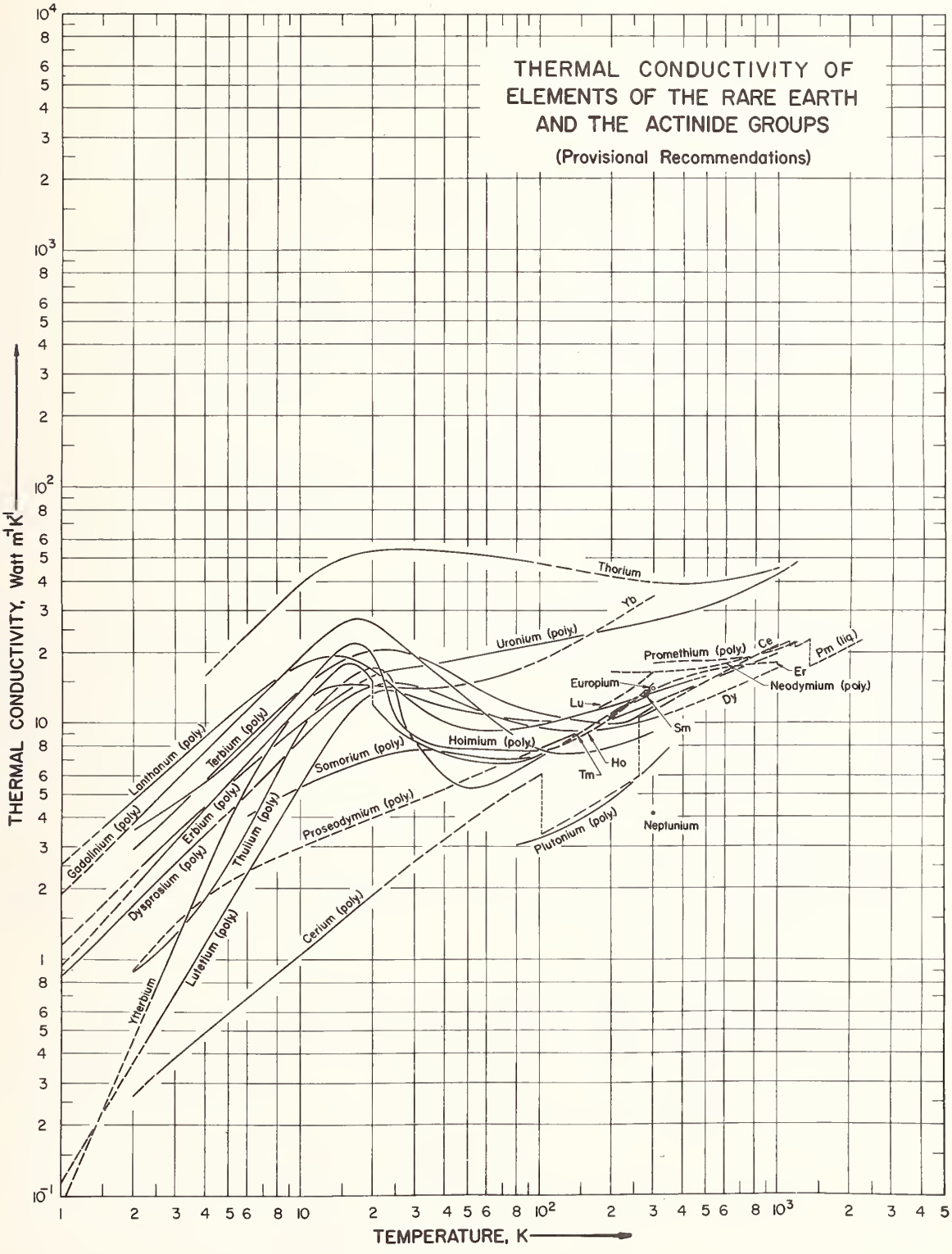

Figure 17. Thermal Conductivity of Elements of the Rare Earth and the Actinide Groups (Provisional Recommendations)

The State of Knowledge Regarding the Thermal Conductivity of the Non-Metallic Elements -- Those Solid at Normal Temperature[1]

C. Y. Ho and R. W. Powell[2]

Thermophysical Properties Research Center, Purdue University, West Lafayette, Indiana 47906

Of the 103 chemical elements, experimental thermal conductivity data are available for 62 metallic elements, 9 non-metallic solids and 11 non-metallic fluids. In this paper, the available thermal conductivity data for the 9 non-metallic solid elements are reviewed. These are arsenic, boron, carbon (in the forms of diamond and graphite), iodine, phosphorous, selenium, silicon, sulfur, and tellurium.

Key words: Amorphous solid, arsenic, boron, carbon, conductivity, diamond, graphite, iodine, liquid phase, non-metallic elements, phosphorus, polycrystal, selenium, single crystal, silicon, sulfur, tellurium, thermal conductivity.

1. Introduction[3]

The present paper reviews the information available for the thermal conductivity of the nine non-metallic elements that are solid at normal temperature. It is complementary to the accompanying paper by Powell and Ho [1][4], and, the two papers seek to give the complete information for the normal solid elements. As before attention is directed to the areas that need to be studied. In the course of this work, earlier TPRC publications [2] have been considerably up-dated and attempts have been made to assess the available results so as to yield most probable values. Similar assessments were previously made for diamond [3] and for graphite [4] but those for amorphous carbon, arsenic, boron, iodine, phosphorus, selenium, silicon, sulfur, and tellurium are new. No information has been located for astatine. As was explained in [1], the present assessments regarding the most probable thermal conductivities should be treated as provisional values for which constructive comments would be welcomed, together with notes of any further relevant information.

Because of the provisional nature of these values it has not seemed desirable to tabulate them at this stage. Graphical presentation of these interim values should suffice for those having expert knowledge of these materials to judge whether the present proposals are reasonable ones, and at the same time the curves will give clear indications of the temperature ranges for which values are available. The forthcoming work on the thermal conductivities of the elements referred to in [1] will of course contain tabulated recommended values.

2. Notes on the Existing Information and Its Assessment

Table 1 is included as an example of the manner in which the experimental information available for the thermal conductivity of a particular material has been tabulated. This is for sulfur, an element for which only 21 sets of experimental data have been located and the relevant information is contained in a table of reasonable size. For graphite there are 582 entries.

---

[1]This paper covers a more restricted field than was originally indicated. Some of the omitted matter has appeared in "Thermal Conductivity of Selected Material," Powell, R.W., Ho, C.Y., and Liley, P.E., National Standard Reference Data System NSRDS-NBS 8 (November 1966).

[2]Head of Reference Data Tables Division and Senior Researcher, respectively.

[3]Much of the "Introduction" of the accompanying paper by R.W. Powell and C.Y. Ho applies equally to this paper but is not repeated.

[4]Figures in brackets indicate the literature references at the end of this paper.

Table 1. Specifications of the Specimens of Sulfur

Curve No.	Ref. No.	Author(s)	Year	Met'd Used	Temp. Range (K)	Reported Error, %	Name and Specimen Designation	Composition (weight percent), Specifications and Remarks
1	5	Kaye, G.W.C. and Higgins, W.F.	1929	L	293-368			Commercial purity; crystalline variety of rhombic aggregate state; specimen prepared at temperature not exceeding 160 C.
2	5	Kaye, G.W.C. and Higgins, W.F.	1929	L	368-383			The above specimen in monoclinic aggregate state.
3	5	Kaye, G.W.C. and Higgins, W.F.	1929	L	388-483			Commercial purity; in liquid state.
4	6	Eucken, A.	1911	L	83,273			Rhombic crystalline sulfur.
5	6	Eucken, A.	1911	L	83,273			Amorphous; made by casting boiling sulfur.
6	7	Slack, G.A.	1965	L	2.6-81		R 124	Single crystal of the stable orthorhombic modification slowly grown from a CS_2 solution at room temperature in one week; sulfur starting material > 99 pure; rod-shaped sample about 0.2 cm in dia and 0.7 cm long; transparent with a yellow color; a few small internal growth flaws visible in the sample; heat flow perpendicular to the c-axis.
7	7	Slack, G.A.	1965	L	3.2-92		R 127	Similar to the above specimen but heat flow parallel to the c-axis.
8	8, 9	Yoshizawa, Y., Sugawara, A., and Yamada, E.	1964	C	285-354	±1		99.98 pure; α(rhombic) sulfur; polycrystalline; crown glass plate used as comparative material, the thermal conductivity of which is given as $k = 0.803 + 0.00054\ t$ with k in kcal m^{-1} $hr^{-1}C^{-1}$ and t in C.
9	9	Sugawara, A.	1965	C	370-389	±1		99.98 pure; β(monoclinic) sulfur; polycrystalline; same comparative material used as above.
10	9	Sugawara, A.	1965	C	395-428	±1		99.98 pure; liquid sulfur; same comparative material used as above.
11	10	Lees, C.H.	1898	L	306,334			4 cm dia x 0.193 cm thick.
12	11, 12	Mogilevskii, B.M. and Chudnovskii, A.F.	1964	P	305-460			Data cover both solid and liquid states.
13	13	Green S.E.	1932	R	277-353			Rhombic crystal; spherical shell specimen with O.D. 10.200 cm and I.D. 5.514 cm; prepared by melting sulfur flowers at 170 C, cast in a brass mould, cooling to complete solidification in about 1.5 hrs, lowering the temperature to about 60 C for 30 min, then allowing to cool in the lagging; density 1.90 g cm^{-3}.
14	13	Green S.E.	1932	R	280-358			Rhombic crystal; spherical shell specimen with O.D. 10.208 cm and I.D. 5.508 cm; prepared by melting sulfur flowers at 127 C poured into a brass mould, heated to 135 C, cooled to the melting point in about 5 hrs, completely solidified after another 40 min; density 1.94 g cm^{-3}.
15	14	Turnbull, A.G.	1959	P	460-574	<±3		Chemically pure; molten specimen contained in a cell made from two thick-walled silver tubes, the liquid annulus has an outer dimension of 28.5 mm dia x 100 mm long and a width of 8 mm; held for 24 hrs at each temperature during measurements.
16	15	Hecht, H.	1904	P	373.2			10.8 cm cubic specimen; density 2.03 g cm^{-3}; thermal conductivity value calculated from measured thermal diffusivity and the specific heat value of 0.187 cal $g^{-1}c^{-1}$.
17	16	Lees, C.H.	1892	C	287.4			Irregular shaped plate specimen 0.0584 cm in thickness; prepared by pressing between two microscope slides having plane surfaces; brass used as comparative material.
18	17	Niven, C. and Geddes, A.E.M.	1912	L	276.7			Thin plate specimen.
19	18	Ioffe, A.V. and Ioffe, A.F.	1952	L	300			Amorphous sulfur.
20	18	Ioffe, A.V. and Ioffe, A.F.	1952	L	300			Single crystal; heat flow along one crystal axis.
21	18	Ioffe, A.V. and Ioffe, A.F.	1952	L	300			Single crystal; heat flow along another crystal axis perpendicular to the above.

In table 1 the numbered references have been altered to correspond with those of this paper. The last column contains the summarized specimen details which were thought to be significant and it seems desirable to comment on the sixth and seventh entries. These relate to measurements by Slack [7] for two single crystals of sulfur, exceeding 99 percent purity; each a rod-shaped specimen about 0.7 cm long and 0.2 cm in diameter, cut from a crystal of the stable orthorhombic modification to give the heat flow perpendicular to the c-axis in No. 6 and in No. 7 parallel to this direction. Slack noted that a few internal growth flaws were visible in the samples studied. Since these samples were tested to temperatures below that of the thermal conductivity maximum, the most important of these facts is the sample size, since the thermal conductivity of a non-metallic single crystal near absolute zero is mainly governed by the boundary scattering. An otherwise similar specimen, cut from the same crystal, but of larger diameter will have a proportionately greater thermal conductivity over the very low temperature region. The crystallite size will behave similarly.

The corresponding logarithmic plot of the temperature variation of the thermal conductivity of sulfur is given in figure 1, and it is of interest to comment first on the two low temperature curves numbered 6 and 7. Over about the range 12 to 90 K the two curves lie within 10 percent crossing over at 25 K. These differences are probably consistent within the experimental uncertainty, but at the maxima and at lower temperatures the differences increase to over 300 percent, the thermal conductivity for the direction parallel to the c-axis appearing greater. However, Slack did not regard these differences as due to true crystal anisotropy, but thought them to result from differences in crystal perfection. Slack reported the confirmation of little if any anisotropy in λ for sulfur by some room temperature measurements on other samples by a comparative measurement of the de Sénarmont type [19], the values so obtained all agreeing to within 20 percent.

The foregoing rather incidental remarks are important in that they introduce some of the precautions involved at low temperatures with this type of work.

Slack's measurements , as shown in curves 6 and 7 of figure 1 stop at about 90 K. He considered radiation transfer to have become a limiting factor in the attainable experimental accuracy, and stated that the measurements of Eucken [6] (curve 4), which link on well with the data of several other workers near room temperature, probably represent the behavior at higher temperatures.

This would leave the measurements for sulfur in a fairly satisfactory state except for two points at 300 K due to A.V. Ioffe and A.F. Ioffe [18]. These are numbered 20 and 21 and are for single crystals having the heat flow along two mutually perpendicular axes. Slack only mentioned this Russian work as a 'Note added in proof' and it is unfortunate that this work came to his notice after his own measurements were completed,for several uncertainties now arise. The ratio for these two axial directions is 1.27 and indicates an anisotropy which exceeds the 20 percent regarded as negligible by Slack. He deduced that the higher value would be for the c-axial direction, and, if so this would agree with his own results at low temperatures but not at his upper temperature limit. As the Russian values are much higher, the question remains, are these on curves which would remain higher to low temperatures, or should Slack's curves flatten out towards these values?

These questions now remain for future work to answer. For the present it has been decided to ignore these Russian values until more evidence is available and to follow the course suggested by Slack. This gives a drop of about 33 percent at the $\alpha \rightarrow \beta$ phase transformation, a constant value for the monoclinic form, which could be subject to further investigation, and another drop of about 18 percent on passing into the liquid phase. Three out of four observers agree with the curve chosen for the liquid phase,and all four,that the phase has a small positive coefficient in this range near the melting point (See [3] or fig. 7).

Much more could be said about individual measurements and other uncertainties would probably arise for each element considered. In this short account , further detailed treatment is impossible and an attempt has been made to convey an overall picture of the present position through figures 2 and 3. Figure 2 illustrates for the three main types of carbon and for the other elements under consideration the number of sets of measurements for which TPRC has information, whilst figure 3 shows the total ranges of temperature that have been covered for each material.

It will be noted that no information is available for astatine and but little for arsenic and iodine. Indeed, knowledge of the thermal conductivity of arsenic is limited to one single measurement at 293 K by Little [20] in 1926, and that of iodine for the solid phase rests on measurements published in 1923 [21] for a narrow range of temperature close to normal. The measurements shown for the range 447 to 693 K relate to the vapor phase of iodine, there being none for the liquid phase, although estimated curves extending to the critical point (785 K), have been proposed [22] for both liquid and vapor. No other measurements for the vapor phase occur, so any other instance where the vertical line of figure 3 exceeds the melting point relates to the liquid phase.

The available data for silicon are shown by means of logarithmic and linear plots in figures 4 and 5. Both figures are included because silicon is an element that has attracted a lot of interest and it seems desirable to comment on the data available at both low and high temperatures. Much of the low temperature data included in figure 4 relate to samples that have been doped to give silicon of either n- or p-type. The location of the thermal conductivity maximum reveals no well-defined dependence on the crystal type. Holland [23] reports the highest maximum value of 5230 $Wm^{-1}deg^{-1}$. This occurs at 22.5 K and is for an n-type single crystal of silicon doped with phosphorus. The same worker is also responsible for the highest value for a p-type crystal, one doped with boron for which his value is 4700 $W\ m^{-1}\ deg^{-1}$ at 24 K.

This figure has been included to illustrate an unusual type of variation in the location of these maxima. For most materials, increase of purity leads to a higher maximum which occurs at a proportionately lower temperature. This type of variation is in fact seen for many of the silicon results where T_m decreases from about 200 to 22.5 K as λ_m increases from 42 to 5230 $Wm^{-1}deg^{-1}$. On the other hand there are maxima which remain in the temperature range 18 to 28 K as λ_m increases from 116 to 5230 $Wm^{-1}deg^{-1}$. In each group there are examples of both n- and p-type silicon, though in the latter group the majority of the samples are of n-type and in the former group the majority are of p-type.

In this low temperature range the most probable curve for pure silicon has been based on Holland's highest curve. Below the lowest temperature his curve has been extrapolated parallel to sets of data by Carruthers, Geballe, Rosenberg, and Ziman [24] as shown by curves 4 and 5 and in this range $\lambda \sim T^{2.9}$, in fair agreement with the T^3 dependence of specific heat.

At 120 K, the upper limit of Holland's measurements on the chosen sample,the curve merges into No. 31 of Glassbrenner and Slack [25]. Their measurements extend almost to the melting point and over much of the high temperature range, shown more clearly in figure 5. They agree with the values of curve 82 due to Fulkerson et al. [26] to within about 4 percent, the latter values being lower. The proposed curve has been drawn intermediately between these two sets of data and has been continued smoothly to the melting point.

No determinations appear to have been reported for the thermal conductivity of liquid silicon, and, in view of the electronic contribution to the thermal conductivity of the solid near the melting point, which is believed to be about 5 percent [25], any estimation for the liquid phase from electrical resistivity data would seem to present considerable uncertainties .

The treatment given the remaining elements has been similar but can only be briefly indicated. The curves that have been previously recommended for diamond and graphite and those which are now provisionally recommended for the other elements are reproduced in figures 6 and 7.

Arsenic: -- The one available measurement is for room temperature only, but should the thermal conductivity of arsenic be required over a wider range, examination of figure 7 suggests that extrapolation in keeping with the form of the other curves could produce some very provisional values.

Boron: -- Values and predictions by Slack [7] have been adopted. His measurements are only for the range 3 to 300 K, but he gave extrapolated values to about 1473 K, the $\alpha \rightarrow \beta$ transformation temperature. At 630 K however some values reported by Morris [27] are some 60 percent greater.

Carbon: -- In the amorphous form the values are low, have a positive coefficient and vary considerably, presumably due to such variables as density, particle size, manufacturing process, etc. No assessment has been attempted. Thermal conductivity of diamond has been reviewed [3]. The very limited data have all been at normal and low temperatures, 320 K being the maximum measurement temperature. Graphite with nearly 600 sets of measurements on its many different forms and grades, and its unusual temperature dependence of thermal conductivity at low and high temperatures, and its higher electrical conductivity is a complex special subject for which reference should be made to an earlier publication [4] in which the general features of the thermal conductivity of graphite have been discussed and separate treatments have been given to pyrolytic graphite and to four commercial grades. Figure 6 shows the tremendous anisotropy of pyrolytic graphite. For a limited range of temperatures above 100 K the thermal conductivity parallel to the layer planes exceeds all known solid materials except diamond, whereas that of pyrolytic graphite in the direction perpendicular to the layer planes is comparable with that of insulators. Between these two curves lie all other grades of graphite. The precise curve at low temperatures for the highly-oriented and well-annealed pyrolytic graphite in the direction perpendicular to the layer planes is largely conjectural since no measurements have been made.

Phosphorus: -- The data of Slack [7] have been accepted for black phosphorus for the range 2.7 to 300 K and those of Turnbull [28] for white phosphorus for temperatures a little above and below the melting point. The latter's data in the liquid phase are preferred over those of Kramer and Schmeiser [29] as his method had appeared to yield satisfactory values for liquid sulfur. Also his values are thought to be in better agreement with simple ' quasi-lattice' theories.

Selenium: -- In the case of selenium the recently published measurements of Adams, Baumann, and Stuke [30] have provided curves for the two main crystal directions. For temperatures above 20 K the thermal conductivity for the direction parallel to the c-axis is about 4 times that for the perpendicular direction. This difference persists to about 100 K, the upper limit of their experiments, and in this temperature range the derived values for polycrystalline selenium show reasonable agreement with a curve due to White, Woods, and Elford [31].

The reeommended curves for the two crystal directions are based on the anisotropy ratio and the highest conducting crystal values of [30] but at low temperatures the values are clearly very dependent on crystal perfection and specimen size. No dimensions are given in [30]. Above 100 K the two curves have been extrapolated in line with other data, turning up at about 350 K.

The two sets of data for the conductivity of liquid selenium differ considerably and a somewhat tentative intermediate curve has been indicated in figure 7.

Tellurium: -- Available data for tellurium also indicate considerable thermal conductivity anisotropy and the two curves shown in figure 7 for the parallel and perpendicular directions have a ratio of about two.

The thermal conductivity of liquid tellurium is far from certain. The proposed curve follows recent values by Benguigui [32], which show liquid tellurium to behave as a semi-metal with a Lorenz function decreasing from 4.4×10^{-8} to 3.2×10^{-8} V^2K^{-2} over the range 743 to 923 K, whereas two earlier sets of measurements [33,34] had indicated much higher values.

3. Summary of Position, with Suggestions for Future Work

The attempt to assess the thermal conductivity data for the non-metallic elements has served to emphasize the value of the additional knowledge that is available for use with metallic elements.

The differences as they apply at present are compared below:

	Metallic Elements	Non-metallic Elements
(a)	At moderate and high temperatures (including liquid phase)	
	$\lambda = LT\rho^{-1}$ approx., where L = Lorenz function, ρ = electrical resistivity	Nothing similar
(b)	At low temperatures	
(1)	Close to absolute zero: $\lambda = L_0 T \rho_0^{-1}$ approx., where L_0 = theoretical Lorenz number, ρ_0 = residual electrical resistivity	Nothing similar
(2)	Over range $0 < T < 1.5\ T_m$: $\lambda = [\alpha' T^n + \beta T^{-1}]^{-1}$ where $\alpha' = \alpha'' (\beta / n\alpha'')^{a/(m+1)}$. See references [3] and [4] for details.	Nothing similar
(c)	Purity and/or perfection increases as: --	
(1)	ρ_{295}/ρ_0 increases	Nothing similar
(2)	β decreases	Nothing similar
	β can be derived from equation of (b) (2) or from $\beta = L_0^{-1}\rho_0$	
(d)	Dependence of λ on sample size: None	At low temperatures (below T_m) λ of a pure crystal increases with size of crystal.

Any suggestions or investigations leading to an acceptable guiding parameter for non-metals would be most useful. At the time when Cezairliyan [35] applied the generalized principle of corresponding states to metallic elements and found the equation given above for the range 0 to 1.5 T_m to hold, he also considered some semi-metals and non-metals. Whereas the various sets of data for bismuth, germanium, silicon, selenium, tellurium, and carbon (graphite) could be similarly correlated in separate curves by plotting the reduced thermal conductivity (λ_T/λ_m) as a function of the reduced temperature (T/T_m), these curves differed amongst themselves as well as from that for the metals. It was concluded that it would be necessary to include some additional parameters to bring these elements collectively or in groups to one or more common curves. This further work is still required.

Until a satisfactory criteria for the net purity and perfection of a non-metallic sample becomes available an element of doubt will exist as to whether a set of measurements made on one sample will be applicable to another sample.

The above are regarded as directions for further work that are common to all non-metallic elements. Some of the thermal conductivity requirements for the individual elements will now be summarized.

Arsenic: -- Measurements for the full temperature range are required to support the single data point at room temperature and any prediction that might be based on this.

Astatine: -- The longest lived isotope of astatine has a half-life of only 8.3 hours, so the thermal conductivity would probably be of academic interest only, and the lack of information is likely to continue.

Boron: -- Boron should be measured above 300 K, the present upper limit. This includes the liquid phase for which no values have been reported.

Carbon: -- Diamond with its high thermal conductivity could be an important material. The proposed values for the three types are based on only a few measurements, all at or below room temperature. More measurements are required and these should be extended to higher temperatures. Graphite in the pyrolytic form requires study to low temperatures for the direction normal to the layer planes. As new forms and distinct grades of graphite are produced new measurements will be required for the full temperature range. Above 3000 K is still a region where some doubt exists.

Iodine: -- Iodine requires measurements over a wide temperature range for both solid and liquid phases. The one available set of values for the solid, reported in 1923, has a negative coefficient that appears unduly large; also measurements have yet to be made for the liquid phase.

Phosphorus: -- Black phosphorus requires further study above 300 K, and white phosphorus below 250 K and check measurements should be included near the solid to liquid transition and well into the liquid phase.

Selenium: -- The present curves for the two main single crystal directions have been extrapolated to temperatures above about 100 K. These require confirmation particularly above about 300 K and well into the liquid phase.

Silicon: -- The solid phase appears to have been adequately covered. No values have been reported for the liquid phase.

Sulfur: -- The data appear to be sufficient for polycrystalline sulfur but new determinations on good single crystals are needed to resolve the differences between the Russian values at room temperature and the extrapolated data of Slack. Should the former be confirmed the measurements on these crystals will be required over the full temperature range.

Tellurium: -- The values adopted for the liquid phase need confirmation.

4. References

[1] Powell, R.W. and Ho, C.Y., The state of knowledge regarding the thermal conductivity of the metallic elements, the preceding paper of these Proceedings.

[2] Touloukian, Y.S., Thermophysical Properties Research Center Data Book, Volume 3, Nonmetallic Elements, Compounds and Mixtures (in Solid State at Normal Temperature and Pressure), Chapter 1, Thermal Conductivity, 457 pages in Chapter 1 as of December 1966.

[3] Powell, R.W., Ho, C.Y., and Liley, P.E., Thermal Conductivity of Selected Materials, National Standard Reference Data System NSRDS-NBS 8 (Nov. 1966).

[4] Ho, C.Y., Powell, R.W., and Liley, P.E., Thermal Conductivity of Selected Materials, Part 2, National Standard Reference Data System NSRDS-NBS 16, in press.

[5] Kaye, G.W.C. and Higgins, W.F., Thermal conductivity of solid and liquid sulfur, Proc. Roy. Soc. (London) A122, 633-46 (1929).

[6] Eucken, A., On the temperature dependence of the thermal conductivity of solid non-metals, Ann. Physik 34(2), 185-221 (1911).

[7] Slack, G.A., Thermal conductivity of elements with complex lattices: B, P, S, Phys. Rev. 139 (2A), A507-15 (1965).

[8] Yoshizawa, Y., Sugawara, A., and Yamada, E., Thermal conductivity of α-sulfur, J. Appl. Phys. 35(4), 1354-5 (1964).

[9] Sugawara, A., Thermal conductivity of sulfur accompanying crystal transition and phase change, J. Appl. Phys. 36(8), 2375-7 (1965).

[10] Lees, C.H., On the thermal conductivities of single and mixed solids and liquids and their variation with temperature, Phil. Trans. Roy. Soc. (London) 191A, 399-440 (1898).

[11] Mogilevskii, B.M. and Chudnovskii, A.F., Measurement of the thermal conductivity of semiconductors by the transient probe method, Inzh.-Fiz. Zh., Akad. Nauk Belorussk. SSR, 7 (12), 23-31 (1964) (Russian).

[12] Mogilevskii, B.M. and Chudnovskii, A.F., Measurement of semiconductor thermal conductivity by a nonsteady probe method, English translation of above, Foreign Technology Div., Wright-Patterson AFB, Ohio, DDC and CFSTI, AD 627 112, FTD-TT-65-1257, TT 66-60371, 1-15 (1966).

[13] Green, S.E., The spherical shell method of determining the thermal conductivity of a thermal insulator, Proc. Phys. Soc. (London) 44, 295-313 (1932).

[14] Turnbull, A.G., Thermal conductivity of molten salts and other liquids, Ph.D. Thesis, Imperial College of Science and Technology. London, 146 pp. (1959).

[15] Hecht, H., Method to determine the thermal conductivity of poorly conducting bodies in sphere and cube form and its performance on marble, glass, sandstone, gypsum and serpentine, basalt, sulfur and coal, Ann. Physik 14, 1008-30 (1904).

[16] Lees, C.H., The thermal conductivity of crystals and other bad conductors, Phil. Trans. Roy. Soc. (London) 183, 481-509 (1892).

[17] Niven, C. and Geddes, A.E.M., On a method of finding the conductivity for heat, Proc. Roy. Soc. (London) 87A, 535-9 (1912).

[18] Ioffe, A.V. and Ioffe, A.F., Simple method of measuring thermal conductivities, Zh. tekh. Fiz. 22 (12), 2005-13 (1952).

[19] de Sénarmont, M.H., Memoir on the conductivity of crystalline substances for heat, Ann. Chim. Phys., 3, 21, 457-70 (1847) and 22, 179-211 (1848); also Compt. Rend., 2, 25, 459-61 (1847).

[20] Little, N.C., Thermomagnetic and galvanomagnetic effects in arsenic, Phys. Rev. 28, 418-22 (1926).

[21] Pochettino, A. and Fulcheris, G., On the electrical and thermal properties of iodine, Atti. Reale Accad. Sci. Turino 58 (14a), 311-20 (1923).

[22] Schaefer, C.A. and Thodos, G., Thermal conductivity of diatomic gases: liquid and gaseous states, A.I.Ch. E. Journal 5(3), 367-372 (1959).

[23] Holland; M.G., Effect of oxygen on the thermal conductivity of silicon, Proc. Intern. Conf. Low Temp. Phys., 7th Toronto, Canada, 1960, 280-4 (1961).

[24] Carruthers, J.R., Geballe, T.H., Rosenberg, H.M., and Ziman, J.M., The thermal conductivity of germanium and silicon between 2 and 300 K, Proc. Roy. Soc. (London) 238A, 502-14 (1957).

[25] Glassbrenner, C.J. and Slack, G.A., Thermal conductivity of silicon and germanium from 3 K to the melting point, Phys. Rev. 134 (4A), A1058-69 (1964).

[26] Fulkerson, W., Moore, J.P., Williams, R.K., Graves, R.S., and McElroy, D.L., Thermal conductivity, electrical resistivity and Seebeck coefficient of silicon from 100 to 1300 K, Phys. Rev., in press.

[27] Morris, R.G., High-temperature thermal conductivity measurements in semiconductors, South Dakota School of Mines and Tech., Status Rept. for 1 Oct. 64 to 30 Sept. 65 under Contract Nonr296401, AD 430 154 (September 1965).

[28] Turnbull, A.G., Thermal conductivity of liquid and solid α-phosphorus, Z. Physik. Chem.(Frankfurt) 42 (3/4), 243-6 (1964).

[29] Kraemer, H. and Schmeiser, K., Thermal conductivity of yellow phosphorus in the temperature range +16 to +80°, Z. Physik. Chem. (Frankfurt)35, 1-9 (1962).

[30] Adams, A.R., Baumann, F., and Stuke, J., Thermal conductivity of selenium and tellurium single crystals and phonon drag of tellurium, Physica Status Solidi 23 (1), K99-K104 (1967).

[31] White, G.K., Woods, S.B., and Elford, M.T., Thermal conductivity of selenium at low temperatures, Phys. Rev. 112 (2), 111-13, (1958).

[32] Benguigui, L., Thermal conductivity of liquid tellurium between 740 and 900 K, Physik Kondensierten Materie 5 (3), 171-77 (1966).

[33] Amirkhanov, Kh. I., Bagdnev, G.B., and Kazhlayev, M.A., Anisotropy of thermal conductivity in single crystals of tellurium, Akad. Nauk. SSSR Doklady 124(3), 554-6, (1959).

[34] Cutler, M. and Mallon, C.E., Thermoelectric study of liquid semiconductor solutions of tellurium and selenium, J. Chem. Phys. 37, 2677-83 (1962).

[35] Cezairliyan, A., Predition of Thermal Conductivity of Metallic Elements and Their Dilute Alloys at Cryogenic Temperatures, Purdue Univ., Thermophysical Properties Research Center, TPRC Rept. 14 (1962); also USAF Rept. ASD-TDR-63-291 (1963).

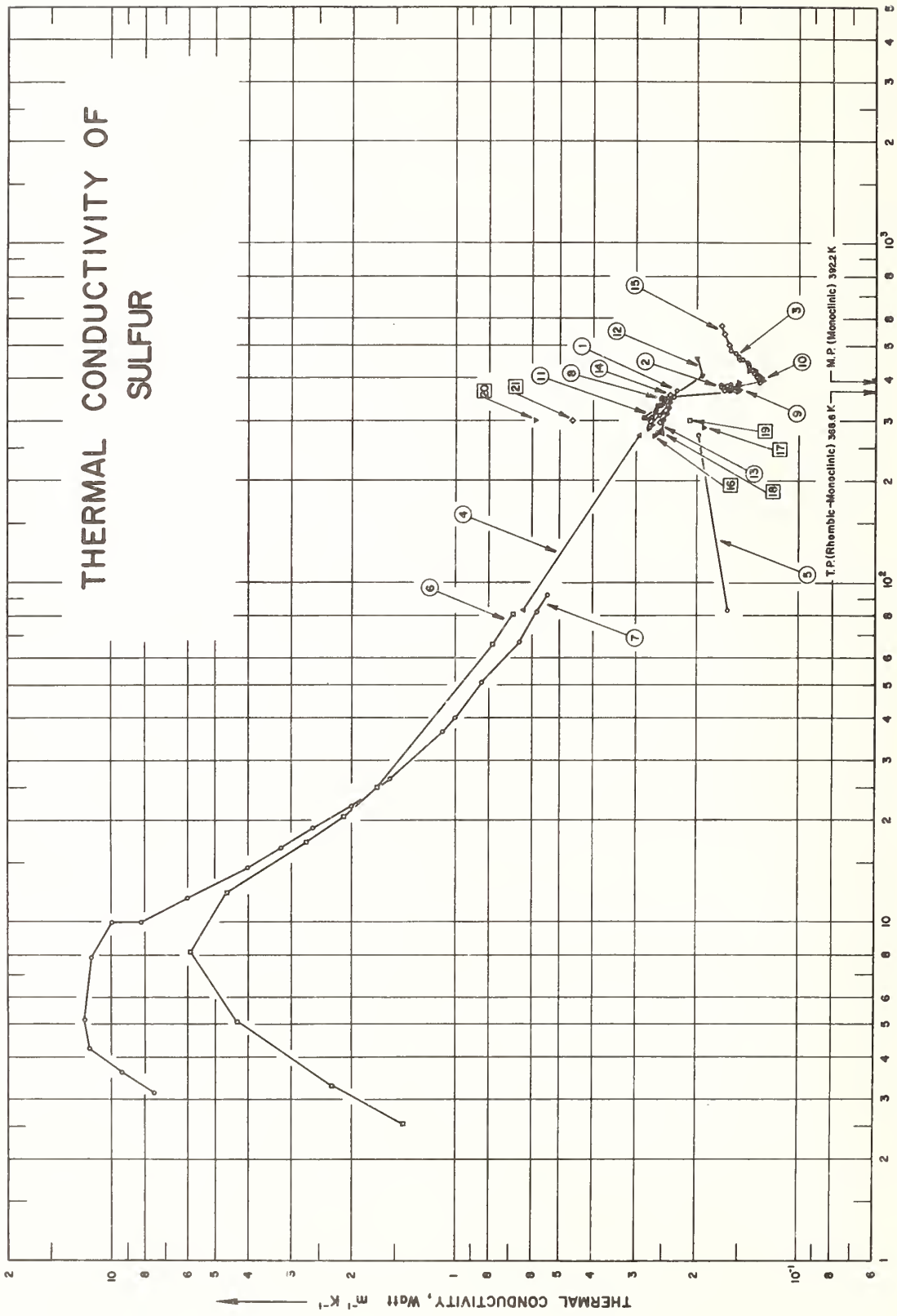

Figure 1. Thermal Conductivity of Sulfur.

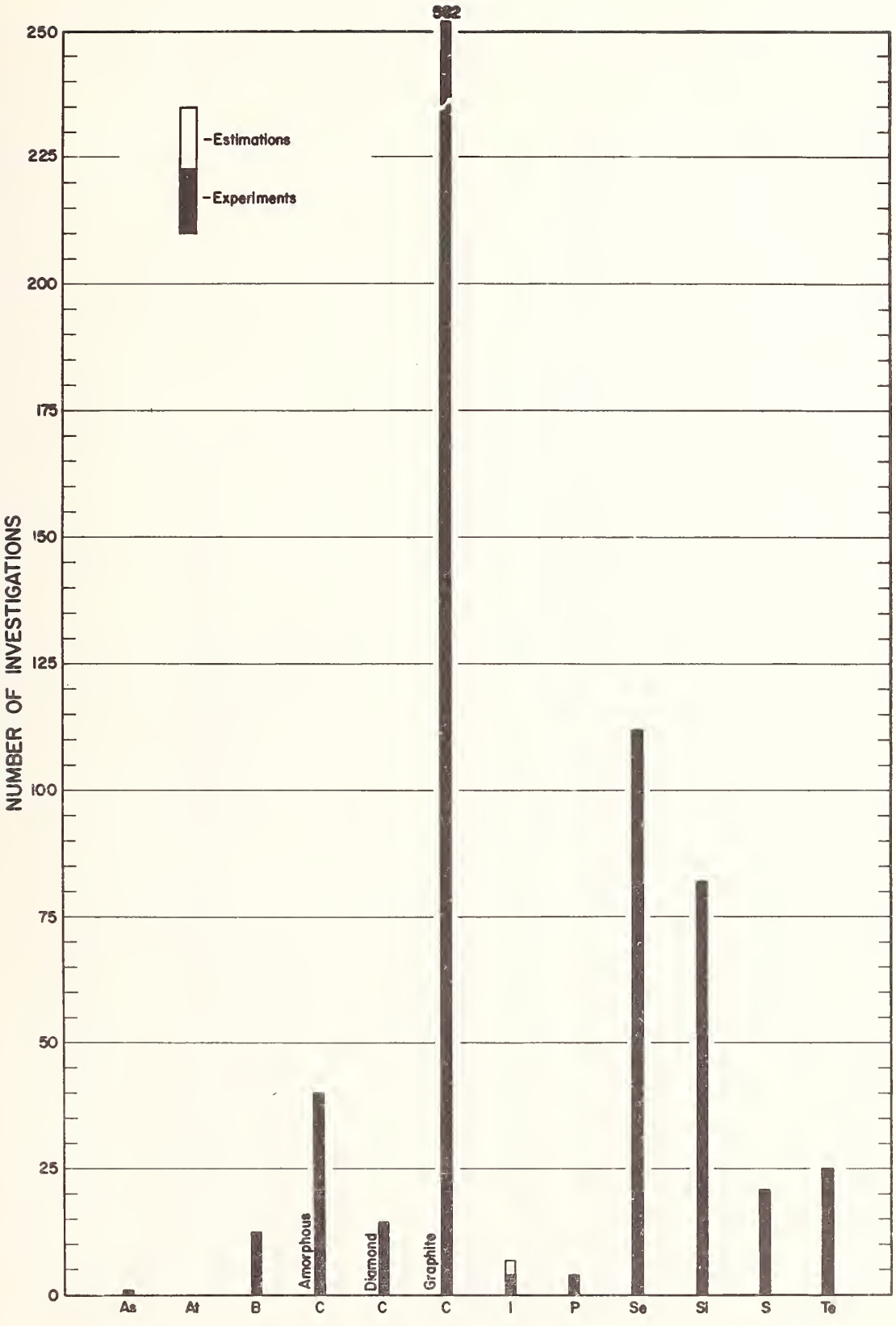

Figure 2. Number of Investigations on the Thermal Conductivity of Non-metallic Solid Elements.

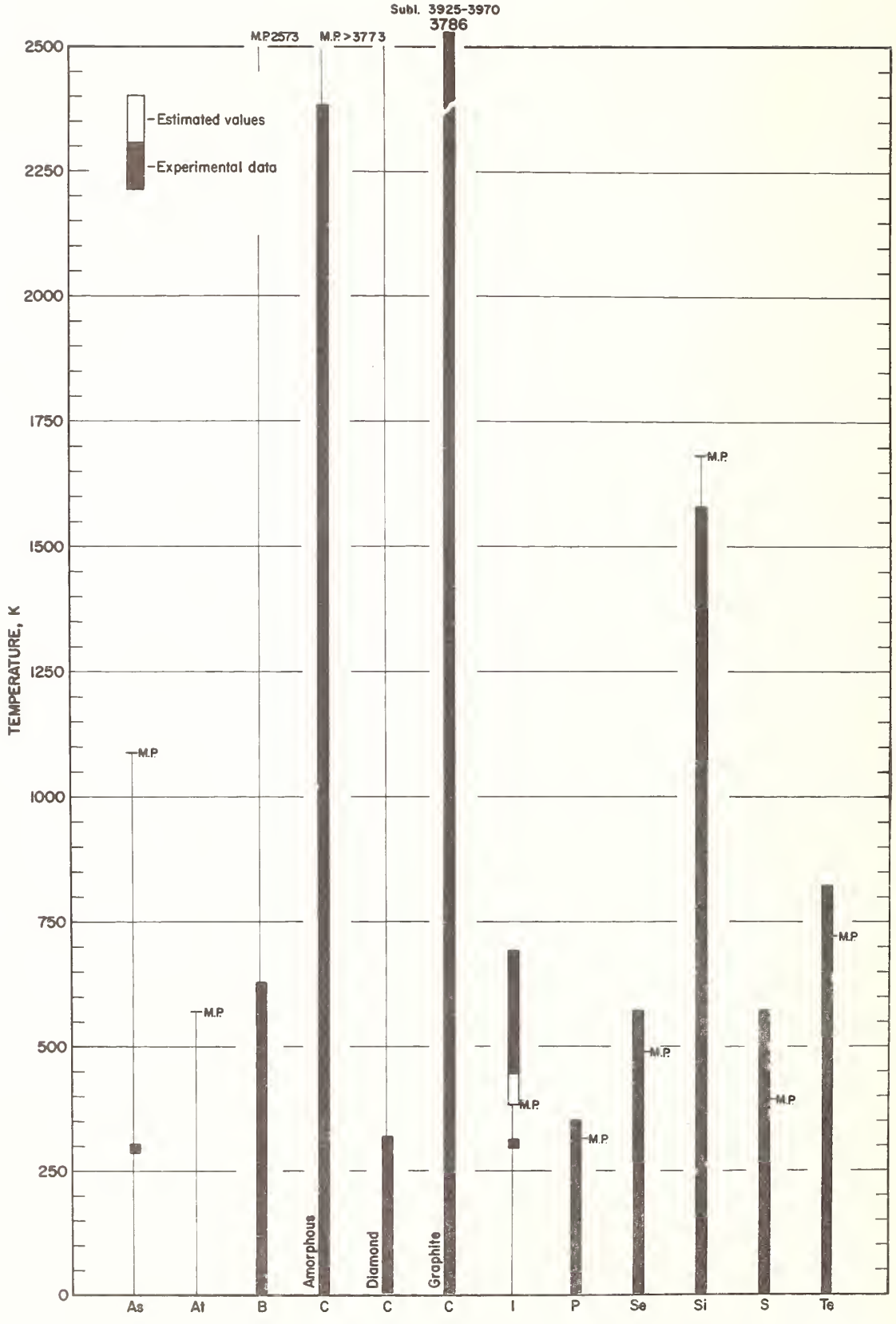

Figure 3. Temperature Range of Available Thermal Conductivity Data for Non-metallic Solid Elements.

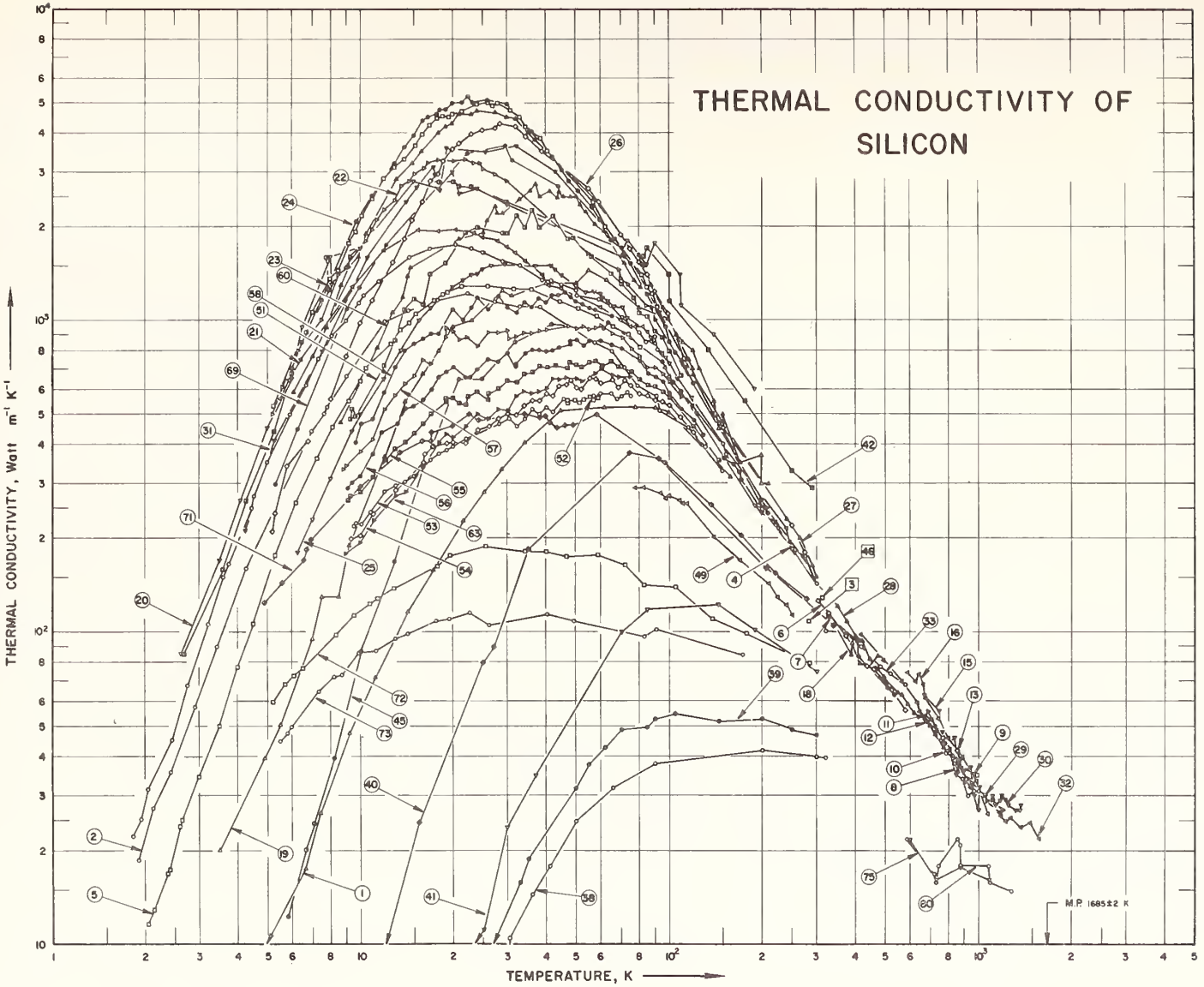

Figure 4. Thermal Conductivity of Silicon (Logarithmic Scales).

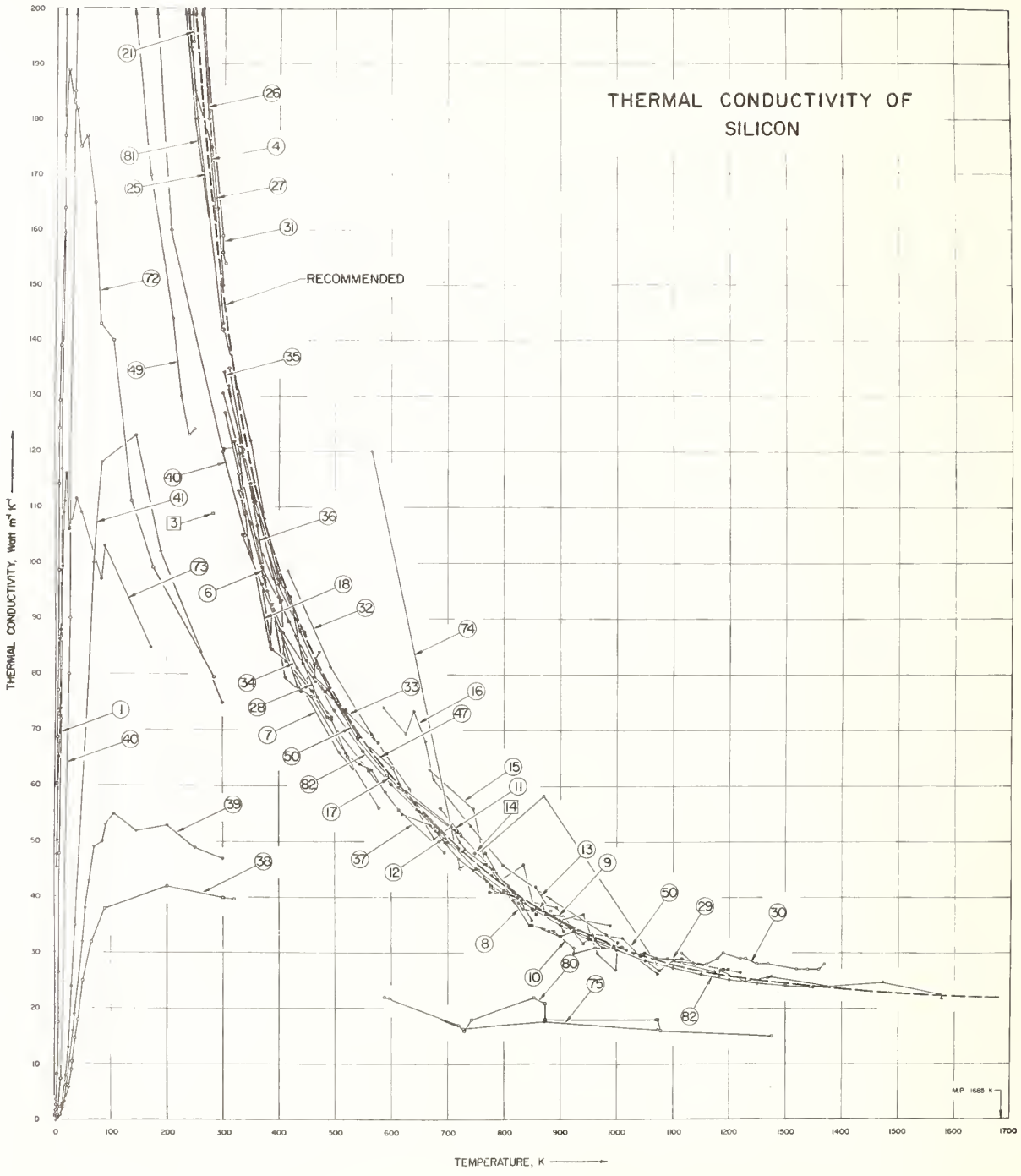

Figure 5. Thermal Conductivity of Silicon (Linear Scales).

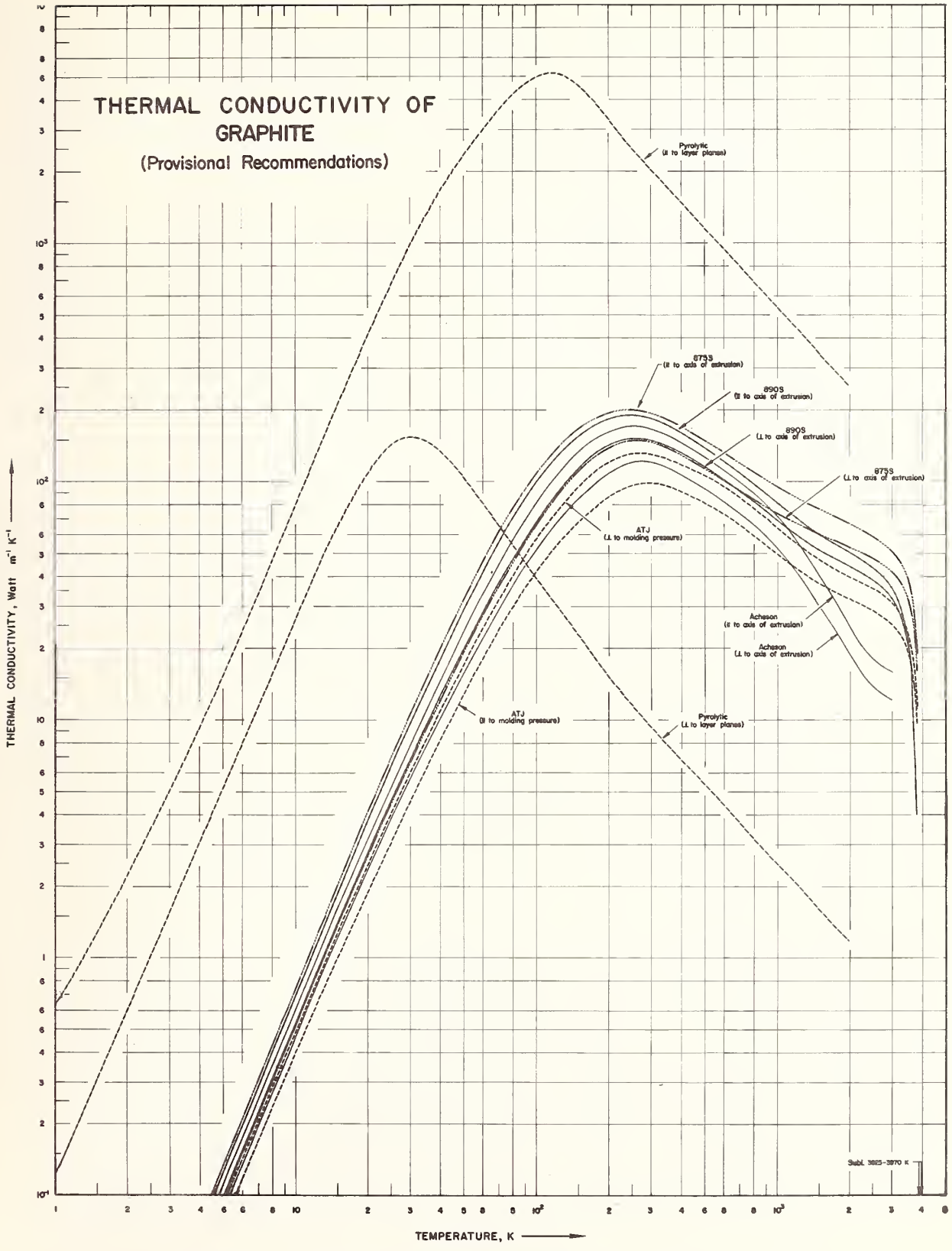

Figure 6. Thermal Conductivity of Graphite: Recommended Curves.

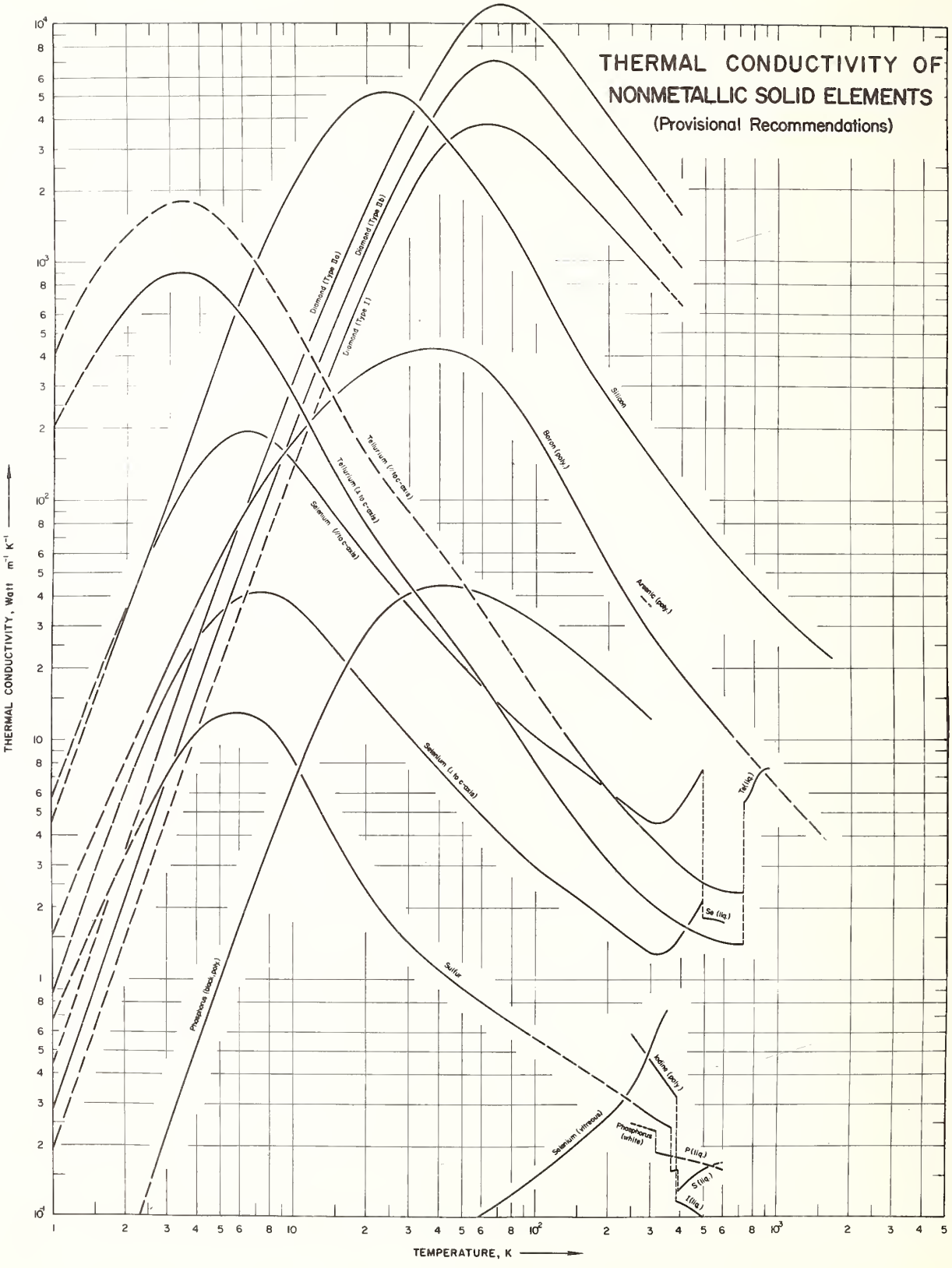

Figure 7. Thermal Conductivity of Non-metallic Solid Elements: Provisional Recommendations.

Some Aspects concerning Thermal Conductivity Data of Liquids and Proposals for New Standard Reference Materials

H. Poltz

Physikalisch-Technische Bundesanstalt,
Braunschweig, Germany

The thermal conductivity of organic liquids poorly absorbing IR-radiation contains a term of measurable magnitude arising from radiative heat transfer. This term can be, depending on the apparative arrangements, between about one and seven per cent of the total thermal conductivity at room temperature and increases like T^3. The influence of the apparative conditions on the temperature coefficient of thermal conductivity is in general considerably greater. Therefore one should, if possible, choose liquids strongly absorbing IR-radiation for standard reference purposes because their thermal conductivity shows a smaller radiative term.

We present thermal conductivity values of some alcohols which have a high IR-absorption. As it was to be expected, the measured values show a small dependence on the thickness of the liquid layer. Therefore we think some of these alcohols well-suited as standard reference materials at moderate temperatures. Their hygroscopic reaction is moderate and very pure products are obtainable in trade. As reference materials for a higher temperature range phthalic acid esters should be taken into consideration.

Key words: Alcohols, conductivity, heat transfer, hydrocarbons, IR-absorption, liquids, organic liquids, phthalic acid esters, radiation, radiative heat transfer, reference materials, standard, temperature coefficient, thermal conductivity.

1. The Radiative Term of Thermal Conductivity

Of the different physical processes contributing simultaneously to the heat transport in a liquid, the radiative heat transfer depends on the thickness of the liquid layer and on the optical qualities of the liquid and the surfaces bordering it. This was shown by measuring thermal conductivities of organic liquids using a guarded parallel plate apparatus by varying the plate distances [1,2][1]. Fig. 1 shows the measured thermal conductivity k_{eff} of two hydrocarbons poorly absorbing and of an alcohol strongly absorbing in the IR-region as a function of the thickness s of the liquid layer. Of the two hydrocarbons, liquid paraffin has a high viscosity. k_{eff} increases for increasing s. It is evident that the increase of k_{eff} depends on the ir-absorption of the liquid in the range of $s<2$ mm and on the viscosity in the range of $s > 2$ mm. Hence a perceptible influence of convection seems to exist only for plate distances of more than 2 mm. Fig. 2 and 3 show the increase of the thermal conductivity and its temperature coefficient respectively within

[1] Figures in brackets indicate the literature references at the end of the text of this paper.

the range from s = 0.4 to 2 mm each for three liquids which have an IR-absorption of different magnitude. The slopes of the curves increase with decreasing IR-absorption coefficients for the liquid.

Calculating the radiative term R of the total thermal conductivity k_{eff} gives the following expression valid for small temperature differences between the plates ($T_1 - T_2 \ll T_2 < T_1$) and the radiative thermal conductivity k_r being small relative to k_{eff} as it is always for liquids at moderate temperatures [3,4]

$$R = \frac{4}{3} \int_{\lambda=0}^{\infty} \frac{n^2}{\chi} \frac{\partial E_r}{\partial T} Y \, d\lambda \qquad (1)$$

n and χ are the refractive index and the absorption coefficient of the liquid, E_r Planck's function, T the absolute temperature, λ the wave length of heat radiation, and Y a function of the optical thickness τ of the liquid layer, and the emissivity ε of the plate surfaces. τ is the product $\chi \times s$.

After introducing wave independent effective mean values for the material quantities contained in it, eq(1) can be transformed into

$$R = k_r Y = \frac{16}{3} \frac{\bar{n}^2}{\bar{\chi}} \sigma T^3 Y \qquad (2)$$

where σ is the Stefan-Boltzmann constant. If the radiation is regularly reflected by the plate surfaces Y becomes

$$Y = 1 - \frac{3}{\tau}(2 - \varepsilon) \int_{x=0}^{1} \frac{1 - \exp(-\tau/x)}{1 + (1 - \varepsilon) \exp(-\tau/x)} x^3 dx \qquad (3)$$

The function Y increases from 0 to 1 when τ rises from 0 to ∞. Hence the influence of surfaces limiting the thickness of a liquid layer results always in diminishing the radiative term of thermal conductivity. Y represents the reduction of the radiative term relative to that existing at a very large optical thickness. A numerical evaluation of Y is presented in [3]. Fig. 4 shows Y as a function of τ and ε. The lowest curve in this diagram represents Y for the hypothetic case of $\varepsilon = 0$ that is the plate surface emitting not the least radiation into the liquid. Hence the distance from the zero line to this curve characterizes the contribution of the inner radiation of the liquid to the heat transfer from plate to plate. The radiative transfer within the medium has its highest value at the midst of the liquid layer and is diminished near the plate surfaces by reflections. The distance from the curve for $\varepsilon = 0$ to one of the upper curves characterizes the contribution of the radiation originally emitted by the plate surfaces to the heat transfer. Regarding the magnitude of ir-absorption of organic liquids one sees that it is very difficult, for experimental reasons, to perform measurements at optical thicknesses of the layer smaller than 0.5. As the emissivity of metallic surfaces is in general smaller than 0.2, figure 4 shows that the contribution to the radiative heat transfer originating in the radiation of the plate surfaces is always small relative to the contribution of the inner radiation of the liquid.

In order to give an idea of the accuracy of eq. (2) for small absorbing liquids, figure 5 shows the increase of the thermal conductivity and its temperature coefficient of toluene at 25°C for rising thicknesses of the liquid layer obtained by measurements and by calculation (dashed curves) using eq (2). The mean value of the absorption index contained in this formula was gained by evaluating an ir-absorption diagram of the liquid. As the refractive index of toluene is not very varying within the range of wave lengths to be considered, we chose the optical value.

Measurements which show the influence of the optical thickness on the thermal conductivity and its temperature coefficient for some poorly absorbing liquids in greater detail are presented in [5].

2. The Problem of Selecting Organic Liquids Suitable for Standard Reference Purposes

There are some organic liquids whose thermal conductivity has been measured by several investigators to a high accuracy over a large temperature range. Moreover they are obtainable in a very pure quality and are nonhygroscopic and relatively resistant in a chemical and thermal sense. Unfortunately most of them belong to the class of hydrocarbons or chlorinated hydrocarbons having no chemical bonds, and therefore these have a low absorption for heat radiation. Hence their thermal conductivity varies due to its radiative term between about one and six per cent of the total value at room temperature depending on apparative conditions.

The radiative term increases proportional to T^3 as eq. (2) shows. Therefore we expect a high value at elevated temperatures for poorly absorbing liquids. To give an idea how much the radiative term may rise within a range up to 300°C for hydrocarbons, we have used measurements on liquid paraffin performed between 25 and 80°C at various thicknesses of the liquid layer [5] to extrapolate to 300°C the curves showing the temperature dependence by applying eq. (2). The result is represented in figure 6. Of course such a wide extrapolation cannot give exact results as there are neglected many facts, e.g., the temperature dependence of the material quantities contained in eq. (2) and calculated as mean values only in the range from 25 to 80°C. Nevertheless we can deduce from the diagram that organic liquids poorly absorbing heat radiation show a radiative term of thermal conductivity too high as to be well-suited for standard reference purposes.

3. Thermal Conductivity Measurements on Alcohols

Equation (2) shows that the radiative term of thermal conductivity is small for such liquids which have a large mean absorption coefficient within the range of IR-radiation. Organic liquids having a very high absorption are the alcohols of a small chain length. Therefore we measured the thermal conductivity of the eight alcohols having from one to four carbon atoms in the region of moderate temperatures varying the thickness of the liquid layer in order to determine the magnitude of the radiative term.

The results of these measurements are presented in the tables 1 to 3 together with mean values calculated by linearly interpolating the measured values as functions of the temperature. The differences between measured and calculated values give an idea of the relative accuracy of the measurements. The precision of the measured values is estimated at about ± 0.5 per cent.

The investigation was made using materials obtainable in trade and suitable for analytic purposes. Table 4 gives some information about the purity of these materials.

There are no impurities contained in the liquids giving rise to a perceptible modification of the measured values. As all these alcohols are hygroscopic, the water percentage of all samples was determined spectroscopically after having finished the measurements. We filled the degassed sample into the evacuated apparatus and then let thoroughly dried air or nitrogen into it in order to eliminate stresses which might have deformed the parallel plates a little bit. When regarding this procedure we could detect no change of the water percentage of the sample after it had been in the apparatus for some days except for ethanol. This alcohol proved to be extremely hygroscopic and it was very difficult to make measurements not influenced by a rising water percentage. In this point, we had a little trouble also with measuring of methanol and tertiary butanol. The hygroscopicity of the other butanols and of the propanols seems to be moderate. Therefore we think it possible to measure their thermal conductivity at moderate temperatures without excluding the atmosphere if the measurements are finished in a short time.

Table 1

Thermal conductivity of propanols and butanols

Thickness of the liquid layer mm	Thermal conductivity $k_{eff} \times 10^3$, W cm^{-1} deg^{-1}								$\frac{d\,k_{eff}}{dT} \times 10^6$ W cm^{-1} deg^{-2}
	10 °C		25 °C		40 °C		55 °C		
	meas.	mean	meas.	mean	meas.	mean	meas.	mean	
					n - Propanol				
0.4581	1.548	1.547	1.511	1.512	1.478	1.478	1.444	1.444	-2.29
0.9578	1.553	1.553	1.518	1.519	1.485	1.485			-2.26
1.9293	1.556	1.556	1.522	1.523	1.490	1.490			-2.21
					iso - Propanol				
0.4581	1.370	1.370	1.340	1.340	1.309	1.309			-2.03
0.9578	1.375	1.375	1.345	1.346	1.316	1.316			-1.95
1.9293	1.378	1.378	1.348	1.349	1.320	1.320			-1.96
					n - Butanol				
0.4581	1.508	1.508	1.473	1.475	1.444	1.442	1.409	1.409	-2.19
0.9578	1.514	1.514	1.482	1.483	1.454	1.452	1.422	1.422	-2.04
1.9293	1.516	1.516	1.486	1.487	1.457	1.457	1.427	1.427	-1.98
					sec. Butanol				
0.4581	1.374	1.373	1.342	1.343	1.313	1.313	1.283	1.283	-2.01
0.9578	1.383	1.382	1.351	1.352	1.322	1.322	1.293	1.292	-1.99
1.9293	1.384	1.383	1.353	1.354	1.324	1.324	1.295	1.295	-1.96
					iso - Butanol				
0.4581	1.331	1.332	1.306	1.306	1.280	1.280	1.255	1.255	-1.70
0.9578	1.337	1.337	1.312	1.313	1.288	1.288	1.264	1.264	-1.62
1.9293	1.339	1.340	1.317	1.317	1.294	1.293	1.269	1.270	-1.56

Table 2
Thermal conductivity of methanol and ethanol

Thickness of the liquid layer	Thermal conductivity $k_{eff} \times 10^3$, W $cm^{-1}deg^{-1}$										$\frac{dk_{eff}}{dT} \times 10^6$	W $cm^{-1}deg^{-2}$
	10 °C		15 °C		20 °C		25 °C		30 °C		40 °C			
mm	meas.	mean	meas.	mean	meas.	mean	meas.	mean	meas.	mean	meas.	mean		
						Methanol								
0.458	2.012	2.011			1.980	1.980			1.948	1.949	1.919	1.918	-3.10	
0.958	2.016	2.016			1.986	1.986			1.954	1.956	1.927	1.926	-3.00	
1.455	2.022	2.021	2.005	2.006	1.993	1.992	1.977	1.977					-2.91	
1.929	2.024	2.025	2.011	2.010	1.995	1.995	1.980	1.980					-2.96	
						Ethanol								
0.458	1.676	1.676			1.645	1.645			1.615	1.615			-3.04	
0.958	1.682	1.682	1.668	1.667			1.636	1.637	1.623	1.622			-2.99	
1.929	1.686	1.686	1.673	1.672	1.658	1.658	1.643	1.643	1.629	1.629			-2.86	

Table 3
Thermal conductivity of tert. Butanol

Thickness of the liquid layer	Thermal conductivity $k_{eff} \times 10^3$, W $cm^{-1}deg^{-1}$										$\frac{dk_{eff}}{dT} \times 10^6$	W $cm^{-1}deg^{-2}$
	30 °C		35 °C		40 °C		45 °C		50 °C			
mm	meas.	mean	meas.	mean	meas.	mean	meas.	mean	meas.	mean		
0.458	1.065	1.065	1.059	1.058	1.051	1.052	1.046	1.045	1.038	1.038	-1.35	
0.958	1.072	1.072			1.059	1.060	1.054	1.054	1.048	1.047	-1.23	
1.455	1.077	1.078			1.066	1.065			1.052	1.052	-1.25	
1.929	1.079	1.078			1.068	1.068	1.062	1.062	1.056	1.057	-1.09	

Table 4

Purity of alcohols used for the measurements

Substances	purity guaranteed %	real purity %	max. water percentage %	real water percentage %	other impurities %
Methanol R.G.[a]	99.0		0.05		
Ethanol, absolute R.G.	99.1		0.2		Methanol 0.1
Propanol - (1) R.G.	99.0		0.05		t-Butanol
iso-Propanol R.G.	99.7	99.8 - 99.9	0.1		
Butanol - (1) R.G.	99.0	99.5 - 99.9	0.2	0.1	
Butanol - (2) for chromatography	98.5	99.8 - 99.9	0.2	0.05	
iso-Butanol R.G.	99.0	99.2 - 99.9	0.05		
t-Butanol for chromatography	99.0	99.8 - 99.9	0.1		Butanol - (2)

[a] R.G. = Reagent Grade

4. Alcohols as Standard Reference Materials at Moderate Temperatures

As a conclusion from our experiences in measuring alcohols, we can say that the propanols and the butanols with exception of tertiary butanol are well fitted for reference purposes. In order to show how much the radiative term of them is reduced by their high IR-absorption we have presented in the same scale the measured dependence of thermal conductivity upon the plate distances for an alcohol and a hydrocarbon each in the figures 7 and 8.

Unfortunately there are not enough thermal conductivity measurements of high accuracy available on alcohols. Table 5 shows a comparison of some values measured by several authors [6 to 15]. We think it necessary to gain more reliable mean values by further measurements.

Table 5

Thermal conductivity of alcohols at 25 °C
measured by several authors

Author	Ref.	Meth-anol	Eth-anol	Propanol n	Propanol iso	Butanol n	Butanol sec.	Butanol iso	Butanol tert.
		Thermal conductivity, W cm^{-1} deg^{-1} x 10^{-3}							
Riedel	[6]	2.01	1.66	1.55	1.40	1.52			
Mason	[7]	2.01	1.61						
Filippov	[8]	2.05	1.70	1.52	1.41	1.44		1.34	
Tsederberg	[9]		1.63						
Challoner	[10]		1.68						
Scheffy	[11]								1.07
Grassmann	[12]		1.64						
Jamieson	[13]	2.01							
Jobst	[14]	1.64	1.62	1.52		1.47			
Tufeu	[15]	2.09	1.73	1.58					
This work		1.97	1.64	1.52	1.34	1.48	1.35	1.31	1.08
		Temperature coefficient, W cm^{-1} deg^{-2} x 10^{-6}							
Riedel	[6]	-3.1	-3.1	-1.1	-1.2	-2.0			
Mason	[7]	-1.3	-5.5						
Filippov	[8]	-2.5	-2.4	-2.1	-1.6	-2.0		-1.3	
Tsederberg	[9]		-2.6						
Challoner	[10]		-3.0						
Scheffy	[11]								-0.3
Grassmann	[12]		-3.3						
Jamieson	[13]	-							
Jobst	[14]	-3.7	-2.8	-2.0		-1.7			
Tufeu	[15]	-3.8	-3.1	-2.4					
This work		-3.0	-3.0	-2.3	-2.0	-2.1	-2.0	-1.6	-1.3

5. Standard Reference Materials for Elevated Temperatures

Because of the radiative term of thermal conductivity rising rapidly with temperature, the necessity is evident to use liquids of high -absorption for reference purposes at elevated temperatures. But there seem to be no measured values of suitable materials sufficiently reliable. We believe that phthalic acid esters are well fitted for these purposes. They are to be obtained in a very high degree of purity. They are nonhygroscopic, nontoxic, liquid at room temperature and have relatively high boiling points. Besides this, they are nonaggressive and resistant to chemical and thermal influences. We hope to present results about their thermal conductivity and its radiative term in some time.

6. References

[1] Fritz, W. and Poltz, H., Absolutbestimmung der Wärmeleitfähigkeit von Flüssigkeiten I - Kritische Versuche an einer neuen Plattenapparatur, Int. J. Heat Mass Transfer 5, 307 (1962).

[2] Poltz, H., Die Wärmeleitfähigkeit von Flüssigkeiten III. Abhängigkeit der Wärmeleitfähigkeit von der Schichtdicke bei organischen Flüssigkeiten, Int. J. Heat Mass Transfer 8, 609 (1965).

[3] Poltz, H., Die Wärmeleitfähigkeit von Flüssigkeiten II. Der Strahlungsanteil der effektiven Wärmeleitfähigkeit, Int. J. Heat Mass Transfer 8, 515 (1965).

[4] Kohler, M., Einfluß der Strahlung auf den Wärmetransport durch eine Flüssigkeitsschicht, Z. Angew. Phys. 18, 356 (1965).

[5] Poltz, H. and Jugel, R., The thermal conductivity of liquids IV - Temperature dependence of thermal conductivity, Int. J. Heat Mass Transfer 10, 1075 (1967).

[6] Riedel, L., Neue Wärmeleitfähigkeitsmessungen an organischen Flüssigkeiten. Chemie Ingr.-Tech. 23, 321, (1951); - Wärmeleitfähigkeitsmessungen an Mischungen verschiedener organischer Verbindungen mit Wasser. Chemie Ingr. Tech. 23, 465 (1951).

[7] Mason, H. L., Thermal conductivity of some industrial liquids from 0 to 100 deg. C. Trans. Amer. Soc. Mech. Engrs. 76, 817 (1954).

[8] Filippov, L. P., Thermal conductivity of fifty organic liquids. Vestnik Moskov, Univ. Ser. Fiz.-Mat. i Estestven. Nauk, 9, 45 (1954).

[9] Tsederberg, N.V. and Timrot, D.L., Experimental determination of the coefficient of thermal conductivity for a 94 per cent volume solution of ethanol for the temperature range -75 to +200 °C. Zh. tekh. Fiz., 25, 2458 (1955).

[10] Challoner, A.R. and Powell R.W., Thermal conductivities of liquids: new determinations for seven liquids and appraisal of existing values, Proc. R. Soc. A 238, 90 (1956).

[11] Scheffy, W.J. and Johnson, E.F., Thermal conductivities of liquids at high temperatures, J. Chem. and Engng. Data 6, 245 (1961).

[12] Grassmann, P., Straumann, W., Widmer, F. and Jobst, W., Measurement of thermal conductivity of liquids by an unsteady state method. In Amer. Soc. Mech. Engrs. Progress in Intern. Res. on Thermodyn. and Transport Prop., pp. 447-453. New York and London: Academic Press (1962).

[13] Jamieson, D.T. and Tudhope, J.S., A simple device for measuring the thermal conductivity of liquids with moderate accuracy. NEL Report No.81. East Kilbride, Glasgow (1963).

[14] Jobst, W., Messung der Wärmeleitfähigkeit von organischen, aliphatischen Flüssigkeiten und von Gasen nach einem instationären Absolutverfahren, Dissertation Eidgenössische Technische Hochschule Zürich, Switzerland (1965).

[15] Tufeu, R., Le Neindre, B. and Johannin, P., Conductibilité thermique de quelques liquides, C.R.Acad. Sc. Paris. 262, 229 (1966).

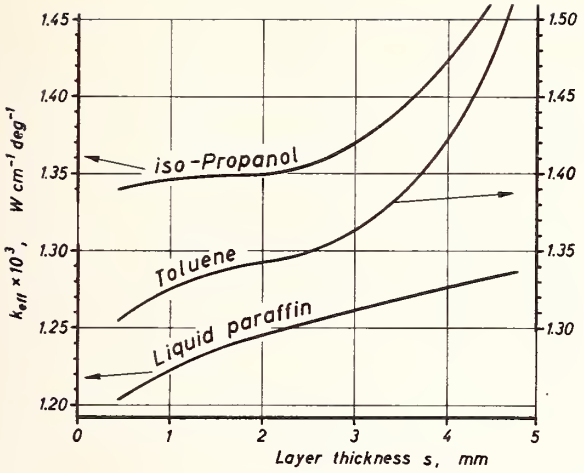

Figure 1. Thermal conductivity k_{eff} as a function of the layer thickness at 25 °C.

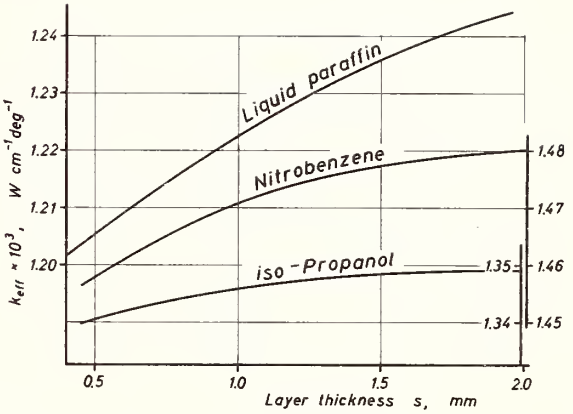

Figure 2. Thermal conductivity k_{eff} as a function of the layer thickness at 25 °C.

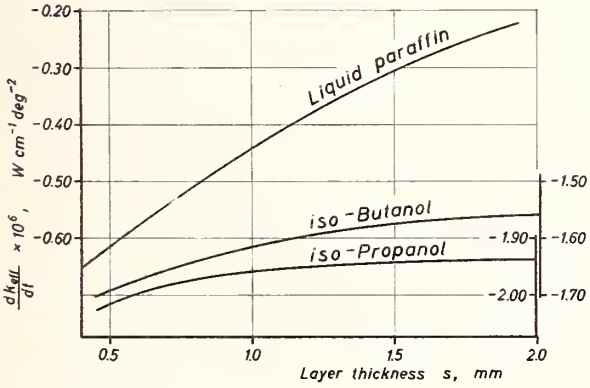

Figure 3. Temperature coefficients of thermal conductivity as functions of the layer thickness at 25 °C.

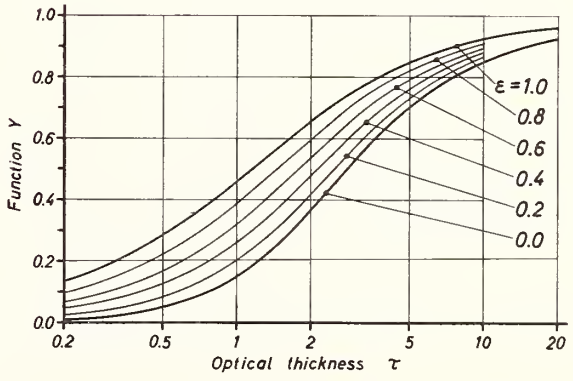

Figure 4. Y as a function of the optical thickness τ

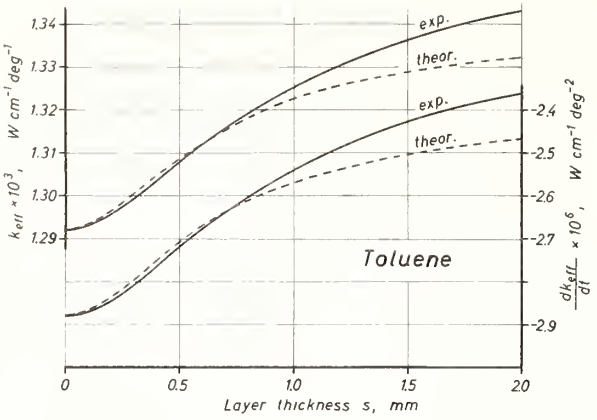

Figure 5. The thermal conductivity of toluene and its temperature coefficient measured and calculated for 25 °C.

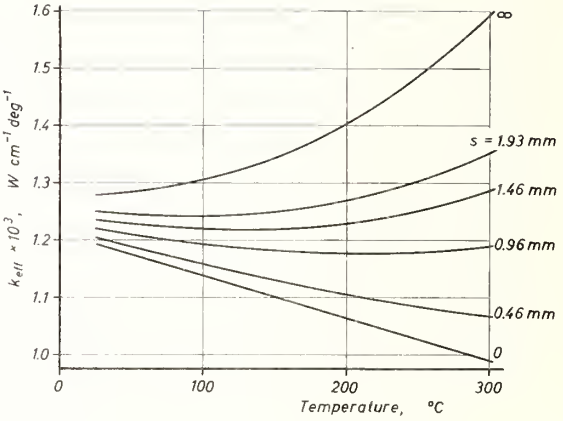

Figure 6. Thermal conductivity of liquid paraffin for several layer thicknesses extrapolated at 300 °C.

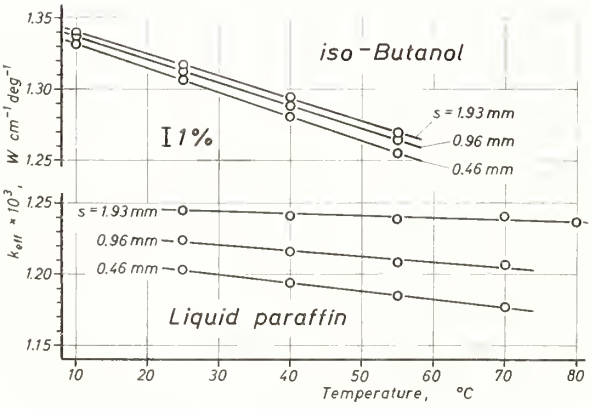

Figure 7. Thermal conductivities of iso-butanol and liquid paraffin at three layer thicknesses.

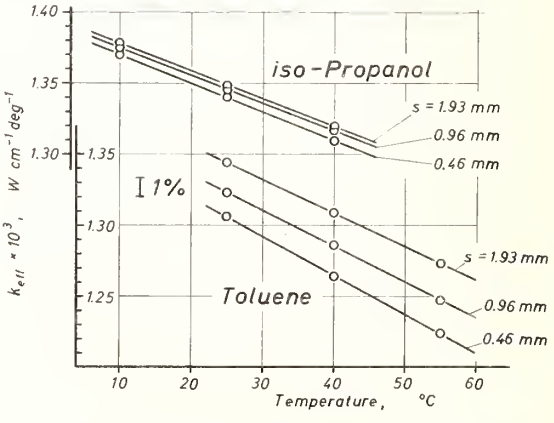

Figure 8. Thermal conductivities of iso-propanol and toluene at three layer thicknesses.

The Thermal Conductivity of Nonmetallic Elements [In liquid or gaseous state at NTP] In Solid, Saturated and Atmospheric Pressure States

P. E. Liley

Thermophysical Properties Research Center
Purdue University
2595 Yeager Road
West Lafayette, Indiana 47906

Information in the literature on the thermal conductivity of argon, bromine, chlorine, deuterium, fluorine, helium, hydrogen, iodine, krypton, neon, nitrogen, oxygen, radon, tritium and xenon for solid, saturated liquid and vapor and gas at atmospheric pressure has been collected and analyzed. Where data were lacking, a variety of estimation methods have been employed to obtain values. Most probable values are suggested and departure plots given where appropriate to show the concordance between different data sets.

Key Words: Conductivity, elements, gases, liquids, recommended values, solids, thermal conductivity, vapors.

Thermal Conductivity of Vitreous Silica: Selected Values[1]

Lois C. K. Carwile and Harold J. Hoge[2]

Pioneering Research Laboratory
U. S. Army Natick Laboratories
Natick, Massachusetts 01760

The published literature on the thermal conductivity of vitreous silica has been assembled and the results critically evaluated. Best values of thermal conductivity as a function of temperature have been selected. These are presented in both graphical and tabular form. They cover the range 80 to 660° K and published data extending from 3° to 2100° K are shown in the graphs. An attempt was made to consult all work that could significantly affect the choice of best values. Published papers were located with the aid of Chemical Abstracts, Physics Abstracts, the Thermophysical Properties Retrieval Guide, and some other general sources. In addition, relevant references in the papers themselves were followed up until a substantially "closed system" had been generated, as shown by the fact that no new references were being turned up.

Key Words: Fused quartz, fused silica, quartz glass, radiative heat transfer, reference material, silica, thermal conductivity, vitreous silica.

1. Introduction

Vitreous silica is an important material in research, and is used to some extent in industry. It is easily obtained in a state of high purity. It is chemically inert to most substances, including many strong acids; hence it is valued as a storage container, and as a reaction vessel for chemicals of the highest purity. It is much used in optical work because of its wide range of transmission. It has excellent elastic properties: it transmits ultrasonic waves with very little absorption of energy (except at low temperatures); and fibers of it, being relatively immune to permanent set, make excellent electrometer suspensions and delicate spring balances. Vitreous silica has a very small coefficient of thermal expansion, hence is highly resistant to thermal shock. As a refractory, it can withstand temperatures of 1300°K (1027°C) for long periods, and higher temperatures for short periods. It is an excellent electrical insulator.

---

[1] This paper contains the material presented in Technical Report 67-7-PR (July 1966) of the U. S. Army Natick Laboratories, with no significant change.

This paper reports research undertaken at the U. S. Army Natick (Mass.) Laboratories and is approved for publication. The findings in this report are not to be construed as an official Department of the Army position.

[2] Member and Head, respectively, of Thermodynamics Group.

Vitreous silica is a noncrystalline material (glass) of the composition SiO_2. It is usually made either from large selected quartz crystals or from very pure quartz sand. It is available in two basic types: clear (transparent) and translucent (satiny, silky). Clear vitreous silica is made by melting large crystals of quartz, and for this reason it is often called fused quartz or quartz glass; however, we prefer to reserve the word quartz for the commonest of the crystalline forms of silica, and to refer to the glass as vitreous silica, fused silica, or silica glass. Sosman [75][3], in his book on silica published in 1927, accepted the name "vitreous silica", and Laufer [76] in a more recent paper recommends it.

When vitreous silica is made from sand, the translucent or satiny type is obtained. The satiny appearance is caused by tiny air bubbles that are trapped when the material is fused, and then are elongated into striations when the material is drawn or worked into useful shapes. The present study is almost entirely concerned with clear, vitreous silica, which contains no trapped bubbles of air or other gas.

Vitreous silica is marketed under the names of fused silica, quartz glass, vitreous silica, and also under a number of trade-mark names. Among these are Amersil, Homosil, Infrasil, and Vitreosil; some of these names refer to special varieties having, for example, high optical transmission in a certain region of the spectrum.

Because vitreous silica is a highly reproducible material with suitable mechanical, chemical, and refractory properties, it has been suggested as a standard material for thermal-conductivity work. However, we believe the large radiative transfer of heat through vitreous silica makes it less desirable than an opaque substance as a thermal-conductivity standard, at least at high temperatures. We will return to this point later.

Characterization. Vitreous silica consists of a network of tetrahedrons of SiO_2, loosely packed. Each silicon atom is tetrahedrally surrounded by 4 oxygen atoms, and each oxygen is shared by 2 silicons; but long-range order is lacking. In a crystal, all corresponding Si-O-Si bond angles are equal, but in the glass this angle varies somewhat; also, according to Warren and Biscoe [77], the orientation of adjacent tetrahedra about these bonds is random in the glass. The X-ray analysis of vitreous silica shows the short-range, near-neighbor order that is characteristic of liquids and glasses, but no order extending over a distance as large as 3 or 4 times a unit-cell dimension.

The density of vitreous silica has a slight dependence on the rate at which the material is cooled from the molten state. Sosman [75] selected 2.203 g cm^{-3} as the best value for the density of clear vitreous silica, and stated that different samples were likely to differ in density by as much as 0.001 percent. Subsequent work gives little reason for differing from Sosman's conclusions. Crawford and Cohen [13] observed both the density and the thermal conductivity of vitreous silica before and after neutron bombardment. Using a hydrostatic method, they found the density at room temperature to be 2.2002 g cm^{-3} before bombardment. This value was increased by 2.7 percent during bombardment, but subsequent annealing substantially restored the original value. The lack of long-range order in vitreous silica is associated with an open molecular structure with numerous vacant sites. These vacant sites reduce the density of vitreous silica to a value about 17 percent less than that of crystalline quartz.

Vitreous silica does not have a sharp melting point. The crystalline form of silica that is stable at the highest temperature is cristobalite [75]; it melts at about 1710°C (1983°K), and becomes a liquid of high viscosity.

Devitrification. The high-temperature limit of usefulness of vitreous silica is generally the temperature at which devitrification (crystallization) occurs, rather than that at which the material begins to soften or melt. Below about 1000°C (1273°K) it shows no tendency to crystallize, but at 1100°C and above, minute crystals gradually form. The crystals become visible when the material is cooled, as they undergo a transformation that gives them a white, chalky appearance. Devitrification is accompanied by a decrease in mechanical strength and an increase in tendency to shatter. It proceeds more rapidly as the temperature is raised; it may be complete in 4 to 8 hours, or it may be a matter of days. Devitrification begins at a surface; it is accelerated by water vapor, by alkalis, and by many other substances. It is retarded when the amount of oxygen in the vitreous silica is slightly less than stoichiometric [78]. High-quality transparent vitreous silica, in the absence of catalysts, has been held at 1300°C (1573°K)

[3] Figures in brackets indicate the literature references at the end of this paper.

for several hours with only a slight cloudiness resulting. The product of devitrification is usually cristobalite, even at temperatures where cristobalite is not the most stable form of silica.

Effects of OH. Although clear vitreous silica made by melting crystals is ordinarily very pure, there are usually traces of metals in it. For some optical work, these traces of metals must be avoided; for this purpose, silica is made by reacting $SiCl_4$ with water and depositing the SiO_2 in the glassy state. Vitreous silica made from $SiCl_4$ is metal-free, but it contains [79] a relatively large amount of OH, which comes from the water formed in the reaction. This OH can amount to more than 0.001 percent by weight, whereas vitreous silica made by melting natural crystals contains only about 3 parts of OH per million. This difference in OH-content causes small changes in density, thermal expansion, index of refraction, and other properties, but perhaps its greatest importance is in spectroscopic experiments that require transmission of the OH frequencies; the presence of OH in the glass causes these frequencies to be absorbed. The effect of OH-content on the thermal conductivity of vitreous silica has not been specifically studied, but presumably it is small in comparison with the scattering of even the better data now available.

Satiny vitreous silica, λ-values. As discussed earlier, satiny vitreous silica contains elongated air bubbles that form striations in the material. Since the selected values in the present paper refer to clear, rather than satiny vitreous silica, we will present here the small amount of information that is available on the difference in thermal conductivity of the clear and satiny varieties. One would expect the striations to reduce the conductivity, especially when the direction of heat flow is perpendicular to the long axes of the striations. However, the effect appears to be rather small. Koenig and co-workers [34] reported measurements on clear vitreous silica, and on satiny material with the heat flow parallel to the striations. These measurements show the λ-values of the satiny type to be about 1 percent below those of the clear material in the range 40 to 120°C. The authors did not consider this difference significant, but we note that it is in the direction to be expected. Later the same group [35] made similar measurements on two new satiny samples, one having the striations parallel, the other perpendicular, to the direction of heat flow. Again, in approximately the same temperature range, one sample had a conductivity about 3 percent lower than the other, but unfortunately the report does not tell us which sample was which. Both of the sets of measurements just referred to were made rather early in an extensive series of investigations. More accurate results were obtained later in the work, but the comparison between clear and satiny vitreous silica does not appear to have been repeated.

2. Selection of the Values

The methods used in evaluating the experimental data, drawing a master curve, and preparing a table of selected values of the thermal conductivity, λ, will now be described. As indicated earlier, the variety of material to which the curve and tables refer is clear (transparent) vitreous silica. In some cases the same set of experimental data has been published in several different papers. In such cases we have selected one of the papers as the primary reference and have listed the others in the group of references "for which another reference is preferred." The governing factors considered in the selection of the primary reference will be found in the annotations to the various references.

Because of the large amount of data on the thermal conductivity of vitreous silica and the wide range of temperature covered, three separate graphs have been used to present the data. All three graphs start at 0°K; one extends upward to 100°K, another to 1000°K, and the third to 2100°K. The results of a particular research are given in one graph but are not duplicated in the others; thus overcrowding of the graphs is avoided.

The values of λ selected and recommended for use are given in Tables 1 and 2, and are represented in Figs. 1, 2, and 3 by heavy solid lines (the master curve). The values were selected by plotting the available data on large-scale graphs similar to Figs. 1, 2, and 3. A master curve was drawn, studied, revised, and tentatively accepted. Values were read from this master curve; they were differenced, smoothed, and checked for consistency with the master curve. When table and curve were smooth and mutually consistent, they were accepted. Table 1 resulted from this process. Table 2 was derived from Table 1 and is consistent with it.

The master curve and the tables extend only from about 80° to about 660°K (-193° to 387°C). At higher temperatures there is a dashed line joining with the master curve and extending it. This extension was derived by using heat-capacity data, and it is believed to represent roughly the thermal conductivity of vitreous silica in the absence of radiative heat transfer. The method of deriving the dashed curve is described later in this report.

Table 1

T	λ	T	λ
	millical		millical
°K	cm sec °C	°K	cm sec °C
80	1.31	380	3.56
	30		5
100	1.61	400	3.61
	27		5
120	1.88	420	3.66
	24		6
140	2.12	440	3.72
	21		5
160	2.33	460	3.77
	19		6
180	2.52	480	3.83
	17		5
200	2.69	500	3.88
	15		5
220	2.84	520	3.93
	13		6
240	2.97	540	3.99
	12		5
260	3.09	560	4.04
	10		6
280	3.19	580	4.10
	9		5
300	3.28	600	4.15
	8		5
320	3.36	620	4.20
	7		4
340	3.43	640	4.24
	7		4
360	3.50	660	4.28
	6		

Table 2

T	λ
	Btu in.
°R	°R ft^{2}hr
150	3.95
	117
200	5.12
	100
250	6.12
	83
300	6.95
	73
350	7.68
	61
400	8.29
	51
450	8.80
	43
500	9.23
	36
550	9.59
	30
600	9.89
	31
650	10.2
	2
700	10.4
	2
750	10.6
	2
800	10.8
	3
850	11.1
	2
900	11.3
	2
950	11.5
	2
1000	11.7
	2
1050	11.9
	2
1100	12.1
	2
1150	12.3
	2
1200	12.5

Data Shown in Fig. 1. Figure 1 extends from 0° to 1000°K. It contains the data from references [1] to [11]; these references include much but not all of the best data for intermediate temperatures.

Although the master curve is based on the data in all three figures, the data of Birch and Clark [1], shown in Fig. 1, are perhaps the most valuable single set of data. These authors used a guarded hot-plate apparatus and a steady-state absolute method. The temperature difference across the sample was usually about 5°K. Each test was run in a nitrogen atmosphere and again in helium, and between the two results the thermal-contact resistances were eliminated.

Considerable weight has been given to the data obtained by Ratcliffe [2], which cover the range 123° to 322°K. Steady-state measurements were made in 3 different apparatuses; each apparatus had the hot plate sandwiched between 2 specimens. Care was taken to reduce or eliminate contact resistance, and corrections were made for lateral heat losses. At least 12 different samples were measured.

Valuable data were obtained by Kamilov [3] from about 89° to about 500°K. The apparatus was contained in a Dewar flask within another flask, with provision for regulating the pressure between the walls of the inner flask. One unusual feature of the apparatus was the type of "thermocouple" used to register temperature equality between the top shield and the hot plate. This " thermocouple" consisted of a copper sheet coated with cuprous oxide; it actuated an electronic temperature controller. The published data represent the averaged results for 4 specimens with different thicknesses.

Kurepin and Platunov [4] described an apparatus for measuring either thermal conductivity or thermal diffusivity over a wide range of temperature. In measuring λ, heat was supplied so as to get a steady rate of temperature rise in the entire sample, for example, 0.10 deg/sec, and the temperature drop across the sample was measured as a function of time. The amount of heat flowing was determined from the known heat capacity and temperature rise of a heat sink, which was a core of Armco iron. Their data appear to be of good accuracy.

Eucken [5] used a steady-state hot-plate method, and obtained surprisingly good results considering that his apparatus appears to have been unguarded.

Vasil'ev [6] used a quasistationary (steady-rise) method for 39 of his plotted points, and a transient method for 2 points. He used radial heat flow in a guarded cylindrical apparatus that did not require a heat sink. Automatic temperature control and recording were used, and the data appear to be good. We note that the data in his Fig. 3 taken from Ratcliffe appear to be incomplete; and those taken from Knapp, to be misplotted.

Kaye and Higgins [7] reported careful measurements by a comparison method, using aluminum bars as the reference material. Data were obtained for 3 samples of vitreous silica; they are 6 to 8 percent lower than our accepted curve.

Kingery and Norton [8] used 2 different methods. The first method employed a prolate spheroidal envelope; it was an absolute, steady-state method. The second method was a comparative one. Their data are about 4 percent higher than our accepted curve; however, the data are valuable because they extend to relatively high temperatures.

Bil' and Avtokratova [9] used vitreous silica as a standard material for testing their apparatus. The values found are about 8 to 15 percent lower than our selected values. Their samples were stated to be of unsatisfactory purity and to contain air pockets.

The results obtained by Scholes [10] and by Koenig [11] were obtained by a comparison method. These values are higher and rise more rapidly with temperature than those we have selected.

Data Shown in Fig. 2. Figure 2 extends from 0° to 100°K. In this range, the work of Berman [12] appears to be the most reliable. He measured 3 samples by a steady-state method, with a radiation-shielded apparatus surrounded by a vacuum jacket. The entire apparatus could be cooled by liquid helium or other coolant.

The λ-values of Crawford and Cohen [13] increase very rapidly with temperature, and do not extrapolate toward the accepted values at higher temperatures as Berman's do. Crawford and Cohen attributed the difference between their values and those of Berman to a difference in the materials tested, but the difference seems rather large for such an explanation.

Data Shown in Fig. 3. Figure 3 extends from 0° to 2100°K. Very good data were reported by Devyatkova, Petrov, Smirnov, and Moizhes [14], over a wide range of temperature. Their work was undertaken to determine the potential usefulness of vitreous silica as a standard of reference for measurements

of thermal conductivity. They used 3 different apparatuses. Temperature gradients were measured by means of thermocouples fastened to metal pins inserted into holes drilled in the samples. Corrections were made for lateral heat losses. Their results have significantly influenced our selection of best values throughout the range for which a master curve and tables have been given. As will be seen below, we believe that radiant energy transfer has caused the results at higher temperatures to represent an apparent rather than true thermal conductivity.

Seemann [15] reported careful work by a radial-flow method with 2 different apparatuses and a single test sample. During measurements, both surfaces of the specimen were in contact with liquid metal: mercury at ordinary temperatures, lead-tin eutectic at higher temperatures. Seemann's results appear to be about 10 percent low in the range of temperatures for which we have drawn a master curve. However, at higher temperatures Seemann's results appear to be among the most successful in avoiding radiant-heat transfer.

Ito [16] also used the radial-flow method. His results are lower than those of most other workers; at the lower end of his range, he is about 20 percent below our master curve. Ito's results as reported by Birch and Clark [1] and by Ratcliffe [2] in the form of straight lines do not agree with the plotted points in Ito's paper; the discrepancy can be explained if we assume that these authors used Ito's equation with temperatures in °K, whereas it is actually for temperatures in °C. Whatever the cause, the discrepancy is substantial.

Vishnevskii and Dzyubenko [17] built a guarded apparatus for measuring λ by a transient method. They report results obtained with this apparatus and also by a steady-state method; the two sets of results show good agreement and are represented by a single curve. However, these values are about 8 percent lower than those of our accepted curve.

An unusual method, involving steep temperature gradients, was used by Wray and Connolly [18] to measure λ of vitreous silica at high temperatures "without radiative effects". Each sample was in the form of a cylindrical rod with a tungsten wire along the axis, so prepared as to have continuous bonding between wire and sample as shown by microscopic examination. The wires were of very small diameter (0.008 cm or less), and served as both heater and thermometer. From the graphs of observed power vs. wire temperature, the slopes were determined; and these slopes were used to find λ by a formula which Wray and Connolly derived theoretically. Their results were presented as smooth curves, and give values of λ at higher temperatures than any other papers that we have located. The curves of Wray and Connolly remain substantially horizontal at higher temperatures, where those of others rise steeply.

Observations at high temperatures were also reported by Lucks, Matolich, and Van Velzor [19]; Kingery and Norton [20]; and Pustovalov [21]. In all these data the steepening rise shows the presence of radiative heat transfer. Most observers made some effort either to reduce or to correct for radiative heat transfer. For example, Lucks, Matolich, and Van Velzor made some experiments with thin low emissivity foil "adjacent to the surface of the transparent solid specimens" (they used a comparison method, with Armco iron as the accepted standard). They found that the λ-values obtained without foil showed a more rapid increase than those obtained with foil, above about 450°C (723°K).

Kingery and Norton used 3 different apparatuses; all employed the comparison method. The paper of Lee and Kingery [64] reports the same work with a somewhat better description of experimental methods.

Pustovalov used an apparatus of cylindrical symmetry, with an axial heater; the positions of the thermocouples in the samples were determined by using X-rays [80]. The λ-values reported are about 25 percent lower than our master curve. It is possible that the porosity of the sample is responsible; Pustovalov gives [69] the apparent porosity of his sample as 1.0 percent; but from his measured density (2.06 g cm^{-3}) and our accepted density (2.204), we calculate a porosity of 6.5 percent.

Also shown in Fig. 3 are the results of Colosky [22], and those of Knapp [23]; these appear to be too high and to rise too steeply.

At the higher temperatures, the data reported by almost all the experimenters lie above the master curve and the dashed curve that extends it upward. As mentioned earlier, this dashed curve represents our estimate of the thermal conductivity of vitreous silica in the absence of radiative heat transfer. The method of obtaining this curve will be described in the next section.

3. Nonradiative Heat Transfer at High Temperatures

Thermal conductivity as defined does not include the transfer of heat by either convection or radiation. However, in many investigations of thermal conductivity some heat transfer by convection or

radiation takes place in the sample. When the amount is small, this transfer is often included with the transfer by conduction, and an apparent thermal conductivity is calculated. In the case of vitreous silica such a procedure is permissible up to about 600°K, but as the temperature increases the radiative heat transfer becomes very large, and it is not desirable to lump it with thermal conductivity.

The problem of radiative heat transfer is of special importance in vitreous silica because the substance is highly transparent. Vitreous silica transmits a wider range of wave lengths than most glasses; the range extends from 0.2 to 4.0 microns, approximately, and in addition there are other bands of transmission or partial transmission at longer wave lengths.

In estimating the ordinary (nonradiative) thermal conductivity of vitreous silica at high temperatures we can follow either of two paths. We can estimate the effect of radiation and substract it from the total observed heat transfer, or, we can assume a relation between thermal conductivity and some other property of the material such as the specific heat c_p, and use this to give us λ.

It is easy to make rough calculations of radiative heat transfer in vitreous silica, but much harder to make accurate ones using the absorption coefficient appropriate for each wave length. We have avoided such difficult and perhaps uncertain calculations by assuming that λ/c_p is a constant. Accepting c_p, we have calculated the nonradiative value of λ, and have checked the results so obtained by some rough calculations of radiative heat transfer that are described in the next section.

It is well known that heat capacity and thermal conductivity are closely related. According to a very simple theory λ is proportional to the product $c_p vl$, where v is the mean velocity of phonons and l their mean free path. Our assumption that λ/c_p is constant is equivalent to assuming that the product vl is constant. This assumption is used simply because no better one is at hand, and no great accuracy is claimed for it. If we were to go beyond the assumption λ/c_p = a constant, we would assume that this quantity decreases somewhat with temperature, because increasing lattice vibrations tend to reduce the mean free path l.

Sosman [reference 75, p. 314] has published a table giving c_p of vitreous silica. Although there are more recent data in some temperature regions than those that Sosman used, his table is convenient for our present purpose because it covers a wide range, extending from 18° to 1973°K. With c_p-values from this table and λ-values from our master curve, the quantity λ/c_p was calculated and plotted vs. T. Throughout the interval 473° to 623°K, this quantity had the value 16.6 mg cm^{-1} sec^{-1}. At both ends of the interval the curve turned upward. The value 16.6 was accepted.

Multiplying Sosman's c_p-values by 16.6 gave the values of λ that are represented by the dashed extension of the master curve in Fig. 3. This dashed curve we believe to be a rough but reasonable estimate of the thermal conductivity of vitreous silica in the absence of radiative heat transfer. It will be seen that the results of Wray and Connolly [18], whose experiments were designed to minimize radiative heat transfer, are in much better agreement with the dashed curve than those of any other investigator.

Sosman's c_p values have a change in slope between 1400° and 1500°K, which shows up in our dashed curve. Whether this change in slope is real or is due to experimental error we do not know. The uncertainty in assuming λ/c_p to be constant is so large that the irregularity in the dashed curve is probably comparatively unimportant.

4. Radiative Heat Transfer

As a check on the values of nonradiative heat transfer obtained as described above, a few calculations of the radiative heat transfer to be expected in vacuum and in our idealized model of vitreous silica have been made. First the "thermal conductivity" of a "slab of vacuum" 1 cm thick, with black-body walls, was calculated. Such a model would account for the radiative heat transfer in a perfectly transparent material and might be useful for a material that was a uniformly gray absorber at all wave lengths. It did not account satisfactorily for the sharp increase in slope shown by the experimental data for vitreous silica, principally because it caused the rise to occur at temperatures that were too low.

Next we tried a slightly more sophisticated model, one in which the sample of 1 cm thickness was considered to be a perfect transmitter for all radiation of wave lengths lying between 0.2 and 4.0 microns, and to be perfectly opaque to all other wave lengths. (Actually, the energy at wave lengths shorter than 0.2 μ was negligible, so a "window" extending from 0 to 4.0 μ would have given the same result.) This model was quite satisfactory. When the radiative "conductivity" of the model was added to the values of the master curve and the dashed curve, the dot-dash curve shown in Fig. 3 was obtained.

This curve is a reasonably good representation of the experimental data in which radiation was important. Note that it comes close to the data of Kingery and Norton, and to those of Lucks, et al. "without foil".

Since the more sophisticated model of radiative transfer and the dashed λ-curve based on c_p are mutually consistent they tend to confirm each other, but even so the breakdown of λ into radiative and nonradiative parts can only be considered a rough approximation.

A few remarks pointing out the weakness of the model used above in the calculation of radiative transmission are in order. Perfect transmission of radiation gives a conductance that is independent of the sample thickness and a conductivity that is proportional to sample thickness. For many wave lengths, vitreous silica is neither a perfect transmitter nor a perfect absorber, but is intermediate, with a mean free path for the radiation that may be of the order of a few millimeters. An individual quantum will, on the average, travel this distance before it is absorbed, but new quanta to replace those absorbed will be generated throughout the glass.

Gardon [81] has summarized the theory of heat transfer within glass by absorption and re-emission of radiation. A radiative thermal conductivity proportional to T^3 and inversely proportional to the absorption coefficient of the glass is found. However, the concept of a radiative thermal conductivity is not very useful because it is applicable only in the interior of large samples and not near the heat source and heat sink (hot plate and cold plate). The boundary conditions when radiative heat transfer is present are normally such that the temperature gradient within the sample is nonuniform, being steeper near the hot and cold plates than elsewhere. We see from this that when the absorption coefficient has any small non-zero value (as well as when it is actually zero) the "radiation conductivity" depends on sample thickness.

Some workers have reduced the effect of radiative heat transfer by using highly reflective metal foil such as aluminum or platinum, placed on either side of the sample, between it and the hot and cold plates. Although this arrangement substantially reduces the amount of radiative heat transfer, it does not eliminate it. Even if the foil had zero emissivity so that heat entered and left the sample only by conduction, a portion of the heat would be converted to radiation within the sample and would travel through the sample in the form of radiation.

5. Vitreous Silica as a Standard of Thermal Conductivity

Clear vitreous silica exhibits many of the characteristics desirable in a standard material for thermal-conductivity measurements. Among these characteristics are its high purity, uniformity, low thermal expansion, and chemical inertness. Vitreous silica has been used as a standard by a number of investigators; among them Benfield [27], Bullard and Niblett [82], Kamilov [3], and R. W. Powell [67]. Noting the wide use of vitreous silica as a calibrating standard, Devyatkova, Petrov, Smirnov, and Moizhes [14] made experiments to examine its suitability for this purpose. Using three different apparatuses in overlapping ranges, they made measurements from 82° to 1166°K. Comparing their data with those of Berman [12], Ratcliffe [2], and Kingery [60], they found good agreement, and concluded that vitreous silica is suitable for use as a standard substance in thermal-conductivity measurements.

Although we agree in part with this conclusion, we believe that the usefulness of clear vitreous silica as a standard is limited to low and moderate temperatures, where radiation is not important. As was brought out in the two preceding sections of this paper, radiative heat transfer in vitreous silica undoubtedly exceeds nonradiative transfer at the higher temperatures. The agreement of the high-temperature data of Devyatkova, et al., with those of Kingery is better than we would expect. The sample used by the first group had a thickness of 1 cm. The thickness of Kingery's sample was probably 2.54 cm. The relative importance of radiation in the two samples would be different and should lead to different apparent values of λ. It is possible that some compensating effect was present that kept the two sets of results in agreement.

Methods of making vitreous silica opaque have been devised, but so far as we are aware there are no measurements of the thermal conductivity of opaque samples. If vitreous silica could be rendered opaque without changing its thermal conductivity, it would make an excellent standard material for use at any temperature up to the point where significant devitrification may occur.

6. Reliability of the Tables

The tabulated values of λ between 150° and 450° K are believed to be accurate to ± 7 percent; near room temperature they may be somewhat better. Below 150° K the uncertainty increases and may reach ± 12 percent. Likewise above 450° K the uncertainty increases and may be as large as ± 15 percent at the upper limit of the table.

7. Data for Conversion of Units

$T\ (°R) = T\ (°K) \times 1.8.$

$T\ (°K) = t\ (°C) + 273.15.$

$T\ (°R) = t\ (°F) + 459.67.$

Watt cm $°K^{-1}cm^{-2}$ = cal cm $°K^{-1}cm^{-2}sec^{-1} \times 4.1840.$

Btu in. $°R^{-1}ft^{-2}hr^{-1}$ = cal cm $°K^{-1}cm^{-2}sec^{-1} \times 2902.9.$

Btu ft. $°R^{-1}ft^{-2}hr^{-1}$ = cal cm $°K^{-1}cm^{-2}sec^{-1} \times 241.91.$

8. Acknowledgment

We are indebted to Mr. Ronald A. Segars of this laboratory for help on various phases of this survey.

9. Annotated References

9.1. Containing Data Plotted in Fig. 1

[1] Birch, Francis, and Clark, Harry, The thermal conductivity of rocks and its dependence upon temperature and composition, Part 1. Am. J. Sci. 238, 529-58 (1940). Values were read from their Fig. 6 and also from their Fig. 7, and agreed within the error of reading. Corresponding values from the two graphs were averaged before being plotted in our Fig. 1.

[2] Ratcliffe, E. H., Thermal conductivities of fused and crystalline quartz. Brit. J. Appl. Phys. 10, 22-5 (1959). In addition to the plotted points of Ratcliffe's "present measurements" in his Fig. 3, we have also accepted the point taken by Ratcliffe from D. W. Butler, "Unpublished data (National Physical Laboratory, 1950)."

[3] Kamilov, I. K., Investigation of the thermal conductivity of solids in the interval from 80 to 500°K. Instr. Exptl. Tech. No. 3, 583-7 (1962). This is a translation of reference [58]. Figure 3 of this paper contains vitreous-silica data in the form of plotted points. We found that the x's represent Kamilov's data; the circles were taken by him from reference [14].

[4] Kurepin, V. V., and Platunov, E. S., Apparatus for rapid wide-temperature thermophysical tests of thermally insulating and semi-conducting materials (dynamic α λ-calorimeter), Izv. Vysshikh Uchebn, Zavendenii, Priborostr. No. 5, 119-26 (1961). Their Fig. 4 contains values of thermal conductivity (λ) and thermal diffusivity (α); we have used only the former.

[5] Eucken, A., The temperature dependence of thermal conductivity of solid nonmetals. Ann. Physik (4) 34, 185-221 (1911). The value for 100°C (373°K) is followed by a question mark in the paper; also it does not agree with the value given by Eucken for the same temperature in a later paper (reference 56). Hence we have omitted this value from our Fig. 1.

[6] Vasil'ev, L. L., Method and apparatus for the determination of the thermophysical properties of heat-insulating materials in the temperature range 80 - 500°K. Inzh.-Fiz. Zhur. 7, No. 5, 76-84 (1964). Thermal-conductivity values are given in his Fig. 3; thermal-diffusivity and specific-heat values are given in his Fig. 4. We have used only the thermal-conductivity data as given in his Fig. 3.

[7] Kaye, G.W.C., and Higgins, W.F., The thermal conductivity of vitreous silica, with a note on crystalline quartz. Proc. Roy. Soc. (London) A 113, 335-51 (1926). We have plotted their results from Table 5.

[8] Kingery, W. D., and Norton, F. H., The Measurement of Thermal Conductivity of Refractory Materials. U. S. At. Energy Comm. Rept. NYO-6444 (June 30, 1954), 16 p.; AD-40873. We have taken the experimental data from Fig. 1 of this report. This figure has been published in several different papers; we have selected this one as our primary reference because the figure in it was the largest. Reference [60], which contains a smaller version of the same figure, contains a fuller description of the work than the present reference.

[9] Bil', V. S. and Avtokratova, N.D., Temperature dependence of the thermal and temperature conductivities of some unfilled polymers. High Temp. 2, 169-75 (1964). This is a translation of reference [49]. The data given in their Fig. 1 have been read off and are plotted in our Fig. 1.

[10] Scholes, William A., Thermal conductivity of bodies of high BeO content. J. Am. Ceram. Soc. 33, 111-7 (1950). The points for vitreous silica given in his Fig. 3 have been read off and are plotted in our Fig. 1.

[11] Koenig, John H., Progress Report No. 4 from September 1 to December 1, 1953, N. J. Ceram. Research Sta., Rutgers Univ., 159 p.; AD-29335. We have selected the data given in engineering units in Table II, p. 6 of this report, for conversion and plotting in our Fig. 1.

9.2. Containing Data Plotted in Fig. 2

[12] Berman, R., The thermal conductivities of some dielectric solids at low temperatures. Proc. Roy. Soc. (London) A 208, 90-108 (1951). We have read off and used the plotted points in the upper section of Fig. 2 of Berman's paper.

[13] Crawford, J. H., Jr. and Cohen, A. F., The effect of fast neutron bombardment on the thermal conductivity of silica glass at low temperature. Bull. Inst. Intern. Froid, Annexe 1958-1 (1958), p. 165-72. These authors give data obtained before irradiation, after irradiation, and after the effects of irradiation have been removed by annealing. The lowest curve in their Fig. 1 represents the data obtained in the unirradiated state and the data obtained after annealing; we have used both of these sets of data.

9.3. Containing Data Plotted in Fig. 3

[14] Devyatkova, E. D., Petrov, A.V., Smirnov, I.A. and Moizhes, B. Ya., Fused quartz as a standard material in heat conductivity measurements. Fiz. Tverdogo Tela 2, 738-46 (1960). Figure 3 of this paper contains 3 sets of data obtained by the authors and 4 sets of data taken from other workers. The data of the authors have been read from this figure. An English translation of the paper exists (reference 55), but it was considered preferable to take the data from the Russian original.

[15] Seemann, Herman E., The thermal and electrical conductivity of fused quartz as a function of temperature. Phys. Rev. 31, 119-29 (1928). The data were read from Fig. 3 of this paper.

[16] Ito, Shuyo, Thermal conductivity of a transparent vitreous silica tube. J. Mazda Co. (Japan) Vol. 4, No. 2, 185-8 (1929). A copy of this paper was obtained for us from The Diet Library, Tokyo, by a Japanese colleague. The experimental points plotted in Fig. 3 were read from the graph in this paper.

[17] Vishnevskii, I.I. and Dzyubenko, M.I., Measurement of the coefficients of thermal conductivity and thermal diffusivity of refractory materials by a transient method. Inzh.-Fiz. Zhur., Akad. Nauk Belorussk. S.S.R. 7, No. 10, 45-8 (1964).

[18] Wray, Kurt L. and Connolly, Thomas J., Thermal conductivity of clear fused silica at high temperatures. J. Appl. Phys. 30, 1702-5 (1959). These authors give λ-values only as the smooth curves plotted in their Fig. 3; values have been read from these curves. Fig. 5 of reference [74] could have been used instead, but there are slight differences in the two figures, and the present paper is presumably the later one. In our Fig. 3, the data for Wray and Connolly have been shown as short sections of smooth curves at 100°-intervals. There is no correspondence between these short sections and any plotted points of Wray and Connolly, since these authors gave their λ-data only as smooth curves.

[19] Lucks, C. F., Matolich, J. and Van Velzor, J.A. The Experimental Measurement of Thermal Conductivities, Specific Heats and Densities of Metallic, Transparent, and Protective Materials, Part III. Wright Air Development Center AF Tech. Rept. 6145, Part III, March 1954. 71 p.; AD-95406. We have used the data for vitreous silica from Tables 7 and 8.

[20] Kingery, W. D. and Norton, F. H., The measurement of thermal conductivity of refractory materials. Quarterly Progress Report for the Period Ending January 1, 1955. U. S. At. Energy Comm. Rept. NYO-6447 (1955), 16 p.; AD-55595. Data are given in Fig. 4 of this paper. They extend from 95 to 1214°C (368 to 1487°K), but not all have been shown in our Fig. 3. Those below 700°C are uniformly spaced, and we have omitted them on the assumption that they represent the same data that are presented in reference [8]. The data at 700°C and above are less regular and we have accepted them as new data. The 3 highest-temperature points in the present reference are omitted because they have λ-values beyond the range of Fig. 3.

[21] Pustovalov, V. V., Change of thermal conductivity of quartz glass in the process of crystallization. Steklo i Keram. 17, No. 5, 28-30 (1960). The plotted points from the top curve in Fig. 3 of this paper have been read off and used in our report. The paper has been translated into English (reference 68).

[22] Colosky, Benjamin P., Thermal conductivity measurements on silica. Bull. Am. Ceram. Soc. 31, 465-6 (1952). Figure 2 contains the experimental data. The two upper curves refer to crystalline quartz. The bottom curve represents data obtained with 3 different samples of vitreous silica. Two of these were clear and one was smoky, but there is no significant difference between the λ-values of the 3 samples. The points for all three have been read from the graph and plotted in our Fig. 3.

[23] Knapp, W. J., Thermal conductivity of nonmetallic single crystals. J. Am. Ceram. Soc. 26, 48-55 (1943). The vitreous-silica data from Table II of this paper are plotted in our Fig. 3, except for the point of highest T and λ, which comes beyond the range of the figure.

9.4. Containing Data Not Plotted in the Figures

These references contain the data judged to be less important than those in references [1] to [23]. The arrangement is alphabetical. Each of the references in this group is followed by a brief annotation, in which the λ-values reported in the paper are included. Numerical values given below are in cal $cm^{-1}sec^{-1}°C^{-1}$.

[24] Ballard, Stanley S., McCarthy, Kathryn A., and Davis, William C., A method for measuring the thermal conductivity of small samples of poorly conducting materials such as optical crystals. Rev. Sci. Instr. 21, 905-7 (1950). A relative method was used, but the specific reference material used in each experiment is not stated. For vitreous silica they found λ = 0.00282 at 41°C, using a "Homosil" sample from the W. C. Heraeus Co.

[25] Barratt, Thomas, Thermal conductivity. Part II: Thermal conductivity of badly-conducting solids. Proc. Phys. Soc. (London) 27, 81-93 (1914). For vitreous silica of density 2.17 $g\ cm^{-3}$, the thermal conductivity was found to be 0.00237 at 20°C, and 0.00255 at 100°C.

[26] Beck, A., A steady state method for the rapid measurement of the thermal conductivity of rocks. J. Sci. Instr. 34, 186-9 (1957). A relative method was used, with brass (calibrated versus crystalline quartz) as the reference material. For vitreous silica at 28°C, the thermal conductivity obtained was 0.00323.

[27] Benfield, A. E., Terrestrial heat flow in Great Britain. Proc. Roy. Soc. (London) A 173, 428-50 (1939). A comparison method was used, with brass bars as the reference material. The brass was calibrated versus crystalline quartz, and the effect of resistance at contact surfaces was eliminated by using 4 samples of different thickness. The value of λ found for vitreous silica (Vitreosil from the Thermal Syndicate) was 0.00317 at 21.1°C.

[28] Bullard, E. C., Heat flow in South Africa. Proc. Roy. Soc. (London) A 173, 474-502 (1939). The thermal conductivity of vitreous silica was measured as a check on the accuracy of the apparatus, which had been calibrated against a crystalline quartz sample. For vitreous silica at 25°C, Bullard found λ = 0.00307.

[29] Crawford, J. H., Jr., and Wittels, M. C., Radiation stability of nonmetals and ceramics. Proc. 2d U.N. Int. Conf. Peaceful Uses Atomic Energy, Vol. 5, p. 300-10, 1958. They report λ = 0.0035 at 30°C; there is also a graph (Fig. 7) of low-temperature values. This graph appears to be identical with one in reference [53]; reference [13] is preferred over both.

[30] Eucken, A., The heat conductivity of ceramic refractory materials. Its calculation from the heat conductivity of the constituents. Forschungsh. 353 (Suppl. Forsch. Gebiete Ingenieurw. B 3, Mar. - Apr. 1932), 16 p. The data in this paper appear to be a selection of values based on previously published work of Eucken [5], Kaye and Higgins [7], and Seemann [15]. However, if this is the case, the values ought to be about 20 percent higher. We cannot be sure that these values are not based in part on new unpublished data obtained by Eucken.

[31] Gafner, G., The application of a transient method to the measurement of the thermal conductivity of rocks and building materials. Brit. J. Appl. Phys. 8, 393-7 (1957). A method of "steady rise" was employed; three samples of vitreous silica were measured in one apparatus and three others in another. The mean of the 6 measurements was λ = 0.00323 with a total spread of 6 percent; the temperature of all the measurements was 30°C.

[32] Jakob, M., The material properties most important in heat transfer. Der Chemie-Ingenieur, A. Eucken and M. Jakob, editors, Akad. Verlag, Leipzig, 1933. Vol. 1, Pt. 1, p. 308-79. The information on vitreous silica, p. 340-1, includes a smooth curve of thermal conductivity vs. temperature, but no plotted points. It seems likely that this curve is based on previously-published work of other authors, but we are not sure that this is the case.

[33] Kaganov, M. A., Lisker, I. S. and Chudnovskii, A. F., Rapid method for determining thermal conductivity of semiconductor materials. Inzh.-Fiz. Zhur., Akad. Nauk B. S. S. R. 4, No. 3, 110-2 (1961). By a transient method they found λ of vitreous silica to be 0.00331, at a temperature that we take to be approximately 12.5°C.

[34] Koenig, John H., Progress Report No. VI from March 1 to June 1, 1952. N.J. Ceram. Research Sta., Rutgers Univ., 98 p.; ATI-163519. This paper is of interest because it contains a comparison of thermal conductivities of clear and silky vitreous silica. For quantitative data on clear vitreous silica we prefer reference [11], in which the measurements were made with improved equipment.

[35] Koenig, John H., Progress Report No. 2 from March 1 to June 1, 1953. N.J. Ceramic Research Sta., Rutgers Univ., 117 p.; AD-13154. This paper contains a comparison of thermal conductivities of silky vitreous silica measured parallel and perpendicular to the striations. Although it is not clear which set of data refers to each form, the data show that there was not much difference between the two.

[36] Luikov, A. V., Vasiliev, L. L. and Shashkov, A. G., A method for the simultaneous determination of all thermal properties of poor heat conductors over the temperature range 80 to 500°K, in Advances in Thermophysical Properties at Extreme Temperatures, and Pressures, Third Symposium on Thermophysical Properties. ASME, Purdue Univ., Mar. 22-25, 1965, Serge Gratch, editor (The American Society of Mechanical Engineers, New York, 1965), p. 314-9. This paper contains some ambiguities or errors that have caused us not to include the data in any of our graphs. The density given for the vitreous silica is 2.650 g cm^{-3}, which is 20 percent higher than accepted values (it is roughly the accepted density for crystalline quartz). The data of other observers, plotted in Fig. 6 of the present reference, appear to be incorrectly given, at least in part. Also the data for vitreous silica in the present reference are from 8 to 17 percent lower than those given by Vasiliev [6] one year earlier.

[37] Milnes, M. V., Low-temperature thermal conductivity apparatus. North American Aviation Inc., Rept. SDL 408, 9 Sept. 1963, 14 p. A sample of vitreous silica was measured, presumably to check out the apparatus. The λ-value found was .0033, and the sample mean temperature, which we computed from the given thermocouple data, was 23.1°C.

[38] Nukiyama, Shiro, The thermal conductivity of glass, chilled glass, quartz, fused quartz (transparent), Bakelite, India-rubber, coal, Isolite, porcelain, slate, granite and marble. Trans. Soc. Mech. Engrs. (Japan) 2, 344-5 (1936). English abstract, ibid., p. S-96, S-97. Three plotted λ-values for vitreous silica are given, covering the range 15 to 33° C. An equation is given that appears to represent the points satisfactorily. The equation gives, at 300°K (26.85°C): λ = 0.00294.

[39] Phillips, L. S., The measurement of thermoelectric properties at high temperatures. J. Sci. Instr. 42, 209-11 (1965). The apparatus was so designed that the Seebeck coefficient, the electrical resistivity, and the thermal conductivity of a specimen could each be measured. The thermal conductivity of vitreous silica was measured in the range 160 to 595°C "to assess the behavior of the apparatus." The results are given in the form of a smooth curve. In view of this, and in view of the fact that the apparatus emphasized rapid operation rather than high accuracy, we have not plotted the results in any of our figures. At the lowest temperature, Phillips' curve is 5 percent below our master curve; at the highest temperature it is 18% above it.

[40] Powell, R. W., Thermal conductivity as a nondestructive testing technique, in Progress in Non-destructive Testing, E. G. Stanford and J. H. Fearon, editors (Heywood and Company, London, 1958), Vol. 1, p. 199-226. The λ-value of vitreous silica at "about 28°C" is given as 0.00330 in Table 4 and again in Table 5. This same value of λ was given earlier by Powell in reference [67]. However, the earlier paper does not give the temperature of the measurement.

[41] Sisman, O., Bopp, C. D. and Towns, R. L., Radiation effects on the thermal conductivity of ceramics. U. S. At. Energy Comm., Oak Ridge Natl. Lab. Rept. ORNL-1852, 33-5 (1955). The value reported for unirradiated vitreous silica is 0.0035, "at about 40°C."

[42] Weeks, James L. and Seifert, Ralph L., Note on the thermal conductivity of synthetic sapphire. J. Am. Ceram. Soc. 35, 15 (1952). Measurements made on a 6-mm rod of vitreous silica from Hanovia Chemical Company yielded 0.0041 at 73°C and 0.0057 at 135°C.

9.5. Containing Data for Which Another Reference is Preferred.

The arrangement is alphabetical.

[43] Barratt, T., and Winter, R. M., The thermal conductivity of wires and rods. Ann. Physik 77, 1-15 (1925). Condensed German translation of 2 papers of Barratt, one of which was reference [25].

[44] Berman, R., Thermal conductivity of glasses at low temperatures. Phys. Rev. 76, 315-6 (1949). This appears to be the place of first publication of Berman's data on vitreous silica. However, we prefer to use the fuller account, reference [12].

[45] Berman, R., The thermal conductivity of disordered solids at low temperatures. Bull. Inst. Intern. Froid. Annexe 1952-1 (1952), p. 13-20. This paper contains a smooth curve for vitreous silica; we prefer to take the data from the plotted points of reference [12].

[46] Berman, R., Thermal conductivity of some polycrystalline solids at low temperatures. Proc. Phys. Soc. (London) A 65, 1029-40 (1952). This paper contains 7 tabulated values of λ of vitreous silica. Six are at low temperatures, and agree with those in reference [12], which is preferred. The remaining value is for room temperature, and we have not found it elsewhere in Berman's published papers; however, it is given to only one significant figure, and we have not used it.

[47] Berman, R., The thermal conductivity of dielectric solids at low temperatures. Advances Phys. (London) 2, 103-40 (1953). This paper contains a smooth curve for vitreous silica. Reference [12] is preferred.

[48] Berman, R., Klemens, P. G., Simon, F. E., and Fry, T. M., Effect of neutron irradiation on the thermal conductivity of a quartz crystal at low temperature. Nature 166, 864-6 (1950). This paper contains a smooth curve of λ versus temperature, taken from an earlier paper of Berman [44]. Reference [12] is preferred.

[49] Bil', V. S. and Avtokratova, N. D., Temperature dependence of thermal conductivity and thermal diffusivity of some unfilled polymers. Teplofiz. Vysokikh Temperatur, Akad. Nauk S. S. S. R. 2, 192-8 (1964). We have not yet obtained a copy of this paper; it is the Russian original of [9].

[50] Bopp, C. D., Sisman, O. and Towns, R. L., Radiation stability of ceramics. U. S. At. Energy Comm. Oak Ridge Natl. Lab. Rept. ORNL-1945 (Aug. 30, 1955), 35-6. Reference [41] is preferred.

[51] Cohen, A. Foner, Low-temperature thermal conductivity in neutron-irradiated vitreous silica. U. S. At. Energy Comm. Oak Ridge Natl. Lab. Rept. ORNL-2413, 70-1 (Aug. 31, 1957). This appears to be the same work as that reported in reference [13], which we prefer.

[52] Cohen, Anna Foner, Low temperature thermal conductivity of nonmetals including radiation effects, in Low Temperature Physics and Chemistry, Proc. Fifth Intern. Conf. on Low Temperature Phys. and Chem. ... 1957, Joseph R. Dillinger, editor (Univ. of Wisconsin Press, Madison 1958), p. 385-8. Reference [13] is preferred.

[53] Cohen, Anna Foner, Low-temperature thermal conductivity in neutron irradiated vitreous silica. J. Appl. Phys. 29, 591-3 (1958). This paper contains less than half as many plotted points as [13], although it covers a greater temperature range. We prefer reference [13], which appears to be a later and better report of the work.

[54] Crawford, J. H.,Jr., and Cohen, A. F., Effect of fast neutron bombardment on the thermal conductivity of silica glass at low temperature. U. S. At. Energy Comm. Oak Ridge Natl. Lab. Rept. ORNL-2614, 43-6 (31 Aug. 1958). This article closely resembles reference [13]; however, the latter is preferred.

[55] Devyamkova, E. D., Pemrov, A. V., Smirnov, I. A., and Moizhes, B. Ya. Fused quartz as a model material in thermal conductivity measurements. Soviet Phys. Solid State 2, 681-8 (1960). English translation of reference [14].

[56] Eucken, A. The heat conductivity of solid materials at low temperatures. Z. Tech. Physik 6, 689-94 (1925). Reference [5] is preferred. The present paper contains a value at 21°K that is not given in reference [5] and another at 373°K that differs from the value given in reference [5]. We have omitted the 21° value of the present report on the assumption that it is not an original determination but an extrapolation, and we have omitted both of the 373° values given by Eucken because they do not agree. The remaining values in the present reference agree with

those in reference [5].

[57] Eucken, A., Thermal conductivity of nonmetals and metals. Physik. Z. 29, 563-6 (1928). We prefer reference [5].

[58] Kamilov, I. K., Investigation of the thermal conductivity of solids in the interval from 80 to 500°K. Pribory i Tekhn. Eksperim. No. 3, 176-9 (May-June 1962). This is the Russian original of reference [3].

[59] Kingery, W. D., Factors affecting thermal stress resistance of ceramic materials. J. Am. Ceram. Soc. 38, 3-15 (1955). This paper contains two numerical λ-values for vitreous silica; however, they appear to be only incidental to the subject of the paper. We prefer reference [8].

[60] Kingery, W. D., Thermal conductivity: XII, Temperature dependence of conductivity for single-phase ceramics. J. Am. Ceram. Soc.38, 251-5 (1955). This paper is similar to reference [8]; it has a better description of experimental techniques than reference [8].

[61] Kingery, W. D., Thermal conductivity: XIV, Conductivity of multicomponent systems. J. Am. Ceram. Soc. 42, 617-27 (1959). Reference [8] is preferred.

[62] Klemens, P. G., The thermal conductivity of dielectric solids at low temperatures (Theoretical). Proc. Roy. Soc. (London) A 208, 108-33 (1951). The λ-data on vitreous silica in Fig. 2 of this paper are from Berman [12]. However, the data in the present reference are less numerous than those in Berman's paper, which we prefer. In addition, the data in the present reference have been "adjusted".

[63] Koenig, John H., Progress Report No. 1 from December 1, 1952 to March 1, 1953. N. J. Ceram. Research Sta., Rutgers Univ., 100 p; AD-5552. This paper contains λ-data for vitreous silica. However, we consider that they are superseded by the data reported in reference [11].

[64] Lee, D. W. and Kingery, W. D., Radiation energy transfer and thermal conductivity of ceramic oxides. J. Am. Ceram. Soc. 43, 594-607 (1960). Reference [20] is preferred. However, the present reference contains a somewhat fuller description of the experiments than reference [20].

[65] Lucks, C. F., Deem, H. W. and Wood, W. D. Thermal properties of six glasses and two graphites. Bull. Am. Ceram. Soc. 39, 313-9 (1960). After studying this paper and plotting the λ-values given for vitreous silica we have concluded that the data are smoothed values taken from the original data of reference [19].

[66] Norton, F. H., Kingery, W. D. "et al.", The measurement of thermal conductivity of refractory materials. U. S. At. Energy Comm. Rept. NYO-3646, 1-8 (July 1, 1953). Reference [8] is preferred. Although the present reference appears to be the earliest report of this work, its graph of the data is smaller than the graph in reference [8].

[67] Powell, R. W., Experiments using a simple thermal comparator for measurement of thermal conductivity, surface roughness and thickness of foils or of surface deposits. J. Sci. Instr. 34, 485-92 (1957). Vitreous silica was one of the materials used in standardizing the apparatus. The λ-value given here is also given in reference [40]. Reference [40] is preferred because it contains the temperature of the measurement, whereas no temperature is given in the present reference.

[68] Pustovalov, V. V., Change in thermal conductivity of quartz glass in the process of crystallization. Translation by A. J. Peat, General Electric Research Lab. Rept. 60-RL-(2525M), September 1960. 8 p. English translation of reference [21]. Graph showing data is smaller than the one in reference [21].

[69] Pustovalov, V. V., Thermal conductivity of some refractory materials. Ogneupory 26, 302-5 (1961). The unsmoothed values of reference [21] are preferred. However, the present paper gives the density of the vitreous-silica sample, from which we computed a greater porosity than that given by Pustovalov.

[70] Ratcliffe, E. H., Preliminary measurements to determine the effect of composition on the thermal conductivity of glass. Phys. Chem. Glasses 1, 103-4 (1960). Reference [2] is preferred. The smooth curve in the present reference agrees with the data in reference [2]. It goes to a higher temperature, but we have assumed that this is an extrapolation of the previous results.

[71] Ratcliffe, E. H., A survey of most probable values for the thermal conductivities of glasses between -150 and 100°C, including new data on twenty-two glasses and a working formula for the calculation of conductivity from composition. Glass Technol. 4, 113-28 (1963). Reference [2] is preferred. The present reference contains a short table of "assessed best" values for vitreous silica. These values average 1.0 percent above our master curve.

[72] Sisman, O., Bopp, C. D. and Towns, R. L., Radiation stability of ceramic materials. U. S. At. Energy Comm. Oak Ridge Natl. Lab. Rept. ORNL-2413 (Aug. 31, 1957), 80-2. Reference [41] is preferred.

[73] Smoke, Edward J. and Koenig, John H., Thermal properties of ceramics. Rutgers Univ. Eng. Research Bull. 40 (Jan. 1958). 53 p. This is a summary of results previously issued in their progress reports. We prefer reference [11] as a source of λ-data on vitreous silica.

[74] Wray, Kurt L., and Connolly, Thomas J., Thermal conductivity of clear fused silica at high temperatures. Avco Research Lab. Res. Rept. 44 (February 1959). 13 p. We prefer reference [18].

Containing No Original Thermal-Conductivity Data on Fused Silica

[75] Sosman, Robert B., The Properties of Silica. (The Chemical Catalog Company. Reinhold Pub. Corp., New York, 1927). 856 p.

[76] Laufer, Jerome S., High silica glass, quartz, and vitreous silica. J. Opt. Soc. Am. 55, 458-60 (1965).

[77] Warren, B. E. and Biscoe, J., The structure of silica glass by X-ray diffraction studies. J. Am. Ceram. Soc. 21, 49-54 (1938).

[78] Wagstaff, F. E., Brown, S. D. and Cutler, I.B. The influence of H_2O and O_2 atmospheres on the crystallization of vitreous silica. Phys. Chem. Glasses 5, 76-81 (1964).

[79] Hetherington, G. and Jack, K. H., Water in vitreous silica. Part I: Influence of 'water' content on the properties of vitreous silica. Phys. Chem. Glasses 3, 129-33 (1962).

[80] Pustovalov, V. V., Determination of thermal conductivity of refractories to 1200° by the method of stationary heat flow. Ogneupory 24, No. 4, 180-5 (1959). Gives a description of the experimental method used by Pustovalov in reference [21].

[81] Gardon, Robert, A review of radiant heat transfer in glass. J. Am. Ceram. Soc. 44, 305-12 (1961).

[82] Bullard, E. C. and Niblett, E. R., Terrestrial heat flow in England. Monthly Notices Roy. Astron. Soc. Geophys. Suppl. 6, 222-38 (1951).

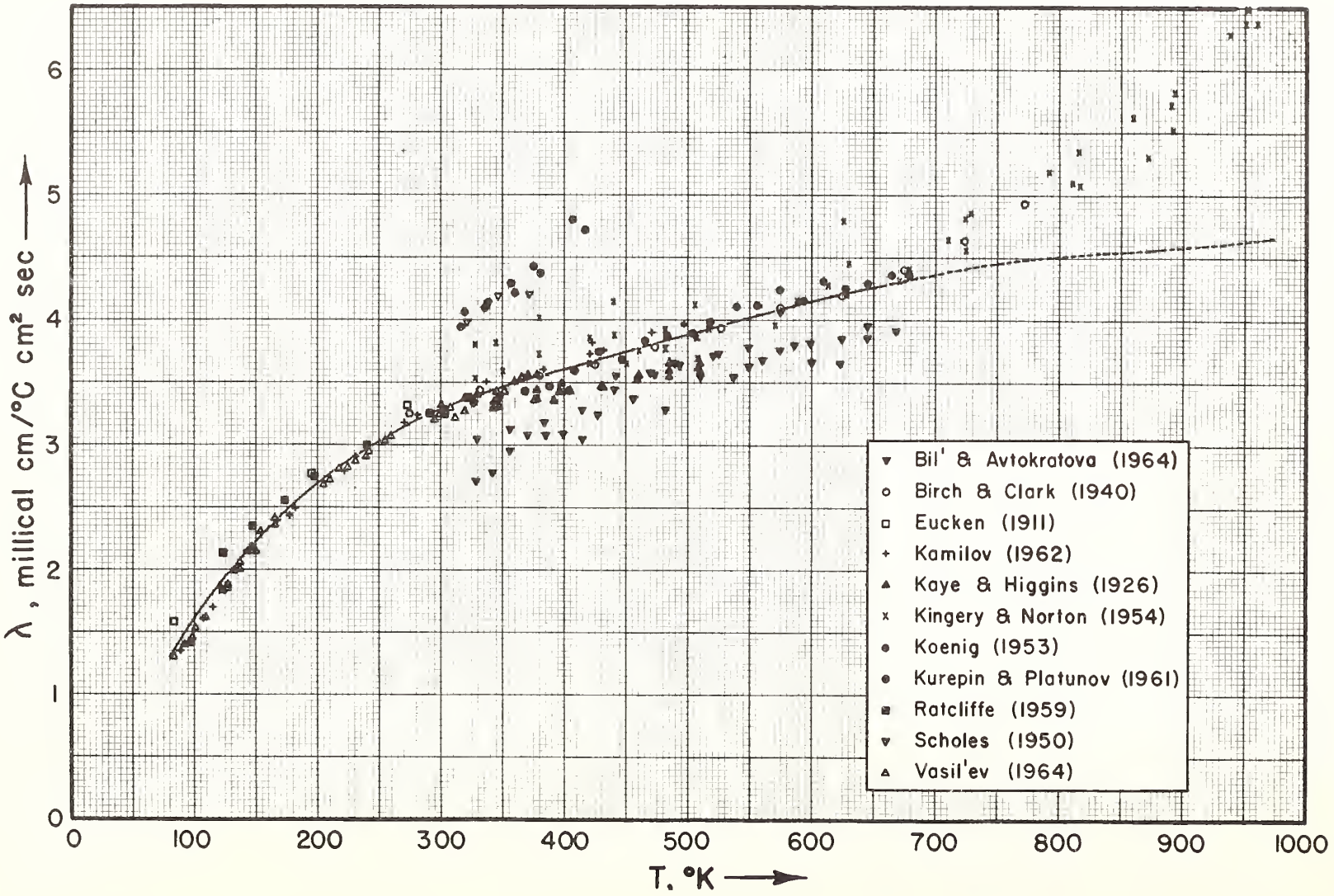

Figure 1. Thermal conductivity data of references [1] to [11].

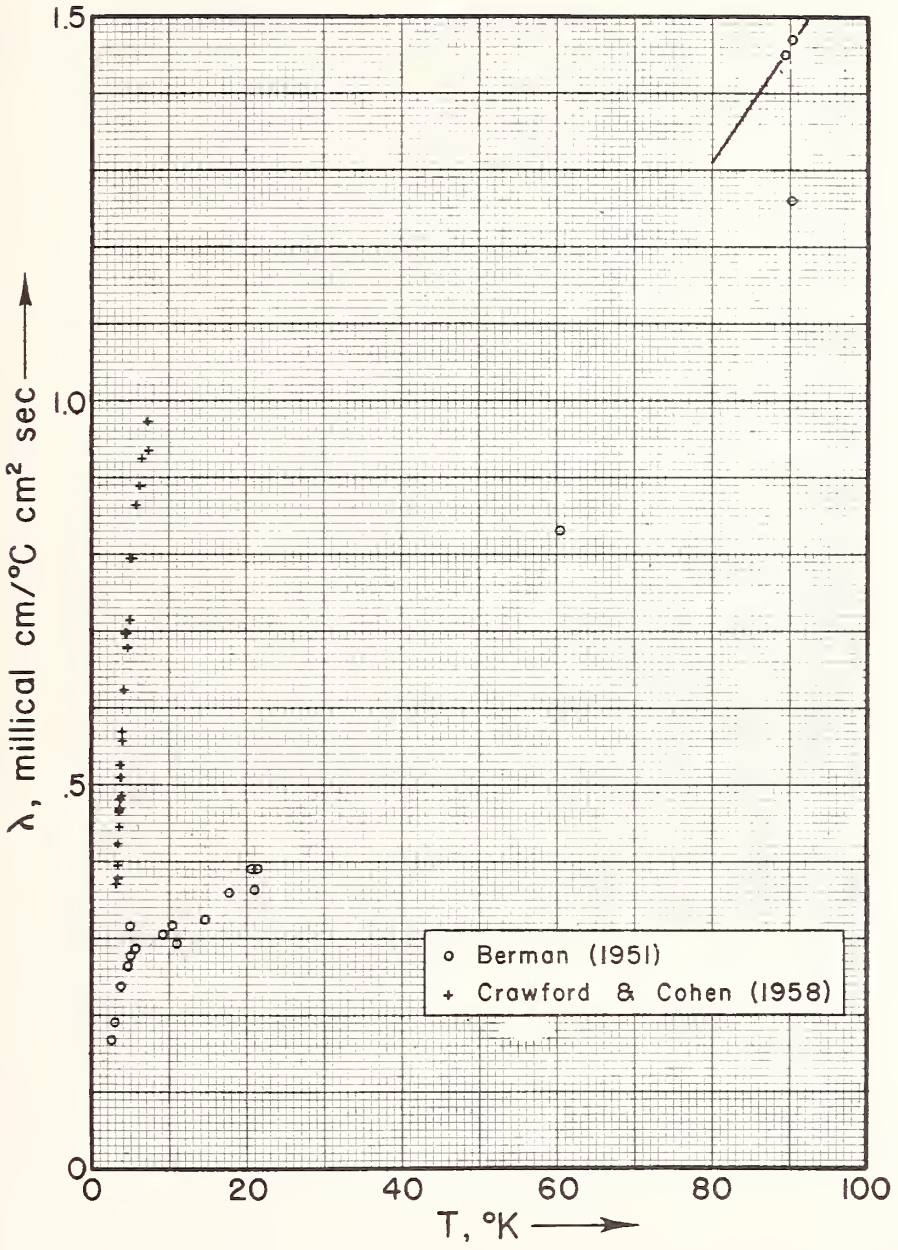

Figure 2. Thermal conductivity data of references [12] and [13] . The master curve begins at 80 °K.

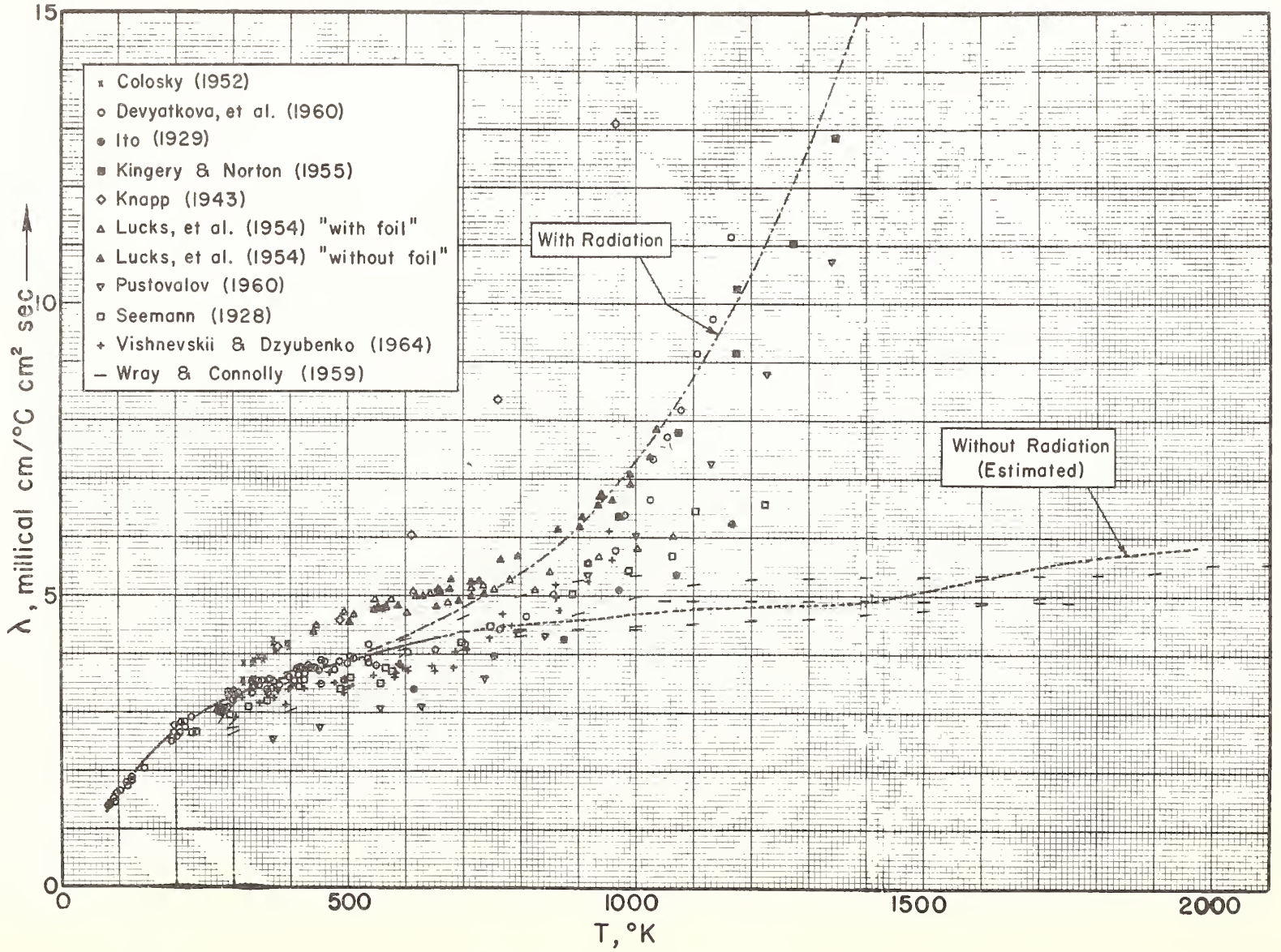

Figure 3. Thermal conductivity data of references [14] to [23].

Development of High Temperature Thermal Conductivity Standards

Alfred E. Wechsler[1]

Arthur D. Little, Inc.
Cambridge, Massachusetts 02140

and

Merrill L. Minges[2]

Air Force Materials Laboratory
Wright-Patterson Air Force Base, Ohio 45433

The continued use of high-temperature materials has led to the requirements for accurate thermal conductivity and thermal diffusivity standards. The program described herein encompasses an analytical and experimental study to establish high-temperature thermal conductivity and thermal diffusivity standards and to test these standards at several property measurement laboratories. Candidate ceramics, intermetallics, metals, and graphites were selected and used in a preliminary laboratory evaluation consisting of heating tests, visual and microscopic examination, and room-temperature thermal conductivity and electrical resistivity measurements. On the basis of test results, alumina, thoria, tungsten, and RVD and AXM-5Q1 graphites were chosen for the laboratory measurement program. Specifications written for these materials and the results of receiving inspection and density measurements of the samples obtained are presented. The status of measurements at participating laboratories is briefly described.

Key Words: Alumina, conductivity standards, diffusivity standards, graphite, high temperature thermophysical properties, thermal conductivity, thermal diffusivity, thoria, tungsten.

1. Introduction

The increased importance of high-temperature materials has led to the requirements for accurate thermal property data for design purposes. Measurements of thermal conductivity and diffusivity have been limited in their applicability by the unavailability of basic reference standards to evaluate and calibrate thermal property measurement apparatus. The selection of calibration standards for use at temperatures up to 1200°C (2200°F) has been proceeding for several years; laboratories have participated in round-robin tests evaluating tentative standard materials, such as Armco iron, Pyrex glass, and Pyroceram Code 9606.

The objectives of this program are to establish high-temperature thermal conductivity and thermal diffusivity standards and to test these standards at several thermal property measurement laboratories. The program is being carried out in two phases: Phase I consisted of the identification, selection, characterization and preliminary evaluation of candidate standard materials. Phase II consists of specification of sample materials, a test program at participating laboratories, and detailed examination of the thermal property data obtained.

This paper summarizes the results of the Phase I program, presents materials specifications and the results of visual examination and density measurements of the samples, and reviews the status of the Phase II laboratory test program.

2. Phase I--Materials Selection and Evaluation

2.1. Preliminary Materials Selection

To initiate the program, we chose potential candidate materials from those for which thermal property measurements had been reported in the literature. Materials which were obviously unsuitable because

[1]Group Leader, Engineering Sciences, Research and Experiments Group.

[2]Technical Manager, Structural Materials

of their low melting points were not considered further. Other materials were rated on a qualitative scale according to criteria such as phase change, melting point, sample reproducibility, availability, isotropy, homogeneity, microstructure stability, vapor pressure, mechanical strength, fabricability, shelf life, and cost. Materials were categorized as ceramics, intermetallics, metals, and graphites to aid their comparison, to provide for selection of potential standards which would cover a broad range of thermal conductivities (0.1 to 100 watt m^{-1} $°C^{-1}$) and to select candidates for use in vacuum, oxidizing, reducing or graphitic environments. The materials chosen for further experimental evaluation were:

Ceramics - Al_2O_3, BeO, $CaZrO_3$, ThO_2, and ZrO_2 (Y_2O_3 stabilized)

Intermetallics - B_4C, SiC, TiC, ZrB_2

Metals - Mo, Mo-30W, Ta, Ta-10W, W

Graphites - Union Carbide Corp. - ATJ, CEQ, and RVD
Pure Carbon Co. - P0-3 and DS-13
Poco Graphite, Inc. - 1924-H
Spear Carbon Co. - 7890
Ultra Carbon Co. - XUT-31 and UF4S

Figures 1 and 2 show the approximate thermal conductivity of these materials as a function of temperature.

2.2. Sample Procurement

Specifications for materials which were not commercial products were established, and samples in sizes and shapes similar to those required for thermal conductivity and diffusivity apparatus were obtained from qualified suppliers. Table 1 shows the materials used, the suppliers and the general sample characteristics. The samples were examined visually upon receipt and compared with the purchase specifications. All samples were accepted for preliminary experimental evaluation, even though some of them differed from the purchase specification.

Table 1. Materials Used in Preliminary Laboratory Evaluation

Sample	Supplier	Sample Size	Remarks
Ceramics			
Alumina	Coors Porcelain Co. Golden, Colorado	(1)	AD-995 composition, polycrystalline, sintered alumina
Beryllia	National Beryllia Corp. Haskell, N. J.	(1)	Berlox composition, 99.5% BeO, polycrystalline, sintered beryllia
	Brush Beryllium Co. Elmore, Ohio	(1)	Thermolox 99.5 composition, polycrystalline, sintered beryllia
Calcium Zirconate	Zirconium Corp. of America Solon, Ohio	(1)	99.5% pure, polycrystalline, sintered material
Zirconia	Zirconium Corp. of America Solon, Ohio	(1)	Polycrystalline, sintered material, stabilized with 12 mole % yttria
Thoria	National Beryllia Corp. Haskell, N. J.	(1)	Thorox composition, 99.5% pure, polycrystalline, sintered material
Intermetallics			
Boron Carbide	Carborundum Co. Niagara Falls, N. Y.	(2)	90+% dense, 76 wt% Boron, pressed samples
Silicon Carbide	Norton Co. Worcester, Mass.	(2)	Crystalon R grade
	Carborundum Co. Niagara Falls, N. Y.	(2)	KT grade
Titanium Carbide	Carborundum Co. Niagara Falls, N. Y.	(2)	95% pure

Titanium Carbide	Norton Co. Worcester, Mass.	(2)	96-98% pure, 79.7% Ti
Zirconium Diboride	Carborundum Co. Niagara Falls, N. Y.	(2)	95% pure, 79% Zr
	Norton Co. Worcester, Mass.	(2)	98% pure, 78% Zr
Metals			
Molybdenum	Climax Molybdenum New York, N. Y.	(1)	Arc melted, wrought bar
Molybdenum-30% Tungsten	Climax Molybdenum New York, N. Y.	(1)	Arc melted, wrought bar
Tantalum	National Research Corp. Cambridge, Mass.	(1)	Arc melted, wrought bar
Tantalum-10% Tungsten	National Research Corp. Cambridge, Mass.	(1)	Arc melted, wrought bar
Tungsten	Fansteel Metallurgical Corp. Chicago, Illinois	3/4" dia bar	Pressed and sintered, wrought bar
	Universal-Cyclops Bridgeville, Penn.	9/16" dia bar	Arc melted, wrought bar
Graphites			
Grade RVD	Union Carbide Corp. Parma, Ohio	5" x 5" x 3"	Density 1.88 gm/cm^3
CEQ	Union Carbide Corp. Parma, Ohio	5" x 5" x 3"	Density 1.53 gm/cm^3
ATJ	Union Carbide Corp. Parma, Ohio	5" x 5" x 3"	Density 1.77 gm/cm^3
7890	Spear Carbon Co. St. Marys, Penn.	5" x 2" x 10"	Density 1.47 gm/cm^3
1924-H	Poco Graphite, Inc. Garland, Texas	1 3/4" dia x 6"	Density 1.84 gm/cm^3
PO-3	Pure Carbon Co. St. Marys, Penn.	1" dia x 2"	Density 1.82 gm/cm^3
XUT-31	Ultra Carbon Co. Bay City, Michigan	1" dia x 12"	Density 1.67 gm/cm^3
UF4S	Ultra Carbon Co. Bay City, Michigan	1" dia x 12"	Density 1.72 gm/cm^3

Sample Size: (1) 2 1/2" dia x 1/2" thick disc with 1/2" dia center hole and 5/8" dia x 1/8" thick disc

(2) 2 1/2" dia x 1/2" thick disc

2.3. Experimental Evaluation

The experimental evaluation program consisted of visual examination of the samples and comparison with the specifications, density measurements, microstructural examination, heating tests, preliminary thermal conductivity measurements, and electrical conductivity measurements. Ceramics, metals, and intermetallics were heated in a vacuum environment at temperatures up to 2200°C (4000°F) for up to 24 hours per test cycle. Graphites were heated in a graphite and atmospheric pressure argon environment at temperatures up to 2300°C (4200°F) for similar durations. Preliminary thermal conductivity measurements were made at room temperature in a cut bar apparatus; measurement precision ranged between $\pm$ 2 and $\pm$ 3%, depending upon the samples used. Electrical resistivity was measured at room temperature and at liquid nitrogen temperature using the d.c. four-point method with an apparatus and instrumentation capable of $\pm$ 1 to $\pm$ 2% precision. The objective of these thermal conductivity and electrical resistivity measurements was to assess changes in the samples caused by heat treatment. Details of the apparatus and test methods are given in the report on the Phase I program [1][3].

[3]Figures in brackets indicate the literature references at the end of this paper.

Among the ceramics, aluminum oxide and thorium oxide were found to be suitable for further evaluation in the standards program because tests indicated that any changes in their structure or thermal properties induced by heat treatment were small and would not affect the application of these materials as standards. Beryllium oxide was rejected from further consideration because of its high vaporization rates in vacuum and because its unpredictable high-temperature reactions could result in toxicity problems. Calcium zirconate was rejected because of its poor sample reproducibility, its significant vaporization at moderate temperatures, and its reaction with refractory metals and ceramics used in typical measurement apparatus. Yttria stabilized zirconia was rejected because of its reaction with refractory metals, its apparent change in physical and chemical composition (resulting in a change in thermal properties) on heating, and its high vaporization rates at high temperatures.

None of the intermetallic candidate materials was found suitable for continued use in the program. Boron carbide was unsatisfactory because the high rate of vaporization at low temperatures causes the preferential vaporization of boron and thus changes its physical and chemical properties. Commercially available silicon carbide was unsatisfactory because of the high rate of vaporization of silicon in vacuum and the accompanying change in chemical composition. Titanium carbide was rejected because of the difficulties in obtaining reproducible samples, lack of control of stoichiometry, and rapid volatilization at moderate temperatures. Zirconium diboride appeared to be the most promising of the intermetallic materials. However, high vaporization rates resulting in a preferential loss of boron, changes in thermal conductivity on heating, and difficulties in obtaining reproducible samples of controlled stoichiometry indicate that this material should not be used as a standard in its present state of development.

Arc cast tungsten was selected as the most suitable candidate metal because heat treatment up to 2200°C (4000°F) did not significantly change its thermal and electrical properties or produce effects known to detract from its use as a standard. Changes in the thermal and electrical properties of arc-melted tantalum after heating were also minimal; however, tungsten was preferred to tantalum because it has greater physical and chemical stability at high temperatures. Molybdenum and molybdenum-30% tungsten were rejected because of their high vaporization rates and their lower maximum use temperatures compared to the other refractory metals. Tantalum-10% tungsten was rejected because of difficulties in obtaining samples of reproducible composition and changes in thermal and electrical properties after heat treatment. Pressed and sintered tungsten was not considered for further use because of intergranular cracking at high temperatures and resultant changes in thermal and electrical properties.

On the basis of our preliminary experimental examination, it was difficult to distinguish between acceptable and non-acceptable graphites. However, available manufacturers' data, the data in the literature, and our experiments indicate that Union Carbide Corporation's grade RVD and Poco Graphite, Inc.'s grade 1924-H are the most suitable materials. Grade RVD is recommended by its homogeneity, reproducibility, and the long experience in its production; its principal disadvantage is anisotropy. Grade 1924-H is very isotropic compared to other graphites.

3. Phase II--Sample Specification, Procurement and Preparation

3.1. Sample Specification and Procurement

The alumina, thoria, and graphite samples for Phase II were to be obtained from the suppliers who provided Phase I samples. The specifications for these materials, except for dimensions, were the same as those used in Phase I. Because of the sample sizes required and the limited availability of large-diameter arc-cast tungsten, samples were obtained from Climax Molybdenum Corp. rather than from Universal-Cyclops Steel Corp. The material specification was almost identical to that used previously.

In Phase I we used a Poco Graphite, Inc., sample designated 1924-H. During the program the designation was changed to AXF-5Q1. (The symbols designate the type and condition of the material: e.g., A indicates fine grain, X indicates graphitization, F indicates the high density range, 5 indicates graphitization at 2500°C, and 1 indicates a purified product.)

The information we received at the completion of Phase I indicated the desirability of using grade AXM-5Q1, to improve sample reproducibility and to make the material more valuable as a standard. Grade AXF-5Q1 is of very high density; the material is available only in small sample sizes and there may be more variation in density across individual sample billets or bars. This grade is produced on a limited basis; but, because of its high density and high mechanical strength, it has been of considerable interest to aerospace companies. Grade AXM-5Q1 is similar in all respects to grade AXF-5Q1 except that the molding pressure is less, the density is lower, and the density-related properties (strength and conductivity) are correspondingly lower. Because grade AXM-5Q1 is available in larger sizes than AXF-5Q1 and should have less variation of properties in a particular billet, it was selected for Phase II. Materials specifications for Phase II are given below:

a. Aluminum Oxide--Coors Porcelain Co.

Aluminum oxide to be used as a standard for determination of thermal conductivity and thermal diffusivity. To ensure homogeneous density and reduce internal stresses the material is to be fabricated

by isostatic pressing. Fired pieces must be free of cracks, visible discolorations or inclusions, and be uniform in color. The microstructure must be uniform within the specification and free of second phase. Fired pieces must conform to the following specification:

Grade	AD 995
Chemical Purity	99.5% Alpha Al_2O_3 (nominal)
Chromium Content	0.20 $\pm$ 0.05%
Sintered Density	3.84 gm/cm^3 typical, 3.80 gm/cm^3 minimum
Water Absorption	Zero
Maximum Average Grain Size	25 microns
Surface Finish	55 micro inches maximum

Edges to be left sharp as ground. A representative analysis of the finished product must be supplied; lot identification and sintering temperature must be given. All samples are to be packed individually to eliminate damage in shipment.

b. Thorium Oxide--National Beryllia Corp.

Thorium oxide to be used as a standard for determination of thermal conductivity and thermal diffusivity. To ensure homogeneous density and reduce internal stresses the material is to be fabricated by isostatic pressing then sintered. The fired pieces must be free of cracks, visible discolorations or inclusions and must be uniform in color. The microstructure must be uniform within the specification and free of second phase. Fired parts must conform to the following specification:

Grade	Thorox
Chemical Purity	99.9% cubic ThO_2 (minimum)
Sintered Density	9.2 $\pm$ 0.1 gm/cc
Water Absorption	1.0% maximum, 0.1% typical
Maximum Average Grain Size	30 microns
Surface Finish	55 micro inches (maximum)

The chemical composition of the starting powder and a representative analysis of the finished product must be supplied; lot identification, sintering time and temperature must be given. All samples are to be packed individually to eliminate damage in shipment.

c. Tungsten--Climax Molybdenum Co.

Arc-cast tungsten--extruded and stress relieved--to be used as a standard for determination of thermal conductivity and thermal diffusivity.

General Composition:

W 99.87% min	Sn less than 20 ppm	Mn less than 10 ppm	Co less than 10 ppm
Mo 0.1% max	Pb less than 20 ppm	Si less than 20 ppm	Al less than 20 ppm
Ni 0.001% max	O_2 less than 30 ppm	Cr less than 10 ppm	Cu less than 10 ppm
Fe 0.003% max	N_2 less than 30 ppm	V less than 10 ppm	Mg less than 10 ppm
C 0.005% max	H_2 less than 5 ppm	Ti less than 10 ppm	

Identification: The material is to be identified according to heat number, the identifying symbol or number to be marked on each rod or bar. The chemical composition of the heat and the conditions of stress relieving are to be given.

Inspection: All samples are to be inspected using a dye-penetrant technique and an ultrasonic technique to assure freedom from defects; the material is to be free of defects such as slivers, cracks, and seams.

d. RVD Graphite--Union Carbide Corp.

RVD graphite to be used as a standard for determination of thermal conductivity and thermal diffusivity. Pieces must be free of cracks and inclusions and conform to the following chemical and

mechanical specifications. The direction of the grain is to be marked on each piece, and the heat or batch number is to be indicated.

Grade	RVD
Characteristic	Two-fold anisotropic
Structural Class	High density
Grain Size Range	Medium
Particle Size	0.016" (maximum)
Density	1.86-1.92 gm/cm^3 (average density 1.89 gm/cm^3)
Electrical Resistivity	1260 $\pm$ 20% micro ohm-cm variation within the lot $\pm$ 10% (measured with grain); 2000 $\pm$ 20% micro ohm-cm variation within the lot $\pm$ 10% (measured across grain)
Coefficient of Thermal Expansion	3.0 x 10^{-6} ($\pm$ 20%) in/in°C variation within the lot $\pm$ 10% (measured across grain); 1.7 x 10^{-6} ($\pm$ 20%) in/in°C variation within the lot $\pm$ 10% (measured with grain)
Process Temperature	2800°C

e. AXM-5Q1 Graphite--Poco Graphite, Inc.

AXM-5Q1 graphite to be used as a standard for determination of thermal conductivity and thermal diffusivity. Pieces must be free of cracks and inclusions and must conform to the following chemical and mechanical specification. The direction of the grain is to be indicated.

Grade	AXM-5Q1 (special density)
Characteristic	Isotropic
Structural Class	Medium density
Grain Size Range	Fine
Particle Size	0.001 inch (maximum)
Density	1.74-1.76 gm/cm^3
Compressive Strength	14,000 psi (minimum)
Electrical Resistivity	1750 $\pm$ 20% micro ohm-cm
Coefficient of Thermal Expansion	6.3 x 10^{-6} in/in°C (room temperature to 100°C)
Process Temperature	2500°C

Alumina and thoria samples were obtained in the sizes required for the apparatus to be used in the participating laboratories (see Section 3.3). Tungsten was ordered as bar stock and machined to the sizes required. Graphites were ordered in billet form and machined to size after non-destructive tests had been completed.

3.2. Sample Inspection and Preparation

The sample materials were visually inspected upon receipt and the densities of finished samples and bulk material were measured. Microstructural examination and chemical analysis of samples are in progress. Significant observations are noted below; Table 2 summarizes density measurements on samples. The samples distributed to test laboratories have been further selected to reduce the density variation.

a. Alumina

Finished alumina samples appeared to be of good quality with minimum surface defects. A slight color variation was noted on disc samples (2" dia x 1/2" thick); more pronounced variation was noted on rod samples (1/4" and 3/8" dia). Dimension tolerances were within the $\pm$ 0.003" specified, and sample flatness was within the specification of 0.002" TIR.

Table 2. Densities of Samples Obtained for Use in Phase II

Size	Number Tested	Average Density gm/cm^3	Average Deviation gm/cm^3	Density Range gm/cm^3
Alumina				
2" dia disc	48	3.807	0.005	3.786-3.824
3/8" dia rod	11	3.782	0.006	3.770-3.794
1/4" dia rod	11	3.801	0.008	3.779-3.823
Thoria				
2" dia disc	55	9.256	0.045	9.137-9.399
3/8" dia rod	10	9.293	0.026	9.24 -9.37
1/4" dia rod	4	9.288	0.033	9.25 -9.34
AXM-5Q1 Graphite				
2" x 4" x 6"	20	1.757	0.006	1.747-1.766
4" dia x 12"	3	1.759	0.007	1.748-1.766

As shown in Table 2, the density of the disc samples is at the low end of the specification range, and the rod samples are in many cases outside the specification range. We have selected specific samples for use in conductivity and diffusivity measurements based upon these values and have attempted to use materials of constant density for different measurement methods, where possible. It should be possible to correct the data obtained for these density variations. Note that within any given type of specimen, good uniformity is obtained.

b. Thoria

Thoria samples were of apparent good quality with minimum surface defects. A color variation from light to dark yellow was observed. Sample edges were sometimes dark and grayish. Principal sample defects were chips on the edges and color centers in several samples. Samples were within the dimension tolerance specified.

As shown in Table 2, the average density values are within the specified limits although several specific samples were outside the range. The density range and average deviations are significantly larger for the thoria samples than for alumina samples.

c. Tungsten

Visual examination of tungsten samples showed no significant defects. Samples were generally within the tolerances specified and were machined to tolerances similar to the alumina and thoria specimens. The measured density of all machined samples was approximately 19.23 gm/cm^3.

d. AXM-5Q1 Graphite

Cursory visual inspection of AXM-5Q1 graphite showed no obvious flaws or defects. As indicated in Table 2, there was little variation in the bulk density of the billets and bars of this material. However, NDT radiometric density determinations carried out at Avco Corporation on these samples showed local variations of up to $\pm$ 4% in density over a single block. To reduce the effects of these variations, we have prepared density maps of the individual graphite billets and bars and carefully selected certain portions for the preparation of samples. Material having the least density variation and a good average value was chosen for sample preparation. Figures 3 and 4 show representative results of NDT tests on cylindrical AXM-5Q1 samples. The variations in density appear to be random on both billets and bars although there are slight trends toward greater density variations near the edges of the samples.

e. RVD Graphite

RVD graphite was obtained as a large billet, approximately 25 x 25 x 45 cm. The billet was cut in three slabs, each 8 cm thick. Visual observation showed no obvious flaws or deficiencies. The bulk density of the three slabs was measured to be 1.84, 1.87 and 1.89 gm/cm^3. NDT radiometric density measurements of the slabs showed good uniformity in the center portion of the slab (i.e., a variation of about $\pm$ 1% in density). The peripheral areas of the sample had higher densities than the center. Samples were selected from the central portions of the slabs to minimize density variations and to obtain a uniform average density.

3.3. Thermal Conductivity and Diffusivity Measurements

Measurements of thermal conductivity and diffusivity, sponsored under this program, are in progress at the laboratories indicated in Table 3. The samples to be measured and the methods used are also

given in the table. Measurements of thermal conductivity of alumina and thoria by a comparative method and of tungsten by a longitudinal heat flow method are planned by the National Bureau of Standards. Measurements of thermal conductivity (and electrical resistivity, where applicable) of the five candidate standards by longitudinal and radial heat flow methods are planned by Oak Ridge National Laboratories. Microscopic and metallurgical examination of samples, combined with chemical analysis will be used both before and after testing to aid the interpretation of the thermal property data.

Table 3. Thermal Property Measurements in Progress in Phase II

Organization	Method	Samples Tested	Temperature Range, °C	Remarks
Thermal Conductivity				
Atomics International	Radial inward heat flow	RVD graphite AXM-5Q1 graphite	1000-2500 1000-2500	Duplicate samples each material
General Electric (Cincinnati)	Radial outward heat flow	Alumina Thoria Tungsten	1000-1800 1000-2200 1000-2500	Duplicate data, duplicate samples each material
Illinois Institute of Technology Research Institute	Radial outward heat flow	Alumina Tungsten	1000-1800 1000-2200	Duplicate samples each material
National Beryllia Corporation	Radial outward heat flow	Thoria	1000-2200	Duplicate samples
Southern Research Institute	Radial inward heat flow and longitudinal heat flow (800-1000°C)	RVD graphite AXM-5Q1 graphite	800-2700 800-2700	Duplicate samples each material; measurements made in 2 orientations with AXM-5Q1 graphite
Thermal Diffusivity				
Atomics International	Laser flash	Alumina Thoria Tungsten RVD graphite AXM-5Q1 graphite	1000-1800 1000-2200 1000-2200 1000-2200 1000-2200	Duplicate samples each material; graphite measurements to be made in 2 perpendicular orientations
Battelle Memorial Institute	Laser flash	Alumina Thoria Tungsten RVD graphite AXM-5Q1 graphite	1000-1800 1000-2200 1000-2200 1000-2200 1000-2200	Duplicate samples each material; graphite measurements to be made in 2 perpendicular orientations

4. Acknowledgments

This work is supported by the Air Force Materials Laboratory, Wright-Patterson Air Force Base, Ohio, under Contract AF 33(615)-2874. The authors gratefully acknowledge the assistance of the many co-workers in the field of thermal property measurements who contributed to the program.

5. References

[1] Wechsler, A. E., Development of high temperature thermal conductivity standards, AFML-TR-66-415, January 1967.

[2] Powell, R. W., Ho, C. Y., and Liley, P. E., Thermal conductivity of selected materials, NSRDS-NBS 8, November 25, 1966.

[3] Goldsmith, A., Hirschhorn, H. J., and Waterman, T. E., Thermophysical properties of solid materials, Vol. III, WADS Technical Report 58-476, Revised Edit., November 1960.

[4] Loser, J. B., Moeller, C. E., and Thompson, M. B., Thermophysical properties of thermal insulating materials, ML-TDR-64-5, April 1964.

[5] Jun, C. K., and Hoch, M., Research on thermal conductivity of tantalum, tungsten, rhenium, Ta-10W, T_{111}, T_{222}, and W-25 Re in the temperature range 1500-2800°K, Contract AF 33(615)-1759, 1966.

[6] Taylor, R. E., and Nakata, M. M., Thermal properties of refractory materials, WADD-TR-60-581, Part IV, November 1963.

[7] Wood, W. D., and Deem, H. W., Thermal properties of high temperature materials, RSIC-202, June 1964.

[8] Neel, D. S., Pears, C. D., and Oglesby, S., The thermal properties of thirteen solid materials to 5000°F or their destruction temperature, WADD-TR-60-924, February 1962.

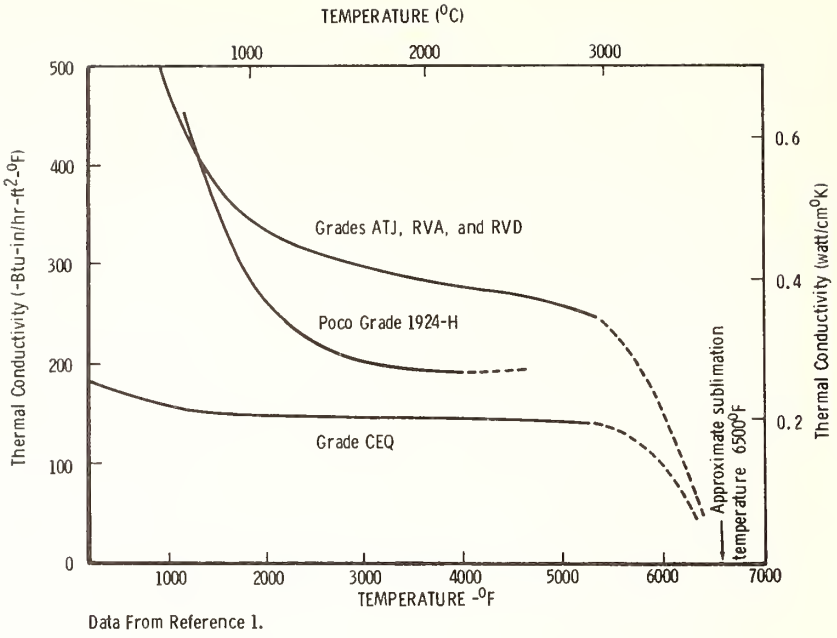

Figure 1 Approximate Thermal Conductivity of Various Grades of Graphite Versus Temperature

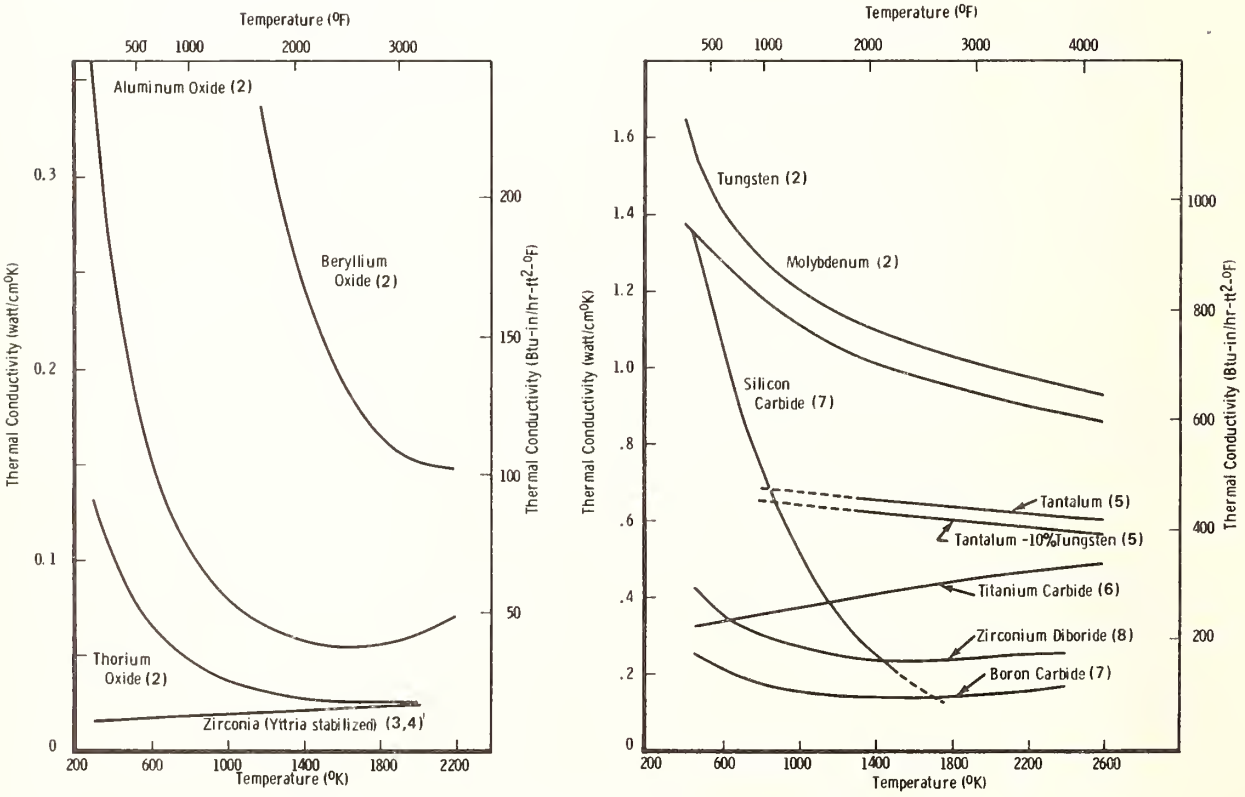

Figure 2 Thermal Conductivity of Candidate Standards

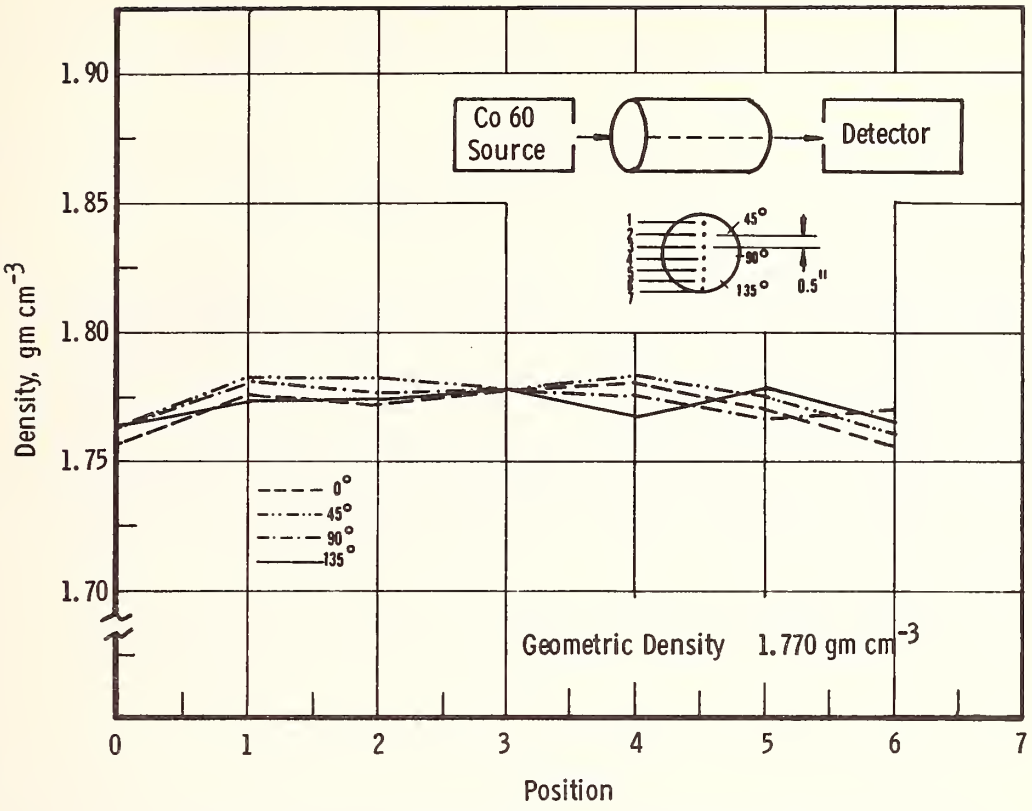

Figure 3 Axial Density Distribution in AXM-5Q1 Graphite

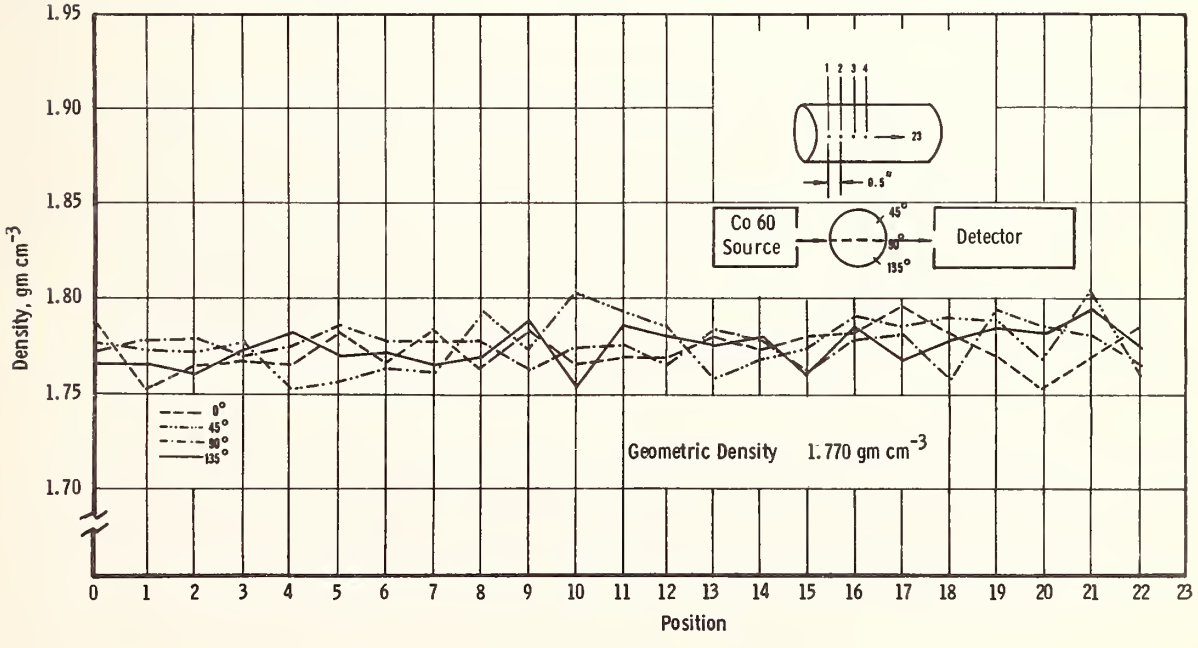

Figure 4 Radial Density Distribution in AXM-5Q1 Graphite

Glass Beads--A Standard for the Low Thermal Conductivity Range?

Alfred E. Wechsler[1]

Arthur D. Little, Inc.
Cambridge, Massachusetts 02140

A measurement standard for low thermal conductivity, suitable for a broad temperature range, is required in the many applications of thermal insulation materials. Glass beads have been suggested as a candidate standard because of their potential reproducibility, thermal stability, and amenability to analysis of the heat transfer mechanisms. Literature thermal conductivity data for several types of evacuated and gas-filled glass bead systems are summarized. Recent measurements using the line heat source and guarded cold plate apparatus are presented. The effects of particle size, temperature, and gas pressure on thermal conductivity are discussed. Considerable discrepancy exists in the conductivity data for evacuated glass bead systems obtained by different methods at different laboratories. The results suggest that variations in the sample preparation and cleanliness, particle size and distribution, as well as apparatus limitations may be the cause of these discrepancies.

Key Words: Comparative method, evacuated powders, glass beads, guarded cold plate method, line heat source method, thermal conductivity, thermal conductivity probe.

1. Introduction

The increased use of powder, fibrous, foam, and multilayer insulations as components of thermal protection systems for low and intermediate temperature applications has led to the requirements for a suitable standard of low thermal conductivity. The present standard used by the National Bureau of Standards and others is a semi-rigid resin bonded fiberglass insulating board with a thermal conductivity of about 0.035 $W\ m^{-1} deg^{-1}$. The need for a standard with a lower conductivity value is shown in Table 1 which summarizes the range of thermal conductivity values of common insulation materials.

Table 1. Thermal Conductivities of Various Insulations

Material	Thermal Conductivity $W\ m^{-1}\ deg^{-1}$
Multilayer Insulations	1.0×10^{-5} to 1.0×10^{-4}
Opacified Evacuated Powders	2.8×10^{-4} to 1.0×10^{-3}
Evacuated Glass Fibers	5.8×10^{-4} to 2.8×10^{-3}
Evacuated Powders	8.5×10^{-4} to 5.8×10^{-3}
Unevacuated Foams, Powders, Fibers	6.0×10^{-3} to 3.6×10^{-2}

The usual criteria of homogeneity, isotropy, reproducibility, and availability apply to the selection of a low thermal conductivity standard. In addition, it is desirable to (1) have a knowledge of the mechanisms of heat transfer in the candidate standard, (2) select a material suitable for use in many types of apparatus over a broad temperature range, and (3) have a single standard that will be applicable to the large conductivity range of many types of insulating materials.

[1]Group Leader, Engineering Sciences, Research and Experiments Group.

Glass beads have been suggested as a candidate standard for this application. They are readily available; their inherent form should lead to homogeneity, isotropy, and reproducibility. They can be used in many types of apparatus because of their small particle size and their fluidity. A large range in thermal conductivity can be obtained by using gas-filled and evacuated beads. However, the reproducibility of thermal conductivity data is questionable, and the effects of particle size, mechanical loading, temperature, and sample preparation procedures on thermal conductivity have not yet been fully established.

The objectives of this paper are to summarize available thermal conductivity data on glass beads, to discuss the factors which cause variations in the data, and to suggest procedures for further work to improve the applicability of glass beads as a thermal conductivity standard.

2. Materials Used

Solid beads or spheres are commercially prepared from soda-lime-silica glass, borosilicate glass, and fused quartz. The first of these has been used most often in thermal conductivity measurements and the data presented in this paper will be restricted to this readily available material.

The principal commercial suppliers of soda-lime-silica glass beads are the 3M Company and Microbeads, Inc. The beads are available in grades with average diameters from about 0.025 mm to 0.5 mm, graded with respect to shape as well as size and size distribution. Manufacturers may designate the beads according to the percentage of "true spheres", typically 65% to 95%. When obtaining glass beads, the material is usually specified by the fraction retained by or passing through standard sieves. Thus, the upper and lower values for bead diameters are established. In practice, however, a small percentage of fines is often found in most samples. For example, Table 2 below gives both manufacturers' size distribution data on two typical bead sizes.

Table 2. Glass Beads Size Distribution--Manufacturers' Data

Bead Type	Percent Retained on U. S. Sieve No.						
	60 (0.25 mm)	70 (0.21 mm)	80 (0.177 mm)	100 (0.149 mm)	120 (0.125 mm)	140 (0.105 mm)	170 (0.088 mm)
710A		0-2		92-100			
100B (200 micron)	10	40	40	10			
1217A					0-2		92-100
120B (120 micron)				0	35	60	5

Properties of the bulk glass which are significant to the use of the glass beads in thermal conductivity measurements are listed in Table 3. Glass beads are supplied in quantities of one to several thousand pounds. Special orders with more narrow size distributions can also be obtained. The beads are relatively clean and free from foreign material when received.

Table 3. Properties of Bulk Glass from Which Glass Beads are Prepared[a]

Density[b]	2.5×10^3 kg/m^3
Hardness	6 (Mohs' scale)
Coefficient of Thermal Expansion	9.5×10^{-6} deg^{-1} (20 to 300°C)
Thermal Conductivity	1.04 W m^{-1} deg^{-1} (room temperature)
Specific Heat	1080 J kg^{-1} deg^{-1}
Modulus of Elasticity	7.5×10^{10} N/m^2
Refractive Index (6200Å)	1.53

[a] From manufacturers' data sheets.

[b] Density of the beads depends upon the packing and size distribution but is usually in the range of 1.45 to 1.55 $\times 10^3$ kg/m^3.

3. Measurement Methods

Table 4 summarizes the methods used by various investigators to measure the thermal conductivity of glass beads, as well as the types and sizes of beads, temperature ranges, and environmental conditions. The thermal conductivity probe, line heat source, and guarded cold plate methods are commonly used techniques well known to most investigators.

Table 4. Methods and Environmental Conditions Used in Measuring Thermal Conductivity of Glass Beads

Investigators	Method	Bead Properties			Temperature	Environmental Conditions
		Type	Diameter mm	Density kg/m^3	°K	
Masamune & Smith[1][2]	Comparative, Lucite disc	3M	0.029-0.470	1500	315	Air and vacuum
Watson[2]	One-dimensional radiative flux	Microbeads	<0.037-0.84	1170-1820	150-350	Vacuum
Messmer[3]	Probe	Microbeads	0.177-0.84	1560-1660	300	Air, vacuum and mechanical load
Wechsler & Simon[4]	Line heat source	Microbeads	0.044-0.062	1420	190-350	Vacuum
Wechsler & Glaser[5]	Probe and guarded cold plate	3M	0.029-0.150	1460	300	Air and vacuum
Salisbury & Glaser[6]	Line heat source	3M	0.050-0.200	1500	300	Vacuum
Arthur D. Little[7]	Guarded cold plate	Microbeads	0.59 -0.84	1590	190-270	Vacuum, N_2, He

The comparative apparatus used by Masamune and Smith [1] consisted of a Lucite disc 3.8 cm in diameter and 1.25 cm thick adjacent to a similar sized sample. One-dimensional heat flow was assumed between hot and cold plates which were in contact with the Lucite disc and sample, respectively. Temperature measurements were made with thermocouples at the Lucite-heat source, Lucite-sample, and sample-heat sink interfaces. The conductivity of the Lucite was taken as 0.205 $W\ m^{-1}\ deg^{-1}$.

In the method used by Watson [2], a sample was placed on a warm temperature bath plate; the top of the sample radiated to a cavity maintained at 77°K. The heat flux emitted from the sample was measured using an 8-14μ filtered infrared photoconductor photometer and the temperature of the sample surface was determined from this emitted energy. From the measured heat flux, bath temperature, sample thickness, and the calculated temperature of the free surface of the sample, the thermal conductivity was then evaluated. Errors in measurement are discussed by each of the investigators cited in Table 4. Generally, this method should have accuracies of from 5 to 20%, although greater accuracy is claimed by several investigators.

The method of sample preparation is not adequately described by most investigators. Messmer [3] resieved, washed, and dried (at 110°C) the beads used in his work. The beads used by Wechsler and Simon [4] were sieved, washed, and baked at 200°C in high vacuum for a prolonged period. Watson [2] washed some of the samples in acetone prior to use. Other investigators provide only limited indications of how the samples were handled, cleaned, and used.

The only common measurement control used in most investigations is bulk density. The measurements are usually gravimetric and are often made during preparing the sample. A desirable characteristic of the glass beads is that they will pack under random filling methods to densities between 1450 and 1550 kg/m^3. Values differing significantly from this range are indicative of a broad size range or errors in measurement.

---

[2]Figures in brackets indicate the literature references at the end of this paper.

4. Measurement Results

In this section, the effects of gas pressure, particle size, temperature, and mechanical loading will be discussed. The results of different investigators will be compared; the discussion will emphasize data obtained at atmospheric pressure and at high vacuum.

4.1. Effect of Gas Pressure

The dependence of thermal conductivity of a powder on gas pressure has been studied for many years [8]. Theoretical and empirical correlations have been developed to predict the contribution of the gas phase to thermal conductivity of the heterogeneous composite [9,10]. The correlations are generally satisfactory in predicting the variation of thermal conductivity with gas type at atmospheric pressure, and in predicting the rate of decrease in thermal conductivity with decreasing gas pressure. The principal discrepancy between available theories and current experiments is in establishing the residual thermal conductivity of the solid when the interstitial gas pressure is reduced to a very low value. The effects of physically or chemically adsorbed gases on this residual conductivity are not well known.

Figure 1 shows data of three investigators on the effect of gas pressure. Unfortunately, the measurements were made with different particle size beads; however, all measurements were near 300°K. The data of Messmer [3] and Wechsler and Glaser [5] are in reasonable agreement. The larger the particle size, the greater the reduction in gas pressure that is required to achieve the equivalent reduction in thermal conductivity. Note that these data are in fair agreement at atmospheric pressure and at low pressures. The variation in conductivity with particle size is in agreement with other data described later. The data of Masamune and Smith [1] agree with the data of Messmer [3] and Wechsler and Glaser [5] at atmospheric pressure but differ greatly at low pressure. This may be a result of the limitations imposed by the design of the comparative apparatus using a relatively high conductivity standard. These data point out two ranges where glass beads may be useful as a possible standard--at atmospheric pressure and at high vacuum. It would be difficult to use the beads as a standard at intermediate gas pressures because of the large slope of the conductivity-pressure curve and the difficulty in accurate pressure measurements within powder systems.

4.2. Effect of Particle Size

Figure 2 shows the data obtained by several investigators at atmospheric pressure and at gas pressures below 10^{-2} torr, where the effects of gas pressure are small. Although there appears to be a wide variation in the data, several definitive conclusions can be drawn.

(1) At atmospheric pressure, the data of all investigators are relatively consistent with respect to the absolute value of thermal conductivity. This is attributed to the large gas conduction contribution at atmospheric pressure. There is only a small increase of thermal conductivity with an increase in particle size.

(2) Under high vacuum conditions, there is considerable variation of thermal conductivity with particle size. The results of Watson [2], Wechsler and Glaser [4], Salisbury and Glaser [6], and Arthur D. Little, Inc.[7] are consistent in both the absolute value of thermal conductivity and the increase of thermal conductivity with increased particle size. Note that the thermal conductivity of beads with very small particle size appears to be higher than that of beads with an intermediate particle size. This can be explained by the different magnitudes of the conduction and radiation contributions to thermal conductivity.

(3) Examination of Figure 2 and Table 4 shows that there is no consistent effect of the source of materials. The comparative method of Masamune and Smith [1] gives higher thermal conductivity values and less effect of particle size on thermal conductivity than any other method. The thermal conductivity probe methods used by Messmer [3] and Wechsler and Glaser [5] give higher thermal conductivity values than the line heat source or guarded flat plate methods. These data suggest that the probe and comparative method may have lower limits of applicability or may yield inaccurate data at low conductivity values. The high value of conductivity for beads with a 193μ diameter obtained by Messmer [3] at 10^{-2} torr does not agree with the other observed trends.

(4) The beads which have been thoroughly cleaned and outgassed at low pressures (Watson [2] and Wechsler and Simon [4]) seem to have lower thermal conductivity values than those for which the preparation method is not specified. This may be a coincidence or it could result from removal of conducting films on the beads by cleaning or prolonged outgassing.

The results suggest that careful sample preparation is necessary to obtain good data and each apparatus and method should be examined to determine the errors involved in measurements of low thermal conductivity materials.

4.3. Effect of Temperature

The effect of temperature on the thermal conductivity of glass beads has been investigated by Watson [2] and Wechsler and Simon [4]. These investigators interpret the conductivity data as the sum

of a term with a constant value, representing the contribution of solid conduction, and a term which has a cubic temperature dependence, representing the contribution of thermal radiation. This approach seems to give consistent results for glass beads as well as other powders. Figure 3 shows typical results of these investigators. Each curve represents the equation:

$$k = B + AT^3 \tag{1}$$

where B is the solid conduction contribution, A is a radiation term--a constant for a given material--k is the effective thermal conductivity, and T is the absolute temperature. Table 5 shows values of these constants as a function of particle size.

Table 5. Radiative and Solid Conduction Contributions to the Thermal Conductivity of Glass Beads

Investigator	Particle Size microns	Radiative Term (A) $W\ m^{-1}\ deg^{-4}$	Solid Conduction Term (B) $W\ m^{-1}\ deg^{-1}$
Watson [2]	840-590	26.6×10^{-11}	-6.6×10^{-5}
	350-250	13.4×10^{-11}	9.5×10^{-5}
	125- 88	8.5×10^{-11}	32.2×10^{-5}
	74- 53	3.4×10^{-11}	70.0×10^{-5}
	<37	6.3×10^{-11}	95.4×10^{-5}
Wechsler & Simon [4]	44- 62	3.0×10^{-11}	46.6×10^{-5}

The general trends of increased solid conduction contribution with increased particle size and decreased radiation contribution with decreased particle size are evident. Relatively good agreement is obtained between the work of these investigators. The two opposing trends can result in apparent anomalies of the effects of particle size on thermal conductivity at very low temperatures. It would be desirable to extend the temperature range of measurement as well as the quantity of data to improve the characterization of the solid conduction and radiation mechanisms.

Little published data are available on the effect of temperature on the thermal conductivity of gas filled glass beads. However, because of the large contribution of gas conduction, the effect of temperature on conductivity of gas filled glass beads should parallel the effect of temperature on gas conductivity.

4.4. Effect of Mechanical Loading

Messmer [3] has investigated the effect of compressive loading on the thermal conductivity of glass beads. Evacuated glass beads of 710μ and 193μ diameter were subjected to external pressures of from 10^5 to 7×10^6 N/m^2 at 300°K. The thermal conductivity of both materials increased with the 1/4 power of the applied external pressure. This differs slightly from the 1/3 power of the external pressure obtained from Hertzian loading analysis. Data obtained on gas filled beads by Messmer [3] show only a small effect of mechanical load because of the large contribution of the gas to the system's thermal conductivity. Preliminary data obtained at Arthur D. Little, Inc. [7] using 710μ diameter evacuated glass beads at 225°K in a guarded cold plate apparatus show that the thermal conductivity increases with about the 1/10 power of the load over the pressure range from 5×10^3 to 3×10^4 N/m^2. The radiation component of thermal conductivity should be almost invariant with loading, whereas the conduction component should increase with the 1/3 power of the load. Depending upon the ratio of solid conduction to radiation, the dependence of thermal conductivity on external load can vary significantly. In most thermal conductivity apparatus, natural mechanical loading of the sample will not be important.

5. Recommendations

Evacuated and gas filled glass beads are a candidate standard for the low thermal conductivity range; however, additional carefully controlled data are required before this material can be accepted as a standard. The following procedures are suggested to assist the further evaluation of glass beads.

(1) Select two or three particle size ranges and distributions for use in subsequent measurements. The size ranges should be chosen so that sieving can be used to obtain the required size distribution rather than more complex separation or classification methods.

(2) Establish a controlled method for cleaning, outgassing, and preparing samples.

(3) Perform repeated thermal conductivity measurements using different methods and apparatus under carefully specified environmental conditions of temperature, temperature gradient, and gas pressure. A temperature range of 100 to 500°K, with temperature gradients of less than 10°K/cm is recommended. Gas pressures should be kept below 10^{-4} torr or at atmospheric pressure. Nitrogen or an inert gas of high purity should be used. Measurements should be made under carefully controlled mechanical load conditions. Density data should be obtained as a control parameter.

(4) Analyze the random and systematic errors in each thermal conductivity method used and report the precision and estimated accuracy of the measurements with the data.

Through the cooperative efforts of the participants of this conference, it may be possible to establish glass beads as a low conductivity standard within several years.

6. Acknowledgments

The author gratefully acknowledges the assistance of Mr. F. Ruccia, Mr. I. Black, Mr. E. Boudreau, and Mr. R. Carroll in obtaining the published and unpublished data at Arthur D. Little, Inc. The help of Professor R. C. Reid of MIT in compiling and examining the data was greatly appreciated.

7. References

[1] Masamune, S., and Smith, J. M., Thermal conductivity of beds of spherical particles, Ind. & Eng. Chem. Fundamentals, 2, No. 2, p 136-142 (1963).

[2] Watson, K., The thermal conductivity measurements of selected silicate powders in vacuum from 150°-350°K, Ph.D. Thesis, California Inst. of Tech., 1964.

[3] Messmer, J., personal communication (1964).

[4] Wechsler, A. E., and Simon, I., Thermal conductivity and dielectric constant of silicate materials, Final Report prepared by Arthur D. Little, Inc., for NASA George C. Marshall Space Flight Center, under Contract NAS8-20076, August 1966.

[5] Wechsler, A. E., and Glaser, P. E., Thermal conductivity of non-metallic materials, Final Report prepared by Arthur D. Little, Inc., for NASA George C. Marshall Space Flight Center, under Contract NAS8-1567, June 1964.

[6] Salisbury, J. W., and Glaser, P. E., editors, Studies of the characteristics of probable lunar surface materials, AFCRL-64-970 (Jan. 1964).

[7] Arthur D. Little, Inc., unpublished work in progress.

[8] Smoluchowski, M., Sur la conductibilite calorifique des corps pulverisis, Bull. Int. L'Acad. Sci. de Cracovie, A129 (1910).

[9] Schotte, W., Thermal conductivity of packed beds, AIChE Journal, 6, 63 (1960).

[10] Everest, A., Glaser, P. E., and Wechsler, A. E., Thermal conductivity of non-metallic materials, Summary Report prepared by Arthur D. Little, Inc., for NASA George C. Marshall Space Flight Center, under Contract NAS8-1567, 27 April 1962.

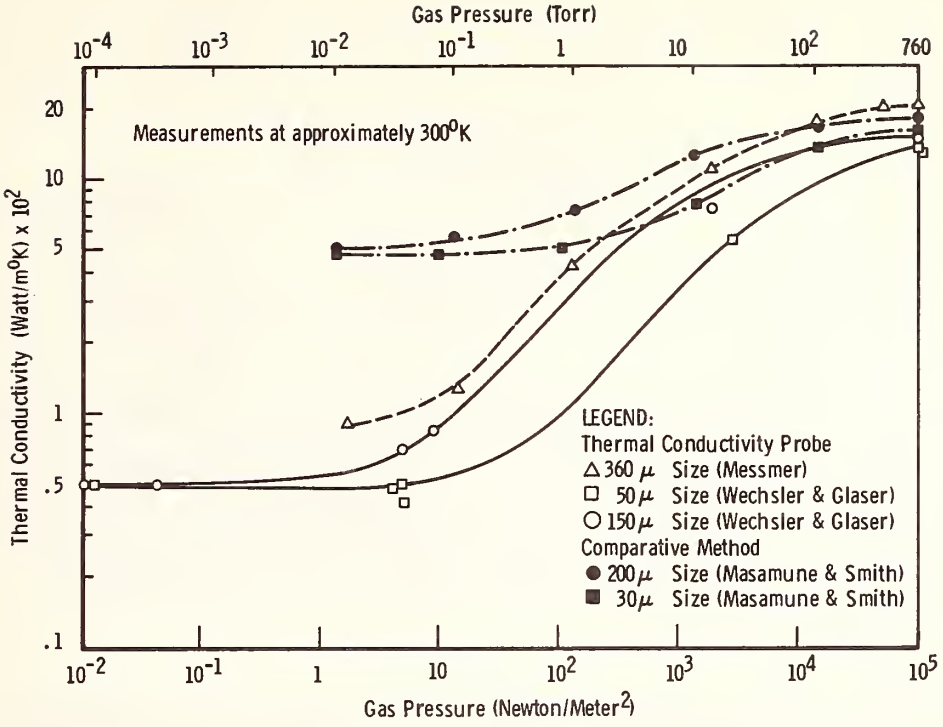

Figure 1 Effect of Gas Pressure on Thermal Conductivity of Glass Beads

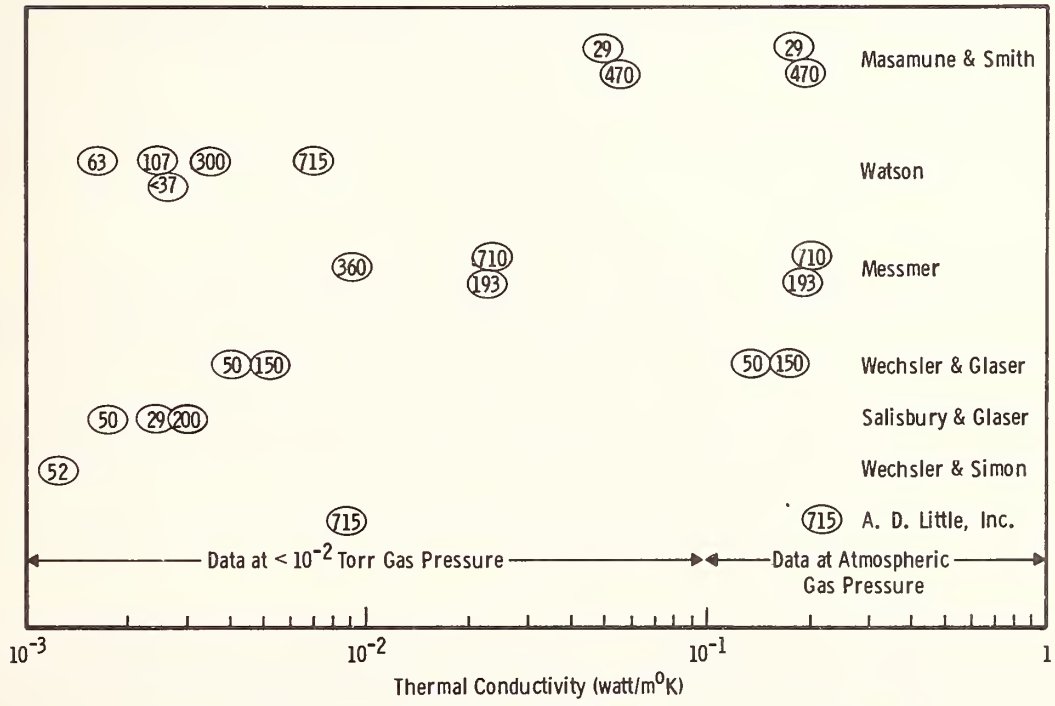

Note: Numbers Refer to Particle Diameter in Microns, All data reported at approximately 300°K.

Figure 2 Effect of Particle Size on Thermal Conductivity

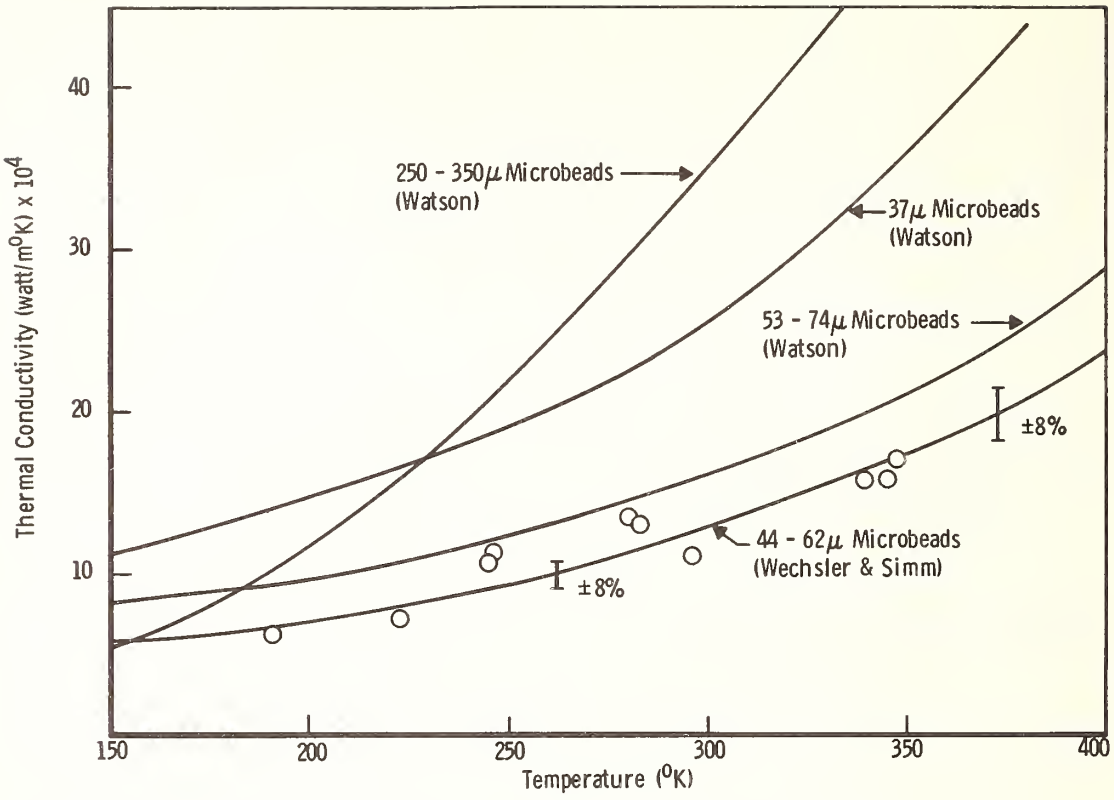

Figure 3 Effect of Temperature on the Thermal Conductivity of Glass Beads

Lattice Thermal Conductivities of Semiconductor Alloys

I. Kudman

RCA Laboratories
Princeton, New Jersey

The lattice thermal conductivities of disordered semiconductor alloys are treated using the phenomenological model derived by Abeles. The thermal conductivity is expressed in terms of the lattice parameters and mean atomic weights of the alloy and its constituents. This treatment is applied to both III-V and IV-VI semiconductor alloy systems. Comparison of the theoretically derived and experimentally determined lattice thermal conductivities are discussed.

Key words: Lattice thermal conductivity, semiconductor alloys.

1. Introduction

Solid solution alloys are ideally suited for studying the effects of defects on thermal transport. The small concentrations of intentionally and unintentionally added impurities have a negligible effect on the thermal conductivity, as compared to that of alloying.

Above the Debye temperature, the thermal conductivity of a semiconductor can be determined, to a fair degree of accuracy, by use of the 3-phonon scattering equation of Leibfried and Schlomann [1][1]. For the case of combined scattering, the relaxation time approximation has been applied with considerable success. The relaxation time approximation of Klemens [2] and Callaway [3] has been used by Abeles [4] to derive a simple phenomenological model to describe the variation of thermal conductivity of semiconductor alloys as functions of both composition and temperature.

It is the purpose of this paper to compare the thermal conductivities derived by the Abeles model to those determined experimentally. The experimental results are given for III-V and IV-VI semiconductor alloy systems.

2. Experimental

The III-V alloy systems; GaAs-InAs, GaSb-GaAs, and GaSb-InSb, were prepared by the zone leveling technique. This procedure consists of moving a molten zone having the liquidus composition through charge material having the isothermally corresponding solidus composition. The IV-VI alloy system, PbTe-PbSe, was prepared by the vertical Bridgman method.

The thermal conductivities were determined from high temperature diffusivity measurements [5]. The specific heats required to convert the thermal diffusivity, K/C_p, into K were obtained from measurements of the III-V compounds [6] and the Dulong-Petit value was used for the PbTe-PbSe alloy system [7].

3. Discussion

3.1 Theory

For temperatures above the Debye temperature, the thermal conductivity of a semiconductor alloy results from the scattering of phonons by mass fluctuation and strain scattering due to alloying and anharmonic phonon-phonon scattering. A phenomenological theory describing the variation of the thermal resistance on alloy composition and temperature has been derived by Abeles [4]. It was assumed that the reciprocal relaxation times depend on frequency ω as ω^4 for strain and mass point defects and as ω^2 for normal and umklapp three-phonon anharmonic processes. The lattice thermal resistance of a disordered

[1] Figures in brackets indicate the literature references at the end of this paper.

semiconductor alloy is given by the expression (reader is referred to reference 4 for a detailed discussion):

$$1/k = [A]\,(TM\Gamma)^{\frac{1}{2}}\,\delta^3 + [B]\,M^{\frac{1}{2}}\,\delta^{7/2}\,T,$$

where

$$[A] = 9.67\times10^{5}\,(1 + 5/9\,\alpha)^{\frac{1}{5}}\,\gamma_1\,\beta^{-2} \qquad (1)$$

$$[B] = 7.08\times10^{-2}\,(1 + 5/9\,\alpha)\,\gamma_1^{\,2}\,\beta^{-3}$$

Here α is the ratio of normal to umklapp scattering rates: γ_1 is the anharmonicity parameter; β is defined by $\beta = \theta M^{\frac{1}{2}}\,\delta^{3/2}$, where θ is the Debye temperature, M is the mass, and $\delta = a/2$ for diamond and zinc-blende lattices, where a is the lattice constant. The disorder parameter $\Gamma = x(1-x)\,[\Delta M/M + \epsilon\,\Delta\delta/\delta]$, where x is the composition, ΔM is the mass difference, $\Delta\delta$ is the difference in lattice constants, and ϵ is the strain term.

The model of Abeles includes two major modifications which have not, in general, been considered in theories of point defect scattering: (1) the inclusion of normal processes and (2) the introduction of a strain term due to atomic misfit. A similar expression was derived by Parrott [8], however, the contribution of strain scattering was not included in the derivation.

The introduction of normal processes was based on the suggestion of Klemens [9] that these processes contribute significantly to the thermal resistance even at high temperatures. While normal processes do not contribute directly to the thermal resistance, they scatter phonons into modes which can then undergo scattering by another mechanism e.g. point defect scattering.

The strain term introduced by Abeles is that due to Klemens [2] in which an impurity is introduced in a simple cubic lattice with only nearest neighbors acting. Abeles then proceeds to treat the scattering in terms of the elastic continum "sphere-in-hole" model and arrives at the definition of Γ given above. The strain term ϵ is assigned a value of 39 based on the impurity model of Klemens.

Although β is readily calculated, ϵ assigned a value of 39, and γ_1 can be determined from the thermal conductivity of the components, it is not obvious how to choose a value for the adjustable parameter α. The thermal resistivity of the Ge-Si alloy system was computed by Abeles and agreement obtained between the theoretical values at 300°K and the experimental data for $\gamma_1 = 1.77$ and $\alpha = 2.5$.

3.2 III-V Compound Alloys

The calculations of the lattice thermal resistivities of disordered semiconductor alloys will now be applied to the III-V compound alloy systems. The strain term ϵ remains unchanged and the adjustable parameter α will be assumed equal to 2.5 as in the base of the Ge-Si alloys. (It must be emphasized that α is an adjustable parameter and may vary from one class of semiconductors to the next, it is used only for the initial calculations since it was successfully applied to the Ge-Si alloys).

Abeles computed the thermal resistivities for two III-V alloys systems assuming γ_1 to be constant, as was found for the Ge-Si alloys. For one system, InAs-InP, the agreement was poor, especially as the InP content increased. While the assumption of a constant γ_1 for Ge-Si alloys is justified on the basis of experimental data, this is not the case for the III-V compounds. In the III-V compounds it was found that the anharmonicity parameter varied significantly from compound to compound [10].[2] γ_1 depends on the mass ratio of the constituent elements in such a manner that compounds with a mass ratio close to unity, e.g., InSb, have large values of γ_1; and those with a large mass ratio, e.g. AlSb have smaller values of γ_1. The variation of $\gamma_1^{\,2}$ as a function of the mass ratio is shown in figure 1.[3]

The variation of the room temperature lattice thermal resistivities of the III-V alloys were computed using the values of α and ϵ given above. The anharmonicity parameter was determined from figure 1 using the average mass ratio of the alloy. The lattice thermal conductivities of the alloys were obtained by subtracting the electronic contribution from the total thermal conductivity. The electronic thermal conductivity was computed for the case of combined polar plus ionized impurity scattering [11].

---

[2] The variation of the anharmonicity parameter given in reference 10 was determined by fitting the experimental data to the 3-phonon equation of Leibfried and Schlomann [1]. The only unknown in this expression was γ, which was found to vary from compound to compound. It was not intended to imply, however, that the parameter γ would depend on the mass ratio rather than the thermal conductivity. Since no theoretical expression is available to explain this behavior, it is convenient to use a varying γ to describe the thermal conductivity of the III-V compounds and their alloys.

[3] Note that $\gamma_1^{\,2}$ eq (1) = $[\gamma + \frac{1}{2}]^2$ (reference 10).

The theoretical curve (dashed line) for the alloy system InAs-GaAs is shown in figure 2 together with the experimental data (crosses), the agreement being better than 20% at all compositions. In view of the assumption made for the value of α, the agreement between theory and experiment is quite good. The value of α necessary to fit the experimental data in figure 2 was determined prior to the computation of the thermal resistivities of the remaining III-V alloy systems. It was pointed out, previously, that α is an adjustable parameter and may vary from one class of semiconductors to another. It is expected, however, that α will not vary greatly from system to system within a particular covalent crystal system such that the value of α determined for the InAs-GaAs system should be applicable to other III-V alloy systems. The best fit was obtained for $\alpha = 1.5$ and shown in figure 2 by the solid line, the agreement being excellent at all compositions.

The thermal resistivities of the alloy systems GaAs-GaSb, GaSb-InSb, and InAs-InP [12] were computed using $\alpha = 1.5$, $\epsilon = 39$, and γ_1 determined from figure 1. The computed curves and experimental results are shown in figures 3,4 and 5 for III-V alloy systems, the agreement being excellent in all cases.

3.3 IV-VI Alloys

The calculation of the thermal resistivity was extended to the IV-VI alloy system PbTe-PbSe which has been investigated in the past for thermoelectric applications [13]. The anharmonicity parameter was determined for the components and then assumed to vary linearly as a function of composition. The parameters α and ϵ were assumed to be the same as the III-V compounds. The electronic contribution to the thermal conductivity was computed for the case of acoustical scattering and subtracted from the total thermal conductivity.

The computed curve and experimental results are shown in figure 6, the agreement, as for the other alloy systems, being excellent at all compositions.

4. Conclusion

It has been quite clearly demonstrated that the theory of Abeles is applicable to a wide range of cubic semiconductor alloys systems. It is apparent that information obtained from one alloy system can be used to obtain greater accuracy in predicting the thermal conductivities of other alloy systems within a class of semiconductors.

The introduction of a strain contribution to the disorder parameter must be considered for all alloy systems as well as the effects of normal processes. For many of the alloy systems discussed above, the strain contribution was considerably greater than the mass fluctuation contribution to the disorder parameter Γ.

5. References

[1] Leibfried, G. and Schlomann, E., Nachr. Akad. Wiss. Gottingen, Math. Physik Kl. IIa 4, 71 (1954).

[2] Klemens, P. G., Proc. Roy. Soc. (London) A208, 108 (1951); Proc. Roy. Soc. (London) A68, 1113 (1955); Phys. Rev. 119, 507 (1960).

[3] Callaway, J., Phys. Rev. 113, 1046 (1959); Callaway, J. and von Baeyer, H. C., Phys. Rev. 120, 1149 (1960).

[4] Abeles, B., Phys. Rev. 131, 1906 (1963).

[5] Abeles, B., Cody, G. D., and Beers, D. S., J. Appl. Phys. 31, 1585 (1960).

[6] Miller, R., unpublished.

[7] Parkinson, D. H., and Quarrington, J. E., Proc. Phys. Soc. A67, 569 (1954).

[8] Parrott, J. E., Proc. Phys. Soc. 81, 726 (1963).

[9] Klemens, P. G. Westinghouse Research Report, 929-8904-R3 (1961); Klemens, P. G., White, G., and Tainsh, R. J., Phil. Mag. 7, 1323 (1962).

[10] Steigmeier, E. F. and Kudman, I. Phys. Rev., 141, 767 (1966).

[11] Amith, A., Kudman, I., and Steigmeier, E.F., Phys. Rev. 138, A1270 (1965).

[12] Bowers, R., Bauerle, J. E., and Cornish, A. J., J. Appl. Phys. 30, 1050 (1959).

[13] Joffe, A. F., Semiconductor Thermoelements and Thermoelectric Cooling (Infosearch Ltd., London 1957).

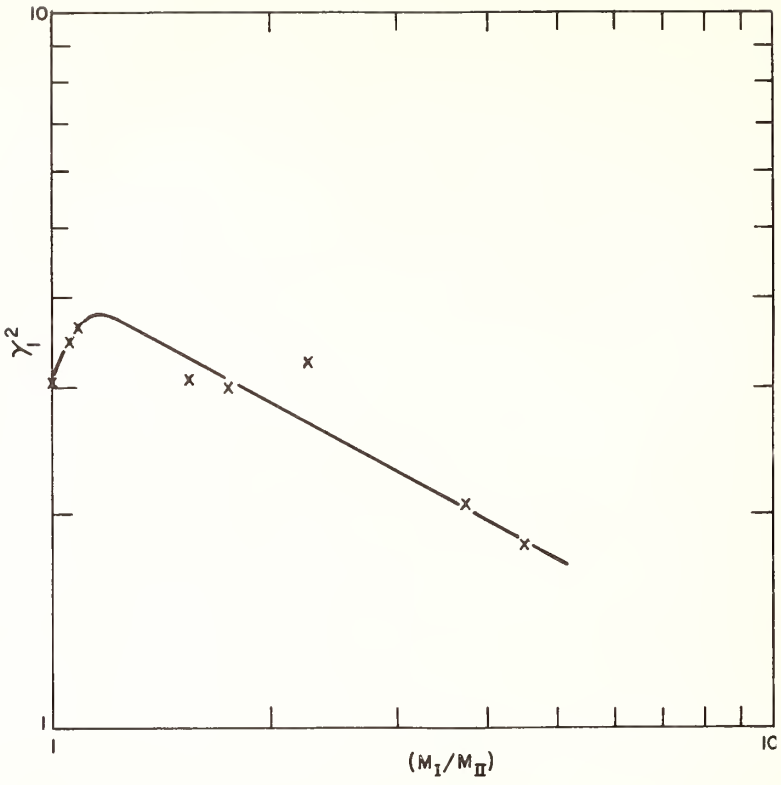

Figure 1 The variation of the square of the anharmonicity parameter γ_1 for the III-V compounds as a function of the mass ratio M_I/M_{II} of the constituent elements. The values shown by crosses are derived experimentally.

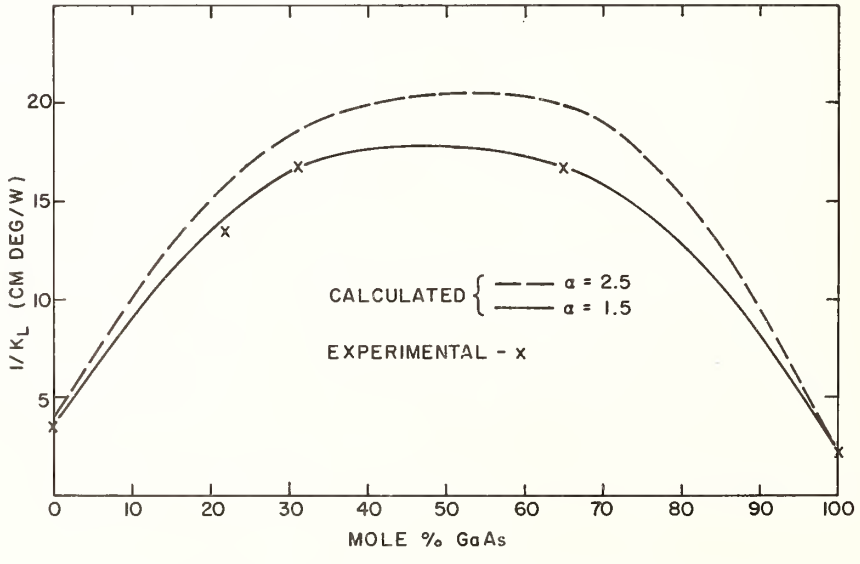

Figure 2 The lattice thermal resistivity at 300°K as a function of composition for GaAs-InAs alloys. Dashed curve (α = 2.5) and solid curve (α = 1.5) computed from eq. 1.

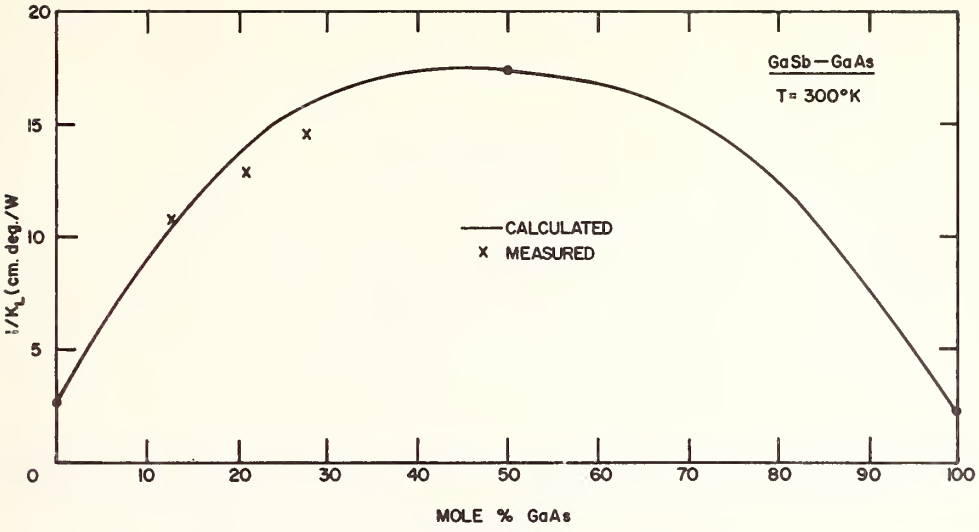

Figure 3 The lattice thermal resistivity at 300°K as a function of composition for GaAs-GaSb alloys. Solid curve computed from eq. 1.

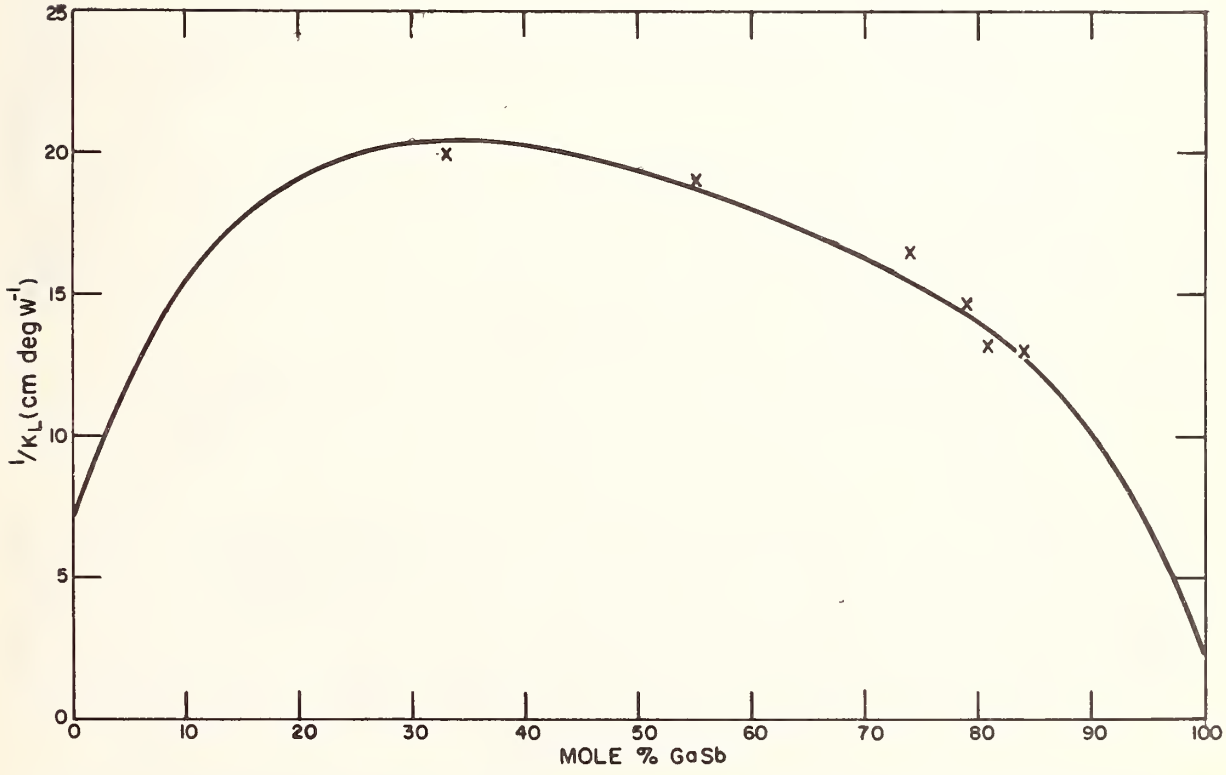

Figure 4 The lattice thermal resistivity at 300°K as a function of composition for GaSb-InSb alloys. Solid curve computed from eq. 1.

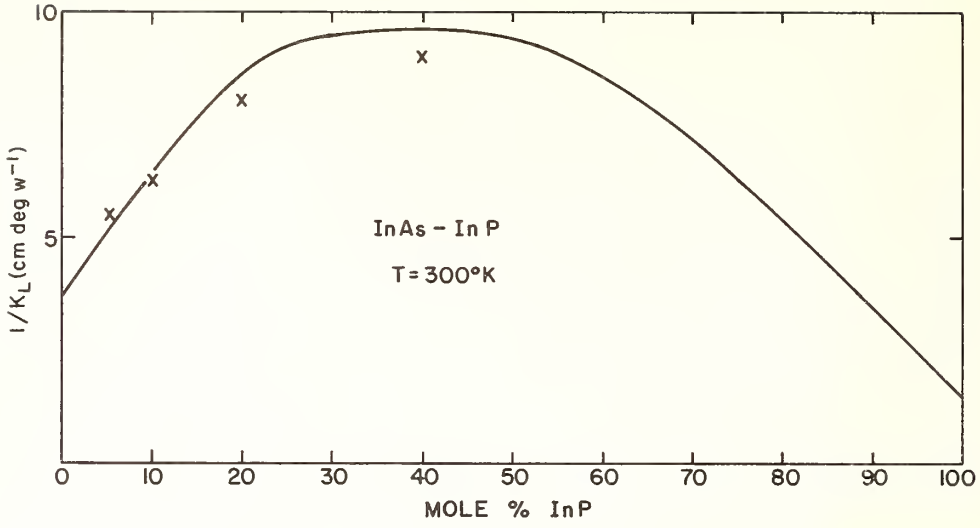

Figure 5 The lattice thermal resistivity at 300°K as a function of composition for InAs-InP alloys. Solid curve computed from eq. 1.

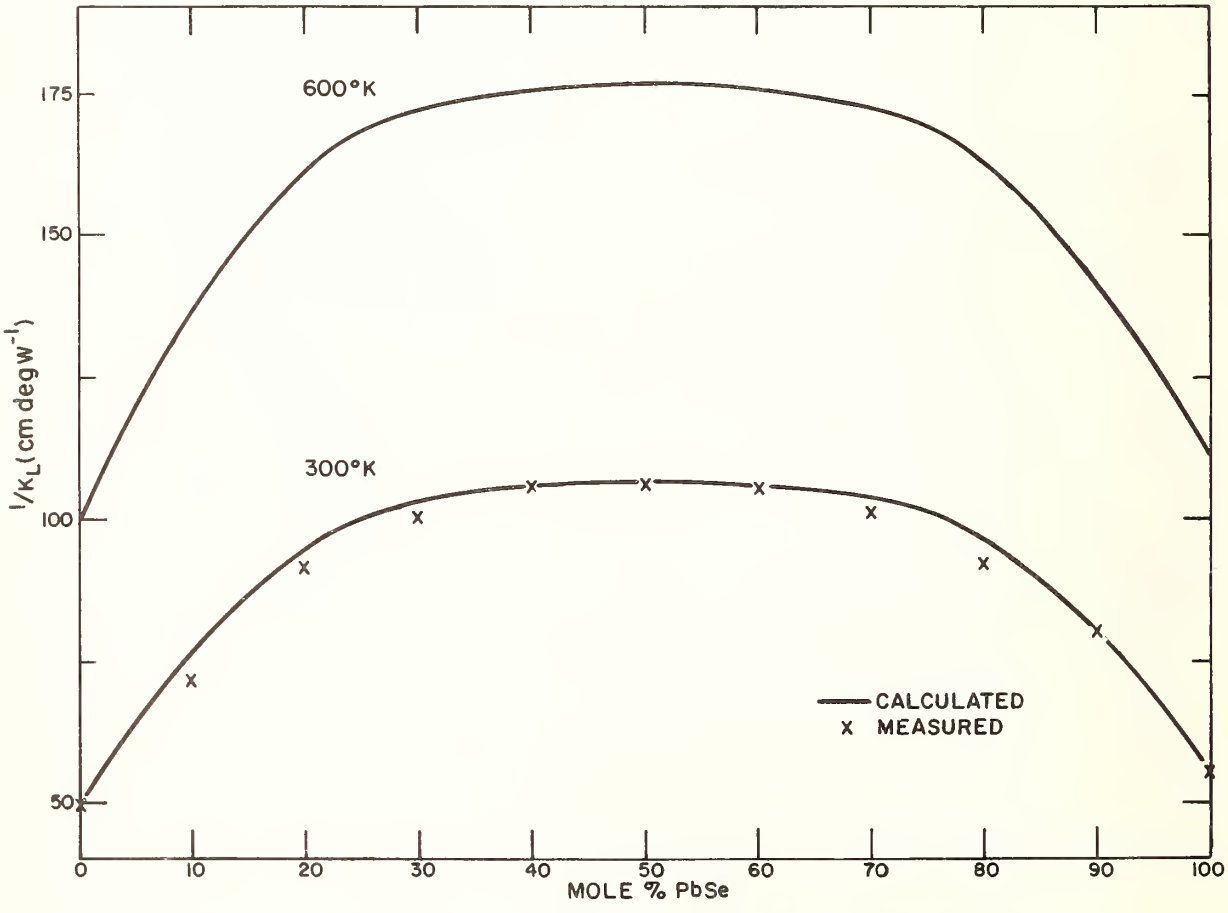

Figure 6 Lattice thermal resistivity at 300°K as a function of composition for PbTe-PbSe alloys. Solid curves at 300 and 600°K computed from eq. 1.

Thermal Conductivity of N-type Germanium from $0.3^{\circ}K$ to $4.2^{\circ}K$[1]

Bruce L. Bird and Norman Pearlman

Department of Physics
Purdue University
Lafayette, Indiana

The thermal conductivity of N-type germanium has been measured between $0.3^{\circ}K$ and $4.2^{\circ}K$. Excellent agreement with the theoretical model of Griffin and Carruthers is found for an Sb doped sample ($N_D = 3.6 \times 10^{15} cm^{-3}$). The model proposed by Keyes, however, is also able to give a reasonable fit for different values of the parameters. Experimental results for an As doped sample ($N_D = 5.3 \times 10^{15} cm^{-3}$) and a P doped sample ($N_D = 2.6 \times 10^{16} cm^{-3}$) are in complete disagreement with both theoretical models. Both samples show a decreased thermal conductivity which varies as T^3 down to the lowest temperature measured with no indication of any resonance scattering.

Key Words: Electron-phonon scattering, low temperature, N-type germanium, point defect, semiconductor, thermal conductivity.

1. Introduction

Previous measurements of the low temperature thermal conductivity of N and P-type germanium [1, 2, 3, 4, 5][2], have shown that shallow donors or acceptors are very strong scatterers of phonons. For example, a concentration of as little as 4×10^{15} Sb donors per cm^{-3}. reduces the thermal conductivity at $2^{\circ}K$ by a factor of eight.

Measurements by Goff and Pearlman [2] on highly doped, highly compensated N-type material as compared with singly doped material having the same concentration of neutral donors indicated that the extra thermal resistance was correlated with the number of neutral donors and not with the total impurity concentration. Thus the phonon scattering occurs because of an interaction with the electron bound to the donor ion not with the donor ion itself. An impurity species effect was also found with Sb being a more effective scatterer of phonons than either As or P at $2^{\circ}K$ for concentrations less than $6 \times 10^{17} cm^{-3}$. For concentrations greater than this the extra thermal resistance becomes species independent.

The scattering process then can be separated into at least two types, one for concentrations in which there is little overlap of the electronic wave functions between neighboring impurities and the other in which the concentration is so large that the interaction of donor electrons leads to the formation of an impurity band. In this article we will only consider the case of low concentration, non-compensated samples for which the donor electrons are assumed to be isolated.

The problem of isolated shallow donors in germanium has been reviewed by Kohn [6]. The electronic energy levels of the bound donor electron were calculated using the effective mass approximation. There is good agreement between theory and experiment for the excited states but not for the ground state. The effective mass approximation predicts that all shallow donors should have an ionization energy of 9.2 milli-electron volts and their ground state should be 4-fold degenerate, neglecting spin. Experimentally it has been found that the donor ground state is split by an amount $4\Delta_c$ producing a singlet ground state and a triply degenerate excited state. The type of chemical impurity determines $4\Delta_c$, thus it is referred to as the "chemical shift" or "valley-orbit" splitting. Table 1 lists the ionization energy (ϵ_i) and chemical shift for some of the shallow donors in germanium, as determined from infrared absorbtion measurements by Reuszer and Fisher [7].

---

[1]Work supported in part by ARPA.

[2]Figures in brackets indicate the literature references at the end of this paper.

Table 1

	Sb	P	As	Effective Mass
ϵ_i(milli-e.v.)	10.19	12.76	14.04	9.2
$4\Delta_c$(milli-e.v.)	0.32	2.83	4.23	0.0
$T_R(^oK) = 4\Delta_c/k$	3.71	32.8	49.1	
$r_o(\text{A}^o)$	44.2	35.3	32.0	65.0
$N_D^m(cm^{-3})$	2.2×10^{16}	4.4×10^{16}	5.8×10^{16}	7.0×10^{15}

Also listed in Table 1 is the effective Bohr radius r_o for an electron in the ground state. It was calculated from the measured ionization energy by using the equations applicable to the hydrogen atom immersed in a medium with dielectric constant K, that is, $\epsilon_i = R(m^*/m)(1/K^2)$ and $r_o = a_o(m/m^*)K$ where $R = 13.6$ e.v. and $a_o = 0.53\text{A}^o$. The dielectric constant for germanium is 16. The value of r_o listed under the effective mass value was obtained by Kohn [6] as a result of a variational calculation to determine ϵ_i.

Fritzsche [8], on the basis of impurity conduction measurements, has suggested that the condition $a/r_o < 5$, where a is an average distance between impurity atoms, $a = (3/4\pi N_D)^{1/3}$, defines the region in which the impurity atoms can be considered isolated. The largest concentration of donors for which this inequality holds, N_D^m, is shown in Table 1.

2. Models Used for Electron-Phonon Scattering

In order to explain the thermal conductivity results Keyes [9] proposed a model in which the scattering arises from the large effect of strain on the energy of the bound donor electron. The electronic energy states have a quadratic dependence on the strain produced by the phonons. This results in scattering of the point defect type $\tau^{-1} \propto \omega^4$. A further dependence on the phonon frequency arises when the phonon wavelength becomes shorter then the diameter of the electronic orbit causing the average strain to approach zero, so that the phonon scattering rapidly decreases as the phonon frequency rises past $\omega \sim v/r_o$. This results in a scattering rate which Keyes expresses in the form

$$\tau_{ep}^{-1}(\omega,p)^K = M(\omega)\, V(v_p)\, F(\omega,p) \tag{1}$$

with

$$M(\omega) = \frac{1}{3^4 \pi d^2}\left[\frac{n_{ex} E_u^4 D_p \omega^4}{(4\Delta_c)^2}\right]$$

$$V(v_p) = \frac{2}{5}\left[\frac{1}{v_1^7} + \frac{1}{v_2^7}\right]$$

and the cutoff factor $F(\omega,p)$ given by

$$F(\omega,p) = \left[1 + (r_o\omega/2v_p)^2\right]^{-8}$$

The anistropy factor D_p has the values

$$D_1 = 4/5 \qquad D_2 = D_3 = 3/5$$

where $p = 1, 2, 3$ indicates the phonon polarization.

In eq. (1) d is the density of germanium, n_{ex} is the concentration of neutral donors, E_u is the shear deformation potential constant, v_1 and v_2 are the velocity of longitudinal and transverse sound waves, and D_p is an anisotropy factor averaged over angle. Keyes expression for the inverse relaxation time is small at low frequencies because of the ω^4 dependence, reaches a maximum at about $\omega = v/r_o$ then rapidly declines due to the cutoff factor $F(\omega,p)$. It is species dependent through its dependence on $4\Delta_c$ and r_o.

In a more detailed calculation, Griffin and Carruthers [10] argued that whereas Keyes treated the electron as moving in the static strain field created by the phonons, the electron actually adjusts to the phonon perturbation with a characteristic frequency $4\Delta_c/\hbar$ which lies in the range of phonon frequencies important for heat conduction. Griffin and Carruthers thus treat the problem in analogy with the resonance fluorescence scattering of photons. During the elastic scattering process the electron undergoes a virtual transition between the singlet and triplet states while the phonons' crystal momentum is changed.

Using this approach Griffin and Carruthers obtained the following expression for the relaxation time

$$\tau_{ep}^{-1}(\omega,p)^{GC} = M'(\omega)\, R(\omega)\, W(\omega, v_p, p)\, B(T) \tag{2}$$

with

$$M'(\omega) = \frac{1}{3^4 \pi d^2}\left[\frac{n_{ex} E_u^4 H_p \omega^4}{(4\Delta_c)^2}\right]$$

$$R(\omega) = (4\Delta_c)^4 / [(\hbar\omega)^2 - (4\Delta_c)^2]^2$$

$$W(\omega, v_p, p) = \left\{\frac{1}{v_p^2 S_p}\left(\frac{1}{S_1 v_1^5} + \frac{3}{2 S_2 v_2^5}\right)\right\}$$

where S_p is related to the cutoff factor $F(\omega,p)$ by $S_p^2 = 1/F(\omega,p)$. H_p is an anistropy factor with the values

$$H_1 = 43/225$$

$$H_2 = 32/225$$

$$H_3 = 40/225$$

and $B(T) = \{B_S(T) + B_T(T)\,[2 + (\hbar\omega/4\Delta_c)^2]\}$.

In equation (2), $B(T)$ is a temperature dependent factor due to thermal excitation of electrons from the singlet to the triplet state. If all electrons are assumed to be in the ground state then $B_S(T) = 1.0$, and $B_T(T) = 0.0$

Comparing eq (1) and (2), the major difference, aside from those arising from different methods of averaging velocities and angular integrations, is the presence of the "true resonance factor" $R(\omega)$ in GC's expression for τ_{ep}^{-1}. Note in the limit of $\hbar\omega << 4\Delta_c$ that $R(\omega)$ approaches one.

3. Thermal Conductivity Integral

In order to compare the theoretical expressions for τ_{ep}^{-1} with the experimental results, the thermal conductivity has been calculated using the form of the thermal conductivity integral as written by Carruthers (equation 3.3)[11], using $\omega_p = v_p q$ and $x = \frac{\hbar\omega}{kT}$

$$\lambda(T) = \left(\frac{k^4 T^3}{6\pi^2 \hbar^3}\right) \sum_p \frac{1}{v_p^2} \int_0^{\theta/T} \frac{e^x x^4}{(e^x - 1)^2}\, \tau_c(x,p)\, dx \tag{3}$$

where the total relaxation time τ_c is given by

$$\tau_c^{-1}(\omega,p) = \tau_B^{-1}(\omega,p) + \tau_I^{-1}(\omega) + \tau_N^{-1}(\omega) + \tau_{ep}^{-1}(\omega,p).$$

The relaxation times included in the total relaxation time τ_c are τ_B, boundary scattering; τ_I, isotope scattering; τ_N, umklapp and normal processes; and τ_{ep}, electron-phonon scattering.

Casimir's [12] relation will be used for boundary scattering but modified to take into account the difference in velocity of the differently polarized waves, i.e., $\tau_B^{-1} = v_p/L_c$. The Casimir length, $L_c = 1.13(A_s)^{1/2}$, defines an effective length associated with a sample whose cross-sectional area is A_s.

Klemens [13] expression for the isotopic relaxation time is given by $\tau_I^{-1} = A\omega^4$ with the constant $A = V_o\Gamma/(4\pi v_s^3)$ in which V_o is the volume per atom, v_s is some average sound velocity, and Γ is a constant determined by the relative abundance of the isotopes and their masses. For germanium $\Gamma = 5.89 \times 10^{-4}$. This results in the theoretical value of A being 2.35×10^{-44} sec.^{3}, assuming $v_s = 3.56 \times 10^5$ cm./sec. as calculated from the Debye temperature at 0°K of 375°K for germanium.

It should be noted that it would be more consistent to take the polarization dependence of the sound velocity into account when using τ_τ^{-1} in the thermal conductivity as was done for boundary scattering. However, in the temperature range of interest, since the isotopic contribution to the thermal resistance is small, the usual approximation of taking A to be equal for all three branches will be followed.

Callaway [14], in his phenomenological development of an appropriate method of combining various scattering processes in the thermal conductivity integral, suggested that scattering due to momentum conserving normal processes could be allowed for by including their relaxation time as part of the total relaxation time τ_c^{-1}. Using Herring's [15] suggested form for the relaxation time for low frequency phonon-phonon scattering ($\tau_N^{-1} \propto \omega^s T^{5-s}$), Callaway was able to fit the thermal conductivity of normal and isotope enriched germanium reasonably well over the range from 2 to 100°K. With $\tau_c^{-1} = v_s/L_c + A\omega^4 + (B_1 + B_2)\omega^2 T^3$ he obtained the best fit with $A = 2.57 \times 10^{-44}$ sec^3 and $(B_1 + B_2) = 2.77 \times 10^{-23}$ sec. deg^{-3}.

4. Description of samples and method of measurement

All germanium samples were cut from the ingot in the form of rectangular prisms with their long axis in the (100) direction perpendicular to the growth axis of the crystal in order to minimize impurity concentration gradients. The impurity concentration listed in Table 2 was determined from the room temperature Hall coefficient.

The samples as cut from the ingot with a diamond saw had approximate dimensions of 5 x 5 x 25 mm. All surfaces were then ground with #280 carborundum powder reducing the sample dimensions to about 4 x 4 x 24 mm. and ensuring diffuse boundary scattering.

Table 2

Sample	n_{ex} (cm^{-3})
Ge - 422A	5.4×10^{13}
Ge(Sb) - 172AI	3.6×10^{15}
Ge(As) - 200A	5.3×10^{15}
Ge(P) - 229A (2)	2.6×10^{16}

Measurements were made in a recirculating He^3 cryostat capable of covering the temperature range from 0.27°K to above 4.2°K. The thermal conductivity was measured using the absolute method with the temperature difference along the sample determined by two germanium thermometers. The germanium thermometers were calibrated each run against the vapour pressure of He^4 and He^3 from 0.7 to 4.2°K. Below 0.7°K a paramagnetic salt, chromic methylammonium alum, was used for calibration. For each sample forty or more data points were taken between 0.3°K and 4.2°K and about 26 calibration points.

The estimated absolute accuracy of λ is ±6% while comparison of λ values for a given run is within ±4% for $T > 2.2$°K and ±2% for $T < 2.2$°K with the exception of the data points for sample Ge(As)-200A above 2.2°K which are uncertain to ±10% because the measured ΔT was too small.

5. Results and Discussion

Representative data for the pure germanium sample, Ge - 422A, are shown in figure 1. GC1 is the curve calculated from eq (3) but setting $\tau_{ep}^{-1} = 0$. The values for normal germanium found by Callaway, i.e., $A = 2.57 \times 10^{-44} sec.^3$ and $(B_1 + B_2) = 2.77 \times 10^{-23} sec^2 deg^{-2}$ were used along with $v_1 = 5.37 \times 10^5$ cm/sec. and $v_2 = v_3 = 3.28 \times 10^5$ cm./sec. as calculated by Hasegawa [16] from the measured elastic constants. The Debye temperature was taken to be $\theta_D = 375^oK$. A least mean square fit of the seven experimental points between 0.37^oK and 0.56^oK to the equation $\lambda = CT^n$ gave $C = 0.1314$ Watt $cm^{-1} deg^{-4}$ and $n = 2.99$. Agreement between values for λ calculated from this equation and the experimental values was better than 0.5% for each point. This value of C gives $L_{exp} = 0.438$ cm. as compared to $L_c = 0.443$ cm. calculated from Casimir's relation, that is, $L_{exp}/L_c = 98.9\%$.

Representative data for the Sb doped sample, Ge(Sb) - 172AI, are also shown in figure 1. Two different runs were made on this sample, as indicated by the squares and triangles, in order to ensure no effect on the measurements due to strains introduced by the method of mounting the sample. The data points indicated by triangles were taken with the sample attached to the He^3 cryostat and to the sample heater with copper clamps. The thermometers were glued to thin, pure germanium slabs which were soldered to the sample. The squares indicate data points taken with the sample attached to the He^3 cryostat and to the sample heater by soldering to a thin slab of tungsten. The mounting of the thermometers was also changed by gluing them directly to the sample. Comparison of the results between 0.3^oK and 1.2^oK of the two mounting methods gave agreement to within 1%.

In all the calculated curves the values for A, $(B_1 + B_2)$, v_1, v_2, and θ_D used for GC1 will be used and the value for L will be taken as $L = .989\ L_c$ in order to be consistent with the results obtained for the pure sample. Also all electrons will be assumed to be in the ground singlet state, i.e., $B(T) = 1.0$ in eq (2).

Curve GC2 in figure 1 was calculated using the Griffin-Carruthers expression for τ_{ep}^{-1} with $E_u = 16.0$ e.v., $4\Delta_c = 0.32 \times 10^{-3}$ e.v., and $r_o = 44\text{Å}$. An excellent fit, within 10%, over the entire temperature range is obtained. Since E_u appears in the expressions for τ_{ep}^{-1} raised to the fourth power, any uncertainty in its value will be important when comparing theory with experiment. This is shown in curve GC2A which has the same values for all parameters except E_u is changed from 16.0 e.v. to 19.0 e.v. Unfortunately values of E_u determined by different experiments [17, 18, 19] cover the range from 15 to 19 e.v. A mean value appears to be around 17 e.v.

In figure 2 the data for Ge(Sb) - 172A(2) is reproduced along with curves K1 and K2 which were obtained by using Keyes' expression for τ_{ep}^{-1}. The same values of E_u, $4\Delta_c$, and r_o used in calculating GC2 were used to calculate K2. If the true resonance factor $R(\omega)$ is replaced by its low frequency limit in GC's expression (eq 2) the calculated curve lies within a few percent of K2. Thus the true resonance factor is what causes the excellent fit of GC2 to the data above 1^oK, suggesting that the mechanism of resonance fluorescence does occur. Unfortunately the strength of this conclusion is weakened somewhat by considering curve K1 which uses the same values for the parameters as GC2 and K2 except that r_o is set equal to the effective mass value of 65Å. This curve agrees with the data down to about 1.4^oK but then deviates to higher values at the lower temperatures. Thus by treating E_u, which is most effective near the maximum in the resonance, and r_o as adjustable parameters one could also obtain a reasonable fit to the experimental results using Keyes' expression for τ_{ep}^{-1}.

Figure 3 shows representative data for an As doped sample, Ge(As)-200A, and a phosphorous doped sample, Ge(P)-229A(2). Curve GC3 is calculated with $4\Delta_c = 4.23 \times 10^{-3}$ e.v. and $r_o = 32.0\text{Å}$ while curve GC4 used $4\Delta_c = 2.83 \times 10^{-3}$ e.v. and $r_o = 35.3\text{Å}$. The surprising result is that neither As or P doped samples exhibit any resonance scattering at all but only a constant added thermal resistance implying a frequency independent scattering mechanism. Both GC3 and GC4 lie somewhat below the experimental points at the high temperature side but then gradually return to the pure sample limit as the temperature is reduced due to the ω^4 dependence of τ_{ep}^{-1}.

In view of these results it is of interest to compare the measurements down to 0.2^oK reported by Carruthers et al. [5] on indium doped samples (10^{14}, 1.9×10^{14}, and $10^{15} cm^{-3}$). The energy level structure for acceptors in germanium is very different from that of donors, consisting of a 4-fold degenerate ground state with the next excited state 6 to 7 milli-e.v. higher. However these samples also gave a decreased thermal conductivity varying as T^3 but the extra thermal resistance was not well correlated with the amount of impurity added. Klemens' [13] expression for the scattering of phonons by grain boundaries gives a frequency independent relaxation time but when applied to germanium leads to a mean free path 10^4 times larger than observed. They therefore surmised that the added impurities may locate preferentially near low angle grain boundaries in germanium and give an enhanced grain boundary scattering.

Ultrasonic attenuation measurements made by Pomerantz [20] on N-type germanium (Sb, As, and P doped) in the temperature range from 5^oK to 50^oK were explained by him as due to the electronic relaxation between the triplet states which had been split in energy because of the strain field created by the ultrasonic wave. Kwok [21] has developed the theory for this process in more detail.

The mechanism proposed by Pomerantz, since it is proportional to the number of electrons occupying the triplet states, would predict negligible phonon scattering for As and P doped germanium in the temperature range from 0.3°K to 4.2°K. (See table 1 for the temperature equivalent, T_R, of $4\Delta_c$.)

In addition to the different effect Sb donors have on the thermal conductivity of germanium as compared with As and P donors, Mathur and Pearlman [3] have found a difference in their behavior on compensation. They found that highly compensated P and As doped samples have an extra thermal resistance which, while correlated with the number of neutral donors, shows an increased thermal resistance as compared to the uncompensated material. This is in contrast to the behavior of Sb doped samples which show a similar or slightly smaller value of the extra thermal resistance upon compensation. Further measurements are in progress on samples with different concentrations, both compensated and uncompensated, to see if these two differences in behavior between Sb doped as compared to As or P doped germanium are correlated.

6. References

[1] J.F. Goff and N. Pearlman, in Proceedings of the 7th International Conference on Low Temperature Physics, edited by G.M. Graham and A.C. Hollis Hullet (University of Toronto Press, Toronto, 1961), p. 284-288.

[2] J.F. Goff and N. Pearlman, Phys. Rev. 140, No. 6A, A2151 (1965).

[3] M.P. Mathur and N. Pearlman, to be published.

[4] J.A. Carruthers, T.H. Geballe, H.M. Rosenberg, and J.M. Ziman, Proc. Royal Soc. (London) 238A, 502 (1957).

[5] J.A. Carruthers, J.F. Cochran, and K. Mendelssohn, Cryogenics, 2, No. 3, 1 (1962).

[6] W. Kohn, in Advances in Solid State Physics, edited by F. Seitz and D. Turnbull (Academic Press Inc., New York, 1957), Vol. 5, p. 258-321.

[7] J.H. Reuszer and P. Fisher, Phys. Rev. 135, No. 4A, A1125 (1964).

[8] H. Fritzsche, J. Phys. Chem. Solids 6, 69 (1958).

[9] R.W. Keyes, Phys. Rev. 122, 1171 (1961).

[10] A. Griffin and P. Carruthers, Phys. Rev. 131, No. 5, 1976 (1963).

[11] P. Carruthers, Rev. Mod. Physics 33, 92 (1961).

[12] H.B.G. Casimir, Physica 5, 495 (1938).

[13] P.G. Klemens, Advances in Solid State Physics, edited by F. Seitz and D. Turnbull (Academic Press Inc., New York, 1958), Vol. 7, p. 1.

[14] J. Callaway, Phys. Rev. 113, 1046 (1959).

[15] C. Herring, Phys. Rev. 95, 954 (1954).

[16] H. Hasegawa, Phys. Rev. 118, 1513 (1960).

[17] B. Tell and G. Weinreich, Phys. Rev. 143, No. 2, 584 (1966).

[18] R.E. Pontinen and T.M. Sanders, Jr., Phys. Rev. 152, No. 2, 850 (1966).

[19] S. Riskaer, Phys. Rev. 152, No. 2, 845 (1966).

[20] M. Pomerantz, Proc. IEEE, 53, No. 10, 1438 (1965).

[21] P.C. Kwock, Phys. Rev. 149, No. 2, 666 (1966).

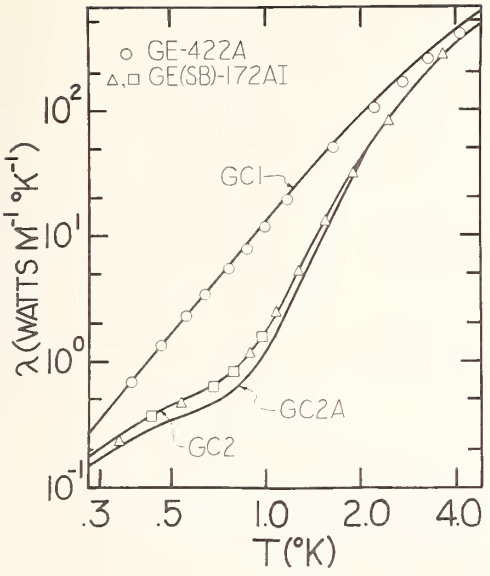

Figure 1. Thermal conductivity of pure and Sb doped germanium.

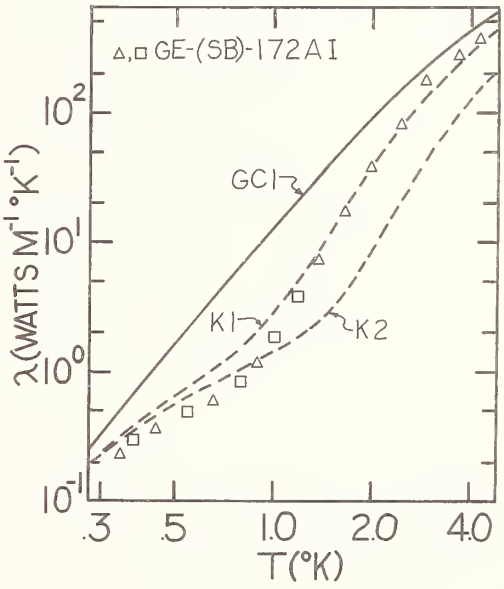

Figure 2. Thermal conductivity of Sb doped germanium.

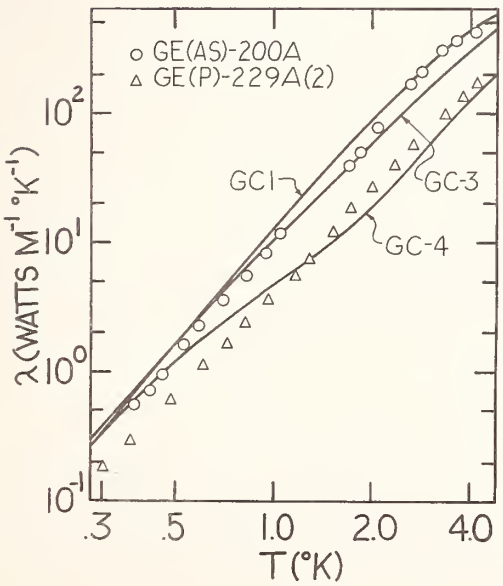

Figure 3. Thermal conductivity of As and P doped germanium.

The Lattice Thermal Conductivity of Bismuth Telluride and Some Bismuth Telluride - Bismuth Selenide Alloys

D. H. Damon and R. W. Ure, Jr.
Westinghouse Research Laboratories
Pittsburgh, Pennsylvania 15235

and

J. Gersi
Westinghouse Atomic Equipment Division
Cheswick, Pennsylvania 15024

The thermal conductivity of a number of samples of Bi_2Te_3, both undoped and doped with excess Te, and Bi_2Te_3 - Bi_2Se_3 alloys has been measured between 80°K and 370°K. Samples grown both by zone-leveling and by the Bridgeman method were used. For all samples the heat flow was parallel to the cleavage plane, perpendicular to the c-axes. Between 80°K and 240°K the total thermal conductivity is separated into a lattice thermal conductivity K_L, and an electronic thermal conductivity, K_e. In agreement with previous results we find $W_L = K_L^{-1} = \beta T + \gamma$. According to theory, β is determined by purely phonon-phonon scattering for small defect concentrations. However, at larger defect concentrations, the value of β is altered by the point defect scattering. For a sample with a small concentration of Bi_2Se_3 (nominally ~2%), the value of β is nearly identical with that found for the Bi_2Te_3 samples; however, for a sample with a nominal concentration of ~10% Bi_2Se_3, the value of β is at least 30% larger. These results can be explained by current theories of phonon scattering by point defects.

Key Words: Alloy semiconductors, bismuth telluride, defects, electrical conductivity, Lorenz number, phonons, scattering, Seebeck coefficient, thermal conductivity, thermoelectric.

1. Introduction

Since Bi_2Te_3 and its alloys are the best thermoelectric materials in the temperature range from below room temperature to about 200°C, the thermal conductivities of these materials have been extensively studied. This work has established many of the factors that determine the phonon mean free path, but was hampered by the lack of an adequate theory of the lattice thermal conductivity at high temperature. This was remedied in the early 60's by the theoretical work of Klemens [1][1] and Parrot [2]. At present data is not available over a wide enough temperature range to test the applicability of this theory to Bi_2Te_3 alloys. We have, therefore, measured the thermal conductivity of a number of $Bi_2Te_{3-x}Se_x$ alloys together with some Bi_2Te_3 samples between 80°K and 380°K. We have compared our results with the predictions of this theory.

The theoretical work referred to above is concerned with the high temperature lattice thermal conductivity of a crystal containing a random distribution of point defects. In Klemens' theory, the lattice thermal conductivity is determined by the scattering of the phonons both by three phonon U-processes and by point defects (Rayleigh scattering). Parrot extended this theory with a detailed study of the effects of three phonon N-processes. This theory gives very definite results for the dependence of the lattice thermal conductivity on both temperature and defect concentration. At small point defect concentrations and high temperatures, one expects the lattice thermal resistivity $W_L = 1/K_L$ to be represented by

$$W_L = W_u + W_o \tag{1}$$

where W_u is the thermal resistivity of the defect free crystal and W_o, independent of T and proportional to the concentration of defects N, is the thermal resistivity due to point defect scattering. At large

[1] Figures in brackets indicate the literature references at the end of this paper.

defect concentrations and lower temperatures, W_L is not separable into two independent terms; instead the theory predicts $K_L \propto T^{-1/2} N^{-1/2}$. Quantitatively, the theory is not complete since the relative strength of the U and N processes remains as an adjustable parameter. Abeles [3] has shown that it gives a very good account of the measured thermal conductivity of Ge-Si alloys and a number of alloys formed from III-V compounds.

Another reason for undertaking this work was to assist the development of a theoretical understanding of the factors which determine the figure of merit of thermoelectric materials. As is shown in many texts [4], the thermoelectric efficiency of a material increases with increasing values of the parameter $(\mu/K_L)\, m^{*\,3/2}$ where m^* is the density of states effective mass, μ is the charge carrier mobility and K_L is the lattice thermal conductivity. Ioffe et al. [5] have proposed that μ/K_L can be increased by alloying a good thermoelectric material with a compound whose atoms have a similar valence electron structure but different atomic mass. Several authors [6],[7] have argued that our present knowledge of semiconductors suggests that we should not expect to find materials with dramatically higher thermoelectric efficiencies than those we now have. Any improvements in thermoelectric devices now depend on obtaining detailed knowledge of the scattering processes that determine the phonon and charge carrier free paths. The purpose of this work was to contribute to the knowledge of phonon scattering by defects in the bismuth telluride materials. The early work on the thermal conductivity of Bi_2Te_3 by Goldsmid [8] and Satherthwaite and Ure [9] was soon followed by many other investigations. These results have been summarized by Goldsmid [10] in a recent review. Much of the present literature describes attempts to produce material of high thermoelectric efficiency and is not concerned in detail with the scattering processes that determine the transport properties. Most of the measurements which have been reported for the lattice thermal conductivity of the alloys have been done over a rather restricted temperature range near 300°K. Three independent investigations [11] have established that the lattice thermal conductivity of $Bi_2Te_{3-x}Se_x$ alloys decreases regularly with increasing concentrations of Se up to a concentration of about 20% Bi_2Se_3. It is generally supposed that scattering of the phonons by the Se atoms is responsible for this effect. In the past two years the results of a comprehensive and systematic investigation of the lattice thermal conductivity of Bi_2Te_3 alloys has been published in a series of papers by a group at the Leningrad Semiconductor Institute [12-15]. They find that the lattice thermal resistivity may be represented by eq (1) for a wide range of solute concentrates and many different solutes. Their data suggest that this relation holds even if W_o is about 75% of W. This result cannot be understood in terms of the Klemens-Parrot theory. We find that the lattice thermal resistivity of the $Bi_2Te_{3-x}Se_x$ alloys may be represented by $W = \beta T + \gamma$ which is of the same functional form of T as eq (1). However, we find that β varies with Se concentration. We will show that our results are predicted by the theory.

In order to separate the measured total thermal conductivity into lattice and electronic parts, we have measured the Seebeck coefficient and electrical resistivity of our samples. We cannot affect this separation with any confidence above 240°K because of the ambipolar electronic thermal conductivity which becomes significant above this temperature. Measurements much below 80°K will not serve the purpose of this investigation since the theory must fail for temperatures below about $\theta/2$ where θ is the Debye temperature. The value of θ for Bi_2Te_3 is 155°K.

The crystal structure of Bi_2Te_3 is $R\bar{3}m$. These materials have a single, very pronounced cleavage plane perpendicular to the c axis, which is the 3-fold rotation axis. The material is anisotropic. However, for the normal electrical resistivity, thermal conductivity and Seebeck coefficient, all directions perpendicular to the c axis are equivalent. That is, if the heat flux or electric current is in the cleavage plane, then the measured κ, α, or ρ is independent of the particular direction in the cleavage plane. All measurements were made with this orientation. Measurements were made on single crystals or on samples containing a few large grains all having their cleavage planes parallel to the long axis of the sample.

2. Experimental Procedure

The apparatus and the experimental procedures used to measure the Seebeck coefficient, α, electrical resistivity, ρ, and thermal conductivity, K, of the Bi_2Te_3 samples have been described in great detail in a previous publication [16]. In brief, a stationary heat flow method was used with copper-constantan thermocouples for thermometers. The ends of the samples were nickel-plated and then soldered between the sink and the sample heater. This heater is surrounded by a guard heater to reduce the radiative heat transmitted from the sample heater. With this guard, the heat loss by radiation from the sample heater is less than 10% of total heat. These radiative losses have been measured and corrections made. The accuracy of the thermal conductivity measurements is 3 to 4%. The precision is somewhat better. Better than 1% reproducibility has been obtained on removing and then replacing a sample in the apparatus. All the samples were roughly of the same size being no smaller than 4 x 5 x 12 mm; it was therefore possible to make accurate measurements of their geometrical form factors.

All samples were prepared by sealing stoichiometric proportions of very pure elements (99.999% purity) in evacuated, graphite-coated vycor tubes. To insure homogeneity, the samples were thoroughly mixed in a rocking furnace maintained at a temperature above that of the melting point of the alloy and then air or water quenched.

Crystals were grown by two methods. Bridgman crystals were made by lowering a previously mixed sample at rates which varied from 0.25 to 1.50 inches/hour through a furnace with a temperature gradient of 100°C/inch near the solid-liquid interface. To achieve this gradient, a vertical tube furnace was mounted over a circulating water bath with a separately controlled auxiliary winding placed in the bottom of the furnace. The resulting ingots were polycrystalline with their cleavage planes oriented parallel to the axis of growth. These ingots were quite homogeneous, the variation of both the electrical resistivity and Seebeck coefficient being no larger than 10% over the central 60% of the ingot.

Single crystal samples were prepared by a horizontal, single-zone-pass technique. A single crystal seed and a slug about 15 cm long were placed in a graphite-coated Lavite boat. The boat was sealed in an evacuated vycor tube and placed in a horizontal position in a zone-levelling apparatus. The entire tube was heated to about 400°C to prevent condensation of tellurium. A molten zone about 2.5 cm long was formed by a narrow heater which could be moved along the boat. This molten zone was brought slightly into the single crystal seed. The zone was then moved along the ingot at a rate of 2 to 4 mm/hr. For Samples 1, 3 and 7, the composition given in Table 1 is the composition of the 15 cm slug. For growth of Sample 2, the following slugs were placed in the Lavite boat: a single crystal seed, a slug 2.5 cm long of composition 37 atomic % Bi - 63 atomic % Te, and a slug 12.5 cm long of stoichiometric Bi_2Te_3. This procedure gives a melt composition of 63 atomic % Te which remains approximately constant as the molten zone is moved through the ingot. With a melt of this composition, the solid contains slight excess Te which makes the crystal n-type [9].

Table 1. Description of the samples used in this investigation. The compositions given are those of the starting material. For all samples, K was measured with the heat flow parallel to the cleavage plane.

Sample Number	Code Number	$R(77^\circ K)$ cm^3C^{-1}	Extrinsic Carrier Concentration cm^{-3}	$\rho(77^\circ K) \times 10^6$ ohm-m	$\alpha(100^\circ K)$ $\mu V/^\circ K$	Preparation and Composition
1	67E4-1	+0.24	2.6×10^{19}	1.56	+ 84	Single zone, Bi_2Te_3 melt, sample Bi rich, single crystal, p-type
2	62AW3-1	-0.79	7.9×10^{18}	1.48	- 94	Single zone, Bi_2Te_3 + excess Te, single crystal, n-type
3	67F-3	+0.192	3.3×10^{19}	1.92	+ 81	Single zone, Bi_2Te_3 + 2 mole % Bi_2Se_3, nearly single crystal, no grains revealed by etching, cleavage not perfect.
4	N-13	-0.30	2.1×10^{19}	3.6	-115	Bridgman, Bi_2Te_3 + 10 mole % Bi_2Se_3 + I doping, etching revealed 6 nearly single crystal grains
5	B-23-B4	--		3.01	-118	Bridgman, Bi_2Te_3 + 10 mole % Bi_2Se_3 + I doping, many small crystallites
6	N-47			3.42	-124	Bridgman, Bi_2Te_3 + 10 mole % Bi_2Se_3 + I doping, many small crystallites
7	N-47Z	-1.46	4.3×10^{18}	11.1	-241	Single zone pass on ingot from which sample 6 was cut, single crystal

Samples were cut from the ingots with a spark cutter. Some of the characteristics of the samples are listed in Table 1. The samples were cut from the ingots and then etched in either a 1:1 $HCl:HNO_3$ etch or a Br etch consisting of a few drops of Br in ~50 cc of methanol. These etches are effective in revealing grain boundaries. They do not reveal small distortions of the crystal within the grains. For example, the etching showed Sample 4 to be composed of four large and two small grains. Upon completion of the thermal conductivity measurements, one grain was cut from the sample and attempts were made to cleave a bar (~1 x 3 x 12 mm) suitable for measurement of the Hall coefficient from this grain. This cleaving showed that the c axis was not in the same direction throughout the grain. However, the c axis did not deviate by more than 5° from the normal to the long dimension of the crystal. This was found to be true for all the samples. For the Bridgman ingots, we were successful in obtaining a good single crystal Hall bar for Sample 4 only. The single zone ingots presented no such problems. These samples were prepared with cleavage planes as two faces of the sample. The other four planes completing the right rectangular parallelepiped were cut with a spark cutter.

3. Experimental Results

Figures 1, 2 and 3 show the measured values of K, α and ρ plotted against temperature, T. Where comparisons can be made, these results are in good agreement with previously published results.

The procedure [17] used for separating the measured thermal conductivity into an electronic thermal conductivity, K_e, and a lattice thermal conductivity, K_L, is well known and only a few brief remarks are required here. One assumes that (1) the scattering of the carriers can be described by a relaxation time that is proportional to the carrier energy raised to some power, i.e., $\tau = \tau_o E^s$, where E is the carrier energy, and (2) the bands are of standard form, i.e., the density of states varies as $E^{1/2}$. One then uses the measured values of α to calculate values of the Fermi energy ζ. The electronic thermal conductivity is then given by $K_e = LT/\rho$ where the Lorenz number, L, is a known function of ζ and s. This procedure is probably reasonably good so long as there is electrical conduction in one band only. At high temperatures there is conduction in both the valence and conduction bands and the electronic thermal conductivity is enhanced by ambipolar diffusion. The calculation of this contribution requires knowledge of several parameters whose values are not well known for the alloys. The results shown in figure 1 clearly show ambipolar contributions to the thermal conductivities of Sample 4 at $380^{\circ}K$ and Sample 7 at $300^{\circ}K$ and suggest that there may be a small contribution in Sample 2 at $300^{\circ}K$. Accordingly, we have restricted our analysis to results at temperatures below $240^{\circ}K$. At $240^{\circ}K$ the value of ζ calculated from α is greater than -0.1 kT for all our samples with the exception of Sample 7. As usual, ζ is measured in hole energy from the valence band edge for the p-type specimens and in electron energy from the conduction band edge for the n-type specimens. Since the energy gaps for these samples are about 8 kT at this temperature, it seems safe to ignore two-band conduction below $240^{\circ}K$.

As shown in figure 3, the electrical resistivity of all the samples increases at least as fast as T between $80^{\circ}K$ and $240^{\circ}K$. This surely indicates that phonon scattering predominates. The simplest theory of electron-phonon scattering in semiconductors would therefore suggest $s = -1/2$. This value, however, does not provide a good account of the temperature dependence of the mobility of the carriers in Bi_2Te_3, particularly for p-type material. Moreover, for the alloys the resistivity is less sensitive to temperature than for the Bi_2Te_3 samples. This suggests that carrier scattering by the solute atoms is not negligible in the alloys. The relaxation time for combined impurity and phonon scattering is not proportional to E^s, but must be represented by a more complicated function of E. For small or moderate charge carrier concentrations, τ is a decreasing function of E for phonon scattering, an increasing function of E for charged impurity scattering, and independent of E for neutral impurity scattering. Qualitatively then, one can study the effect of impurity scattering by calculating K_e using $\tau = \tau_o E^s$ with values of s in the range -1/2 to 3/2. It will be appreciated that at present we cannot calculate very accurate values of K_e.

Figure 4 shows the temperature dependence of $W_L = 1/K_L = 1/(K-K_e)$ calculated from the measured values of K and the calculated values of K_e. With the exception of Sample 4, we have used $s = -1/2$. For Sample 4 two results are shown, one for $s = -1/2$ and one for $s = +1/2$. Within experimental error and considering the uncertainty in the values of K_e, the experimental results may be represented by $W = \beta T + \gamma$. If K_e is calculated using $s = -1/2$, then β has the following values: Samples 1 and 2 (Bi_2Te_3) $\beta = 2.0 \times 10^{-3}$; Sample 3 ($Bi_2Te_3$ + 2% Bi_2Se_3) $\beta = 2.2 \times 10^{-3}$; Samples 4, 5, 6 ($Bi_2Te_3$ + 10% Bi_2Se_3 + I) $\beta = 2.7 \times 10^{-3}$; Sample 7 $\beta = 2.6 \times 10^{-3}$ mW^{-1}. We observe that this difference cannot be attributed to improper values of K_e. If there is any significant difference between the energy dependence of the τ's for the Bi_2Te_3 samples and for the alloys containing 10% Bi_2Se_3, then the τ for the latter samples should be a less rapidly decreasing function of E than the τ for the Bi_2Te_3 samples. As shown by the results with $s = +1/2$, this difference would result in an even larger difference between the values of β.

4. Discussion

For the case of phonon scattering by three phonon U-processes combined with scattering by a random distribution of point defects, Klemens [1] obtained the formula

$$K_L = K_u \frac{\omega_o}{\omega_D} \tan^{-1}\left(\frac{\omega_D}{\omega_o}\right) \qquad (2)$$

for the lattice thermal conductivity. In this expression ω_D is the Debye frequency, ω_o is the phonon frequency at which the scattering rates for the two processes are equal and K_u is the lattice thermal conductivity of the defect-free crystal. If we have $K_u = K_o T^{-1}$ with K_o independent of T, then ω_o is proportional to $T^{1/2}\ N^{-1/2}$ where N is the concentration of defects as shown by Klemens [1]. Figure 5 shows a plot of $W_L = 1/K_L$ calculated from this formula for various values of N. Both T, W_L and N are in arbitrary units. The lowest line $W = W_u = T/K_o$ shows the thermal resistivity of the defect-free material. For small defect concentrations, i.e., $\omega_o \gg \omega_D$, eq (2) may be written $W_L = W_u + W_o$ with $W_o = (W_u/3)(\omega_D/\omega_o)^2$ which is independent of T and proportional to N. This behavior is shown by the curve labeled N = 1. As shown by the curves labeled N = 4 and N = 9, W_L cannot be approximated by eq (1) with W_u independent of N for larger values of N. However, this figure clearly shows that over a small range of temperatures the curvature in a plot of measured values of W_L vs. T would not be observed. One would represent all the results between say T = 10 and T = 30 by equations of the form $W_L = \beta T + \gamma$ with both β and γ increasing with N. This, we suggest, is the explanation of our experimental results shown in figure 4. Moreover, the results shown in figure 4 do not exactly fit the straight lines. Because of experimental error and the uncertainty in K_e, we do not claim that the curvature indicated by our results is well established but it certainly is of the form predicted by eq (2).

An attempt to give a quantitative account of the experimental results is beset with many difficulties. The uncertainty in the values of K_e has already been described. The use of $K_u = K_o T^{-1}$ is certainly not completely correct. Ioffe has pointed out that the equation $W_u = (1/K_o)(T - \theta/3)$ might better represent the high temperature ($T \gtrsim \theta$) lattice thermal resistivity of a defect-free material. Goldsmid [17] has reported that neither formula is perfectly satisfactory for Bi_2Te_3. The value of K_o calculated from the results shown in figure 4 for Samples 1 and 2 is 5.0×10^2 $W m^{-1}$, in good agreement with the value reported by Satherthwaite and Ure [9] but about 14% larger than the value found by Walker [18]. The data for Samples 1 and 2 do not answer the question of how to represent W_u as a function of T since these are not completely defect-free samples. No foreign atoms have been added to these samples but they contain defects, such as vacancies, interstitials, atoms on wrong sites, and dislocations, which are effective phonon scatterers. The value of K_u should vary with Se concentration. However, if it is permissible to use a virtual crystal model, this is a very small effect, since the lattice thermal conductivity of Bi_2Se_3 is only about 1.3 times that of Bi_2Te_3 [10].

The compositions given in Table 1 are those of the starting material and are not necessarily those of the samples measured. Samples 4, 5 and 6 contain I added to maintain a high carrier concentration. A quantitative account of the measured values of W_L would necessitate the separation of the scattering due to Se from that due to I since iodine is an effective phonon-scatterer in Bi_2Te_3. The addition of I to the 10 mole % Bi_2Se_3 samples was necessary for the following reason. Bi_2Te_3 crystallized from a stoichiometric melt is p-type (Bi rich). As stoichiometric amounts of Bi_2Se_3 are added, the extrinsic hole concentration decreases until, for a composition of ~20 mole % Bi_2Se_3, the materials become n-type [19]. If the iodine had not been added to the samples containing ~10 mole % Bi_2Se_3, then their extrinsic hole concentrations would have been small and the uncertainty in K_e due to ambipolar diffusion would have been encountered at lower temperatures. This is seen in the results for Sample 7. The values of R, ρ and α given in Table 1 show that a large fraction of the iodine was lost in the process of growing Sample 7 from the material from which Sample 6 was cut. The value of W_L for Sample 7 at 240°K (figure 4) is almost certainly incorrect because an ambipolar contribution is an important part of K_e at this temperature. At lower temperatures the temperature dependence of W_L for Sample 7 is not qualitatively different from that for Samples 4, 5 and 6 (we know that at least part of this reduction in defect concentration is due to the loss of iodine). We can then conclude that there is no difference between the lattice thermal conductivities of the Bridgman and single-zone grown alloys for $T > 80°$ and Se concentrations below 10 mole % other than that caused by different point defect concentrations.

Despite these uncertainties, it nevertheless seems worthwhile to try to fit the Klemens formula to the data. For Ge-Si alloys, it is known that this formula does not give a good account of the temperature dependence of K_L. As shown by Parrot [2] and Abeles [3], the theory can be brought into reasonable agreement with experimental results only when the effect of N-processes are also included. Therefore, it is of interest to see if the formula can do somewhat more than predict the qualitative changes in the temperature dependence of the thermal resistivity of the alloys. By taking $W_o = (W_u/3)(\omega_D/\omega_o)^2$, eq (2) becomes

$$K_L = K_u \sqrt{\frac{W_u}{3W_o}} \tan^{-1} \sqrt{\frac{3W_o}{W_u}} \ . \qquad (3)$$

We assume that $W_u = 2 \times 10^{-3}\ T\ {}^{o}K\ mW^{-1}$ is the same for all specimens, ignoring the small change in W_u

with the addition of Bi_2Se_3 predicted by the virtual crystal model. With the choice of $W_o = 0.18$ and 0.59 m $^oK\ W^{-1}$ for Samples 3 and 4 respectively, figure 6 shows that the formula gives an excellent account of the experimental results. At first thought, the ratio $59/18 \approx 3.3$ does not seem large enough. Sample 4 should contain roughly 5 times as much Se as Sample 3, as well as some iodine that is absent from Sample 3. However, we do know that there must also be a difference in the vacancy/interstitial concentrations between the two samples and until the effect of this difference is understood, a final judgement must be reserved. This fit of the Klemens formula suggests that the N-processes may be of relatively less importance to the high temperature thermal conductivity of Bi_2Te_3 alloys than to the Ge-Si alloys. This would seem to be a reasonable result. It is known [20] that the Leibfried-Schloemann formula overestimates the lattice thermal conductivity of both elements and compounds. However, the discrepancy is larger for compounds than for elements (in the case of Ge, Si and Bi_2Te_3, the Leibfried-Schloemann formula overestimates the lattice thermal conductivity by factors of 2.1, 1.5 and 5.1 respectively). Klemens suggested [20] that this is the result of additional U-processes arising from the extra zone boundaries in the compounds. If this is correct, then we might expect that the ratio of the strengths of U to N processes would be larger in the Bi_2Te_3 alloys than in the Ge-Si alloys. However, N-processes are most effective when the point defect scattering is dominant and this is not the case even for Samples 4, 5 and 6 at 80^oK. For Sample 4 at 80^oK, $\omega_D/\omega_o \approx 3.3$ whereas Ge-Si alloys have been measured for which $\omega_D/\omega_o \approx 13$. It must, therefore, be recognized that we have not put the Klemens formula to an exacting test.

In figure 4 we have included a line labeled "Lenningrad". This represents the results found by the group at the Lenningrad Semiconductor Institute [12-15] for a sample of 97% Bi_2Te_3 + 3% Sb_2S_3. Moreover, they find dW_L/dT to be independent of defect concentrations for samples containing as much as 9 mole % Sb_2S_3 so that their results can all be represented by $W = W_u + W_o$ even when $W_o > W_u$. We do not understand their results but it seems quite clear that point defect scattering alone cannot account for the changes in K_L that they have produced by alloying Bi_2Te_3 with Sb_2S_3. They also claim the same type of results for Bi_2Te_3 - Bi_2Se_3 alloys for samples containing as much as 8% Bi_2Se_3. Our results clearly disagree with theirs. It does not seem possible to understand their results in terms of the current theory of point defect scattering.

In summary, the lattice thermal conductivity of Bi_2Te_3 alloys containing as much as 10 mole % Bi_2Se_3 is determined only by the chemical composition of the sample. The experimental results are in excellent qualitative agreement with the theory that treats the phonons as being scattered both by three phonon processes and by a random array of point defects. Quantitative comparison of theory and experiment must await the solution of a number of problems. However, our preliminary attempts to fit the theory to the experimental results suggests that good quantitative agreement between theory and experiment will be found.

5. Acknowledgment

The authors thank P. Piotrowski and D. Zupon for assistance with the sample preparation and the measurements.

6. References

[1] P.G. Klemens, Phys. Rev. 119, 507 (1960).

[2] J.E. Parrot, Proc. Phys. Soc. 81, 726 (1963).

[3] B. Abeles, Phys. Rev. 131, 1906 (1963).

[4] For example see, Thermoelectricity: Science and Engineering, eds. R.R. Heikes and R.W. Ure, Jr. (Interscience. New York, 1961).

[5] A.F. Ioffe, S.V. Airapetiants, A.V. Ioffe, N.V. Kolomoets and L.S. Stilbans, Doklady Akad. Nauk SSSR 106, 981 (1956); English translation: Russian Literature Survey: SEM-1-56 (Infosearch, London, 1956). For a discussion of this argument, see Ref. 4, p. 383.

[6] H.J. Goldsmid, Thermoelectric Refrigeration (Plenum Press, New York, 1964), p. 130.

[7] R.W. Ure, Jr., Proc. of the IEEE/AIAA Thermoelectric Specialists Conf., Washington, D.C., May 17, 1966 (Inst. of Electrical & Electronic Engineers, New York, 1966), Paper No. 11; Adv. Energy Conversion, to be published.

[8] H.J. Goldsmid, Proc. Phys. Soc. B69, 203 (1956).

[9] C.B. Satherthwaite and R.W. Ure, Jr., Phys. Rev. 108, 1164 (1957).

[10] H.J. Goldsmid in Materials Used in Semiconductor Devices, ed. C.A. Hogarth (Interscience Publishers, New York, 1965), p. 165ff.

[11] See Ref. 10 for a discussion of these results and references to the original work.

[12] E.A. Gurieva, V.A. Kutasov and I.A. Smirnov, Sov. Phys. - Solid State 6, 1945 (1965).

[13] V.A. Kutasov, B.Y. Moizhes and I.A. Smirnov, Sov. Phys. - Solid State 7, 845 (1965).

[14] E.A. Gurieva, A.I. Zaslavski, V.A. Kutasov and I.A. Smirnov, Sov. Phys. - Solid State 7, 978 (1965).

[15] V.A. Kutasov and I.A. Smirnov, Sov. Phys. - Solid State 8, 2153 (1967).

[16] D.H. Damon, J. Appl. Phys. 37, 3181 (1966).

[17] H.J. Goldsmid, Proc. Phys. Soc. 72, 17 (1958).

[18] P.A. Walker, Proc. Phys. Soc. 76, 113 (1960).

[19] U. Birkholtz, Z. Naturforsch 13a, 780 (1958).

[20] P.G. Klemens in Solid State Physics, eds. F. Seitz and D. Turnbull (Academic Press, New York, 1958), Vol. 7, p. 46ff.

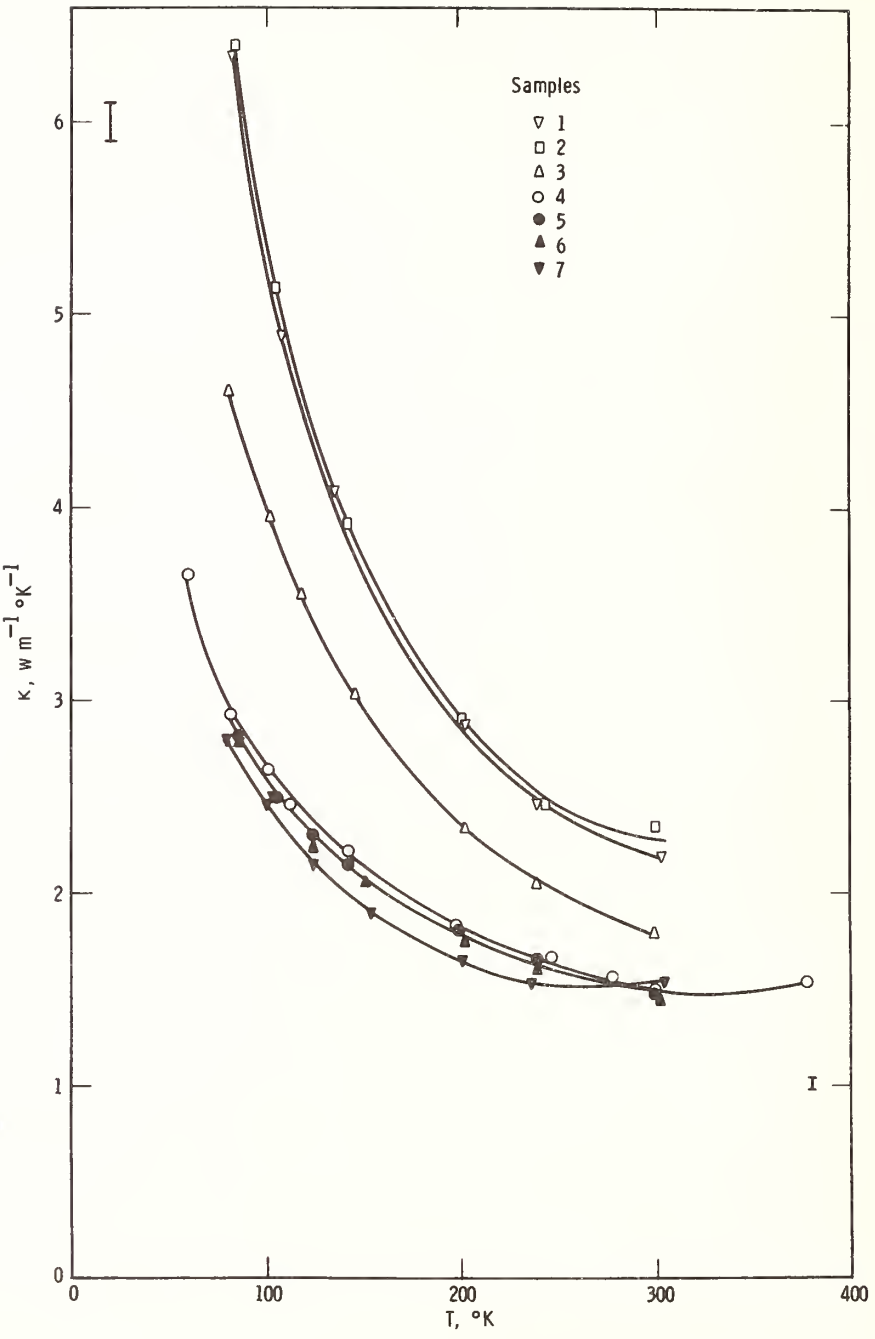

Fig. 1 Measured values of the thermal conductivity, K, plotted against absolute temperature, T.

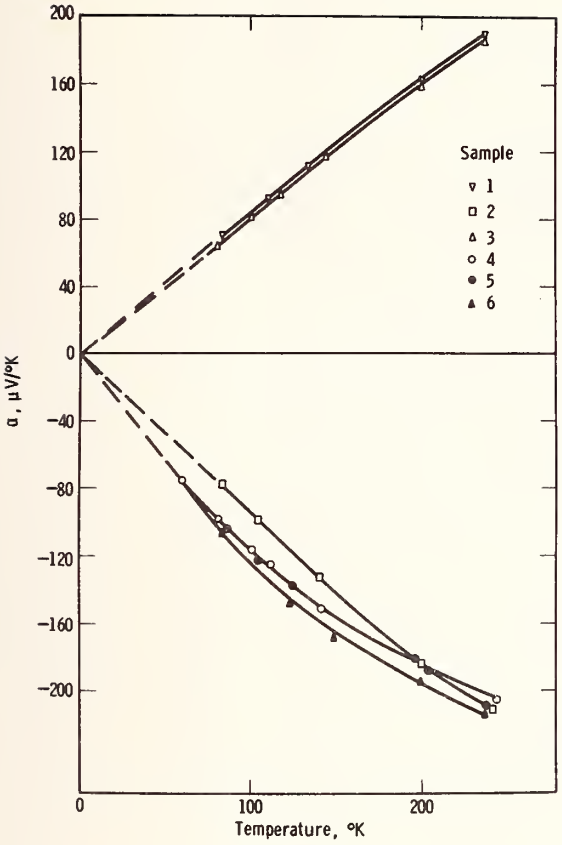

Fig. 2 Measured values of the Seebeck coefficient, α, plotted against absolute temperature, T.

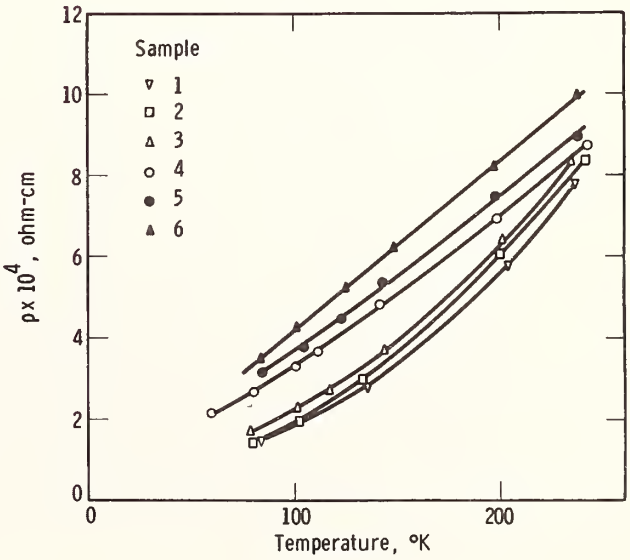

Fig. 3 Measured values of the electrical resistivity, ρ, plotted against absolute temperature, T.

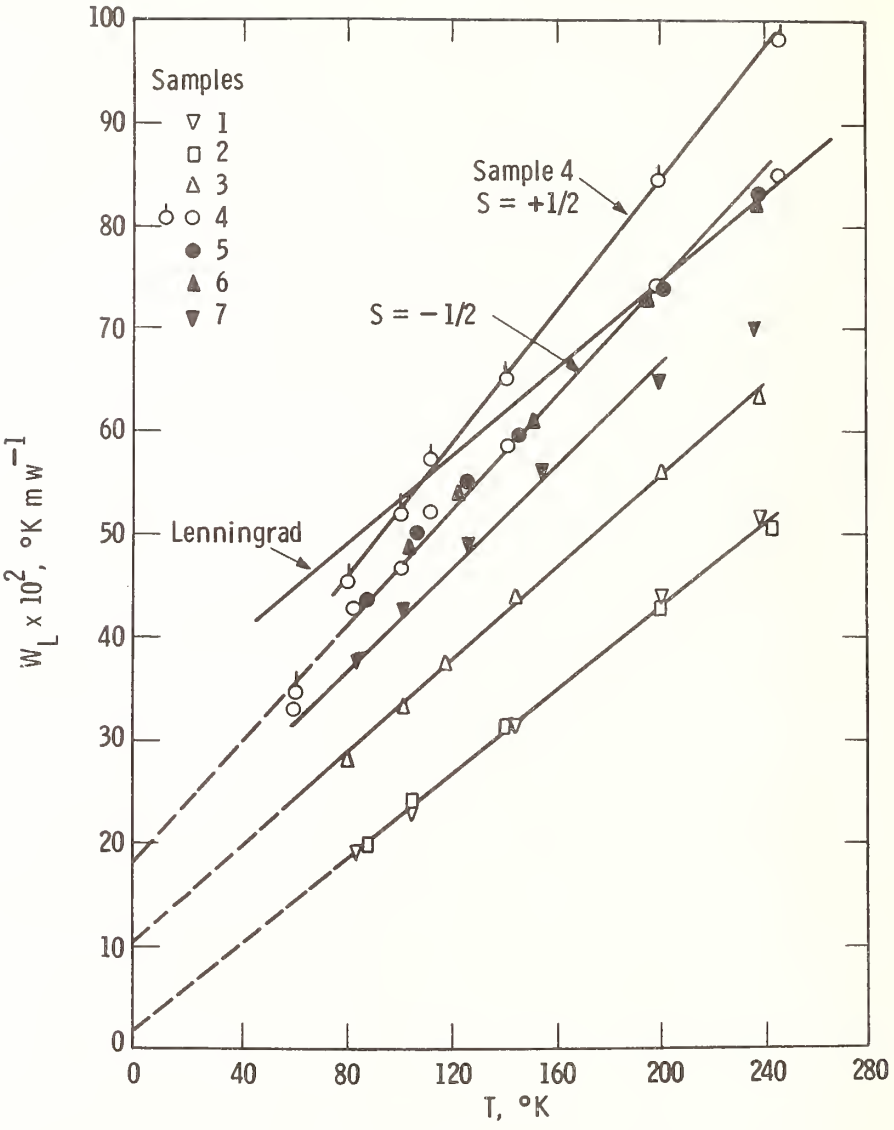

Fig. 4 Values of the lattice thermal resistivity, W_L, plotted against absolute temperature, T. W_L is calculated from $W_L = 1/K_T$ and K_L is calculated from $K_L = K-K_e$ where K_e is the electronic thermal conductivity computed from the measured values of ρ and a Lorenz number deduced from the measured values of α. All values of the Lorenz number were calculated assuming s = -1/2 with the exception of the curve labeled s = +1/2 for Sample 4 (see text). The line labeled "Lenningrad" shows the results given in reference [13] for a sample of 97% Bi_2Te_3 + 3% Sb_2S_3.

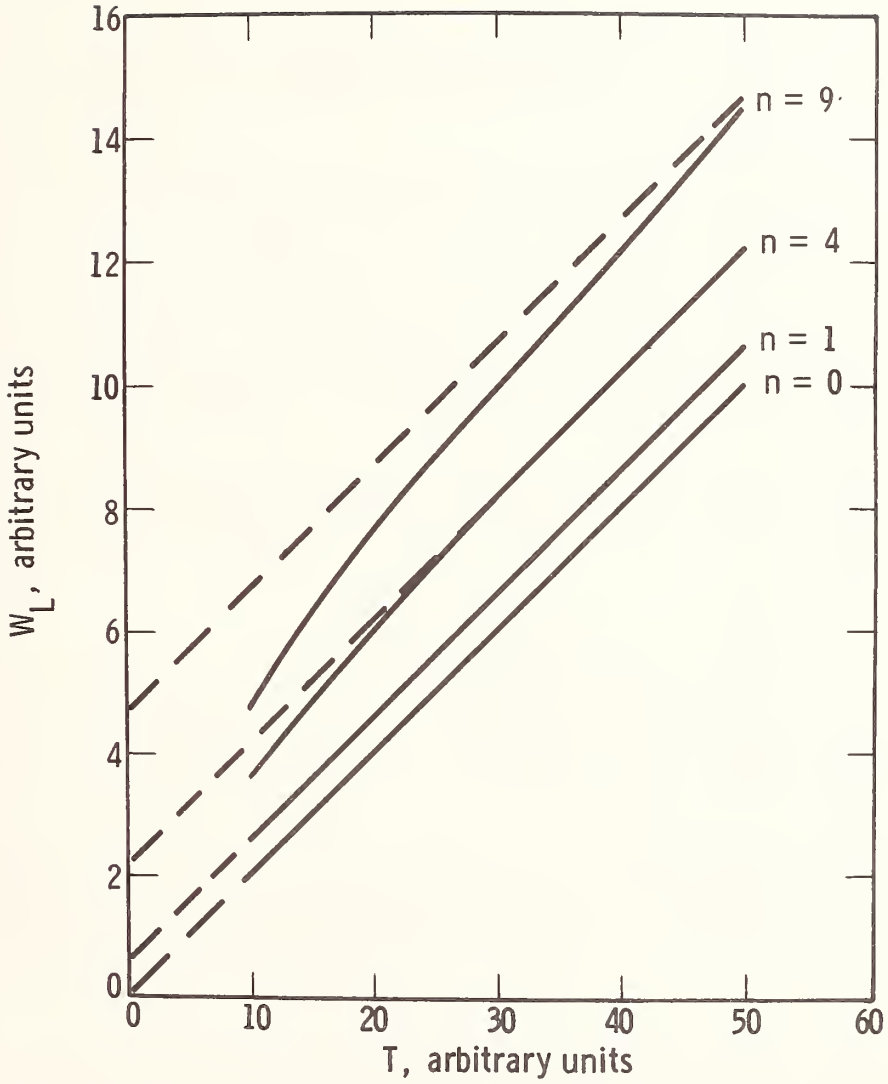

Fig. 5 The variation of the lattice thermal resistivity, W_L, with temperature, T, and defect concentration, n, predicted by the Klemens formula (eq 2). W_L, T and n are in arbitrary units. The lowest curve shows the variation of W_u, the lattice thermal resistivity of the defect-free crystal; the upper curves show the effects of adding point defects.

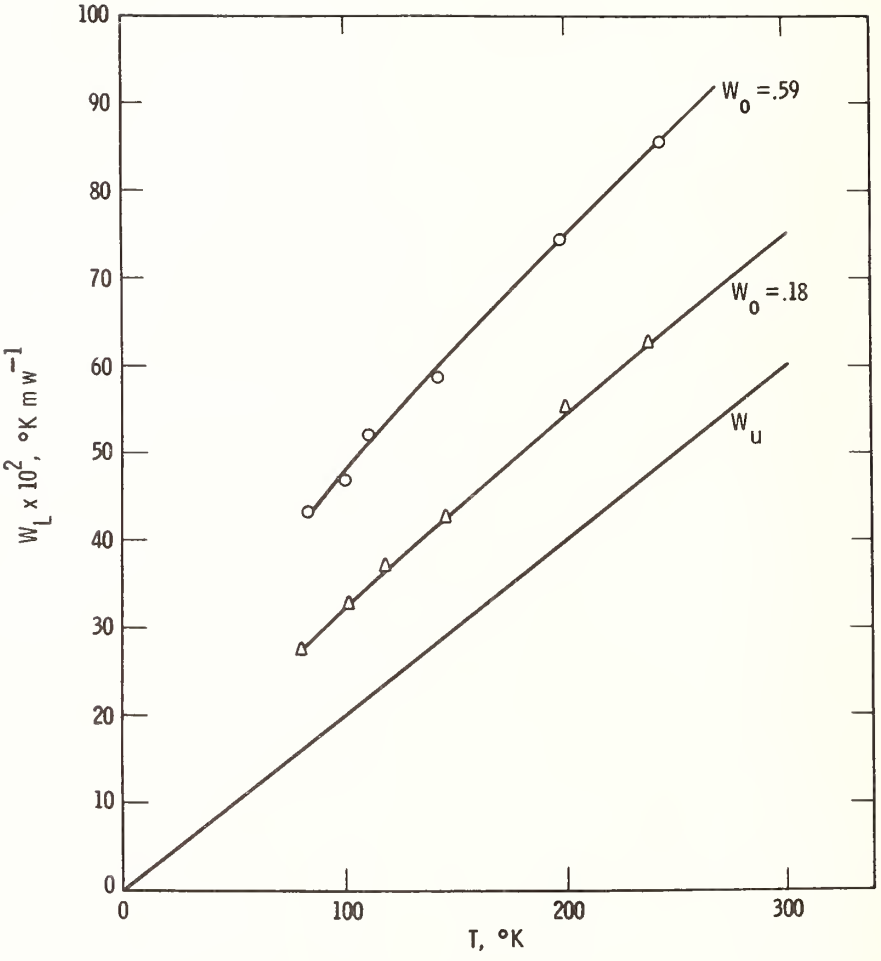

Fig. 6 The fit of the Klemens formula (eq 3) to the measured values of W_L for Samples 3 and 4. The points are the same as those shown in figure 4. The curves have been calculated from equation 3 with the assumption $W_u = 0.002\ T\ ^{o}K\ m\ W^{-1}$ for pure Bi_2Te_3.

Thermal Conductivity of Cadmium Arsenide from 60 to 400°K

D. P. Spitzer

American Cyanamid Company
Stamford, Connecticut 06904

Measurements of the thermal conductivity of Cd_3As_2 have been extended to lower temperatures than previously reported [1][1]. It now appears, contrary to an earlier interpretation, that the lattice thermal conductivity of either undoped, Cu-doped, or Se-doped Cd_3As_2 is 1.4 ± 0.2 W m^{-1} deg^{-1} (14 ± 2 mW cm^{-1} deg^{-1}) over the whole stated range of temperature, and total thermal conductivities are anomalously low because of electronic components that are much less than given by the Wiedemann-Franz law. Similar results have been reported for Ag_2Se, HgSe, and PbTe at low temperatures, and may be explained by assuming inelastic scattering mechanisms, probably of electrons by electrons. Inelastic scattering processes probably occur in many semiconductors, but the effects are clearly noticeable only in materials with high carrier mobility and low lattice thermal conductivity.

Key Words: Cadmium arsenide, electron-electron scattering, electronic thermal conductivity, inelastic electron scattering, lattice thermal conductivity, Lorenz number, thermal conductivity, thermal resistivity.

1. Introduction

An earlier publication from our laboratories presented thermal and electrical conductivities for over thirty variously-doped samples of Cd_3As_2 at room temperature and for three representative samples from 240 to 400°K [1]. At that time, low thermal conductivities of undoped samples (and some doped ones) were ascribed to low lattice components, due to unusually effective phonon scattering by a lattice defect (As vacancy). Cd_3As_2 doped with Se, which increased the charge carrier concentration but decreased carrier mobility, had normal thermal conductivities in accordance with the Wiedemann-Franz law.

It appeared that more information on the cause of the low thermal conductivities might be obtained from thermal conductivity measurements at lower temperatures, on both undoped and Se-doped Cd_3As_2. The small differences in lattice thermal conductivity found in [1] should be much greater at lower temperatures if the postulated explanation were correct (namely, the Se was assumed to fill up anion vacancies thought to be normally present in undoped Cd_3As_2 so that the usual $1/T$ law is found for lattice thermal conductivity instead of the temperature independent conductivity that results from impurity scattering).

2. Experimental

The samples used were polycrystalline pieces, a few millimeters on a side, cut from ingots made by fusion of the elements in vacuum, as described previously [1]. In addition to the samples described in [1], we attempted to make Cd_3As_2 with a smaller number of carriers by zone-refining, as reported by Ugai and Zyubina [2]. Cd_3As_2 was completely sealed in a graphite tube, except for a small hole through which it could be evacuated, and this in turn was sealed in a Vycor tube. A molten zone about two centimeters wide was passed through the 20 cm long sample at the rate of 2.5 cm/hr. After forty such passes, no significant variation in carrier concentration along the length of the sample was found. Swiggard [3] recently reported that zone-refining of Cd_3As_2 under conditions where vaporization was eliminated reduced the number of carriers by only a factor of two. Appreciable sublimation had taken place in our case, and this might have evened out otherwise small differences in concentration.

Measurements of thermal conductivities at room temperature and below were made in an apparatus designed to fit into a helium dewar with only a 1.27 cm (0.5 inch) diameter sample chamber. The arrangement used is illustrated in figure 1. The steady heat applied at the bottom end of the sample was cal-

[1] Figures in brackets indicate the literature references at the end of this paper.

culated directly from the current and voltage across the resistor which was used as a heater. A correction was made for radiation losses from the heater block surface (this surface was intentionally blackened so that its approximate emissivity would be known). This correction ranged from about 10% at room temperature to less than 0.5% at 100°K. Another correction was made for conduction through the leads connected to the heat source and through the thermocouple wires; this was 2-5% of the total heat and essentially independent of temperature. The thermal conductivity of the sample is simply the corrected heat input divided by the resultant temperature difference across the sample, and multiplied by the ratio of the sample's length to its cross-sectional area.

Measurements on samples of Inconel 702 of known thermal conductivity gave results that were correct within ± 5%, at least down to about 80°K. The measurements on the Cd_3As_2 samples, however, were generally reproducible only to within 10%. At lower temperatures, the temperature of the heat sink drifted too much to permit accurate measurements of the temperature difference across the sample (the heat capacity of the copper sink decreases by more than a factor of ten between 80 and 20°K). It is likely that this difficulty could be corrected by using metal instead of polytetrafluoroethylene rings around the sink.

Electrical conductivity and Seebeck coefficient were measured on the same set-up, after moving the position of only one lead (from the end of the heater resistor to the copper block around it).

3. Results

Total and lattice thermal conductivities for one undoped, one Cu-doped, and two Se-doped samples of Cd_3As_2 are given in figures 2 and 3. For the undoped and Cu-doped samples, the two lattice conductivities given result from two different estimates of the electronic thermal conductivity, as described below. The lattice conductivity is simply the difference between the measured total thermal conductivity and the calculated electronic thermal conductivity.

Electrical conductivities for the four samples are given in figure 4. Seebeck coefficients varied smoothly from about 15 μV/°K at 60°K to 70-80 μV/°K at 400°K for undoped or Cu-doped Cd_3As_2. At these same temperatures, the Seebeck coefficients for the Se-doped samples were about 10 and 40 μV/°K, respectively.

Measurements which were obtained down to about 20°K on the present samples did indicate that total thermal conductivities continued to decrease with decreasing temperature, as expected from $\lambda_e \propto L\sigma T$ and the decreasing lattice heat capacity term. The scatter in these data became quite bad at these lower temperatures, however, and such data are not included here. More accurate measurements at lower temperatures are not expected to affect the interpretation of the results to be presented.

From [1] it is known that there is very little change in total or lattice thermal conductivity between 300 and 400°K, for all Cd_3As_2 samples. (Unfortunately, the measurements reported here were not made on the identical samples used in [1]; the Cu-doped sample was from the same ingot, however, and the other samples were from different ingots, but prepared under identical conditions.) In figure 2 of [1], λ_L for a Se-doped sample is shown to be increasing with decreasing temperature, but it is now thought that a greater uncertainty should be admitted for this λ_L, because of the large electronic component. It is significant that the points for this λ_L fall in the range 1.4 ± 0.4 W m^{-1} deg^{-1}, where the mean value is the same as that found here.

Thermal conductivity of Cd_3As_2 in the temperature range 80-380°K has also been recently reported by Giraudier [4]. The thermal and electrical conductivities of his sample are about twice those of our undoped sample. Giraudier's thermal conductivities seem generally too high, especially above 300°K, where the thermal conductivity is shown to be increasing considerably with temperature. The lattice conductivity can hardly be increasing, and the electronic conductivity should be nearly independent of temperature. Below 300°K, good agreement with our λ_L of 1.4 W m^{-1} deg^{-1} is obtained only if an L as high as $3.1(k/e)^2$ is assumed (k is Boltzmann's constant and e is the electronic charge). This is reasonable only if the carrier concentration is much higher than for our samples, but this is not known.

A description of the calculation of the electronic thermal conductivity has been given in the earlier publication [1]. This is calculated as usual from the electrical conductivity and the Lorenz constant. L is determined from a knowledge of the carrier scattering mechanism, as given by temperature dependence of mobility, and from the position of the Fermi level, calculated from the Seebeck coefficient.

According to our calculations and those of others [5], even undoped Cd_3As_2 is quite degenerate, with a Fermi level about 0.12 eV (~ 5kT at 300°K) above the bottom of the conduction band and not much dependent on temperature. Consequently, L calculated as above for undoped Cd_3As_2 is near the $L_o = (\pi^2/3)(k/e)^2$ value that applies to a completely degenerate conductor, namely, $L \sim 3.0(k/e)^2$ at 300°K [1]. Similarly, $L \sim 2.9(k/e)^2$ was found for the Cu-doped Cd_3As_2 and $L \sim 3.1(k/e)^2$ for Se-doped Cd_3As_2. Using these values for L gives the λ'_L curves for samples 1 and 2 (fig. 2) and the λ_L values for samples 3 and 4 (fig. 3). The λ_L curves for samples 1 and 2 result from taking $L = 2.0(k/e)^2$ instead. It is thought to be just coincidental that this is the L for the completely non-degenerate case.

4. Discussion

There is now considerably more evidence for anomalously low electronic thermal conductivities than for low lattice thermal conductivities: (1) The anomaly decreases as electrical conductivity decreases. (2) It is now found the λ_L is independent of temperature for Se-doped as well as undoped Cd_3As_2. This means that our explanation as to why Se-doping apparently increased lattice thermal conductivity (i.e., Se atoms were thought to fill up As vacancies) has no support. (3) The λ_L for all of our samples are identical over the entire temperature range if we assume that the Lorenz number for undoped (or Cu-doped) Cd_3As_2 is a low $2(k/e)^2$. (4) λ_L = 1.2 W m^{-1} deg^{-1} at 80°K has been found by Goldsmid [6] from measurements utilizing a magnetic field to directly eliminate the electronic thermal conductivity. This is in good agreement with our value of 1.4 ± 0.2 W m^{-1} deg^{-1} found when a low electronic thermal conductivity is assumed. Such measurements using magnetic fields will ultimately provide the most direct separation of lattice and electronic thermal conductivity.

As more data become available on thermal conductivities of materials that have comparable lattice and electronic thermal conductivities, it appears that adherence to the Wiedemann-Franz law, with Lorenz numbers calculated as indicated above, is the exception rather than the rule. There are presently only a handful of materials for which measurements of thermal conductivity have been made on samples of varying electrical conductivity. Besides Cd_3As_2, this list includes Bi_2Te_3 [7], Ag_2Te [8], Ag_2Se [9, 10], SnTe [11], InAs [12], HgSe [13], and PbTe [14, 15, 16] (some such data are also available for Bi_2Se_3 [17] but are too limited to permit definite conclusions regarding scattering mechanism). Most of these materials clearly show considerable deviations from the electronic thermal conductivity when calculated as previously mentioned.

Perhaps Bi_2Te_3 is the only compound on the above list that closely obeys the Wiedemann-Franz law. Low values for total thermal conductivity have been found for some samples of Bi_2Te_3 [7], but this has quite conclusively been shown to be due to a low lattice component (caused by a large phonon scattering cross-section for the halogen ion dopants used).

Available data for Ag_2Te [8] do not extend to very high electrical conductivities and could be fit equally well with a lower Lorenz number if it is assumed that the samples with the lowest electrical conductivities have a lattice component that is about 0.2 W m^{-1} deg^{-1} less than for the other samples (this seems reasonable because some of these samples are stated to be defective in silver and the low electrical conductivity of the others suggests that they are more than usually disordered).

SnTe is different from the other materials in the list above in that it has a rather low carrier mobility and is not a good thermoelectric material. The carrier concentrations in the SnTe samples [11] were at least a factor of ten greater than for the other materials in the list. Here the Lorenz numbers were found to be generally greater than L_o. It was suggested that there was a connection between the behavior of the Lorenz number and a band structure involving two valence bands, but the physical processes involved could not be identified. The anomaly in the electronic thermal conductivity of SnTe is almost certainly quite different from that in Cd_3As_2 in any event.

Cd_3As_2, PbTe, Ag_2Se, HgSe, and InAs all definitely exhibit anomalously low Lorenz numbers, at least over some range of temperature and carrier concentration. It seems likely that some type of inelastic electron scattering is responsible for the low Lorenz numbers in all of these materials. In some cases the inelastic electron scattering may be caused by optical phonons and in other cases may be caused by other electrons. At room temperature, Lorenz numbers are markedly low only for Cd_3As_2 and Ag_2Se. No explanation has been given for Ag_2Se, but its behavior is generally more similar to Cd_3As_2 than to any of the other materials mentioned.

InAs has such a high lattice thermal conductivity that accurate experimental determination of the electronic component has not been possible. Thermal conductivity measurements on highly doped InAs have been reported [12] only for the temperature range 300-700°K, and even at these temperatures the lattice conductivity is fairly high and the electronic contribution is rather uncertain. The electronic component is definitely lower than expected and can be at least partly accounted for by scattering of electrons by optical phonons; a reduction in L to $0.60L_o$ was calculated for scattering by optical phonons.

The most unequivocal separation of electronic and lattice thermal conductivities is obtained by measurement of thermal conductivity with and without a strong magnetic field. The latter measurement gives the lattice conductivity directly, and the difference of the two measurements is the electronic component. Such measurements have been made for PbTe and HgSe at low temperatures (below 300°K). The HgSe samples [13] were all very degenerate, with the Fermi level being 7-30 kT above the bottom of the conduction band. The Lorenz number was found to be only about 70% and 45% of L_o at 95 and 205°K, respectively. Since there was also previous evidence that optical phonons were involved in the scattering processes, it was suggested that the low Lorenz numbers were associated with the inelastic nature of the electron scattering by the optical phonons (as was done for InAs above). No quantitative analysis was attempted. It is generally agreed that scattering of electrons in Cd_3As_2 is predominantly by acoustic phonons [18, 19, 5], and it is unlikely that the explanation given for HgSe applies to Cd_3As_2.

Measurements on PbTe [15, 16] were made on somewhat less degenerate samples, with Fermi levels about 2-12 kT above the bottom of the conduction band. Low Lorenz numbers were found below room temperature, with a minimum of about $0.6L_o$ in the vicinity of 100°K, for samples with carrier concentration in the range 10^{24} to 10^{25} m^{-3} (10^{18} to 10^{19} cm^{-3}). The low Lorenz numbers were explained on the basis of electron-electron collisions, which had also been satisfactorily used to explain thermoelectric power data for PbTe [20].

Equation (1) is given by Moizhes and Ravich [20] for the thermal resistivity due to electron-electron scattering:

$$\frac{W_{ee}}{W_o} = \frac{3\pi^4 e^3 (kT)^2 r_s unN}{5\epsilon_\infty^2 \hbar^3 v_F^4 k_F^2} \tag{1}$$

Here W_o is the thermal resistivity associated with elastic scattering mechanisms, as given by the Wiedemann-Franz law, k_F is the average crystal momentum at the Fermi level,

$$k_F = (3\pi^2 n/N)^{1/3} \tag{2}$$

v_F is the velocity corresponding to this crystal momentum, N is the number of energy ellipsoids, r_s is the screening radius,

$$r_s = (\epsilon_\infty / 4\pi e^2 \rho)^{1/2} \tag{3}$$

ρ is the density of states, u is the electron mobility, and ϵ_∞ is the high frequency dielectric constant. Using eq (1), Moizhes and Ravich find $W_{ee}/W_o = 1.0$ at 77°K, in excellent agreement with the value of 0.7 required to explain their experimental data. In repeating this calculation, we obtain a value of 9.3 instead of 1.0 for W_{ee}/W_o. Moizhes and Ravich, however, did not explicitly state what value they used for the effective mass (which enters into v_F), and it may be that they used something other than the 0.12 m_o that we used. One cannot really expect such good agreement as is claimed, anyway, and it is significant enough that the calculation gives the right order of magnitude.

The same calculation may readily be made for Cd_3As_2. Using values of $n = 2 \cdot 10^{24}$ m^{-3}, $\rho = 1.7 \cdot 10^{25}$ $(eV)^{-1}$ m^{-3}, $\epsilon_\infty = 16.3$ [21], $u = 3.0$ m^2 V^{-1} sec^{-1}, $m = 0.05$ m_o, eq (1) gives $W_{ee}/W_o = 2.2$ at 77°K, which is of the same order of magnitude as for PbTe.

The form of eq (1) also agrees with the temperature dependence of the electron-electron resistance in PbTe below about 100°K, i.e., W_{ee} decreases with decreasing temperature. Our data on Cd_3As_2 do not go to low enough temperatures to make a comparison. For PbTe above 100°K, however, the experimental W_{ee} decreases with increasing temperature, contrary to eq (1). This is ascribed in [16] to the sample becoming non-degenerate, but this seems doubtful. For Cd_3As_2, the extra thermal resistivity is practically independent of temperature.

If the v_F and k_F are expressed in terms of n in eq (1), it is seen that W_{ee} should decrease with increasing n (W_{ee} does not, on the contrary, increase indefinitely as n decreases, since n must always be large enough for degenerate statistics to apply). This dependence on n was actually observed for PbTe, and this agrees qualitatively with our results on Cd_3As_2. Namely, the Se-doped Cd_3As_2 samples with about six times the number of carriers as the undoped samples do not show the extra thermal resistivity that the undoped samples do. (However, the fact that the mobility dependence on temperature is less for Se-doped Cd_3As_2 ($u \propto T^{-1/2}$) than for undoped Cd_3As_2 ($u \propto T^{-1}$) suggests that impurity scattering is greater in the Se-doped samples, and this may also lead to a higher Lorenz number.)

As pointed out in [21], an equation similar to (1) is given by Ziman [22], for W_{ee} only:

$$W_{ee} = (9/40)(\pi^2)(e^4 T / v_F E_F^3)(R/q) \tag{4}$$

where E_F is the Fermi energy, R is the same as k_F with N = 1, and q is the same as $1/r_s$ with $\epsilon_\infty = 1$. Using the same numbers for Cd_3As_2 as above, eq (4) yields $W_{ee} = 5$ m deg W^{-1}, approximately, at room temperature. The extra thermal resistance found experimentally is about 0.3 m deg W^{-1} over our whole temperature range. Ziman recognizes that eq (4) overestimates the electron-electron thermal resistance.

This may be due in part to the neglect of the dielectric constant of the material; a high dielectric constant would be expected to decrease the strength of the interaction between electrons and result in a lower W_{ee}. It is most significant, however, that the W_{ee} calculated for Cd_3As_2 is a factor of 10^4 larger than that quoted by Ziman for a typical metal (sodium). This is seen to be primarily connected with the much lower Fermi energy of the semiconductor. According to Ziman [22], the mean free path for electron-electron collisions is proportional to $(E_F/kT)^2$, i.e., collisions are much more likely in the material with the lower Fermi energy.

5. Conclusions

It appears that inelastic scattering processes occur in many semiconductors, but the effects are clearly noticeable only in materials with high carrier mobility and low lattice thermal conductivity. Inelastic scattering of electrons may be caused by either optical phonons or by other electrons. Scattering by optical phonons has been invoked to explain the electronic thermal conductivity of HgSe and InAs, while electron-electron scattering qualitatively explains the behavior of the electronic thermal conductivity in PbTe below 100°K and gives at least the right order of magnitude for the extra thermal resistance in Cd_3As_2. The band structure of Cd_3As_2 is thought not to be simple, and it has been proposed [18, 23] that there are two conduction bands with different effective masses. Such details may be important for the electronic thermal conductivity. It is hoped that the approximations presently available for calculating inelastic scattering processes can be improved and that more direct measurements of electronic thermal resistance in semiconductors will be made.

If one expresses all parameters in eq (1) in terms of effective mass and carrier concentration (taking u proportional to $T^{-3/2}\, m^{*-5/2}$ and ρ proportional to $m^* n^{1/3}$), then

$$W_{ee}/W_o \propto (T^{1/2} m^*)/(\epsilon^{3/2} n^{7/6}) \qquad (5)$$

The ratio $m^*/\epsilon^{3/2}$ varies from one semiconductor to another by, at most, a factor of about ten; for thermoelectric materials only, the variation is just a factor of two. Hence W_{ee} may be significant in any semiconductor that is degenerate at a relatively low carrier concentration, i.e., one that has a low effective mass.

The lattice thermal conductivity of Cd_3As_2 has been rather ignored here. In a way, the interpretation of our data is straightforward since the temperature independence of the lattice thermal conductivity clearly indicates that the phonon scattering is predominantly by impurities, both for undoped and doped Cd_3As_2. The impurities must be lattice defects, and are still presumed to be arsenic vacancies; there is still no direct evidence on this point, however.

6. Acknowledgements

We wish to thank Mr. S. B. Hladky for his part in development of the experimental apparatus and Mr. D. L. Wiegand for preparation of the samples and assistance with measurements.

7. References

[1] Spitzer, D. P., Castellion, G. A., and Haacke, G., J. Appl. Phys. 37, 3795 (1966).

[2] Ugai, Ya. A. and Zyubina, T. A., Inorganic Materials 1, 790 (1965).

[3] Swiggard, E., J. Electrochem. Soc. 114, 976 (1967).

[4] Giraudier, L., J. Phys. (Paris) 26, 129A (1965).

[5] For example: Zdanowicz, W., Acta Phys. Polon. 20, 647 (1961).

[6] Goldsmid, H. J., private communication.

[7] Goldsmid, H. J., Proc. Roy. Soc. (London) 72, 17 (1959).

[8] Taylor, P. F. and Wood, C., J. Appl. Phys. 32, 1 (1961).

[9] Conn, J. B. and Taylor, R. C., J. Electrochem. Soc. 107, 977 (1960).

[10] Busch, G., Hilti, B., and Steigmeier, E., Z. Naturforsch. 16a, 627 (1961).

[11] Damon, D. H., J. Appl. Phys. 37, 3181 (1966).

[12] Sheard, F. W., Phil. Mag. 5, 887 (1960).

[13] Aliev, S. A., Korenblit, L. L. and Shalyt, S. S., Soviet Phys. - Solid State 8, 565 (1966).

[14] Devyatkova, E. D., Soviet Phys. - Tech. Phys. 2, 414 (1957).

[15] Muzhdaba, V. M. and Shalyt, S. S., Soviet Phys. - Solid State 8, 2997 (1966).

[16] Ravich, Yu. I., Smirnov, I. A., and Tikhonov, V. V., Soviet Phys. - Semiconductors 1, 163 (1967).

[17] Hashimoto, K., Mem. Fac. Sci. Kyushu Univ., Ser. B, 2, 187 (1958) (Quoted by Drabble, J. R. and Goldsmid, H. J., Thermal Conduction in Semiconductors (Pergamon Press, (1961).

[18] Sexer, N., Phys. Status Solidi 14, K43 (1966).

[19] Sexer, N., J. Phys. Radium 22, 807 (1961).

[20] Moizhes, B. Ya. and Ravich, Yu. I., Soviet Phys. - Semiconductors 1, 149 (1967).

[21] Haidemenakis, E. D., Balkanski, M., Palik, E. D., and Tavernier, J., Bull. Am. Phys. Soc. 11, 401 (1966).

[22] Ziman, J. M., Electron and Phonons, p. 417 (Clarendon Press, 1960).

[23] Sexer, N., Phys. Status Solidi 21, 225 (1967).

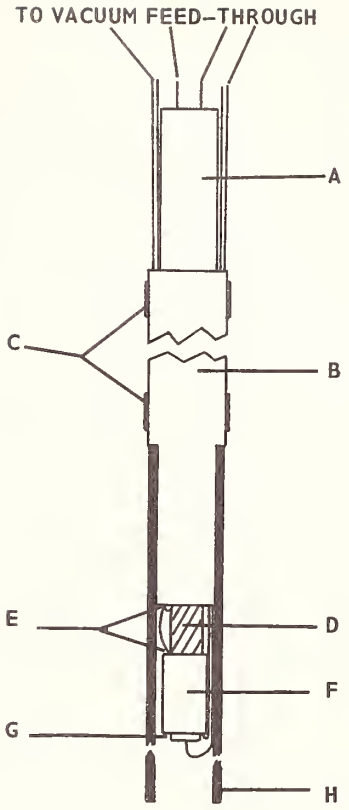

Figure 1. Thermal conductivity apparatus.
A - main heater; B - copper heat sink;
C - polytetrafluoroethylene spacers;
D - sample ; E - copper-constantan thermocouples; F - copper heater block; G - heater resistor (Corning glass); H - brass shield.
The diameter of the body of the apparatus is 1.20 cm, and the overall length is about 18 cm.

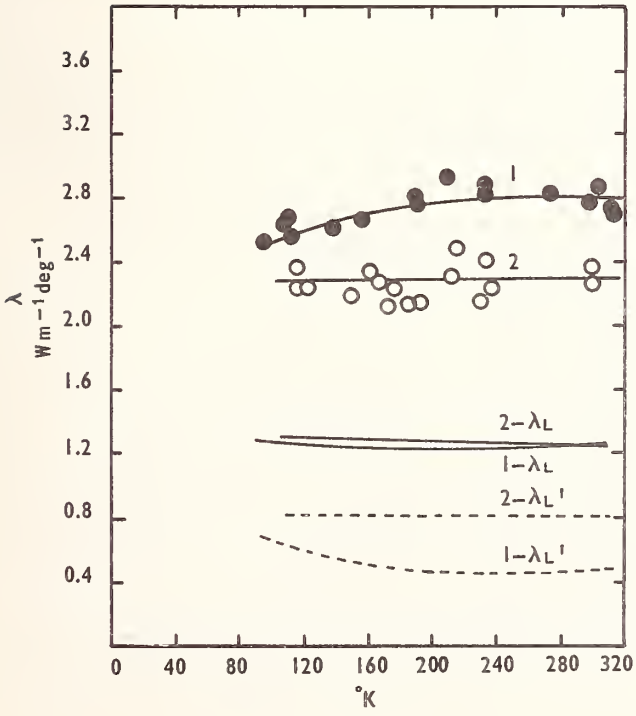

Figure 2. Total and lattice thermal conductivities of (1) Cd_3As_2 ($2 \cdot 10^{24}$ electrons/m^3) and (2) Cd_3As_2 + 0.1 wt. % Cu ($1.6 \cdot 10^{24}$ electrons/m^3) as a function of temperature.

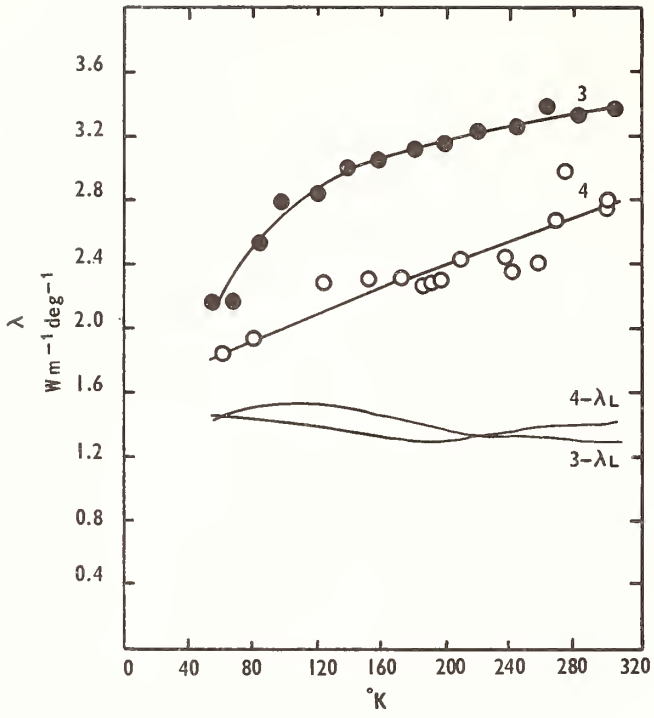

Figure 3. Total and lattice thermal conductivities of two different samples of Cd_3As_2 + 1.0 wt. % Se (about $1.5 \cdot 10^{25}$ electrons/m^3 for both samples) as a function of temperature.

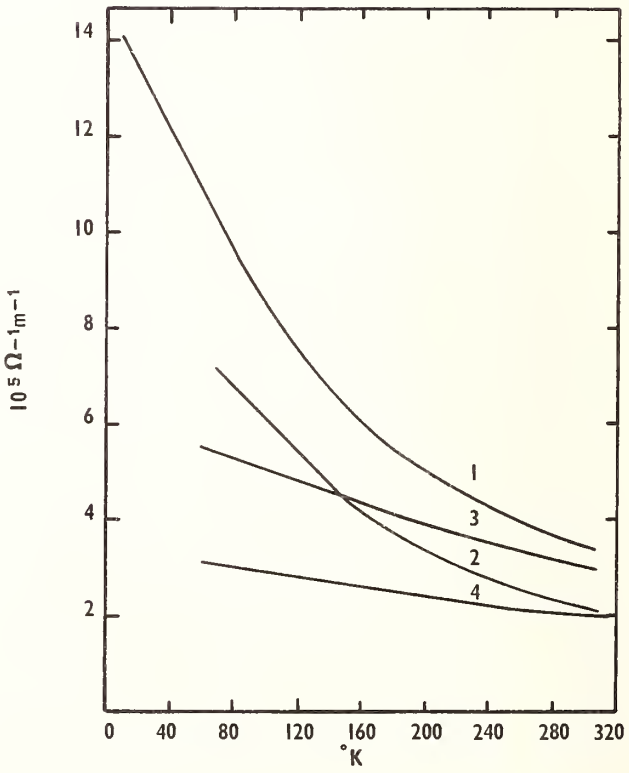

Figure 4. Electrical conductivities versus temperature for the samples of figures 2 and 3.

Measurement of Dislocation Phonon Scattering in Alloys

P. Charsley, A.D.W. Leaver and J.A.M. Salter

Department of Physics, University of Surrey
Battersea Park Road, London, S.W. 11.
England

Measurement of thermal conductivity between 1.5 and 4.2°K combined with the determination of dislocation density by transmission electron microscopy yielded values for dislocation phonon scattering in three copper aluminium alloys, and one copper zinc alloy. The results indicated that dislocation phonon scattering in copper alloys depends on both the type and amount of solute, and that the effects of dislocation arrangement are small. More careful experiments to detect any effect due to dislocation arrangements have been carried out. An experiment to measure the thermal conductivities of a deformed 12 at.% copper-aluminium alloy while held under tension near its flow stress, and while released, indicated no difference between the two cases. In an experiment on a deformed single crystal of a 12 at.% copper-aluminium alloy, a small effect ascribed to an anisotropy in the scattering of phonons by screw dislocations has been found. In both these experiments the λ/T against T graphs showed a kink at about 3°K. This may be explained by considering the scattering of phonons from edge dislocation dipoles.

Key Words: anisotropy, copper alloys, dislocations, lattice conductivity, phonon scattering.

1. Introduction

At liquid helium temperatures the thermal conductivity of annealed copper alloys with residual resistivities less than about 0.1 μΩm can be well represented by

$$\lambda = AT + BT^2 \tag{1}$$

where the quadratic term is entirely due to lattice conduction; its magnitude is limited by electron-phonon scattering which has the same dependence on phonon wave number q as the expected scattering due to individual dislocations. So the effect of plastic deformation is to reduce the value of B in eq (1). Changes in B^{-1} give values of $W_d T^2$ which is a measure of the extra thermal resistivity due to the dislocations introduced.

From measurements of $W_d T^2$ combined with the determination of dislocation densities N_d using transmission electron microscopy we have obtained values for

$$\sigma = \frac{W_d T^2}{N_d} \tag{2}$$

for some α phase copper aluminium alloys. The results, which have been submitted for publication elsewhere (1)[1], were that σ varied from $1.0 \pm .3 \times 10^{-13}$ W^{-1} m^3 deg^3 for a 2 at.% alloy to $2.1 \pm .7 \times 10^{-13}$ W^{-1} m^3 deg^3 for a 12 at.% alloy. We thought that this variation was due to the marked changes in dislocation structures with aluminium content which is observed in these alloys (2). The 12 at.% alloy has a low stacking fault energy and the dislocation structure is quite regular with the frequent occurrence of rows of dislocations of the same sign. In the 2 at.% alloy the dislocations are very tangled. It seemed possible that the higher value of σ in the 12 at.% alloy was due to the effect of dislocation pile ups. This was suggested previously by Klemens (3) as a possible explanation of the discrepancies which exist between theoretical and experimental values of σ. However, 70-30 α brass has a dislocation structure in the deformed state very similar to that found in our 12 at.% copper aluminium alloy, and the value of σ obtained by Lomer and Rosenberg was about 0.5×10^{-13} W^{-1} m^3 deg^3, (4). Believing this might be in error we made a similar measurement and

[1] Figures in brackets indicate the literature references at the end of this paper.

obtained a value for α brass of $0.4 \pm .2 \times 10^{-13}$ W^{-1} m^3 deg^3. We therefore suggested that the values of σ obtained in copper alloys depend upon both the type and amount of solute present, and that they appear to be substantially independent of dislocation arrangement.

Because this conclusion seems at variance with the strain field model for dislocation-phonon scattering we have carried out some further experiments to investigate the effect of pile ups and dislocation arrangements on the lattice thermal conductivity of a 12 at.% copper-aluminium alloy.

2. The Specimens

The alloy of nominal composition 12 at.% was prepared and analysed by the International Research and Development Co. as described previously (5). The mean composition of the ingot from which all the specimens were made was 11.3 at.% aluminium in copper.

Single crystals were grown in graphite moulds using the Bridgman technique. The polycrystalline specimens used in the under stress experiment described below were turned out from as received material and annealed for about 15 hours at 750°C before use.

3. The Experiment to Detect Pile-Ups

3.1 The Idea

The strain field of a dislocation pile-up depends upon the spacing of the dislocations in it. This can be altered by applying an external stress. The phonons are scattered by the strain field, so that if pile-ups in any number are present one might expect to find a difference between the lattice thermal conductivities of a deformed specimen while in a relaxed state and while held under tension. Since the effect of a stress is to decrease the average spacing between dislocations in a pile-up it is to be expected that a specimen under stress will have a lower conductivity than a relaxed specimen. To perform such an experiment the specimen must be constrained by a jig, and at the same time the thermal conductivity measured.

3.2 The Techniques Used in the Under-Stress Experiments

It was decided to use a jig of very high thermal conductance and to supply the heat to the specimen from the centre. Thus the two ends of the specimen are maintained at equal temperatures. The jig is shown in figure 1. Stainless steel threaded end pieces E were brazed on to the specimen S, these served both to take the nuts N, and to enable the specimen to be fitted into a tensile machine. The thermal contact from the ends of the specimen to the copper jig J were made by soldering copper wires w between them and the jig corners. The connection of the jig to the heat sink was made by a 3 mm diameter copper wire W from the centre of the cross piece B. The specimen, with a heater H and thermometers T_1 and T_2 attached as shown, was fitted in the jig and then mounted in a tensile machine. After a suitable amount of plastic deformation, and with the stress still applied, the nuts N were tightened until the stress registered on the tensile machine had dropped to zero.

The specimen is then held in the jig under tension near the flow stress, and when mounted in the cryostat and cooled to 4.2°K remains in this condition. We believe this to be the case because:

(a) Separate experiments in the tensile machine indicated that after an initial load drop of about 2% of the flow stress no load relaxation in the specimen and end pieces occurred over periods of up to 12 hours.

(b) The differential contraction between specimen and jig which occurs on cooling is of such a sign as to cause further plastic deformation.

The cryostat was similar to one previously described (5). Measurements of $\dot{Q}$ and ΔT, the temperature difference down one half of the specimen, were made between 1.5 and 4.2°K. The system was then warmed to room temperature, the nuts N loosened and removed, and the measurement of $\dot{Q}$ and ΔT repeated. For a symmetrical arrangement λ is easily calculated since half the heat produced in the heater goes in each direction; but in any case λ may be calculated knowing the size factor of the gauge length and the relative size factors of the two halves of the specimen between the heater tag and the points where the wires w are attached. A comparison of the values of λ determined in this way for a relaxed specimen in the jig with the values obtained by the standard method for the same specimen removed from the jig gave results which agreed to within 1% of λ.

4. The Experiment to Detect Anisotropy

4.1 The Idea

This is similar to the experiment carried out by Moss (6) on non-metallic crystals. We tried to prepare from a deformed single crystal specimens in which the angle between the heat current and the dislocation lines differed. This experiment is very difficult in a face centred cubic material because one must limit plastic deformation as much as possible to one slip system. This in turn limits the dislocation densities which can be introduced, and one is trying to detect small changes in $W_d T^2$ against a relatively large background of electron-phonon scattering.

4.2 Specimen Preparation

Figure 2 shows diagrammatically a single crystal of 12 at.% copper-aluminium of dimensions .2 x 10 x 2.5 cm. The operative slip plane containing the primary burgers vector $\underline{b}$ is shown. $\underline{b}$ made an angle of 10^{o} with the trace of the slip plane on the thin face of the crystal. This crystal was deformed in tension as much as possible consistent with only one slip system operating. This was judged from the absence of a significant number of slip lines on any but the primary system. (In this connection it is worth noting that Steeds and Hazzledine (7) measured the relative densities of primary and secondary dislocations in a 10 at.% copper-aluminium alloy after 45% shear strain. They found that the density of the primary dislocations was about four times that of the secondary dislocations.) Then the directions in the crystal of the primary edge and screw dislocations may be determined. Two specimens of the shape shown in figure 2 complete with thermometer tags T were obtained by cutting perpendicular to the large face ABCD of the crystal. This was done by spark machining. In one specimen, referred to here-after as cross 1, the orientation of the cross was chosen such that the primary edge dislocations made equal angles with both arms $A_1 A_2$ and $B_1 B_2$. The angle between the screw dislocations and these two directions however differed. In cross 2 the situation with regard to the edge and screw dislocations was reversed. Thus a comparison of the thermal conductivities of the two arms of cross 1 or of the two arms of cross 2 will show any anisotropy in the scattering of phonons by screw and edge dislocations respectively.

One arm of each cross made an angle of about 30^{o} with the tensile axis so that it is reasonable to assume equal mean dislocation densities and the same dislocation structures for both arms of any one cross.

5. Results

5.1 The Jig Experiment

The results for the measurements done in the jig are shown in figure 3. The upper set of points is for the single crystal. This had been deformed about 20% in tension to a stress of 7 kg mm^{-2}. The lower set of points is for the polycrystal which was deformed by about 5% at a stress of 20 kg mm^{-2} For both specimens the open circles refer to the relaxed condition. Note that the ordinates for the two specimens are shifted relative to one another.

The vertical arrows on the graph indicate $\pm$ 1% $\frac{\lambda}{T}$ and within this range, (a) there is no significant difference between the measurements under stress or relaxed for either the poly or the single crystal, and (b) straight lines may be drawn through the points. However, the scatter on the individual curves is considerably less than $\pm$ 1%, and in the case of the polycrystal the relaxed measurements give lower values throughout the temperature range. This is the opposite of what one would expect for pile-ups, and any change in size factor caused by the elastic deformation of the specimen under tension can only increase this difference. Moreover, if one joins up the points the λ/T against T plots appear as a curve for the single crystal under stress, but more like a kinked straight line for the remaining three sets of points.

5.2 The Anisotropy Experiment

The flat single crystal was deformed about 25% in tension at a flow stress of 6 kg mm^{-2}. This took the crystal through stage I of the work hardening curve and into the beginning of stage II. The table below gives the angles between the heat current and the primary edge and screw dislocations for each cross. The edges in cross 1 were not at exactly the same angle due to the rotation of the crystal axis during deformation.

Table 1. The angles between the primary dislocations and the heat flow for the directions measured. The graphical symbols used in figure 4 are also given.

	Cross 1		Cross 2	
	$A_1 A_2$	$B_1 B_2$	$A_1 A_2$	$B_1 B_2$
Angle to Edges	55^o	63^o	80^o	46^o
Angle to Screws	35^o	73^o	52^o	52^o
Graphical Symbol	○	□	▽	×

The results of the thermal conductivity measurements are shown in figure 4. The graphical symbols used are indicated in table 1, and the points for cross 2 are shown displaced to the right by 0.6^oK. Almost all the points can be made to lie within ± 1% λ/T of the same straight line. Taken at their face value each set of points is better represented by a kinked straight line as drawn in figure 4. The results for cross 2 indicate that there is no detectable anisotropy due to edge dislocations. The vertical difference between the results for the two arms of cross 1 cannot be considered significant since each direction involves the measurement of a different size factor. Nevertheless, for cross 1 in the region above about 3^oK, the points for arm A_1A_2 lie on a line of greater slope than those for arm B_1B_2. This would be consistent with an anisotropy in the scattering of phonons by screw dislocations.

5.3 Evidence that the Kink is Real

The drawing of other than straight lines through the points for the λ/T against T plots needs justification. The effect looks like a systematic error. It cannot be due to the superfluid transition in liquid helium because it occurs well above this. We measured cross 1 in the direction A_1A_2 in a different cryostat using different thermometers and heater. The two sets of measurements are shown in figure 5. They agree extremely well. Recent measurements in this latter cryostat of the thermal conductivity of an annealed and deformed 2 at.% alloy gave very good straight lines in both cases with all the points within ± 0.2% λ/T of the lines. We are at present carrying out further test experiments.

6. Discussion

No effect corresponding to the expected behaviour of dislocation pile-ups was observed in the jig experiments. For the polycrystal the difference between the two measurements, under stress and relaxed, could be significant but it is in the opposite direction to that expected.

The limitations on the dislocation density which can be introduced in the anisotropy experiments together with the results obtained indicate perhaps the unsuitability of a face centred cubic alloy. The experiment might be better done using an alloy with a hexagonal close packed structure in which slip only occurred on the basal planes. Nevertheless, considering the results for cross 1 in the temperature region above the kink there is a difference in the slopes of the λ/T against T plots for the two arms. The smaller slope occurs for direction B_1B_2 in which the screw dislocations make a greater angle with the heat flow in agreement with the expected behaviour (6).

There still remains the kink in the λ/T against T graphs which occurs in all the specimens. This kink is not present in annealed and deformed alloys of 2 at.% copper-aluminium. We believe that it may be due to the presence of large numbers of dislocation dipoles in the deformed 12 at.% alloy. The deformation of annealed single crystals of this alloy in the early stages proceeds by the formation of localized bands of slip, separated by regions in which comparatively little or no slip has occurred. As the deformation proceeds the bands get wider and fresh bands appear until at the end of stage I the crystal is uniformly covered with slip. Recently Mitchell et al (8) studied the dislocation structure of these bands in an 8 at.% copper-aluminium alloy in the first few percent of plastic deformation. They found that the dislocations in the bands of deformation were present in the form of interleaved pile-ups of parallel positive and negative edge dislocations. The distance between the glide planes on which the adjacent groups of dislocations of opposite sign occurred varied from about 50 angstroms to a few microns. Steeds and Hazzledine (7) also found large numbers of dipole groups in their 10 at.% alloy.

The effect of dipoles on lattice thermal conductivity has been discussed by Moss (6); it depends upon the relative sizes of the dipole spacing d and the dominant phonon wave length given by $\ell = 0.6\, a\, \frac{\theta}{T}$ where a is the lattice spacing and θ the Debye temperature. For $\ell \ll d$ the phonons see a dipole as separate dislocations giving the usual q^{-1} wave number dependence for the dislocation phonon scattering relaxation time. For $\ell \gg d$, the phonons see the equivalent of a line of point defects, the relaxation time is proportional to q^{-3}, and the scattering is less effective than that from two isolated dislocations for the same ℓ.

For a fixed value of d, as the temperature is lowered, there will come a point where the phonons will begin to see the dipole aspect of the dislocation arrangement. The phonon scattering will then begin to decrease from the value expected for a random arrangement of dislocations sufficient to account for the phonon scattering at higher temperatures. Correspondingly the values of λ/T will begin to lie above a line extrapolated from the higher temperatures.

Moss (6) has suggested that this change will begin when $\ell \simeq 2d$. In our alloys the kink occurs at about $3^{\circ}K$ where the dominant phonon wavelength is about 200 angstroms. So to account for the effect observed, the majority of the dipoles must have a spacing of about 100 angstroms. This is consistent with the available electron microscope evidence. What one might expect to happen at lower temperatures is that the λ/T against T plots would turn again, but in the opposite direction to a line whose slope would correspond to the scattering from electrons and the residual density of randomly distributed dislocations.

The effect of an external stress on a sheet of dislocation dipoles will be to move one set of dislocations relative to the other but not to change the relative spacing of dislocations of a given sign. Thus a null effect in the under-stress experiment is readily explained on the assumption that the majority of the piled-up groups of dislocations exist in dipole sheets. The effect in the 'wrong' direction might be explainable in terms of an overall decrease in dipole spacings under the action of the applied stress.

With regard to our values for $\sigma(1)$. Neglecting the existence of the kink in deformed copper-aluminium alloys of the higher compositions could lead to an over estimate of the values of $W_d T^2$ obtained. At the worst, the values we obtained would be one-and-a-half times too big.

7. References

(1) Charsley, P., Salter, J.A.M. and Leaver, A.D.W. An experimental investigation of dislocation-phonon scattering in some copper alloys. Submitted to phys. stat. sol for publication.

(2) Swann, P.R. and Nutting, J. The influence of stacking-fault energy on the modes of deformation of polycrystalline copper alloys. J.Inst. Met. 90 133 (1961)

(3) P.G. Klemens. Thermal conductivity and lattice vibrational modes. Solid State Physics 7 1 (1958)

(4) Lomer, J.N. and Rosenberg, H.M. The detection of dislocations by low temperature heat conductivity measurements. Phil. Mag. 4 467 (1959)

(5) Charsley, P. and Salter, J.A.M. The lattice thermal conductivities of annealed copper-aluminium alloys. phys. stat. sol. 10 575 (1965)

(6) Moss, M. Effect of plastic deformation on the thermal conductivity of calcium fluoride and lithium fluoride. J. Appl. Phys. 36, 3308 (1965)

(7) Steeds, J.W. and Hazzledine, P.M. Dislocation configurations in deformed copper and copper 10 at.% aluminium alloy. Disc. of Faraday Soc. 38 103 (1964)

(8) Mitchell, J.W., Chevrier, J.C., Hockey, B.J. and Monaghan, J.P. Jr. The nature and formation of bands of deformation in single crystals of α-phase copper aluminium alloys. Can. J. Phys. 45 453 (1967)

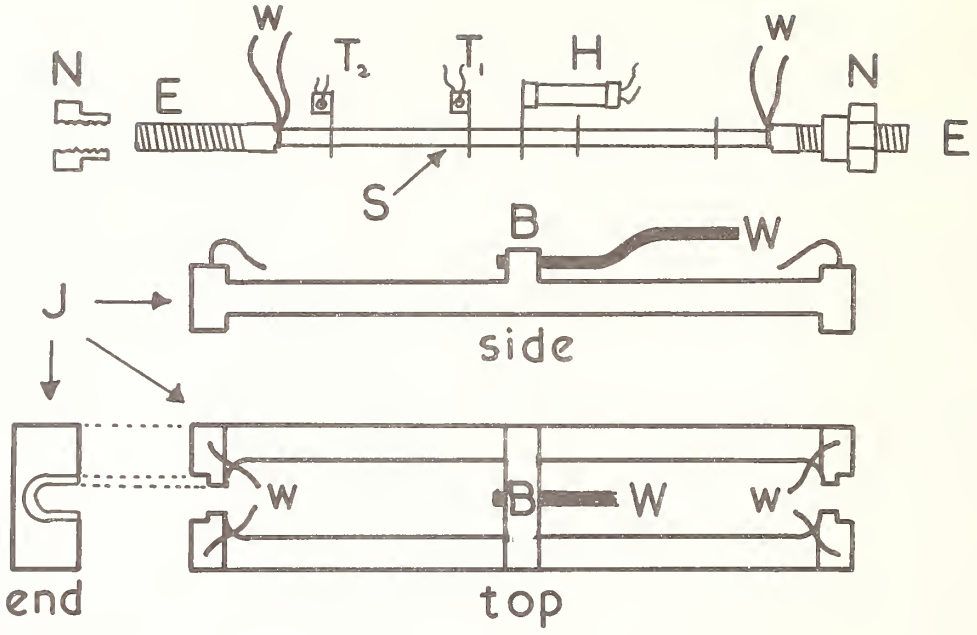

Figure 1 The specimen and jig. See section 3.2 of the text for explanation.

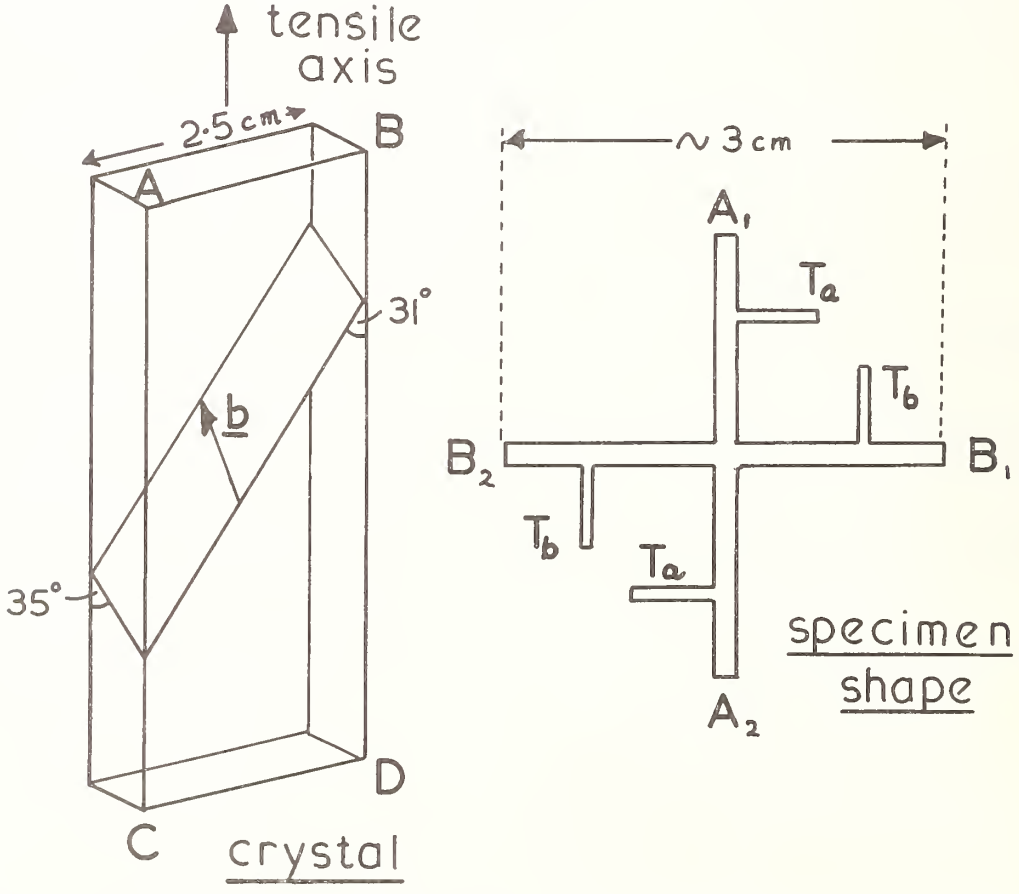

Figure 2 The single crystal and specimen shape. The trace of the primary slip plane on the crystal faces is shown. b is the primary burgers vector.

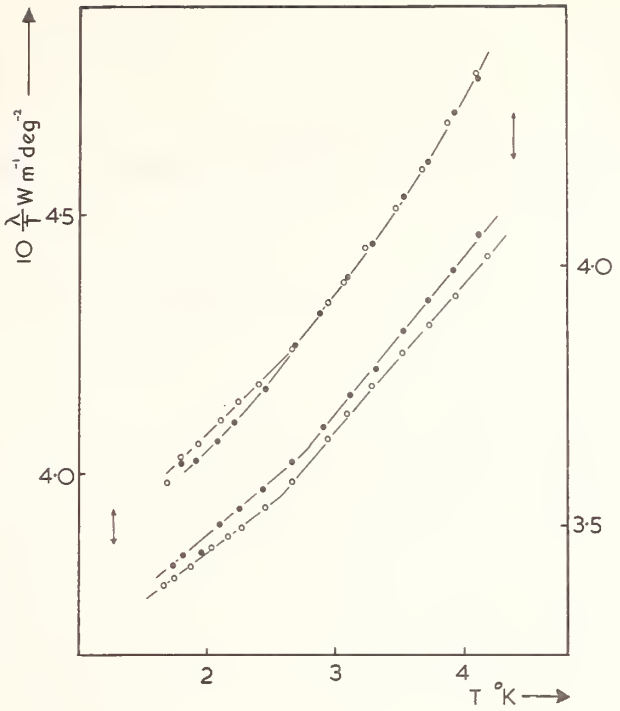

Figure 3 $\frac{\lambda}{T}$ against T for the specimens measured in the jig. The open circles are for the relaxed condition. The lower set of points and the right hand $\frac{\lambda}{T}$ axis refer to the polycrystal.

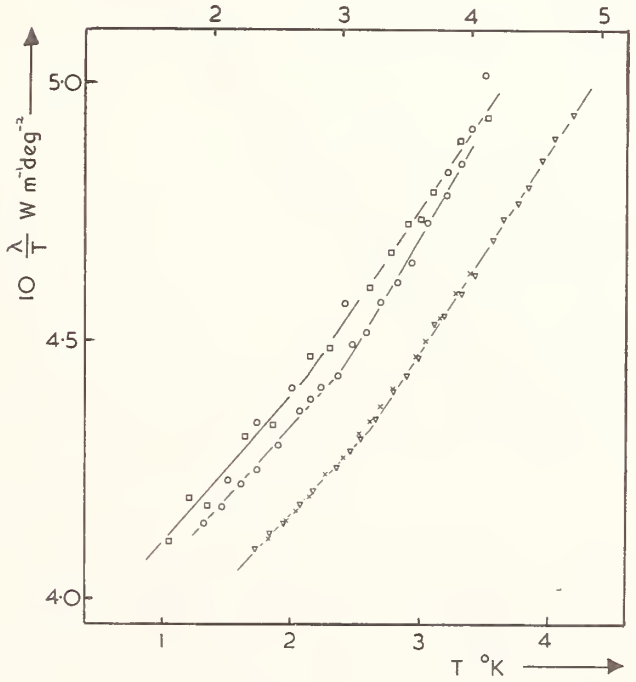

Figure 4 $\frac{\lambda}{T}$ against T for the cross shaped specimens. The lower temperature scale refers to the right hand set of points which are for the two directions of cross 2. For a further indication of which points refer to which directions see table 1 in section 5.2.

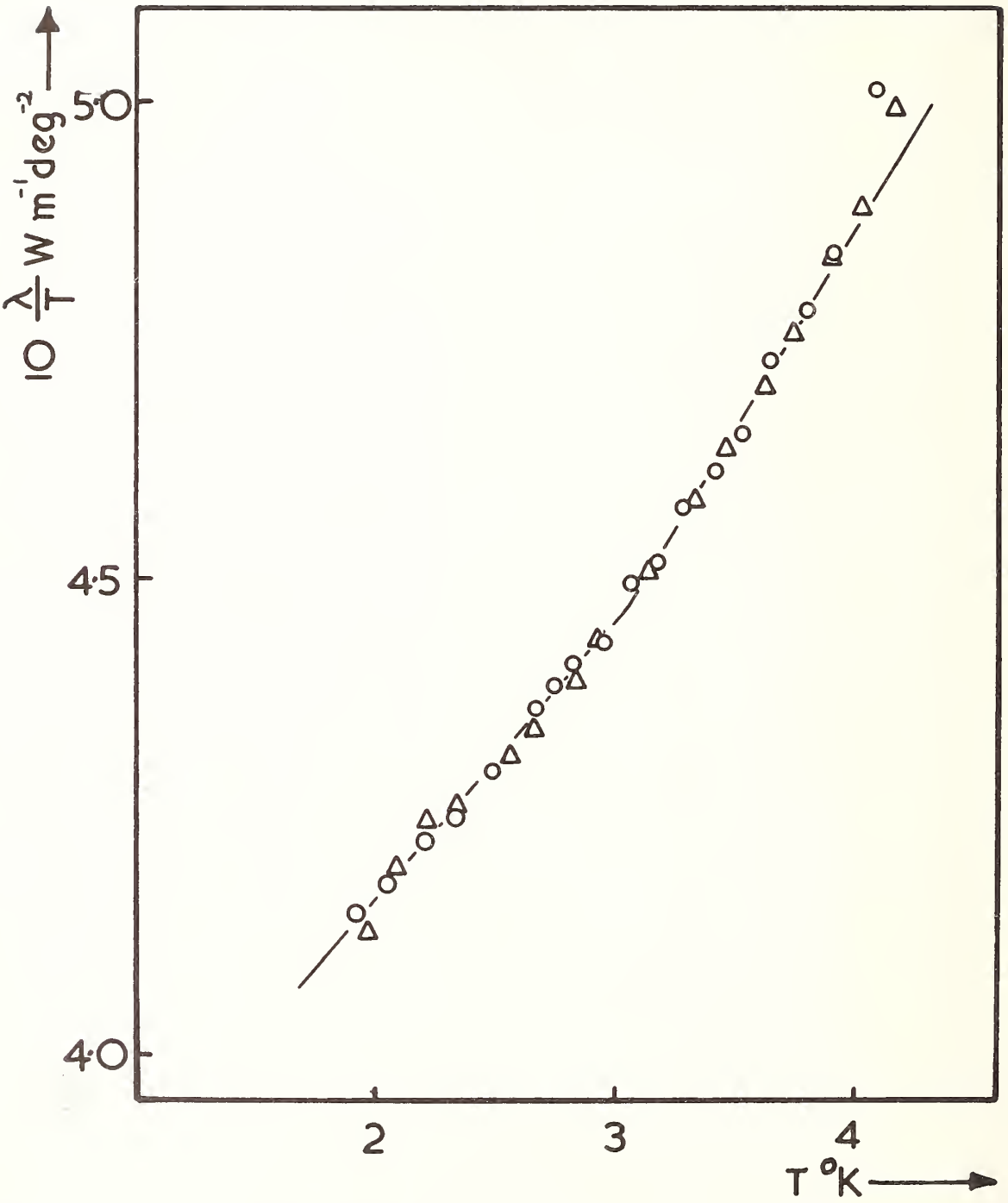

Figure 5 $\frac{\lambda}{T}$ against T for the direction A_1A_2 of cross 1 measured in two different cryostats. The triangles refer to the second cryostat.

The Thermal Resistivity Resulting From the Combined Scattering of Phonons by Edge Dislocation Dipoles and by Normal Processes

P. P. Gruner

Boeing Scientific Research Laboratories
P.O. Box 3981
Seattle, Washington 98124

The thermal resistivity due to the scattering of phonons by edge dislocation dipoles and by normal three-phonon processes has been calculated. Deviations from the normal T^{-2} - dependence of the resistivity (T:absolute temperature), which is due to the scattering of phonons by isolated dislocations, occur at temperatures where the dominant wavelength of the phonons is larger than the distance between the two dislocations of the dipole. It is found that the resistivity becomes independent of the temperature in the neighborhood of $T \sim 0$ and remains finite at T=0. Towards high temperatures the resistivity due to dipoles approaches asymptotically the resistivity which is due to isolated dislocations. Numerical results were obtained with the material constants of copper. The temperature above which the resistivity differs less than 10 % from the asymptotic value is given by $T=370\ (|\vec{B}|/R)$ °K ($\vec{B}$:Burgers vector, R:dislocation distance).

The interactions of the phonons with the dipoles were treated by non-linear elasticity theory which includes also the normal three-phonon interaction. The Boltzmann equation was solved with the variational method.

Key Words: Boltzmann equation, edge dislocation dipole, lattice thermal conductivity, non-linear elasticity theory, normal processes, variational method.

1. Introduction

The possibility to distinguish between different kinds of lattice defects by measurements of the lattice thermal conductivity as a function of the temperature is based on two facts. Firstly, the scattering cross-sections of various kinds of defects are characteristic functions of the phonon wavelength. Secondly, the phonon spectrum depends at low temperatures strongly on the temperature. On account of these features the thermal resistivities due to various kinds of defects show characteristic temperature dependencies.

Yet, the thermal resistivity does not only depend on the type of the scatterers, it also depends on the arrangement of the defects. If the defects are far apart from each other and are distributed in a random manner then the scattering is incoherent. Then, the total scattering cross-section of a particular kind of defect is simply the sum of the single scattering cross-sections. In case of deviations from a random distribution of defects, the various phases of the scattered waves must be taken into account; the scattering cross-section contains a coherent part as well as an incoherent part. The contribution due to the coherent scattering will be significant if the distance between the defects is comparable with the dominant phonon wavelength.

Investigations of the thermal resistivity due to pile-ups of screw dislocations [1][1] and of edge dislocations [2] show that coherent scattering is not negligible below a certain temperature. The coherent part of the scattering gives rise to an increase in the resistivity. It also leads to deviations from the normal quadratic temperature dependence of the thermal conductivity, which arises from scattering of phonons by randomly distributed dislocations. In order to give a value for the temperature[2] below which the arrangement of the dislocations becomes significant, we mention the result which was obtained for a group of dislocations piled up under a stress against an obstacle. In case of screw dislocations, the arrangement becomes significant below 2.5°K. The corresponding value for edge dislocations is 13.5°K. These data were calculated with the material constants of copper. The resolved shear stress was assumed to be 10^{-3} G (G:shear modulus). The number of dislocations within the group was 15.

[1] Figures in brackets indicate the literature references at the end of this paper.

[2] The limiting temperature is defined as that temperature above which the relative difference between the resistivity due to randomly distributed dislocations and due to dislocation groups is smaller than 10%.

Another important example where the resistivity strongly depends on the arrangement of the dislocations is the dipole configuration. In this case two parallel edge dislocations of opposite signs are separated by a distance R which is small compared with other dislocation distances. A few qualitative conclusions on the thermal resistivity due to this kind of defect can be drawn without calculation. The lattice thermal conductivity which is limited by a dislocation dipole must be one half of the conductivity which is limited by an isolated dislocation if the distance between the two dislocations is sufficiently large. At high temperatures, where most of the energy is transported by phonons with wavelengths shorter than the distance R , one expects also the resistivity due to a dipole to be twice that which is due to a single dislocation. If the distance R is small, however, parts of the strain fields cancel since the two dislocations have opposite signs. Hence, decreasing distances between the dislocations of a dipole lead to a reduction of the resistivity. Thus, whereas in case of phonon scattering by dislocation pile-ups the resistivity increases with decreasing separation between the dislocations, the contrary is true in case of the phonon-dislocation dipole interaction.

Before presenting an outline of the theory which was used for the calculation of the thermal resistivity, we anticipate a result of the following calculations concerning the convergence of the conductivity integral. It turns out that the scattering by dipoles alone is not strong enough in order to produce a non-zero resistivity. The partial cancellation of the strain fields gives rise to a rapid drop of the scattering strength for long wavelength phonons. On account of this decrease of scattering strength the energy current carried by the low frequency phonons will not reach a stationary state. A natural way out of this situation is given by taking into account the normal three-phonon interactions. These latter interactions contain processes which diminish the rapid drop of the scattering strength for long wavelength phonons [3].

It must be noted that the normal processes themselves cannot produce a non-zero resistance, as was first shown by Peierls [4]. The conservation of the quasi-momentum of the phonon gas, which is a characteristic feature of these interactions, prevents the phonons from reaching a stationary state. But, in connection with the phonon scattering by lattice defects, which destroys the conservation of the momentum, the normal processes are important.

2. Outline of the Theory

2.1 The Classical Hamiltonian of the Lattice Vibrations

We are interested in the scattering of phonons at low temperatures. In this temperature region the wavelengths of the excited phonons are large compared with the lattice constant. We can therefore treat the dynamics of the lattice waves with continuum theory. For convenience we shall restrict ourselves to an isotropic continuum. The interactions between the lattice waves and the defects are in this model treated by deviations from Hooke's law. We shall take into account deviations from Hooke's law up to terms which are quadratic in the strains. Bross [5] showed that the potential energy density of the lattice vibrations in an isotropic continuum which contains lattice defects is of the form

$$\Psi = \Psi\left\{A_i;\ \varepsilon_I,\ \varepsilon_{II};\ \gamma_I,\ \gamma_{II},\ \gamma_{III};\ (\varepsilon\gamma)_{II},\ (\varepsilon\varepsilon\gamma)_{III},\ (\varepsilon\gamma\gamma)_{III}\right\} \tag{2.1a}$$

if one retains only terms up to the order $\varepsilon^n \gamma^{3-n}$ (n=0,1,2,3). ε and γ are the strains produced by the defects and by the lattice vibrations, respectively. The subscripts I, II, and III refer to first, second, and third invariants of the strain tensors. Consistent with the above approximation is that the strains which enter eq (2.1a) are those which are calculated with linear elasticity theory. A_1 and A_2 are the constants of the linear theory, whereas the constants of the non-linear theory are denoted by A_3, A_4, and A_5. The A_i are related to Lamé's constants λ and μ and to Murnaghan's constants [6] l, m, and n by

$$A_1=(\lambda+2\mu)/2,\ A_2=-2\mu,\ A_3=(1+2m)/3,\ A_4=-2m,\ A_5=n\ . \tag{2.1b}$$

The Hamiltonian of the lattice vibrations is

$$H = (1/2)\int \rho\ (\dot{\vec{s}})^2 dV + \int \Psi\ dV\ . \tag{2.2}$$

It must be noted that all quantities in eq (2.2) refer to the statically deformed state which is produced by the lattice defects alone. ρ is the mass density and $\vec{s}$ is the displacement of the volume element dV due to the lattice vibrations.

2.2 Quantum Mechanics of the Phonon Interactions

The transition to quantum mechanics is done in the usual way. The displacement field which results from the lattice vibrations is decomposed in a set of normal modes. The complex normal coordinates $a^+(\vec{k},j)$ and $a(\vec{k},j)$, which are in the classical case amplitudes of plane waves (with wave vector $\vec{k}$ and polarization index j), are in quantum mechanics operators. These operators create or annihilate a phonon if they are applied to a wave function ψ which describes the state of the phonon gas[3]:

$$a^+(\vec{k})\ \psi\ (N_{\vec{k}}) = (N_{\vec{k}}+1)^{1/2}\ \psi\ (N_{\vec{k}}+1)\ , \tag{2.3a}$$

$$a(\vec{k})\ \psi\ (N_{\vec{k}}) = (N_{\vec{k}})^{1/2}\ \psi\ (N_{\vec{k}}-1)\ . \tag{2.3b}$$

$N_{\vec{k}}$ is the number of phonons in the mode $\vec{k}$. The Hamilton operator which corresponds to eq (2.2) can be written as

$$H = H_0 + V_D + V_N \tag{2.4a}$$

with the Hamilton operator of the undisturbed phonon gas[4]

$$H_0 = \sum_{\vec{k}} \hbar\omega(\vec{k})\ \left\{a^+(\vec{k})a(\vec{k}) + 1/2\right\}\ . \tag{2.4b}$$

The frequency $\omega(\vec{k})$ of the mode $\vec{k}$ is in the continuum approximation given by

$$\omega(\vec{k}) = v|\vec{k}|\ . \tag{2.4c}$$

The sound velocity, denoted by v, can have two different values, one for the longitudinal waves and another for the transversal waves. V_D and V_N are the operators for the phonon-defect interaction and the normal three-phonon interaction. The phonon-defect operator can be represented in the form

$$V_D = \sum_{\vec{k},\vec{k}'} V(\vec{k},\vec{k}')\ a^+(\vec{k})a(\vec{k}') + \text{other terms quadratic in the operators } a \tag{2.4d}$$

with

$$V(\vec{k},\vec{k}') = A_i\ [\vec{e}(\vec{k})\cdot\vec{e}(\vec{k}')]\ (\vec{k}\cdot\vec{k}')\ \tilde{\varepsilon}_I(\vec{g}) + \cdots\ . \tag{2.4e}$$

$\vec{e}(\vec{k})$ is a polarization vector and $\tilde{\varepsilon}$ is the Fourier transform of ε. The coefficients $V(\vec{k},\vec{k}')$ vanish, unless

$$\vec{k} + \vec{k}' + \vec{g} = 0. \tag{2.4f}$$

Equation (2.4f) shows that the wave vector is not conserved in collisions of the phonons with defects. The consequence is that the quasi-momentum of the phonon gas will be changed in the phonon-defect interaction. The phonon-phonon interaction operator can be written as

$$V_N = \sum_{\vec{k},\vec{k}',\vec{k}''} V(\vec{k},\vec{k}',\vec{k}'')a^+(\vec{k})a^+(\vec{k}')a(\vec{k}'') + \text{other terms cubic in the operators } a. \tag{2.4g}$$

---

[3] In the following equations we denote the mode $(\vec{k},j)$ by $\vec{k}$.

[4] $\hbar$ is Planck's constant divided by 2π

The coefficient $V(\vec{k},\vec{k}',\vec{k}'')$ is a function of products between polarization vectors and wave vectors and does not contain the strain field of the defects. $V(\vec{k},\vec{k}',\vec{k}'')$ vanishes, unless

$$\vec{k} + \vec{k}' + \vec{k}'' = 0 \quad . \tag{2.4h}$$

Both coefficients, $V(\vec{k},\vec{k}')$ and $V(\vec{k},\vec{k}',\vec{k}'')$, are explicitly represented in Reference [5]. Scattering processes of the type (2.4h) are called normal processes. As already mentioned, the quasi-momentum of a phonon gas in which the phonons interact only by normal processes is conserved. This conservation has the consequence that the thermal conductivity is infinite if the phonons were not in addition scattered by those processes (eq(2.4f)) which destroy the conservation of the quasi-momentum.

The operators V_D and V_N, if acting on the wave function ψ, cause transitions from one phonon state to another. The probability rate for those transitions can be calculated with the help of time dependent perturbation theory. Having the probability rate, one calculates the total rate of change of the number of phonons in mode $\vec{k}$. The result can be written in the following form:

$$\begin{aligned}(d\bar{N}_{\vec{k}}/dt)_{\text{collision}} &= \sum_{\vec{k}'} W(\vec{k},-\vec{k}')(\bar{N}_{\vec{k}}',-\bar{N}_{\vec{k}}) \\ &+ \sum_{\vec{k}',\vec{k}''} W(\vec{k},\vec{k}',-\vec{k}'')[(\bar{N}_{\vec{k}}+1)(\bar{N}_{\vec{k}}'+1)\bar{N}_{\vec{k}}'' - \bar{N}_{\vec{k}}\bar{N}_{\vec{k}}'(\bar{N}_{\vec{k}}''+1)] \\ &+ \text{two similar expressions} \quad .\end{aligned} \tag{2.5a}$$

$\bar{N}_{\vec{k}}$ is the mean number of phonons in the mode $\vec{k}$ and is defined by

$$\bar{N}_{\vec{k}} = \sum N_{\vec{k}} P(\ldots N_{\vec{k}}\ldots,\ldots\tilde{N}_{\vec{k}}\ldots,t) \quad , \tag{2.5b}$$

where the summation runs over all phonon states $(\ldots N_{\vec{k}}\ldots)$. P obeys the master equation and is the probability of finding $N_{\vec{k}}$ phonons at a time t in mode $\vec{k}$ if there were $\tilde{N}_{\vec{k}}$ phonons in the same mode at $t=0$. The quantities $W(\vec{k},-\vec{k}')$ are, except for the mean phonon numbers $\bar{N}_{\vec{k}}$, equal to the probability per unit time for a transition from mode $\vec{k}$ to mode $\vec{k}'$ which is caused by the phonon-defect interaction. It is

$$W(\vec{k},-\vec{k}')=2\pi(2\pi)^6(V_0\rho_0)^{-2}|V(\vec{k},-\vec{k}')|^2[\omega(\vec{k})\omega(\vec{k}')]^{-1}\delta\left\{\omega(\vec{k})-\omega(\vec{k}')\right\}, \tag{2.5c}$$

where V_0 and ρ_0 are the crystal volume and the mass density in the undeformed state, respectively. Equation (2.5c) shows that the scattering by static defects is elastic, i.e., the energy of the incident phonon must be equal to the energy of the scattered phonon:

$$\hbar\omega(\vec{k}) = \hbar\omega(\vec{k}') \quad . \tag{2.6}$$

The transitions due to normal processes between three phonon states are governed by two selection rules which follow from the corresponding transition probabilities [5]. One of the selection rules we have already met in eq (2.4h). For transitions in which, for example, one phonon of mode $\vec{k}''$ is annihilated and one phonon in each of the modes $\vec{k}$ and $\vec{k}'$ is created, eq (2.4h) reads

$$\vec{k}'' = \vec{k} + \vec{k}' \quad . \tag{2.7a}$$

On the other hand, the transition probability per unit time, $W(\vec{k},\vec{k}',-\vec{k}'')$, for the processes under consideration vanishes, unless

$$\omega(\vec{k}'') = \omega(\vec{k}) + \omega(\vec{k}') \quad . \tag{2.7b}$$

The consequences of the selection rules (2.7) will be discussed later on.

2.3 The Transport Equation

A temperature gradient changes the distribution of the phonons in thermal equilibrium[5],

$$\bar{\bar{N}}_{\vec{k}} = [\exp(\hbar\omega/KT) - 1]^{-1} , \tag{2.8}$$

until, on account of the various scattering mechanisms, a stationary state is reached. The change of the mean phonon numbers, $\bar{N}_{\vec{k}}$, per unit time which is caused by the field of the temperature gradient is

$$\dot{\bar{N}}_{\vec{k}}|_{field} = - [\vec{v}(\vec{k})\cdot \mathrm{grad}T](\partial\bar{\bar{N}}_{\vec{k}}/\partial T) , \tag{2.9}$$

where $\vec{v}(\vec{k})$ is the group velocity. In the stationary state the total rate of change of the mean phonon numbers must vanish. This yields

$$\dot{\bar{N}}_{\vec{k}}|_{field} + \dot{\bar{N}}_{\vec{k}}|_{collision} = 0 . \tag{2.10}$$

The Boltzmann equation (2.10) is an integral equation for the mean phonon numbers $\bar{N}_{\vec{k}}$. It is convenient to subtract from the occupation numbers $\bar{N}_{\vec{k}}$ of the stationary state their thermal equilibrium value and to write

$$\bar{N}_{\vec{k}} - \bar{\bar{N}}_{\vec{k}} = (1/T)(\vec{X}_{\vec{k}}\cdot \mathrm{grad}T)(\partial\bar{\bar{N}}_{\vec{k}}/\partial\hbar\omega) . \tag{2.11}$$

The unknown vector function $\vec{X}_{\vec{k}}$ must be obtained by solving the integral equation (2.10). If we know $\vec{X}_{\vec{k}}$, we find from the energy current density

$$\vec{q} = (1/V_0) \sum_{\vec{k}} \hbar\omega(\vec{k})\bar{N}_{\vec{k}}\vec{v}(\vec{k}) = (1/V_0T) \sum_{\vec{k}} \hbar\omega(\vec{k})\vec{v}(\vec{k})[\vec{X}_{\vec{k}}\cdot \mathrm{grad}T](\partial\bar{\bar{N}}_{\vec{k}}/\partial\hbar\omega) \tag{2.12a}$$

the tensor of the thermal conductivity

$$\kappa = -(1/TV_0) \sum_{\vec{k}} \hbar\omega(\partial\bar{\bar{N}}_{\vec{k}}/\partial\hbar\omega)\ \vec{v}(\vec{k})\vec{X}_{\vec{k}} . \tag{2.12b}$$

2.4 Approximate Solution of the Transport Equation

Usually, the transport problem has been solved by introducing the concept of relaxation times [7]. This approximation, however, is doubtful in case of the normal three-phonon interaction. Callaway [8] showed, by taking into account the fact that the quasi-momentum of the phonon gas is conserved in normal three-phonon collisions, how one has to modify the concept of relaxation times. A justification of Callaway's method was given by Krumhansl [9]. But, even if the introduction of relaxation times is justified, it is often not easy to calculate them in a rigorous way. In order to avoid the shortcomings of the relaxation time approximation, we used the variational method for the solution of the transport equation. This method allows to control the approximations which are made and permits to distinguish between different polarization branches. No distinction between phonons in different polarization states is made in the relaxation time approach.

We describe now, in short, the variational method. Substituting eq (2.11) into eq (2.10) yields

$$L\{\vec{X}_{\vec{k}}\} = \hbar\omega(\partial\bar{\bar{N}}_{\vec{k}}/\partial\hbar\omega)\vec{v}(\vec{k}) . \tag{2.13}$$

---

[5] K is Boltzmann's constant

The linear integral operator L, which we shall not present here, can easily be found from the right hand side of eq (2.5a)[6]. With eq (2.13) the tensor of the thermal conductivity (2.12b) can be written as

$$\kappa = - (1/TV_0) \sum_{\vec{k}} \vec{X}_{\vec{k}} L\left\{\vec{X}_{\vec{k}}\right\} . \tag{2.14}$$

On account of the symmetry of the transition probabilities $W(\vec{k},\vec{k}')$ and $W(\vec{k},\vec{k}',\vec{k}'')$, with respect to the indices $\vec{k}$, $\vec{k}'$, and $\vec{k}''$, one can show that for two arbitrary functions Y_1 and Y_2

$$\sum_{\vec{k}} Y_1 L\left\{Y_2\right\} = \sum_{\vec{k}} Y_2 L\left\{Y_1\right\} , \tag{2.15a}$$

and that

$$- \sum_{\vec{k}} Y L\left\{Y\right\} \geq 0. \tag{2.15b}$$

We choose now some arbitrary vector function $\vec{Z}(\vec{k})$, which will be specified later on, on which we impose the conditions

$$\vec{Z}(-\vec{k}) = - \vec{Z}(\vec{k}) \tag{2.16a}$$

and

$$\sum_{\vec{k}} Z_i(\vec{k}) L\left\{Z_i(\vec{k})\right\} = \sum_{\vec{k}} \hbar\omega(\partial\bar{\bar{N}}/\partial\hbar\omega) v_i(\vec{k}) Z_i(\vec{k}) = \sum_{\vec{k}} Z_i(\vec{k}) L\left\{X_i(\vec{k})\right\} \tag{2.16b}$$

Condition (2.16a) is chosen since only the odd part of $\vec{Z}(\vec{k})$ contributes to the conductivity (2.12b). On account of the condition (2.16b) and eqs (2.15a) and (2.15b), it follows that among all vector functions $\vec{Z}(\vec{k})$ the exact solution $\vec{X}(\vec{k})$ leads to a maximum of the expression $- \sum Z_i L\{Z_i\}$. One finds

$$- \sum_{\vec{k}} Z_i(\vec{k}) L\left\{Z_i(\vec{k})\right\} \leq - \sum_{\vec{k}} X_i(\vec{k}) L\left\{X_i(\vec{k})\right\} . \tag{2.17}$$

From this inequality it follows that among all arbitrary functions $\vec{Z}(\vec{k})$ those which make the left hand side of (2.17) a maximum lead together with eq (2.12b) to the exact diagonal components of the conductivity tensor. We choose as a trail function the expansion

$$\vec{Z}(\vec{k}) = \sum_{r=0}^{\infty} \sum_{n=1}^{\infty} \sum_{m=-n}^{n} \vec{Z}(j,m,n,r)(\hbar\omega)^r Y_{nm}(\Theta,\phi) . \tag{2.18}$$

Since $\vec{Z}(\vec{k})$ depends, according to our convention that $\vec{k}$ stands for $\vec{k}$ and j, on the polarization branch, the expansion coefficients $\vec{Z}(j,m,n,r)$ depend also on the polarization. The spherical angles Θ and ϕ determine the direction of the wave vector $\vec{k}$. Y_{nm} are normalized spherical harmonics. Substitution of the trial function (2.18) into eq (2.17) and variation of the coefficients $\vec{Z}(j,m,n,r)$ under the conditions (2.16a) and (2.16b), yields the following system of equations

$$\sum_{\nu'} M(\nu,\nu')\vec{Z}(\nu') = \vec{N}(\nu) , \tag{2.19}$$

---

[6] The sum $\sum_{\vec{k}}$ ...is in the usual way replaced by $(V_0/(2\pi)^3 \int$ ...d^3k

where ν stands for (j,m,n,r). The matrix M contains all information on the scattering mechanisms. If more than one scattering mechanism is present then M is equal to the sum of the matrices which belong to each scattering mechanism. In our present case, M contains two parts. One part is due to the phonon-dipole interaction, the other part belongs to the normal processes[7]. The matrix M for defects and the vector matrix $\vec{N}$ are represented in the Appendix. From eqs (2.12b) and (2.19) and the expansion (2.18) we find for the thermal conductivity:

$$\kappa = - (1/TV_0) \sum_{\nu} \vec{N}(\nu)\, \vec{Z}(\nu) \quad . \tag{2.20}$$

3. Application of the Theory to the Scattering of Phonons by Edge Dislocation Dipoles

We shall not present the calculations in detail and shall rather restrict ourselves to a few remarks which will be needed in the following discussion of the results. We consider two parallel edge dislocations of opposite signs, as shown in Figure 1. The dislocation lines are parallel to the z-axis and have Burgers vectors in the direction of the positive x-axis. The vector $\vec{R}$ and the x_1-axis enclose the angle ϕ_0. As already mentioned, the strains ε in the energy density (2.1a) are those which are given by linear elasticity theory. The composed strain field of the two dislocations is then simply the sum of the single strain fields. Taking the Fourier transform of the composed strain field, one finds

$$\tilde{\varepsilon}(\vec{g}) = \tilde{\varepsilon}^S(\vec{g}) \, [1 - \exp(i\vec{g}\cdot\vec{R})] \quad , \tag{3.1a}$$

where the Fourier transform of the strain component mn due to a single edge dislocation is [10]

$$\tilde{\varepsilon}^S_{mn} = \frac{i|\vec{b}|}{(2\pi)^{3/2}} \frac{g_2}{g^2} \delta(g_3) \left\{ \delta_{mn} - \delta_{m3}\delta_{n3} - \frac{1}{1-\nu} \frac{g_m g_n}{g^2} \right\} . \tag{3.1b}$$

ν is Poission's ratio. Substitution of eq (3.1a) into eq (2.4e) yields together with eqs (2.4d) and (2.5c)

$$W(\vec{k},-\vec{k}') = W^S(\vec{k},-\vec{k}') \cdot 2 \cdot \left\{ 1 - \cos\left[(\vec{k}-\vec{k}')\cdot\vec{R}\right] \right\} \quad , \tag{3.2a}$$

where $W^S(\vec{k},-\vec{k}')$ is proportional to the transition probability per unit time that a phonon will be scattered from mode $\vec{k}$ into mode $\vec{k}'$ due to the interaction of the lattice waves with a single dislocation. The latter transition probability can be written in the form

$$W^S(\vec{k},-\vec{k}') = (1/k)\delta\,[k_3/k - k'_3/k]\,\delta[\omega(\vec{k})-\omega(\vec{k}')]\cdot F \tag{3.2b}$$

with

$$k = |\vec{k}| . \tag{3.2c}$$

The function F contains the spherical angles Θ,ϕ and Θ', ϕ' of the wave vectors $\vec{k}$ and $\vec{k}'$ and the elastic constants. The structure factor in eq (3.2a), resulting from the different positions of the scattering centers, may be omitted if the distance R between the dislocations is very large. Then $W(\vec{k},-\vec{k}') = 2\, W^S(\vec{k},-\vec{k}') \propto 1/k$. In this case the resistivity will be equal to twice the resistivity which is due to a single dislocation. For values of kR which are small compared with 1, however, the wave vector dependence of $W(\vec{k},-\vec{k}')$ is quite different. One finds that $W(\vec{k},-\vec{k}') \propto kR^2$, for $kR \ll 1$. From the Boltzmann equation (2.10) and the related equations we find that the deviations $\vec{X}(\vec{k})$ of the occupation numbers from their thermal equilibrium values must be proportional to $1/(kR)^2$ for small k. With this wave vector dependence of the $\vec{X}(\vec{k})$ the conductivity (2.12b) diverges at $k \sim 0$. In order to avoid that singularity we included the normal processes. The results will be discussed in the next section.

[7] The explicit form of the matrix M for normal processes can be found in Reference [5].

4. Results and Discussion

4.1 Scattering of Phonons by Edge Dislocation Dipoles and by Normal Processes

We have seen that the thermal resistivity is zero if the phonons were scattered only by dipoles. The inclusion of the normal processes changes this situation completely. It was shown in Reference [3] that the normal three-phonon interactions contain in an isotropic continuum two kinds of interactions. On account of the conservation of energy (2.7b), the sum of the energies of two interacting phonons ($\hbar\omega+\hbar\omega'$) must be equal to $\hbar\omega''$. The conservation of the quasi-momentum of the phonon gas, expressed by eq (2.7a), on the other hand, imposes certain restrictions on the possible values of ω'. For example, if the phonons $\hbar\omega$ and $\hbar\omega'$ belong to transversal branches and if the phonon $\hbar\omega''$ belongs to a longitudinal branch, then ω' depends on ω. The studies of the possible normal processes in a continuum [3] showed that processes for which ω' does not depend on ω- energetically unlimited processes-yield a rate of change of the mean phonon numbers (2.5a) which is proportional to ω for $\omega\to 0$. The other kind of interaction, for which ω' is a function of ω, yields $\partial\bar{N}/\partial t\propto\omega^4$. According to the last section, the rate of change of the phonon numbers due to the phonon-dipole interaction is proportional to ω^3, for $\omega\to 0$, and becomes insignificant at $\omega\sim 0$ if compared with $\partial\bar{N}/\partial t$ which results from energetically unlimited normal processes. Hence, at small frequencies, the frequency dependence of the deviations $\vec{X}(\vec{k})$ of the phonon numbers from their thermal equilibrium values is governed by energetically unlimited processes. Then, as follows from the Boltzmann equation, the $\vec{X}(\vec{k})$ are independent of the frequency. The consequence is that the thermal conductivity will no longer have a singularity at $\omega=0$. We note, that we already used in eq (2.18) the result that $\vec{X}(\vec{k})$ is independent of ω, for $\omega\to 0$ (the power series starts with r=0).

We shall not go into details of the integrations which must be carried out in order to get numerical values for the matrices M. We only point out that for the normal processes the matrix elements of M depend on each other. One finds, as a consequence of the two selection rules (2.7a) and (2.7b), that

$$M(j,m,1,r;L,-m,1,1) + (v_L/v_T)M(j,m,1,r;T,-m,1,1) = 0. \tag{4.1}$$

Here L and T stand for longitudinal and transversal branches. v_L and v_T are the corresponding sound velocities. On account of eq (4.1) the determinant of $\underset{\sim}{M}$ vanishes identically. If normal processes are the only scattering mechanisms then the vector $\vec{Z}(\nu)$ in eq (2.19) is infinite and the thermal resistance is zero, as mentioned earlier.

4.2 The Thermal Conductivity Limited by Dipoles and by Normal Processes

We consider the dislocation arrangement of Figure 1. Let ϕ_0 be equal to $\pi/4$. The resistivity for configurations with other angles has also been calculated. Since the main features of the temperature behaviour of the thermal conductivity do not change very much with varying angles ϕ_0, we shall discuss here only the 45 degree case. Note, that the shear stress in the glide plane of a dislocation due to the other dislocation vanishes. Hence, this configuration is stable with respect to gliding.

The conductivity has been calculated with the elastic constants of copper. Numerical values of the elastic constants can be found in Reference [11]. In Figures 2 through 4, we have plotted the components of the reduced thermal conductivity $\tilde{\kappa}$, which is defined by

$$\tilde{\kappa} = \kappa[K^2\rho_0\, v_T^3/(hb^2N_D)]^{1/2}, \tag{4.2}$$

versus the reduced temperature

$$\tilde{T} = KT(\rho_o h^3\, v_T^5\, b^2\, N_D)^{-1/4} \tag{4.3}$$

N_D is the number of dislocation pairs per cm^2 perpendicular to the x_1, x_2-plane; h is Planck's constant and b is the absolute value of the Burgers vector. The parameter

$$p = (b^2 N_D)^{1/4}(R/b) \tag{4.4}$$

is a measure for the distance between the two dislocations of a dipole.

Figures 2,3, and 4 show the components[8] $\tilde{\kappa}_{xx}$, $\tilde{\kappa}_{yy}$, and $-\tilde{\kappa}_{xy}$, respectively. The component $\tilde{\kappa}_{zz}$ is infinite since the z-component of the wave vectors is conserved (see eq (3.2b)). We note that the xy-component is negative. This means that a temperature gradient in positive y-direction produces a positive heat current component in x-direction. The component $\tilde{\kappa}_{xy}$ appears since in this configuration the x and y axes are not principal axes of the conductivity "ellipsoid". In the case of isolated edge dislocations parallel to the z-axis and with Burgers vectors parallel to the x-axis only $\tilde{\kappa}_{xx}$ and $\tilde{\kappa}_{yy}$ do not vanish, except for $\tilde{\kappa}_{zz}$.

Curve 1 in Figures 2 and 3 shows the components $\tilde{\kappa}_{xx}$ and $\tilde{\kappa}_{yy}$, respectively, of the conductivity which is limited by isolated dislocations and normal processes. These components are at low and high temperatures proportional to T^2. The magnitude of the conductivity at low temperatures, however, is larger than that at high temperatures. This difference is due to a change in slope of the conductivity at intermediate temperatures, which results from the three-phonon interactions [3]. In case of phonon scattering by dipoles and by normal processes the conductivity approaches asymptotically curve 1 for increasing temperatures or increasing distances R. This follows immediately from the transition probability (3.2a) which approaches for large products ωR the transition probability due to two isolated dislocations.

At very low temperatures, the conductivity limited by dipoles and normal processes is independent of the temperature and has a finite value at T=0. The magnitude of the conductivity in this temperature region is inversely proportional to the square of the distance R. As expected, the conductivity increases on account of the reduction in scattering strength which is due to the partial cancellation of the strain fields.

At intermediate temperatures, we find a minimum in the conductivity if the distance R is sufficiently small (p small). The reason for the occurrence of this minimum follows from the transition probability (3.2a) which has a main maximum for values of $kR \sim \pi/2$. If the temperature is such that the maximum of the phonon distribution coincides with the main maximum of the transition probability then the resistivity will have a maximum. An increase in R will shift the main maximum of the transition probability towards smaller k values. Hence, the minimum of the conductivity occurs at lower temperatures. The minimum disappears if the distance R becomes too large. Increasing R leads to a reduction of the width of the main maximum. The consequence is that the number of phonon states which are affected by an enhanced scattering is reduced.

The $-\tilde{\kappa}_{xy}$ component, shown in Figure 4, is at very low temperatures also independent of the temperature and proportional to $1/R^2$ and drops at high temperatures very rapidly to zero. Note, that in case of phonon scattering by isolated dislocations, which are parallel to the z-axis and which have Burgersvectors parallel to the x-axis, the component $\tilde{\kappa}_{xy}$ is zero.

The temperature above which the difference between the thermal conductivity limited by dipoles, κ_D, and the conductivity limited by isolated dislocations, κ_S, is smaller than $\kappa_S/10$ has been calculated for the xx-component of κ. It is found that this limit lies at a temperature $T_{limit} = 370\ b/R°K$.

5. Conclusion

The influence of edge dislocation dipoles on the lattice thermal conductivity has been studied in an isotropic continuum. The scattering of phonons by normal processes was included in the calculations in order to get finite results for the thermal conductivity. Deviations from the normal T^2-dependence of the conductivity, which is found if the phonons are scattered by isolated dislocations, appear below a certain temperature. This temperature depends on the distance between the two dislocations of a dipole. The conductivity is independent of the temperature at $T \sim 0$ and reached a finite value at T=0.

[8] It is $x = x_1$, $y = x_2$ and $z = x_3$.

6. References

[1] Gruner, P., Zeitschr. Naturforsch. 20a, Heft 12, 1626 (1965).

[2] Bross, H., Zeitschr. Phys. 189, 33 (1966).

[3] Bross, H., Gruner, P., and Kirschenmann, P., Zeitschr. Naturforsch, 20a, Heft 12, 1612 (1965).

[4] Peierls, R.E., Quantum Theory of Solids, Oxford Clarendon (1955).

[5] Bross, H., Phys. Stat. Sol. 2, 481 (1962).

[6] Murnaghan, F. D., Finite Deformation of an Elastic Solid, John Wiley and Sons, Inc., New York (1951).

[7] Klemens, P.G., Solid State Physics, Vol. 7, Academic Press, New York (1958).

[8] Callaway, J., Phys. Rev. 113, 1046 (1958)

[9] Krumhausl, J. A., Proc. Phys. Soc. 85, 921 (1965)

[10] Bross, H., Seeger, A., and Haberkorn, R., Phys. Stat. Sol. 3, 1126 (1963)

[11] Seeger, A., Buck, O., Zeitschr. Naturforsch. 15a, Heft 12, 1056 (1960)

7. Appendix

The matrix M for static defects is given by

$$-KT[(2\pi)^3/V_0]^2 M(j,m,n,r;j',m',n',r') = \sum_{j''} \iint W(j,\vec{k};j'',-\vec{k}')[\bar{\bar{N}}(j,\vec{k})+1]\bar{\bar{N}}(j,\vec{k})[\hbar\omega(j,\vec{k})]^r Y_{nm}(\Theta,\phi)$$

$$\left\{\delta^{jj'}[\hbar\omega(j,\vec{k})]^{r'} Y_{n'm'}(\Theta,\phi) - \delta^{j'j''}[\hbar\omega(j',\vec{k}')]^{r'} Y_{n'm'}(\Theta',\phi')\right\} d^3k d^3k' .$$

The vector matrix $\vec{N}$ is given by

$$-KT[(2\pi)^3/V_0]\vec{N}(j,m,n,r) = \int [\bar{\bar{N}}(j,\vec{k})+1]\bar{\bar{N}}(j,\vec{k})[\hbar\omega(j,\vec{k})]^{r+1} \vec{v}(j,\vec{k}) Y_{nm}(\Theta,\phi)\, d^3k \quad .$$

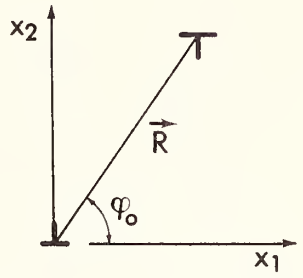

Figure 1: Dislocation Dipole Arrangement

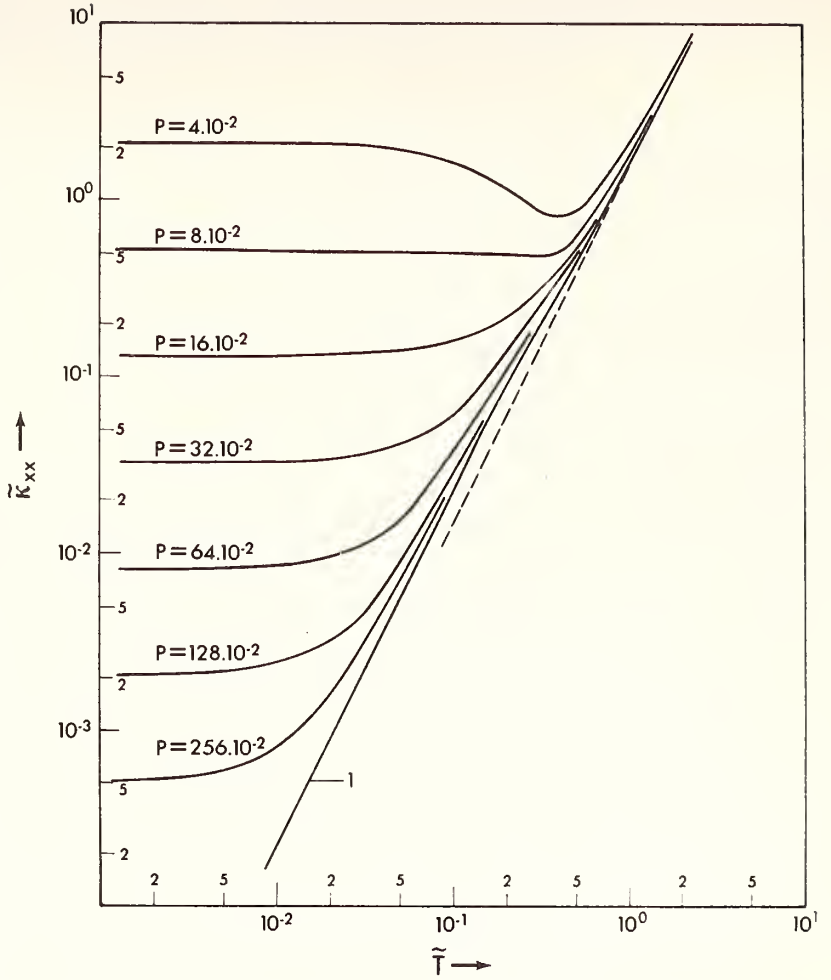

Figure 2: Reduced xx-Component of the Lattice Thermal Conductivity in Copper Limited by Edge Dislocation Dipoles and by Normal Processes

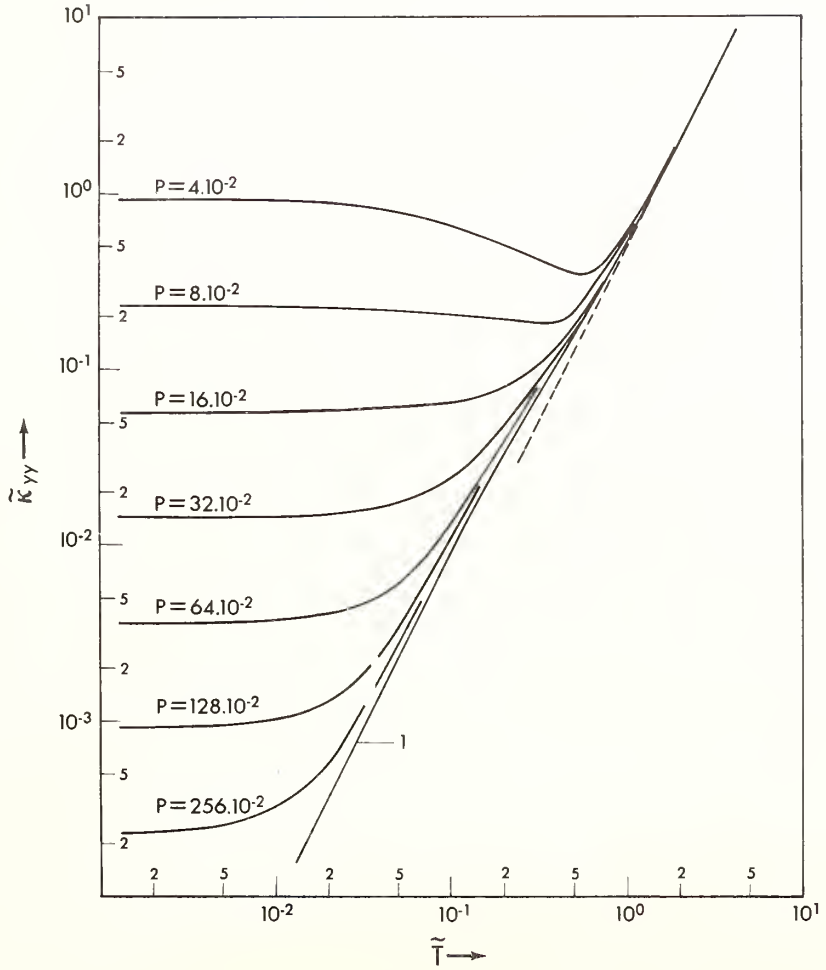

Figure 3: Reduced yy-Component of the Lattice Thermal Conductivity in Copper Limited by Edge Dislocation Dipoles and by Normal Processes

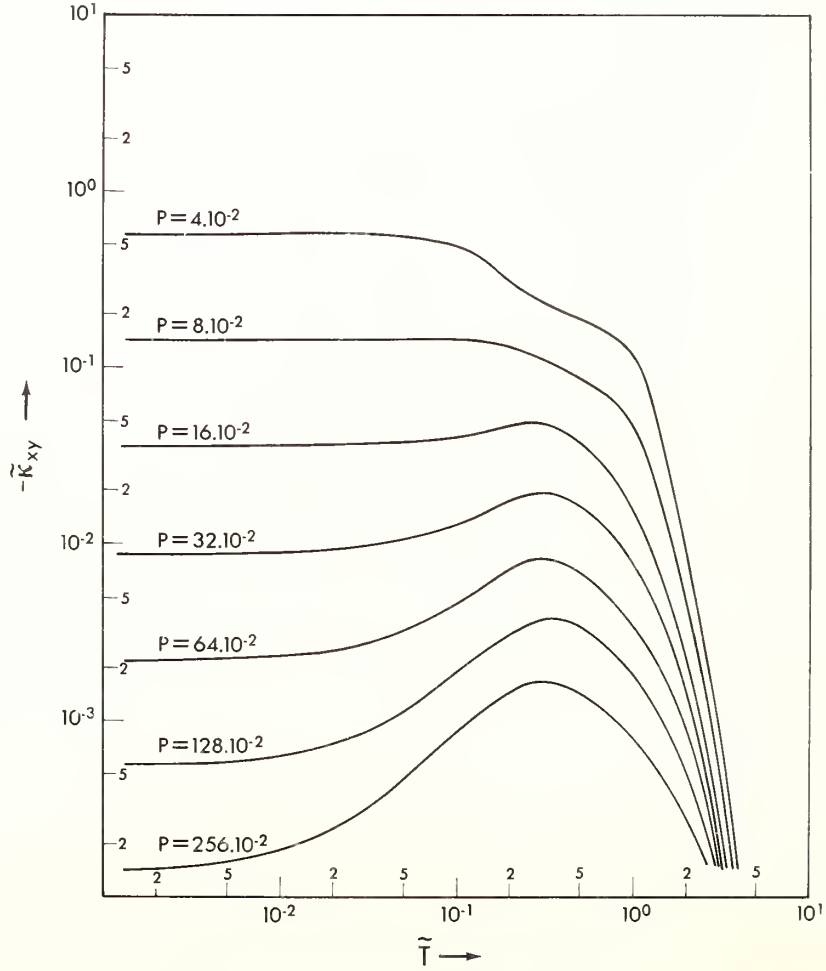

Figure 4: Negative Reduced xy-Component of the Lattice Thermal Conductivity in Copper Limited by Edge Dislocation Dipoles and by Normal Processes

Thermal Diffusivity Measurements With Stationary Waves Method

A. Sacchi, V. Ferro, C. Codegone[1]

Istituto di Fisica Tecnica
del Politecnico di Torino (Italy)

Stationary thermal waves have been obtained by means of a suitable control device in a system consisting of two equal plane samples. These samples have been pressed together, so as to obtain a good contact, while a thin plate with controlled electric heating and a refrigerated sink were successively pressed on the outside surfaces of the samples. When half-wave stationary conditions have been established in the system, the phase difference between the temperature oscillations of the two surfaces of each sample attains the value π. Then the thermal diffusivity a of the sample material is given by the simple relation:

$$a = \frac{f \ell^2}{\pi}$$

where f is the wave frequency and ℓ is the sample thickness.

Key Words: Thermal diffusivity.

1. Introduction

The knowledge of thermal diffusivity is important in the heat transmission problems having unsteady state conditions. This parameter can be evaluated indirectly from the measurement of the thermal conductivity λ, of specific mass ρ and of specific heat c, but the relative error of the results in the sum of the errors of λ, ρ and c.

Other methods allow the direct evaluation of thermal diffusivity a producing suitable thermal fields variable in time [1][2][2].

This work, which belongs to the second group, consists of making the sample oscillate thermally in a half-wave mode. The thermal diffusivity is then given by $a = f \ell^2/\pi$, where ℓ is the sample thickness (m), and f is the oscillation frequency (s^{-1}). Note that this relation is a function only of the kinematic quantities which characterize the dimensions of a (m^2/s).

2. Theory

The theory of the process is the following. Two identical plane layers of the tested material are placed in face to face contact with each other and their outer surfaces are subjected to the same temperatures. Assuming the origin of x to be on the contact surface (through which no thermal flux flows), the following equation is obtained if the material may be supposed homogeneous and isotropic, initial conditions being taken as zero:

$$\frac{\Theta}{\Theta_\ell} = \frac{\Theta}{\Theta_{-\ell}} = \frac{\cosh(qx)}{\sinh(q\ell)} \qquad (1)$$

---

[1] Assistants and Professor of Technical Physics.

[2] Figures in brackets indicate the literature references at the end of this paper.

where:

Θ is the Laplace transform of temperature θ in a general surface at abscissa x ;
$\Theta_\ell = \Theta_{-\ell}$ is the Laplace transform of temperature at the outer surfaces of the layers;
ℓ is the layer thickness;
$q = \sqrt{p/a}$ (p is the auxiliary variable introduced by the transform and a is the thermal diffusivity of the material).

The temperature θ_o on the contact surface is defined by its Laplace transform:

$$\frac{\Theta_o}{\Theta_\ell} = \frac{1}{\cosh (q\ell)} = G (p) \tag{2}$$

Equation (2) gives the layer transmission function between the outer ($x = + \ell$) and the inner ($x = 0$) surfaces which is defined in the servomechanism theory as the ratio between the Laplace transform of dependent output variable Θ_o and independent input variable Θ_ℓ.

By using a special automatic control system, a proportional ratio between θ_o and θ_ℓ can be given by the following equation:

$$\theta_\ell = \theta_{-\ell} = H \theta_o \tag{3}$$

where H is a real constant.

Equation (3) is equivalent to the following:

$$\Theta_\ell = H \Theta_o \tag{4}$$

The system obtained in this manner (figures 1a and 1b) is a feedback system. It is unstable when the open circuit gain is:

$$G (p) \cdot H = -1 \tag{5}$$

Equation (5) is both modulus and phase valid. It can therefore be divided into the following equalities:

$$| G (p) \cdot H | = 1 ; \qquad \arg \left[G (p) \cdot H \right] = (2n + 1)\pi \tag{6}$$

in which n is an arbitrary whole number.

Equations (6) and (2) lead to the following:

$$H = \left| \cosh (q\ell) \right| ; \qquad \arg \left[\frac{1}{\cosh (q\ell)} \right] = (2n + 1)\pi \tag{7}$$

Persistent oscillations are introduced into the system, if $\omega = 2\pi f = 2\pi/T$ (f being the oscillation frequency and T the oscillation period) when $p = j\omega$. It follows that:

$$q\ell = \ell \sqrt{\frac{p}{a}} = \ell \sqrt{\frac{j\omega}{a}} = (1 + j)\ell \sqrt{\frac{\omega}{2a}} ,$$

from which:

$$R (q\ell) = I (q\ell) = \ell \sqrt{\frac{\omega}{2a}} \tag{8}$$

where $R (q\ell)$ and $I (q\ell)$ are respectively the real and imaginary parts of $q\ell$.

Therefore, considering eq (8), the solution of eq (7) when n = 0 is:

$$H = 11.592 = 10.541 \quad dB \tag{9}$$

$$R(q\ell) = \pi \; ; \quad I(q\ell) = \pi \tag{10}$$

Equating (8) and (10) we obtain:

$$\omega = \frac{2\pi^2 a}{\ell^2} \; ; \quad T = \frac{\ell^2}{\pi a} \; ; \quad f = \frac{\pi a}{\ell^2} \tag{11}$$

Consequently ω, T and f are established uniquely and the system oscillates sinusoidally with a halfwave resonance. Figures 2a and 2b show the amplitude of the temperature oscillations as a function of abscissa x and θ_o and θ_1 versus time.

Multiple halfwave oscillations (n = 1,2,3...) are greatly attenuated since the condition defined by the first part of equation (7) is not applicable in these cases.

As defined by equation (9), H is a constant and does not depend on layer material. It can be set permanently on the unit main control system. Diffusivity a can be calculated by equation (11) from the excited oscillations.

3. Experimental Details

The described method is applied to measurements of thermal insulating material diffusivity. A first unit operational diagram is illustrated in figures 3a, 3b, 3c and 3d. Figure 3a gives the refrigerator installation diagram; figure 3b shows the specimen (submitted to thermal oscillations) with the control equipment which has been conceived by the first of us, while figure 3c shows the positioning on the sample of the thermocouples used to record collected data.

The tested material (figure 3b) which is made up into two identical specimens (1) measuring 500 x 500 mm with an interposed thermocouple, is placed between two 1 mm thick micanite sheets (2) with nickel-chrome plate heating resistors.

The setup is enclosed within two ethyl alcohol circulation tanks (3) and brought to a temperature of about -40 °C by means of the refrigerator shown in figure 3a. The two 1 mm thick asbestos board layers (4) separate the alcohol circulation tanks from the heating elements. The thickness of the asbestos boards has been experimentally defined so as to reach a sufficiently close heating and cooling rate balance.

The two 1 mm thick aluminum sheets (5) are placed between the heating elements and the tested specimens, in order to equalize the surface temperature distribution. Heating elements (2) and aluminum sheets (5) each consist of a central 250 x 250 mm section and of a guard ring.

The temperatures at the contact surfaces of the two layers and at one of their outer surfaces (e.g. the upper one) are measured by two thermocouples. The differences between these readings and a reference level, set by a dc mV generator (6), are monitored by two deviation amplifiers (7) whose series outputs are the input of the regulator R_1 which is used to feed the central area of the upper heater.

By suitably adjusting the deviation amplifiers' gain factors, the ratio H between the amplitude of upper and contact surface oscillations can reach the value shown by equation (9).

Three other control systems R_2, R_3 and R_4 (which utilize the deviation amplifiers (8)) ensure temperature equality on the remaining areas of heating plates (upper peripheral, central and lower peripheral) with the upper central plate.

The above mentioned control systems are of the derivative-integral proportional action (p.i.d.) type with an operational amplifier calculation circuit, a magnetic amplifier and a saturable reactor power circuit.

The ethyl-alcohol supply unit (cfr. fig. 3a) consists of the reservoir (9), the circulation pump (10), and the heat exchanger (11), which is the evaporator of a Freon 22 circuit having the compressor (12), the condenser (13), and the expansion valve (14). Thermostatic regulator T_1 controls the reservoir temperature by actuating the compressor (12).

This whole assembly is placed inside the refrigerating room (15), cooled by an F 22 circuit consisting of the compressor (17), the condenser (18) the expansion valve (19), the evaporator (16) and the thermostatic regulator T_2.

A multipoint recorder measures temperature trends by means of 0.2 mm Cu-Const thermocouples, connected as shown in figure 3c.

The second apparatus used for thermal diffusivity measurements at temperatures above + 30°C is reported in figure 3e. Heating elements are obtained with infrared lamps suitably placed to obtain a flat flux distribution on the external surfaces of the samples. The cooling of the same surfaces is obtained by natural or forced air convection and by radiation into the ambient.

4. Results and Conclusions

Experimental results are reported in figures 4 and 5 and in table 1. Figure 4 shows an example of temperature recordings in which the 1/2 wave oscillation is apparent.

The tested sample was a 500 x 500 x 50 mm layer of expanded phenolic resin with apparent specific mass $\rho = 32.7$ kg/m^3, and an average cell diameter of 0,2 mm.

In this case the resonance frequency is:

$$f = \frac{1}{T} = 0.943 \text{ mHz},$$

and the diffusivity from eq (11) is:

$$a = \frac{\ell^2 f}{\pi} = 7.50 \times 10^{-7} \text{m}^2/\text{s} \qquad (12)$$

The value of a, calculated for the same material, according to the usual definition

$$a = \frac{\lambda}{\rho c} \qquad (13)$$

where λ = thermal conductivity = 0.0295 W m^{-1} °C^{-1} at the mean temperature $\theta_m = 0$°C;

ρ = apparent specific mass = 32.7 kg/m^3;

c = specific heat = 1170 J/(kg °C) at the same mean temperature of 0°C (values experimentally evaluated) yields $a = 7.50 \times 10^{-7}$ m^2/s, which shows a 2.6% difference with respect to the value measured with this direct method.

A series of thermal diffusivity measurements was carried out on expanded phenolic resin, polystyrene, and F 12 expanded urethane foam (figure 5) at different temperatures in the -30 to +45°C range. The temperature oscillation amplitude was kept within ± 5°C.

In some tests the diffusivity a was also deduced by the direct-measured values of λ, ρ and c. The value of a defined by equation (13) is subject to the experimental errors of the measure of λ, ρ and c, whereas the value of a defined by equation (11) depends only on frequency and length measurements which are more exact than the calorimetric measurements.

5. References

[1] Carslaw, H. S., and Jaeger, J. C., Conduction of Heat in Solids, 2nd ed., p. 403, (Clarendon Press, Oxford, 1959).

[2] Codegone, C., Ferro, V., and Sacchi, A., Experiments on Thermal Oscillations Through Insulating Materials, Supplement au Bulletin de l'Inst. Int. du Froid Annexe 1966-2, 23-37.

TABLE I

Tested Materials	θ_m	λ	ρ	c	$a=\frac{\lambda}{\rho c}$	T	f	ℓ	$a=\frac{\ell^2}{\pi T}$
	^aC	$\frac{W}{m\,^aC}$	$\frac{kg}{m^3}$	$\frac{kJ}{kg\,^aC}$	$10^{-7}\frac{m^2}{s}$	s	m Hz	m	$10^{-7}\frac{m^2}{s}$
Expanded	-28.5		14.96			520	1.92	0.05	15.3
Palystyrene	-18.5		"			500	2	"	15.9
	-10		"			485	2.06	"	16.4
	0	0.032	"	1.215	17.6	463	2.20	"	17.2
	+20		"			421	2.375	"	18.9
	+45	0.038	14.8	1.215	21.2	390	2.56	"	20.4
	+45	0.038	12.1	1.215	25.9	1270	0.786	0.10	25
Expanded	-30		32.7			1188	0.842	0.05	6.70
phenalic	-20		"			1158	0.863	"	6.85
resin	-10		"			1105	0.905	"	7.20
	0	0.0295	"	1.170	7.70	1059	0.944	"	7.50
	+20		"			912	1.10	"	8.76
	+45		"			720	1.39	"	11.05
	+45	0.044	46.8	1.170	8.02	978	1.02	0.05	8.10
F 12 expanded	-20	0.0196	36.9			2415	0.414	0.051	3.43
urethane	0	0.0180	"			2855	0.350	"	2.90
foam	+25.5	0.0186	"			2715	0.368	"	3.05
	+63	0.0237	"	1.385	4.63	1785	0.560	"	4.64

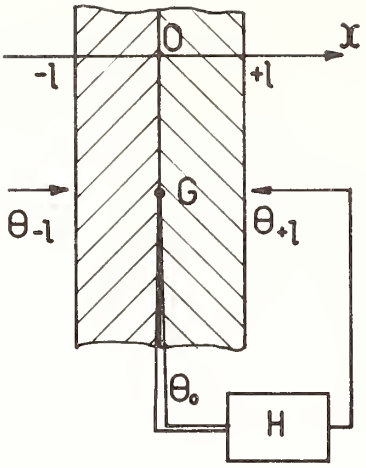

Fig. 1a Thermal system diagram.

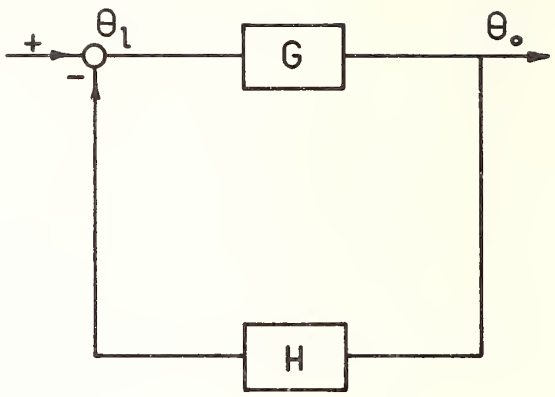

Fig. 1b Feedback system block diagram.

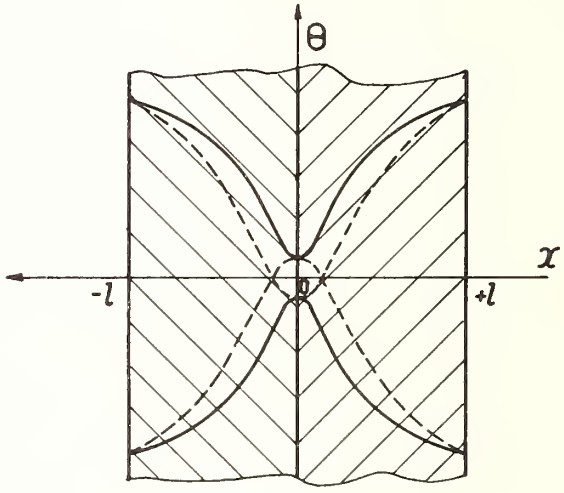

Fig. 2a Amplitude of oscillations as a function of x.

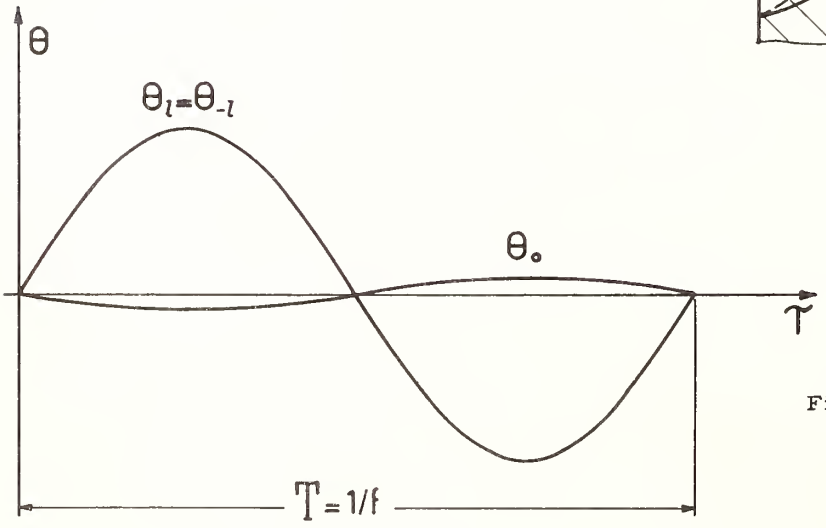

Fig. 2b θ_{o1}, θ_{ℓ} and θ_{ℓ} temperatures versus time.

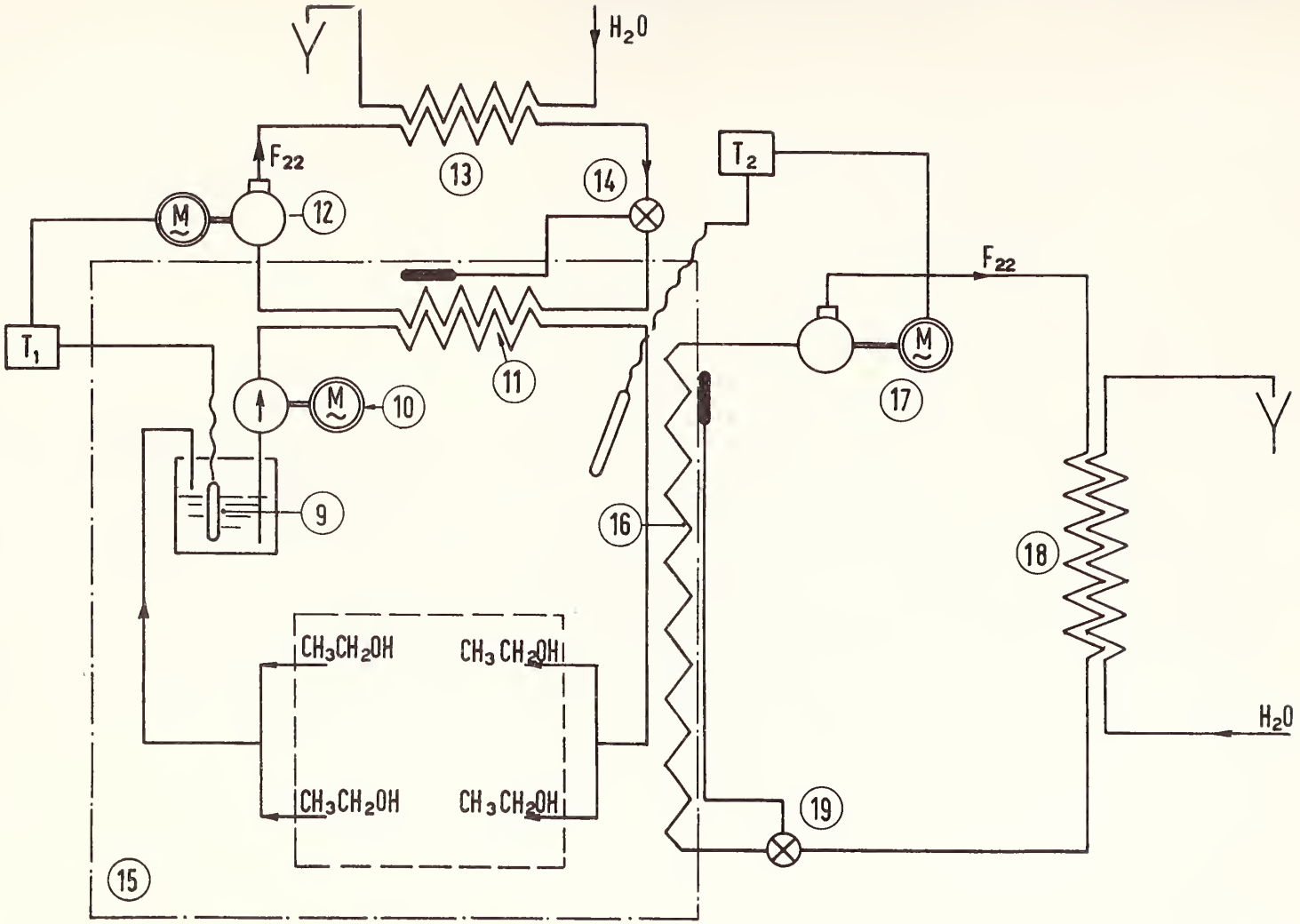

Fig. 3a Refrigerator installation diagram

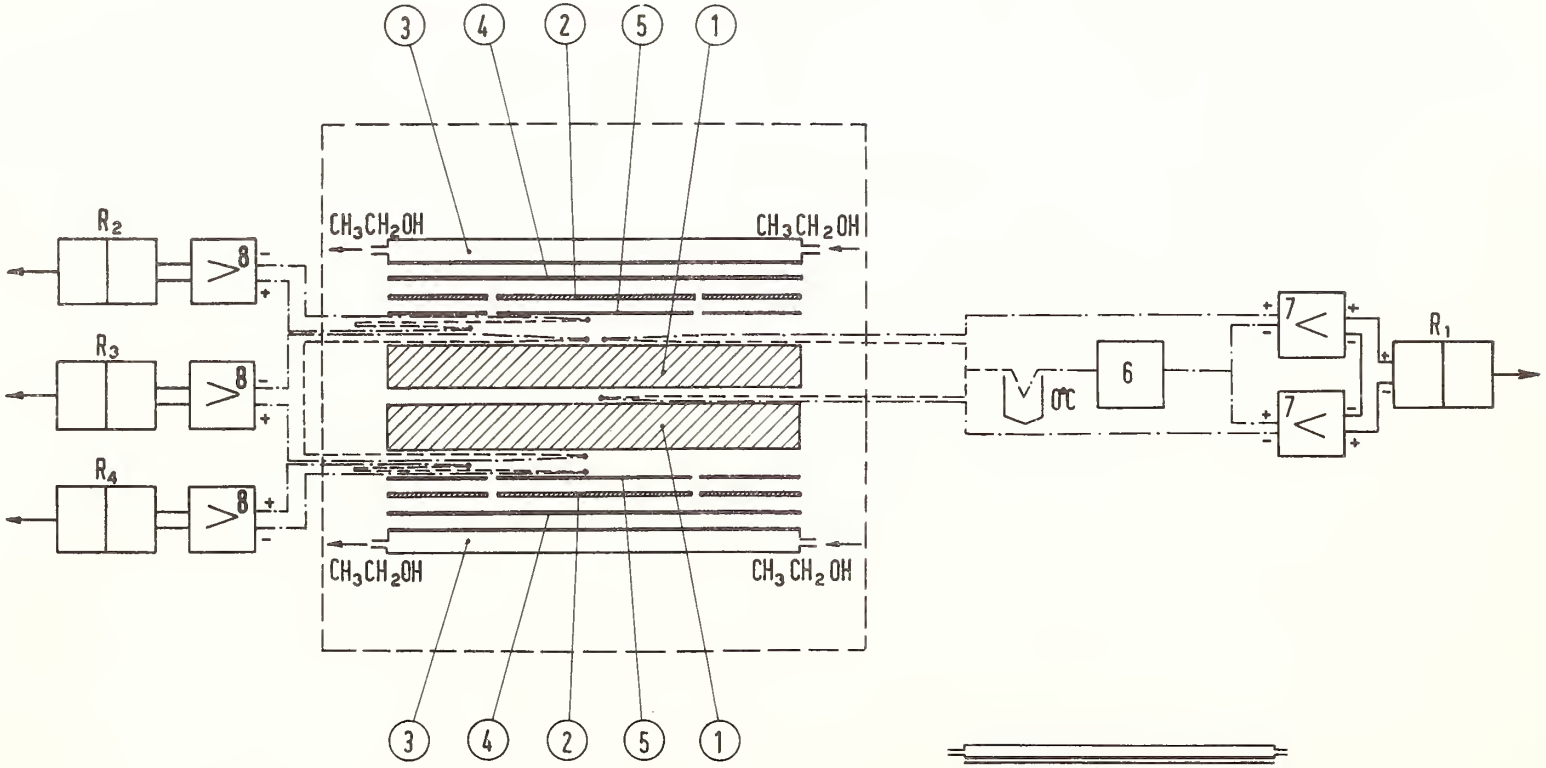

Fig. 3b Operational diagram of the device with control equipment.

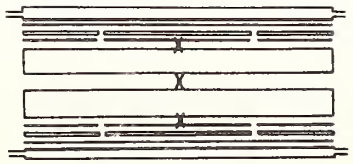

Fig. 3c Positioning of the thermocouples used to record collected data.

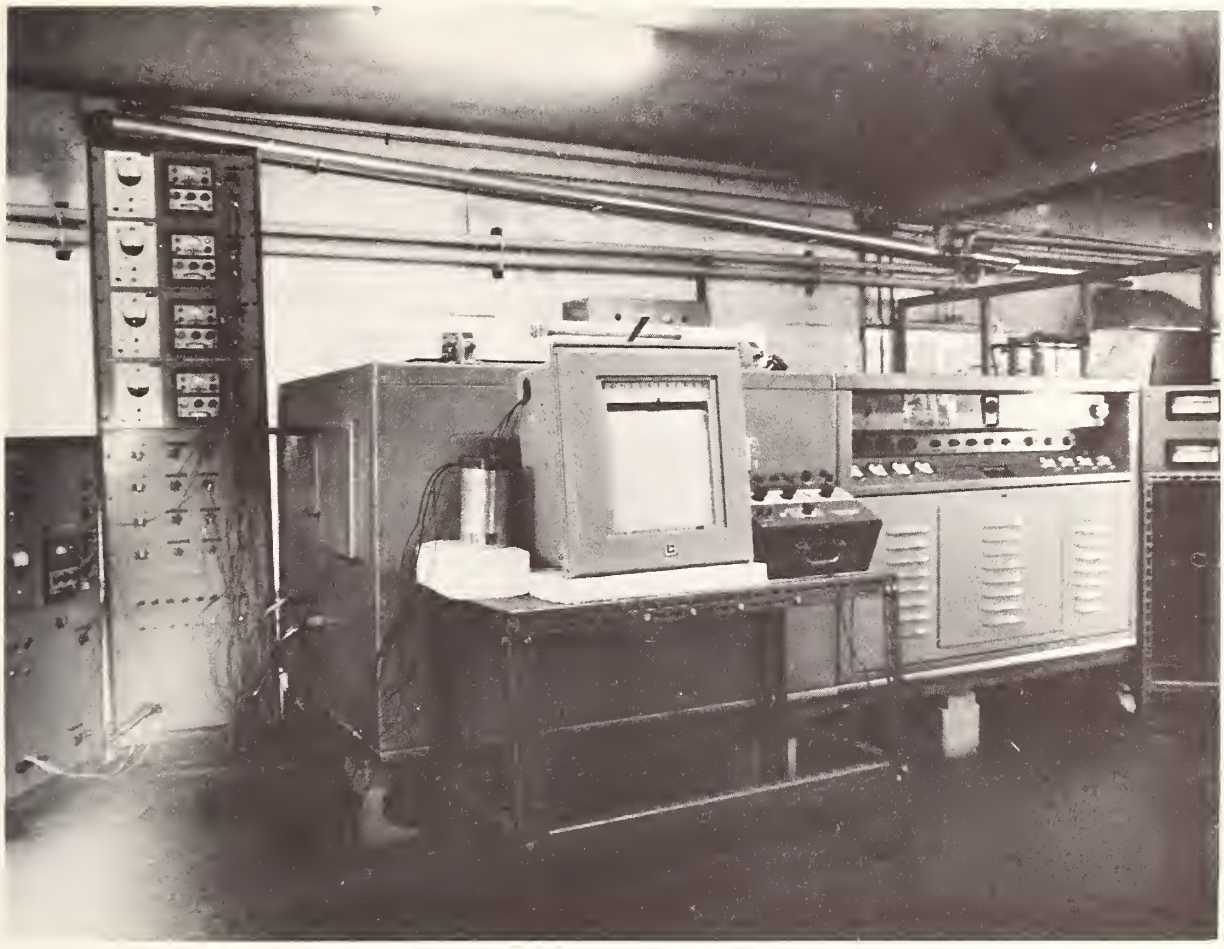

Fig. 3d Testing apparatus picture

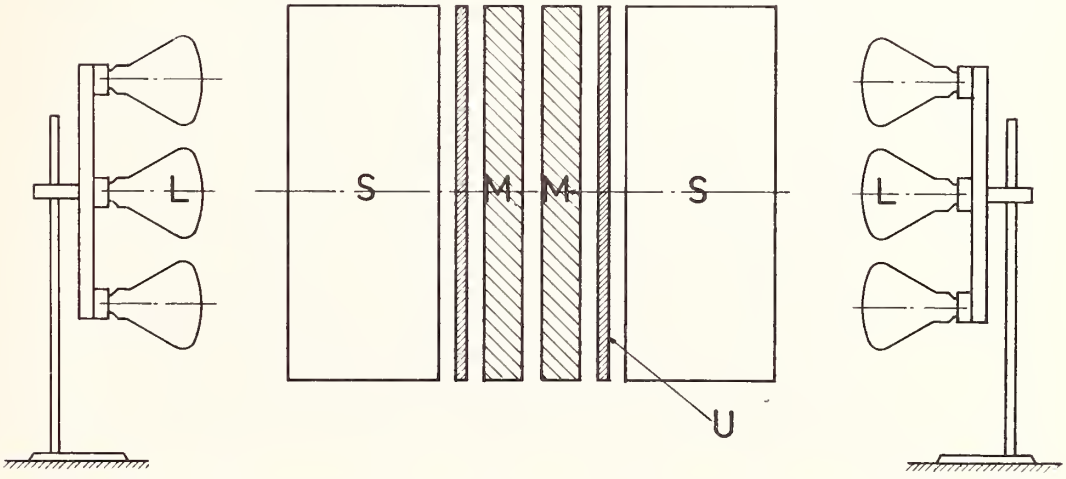

Fig. 3e Device of the second equipment: L infrared lamps, M specimens, U black alluminium sheets to uniformize temperature distribution, S reflecting lateral screcn to concentrate radiation flux.

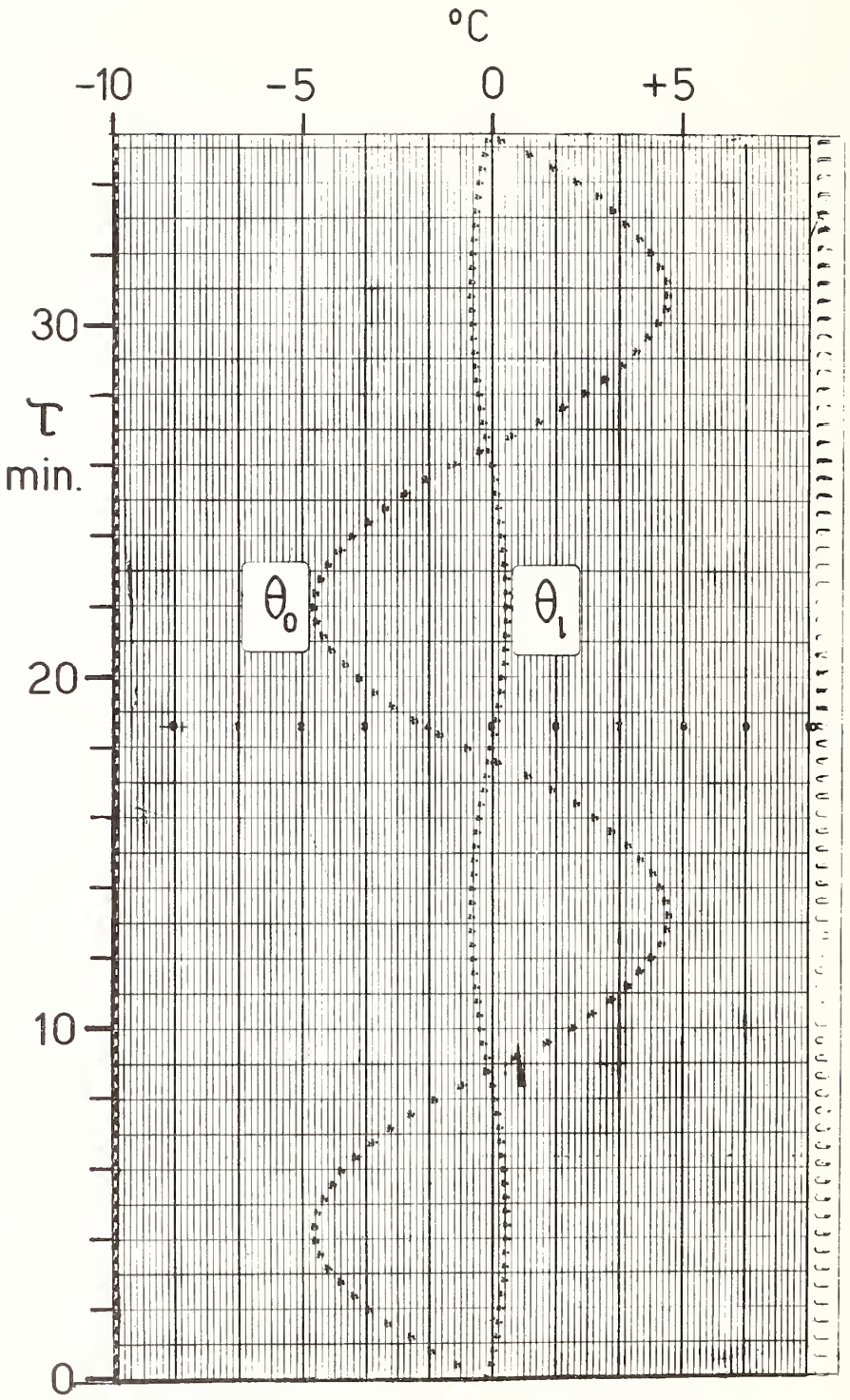

Fig. 4 Thermal oscillation recording of expanded phenolic resin ρ = = 32.7 kg/m^3; θ_m = 0°C

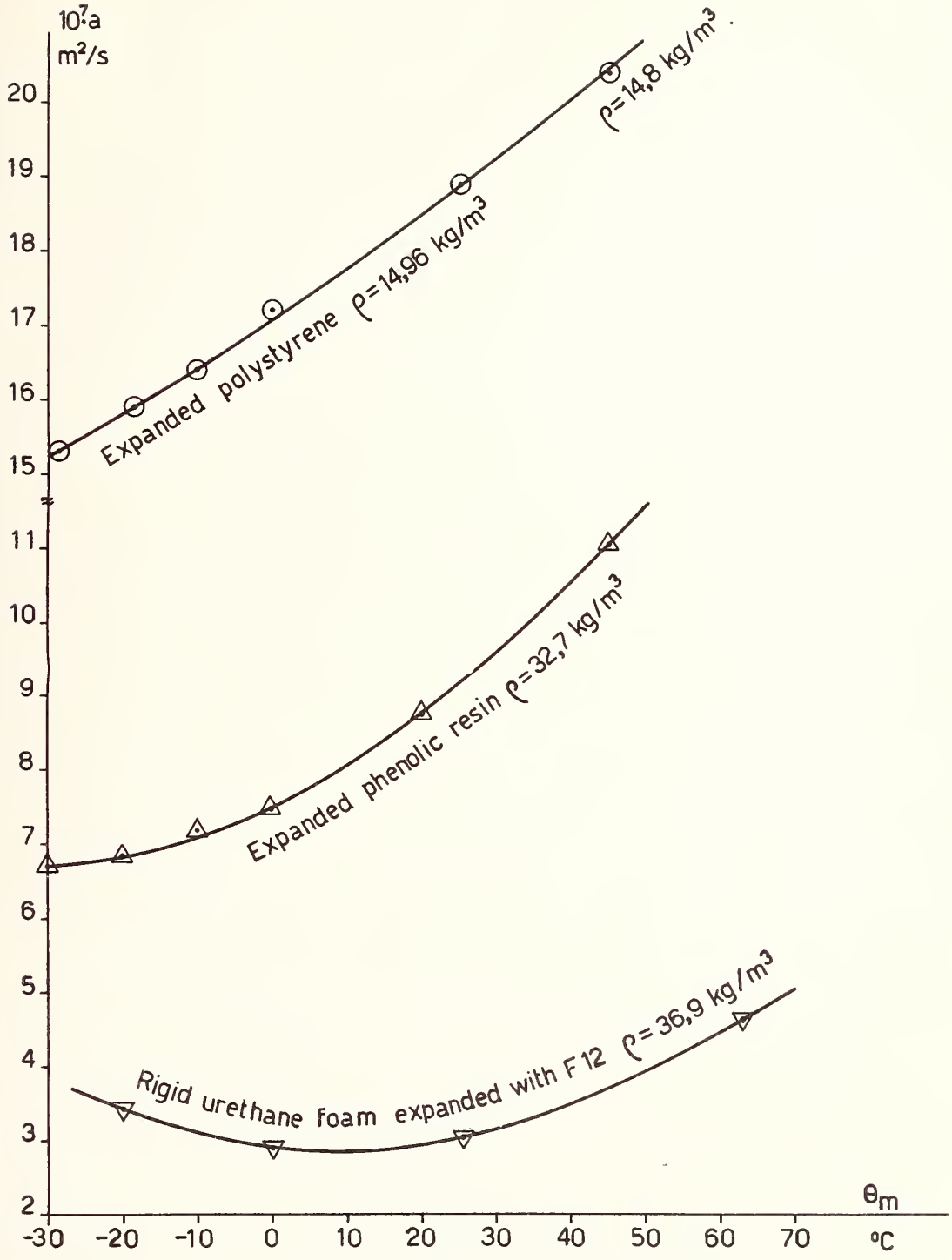

Fig. 5 Thermal diffusivity of tested materials vs the mean temperature

Rotating Thermal Field

C. Codegone, V. Ferro, A. Sacchi[1]

Istituto di Fisica Tecnica - Politecnico
Turin - (Italy)

Experiments are described in which a rotating thermal field has been obtained by superposing two perpendicular thermal fields which have sinusoidal oscillations and a $\pi/2$ phase difference. The experimental apparatus utilized a sample of expanded phenolic resin in the form of a long prism with square cross-section. The $\pi/2$ phase differences of the oscillations have been obtained by means of a suitable wave generator and four temperature control systems. Two infrared lamps for each side of the prism form the radiant energy sources. Following the theory of the phonomenon summarized here, the range of frequencies of the oscillations was chosen to be 10^{-4} to 10^{-5} Hz. Recordings of the thermal waves and of the rotating field are shown and some developments and possible applications are indicated.

Key Words: Rotating thermal field, thermal wave propagation.

1. Theory of the Phenomenon

On all the four sides of a square base parallelepiped prism (fig. 1) made out of homogeneous and isotropic material, four sinusoidal temperature waves are applied:

$$\theta_n = \Theta_\ell \sin [\omega t + (n - 1)\, \pi/2] \tag{1}$$

where $n = 1,2,3,4$.

The applied waves therefore have identical amplitudes Θ_ℓ and frequencies $f = \omega/2\pi$, and each of them has a $\pi/2$ phase difference from the preceding wave when examined successively in one direction (e.e. clockwise) around the specimen.

A prism sufficiently elongated in the direction perpendicular to the lines of thermal flux is assumed (figure 1). Therefore the effects of thermal dispersions on the extreme unheated sides (B_1) and (B_2) may be neglected in the middle square section (A) (these sides are well insulated anyway). In the middle section there is a two dimensional temperature field which is a superposition of components H_x and H_y, where H_x and H_y are the two perpendicular components due to the four externally applied thermal waves.

A stabilized state of oscillations can now be considered in which the amplitudes of the imposed temperatures are sufficiently limited (10 - 15°C), so that in such a range, the thermal properties of the medium, seat of the studied phenomenon, may be held constant.

Under such conditions the unidimensional problem then consists of a sinusoidal thermal field defined by the gradient $H_s = \partial\theta_n/\partial s$ ($s = x,y$) along any of the two directions parallel to the sides ℓ of section (A).

Choosing for instance the direction of the x axis, the said field is assumed to be produced by the two sinusoidal temperature waves applied to the faces perpendicular to the chosen direction:

$$\theta_1 = \Theta_\ell \sin \omega t \tag{2}$$

$$\theta_2 = \Theta_\ell \sin (\omega t + \pi) \tag{3}$$

---

[1] Professor and Assistants of Technical Physics, respectively.

which have the same amplitude and frequency and are out of phase with one another.

If the thickness ℓ is sufficiently small compared to the wavelength $\lambda = 2\sqrt{\pi\, a\, T}$ of the thermal wave in the medium under consideration (a = thermal diffusivity, T = period of oscillation), we can assume that the waves propagate in such thickness without appreciable attenuation and phase lag [2][2]. Consequently a linear distribution of temperature will exist (fig. 2), while with respect to time the field will vary sinusoidally according to the relation:

$$H_x = \frac{\partial \vartheta_1}{\partial x} = \frac{2\Theta_\ell}{\ell} \sin \omega t \,, \tag{4}$$

where the origin is on the middle plane and the positive x trend is as marked in figure 2.

Two unidimensional thermal fields are now superposed in the prism under consideration:

$$H_x = \frac{\partial \theta_1}{\partial x} = \frac{2\Theta_\ell}{\ell} \sin \omega t \tag{4}$$

$$H_y = \frac{\partial \theta_2}{\partial y} = \frac{2\Theta_\ell}{\ell} \cos \omega t \tag{5}$$

which are perpendicular and out of phase with one another.

In the middle section (A), the thermal field resulting from the vectorial sum of H_x and H_y will rotate with angular velocity ω and have magnitude $2\,\Theta_\ell/\ell$, and in the complex plane can be represented by the rotating vector (fig. 3):

$$\vec{H} = H_y + j\, H_x = \frac{2\Theta_\ell}{\ell} e^{j\omega t} \,. \tag{6}$$

In fact, considering (4) and (5) as parametric equations of the resulting field and eliminating ωt, we obtain the ordinary equation of the circular trajectory of the point of the resultant rotating vector:

$$H_x^2 + H_y^2 = 4\,\Theta_\ell^2 / \ell^2 \,. \tag{7}$$

In the general case where the thermal field components H_x and H_y have different amplitudes, the parametric equations of these components are [3]:

$$H_x = \frac{2\Theta_x}{\ell} \sin \omega t = a \sin \omega t \tag{8}$$

$$H_y = \frac{2\Theta_y}{\ell} \cos (\omega t + \varphi) = b \cos (\omega t + \varphi) \tag{9}$$

where Θ_x and Θ_y are the amplitudes of the externally applied thermal waves in the x and y direction respectively, and φ is the phase angle between the components H_x and H_y. The equation of the resulting trajectory is an ellipse:

---

[2] Figures in brackets indicate the literature references at the end of this paper.

In this manner v''_4 (and consequently θ_4) has the same time dependence as v'_4.

For zone 2, which is opposed to zone 4 (fig. 5b), the regulation unit maintains constant $v''_2 + v'_2$ at the value 3 mV, so that $v'_2 = v'_4$, v''_2 (and consequently θ_2) oscillates out of phase with respect to v'_2 (and to θ_4), but always in the neighborhood of the constant of 2.5 mV (the equivalent of the temperature on the axis of the specimen). Temperatures θ_1 and θ_3, starting from a signal on the oscillator having a phase lag of $\pi/2$ with respect to v'_4, present a phase lag of $\pi/2$ in comparison to θ_2 and θ_4 respectively. If v'_1 lags behind v'_4 the thermal field rotates clockwise, if v'_1 anticipates v'_4 the thermal field rotates counterclockwise.

3. Results of Experimental Observations and Measurements

In figure 6, recordings are given of temperature waves imposed on the four sides 1,2,3 and 4 of the prism specimen in the case when all the waves have the same amplitude ($\Theta_x = \Theta_y = \Theta_\ell$), and waves on adjacent sides have a $\pi/2$ phase difference. The mean temperature θ_o of the oscillations is constant and equal to +60°C, the value imposed on the axis of the prism.

Figure 7 illustrates the position of thermocouples a, b, and o, used for detecting thermal fields, in the interior and on the middle plane of the specimen. Couples a, b are positioned on the diagonals 15 mm from the axis, i.e. the position where the couple o is placed. This distance of 15 mm must be sufficiently small when compared to the thermal wavelength λ used in the experiments, for previously mentioned reasons. Operating with a period $T = 6$ hours, the wavelength is $\lambda = 2\sqrt{\pi\, a\, T} = 520$ mm, assuming for the present specimen of expanded phenolic resin, according to preceding measurements [1], that $a = 12 \cdot 10^{-7}$ m^2/s.

In figure 8 the connections of the thermocouples for detecting the field are indicated together with the connections between them and the XY plotter. Due to the particular symmetry in positioning of sensitive elements, it follows, that the pair a - o of thermocouples, connected in series, gives the thermal gradient $\partial\theta/\partial X$ which oscillates sinusoidally with time along the X axis, while the second pair b - o gives the thermal gradient $\partial\theta/\partial Y$, perpendicular to the first and a sinusoidal function of time in the direction of Y axis. These gradients, analogous to the thermal fields H_x and H_y mentioned in paragraph 1, are fed into a twin axial XY plotter, in which the motion of the writing pen is directed by one of the thermal fields and the motion of the paper sheet by the other one.

In this manner (fig. 9) the recording of the field resulting from the superposition of the two perpendicular fields oscillating $\pi/2$ out of phase is obtained. From the recording we can observe a field rotating with an angular velocity $\omega \cong 2.9 \times 10^{-4}$ rad/s. The trajectory of the point of the vector representative of the field is practically circular and has the following radius:

$$\frac{\Delta\Theta_{1,3}}{\Delta x} = \frac{\Delta\Theta_{2,4}}{\Delta y} = 2.2\,°\text{C/cm} .$$

With an imposed wave amplitude of 12°C, the amplitude of the thermal field should become, according to eqs. (4), (5), and the assumption of a linear temperature variation within the specimen and therefore of propagation without attenuation, $2\Theta_\ell/\ell = 2.4$°C/cm. This value is nearly 10% greater than the experimental value.

Figure 10 shows a recording of the unidimensional thermal field $\Delta\theta_{1,3}/\Delta x$ alone; the temperature on sides 2 and 4 (constant at the value $\theta_o = +60$°C) and the amplitude and period of temperature waves imposed on faces 1 and 3 (fig. 11) are the same as those already mentioned regarding figure 6. In this recording, which was linear as expected, the thermocouple pair a - o was connected to the X axis and the pair b - o to the Y axis of the XY plotter. Figures 12a and 12b show respectively the general view of the apparatus and the prism mounted in place.

Further experiments could be executed using different amplitudes and frequencies of the imposed temperature waves and choosing different phases for the perpendicular thermal fields. This would enable evaluation of thermal properties of materials, such as thermal diffusivity and the attenuation constant, as in order to detect eventual anisotropies in the same materials. In other experiments we should also be able to verify with thermal fields the general properties of oscillatory phenomena. For example, thermo- and galvano-magnetic effects could be investigated with a superposition of magnetic and thermal fields in electrical conductors and semiconductors. Since the rotation of the thermal field is actuated by means of fixed apparatuses which are external to the medium being studied, we may foresee other applications, for instance to the processes of zone fusion for the purification of metals.

$$\frac{H_x^2}{a^2} + \frac{H_x^2}{b^2} + \frac{2H_x H_y}{ab} \sin\varphi = \cos^2\varphi \,. \tag{10}$$

The resulting field still rotates with angular velocity ω, and the ratio of the semiaxes is:

$$\frac{a}{b} = \tan\psi \tag{11}$$

where ψ is:

$$\sin 2\psi = \frac{-2ab}{a^2 + b^2} \cos\varphi \,. \tag{12}$$

and the azimuth χ is:

$$\chi = \frac{1}{2} \arctan\left(\frac{-2ab}{a^2 + b^2} \sin\varphi \right) \,. \tag{13}$$

2. Description of the Experimental Apparatus

The experiments were made on a prismatic specimen of expanded phenolic resin of dimensions 100 x 100 x 45 mm, having eleven 0.2 mm diameter Cu-Constantan thermocouples[3], according to the schemes of figures 4a and 4b. Four of these couples, each placed on one of the sides of the specimen, are used for the automatic regulation; four others, side by side with the ones above, are connected to a temperature recorder for controlling the imposed oscillations; the remaining three, positioned inside the specimen, are used for detecting the rotating thermal field and are connected to an XY recorder.

The sides of the specimen are covered by four externally blackened aluminum plates of dimensions 95 x 400 x 4 mm, which are used for the purpose of making the surface temperatures uniform. The complete specimen assembly was positioned inside a support structure bearing polished aluminum shields to direct radiating energy fluxes, emitted by each group of infrared radiation lamps L, onto the corresponding surface of the specimen. Four automatic regulators R feed the groups of lamps in such a manner as to cause the temperature in the center of all four sides of the prism to vary sinusoidally with the same amplitude, and such that there is a $\pi/2$ phase difference between the variations of adjacent sides in a clockwise sense around the specimen.

The programming apparatus G of the thermal oscillations is a function generator producing two sinusoidal signals of variable amplitude and phase lag, respectively 0 to 10 V and 0 to 2π.

Each signal, used as a program by two opposed sides, was suitably reduced in amplitude through a dividing resistance P (fig. 4a), so as to reduce the amplitude of the e.m.f. to ± 0.5 mV around the set value of 0.5 mV. This e.m.f. amplitude is equivalent to 12°C of amplitude of temperature oscillation, for the given type of thermocouples. In this temperature range the linearization of the characteristic curve of the thermocouples results in an error of less than 0.1°C. The e.m.f. extracted from the dividing resistance is alternatively added to and subtracted from the signal given by the couples of the opposing faces, and the resulting signals are sent to the regulation units which feed the related infrared radiation heaters.

On the basis of figures 4a and 4b, figure 5a presents the evolution in time of the e.m.f. related to the regulation of zones 4 and 2, which are connected to the same signal from generator G.

The e.m.f. v'_4 extracted from dividing resistance P , is subtracted from v''_4, given by the thermocouple of zone 4, and $v''_4 - v'_4$ is sent into regulation unit R4, which suitably feeds the heaters of the relative zone in order to maintain the e.m.f. corresponding to the said zone at the constant value 2 mV.

---

[3] Systematic experiments, executed with various diameters of thermocouple joints and with various frequencies, indicated that in the foresaid conditions, the influence of the thermal capacity of the joints on the results of the measurements is not detectable by the registering apparatus.

4. References

[1] Codegone,C., Ferro, V., and Sacchi, A., Prove di risonanza di oscillazioni termiche, - Atti Accademia delle Scienze di Torino 100, 377-388, (1965/66). Ancora sulle oscillazioni termiche in piane, - Atti Accademia Scienze di Torino 100, 627-634, (1965/66).

[2] Grober, H., and Erk, S., Die Grundgesetze der Warmeubertragung, J. Springer, Berlin 81, (1933).

[3] Perucca, E., Fisica generale e sperimentale, U.T.E.T., Vol. 1, Torino, 128, (1949).

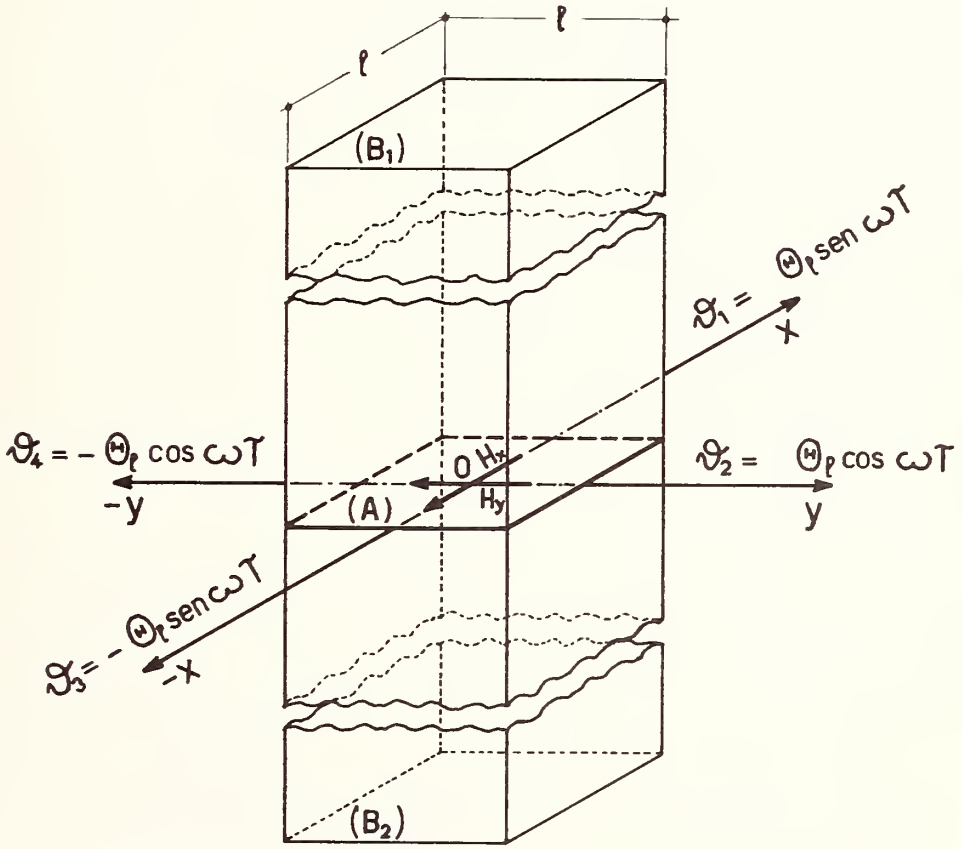

Figure 1

Scheme of the principle for the actuation of a bidimensional thermal field in the prismatic specimen of the considered material.

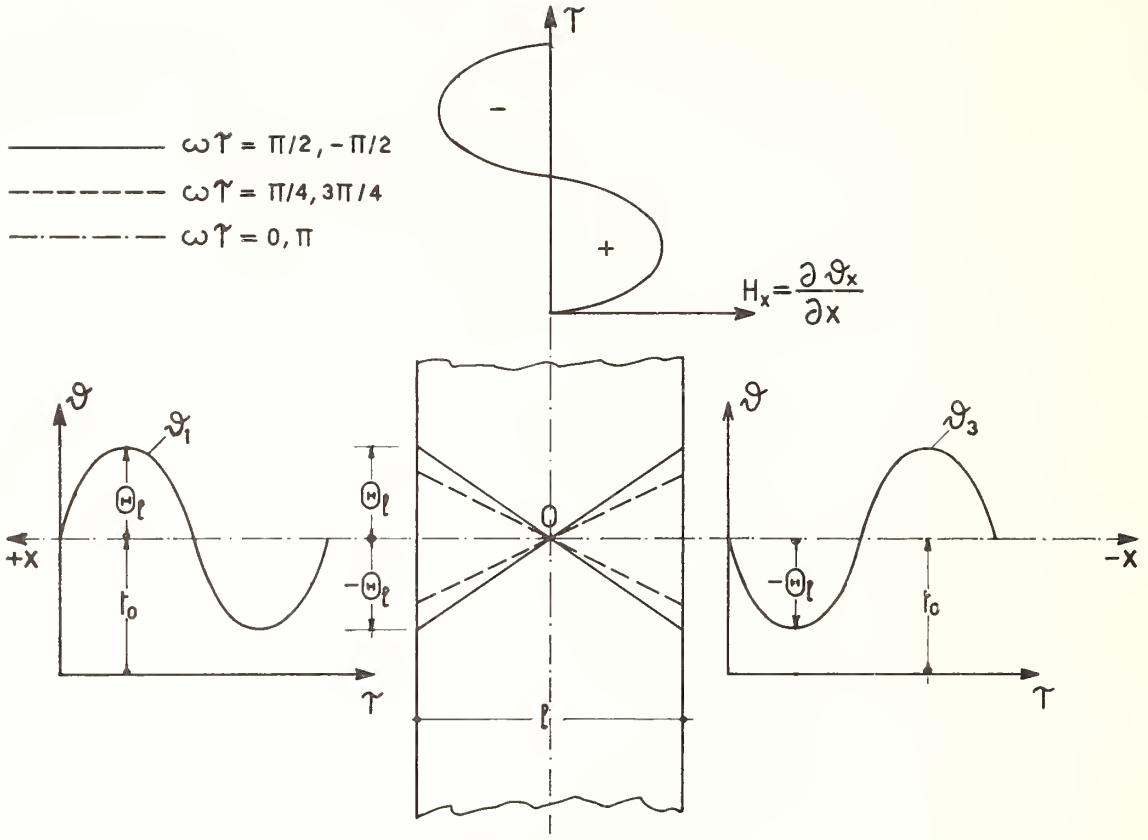

Figure 2

Thermal unidimensional field in a slab with linear distribution of temperature along the thickness of the same.

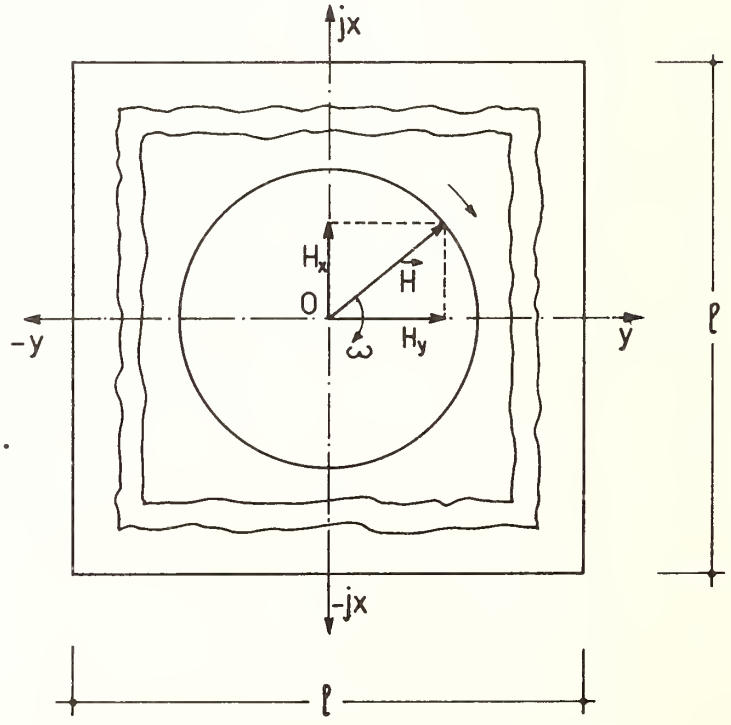

Figure 3
Rotating thermal field in a transversal section of the prism.

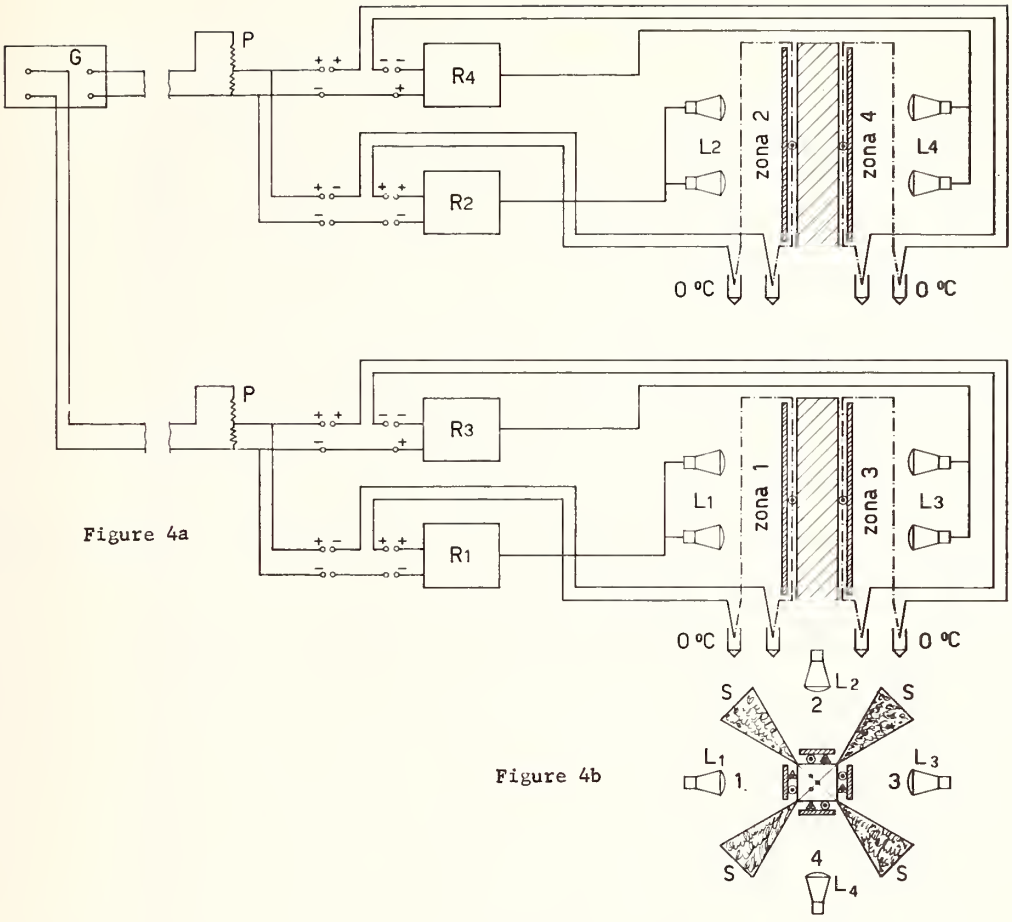

Figure 4a

Figure 4b

Figure 4a

Functional scheme of the experimental apparatus.

G = wave generator

L = infrared radiation lamps

P = partition resistance

R = P.I.D. action regulators with magnetic power amplifiers.

Figure 4b

Transversal section of the specimen with schematic indication of thermo couple used for:

○ regulation

Δ recording

● XY recording

S = polished aluminum shields filled by insulating material.

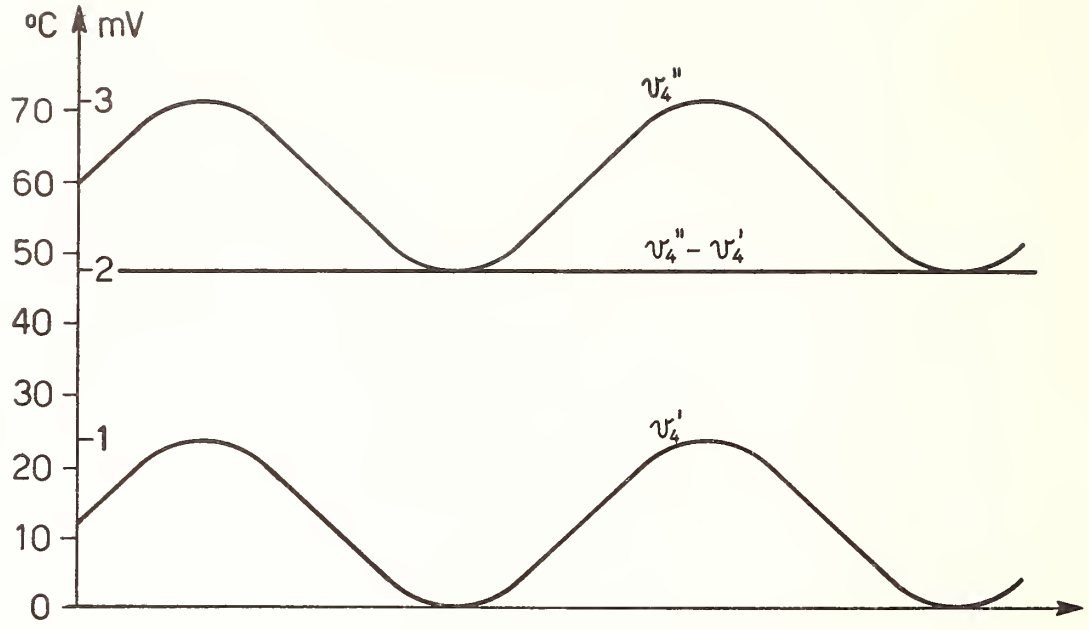

Figure 5a

Bearing of e.m.f. relative to the regulation of zone 4.

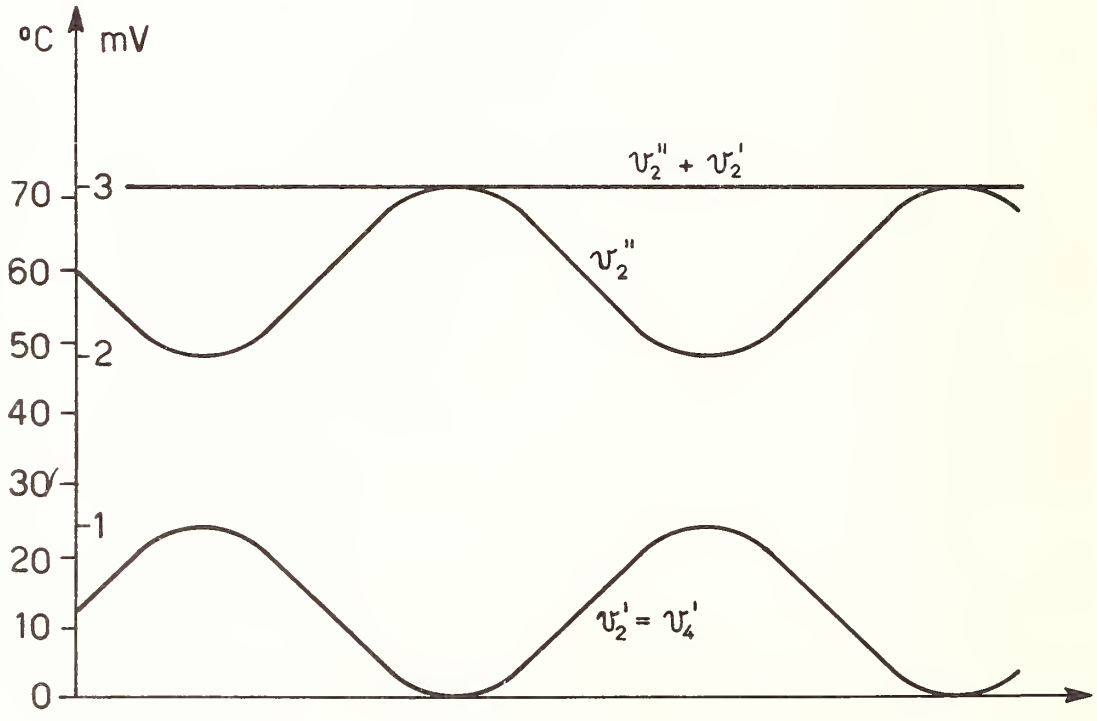

Figure 5b

Bearing of e.m.f. relative to the regulation of zone 2.

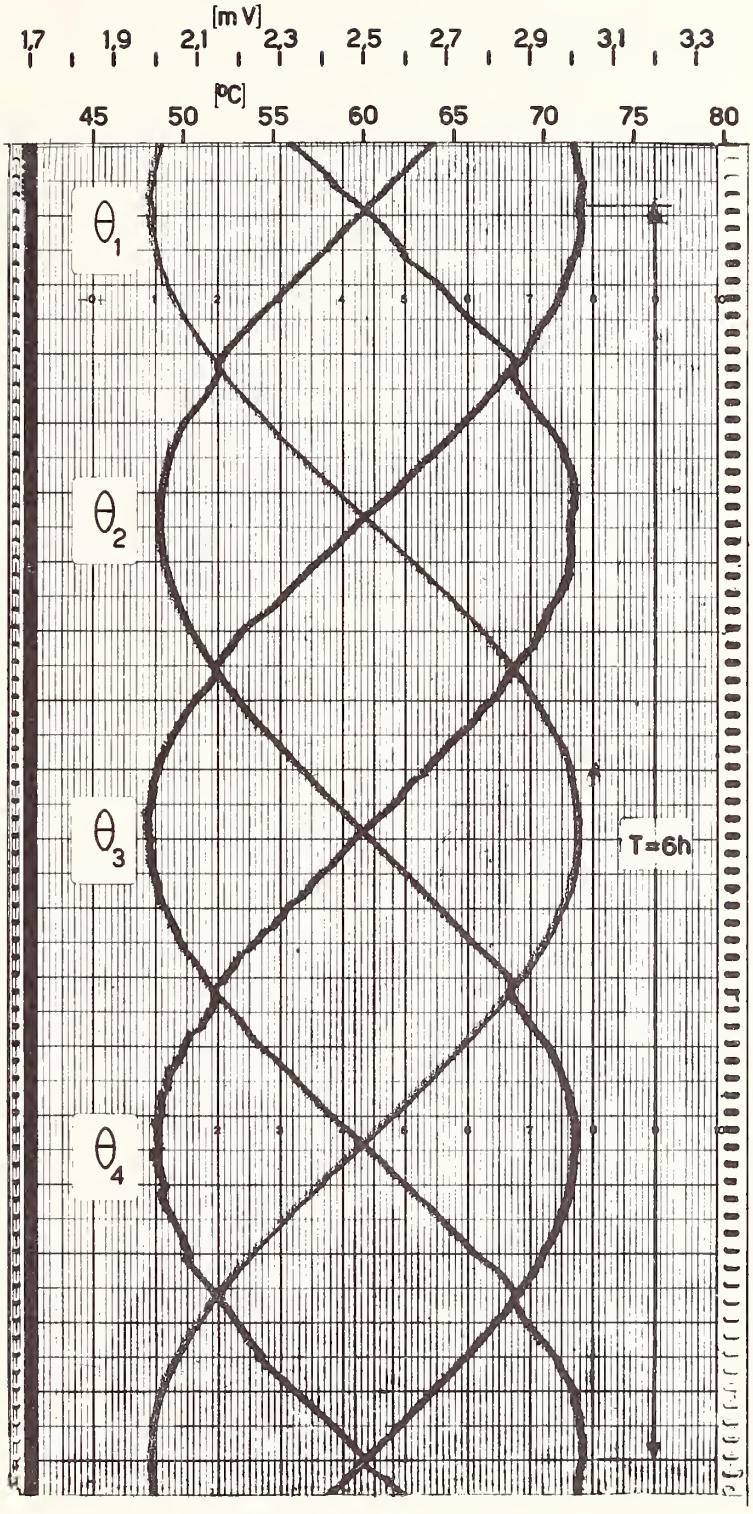

Figure 6

Recording in time of the waves of temperature $\theta_1, \theta_2, \theta_3, \theta_4$ imposed on the four sides of the prism (see fig. 1) for a period T = 6 hs.

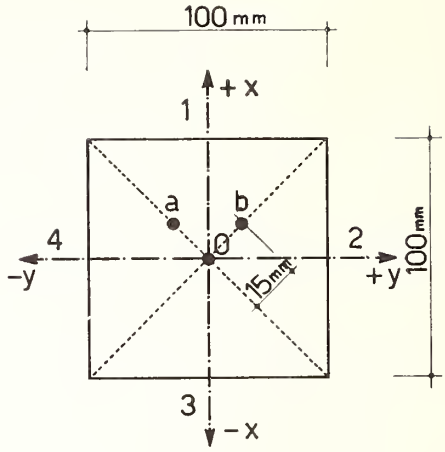

Figure 7

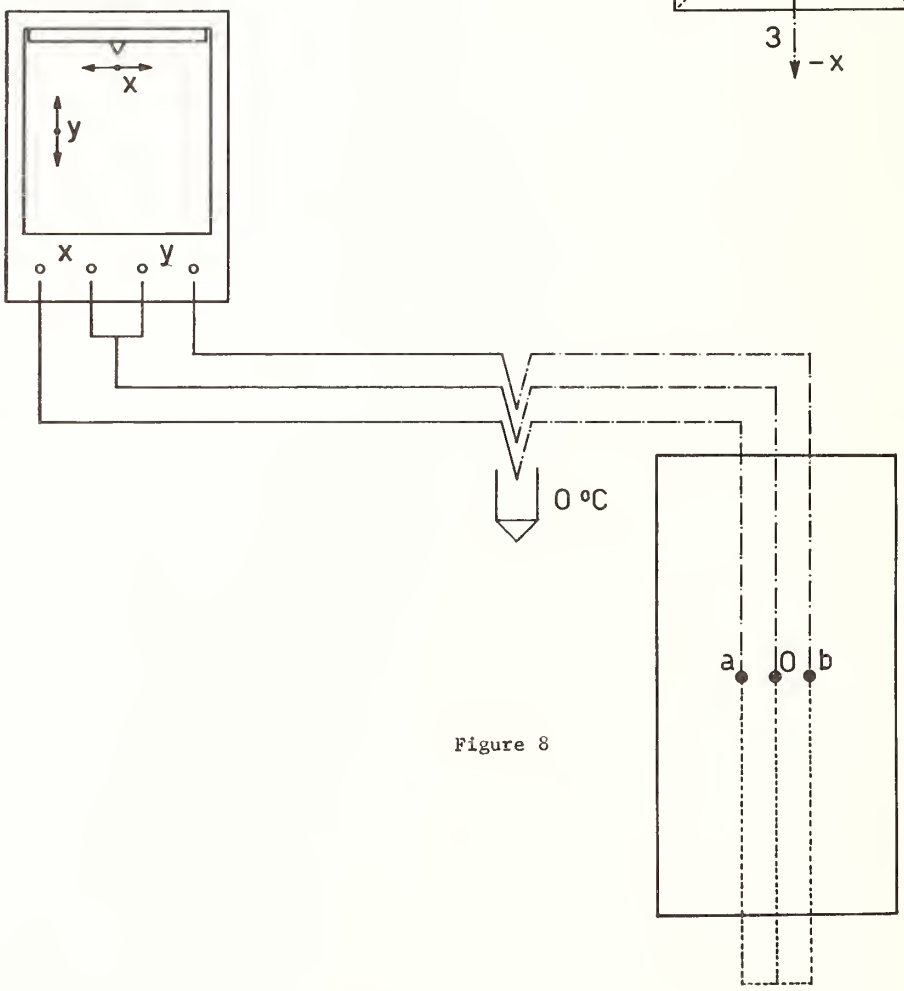

Figure 8

Figure 7

Position of the thermocouples in the transversal section of the specimen for the detection of the rotating thermal field $\vec{H}$.

Figure 8

Scheme of the connections of the couples in figure 7 to the XY plotter for the field $\vec{H}$.

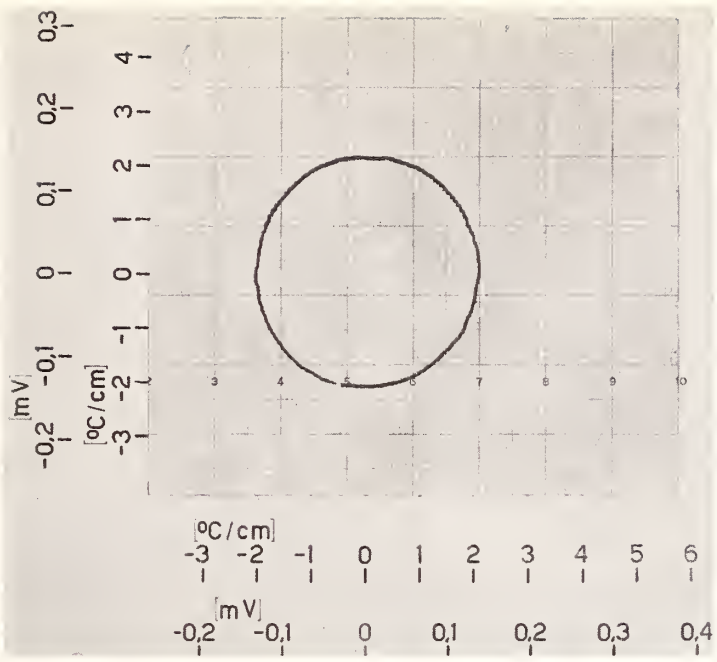

Figure 9

Recording of the thermal rotating field $\vec{H}$ in the section of figure 7, imposing on the external sides the waves of figure 6 .

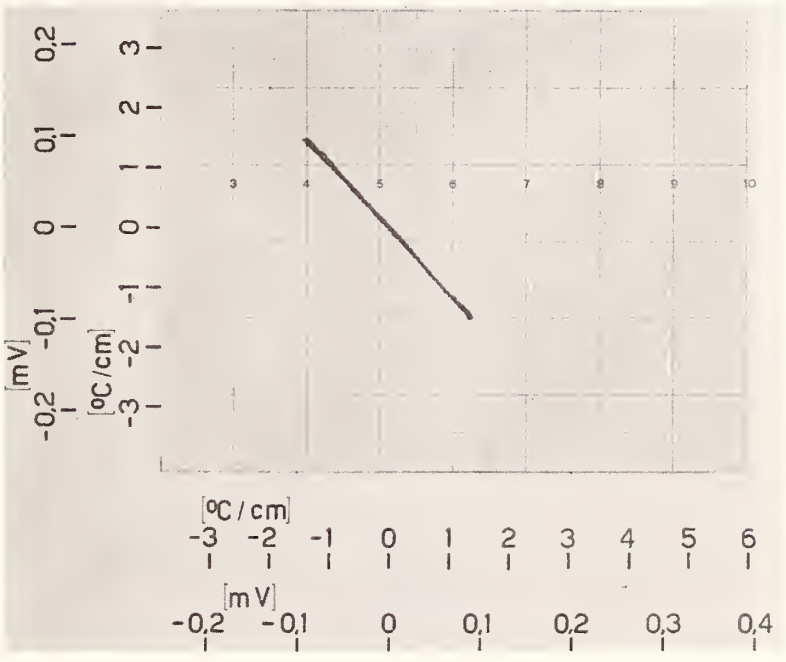

Figure 10

Recording of the unidimensional thermal field H_x, with connections to XY plotter as in figure 8.

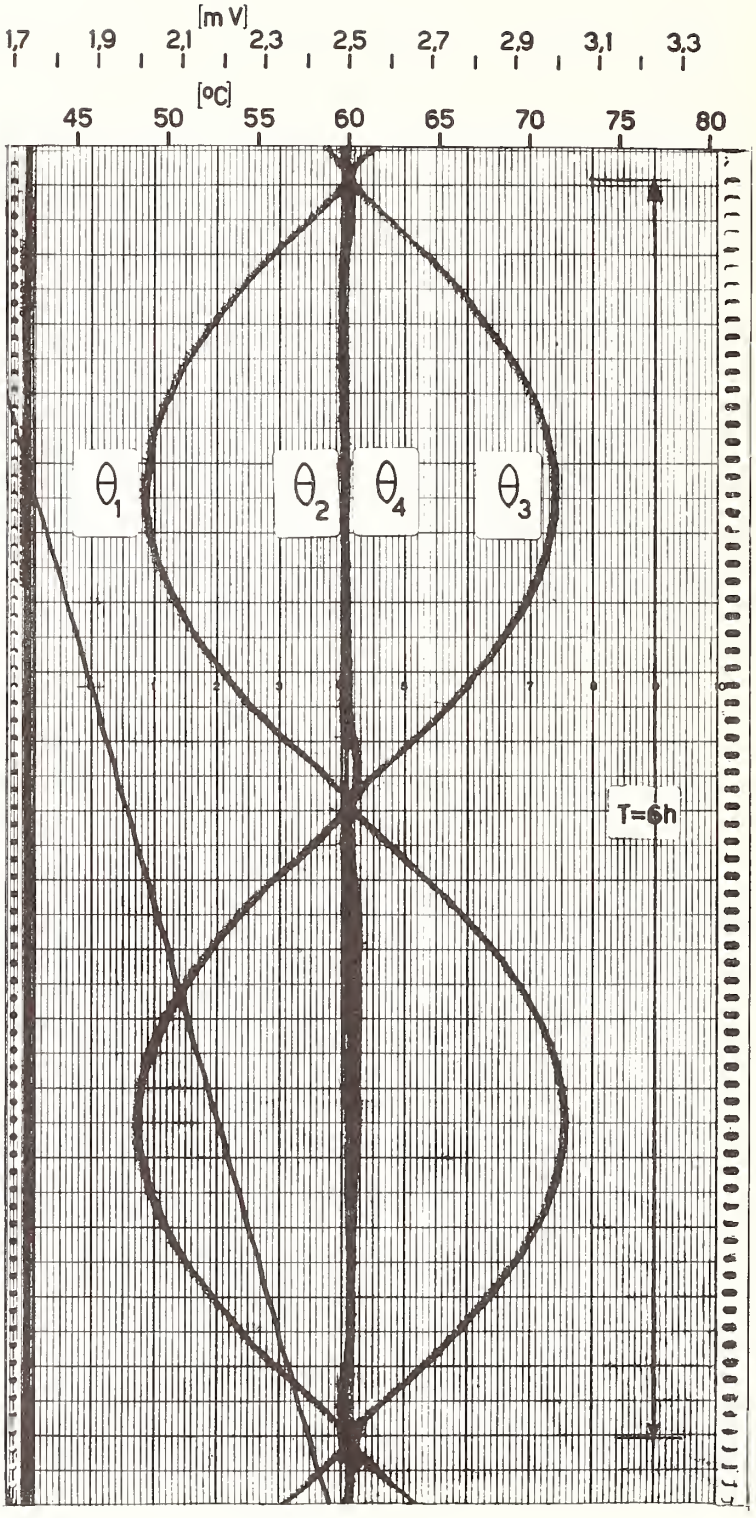

Figure 11

Recording in time of temperature waves θ_1 and θ_3 imposed on sides 1 and 3 of the prism, for detecting unidimensional field H_x, the value of temperature on sides 2 and 4 is equal $\theta_2 = \theta_4 = \theta_o = +60°C$.

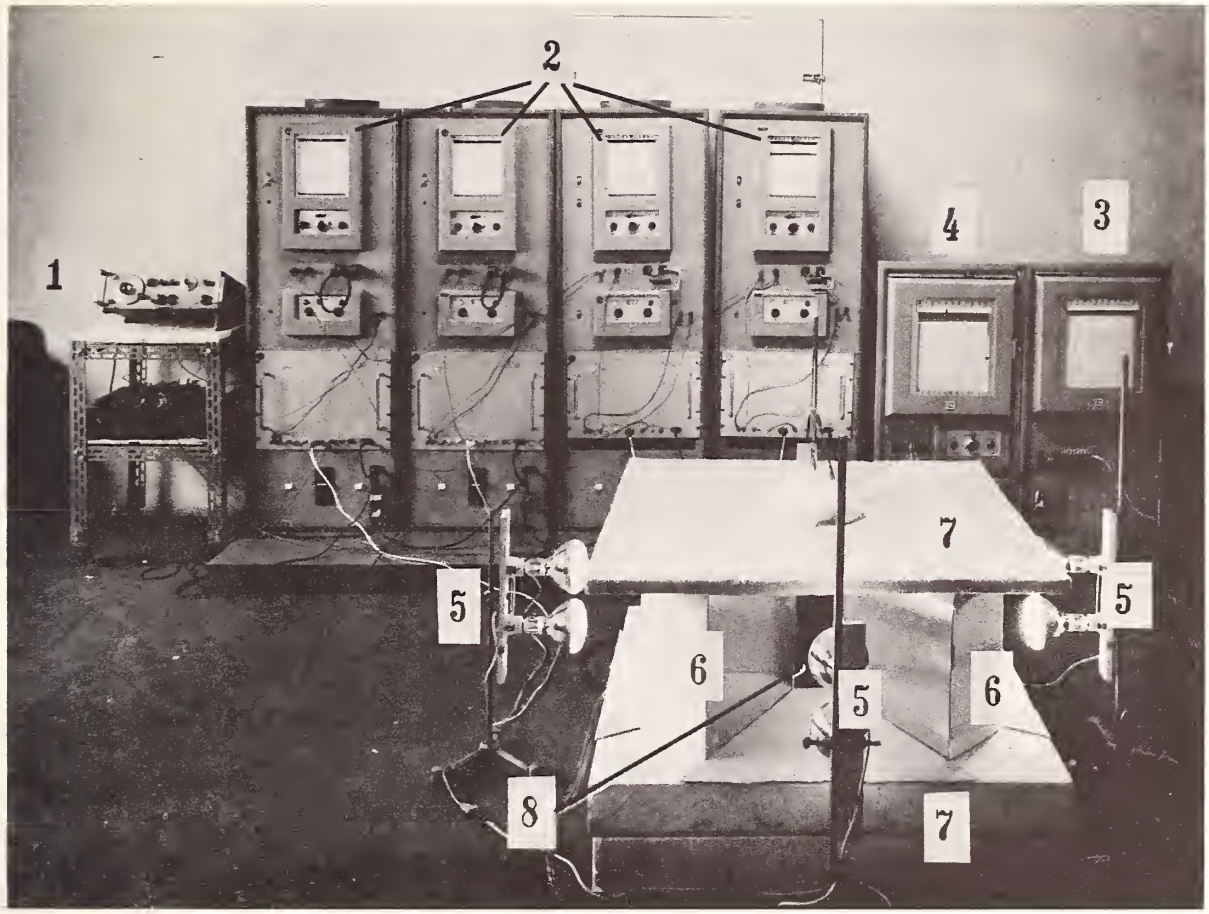

Figure 12a

Photographic view of the experimental apparatus.

1 - Wave generator

2 - Regulators of imposed thermal waves

3 - Recorder of imposed thermal waves

4 - XY plotter

5 - Lamps

6 - Vertical shields

7 - Horizontal shields

8 - Prism, seat of rotating thermal field.

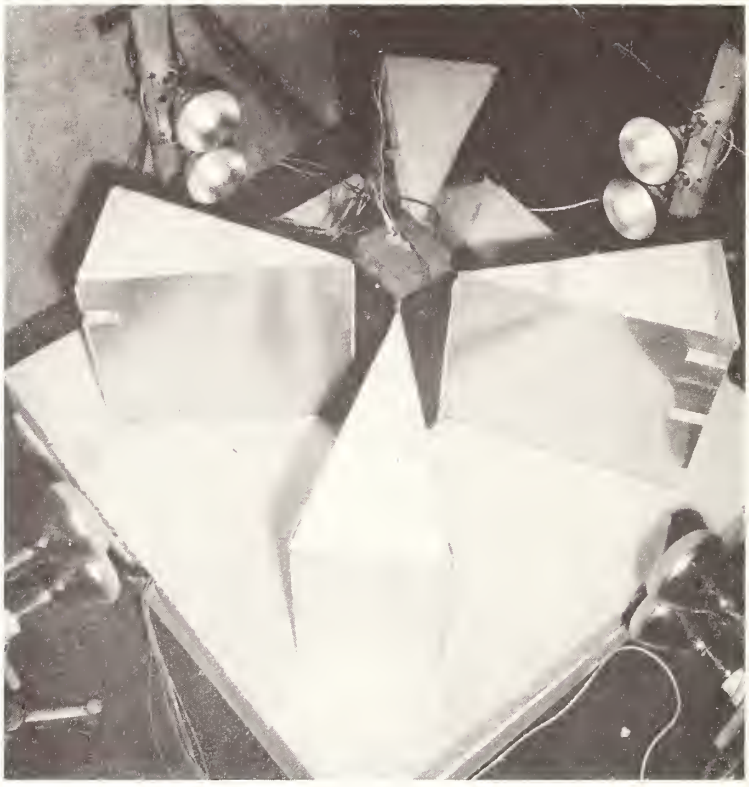

Figure 12b

Photographic view of the prismatic specimen, seat of rotating thermal field with basal and side shields.

Thermal Attenuation through Homogeneous and Multilayer Slabs in Steady Periodic Conditions - Theory and Experiments

V. Ferro, A. Sacchi and C. Codegone[1]

Istituto di Fisica Tecnica - Politecnico
10129 - Turin - (Italy)

Tests of thermal oscillation through homogeneous or multilayer slabs have been carried out on a device consisting of two equal and plane samples with and without thermal capacity interposed. By a suitable control system identical, sinusoidal temperature oscillations have been imposed onto both external surfaces of the device and recorded, and the temperature oscillations received at the internal surfaces have been recorded. With a proper test arrangement, reduction factors of temperature waves at various frequencies have been found by this method, and the characteristic parameters of the thermal propagation through the homogeneous or composite slabs have been experimentally determined. The experimental results have been compared with those one can calculate from the theory of periodic thermal conduction through slabs.

Key Words: Attenuation through slabs, characteristic parameters of periodic conduction, periodic thermal waves.

1. Introduction

The study of the transmission of thermal steady waves through homogeneous or multilayer slabs has been carried out by several authors in the past[1 - 6][2] and more recently by others[7 - 11].

In this work an experimental apparatus is examined to evaluate the attenuation and the phase difference of thermal sinusoidal waves through a simple or a composite slab with and without thermal capacity in series to the same slab.

Parameters are obtained from these tests which fully characterize the behaviour of the slabs in periodic thermal conditions, and moreover the field of agreement of theory with the experimental results is determined.

2. Theory of the Phenomenon

2.1. Homogeneous Slab

The Fourier equation for the one-dimensional heat flow through a flat and homogeneous slab infinitely extended in the direction normal to its thickness and which is free of heat sources or sinks, is expressed through the Laplace transform Θ of the temperature θ, by the well-known relation:

$$\frac{d^2\Theta}{dx^2} = \frac{1}{a} p\Theta \qquad (1)$$

---

[1]Assistants and Professor of Technical Physics, respectively.

[2]Figures in brackets indicate the literature references at the end of this paper.

where x is the abscissa of the generic isothermal plane surface, $\underline{a}$ is the thermal diffusivity and p the auxiliary variable introduced by the transformation. If a thermal capacity $2C_i$, referred to the unit surface and expressed in $kJm^{-2}°C^{-1}$ is put in the middle of the slab, eq (1) is still valid with the following boundary conditions transformed according to Laplace, (fig. 1):

$$\text{at } x = \pm \ell \qquad \Theta = \Theta_\ell = \Theta_{-\ell} \tag{2}$$

$$\text{at } x = 0 \qquad \lambda \left(\frac{d\,\Theta}{dx}\right)_{x=0} = C_i p\, \Theta_o = -\Phi_o, \tag{3}$$

where ℓ is the thickness of the slab and λ is the thermal conductivity of the material, and Φ represents the Laplace transform of the flux φ.

When the temperature changes on the external surfaces of the slab are sinusoidal with pulsation $\omega = 2\pi f$, the steady state solution of eq (1) with $p = j\omega$ ($j = \sqrt{-1}$) and with the boundary conditions (2) and (3), becomes:

$$\Theta = \Theta_o \cos h \{(1 + j) \times [\omega/2a]^{1/2}\} + j\omega C_i Z_\infty \Theta_o \sin h \{(1 + j) \times [\omega/(2a)]^{1/2}\} = A\Theta_o + Bj\omega C_i \Theta_o \tag{4}$$

where the expressions for A and B are obvious from eq (4). The heat flux in the slab is given by

$$\varphi = -\lambda \partial\theta/\partial x \tag{5}$$

and its Laplace transform for this case is:

$$\begin{aligned} \Phi &= [\Phi_o/j\omega C_i Z_\infty)]\{\sinh \ (1 + j) \times [\omega/(2a)]^{1/2} + \Phi_o \cosh \ \{(1 + j) \times [\omega/(2a)]^{1/2}\} \\ &= C \frac{\Phi_o}{j\omega C_i} + D\Phi_o. \end{aligned} \tag{6}$$

where $Z_\infty = (1 - j)/\sqrt{2\omega\lambda\rho c}$ (ρ = density [$kg\ m^{-3}$] and c = specific heat [$Jkg^{-1}°C^{-1}$] is the characteristic thermal impedance of the medium which is assumed to be infinitely extended in the x-direction, and through which the thermal wave propagates. The expression for the parameters A and B are easily deduced from eq (4). The expressions for C and D result from eq (6) and for a homogeneous slab are: $A = D$ and $B = CZ_\infty^2$.

Developing eqs (4) and (6), and separating the real part from the imaginary part yield the reduction factors σ of temperature and heat flux oxcillations through the slab between the surfaces $x = \pm \ell$ and $x = 0$. We obtain for the moduli of σ:

$$|\sigma_\theta| = \Theta_o/\Theta_\ell = \theta_o/\theta_\ell = [(M_1 + R\epsilon M_2)^2 + (N_1 + R\epsilon N_2)^2]^{-1/2} \tag{7}$$

$$|\sigma_\varphi| = \Theta_o/\Theta_\ell = \varphi_o/\varphi_\ell = \{[M_1 + N_2/(2\epsilon R)]^2 + [(N_1 - M_2/(2\epsilon R)^2]\}^{-1/2} \tag{8}$$

where:

$\epsilon = \ell[\omega/2a]^{1/2}$ $\qquad$ $R = C_i/(\rho c \ell)$

$M_1 = \cos h\epsilon \cos\epsilon$ $\qquad$ $M_2 = \sinh\epsilon\cos\epsilon - \cosh\epsilon \sin\epsilon$

$N_1 = \sinh\epsilon \sin\epsilon$ $\qquad$ $N_2 = \sinh\epsilon \cos\epsilon - \cosh\epsilon \sin\epsilon$

In logarithmic units, according to electrotechnical notations, the relations (7) and (8) become, in terms of the attenuation α:

$$\alpha_\theta = 20 \log_{10}\left(1/|\sigma_\theta|\right) \qquad \alpha_\varphi = 20 \log_{10}\left(1/|\sigma_\varphi|\right) \qquad (9), (10)$$

The phase differences ψ of the temperature and flux waves between the same surfaces are:

$$\psi_\theta = \arctan(\Theta_\ell/\Theta_o) = \arctan(\theta_\ell/\theta_o) = \arctan\left[(N_1 + R\varepsilon N_2)/(M_1 + R\varepsilon M_2)\right] \qquad (11)$$

$$\psi_\varphi = \arctan(\Phi_\ell/\Phi_o) = \arctan(\varphi_\ell/\varphi_o) = \arctan\left\{[N_1 + M_2/(2\varepsilon R)]/[M_1 + N_2/(2\varepsilon R)]\right\} \qquad (12)$$

One can observe that the eqs. (7), (8), (11) and (12) become, when R = 0 and thus $C_i = 0$:

$$|\sigma_{o,\theta}| = (M_1^2 + N_1^2)^{-1/2} \qquad \sigma_{o,\varphi} = 0 \qquad (13), (14)$$

$$\psi_{o,\theta} = \arctan(\tanh\varepsilon \tan\varepsilon) \qquad (15)$$

$$\psi_{o,\varphi} = \arctan\left[(\tanh\varepsilon \cot\varepsilon - 1)/(\tanh\varepsilon \cot\varepsilon + 1)\right] \qquad (16)$$

If R = 0 and $\varepsilon > 1$, eqs. (9), (11) and (12) can be written:

$$\alpha_{o,\theta} = 8.686\varepsilon - 6.02 \quad [\text{db}] \qquad (17)$$

$$\psi_{o,\theta} \cong \varepsilon \qquad \psi_{o,\varphi} \cong (1 - \tan\varepsilon)/(1 + \tan\varepsilon) \qquad (18), (19)$$

and, if $\varepsilon = \pi$, the eqs. (17), (18) and (19) are simply:

$$\alpha_{o,\theta} = 21.082 \qquad \psi_{o,\theta} = \pi \qquad \psi_{o,\varphi} = \pi/4 \qquad (20), (21), (22)$$

which represent half-wave stationary conditions through the slab and in this case the pulsation $\omega = 2\pi^2 a/\ell^2$ results [12].

In figures 2,3 and 4 eqs (7)-(19) are plotted versus the non-dimensional parameters ε and R.

2.2. Multilayer Slabs

Theoretical analysis, performed by several authors [5], [6], [13], has established that the composite slabs, made of several sublayers of homogeneous isotropic materials arranged normally to flow lines, may be treated as a cascade of four-terminal networks if the boundary effects are negligible. Of course, each four-terminal network of the cascade is supposed to be passive, linear, and bilateral, and moreover the wave amplitudes are assumed relatively small so that the thermal diffusivity may be considered a constant and hence the superposition of the effects due to different frequencies is appliable.

The discussion is carried out generally using the theory of complex variable functions. We indicate a generical frequency $f_\nu = \omega_\nu/(2\pi) = 1/\tau_\nu$ (ω_ν = angular frequency, τ_ν = wave period, $\nu = 1,2,\ldots, k,\ldots$ is the progressive number of the various frequencies), $\theta_{o\nu}$ and $\varphi_{o\nu}$ are the sinusoidal components of temperature and thermal flux at the external surface S_o of the composite slab ($\varphi_{o\nu}$ being referred to the unit face area of the slab) and $\theta_{n\nu}$ and $\varphi_{n\nu}$ are the same quantities referred to the opposite surface S_n. We thus obtain, using matrix formulation:

$$\begin{vmatrix} \theta_{o\nu} \\ \varphi_{o\nu} \end{vmatrix} = \begin{vmatrix} \Theta_{o\nu} \\ \Phi_{o\nu} \end{vmatrix} = \prod_{m=1}^{n} \begin{vmatrix} a_{m\nu} & b_{m\nu} \\ c_{m\nu} & d_{m\nu} \end{vmatrix} \begin{vmatrix} \theta_{n\nu} \\ \varphi_{n\nu} \end{vmatrix} = \begin{vmatrix} A_\nu & B_\nu \\ C_\nu & D_\nu \end{vmatrix} \begin{vmatrix} \theta_{n\nu} \\ \varphi_{n\nu} \end{vmatrix} = \begin{vmatrix} A_\nu & B_\nu \\ C_\nu & D_\nu \end{vmatrix} \begin{vmatrix} \Theta_{n\nu} \\ \Phi_{n\nu} \end{vmatrix} \tag{23}$$

where $a_{m\nu}$, $b_{m\nu}$, $c_{m\nu}$ and $d_{m\nu}$ are suitable complex constants like those given in eqs. (4) and (6) and are related to the m-th homogeneous sublayer at the frequency f_ν, n is the number of the sublayers and $\prod$ the symbol of product. A_ν , B_ν , C_ν and D_ν may be held as characteristic parameters of the multilayer slab at the frequency f_ν. We remember that in the sinusoidal case yields in general $\theta_\nu = \Theta_\nu \, e^{j\omega_\nu t}$ and $\varphi_\nu = \Phi_\nu \, e^{j\omega_\nu t}$.

According to the methods used in all branches of electrotechnics where similar problems are met, the positive direction assigned to the heat flows $\varphi_{o\nu}$ and $\varphi_{n\nu}$ is the same direction of the thermal wave transmission, namely from the surface to which temperature oscillations are applied toward the surface which is consequently affected. Any change in the direction of the thermal waves causes the flow sign to change, thus yielding:

$$\begin{vmatrix} \theta_{n\nu} \\ \varphi_{n\nu} \end{vmatrix} = \begin{vmatrix} D_\nu & B_\nu \\ C_\nu & A_\nu \end{vmatrix} \begin{vmatrix} \theta_{o\nu} \\ \varphi_{o\nu} \end{vmatrix} \tag{24}$$

since the parameters A_ν, B_ν, C_ν and D_ν, just as $a_{m\nu}$, $b_{m\nu}$, $c_{m\nu}$ and $d_{m\nu}$, must satisfy the unimodularity condition, which is satisfied by any linear, bilateral, and passive system:

$$A_\nu \, D_\nu - B_\nu \, C_\nu = 1 \, . \tag{25}$$

These parameters are complex quantities: only three of them are independent, and the fourth is determined from the others by eqs. (25); the number of independent quantities becomes two in the case of slabs having a symmetric arrangement of the layers, because we have now:

$$A_\nu = D_\nu \, . \tag{26}$$

The parameters uniquely define, at a given frequency f_ν, the behavior of the composite slab which is subject to temperature oscillations.

For instance, if we assume that the surface S_o is bounded by an outside ambient (h_e being the corresponding film coefficient) and the surface S_n is in contact with an inside ambient (h_i being the corresponding film coefficient), we have:

$$\begin{vmatrix} \theta_{e\nu} \\ \varphi_{e\nu} \end{vmatrix} = \begin{vmatrix} 1 & -1/h_e \\ 0 & 1 \end{vmatrix} \begin{vmatrix} A_\nu & B_\nu \\ C_\nu & D_\nu \end{vmatrix} \begin{vmatrix} 1 & -1/h_i \\ 0 & 1 \end{vmatrix} \begin{vmatrix} \theta_{i\nu} \\ \varphi_{i\nu} \end{vmatrix} = \begin{vmatrix} E_\nu & F_\nu \\ G_\nu & H_\nu \end{vmatrix} \begin{vmatrix} \theta_{i\nu} \\ \varphi_{i\nu} \end{vmatrix} \tag{27}$$

where at a given frequency f_ν, $\varphi_{e\nu}$ and $\varphi_{i\nu}$ are the thermal fluxes referred to the outside and to the inside ambients respectively, and $\theta_{e\nu}$ and $\theta_{i\nu}$ are the corresponding temperature values.

All quantities involved and previously defined have in practice a periodic behaviour which is generally not sinusoidal. They can, however, be expanded in Fourier series, each of which yields a sum of a constant term, a fundamental frequency wave term, and successive harmonic terms. The characteristic parameters should then be evaluated both for the direct or constant component and for each of the various sinusoidal components of the periodic wave, repeating the above discussion about the composite slab behaviour for each frequency. With this purpose in mind, an experimental method which has been set up for the measurement of these complex quantities, is now described.

3. Principles of the Experimental Method

Neglecting the film heat resistances, the parameters which fully describe the thermal behaviour of a multilayer slab at a given frequency are those called A_ν , B_ν , C_ν and D_ν in eq (23). Since, according to eq (25) only three of them are independent, three experimental measurements will be sufficient to evaluate all of them. Moreover we want to avoid a direct measurement of the oscillating heat flux, which is very difficult.

The homogeneous slab, which is characterized by the parameters $A = D$, B and C of eqs. (4) and (6) [or $a_{m\nu} = d_{m\nu}$ and $c_{m\nu}$ of eq. (23)], can be considered a particular case of the multilayer slab. Accordingly we designed the following sequence of experiments, each of them leading to the evaluation of one parameter at a given frequency.

3.1. Measurement of A_ν

Two identical slabs are placed close to each other so that the surfaces S_n are in mutual contact (fig. 5a). A sinusoidal temperature oscillation $\theta_{o\nu}$ is imposed on both surfaces S_o and the temperature $\theta_{n\nu}$ is recorded at the facing internal surfaces S_n. This arrangement corresponds to the boundary condition $\varphi_{n\nu} = 0$. The ratio $\theta_{o\nu}/\theta_{n\nu}$ is a complex number whose modulus is the inverse of the reduction factor of the amplitudes of the sinusoidal oscillations, and whose argument is the phase difference between these oscillations. Equation (23) then yields:

$$A_\nu = \frac{\theta_{o\nu}}{\theta_{n\nu}} = \frac{\Theta_{o\nu}}{\Theta_{n\nu}} \tag{28}$$

For a homogeneous slab the boundary condition is $\varphi_{o\nu} = 0$ and remembering eq (4) for $C_i = 0$ and $x = \ell$, we have:

$$1/|\sigma_{\nu\theta}| = a_\nu = \theta_{\ell\nu} / \theta_{o\nu} = \Theta_{\ell\nu} / \Theta_{o\nu} = \cosh[(1+j)\varepsilon_\nu] \tag{29}$$

3.2. Measurement of B_ν

The same arrangement of the previous experiment is kept, and a thin conducting layer is inserted between the internal facing surfaces S_n so that it is in good thermal contact with them. This layer must present a thermal diffusivity much higher than that of the multilayer slab under test. It has a known thermal capacity $2C_i$ and it is provided with suitable notches to avoid heat conduction from the center toward the periphery (fig. 5b). A sinusoidal temperature oscillation $\theta_{o\nu}$ is imposed on both outside surfaces S_o and the temperature $\theta_{n\nu}$ at the inside surfaces S_n is recorded.

In this case we have:

$$\varphi_{n\nu} = j\omega_\nu C_i \theta_{n\nu}$$

and from the first of eqs. (23) it follows that:

$$\theta_{o\nu} = A_\nu \theta_{n\nu} + jB_\nu \omega_\nu C_i \theta_{n\nu} .$$

So we obtain:

$$B_\nu = \frac{\theta_{o\nu}/\theta_{n\nu} - A_\nu}{j\omega_\nu C_i} \tag{30}$$

Similarly in a homogeneous slab, for $x = \ell$, eq (4) holds and therefore we have:

$$b_\nu = \frac{\Theta_{\ell\nu}/\Theta_{o\nu} - a_\nu}{j\omega_\nu C_i} = \frac{\Theta_{\ell\nu}/\Theta_{o\nu} - \cosh[(1+j)\varepsilon_\nu]}{j\omega_\nu C_i} = Z_{\infty\nu} \sinh[(1+j)\varepsilon_\nu] . \tag{31}$$

3.3. Measurement of D_ν

Both slab elements are reversed (fig. 5c), so that the surfaces S_o are in mutual contact and we then proceed according to section 3.1. The temperature oscillation $\theta_{n\nu}$ is applied to the outer surfaces S_n and the corresponding oscillation $\theta_{o\nu}$ is now recorded at the facing surfaces S_o. From eq (24), remembering that with this arrangement $\varphi_{o\nu} = 0$, we obtain:

$$D_\nu = \frac{\theta_{n\nu}}{\theta_{o\nu}} \tag{32}$$

If the slab is symmetric, it follows $A_\nu = D_\nu$ and the test shown in this section is not necessary. This is also true for the case of a homogeneous slab, where $a_\nu = d_\nu$. The parameter C_ν can now be evaluated from eq (25). For a homogeneous slab it is simply $c_\nu = b_\nu / Z_{\infty\nu}^2$.

4. Description of the Experimental Equipment

The equipment used to perform the experiments on the multilayers slabs is shown schematically in figure 6. Slab samples M_1 and M_2, placed according to one of the arrangements described in the preceding section, are fastened between two metal plates 6a and 6b with guard rings 3a and 3b. The plates and the rings are equipped with nickel-chrome heating resistances 2a, 2b, 5a and 5b, and face the outer surfaces of the sample layers M_1, which are in good thermal contact with them.

Two cooling tanks, 1a and 1b, are located next to the heating plates. Each one of them faces the heating elements and has a copper plate (size 500 x 500 x 10 mm) which is kept isothermal by circulating water or methyl alcohol at a temperature about 25-40°C lower than the mean temperature of the heating elements. The temperature value in the range 25-40°C is chosen as a function of the wave frequency. The temperature of the cooling tanks is kept at a value much lower than the oscillating temperature minimum, while the control systems deliver the power required to impose the programmed temperature oscillation on the slab surfaces. Two asbestos sheets, 4a and 4b, separate the cooling tanks from the heating plates. The temperature oscillation amplitudes must have limited values ($\approx$5-10°C), so that the transport parameters can be considered constant and therefore the heat flux equations linear, as it was assumed in the previous sections.

A sinusoidal wave generator G, with pre-arrangeable amplitude and frequency, causes the temperature to oscillate at the central heating unit (5a and 5b) through two control systems R_1 and R_5, whereas the two guard sections 2a and 2b follow the temperature of the corresponding heating unit by means of two differential thermocouples, which are connected to control units R_6 and R_7 respectively.

In order to avoid errors due to heat losses at the edges when the composite slab includes some good conductor layer, or in some instances a layer with a thermal diffusivity higher than others in the sample, the influence of the conducting layer is compensated for on an average by means of the peripheral heating resistances r_2 and r_3, controlled by the systems R_2 and R_3. These control systems operate so as to equalize the temperatures of the center and of the periphery of the conducting layer, which has a thermal capacity of $2C_i$. An additional control element R_4 eliminates the heat losses at the edges of the thermal capacity $2C_i$ by means of a peripheral heating resistance r_4 and a cooling pipe 7.

The thermal capacity $2C_i$ is built of an aluminum plate 1 mm thick [$C_i = 1195\ Jm^{-2}°C^{-1}$] or 2 mm thick [$C_i = 2390\ Jm^{-2}°C^{-1}$] or 4 mm thick [$C_i = 4780\ Jm^{-2}°C^{-1}$], which is suitably divided in concentric squares separated by air annuli to further reduce the peripheral heat losses.

All control systems used are of the P.I.D. (proportional, integral and differential) type, with final power amplifiers. The whole assembly, including samples, heating units, and cooling tanks, is tightened in the thermal flux direction and is thermally insulated on the peripheral surfaces with fiberglass. It is then placed in a usual room for oscillating tests at mean temperature in the range +40 to +60°C, or in a refrigerated box with dried atmosphere for tests at a mean temperature of about 0°C or lower. In this second case the box is kept at the average temperature of the programmed thermal oscillation by means of a suitable control system. Chromel-Alumel thermocouples (0.32 mm dia.) are located on outer and inner surfaces of the slab samples and in the middle of the system within suitable grooves. They follow in part an isothermal path and are connected to a multipoint potentiometric recorder T.

This experimental apparatus is obviously also employed for tests on homogeneous slabs. A modification of this device uses a radiant heating source [12], [14] instead of a conducting heating source like plates 6a, b and 3a, b of figure 6.

5. Experimental Results

5.1. Homogeneous Slabs

Figures 7a and 7b reproduce the recordings of the imposed temperature wave θ_ℓ and of the transmitted wave θ_ρ, obtained for a sample of rigid polyurethane foam, with and without thermal capacity C_i in series. Three types of synthetic expanded materials were tested: polystyrene, phenolic resin and polyurethane.

Through the experimental measurements of the equivalent thermal conductivity λ, the apparent density ρ, and the equivalent specific heat c[3], the diffusivity value a and therefore the value of the dimensionless parameter ε were deduced for the samples tested. From this value of ε and through the theoretical relationships (7), (9), (11), (13), (15), (17), (18), we have plotted the curves of the attenuation (or reduction factor) and the phase difference, which in figures 8-11 are compared with the experimental values obtained by means of the assembly described in the previous paragraph. The results also confirm the validity of the previous relationships and the admissibility of the expression $a = \lambda/(\rho c)$ of the thermal diffusivity for expanded insulating materials, in which temperature oscillations of limited amplitudes (~5-10°C) occur. These materials are microscopically non-homogeneous, insofar as they are composed of small cells, where the conduction phenomenon is coupled with radiation and convection phenomena. The latter indeed is rather limited, being questionable for materials of low gas permeability. Tables 1, 2 and 3 show the physical properties of tested materials and the wave periods, which have been used to calculate the theoretical curves. Further results are given in reference [15]. The wave periods in these tables are also the same as those of the tests.

Table 1. Expanded Phenolic Resin.

Mean temperature of the slab	$\theta_m = +45$	°C
Slab thickness	$2\ell = 0.1$	m
Equivalent thermal conductivity at +45°C	$\lambda = 0.042$	$Wm^{-1}{}^\circ C^{-1}$
Equivalent specific heat at +45°C	$c = 1.17$	$kJ\ kg^{-1}{}^\circ C^{-1}$
Apparent density	$\rho = 42.6$	kgm^{-3}
Diffusivity	$a = \lambda/(\rho c) = 8.43 \cdot 10^{-7}$	$m^2\ s^{-1}$
Thermal capacity	$C_i = 0, 1.195, 2.390, 4.780$	$kJm^{-2}{}^\circ C^{-1}$
$R = C_i/(\rho c 1) =$	$= 0, 0.48, 0.96, 1.92$	
Period	$\tau = 0.5, 1, 2, 3$	hours

Table 2. Expanded Polystyrene.

Mean temperature of the slab	$\theta_m = +45°C$	°C
Slab thickness	$2\ell = 0.1$	m
Equivalent thermal conductivity at +45°C	$\lambda = 0.038$	$Wm^{-1}{}^\circ C^{-1}$
Equivalent specific heat at +45°C	$c = 1.215$	$kJ\ kg^{-1}{}^\circ C^{-1}$
Apparent density	$\rho = 14.6$	$kg\ m^{-3}$
Diffusivity	$a = \lambda/(\rho c) = 21.2 \cdot 10^{-7}$	$m^2\ s^{-1}$
Thermal capacity	$C_i = 0, 1.195, 2.390, 4.780$	$kJ\ m^{-2}{}^\circ C^{-1}$
$R = C_i/(\rho c 1) =$	$= 0, 1.35, 2.70, 5.40$	
Period	$\tau = 0.5, 1, 2, 3$	hours

[3] We speak of equivalent or apparent transport property because we have an expanded, porous material as a sample.

Table 3. Rigid Polyurethane Foam (Expanded with F12).

Mean temperature of the slab	$\theta_m = +63°C$	°C
Slab thickness	$2\ell = 0.102$	m
Equivalent thermal conductivity at +63°C	$\lambda = 0.102$	$W\ m^{-1}{}^{\circ}C^{-1}$
Equivalent specific heat at +63°C	$c = 1.385$	$kJ\ kg^{-1}{}^{\circ}C^{-1}$
Apparent density	$\rho = 36.9$	$kg\ m^{-3}$
Diffusivity	$a = \lambda/(\rho c) = 4.64 \cdot 10^{-7}$	$m^2\ s^{-1}$
Thermal capacity	$C_i = 0, 2.390, 4.780$	$kJ\ m^{-2}{}^{\circ}C^{-1}$
$R = C_i/(\rho c 1) =$	$= 0, 0.92, 1.84$	
Period	$\tau = 1, 2.5, 6$	hours

5.2. Multilayer Slabs

Some types of multilayer slabs have been examined, and their characteristics are listed in table 4. The experiments outlined in sections 3.1. and 3.2. have been performed on symmetric samples, where as those explained in sections 3.1., 3.2. and 3.3. were performed on asymmetric samples.

The imposed thermal wave has a mean temperature value of about +40°C and an amplitude in the range ± 5-7°C[4]. The moduli and the phase differences of the reduction factor σ, which have been found by the experiments, are given in table 5. According to eqs (28), (30), (32) and (25) the characteristic parameters A_ν, B_ν, C_ν, D_ν of multilayer slabs have been determined. The value of B_ν has been taken as the average between the values of $B_{2\nu}$ and $B_{4\nu}$ relative to the two different thermal capacities [$B_{2\nu}$ with $C_i = 2390\ J\ m^{-2}{}^{\circ}C^{-1}$ and $B_{4\nu}$ with $C_i = 4780\ J\ m^{-2}{}^{\circ}C^{-1}$]. The results are listed in table 6; in figure 12 are given some recordings of the temperature waves.

Afterwards numerical calculations have been made to check the agreement between theoretical and experimental values of the oversaid parameters. The theoretical values for the various tested slabs have been calculated following the theory given in a preceding paper [16] and assuming the quantities given in table 4. The calculated values are listed in table 7. Further results are given in reference [17]. In the range of temperature amplitudes chosen the agreement between theoretical and experimental values is satisfactory, considering that the slabs examined are made of usual building material.

---

[4] To evaluate the influence of the thermal joint capacities on the attenuation and on the phase lag, some experiments have been made with wire of diameters 0.32, 0.5 and 1.02 mm, at frequencies in the range 1×10^{-3} to 1×10^{-4} Hz. In this range and with the wire of diameter 0.32 mm the influence of the said capacity is not detectable by the recorders.

Table 4. Properties of the Tested Multilayer Slabs.

Slab	Layer	Materiol	ℓ	λ	ρ	c	q (a)	arrangement of the layer
-	-	-	m	$W m^{-1} {}^{o}C^{-1}$	$kg\ m^{-3}$	$J kg^{-1} {}^{o}C^{-1}$	$W m^{-2} {}^{o}C^{-1}$	
1	1	Eternit	0.02	0.55	1850	930		asymmetric
	2	Expanded polystyrene	0.018	0.041	12.3	1215	2.11	
2	1	Expanded polystyrene	0.018	0.041	12.3	1215	2.11	
	2	Eternit	0.02	0.55	1850	930		
3	1	Eternit	0.005	0.55	1880	930		symmetric
	2	Expanded polystyrene	0.019	0.041	13	1215	2.08	
	3	Eternit	0.005	0.55	1880	930		
4	1	Eternit	0.0035	0.55	1600	930		symmetric
	2	Acalorit (b)	0.021	0.12	700	1000	5.33	
	3	Eternit	0.0035	0.55	1600	930		

(a), q = equivalent thermal conductance.

(b), Acalorit is cement-asbestos material with ρ = 600 - 800 $kg\ m^{-3}$.

Table 5. Experimental Reduction Factor and Phase Difference.

Slab	τ_ν Period	Test 3.1. A_ν		Test 3.2. C_i = 2390 $J\ m^{-2} {}^{o}C^{-1}$		Test 3.2. C_i = 4780 $J\ m^{-2} {}^{o}C^{-1}$		Test 3.3. D_ν	
		$\lvert\vartheta_{o\nu}/\vartheta_{n\nu}\rvert$	$\angle\vartheta_{o\nu}/\vartheta_{n\nu}$	$\lvert\vartheta_{o\nu}/\vartheta_{n\nu}\rvert$	$\angle\vartheta_{o\nu}/\vartheta_{n\nu}$	$\lvert\vartheta_{o\nu}/\vartheta_{n\nu}\rvert$	$\angle\vartheta_{o\nu}/\vartheta_{n\nu}$	$\lvert\vartheta_{n\nu}/\vartheta_{o\nu}\rvert$	$\angle\vartheta_{n\nu}/\vartheta_{o\nu}$
-	hours	-	rad	-	rad	-	rad	-	rad
1	2.5	11.30	1.49	12.03	1.52	12.78	1.55	1.17	0.49
	6	5.41	1.35	5.71	1.37	6.03	1.39	1.03	0.20
	15	2.26	1.11	2.37	1.14	2.48	1.15	1.02	0.11
2	2.5	1.17	0.49	1.49	1.00	2.07	1.37	11.30	1.49
	6	1.03	0.20	1.10	0.51	1.27	0.77	5.41	1.35
	15	1.02	0.11	1.024	0.25	1.04	0.38	2.26	1.11
3	1	7.63	1.49	9.6	1.54	11.5	1.58	-	-
	2.5	3.03	1.13	3.78	1.24	4.50	1.30	-	-
	6	1.56	0.84	1.82	0.98	2.13	1.07	-	-
4	1	3.70	1.76	4.63	1.89	5.4	2.05	-	-
	2.5	1.73	1.16	1.98	1.26	2.24	1.35	-	-
	6	1.22	0.61	1.29	0.70	1.36	0.78	-	-

Table 6. Experimental Characteristic Parameters of Multilayer Slabs (a).

Slab	τ_ν	$B_{2\nu}$		$B_{4\nu}$		B_ν		C_ν	
		mod	arg	mod	arg	mod	arg	mod	arg
-	hours	$m^{2o}C\,W^{-1}$	rad	$m^{2o}C\,W^{-1}$	rad	$m^{2o}C\,W^{-1}$	rad	$W\,m^{-2o}C^{-1}$	rad
1	2.5	0.485	0.380	0.479	0.416	0.482	0.398	28.3	1.66
	6	0.460	0.143	0.475	0.153	0.468	0.148	12.1	1.56
	15	0.467	0.116	0.471	0.143	0.469	0.130	4.63	1.53
2	2.5	0.443	0.313	0.484	0.393	0.464	0.353	29.4	1.70
	6	0.483	0.148	0.454	0.156	0.469	0.152	12.0	1.55
	15	0.514	0.153	0.500	0.173	0.507	0.163	4.28	1.50
3	1	0.485	0.183	0.478	0.185	0.482	0.184	123	2.79
	2.5	0.500	0.078	0.479	0.046	0.490	0.062	20.1	2.28
	6	0.505	0.078	0.508	0.026	0.507	0.052	5.40	2.01
4	1	0.258	0.785	0.238	0.842	0.248	0.814	58.7	2.71
	2.5	0.190	0.292	0.191	0.328	0.191	0.310	19.6	2.21
	6	0.191	0.101	0.186	0.127	0.189	0.114	7.83	1.79

(a) The values of A_ν and D_ν are listed in table V .

Table 7. Theoretical Characteristic Parameters of Multilayer Slabs.

Slab	τ_ν	A_ν		B_ν		C_ν		D_ν	
		mod	arg	mod	arg	mod	arg	mod	arg
-	hours	-	rad	$m^{2o}C\,W^{-1}$	rad	$W\,m^{-2}\,{}^oC$	rad	-	rad
1	2.5	12.35	1.596	0.492	0.405	27.9	1.718	1.067	0.473
	6	4.967	1.393	0.480	0.150	10.8	1.639	1.012	0.206
	15	2.074	1.052	0.472	0.134	4.03	1.524	1.002	0.099
2	2.5	1.067	0.473	0.492	0.405	27.9	1.718	12.35	1.596
	6	1.012	0.206	0.480	0.150	10.8	1.639	4.967	1.393
	15	1.002	0.099	0.472	0.134	4.03	1.524	2.074	1.052
3	1	7.33	1.547	0.484	0.180	113	2.909	7.33	1.547
	2.5	3.09	1.254	0.495	0.061	21.0	2.497	3.09	1.254
	6	1.68	0.91	0.497	0.044	6.30	2.037	1.68	0.910
4	1	3.683	1.760	0.214	0.710	68.2	2.793	3.683	1.760
	2.5	1.709	1.205	0.193	0.340	19.2	2.237	1.709	1.205
	6	1.150	0.613	0.183	0.130	7.37	1.839	1.150	0.613

6. References

[1] Broeber H., Erk, S., Die Grundgesetze der Wärmeübertragung, Springer Verlag, Berlin, 70, (1933).

[2] Alford, J. S., Ryan, J.E., Urban P.O., Effect of Heat Storage and Variation in Outdoor Temperature and Solar Intensity on Heat Transfer Through Walls, Ashve Transaction, 45, 369, (1939).

[3] Marmet Ph., Etude du regime thermique sinusoidal des murs et des locaux par voie'analogie électrique, Compte Rendu du Septième Congrès International du Chauffage, Ventilation et du Conditionnement, Paris, 236-302, (1947).

[4] Mackey, C. O., Wright, L. T., Periodic Heat Flow.Homogeneous Walls, Heating, Piping, 16, 546-555, (1944). Periodic Heat Flow.Composite Walls or Roofs, Heating, Piping, 18, 107-110, (1946).

[5] Carslaw, H. S., Jaeger, J. C., Conduction of Heat in Solids, Clarendon Press, Oxford, 88, (1948).

[6] Mattarolo, L., Analogia elettrica e metodo dei quadripoli in problemi di trasmissione termica, La Termotecnica, Vol. VI, 355-363, (1952).

[7] Barducci, I., Calcolo approssimato dell'attenuazione termica di pareti in regime periodico, sotto condizioni più generali di quelle di Alford, Ryan e Urban, Quaderni di Fisica Tecnica n. 2, Università di Roma, Facoltà di Ingegneria, (1964).

[8] Choudhury, N. K. D., Warsi, Z. U. A., Weighing Function and Transient Thermal Response of Buildings. Part I, Homogeneous Structure, Int. Journal of Heat and Mass Transfer, 7, 1309-1321, (1964).

[9] Warsi, Z. U. A., Choudhury, N. K. D., Weighing Function and Transient Thermal Response of Buildings, Part II, Composite Structure, Int. Journal of Heat and Mass Transfer, 7, 1322-1334, (1964).

[10] Columba, M., Lo Giudice, G., Trasmissione del calore in regime periodico negli edifici, Calcolo Numerico, Atti Accademia di Scienze, Lettere ed Arti di Palermo, Serie IV, Vol. XXV, Parte 1, 267-322, (1964-65).

[11] Sacchi, A., Sul Calcolo della attenuazione termica di pareti in regime periodico, La Termotecnica, Vol. XX, 60-65, (1966).

[12] Ferro, V., Sacchi, A., Oscillazioni termiche in pareti semplici anche in condizioni di risonanza, La Termotecnica, Ricerche n. 16, Vol. XX, 8, (1966).

[13] Vodicka, V., Conduction of Fluctuating Heat Flow in a Wall Consisting of Many Layers, Applied Scientific Research, Vol. A-V, 108-114, (1956).

[14] Ferro, V., Sacchi, A., Oscillazioni termiche in pareti composete, La Termotecnica, Ricerche n. 16, Vol. XX, 22, (1966).

[15] Codegone, C., Ferro, V., Sacchi, A., Experiments on Thermal Oscillations through Insulating Materials, Supplement au Bull.del'Inst. Int. du Froid, Annexe, 175, (1966-2).

[16] Boffa, C., Ferro, V., Sacchi, A., Tabelle numeriche per il calcolo rapido dei parametri caratteristici di pareti composte, La Termotecnica, Ricerche n. 16, Vol. XX, 52, (1966).

[17] Codegone, C., Ferro, V., Sacchi, A., Thermal Oscillations through Walls, Comm. 2, XII^{e} Congres International du Froid, Madrid, (1967).

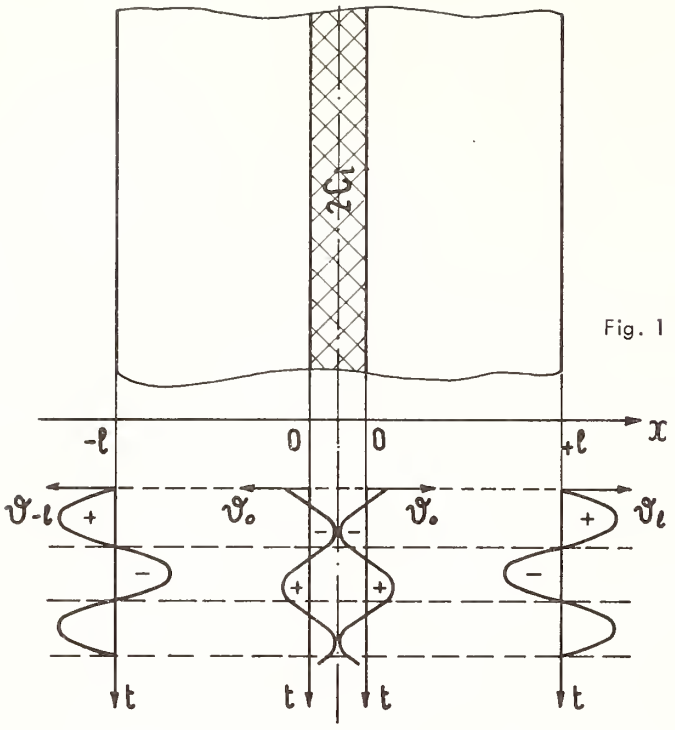

Fig. 1 Thermal test diagram with interposed capacity 2 C_i

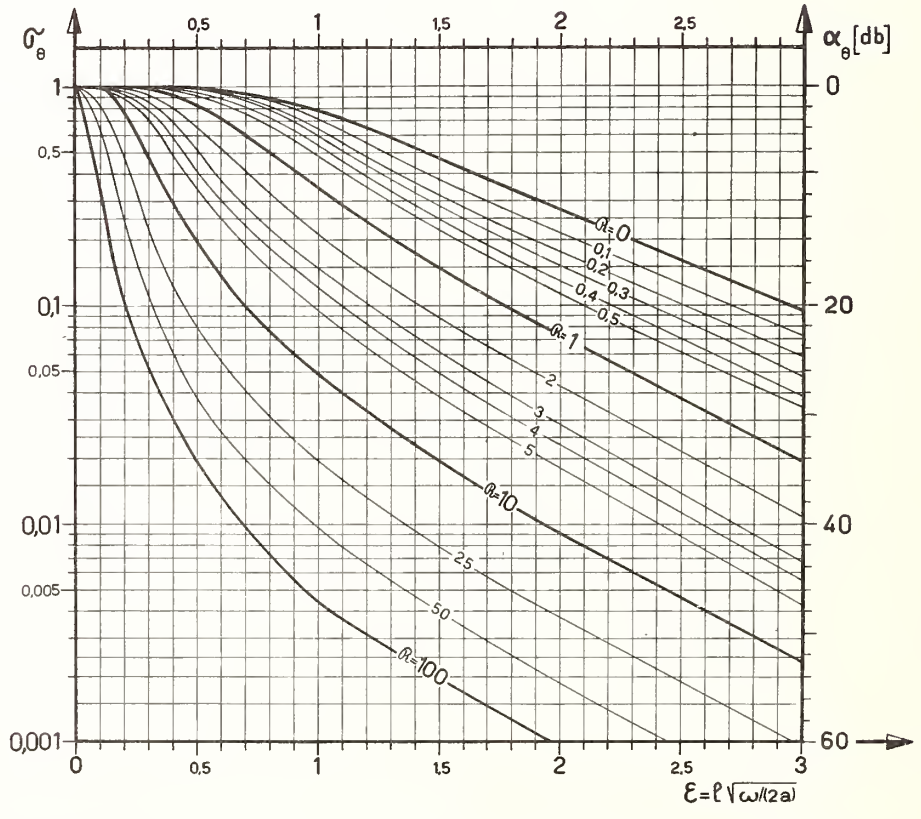

Fig. 2 Reduction factor modulus $|\sigma_\vartheta|$ and attenuation α_ϑ of temperature oscillations vs. adimensional parameters ε and R.

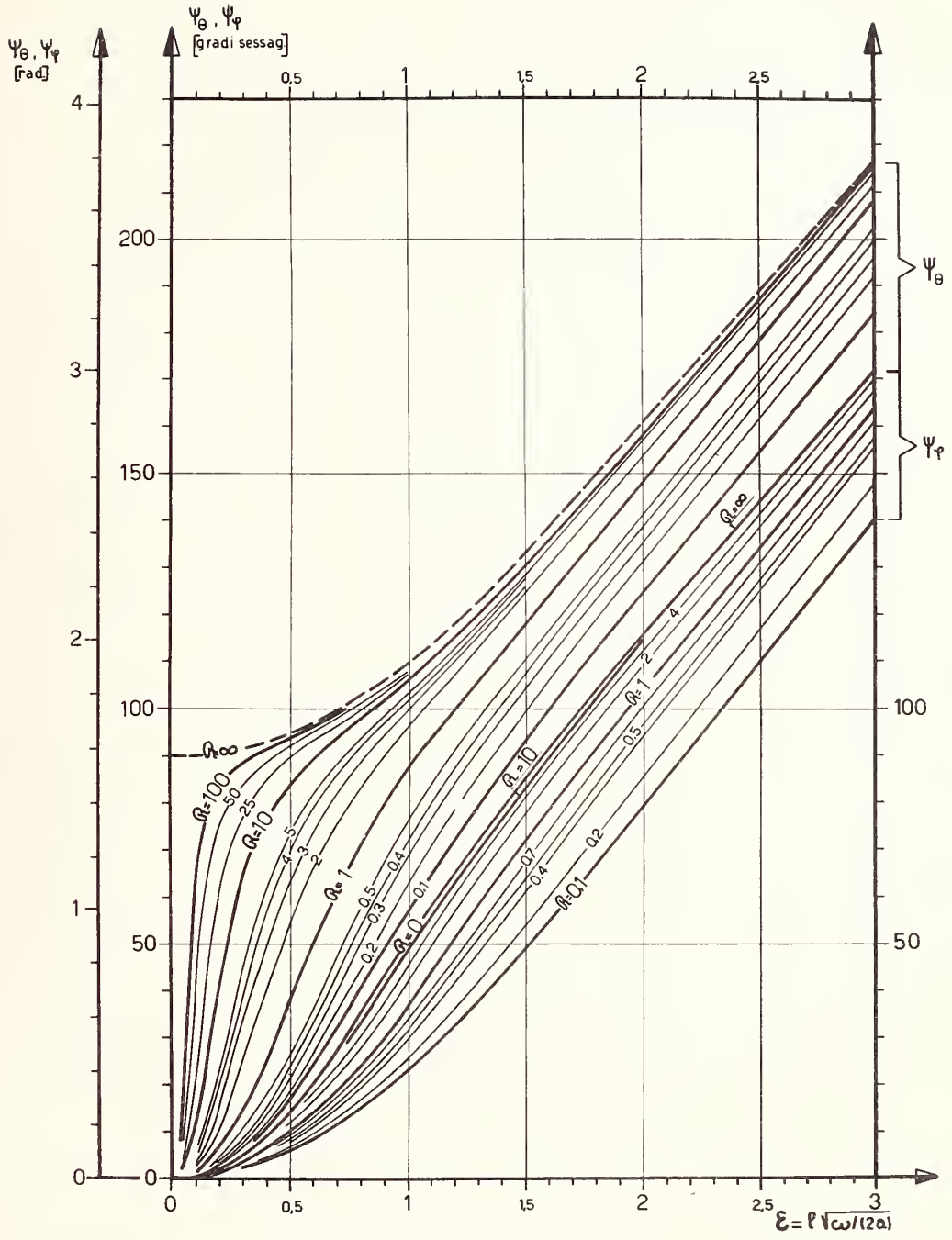

Fig. 3 Phase difference Ψ_ϑ and Ψ_φ vs. adimensional parameters ε and R.

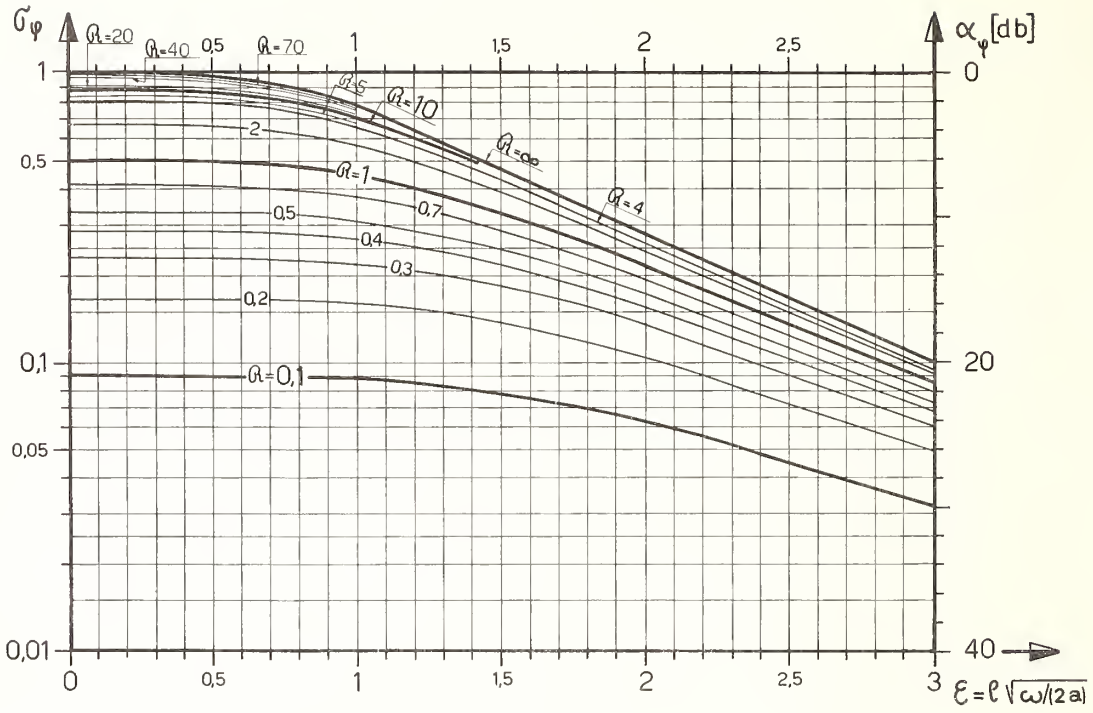

Fig. 4 Reduction factor modulus $|\sigma\varphi|$ and attenuation $\psi\varphi$ of thermal flux oscillations vs. adimensional parameters ε and R.

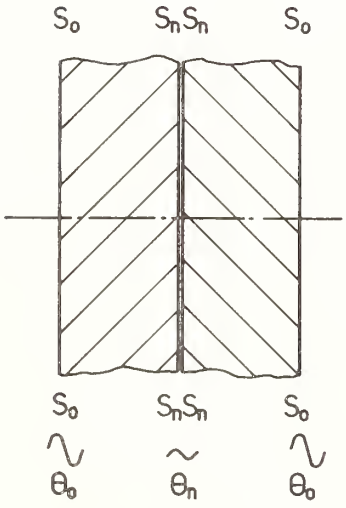

Figure 5a. Thermal test diagram to measure the parameter A_ν .

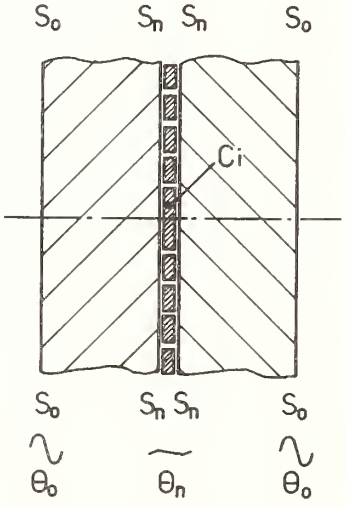

Figure 5b. Thermal test diagram to measure the parameter B_ν .

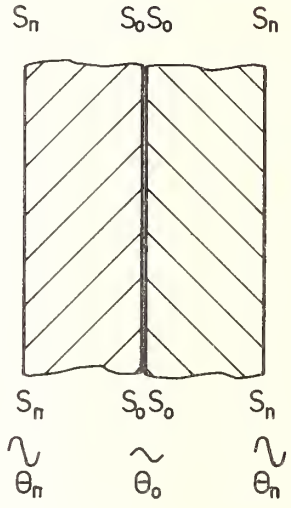

Figure 5c. Thermal test diagram to measure the parameter D_ν .

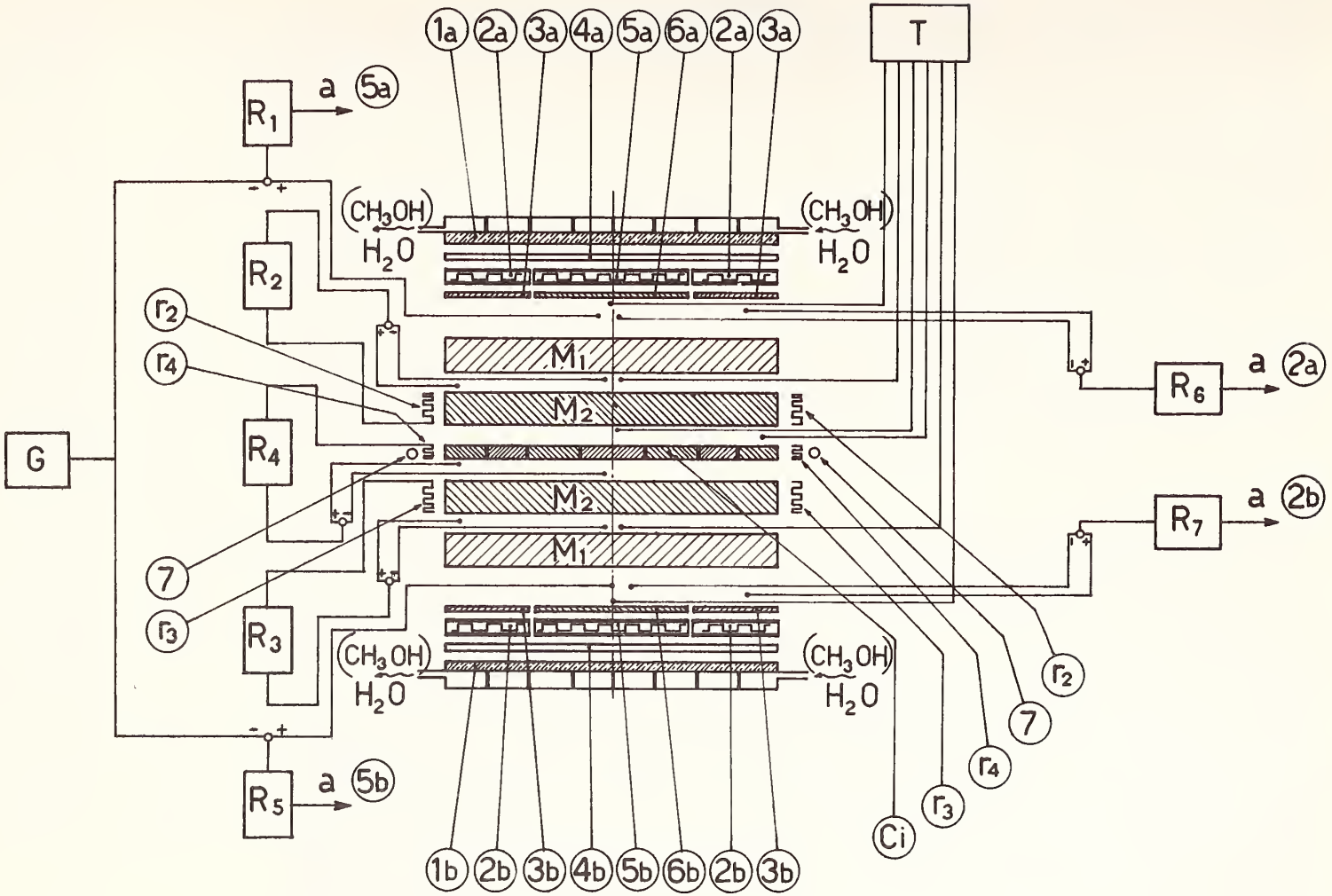

Fig. 6 Operational diagram of the test apparatus with measuring and control system.

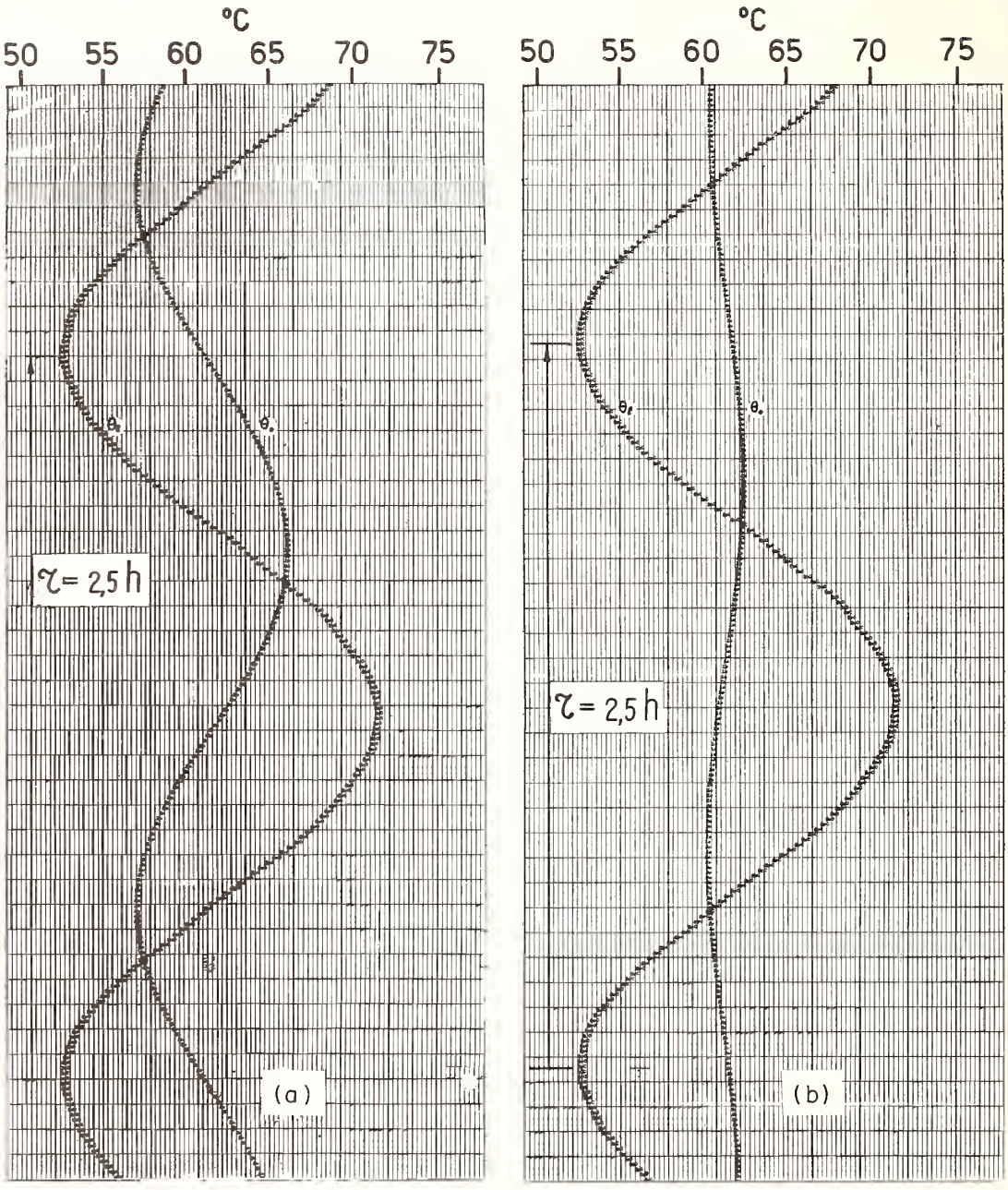

Fig. 7-a Recording of the imposed temperature waves $\vartheta_{\ell} = \vartheta_{\ell}$ and of the recorded wave ϑ_o tested material: rigid urethane foam expanded with F 12 - $|\vartheta_o / \vartheta_{\ell}| = 0.49$; arg $(\vartheta_o / \vartheta_{\ell}) = 1.40$ rad; Period $\tau = 2.5$ h.

Fig. 7-b Recording of the imposed temperature waves $\vartheta_{\ell} = \vartheta_{\ell}$ and of the received waves ϑ_o with interposed thermal capacity $C_i = 4.780$ kJ m^{-2} °C^{-1}-tested material: the same of Fig. 7-a. $|\vartheta_o / \vartheta_{\ell}| = 0.108$; arg $(\vartheta_o / \vartheta_{\ell}) = 1.92$ rad; Period $\tau = 2.5$ h.

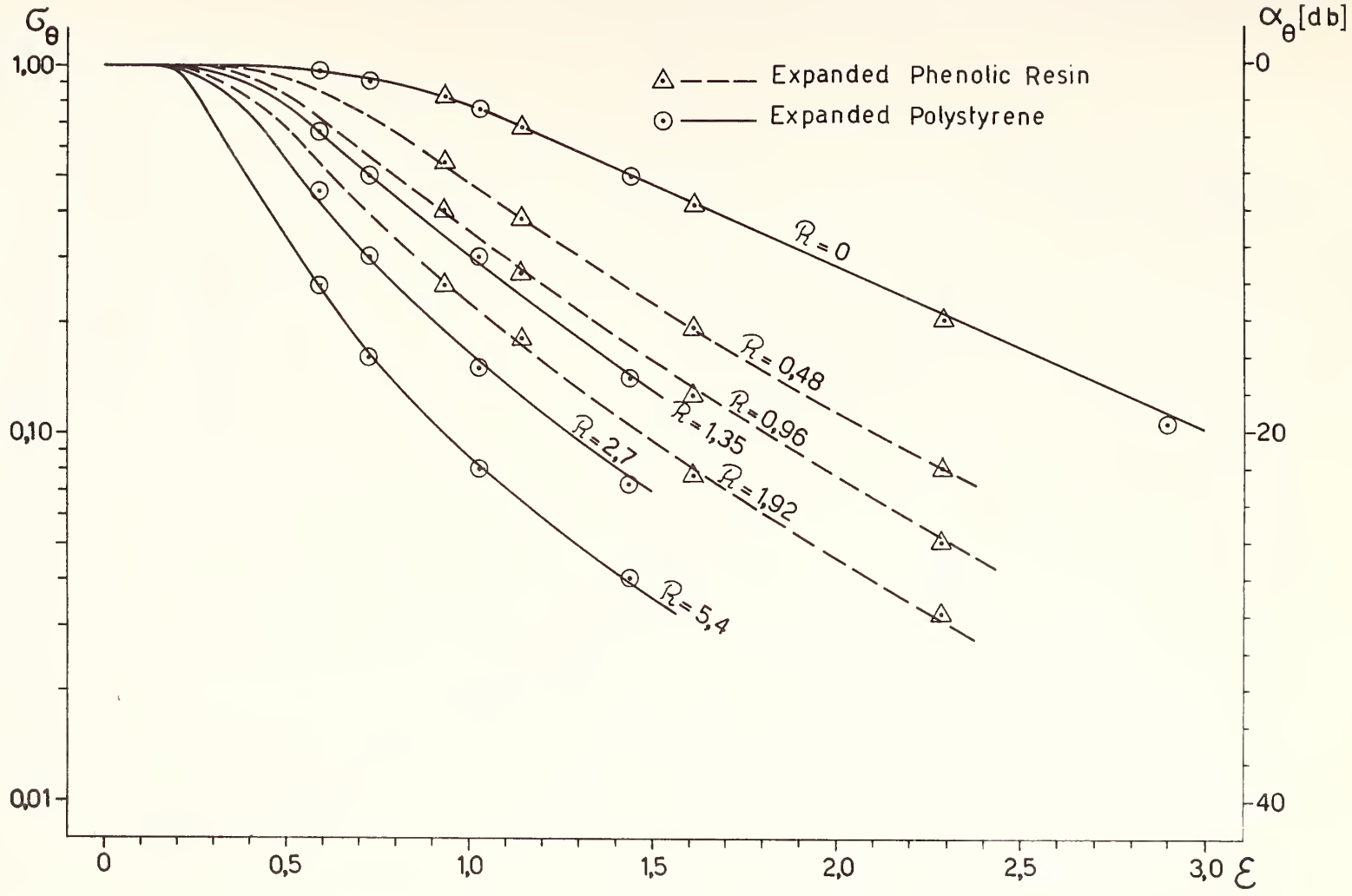

Fig. 8 Theorical curves and experimental values of $|\sigma_\vartheta|$ and α_ϑ vs. adimensional parameters ε and R for the tested slabs of phenolic expanded resin ($\rho = 42.6\ kg/m^3$) and expanded polystyrene ($\rho = 14.6\ kg/m^3$). Mean temperature of the slab $\vartheta_m = +45\ ^\circ C$.

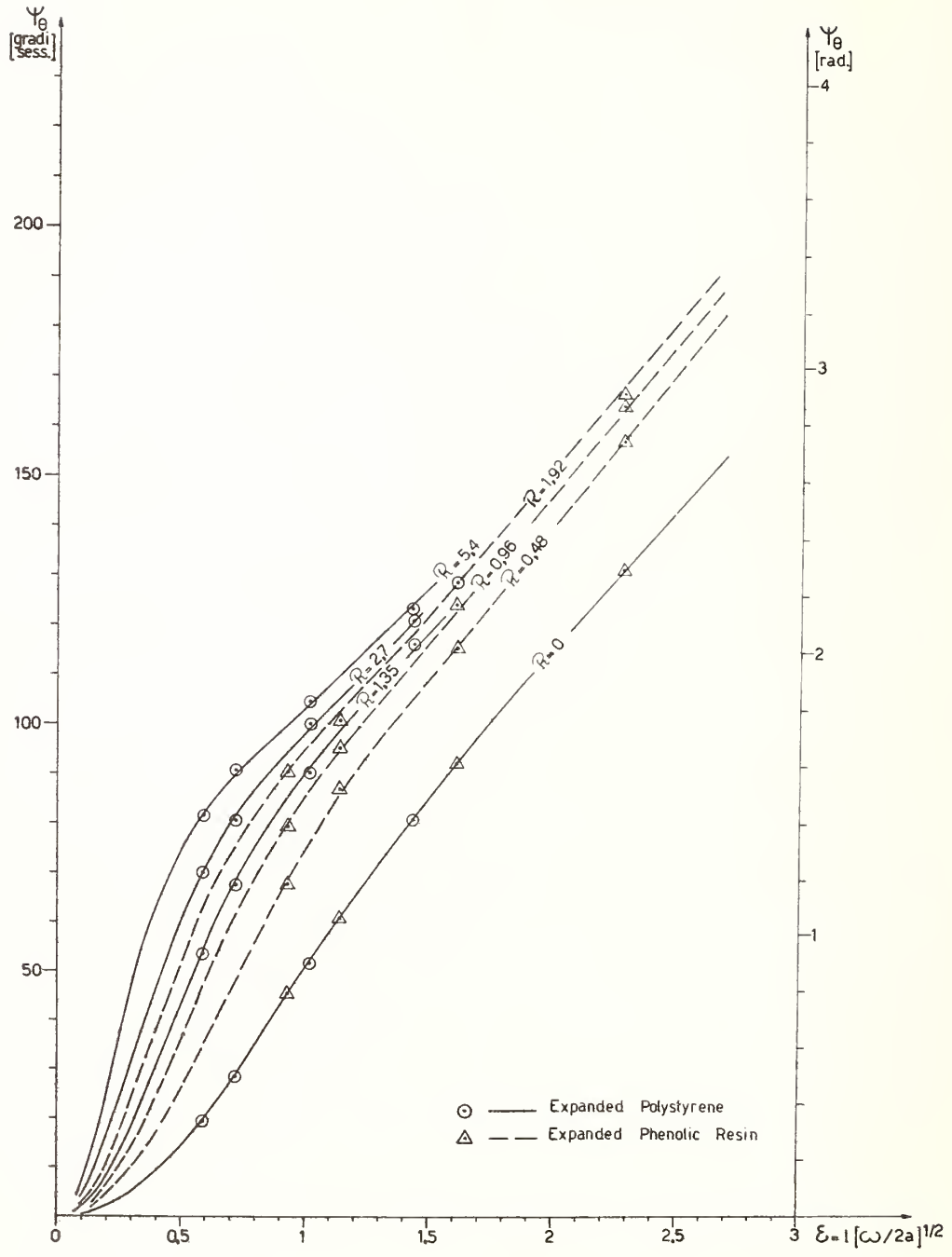

Fig. 9 Theoretical curves and experimental values of ψ_ϑ vs. adimensional parameter ε and R for the same slabs and mean temperature of fig. 8.

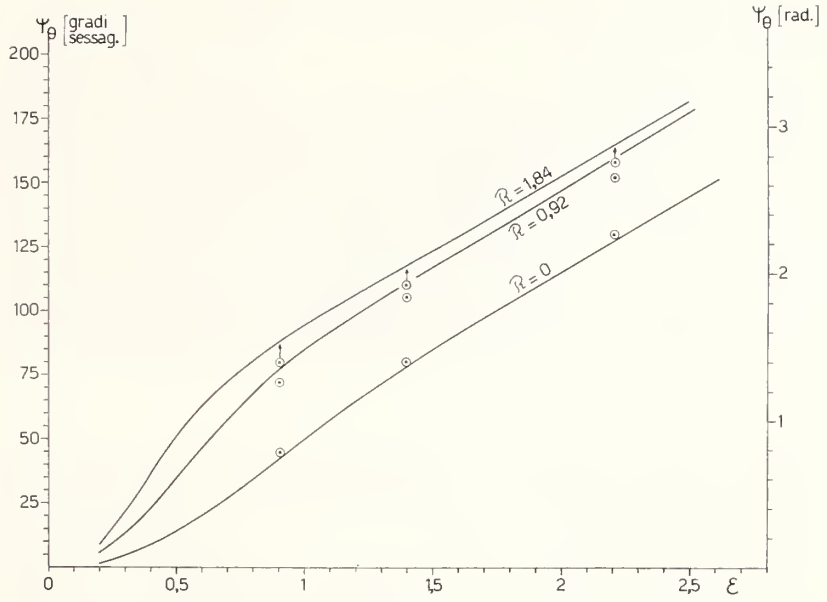

Fig. 10 Like fig. 8 but the slab tested is rigid urethane foam expanded with F 12 (ρ = 36.9 kg/m^3) and the mean temperature is ϑ_m = + 63 °C.

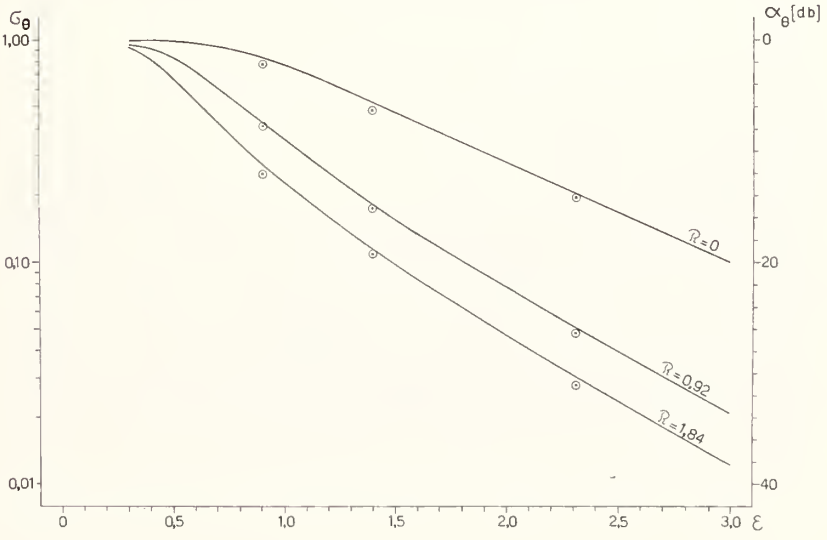

Fig. 11 Like fig. 9 for the same material of fig. 10.

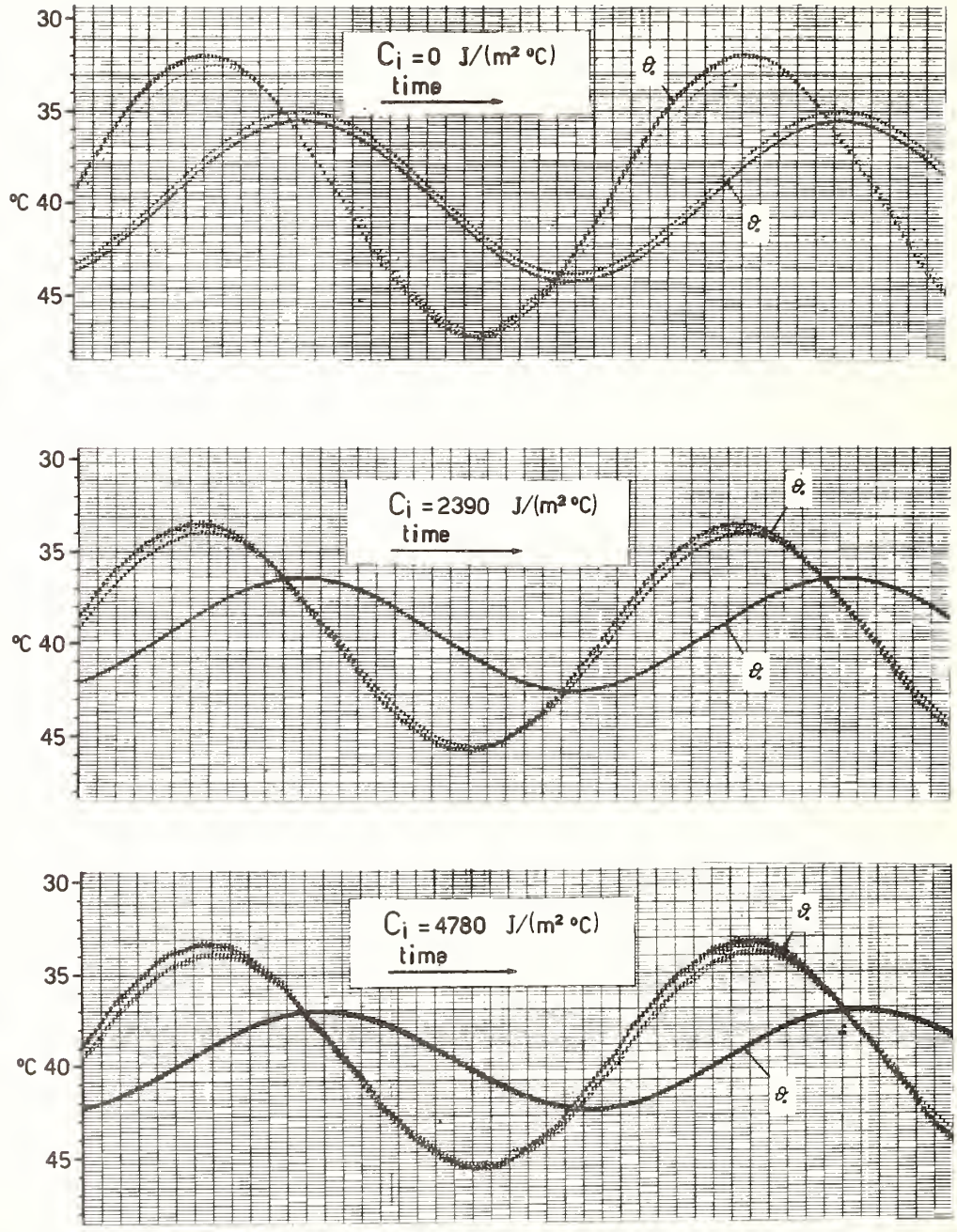

Fig. 12 Recordings of imposed temperature waves ϑ_o and received ϑ_n in the case of multilayer slab N° 3 and for the period τ = 2.5 h. The intermediate wave recorded between ϑ_o and ϑ_n corresponds to the temperature of the sublayer surfaces.

Heat Losses In a Cut-Bar Apparatus: Experimental-Analytical Comparisons

Merrill L. Minges

U. S. Air Force Materials Laboratory
Wright-Patterson Air Force Base
Dayton, Ohio 45433

In connection with thermal conductivity measurements on beryllium oxide, data on heat exchange between the specimen-meter bar column and the surrounding insulation were obtained. These data consisted of measured differences in the flux through the Armco iron meter bars position above and below the beryllium oxide thermal conductivity specimen and in the variation of the flux in the specimen-meter bar column as the guard heater temperature distribution was varied. Analytical predictions of the heat exchange between the specimen-meter bar column and the insulation were made by first generating an equation for the temperature field in the insulation with the various boundary temperatures observed experimentally, and then deriving an expression for the radial temperature gradient at the specimen column-insulation interface. Integration of this equation with respect to the axial coordinate leads directly to an expression for the predicted heat exchange which was then used to generate values for comparison with the experimental results. No measurements of the thermal insulation conductivity were made in this investigation, thus some discussion is given as to the rationale used for estimating this conductivity from data available in the literature. The comparisons of predicted and measured heat exchange values show inconsistencies in some cases. Although the source of these differences is not entirely clear, it appears that uncertainties in the true temperature distribution along the insulation boundaries are the largest source of error.

Key Words: Boundary value analysis, comparative conductivity, heat losses, thermal conductivity, thermal insulation.

1. Introduction

At the 4th Thermal Conductivity Conference the design of an apparatus for the measurement of thermal conductivity by the comparative method was described (1)[1]. Results of conductivity and thermal contact resistance measurements were presented the following year (2). One of the important features of this equipment was a fairly large ratio of lateral insulation diameter to specimen diameter (d_i/d_s= 6.0). This ratio was purposely chosen considerably greater than the optimum value so that guarding requirements could be relaxed. Using a simplified heat transfer analysis it was concluded that this approach was acceptable as long as the specimens had a conductivity level at least 100 times that of the insulation. For the alumina bubble insulation-beryllium oxide specimen combination studied here, this ratio varied from about 5.0×10^{-5} at room temperature to about 7.4×10^{-3} at 1000°C.

In order to substantiate the apparatus design rationale an analytical analysis of heat losses was conducted, the results then being compared with experimental measurements of heat losses. The experimental heat loss data consisted of measured differences between the heat flux through each of the meter bars as a function of variations in the absolute temperature level and variations in the guard heater temperature distribution. The next section briefly sketches the analytical analysis. The final section of the paper compares the experimental results with the predicted values of heat exchange between the insulation and the specimen column.

[1] Figures in parentheses indicate the literature references at the end of this paper.

2. Analytical Development

In order to arrive at an analytically exact prediction of the heat exchange between the specimen column and the insulation surrounding it, it is necessary to have an expression for the radial temperature gradient at the column surface as a function of the axial coordinate. If this is available then an equation of the following form can be applied,

$$q_{loss} = 2\pi r_o \int_o^L K_i \left(\frac{\partial T}{\partial r}\right)_{r=a} dz \qquad (1)$$

where,

r_o = SPECIMEN RADIUS

L = SPECIMEN COLUMN LENGTH

The expression for $\left(\frac{\partial T}{\partial r}\right)_{r=a}$ was obtained by developing a general equation for the temperature field in the annular insulation region surrounding the specimens and performing the indicated differentiation. This temperature field equation was constructed by superposition of solutions for the steady-state boundary value system made up of the insulation region with its surface temperature distributions. The most general solution developed for this axi-symmetric system was for arbitrary temperature distributions $f_o(z), f_1(z), f_2(r)$ along the inner and outer cylindrical boundaries and the upper surface boundary, respectively. The lower surface boundary was assumed to be at a constant temperature, T = 0, although this is essentially a temperature field normalization condition which could very easily be relaxed. A sketch of the system and these boundary conditions is given in figure 1.

BOUNDARY CONDITIONS

(1) $r = r_o$ Z, $T = f_o(Z)$

(2) $r = r_1$ Z, $T = f_1(Z)$

(3) $r_o \le r \le r_1$, $Z = 0$, $T = 0$

(4) $r_o \le r \le r_1$, $Z = L$, $T = f_2(r)$

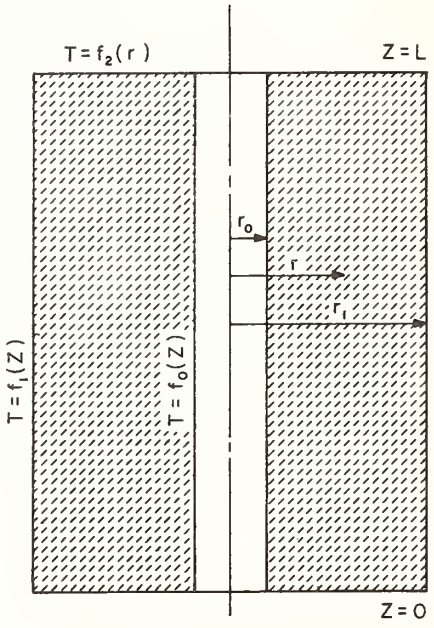

FIGURE 1 - Insulation Segment and Boundary Conditions

Because the governing differential equation, $\nabla^2 T = 0$, is linear (i.e., $k_i = f(T,r,z)$) the various boundary conditions were considered separately, the solution for each then added

to give the required result. A solution was developed for boundary conditions 1 and 2 simultaneously and then a solution for boundary condition 4.

The solution of Laplace's equation in cylindrical coordinates for the axi-symmetric case is performed by separation of variables with integration of the resulting total differential equations. For the case when the boundary conditions are a function of the axial coordinate (B.C. 1 and 2) the general product solution is in terms of sin (z) and modified zero order Bessel functions of the first and second kind, I_o (r) and K_o (r). When the boundary conditions are a function of the radial coordinate (B.C. 4) the general product solution is in terms of the hyperbolic function sinh (z) and zero order Bessel functions of the first and second kind, J_o (r) and Y_o (r).

Considering first the analysis involving boundary conditions 1 and 2, separation of variables leads to the following general solution of Laplace's equation,

$$T(r,z) = \left[A' I_o(\lambda r) + B' K_o(\lambda r) \right] \left[C' \cos(\lambda z) + D' \sin(\lambda z) \right] \tag{2}$$

where,

$$A', B', C', D' = \text{CONSTANTS}$$

The T = 0 boundary condition along the surface z = 0 lead to the requirement that

$$C' = 0$$

The T = 0 boundary condition along the surface z = L lead to the following eigen-value restrictions on the parameter λ .

$$\lambda_n = {}^{n\pi}/_{L}\,, \quad n = 0, 1, 2, \cdots\cdots$$

Thus a particular solution of the differential equation becomes,

$$T(r,z)_n = \left[E'_n I_o\left(\frac{n\pi r}{L}\right) + F'_n K_o\left(\frac{n\pi r}{L}\right) \right] \sin\left(\frac{n\pi z}{L}\right) \tag{3}$$

The constants in this equation are now subscripted as E_n and F_n since there is a solution for each value of n.

In order to satisfy boundary conditions 1 and 2 it is necessary to utilize an infinite series solution of the differential equation constructed as a linear combination of solutions of the above form,

$$T(r,z) = \sum_{n=1}^{\infty} T(r,z)_n \tag{4}$$

This linear combination is also a solution of the original differential equation. After regrouping of the constants in cylindrical function form the infinite series solution can be

written as,

$$T(r,z) = \sum \frac{\varrho\left(\frac{n\pi r_1}{L}\right) G_n(r, r_o) + \varrho\left(\frac{n\pi r_o}{L}\right) G_n(r_1, r)}{G_n(r_1, r_2)} \sin\left(\frac{n\pi z}{L}\right) \tag{5}$$

where,

$$\varrho\left(\frac{n\pi r_o}{L}\right) = E_n' I_o\left(\frac{n\pi r_o}{L}\right) + F_n' K_o\left(\frac{n\pi r_o}{L}\right)$$

$$G_n(r_i, r_j) = I_o\left(\frac{n\pi r_i}{L}\right) K_o\left(\frac{n\pi r_j}{L}\right) - I_o\left(\frac{n\pi r_j}{L}\right) K_o\left(\frac{n\pi r_i}{L}\right)$$

Substituting B.C. 1 and 2 in the above equation and developing the Fourier coefficient integral conditions in the usual way for this orthogonal family (3) leads to the following general solution of the differential equation meeting boundary conditions 1 and 2,

$$T(r,z) = \frac{2}{L} \sum_{n=1}^{\infty} \frac{\sin\left(\frac{n\pi z}{L}\right)}{G_n(r_1, r_o)} \left\{ G_n(r, r_o) \int_0^L f_1(z) \sin\left(\frac{n\pi z}{L}\right) dz + G_n(r_1, r) \int_0^L f_o(z) \sin\left(\frac{n\pi z}{L}\right) dz \right\} \tag{6}$$

Considering now the solution involving boundary condition 4, separation of variables leads to the following general solution of Laplace's equation,

$$T(r,z) = \left[A J_o(\kappa r) + B Y_o(\kappa r) \right] \left[C \cosh(\kappa z) + D \sinh(\kappa z) \right] \tag{7}$$

where,

A, B, C, D, = CONSTANTS

The T = 0 boundary condition along the surface z = 0 leads to the requirement that

$$C = 0$$

Applying the boundary conditions

$$r = r_o, \; Z, \; T = 0$$

$$r = r_1, \; Z, \; T = 0$$

and eliminating the constants A and B from the equations that result leads to the following condition which must be fulfilled:

$$Y_0(\kappa r_0) J_0(\kappa r_1) - Y_0(\kappa r_1) J_0(\kappa r_0) = 0 \tag{8}$$

The above condition is met by an infinite number of eigenvalues, κ_n , which are the positive roots of this equation. Introducing cylindrical function notation,

$$U_0(\kappa_n; r_0; r_1) \equiv J_0(\kappa_n r_0) Y_0(\kappa_n r_1) - J_0(\kappa_n r_1) Y_0(\kappa_n r_0) \tag{9}$$

the eigenvalues, κ_n , are defined by

$$U_0(\kappa_n; r_0; r_1) = 0, \qquad n = 1, 2, 3, \cdots\cdots \tag{10}$$

Thus a particular solution of the differential equation becomes

$$T(r, z)_n = \left[A_n J_0(\kappa_n r) + B_n J_0(\kappa_n r) \right] \left[D_n \sin h(\kappa_n z) \right] \tag{11}$$

where again the constants are subscripted to reflect the family of solutions represented by the eignevalues, κ_n .

Writing the corresponding infinite series solution and recasting the form of the constants leads to the following representation for $T(r,z)$,

$$T(r, z) = \sum_{n=1}^{\infty} \frac{R(\kappa_n r_1)\left[U_0(\kappa_n; r_0; r)\right] + R(\kappa_n r_0)\left[U_0(\kappa_n; r; r_1)\right]}{U_0(\kappa_n; r_0; r_1)} \sin h(\kappa_n z) \tag{12}$$

where,

$$R(\kappa_n r) = E_n J_0(\kappa_n r) + F_n Y_0(\kappa_n r)$$

Substituting B.C. 4 in the above equation and developing the Fourier coefficient integral conditions leads to the general solution given below in eq (13) as a cylindrical function Fourier series. The norm $N\{U_0(r)\}$ for this class of orthogonal functions is found by applying Lommel integral relations.

$$T(r,z) = \frac{\pi^2}{2} \sum_{n=1}^{\infty} \frac{K_n^2 J^2(K_n r_0) U_0(\kappa_n; r; r_1) \sin h(K_n z)}{\left[J_0^2(\kappa_n r_0) - J_0^2(\kappa_n r_1) \right] \sinh(\kappa_n L)} \int_{r=r_0}^{r=r_1} r f_2(r) U_0(\kappa_n; r; r_1) dr \tag{13}$$

The general solution of the original differential equation meeting all the boundary conditions given in figure 1 is simply the sum of eqs (6) and (13).

For this particular experimental arrangement, boundary condition 4 is not arbitrary. The constraint on $f_2(r)$ is of a physical nature rather than mathematical. If $f_1(L)$ and $f_0(L)$ are the temperatures on the z = L plane at points r = r_i and r = r_o respectively, then it can be easily shown that to satisfy $\nabla^2 T = 0$,

$$f_2(r) = f_0(L) + \left[f_1(L) - f_0(L)\right] \ln\left(\frac{r}{r_o}\right) \Big/ \ln\left(\frac{r_i}{r_o}\right) \tag{14}$$

Based on the experimental temperature distribution measurements $f_0(z)$ and $f_1(z)$ can be quite accurately represented in the form,

$$f_0(z) = T_0(1-\alpha) + \alpha T_{L0} \tag{15}$$

$$f_1(z) = T_1(1-\alpha) + \alpha T_{L1} \tag{16}$$

where,

$$\alpha = z/L$$

$$T_0 \equiv f_0(0), \qquad T_{L0} \equiv f_0(L)$$

$$T_{L1} \equiv f_1(L)$$

Using eqs (14)-(16) for explicit evaluation of the various Fourier coefficient integrals leads to the following equation for the temperature distribution in the insulation segment.

$$T(r,z) = \frac{\pi}{\ln\left(\frac{r_i}{r_o}\right)} \sum_{n=1}^{\infty} \left[\frac{J_0(\kappa_n r_o) u_0(\kappa_n; r; r_o) \operatorname{SIN} h(\kappa_n z)}{\left[J_0^2(\kappa_n r_o) - J_0^2(\kappa_n r_i)\right] \operatorname{SIN} h(\kappa_n L)} \right] \times$$

$$\left[\left\{ T_{L0} \ln\left(\frac{r_i}{r_o}\right)(1 + \ln r_o) - T_{L1} \ln(r_o) \right\} \left\{ J_0(\kappa_n r_o) - J_0(\kappa_n r_i) \right\} + (T_{L1} - T_{L0}) \left\{ J_0(\kappa_n r_o) \ln r_i - J_0(\kappa_n r_i) \ln r_o \right\} \right]$$

$$+ \frac{2}{L} \sum_{n=1}^{\infty} \frac{\operatorname{SIN}\left(\frac{n\pi z}{L}\right)}{G_n(r_i; r_o)} \left\{ G_n(r; r_o)\left(\frac{L}{n\pi}\right)\left[T_1 - T_{L1}(-1)^n\right] + G_n(r_i; r)\left(\frac{L}{n\pi}\right)\left[T_0 - T_{L0}(-1)^n\right] \right\}$$

(17)

Equation (1) is now applied to determine the total heat exchange between the composite specimen bar and the insulation. In using this equation it was assumed that the insulation thermal conductivity, K_i , was temperature and position independent. A temperature and spatially dependent conductivity could be introduced in evaluating the eq (1) integral although it is important to bear in mind that this is still only an approximation since the use of the condition $\nabla^2 T = 0$ implies temperature independent properties.

The final result of the substitution and integration of eq (1) is as follows:

$$q_{loss} = 2\pi r_o k_i \int_o^L \left(\frac{\delta T}{\delta r}\right)_{r=r_o} dZ =$$

$$2\pi r_o k_i \left\{ 2\sum_{n=1}^{\infty} \left[\frac{G_n'(r_o;r_o)}{G_n(r_i;r_o)} \left\{ T_i - T_{Li}(-1)^n \right\} + \frac{G_n'(r_o;r_i)}{G_n(r_i;r_o)} \left\{ T_o - T_{Lo}(-1)^n \right\} \right] \left\{ \frac{1-(-1)^n}{n\pi} \right\} \right.$$

$$\left. - \frac{2}{r_o \ln\left(\frac{r_i}{r_o}\right)} \sum_{n=1}^{\infty} \xi_n \eta_n \frac{J_o(\kappa_n r_i)}{J_o(\kappa_n r_o)} \left[\frac{\cosh(\kappa_n L) - 1}{\kappa_n} \right] \right.$$

(18)

Where,

$$\xi_n = J_o(\kappa_n r_o) \Big/ \left[\left\{ J_o^2(\kappa_n r_o) - J_o^2(\kappa_n r_i) \right\} \sinh(\kappa_n L) \right]$$

$$\eta_n = \left[T_{Lo} \ln\left(\frac{r_i}{r_o}\right) \left\{ 1 + \ln r_o \right\} - T_{Li} \ln r_o \right] \left[J_o(\kappa_n r_o) - J_o(\kappa_n r_i) \right]$$

$$+ (T_{Li} - T_{Lo}) \left\{ J_o(\kappa_n r_o) \ln r_i - J_o(\kappa_n r_i) \ln r_o \right\}$$

$$G_n'(r_i;r_j) = I_1\left(\frac{n\pi r_i}{L}\right) K_o\left(\frac{n\pi r_j}{L}\right) + I_o\left(\frac{n\pi r_j}{L}\right) K_1\left(\frac{n\pi r_i}{L}\right)$$

Alternate terms of the first summation are zero due to the factor $\left[1-(-1)^n\right]$ hence only odd values of n need be considered. In the second summation determination of the eigenvalues, κ_n , as defined by eq (10) is necessary. An infinite series approximation given by Gray and Mathews (4) was applied; limited tabulations are also found in Jahnke and Emde (5). The first few roots are given in Table 1 for the case where $r_1/r_2 = 6.0$. For $n > 6$, the roots are given to within 0.1% by eq (19),

$$\kappa_n r_o = n\pi/5 \tag{19}$$

Table 1 - Positive Roots of $U_o(\kappa_n; r_o; r_i) = 0$ When $r_i / r_o = 6.0$

n	$r_o \kappa_n$	n	$r_o \kappa_n$
1	0.226	5	3.134
2	1.233	6	3.764
3	1.874	7	4.393
4	2.506	8	5.023

IBM 7094 evaluation of eq (18), discussion of convergence characteristics and comparison with experimental heat loss measurements is given in the next section.

3. Experimental-Analytical Comparisons

In evaluating the series in eq (18) term by term print out of the computer results was employed to study convergence characteristics. Hand calculation of several terms was also run to check the computer results. The first series was carried to n = 40. For $n > 20$ the terms contributed no more than 0.3% to the sum. In the case of the second series the first term in the summation, represented by κ_1 , varied between 70% and 93% of the series sum. Subsequent terms alternated sign with decreasing magnitude, as might be expected for a series having linear $J_o(K_n r)$ factors. Terms through κ_9 were evaluated to obtain a sum varying less than 1% with inclusion of higher terms.

Equation (18) requires values of the thermal insulation conductivity. This conductivity was not measured in the investigation, thus it was necessary to estimate values from data in the literature. Literature data on alumina powders are reported for a range of densities and particle sizes. Extrapolation of the data to other ranges of density or particle size is not straightforward because of the high radiative contribution to the total thermal conductivity. The data of Laubitz (7) was found to be particularly useful since the solid conduction and radiation contributions to the effective conductivity were presented separately as a function of temperature. Further, the data were found to be consistent with other alumina powder data in the same density and particle size range (8,9).

The results of Laubitz, measured in vacuum, on a powder with density of 1.77 gms/cm^3 and particle sizes in the range 300-420 μ is given as curve (1) in figure 2. This particle size range encompasses the average particle diameter of the alumina bubbles used here, $\bar{d} = 396\ \mu$. The alumina bubbles have a lower density, however, the average value being 1.01 gms/cm^3. The bubbles are hollow but since the radiative contribution is essentially size dependent, (see eq (2), ref. 7), it was assumed that this contribution was the same as that inferred by Laubitz for material having the same particle size range as the alumina bubbles (curve (2), fig 2). The solid conduction contribution for the alumina bubbles was calculated by reducing that measured by Laubitz in the ratio 1.01/1.77. The estimated effective conductivity for the alumina bubbles, found by adding the conductive and radiative contributions, is given as curve (3) in figure 2. That this curve is of the right order of magnitude is demonstrated by the dotted curve in the figure. This curve gives vacuum environment conductivity results by Wechsler and Glaser (10)for an alumina bubble/graphite fiber composite.

Using curve (3), figure 2, and the experimental temperature distribution data given in Table 2, eq (18) was evaluated.

Table 2. Insulation Segment Temperature Distribution Data

Data Point	T_{L1}(°C)	T_1(°C)	T_{Lo}(°C)	T_o(°C)	$\bar{T}_i$(°C)	$\bar{k}_i$ $\frac{W}{m\ deg}$
1	105.2	44.6	74.0	28.1	74.9	0.0115
2	145.0	55.3	120.5	43.9	100.2	0.0144
3	363.9	181.9	397.7	73.9	272.9	0.0259
4	437.4	216.2	502.2	80.6	326.8	0.0302
5	479.0	237.2	510.0	86.7	358.1	0.0332
6	531.3	257.2	522.2	90.0	394.3	0.0374
7	571.1	264.7	657.2	86.7	418.0	0.0418
8	651.3	278.5	836.5	45.6	461.8	0.0475
9	723.0	282.9	1042.5	15.6	503.2	0.0548

The comparison between the experimental heat loss measurements and those predicted by eq (18) are presented in Table 3 as percentages of the average heat flux in the specimen column. Positive values represent heat flow from the specimens into the insulation. If $(T_{BeO})_m$ is the mid-point temperature of the beryllium oxide specimen and T_{guard} is the guard heater temperature at the same axial position, then $(T_{guard}/(T_{BeO})_m - 1)100$ is the percentage by which the guard temperature exceeds that of the BeO specimen; this quantity will be termed the guard mismatch. For data points 4 - 6, the mean temperature of the BeO was held approximately constant while the guard mismatch varied from 8 to 23%. As seen in Table 3 the heat exchange between specimen column and insulation varied only 1.3% as observed experimentally and 2.9% according to the

analytical prediction. Thus thermal guarding of the specimen column does have an effect on the heat flowing in the column but the effect is not of high sensitivity. The experimental conductivity data was obtained with guard mismatching ranging from +23% to -11%. Across this wide range the average heat exchange between insulation and specimen column was 4.7%.

Table 3. Experimental-Analytical Heat Exchange Values

Data Point	Average Heat Flux in the Specimen Column(W)	Predicted Value	Experimental Value
1	11.0	2.6%	5.4%
2	18.4	2.8	6.4
3	56.6	7.1	5.5
4	67.6	9.0	5.4
5	67.5	10.0	5.4
6	67.2	11.9	4.1
7	81.0	14.0	4.0
8	103.8	16.8	-1.1
9	130.0	19.7	-5.5

It is important to note that there is some uncertainty in the experimental heat exchange values. For data points 4 and above these exchange values are obtained by taking the difference between large heat flux values, hence uncertainty in these fluxes greatly accentuates uncertainties in the heat exchange values. For low temperature data points the principal uncertainty in the heat exchange values is the error in the temperature gradient determinations in the meter bars above and below the BeO specimen. This uncertainty is particularly important here where the overall temperature drops in the meter bars are relatively low.

The change in sign of the experimental heat exchange values for the higher temperature data points are internally consistent. That is, in those cases where the exchange is positive (heat flow into the insulation), the thermocouples on the specimen surface give lower readings than those in the same plane at the specimen centerline. When the experimentally observed heat exchange values change sign, the surface thermocouples are found to read higher than the corresponding centerline couples.

Now comparing the experimental heat exchange values with the analytical predictions, based on the uncertainties in the experimental values discussed above, the predictions are consistent at least through data point 7.

The last two data point comparisons in Table 3 require further elaboration. Examining the experimental thermocouple data, there is an uncertainty of the gradient in the meter bars of 3.1%. In the cases where the measured heat exchange is near zero and going negative this uncertainty in the meter bar gradient introduces a particularly large uncertainty in the heat exchange value. The range for data point 8 is from -1.1% to +2.8% while for data point 9 it is from -5.5% to -2.2%. Further, the magnitude of the heat exchange is large here compared with the low temperature cases. For data points 8 and 9 this radial flux is from 10 to 12 times that for data point 1. For these higher temperature data points, the comparatively high radial fluxes introduce the possibility of significant temperature drops at the specimen-insulation interfaces and the insulation-guard heater interface. These temperature discontinuities result from the contact resistance associated with the interfaces and become significant when the radial flux is large. Assuming a conservatively high interface thermal contact conductance of 20 BTU/hr-ft^2-^{o}F, the interfacial temperature drop is at least 20^{o}F for the last two data points in Table 3. This factor is significant with respect to the analytical predictions because the temperature distributions used in evaluating eq (18) were not measured directly in the insulation but in the specimen column and the guard heater ring. This is certainly one of the largest factors in the disagreement between the heat exchange values for the high temperature data points.

In general the heat exchange predictions are of the right magnitude. However, it is apparent that to provide a more rigorous test of heat exchange predictions it would be necessary to conduct extensive measurements with that specific aim in mind. Such measurements would be most difficult to perform due to the necessity of accurately measuring temperatures directly in the low density insulation material.

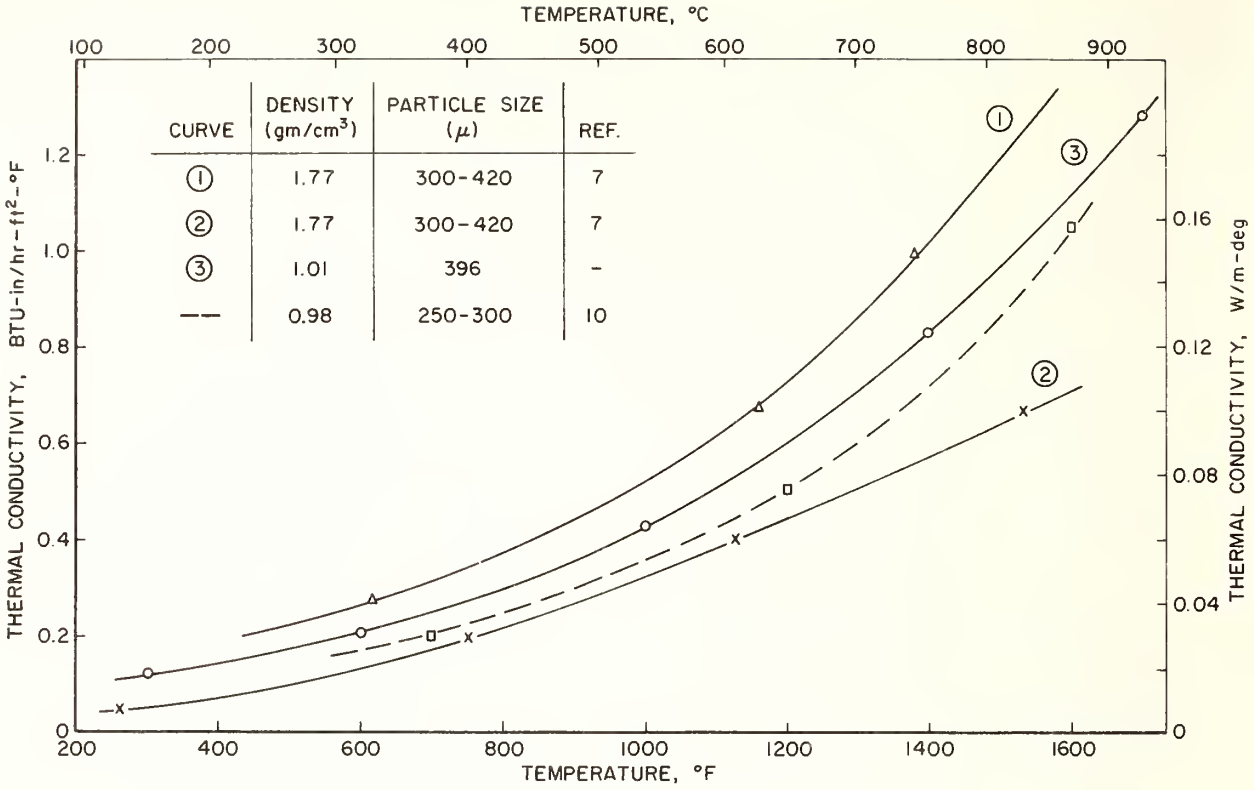

FIGURE 2 - Thermal Insulation Conductivity Comparisons

4. Nomenclature

Because the final write-up for this paper was completed before the information on units and nomenclature was available, the symbols are not entirely consistent with those of the Proceedings. The following listing gives symbol designations unique to this paper.

k	Thermal Conductivity
λ_n, $\mathcal{K}_n$	Eigenvalue Parameters
q	Heat Flux

5. References

(1) Minges, M.L., "Comparative Conductivity and Thermal Contact Resistance Measurements", p. IV-B-20 to IV-B-31, Proc 4th Thermal Cond Conf, (1964).

(2) Minges, M.L. and Denman, G.L., "Progress Report, AFML Thermal Properties Group", Proc Fifth Thermal Cond Conf, II, (1965).

(3) Kreyszig, E., Advanced Engineering Mathematics, John Wiley and Sons, New York, N.Y., (1962).

(4) Gray, A. and Mathews, G.B., A Treatise on Bessel Functions, p. 260, MacMillan and Co., Ltd., London, (1931).

(5) Jahnke, E., Emde, F., Funktionentafeln, p. 205, Dover Publications, New York, N.Y., (1945).

(6) Norton Company, Worcester, Mass., Data Sheets, Aluminum Oxide Bubbles, Product E-163.

(7) Laubitz, M.J., "A Note on the Thermal Conductivity of Powders in Vacuum", Proc Third Conf Thermal Cond, II, p. 628-635, (1963).

(8) Godbee, H.W., Ziegler, W.T., "The Thermal Conductivity of MgO, Al_2O_3, and ZrO_2 Powders to 850°C", Proc Third Conf Thermal Cond, II, p. 557-612, (1963).

(9) Flynn, D.R., J. Res NBS-C, Engrg and Inst., 67C(2), p. 129-137, (1963).

(10) Wechsler, A.E., Glaser, P.E., "Investigation of the Thermal Properties of High Temperature Insulating Materials", ASD-TDR-63-574, 91, (1963)

Application of Neutron Diffusion Theory Techniques to Solution of the Conduction Equation

I. Catton and J. R. Lilley

Douglas Aircraft Company
Santa Monica, California

Computer codes for neutronic analysis of nuclear reactor cores have developed in parallel with, and sometimes spurred the development of, improved electronic computers. While this large effort has yielded spectacular increases in the efficiency with which the neutron diffusion equation can be solved, the diffusion of these techniques into heat conduction codes has not continued apace. This paper reports on the application to the conduction equation of techniques commonly used to solve Poisson's equation for neutron diffusion in one and two dimensions. Specifically, a non-iterative solution to the one-dimensional steady state equation is described, as well as comparisons of the Liebman, Aitken and Young-Frankel methods as applied to two-dimensional problems.

Conduction from a Finite-Size Moving Heat Source Applied to Radioisotope Capsule Self-Burial[1]

C. R. Easton[2]

Nuclear Technology and Subsystems
Research and Development
Missile and Space Systems Division
Douglas Aircraft Company
Santa Monica, California 90405

The re-entry of a radioisotope heat source and its impact on the Earth's surface may result in burial of the source in soil. Internal heat generation may increase the temperature of the capsule and the surrounding soil enough to melt the soil and initiate capsule self-burial. Analytical studies of heat conduction from a finite, moving heat source were conducted to determine the conditions under which self-burial occurs, the magnitude of self-burial velocity, and the parameters important to self-burial. Configurations studied were a point source, a constant-temperature spherical-shell source, and a finite-line source. For one typical case, self-burial was initiated at a capsule power density of 2.2×10^{-6} W/m^3. The self-burial velocities were on the order of 10^{-5} m/s or less. The dimensionless groups found to control self-burial are

$$\left(\frac{\text{Velocity} * \text{capsule radius}}{2 * \text{thermal diffusivity}}\right)$$

$$\left(\frac{\text{Heat source strength}}{4\pi * \text{radius} * \text{thermal conductivity} * \text{soil-melting temperature}}\right)$$

and, for the cylindrical capsules, the length-to-diameter ratio.

Key Words: Analytical, cylindrical, finite, heat conduction, heat source, moving source, radioisotope, self-burial, spherical.

1. Problem Statement

The application of radioisotope heat sources to electric-power systems used in space vehicles poses a safety problem because random re-entry and impact on the Earth's surface may occur. A heat source designed to re-enter intact possesses terminal velocities high enough to result in impact burial for some soil conditions and capsule designs. The power-systems of many capsules have a sufficiently high power density to melt the surrounding soil if they are partially or totally buried. If the capsule is denser than the soil, which is usually the case, it will sink through the molten soil and bury itself.

The answers to questions concerning recovery, possible contamination of underground water, and self-burial as a passive disposal mechanism depend on an understanding of the initiation and rate of self-burial. Finally, to design for or against self-burial, one needs to know what parameters and dimensionless groupings affect self-burial and how.

An analytical solution to self-burial will clarify these problems. The solution involves the treatment of a finite-size, moving heat source. The assumptions necessary for this solution degrade its accuracy, but the speed and ease of obtaining answers and the understanding achieved more than compensate

---

[1] Credit: This work was conducted by the Douglas Missiles and Space Systems Division under Independent Research and Development Account No. 81311-006.

[2] Mechanical Engineer

for this shortcoming. One necessary assumption is that the soil has constant thermal properties. This assumption linearizes the governing differential equations to make a solution possible. It is also assumed that the temperature field surrounding the capsule as seen from the capsule is steady. This assumption implies an infinite, homogeneous medium with constant self-burial velocity. Temperature falls rapidly to the front and sides of the capsule, making it reasonable to assume a homogeneous medium. Data of Jeffers and Baker [1][3] show transient times of about 4 hours for a constant-power electric heater buried in soil. The self-burial velocities reported here are of the order of 10^{-5} m/s or less. The capsule can move through the region of important temperature effects in about the same time it takes to initiate motion. Hence, the portion of the transient during which motion of the capsule occurs should be small, compared to the portion which initiates motion. It is then reasonable to consider only steady motion of the capsule.

Observing the capsule from a distance, one would see a monopole (caused by the internal heat generation) and superimposed dipoles (caused by the melting and refreezing of the soil and by the distributed source). The strength of the melting-freezing dipole is sharply reduced because the high thermal conductivity of the capsule makes it nearly a thermal short circuit for the dipole. The opposite effect applies to the distributed source dipole. One can normally neglect dipole effects in the presence of a monopole. Such an assumption will be shown invalid for the present case because of the inhomogeneity caused by the capsule in the soil medium. It will be assumed instead that the high thermal conductivity of the capsule dominates all multipole effects. Additional discussion of this assumption is presented with the analysis of a monopole heat source.

The problem then becomes that of solving for the motion of a finite heat source in an infinite, homogeneous medium of constant properties. The motion is to be along a straight line and such that the temperature at a fixed distance in front of the capsule center is a specified constant, i.e., the soil melting temperature.

2. Basic Equations

The development of the basic differential equation for a moving heat source is a textbook problem discussed by Eckert and Drake [2] and others. The transient heat conduction equation,

$$\frac{\partial T}{\partial t} = \alpha \nabla^2 T \tag{1}$$

is the starting point. In eq (1), T is the temperature excess over the surroundings, t is the time, α is the thermal diffusivity, and ∇^2 is the Laplacian operator. The motion is assumed to be in the x direction. Placing

$$\xi = x - Ut \tag{2}$$

transforms eq (1) to coordinates moving with the source, if U is the speed of the source. Considering steady state only, the transformed equation is

$$\nabla_\xi^2 T = -\frac{U}{\alpha} \frac{\partial T}{\partial \xi} , \tag{3}$$

where ∇_ξ^2 is the Laplacian operator in the new coordinates. Equation (3) has a solution of the form

$$T = e^{-\frac{U\xi}{2\alpha}} f(\xi, y, z) , \tag{4}$$

where f satisfies

$$\nabla_\xi^2 f = \left(\frac{U}{2\alpha}\right)^2 f \quad . \tag{5}$$

Equation (5) is the basic differential equation for this study.

---

[3] Figures in brackets indicate the literature references at the end of this paper.

2.1. Solution for a Monopole

For a monopole, f has no angular dependence. The solution follows the Eckert and Drake concept. In spherical coordinates, eq (5) becomes,

$$\frac{d^2f}{dr^2} + \frac{2}{r}\frac{df}{dr} - \left(\frac{U}{2\alpha}\right)^2 f = 0 \quad . \tag{6}$$

This equation has a general solution of the form

$$f = \frac{1}{r}\left[C_1 e^{\frac{Ur}{2\alpha}} + C_2 e^{-\frac{Ur}{2\alpha}}\right] \quad . \tag{7}$$

Substituting from eq (7) into eq (4) gives

$$T = \frac{e}{r}^{-\frac{U\xi}{2\alpha}}\left[C_1 e^{\frac{Ur}{2\alpha}} + C_2 e^{-\frac{Ur}{2\alpha}}\right] \quad . \tag{8}$$

Boundary conditions are

$$\left.\begin{array}{l} r\to\infty,\ T\to 0 \\ r\to 0,\ \dfrac{\partial T}{\partial r} \to -\dfrac{Q}{4\pi r^2 k} \end{array}\right\} \quad , \tag{9}$$

where

Q = Heat source strength

k = Soil thermal conductivity

The first boundary condition gives $C_1 = 0$, while the second gives

$$C_2 = \frac{Q}{4\pi k} \quad , \tag{10}$$

since $r = 0$ implies $\xi = 0$.

The solution for temperature is

$$T = \frac{Q}{4\pi k r} e^{-\frac{U}{2\alpha}(r+\xi)} \tag{11}$$

For a capsule of radius, r_o, the temperature at $\xi = r = r_o$ is T_m, the soil melting temperature. The self-burial speed is found by solving eq (11) for U with the above conditions applied

$$U = \begin{cases} \dfrac{\alpha}{r_o}\ln\left(\dfrac{Q}{4\pi r_o k T_m}\right), & Q > 4\pi r_o k T_m \\ 0 \quad , & Q \le 4\pi r_o k T_m \end{cases} \tag{12}$$

The maximum heat-source strength that will not cause self-burial is given by

$$Q_m = 4\pi r_o k T_m \quad . \tag{13}$$

A value of self-burial speed can be calculated by assuming the following parameters:

Soil density = 1,600 kg/m^3
Soil specific heat = 840 J kg^{-1} deg^{-1}
Soil conductivity = 0.35 W m^{-1} deg^{-1}
Source strength = 400 W
Soil melting temperature = 1,330 deg K above ambient
Capsule radius = 0.025 m

The self-burial speed for these values is

$$U = 1.1 \times 10^{-5} \text{ m/s} \quad . \tag{14}$$

The maximum value of heat-source strength, Q_m, which will not cause self-burial is 150 W. The temperature difference between the bottom and the top of the capsule, T, is approximately equal to 2,200 deg. Such a large temperature difference could clearly not be tolerated by a real capsule. However, conduction through the capsule should substantially reduce this temperature difference.

An estimate of the true temperature difference can be easily formed using the following idealizations: (1) conduction takes place in the cladding only, (2) all internally generated heat is delivered uniformly to the cladding, (3) all heat transferred to the soil is transferred uniformly over the lower hemisphere, and (4) all heat liberated by freezing is transferred uniformly to the upper hemisphere to be conducted to the lower hemisphere.

These assumptions result in the differential equation,

$$\frac{d}{d\theta}\left(\sin\theta \frac{dT}{d\theta}\right) = -\frac{q r_o^2 \sin\theta}{b\, k_c} \quad , \tag{15}$$

where

$$q = \frac{Q}{4\pi r_o^2} + \frac{\rho_s U Q_f}{2} \quad , \tag{16}$$

and θ is the polar angle, b is the cladding thickness, k_c is the cladding thermal conductivity, ρ_s is the soil density, and Q_f is the soil heat-of-fusion.

Equation (15) is integrated separately for the upper and lower regions with boundary and matching conditions.

$$\left.\begin{aligned} \left.\frac{\partial T}{\partial \theta}\right|_{\theta=0,\,\pi} &= 0 \\ T_\ell\left(\frac{\pi}{2}\right) &= T_u\left(\frac{\pi}{2}\right) \\ T_\ell(0) &= T_m \end{aligned}\right\} \tag{17}$$

Integrating and applying conditions of eq (17) gives,

$$T_{\ell,u} = \frac{r_o^2}{bk_c} \left\{ q_u \ell n\,(2) + q_{\ell,u} \left[\ell n\,(\sin\theta) - C\,\ell n\,(\csc\theta - \cot\theta) \right] \right\} \quad , \tag{18}$$

where C = +1 for the lower half and -1 for the upper half.

Solving for the temperature difference gives,

$$\Delta T = T_u(\pi) - T_\ell(0) = \frac{2\,\ell n(2) r_o^2}{bk_c} \left(\frac{Q}{4\pi r_o^2} + \frac{\rho_s U Q_f}{2} \right) \quad . \tag{19}$$

Using the previous values plus

$$\begin{aligned} k_c &= 52.5 \text{ W m}^{-1} \text{ deg}^{-1} \\ b &= 0.0051 \text{ m} \end{aligned} \quad ,$$

the estimated temperature difference is

$$\Delta T \simeq 170 + 2.5 \times 10^{-5} Q_f \text{ deg} \quad . \tag{20}$$

The heat-of-fusion will vary for different soils but should always be less than $2.3\ 10^6$ J/kg. Equation (20) then shows two important results. First, the true capsule is much closer to an isothermal finite source than to a monopole. Second, the dipole effect of melting and freezing of the soil is of much less importance than the dipole effect of the distributed source.

2.2. Solution for an Isothermal Sphere

An isothermal sphere is a relatively easy solution to form and it should closely approximate the behavior of a real capsule. Equation (5) is still appropriate,

$$\nabla_\xi^2 f = \left(\frac{U}{2\alpha} \right)^2 f \quad . \tag{5}$$

This equation yields to separation of variables and gives, for a particular solution,

$$T_p = e^{-Arx} \left[C_3\, i_p(Ar) + C_4\, k_p(Ar) \right] \left[C_5\, P_p(x) + C_6\, Q_p(x) \right] \quad , \tag{21}$$

where the C's are arbitrary constants, i_p and k_p are spherical hyperbolic Bessel's functions, P_p and Q_p are Legendre polynominals, and

$$\left.\begin{aligned} x &= \cos\theta \\ A &= \frac{U}{2\alpha} \end{aligned}\right\} \quad . \tag{22}$$

Appropriate boundary conditions are that T be finite everywhere outside the capsule and constant on the surface of the capsule. The first condition forces C_3 to be zero, and no gain in generality results from retaining the Q_p with polar symmetry. A summation of particular solutions is required to meet the second boundary condition,

$$T = C \sum_{p=0}^{\infty} C_p e^{-Arx} k_p(Ar)\, P_p(x) \quad . \tag{23}$$

Applying the second boundary condition to eq (23) gives

$$T = T_m e^{-Arx} \sum_{p=o}^{\infty} \left(\frac{2p+1}{2}\right) \frac{k_p(Ar)}{k_p(Ar_o)} P_p(x)\, G_p(Ar_o) \quad , \tag{24}$$

where

$$G_p(\eta) = \frac{1}{2^p} \sum_{\ell=o}^{\left[\frac{p}{2}\right]} \frac{(-1)^\ell (2p-\ell)!}{\ell!(p-\ell)!\eta^{(p-\ell+1)}} \left[e^{-\eta} \sum_{t=o}^{p-\ell} \frac{\eta^t}{t!} - e^{\eta} \sum_{t=o}^{p-\ell} \frac{(-\eta)^t}{t!} \right] .$$

The most desirable form of eq (24) is that which relates the internal heat generation to the self-burial speed. This form is obtained by setting the surface integral of the normal derivative of eq (24) equal to the heat-generation rate divided by conductivity. The resultant equation is

$$Q = \pi r_o\, kT_m \sum_{p=o}^{\infty} (-1)^p (2p+1) \left[\frac{Ar_o\, k_{p+1}(Ar_o)}{k_p(Ar_o)} - p \right] G_p^2(Ar_o) \quad . \tag{25}$$

For A = 0, eq (25) reduces to eq (13).

The dimensionless forms of eqs (12) and (25) are found by setting

$$\left.\begin{aligned} Z &= Ar_o \\ q &= \frac{Q}{2\pi r_o\, kT_m} = \frac{Q}{Q_m} \end{aligned}\right\} \quad . \tag{26}$$

The variable, Z, can be considered to be a ratio of a characteristic dimension to a wave length of the disturbance caused by motion of the source.

Equations (12) and (25), in dimensionless form, are

$$Z = \begin{cases} (\ell n\, q)/2, & q > 1 \\ 0 \quad , & q \le 1 \end{cases} \tag{27}$$

$$q = \sum_{p=o}^{\infty} (-1)^p (2p+1) \left(\frac{Zk_{p+1}(Z)}{k_p(Z)} - p \right) G_p^2(Z) \quad . \tag{28}$$

These equations are shown graphically in figure 1. The two equations show different magnitudes and functional forms. Also shown is an estimate of the self-burial speed of a real capsule. To form this estimate, it is assumed that the difference between the monopole and the isothermal sphere is caused by the unrestrained temperature away from the forward stagnation point of the monopole. The heat carried away by the excess of temperature can be estimated by

$$q_e = \frac{Za^2}{2} (e^{nZ} - 1) \quad , \tag{29}$$

where a is a multiplier on the capsule radius representing the effective radius of excess heating, and n is a number representing the average excess temperature. At the capsule surface, n has a range from 1 to 2. Assuming n = 1.5, a can be calculated from the data of figure 1. The variation of a with Z is shown in figure 2. The dashed curve in figure 2 is from the family

$$a = 1 + \frac{C}{Z} \quad , \tag{30}$$

which we might expect a to follow, analogous to Mach waves in supersonic flow.

It is appropriate to choose n = 0.24 to estimate the self-burial speed of a real capsule, as this value gives the appropriate temperature difference across the capsule. This value of n should be an upper limit since the temperature excess is a high estimate. The deviation from the isothermal sphere is not negligible, but the error in estimating the self-burial velocity of the real spherical capsule is felt to be small.

There is no need to pursue spherical models further. It is more desirable to consider cylindrical models because these better approximate real capsules.

2.3. Solution of Finite Cylinder Capsules

The model chosen for analysis of cylindrical capsules is a finite-line integral of monopole heat sources. The capsule is assumed to have its axis horizontal. Figure 3 shows the manner in which eq (11) is used as an integrating kernel for the model. In dimensionless form, the line integral is

$$\tau = \frac{4\pi r_o \, kT}{Q/\ell} = \int_o^{\ell} \frac{e^{-Z\left(1 + \sqrt{1 + \eta^2}\right)}}{\sqrt{1 + \eta^2}} \, d\eta \quad , \tag{31}$$

where ℓ is the capsule L/D and the other variables are as previously defined. The relationship between heat flux and self-burial velocity is

$$q' = \frac{Q/\ell}{4\pi r_o \, kT_m} = \frac{e^{Z}}{\displaystyle\int_o^{\ell} \frac{e^{-Z\sqrt{1 + \eta^2}}}{\sqrt{1 + \eta^2}} \, d\eta} \quad . \tag{32}$$

Equation (32) can be integrated for the limiting case of zero self-burial velocity. The result is

$$q'_m = \frac{1}{\log_e \left[\ell + \sqrt{1 + \ell^2}\right]} \quad . \tag{33}$$

The limiting case of infinite L/D is found from eq (5) solved in cylindrical coordinates. The solution is similar, except that hyperbolic Bessel's functions appear in lieu of exponentials. The result is

$$q'_\infty = \frac{e^{Z}}{K_o(Z)} \quad . \tag{34}$$

There is no minimum value of q' for the infinite cylinder, analogous to Q_m. The fallacy of assuming an infinite cylinder is thus underscored.

The general case of eq (32) must be integrated numerically. The result is given in figure 4, with the zero line calculated from eq (33) and the asymptotic limit from eq (34). Only for large self-burial speed does the heat-source strength approach the asymptotic limit by an L/D of 20. The finite length of a real capsule will be an important consideration.

The solution for the case of a finite, isothermal cylinder is very difficult. It would probably be as easy to develop a generalized computer program to solve the problem with capsule internal conduction,

melting and freezing, and variable thermal properties as it would be to solve the case of the isothermal cylinder. This course is recommended should further pursuit of this subject prove warranted.

The correlation between the monopole and the isothermal sphere can be used to estimate the behavior of an isothermal cylinder. The value of n should be somewhat larger for a cylinder than for a sphere. Assuming n = 1.6, the equation for the excess source is

$$q_e' = \frac{Za}{2\pi}(e^{nZ} - 1) \quad . \tag{35}$$

Figure 5 shows the line source and estimated isothermal cylinder for a capsule L/D of 12. The deviation of the line-source model from the isothermal-cylinder model is estimated to be much less important than for the comparable spherical cases. This result can be attributed to the smaller relative area encompassed by the dimension $r_o a$ in the case of the cylinder. Although the excess of temperature is the same for both cases, the mass of soil involved is much less for the cylinder, therefore the excess of heat removed is much less.

3. Conclusions

Self-burial is a real possibility for a radioisotope capsule on the ground. The maximum heat-source strength which will not bury itself after an initial burial is easily shown to be

$$Q_m = 4\pi r_o k T_m \tag{36}$$

$$Q_m' = \frac{4\pi L k T_m}{\log_e \left[\ell + \sqrt{1 + \ell^2}\right]} \tag{37}$$

for the spherical and cylindrical capsules, respectively. Expressions for the relationship between heat-source strength and self-burial speed were derived for idealized conditions. The solutions were demonstrated to be reasonably accurate within the limitations of steady-state, homogeneous medium and constant properties.

It is recommended that the capsule designer study the effect of self-burial on capsule design from the standpoint of passive disposal, potential hazards, and recovery. If designing for self-burial is desirable and practical, a computer program should be developed to solve the general equations and provide design data.

4. References

[1] Jeffers, S. L. and Baker, F. L., Private Communication, Sandia Corporation, Aerospace Nuclear Safety Group.

[2] Eckert, E. R. G. and Drake, R. M., Heat and Mass Transfer, (McGraw-Hill, 1959).

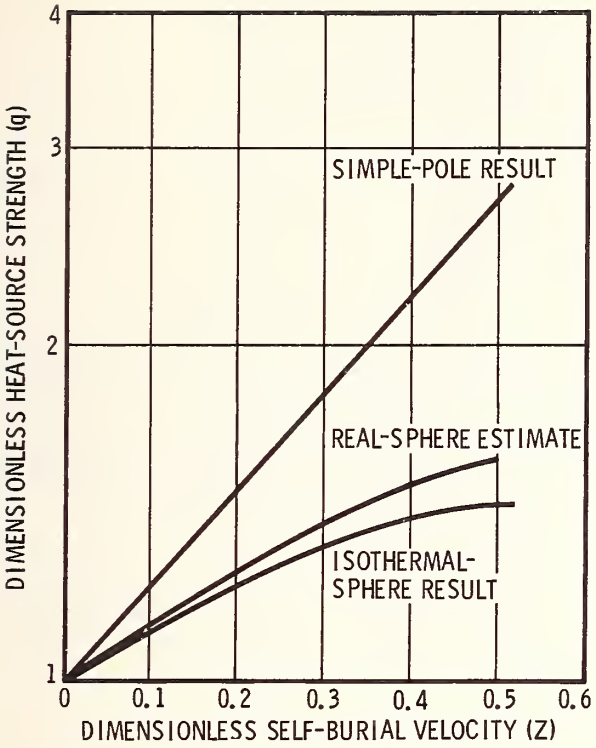

Figure 1. Dimensionless self-burial velocity.

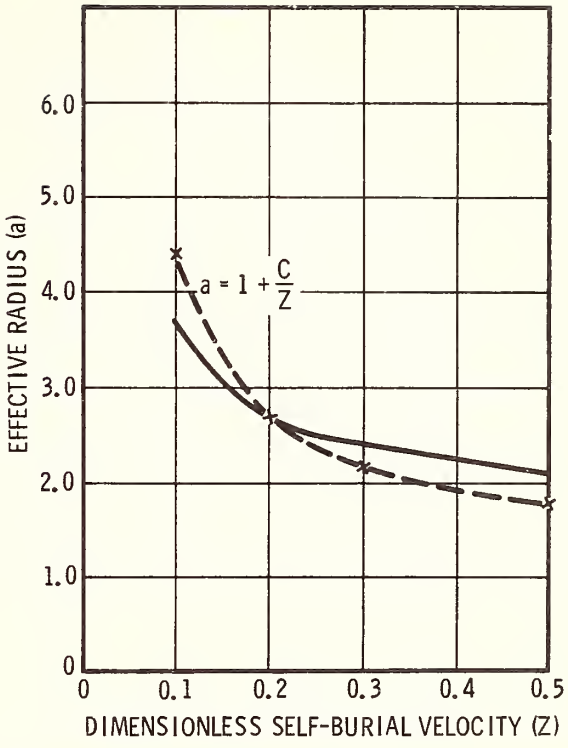

Figure 2. Effective radius of excess heating.

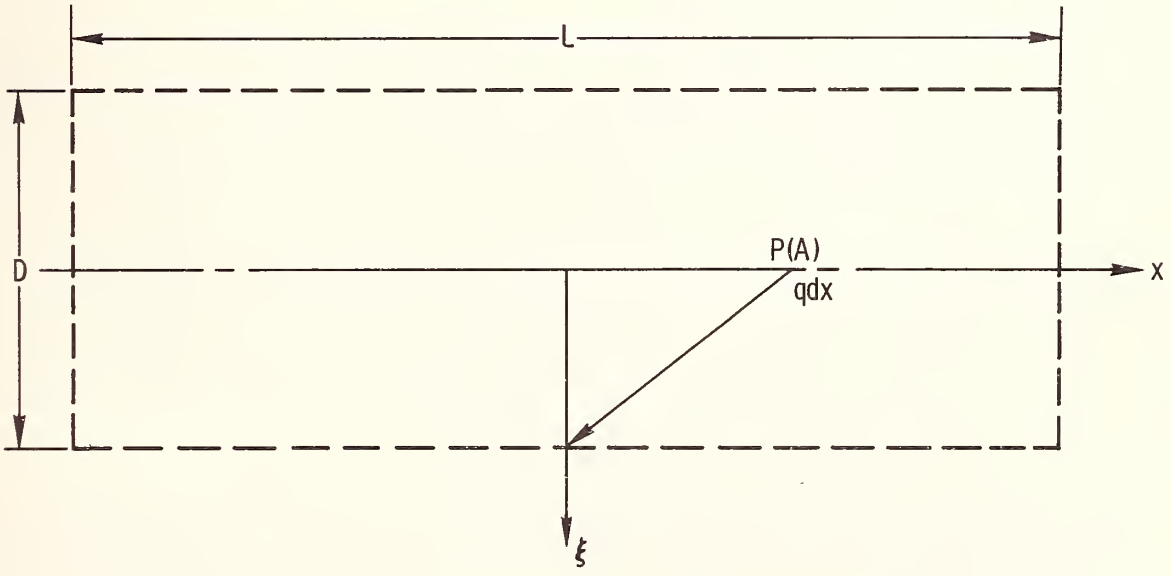

Figure 3. Continuous-line-source model of cylindrical capsule.

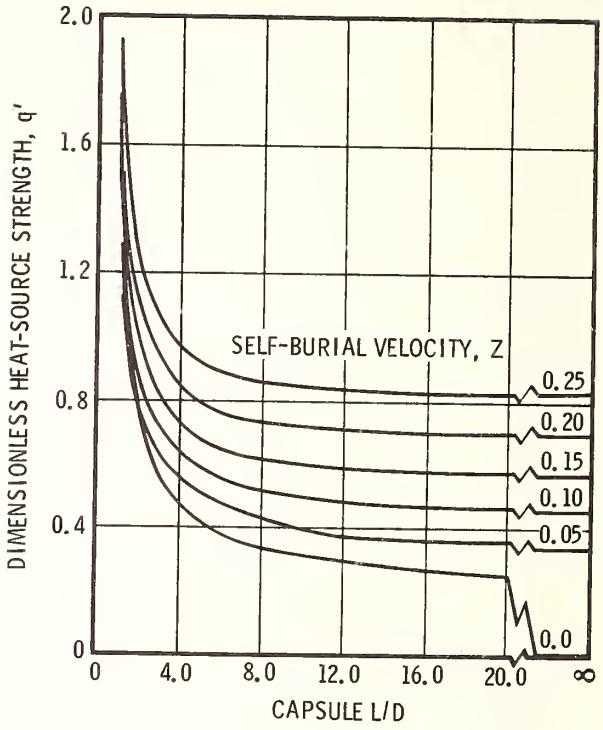

Figure 4. Effect of capsule length-to-diameter ratio on heat-source strength per unit.

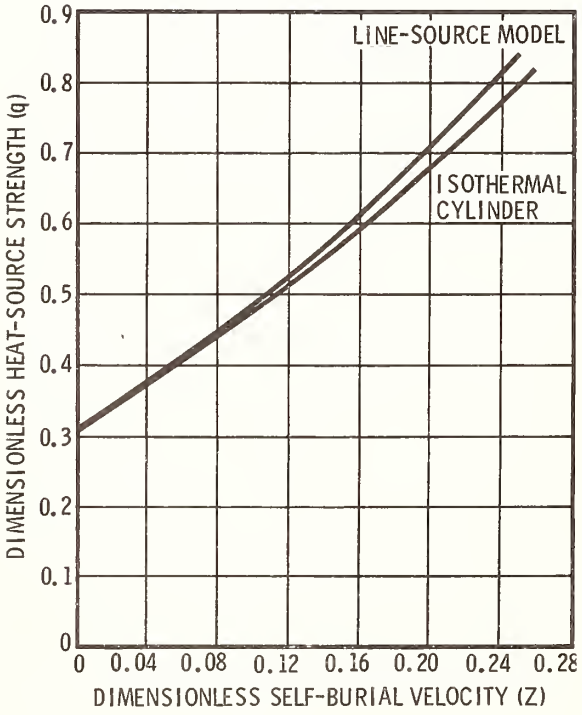

Figure 5. Estimate of self-burial velocity of an isothermal cylinder with L/D = 12.

Evaluation of Steady-Periodic Heat Flow Method for Measuring the Thermal Diffusivity of Materials with Temperature-Dependent Properties

C. J. Shirtliffe and D. G. Stephenson

Division of Building Research
National Research Council of Canada
Ottawa

Temperatures in a material with temperature-dependent properties were calculated by finite difference methods. The calculated values were analyzed for harmonic content and used with the solution to the linear form of the heat conduction equations to determine the mean value of thermal diffusivity. Errors in determining the mean properties were calculated and the distortion produced by the temperature dependence was tabulated. Distortion of the temperature waves in the material places limitations on the use of the method for moist materials. The main harmonic content was found to have little distortion so long as only odd harmonics were present in the boundary conditions. Accuracy of the method was established for the configuration and range of parameters anticipated for moist building materials.

Key Words: Dry materials, infinite slabs, moist materials, periodic heat flow, temperature dependence, thermal conductivity, thermal diffusivity.

1. Introduction

Water migrates when a temperature gradient is applied to a moist porous material. This fact has to be borne in mind when designing experiments to measure the thermal properties of moist materials. The movement of moisture contributes to the heat transfer and it makes the apparent thermal properties quite dependent on the temperature and moisture content of the sample. It also causes the moisture distribution through the sample to change during the course of an experiment making it difficult to say what moisture content and temperature correspond to the measured conductivity or diffusivity. This problem is alleviated by using steady periodic boundary conditions because this makes the time average condition of the sample constant.

The Angstrom method has been used, therefore, to measure the thermal diffusivity of moist materials (1, 2),[1] but it has never been established that the method gives true mean values, even for "dry" materials, when the thermal properties are temperature dependent. The objective of this study was to determine the magnitude of the errors that might occur when the Angstrom method was used to measure the thermal diffusivity of materials that contain moisture.

2. Method of Determining Errors

The error inherent in the Angstrom method was checked in the following way: (i) the temperatures at different locations through a sample were calculated for steady periodic boundary conditions assuming that the thermal properties of the sample varied in a particular way with variations of temperature; (ii) the calculated temperatures were used to compute a mean value of thermal diffusivity just as if they had been obtained by experiment; and (iii) the resulting "experimental" value of diffusivity was compared with the "correct" mean value, i. e. the mean of the values used in the

[1] Figures in parentheses indicate the literature references at the end of this paper.

original calculations; the difference was the error inherent in the method of calculating a mean value from experimental results.

The initial calculations were made using the finite difference equations given in Appendix I. This numerical approach was used because no exact analytical solution was known that would permit the simulation of an experimental set-up: quasi-linear approximate methods were tried but there was no sure way of knowing when the calculated results began to have a non-negligible error. The purely numerical results could be made as accurate as required by using finer increments in space and time and the accuracy could be checked by comparing results for successively smaller increments. This study indicated that there is an optimum value of the inverse Fourier number, $1/F_o = (\Delta x)^2/a\Delta t$, at about 6 where "a" is the thermal diffusivity. Values of Δx and Δt were selected, therefore, so as to make this parameter close to six when "a" was at its mean value. This also ensured that the finite difference expressions remained stable since the stability limit is $1/F_o > 2$; in no case did "a" vary by as much as a factor of 3 from its mean value.

The results of the finite difference calculations were first analyzed to determine the mean value and the amplitude and phase of the main harmonic of the temperature at those locations where temperatures would normally be measured. The main harmonic component of each of these temperatures was then used to calculate the experimental value of "a." The formulas used for this computation are given in Appendix II. These equations are based on the premise that the thermal properties of the sample are independent of temperature; it is this simplifying assumption that causes an error in the calculated value of diffusivity.

The errors associated with all the numerical calculations were determined by comparing the "experimental" results with the "correct" values for a case where there was no variation of the properties with temperature. This showed that the error was less than 0.003 per cent.

3. Scope of Study

The initial study was limited to problems subject to the three following conditions:

(i) two identical, two-dimensional slabs
(ii) properties varying linearly with temperature

$$\lambda = \lambda_o (1 + \alpha\theta); \quad dc = dc_o (1 + \beta\theta)$$

where d is density, α and β are the temperature coefficients, λ_o and dc_o are the mean values;

(iii) boundary conditions

1. $\theta_1 = E_1 \sin wt$ and $\theta_2 = E_2 \sin (wt + \Delta_o)$

where $w = 2\pi/p$, circular frequency, Δ_o is a phase shift, p is the period

or

2. Square waves; $\pm E_1$ and $\pm E_2$; $\Delta_o = 0$ or 180°.

The range of the variables investigated was:

$a = 2.6 \times 10^{-8}$ m^2/s and 2.6×10^{-7} m^2/s (0.001 and 0.01 ft^2/hr)

E_1 and E_2 = 2.8 to 28 C (5 to 50 F)

$p = 7.2 \times 10^2$ to 3.6×10^4 sec (0.2 to 10 hr)

α and β = -0.036 to +0.036 deg C^{-1} (-0.02 to +0.02 deg F^{-1})

The boundary conditions were selected so as to have no even harmonics. A quasi-linear analysis, to be published later, showed that this type of boundary condition should produce the best results.

4. Results

4.1 Distortion of Wave Form

The temperature dependence of the properties caused a distortion of the temperature wave form in the material. Tables 1 and 2 summarize some of the results for one set of boundary conditions. Distortion occurs for both sine-wave and square-wave boundary conditions.

Table 1. Effects of Temperature Dependence of Properties on the Temperature Variation in a Slab

Tabulated results for:

- centerline of slab
- 13.9 deg C amplitude
- 1 hr period
- $1/F_o = 5.9$
- 5th cycle results
- thickness = 0.061 m
- square-waves
- in phase
- 1000 steps/cycle
- $a_o = 2.58 \times 10^{-7}\ m^2/s$
- zero mean temp. at surfaces

Temp. Coefficients		Average Temp.	Main Harmonic		Second Harmonic		Error in a_o **
$\alpha \times 10^3$	$\beta \times 10^3$	°C	Amplitude, °C	Phase	Amplitude, °C	Phase	%
0.0*	0.0*	0.000*	6.172*	-102.22*	0.000*	-	-
0.0	0.0	0.002	6.172	-102.22	0.00005	10.88	+0.002
0.0	-3.6	-0.00050	6.172	-102.22	0.077	101.58	-0.005
0.0	-7.2	-0.0011	6.172	-102.20	0.156	101.64	+0.018
0.0	7.2	0.0011	6.172	-102.20	0.156	-78.28	+0.018
3.6	0.0	0.307	6.172	-102.17	0.040	143.48	-0.020
-3.6	0.0	-0.307	6.172	-102.17	0.040	-36.38	-0.020
-7.2	0.0	-0.612	6.167	-102.07	0.080	-34.20	-0.040
3.6	-3.6	0.301	6.178	-102.12	0.091	118.60	-0.080
3.6	3.6	0.312	6.167	-102.22	0.038	122.10	+0.011
-3.6	-3.6	-0.312	6.167	-102.22	0.038	57.74	-0.011
-3.6	-7.2	-0.317	6.161	-102.26	0.089	84.18	-0.182
3.6	7.2	-0.317	6.161	-102.26	0.089	-95.73	-0.182
7.2	-3.6	0.604	6.183	-101.92	0.546	-175.47	-0.112
7.2	3.6	0.618	6.156	-102.12	0.053	170.28	-0.268
7.2	7.2	0.623	6.150	-102.12	0.076	122.15	+0.444
-7.2	-7.2	-0.623	6.144	-102.22	0.077	57.77	+0.444
36.0	-36.0	2.797	6.644	-92.07	1.006	132.24	-7.55
36.0	36.0	2.963	5.617	-102.14	0.283	-123.63	+10.2

* Solutions for constant properties
** from real part of eq (3), Appendix II

The temperature dependence of the properties gives rise to a non-zero average temperature at the internal points, even though the average boundary temperatures are zero. Typical profiles are given in figure 1. Table 1 shows that, for the conditions studied, this effect is less than 20 per cent of the amplitude of the main harmonic. The distortion in the mean temperature depends primarily on the coefficient α and varies linearly with it.

Table 2. Effects of Frequency on the Temperature Variation in a Slab with Temperature Dependent Properties (non-metal; 5 cm thickness)

α = 0.0036/°C
L = 0.061 m
13.9 deg C sine waves, zero mean
18 slices, $1/F_o$ = 6.2, 5th cycle results
Boundaries at 0 mean temperature

β = 0.0072 /deg C
a = 2.58×10^{-7} m^2/s
120° phase shift

Results for the Centerline

Period hr	Mean Temp, °C	Main Harmonic		Second Harmonic	
		Ampl, °C	Phase	Ampl, °C	Phase
1.0	0.171	2.42	-162.24	0.0218	131.84
0.5	0.179	1.12	156.43	0.0050	36.91
0.2	0.193	0.25	75.35	0.0012	-2.34

Distortion of the main harmonic is primarily affected by the coefficient α as shown by Tables 1 and 2. These are relatively small and it can be inferred that the fundamental frequency can be used to obtain good approximations to the mean thermal diffusivity. The error in the main harmonic is also affected by β, θ max, and the period.

The temperature dependence of properties produced even harmonics at internal points. The second harmonic content (Tables 1 and 2) depends on both the temperature coefficients. The amplitude of the second harmonic is more than 15 per cent of the main harmonic for the worst case shown.

Results not shown indicate that the odd harmonics of square-wave boundary conditions have distortion similar to the main harmonic, but because of the fewer number of points used in the harmonic analysis, they have more inherent errors.

The frequency has a marked effect on the distortion (Table 2). The distortion of the average temperature increases with frequency, but the relative amplitude of the second harmonic decreases. No exact explanation can be offered for this at present.

The relative phase of the boundary temperatures affects the results. The effect is second order for mean temperature as shown in figure 1. The second harmonic distortion is worse when the boundary temperatures are in phase than when they are 180° out of phase.

4.2 Errors in Determination of Thermal Diffusivity

The results of a quasi-linear analysis, to be published later, and the basic form of the finite difference equation, given in Appendix I, indicated that the errors are functions of α, β, $\alpha - \beta$ and $\alpha + \beta$ and sums and products of these parameters. These relationships were checked for the results of the finite difference calculations by plotting error in determining thermal diffusivity against the same combinations of α and β.

A summary of the most important characteristics of the error in the determination of the thermal diffusivity is given in figures 1 and 2 for a = 2.58×10^{-7} m^2/s (0.01 ft^2/ hr), and, $\pm$ 13.9 C (25 F) square-wave boundary conditions. The error for a thermal diffusivity of $2.58 \times 10^{-8} m^2$/sec was similar.

Figure 2 gives the errors in determining the thermal diffusivity from the real part of eq (3) in Appendix II while figure 3 gives the error when they are determined from the imaginary part of the equation. The errors are smaller using the real part, except when $\alpha = \beta$, i.e. when the thermal diffusivity is a constant. The slope of the curves indicates that the error terms are essentially quadratic functions of α and β. Figures 2 and 3 are not exact, expecially at the lower values, because of the

finite difference error in the calculations.

Typical values for the temperature coefficients, α and β, for dry materials are given in Table 3. The range in α is from -0.01 to +0.01 per deg K and β from -0.003 to +0.004 per deg K. Values for moist materials are unknown, but a rough estimate would be, -0.02 to +0.02 per deg K for α and -0.005 to +0.005 for β.

Table 3. Typical Values for the Temperature Coefficients of Thermal Conductivity and Thermal Diffusivity of Dry Solids at Temperatures Above 100°K

Type of Material	Temperature Coefficient α per deg. C	Temperature Coefficient β per deg. C
metals	-0.010 to +0.010 (rare 0.020)	-0.003 to +0.004
non-metals	0 to 0.004 (rare 0.020)	-0.0003 to +0.003
semi-conductors	-0.006 to +0.006	-0.0003 to +0.003

(Data from American Institute of Physics Handbook, 2nd Edition)

The errors in determining thermal diffusivity in the range considered can be estimated from figures 2 and 3, as being less than 1 per cent for dry materials and 3 per cent for moist materials using the real part of the linear solution, and less than 2 and 6 per cent, respectively, using the imaginary part of the linear solutions.

5. Conclusions

Distortion produced by the temperature dependence of thermal properties places limitations on the use of steady-periodic methods for measuring the thermal properties of moist materials. The steady mean temperature gradient can be expected to produce a nonuniform mean moisture content in the material. The method has advantages, however, over other methods since the mean gradient is only a small fraction of the maximum temperature variation in the material.

The main harmonic must be found by accurate harmonic analysis because of the harmonic distortion that is introduced by the temperature dependence of the thermal properties.

The mean thermal diffusivity of the material determined from the main harmonic has some error but the accuracy of the method is adequate for most purposes even for large temperature dependence. Steady periodic methods can, therefore, be used to determine the thermal diffusivity of normal dry materials. Errors due to the temperature dependence can be estimated from the curves in figures 2 and 3.

6. References

(1) Higashi, A. On the thermal conductivity of soil, with special reference to that of frozen soil, Trans. Amer. Geophys. Union, 34, 5, (1963).

(2) Jackson, R. D. and Kirkham, D. Method of measurement of the real diffusivity of moist soil. Proc. Soil Sci. Amer., 22, 6, (1958).

(3) Carslaw, H. S. and Jaeger, J. C. Conduction of heat in solids. 2nd Edition, Oxford Press.

(4) Shirtliffe, C. J. and Stephenson, D. G. The determination of the thermal diffusivity and conductivity of materials subjected to periodic temperature variations. NRC/DBR, Computer Program No. 12 (1962).

Appendix I

1. Finite Difference Solution

1.1 Basic Equation

The basic equation approximated by the finite differences was

$$\frac{\partial \theta}{\partial t} = \frac{1}{cd} \frac{\partial}{\partial x} \left(\lambda \frac{\partial \theta}{\partial x} \right) \tag{1}$$

with: zero initial conditions, periodic boundary temperature, cd and λ functions of temperature.

1.2 Finite Differences

Central difference approximations were used to approximate the derivatives, yielding

$$\theta\ (n, t + \Delta t) = \theta\ (n, t) + \frac{\Delta t}{\Delta x^2 dc(n)} \left[\left(\frac{\lambda\ (n-1) + 4\lambda\ (n) - \lambda\ (n+1)}{4} \right) \cdot \theta\ (n-1, t) - 2\lambda\ (n)\ \theta\ (n, t) \right.$$

$$\left. + \left(\frac{\lambda\ (n+1) + 4\lambda\ (n) - \lambda\ (n-1)}{4} \right) \cdot \theta\ (n+1, t) \right]_t \tag{2}$$

where: dc and λ are arbitrary functions of temperature, n indicates the node point, Δt indicates the time step.

If $\lambda = \lambda_o (1 + \alpha\theta)$ and $cd = c_o d (1 + \beta\theta)$, eq (2) reduces to

$$\theta\ (n, t + \Delta t) = \theta\ (n, t) + a_o \frac{\Delta t}{\Delta x^2} \left[H - \left(\frac{(\beta - \alpha)\ \theta\ (n, t)}{1 + \beta\theta\ (n, t)} \right) H - \frac{\alpha \left(\theta (n+1, t) - \theta\ (n-1, t) \right)^2}{4 \left(1 + \beta\theta\ (n, t) \right)} \right]$$

where $H = \left(\theta\ (n+1, t) - 2\theta\ (n, t) + \theta\ (n-1, t) \right)$ and is the form for constant properties and $\Delta x^2 / a_o \Delta t$ is the normal non-dimensional inverse Fourier number, $1/F_o$.

The second term is maximum when $\alpha = -\beta$.

Appendix II

2. Linear Solution for Two Slabs

2.1 General

The solution for the temperature variation in an infinite slab of a material of constant properties with periodic boundary temperatures is given in Carslaw and Jaeger (3). In terms of the temperature at three points in the material, and in matrix notation the solution is

$$\begin{bmatrix} \theta_1 \\ q_1 \end{bmatrix} = \begin{bmatrix} A & B \\ D & A \end{bmatrix} \cdot \begin{bmatrix} \theta_2 \\ q_2 \end{bmatrix} \tag{1}$$

and

$$\begin{bmatrix} \theta_2 \\ q_2 \end{bmatrix} = \begin{bmatrix} A^* & B^* \\ D^* & A^* \end{bmatrix} \cdot \begin{bmatrix} \theta_3 \\ q_3 \end{bmatrix} \tag{2}$$

where θ_1, θ_2, and θ_3 are periodic temperatures at points 1, 2, and 3; q_1, q_2, and q_3 are the periodic heat fluxes at points 1, 2, and 3, and

$$A = \cosh (1 + i)\,\Phi \qquad B = \frac{R \sinh (1 + i)\,\Phi}{(1 + i)\,\Phi} \qquad D = \frac{(1 + i)\,\Phi \sinh (1 + i)\,\Phi}{R}$$

where $\Phi = (\pi L^2/aP)^{\frac{1}{2}}$, $R = L/\lambda$, L = distance between respective points, λ = thermal conductivity, a = thermal diffusivity $= \lambda/dc$, P = period, d = density, c = specific heat per unit mass, and * refers to functions for the slab between points 2 and 3.

Equations (1) and (2) hold for all pure harmonics of the boundary conditions when the properties are constants.

2.2 Similar Slabs

For the case where the three temperatures are measured at evenly spaced points in a homogeneous material, the equations can be combined to give the following expression for the thermal diffusivity (Shirtliffe and Stephenson (4)):

$$(1 + i)\,\Phi = \cosh^{-1}\left(\frac{\theta_1 + \theta_3}{2\theta_2}\right) \tag{3}$$

Values of Φ can be obtained for both the real and imaginary part of the equation and the two values should be equal. This configuration can be used as an absolute method for finding the thermal diffusivity of a material.

2.3 Dissimilar Slabs

For two slabs of dissimilar material in contact at plane 2, the properties of the slab of material between points 1 and 2 can be found if the properties of the material between points 2 and 3 are known. Again from Ref (4) we obtain

$$\frac{\theta_1}{\theta_2} = A + B\left(\frac{q_2}{\theta_2}\right) \tag{4}$$

where

$$\frac{q_2}{\theta_2} = \frac{A^*}{B^*} + \frac{1}{B^*}\left(\frac{\theta_3}{\theta_2}\right). \tag{5}$$

The second equation shows that the reference slab is used as a "heat meter." When eq (5) is substituted in eq (4), the complex equation for θ_1/θ_2 contains the two unknowns R and Φ, or λ and a. These can be found from the real and imaginary parts of the equation. The solution has been done on a digital computer using standard numerical techniques.

2.4 Application of Equations

Apparatus based on these equations has been built and used at intervals over the past eight years. The results from the experimental investigation including considerable error analysis will be published elsewhere.

Computer analysis was found necessary to adequately handle the harmonic analysis of the temperature waves to solve the equations, and for error analysis.

This paper is a contribution from the Division of Building Research, National Research Council of Canada, and is published with the approval of the Director of the Division.

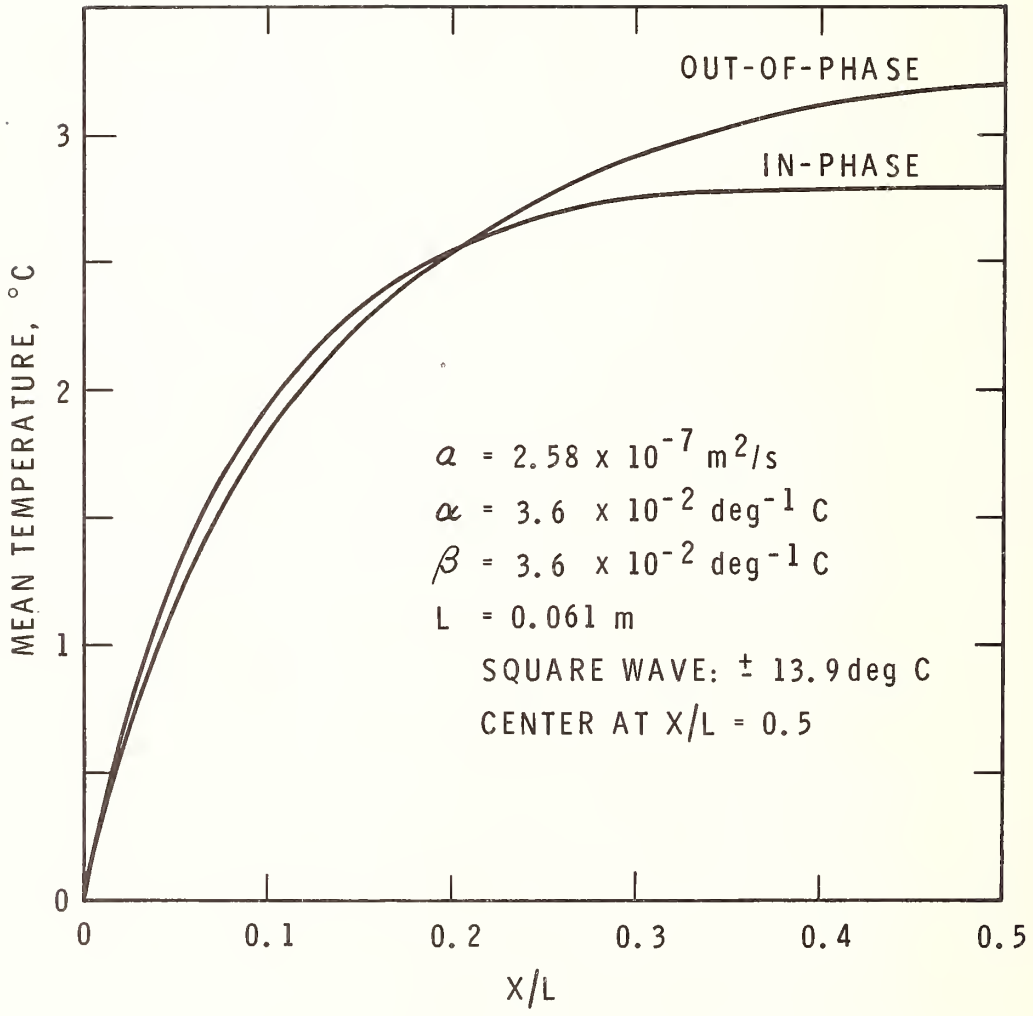

Figure 1 Mean Temperature Profile Produced by Temperature Dependence of Properties for Conditions Given.

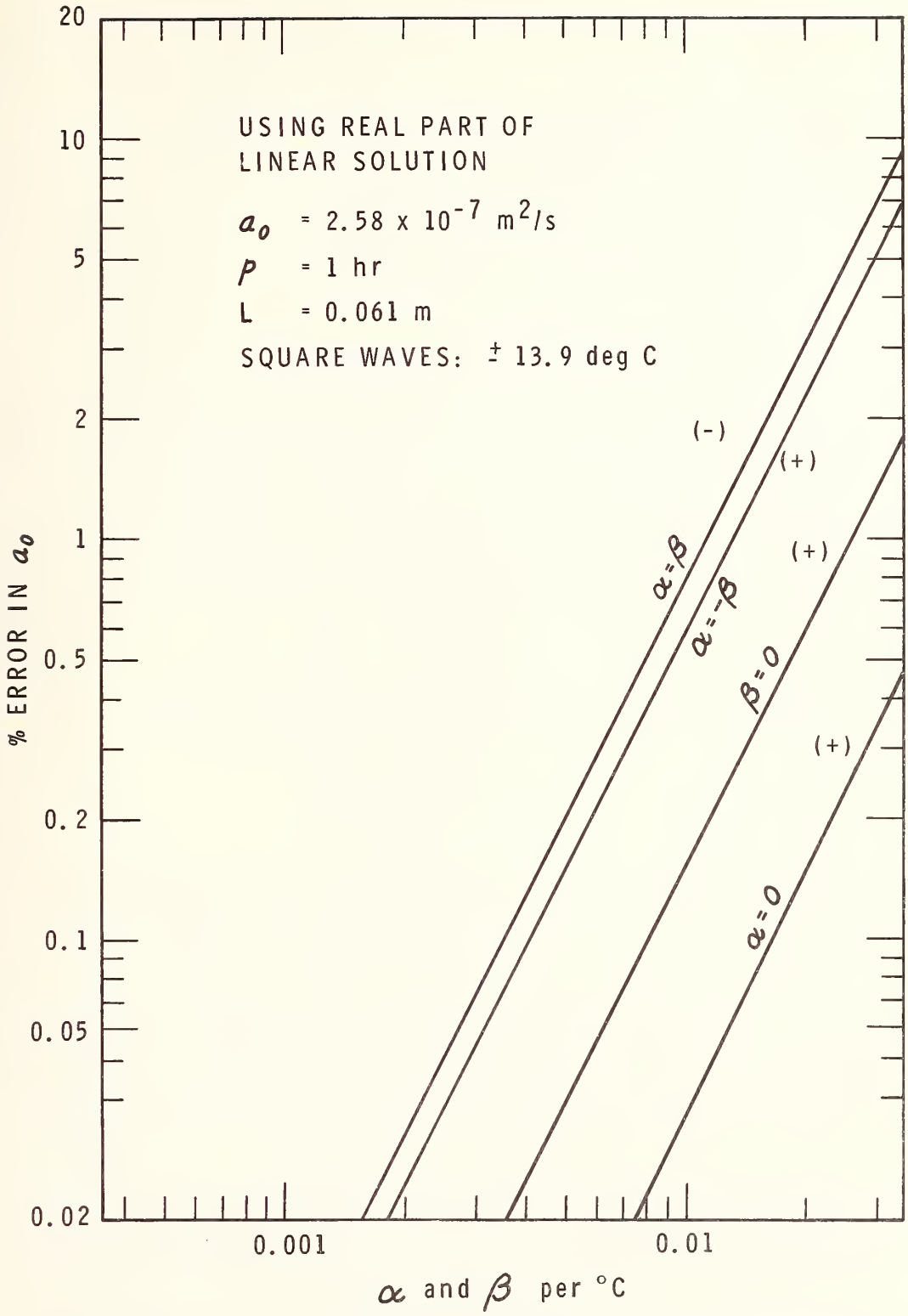

Figure 2 Error in Determining a_o Using Real Part of Linear Solution and for Particular Combinations of α and β.

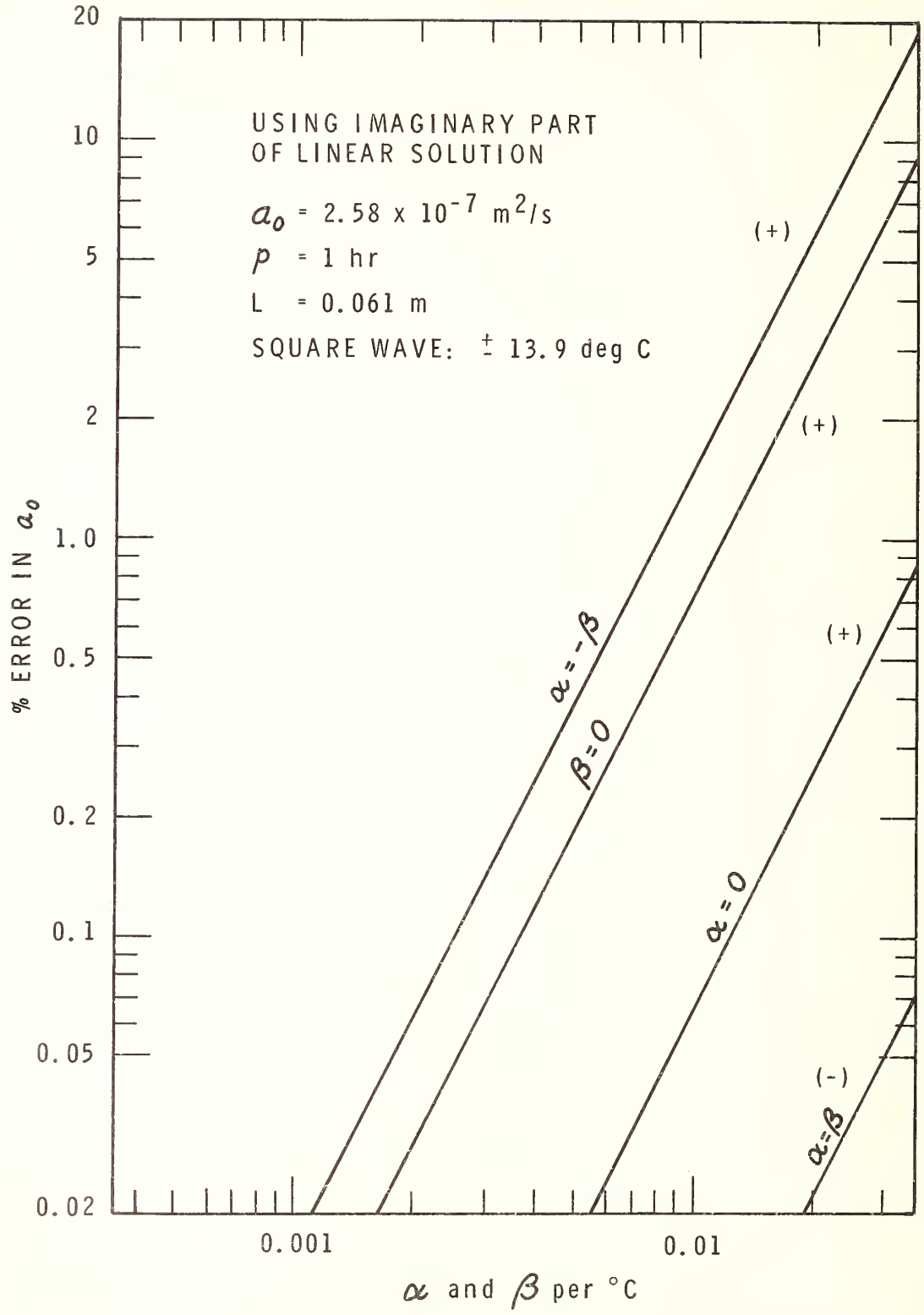

Figure 3 Error in Determining a_o Using Imaginary Part of Linear Solution and for Particular Combinations of α and β.

Comparison of Modes of Operation for Guarded Hot Plate Apparatus with Emphasis on Transient Characteristics

C. J. Shirtliffe and H. W. Orr

Division of Building Research
National Research Council of Canada
Ottawa, Canada

The constant heat flux and constant temperature modes of operation of the guarded hot plate apparatus are compared and the existence of an optimum heat flux boundary condition is examined. The step response equations for the different modes and for various preconditioning temperatures are tabulated and presented in graphical form. Optimum preconditioning temperatures are determined. Effects of disturbances and plate capacity are discussed and control and measurement problems compared. A hybrid mode of operation is suggested. The extension of the results to the use of heat meters and transient heat flow apparatus is discussed. Constant temperature or a hybrid mode of operation is found to be the most practical. The response times can be an order of magnitude less than constant heat flux operation. Use of the guarded hot plate apparatus in the constant temperature mode is suggested for other measurements.

Key Words: Guarded hot plate, heat meters, modes, optimum boundary conditions, response time, thermal conductivity, thermal diffusivity, transient errors, transient heat flow.

1. Introduction

Historically, the guarded hot plate apparatus (1)[1] is a "Standards Lab" type instrument where the emphasis is on accuracy rather than on minimizing the duration of the test. The transient heat flow characteristics and control problems have therefore been neglected. Other types of apparatus have been evolved for short duration tests of lesser accuracy.

It was believed that the standard guarded hot plate apparatus was much more versatile than assumed and that with the proper control system and measurement techniques its use could be extended to rapid, high accuracy testing. The apparatus was thought to offer advantages in the transient heat flow area and for use in conjunction with heat meters. Also, since the guarded hot plate apparatus is being proposed for testing "super" insulations with extremely long response times, it was believed that the control mode that is optimum in terms of speed and accuracy should be determined and the response functions tabulated to allow estimation of the time to reach an adequate steady state condition.

The guard balance is assumed to be controlled automatically in this analysis so that it does not introduce additional disturbances into the system. This is believed to be a reasonable assumption as most laboratories have provided this type of control for their apparatus. The temperature of the cold plate is assumed to be constant.

---

[1] Figures in parentheses indicate the literature references at the end of this paper.

2. Modes of Operation and Transient Characteristics

Two modes of control of the hot plate in the guarded hot plate apparatus are in general use. For the simplest and most widely used the plate is supplied with constant power, thereby producing a constant heat flux at the surface of the plate. The second, less widely used, method is to keep the temperature of the hot plate constant by controlling the power with a temperature controller. The latter method was used by Sommers (2) for "high speed" tests, but has not been widely used because of the extra equipment involved and the lack of knowledge of the relative advantages and problems of this mode compared to the constant heat flux mode.

2.1. Constant Heat Flux Operation

The usual sequence of events in performing a test with the guarded hot plate apparatus with constant heat flux from the hot plate is as follows:

(i) The sample is conditioned to the mean temperature of the test

(ii) The cold plates are at the required temperature

(iii) No power is being supplied to the hot plate and it is not at the required test temperature

(iv) The thermal conductivity and, therefore, the power to the test area are estimated

(v) The sample is placed in the plates, the power to the test area increased for an unspecified period of time, to heat up the plate and the sample, then reduced to the estimated power. The conditions then are allowed to reach steady state

(vi) Additional adjustments of the power are usually necessary and disturbances must settle out.

There has been no easy way to estimate the time required to reach the steady state condition using this procedure.

2.2. Constant Temperature Operation

The usual sequence of operations for use with the hot plate at a controlled temperature is as follows:

(i) The sample is conditioned to the mean temperature of the test

(ii) Both the hot and cold plates are at the required temperatures

(iii) The sample is placed in the apparatus and the test area power increases automatically to supply the required heat and then drops to the steady state value.

It should be noted that no guessing or second adjustments are required.

2.3. Optimum Boundary Conditions

Constant temperature operation is easier than constant heat flux operation, and probably faster, but the question remains as to whether there is a boundary condition that will give even faster response.

Assuming there is a better, nonconstant, heat flux boundary condition, $F(t)$, where t is time, and the appropriate unit step response of the sample is $V(x, t)$, the surface temperature of the hot plate can be written as given in ref. (3).

$$\theta(x,t) = \int_0^t F(t-t')\ V_t\ (x,t')\ d\ t'$$

where t' is the dummy time variable, and subscript t indicates the time derivative.

By normal response factor methods, $F(t)$ can be found for any desired response. Since the answer depends, however on the step response of the sample, $V(x, t)$, which is a function of the unknown thermal properties, there is no practical way to find this optimum condition for thermal conductivity apparatus. The most practical boundary conditions would appear to be the constant temperature boundary condition, since it is the only boundary condition that can be specified without regard to sample properties.

2.4. Response Times

The theoretical solutions to the heat transfer problems corresponding to the constant temperature and constant heat flux modes of operation are given in Appendix I. The solutions have been derived in nondimensional form to make them general. The temperature is nondimensionalized as shown in Appendix I to be zero at the cold plate and 1 at the hot plate under steady state conditions. The nondimensional heat flux is also 1 under steady conditions. Time zero is referred to as the time at which the boundary conditions are applied, that is, the test is started, and is nondimensionalized by the thermal diffusivity "a" and the thickness, L.

The solutions are given in general form and also for specific locations in the sample at which the measurements are to be made for determining the thermal conductivity, since it is these values that must approach steady state before the measurements can be made accurately.

The response time of a sample is defined here to mean the time required for the uncontrolled, or unspecified, variable at the hot plate to reach an adequate steady state so as to give an error in the measurement of thermal conductivity of less than the specified value. A curve of error in the measurement versus time will result for each mode. The equations for error are given in Appendix II.

Response times for the constant temperature and constant heat flux modes with the initial temperature equal to the steady mean temperature, $W = 0.5$, are given in figure 1. The response time for constant temperature mode is seen to be almost an order of magnitude less than for the constant heat flux mode when the errors are small.

The response times for specimens at various initial temperatures, W, are shown in figures 2 and 3, for values of $W = 0$, the cold plate temperature, to $W = 1$, the hot plate temperature. In each mode there is an optimum value of W at which the response time is least. The error reverses sign, that is, overshoots, when the initial temperature is greater than 0.5 for the constant temperature mode and 0.635 for the constant heat flux mode, and the negative portion of the curve can govern the response time of a test. The optimum values of the initial temperature, W, are therefore approximately 0.52 and 0.64, respectively, for the two modes. The response times for the two modes at the optimum W are approximately the same. The response time for the constant flux mode at optimum conditioning is an order of magnitude less than that for conditioning to the mean temperature; this can be useful in cases where the thermal conductivity of a specimen is being checked and the steady state heat flux can be determined beforehand. If the thermal conductivity is not known then the final hot plate temperature and therefore the optimum W cannot be determined.

The equations and figures do not take into account the heat storage capacity of the plates, the three-dimensional nature of the heat flow, or the temperature dependence of the properties. It should therefore be recognized that the equations and figures are only a guide to the actual response time and that checks should be made on the applicability of the figures to any particular apparatus by testing samples of known thermal diffusivity.

A test was made on a foam polystyrene sample, 2.5 cm thick with a 20- by 20-cm guarded hot plate to compare the theoretical response times to the actual values. For constant heat flux operation, the response time to $\frac{1}{2}$ per cent error was less than 15 sec, when the hot plate was preheated to the steady state temperature, and over 10 hr when the plate was not preheated. In each case the exact constant heat flux was used to obtain the desired hot plate temperature. The theoretical value was approximately 40 sec for the specimen. In constant temperature mode the measured response time was approximately 70 sec. The response curves are, therefore, better estimations of the actual response times for the constant temperature mode than the constant heat flux mode.

2.5. Measurement Problems

Each mode of operation has inherent measuring problems. The constant heat flux mode of operation has such long response times that the true steady state value can be difficult to recognize. Measurements must be made over an extended period to ensure that it has been reached. The constant temperature mode of operation requires that the temperature of the hot plate be controlled, by controlling the power to the heater. The steady state power to the heater will, by definition, vary a small amount with time. It is necessary to average the power over a sufficient length of time to obtain the mean values. The averaging time will depend on the controller characteristics and the temperature sensor. The problem of averaging can be eased considerably by using a strip chart recorder, automatic data logger, or a signal averaging circuit.

2.6. Hybrid Mode

The best of both methods can be obtained by starting the test in the constant temperature mode and switching later to the constant heat flux mode. This hybrid mode of operation requires a signal averager and is accomplished by starting in the constant temperature mode, monitoring the average power supply voltage, and when it becomes sufficiently constant, setting the output of the controller to that value, and switching the controller to manual mode, thereby supplying constant heat flux to the hot plate. Depending on the success of the transfer to constant heat flux operation, the measurement can be made with a short settling time, and with normal measuring instruments.

2.7. Disturbances and Readjustments

If the temperature or the heat flux of the hot plate must be readjusted so as to conform to a standard test condition, or if it is disturbed, the time for the transient to settle can be estimated from the response time curves. A change in a parameter at one surface corresponds to the case of a change at the surface and zero initial temperature. The error that the disturbance produces in the steady state value should be used in determining the response time. For example, a 10 per cent change need only settle to 10 per cent of its final value to produce a 1 per cent error in the measurement.

2.8. Plate Capacitance

The hot plate assembly can have more than 100 times the thermal capacitance of the sample and can therefore be the major factor in determining response time (3). Failure to preheat the hot-plate assembly to the desired temperature can greatly extend the test, especially for the constant heat flux mode where the small source of heat must raise the temperature of the large thermal mass. The increase in response time, or lag, decreases as the conductance of samples increases, and can vary from a few seconds to many hours. For constant temperature operation, the hot plate is normally at the required temperature and the thermal mass can be used to advantage to supplement the heater capacity in heating the specimen. In the hybrid mode, the thermal capacitance is helpful during the constant temperature interval and detrimental in the constant heat flux interval.

2.9. Characteristics of Control Systems for Hot Plates

It has been found that the response time for the normal design of hot plates and normal samples is so great that reset is required, i. e. integral action with "anti-windup" feature along with the proportional action in the controller. The sudden changes in power output required when high capacitance samples are placed in the apparatus make it desirable to have rate, i. e. derivative action, as well. Proper design of the hot plate and placement of the temperature sensor can decrease the lags in the control system and ease these requirements.

2.10. Further Refinement

If the shortest possible test time is required, there is no reason why the samples cannot be preconditioned to the proper temperature gradient in a large, simplified pair of temperature

controlled plates. The samples could then be tested rapidly in an apparatus operated in the constant temperature mode.

3. Application to Heat Meter Apparatus

The guarded hot plate apparatus, when operated in the constant temperature mode, forms the basic configuration required for measuring thermal conductivity with a heat meter; the advantage of this heat meter method is the simplicity of the measurements.

The solutions in Appendix I can be applied to the heat meter apparatus as well, as long as the heat meter is thin and has a low thermal capacitance. Equations (5), (6), and (7) of Appendix I show that there are three locations in a sample where optimum response without overshoot can be attained. The locations and relevant conditions are listed below.

Test Conditions

(i) the sample is conditioned to a uniform temperature

(ii) the temperature of the hot and cold plates are controlled.

Locations and Initial Temperatures

(i) at the hot surface - sample at the mean temperature

(ii) at the cold surface - sample at the mean temperature

(iii) at the center of the sample - any uniform temperature.

The third location, at the center of the sample, is not only ideal in terms of response but also provides some isolation from any small independent disturbances at the plates and, ideally, does not require the sample to be conditioned to any specific temperature. The initial temperature must be uniform or at least symmetric about the center point. If there is the possibility that thermal conductivity is a function of temperature, the center position affords the proper location to indicate if the temperature has deviated from the mean value. The center position requires two identical samples. Lang (4) has developed an apparatus with the heat meter in this location but it is not clear if all the advantages were recognized. Norris and Fitzroy (5) gave the theoretical justification for the method.

4. Extension to Transient Measurement Conditions

Beck (6) has determined the optimum configuration for transient heat flow apparatus for simultaneous determination of thermal conductivity and specific heat. When the thermal conductivity is low, the optimum configuration is a large thermal mass "cold plate," preconditioned but not continuously cooled, and a constant temperature warm side with heat flux metered. The cold plate is insulated on all but the active surface. The thermal properties are inferred from the cold plate temperature and the hot side heat flux, using a "nonlinear estimation" procedure. The guarded hot plate apparatus with temperature controlled hot plate can be modified to attain the required configuration; this allows the extension of the apparatus to measurement of both thermal conductivity and specific heat.

With samples of high thermal conductivity, the optimum configuration at the cold plate remains the same while that of the hot side condition is zero heat flux. Thermal properties are inferred from temperatures measured on the two sides by the same procedure. By removing the hot plate from the guarded hot plate apparatus, this condition can be accomplished.

Further work should be considered on the adaptation of the guarded hot plate apparatus to this type of measurement, and a study of the sources of error. Modification in design of the hot and cold plates might be required to make them "universal," or interchangeable plates might be considered.

5. Conclusion

The constant temperature and hybrid modes of operation have been shown to be the most practical for the guarded hot plate apparatus. The response times can be an order of magnitude better than for constant heat flux operation. The figures presented can be used as a guide to estimate the time required to reach an adequate steady state.

Guarded hot plate apparatus with temperature-controlled plates can be used for rapid measurements, either alone or in conjunction with a heat meter. The apparatus also might be used for the simultaneous determination of thermal conductivity and thermal diffusivity.

This report is a contribution from the Division of Building Research, National Research Council of Canada, and is published with the approval of the Director of the Division.

6. References

(1) Method of test for thermal conductivity of materials by means of the guarded hot plate (C177-63. Book of ASTM Standards, 1963, Part 3.

(2) Somers, E. V., High-speed guarded hot plate apparatus for thermal conductivity of thermal insulation. Trans., ASME, 78, August 1956, p. 1191-6.

(3) Churchill, R. V., Operational mathematics, Second Edition, McGraw-Hill Book Co. Inc., New York, 1958.

(4) Lang, D. L., A quick thermal conductivity test on insulating materials, ASTM Bulletin No. 216, September 1965, p. 58-60.

(5) Norris, R. H. and Fitzroy, (Mrs.) Nancy D., A quick thermal conductivity test on insulating materials, Materials Research and Standards, VI, September 1961, p. 727-729.

(6) Beck, J. V., The optimum analytical design of transient experiments for simultaneous determinations of thermal conductivity and specific heat. Michigan State University, Ph. D., 1964 Engineering, Mechanical.

Appendix I

Response Times for an Infinite Slab

1. Basic Equation

The nondimensionalized heat equation for an infinite slab with uniform boundary conditions is

$$\frac{\partial^2 \theta}{\partial X^2} = \frac{\partial \theta}{\partial \tau}$$

where $\theta = \left[T(x,t) - T(0,\infty)\right] / \left[T(L,\infty) - T(0,\infty)\right]$

$X = x/L$, $\tau = a\,t/L^2$, L = the thickness of the slab, x = the space variable, running from 0 to L, t = time, a = the thermal diffusivity.

The nondimensionalized heat flux is written as

$$\frac{q}{q_1} = \frac{\partial \theta}{\partial X}$$

where q = heat flux, q_1 = the steady state heat flux $\left(-\lambda \left[T(L,\infty) - T(0,\infty)\right] / L\right)$,
λ = the thermal conductivity, ∞ = indicates the steady state value.

1.1. Boundary Conditions (B.C.)[2]

Constant temperature at $X = 0$

$$\theta(0, \tau) = 0.$$

Two separate boundary conditions at $X = 1$ will be considered:

(i) Constant temperature: $\theta(1, \tau) = 1$, and

(ii) Constant heat flux: $\left.\frac{\partial \theta}{\partial X}\right)_{1, \tau} = 1.$

In each case the steady state temperature difference and steady state heat flux are equal to unity.

1.2. Initial Conditions

The following uniform initial condition is assumed:

$$\theta(X, 0) = W$$

where W is a finite constant.

1.3. Solutions to Basic Problem

Solutions have been determined using basic solutions and the "Superposition Principle" as given by Churchill (3).

The solutions are given in terms of the variable not specified at $X = 1$, that is, in terms of heat flux for constant temperature boundary condition, and in terms of temperature for the constant heat flux boundary condition. The solutions are first given in general form, then for special cases with X, or both X and W, specified. Tables of the functions may be obtained by writing the authors directly.

(1) General Form of Solutions

(a) Constant Temperature B.C.

$$\left.\frac{\partial \theta}{\partial X}\right)_{1, \tau} = 1 + 2 \sum_{n=1}^{\infty} (-1)^n \cdot \cos (A_n X) \cdot \exp(-A_n^2 \tau) + 4W \sum_{n=1}^{\infty} \cos (B_n X) \cdot \exp(-B_n^2 \tau) \qquad (1)$$

where $A_n = n\pi$, $B_n = (2n-1)\pi$, exp ( ) is the exponential function, $e^{(\ )}$

(b) Constant Heat Flux B.C.

$$\theta(X, \tau) = X - 8 \sum_{n=1}^{\infty} \left[(-1)^{n-1}/B_n^2\right] \cdot \sin (B_n X/2) \cdot \exp(-B_n^2 \tau/4)$$

$$+ 4W \sum_{n=1}^{\infty} (1/B_n) \cdot \sin(B_n X/2) \cdot \exp(-B_n^2 \tau/4) \qquad (2)$$

---

[2] Boundary conditions will be abbreviated as B.C.

(2) Special Cases

(a) Constant Temperature B.C., with X = 1

$$\left.\frac{\partial\theta}{\partial X}\right)_{1,\tau} = 1 + 2\sum_{n=1}^{\infty} \exp(-A_n^2\tau) - 4W\sum_{n=1}^{\infty} \exp(-B_n^2\tau) \tag{3}$$

(b) Constant Heat Flux B.C., with X = 1

$$\theta(1,\tau) = 1 - 8\sum_{n=1}^{\infty} (1/B_n^2) \cdot \exp(-B_n^2\tau/4) + 4W\sum_{n=1}^{\infty} \left[(-1)^{n-1}/B_n\right] \cdot \exp(-B_n^2\tau/4) \tag{4}$$

(c) Constant Temperature B.C., with X = 0.5, W finite

$$\left.\frac{\partial\theta}{\partial X}\right)_{0.5,\tau} = 1 + 2\sum_{n=1}^{\infty} \exp(-4A_n^2\tau) \tag{5}$$

(d) Constant Temperature B.C., with X = 1, W = 0.5

$$\left.\frac{\partial\theta}{\partial X}\right)_{0.5,\tau} = \text{right-hand side of eq (5)} \tag{6}$$

(e) Constant Temperature B.C., with X = 0, W = 0.5

$$\left.\frac{\partial\theta}{\partial X}\right)_{0,\tau} = \text{right-hand side of eq (5)} \tag{7}$$

(f) Constant Temperature, with X = 1, W = 1

$$\left.\frac{\partial\theta}{\partial X}\right)_{1,\tau} = 1 + 2\sum_{n=1}^{\infty} (-1)^n \cdot \exp(-A_n^2\tau) \tag{8}$$

2. Calculation of Errors

Errors in determination of thermal conductivity, if measurements are made before steady state conditions are attained, are derived below.

2.1. Constant Temperature B.C.

Error at time τ and position X.

$$\text{Error} = \frac{q(X,\tau) - q(X,\infty)}{q(X,\infty)}$$

$$= \left.\frac{\partial\theta}{\partial X}\right)_{X,\tau} - 1$$

since $\dfrac{q(X,\tau)}{q(X,\infty)} = \left.\dfrac{\partial\theta}{\partial X}\right)_{X,\tau}$, and $\left.\dfrac{\partial\theta}{\partial X}\right)_{X,\infty} = 1$

2.2. Constant Heat Flux B.C.

Error at time τ and at position X

$$\text{Error} = \frac{\left[\theta(X,\infty) - \theta(0,\infty)\right]}{\left[\theta(X,\tau) - \theta(0,\tau)\right]} - 1$$

$$= \frac{1}{\theta(X,\tau)} - 1$$

$$= \frac{1}{\theta(1,\tau)} - 1 \quad \text{at} \quad X = 1$$

since $\theta(0,\tau) = 0$, all τ, and $\theta(X,\infty) = X$.

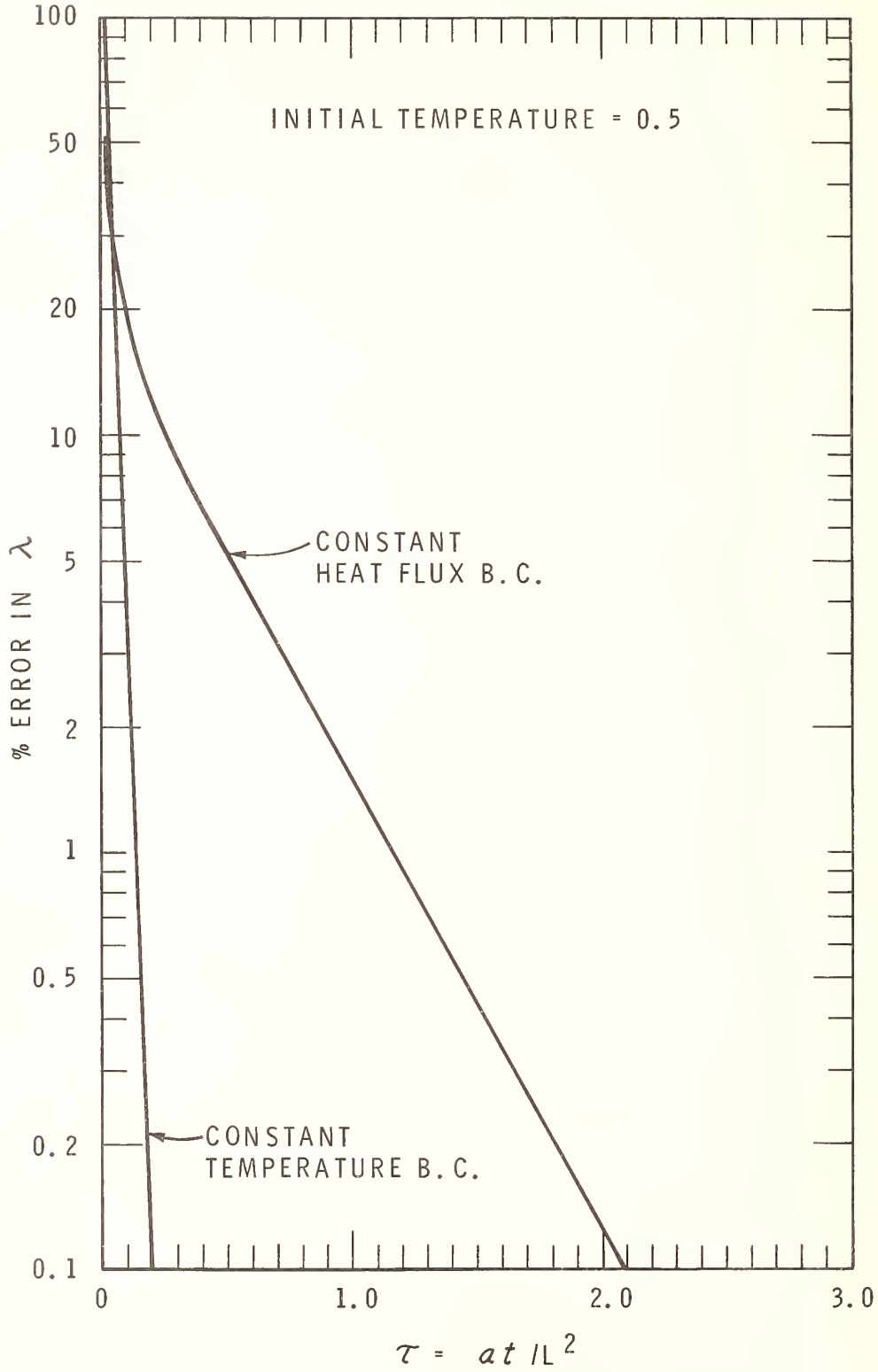

Figure 1 Response Times for Measuring Thermal Conductivity
- Error at Time τ After Start of Test
- Constant Temp. and Constant Heat Flux Modes
- Initial Temp., W = 0.5

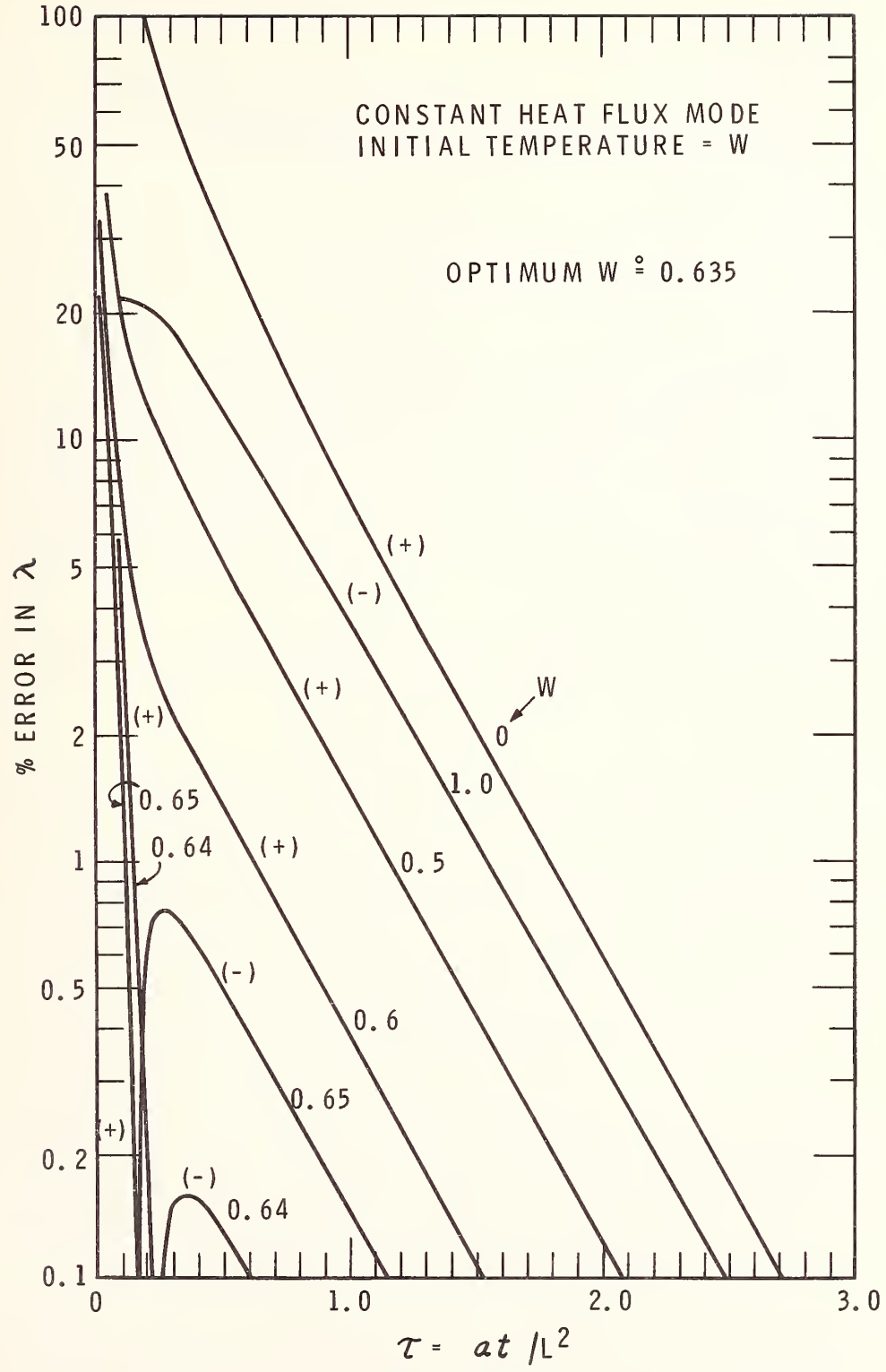

Figure 2 Response Times for Measuring Thermal Conductivity
- Error at Time τ After Start of Test
- Constant Heat Flux Mode
- Initial Temp., W = 0 to 1.0

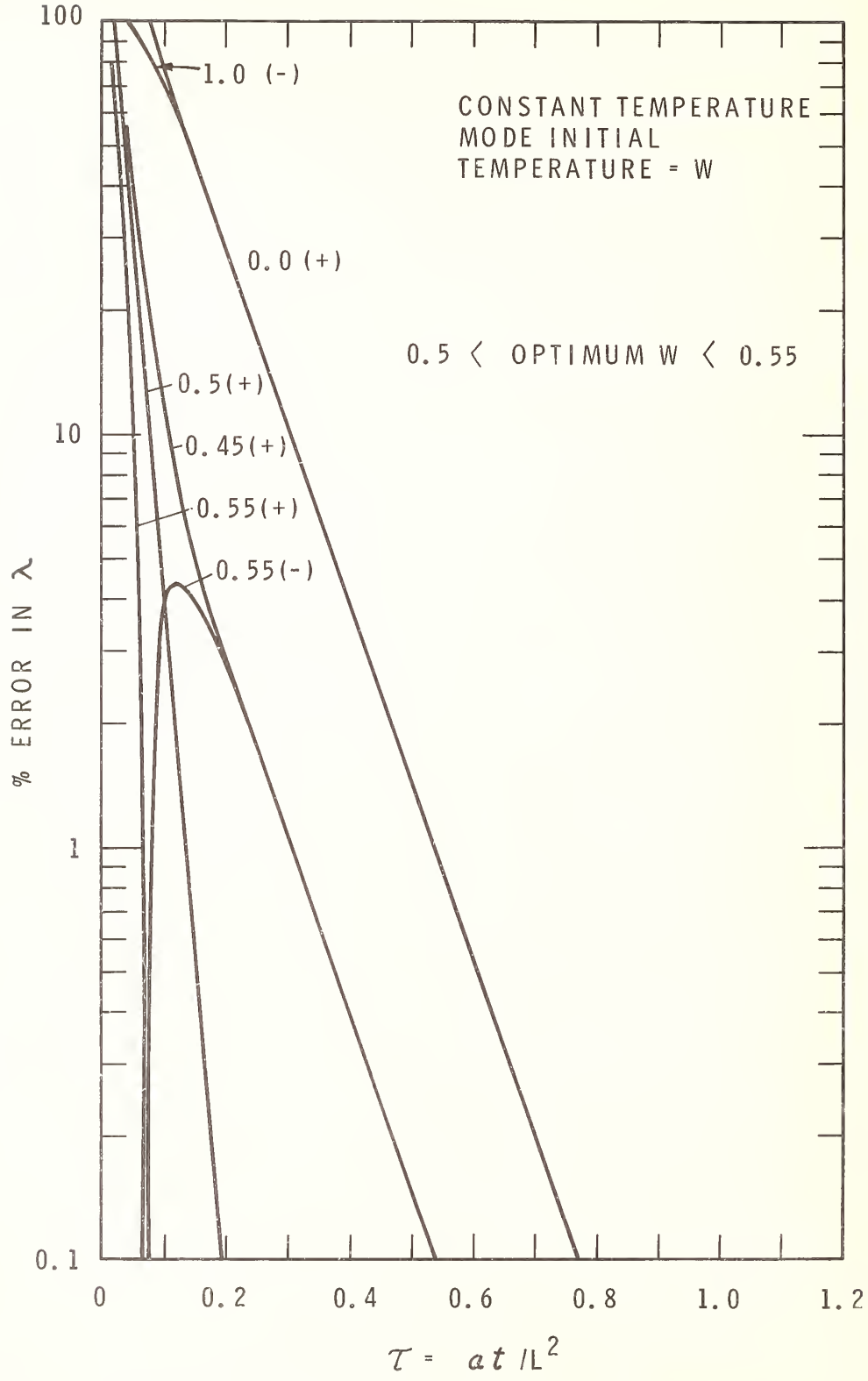

Figure 3 Response Times for Measuring Thermal Conductivity
- Error at Time τ After Start of Test
- Constant Temp. Mode
- Initial Temp., W = 0 to 1.0

METHOD FOR MEASURING TOTAL HEMISPHERIC EMISSIVITY OF PLANE SURFACES WITH CONVENTIONAL THERMAL CONDUCTIVITY APPARATUS

Nathaniel E. Hager, Jr.

Research & Development Center
Armstrong Cork Company
Lancaster, Pennsylvania

The conductance of an air space bounded by two large horizontal parallel plane surfaces is measured in conventional thermal conductivity apparatus. Convection is kept unimportant by having the hotter surface on top, and conduction of heat by the air is subtracted from the measurement to obtain a value for the net radiation exchange. When the two surfaces are identical, this value is used to compute their total hemispheric emissivity. A high-emissivity surface so measured is retained as a standard, and single samples of other surfaces are then tested by placing them in the opposite position. It is estimated that use of this technique with the Northrup thermal conductivity apparatus yields emissivity values accurate to within 0.015.

Key words: Emissivity, heat transfer, surface properties, thermal conductivity, thermal properties, thermal radiation.

1. Introduction

Infrared radiation plays an important and sometimes dominant role in practical heat transfer problems. To calculate the rate at which thermal energy is emitted, one usually needs to know the total hemispheric emissivity of surfaces in the temperature range found in the normal environment.

The literature describes apparatus for producing detailed data on the directional and spectral characteristics of emitting surfaces (1,2,3,4)[1]. Such data are ideal for checking emission theories, but they must be integrated to get values useful for engineering and apparatus design purposes. There remains a practical need for simpler apparatus which directly produces integrated values.

A number of techniques have been described for direct measurement of total hemispheric emissivities of wires (5), spheres (6), and cylinders (7); the samples are heated electrically in evacuated chambers, and emissivity determinations are made by observing the rate of energy loss to the enclosing surfaces. Worthing has used a parallel-plate-in-vacuum method (8); one plate is held at a fixed temperature, and the heating rate and heat capacity of a second plate are used to compute the radiant exchange between the enclosed surfaces.

The method described here also employs parallel plates, but it does not require evacuation. The thermal conductance of an air space between two parallel plane surfaces is measured in conventional thermal conductivity apparatus of the type described by Northrup (4). The apparatus produces total hemispheric emissivity values of coatings, sheets, and surfaces of thin slabs with sufficient accuracy for most design purposes. Calibrated black body sources and delicate radiometric devices are not needed, and temperature-controlled shielding devices are not required for eliminating background interference even when the sample is approximately at room temperature.

2. Theory

Elementary heat transfer theory suggests an idealized experiment for determining emissivity values for infinite plane samples. This experiment is described in the following discussion. Later, real apparatus is described which puts the experiment on a practical basis; i.e., steps are taken to permit measurements to be made with samples of limited size.

---

[1] Figures in brackets indicate the literature references at the end of this paper.

2.1. Idealized Experiment

A volume of air is enclosed, as shown in figure 1, between two infinite horizontal isothermal planes. A calibrated slab of thermal insulating board is placed immediately below the air space. The top surface of the assembly is heated uniformly to temperature T_h while the bottom surface is held at a lower temperature T_o. Under steady-state conditions the interface between the air space and the board assumes a temperature T_c. The heat flux q through the air space is the same as that through the board and is given by the equation

$$q = \frac{k_o \Delta T_o}{D_o} , \tag{1}$$

where k_o and D_o are known values of the thermal conductivity and thickness of the board, and $\Delta T_o = T_c - T_o$.

Since the upper plane is at a higher temperature than the lower, heat is transferred downward through the air space by gaseous conduction and thermal radiation, and convection is negligible. Assuming that the separation between planes is so small that no appreciable amount of radiation is absorbed by the air in passing from the one plane to the other, the conduction and the radiation processes are independent, and the total heat flux through the air space may be broken down into two components as indicated by the equation

$$q = q_a + q_r , \tag{2}$$

where q_a is the heat conducted by the air, and q_r is the net thermal radiation exchange between surfaces.

If the thermal conductivity of the air is k_a, and the distance between the enclosing surfaces is D, then the gas conducted heat is calculated from the equation

$$q_a = \frac{k_a \Delta T}{D} , \tag{3}$$

where $\Delta T = T_h - T_c$.

According to standard texts (9), the net radiation exchange is given by the equation

$$q_r = \frac{4 \sigma \bar{T}^3 \Delta T}{\frac{1}{\epsilon_h} + \frac{1}{\epsilon_c} - 1} , \tag{4}$$

where ϵ_h and ϵ_c are respectively the emissivities of the "hot" and "cold" surfaces bounding the air space, σ is the Stefan radiation constant, and $\bar{T}$ is the mean absolute temperature of the air space. For this equation to be valid, the emissivity of each surface must equal its absorptivity for that radiation emitted by the opposite surface. This means that the surfaces must be "gray", or ΔT must be small. Combining the above equations, and solving for ϵ_h yields the equation

$$\epsilon_h = \frac{1}{1 - \frac{1}{\epsilon_c} + \frac{4 \sigma \bar{T}^3}{\frac{k_o \Delta T_o}{D_o \Delta T} - \frac{k_a}{D}}} .$$

If the emissivity of the one surface ϵ_c is known, then, since all other factors on the right-hand side are known or can be measured, the emissivity of the other surface ϵ_h can be calculated. If the emissivity of neither surface is known, but both surfaces are known to have the same emissivity, so that $\epsilon_c = \epsilon_h$, then the equation can be re-solved to get an expression for the emissivity common to the two surfaces.

2.2 Practical Experiment

Experience with conventional thermal conductivity apparatus suggests that the idealized experiment is closely approximated by the configuration sketched in figure 2. Heavy horizontal high-conductivity plates, one electrically heated and the other kept at a cooler temperature, are used to form nearly isothermal surfaces. The plates are square with edge length L. A calibrated slab of insulating board having thickness D_o rests on the lower plate, and the upper plate is supported at a distance D above the upper surface of the slab.

The choice of design depends on selecting values for D_o and D, and then sizing L, in view of the magnitude of D_o and D, so that the heat flow in the central region of the system is essentially the same as it would be if L were infinite. The reasoning involved in making these choices is included in a paper being prepared for later publication, and only the results are stated here.

Experience suggests that about 2.5 cm is a good value to take for D_o and D. It is estimated from published data (10) that, as long as D does not exceed this value, the absorption of radiation by normal room air does not affect the practical experiment. Both analysis and experiment show that the infinite plane theory is approximately valid within the central portions of the finite plate system when L is at least twelve times as large as D, and when at least one of the surfaces enclosing the air space emits with characteristics approximating those of an ideal black surface.

3. Apparatus and Procedure

Apparatus constructed along the lines discussed, as shown in figure 3(a), consists of a simple Northrup thermal conductivity apparatus, and a special emissivity cell. The latter unit is positioned between an electrically-heated plate and the calibrated insulation slab; the hot and cold plates are about 30.5 cm square and are made of 6.35-mm and 12.7-mm aluminum respectively.

3.1. Emissivity Cell Construction

The emissivity cell detailed in figure 3(b) nominally measures 30.5 x 30.5 x 2.54-cm, and consists of a plywood frame covered on one side with a tightly stretched sheet of 0.15-mm paper. At the center of the paper sheet is mounted a 12 x 12 x 0.05-mm platelet made of edge-welded copper-Constantan thermocouple ribbon. The paper and the central platelet are sprayed with flat black enamel, and the lower surface of the hot plate is treated with the same material. In the latest version of the cell, the interior surfaces of the sides of the frame are lined with 5-μ aluminum foil.

3.2. Standard Slab Selection

The standard slab is 0.295-g/cm^3 corkboard (11) which is sanded to obtain plane surfaces and a uniform thickness of about 2.54 cm. This board has maintained its thermal conductivity to within 2% of the original value measured five years ago, and according to the experience of workers elsewhere in this laboratory, similar slabs have been found to be at least this stable over even longer periods of time (12).

3.3 Standard Surface Calibration

To calibrate the black surface in the emissivity cell, the apparatus is run as described with the two surfaces having identical coatings. To make sure that the emissivities of the two surfaces are identical, it is necessary to make sure that the emissivity is characteristic of the coating and is not affected by the base. Assurance is obtained that this is the case by building up the coating on one surface at a time with several applications until successive applications lead to no further change in emissivity measurements.

The heater power is adjusted so that the temperature difference between hot and cold plates is between 10 and 20 deg. After the apparatus has come to thermal equilibrium, which usually takes 6 to 8 hours, the temperature differences across the standard slab and the emissivity cell are read, and the temperature of the hot plate is measured. These data, along with known parameters associated with the standard slab and the test cell, are substituted into eq (5) to obtain the emissivity value shown in the first row of table 1. Note that this value is obtained before the cell is lined with aluminum foil.

Table 1. Emissivity values measured for standard surface.

Emissivity Cell Condition	Number of Tests	ϵ
Unlined	11	0.914 ± 0.003
Lined with Foil	4	0.928 ± 0.005

3.4. Performance Tests

Several tests are run for the purpose of establishing the extent to which the finite plate system approximates the ideal infinite plate system. The first test is to add the aluminum foil lining. This produces an effect comparable to increasing the extent of the surfaces facing the air space. The value shown in the table indicates that a 1.5% increase in measured emissivity values results from using the foil. Because increasing the effective size of the surfaces makes such a small difference, it is concluded that, at least at the center of the cell where the measurement is made, the radiant flux is close to the infinite plane ideal.

Other tests demonstrate the degree of uniformity of the temperature of the median plane, or the plane defined by the paper surface in the emissivity cell. At a distance of 6 cm from the center, the temperature is only 0.02 deg lower than at the center, and at a distance of 11.5 cm, it is 0.15 deg lower. These data can be used to show that, in the central region, lateral heat flow has little effect on the over-all transfer of heat from the heated plate to the median plane; i.e., the conducted heat flows uniformly perpendicular to the plates in the central region. These tests have led to the belief that heat flows through the center of the emissivity cell nearly as it would in the infinite plate case.

3.5. Accuracy

In view of the accuracy with which the parameters of the system are known, it is estimated that the probable absolute error in the measurements does not exceed 0.014 when the foil-lined cell is used. As noted in the table, the spread in measured values is somewhat less than the estimated error.

3.6. Test Surface Techniques

After the standard surface in the emissivity cell is calibrated, other surfaces are measured by mounting them on the hot plate, measuring the conductance of the air space, and using eq (5) to obtain the emissivity.

When measuring the emissivity of a surface of a thin sheet, the sheet is stretched over the hot plate or mounted with thin double-faced pressure-sensitive tape. Coatings are put on a thin metal foil or other thin base material, which is in turn mounted to the hot plate. The surface of sheets which do not have negligible thermal resistance can also be tested, provided appropriate corrections are made in the evaluation.

3.7. Results Compared with Published Measurements

Some verification of the correctness of the described method is obtained by comparing measured values with values tabulated in the literature. It is difficult to do this with a high degree of exactness because surface condition is so important in most cases, and because it is difficult to reproduce surfaces measured by others. Nevertheless certain surfaces may be expected to have emissivity values falling within limited ranges, and some degree of checking is possible. Table 2 shows the comparison. Especially important is the fact that appropriately low emissivity values are obtained with reflective surfaces. This helps to establish the fact that convection heat transfer has indeed been made unimportant by using the horizontal configuration with the hotter surface on top.

Table 2. Experimental emissivity values compared with published values.

Surface	T(°C)	New Apparatus	Published (a,b)
Commercial aluminum paint	44	0.28	-
Various aluminum paints	24-38	0.20-0.60	0.27-0.67
Flat black alkyd enamel	38	0.928	-
Black lacquer	38	-	0.87-0.98
Commercial aluminum foil	38	0.065	-
Commercial aluminum foil and sheet goods	38	-	0.055-0.11

(a) W. H. MacAdams, "Heat Transmission".
(b) G. B. Wilkes, "Heat Insulation".

4. References

(1) Maki, A. G., Stair, R., and Johnston, R. G. J. Research Natl. Bur. Standards 64C, 99 (1960).

(2) Maki, A. G., and Plyler, E. K., J. Research Natl. Bur. Standards 66C, 283 (1962).

(3) McDermott, P. F., Rev. Sci. Instr. 8, 185 (1937).

(4) Wilkes, G. B., "Heat Insulation", (John Wiley and Sons, Inc., New York, 1950).

(5) Davisson, C. and Weeks, J. R., J. Opt. Soc. Am. and Rev. Sci. Instr. 8, 581 (1924).

(6) Gest, G., J. Opt. Soc. Am. 39, 1009 (1949).

(7) Fulk, M. M., and Reynolds, M. M., J. Appl. Phys. 28, 1464 (1957).

(8) Worthing, A. G., J. Opt. Soc. Am. 30, 91 (1940).

(9) Jakob, Max, "Heat Transfer", (John Wiley and Sons, Inc., New York, 1957), Vol. II, p. 3.

(10) McAdams, W. H., "Heat Transmission", (McGraw-Hill Book Company, Inc., New York 1954), pp. 85-88.

(11) Vibracork, Armstrong Cork Company, Lancaster, Pa.

(12) Private Communication, Z. Zabawsky, Physical Standards Department, Research and Development Center, Armstrong Cork Company.

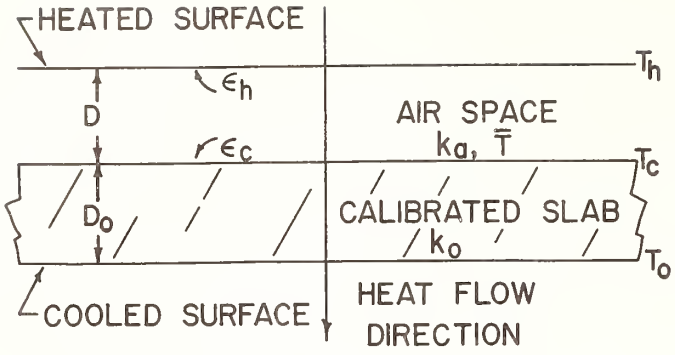

Figure 1. Schematic view of idealized experiment.

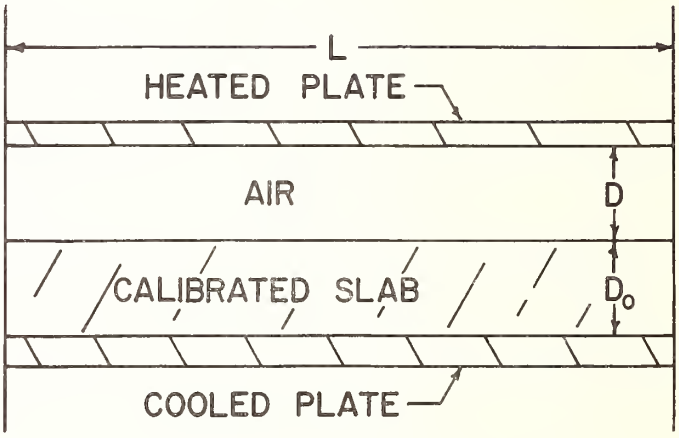

Figure 2. Schematic view of practical apparatus.

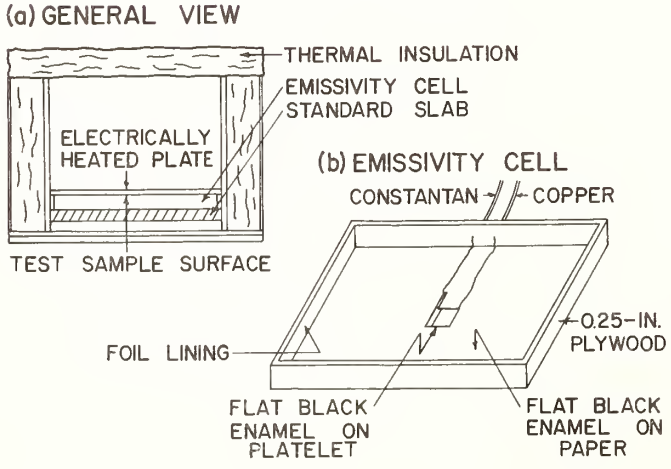

Figure 3. Sketches of apparatus.

Heat Pulse Experiments and the Study of Thermal Transport at Low Temperatures

R. J. von Gutfeld

IBM Watson Research Center
Yorktown Heights, New York

Heat pulse propagation experiments in solids offer a relatively simple and direct method for determining (1) the thermal carrier mean free path from the shape of the detected pulse and (2) the carrier velocity from the first arrival time of the thermal signal. In dielectric samples this gives rise to the phonon mean free path and the phonon energy velocities. In metal samples, the electron mean free path and the Fermi velocity are obtained. Recent heat pulse experiments on sapphire and gallium will be described to illustrate the technique and its usefulness in the study of thermal transport properties.[1]

Key Words: Electron and phonon mean free path, electrons-scattering, Fermi velocity, gallium, heat conduction, sapphire.

[1]Full test to appear in W. P. Mason, Physical Acoustics Vol. V, (Adademic Press, New York, 1968). Preliminary results were reported by the author and A. H. Nethercot, Jr., in Phys. Rev. Letters 12, 641 (1964) and 18, 855 (1967).

Deviations from Matthiessen's Rule in the Low Temperature Thermal and Electrical Resistivities of Very Pure Copper

J. T. Schriempf

Metallurgy Division
Naval Research Laboratory
Washington, D. C. 20390

Measurements have been made of the electrical and thermal resistivities of copper at temperatures from 2 to 20°K. The ratios of room temperature to helium temperature electrical resistivities of the three specimens studied ranged from 1000 to 3000. In both the electrical and thermal resistivities, deviations from Matthiessen's rule of the order of 100% were observed. These results are consistent with recent work by Dugdale and Basinski[1][1] which indicates that the deviations from Matthiessen's rule can be very large when metallic impurities are the major source of the residual resistivities.

Key Words: Copper, electrical conductivity, Lorenz number, Matthiessen's rule, thermal conductivity.

1. Introduction

Matthiessen's rule assumes that the experimentally observed electrical resistivity (ρ_{exp}) of a metallic specimen can be written as:

$$\rho_{exp} = \rho_o + \rho_i, \tag{1}$$

where ρ_o is that portion of the electrical resistivity which is due to electrons scattering from impurities and imperfections, and ρ_i is the portion of the electrical resistivity which is characteristic of the ideally pure metal. In pure metals it is a good assumption that the thermal transport is due entirely to the motion of the electrons, and in this case, Matthiessen's rule can be extended to the experimentally observed thermal resistivity (w_{exp}), or

$$w_{exp} = w_o + w_i, \tag{2}$$

where w_o and w_i are the thermal analogues of ρ_o and ρ_i. Since changes in atomic volume are small at the temperatures of interest here (below 20°K), ρ_o is independent of temperature. Furthermore, ρ_o and w_o are related according to the Wiedemann-Franz law,

$$L_o = \frac{\rho_o}{w_o T} \tag{3}$$

---

[1] Figures in brackets indicate the literature references at the end of this paper.

where L_o is the Lorenz number and has the theoretical value, $L_{th} = 2.443 \times 10^{-8}$ V^2/deg^2.

Although the Wiedemann-Franz law as used in eq (3) has been well established in pure metals, Matthiessen's rule is seldom strictly obeyed [2]. Furthermore, if one takes

$$\Delta_\rho = \rho_{exp} - \rho_i - \rho_o \tag{4}$$

and

$$\Delta_w = w_{exp} - w_i - w_o \tag{5}$$

as the deviations from Matthiessen's rule for the electrical and thermal resistivities, respectively, it can be shown that the deviations are always positive [2]. Although several workers [1,3,4] have studied these deviations in copper, a careful comparison of the thermal and electrical deviations has not heretofore been done. The data presented below permit a comparison of these deviations at temperatures below 20°K for copper specimens with ratios of room temperature to helium temperature resistivities of the order of 1000 to 3000.

2. Experimental

The apparatus used to measure the electrical and thermal resistivities of the copper specimens from ~ 2.5° to 20°K has already been described [5]. In this apparatus both thermal and electrical contact is made at each end of a specimen by a single copper clamp, so that a single geometric factor determines the net thermal, as well as the net electrical, resistance. Thus the apparatus permits the measurement of both the electrical and thermal resistivities on exactly the same specimen.

Three copper specimens were prepared from American Smelting and Refining Company copper rod of spectrographic purity (99.999%). Specimen Cu 1 was swaged from the stock diameter of 3/8 inch to 0.125 inch diameter, annealed for 12 hr at 1000°C in air at a pressure of about 10^{-3} torr, and etched to a final diameter of 0.119 inch. Specimen Cu 2 was made from the same stock by swaging to a diameter of about 0.080 inch. This specimen was etched heavily in 50% nitric acid between steps in the swaging process to reduce surface contamination. Finally, the specimen was etched to a diameter of about 0.076 inch and annealed for 3 hr at 530°C in a vacuum of about 1×10^{-6} torr. After measurements were completed on specimen Cu 2, it was annealed for about 22 hours at 1000°C in an atmosphere achieved by using a continuous air leak to reduce the 1×10^{-6} torr vacuum to 5×10^{-4} torr. This "oxidized" specimen, labeled Cu 2-0, was found to have a slightly larger diameter than Cu 2. Metallographic examination of Cu 2-0 revealed the presence of "holes", presumably pockets of copper oxide formed during the oxidation annealing process. No indication of oxide pockets was found in Cu 1 or in a test piece prepared by the same technique used for Cu 2. Spectrographic examination of the three specimens verified the 99.999% purity of specimens Cu 2 and Cu 2-0, but indicated about 0.01% Mn in Cu 1. The presence of 0.01% Mn in Cu 1 was confirmed by colorimetric chemical analysis.

Geometric shape factors for Cu 1 and Cu 2 were obtained from optical comparator measurements of diameters and distances between contacts. The shape factor for Cu 2-0 was obtained by assuming its electrical resistivity at 24°C was identical to that of Cu 2. Errors introduced in the determination of specimen geometry are estimated to be no greater than 2%. Apart from errors in the shape factors, errors in the measurement are estimated to be no greater than ± 1%.

3. Results and Discussion

The values of ρ_o and w_oT obtained by extrapolation of the data to 0°K are shown in Table 1, along with other pertinent characteristics of the three specimens. In the case of ρ_o, the extrapolation ignored a small minimum (of the order of 1/2%) in the ρ-T curve which occurred at about 5°K for specimens Cu 1 and Cu 2. It is noteworthy that the values of L_o for all three specimens are within 2% of the theoretical value. This is in agreement with results of Tainsh and White [6] on a specimen of comparable purity, and is in marked contrast with earlier results by Powell, Roder, and Hall [4]. In view of the sound theoretical and extensive experimental evidence which indicates $L_o = L_{th}$ in good metallic conductors of high purity [2], it is felt that the value of L_o obtained

by Powell, Roder, and Hall must not be correct for high purity copper.

Table 1. Characteristics of copper specimens.

Specimen	$\rho_o x10^{11}$ Ωm	$\rho_{24°C} x10^8$ Ωm	$w_o T x10^4$ m deg^2/w	$L_o x10^8$ V^2/deg^2	Annealing temp. °C	Annealing pressure torr	Annealing time hr	Metallic impurities ppm
Cu 1	1.73	1.77	7.20	2.40	1000	$\sim 10^{-3}$	12	100 (Mn)
Cu 2	.579	1.69	2.34	2.47	530	10^{-6}	3	<10
Cu 2-0(a)	1.12	1.69	4.52	2.48	1000	$5x10^{-4}$	22	<10

(a) Shape factor obtained by assuming $\rho_{24°C}$ to be equal to that of Cu 2.

In figure 1, the thermal and electrical resistivity data for all three specimens are shown in logarithmic plots of $w_{exp}-w_o$ and $\rho_{exp}-\rho_o$ versus temperature. Also indicated in figure 1 by a dotted line are the thermal data of Powell, Roder, and Hall for a specimen of $\rho_o \sim 1.2x10^{-11}$ Ωm. Our data on specimen Cu 2-0, which has $\rho_o \sim 1.1x10^{-11}$Ωm, is in quite good agreement with the Powell, Roder, and Hall results above, say, 15°K. The lack of agreement at lower temperatures is consistent with Powell, Roder, and Hall's observation of $L_o < L_{th}$. The observed temperature dependence of the electrical resistivity is approximately $T^{4.6}$ for all three specimens at temperatures from about 5° to 20°K. For the thermal resistivity, the observed temperature dependence is roughly T^2 near 20°K, but becomes weaker with decreasing temperature, approaching $T^{1.7}$ for Cu 2 and $T^{1.0}$ for Cu 2-0.

In order to establish the deviations from Matthiessen's rule, as defined in eqs (4) and (5), a knowledge of ρ_i and w_i is necessary. The usual practice is to assume that Δ_ρ and Δ_w are essentially zero in the most pure specimen; thus in this work

$$\rho_i = (\rho_{exp}-\rho_o)_{Cu\ 2} \tag{6}$$

and

$$w_i = (w_{exp}-w_o)_{Cu\ 2}. \tag{7}$$

With assumptions (6) and (7) then, the data in figure 1 indicate that Δ_w and Δ_ρ are much larger in specimen Cu 1 than in specimen Cu 2-0. Recent work by Dugdale and Basinski [4] with dilute alloys of Au, Ge, and Sn in Cu indicates that the deviations from Matthiessen's rule might be much larger in the case where impurities are the major source of ρ_o and w_o than in the case where dislocations are the source of ρ_o and w_o. Thus it is tempting, although by no means conclusive, to claim that the ρ_o and w_o of specimen Cu 1 are due primarily to the Mn impurity, while Cu 2-0 exhibits a ρ_o and w_o due chiefly to dislocations.

In both the present work and in Dugdale and Basinski's studies, the ideal resistivities were found by assuming Δ_ρ and Δ_w to be negligible in the purest specimen. However, all the specimens used in the present study were quite pure by current standards, and yet significant deviations from Matthiessen's rule were found among them. Therefore, any conclusions from studies of this nature are strongly influenced by the characteristics of the specimen chosen as the "ideal" specimen. Nevertheless, the present investigation, in agreement with Dugdale and Basinski's studies, indicates that very small amounts of metallic impurities can cause extremely large deviations from Matthiessen's rule in copper at low temperatures.

4. Acknowledgments

The author is indebted to G. Picklo for performing the spectrographic and chemical analyses, and to R. Meussner and the Metallurgy Division metallography section for the metallographic examinations of the specimens.

5. References

[1] Dugdale, J. S., and Basinski, Z. S., Phys. Rev. 157, 552 (1967).

[2] Klemens, P. G., Handbuch der Physik 14, 198 (1956).

[3] White, G. K., Australian J. Phys. 6, 397 (1953).

[4] Powell, R. L., Roder, H. M., and Hall, W. J., Phys. Rev. 115, 314 (1959).

[5] Schriempf, J. T., Sixth Conference on Thermal Conductivity, Dayton, Ohio, p. 615 (1966).

[6] White, G. K., and Tainsh, R. J., Phys. Rev. 119, 1869 (1960).

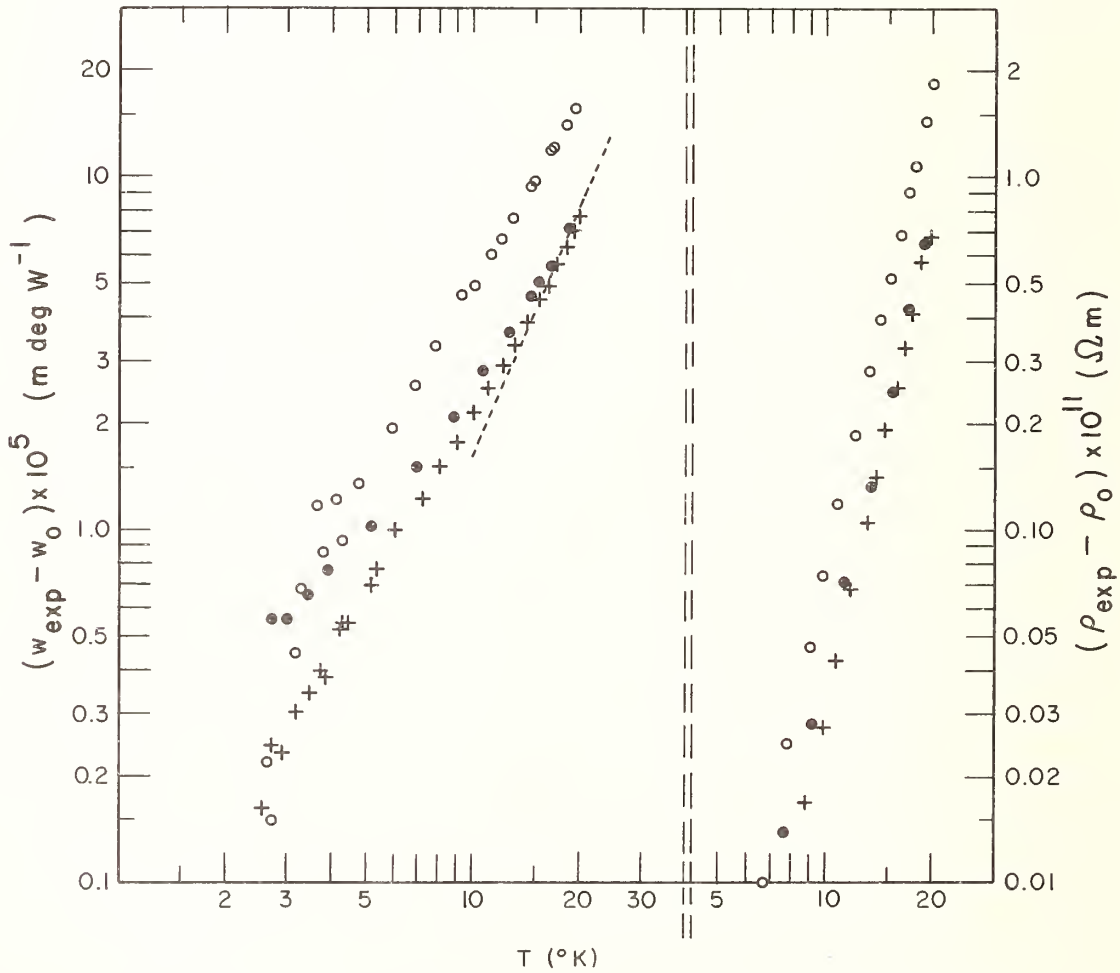

Figure 1 - Thermal and electrical resistivities of copper. For each specimen, ρ_o and w_o were obtained by extrapolation of the data to 0°K. The results for specimen Cu 1 are indicated by o, Cu 2 by +, and Cu 2-0 by •. The dotted line indicates data of Powell, et al. [4] for a specimen with a ρ_o comparable to the ρ_o of Cu 2-0.

Thermal Conduction in Bismuth at Liquid Helium Temperatures- Effects at Intermediate Fields[1]

S. M. Bhagat and B. Winer

University of Maryland
College Park, Maryland

Recent measurements [1][2] on the thermal conductivity of high purity bismuth single crystal samples have shown that for $1.3<T<2°K$ the conduction is mainly due to phonons. In addition, while boundary scattering is predominant, there is a sizeable contribution due to scattering by electrons. Application of a transverse magnetic field showed that the field dependence should be divided into three regions: (i) low field region: 0-100 Oe, the thermal conductivity decreases very rapidly; the decrease being almost certainly due to the "wiping out" of the small electronic contribution, (ii) intermediate field region: 100-1000 Oe, a slow decrease in the thermal conductivity (not studied in any detail in Ref. 1), (iii) high field region: above 2000 Oe, de Haas van Alphen oscillations are observed. The present paper is concerned with further measurements in region (ii). The slow reduction is essentially confirmed and it is proposed that this is related to additional scattering of phonons by electrons when the Landau Level separation is comparable to a typical phonon frequency.

Key Words: Bismuth, electron scattering, intermediate magnetic fields, Landau levels, thermal conductivity.

1. Introduction

Recently, we have reported some rather precise measurements [1] on the thermal conductivity, λ, of high purity single crystal samples of Bi in the range $1.3<T<2°K$. Measurements were made both at zero field and as a function of magnetic field (H) applied transverse to the direction of heat flux. The main conclusions of the investigation were:

(a) the conduction is mainly due to phonons;

(b) at 1.3°K the electron contribution (as evidenced by the rapid reduction in λ on application of (H) amounts to about 5% of the total λ for the purest specimens;

(c) while boundary scattering is predominant, effects due to scattering by electrons are also sizeable since, firstly, de Haas van Alphen type oscillations are observed, secondly, the temperature dependence of λ is significantly different from T^3; and thirdly, the temperature dependence of λ is anisotropic.

In observing the dependence on H it was further noted that for $100<H<1000$ Oe the value of λ reduced very slowly. The present work was undertaken to further elucidate this behavior. Although the results are still rather preliminary, the slow reduction is essentially confirmed. At 1.34°K, the only temperature at which these measurements have been made so far, this reduction amounts to only 1/2% of the value of λ at zero field.

2. Method and Results

The measurements were made essentially as described in Ref. [1]. However, a slightly different procedure was used for calibrating the resistance thermometers in an applied field. Since the effect was expected to be very small, it was not possible to use any techniques requiring extrapolation. The bath temperature was stabilized at some temperature, say T_0, and a thermal gradient was established across the sample so that the thermometers read T_1 and T_2. Then the field was swept and data taken. Subsequently, the bath temperature was stabilized to the zero field values of T_1 and T_2 successively (with no heat flow

[1]Work supported in part by the Advanced Research Projects Agency.

[2]Figures in brackets indicate the literature references at the end of this paper.

into the sample) and the values of the resistors measured as a function of field. This field dependence was found to be highly repeatable and free from any hysteresis effects.

Figs. 1 (H|| Bis) and 2 (H|| Trig) show the variation of $[\lambda(H)-\lambda(0)]/\lambda(0)$ at 1.3416°K for a binary sample. The two sets of data are intended to show the effects of sample deterioration between runs. Firstly, the region of initial fall broadens out in field and secondly the total fall itself is reduced. However, the slow fall region is essentially unaltered. The broadening of the initial fall region can be very easily understood by using arguments familiar from the theory of magnetoresistance. At the conclusion of the thermal conductivity runs the residual resistivity ratio of this sample was measured to be $\rho_{300}/\rho_{1.3} \simeq 250$.

3. Discussion

As is well known the application of a magnetic field leads to the establishment of Landau levels; i.e. the electrons bunch up in levels whose separation is equal to $\hbar\omega_c$, where $\hbar\omega_c = eH/m^*c$. In the case of Bi one finds that the separation between the levels becomes $\sim k$ (the Boltzmann constant) for fields of the order of 100 Oe. It is therefore very tempting to suggest that the reduction in λ observed by us for fields larger than 100 Oe is caused by enhanced scattering of phonons by electron transitions between Landau levels. In other words, since the density-of-states is peaked at the Landau level energies one should expect additional phonon absorption. A very naive picture will indicate that this additional scattering may give an enhancement in scattering by electrons on the order of $\hbar\omega_c/E_f$ where E_f is the Fermi energy; about 1 to 2% for Bi at $H \sim 10^2$ Oe. Since the electron scattering term (see Ref. 1) amounts to only a few percent of the total thermal resistivity, this will qualitatively account for the effect observed by us.

We are thankful to Dr. J. R. Anderson for some useful discussions.

4. References

[1] Bhagat, S. M. and Manchon, D. D., Jr., Heat Transport in Bismuth at Liquid-Helium Temperatures, Phys. Rev. 164(3), 966(1967).

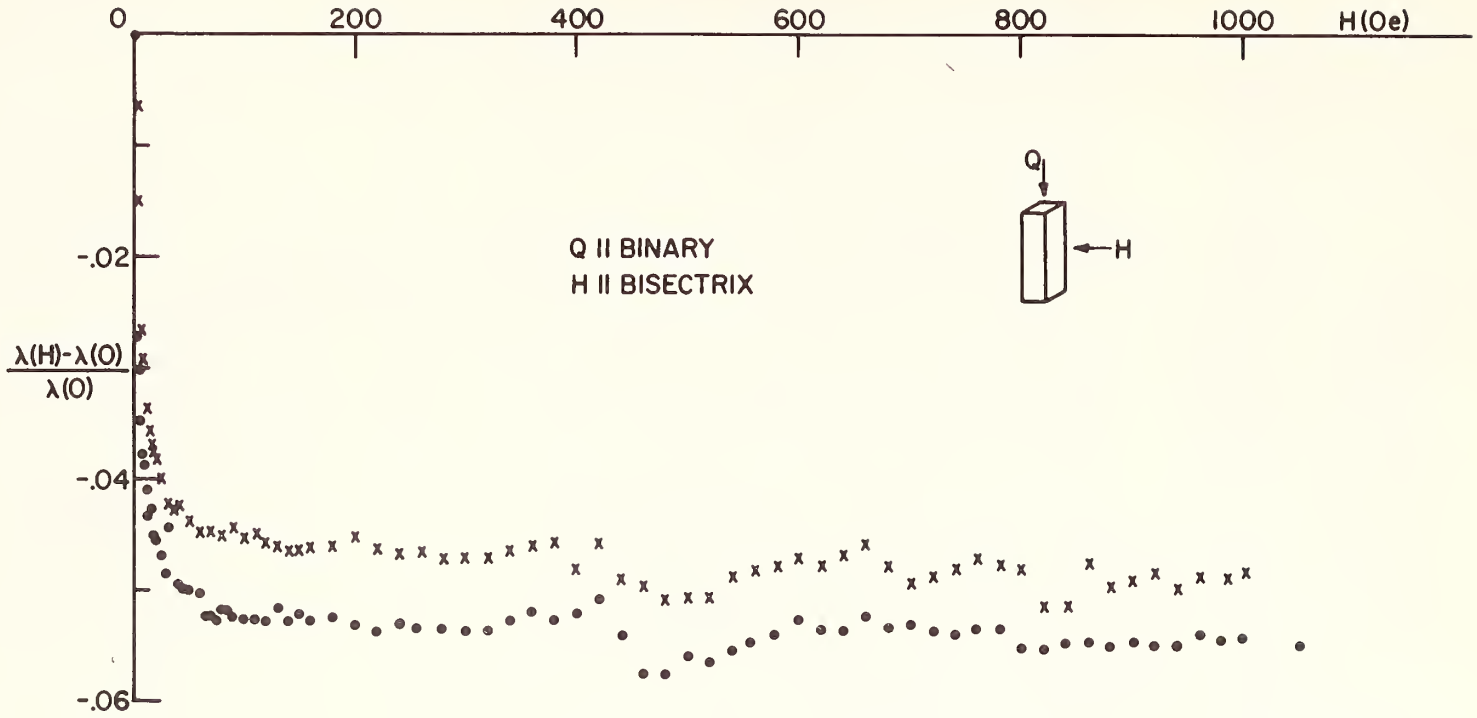

Fig. 1 Variation of the thermal conductivity of bismuth in a transverse applied field when direction of heat flow is along binary axis and field is along bisectrix axis. The full circles and the crosses refer to two separate runs (see text).

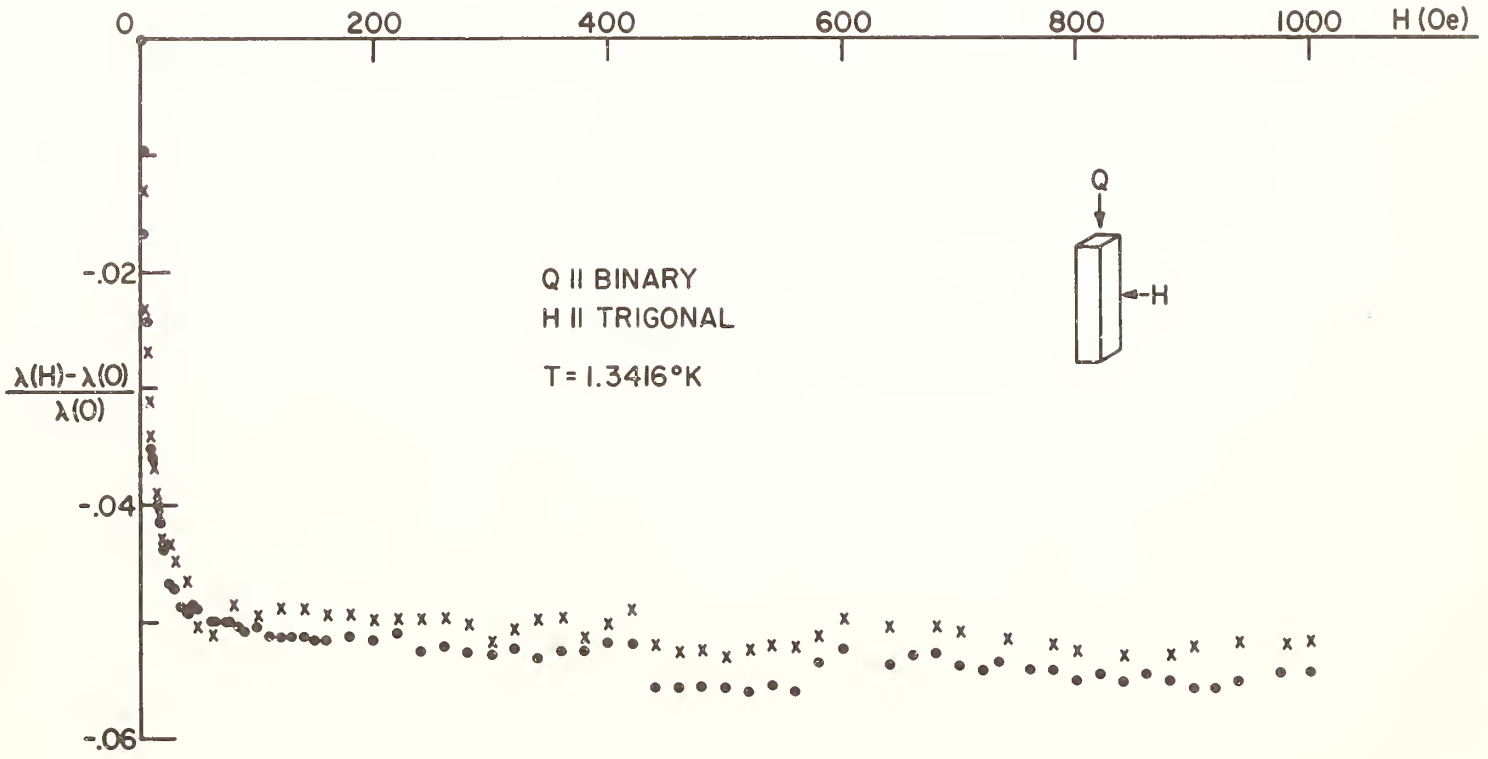

Fig. 2 Variation of the thermal conductivity of bismuth in a transverse applied field when direction of heat flow is along binary axis and field is along trigonal axis. The full circles and the crosses refer to two separate runs (see text).

Thermal Conductivity of Pure and Impure Tin in the Normal and Superconducting States[1]

C. A. Reynolds, J. E. Gueths,[2] F. V. Burckbuchler
N. N. Clark,[3] D. Markowitz, G. J. Pearson,[4] R. H. Bartram, and C. W. Ulbrich[5]
Physics Department and Institute of Materials Science
University of Connecticut
Storrs, Connecticut 06268

Measurements of the normal- and superconducting-state thermal conductivities (K^n and K^s) were made on two pure (99.999%) and twenty lightly doped tin specimens. Nine polycrystalline samples contained mercury, lead or bismuth impurity up to 1 at. % . Eleven single crystal samples containing up to 0.3 at. % cadmium were measured with the heat current nearly perpendicular to the tin tetrad axis. The lattice component in the normal state, K_g^n , is fractionally very small, but is enhanced in the superconducting state, K_g^s; the data admit to analysis in terms of the "universal curve" formalism of Lindenfeld and Pennebaker for, K_g^n , and the theory of Bardeen, Rickayzen and Tewordt for K_g^s/K_g^n . The electronic component in the normal state, K_e^n , is assumed to be of the conventional form $(\beta/T + \alpha T^2)^{-1}$. The ratio, ρ_o/β , where ρ_o is the residual resistivity, is found to be independent of impurity content and in agreement with the theoretical Lorenz number. The anisotropy of β is found to be similar to that of ρ_o . The variation of α was studied as a function of impurity concentration and found to increase monotonically with concentration, as reported by previous investigators. Comparison of some of our K_e^s/K_e^n data with the theory of Kadanoff and Martin produced an apparent contradiction to Anderson's theorem. This prompted us to formulate a theory, based on features taken from the work of Markowitz and Kadanoff and of Hohenberg, of the effect of energy gap anisotropy on K_e^s . An expression was developed for K_e^s/K_e^n as a function of crystal orientation, temperature, and mean free path. The gap edge, which is central to thermal conductivity, is rendered isotropic by impurities well before their effect is felt on quantities such as the average gap or transition temperature. The theory is found to reproduce the qualitative features of our data, as well as that of Guenault for pure tin, but it under-estimates the magnitude of the anisotropy effect by about a factor of two. From the isotropic theory of Kadanoff and Martin and Guenault's data we have estimated the effective gaps parallel and perpendicular to the tin tetrad axis. Using the picture of the Fermi surface proposed by Klemens, we have calculated the average gap after anisotropy has been washed out and found that our data is in good agreement with theory when the gap variation is determined in this semi-empirical way.

Key Words: Electrical conductivity, Lorenz number, superconducting energy gap, superconductor, thermal conductivity, tin, tin alloys.

1. Full text has been published as follows:

J. E. Gueths, N. N. Clark, D. Markowitz, F. V. Burckbuchler and C. A. Reynolds, Phys. Rev. 163(2), 364 (1967).
G. J. Pearson, C. W. Ulbrich, J. E. Gueths, M. A. Mitchell and C. A. Reynolds, Phys. Rev. 154, 329 (1967).
C. W. Ulbrich, D. Markowitz, R. H. Bartram, and C. A. Reynolds, Phys. Rev. 154, 338 (1967).

---

[1]Supported by U. S. Air Force Office of Scientific Research grant AF-AFOSR-474-67 and Office of Naval Research Contract NONR2967 (00)
[2]Wisconsin State University, Oshkosh, Wisconsin. (Present address)
[3]Present address: Universidad de Costa Rica, San Jose, Costa Rica.
[4]Present address: Eastman Kodak, Rochester, New York.
[5]Present address: Clemson University, Clemson, South Carolina

2. References

1. P. Lindenfeld and W. B. Pennebaker, Phys. Rev. 127, 1881 (1962).

2. J. Bardeen, G. Rickayzen, and L. Tewordt, Phys. Rev. 113, 982 (1959).

3. Leo P. Kadanoff and Paul C. Martin, Phys. Rev. 124, 670 (1961).

4. P. W. Anderson, J. Phys. Chem. Solids 11, 26 (1959).

5. D. Markowitz and L. P. Kadanoff, Phys. Rev. 131, 563 (1963).

6. P. Hohenberg, Zh. Eksperim. i Teor. Fiz. 45, 1208 (1963) (English transl.: Soviet Phys.-JETP 18, 834 (1964)).

7. A. M. Guenault, Proc. Roy. Soc. (London) A262, 420 (1961).

8. P. G. Klemens, C. Van Baarle and F. W. Gorter, Physica, 30, 1470 (1964).

Temperature Dependence of the Lattice Thermal Conductivity of Copper-Nickel Alloys at Low Temperatures

J. C. Erdmann and J. A. Jahoda[1]

Boeing Scientific Research Laboratories
P.O. Box 3981
Seattle, Washington 98124

The lattice thermal conductivity of copper-nickel alloys at low temperatures deviates systematically from the ordinary T^2 - dependence. This deviation is small in the alloys containing only very little nickel. For higher concentrations of nickel, however, the temperature dependence approaches T^1 in the liquid helium temperature range. Only for very nickel-rich alloys a temperature dependence of the lattice conductivity like T^2 is found.

These findings result from experiments with polycrystals as well as single crystals. The behavior of the alloys with more than 50 percent copper can be understood in terms of Pippard's simple relaxation model for the ultrasonic attenuation by s-electrons. Zimmerman and Lindenfeld and Pennebaker have already in this way interpreted similar results in other alloy systems. To understand the behavior of the nickel-rich alloys, however, Pippard's model has to be extended to include d-electrons. Such an extended model has been applied. We find that consistency with experimental results exists, if the mean free path of the d-electrons is up to one order of magnitude smaller than the mean free path of the s-electrons. Other conclusions concern the ratios of the effective masses and the relaxation rates.

Key Words: Copper-nickel alloys, electrical conductivity, electron mean free path, thermal conductivity.

1. Introduction

The lattice thermal conductivity of copper-nickel alloys at low temperatures is interesting mainly for the following reason: The mean free path ℓ of the electrons can become small enough so that its product with the predominant phonon wave number q is smaller than unity. This situation is usually met in studies of the ultrasonic attenuation by electrons. Pippard [1][2] has given a theory of this effect, also applicable for the case $q\ell>1$. The value of Pippard's theory for investigations of the lattice thermal conductivity lies in the fact, that the coefficient of ultrasonic attenuation can be regarded as the reciprocal of the phonon mean free path. It is then possible to study the transition of the lattice thermal conductivity from the regime $q\ell>1$ (ordinarily valid for thermal phonons) to the regime $q\ell<1$ (often characteristic for ultrasonic experiments). This transition means a breakdown of the adiabatic principle, as discussed by Ziman [2], but the arising theoretical difficulties are avoided by Pippard's approach, unlike the usual treatment of electron-phonon scattering in terms of well-defined quantum states.

Zimmerman [3] and Lindenfeld and Pennebaker [4] have shown by investigations of various alloys that the low temperature lattice thermal conductivity, if limited by the electron-phonon interaction, varies

(a) as the square of the temperature, if $q\ell \gg 1$ (longitudinal modes);

(b) as the cube of the temperature, if $q\ell \gg 1$ (transversal modes);

(c) proportional to the temperature, if $q\ell \ll 1$ (all modes).

At least the cases (a) and (c) seem to be well verified.

---

[1] Staff Members

[2] Figures in brackets indicate the literature references at the end of this paper.

As in the case of palladium-silver alloys, recently investigated by Fletcher and Greig [5], the interest in the thermal conductivity of the copper-nickel system is enhanced by considerations of the important role of d-electrons. We shall concentrate on this topic and show that certain specific features of our results can be best explained in terms of the contributions by d-electrons. In particular we can conclude that the mean free path of the d-electrons is substantially smaller than that of the s-electrons, so that the d-electrons remain in the "ultrasonic" regime $q\ell_d < 1$ for most of the nickel-rich alloys.

The chosen alloys lend themselves well to this type of investigation, because they form a continuous series of solid solutions without miscibility gap. Furthermore, the Fermi-surfaces of copper and nickel have been investigated extensively [6 - 9].

2. Experiments

2.1. Sample Preparation

Eleven specimens have been investigated, three of them single crystals. Their composition and residual resistivity are listed in Table 1. The single crystals were purchased from Materials Research Corp. They were prepared by electron beam float zoning, 12 cm long, 6.0 - 7.5 mm diameter. The polycrystalline alloys, together with their chemical analysis and spectrographic surveys were provided by the courtesy of the International Nickel Company, Inc. The vacuum cast ingots were hammer forged, hot rolled to 18 mm diameter and rough turned. The rough turned bars were swaged to 10 mm diameter. Intermediate annealing was performed at 930°C when necessary. These specimens were finally machined to size, 10 cm long, 5.0 mm diameter. They were annealed for 24 hrs. in the argon furnace and allowed to cool slowly.

Table 1. Composition in weight percent and electrical residual resistivity ρ_o in μΩcm of the investigated specimens. s.c. - single crystal, p.c. - polycrystal

Notation	Type	Composition	ρ_o μΩcm
Cu 98	s.c.	2.29 Ni, bal. Cu	2.17
Cu 96	s.c.	4.05 Ni, bal. Cu	4.95
Cu 91	p.c.	9.30 Ni, 0.025 Al, bal. Cu	11.22
Cu 72	p.c.	27.96 Ni, 0.023 Al, bal. Cu	33.38
Cu 49	p.c.	50.50 Ni, 0.030 Al, bal. Cu	46.10
Ni 65	p.c.	64.87 Ni, 0.051 Al, bal. Cu	27.62
Ni 85	p.c.	84.70 Ni, 0.054 Al, bal. Cu	11.14
Ni 90	p.c.	90.24 Ni, 0.060 Al, bal. Cu	8.24
Ni 91(a)	p.c.	91.05 Ni, 0.046 Al, bal. Cu	15.88
Ni 96	p.c.	95.60 Ni, bal. Cu	3.91
Ni 98	s.c.	99.35 Ni, bal. Cu	0.907
Ni 98(b)	p.c.	97.97 Ni, bal. Cu	1.66

(a) the large value of ρ_o suggests a different composition, appr. 80 percent Ni
(b) no thermal conductivity data

2.2. Measurements

All measurements were performed in the apparatus described previously [10]. One end of the cylindrical specimen was soldered to the heat sink, variable in temperature. To the other end a heater was connected, and the temperature difference along the rod was measured by means of a differential gas thermometer. The electrical resistance also was measured. The vacuum of the specimen chamber was 10^{-6} mm Hg.

3. Results

The thermal conductivity of the eleven specimens listed in Table 1 was measured at temperatures between 4.2°K and approximately 40°K. Below 20-30°K all alloys are well within the range of residual electrical resistivity [10], so that the Wiedemann-Franz-law can be regarded as valid ($L = 2.45 \cdot 10^{-8}$ V^2/deg^2). The total thermal conductivity of the alloys and its electronic and lattice component found by using the Wiedemann-Franz-law are listed in Tables 2-12. The lattice thermal conductivity of the

alloys is plotted in figures 1-4.

Tables 2-12. Ambient temperature in deg K, total thermal conductivity k, its electronic part k_e, and its lattice part k_{ph} in 10^{-3} $Wcm^{-1}deg^{-1}$ for the various specimens. The data for k are entered as measured, k is determined from ρ (see Table 1) using the Wiedemann-Franz law with $L = 2.45 \cdot 10^{-8}$ V^2 deg^{-2}. The limit of the validity range of this separation method is indicated where necessary. The exponent n expresses the temperature dependence of the lattice part between 4.2° and 20°K.

Table 2: Cu 98

n=2.00			
T	k	k_e	k_{ph}
4.23	71.52	47.92	23.60
5.92	109.9	66.95	42.92
6.59	120.4	74.60	45.81
7.41	154.5	83.87	70.58
8.21	172.8	93.43	79.41
9.31	217.2	105.4	111.8
10.34	243.6	117.0	126.6
11.41	296.2	129.1	167.1
12.59	338.1	142.4	195.7
14.01	391.8	158.5	233.3
15.83	458.5	179.2	279.3
18.85	630.9	213.3	417.6
19.34	604.7	218.9	385.8
22.03	679.0	249.3	429.7
24.34	781.3	275.4	505.9
29.54	878.2	334.3	543.9
36.04	1051.	407.8	643.1
39.74	1157.	449.8	707.1
44.93	1227.	508.5	718.8
49.18	1243.	556.6	687.2
55.33	1423.	626.1	797.1
62.73	1411.	709.9	701.8
70.02	1503.	792.4	710.1

Table 3: Cu 96

n=2.00			
T	k	k_e	k_{ph}
4.24	36.68	20.98	15.70
4.24	38.15	20.97	17.18
4.21	35.93	20.83	15.10
5.19	48.91	25.65	23.26
5.42	53.96	26.83	27.13
5.82	60.68	28.80	31.88
6.12	66.59	30.28	36.31
6.41	69.22	31.70	37.52
6.73	71.27	33.30	37.97
7.35	85.36	36.35	49.01
7.78	93.44	38.50	54.94
8.67	110.6	42.90	67.73
9.92	133.0	49.08	83.94
10.44	151.7	51.66	100.0
10.93	160.0	54.06	105.9
11.99	182.4	59.29	123.1
12.63	211.7	62.45	149.2
13.53	220.7	66.94	153.8
14.52	258.7	71.83	186.8
16.02	293.0	79.24	213.8
17.30	318.9	85.58	233.3
17.25	322.8	85.33	237.5
20.02	393.3	99.00	294.3
21.52	436.3	106.5	329.8
23.53	489.3	116.4	372.9
25.02	488.5	123.8	364.7
27.99	603.8	138.5	465.3
31.02	590.3	153.4	436.9
39.03	701.9	193.0	508.8
51.02	848.4	252.4	596.0

Table 4: Cu 91

n=1.97			
T	k	k_e	k_{ph}
4.24	20.86	9.27	11.59
4.52	23.36	9.88	13.49
4.67	23.80	10.20	13.60
4.87	26.87	10.63	16.24
5.12	28.65	11.17	17.46
5.32	31.50	11.72	19.77
5.54	32.77	12.09	20.68
6.62	42.32	14.46	27.86
7.08	49.28	15.45	33.83
7.63	53.62	16.67	36.94
8.01	57.64	17.50	40.14
8.54	66.06	18.66	47.40
9.20	69.58	20.10	49.48
9.69	80.15	21.17	58.98
10.89	98.52	23.79	74.73
11.76	110.2	25.69	84.46
13.25	147.5	28.94	118.6
15.02	170.4	32.81	137.6
16.36	183.4	35.74	147.7
18.21	216.5	39.78	176.7
19.88	250.2	43.43	206.8
22.07	265.5	48.20	217.3
23.78	286.7	51.93	234.8
25.30	334.0	55.26	278.8
26.99	345.7	58.95	286.8
32.11	375.5	70.15	305.3
36.22	449.8	79.11	370.7
41.07	431.2	89.71	341.5
49.92	510.2	109.0	401.2
60.23	534.3	131.5	402.7
70.92	566.4	154.9	411.5

Table 5: Cu 72

n=1.60			
T	k	k_e	k_{ph}
4.24	16.05	3.11	12.94
4.59	19.00	3.37	15.63
4.91	20.88	3.60	17.28
5.09	20.53	3.73	16.79
5.43	25.33	3.99	21.34
5.83	27.71	4.28	23.43
6.16	27.75	4.52	23.23
6.27	30.86	4.61	26.25
6.66	33.57	4.89	28.68
7.01	36.26	5.15	31.12
7.43	37.54	5.45	32.09
7.99	43.52	5.86	37.66
8.51	43.79	6.24	37.55
9.06	50.21	6.65	43.56
10.03	61.43	7.36	54.05
10.68	67.42	7.84	59.59
11.78	84.89	8.64	76.25

Table 6: Cu 49

n=1.15			
T	k	k_e	k_{ph}
4.23	15.30	2.24	13.06
4.68	17.20	2.48	14.72
4.68	16.80	2.48	14.32
5.25	16.79	2.79	14.00
5.60	18.86	2.97	15.89
6.30	22.79	3.35	19.44
6.30	24.59	3.35	21.24
7.00	26.30	3.72	22.58
7.00	26.90	3.72	23.18
8.05	30.13	4.28	25.85
9.05	36.09	4.81	31.28
10.50	39.01	5.53	33.48
10.50	43.30	5.53	37.77
10.50	42.20	5.53	36.67
10.50	40.80	5.53	35.27
12.10	50.82	6.43	44.39
16.80	74.80	8.92	65.88

Table 7: Ni 65

n=1.26			
T	k	k_e	k_{ph}
4.24	15.74	3.76	11.98
4.24	15.74	3.76	11.98
4.43	16.46	3.93	12.53
4.49	16.86	3.98	12.86
4.74	18.26	4.20	14.06
4.89	18.51	4.34	14.17
5.23	20.61	4.64	15.96
5.44	22.27	4.83	17.44
5.57	23.49	4.94	18.55
5.82	23.66	5.16	18.49
6.10	22.07	5.41	16.66
6.31	26.18	5.60	20.59
6.41	27.26	5.69	21.57
6.42	26.97	5.69	21.27
6.67	27.25	5.92	21.34
7.27	30.29	6.45	23.84
7.37	27.86	6.54	21.31

Table 5 (continued)

12.38	82.90	9.08	73.81
12.85	87.26	9.43	77.83
13.01	83.80	9.55	74.26
14.25	108.6	10.46	98.16
14.28	99.80	10.48	89.32
15.50	116.6	11.38	105.2
16.52	115.6	12.12	103.5
17.54	128.7	12.87	115.8
18.40	137.1	13.50	123.6
19.95	161.9	14.65	147.3
19.96	142.1	14.65	127.5
21.53	152.1	15.80	136.3
23.24	177.9	17.05	160.9
25.08	195.1	18.41	176.7
25.13	196.4	18.44	177.9
26.99	222.5	19.81	202.7
26.99	217.9	19.81	198.1
28.65	249.2	21.03	228.2
34.95	283.5	25.65	257.8
35.02	306.5	25.71	280.8
38.22	291.0	28.06	262.9
42.05	306.2	30.86	275.3
47.37	322.8	34.77	288.0
54.04	359.3	39.66	319.6

Table 6 (continued)

20.00	90.25	10.62	79.63
24.00	111.9	12.74	99.16
30.40	135.0	16.14	118.8
35.00	142.5	18.58	123.9
45.00	155.0	23.90	131.1

Table 7 (continued)

7.37	30.70	6.54	24.16
7.67	31.15	6.81	24.35
8.00	31.69	7.10	24.59
8.26	36.57	7.32	29.25
8.55	38.30	7.58	30.71
8.86	37.21	7.86	29.35
9.32	37.74	8.27	29.48
9.34	43.25	8.28	34.97
9.64	41.25	8.55	32.70
10.46	43.26	9.28	33.98
10.81	52.79	9.59	43.20
11.48	52.54	10.19	42.35
12.51	53.15	11.10	42.04
12.54	60.14	11.12	49.02
13.76	59.26	12.20	47.06
15.27	76.94	13.54	63.40
16.98	84.52	15.06	69.46
18.54	95.62	16.45	79.17
20.18	102.7	17.91	84.83
21.49	100.5	19.06	81.46
24.07	114.6	21.36	93.28
26.57	124.7	23.57	101.1
29.13	137.0	25.84	111.2
32.97	139.9	29.25	110.65
44.23	188.9	39.23	149.7
54.16	197.7	48.05	149.7
65.34	219.58	57.96	161.6

Table 8: Ni 85

n=1.33

T	k	k_e	k_{ph}
4.22	17.54	9.27	8.27
4.24	17.57	9.32	8.25
4.39	17.90	9.64	8.26
4.52	19.79	9.95	9.84
5.03	20.63	11.07	9.56
5.31	22.86	11.68	11.18
5.83	25.57	12.81	12.75
6.21	26.16	13.66	12.50
6.29	27.76	13.84	13.92
6.39	26.94	14.05	12.89
6.67	29.90	14.66	15.24
6.99	30.97	15.37	15.60
7.34	33.96	16.13	17.82
7.69	34.67	16.90	17.77
7.94	35.24	17.47	17.77
8.63	40.01	18.98	21.03
9.01	41.08	19.81	21.27
9.93	43.98	21.84	22.13
10.00	45.94	21.98	23.95
11.04	53.96	24.28	29.68
12.11	56.98	26.64	30.34
12.51	61.79	27.54	34.25
13.97	72.31	30.73	41.59
15.72	81.92	34.57	47.35
17.51	89.10	38.51	50.59
19.42	105.8	42.70	63.07
21.03	114.8	46.25	68.60
22.50	123.3	49.48	73.82
24.97	146.3	54.91	91.36
27.24	157.2	59.91	97.27

Table 9: Ni 90

n=1.34

T	k	k_e	k_{ph}
4.22	19.75	12.56	7.19
4.23	19.44	12.58	6.85
4.32	20.31	12.85	7.46
4.42	20.20	13.14	7.05
4.56	21.01	13.56	7.45
4.71	21.89	13.99	7.91
4.87	22.39	14.46	7.92
5.37	26.47	15.97	10.50
5.61	27.10	16.68	10.42
5.82	29.56	17.31	12.25
6.22	29.29	18.50	10.78
6.60	32.42	19.61	12.85
6.93	34.04	20.60	13.44
7.40	36.81	21.99	14.86
7.54	38.66	22.42	16.23
7.97	40.42	23.73	16.69
8.51	42.77	25.31	17.46
9.78	49.52	29.06	20.45
10.29	53.82	30.58	23.23
10.91	58.78	32.44	26.34
11.96	63.74	35.55	28.19
12.55	73.14	37.31	35.83
13.93	85.51	41.41	44.10
13.54	73.86	40.25	33.61
15.29	89.23	45.46	43.77
17.41	103.1	51.75	51.30
18.91	113.9	56.23	57.67
20.49	125.6	60.92	64.65
24.06	147.8	71.54	76.28
26.07	170.1	77.51	92.55

Table 10: Ni 91

n=1.30

T	k	k_e	k_{ph}
4.23	12.14	6.53	5.61
4.24	12.47	6.54	5.93
4.28	12.13	6.60	5.53
4.55	13.73	7.01	6.72
4.82	14.49	7.44	7.04
5.00	15.52	7.72	7.80
5.01	16.05	7.73	8.32
5.49	17.76	8.48	9.28
5.87	19.18	9.06	10.12
6.16	19.92	9.51	10.41
6.74	23.80	10.39	13.40
6.92	23.59	10.68	12.91
7.69	25.34	11.86	13.47
8.16	28.34	12.59	15.75
8.85	32.38	13.66	18.73
9.17	31.24	14.15	17.09
9.87	34.36	15.23	19.12
10.57	36.25	16.30	19.95
10.94	41.72	16.88	24.84
12.00	44.42	18.51	25.91
13.02	47.64	20.09	27.55
14.58	55.88	22.49	33.40
15.78	61.51	24.35	37.16
16.63	65.61	25.65	39.96
18.77	68.10	28.96	39.15
21.20	86.18	32.71	53.47
23.20	95.09	35.80	59.29
24.88	106.4	38.38	68.05
25.11	105.1	38.74	66.38
26.35	115.9	40.66	75.20

Table 8 (continued)

29.51	175.9	64.89	111.0
31.75	176.2	69.83	106.4
33.65	194.6	74.00	120.6
36.88	203.7	81.10	122.6
39.54	222.2	86.95	135.3
43.99	245.6	96.73	148.9
48.31	254.8	106.2	148.6
49.43	239.6	108.7	130.9
53.18	278.9	116.9	162.0

Table 9 (continued)

28.14	180.0	83.66	96.32
30.55	181.6	90.83	90.81
39.00	262.7	115.9	146.7

Table 10 (continued)

29.07	142.3	44.84	97.47
31.14	135.0	48.05	86.91
35.05	136.7	54.07	82.57
40.70	185.1	62.79	122.3
50.74	217.8	78.28	139.5
60.58	205.4	93.47	111.9

Table 11: Ni 96

n=2.0			
T	k	k_e	k_{ph}
4.31	31.81	27.04	4.77
4.44	31.38	27.83	3.55
4.58	31.76	28.70	3.05
4.72	33.07	29.57	3.50
5.42	38.43	34.00	4.43
6.47	46.48	40.57	5.91
7.03	57.28	44.07	13.21
7.03	55.06	44.07	10.99
8.15	63.17	51.07	12.10
9.58	64.79	60.04	14.75
11.64	95.97	72.94	23.03
13.82	118.2	86.65	31.55
19.70	174.4	123.5	50.89
24.95	230.3	156.4	73.94
32.08	284.3	201.1	83.17
41.96	372.6	263.0	109.6

Table 12: Ni 98

n=2.0			
T	k	k_e	k_{ph}
4.23	117.76	114.28	3.47
4.24	118.56	114.62	3.93
4.25	117.90	114.80	3.10
4.51	126.77	121.88	4.89
4.68	129.63	126.43	3.20
5.23	146.68	141.40	5.27
5.73	159.70	154.88	4.82
6.32	178.82	170.72	8.10
7.59	219.94	205.03	14.9
8.48	246.74	229.05	17.7
8.95	254.04	241.79	12.2
9.50	274.17	256.57	17.6
10.49	308.26	283.47	24.8
10.82	314.79	292.37	22.4
11.39	342.95	307.72	35.2
11.69	352.36	315.87	36.5
11.87	356.84	320.75	36.1
13.39	401.89	361.79	40.1
13.78	418.33	372.11	46.2
15.83	472.75	427.69	45.1
16.65	509.85	449.66	60.2
17.94	557.49	484.73	72.8
18.87	574.12	509.83	64.3
20.66	615.05	558.11	56.9
21.86	655.45	590.48	65.0
24.25	754.88	654.93	100.
26.75	844.70	722.66	122.
28.09	845.98	758.76	87.2

The temperature dependence of the lattice thermal conductivity in the temperature range between 4.2°K and 20°K can be well described as T^n by a single power n of the temperature T. The value of n varies from alloy to alloy and is included in tables 2-12. It is also plotted vs. the composition in figure 5. The same figure also contains the value of the lattice thermal conductivity at 4.2°K as a function of the composition. The following features of the two curves are conspicuous:

(a) The exponent n decreases from the value 2.0 for pure copper to about 1.1 for Cu50-Ni50.

(b) For very nickel-rich alloys again a value n=2 is found.

(c) In the composition range Cu50-Ni50 to Cu10-Ni90 the exponent n varies only from 1.1 to about 1.3. The lack of symmetry with composition about Cu50-Ni50 is obvious.

(d) The lattice thermal conductivity of copper is about 7.5 times larger than that of nickel.

(e) The lattice thermal conductivity of copper decreases rapidly with the addition of nickel, while the lattice thermal conductivity of the two most nickel-rich alloys is approximately constant.

(f) For intermediate compositions, the lattice thermal conductivity is largest at the composition Cu40-Ni60. It drops continuously on the nickel-rich side of the alloy system. On the copper-

rich side this drop is also observable, but it interferes with the effect described in (e).

4. Discussion

The ratio of the lattice thermal conductivity to the total measured thermal conductivity at 4.2°K is plotted vs. the alloy composition in figure 6. One notices that for most of the alloys this ratio is larger than 60 percent. We think that this extraordinary enhancement of the lattice component is basically caused by the incomplete electron-phonon interaction which is typical for a situation where the electron mean free path ℓ is smaller than the wave length of the phonons with the predominant wave number q, i.e. where $q\ell < 1$. The theory of this interaction has been given by Pippard [1] for the coefficient of ultrasonic attenuation. It is, however, also relevant to the thermal conductivity, because the attenuation coefficient can be regarded as the reciprocal phonon mean free path. Some of the consequences of Pippard's theory have already been summarized in the Introduction.

Indeed, the product $q\ell$ is smaller than unity for most of the copper-nickel alloys. We find this result, shown in figure 7, if we calculate $q\ell$ from the known values of the electrical conductivity σ. The predominant phonon wave number is approximately [11]

$$q = 2\,KT/(\hbar v_s) \tag{1}$$

(K - Boltzmann constant, T - abs. temperature, $\hbar = h/2\pi$ - Planck's constant, v_s - sound velocity). We shall assume that the electrical conductivity arises from contributions by s- as well as d-electrons, but most of the current is always carried by the s-electrons [12], thus $\sigma \approx \sigma_s$, where

$$\sigma_s = e^2 \tau_s n_s / m_s \tag{2}$$

(τ_s - relaxation time of the s-electrons, n_s - number of s-electrons per atom, m_s - effective mass of the s-electrons). If we assume spherical energy surfaces, we can rewrite eq (2) as

$$\sigma_s = \frac{e^2 \ell_s}{12\pi^3 \hbar} S_{Fs} \quad , \tag{3}$$

where S_{Fs} is the area of the Fermi-surface occupied by the s-electrons (e - electronic charge). From eqs (1) and (3) there follows

$$q\ell_s = 24\pi^3 \,(KT/e^2 v_s) \cdot (\sigma_s / S_{Fs}) \quad . \tag{4}$$

The number of s-electrons per atom n_s for a particular copper-nickel alloy is fairly well known from magnetic measurements [13]. It drops from 1.0 in copper to about 0.6 in Cu60-Ni40 and retains the value 0.6 approximately for the rest of the system. The area of the Fermi-surface S_{Fs} is approximately proportional to $n_s^{2/3}$. For pure copper its value is 23.3 $Å^{-2}$ in the approximation of spherical energy surfaces [14], and 23.0 $Å^{-2}$ if we use Garcia Moliner's nonspherical representation [15], calculated to fit Pippard's experimental results [6].

The number of d-electrons, on the other hand, increases from 0.0 in Cu60-Ni40 to 0.6 per atom in nickel [13]. Hence, in nickel their number is equal to the number of s-electrons. But since the mass ratio of d- and s- electrons may be of order 10 or larger, as one can conclude from specific heat measurements [16], the contribution of the d-electrons to the electrical conductivity is quite small, so that we cannot derive their mean free path from σ.

The situation is different in the case of the ultrasonic attenuation α by electrons, which is given by the expression [1]

$$\alpha_{long} = \frac{nm}{dv_s \tau} \left[\frac{q^2 \ell^2 \tan^{-1}(q\ell)}{3[q\ell - \tan^{-1}(q\ell)]} - 1 \right] \tag{5}$$

for the longitudinal waves and by

$$\alpha_{trans} = \frac{2nm(q\ell)^3}{3dv_s \tau} \{[(q\ell)^2 + 1]\tan^{-1}(q\ell) - q\ell\}^{-1} \tag{5a}$$

for transversal waves. It is important to note that these expressions for the attenuation result as integrals over a spherical Fermi-surface. They have been derived for s-electrons, but it can be shown that the same expressions are obtained for a spherical pocket for d-electrons. Provided $\tau_s \gtrsim \tau_d$, it is then obvious from eqs (5) and (5a) that d-electrons can contribute significantly to α *because* of their large effective mass.

Let us write, using an obvious notation,

$$\alpha = \bar{\alpha}_s(q\ell_s) + \bar{\alpha}_d(q\ell_d) \quad . \tag{6}$$

The bar indicates some modification of α due to s-d or d-s - scattering, respectively. Other modifications may arise, because the d-electrons may not occupy separate pockets, but rather deep depressions of the main sheet of the Fermi-surface, as it seems to be the case in nickel [7-9]. For a first approximation we assume $\alpha_i \approx \bar{\alpha}_i$. If we now take α as the reciprocal phonon mean free path, we can calculate the lattice thermal conductivity (compare with Ref. [4]):

$$k_{long} = \frac{1}{6\pi^2} \frac{K^3}{\hbar^2} \frac{T^2}{\ell_s v_{slong}} \int_0^\infty c_s/\alpha_{long}(c_s,c_d) \cdot f(x)\, dx \quad , \tag{7}$$

$$k_{trans} = \frac{1}{3\pi^2} \frac{K^3}{\hbar^2} \frac{T^2}{\ell_s v_{strans}} \int_0^\infty c_s/\alpha_{trans}(c_s,c_d) \cdot f(x)\, dx \quad , \tag{8}$$

where

$$c_s = q\ell_s \quad , \quad c_d = q\ell_d, \quad f(x) = e^x x^3 (e^x-1)^{-2} \quad , \quad x = \frac{\hbar q v_s}{KT} \quad ,$$

and

$$v_{slong} = 5 \cdot 10^5 \text{ cm s}^{-1} \quad , \quad v_{strans} = 2.5 \cdot 10^5 \text{ cm s}^{-1} \quad .$$

In eqs (7) and (8) we use the calculated values for ℓ_s (fig. 7) The appearance of ℓ_s in the denominator in the expressions (7) and (8) explains in principle the observation (f) mentioned under "Results".

We do not expect that such a crude approach results in good absolute values of the lattice conductivity. The exponent n expressing the temperature dependence, however, should be less affected by wrong scaling constants. Following the Pippard theory consequently, we should add the two components (7) and (8), in order to obtain the total lattice conductivity. This amounts to the assumption of equally strong interaction of the conduction electrons with both longitudinal and transversal vibrational modes (Makinson scheme). The other case often discussed in the literature [17], is restricted to the interaction of electrons with longitudinal modes only (Bloch scheme). The transversal modes are coupled to the longitudinal modes by at least the normal phonon-phonon processes. If we calculate the temperature exponent n from eqs. (7) and (8) for both the Makinson and the Bloch scheme, we find that the former appears to represent the results for the most copper-rich alloys better, while the latter seems to apply better to the rest of the system, i.e. to most of the alloys. This is particularly obvious for the alloy Cu49-Ni51. The calculated exponent n is plotted in figure 8 vs. the alloy composition. This curve should be compared with the corresponding curve in figure 5. It seems that with approximately equal relaxation times for s- and d-electrons, a large mass ratio, and a small ratio of the Fermi-velocities, the experimental data for the alloys containing more than 40 percent nickel can be fairly well fitted by the theoretical values of n , if only longitudinal modes are considered. Since

$$\frac{q\ell_d}{q\ell_s} = \frac{v_{Fd}}{v_{Fs}} \frac{\tau_d}{\tau_s} \quad , \tag{9}$$

where v_{Fs} and v_{Fd} denote the Fermi-velocities of the s- and d-electrons, respectively, we can conclude (or confirm) that the mean free path of the d-electrons must be significantly smaller than the mean free path of the s-electrons. It also means that below 10°K the lattice conductivity of the nickel-rich alloys, including those containing only a few percent copper, belongs to the regime $q\ell_d < 1$, although there may be $q\ell_s > 1$. This situation has been indicated in figure 7.

The results are not so satisfactory for the copper-rich alloys, although inclusion of the transversal modes brings some improvement. It is interesting that in this composition range where it is difficult to fit the exponent n, the lattice conductivity drops rather rapidly for even small additions of solute (Fig. 5). This effect is typical for copper- and silver-rich alloys and has been given particular attention by Tainsh and White [19]. The true causes of this effect, however, are still rather uncertain, although the most likely cause might have to be found in variations of the electron-phonon interaction itself.

The fact that the lattice conductivity of nickel is so much smaller than that of copper [observation (d)] can be explained by the arguments used by Fletcher and Greig [5] who made a similar observation in the silver-palladium system. They explain the low value of the lattice conductivity in transition metals by the effectiveness of s-d and d-d electron transitions. We think that the copper-nickel system should behave correspondingly.

5. Summary

The temperature dependence of the lattice conductivity of well-annealed copper-nickel alloys can be understood through Pippard's theory of the ultrasonic attenuation by electrons. When extended to include d-electrons, this model explains several basic observations. The most important result, however, is the sensitivity of the lattice conductivity to properties of the d-electrons (quite unlike the electrical conductivity), particularly, if their effective mass is large. The experiments confirm that the ratio of the mean free paths of d- and s-electrons in nickel-rich alloys is appr. 0.1, and that the mass ratio is appr. 10.

6. References

[1] Pippard, A. B., Ultrasonic attenuation in metals, Phil. Mag. 46, 1104 (1955).

[2] Ziman, J. M., Electrons and Phonons, Ch. 5.12 (Clarendon Press, Oxford, 1960).

[3] Zimmerman, J. E., Low-temperature lattice heat conduction in high-resistivity alloys, J. Phys. Chem. Solids 11, 299 (1959).

[4] Lindenfeld, P. and Pennebaker, W. B., Lattice conductivity of copper alloys, Phys. Rev. 127, 1881 (1962).

[5] Fletcher, R. and Greig, D., The lattice thermal conductivity of some palladium and platinum alloys, Phil Mag. 16, 303 (1967).

[6] Pippard, A. B., An experimental determination of the Fermi surface in copper, Phil. Trans. Roy. Soc. A250, 325 (1957).

[7] Ehrenreich, H., Phillipp, H.R., and Olechna, D. J., Optical properties and Fermi surface of nickel, Phys. Rev. 131, 2469 (1963).

[8] Tsui, D. C. and Stark, R. W., De Haas-Van Alphen effect in ferromagnetic nickel, Phys. Rev. Letters 17, 871 (1966).

[9] Hanus, J., Feinleib, J., and Scouler, W. J., Low-energy interband transitions and band structure in nickel, Phys. Rev. Letters 19, 16 (1967).

[10] Schroeder, P. A., Wolf, R., and Woollam, J.A., Thermopowers and resistivities of silver-palladium and copper-nickel alloys, Phys. Rev. 138A, 105 (1965).

[11] See Ref. 2, p. 307.

[12] Jones, H., Theory of electrical and thermal conductivity in metals, in Handbuch der Physik, edited by S. Flugge (Springer - Verlag, Berlin, 1956), Vol. 19, p. 265.

[13] Van Elst, H. C., Labach, B., and Van Den Berg, G. J., The magnetization of some nickel alloys in magnetic fields up to 15 kOe between 0°K and 300°K, Physica 28, 1297 (1962).

[14] See Ref. 2, p. 114.

[15] Garcia Moliner, F., On the Fermi surface of copper, Phil. Mag. 3, 207 (1957).

[16] Keesom, W.H. and Kurrelmeyer, B., Specific heats of alloys of nickel with copper and with iron from 1.2° to 20°K, Physica 7, 1003 (1940).

[17] Klemens, P. G., Thermal conductivity of solids at low tempertures, in Handbuch der Physik, edited by S. Flugge (Springer-Verlag. Berlin, 1956), Vol. 14, p. 198.

[18] Rosenberg, H. M., Low Temperature Solid State Physics, p. 123 (Clarendon Press, Oxford, 1963).

[19] Tainsh, R. J. and White, G. K., Lattice thermal conductivity of copper- and silver-alloys at low temperatures, J. Phys. Chem. Solids 23, 1329 (1962).

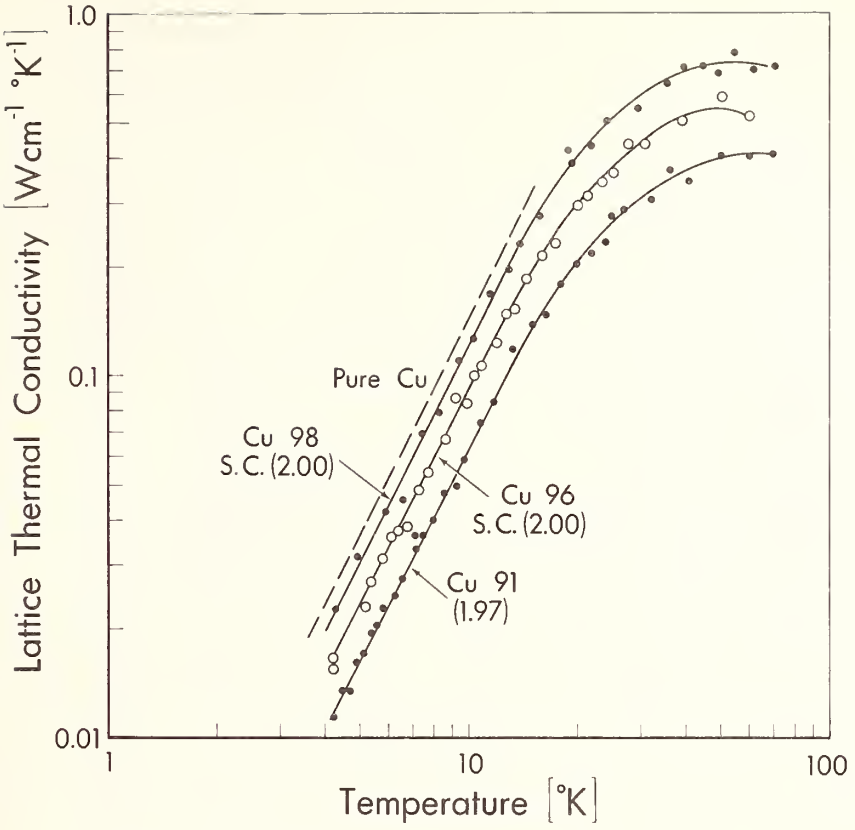

Figure 1: The lattice thermal conductivity vs. the abs. temperature of the alloys Cu98, Cu96, Cu91. The broken line refers to pure copper and has been taken from the literature [18]. Single crystals are denoted by s. c.

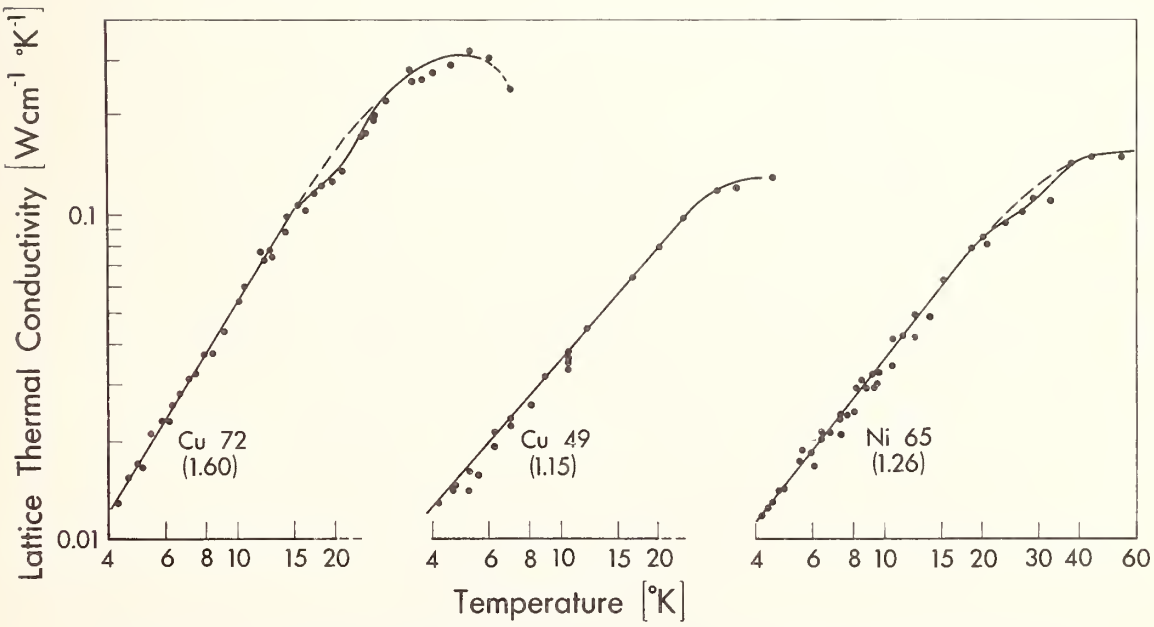

Figure 2: The lattice conductivity vs. temperature of the alloys Cu72, Cu49, Ni65.

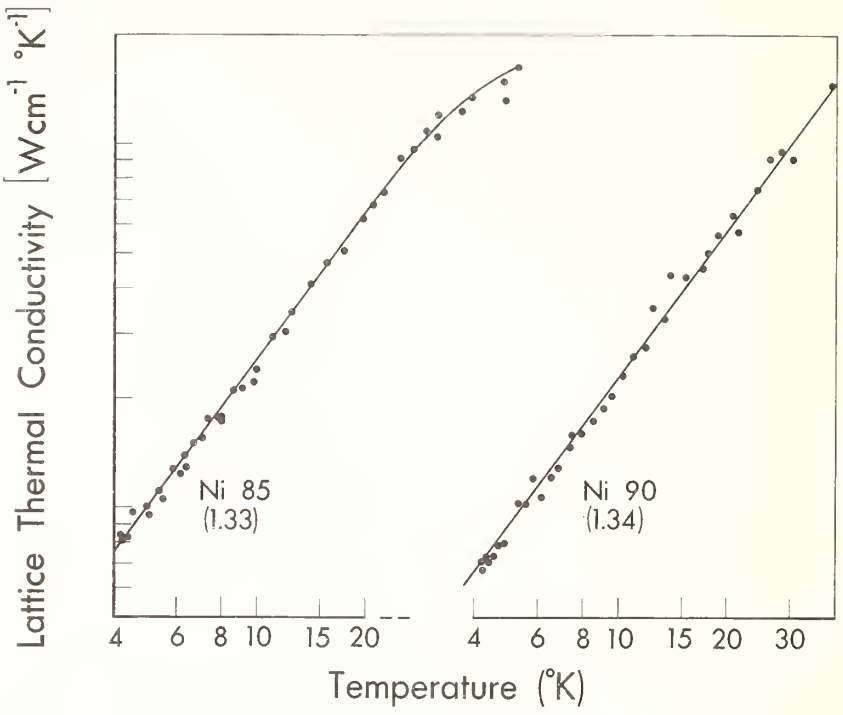

Figure 3: The lattice conductivity vs. temperature of the alloys Ni85, Ni90.

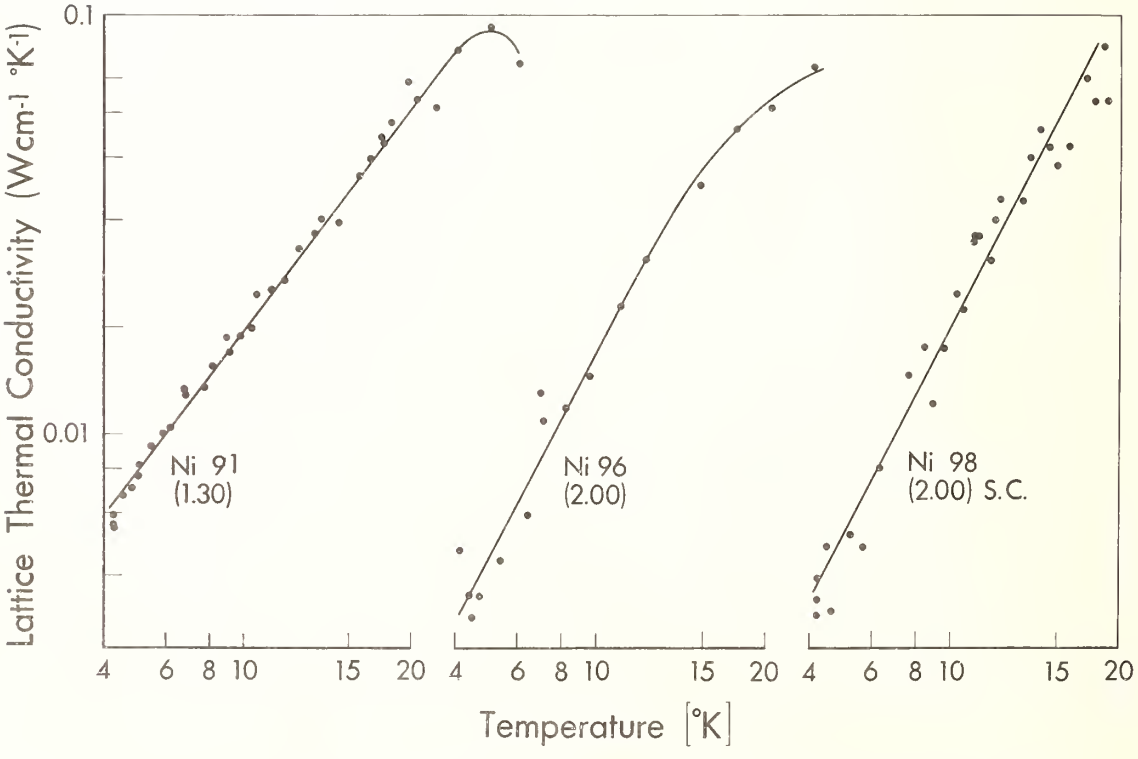

Figure 4: The lattice conductivity vs. temperature of the alloys Ni91, Ni96, Ni98.

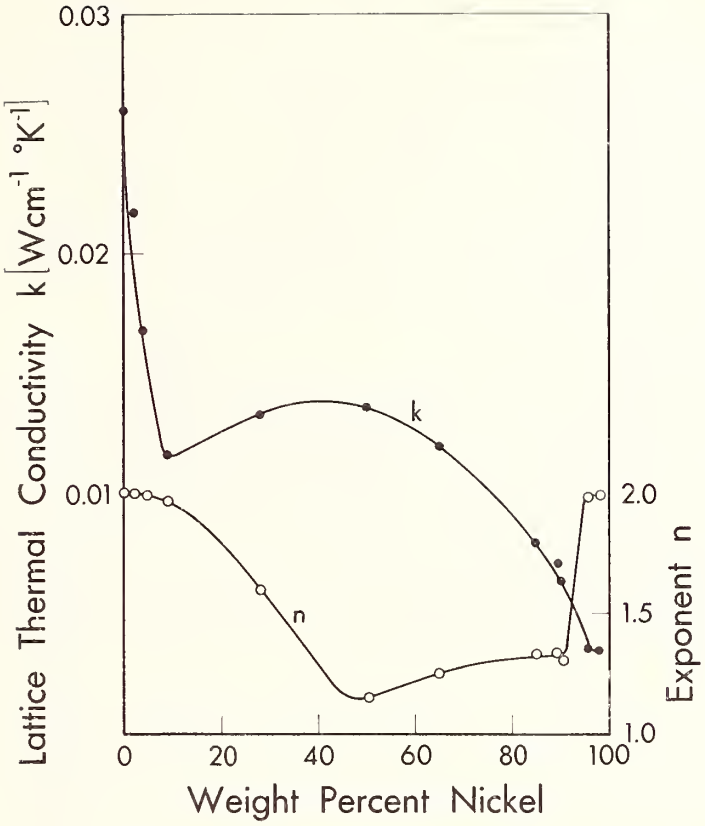

Figure 5: The lattice thermal conductivity at 4.2°K and its temperature exponent n vs. alloy composition of the copper-nickel system.

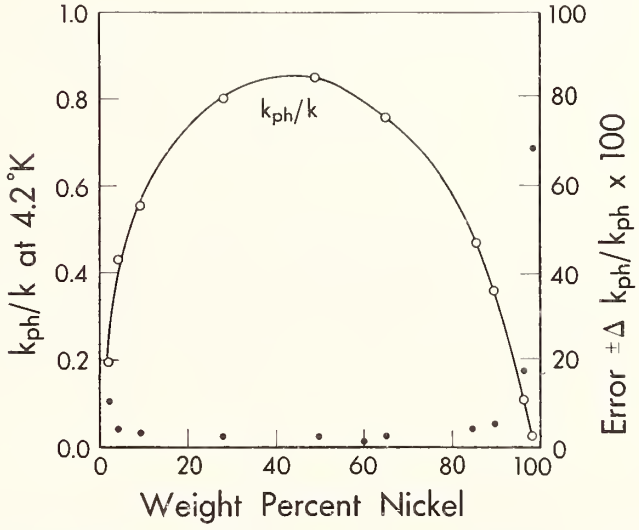

Figure 6: The ratio of the lattice thermal conductivity to the total measured thermal conductivity at 4.2°K vs. alloy composition.

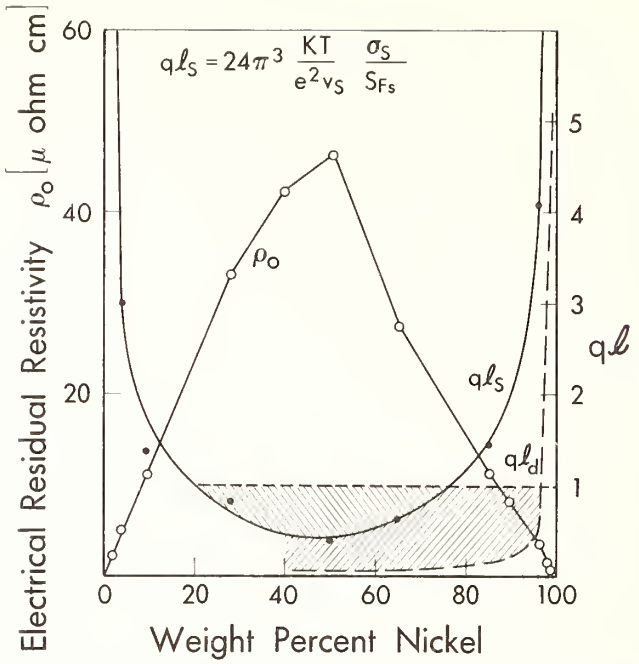

Figure 7: The residual electrical resistivity ρ_o and the product of the predominant phonon wave number q at 4.2°K and the electron mean free path ℓ vs. alloy composition. $q\ell_d = 0.1\, q\ell_s$. The curve for $q\ell_s$ has been calculated from ρ_o using the equation shown ($\rho_o \approx \sigma_s^{-1}$). The shaded areas indicate the regime $q\ell < 1$.

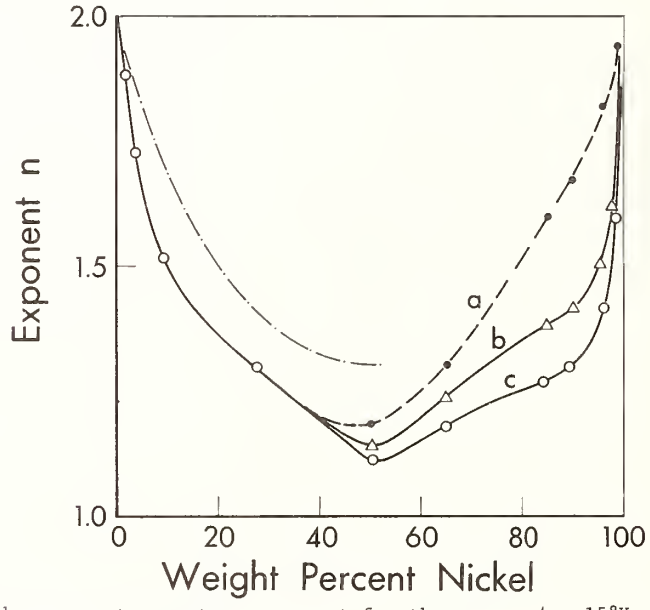

Figure 8: The calculated average temperature exponent for the range 4 - 15°K vs. alloy composition. $\tau_d/\tau_s = 1.2$. Electron concentrations: $n_s = x_{Cu} - 0.6$, $n_d = 0$ for $x_{Cu} \geq 0.6$, $n_d = 0.6 - x_{Cu}$, $n_s = 0.6$ for $x_{Cu} \leq 0.6$.

(a) $m_d/m_s = 0$,

(b) $m_d/m_s = 10$, $v_{Fd}/v_{Fs} = 0.3$

(c) $m_d/m_s = 50$, $V_{Fd}/v_{Fs} = 0.1$

} interaction with longitudinal modes only

broken line: interaction with longitudinal and transversal modes.

Thermal Conductivity of Aerospace Alloys at Cryogenic Temperatures[1]

J. G. Hust, D. H. Weitzel and Robert L. Powell

Cryogenics Division
Institute for Materials Research
National Bureau of Standards
Boulder, Colorado 80302

An apparatus for measurement of thermal conductivity, electrical resistivity, and thermopower of metals and alloys is described. This apparatus, a modified version of the one used earlier in this laboratory, utilizes the steady-state, axial heat flow method. The samples are cylindrical rods about 23 cm long, and from 0.1 to 1.0 cm^2 in cross-sectional area. Included is a discussion about radiation induced errors, thermometry, and temperature control methods. Results on thermal conductivity, electrical resistivity, Lorenz ratio, and thermopower (with respect to normal-silver) are reported for titanium and aluminum alloys from 4° to 300°Kelvin. The data uncertainty is estimated to be about 1% below 120°K, but up to about 5% near 300°K when radiation effects become important.

Key Words: Aluminum alloy, electrical conductivity, Lorenz ratio, thermal conductivity, thermopower, thermoelectric power, titanium alloy.

1. Introduction

The development of new materials for the aerospace industry has created a demand for data on the thermal and electrical properties of these alloys. To help satisfy the immediate needs for these data we are making thermal and electrical conductivity measurements from liquid helium temperatures to near room temperature on several alloys. Later more accurate measurements will be made on several materials to establish them as standard reference materials. Measured standard reference materials may be used to verify the accuracy of new thermal conductivity apparatus or as reference standards in comparative apparatus. The availability of measured standard reference materials should encourage more laboratories to enter this field of measurement.

Thermal data of technically important solids accurate to about 5% satisfy current demands. However, since future demands will likely become more stringent and because standard reference material data are also desired, this program is directed toward the acquisition of data which are accurate to within 1%. Thermal conductivity data accurate to within 1% are difficult to obtain for poor conducting alloys such as titanium A-110AT and especially difficult at temperatures above approximately 120°K.

This paper describes the method of measurement and the apparatus. Included are data for titanium A-110AT and aluminum 7039, along with a brief discussion of errors.

---

[1] This work was supported by NASA, (Space Nuclear Propulsion Office) Contract R-45.

2. Method of Measurement

Of the many methods described in the literature for the measurement of thermal conductivity, probably the simplest both conceptually and mechanically is the axial heat flow method. In this configuration the sample is in the form of a rod with constant cross-sectional area and the heat flow is one-dimensional along the axis of the rod. The defining equation for one-dimensional heat flow is

$$\dot{Q} = -\lambda A \frac{dT}{dX} \tag{1}$$

where $\dot{Q}$ is the rate of heat flow thru the rod; λ is thermal conductivity of the rod at temperature, T; A is cross-sectional area of rod; and dT/dX is the temperature gradient along the rod. The rate of heat flow, $\dot{Q}$, and area, A, are measured directly while the temperature gradient dT/dX can only be approximated from a finite number of measured values of T and X along the sample. For most apparatus there are only two or three points at which T and X are measured; in ours there are eight.

One can approximate the temperature gradient, dT/dX, by $\Delta T/\Delta X$. The quantity ΔT is the temperature difference between two adjacent measured points separated by a distance ΔX. This approximation of dT/dX has the advantage of simplicity but the disadvantage of being mathematically accurate only if the increments ΔT are small or if λ is independent of temperature. However, if ΔT is too small, it will be inaccurate due to measurement errors. A second method of obtaining the temperature gradient is as follows. The T, X points are represented by a function T = T(X) which in turn is differentiated to obtain the approximate temperature gradient, T'(X) = dT/dX. Caution must be exercised in choosing the function T(X) and in determining its parameters to avoid introducing serious fitting errors, particularly in the slope.

3. Apparatus

The apparatus (Fig. 1) used in this experiment is essentially the same as that used earlier at this laboratory by R. L. Powell, et al [1].[2] The present system differs from the earlier ones principally by the addition of the floating sink and its automatic temperature controls. The floating sink allows greater flexibility in setting the temperature of the top of the sample. The temperature of the floating sink is automatically stabilized, thus greatly reducing drift of the sample temperature because of bath temperature drift. The temperature of the shell (0.5 mm thick stainless steel) surrounding the sample is automatically controlled to be the same as the temperature of the sample at the bottom thermocouple station. Three trim heaters spaced evenly along the shell enable one to match the shell and sample temperatures at these locations as well. Since the top of the shell is in good thermal contact with the sample thru the floating sink block, it is possible to closely match the shell temperature to the sample temperature at a total of five points. This adjustment reduces conduction losses thru the leads connected to the sample as well as thermal radiation losses. The measuring thermocouples and the shell-to-sample differential thermocouples (both Chromel vs Au + 0.07% Fe) are electrically insulated from the sample and the shell. A typical thermocouple mount is illustrated in figure 2. Thermal contact, while still maintaining electrical insulation, is obtained with epoxy cement and Apiezen N grease as shown in figure 2.

This apparatus is designed to measure also the thermopower and the electrical resistivity of the sample. The thermopower is determined by measuring the Seebeck voltage between the top and bottom thermocouple holders using 36 AWG "normal" silver wires. The absolute thermopower of normal silver has been determined; it is small compared to most metals and alloys. Electrical resistivity is determined by passing a known current through the sample (from the sample heater thru the sample to the system ground) and measuring the voltage drop across the sample between the top and bottom thermocouple mounts. The Seebeck voltage is subtracted from the total voltage drop to obtain the resistivity voltage drop.

---

[2] Figures in brackets indicate the literature references at the end of this paper.

4. Samples

Two alloys were investigated: titanium alloy A-110AT (annealed) and aluminum alloy 7039-T61. The aluminum sample was ground into a cylinder with 0.1 cm^2 cross-sectional area and 23 cm length. It was supplied by ACF Industries, Inc., Albuquerque, New Mexico with a chemical analysis as follows:

Mn	Si	Ni	Cr	Cu	Fe	Ti	Be	Zn	Mg	Al
.23%	<.10	<.02	0.20	<.10	<.15	0.018	<.001	3.60	2.55	Balance

The heat treatment T-61 was in compliance with Kaiser Aluminum and Chemical Company proprietary heat treatment procedure. The titanium sample was ground into a cylinder of 1.0 cm^2 cross section and 23 cm length. It was supplied by Crucible Steel Company of America, Syracuse, New York with the following chemical analysis:

C	Fe	N	Al	H	Sn	Ti
0.07%	0.20	0.01	5.5	0.0158	2.5	Balance

The hardness and grain size of these samples will also be determined and reported in a later publication for more complete characterization of the samples.

5. Results and Discussion

The thermal conductivity, electrical resistivity, and thermopower of titanium alloy A-110AT and Al-7039 were measured from 5 to 300°K and their values are given in figures 3 thru 8. The Lorenz ratios were calculated from these data and are plotted in figures 9 and 10.

Since Ti A-110AT was the first sample investigated with this redesigned apparatus, more runs than normal were conducted to determine the precision and reproducibility of these measurements. The temperature ranges of these runs were adjusted to obtain considerable overlapping between runs not only for a given bath but also between baths, e.g., some runs using a L-He bath overlap runs using L-H_2 bath. The aluminum sample was measured over the same temperature range as the titanium sample but there was less overlap in each range and therefore fewer runs were required. The number of runs and temperature range investigated with the indicated baths are given below.

	Number of Runs		Temperature range	
Bath	Ti A-110AT	Al-7039	Ti A-110AT	Al-7039
LHe	7	4	5 - 32°K	5 - 28°K
LH_2	7	4	23 - 105°K	21 - 72°K
LN_2	10	6	66 - 150°K	72 - 210°K
CO_2 and Ethanol	3	2	199 - 236°K	198 - 225°K
Ice and Water	1	2	280 - 300°K	280 - 296°K

The scatter in the data for the individual runs and the deviation between overlapping runs are both less than 1% below 120°K. From 120 to 200°K slightly higher deviations are observed and are attributed to the presence of thermal radiation errors.

At the higher temperatures (between 200 and 300°K) the thermal conductivity curve as defined by each run contains a slight bump with the highest point corresponding to about the middle of the sample. This bump can be explained by considering the presence of a parallel path due to thermal radiation. Due to the symmetry of the sample and shield and the temperature distribution of each, the bottom of the sample (hot end) should experience a net loss of energy while the top should gain energy. Thus the calculated $\dot{Q}$ is more nearly correct nearest the heater, becomes progressively larger toward the middle of the sample, and becomes more nearly correct beyond the middle of the sample approaching the top end. Such an error in $\dot{Q}$ would tend to produce the observed bumps.

For Ti A-110AT the magnitudes of these "radiation" bumps are about 2% at 200°K and 6% at 300°K, while for Al-7039 the bump is masked by the scatter, i.e., less than 0.5%, at 200°K and is about 1% at 300°K. In an attempt to confirm that these bumps are caused by thermal radiation, a radiation shield composed of loosely packed glass wool was placed around the Al-7039 sample. An ice-bath run was repeated with this radiation shield in place and resulted in thermal conductivity values 6% lower than with no radiation shield. No bump is observed in these data. The measured thermal conductivity of Ti-A110AT at 300°K was lowered by 13% by the presence of the glass wool radiation shield. At 200°K the measured decrease was 6%, while at 115°K only a 1% decrease was observed. At 20°K the presence of the glass wool packing did not affect the measured value within the scatter of data. It is concluded that the size of the "bump" does not directly indicate the magnitude of the radiation errors, but the presence of the bump is direct evidence that radiation errors exist. The data presented in figures 3 thru 10 are consistent with the measurements made with the glass wool packing in the apparatus.

The present results have been computed with an estimated sensitivity curve for the Chromel vs Au + 0.07 atomic percent Fe thermocouples. This estimated curve may be systematically inaccurate by as much as 2% and adds directly to the uncertainty of the thermal conductivity data. The sensitivity of this thermocouple has been measured at this laboratory and the final data will soon be available. At that time thermal conductivity values will be recomputed using these more reliable data. The final computation will also be based on more refined data reduction techniques and will contain small corrections which have not been included yet. It is anticipated however that these changes will amount to no more than approximately 3%.

The details of these measurements, including a complete error analysis, will follow in a later publication.

6. References

[1] Powell, Robert L., Rogers, W. M., and Coffin, D. O., An Apparatus for Measurement of Thermal Conductivity of Solids at Low Temperatures, J. Res. NBS 59, No. 5, 349-55 (1957); RP 2805.

Added by the editorial reviewer: The use in this paper of trade names of specific products, though contrary to usual NBS practice, is essential to a proper understanding of the work presented. Their use in no way implies any approval, endorsement, or recommendation by NBS.

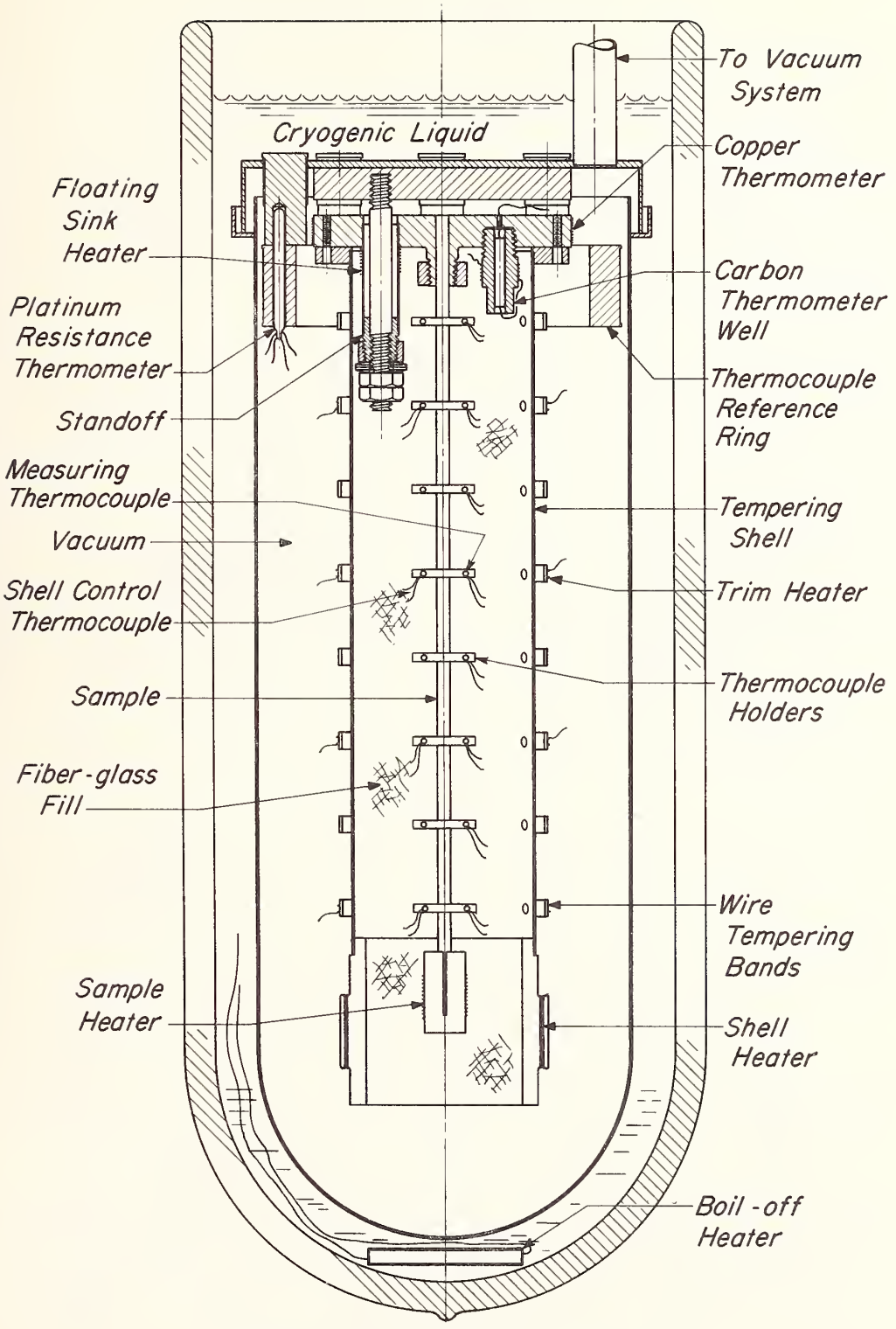

Figure 1. Thermal Conductivity Apparatus.

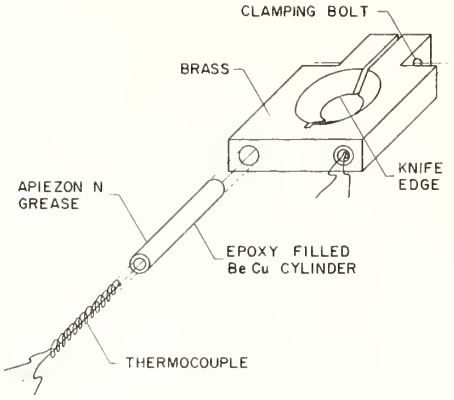

Figure 2. Thermocouple mount.

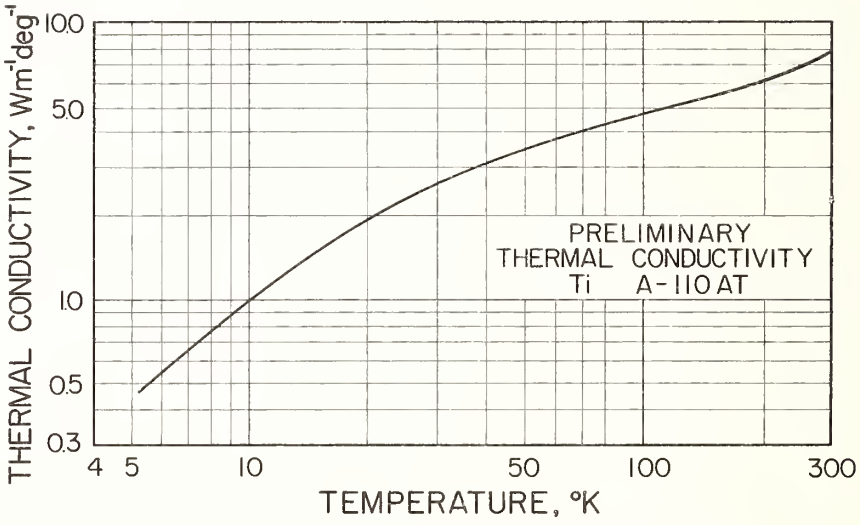

Figure 3. Thermal Conductivity of titanium alloy A-110AT.

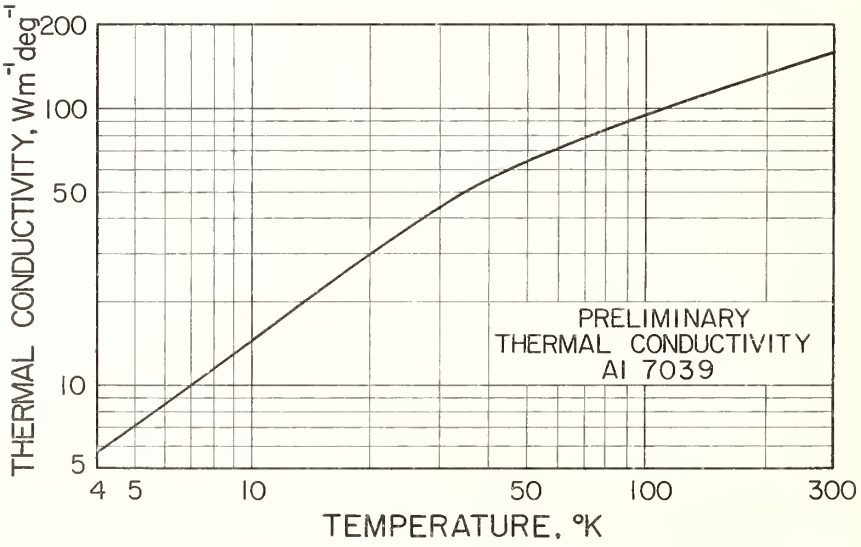

Figure 4. Thermal Conductivity of aluminum alloy 7039.

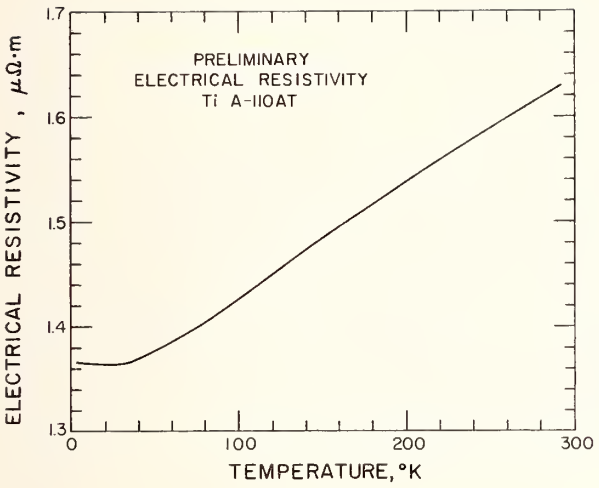

Figure 5. Electrical resistivity of titanium alloy A-110AT.

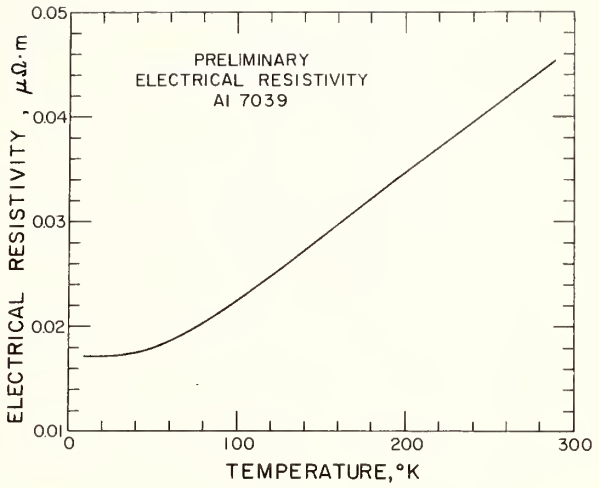

Figure 6. Electrical resistivity of aluminum alloy 7039.

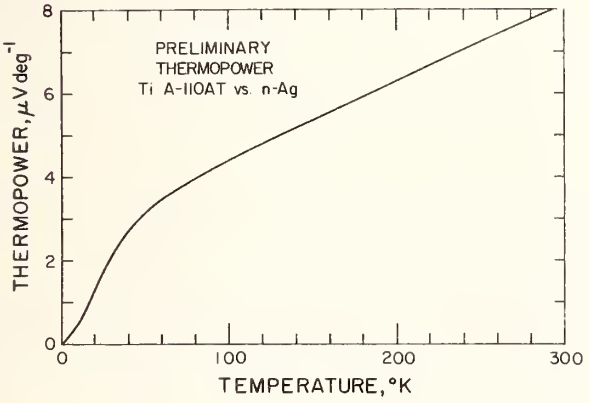

Figure 7. Thermopower of titanium alloy A-110AT. (vs. normal silver).

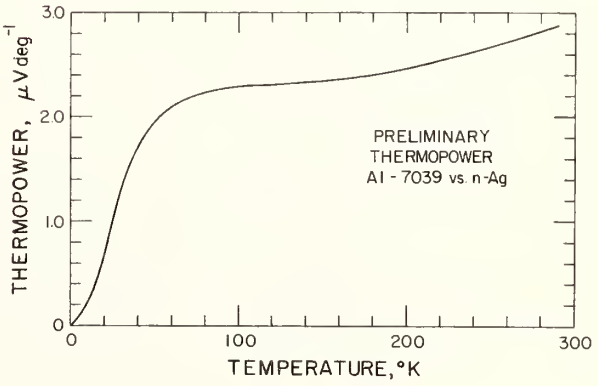

Figure 8. Thermopower of aluminum alloy 7039 (vs. normal silver).

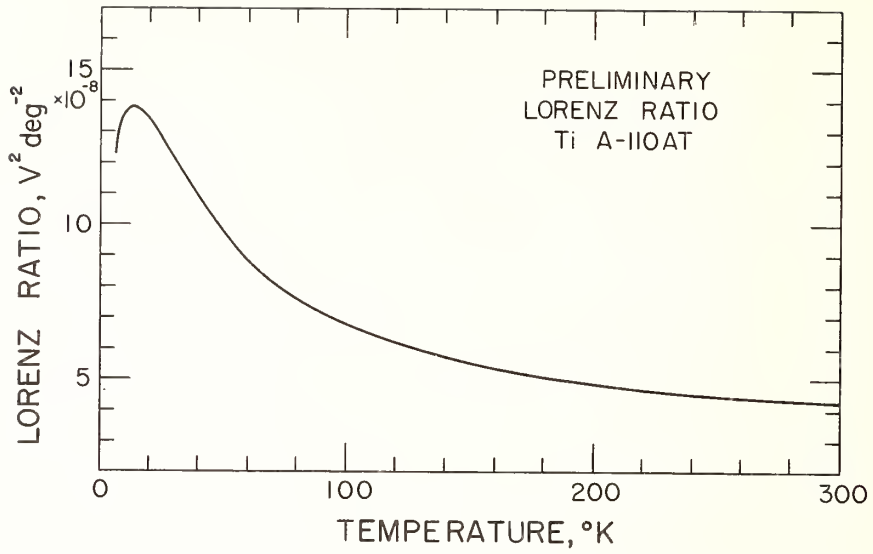

Figure 9. Lorenz ratio of titanium alloy A-110AT.

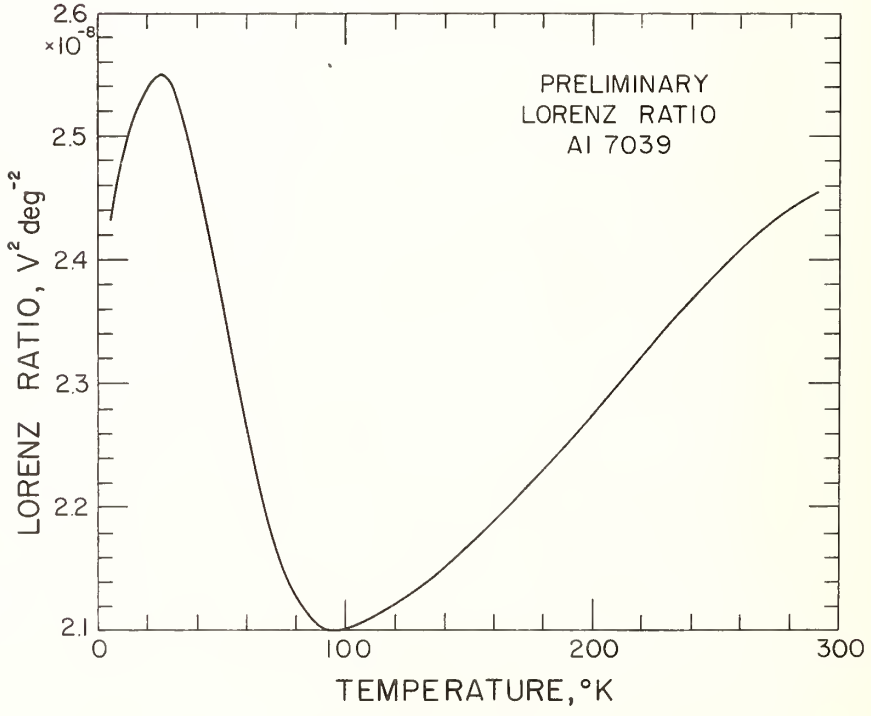

Figure 10. Lorenz ratio of aluminum alloy 7039.

Physical Properties of Indium from 77 to 350 °K[1]

M. Barisoni, R. K. Williams, and D. L. McElroy

Metals and Ceramics Division
Oak Ridge National Laboratory
Oak Ridge, Tennessee 37830

The electrical resistivity, thermal conductivity, and Seebeck coefficient of three high-purity indium specimens were studied between 80 to 400 °K in a guarded longitudinal heat flow apparatus. Two of the three specimens were single crystals of known orientation and data obtained from these samples were used to extract values for the transport properties along the two principal crystallographic axes. The third sample was a coarse-grained polycrystal. Electrical resistivity data are in reasonable agreement with the temperature variations reported for high-purity indium resistance thermometers and application of the results of this study to the behavior of resistance thermometers is discussed. The thermal conductivity data for all samples are consistently lower than values which had been obtained in another investigation, and the differences do not correlate with the differences in the electrical resistivity measurements.

Key Words: Electrical resistivity, indium, Lorenz function, resistance thermometer, Seebeck coefficient, thermal conductivity.

1. Introduction

Indium is a tetragonal metal and its transport properties are expected to vary with crystallographic direction. For a tetragonal crystal, this variation can be described in terms of two independent components along the [001] and [100] axes [1][2]. The properties are isotropic when measured parallel to the (001) plane, so it is common practice to speak of two principal values perpendicular and parallel to the [001] axis. Determination of these two principal components is the first prerequisite for understanding the behavior of this anisotropic metal. This study of the transport properties of indium was undertaken for two principal reasons:

(1) To further refine the knowledge of the thermal conductivity and electrical resistivity of this element and attempt to determine the relative importance of the electronic and phonon heat transfer components.

(2) To determine the effects of crystal anisotropy on the transport properties over a fairly broad temperature range. It was thought that this information would be especially applicable to defining the variability of indium resistance thermometers.

Initially, it was also felt that indium would form a relatively simple starting point for a series of measurements on anisotropic elements because of its low Debye temperature (approx 110 °K) and availability in relatively pure form. The difficulties which were encountered with plastic deformation soon dispelled this illusion but the measurements, which define the small anisotropy fairly well, do form a good basis for further studies in this area.

2. Specimen Characteristics

The three high-purity indium specimens were obtained from Semi Elements, Inc., Saxonburg, Pennsylvania. All three specimens were in rod form, 0.79 cm in diameter and 7.6 cm long and were produced from one lot of starting material. Two of the samples, designated SC-A and SC-C were differently oriented single crystals and one (PC) was a fairly coarse-grained polycrystalline rod.

---

[1]Research sponsored by the U.S. Atomic Energy Commission under contract with the Union Carbide Corporation.

[2]Figures in brackets indicate the literature references at the end of this paper.

Samples for metallurgical evaluation were obtained from each specimen after the experiments had been completed. The results of a semiquantitative spectrographic analysis are compared to results supplied by the Vendor in table 1. The analyses indicated that the total metallic impurity content of the specimens was less than about 100 ppm, and that the impurity content did not vary much from sample to sample. The electrical resistivity ratios shown in table 2, $\rho_{273}/\rho_{4.2}$, are all greater than 7.6×10^3 and give a qualitative indication of the sample purity. The residual resistivities indicate that impurity effects should contribute a maximum of about 0.06% of the total resistivity at 77°K, the lowest temperature which could be obtained in the apparatus.

Table 1. Chemical analysis of indium specimens.

Element	Semiquantitative[a] Spectrographic Analysis (ppm)		
	Sample SC-A	Sample PC	Mfg. Analysis
Ag	20[b]	30[b]	
Al	0.7	0.2	
B	0.1	0.3	
Bi	2	0.5	
Ca	4	1	
Cd	4	10	1
Co	0.05	0.05	
Cr	0.5	1.5	
Cu	2	2	< 1
Fe	1.5	5	
K	4	1	
Mg	0.2	0.2	< 1
Mn	0.5	0.5	
Na	0.6	2	
Ni	0.8	0.08	
Pb	1	4	
Sc	0.5	1	
Si	15[b]	1.5	< 1
Sn			1
Th	0.6	2	
Ti	2	0.4	
Tl	2	7	< 1
Zn	1	30[b]	
S	2	7	

[a]Accuracy about ±50%.

[b]Value may be fictitiously high.

Table 2. Characteristics of indium specimens.

Sample	Density (g/cm^3)	Resistivity Ratio ($\rho_{273}/\rho_{4.2}$)	Hardness DPH (Kg/mm^2)
PC	7.28_1	10.7×10^3	0.7 ($\theta = 50°$)[a]
			0.9 ($\theta = 62°$)
			1.0 ($\theta = 75°$)
SC-A	7.28_5	10.9×10^3	
SC-C	7.28_5	7.6×10^3	

[a]θ is defined as the angle between the rod axis and the [001] direction.

Density data were obtained by immersing the samples in degassed, distilled water and are shown in table 2. These results indicate that the samples were free of voids and close to the reported value (7.28 g/cm^3) [2].

The microstructure of the polycrystalline sample is shown in figure 1. This examination was carried out by supporting the cut specimen in paraffin, removing the distorted surface layer by repeatedly etching with concentrated nitric acid and using Villella's reagent for the final metallographic etch. The sample was found to be free of inclusions and to have an average grain diameter of about 0.28 cm. This grain size represents a significant fraction of the sample diameter and the sample thus does not represent a true, randomly oriented, isotropic polycrystal.

The orientations of the two single crystals were determined from back-reflection Laue photographs, and three or more patterns were obtained on each sample at different axial and angular positions. The patterns were indexed on the body-centered tetragonal cell and showed that the average angles between the sample axis and the [001] crystallographic axis were 81.5 and 41.5° in samples SC-A and SC-C, respectively. Based on the internal consistency and reproducibility of the data, the uncertainties associated with these angles were taken to be about ±2 deg.

Back-reflection Laue photographs were also used to confirm the microstructure shown in figure 1. These patterns, obtained with a 0.05-cm-diam beam, showed that the grains which were observed were indeed single crystals and that some subgrain boundaries may have been present.

Hardness data were obtained on three differently oriented grains of the section and are presented in table 2. The orientations of these grains were determined from the back-reflection Laue patterns, and the hardness numbers indicate that the hardness increases as the plane of the grain approaches the (100) orientation.

After the experiments had been completed, the two single-crystal specimens were reexamined to determine if they had been deformed during the experiments. X-ray diffraction patterns and macro-etching were used to make these checks and no evidence of deformation could be found in sample SC-A. A band of slip lines was, however, found on sample SC-C. These lines extended over about 1.5 cm at one end of the specimen and Laue patterns on this area indicated that local deformation and/or recrystallization had taken place, probably within rather localized regions. The results from this sample, which also had a lower resistivity ratio than the other two must be less valid than the results from sample SC-A. Their use can, however, be justified on the basis that the Laue photographs did not show a change in the crystal orientation, indicating that the deformation did not extend over a large portion of the sample.

3. Experimental Procedure

The thermal conductivity, electrical resistivity, and Seebeck coefficient measurements were made in the apparatus which has been described by Moore et al. [3]. With this apparatus the thermal conductivity and Seebeck coefficient were determined under guarded axial heat flow conditions and the electrical resistivity is measured with the standard four-probe direct-current method. A general view of the apparatus is shown in figure 2. A detailed error analysis presented by Moore et al. [3] is summarized in table 3. The analysis indicates total determinate errors for λ, ρ, and S ($\overline{\text{In-const}}$) of ±1.86%, ±0.6%, and ±1.5%, respectively. Since the resistivities and thermal conductivities parallel and perpendicular to the [001] axis ($\rho_\perp$, $\rho_\parallel$, $\lambda_\perp$, $\lambda_\parallel$) were obtained from a knowledge of the orientations of the two single crystals, the uncertainty in the orientation, ±2°, enlarged the maximum errors associated with these values (table 3). This additional error would amount to a maximum of ±0.06%. Analysis of this error also indicates the importance of obtaining values on a large number of single crystals which differ widely in orientation.

The procedure for determining the absolute Seebeck coefficient of indium from the experimentally determined $S_{\text{In-const}}$ values has also been described by Moore et al. [3], who pointed out the large absolute errors which arise from taking the difference between two large values, $S_{\text{In-const}}$ and $S_{\text{const-Pt}}$.

Some minor modifications of the technique were introduced to solve problems which were due to the extremely poor mechanical properties of indium. The 5-mil-diam Chromel-P vs Constantan thermocouples were attached to the specimen by forcing the ends of the individual wires into the surface of the specimen a distance of about three wire diameters. The wires entered the surface of the samples at an angle of about 90°. The entrance points of the two wires were located about two diameters apart and the measuring junctions were thus made through the indium specimen. The mechanical stability of the junction was considerably improved by cementing both leads to the specimen with a drop of nonconducting epoxy resin. The specimens were attached to the removable copper base with conducting epoxy. This material provided a satisfactory mechanical, thermal and electrical contact and eliminated the clamping arrangement shown in figure 2 which would have deformed the soft indium specimens.

The specimen diameters were determined with an optical comparator. The polycrystalline specimen was quite uniform, showing a maximum variation of 0.2% but the surfaces of the two single-crystal specimens were pitted and had maximum variations of 0.3%. The dimensions used for computing the

Table 3. Summation of measurement errors.

	ρ	$S_{spec-co}$	λ
Temperature measurement			
Uncertainty of measurement temperature	±0.1°K	±0.1°K	±0.1°K
Uncertainty of ΔT measurement (%)		±1.0	±1.0
Dimensional measurement (%)			
Distance between thermocouples	< ±0.36		< ±0.36
Area	±0.13		±0.13
Power measurement (%)			
Measurement of E and I			< ±0.17
Power loss down leads			< ±0.2
Uncertainty in voltage (%)			
Between similar legs of thermocouple Nos. 2 and 3	±0.1	±0.5	
TOTALS	±0.6%	±1.5%	±1.86%
Repeatability without system change	±0.1%	±0.1%	±0.15%

electrical resistivity and thermal conductivity were obtained by averaging a large number of determinations. The effective distances between the thermocouples (and voltage probes) were obtained from knife-edge measurements. The knife edge measurements were not completely satisfactory, one sample (SC-C) was damaged by knife cuts approximately 0.1 cm deep.

4. Experimental Results

The data reported were obtained from six separate assemblies of the apparatus. Sample SC-A was instrumented twice but, except for three electrical resistivity values all of the data reported for it are from one run. All of the data for samples SC-C were obtained from one run. Three runs were made with the polycrystalline specimen. Some Seebeck coefficient data were obtained during all three of these latter runs, electrical resistivity data were only taken during the first and second runs, and thermal conductivity data were obtained during the first and third runs. The limited amount of thermal conductivity data obtained during the second run on the polycrystalline specimen were discarded because difficulties with thermal grounds made it impossible to maintain a satisfactory temperature match between the specimen and guard cylinder.

4.1. Electrical Resistivity Data

The raw electrical resistivity data can be manipulated in a number of ways, so it seems pertinent to describe the sequence which we employed. The data obtained were first fitted to an empirical equation of the form:

$$\rho = A + BT + CT^2 + DT^3 \qquad (1)$$

and are shown in a difference plot, figure 3. The data shown in this figure were not corrected for volume changes on cooling and were not resolved along the crystal axes. The empirical equation can be seen to give adequate descriptions of all the results and the values for the constants are shown in table 4. The data for sample PC show the largest scatter from the equation, about ± 0.2%, and the results for the two single crystal samples vary by ±0.1% or less.

The individual data points were also corrected for the change from the room temperature volume ("corrected" data) and fitted to eq (1). The expansion data of Smith and Schneider [4] were used to make the adjustments for the single crystals. An average volumetric coefficient of expansion [5] was used for sample PC and the principal expansion coefficient data were used for the two single crystals [4]. Values for the coefficients [eq (1)] obtained for the corrected data on all three samples are also shown

Table 4. List of the equations used to fit the experimental results.

Sample PC

$$\rho(T) = -0.3728 + 2.6053 \times 10^{-2}T + 5.9102 \times 10^{-6}T^2 + 3.9432 \times 10^{-8}T^3$$

$$\rho^a(T) = -0.3792 + 2.6029 \times 10^{-2}T + 5.2866 \times 10^{-6}T^2 + 4.2080 \times 10^{-8}T^3$$

$$\lambda(T) = 1.0432 - 7.9987 \times 10^{-4}T - 0.9938 \times 10^{-7}T^2$$

$$\lambda^a(T) = 1.0472 - 7.6755 \times 10^{-4}T - 2.8227 \times 10^{-7}T^2$$

Sample SC-A

$$\rho(T) = -0.3228 + 2.4642 \times 10^{-2}T + 1.6382 \times 10^{-5}T^2 + 2.3961 \times 10^{-8}T^3$$

$$\rho^a(T) = -0.3416 + 2.5066 \times 10^{-2}T + 1.5733 \times 10^{-5}T^2 + 2.2107 \times 10^{-8}T^3$$

$$\lambda(T) = 1.0502 - 9.3418 \times 10^{-4}T + 2.1528 \times 10^{-7}T^2$$

$$\lambda^a(T) = 1.0445 - 9.4793 \times 10^{-4}T + 3.2207 \times 10^{-7}T^2$$

Sample SC-C

$$\rho(T) = -0.2681 + 2.4051 \times 10^{-2}T + 1.8256 \times 10^{-5}T^2 + 1.5357 \times 10^{-8}T^3$$

$$\rho^a(T) = -0.2358 + 2.3256 \times 10^{-2}T + 2.2523 \times 10^{-5}T^2 + 0.8683 \times 10^{-8}T^3$$

$$\lambda(T) = 1.0216 - 6.9767 \times 10^{-4}T - 1.1767 \times 10^{-7}T^2$$

$$\lambda^a(T) = 1.0284 - 7.2824 \times 10^{-4}T - 0.9020 \times 10^{-7}T^2$$

Electrical resistivity and thermal conductivity along the principal axis ([001] direction):

$$\rho(T) = -0.2236 + 2.3570 \times 10^{-2}T + 1.9782 \times 10^{-5}T^2 + 0.8351 \times 10^{-8}T^3$$

$$\rho^a(T) = -0.1417 + 2.1648 \times 10^{-2}T + 2.8958 \times 10^{-5}T^2 - 0.3989 \times 10^{-8}T^3$$

$$\lambda(T) = 0.9983 - 5.0509 \times 10^{-4}T - 3.8878 \times 10^{-7}T^2$$

$$\lambda^a(T) = 1.0154 - 5.4935 \times 10^{-4}T - 4.2590 \times 10^{-7}T^2$$

Electrical resistivity and thermal conductivity along any directions normal to the principal [001] axis:

$$\rho(T) = -0.3250 + 2.4670 \times 10^{-2}T + 1.6305 \times 10^{-5}T^2 + 2.4310 \times 10^{-8}T^3$$

$$\rho^a(T) = -0.3560 + 2.5310 \times 10^{-2}T + 1.4300 \times 10^{-5}T^2 + 2.4877 \times 10^{-8}T^3$$

$$\lambda(T) = 1.0514 - 9.4377 \times 10^{-4}T + 2.2878 \times 10^{-7}T^2$$

$$\lambda^a(T) = 1.0451 - 9.5684 \times 10^{-4}T + 3.3879 \times 10^{-7}T^2$$

Electrical resistivity and thermal conductivity calculated for an isotropic polycrystal

$$\rho(T) = -0.2912 + 2.4303 \times 10^{-2}T + 1.7464 \times 10^{-5}T^2 + 1.8990 \times 10^{-8}T^3$$

$$\rho^a(T) = -0.2846 + 2.4089 \times 10^{-2}T + 1.9186 \times 10^{-5}T^2 + 1.5255 \times 10^{-8}T^3$$

$$\lambda(T) = 1.0337 - 7.9754 \times 10^{-4}T + 0.6878 \times 10^{-7}T^2$$

$$\lambda^a(T) = 1.0352 - 8.2101 \times 10^{-4}T + 0.8356 \times 10^{-7}T^2$$

[a]Experimental results corrected for thermal volume changes.

in table 4. The importance of this correction for indium should be noted. At the lowest temperature (77°K) the volume change correction changes the resistivity of sample PC by −0.6%, while the values for samples SC-A and SC-C are changed by +0.5% and −0.5%, respectively.

Empirical equations for the principal resistivities ($\rho_\perp$ and $\rho_\parallel$) were obtained from the coefficients [eq (1)] for samples SC-A and SC-C. These calculations were carried out with the standard orientation formula [6] using the crystal orientations obtained from the x-ray patterns. Empirical coefficients were generated for both uncorrected and corrected smoothed results. The four sets of empirical coefficients obtained for the two principal resistivities are also shown in table 4.

Finally, two sets of empirical temperature coefficients for isotropic polycrystalline indium were generated from the equations for the principal resistivities. These calculations were based on the formula for the resistivity of a randomly oriented polycrystal [6]. These two equations, which refer to corrected and uncorrected data are shown in table 4.

Smoothed values for the thermal conductivity, electrical resistivity and Seebeck coefficient at 20° intervals are shown in table 5. The data for the thermal conductivity and electrical resistivity are corrected for volume change effects and were obtained from the empirical equations shown in table 4. Data calculated for isotropic polycrystalline indium are included and should be compared to the results for sample PC. The absolute Seebeck coefficient values were obtained by graphically smoothing the experimental data.

One additional point on the calculation of resistivity values for isotropic polycrystalline indium should be considered. For anisotropic materials, it has been shown [1,6] that the resistivity of a randomly oriented polycrystal should depend on the sample geometry and thus is not uniquely related to the principal resistivities. Two limiting cases have been treated, the difference between the two developments being whether the electric field or current density vector is assumed parallel to the sample axis. The treatments also apply to thermal conductivity values, but for indium, which has a small anisotropy ratio, both averaging formulas yield essentially identical results (within ±0.02%). The calculated average thermal conductivity and electrical resistivity values shown in table 5 are therefore not sensitive to this variable. The effect cannot, however, be neglected for materials with large anisotropy ratios. In these substances the concept of an average conductivity or resistivity for an isotropic polycrystalline sample is most nebulous [7] because the measured values would depend upon the length to diameter ratio of the specimen.

The general behavior of the smoothed corrected electrical resistivity data is shown in figure 4. All three curves are concave upward, and the difference between the principal resistivities, which is nearly constant at the lowest temperatures, progressively increases at higher temperatures. The electrical resistivity values obtained in this study can be compared to the results of several previous investigations. Powell *et al.* [8] have reported electrical resistivity and thermal conductivity data for a fairly pure polycrystalline indium specimen from 73 to 393°K, Olsen [9] has listed values for the principal resistivities ($\rho_\perp$ and $\rho_\parallel$) at 273°K and several investigators [10,11,12] have described the characteristics of indium resistance thermometers. The volume change corrections were not used for these comparisons because the other investigators did not employ this correction.

The resistivity values reported by Powell *et al.* [8] are consistently higher than the values found for our polycrystal or calculated from the two principal resistivities. The differences decrease from a maximum of 4.7% at 80°K to only about 0.5% at the ice point. The latter value is easily within the combined errors of the two experiments, but at lower temperature, the differences are real. An alternate way to describe the difference is to note that up to about 225°K the separation in the resistivity values is essentially a constant, equal to about 0.07–0.08 μΩ·cm. This difference is qualitatively consistent with an impurity effect and inconsistent with an anisotropy effect. The latter conclusion is based on the fact that, without the contraction correction, the two characteristic electrical resistivities tend to approach the same curve at low temperatures. The hypothesized impurity effect can be further tested by comparing the measured resistivity difference with a value which can be estimated from the sample purity. The data of Aleksandrov [12a], who studied the effects of impurity additions on the resistivity ratio of indium were used for this calculation, which yields a Matthiessen resistivity difference of about 0.01 μΩ·cm. This value, which is only 15% of the observed electrical resistivity difference, does not confirm this explanation, and thus the resistivity discrepancy cannot definitely be ascribed to sample purity effects.

The ice point principal resistivities and anisotropy ratio given by Olsen [9] are in reasonably good agreement with the results of this study. Both studies indicate that the electrical resistivity parallel to the [001] axis is lower than the resistivities parallel to the [100] and [010] axes. Data obtained in this study yield an ice point anisotropy ratio ($\rho_\perp/\rho_\parallel$) of 1.034, while the data described by Olsen indicate a ratio of 1.05. The ice point resistivity values of Olsen are 0.6 and 2.2% higher than the values that we obtained for the [001] and ⟨100⟩ directions. All attempts to resolve these differences were frustrated because the original data publication could not be traced.

Table 5. Smooth data corrected for thermal expansion.

Temperature (°K)	Normal to the Principal Direction [001]			Parallel to the Principal Direction [001]			Theoretical Polycrystal		Specimen PC		
	$\rho_{\perp}$ μΩ·cm	$\lambda_{\perp}$ W $cm^{-1}deg^{-1}$	$S_{\perp}$ μV/deg	$\rho_{\parallel}$ μΩ·cm	$\lambda_{\parallel}$ W $cm^{-1}deg^{-1}$	$S_{\parallel}$ μV/deg	$\bar{\rho}$ μΩ·cm	$\bar{\lambda}$ W $cm^{-1}deg^{-1}$	ρ_{PC} μΩ·cm	λ_{PC} W $cm^{-1}deg^{-1}$	S_{PC} μV/deg
80	1.7731	0.9707	+0.33	1.7734	0.9687	−0.26	1.7731	0.9700	1.7584	0.9840	+0.23
100	2.3429	0.9528	0.66	2.3087	0.9562	+0.05	2.3314	0.9539	2.3186	0.9676	0.56
120	2.9301	0.9351	0.96	2.8661	0.9433	0.39	2.9087	0.9379	2.8930	0.9510	0.86
140	3.5359	0.9178	1.24	3.4456	0.9301	0.67	3.5058	0.9219	3.4838	0.9342	1.12
160	4.1616	0.9007	1.48	4.0470	0.9166	0.98	4.1233	0.9060	4.0929	0.9172	1.33
180	4.8082	0.8838	1.69	4.6699	0.9027	1.24	4.7620	0.8901	4.7225	0.8999	1.52
200	5.4770	0.8673	1.85	5.3143	0.8885	1.48	5.4227	0.8743	5.3744	0.8824	1.68
220	6.1692	0.8510	1.96	5.9799	0.8739	1.81	6.1060	0.8586	6.0508	0.8647	1.80
240	6.8860	0.8350	2.02	6.6666	0.8590	1.87	6.8127	0.8430	6.7536	0.8467	1.87
260	7.6285	0.8192	2.02	7.3742	0.8438	2.00	7.5436	0.8274	7.4849	0.8286	1.88
280	8.3980	0.8037	1.98	8.1025	0.8282	2.01	8.2994	0.8119	8.2466	0.8102	1.82
300	9.1957	0.7885	1.85	8.8512	0.8123	1.85	9.0807	0.7964	9.0408	0.7915	1.68
320	10.0227	0.7736	1.70	9.6202	0.7960	1.70	9.8884	0.7810	9.8696[a]	0.7727	1.46
340	10.8802	0.7589	1.46	10.4094	0.7794	1.46	10.7231	0.7657	10.7349[a]	0.7536[a]	
350	11.3208[a]	0.7517[a]		10.8114[a]	0.7709[a]		11.1509[a]	0.7581[a]			

[a]Extrapolated value.

The results of this study are compared to resistance-temperature characteristics of indium thermometers in figure 5. Resistance ratio values calculated for an ideal, isotropic polycrystal form the base line for this plot and the resistance ratios derived from the two principal resistivities define the outer limits of variations which could be expected from anisotropy effects. None of the data shown were corrected for the residual resistivities. Based on the thermometer sensitivity, $d(R/R_0)/dT$, the width of the anisotropy band decreases from about 3.1° at 100°K to 1.9° at 250°K, and illustrates the necessity for thermometer stabilization and calibration. The resistivity values of Powell et al. [8], which fell outside the anisotropy envelope, were not included in the plot. The temperature dependences found by White and Woods [10], Yates [11], and values for our polycrystalline specimen are seen to be in good agreement and to be consistent with only a small amount of anisotropy. This plot also offers a possible explanation for the results of Swenson [12], which had been thought to be anomalous [11]. Swenson's results are in good agreement with the curve for an [001] oriented wire, and these results thus indicate the importance of anisotropy effects for indium resistance thermometers.

4.2. Thermal Conductivity Data

Treatment of the thermal conductivity data for the three specimens followed the procedure outlined for the electrical resistivity results. The empirical equation chosen was:

$$\lambda = A - BT \pm CT^2 \ . \qquad (2)$$

The fit of the uncorrected data to this equation is shown in figure 3. The equation works rather well at temperatures above about 150°K, but small systematic deviations appear at lower temperatures. Equations for the actual samples, principal conductivities and conductivity of isotropic indium, both corrected and uncorrected for volume changes are shown in table 4.

The temperature and orientation dependence of the smoothed, corrected thermal conductivity values are shown in figure 6. The curves for the two principal conductivities are nearly parallel at high temperatures and converge at about 80°K. The maximum anisotropy effect is only about 2.5%, which is within the combined uncertainties of the two measurements. The anisotropy of the thermal conductivity is thus not well defined, but the magnitude and direction of the observed effect is consistent with the anisotropy of the electrical resistivity. The curve for the polycrystalline specimen follows the trend shown by the principal conductivities but lies slightly above the latter values at the lowest temperatures. This difference is also well within the combined uncertainties of the two measurements and does not seem to be due to difficulties with the volume change correction because the electrical resistivity does not show this behavior.

Powell et al. [8] have reported values for the thermal conductivity of a polycrystalline indium specimen from 73 to 393°K and these values are compared to the results of this investigation in figure 6. This comparison shows that the values of Powell et al. are consistently larger than all of the results of this study, the difference decreasing from about 10.5% at 78°K to 4.3% at room temperature. The curves for the principal conductivities show that the difference cannot be attributed to preferred orientation effects, and the resistivity values of Powell et al., which are consistently higher than the data from this study, show that the difference is inconsistent with the difference in sample purity. By elimination, then, the discrepancy must be attributed to experimental difficulties. The results of the present study are supported by an intercomparison of results on platinum specimens which has been summarized by Flynn [13]. This summary shows that the data due to Powell [14] are also consistently higher than the values from other laboratories in this temperature range and the measurements of Moore [15] on Powell's platinum specimen indicate that the difference cannot be attributed to sample variations.

4.3. Seebeck Coefficient

Values for the absolute Seebeck coefficient of indium are shown in figure 7 and table 5. These data were obtained from the measured Seebeck coefficients ($S_{In\text{-}const}$), values for the Seebeck coefficient of constantan with respect to platinum [15] and the absolute Seebeck coefficient of platinum [16]. The absolute Seebeck coefficient of indium appears to be small and positive throughout the range of the measurements, but the total uncertainties are so large that even the sign of the coefficient is not well established. Including estimated uncertainties for $S_{Const\text{-}Pt}$ and S_{Pt}, the total maximum error for the data would vary from ±130% at 100°K to ±50% at 300°K. The anisotropy effect ($S_{\perp}-S_{\parallel}$) found from these data is, of course, better defined at a given temperature because most of the errors must have the same effect on both coefficients. Analysis of the errors associated with the difference, $S_{\perp}-S_{\parallel}$, indicates this quantity may be significant. It should be noted that the Seebeck coefficient apparently becomes more isotropic as the temperature increases, which is opposite to the trend shown by the electrical resistivity and thermal conductivity.

5. Discussion of Results

Although no theory of the transport properties of anisotropic metals has been developed [17], it is interesting to see what sort of conclusions can be drawn from using the simple theories for isotropic metals. Applying the modified Bloch-Grüneisen [3] equation to the electrical resistivity results offers one such test. This equation, which gives a good description of the electrical resistivity-temperature behavior of many metals [6], reduces to a simple polynomial in the temperature range studied ($0.72\theta_D$ to $3.18\theta_D$):

$$\rho = \frac{A_1}{T} + A_2 T + A_3 T^2 \ . \tag{3}$$

The A_3 term, which arises from the temperature variation of the Debye temperature, should be related to the dominant linear term:

$$A_3 \cong 2\alpha_v \gamma A_2 \ , \tag{4}$$

where

α_v = volumetric expansion coefficient, and
γ = Grüneisen constant.

Also, the A_1 term should amount to only a few percent of the total over the reduced temperature range of interest. As shown by table 6, the smoothed, corrected resistivity values from table 5 fit this equation rather well. The A_1 term is seen to contribute a maximum of about 5% of the total resistivity at 100°K and the maximum variation of the linear coefficient (A_2) is only about 4%.

Table 6. Least-squares values for modified Bloch-Grüneisen equation.[a]

Resistivity Data	A_1	A_2	A_3	Maximum Deviation at Temperature	
				(%)	(°K)
Parallel to [001]	−8.716	2.117×10^{-2}	2.805×10^{-5}	0.5	80
Perpendicular to [001]	−10.214	2.131×10^{-2}	3.160×10^{-5}	0.3	80
Theoretical polycrystal	−9.720	2.126×10^{-2}	3.041×10^{-5}	0.06	140
Experimental polycrystal	−5.671	2.051×10^{-2}	3.244×10^{-5}	1.08	80

[a]Data from Table 5.

Examination of the coefficients obtained for the two principal directions shows that the anisotropy arises almost exclusively from the A_3 term. The ratio of the first two terms $(A_1/T + A_2T)_\perp/(A_1/T + A_2T)_\parallel$ varies from 0.995 at 80°K to 1.006 at 350°K while the anisotropy ratio varies from 1.000 to 1.045. The theoretical expression for the A_3 term [eq (4)] does not allow for an anisotropy effect, but if one takes the liberty of replacing α_v with the two principal expansion coefficients, the term can at least correlate the signs of the resistivity and linear thermal expansion anisotropies [4]. This correlation, which is not valid for all metals, has of course been recognized for some time [18]. This is about as far as the point can be pressed, the eq (4) could not be expected to hold for indium which has a very anisotropic thermal expansion coefficient and the magnitude of the A_3 term cannot be quantitatively predicted from the measured Grüneisen constant and average volumetric expansion coefficient. Adopting the A_2 and A_3 values for the theoretical polycrystal (table 6) and taking $\alpha_v = 90 \times 10^{-6}$ °K^{-1}, $\gamma = 2.4$ [5] yields:

$$\frac{A_3}{2\alpha_v \gamma A_2} = 3.31. \tag{4a}$$

A reduced Wiedemann-Franz ratio plot for indium is shown in figure 8. The ±2% error band associated with this ratio makes it impossible to reach any conclusions about the isotropy of the electronic Lorenz

number for indium. Values for copper [3,19] are included for comparison, and the striking similarity gives one indication that indium, like copper, is a dominant electronic conductor. Estimates of the phonon conductivity from the Leibfried and Schlömann equation [20] are also consistent with this hypothesis. Strictly speaking, this treatment should not be applied to a material with an anisotropic lattice conductivity, but since the values required were only estimates, this difficulty was ignored. The equation has been shown to consistently over estimate the lattice conductivity of insulators [21], and this tendency was further enhanced by choosing a Debye temperature and Grüneisen constant from the extremes of the reported ranges [5]. This leads to an expression for the maximum lattice thermal conductivity:

$$(\lambda_L)_{max} = \frac{4.7}{T} . \qquad (5)$$

The maximum phonon conductivity estimates correspond to 6 and 1.5% of the total conductivities at 80 and 350°K. The lattice conductivity of copper has been determined at temperatures up to about 100°K [21], and extrapolation of these results to higher temperatures shows that the relative importance of the lattice conductivity is about equal in the two metals. For copper, the extrapolated lattice conductivity amounts to 4 and 1.3% of the total at reduced temperatures (T/θ_0) corresponding to 80 and 350°K for indium.

The W-F ratio behavior for indium thus seems to be predominately due to the electronic thermal conductivity. The decrease in this ratio at lower temperatures would be attributed to inelastic electron-phonon scattering and the fact that the ratio approaches, but does not equal, the Sommerfeld value would indicate that the Lorenz number deviations, which are being found in many transition metals [22], are not present. The resistivity and thermal conductivity data for indium fit the Sondheimer-Wilson theory [23] quite well if an effective free electron concentration of about 1 electron per 4 atoms is chosen. This result is quite similar to the value for copper [19] but is not quite so disturbing because indium is not a monovalent metal. Also, Pimentel and Sheline [24] have derived a concentration of 1 electron per 2 atoms for indium from low temperature specific heat and thermoelectric power measurements.

6. Conclusions

Analysis of the data obtained during this study has led to several conclusions about the behavior of the physical properties of indium:

1. The thermal conductivity is principally due to electronic transport and the values obtained are somewhat lower than previous literature values.

2. The effects of crystal anisotropy on the electrical resistivity and thermal conductivity are rather small and the anisotropy ratios observed for the two properties are internally consistent $\left(\frac{\rho_\perp}{\rho_\parallel} \approx \frac{\lambda_\parallel}{\lambda_\perp}\right)$.

3. The anisotropy ratios for the thermal conductivity and electrical resistivity increase with increasing temperature, a trend which is also shown by the thermal expansion coefficients.

4. Measurements of the electrical resistivity anisotropy are useful for interpreting the variability of indium resistance thermometers.

5. The absolute Seebeck coefficient is small over the whole temperature range studied, probably positive, and, the anisotropy effect observed, if real, has a temperature dependence opposite that of the electrical resistivity and thermal conductivity.

7. References

[1] Nye, J. F., Physical Properties of Crystals, p. 195, Oxford University Press, London, 1960.

[2] American Institute of Physics Handbook, 2nd ed., p.2-20, McGraw-Hill, New York, 1963.

[3] Moore, J. P., McElroy, D. L., and Graves, R. S., Canadian Journal of Physics (to be published in December 1967).

[4] Smith, J. F. and Schneider, V. L., J. Less-Common Metals 7, 17 (1964).

[5] Gschneidner, K. A., Solid State Phys. 16, 314 (1964).

[6] Meaden, G. T., Electrical Resistance of Metals, p. 8, Plenum Press, New York, 1965.

[7] Powell, R. W., Phys. Letters 24A, 445 (1967).

[8] Powell, R. W., Woodman, M. J., Tye, R. P., Phil. Mag. 7, 1183 (1962).

[9] Olsen, J. L., Electron Transport in Metals, Interscience Publishers, p. 107, Wiley, New York, 1962.

[10] White, G. K. and Woods, S. B., Rev. Sci. Instr. 28, 638 (1957).

[11] Yates, B. and Panter, C. H., J. Sci. Instr. 38, 196 (1961).

[12] Swenson, C. H., Phys. Rev. 100(6), 1607 (1955).

[12a] Aleksandrov, B. N., Zh. Eksperim. I. Teor. Fiz. 43, 399 (1962).

[13] Flynn, D. R. and O'Hagan, M. E., J. Research NBS 71C, 255 (1967).

[14] Powell, R. W. and Tye, R. P., Brit. J. Appl. Phys. 14, 662 (1963).

[15] Moore, J. P., private communication.

[16] Cusack, N. and Kendall P., Proc. Phys. Soc. (London) 72, 898 (1958).

[17] Ziman, J. M., Electrons and Phonons, p. 396, Oxford University Press, London, 1963.

[18] Boas, W. and Mackenzie, J. K., Progr. Metal Phys. 2, 90 (1950).

[19] Laubitz, M. J., Canadian Journal of Physics (to be published in December 1967).

[20] Fulkerson, W., private communication.

[21] Klemens, P. G., Solid State Phys. 7, 47 (1958).

[22] Fulkerson, W. and Williams, R. K., Proceedings of the Sixth Conference on Thermal Conductivity, p. 807, Materials Application Division, Air Force Materials Laboratory, Wright-Patterson Air Force Base, Ohio, 1966.

[23] Wilson, A. H., The Theory of Metals, p. 290 University Press, Cambridge, 1958.

[24] Pimentel, G. C. and Sheline, R. K., J. Chem. Phys. 17(7), 644 (1949).

[25]* Roizin, N. M., Mostovlyanskii, N.S., and Strod, R. K., Trans. Solid State Phys. USSR 5, 887 (1963).

[26]* Roizin, N. M., Fiz. Metall. Metalloved 15, 800 (1963).

*These are two additional references on the thermal conductivity of indium.

Figure 1. Indium sample PC. 10X.

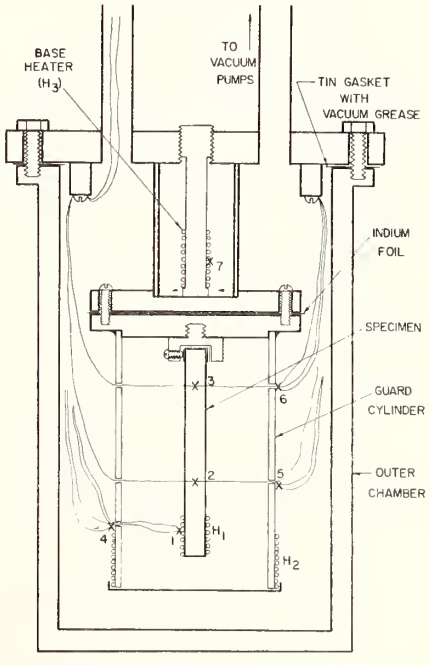

Figure 2. Schematic of ORNL longitudinal heat flow apparatus.

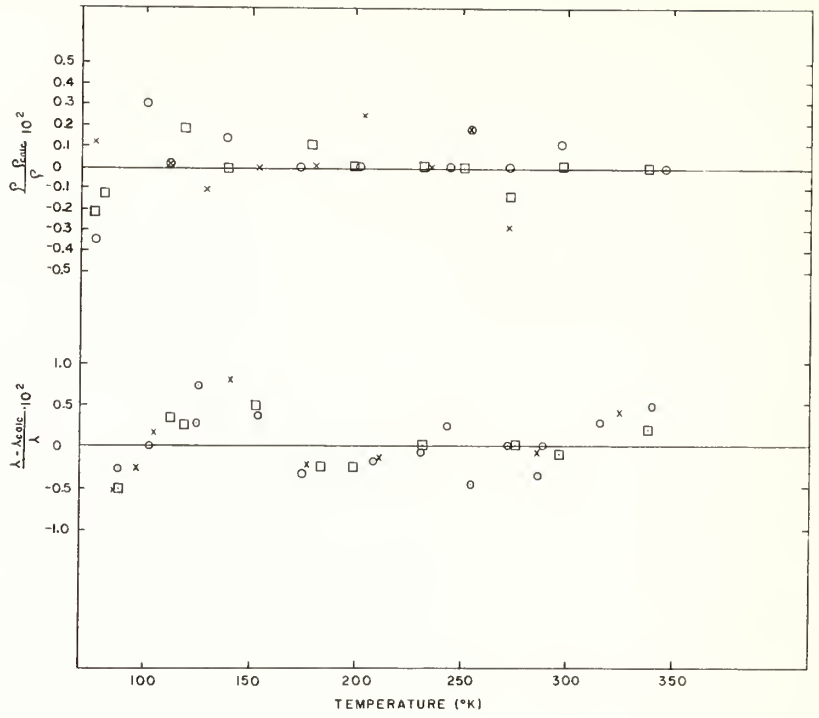

Figure 3. Deviation of the Experimental Electrical Resistivity and Thermal Conductivity Data from the Empirical eqs (1 and 2). ⊗ PC Run 1; × PC Run 2; ⊡ SC-A; ⊙ SC-C.

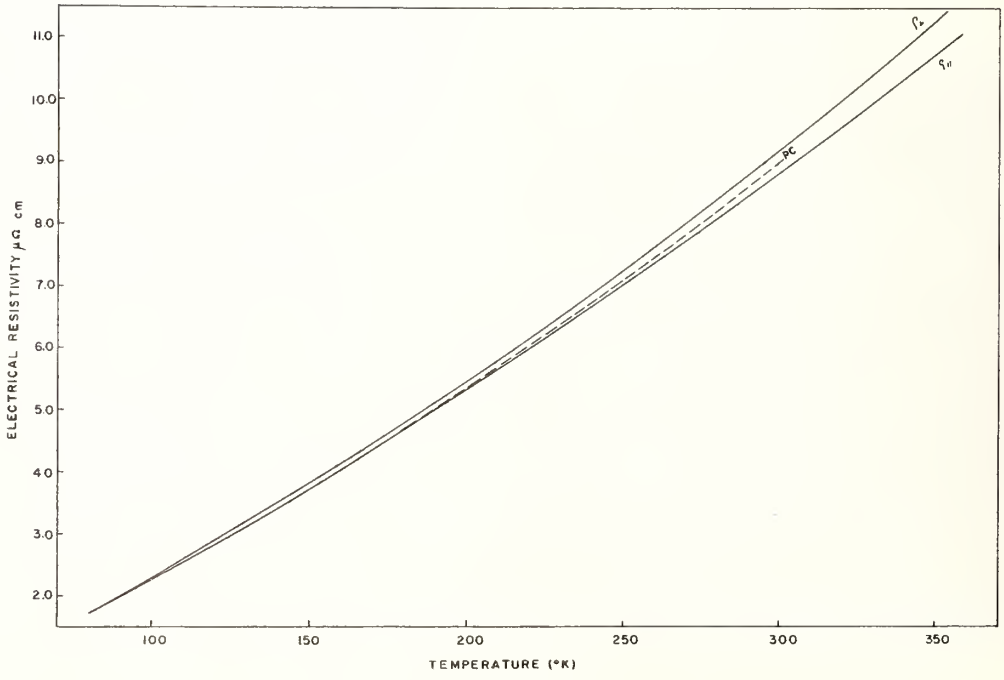

Figure 4. Effects of Temperature and Crystal Anisotropy on the Electrical Resistivity of Indium.

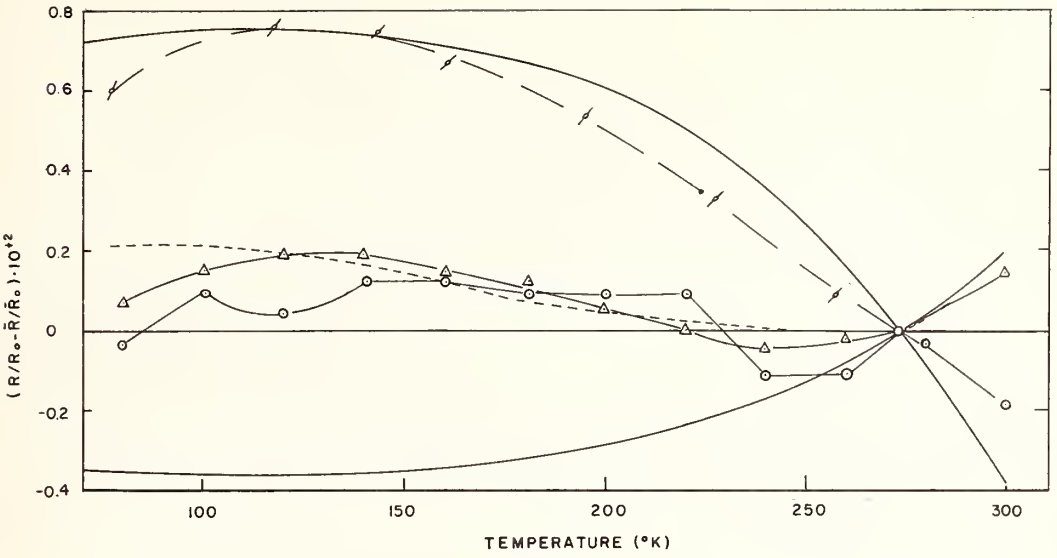

Figure 5. Deviation of R/R_0 Values for Indium Resistance Thermometers from Values Calculated for an Isotropic Polycrystal. R_0 is the ice point resistance. Upper bold curve is for R/R_0 parallel to [001]; lower bold curve is for R/R_0 perpendicular to [001]. △ Sample PC; ⊙ White and Woods; - - - - Yates [11]; ϕ Swenson [12].

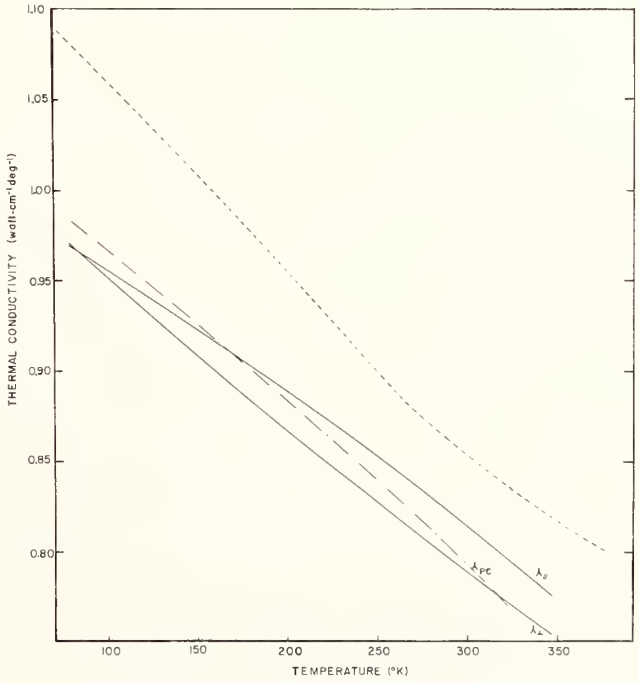

Figure 6. Effects of Temperature and Crystal Anisotropy on the Thermal Conductivity of Indium Lower curves from present study. - - - - Powell, Woodman, and Tye [8].

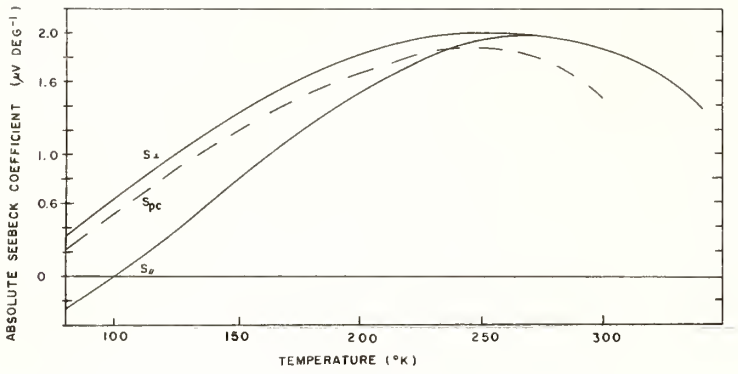

Figure 7. Effects of temperature and crystal anisotropy on the absolute Seebeck coefficient of indium.

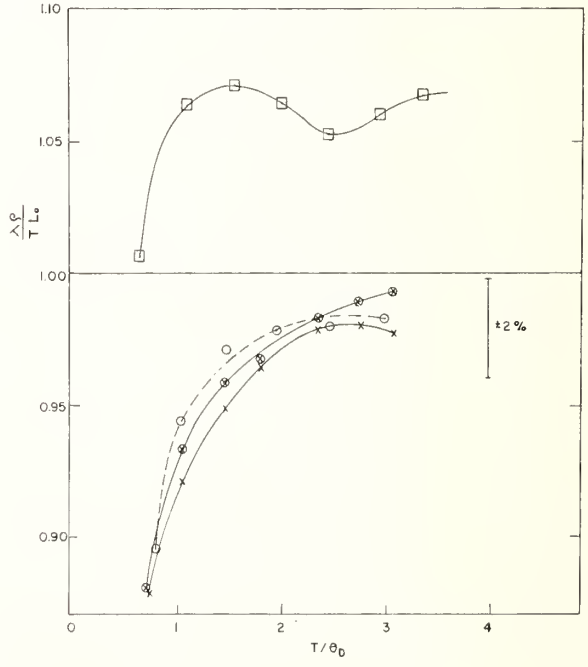

Figure 8. Reduced Wiedmann-Franz ratio plot for indium and copper. Indium θ_D = 110 °K; copper θ_D 300 °K. ⊙ copper [3,19]; ⊡ polycrystalline indium, Powell, Woodman, and Tye [8]; ⊗ indium perpendicular to [001], present study; X indium parallel to [100], present study.

Thermal Conductivity of Aluminum Between About 78 and 373°K

K. E. Wilkes and R. W. Powell[1]

Thermophysical Properties Research Center
Purdue University
West Lafayette, Indiana

An apparatus is described which employs the absolute longitudinal method and permits the measurement of the thermal conductivity of metals in the intermediate low temperature range between the boiling point of nitrogen and the steam point. Results are given for reasonably pure samples of iron and of aluminum.

Key Words: Aluminum, conductivity, electrical resistivity, iron, resistivity, thermal conductivity.

1. Introduction

Recently, considerable attention has been focused on the possibility of a minimum in the thermal conductivity vs. temperature relationship for aluminum in the intermediate low temperature range. The purpose of this investigation was to explore this minimum by measurements on a very pure specimen of aluminum. The results presented here are for an unannealed specimen. Later work will be directed at measuring this effect in an annealed specimen and in specimens with known amounts of impurities.

2. Apparatus

The apparatus used for these measurements is very similar to the one used by Powell, et.al.[1][2]. A schematic of the apparatus is shown in Figure 1. It consists of an internally polished cylindrical chamber connected to a vacuum system capable of producing vacua of the order of 5×10^{-5} torr. The specimen is fitted in a heavy brass base and the chamber is immersed in liquid nitrogen, dry ice and acetone, ice and water, or water. For measurements at intermediate temperatures below the ice point, an auxiliary heated container filled with either isopentane or acetone surrounds the chamber and this in turn is surrounded by either liquid nitrogen or dry ice and acetone.

Heat is supplied electrically at the free end of the rod. For the preliminary measurements on iron, the heater consisted of nichrome wire wound on a thin layer of mica around the end of the rod and then covered with aluminum foil. This proved to be unsatisfactory in that the temperature of the aluminum foil was much higher than that of the specimen, thus introducing large radiation errors. For the measurements on aluminum, the heater consisted of helical coils of 38 gauge nichrome wire insulated by alumina tubing and inserted in a small cylinder of aluminum which was then cemented to the end of the rod. The entire heater was then covered with aluminum foil to minimize radiative losses. Current leads were made of 24 gauge nichrome and two sets of 38 gauge constantan potential leads were spot welded to them. The two constantan leads on each current lead could then be read differentially to determine the amount of heat flowing along the current leads. This type of heater is much like that described by Laubitz[2], and later used by Flynn and O'Hagan[3]. Chromel-contantan thermocouples were pinned by a pencil point into small holes, located at points about 1.9, 5.0, and 8.1 cm. from the free end of the aluminum rod. Other thermocouples were attached to the heater, one of the support rods, the inside wall of the can, and several places on the outside of the can. All thermocouples and leads from the specimen were securely tied to one of the support rods in order to minimize heat losses.

---

[1] Graduate Research Assistant and Senior Researcher, respectively.
[2] Figures in brackets indicate the literature references at the end of this paper.

3. Procedure

The specimen was first suspended freely and heat was supplied in order to determine the amount of heat lost by radiation from the specimen. Next, the specimen was fitted into the brass base and an equilibrium gradient was measured with no heat supplied to the specimen. Then heat was supplied in order to create a temperature difference of about 5°C between the two outside thermocouples. Measurements were made after equilibrium was established, usually after several hours. All temperature and voltage measurements were made with a Leeds and Northrup six-dial potentiometer.

The thermal conductivity was determined by using the difference of that gradient with heat supplied and that without heat supplied to the specimen. Corrections were made for radiation losses, heat either gained or lost through the current leads, and heat lost by conduction through the other leads. The relative amount of these heat losses are summarized in Table 1.

Table 1. Summary of Minor Heat Losses.

Specimen	Radiation Heat Losses				Heat Flow In Current Leads	Heat Flow In Other Leads
	373°K	273°K	195°K	88°K		
Aluminum	2.5%	1.0%	0.4%	.04%	.5%	.05%
Iron	--	1.9%	--	--	1%	.09%

4. Preliminary Measurements

Since these were the first measurements made with this apparatus, a preliminary check on its accuracy was made by measuring the thermal conductivity of a specimen of pure iron near 273°K. The specimen was a rod of 99.96% iron, 1.25 cm in diameter and 10.44 cm. long. At 25°C, its density was 7871 kg m^{-3}. The electrical resistivity was found to be .0900$\mu\Omega$-m. at 273°K, and .1044$\mu\Omega$-m at 302°K. At 280°K, its thermal conductivity was found to be 81.5 $Wm^{-1}deg^{-1}$. This compares well with literature values of from 80.5 to 82.5 $Wm^{-1}deg^{-1}$ [4].

5. Measurements on Aluminum

Next, a series of measurements were made on a polycrystalline aluminum rod which was 1.225 cm. in diameter and 10.16 cm. long. The specimen was supplied by Advanced Research Materials with a stated analysis of .5ppm. Cu, .5ppm. Si, and .1ppm Mg, indicating 99.99989% Al by difference. It was measured in the unannealed state as received from the supplier. Its density was 2698 kgm^{-3} at 23°C and its electrical resistivity was .02425 $\mu\Omega$-m at 273°K and .00221 $\mu\Omega$-m at 77°K.

The results of this series of measurements are shown in Figures 2 and 3. In Figure 2, the calculations were based on the table of emf vs. temperature for chromel-constantan thermocouples which was generated by the Oak Ridge National Laboratory[5] and was based on NBS Circular 561. This curve shows a minimum of a little over 2% at about 180°K, with a maximum at about 330°K. However, at the lowest temperatures measured, liquid nitrogen temperatures, the output of the thermocouples was around 8710μv. This corresponds to a deviation of about 107μv, from the above table by using the boiling point of liquid nitrogen, corrected for atmospheric pressure.

Later, it was called to the authors' attention by Dr. R. L. Powell that newer thermocouple tables exist[6]. At the lowest temperatures, the thermocouples deviated from these tables by about 57μv, the actual temperature being read with a platinum resistance thermometer. The thermocouples were then calibrated in the region below the ice point by using the resistance thermometer and the above tables. In this way, a temperature vs. emf table was established for our particular thermocouples. The results of the calculations based on this table are shown in Figure 3. The calculations above the ice point are based on the ORNL tables with a calibration against a platinum-rhodium

thermocouple. This curve shows a minimum of about 2% at about 220°K and a maximum at about 330°K. By comparing Figures 2 and 3, it is seen that the influence of the proper calibration is to shift the minimum to a higher temperature and to make the calculated thermal conductivity higher as one goes to lower temperatures. At the lowest temperature, the thermal conductivity is changed from 328.4 at 84.6°K to 348.0 at 88.2°K, a change of around 6%.

Both the above curves, along with the results of previous workers are plotted on an enlarged scale in Figure 4. Curve 1 is the results obtained by NBS[7]. No specimen characterization is available for this data. This curve shows a minimum of a little over 2% at about 240°K. Curve 2 shows the results of measurements by Powell, Tye and Woodman [8], on a specimen of 99.993% Al. Here, the minimum is about 8% and occurs at about 220°K. Curve 4 shows the results of measurements by Moore, McElroy, and Barisoni [9] on a specimen of 99.999% Al. It indicates a minimum of about 10% at 160°K. Curves 4 and 5 are the results of the present work both before and after account was taken of the thermocouple calibration.

From these curves, although all agree in indicating a thermal conductivity minimum below room temperature and a maximum above, it is seen that serious discrepancies exist in the individual data. The present work agrees most closely to the results obtained by NBS. Some indication of the importance of the thermocouple calibration has been shown and it is hoped that the proposed further measurements will help to provide more definite information on the influence of sample purity.

6. Acknowledgment

The above work has been carried out at the Thermophysical Properties Research Center and forms part of a program supported by the National Science Foundation to whom grateful acknowledgment is made.

7. References

[1] Powell, R.W., Tye, R.P., and Woodman, M.J., The Thermal Conductivity and Electrical Resistivity of Rhenium, J. Less-Common Metals, 5, pp. 49-55 (1963).

[2] Laubitz, M.J., The Unmatched Guard Method of Measuring Thermal Conductivity, II. The Guardless Method, Can. J. Phys., 43, pp. 232 (1965).

[3] Flynn, D.R., and O'Hagan, M.E., Measurements of the Thermal Conductivity and Electrical Resistivity of Platinum from 100 to 900°C, J. Res. NBS 71C, 255 (1967).

[4] Powell, R.W., Ho, C.Y., and Liley, P.E., Thermal Conductivity of Selected Materials, NSRDS-NBS 8 (Nov., 1966).

[5] Adams, R.K., and Davisson, E.G., "Smoothed Thermocouple Tables of Extended Significance (°C), Chromel-Constantan Thermocouples," ORNL-3649, vol. 2, Sec. 2.6.

[6] Powell, R.L., and Sparks, LL., Final Report on Thermometry Project, NBS Report 9249 (June, 1966).

[7] Flynn, D.R., private communication.

[8] Powell,R.W., Tye, R.P., and Woodman, M.J., The Thermal Conductivity of Pure and Alloyed Aluminum, I. Solid Aluminum as a Reference Material, Advances in Thermophysical Properties at Extreme Temperatures and Pressures, ASME, pp. 277-288 (1965).

[9] Moore,J.P., McElroy, D.L., and Barisoni, M., Thermal Conductivity Measurements between 78 and 340°K on Aluminum, Iron,Platinum and Tungsten, Proceedings of the Sixth Conference on Thermal Conductivity, pp. 737-778 (1966).

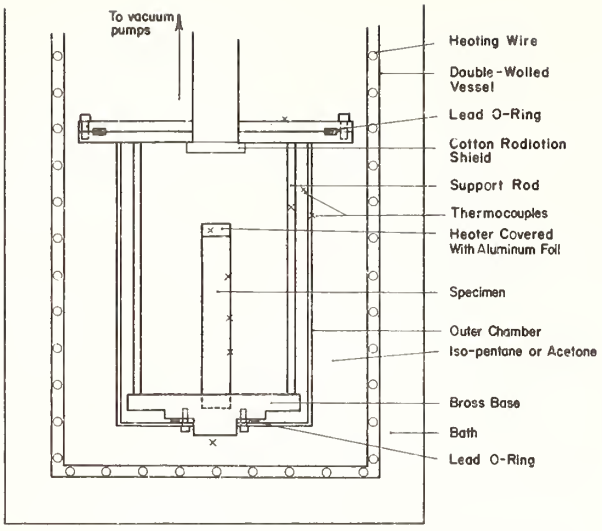

Figure 1. TPRC low temperature apparatus.

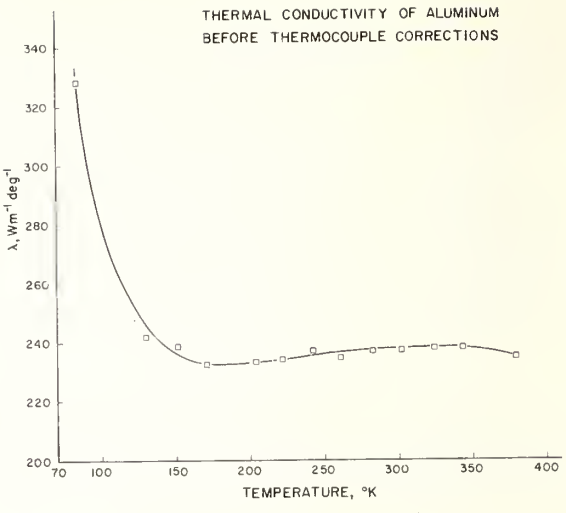

Figure 2. Thermal conductivity of aluminum before thermocouple corrections.

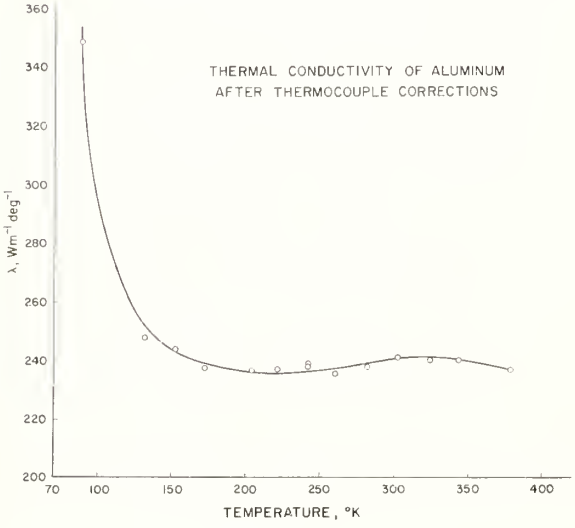

Figure 3. Thermal conductivity of aluminum after thermocouple corrections.

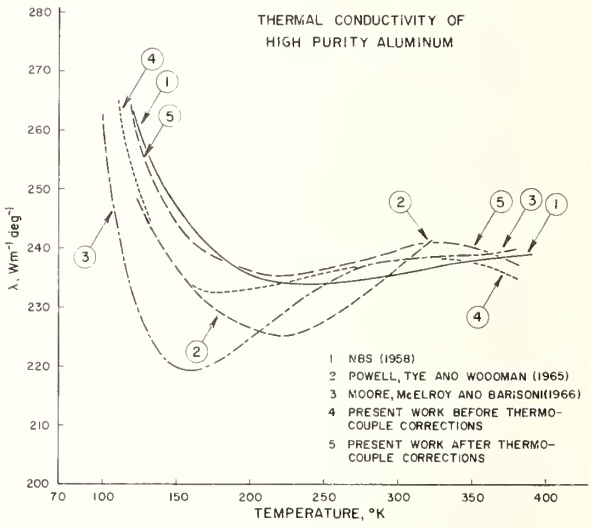

Figure 4. Thermal conductivity of high purity aluminum.

Physical Properties of Chromium from 77 to 400 °K[1]

J. P. Moore, R. K. Williams, and D. L. McElroy

Metals and Ceramics Division, Oak Ridge National Laboratory
Oak Ridge, Tennessee 37830

The electrical resistivity, thermal conductivity, and absolute Seebeck coefficient of two high-purity chromium specimens were measured from 77 to 400 °K. No anomaly was observed in any of these properties in the region of 122 °K, where a local minimum occurs in the elastic constants. At the Néel temperature the Seebeck coefficient and the electrical resistivity drop sharply and the thermal conductivity has a broad shallow minimum. In addition, the electrical resistivity between 310 and 317 °K was also found to be sensitive to temperature gradients. Within experimental accuracy limits, these properties do not show hysteresis near the Néel temperature on thermal cycling from 77 to 400 °K.

Key Words: Electrical resistivity, thermal conductivity, Seebeck coefficient, chromium, Lorenz function, Néel temperature.

1. Introduction

Many properties of chromium have been investigated in the vicinity of the antiferromagnetic-paramagnetic transition at approximately 312 °K. Bolef and De Klerk [1][2] have observed local minima in the elastic constants at 120 and 310 °K as well as a deep local minimum in the coefficient of thermal expansion at 310 °K. Magnetic susceptibility measurements by Collings et al. [2] indicate a local maximum at 312.2 ± 0.5 °K and Beaumont et al. [3] report a peak of about 2.5% in the specific heat at 311.7 °K.

Arajs et al. [4] have measured the electrical resistivity of a chromium single crystal from 4 to 330 °K. Their results do not indicate an anomaly in ρ around 120 °K but do show a distinct local minimum at the Néel temperature, T_N. Their results show some hysteresis at the Néel temperature presumably caused by thermal cycling between 4.2 and 370 °K.

The thermal conductivity (λ) of chromium has been measured above 323 °K by Powell and Tye [5] and by Lucks and Deem [6] and below 150 °K by several investigators including Harper et al. [7]. There has not, however, been a careful study of the λ behavior at the Néel temperature nor do any measurements exist between 150 and 300 °K to connect smoothly with high- and low-temperature data.

The experiment described in this paper was initiated to measure the electrical resistivity, the thermal conductivity, and the absolute Seebeck coefficient(S) of chromium simultaneously from 77 to 400 °K. We were especially interested in the exact behavior of λ at the Néel temperature since the ρ data of Arajs et al. [4] indicate a local minimum might occur in λ if the electronic component of λ were dominant.

2. Specimen Characteristics

Two samples, designated A and B, were used for this study. Iodide chromium crystals, purchased from the Chromalloy Corporation, West Nyak, New York, were used as the starting material for both

[1] Research sponsored by the U.S. Atomic Energy Commission under contract with the Union Carbide Corporation.

[2] Figures in brackets indicate the literature references at the end of this paper.

samples. The samples were produced by different techniques and different lots of crystals were used. Sample A was produced by compacting the cleaned crystals, sealing them in an evacuated steel jacket and hot extruding the assembly. The extrusion, which was carried out at the Battelle Memorial Institute, Columbus, Ohio, was recommended as the best available method for producing dense, high-purity, polycrystalline chromium. The extruded rod produced by BMI was 60 cm long and 1.6 cm in diameter. The second sample (B) was produced in our laboratory by inert gas tungsten electrode arc melting. In this method the crystals are first consolidated into a disc-shaped ingot and this ingot is drop-cast into a rod. The rod produced by this method was approximately 15 cm long and 1.6 cm in diameter.

Both samples, which were 7.7 cm long by 0.96-cm diameter, were machined from the two large diameter rods that yielded extra samples for chemical and metallographic evaluation. A summary of the chemical analysis is shown in table 1. These results indicate that both samples were 99.98+% pure and the

Table 1. Chemical analysis of chromium specimens

Element	Sample A (Extruded)	Sample B (Cast)	Manufacturing Analysis Crystals for Sample B (Lot 613)
	Semi-quantitative spectrographic analysis – ppm		
Ag	1	<0.5(a)	
Al	x(b)	x	0.3
As	1	<0.1	
Au	x	x	
B	3	1	
Ba	2	<0.5	
Be	x	x	
Bi	<0.4	<0.4	
Ca	6	0.6	0.1
Nb	0.4	0.2	
Cd	<0.8	<0.8	
Co	<0.3	3	
Cu	2	5	0.1
Fe	30	3	18
Ga	<20	<20	
Ge	<0.2	<0.2	
Hg	<1	<1	
In	<0.2	<0.2	
K	0.4	4	
Li	<0.1	<0.1	
Mg	<20	<0.2	0.3
Mn	10	0.3	0.1
Mo	<0.5	8	
Na	<0.2	<0.2	
Ni	<0.5	5	0.3
P	<1	<0.1	
Pb	2	<0.8	
Pd	<1	<1	
Pt	<10	<3	
Rn	<0.1	<1	
Ru	<1	<1	
Sb	<1	<1	
S	15	5	
Si	5	5	<10
Sn	<1	<1	
Sr	<0.5	<2	
Ta	x	x	
Te	<1'	<1	
Ti	0.5	0.1	
Tl	<1	<1	
U	<1	<1	
V	3	3	0.3
W	<1	<1	
Zn	<2	<2	
Zr	<1	<1	
calculated			

Element	Sample A (Extruded)	Sample B (Cast)	Manufacturing Analysis Crystals for Sample B (Lot 613)
		Vacuum Fusion Analysis — ppm	
H	5	9	0.2
N	3	28	0.1
O	14	6	5
		Combustion Analysis — ppm	
C	70	60	10
		Resistivity ratio	
$\rho_{273}/\rho_{4.2}$	280	58	

(a) Detection limit — all elements quoted as < ppm.
(b) Masked.

----------chemical differences between the two specimens are rather small. The manufacturers analysis of the iodide chromium crystals which were used for sample B are also included, and the differences between these results and the corresponding values for the casting may be due to contamination during processing. The electrical resistivity ratios, $\rho_{273\ ^\circ K}/\rho_{4.2\ ^\circ K}$ are also shown in table 1. For many metals, values of this ratio give a qualitative indication of the specimen purity, but magnetic phenomena are known to cloud this interpretation [8] in iron. The antiferromagnetic behavior of chromium might also cause difficulties but this point does not seem to have been studied. If this possibility is discounted or assumed to produce a constant effect for both specimens, the data indicate that sample A was significantly superior to sample B. This conclusion does not correlate with the chemically analyzed total impurity contents.

Figures 1 and 2 show that the microstructures of the two specimens were quite different. Longitudinal and transverse sections of a sample corresponding to specimen A were examined, and transverse sections from both ends of sample B were viewed. All of the sections were studied in the as-polished and etched conditions. Examination of the polished sections showed that only a few (<0.1 vol %) small inclusions were present in the samples. There appeared to be some tendency for the inclusions to favor grain-boundaries and, in sample A, a few longitudinal stringers of inclusions were observed. Etching revealed that the grain sizes of the two specimens were quite different. Specimen A had a fairly uniform, fine-grained structure and this observation, along with some evidences of grain growth phenomena indicate that no residual plastic deformation was present. Sample B had very coarse grains and some evidence of subgrain formation could be detected near the centers of the sections. Radial and axial grain size variations were present in this sample but these variations were much smaller than the difference between the grain sizes of samples A and B. Hardness and grain-size measurements were also obtained and are summarized in table 2. The hardness measurements give another indication of sample quality and the values for sample A, which agree well with reported values for recrystallized iodide chromium (see Edwards et al. [9]), also indicate that the samples were well annealed. The densities of the specimens were obtained by the immersion method, using distilled, degassed water. Samples A and B were found to have densities of 7.19 and 7.15 g/cm^3, and it is presumed that the 0.6% difference was due to the presence of voids in the cast sample (B). The value for

Table 2. Summary of Hardness and Grain Size Results for Chromium Samples

	Hardness Number kg/mm^2 (Diamond pyramid, 1 kg load)	Average Grain Diameter (microns)
Sample A — Longitudinal	121	63
Transverse	120	
Sample B — Transverse — Top	123	840
— Bottom	123	440

sample A is less than the x-ray density (7.22 g/cm^3) [10], but is in agreement with a value tabulated for polycrystalline chromium [11]. No voids were observed during the microscopic examination of the samples, but a single void was present at one end of the cast sample. The specimen heater was wrapped on this end of the specimen so that it would not affect the results.

3. Apparatus Description

A guarded-longitudinal technique described by Moore et al. [12] was used to determine ρ, S, and λ over the temperature range from 77 to 400 °K. This technique has most probable errors of ±0.38%, ±2.0%, and ±1.2% for ρ, S, and λ, respectively.

The absolute Seebeck coefficient of Cr-A was determined by measuring the emf between the Constantan legs of the two Chromel-Constantan thermocouples and using a calibration curve relating the Constantan to platinum. The absolute Seebeck of platinum as determined by Cusack and Kendall [13] was then used to calculate the absolute Seebeck coefficient of Cr-A. This method was also used on Cr-B; but, in addition, two platinum wires were attached to the sample near the thermocouple junctions to enable measurements of the Seebeck coefficient with respect to platinum directly.

4. Presentation of Results

4.1 Electrical Resistivity

Smoothed values of ρ, λ, and S are given in table 3 for both chromium samples. The electrical resistivity from 4.2 to 375 °K is shown in figure 3. The electrical resistivity of both samples increases with increasing temperature up to the antiferromagnetic-paramagnetic transition at the Néel temperature of about 311 °K. The ρ of each specimen has a distinct local maximum and minimum in the region of the Néel temperature. Values obtained on Cr-A in the vicinity of 122 °K indicate that the possible spin flip which occurs around 122 °K does not have a noticeable effect on ρ.

Table 3. Smoothed values of ρ, S, and λ for chromium

	Chromium A (a)			Chromium B (a)		
T(°K)	$\rho \times 10^8$ (Ω-m)	$\lambda \times 10^{-2}$ W m^{-1} deg^{-1}	S(μV deg^{-1})	$\rho \times 10^8$ (Ω-m)	$\lambda \times 10^{-2}$ (W m^{-1} deg^{-1})	S(μV deg^{-1})
80	0.860	-	-	1.060	-	-
90	1.225	1.697	3.48	1.445	1.522	5.27
100	1.630	1.593	3.95	1.860	1.453	5.45
120	2.605	1.439	4.97	2.860	1.343	6.04
140	3.760	1.327	6.25	4.050	1.259	7.06
160	5.000	1.241	7.85	5.295	1.187	8.55
180	6.315	1.171	9.92	6.575	1.122	10.62
200	7.545	1.111	12.42	7.830	1.066	12.92
220	8.790	1.061	15.16	9.100	1.020	15.70
240	10.015	1.019	18.13	10.300	0.983	18.30
260	11.095	0.984	20.52	11.385	0.954	20.58
280	12.030	0.957	22.00	12.270	0.930	21.90
300	12.710	0.935	21.63	12.880	0.915	21.65
304	12.792	0.934	21.40	12.946	0.915	21.25
306	12.813	0.934	21.20	12.961	0.916	20.95
308	12.816	0.934	20.80	12.958	0.916	20.50
310	12.791	0.934	20.10	12.931	0.916	19.83
312	12.772	0.934	19.40	12.900	0.916	19.00
314	12.780	0.934	18.75	12.898	0.917	18.60
316	12.808	0.934	18.50	12.940	0.918	18.40
320	12.925	0.934	18.20	13.080	0.918	18.20
340	13.605	0.932	17.65	13.765	0.917	17.60
360	14.340	0.928	17.20	14.470	0.913	17.16
380	15.085	0.920	16.80	15.200	0.906	16.77
400	15.845	0.910	16.42	15.935	0.900	16.41

(a) The smoothed ρ and λ data have not been corrected for thermal expansion. Over the range from 80 to 400°K the correction would amount to less than 0.1%.

The ρ of Cr-A is lower than that of Cr-B over the entire temperature range. The difference amounts to about 13% at 100°K and decreases to 0.6% at 400°K. This difference cannot be explained in terms of normal specimen characteristics such as impurity content or density since the two specimens are quite similar in those respects. If anything, Cr-A has a slightly higher total impurity concentration than Cr-B and this is in the wrong direction to explain the ρ difference. The relative grain sizes of the two samples is also in the wrong direction to have a pertinent effect.

The region around the Néel temperature is shown in greater detail in the inset of Fig. 3. In contrast to the results obtained by Arajs et al. [4] on a single crystal of chromium, our results show no hysteresis outside our maximum imprecision (±0.1%). During one heating cycle, Arajs et al. observed a 3% decrease in ρ at the Néel temperature and a 1.3% decrease on a subsequent heating cycle and this compares to the 0.5% decrease observed in our samples when the specimen had a 0.014 °K m^{-1} gradient and about 1% when the specimen was isothermal.

From 310 to 317 °K the electrical resistivity is sensitive to the presence of a temperature gradient. The results indicated by the solid line were obtained simultaneously with the λ and S measurements when a 0.014 °K m^{-1} gradient existed along the rod.[3] The dashed line for each specimen denotes measurements obtained when the sample was isothermal. The difference between the two curves for each specimen was a maximum of about 0.4% at 312.9 °K. The ρ data obtained with a gradient can be explained to within 0.2% based on an averaging of the isothermal ρ curve. Possibly, if we could reduce the maximum imprecision on each curve (about ±0.1% for this data), the difference might be totally attributable to a gradient averaging. At all other temperatures, that is, below 310 °K and above 317 °K, the results were not sensitive to the presence of a thermal gradient.

Since the thermal gradient was generated with a radially wound heater on one end of the specimen, a small longitudinal magnetic field was unavoidably applied to the specimen while the gradient was present. To insure that the small magnetic field was not causing the apparent resistivity difference, we applied an external magnetic field to Cr-B and took ρ data while the sample was isothermal. Although the external field was some 25 times the field from the specimen heater, the isothermal ρ data was unchanged. We feel, therefore, that the small magnetic field present when there was a gradient along the rod had a negligible effect on the results.

The electrical resistivity of our Cr-A is compared to the results of previous investigators in figure 4. This figure shows the difference in ρ between the other measurements and our results on Cr-A as a function of temperature. Many of the existing ρ data on chromium are very high due to low sample density and/or impurity content and we have not considered these data in making this comparison plot.

The ρ of Cr-A is lower than any chromium reported-to-date except for one run by Arajs et al. [4] which crosses the base line above 300 °K. The ρ of chromium definitely does not obey Matthieson's rule since none of the curves are parallel. The relative behavior of the various results is rather amazing if we generously assume that the results are all accurate. The two sets of data which behave most remarkably are the results of Powell and Tye [5] and Arajs et al. [4]. Powell and Tye's results on their high density electrodeposited sample (annealed at 1410 °C) are in good agreement with our results at low temperatures but are about 8% higher than ours above 300 °K. Conversely, the data of Arajs et al. are extremely high at low temperatures and almost converge with ours above 300 °K. Data reported by White and Woods [14] on an annealed, recrystallized sample are in very good agreement with our results on Cr-A below 100 °K but are higher above 100 °K. The data reported by White and Woods were obtained from sample 5 studied by Harper et al. [7]. There are two curves on figure 4 representing data obtained by De Morton [15] on a heavily cold-worked chromium wire and the same wire after annealing at 700°C in a vacuum of 2×10^{-4} mm of mercury. De Morton's data indicated that ρ of the annealed chromium was higher than ρ of the cold worked chromium below the Néel temperature. Above the Néel temperature the cold-worked chromium had the higher electrical resistivity. This behavior appears anomalous especially considering the results which Harper et al. [7] obtained on cold-worked chromium specimens. Their data showed that ρ at 4.2 °K decreased from 0.255×10^{-8} Ωm for a cold-worked sample to 0.055×10^{-8} Ωm for an annealed fully recrystallized sample. There is a possibility that De Morton's wire sample became contaminated during the annealing in the relatively poor vacuum which could possibly have caused an upward shift of the annealed sample ρ over the entire temperature range. A sample diameter decrease due to chromium evaporation could also cause the same effect.

4.2 Seebeck Coefficient

The absolute Seebeck coefficient for both chromium samples is shown in figure 5. The coefficient for both specimens shows a rapid increase with increasing temperature up to about 287 °K where the

---

[3] The smoothed values of ρ in table 3 represent results obtained with a thermal gradient.

values reach a maximum. A continuous decrease of about 20% occurs in the region of the Néel temperature. There is a large difference between the two samples at low temperatures but this difference disappears above 250 °K. The difference in S at low temperatures is consistent with the ρ difference in reflecting an impurity-like effect. The lower curve in figure 5 represents data obtained by Potter [16] on a chromium of unspecified character.

4.3 Thermal Conductivity

The thermal conductivity results for Cr-A and Cr-B are shown in figure 6. The thermal conductivity of both specimens decreases with increasing temperature to 300 °K where a broad shallow minimum is observed. Above 340 °K λ decreases slowly with increasing temperature. The many data points taken on Cr-A in the region of 122 °K indicate that any anomaly in λ was less than the maximum imprecision (≈ ±1/4%) of the measurements. The λ results from the two specimens differ by about 11% at 90 °K and 1.1% at 400 °K with Cr-A being higher over the entire temperature range. The large difference between the two samples at 90 °K and the convergence at higher temperatures appears to reflect an impurity concentration effect. We attempted to measure with a very small gradient to determine if λ was sensitive to the thermal gradient in the vicinity of the Néel temperature. With the markedly reduced gradient, however, the λ results were too imprecise to resolve a 0.4% difference.

Our results are compared to those of previous investigators with a percentage deviation plot in figure 7. Our λ results on Cr-A, which are used for a basis, are higher than any reported data on chromium. The only high-temperature data which overlaps our measurements are those of Powell and Tye [5]. At 323 °K their results on a high-density electrodeposited sample of chromium are about 8% below λ of Cr-A. If the electronic component of λ were dominant, this difference would be expected since their reported ρ on the same sample is about 8% higher than the ρ of Cr-A. The comparison plot includes three sets of data obtained by Harper et al. [7] on chromium specimens with various amounts of cold working. Although their low-temperature λ results (<50 °K) relate well with the sample residual resistivities (ρ_o = electrical resistivity at 4.2 °K), the λ results which overlap our measurement range do not. Their specimen with the lowest ρ_o has the lowest measured values of λ from 90 to 120 °K.

5. Discussion of Results

5.1 Seebeck Coefficient

The various aspects of the Seebeck coefficient results can be discussed with respect to the equation[4]

$$S = \frac{\pi^2}{3}\frac{k^2}{e} T \left[\frac{1}{\sigma(\epsilon)}\frac{\partial\sigma(\epsilon)}{\partial\epsilon}\right]_{\epsilon = \zeta} \qquad (1)$$

given by Ziman [17] where k is Boltzmann's constant, e is the electronic charge, T is the absolute temperature and σ(ε) is the electrical conductivity if the Fermi energy were ε and ζ is the Fermi energy. Ziman [17] and Fulkerson et al. [18] have shown that this equation can be extended to explain the deviations between the S values of the samples at low temperatures and their convergence with increasing temperature in terms of the ρ differences. They obtain

$$\Delta S \approx -\frac{\pi^2 k^2 T}{3e}\left(\frac{\partial \ell n\, \Delta\rho}{\partial\epsilon}\right)_{\epsilon = \zeta}\frac{\Delta\rho}{\rho_r} \qquad (2)$$

where, in this case, Δρ is the resistivity difference between Cr-A and Cr-B and ρ_r is the resistivity of Cr-A. Since $\frac{\Delta\rho}{\rho_r}$ decreases with increasing temperature, the convergent behavior of the S values with increasing temperature is not surprising. Fulkerson et al. [18] present S data on two iron samples of different purity which behave similarly.

---

[4] Actually eq (1) is not valid at low temperatures ($T < \theta_D$ where θ_D is the Debye temperature). Ziman [17] gives a low-temperature expression for S which depends on the Lorenz function and approaches eq (1) only when L approaches L_o (2.443×10^{-8} V^2 $°K^{-2}$). In view of this we shall limit our use of eq (1) to a comparison of the two chromium samples.

Fine et al. [19] obtained S results by taking the first derivative of a curve for the total emf of chromium vs platinum and they indicate a discontinuity in S at T_N. Our S data are not sufficient to indicate whether or not S is discontinuous at the Néel temperature. The measured values indicate that S is continuous but this may only be apparent since the thermal gradient necessary for measuring S dictates the measurement of an average S over a small temperature range. With a gradient as small as 0.014 °K m^{-1} (about 5 °K between the two measuring thermocouples) S still appeared to be continuous; however, the decrease was as much as 5% in one degree of temperature change. In addition, there may be an unresolvable effect of the thermal gradient on S analogous to the ρ results.

5.2 Thermal Conductivity

The total thermal conductivity of a metal can be expressed as

$$\lambda = \lambda_e + \lambda_g \tag{3}$$

where λ_e is the component carried by the electrons and therefore related to the electrical conductivity, $\sigma = \frac{1}{\rho}$, and λ_g is the component associated with the lattice vibrations. The electronic component can be related to ρ with the Lorenz function L to yield

$$\lambda = \frac{LT}{\rho} + \lambda_g \, . \tag{4}$$

Several values for the Lorenz function (L) have been theoretically predicted. The Sommerfeld value ($L_o = 2.443 \times 10^{-8}$) should apply to a completely degenerate electron gas at high temperatures and seems to be reasonably well attained in the alkali and noble metals. In transition metals, however, the validity of L_o is in doubt and several possible reasons for high-temperature deviations have been suggested. These have been discussed by Fulkerson and Williams [20]. Since the expression for L obtained from solution of the Boltzmann equation is an infinite series, higher order terms above the first term (L_o) may be nonnegligible. Keeping the first three terms, L can be written for high temperatures as

$$L = L_o - S^2 + \frac{8\pi^4}{45} \frac{k^4 T^2}{e^2} \frac{1}{\sigma(\epsilon)} \frac{\partial^2 \sigma(\epsilon)}{\partial \epsilon^2}\bigg|_{\epsilon = \zeta} \tag{5}$$

Thus a value for L above or below L_o could occur depending on the sign and magnitude of $\frac{\partial^2 \sigma(\epsilon)}{\partial \epsilon^2}\Big|_{\epsilon = \zeta}$. If λ_g is assumed to be zero and an experimental L calculated using experimental data for ρ and λ and eq (4), we find that the experimental L is 3.95×10^{-8} at 300 °K. This is much greater than the value of L_o and indicates that $L > L_o$ and/or λ_g is not negligible.

Values of λ_g have been calculated by Fulkerson [21] using a modified Leibfried-Schlömann [22] equation to account for the three phonon Umklapp thermal resistivity and an equation from Ziman [17] to account for the electron-phonon thermal resistivity. The most significant aspect of the calculations is that λ_g can vary from almost zero to values higher than λ. Thus, this approach seems futile for determining λ_g and λ_e.

Fulkerson and Williams [20] outline an approach which involves fitting experimental ρ and λ data to eq (4) with the assumptions that L is constant and

$$\lambda_g = \frac{A}{T} \tag{6}$$

or

$$\lambda_g = \frac{B}{T} + \frac{C}{T^2} \, . \tag{7}$$

Equation (6) is of the form predicted by the modified Leibfried-Schlömann equation and eq (7) is of the form experimentally observed on many electrical insulators. If we assume that λ_g is given by eq (6), then eq (4) becomes

$$\lambda T = \frac{LT^2}{\rho} + A \ . \tag{8}$$

This equation indicates that a plot of λT vs T^2/ρ would be useful in determining an experimental value for L and A. This type plot is shown in figure 8 for chromium. The high-temperature data of Powell and Tye on their sample annealed at 1410 °C is also plotted. From 200 to 1300 °K all points are within ±3% of the straight line which yields $L \approx 2.80 \times 10^{-8}$ and $A = 8000$ W m^{-1}. These values are similar to ones obtained on W by Fulkerson and Williams [20]. The above result for A indicates that at 300 °K, $\lambda_e \approx 66.8$ W m^{-1} and $\lambda_g \approx 26.7$ W m^{-1}. To look at the behavior of L at T_N (where the actual data shows a small deviation from the line in figure 8) we have calculated L for Cr-A using eq (8) with an A of 8000 W m^{-1} and an A of zero corresponding to a λ_g of zero. The results are shown in figure 9. Although the value of L is definitely in severe doubt because of the uncertainty in λ_g, a distinct slope change occurs in L when we assume a smooth behavior for λ_g. We could just as well assume a smooth or constant value for L and calculate a λ_g which would show a large slope change at T_N. This implies that the Lorenz function and/or λ_g must be irregular at T_N.

To obtain a better idea of the location of T_N of Cr-A we have calculated the first derivative of each property with respect to temperature and plotted the results in figure 10. Hall coefficient data from De Vries and Ratherau [23] were used to calculate $\Delta R_H/\Delta T$. The slopes of all the properties have extreme values between 309 and 311 °K with the exception of the isothermal σ data which appears to peak at 311.5 °K. This indicates that the Néel temperature location can be determined most easily by observing the derivative of the property with respect to T as a function of T. The range of temperature for the maximum slope change for S, L, and the σ data obtained during gradient conditions may be caused by the presence of the thermal gradient and this somewhat complicates location of T_N.

The large difference in the properties of the two chromium samples at low temperatures is not understood. All the ρ and λ data indicate that Cr-A is superior to Cr-B in being closer to an ideal, defect-free material. The chemical analysis, however, indicates that Cr-B has lower total impurity concentrations than Cr-A so that this does not appear to be a factor. The difference in the properties cannot be attributed to cold working effects since Cr-B was obtained from a casting and Cr-A was hot extruded and the hardness of both specimens was consistent with values for well annealed chromium. There are two possible reasons for the discrepancy. There might be a particular impurity present in Cr-B (N_2 possibly) which has a large effect on the transport properties, or the impurities might be in solution in Cr-B and in fine precipitates in Cr-A. We plan to investigate this problem further with a series of heat treatment experiments on the two samples.

Based on these differences we are not convinced that our results, even on Cr-A, are representative of those of ideal high-purity chromium, although the results do indicate that Cr-A is the best sample studied to date.

6. Conclusions

The results of ρ, λ, and S measurements on the two chromium specimens permit the following conclusions:

1. Although the two chromium samples used for this study were almost identical chemically, their properties differ significantly at low temperatures.

2. The electrical resistivity has a local maximum and minimum at T_N. The ρ of both samples of chromium was sensitive to the presence of a thermal gradient from 310 to 317 °K. The ρ of the chromium samples does not obey Matthieson's rule.

3. There was no hysteresis observed in ρ, λ, or S around T_N on thermal cycling between 77 and 400 °K.

4. The Seebeck coefficients of both chromium samples are large and positive and both exhibit a sharp decrease at T_N.

5. The thermal conductivity of chromium decreases with increasing temperature and has a broad shallow minimum at T_N. The lattice component of λ is probably significant in magnitude compared to λ_e.

6. The first derivatives of S, $\frac{1}{\rho}$, and L with respect to temperature have extreme values at the Néel temperature. This appears to be the most sensitive approach for determining T_N from transport property data.

7. The behavior of λ at T_N cannot be explained in terms of the ρ behavior assuming a uniform behavior for L and λ_g at T_N. Thus L and/or λ_g must be irregular at T_N.

7. References

[1] Bolef, D. I. and De Klerk, J., Phys. Rev. 129(3), 1063 (1963).

[2] Collings, E. W., Hedgcock, F. T. and Siddiqi, A., Phil. Mag. 6, 155 (1961).

[3] Beaumont, R. H., Chihara, H. and Morrison, J. A., Phil. Mag. 5, 188 (1960).

[4] Arajs, Sigurds, Colvin, R. V. and Marinkowski, M. J., J. Less Common Metals 4, 46 (1962).

[5] Powell, R. W. and Tye, R. P., J. Inst. Metals 85, 185 (1957).

[6] Lucks, C. F. and Deem, H. W., WADC TR 55-496 [AD 97 185].

[7] Harper, A. F. A., Kemp, W. R. G., Klemens, P. G., Tainsh, R. J. and White, G. K., Phil. Mag, 2, 577 (1957).

[8] Schindler, A. I. and La Roy, B. C., J. Appl. Phys. 9(37), 3610 (1966).

[9] Edwards, A. R., Nish, J. I. and Wain, H. L., Met. Rev. 4(16), 403 (1959).

[10] American Institute of Physics Handbook, 2nd Ed., 1963, p. 2-20.

[11] Metals Handbook, 8th Ed., 1961, p. 44.

[12] Moore, J. P., McElroy, D. L. and Graves, R. S., Can. J. Phys., Dec. 1967.

[13] Cusack, N. and Kendall, P., Proc. Phys. Soc. (London) 72, 898 (1958).

[14] White, G. K. and Woods, S. B., Phil. Trans. Roy. Soc. London, Ser. A, 251, 273 (1959).

[15] De Morton, M. E., Nature 181, 477 (1958).

[16] Potter, H. H., Proc. Phys. Soc. 53, 695 (1941).

[17] Ziman, J. M., Electrons and Phonons, (Oxford University Press, 1960).

[18] Fulkerson, W., Moore, J. P. and McElroy, D. L., J. Appl. Phys. 37(7), 2636 (1966).

[19] Fine, M. E., Greiner, E. S. and Ellis, W.C., J. Metals, Trans. Met. Soc. AIME 191, 56 (1951).

[20] Fulkerson, W. and Williams, R. K., Proc. Sixth Conf. on Thermal Conductivity, Dayton, Ohio, October 18-22, 1966, p. 807, 1966.

[21] Fulkerson, W., private communication, 1967.

[22] Leibfried, G. and Schlömann, E., Akad. Wiss. Göttingen Mat.-Physik. Kl.IIA, 71 (1954) (translation obtainable from Technical Library Research Service, Purchase Order B4B-60150, Letter Release S-70).

[23] De Vries, G. and Ratherau, G. W., Phys. Chem. Solids 2, 339 (1957).

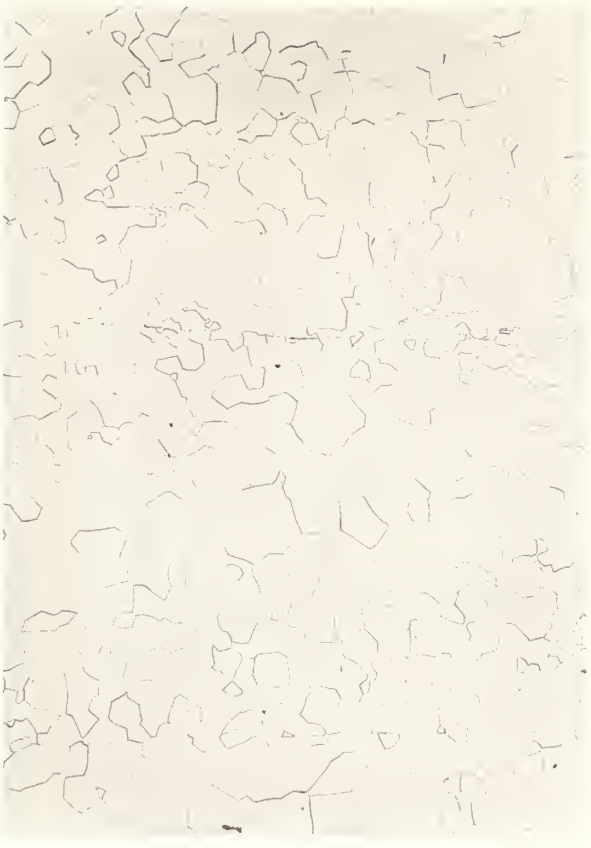

Figure 1. Photomicrograph of Cr-A, 38X, longitudinal section, etchant: 80 ml H_2O, 10 g KOH, 10 g $K_3Fe(CN)_6$.

Figure 2. Photomicrograph of Cr-B, 38X, transverse section, etchant: 80 ml H_2O, 10 g KOH, 10 g $K_3Fe(CN)_6$.

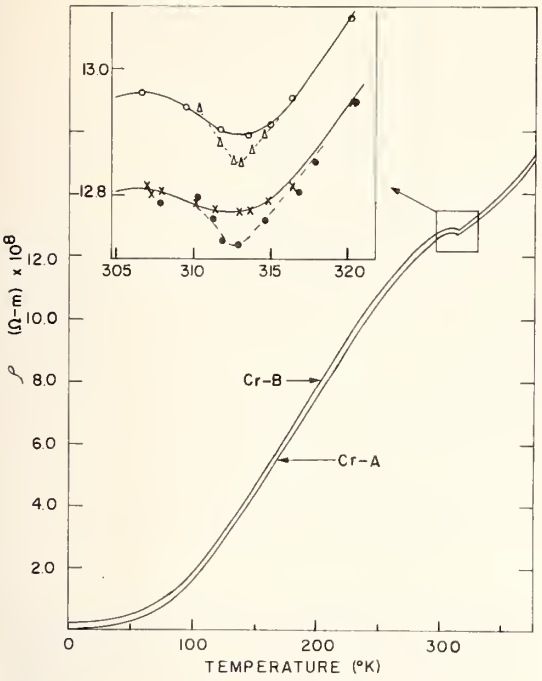

Figure 3. Electrical resistivity of Cr-A, and Cr-B versus temperature. ○: Cr-B with 0.014 $^{o}K\ m^{-1}$ gradient. △: Cr-B isothermal; X: Cr-A with 0.014 $^{o}K\ m^{-1}$ gradient; ●: Cr-A isothermal.

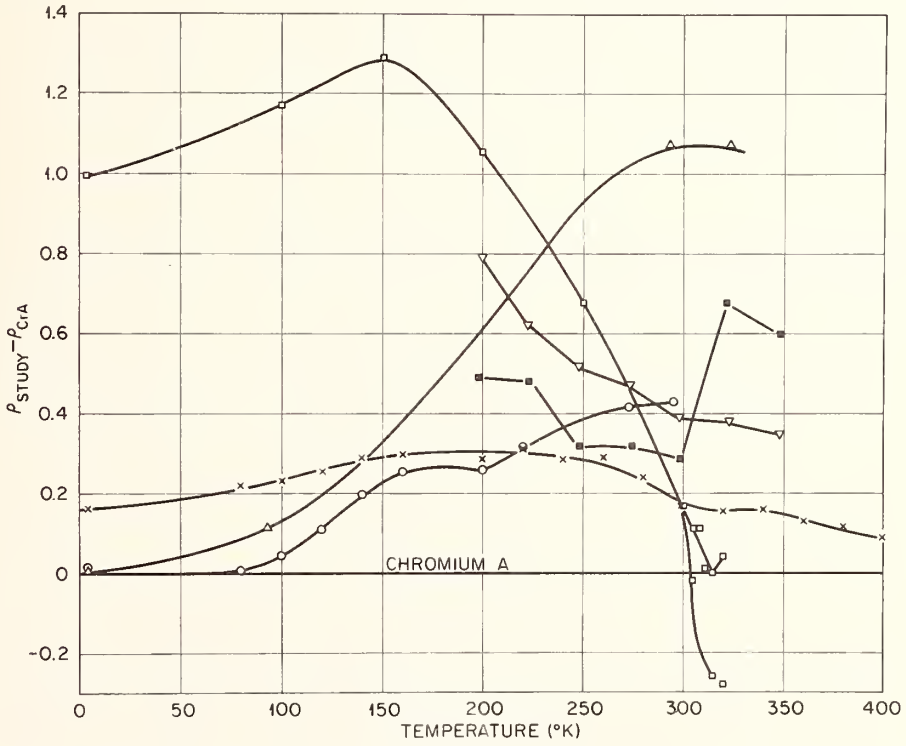

Figure 4. Deviation Plot Showing Difference Between ρ Results of Other Investigators and Cr-A., X:Cr-B; □ :Arajs et al. [4]; △ :Powell and Tye [5]; ○ :White and Woods [14]; ⊠ :De Morton [15] Cold Worked Sample; ▽ :De Morton [15] Sample Annealed at 973 °K for 2 x 10^{-4} mm of Hg.

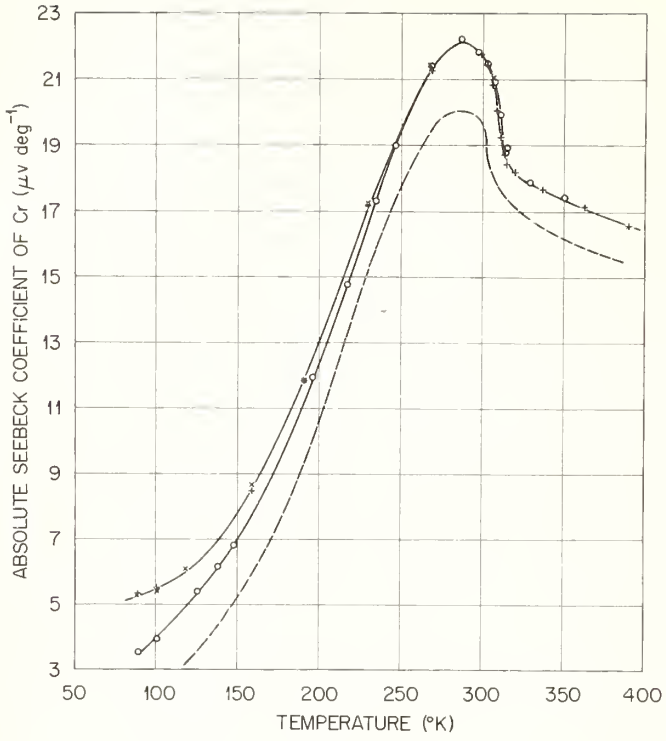

Figure 5. Absolute Seebeck coefficient of chromium. X: Cr-B using constantan leads; + : Cr-B using platinum leads; O : Cr-A using constantan leads; ----: Potter [16].

Figure 6. Thermal conductivity of chromium from 90 to 400 °K. X: Cr-A; O : Cr-B.

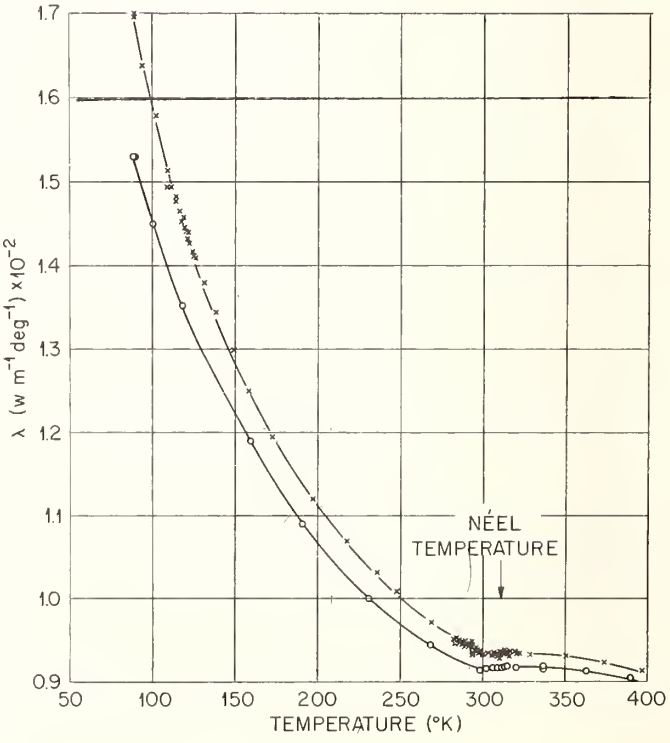

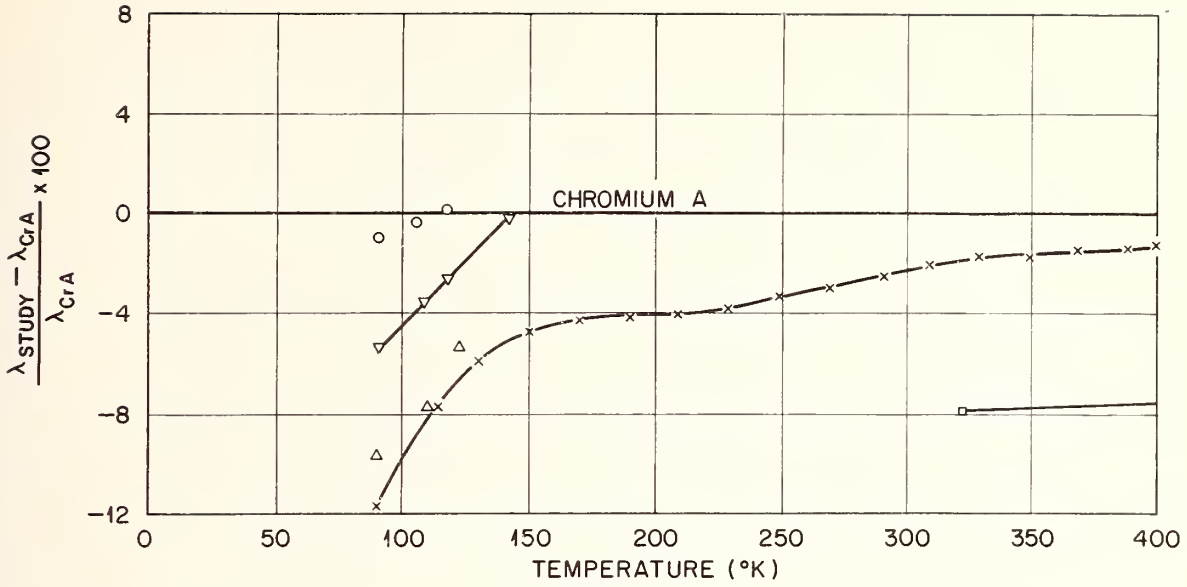

Figure 7. Percentage Deviation of Other λ Results from Results on Cr-A. X:Cr-B; ▽ :Harper et al. [7] on Cold Worked Sample with $\rho_o = 0.255 \times 10^{-8}$ Ωm; ○ :Harper et al. [7] on Cold Worked Sample with $\rho_o = 0.181 \times 10^{-8}$ Ωm; △ :Harper et al. [7] on Annealed Sample with $\rho_o = 0.055 \times 10^{-8}$ Ωm; □ :Powell and Tye [5] on Annealed Electrodeposited Sample.

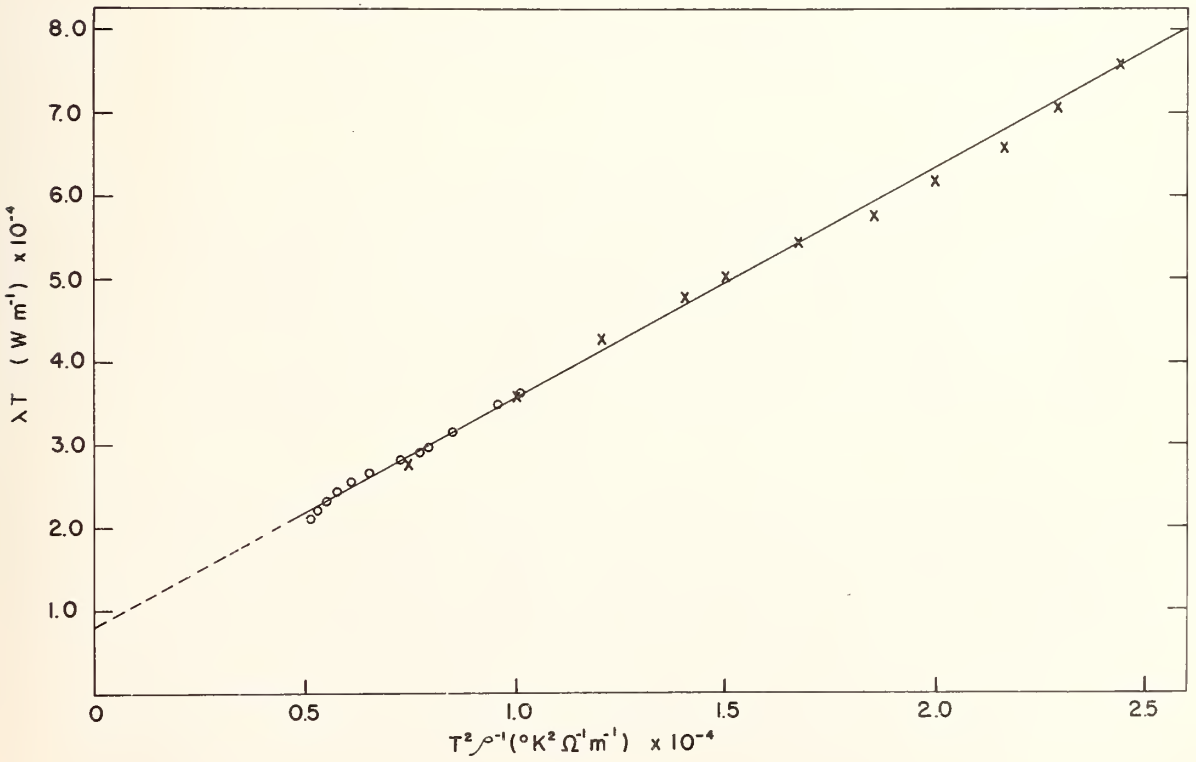

Figure 8. λT versus $T^2\rho^{-1}$ for Chromium; ○ :ORNL Results on Cr-A; X:Powell and Tye [5].

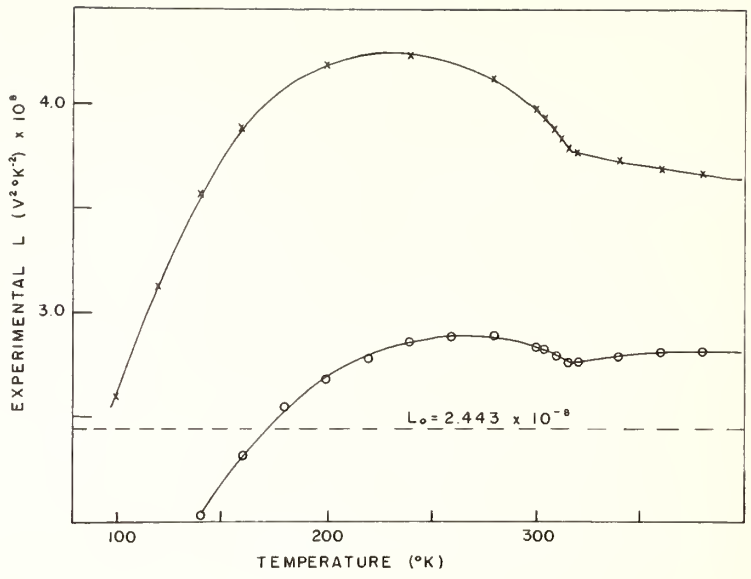

Figure 9. Experimental Lorenz Function for Chromium. X:Calculated using eq (8) with A = 0; O:calculated using eq (8) with A = 8000 W m^{-1}.

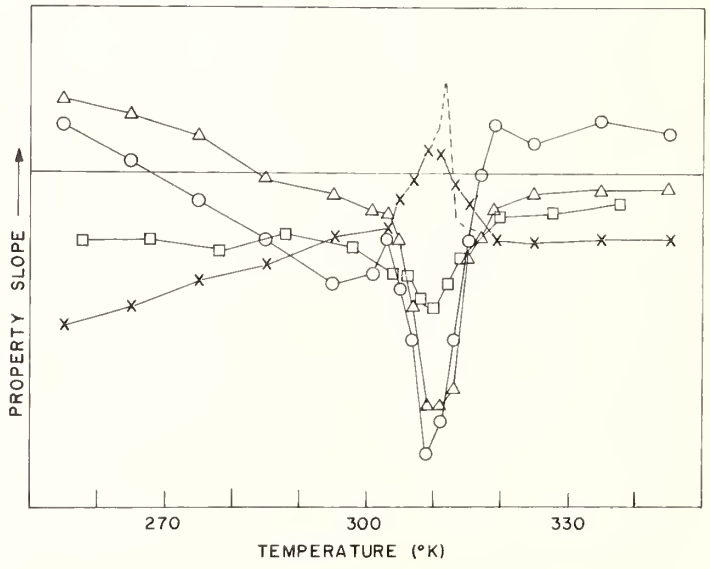

Figure 10. First Derivative of σ,S, L, and Hall Coefficient with Respect to Temperature. □ :Hall coefficient data from De Vries and Ratherau [23]; X: σ of Cr-A when sample under a gradient of 0.014 °K m^{-1}; ------: σ of Cr-A when sample was isothermal; O :Lorenz function from eq (8) with A = 8000 W m^{-1}; Δ :Seebeck coefficient of Cr-A.

The Thermal Conductivity of Chromium Above and Below the Néel Temperature - An Analysis

J. F. Goff[1]

U. S. Naval Ordnance Laboratory
White Oak, Silver Spring, Maryland 20910

Measurements of the thermal conductivity of polycrystalline Cr between 2°K and 290°K indicate that at the higher temperatures it increases. As a result the measured Lorenz No. L shows a T^2 departure from the Sommerfeld value L_o in the temperature range between 120°K and 280°K. The Method of Moments promulgated by Klemens predicts that this departure is due to a second order term in the expansion of the specific conductivity $\sigma(E)$ about the Fermi level. Previous measurements made by Powell and Tye between 323°K and 1273°K found that L was greater than L_o over the whole range of temperature but decreased as the temperature was raised. Consequently ΔL has been calculated for a model in which $\sigma(E)$ has a parabolic well symmetrically arranged about the Fermi level but with a finite width E_o. The calculations give reasonable agreement with the data between 120°K and 1000°K if E_o is allowed to decrease during the antiferromagnetic-paramagnetic change at the Néel temperature. A surprising result is that a parameter of the model - which is related to the constant of the parabolic well - is independent of magnetic changes taking place at the Néel temperature.

Key Words: chromium, electrical resistivity, Lorenz No., Néel temperature, thermal conductivity.

1. Introduction

Both of the most recently reported measurements of the thermal conductivity λ of Cr [1,2][2] indicate that it is anomalously large above 90°K; that is, the Lorenz No. L found from these data is much larger than the expected Sommerfeld value [3] $L = 2.4453 \times 10^{-8} (V/deg)^2$. The low temperature measurements were made on a series of polycrystals between about 2°K and 150°K by Harper et al [1]. Above 90°K the Lorenz No. constructed from their data becomes rapidly greater than L_o. The high temperature measurements were made on a well-annealed, electrolytically deposited sample between 323°K and 1273°K by Powell and Tye [2]. They found that L was anomalously larger over the whole temperature range and attempted to ascribe this anomaly to a lattice component of the thermal conductivity. They concluded that this lattice component would itself have to be anomalously large.

The present measurement [4] of λ and the electrical resistivity ρ over the range 2°K to 291°K confirms this anomaly. At the higher temperatures λ begins to increase, the concomitant L becomes larger than L_o, and this extra $\Delta L = L - L_o$ varies as T^2 between 120°K and 280°K. This temperature dependence is exactly the prediction of the second order extension of the simple theory of electrical conduction which has been made by Klemens [5]. Thus, the purpose of this paper is to show that it is possible to combine these measurements with those of Powell and Tye [2] to develop a model which explains the anomalous thermal conduction without the assumption of a lattice component.

---

[1] Physicist.

[2] Figures in brackets indicate the literature references at the end of this paper.

2. Apparatus

The apparatus has been described previously [6]. The salient features are: 1. A gas thermometer which is used as a calibration standard in the temperature ranges where liquid gas standards are not readily available, 2. a radiation shield which is thermally anchored to the base of the sample so that the thermal environment is nearly the same as the temperature gradient in the sample itself, and 3. electrical connections made of two meter lengths of #40 copper wire thermally anchored to the sample base to minimize conduction losses. Since the previous description [6], there have been four changes made in the apparatus. The sample heater is now a 2000 ohm, ½ watt, metal film resistor which is sealed into a copper block with glyptal enamel. The thermocouple which is used to measure the temperature gradient between 60°K and 300°K has been changed to a Au-2.11 at % Co: Manganin couple to minimize thermal conduction losses. The temperature gradient in the 4°K to 60°K range is measured by two Allen-Bradley 100 ohm, 1/10 watt carbon resistors that are calibrated at 4.2°K and 77°K connected by a straight line on a modified Clement and Quinell plot [7]. Finally, pressure contacts are used in the sample mounting.

The justification of the calibration procedure in the 4°K to 60°K range is threefold. Further calibration of the carbon resistors at lower temperatures against the vapor pressure of liquid He and at higher ones against the gas thermometer indicate a linear Clement and Quinell plot at temperatures up to 120°K. Secondly the data taken with these thermometers at the lower temperatures agree well with the data taken at the higher ones with the thermocouple. Finally, the data taken in this way agree with theoretical predictions.

The data are taken in several ways to obviate systematic errors. No attempt is made to maintain the same size temperature gradient. Some of the data are taken by heating above the liquid He bath and others are taken by allowing the apparatus to drift up in temperature after the bath has boiled away. These data agree with each other within a few percent. The same temperature gradient is used in determining the thermoelectric power of the sample. Since this quantity has a different temperature dependence than λ, it would be difficult for a systematic error to hide in both sets of data. At the very highest temperatures the thermoelectric power measured with this temperature difference agrees with the published data of Møller et al [8] within 1%.

An estimate of radiation losses at the higher temperatures has been made by assuming a gradient between the sample and the radiation shield that is about 10 times the measured gradient. The calculated error in that case is 10% at 300°K and 3% at 200°K. Therefore it is assumed that radiation losses can be ignored.

3. Sample

The sample was cast in an oxygen-free copper boat by melting with an argon arc. It was polycrystalline with a resistivity ratio $\rho(297°K)/\rho(4°K) = 72$. It was annealed in a vacuum at 900°C for 24 hours and then ground to size. The dimensions between thermometers were approximately 4mm x 4 mm x 35mm.

Electrolytic Cr was used. It has been analysed as follows (in weight percent): Cr - 99.92%, Mn - 0.004%, Fe - 0.005%, Mg - 0.002%, Cu - 0.003%, and the balance mostly S, P, Ni, and Mn.

4. Data

4.1 Thermal Conductivity

The thermal conductivity data for this measurement are shown plotted in figure 1 together with those data that have been previously reported for similar samples [1,2]. The lower temperature data were obtained by Harper et al [1] from an as-cast sample with a partial anneal (sample #2). It has a residual resistivity $\rho_o = 1.81 \times 10^{-9}$ ohm-m which is almost the same as that of the present sample for which $\rho_o = 1.83 \times 10^{-9}$ ohm-m. The high temperature data were obtained by Powell and Tye [2] from an electrolytically deposited sample that had been annealed at 1410°C.

Both λ_{max} and ρ_o depend on the quality of the sample. These two quantities are shown plotted against each other in figure 2 where it is seen that the present measurement agrees well in this respect with the data of Harper et al [1]. The reason for the different temperature dependences of the two samples shown in figure 1 is not understood. However, it will be shown that the present data agree with the theoretical

prediction of the temperature dependence of the thermal resistivity [9] due to phonon scattering, w_i.

In an elemental metal of reasonable purity, one expects λ to be due to electrons; that is $\lambda = \lambda_e$. At low temperatures where the electron distribution is surely degenerate the thermal analog to Matthiessen's Rule should hold; the thermal resistance is the sum of the residual and ideal thermal resistivities:

$$w = \lambda_e^{-1} = w_o + w_i \ . \tag{4-1}$$

w_o can be calculated from L_o and the measured value of ρ_o:

$$w_o = (\rho_o/L_o)T^{-1} \ . \tag{4-2}$$

The temperature dependence of w_i separated from w in this way is plotted in figure 3. Between 60°K and 90°K the measured values of $w_i \propto T^2$, the dependence predicted by theory.

Both of these measurements indicate that below 30°K w_i is greater than would be expected, although the temperature dependences differ in the two cases. The source of this extra resistivity is not known and will not be pursued in this paper.

From the point of view of this paper the important phenomenon is the increase of λ above 200°K. It will be shown that this effect is electronic. It is unfortunate that it was not possible to measure through the Néel temperature [10] $T_N = 313.0$°K with the present apparatus because one would like to know if the data would join those of Powell and Tye. It would seem reasonable to expect a discontinuity in λ since one is observed in ρ [11].

4.2. Electrical Resistivity

The electrical resistivity ρ of the sample was measured in the range from 1.2°K to 297°K. The residual resistivity ρ_o was computed to have an average value of 1.834×10^{-9} ohm-m on the basis of nine measurements made between 1.2°K and 12.9°K.

If it is assumed that Matthiessen's Rule holds:

$$\rho = \rho_o + \rho_i \tag{4-3}$$

where ρ_i is the ideal component, it is possible to compute ρ_i from the data. These data are shown in figure 4 as the circles. The solid line comes from the much more accurate data of Arajs and Dunmyre [10]. The agreement between the two sets of data supports the contention that method used to calibrate the carbon resistors at low temperatures is accurate to a fraction of a degree because these same calibrated resistors were used to determine the temperature of the electrical resistivity data.

The temperature dependence of ρ_i shown in figure 4 is completely anomalous. At low temperatures where one expects [12] $\rho_i \propto T^5$, a $T^{3.2}$ dependence is actually found. This latter dependence has been taken to indicate a predominant proportion of inter-band scattering [1]. At the higher temperatures where a T^1 dependence is expected [12], $\rho_i \propto T^{1.8}$. It is not the purpose of the paper to discuss this anomaly, but it seems reasonable to suppose that it indicates a large proportion of electron-electron scattering, which is expected to give a T^2 behavior [13]. The small anomaly occurring at the Néel temperature itself has been well studied [10,11].

4.3. Lorenz Number

The Lorenz No. $L = \lambda\rho/T$ has been computed from values of λ and ρ taken from the best smooth lines drawn through the data. This value is shown in figure 5 along with values for the other two comparable samples [1,2]. The circles are the actual values given by Powell and Tye in their paper [2], while the dashed line was constructed from Harper et al's data [1] for λ and ρ_o and the values of ρ_i shown in figure 4.

In normal metals L is expected to equal L_o whenever there are no other thermal conduction mechanisms and the electronic scattering processes are elastic. The effect of other conduction mechanisms such as lattice conduction is to increase L because then $\lambda = \lambda_e + \lambda_g$. On the other hand the effect of inelasticity is to make $L < L_o$, a condition that obtains generally at intermediate temperatures. In the

present case the behavior of L below 90°K is qualitatively similar to normal metallic behavior with $\lambda = \lambda_e$ only. Now if there is no appreciable lattice thermal conductivity λ_g at these low temperatures, it is unlikely that there would be any at the higher ones because the maximum value of λ_g is expected at approximately $T = \theta/20$ where the Debye temperature [14] $\theta(Cr) = 402°K$. On the other hand Klemens [5] has pointed out that semimetals depart from normal metallic behavior as the temperature increases because the energy KT embraces more of the overlapping band structure. Therefore it is the purpose of this paper to show that the abnormally large values of L above 90°K can be reasonably ascribed to the effects of a semimetallic - or more simply - a complicated band structure. For this purpose it is more instructive to treat ΔL shown in Figure 6. The striking feature is that between about 120°K and 280°K $\Delta L \propto T^2$.

5. Analysis

5.1. Method of Moments

The Method of Moments (hereafter MM) as promulgated by Klemens [5] is a way of treating the electronic Boltzmann equations so that the resulting transport coefficients become expressed in forms that are tractable when applied to substances with complicated Fermi surfaces. The essence of the method is to focus the effect of such complicated surfaces on the integrations over energy that occur in all of the transport integrals. It becomes possible to expand the integrands of these integrals about the Fermi energy and then to allow the data to determine the first derivatives of the expansions.

The MM represents the integration over a constant energy surface by the specific conductivity $\sigma(\epsilon)$ where $\epsilon = E/KT$ is the reduced energy. Then if it is assumed that a relaxation time exists which is the same for both thermal and electrical processes and that the phonon system is in equilibrium, the transport coefficients of interest to this paper become:

electrical conductivity $$\sigma = M_0 \tag{5-1a}$$

thermal conductivity $$\lambda_e = \left(\frac{K}{e}\right)^2 T \left(M_2 - \frac{M_1^2}{M_0}\right) \tag{5-1b}$$

Lorenz No. $$L = \left(\frac{K}{e}\right)^2 \left(\frac{M_2}{M_0}\right) - S^2 \ . \tag{5-1c}$$

M_n is the n'th moment of $\sigma(\epsilon)$.

$$M_n = - \int_{-\infty}^{+\infty} \epsilon^n \sigma(\epsilon) \ \frac{\partial f_o}{\partial \epsilon} \ d\epsilon \tag{5-2}$$

where f_o is the Fermi-Dirac distribution function. It is possible to neglect the S^2 term in eq (5-1c) (and similarly the M_1^2 term in (5-1b)) because $M_2/M_0 > 1$, $(K/e)^2 = 86.3$ μV/deg, and $S_{max}(Cr) = 21$ μV/deg at 300°K [8]. This neglection is about a 6% error. In the following formulae these terms will no longer be included.

In the transport properties of metals one is concerned with the distribution of electrons about the Fermi surface. Therefore this surface is chosen as the energy zero and $\sigma(\epsilon)$ is expanded in a McLauran series about it.

$$\sigma(\epsilon) = \sigma_0 + \sigma_1 \epsilon + \frac{\sigma_2}{2} \epsilon^2 + \frac{\sigma_3}{6} \epsilon^3 + \cdots \tag{5-3}$$

where $\sigma_m = (\partial^m \sigma / \partial \epsilon^m)_0$. If only the first σ_m which makes M_n non-vanishing is retained these coefficients have normal metallic form. If the second non-vanishing term is retained, these coefficients become

$$\sigma = \sigma_0 + \frac{\pi^2}{6} \ \sigma_2 \tag{5-4a}$$

$$\lambda_e \approx \left(\frac{K}{e}\right)^2 T \left[\frac{\pi^2}{3}\sigma_0 + \frac{7\pi^4}{30}\sigma_2\right] \tag{5-4b}$$

$$L \approx \frac{\pi^2}{3}\left(\frac{K}{e}\right)^2 \left(1 + \frac{7\pi^2}{10}\frac{\sigma_2}{\sigma_0}\right) / \left(1 + \frac{\pi^2}{6}\frac{\sigma_2}{\sigma_0}\right) . \tag{5-4c}$$

These formulae are expressed in terms of the reduced energy ϵ; the σ_m depend implicitly on temperature. The temperature dependence of these second order corrections becomes explicit if they are rewritten in terms of the energy E. It is easy to see by comparing expansions of $\sigma(E)$ and $\sigma(\epsilon)$ that

$$(KT)^m \sigma_{mE} = \sigma_m . \tag{5-5}$$

Properly speaking L is not a transport coefficient, but since $L = \lambda\rho/T$ it has the advantage that it has the constant value $L_o = (\pi^2/3)(K/e)^2$ for a normal metal whenever the assumptions made at the beginning of this section apply. Therefore the second order effects are most easily seen in $\Delta L = L - L_o$:

$$\frac{\Delta L}{L_o} = \left(\frac{16}{15}\right)\left(\frac{\sigma_{2E}}{2\sigma_{0E}}\right)(\pi K)^2 T^2 / \left[1 + \frac{\pi^2}{3}K^2\left(\frac{\sigma_{2E}}{2\sigma_{0E}}\right)T^2\right] \tag{5-6}$$

which has a saturation value of 7.815×10^{-8} $(V/deg)^2$, a value which is 3.2 times L_o.

The assumptions made in MM can be expected to apply to metals at temperatures of the order of 100°K or more, and it is seen in figure 6 that the temperature dependence of ΔL is exactly the initial temperature dependence of eq(5-6):

$$\frac{\Delta L}{L_o} \approx \left(\frac{16}{15}\right)\left(\frac{\sigma_{2E}}{2\sigma_{0E}}\right)(\pi K)^2 T^2 \tag{5-7}$$

The quantity $C = (\sigma_{2E}/2\sigma_{0E})$ has been determined from the data to be 195 (electron volts)$^{-2}$. This is a very interesting quantity not only because it is temperature independent below T_n, but it will be shown in the next section that the same number is found from the data above T_n.

5.2 Model

Since second order terms in the $\sigma(E)$ expansion cause $\Delta L > 0$, the non-zero values of ΔL above T_n found by Powell and Tye [2] and shown in figure 6 suggest that these terms still exist at these high temperatures but in a vestigial manner. That is, these second order terms extend only over a limited range of energy E_o; and as the temperature increases the normal portion of $\sigma(E)$ outside this range becomes more important. Therefore the model shown in figure 7 by the solid line is suggested by the data, and ΔL will be calculated for it.

For even values of n the moment integrals of eq (5-2) become

$$M_n = \left\{\sigma_{10}F_n(\epsilon_o) + \sigma_{20}[F_n(\infty) - F_n(\epsilon_o)] + \frac{\sigma_2}{2}F_{n+2}(\epsilon_o)\right\} . \tag{5-8}$$

The $F_n(\epsilon_o)$ are the Fermi-Dirac integrals in the finite interval ϵ_o,

$$F_n(\epsilon_o) = -\int_{-\frac{\epsilon_o}{2}}^{-\frac{\epsilon_o}{2}} \epsilon^n \frac{\partial f_o}{\partial \epsilon} d\epsilon \tag{5-9}$$

It is convenient to define a new function $G(\epsilon_o)$

$$G_n(\epsilon_o) = M_n/\sigma_{10} \tag{5-10}$$

because then σ_{10}, which yields the normal metallic electrical conductivity at low temperatures and so contains unknown temperature dependences implicitly cancels out of L. The transport coefficients are

$$\sigma = \sigma_{10}(T)\, G_o(\varepsilon_o) \tag{5-11a}$$

$$\lambda_e = \sigma_{10}(T)\, T \left(\frac{K}{e}\right)^2 G_2(\varepsilon_o) \tag{5-11b}$$

$$L = \left(\frac{K}{e}\right)^2 \frac{G_2(\varepsilon_o)}{G_o(\varepsilon_o)} \tag{5-11c}$$

These coefficients contain two constants which must be determined from the data. The first, $a = \sigma_{20}/\sigma_{10}$, is the ratio of the zero'th derivitive outside the parabolic well to that inside. The second is the energy width of the well E_o. These constants are related to the quantity C defined by the previous section; $C = 4(a - 1)/E_o^2$.

The model was calculated on the CEIR computor by first computing the $F_n(\varepsilon_o)$ by a three point Gaussian integration with 100 intervals and then storing these in a list to compute $G_n(\varepsilon_o)$ for various values of a. It is somewhat surprising that the $F_n(\varepsilon_o)$ do not approach their saturation values $F_n(\infty)$ until the interval $\varepsilon_o/2$ attains rather high values: $n = 0$, $\varepsilon_o/2 = 16$; $n = 2$, $\varepsilon_o/2 = 20$; $n = 4$, $\varepsilon_o/2 = 26$. As a result the effect of E_o is seen in the coefficients 5-11 at temperatures for which $KT \ll E_o$.

The results of these calculations are shown in figure 8 where the reduced $\Delta L/(K/e)^2 = \Delta L_r$ are plotted against KT/E_o for a series of a. The shape of the high temperature portion of the curve is sensitive to the form of σ_{20}, and the agreement of Powell and Tye's data with the model implies that σ_{20} is indeed rather independent of KT/E_o up to 1000°K. At low temperatures $|E| > E_o/2$ do not affect the transport coefficient, and it is possible to state only that the data must fall somewhere in the cross-hatched region of the figure.

The very interesting result of the model is that the value of C computed from the parameters needed to fit Powell and Tye's data is in excellent agreement with the value obtained from the low temperature data. E_o was found to be 0.188 electron-volts and a to be 2.7. These parameters give a value of C of 192 (electron-volts)$^{-2}$.

6. Conclusion

Since the thermal conductivity data were taken on different samples below and above T_n, there must be some reservations in any conclusions reached from the analysis. However, it is well known that there is an anomaly in $\rho(10,11)$ at T_n, and therefore one would expect an anomaly in either λ or L.

Calculations based on the high temperature model shown in figure 7 predict that ΔL_r vs KT/E_o should be a continuous curve like those shown in figure 8 by the family of curves. It is not possible for the data to fit on one such line, and so in the vicinity of T_n the two parameters a and E_o must decrease as T increases. It is a surprising result of the calculations that $C = (\sigma_{2E}/2\sigma_{0E})$ - which is sort of the parabolic constant of the well - is independent of the changes occurring at the Néel temperature. As is shown in figure 7 the change in $\sigma(E)$ at T_n amounts to an enormous decrease in the height of the parabolic well, which is itself unchanged.

What can be the meaning of such a result? Since $\sigma(E)$ can be considered as a product of the density-of-states (hereafter DS) and a carrier mobility [5], there are two possible sources of explaination: scattering or band structure. However the very fact that the parameters of the model are temperature independent suggests that they represent band parameters. The energy $E_o = 0.188$ electron-volts corresponds to 0.0120 rydbergs, an energy which is comparable to parabolic type wells in the computed DS of transition metals [15,16]. Then if such an interpretation be correct, one would expect to find $\Delta L > 0$ in other transition metals at the higher temperatures.

It has been pointed out by the author [17] that considerations of the transport coefficients from the multiband point of view indicate that they represent different portions of the Fermi surface. The conductivities are weighted toward those portions of the surface which have large carrier occupations and rather pedestrian mobilities when compared with the Hall coefficient and Thermoelectric power. Thus, the DS of interest is not the total DS but more likely the DS in some principal direction of the Brillouin zone. One can then guess that in Cr the principal electron conduction is occurring in those portions of the Fermi surface which are relatively unaffected by the disappearance of the magnetic Brillouin zone planes at T_n. Therefore C is unchanged, but there is some reshuffleling of DS which corresponds to a large decrease of a with a concomitant small change in ρ.

This interpretation is quite speculative. However, the very real possibility exists that measurements of thermal conductivity at high temperatures in pure metals can give some insight into the Fermi surface at these temperatures.

7. Acknowledgements

The author would like to thank Dr. P. G. Klemens for a very helpful discussion. Also, he appreciates the help given by A. C. Verbalis in the computorized analysis and W. J. Buehler in preparing the sample.

8. References

[1] A. F. A. Harper, W. R. G. Kemp, P. G. Klemens, R. J. Tainsh, and G. K. White; Phil. Mag. 2, 577 (1957).

[2] R. W. Powell and R. P. Tye, J. Inst. of Metals 85, 185 (1956-57).

[3] J. M. Ziman, Electrons and Phonons Oxford: Clarendon Press, 1960.

[4] J. F. Goff, Bull. Am. Phys. Soc. 12, 348 (1967).

[5] P. G. Klemens, to be published.

[6] J. F. Goff, J. Appl. Phys. 35, 2919 (1964).

[7] J. P. Clement in "Temperature - Its Measurement and Control in Science and Industry" edited by H. C. Wolfe, Rheinhold: Hew York, 1955, p. 382.

[8] H. B. Møller, A. L. Trego, and A. R. Mackintosh, Sol. State Comm. 3, 137 (1965).

[9] P. G. Klemens, Solid State Phys. 7, 1 (1958).

[10] S. Arajs and G. R. Dunmyre, J. Appl. Phys. 36, 3555 (1965).

[11] S. Arajs, R. V. Colvin, M. J. Marcinkowski; J. Less-Comm. Metals 4, 46 (1962).

[12] J. M. Ziman op. cit. p. 334.

[13] N.F. Mott, Adv. in Phys. 13, 325 (1964).

[14] I. Estermann, S. A. Friedberg, and J. E. Goldman; Phys. Rev. 87, 582 (1952).

[15] M. Asdente and J. Friedel, Phys. Rev. 124, 384 (1961).

[16] L. F. Mattheiss, Phys. Rev. 139, A1893 (1965).

[17] J. F. Goff, submitted to J. Appl. Phys.

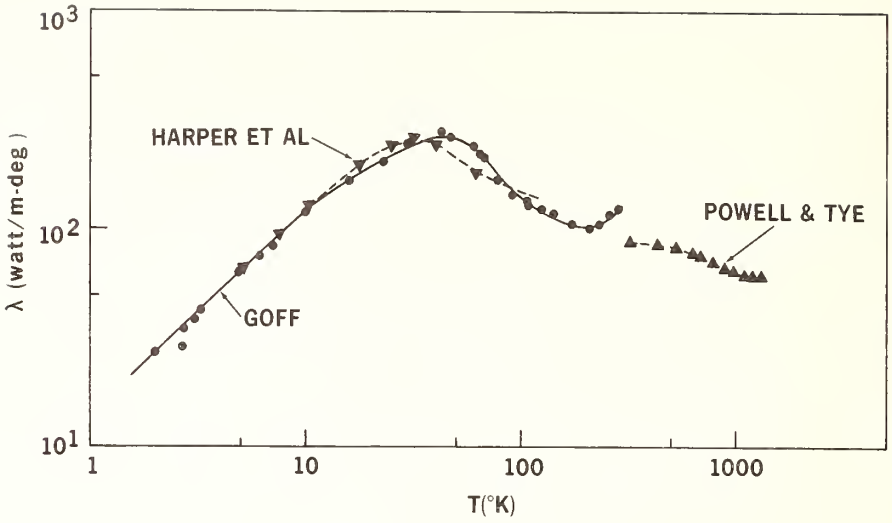

Figure 1. The thermal conductivity λ of chromium vs temperatures. The solid line is the present measurement; the dashed line is for other measurements of comparable samples. At low temperatures these data are for sample #2 of Harper et al [1]. At high temperatures the data are for Powell and Tye's sample [2] which was annealed at 1410°C.

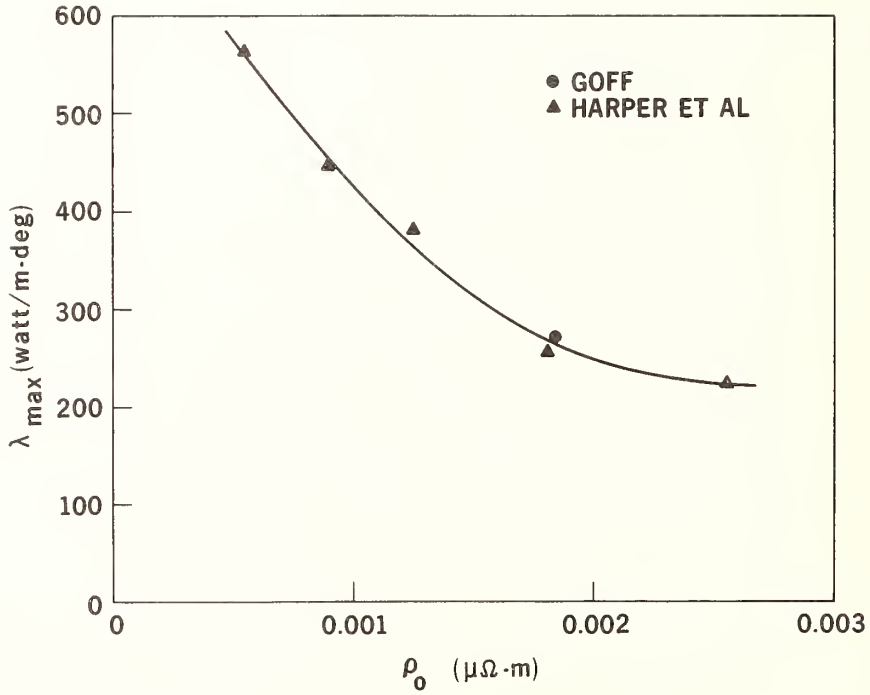

Figure 2. The maximum value of the thermal conductivity compared with the residual resistivity.

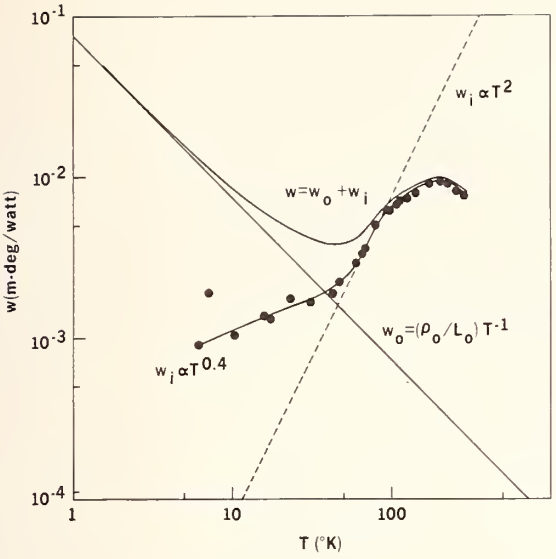

Figure 3. The thermal resistivity vs temperature. The circles are the values of the ideal thermal resistivity computed from the actual data.

Figure 4. The ideal electrical resistivity. The circles are the data taken for this measurement. The solid line is taken from the data of Arajs and Dunmyre [10] .

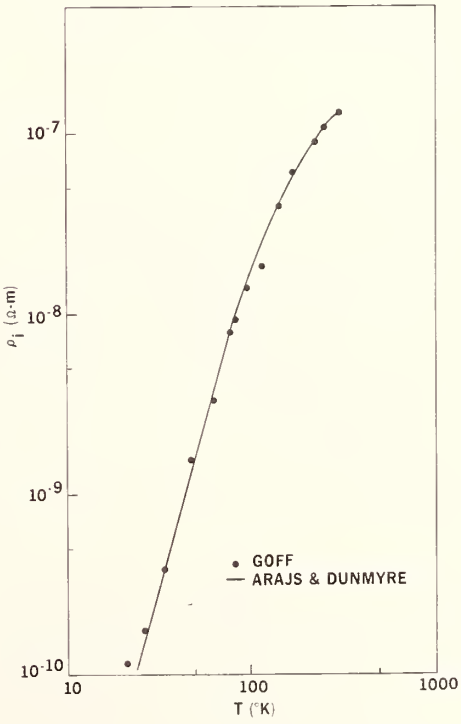

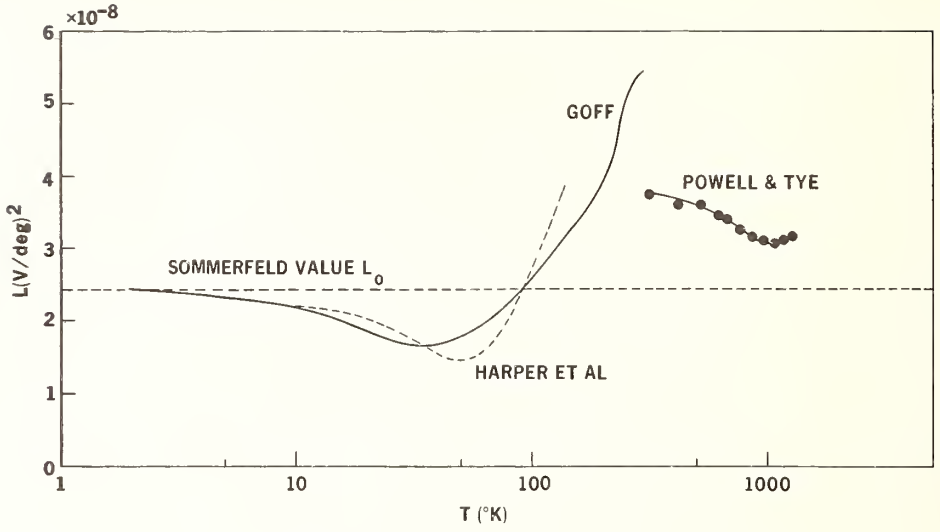

Figure 5. The Lorenz No. vs temperature.

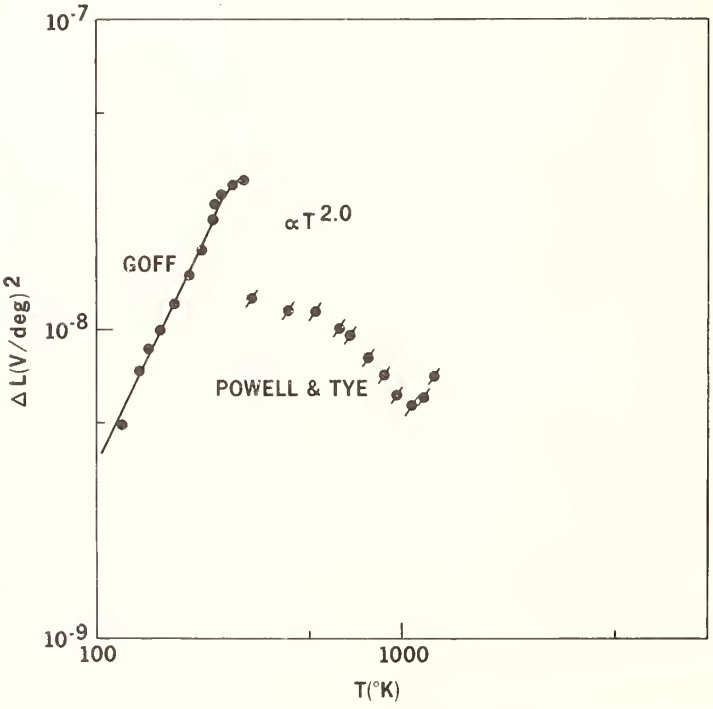

Figure 6. The extra value of the Lorenz No. vs temperature.

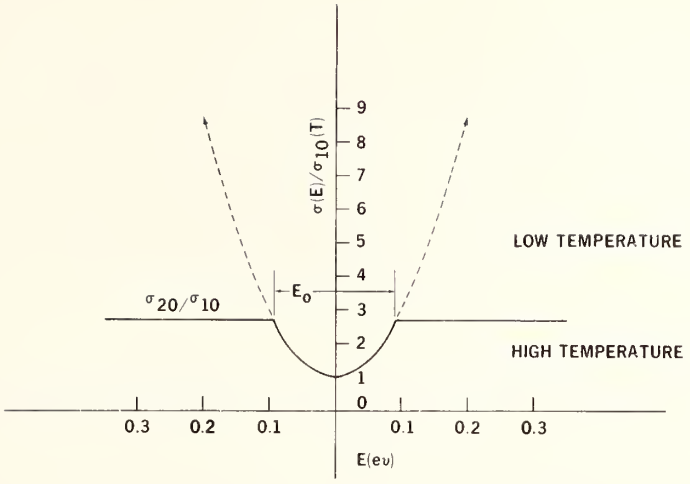

Figure 7. The specific conductivity $\sigma(E)$ deduced from the data. The solid line applies to temperatures greater than the Néel temperature and the dashed line to those less than it.

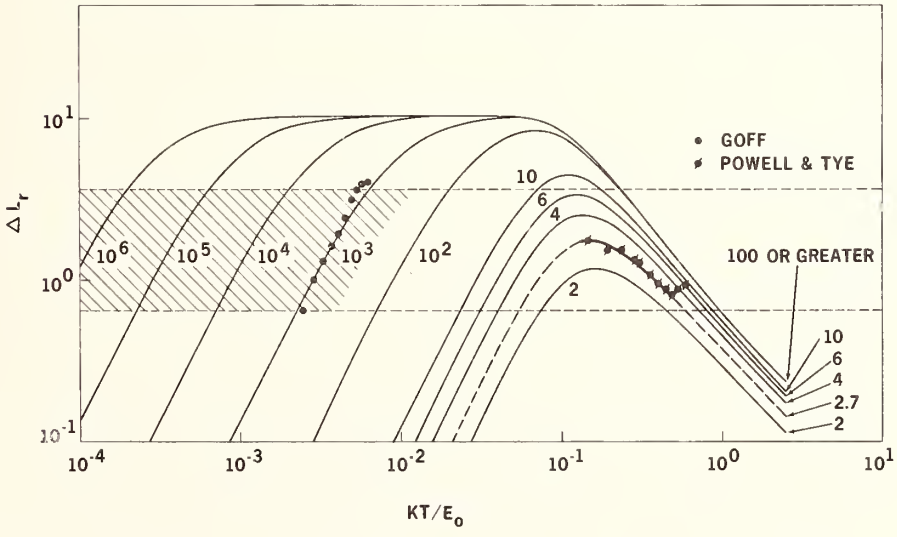

Figure 8. The reduced value of the departure of the Lorenz No. from the Sommerfeld value: $\Delta L_r = (L - L_o)/(K/e)^2$ shown by the family of smooth curves. The data are plotted in terms of the model.

Thermal Conductivity of a Round-Robin Armco Iron Sample

D. C. Larsen and R. W. Powell

Thermophysical Properties Research Center
Purdue University
West Lafayette, Indiana

An apparatus employing a steady state longitudinal heat flow method with matched guarding is described for the determination of the thermal conductivity of good conducting solids in the temperature range 50-800 °C.

The heat outflow from the sample is measured absolutely using a water flow calorimeter in the moderate temperature (50-300 °C) version of the apparatus. The high temperature (200-800 °C) apparatus can be evacuated, and the calorimeter heat sink eliminated. In both instances the heat is supplied electrically and is directly measurable.

The material being investigated is Armco Iron, the specimen being one originally supplied by BMI as a part of the Round-Robin investigation.

Key Words: Armco iron, iron, longitudinal heat flow method, metals, thermal conductivity.

High Temperature Transport Properties of Some Platinel Alloys

M. J. Laubitz and M. P. van der Meer

Division of Applied Physics
National Research Council
Ottawa, Canada

We have measured the transport properties (thermal conductivity, electrical resistivity, and thermoelectric power vs. Pt) of two Pt-Pd-Au and one Pd-Au alloy in the temperature range of 300 to 1200 °K. Using literature values for the phonon conductivities, and for the absolute thermoelectric power of Pt, we have calculated the (electronic) Lorenz function, L_e, and compared it to the theoretically expected value of $(L_o - S^2)$, where L_o is the standard Lorenz number, and S is the absolute thermoelectric power of the material. For the two three-component alloys, L_e is nearly a linear function increasing with temperature, exceeding in magnitude its expected value over the whole temperature range covered, in much the same fashion as in pure Pt and, probably, pure Pd. For the two-component alloy, L_e is larger than its expected value, but approaches it at higher temperatures. The behaviour observed for these alloys contrasts remarkably with that reported by Flynn for Pt-40%Rh.

Key Words: Electrical resistivity, Lorenz function, Pd-Pt-Au alloys, Platinel, thermal conductivity, thermal expansion, thermoelectric power, Wiedemann-Franz ratio.

1. Introduction

In retrospect, many cogent reasons could be adduced for our undertaking the investigations herein described. The true reasons, we must blushingly admit, were rather prosaic: having been supplied with the samples, gratis, by Engelhard Industries, whose interest in the properties of Platinel alloys is more easily appreciated than ours, we measured their transport properties, fully expecting to obtain results analogous to those reported by Flynn [1][1] for Pt-40%Rh. Our results, which differ strikingly from those of Flynn, came to us therefore as a surprise. They further confirm the fact, which even some theoreticians appear to be beginning to appreciate, that the relation between the thermal and electrical conductivities at high temperatures for the transition metals, particularly of the VIII group, is not simply a matter of the Wiedemann-Franz law with the standard Lorenz number, L_o, or even $(L_o - S^2)$. At this stage, we do not know precisely why the Lorenz function of these metals should depart in the observed manner from its standard value, particularly considering that it is the latter which is found in the monovalent metals [2],[3], and even in some polyvalent ones [4]. Therefore, rather than waste space on some second-hand, general, and rather meaningless comments on the "two-band nature" of the transition metals, we shall refrain from any theoretical discussion whatsoever, and restrict ourselves simply to the presentation of the experimental results.

2. Samples and Method

Engelhard Industries have kindly supplied us with three alloys, labelled 5330, 5355, and 7674. These are alloys used for the Platinel I and II thermocouples, and are identified in that way in table 1, which also contains the nominal and actual composition of these alloys. In that table we have also given the residual resistivity ratios

[1]Figures in brackets indicate the literature references at the end of this paper.

measured on our specimens; these indicate that the transport properties are dominated by impurity scattering right up to room temperature.

Table 1. Description of the specimens

Alloy designation	Alternate alloy designation	Use in Platinel thermocouples	Composition			$\frac{\rho(273)}{\rho(4)}$
			Nom. wt % Pd-Pt-Au	Nom. at % Pd-Pt-Au	Actual wt % Pd-Pt-Au	
7674	Platinel 1503	neg. element of I and II	35-0-65	50-0-50	34.95-0-65.05	1.133
5330	Platinel 1786	pos. element of I	83-14-3	90-8-2	83.00-13.95-3.05	1.950
5355	Platinel 1813	pos. element of II	55-31-14	69-21-10	55.0-31.4-13.6	1.289

We have received two specimens from each alloy. One, a composite, approximately 1.2 cm in diameter and 10 cm long, was used for the measurement of the thermal conductivity by the "Guardless" method, previously described by us in detail [5],[6]. The second, a thin rod 0.178 cm in diameter and 20 cm long, was used for the measurement of the electrical resistivity, by a method described in [6]. The thermoelectric power with respect to reference grade platinum (Engelhard Ind.) was measured on both specimens of each alloy, and was used as a cross-check on alloy homogeneity.

We have also measured the total thermal expansion of the composite specimens, $\alpha(T) = (\ell(T)-\ell_o)/\ell_o$, where $\ell(T)$ is the length of the specimen at temperature T, and ℓ_o is its length at room temperature. The measurements were made in a silica push-rod dilatometer; their chief purpose was to provide information necessary for a correction that we have to apply in our method of measuring thermal conductivity [5], and having measured it, we decided to include it here as possibly useful information on the alloys.

3. Results

All the properties have been measured, after specimen annealing, in several cycles of increasing and decreasing temperature. The composite specimens have been annealed at a temperature of between 800 and 900 °K for about 60 hours; the small specimens have been annealed at a higher temperature, of about 1100 °K, but for a shorter time, about 15 hours. The annealing was done in situ, after the specimens have been assembled in the measuring apparatus.

The experimental results obtained, uncorrected for thermal expansion in the case of the thermal conductivity and electrical resistivity, were analysed by a computer in terms of polynomial functions of the absolute temperature, T,

$$f(T) = A + BT + CT^2 + DT^3 + \cdots$$

The coefficients for best fit (i.e. one for which a subsequent increase in the number of terms produces no substantial improvement in the rms deviations, taking account of the increase in the number of degrees of freedom) are given in table 2 for all the properties measured. In that table, we also give the number of points measured for each property, N, the rms deviation of the experimental points from the curves, the temperature range which the equations cover, and the estimated error of our results. The last we consider to be the maximum determinable error, that is the maximum possible error in the results due to all the causes of which we are aware.

For the two three-component alloys, 5330 and 5355, the thermoelectric power measured on the small and large specimens agreed within the scatter of the results for each, and all the results were grouped together for the analysis. This was not the case for the two-component alloy, 7674; for this alloy, not only was there a significant difference between the small and large specimens, but in the large one itself there was a significant difference between its two halves. We have analysed each of these separately, and have given the results in table 2 marked S(s) for the small specimen, and S(l) and S(r) for the two halves of the large one. We have also encountered greater difficulty with the 7674 alloy than with any of the other ones as far as reproducibility in the other transport properties is concerned, which is reflected directly in the larger experimental scatter of the results, as shown by the rms deviations in table 2. However, we have not been able to observe any consistent relation between any of the measured properties and the limited thermal history of the specimens.

Table 2. Experimental results. A, B, C, and D are coefficients of polynomial fit in temperature, in K. Units are: thermal conductivity (λ) - w m^{-1} K^{-1}; electrical resistivity (ρ) - $\mu\Omega$-m; total thermal expansion (α) - %; thermoelectric power vs. Pt (S) - μV/K. λ and ρ not corrected for thermal expansion.

Alloy	Q'ty	A	B × 10^3	C × 10^6	D × 10^9	N	rms deviation	Estimated error + , -	Temperature range
7674	λ	5.84	100.13	-31.86	-	52	2.0 %	3.5 %	300-1150
	ρ	0.2236	0.0548	0.0202	-	18	0.55 "	0.5 "	300-1350
	α	- 0.355	1.186	0.043	-	17	1.1 "	2 "	300-1200
	S(s)	9.47	88.70	-68.97	15.33	15	0.25 μV/K	1 μV/K	300-1300
	S(l)	14.22	56.03	-28.07	-	14	0.26 "	1 "	400-1100
	S(r)	12.62	66.49	-34.84	-	12	0.33 "	1 "	400-1100
5330	λ	27.66	49.47	1.31	-	18	1.6 %	3 %	300-1000
	ρ	0.0808	0.3803	- 0.0774	-	21	0.16 "	0.5 "	300-1350
	α	- 0.304	0.979	0.214	-	16	1.3 "	2 "	300-1100
	S	2.29	-30.17	46.81	-15.70	38	0.05 μV/K	0.2 μV/K	300-1350
5355	λ	10.66	58.69	- 7.25	-	20	1.5 %	3 %	300-1200
	ρ	0.2232	0.3097	- 0.0578	-	21	0.06 "	0.5 "	300-1200
	α	- 0.292	0.929	0.205	-	20	1.1 "	2 "	300-1200
	S	7.25	-40.03	53.03	-18.58	35	0.06 μV/K	0.2 μV/K	300-1300

Figures 1 and 2 illustrate our smoothed results for the thermal conductivity and electrical resistivity as a function of temperature. For comparison, we have included the results for pure Pt [6],[7], pure Pd [8], and also the Pt-40%Rh alloy reported by Flynn [1]. Figure 3 shows the absolute thermoelectric powers of all these metals; the values for Au, Pd, and Pt we have taken from Cusack and Kendall [9], the last also being used for converting the observed thermoelectric powers of our alloys into absolute values. The thermoelectric power of Pt-40%Rh we have calculated from values kindly given us by Dr. R. E. Bedford of our laboratory.

Figure 4 gives the calculated Wiedemann-Franz ratio for the metals, $L_t/L_o = \lambda_t \rho / T L_o$, where λ_t is the total (measured) thermal conductivity, and L_o the standard Lorenz number (2.443×10^{-8} $(V/K)^2$). Figure 5 shows the ratio of the electronic Lorenz function, L_e, to L_o, where $L_e/L_o = \lambda_e \rho / (L_o T)$, λ_e being the electronic conductivity. We have calculated the latter by subtracting an estimated phonon conductivity, λ_p, from the total one, assuming $\lambda_p = 6/T$ for all the metals shown in the diagram. We have selected the λ_p on the basis of the work of Fletcher and Greig [10], who observed approximately this value for the high temperature phonon conductivity for sets of Pd-Ag, Pt-Au, and Pt-Ir alloys, roughly independent of alloy composition and concentration.

Finally, figure 6 gives the ratio of L_e to $(L_o - S^2)$, which is supposed to be a better approximation to the high temperature limiting value of L_e than L_o by itself is.

4. Discussion

Disturbed by the range of values that we have obtained for the thermoelectric power for the alloy 7674, we have attempted to compare our results with such values as we could find in literature. Olsen and Freeze [11], for instance, give total emf's between the temperature T and the ice-point for each of the legs of the Platinel II thermocouple relative to Pt 27. Integrating the equations for our corresponding alloys, we find very good agreement for 5355, the difference between our results and those of Olsen and Freeze corresponding to 0.03 μV/K, well within our experimental error. For the small sample of 7674, we find a difference corresponding to -0.8 μV/K, still less than our estimated error; the two halves of our large specimen, however, give thermoelectric powers that differ by an equivalent of some -1.5 and -4 μV/K.

To obtain a comparison for our 5330 alloy, we integrated an equation representing the difference between that alloy and 5355, and compared it with the differences in the tabulated values given by Zysk [12] for the total emf's of Platinel I and II. The differences between our results and those given by Zysk are somewhat erratic, but, on the average, corresponded to 0.34 μV/K, which is within the combined error of our own results.

On balance, therefore, our results for the alloys 5355 and 5330 agree well with literature values, as do those for our small specimen of the alloy 7674. We do not know why the large specimen of the last showed such variable behaviour. Besides the possibility of experimental error, which we think unlikely, two other factors may enter: 1) effects of ordering, which have been observed in Pd-Cu alloys [13] and Pd-Ag alloys [14], at the same atomic composition as 7674. Our specimens did not receive identical heat treatments, nor did our large specimen receive the type of annealing usually given to Platinel thermocouples; differences in thermoelectric powers could therefore arise due to different degrees of ordering. Corresponding differences should then occur in both the thermal conductivity and the electrical resistivity, and as these could be quite large [13], our calculated Lorenz function, obtained from combining results from two dissimilarly ordered alloys, could be seriously in error. 2) small but genuine composition differences between the large and small specimens, perhaps brought about by our heat treatment or handling. Chen and Nicholson [14], for instance, have shown a very prominent peak in the thermoelectric power of Pd-Ag alloys at the 50-50 at % level; if similar effects exist in the Pd-Au family, then very small composition changes could produce the effects that we have observed. Small compositional changes should not affect seriously the other transport properties. In this case, therefore, we should expect our calculated Lorenz function to be accurate to about 4%.

As far as the thermal conductivity and electrical resistivity is concerned, we find that we have little to say: on the one hand, the "description" of the results is already contained in figures 1 to 6, and there seems little point in repeating it here verbally; on the other hand, we can offer no "explanation" of the behaviour observed, at least not at this stage. We have, however, undertaken further research, of a more systematic nature than heretofore, and we may, hopefully, reach some conclusion in this respect in the future.

5. Acknowledgments

We are grateful to Engelhard Industries, Inc., in Newark, New Jersey, for machining and lending us the specimens used in this work; in particular, we should like to acknowledge the cooperation of Mr. E. D. Zysk, of their Research and Development Division.

6. References

[1] Flynn, D. R., Thermal conductivity, electrical resistivity, and Lorenz function for a 60% Pt-40% Rh alloy, as quoted in the Thermophysical Properties Research Data Books, V.I, p.1253 (1964).

[2] Laubitz, M. J., Transport properties of pure metals at high temperatures; I-Copper, to be published in Can. J. Phys., November 1967.

[3] Laubitz, M. J., Ditto: II-Gold, submitted for publication to the Can. J. Phys.

[4] Powell, R. W., Tye, R. P., and Woodman, M. J., The thermal conductivity of pure and alloyed aluminum; I - Solid aluminum as a reference material, Adv. in Thermophys. Prop. at Ext. Temp. and Press., A.S.M.E. (1965), p.277.

[5] Laubitz, M. J., The unmatched guard method of measuring thermal conductivity; II - the guardless method, Can. J. Phys. 43, 227 (1967).

[6] Laubitz, M. J. and van der Meer, M. P., The thermal conductivity of platinum between 300 and 1000 °K, Can. J. Phys. 44, 3173 (1966).

[7] O'Hagan, M. E., Measurements of the thermal conductivity and electrical resistivity of platinum from 373 to 1373 °K, Doctor of Science thesis, George Washington University, Washington, D.C. (1966).

[8] Powell, R. W., Tye, R. P., and Woodman, M. J., Thermal conductivities and electrical resistivities of the platinum metals, Plat. Met. Rev. 6, 138 (1962).

[9] Cusack, N. and Kendall, P., The absolute scale of thermoelectric power at high temperatures, Proc. Phys. Soc. 72A, 898 (1958).

[10] Fletcher, R. and Greig, D., The lattice thermal conductivity of some palladium and platinum alloys, Phil. Mag. 16, 303 (1967).

[11] Olsen, L. O. and Freeze, P. D., Reference tables for the Platinel II thermocouple, J. Res. N.B.S. 68C, 263 (1964).

[12] Zysk, E. D., A review of recent work with the Platinel thermocouple, Engelhard Ind. Tech. Bull. 4, 5 (1963).

[13] Pott, F. Ph., Untersuchungen zum Wiedemann-Franz-Lorenzschen Gesetz an ungeordneten und geordneten Phasen der Kupfer-Palladium-Legierungsreihe, Z. Naturforschg. 13a, 215 (1958).

[14] Chen, W-K. and Nicholson, M. E., The influence of annealing on the electrical properties of cold-worked Ag-Pd alloys, Acta Met. 12, 687 (1964).

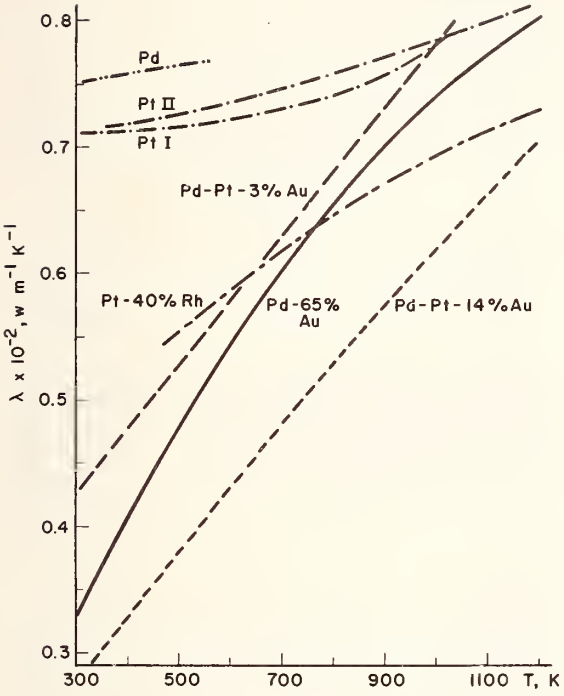

Figure 1. Smoothed values of the thermal conductivity as a function of temperature. References: Pd - [8]; Pt I - [6]; Pt II - [7]; Pt-40% Rh - [1].

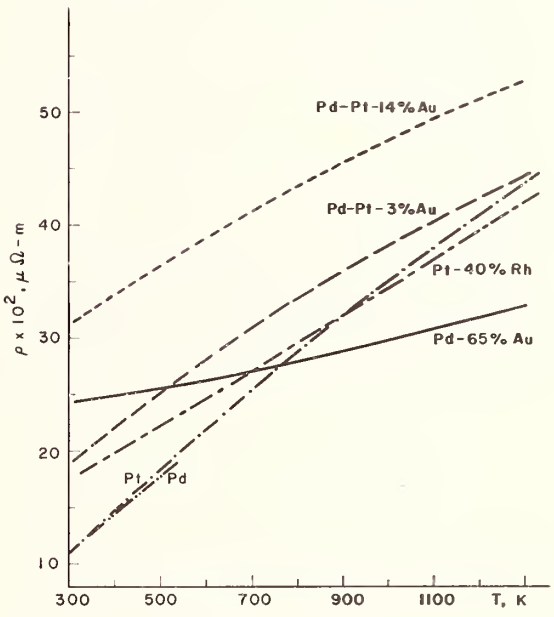

Figure 2. Smoothed values of electrical resistivity as a function of temperature. References: Pd - [8]; Pt - [6]; Pt-40% Rh - [1].

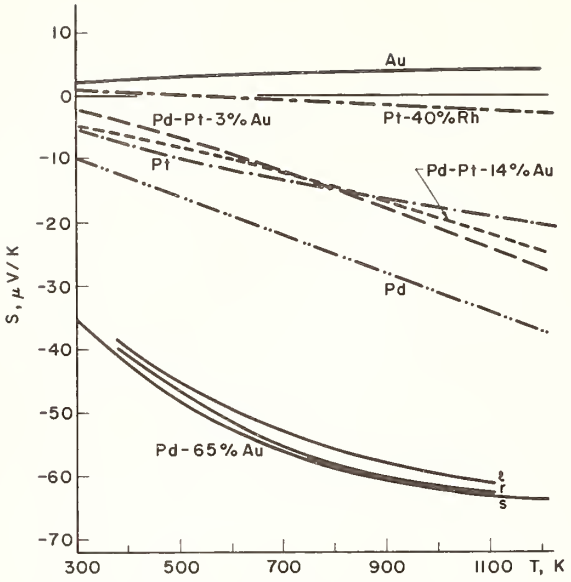

Figure 3. Absolute thermoelectric power as a function of temperature. References: Au, Pd, Pt - [9]; s, l, and r indicate respectively the thermoelectric power of the small specimen, and of the two halves of the large specimen of alloy 7674.

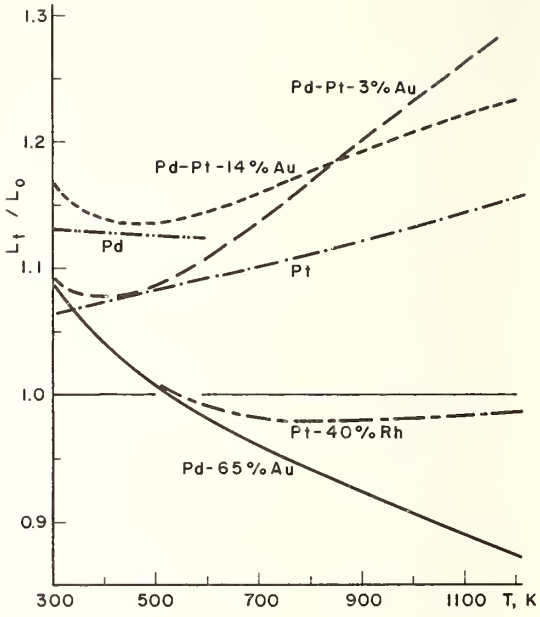

Figure 4. The Wiedemann-Franz ratio, L_t, as a function of temperature.

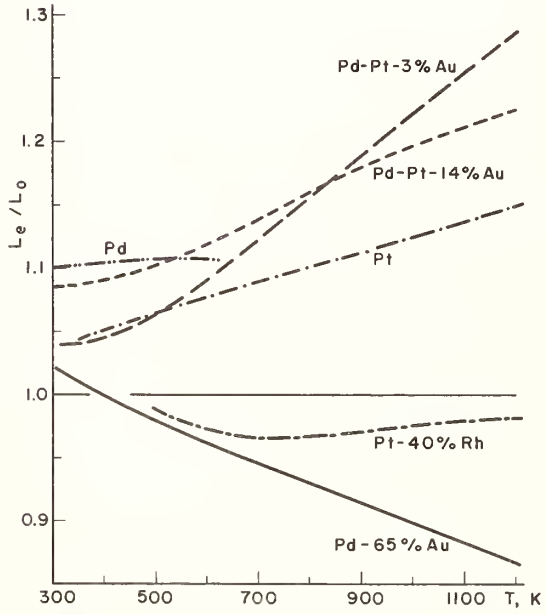

Figure 5. The ratio of the Lorenz function, L_e, to the Lorenz number, L_o, as a function of temperature.

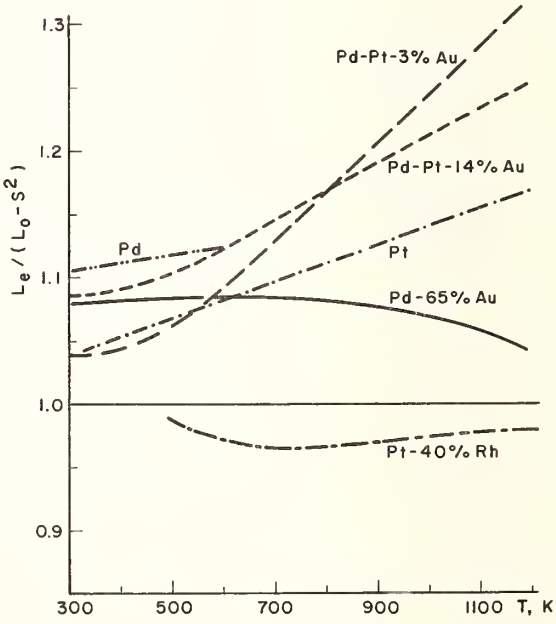

Figure 6. The ratio of the Lorenz function, L_e, to $(L_o - S^2)$, as a function of temperature.

The Thermal Diffusivity of Gold

H. R. Shanks, M. M. Burns and G. C. Danielson

Institute for Atomic Research and Department of Physics
Iowa State University, Ames, Iowa 50010

The thermal diffusivities of four gold samples have been measured from 325 to 1225°K. The sample purities varied from about 95 to 99.999% and the resistivity ratios from 3 to 600. The thermal diffusivity of gold was found to be sensitive to the impurity concentration. The thermal diffusivity data were combined with published specific heat data to obtain thermal conductivity values. Electrical resistivity and Seebeck coefficient measurements were also made on the samples.

Key Words: Gold, Lorenz number, Seebeck coefficient, thermal conductivity, thermal diffusivity.

1. Introduction

Recently there has been increasing interest in understanding the high temperature thermal conductivity of metals. In order to do so, much additional accurate data is needed on the simpler metals such as Cu, Ag, and Au. Thermal diffusivity data on a series of gold samples of different purities are reported here. Gold was chosen because of the availability of reasonably pure samples and the almost total lack of published thermal conductivity data above 300°K.

2. Measurements

The thermal diffusivity measurements were made by a modified Angstrom method. The techniques and equipment which were used for these measurements have been described previously [1, 2][1]. The three sample thermocouples consisted of 0.025 cm diam Pt and Pt/10% Rh wires spot welded to the gold sample. Current for electrical resistivity measurements was applied to the sample through 0.061 cm diam Pt wires spot welded to the sample ends. The apparent electrical resistivity was measured after each measurement of thermal diffusivity by a standard 4-wire technique. Two of the Pt thermocouple wires were used as voltage probes. The thermal diffusivity measurements were made with the samples in one atmosphere of helium and with a 2.5°K amplitude 30 sec period temperature sine wave.

The absolute Seebeck coefficients of the samples were measured by a method described by Heller and Danielson [3]. Two of the thermocouples welded to the sample for thermal diffusivity measurements were used for the Seebeck coefficient measurements. The wires were reconnected externally so that the instantaneous voltage developed across the Pt - Au - Pt junctions could be plotted as a function of the voltage across the Pt/10% Rh - Au - Pt/10% Rh junctions on an x-y recorder.

The 30 sec period sine wave used for thermal diffusivity measurements was also used to supply the varying temperature gradient for the Seebeck coefficient measurements. The absolute Seebeck coefficient of gold could then be calculated from the absolute Seebeck coefficient of platinum reported by Cusack and Kendall [4] and the Pt - Pt/10% Rh thermocouple tables published by Adams and Davisson [5].

3. Samples

Four gold samples of different purity were obtained from four different sources in the form of rods 0.35 cm in diam and 30 cm long. Table 1 lists the samples, the manufacturer, the purity stated by the manufacturer and our measured values for the ratio of the electrical resistivity at 300°K to the electrical resistivity at 4.2°K after the samples had been annealed at 1225°K for 1 hr.

[1] Figures in brackets indicate the literature references at the end of this paper.

Table 1. Sample Characterization.

Sample	Manufacturer	Purity	$R_{300}/R_{4.2}$
Au 1	Johnson, Matthey and Co.	99.999%	600
Au 2	Sigmund Cohn	99.99%	310
Au 3	Aremco	99.9999%	110
Au 4	Mint Gold	-	3

4. Results

The thermal diffusivity results for the four samples are shown in fig. 1. Each point represents the average of two diffusivity values obtained from the two thermocouple combinations at a given temperature. The deviation of the points for each sample from a smooth curve drawn through them was less than 1.5%. The thermal diffusivity was dependent on the purity of the sample and decreased with increasing impurity concentration. For the most impure sample, Mint gold, the thermal diffusivity was found to go through a maximum value at about 725°K.

The electrical resistivities of the four samples are shown in fig. 2. The electrical resistivities of the two samples of highest purity were the same, and were lower than the values for the other two samples. The electrical resistivity versus temperature curve for Au 4 is higher than, and not parallel to, the curves for the other three samples. This difference between the curves implies a high impurity concentration and also a violation of Matthiessen's rule.

The Seebeck coefficients for the four gold samples are shown in fig. 3. The data for the gold samples are based on the absolute Seebeck coefficient of platinum reported by Cusack and Kendall [4]. They report an accuracy of ± 5% for their platinum data. The absolute Seebeck coefficients for samples Au 1, Au 2, and Au 3 agreed within ± 2% over the entire temperature range; and since the differences in the data for the three samples were less than the total errors for the measurements, the values were averaged to give one curve of Seebeck coefficient versus temperature. As expected the results for Mint gold were considerably lower and approached the values observed for the other three samples only at the highest temperatures.

5. Discussion

The thermal diffusivities (fig. 1) of the two highest purity samples, Au 1 and Au 2, which have resistivity ratios of 600 and 310, respectively, differ by only 0.7% at 350°K and by 3% at 1225°K. Since the errors in the measurement are about 2%, it is difficult to report any real difference in the thermal diffusivities of the two samples, although the higher purity sample appears to have a higher thermal diffusivity.

Au 3, with a resistivity ratio of 110, has a thermal diffusivity 7% lower than Au 1 at 350°K. This difference represents a real change in thermal diffusivity with purity. For the most impure sample, Au 4, the thermal diffusivity at 350°K is 36% below the value observed for Au 1, the most pure sample. The shape of the thermal diffusivity versus temperature curve for Au 4 is different from the shape of the other sample curves and represents the effect of large amount of impurities on the thermal diffusivity.

The thermal conductivities of the four samples were obtained from the product of the measured values of thermal diffusivity and the published values of density and specific heat. A constant density [6] of 19.30 gm/cm^3 was used. The specific heat results of Jaeger, Rosenbohm, and Bottema [7] were used in the calculation since their data is the most recent published and, if extrapolated to low temperatures, connects smoothly to the data of Geballe and Giauque [8]. Figure 4 shows the thermal conductivities calculated for each of the four samples and also shows data reported by Mikryukov [9]. The data reported by Mikryukov [9] is on a polycrystalline sample of gold with a reported purity of 99.99%.

The thermal conductivity curves reflect the same differences in purity observed in the thermal diffusivity data because the same specific heat values were used for all samples. This is probably justified for the three samples of highest purity since the specific heat is usually rather insensitive to small amounts of impurities. It may not be valid to use the specific heat for pure gold to calculate the thermal conductivity of Au 4 which has a high impurity concentration. The smoothed thermal diffusivity, the thermal conductivity, the electrical resistivity and Seebeck coefficient for Au 1 are given in table 2. These results represent our best values for the properties of pure gold.

Table 2. Transport properties of pure gold

Temperature °K	Thermal Diffusivity cm^2/sec	Thermal Conductivity watts/cm-deg	Electrical Resistivity ohm-cm	Seebeck Coefficient $\mu V/deg$
325	1.140	2.97	2.43	1.93
400	1.121	2.96	3.05	2.37
500	1.093	2.94	3.93	2.83
600	1.062	2.92	4.84	3.15
700	1.028	2.90	5.76	3.35
800	0.994	2.86	6.75	3.51
900	0.954	2.82	7.76	3.67
1000	0.920	2.78	8.89	3.85
1100	0.874	2.73	10.06	4.03
1200	0.826	2.66	11.35	4.29

The apparent Lorenz numbers were calculated from the thermal conductivity and electrical resistivity data. The resulting curves are shown in fig. 5. The curves for all four samples are in good agreement and, at high temperatures, are all within ± 7% of the theoretical value of 2.45×10^{-8} $V^2/°K^2$.

6. Conclusions

The thermal diffusivities of four gold samples with resistivity ratios ranging from 600 down to 3 have been measured from 325 to 1225°K. The thermal diffusivity values and published specific heat values were used to calculate the thermal conductivities. The thermal conductivities for the samples of higher purity are in good agreement with data on gold reported by Mikryukov [9]. The calculated Lorenz numbers agree well with theory.

7. References

[1] Sidles, P. H. and Danielson, G. C., Thermal diffusivity measurements at high temperatures, In Thermoelectricity, P. H. Egli, Ed., Chap. 16, p. 270 (John Wiley and Sons, 1960).

[2] Martin, J. J., Sidles, P. H., and Danielson, G. C., J. Appl. Phys. 38 3075 (1967).

[3] Heller, M. W. and Danielson, G. C., J. Phys. Chem. Solids 23 601 (1962).

[4] Cusack, N. and Kendall, P., Proc. Phys. Soc. London 72 898 (1958).

[5] Adams, R. K. and Davisson, E. C., ORNL-3649 Vol. 2, Section 2.1 (1965).

[6] Seybold, A. U., USAEC Publ. AECD 2434 (1943).

[7] Jaeger, F. M., Rosenbohm, E., and Bottema, J. A., Pro. Acad. Sci. (Amsterdam) 35 772 (1932).

[8] Geballe, T. H. and Giauque, W. F., J. Am. Chem. Soc. 74 2368 (1952).

[9] Mikryukov, V. E., Vestnik Moskov. Univ. Ser. Mat. Mekh, Astron. Fiz, i Khim., 12 (6) 57 (1957).

[10] Rudnitskii, A. A., AEC-tr-3724 (July, 1959), translated from a publication of the publishing house of the Academy of Sciences, U.S.S.R. (Moscow, 1956).

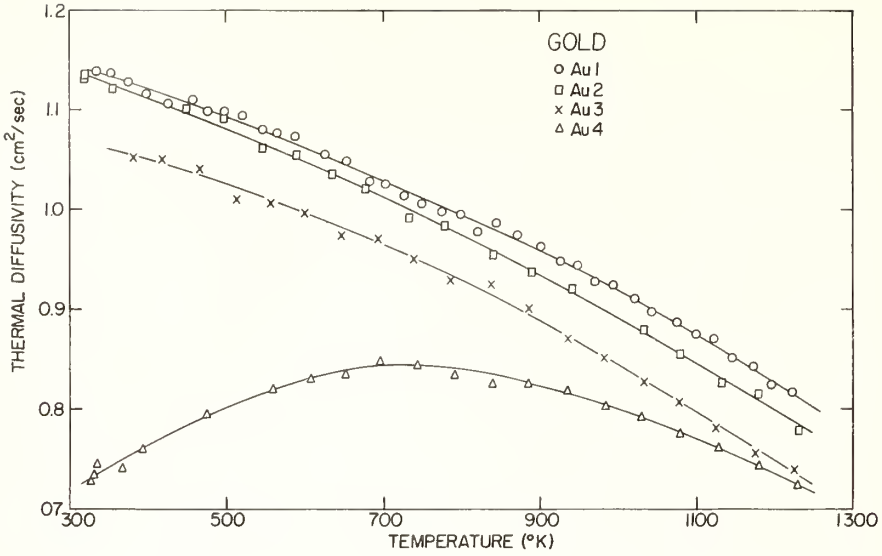

Figure 1. The thermal diffusivity of gold as a function of temperature. The data show the effect of different amounts of impurities with Au 1 the most pure sample and Au 4 the most impure sample.

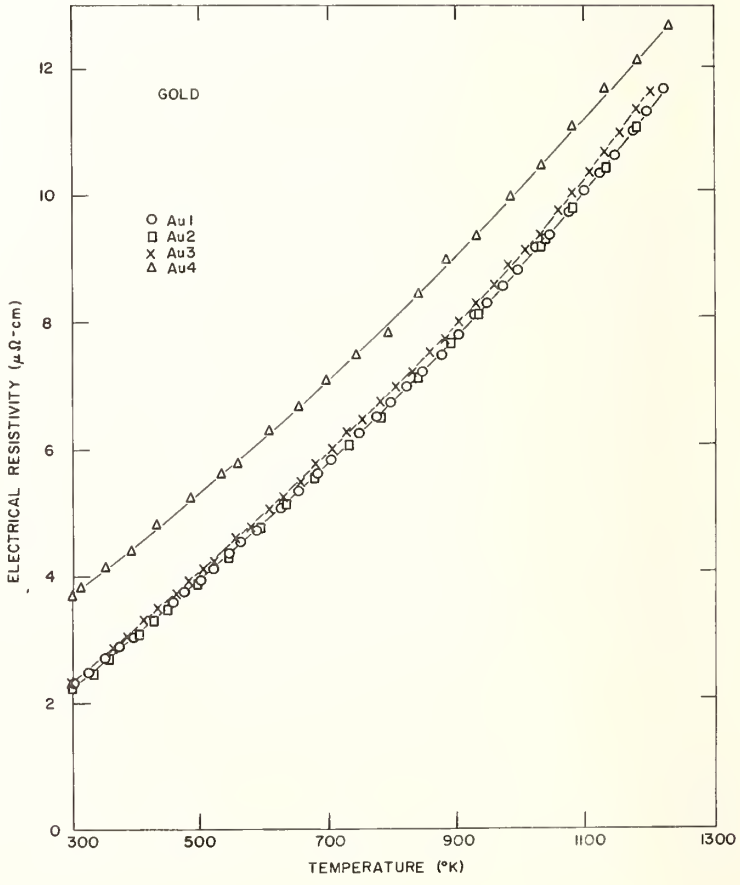

Figure 2. The electrical resistivity of gold as a function of temperature above 300 °K.

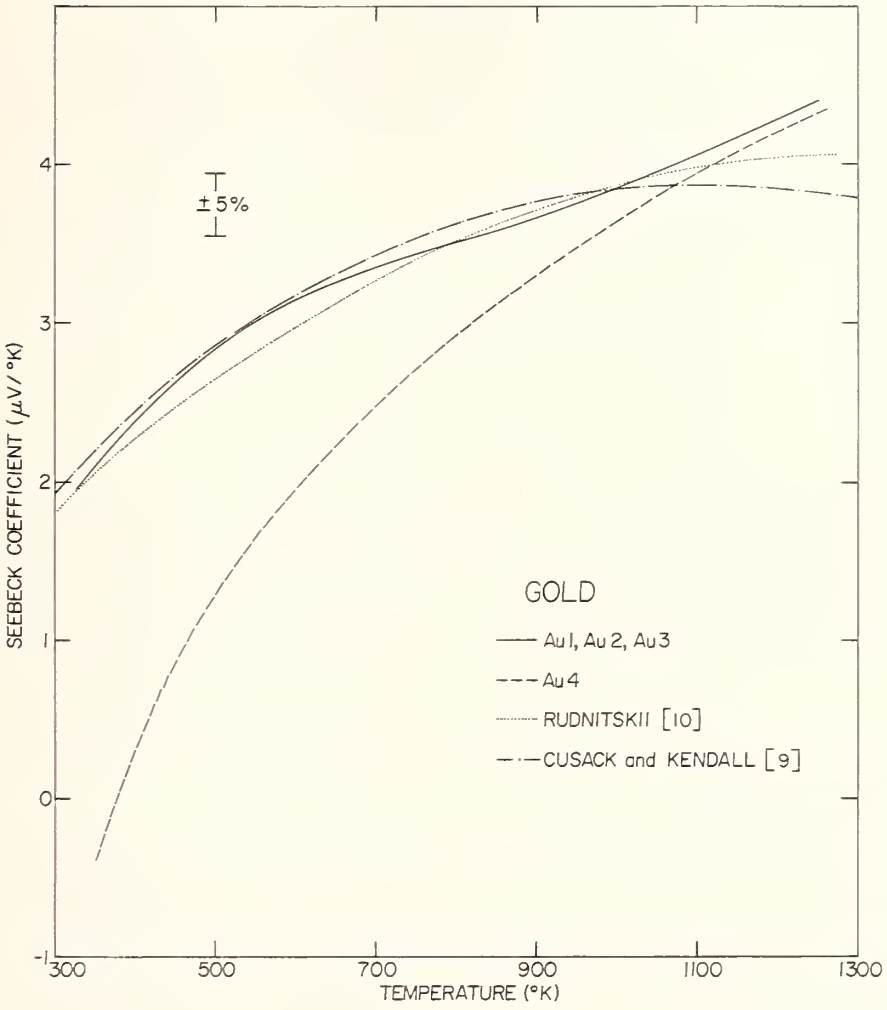

Figure 3. The Seebeck coefficient of gold as a function of temperature. The effect of large amounts of impurities on the Seebeck coefficient can be seen in the data for Au 4.

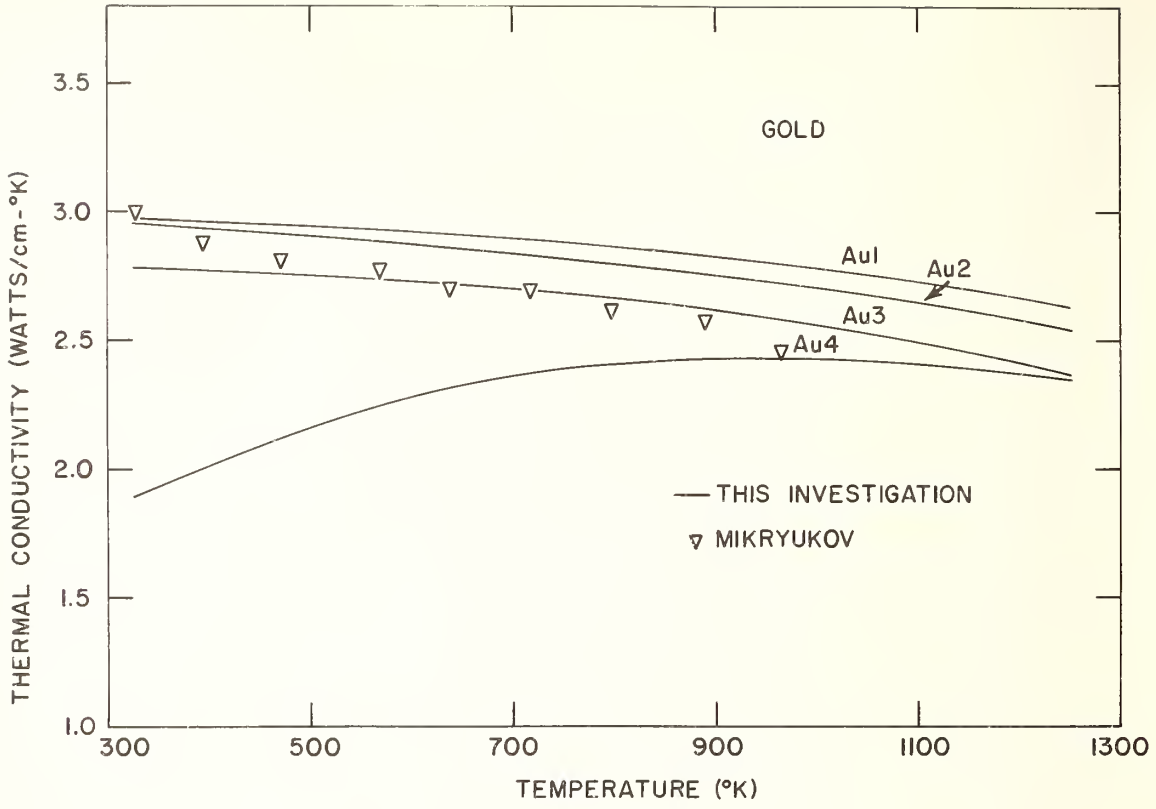

Figure 4. The thermal conductivity of gold as a function of temperature.

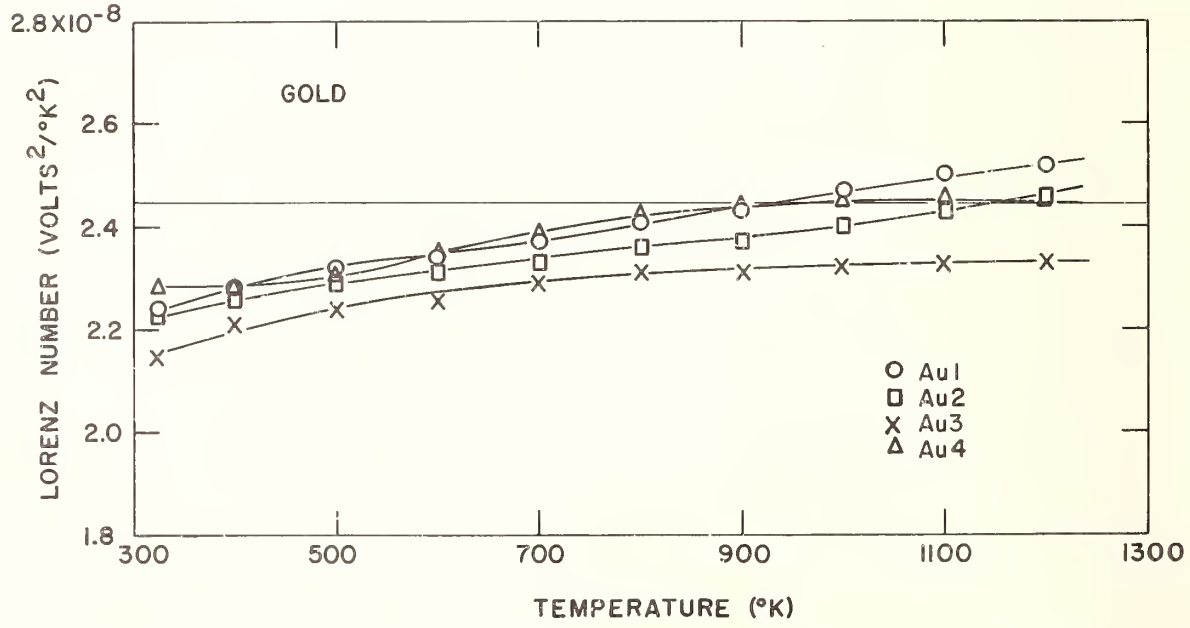

Figure 5. The apparent Lorenz number as a function of temperature for gold. The Wiedemann-Franz law predicts a constant Lorenz number of 2.45×10^{-8} V^2/K^2.

Experimental Determination of the Thermal Conductivity of Solids Between 90 and 200 °K [1]

J. G. Androulakis and R. L. Kosson [2]

Thermodynamics Section
Grumman Aircraft Engineering Corporation
Bethpage, New York

An apparatus to measure the thermal conductivity of solids from 90 to 200 °K is described. This apparatus is based on the axial flow technique. The samples are bars of circular, square, or rectangular cross section. By varying sample geometry, the thermal conductivity of poorly conductive materials and very highly conductive materials can be determined. Experimental data, curves of conductivity vs. temperature, are presented for some metals and plastics. A detailed error analysis identifying important parameters is included.

Key Words: Conductivity, thermal conductivity, measurement apparatus, stainless steels, Teflon, Nylon

1. Introduction

The apparatus developed to measure the thermal conductivity of solids in the temperature range from 90 to 200 °K is based on the conventional axial flow bar method. With this technique the sample, electrically heated at one end, conducts to a liquid nitrogen reservoir at the other end. It is suspended inside a radiation shield guard heater assembly with the radiation shield having approximately the same temperature distribution as the sample. The conductivity is determined from the difference in temperature between any two points, the heat input to the sample heater, and the known geometry of the sample.

The apparatus is similar in concept to many others previously used for low-temperature conductivity determination [1][2][3], but differs significantly in detail design and instrumentation.

Applicability of this method to the determination of the thermal conductivity of both poorly conductive materials and highly conductive materials was evaluated and an optimum sample geometry was defined in each case.

2. Experimental Arrangement

The apparatus is shown schematically in Fig. 1 (see also Figs. 2 through 4). It consists of a central assembly, the conductivity rig proper surrounded by a liquid nitrogen cold wall jacket. Both are suspended coaxially from the top cover of an external vacuum chamber by means of the inlet and outlet flow pipes.

The central assembly consists of an upper liquid nitrogen reservoir to which is attached, through a copper block, a radiation shield and guard heater assembly. The specimen is suspended vertically inside the radiation shield by means of a copper plate to which it is attached by one central screw. This plate is housed inside the shield upper flange which is screwed to the copper sink. An upper heater is housed inside a groove in the copper sink.

---

[1] This effort was performed under the sponsorship of the Grumman Aircraft Engineering Corp. Advanced Development Program, Project No. AD 04-03.

[2] Thermodynamics Engineer and Thermophysics Group Leader, respectively.

[3] Figures in brackets indicate literature references cited at the end of this paper.

Various radiation shields are used to fit particular sample geometries. They are of stainless steel or tantalum sheet with a highly polished inner surface to minimize radiation exchange with the sample. A typical stainless steel construction is shown schematically in Fig. 2a. The miniature heater supplying heat to the specimen is illustrated in Fig. 2b.

After preparation, the sample is inserted inside the radiation shield through the top flange and the whole assembly is attached to the copper block. All mating surfaces are covered with a thin layer of silicone grease to provide better thermal contact. The sample is from 0.076 to 0.23 m long and from 0.0064 to 0.0190 m in diameter (or of equivalent square or rectangular section.)

For measurement of voltage and temperature, fine-diameter insulated wires are used (0.51×10^{-4} to 1.27×10^{-4} m) in order to minimize the conduction loss.

The temperature is measured by copper-constantan thermocouples. They are either soldered directly to the sample or, when soldering is not possible, the junction is buried in the sample and secured in place by a low temperature cement or some mechanical process. The thermocouple output voltage is measured with a Leeds and Northrup type K-3 potentiometer. The power input to the sample heater is supplied by a variable transformer, and is determined from measurements of the current and the voltage drop across the heater. The voltage terminals are near the heater to avoid introducing the I^2R losses of the power leads into the power measurement. The sample heater current is measured from the voltage drop across a standard resistor. The voltage drop across the sample heater and the standard resistor are measured with the Fluke differential dc-ac voltmeter model 887AB. The power inputs to the guard heaters are monitored manually by variable transformers. In some cases, in order to avoid frequent intervention by the operator, the differential temperature between the sample heater and the bottom guard heater is controlled by a closed feedback control loop using a three-mode control action. This control loop continuously adjusts the power input to the guard heater and keeps the temperature difference less than 0.1 °K.

3. Experimental Procedure

The temperature along the sample is measured at equal distances ranging from 0.0064 to 0.051 m, depending on the thermal conductivity of the material. For high-conductivity materials a small ratio A/Z of the cross-sectional area A to the distance Z between thermocouples usually will be adequate for accurate determination of the thermal conductivity. For low-conductivity materials a large value of A/Z is used consistent with minimum measurable power dissipation and maximum temperature interval within which an average value of the thermal conductivity is to be determined.

The sample temperature is measured at three or more points depending on the length of the sample. At low energy levels, the choice of the sample length is greatly influenced by uncertainty in the heat measurement due to heat losses or gains by conduction through the thermocouple wires and by radiation exchange with the radiation shield. This uncertainty, however, becomes insignificant with increased power applied to the sample. Also, the time required to reach a stable thermal balance has some influence on the choice of the sample length.

For plastics, in general, a sample length of 0.076 m is chosen with temperatures measured at two or three points. For metals, a length of 0.13 to 0.23 m is chosen, with thermocouples spaced 0.025 to 0.051 m apart.

The temperature of the radiation shield is measured at the midpoint and is kept within 6 °K of the temperature of the corresponding point at the sample by the use of two guard heaters. In some cases it is necessary to minimize the radiation losses to the cold wall jacket. This is done by loosely wrapping a number of superinsulation foils around the radiation shield.

The conduction loss or gain through the thermocouple wires is minimized by leaving a loose 0.25 m length of wire between the sample and the radiation shield, and by thermally grounding another 0.30 m of wire at the corresponding temperature on the shield. Similarly, the conduction loss or gain through the power leads is minimized by wrapping enough length of wire around the bottom guard heater.

During operation, after the vacuum chamber is evacuated, the two reservoirs are filled with liquid nitrogen. Dry helium is then introduced in the chamber to rapidly cool the sample to a uniform temperature near that of liquid nitrogen. The chamber is

re-evacuated and, after a stable condition is reached, the specimen heater is turned on, with subsequent operation of the bottom guard heater. The upper guard heater is used occasionally to minimize the temperature gradient in the copper block at high heat fluxes but is mainly provided to raise the sink temperature when measurements are made at higher sample temperatures. Unless this is done, for a given thermocouple spacing the temperature gradient between two measured points becomes very large at high power inputs. Measurements are made in a vacuum between 1.33 x 10-5 and 1.33 x 10-6 N/m 2.

4. Conductivity Determination

For each experiment, the conductivity is determined at one or more average temperatures depending on the number of thermocouples. The simplified one-dimensional steady state heat balance equation used to determine the thermal conductivity from the measured values is:

$$P = VI = \lambda \frac{A}{Z} \Delta T \tag{1}$$

where: P = power applied to the sample heater, V = voltage drop across the sample heater, I = current, ΔT = temperature difference between two points, λ = average value of the thermal conductivity in the temperature interval ΔT.

Corrections due to inherent errors of the apparatus are not applied to the calculated conductivity value from eq. (1). An error evaluation (presented below) shows that experimental conditions and sample geometry can be chosen to bring the uncertainty of the experimental value down to a value of about 8% at 90 °K and 5% at 200 °K.

5. Error Evaluation

5.1 Analysis

The following analysis considers the errors involved in using equation (1) to compute the value of the thermal conductivity, as well as the errors involved in measuring the basic physical quantities of a thermal conductivity sample.

The most general heat balance expression for the sample is:

$$P = \int_A \lambda(T) \frac{\partial T}{\partial Z} dA + Q_\ell + wc_p\dot{T} \tag{2}$$

where: $\frac{\partial T}{\partial Z}$ = temperature gradient in the axial direction, Q_ℓ = energy loss through the lead wires, residual gas and by radiation heat transfer, w = mass of measured portion, c_p = specific heat, $\dot{T}$ = rate of change of sample temperature with time at the moment of measurement. The integral can be replaced with the one-dimensional equivalent expression $\lambda(T)A\, dT/dZ$ since the temperature variation over any cross-section where measurements are made is kept negligible (less than 0.1 °K) by the radiation shielding. Furthermore, in order that $\lambda(T)A\, dT/dZ = \lambda A\, \Delta T/Z$, ΔT should be kept relatively small so that errors due to non-linear terms in $\lambda(T)$ will be small. Temperature differences from 8 to 28 deg. are established between measured distances, depending on the thermal conductivity of the material and the temperature.

Eq (2) becomes:

$$P = \lambda A \frac{\Delta T}{Z} + Q_\ell + wc_p\dot{T} \tag{3}$$

Equation (3) gives after differentiation and rearrangement:

$$\frac{\delta\lambda}{\lambda} = \frac{\delta Z}{Z} - \frac{\delta A}{A} - \frac{\delta \Delta T}{\Delta T} + \frac{\delta P - \delta Q_\ell - wc_p\, \delta\dot{T} - \delta(wc_p)\dot{T}}{\lambda A\, Z^{-1}\, \Delta T} \tag{4}$$

For the evaluation of λ, eq (3) is reduced to eq (1), setting $Q_\ell = \dot{T} = 0$. Equation (4) then becomes:

$$\frac{\delta\lambda}{\lambda} = \frac{\delta P}{P} - \frac{\delta A}{A} + \frac{\delta Z}{Z} - \frac{\delta \Delta T}{\Delta T} - \frac{\delta Q_{\ell}}{P} - \frac{wc_p \delta \dot{T}}{P} \qquad (5)$$

Since the errors in P, A, Z, and ΔT are random while errors due to Q_{ℓ} and $\dot{T}$ are systematic, the total error can be better approximated by

$$\frac{\delta\lambda}{\lambda} = \left[\left(\frac{\delta A}{A}\right)^2 + \left(\frac{\delta Z}{Z}\right)^2 + \left(\frac{\delta P}{P}^2\right) + \left(\frac{\delta \Delta T}{\Delta T}\right)^2 \right]^{1/2} + \frac{\delta Q_{\ell}}{P} + \frac{wc_p \delta \dot{T}}{P} \qquad (6)$$

Each linear dimension is measured with an accuracy of ±0.3%. This gives a cumulative error of the measured portion of the sample of:

$$\left(\frac{\delta A}{A}\right)^2 + \left(\frac{\delta Z}{Z}\right)^2 = \left(2\,\frac{\delta D}{D}\right)^2 + \left(\frac{\delta Z}{Z}\right)^2 = (2 \times .3)^2 + (.3)^2 = (.67\%)^2 \qquad (7)$$

The power measurement error contains the contribution to the total error due to the accuracy of the readout instruments for voltage and current. The accuracy of the Fluke high input impedance vacuum tube voltmeter is ±0.05% and the overall accuracy of the precision portable shunt (used with the Fluke) is ±0.25%. In addition, there is an error of the order of 0.3% in the current and the voltage measurements because of waveform deformation. Thus

$$\left(\frac{\delta P}{P}\right)^2 = \left(\frac{\delta I}{I}\right)^2 + \left(\frac{\delta V}{V}\right)^2 = (0.25 + 0.30)^2 + (0.05 + 0.30)^2 = (0.65\%)^2 \qquad (8)$$

Equation (5) shows the uncertainty in the differential temperature measurement to increase rapidly with decreasing temperature interval ΔT. The limit of error of the copper-constantan thermocouples using premium grade wire is ±1% within the temperature range 89 to 215 °K. Therefore, the absolute error $\delta\Delta T$ increases with decreasing temperatures.

The expression for the differential temperature measurement error is

$$\left(\frac{\delta \Delta T}{\Delta T}\right)^2 = \frac{(\delta T_i)^2 + (\delta T_{i+1})^2}{(T_i - T_{i+1})^2} \qquad (9)$$

where i and i+1 refer to successive thermocouples on the sample. This error is plotted in Fig. 5.

The importance of keeping the temperature intervals small enough so that the thermal conductivity may be considered linear in T within the interval ΔT has been previously noted. In order to keep a temperature interval small with an acceptable uncertainty on the differential temperature measurement at the same time, an average value of the thermal conductivity is determined from measurements on two or more spans, in successive tests, arranged so that each span is evaluated at the same mean temperature and with approximately the same differential temperature. This is accomplished by using the upper guard heater or increasing sample heater power. The error shown in Fig. 5 would then be divided by the number of spans used.

The thermocouple readings are checked at ambient and at near liquid nitrogen temperatures (before heat is applied to the sample). The thermocouples respond nearly uniformly at both temperatures, indicating that errors are probably in the same direction. Therefore the differential temperature error is smaller than the values indicated in Fig. 5. Accuracy can be further improved by using calibrated thermocouples.

Heat flow through the thermocouple wires towards or away from the junction causes a temperature measurement error. This is minimized by thermally grounding the thermocouple wires to the radiation shield.

The term $\delta Q_{\ell} = \delta Q_g + \delta Q_w + \delta Q_r$, where Q_g is heat leakage through the residual gas Q_w is heat leakage through lead wires and Q_r is heat leakage by radiation.

The heat loss by convection is generally neglected for vacuum pressures $\leq 1.33 \times 10^{-2}$ N/m^2. Thus, Qg contains only heat loss by gas conduction.

Using the procedure indicated in Ref. [3]; at systems pressures below 0.13 N/m^2, this gas conduction is given by:

$$\delta Q_g = 2.426 \times 10^{-4} \quad A_s \quad \frac{\gamma + 1}{\gamma - 1} \frac{p}{\sqrt{MT}} (T_s - T_o) \qquad (10)$$

with accommodation coefficients $a_s = a_o = 1$, where: δQ_g is heat transfer in watts, A is surface area in cm^2, γ is ratio of specific heats, p is pressure in microns of mercury, T is temperature in degrees Kelvin, and M is molecular weight of residual gas.

Subscripts "s" and "o" refer to sample and cold wall respectively. The temperature T without subscript is measured at the gauge that measures the pressure p.

The heat leaks by gas conduction are greatest at the upper limit of sample temperature. However $\delta Q_g/P$ depends also on the power input to the sample, which is a minimum at the lowest temperature. For T_o = 77°K, T = 300°K, p = 0.001 microns, A_s = 68.5 cm^2 (maximum sample surface), γ = 1.41 and M = 28.8, $\delta Q_g/P$ is evaluated for minimum sample heat inputs of P = 0.0293W at 89°K and P = 0.293W at 200°K, yielding $\delta Q_g/P$ values of .0043% and .0044% respectively. This maximum error applies on the measured portion nearest the sink, since heat loss errors accumulate proceeding away from the sample heater.

The conduction loss through the lead wires (neglecting radiation from the surface of the wires) may be estimated from:

$$\delta Q_w = \sum \frac{\lambda A_w}{Z_w} \quad \Delta T_w \qquad (11)$$

where subscript w refers to the wire.

The thermocouple wires and power leads are thermally grounded around the radiation shield and bottom guard heater with a 0.254 m free length of wire between the sample and shield (see experimental procedure).

The maximum allowed temperature gradient between the radiation shield and the sample is ≤ 5.6 deg for long samples of average or high conductivity and ≤ 2.8 deg for short samples of low conductivity. The maximum temperature gradient $\Delta T_w/Z_w$ through the wire is then 22 deg/m for average or high conductivity samples and 11 deg/m for low conductivity samples. The quantities δQ_w and $\delta Q_w/P$ are greatest at the lower limit of temperature at which measurements are made, since at that temperature the thermal conductivity of the copper is the largest and the power input to the sample P is the smallest.

Table 1 shows an estimate of the heat leak $\delta Q_w/P$ for two different conditions of sample testing. Thermal conductivity values [3] of the wires at a temperature of 89°K, are: λ(copper) = 510 W m^{-1} deg^{-1}; λ(constantan) = 19.6 W m^{-1} deg^{-1}.

Table 1. Heat Leak for Two Test Cases at 89° K

Number of 1.27×10^{-4} m dia. wires	$\frac{\Delta T_W}{Z_W}$ deg/m	Q_W Watts	Minimum power input to the sample P Watts	$\frac{Q_W}{P}$ %
14 (6 copper-constantan thermocouples, 2 copper power leads)	22	0.116×10^{-2}	0.073	1.59
8 (3 copper-constantan thermocouples, 2 copper power leads)	11	0.036×10^{-2}	0.0293	1.23

This maximum error occurs for the measured portion nearest the sink, since the heat leak errors are cumulative proceeding away from the sample heater. At 200°K, power input to the sample is 10 times as great, so the Q_W/P values are approximately 1/10 as large.

The radiation loss δQ_r is estimated for isothermal surfaces using the long concentric cylinder relation. End effects are neglected since the shield is relatively close fitting and the annular gap is small compared with the axial length.

Tables 2 and 3 represent two cases of sample testing.

Table 2. Long samples of average or high conductivity with maximum differential temperature of 5.6 deg between sample and radiation shield, sample exposed area to radiation, $A_S = 64.5 \times 10^{-4}$ m^2 and a total hemispherical emittance of the surface of the sample and shield respectively, $\epsilon_s = 0.2$ and $\epsilon_r = 0.2$

Average Sample Temperature deg k	δQ_r - Watts	Minimum Power Input to the Sample P - Watts	$\frac{\delta Q_r}{P}$ %
89	0.083×10^{-2}	0.073	1.13
200	0.98×10^{-2}	0.73	1.34

Table 3. Short samples of low conductivity with maximum differential temperature of 2.8 deg between points on the sample and radiation shield and $A_S = 45.2 \times 10^{-4}$ m^2, $\epsilon_s = 0.6$, $\epsilon_r = 0.2$

Average Sample Temperature deg K	δQ_r - Watts	Minimum Power Input to the Sample P - Watts	$\frac{\delta Q_r}{P}$ %
89	0.0434×10^{-2}	0.0293	1.48
200	0.510×10^{-2}	0.293	1.74

This maximum error occurs for the measured portion nearest the sink since the effect of heat leaks by radiation is cumulative proceeding away from the sample heater.

It is important to note that when the upper heater is used to bring the temperature of the sink to a higher value (instead of increasing the heat input to the sample) for measurements of the conductivity at higher temperatures, the percentage

error $\delta Q_r/P$ increases, since P remains small. In such cases, the heat leak δQ_r must be kept small by decreasing the temperature difference between the radiation shield and the sample, or finding some other compromise solution towards a minimum error.

The error due to the changing of internal energy may be written:

$$\frac{wc_p\ \delta\dot{T}}{P} = \frac{Z^2 c_p d\ \delta\dot{T}}{\lambda\Delta T} \qquad (12)$$

where d is the density of the material.

Tables 4 and 5 show this error for two test conditions.

Table 4. Stainless steel rod of D = 0.95×10^{-2} m, measured portion length: Z = 5.1×10^{-2} m, d = 7850 kg/m^3, specific heat [3] c_p = 414 $Jkg^{-1}\ deg^{-1}$ at 200 °K and c_p = 209 $Jkg^{-1}\ deg^{-1}$ at 89 °K. Assume that at the moment of measurement the temperature at all points of the measured portion changes uniformly at the rate of $\dot{T}$ = 0.11 deg/hr

Average Temperature of the measured portion deg K	$wc_p\ \delta\dot{T}$ Watts	Minimum power input to the sample P Watts	$wc_p\ \delta\dot{T}/P$ %
89	0.182×10^{-3}	0.073	0.25
200	0.361×10^{-3}	0.73	0.049

Table 5. Teflon rod of D = 0.019 m, Z = 0.013 m, d = 2130 Kg/m^3, specific heat [3] c_p = 695 $Jkg^{-1}\ deg^{-1}$ at 200 °K and c_p = 356 $Jkg^{-1}\ deg^{-1}$ at 89 °K. Assume at the moment of measurement $\delta\dot{T}$ = 0.11 deg/hr

Average Temperature of the measured portion deg K	$wc_p\ \delta\dot{T}$ Watts	Minimum power input to the sample P - Watts	$\frac{wc_p\ \delta\dot{T}}{P}$ %
89	0.085×10^{-3}	0.0293	0.29
200	0.167×10^{-3}	0.293	0.057

5.2 Summary of Errors

An estimate of the total error is summarized below, as calculated using eq (6).

The largest single source of error is that due to the measurement of the differential temperature which is assumed not to exceed 5% at 89°K and 3% at 200°K (either by keeping large temperature intervals or by using more than one span as noted previously).

Table 6. Estimate of Total Error

Average Temperature, deg K	$\frac{\delta\lambda}{\lambda}$	
	Average or High Conductivity Samples	Low Conductivity Samples
89	8.06 %	8.09 %
200	4.68	5.07

6. Experimental Results

Some of the experimental results for steels and plastics are presented in Figures 6 to 8.

For all steels, except the 410 stainless steel, the thermal conductivity determined in this apparatus is in close agreement with values reported in [3] and [4]. For the 410 S.S. the variation of the conductivity with temperature follows the same trend, however, the values are 10% lower than those reported in [4].

The thermal conductivity of the Teflon rod near liquid nitrogen temperature compares satisfactorily with the value reported in [5].

7. References

1 Ziegler, W. T., Mullins, J. C. and Hwa S.C.P., "Specific Heat and Thermal Conductivity of Four Commercial Titanium Alloys", Advances in Cryogenic Engineering, Volume 8.

2 Tyler, W. W., Nesbitt, L. B., and Wilson A. C. Jr., J. Metals 1104 (Sept. 1953)

3 Scott, R. B., Cryogenic Engineering, D. Van Nostrand Co., N.Y., 1959.

4 Powell, R. L. and Blanpied, W. A., "Thermal Conductivity of Metals and Alloys at Low Temperatures", National Bureau of Standards Circular 556.

5 Chelton, D. B. and Mann D. B., "Cryogenic Data Book", National Bureau of Standards Cryogenic Engineering Laboratory, Boulder, Colorado, May 15, 1956.

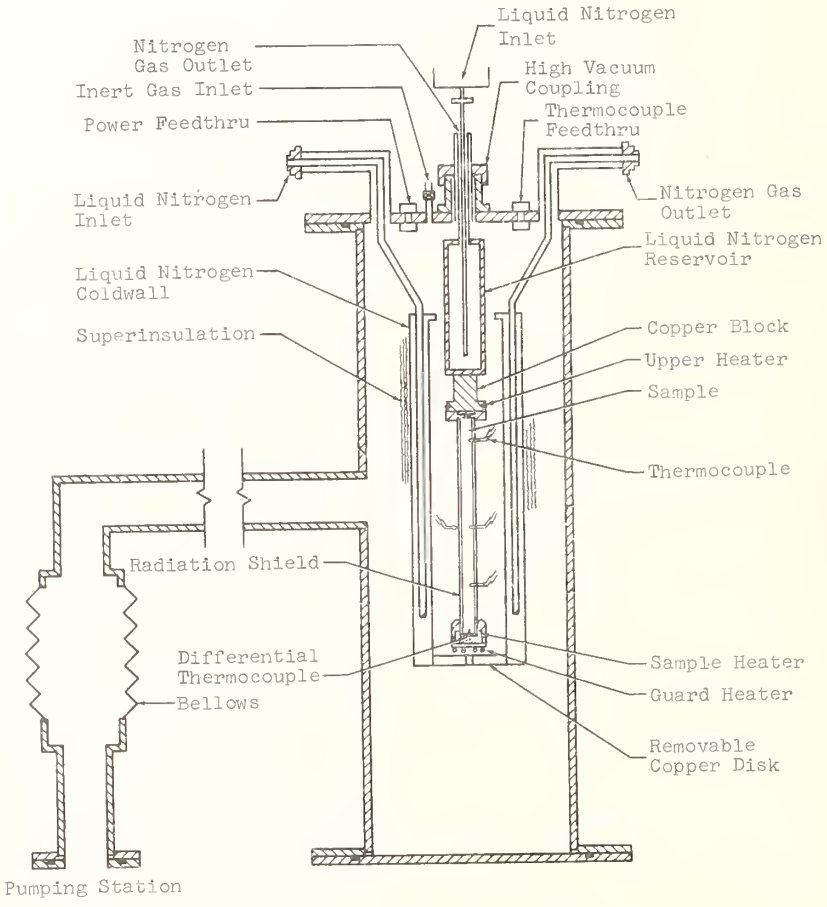

Fig. 1. Schematic drawing of the apparatus

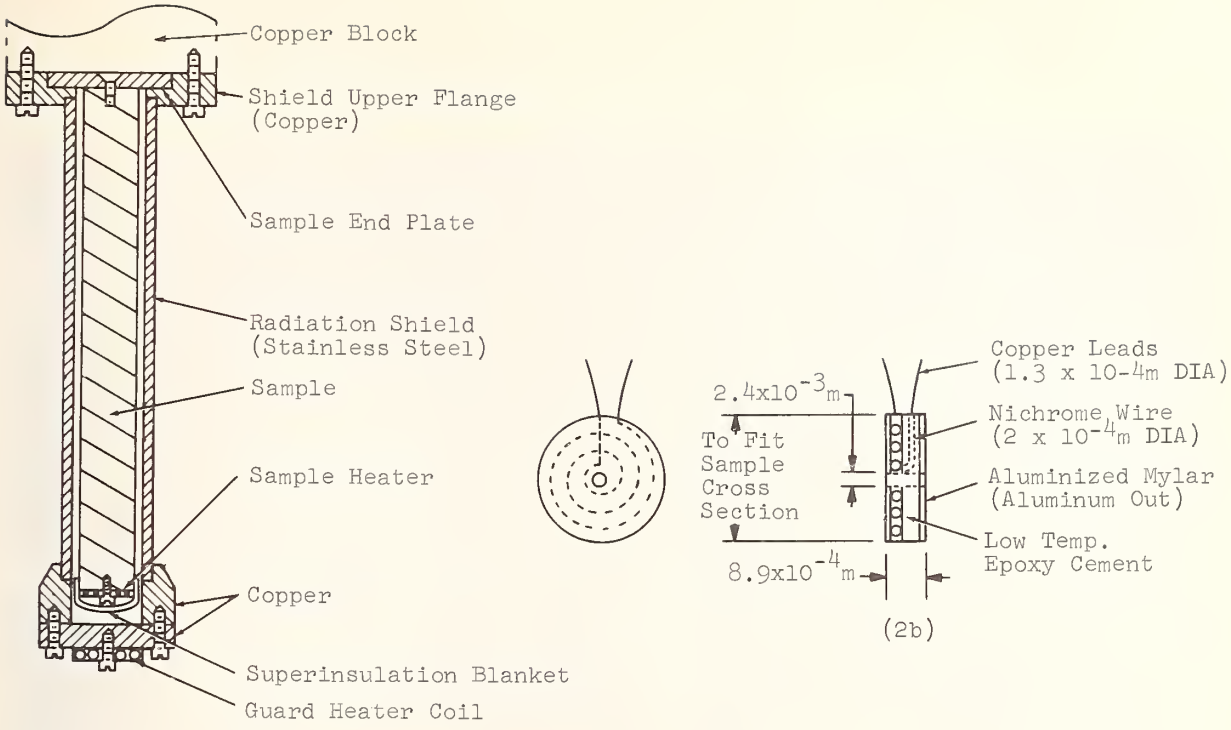

Fig. 2. Radiation shield and guard heater assembly (2a) and sample heater (2b)

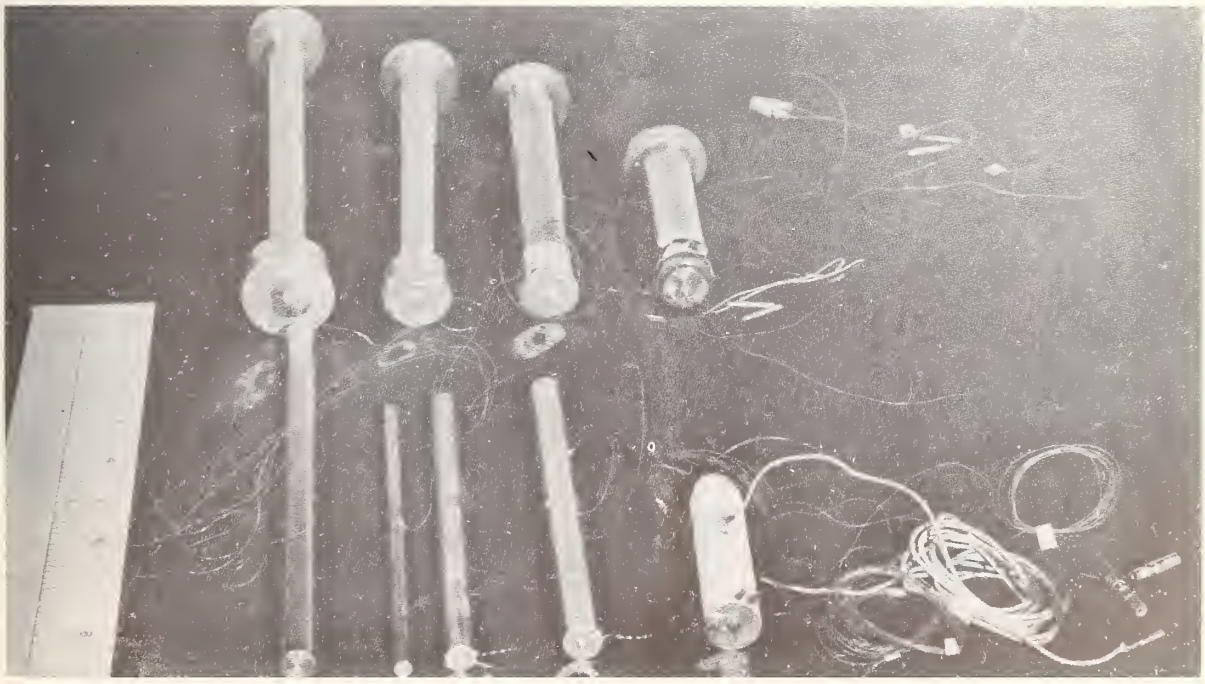

On the top are shown various radiation shields and bottom guard heaters assemblies. On the bottom are wired samples. The three samples on the right are shown with heaters in place.

Fig. 3. Wired shields and samples

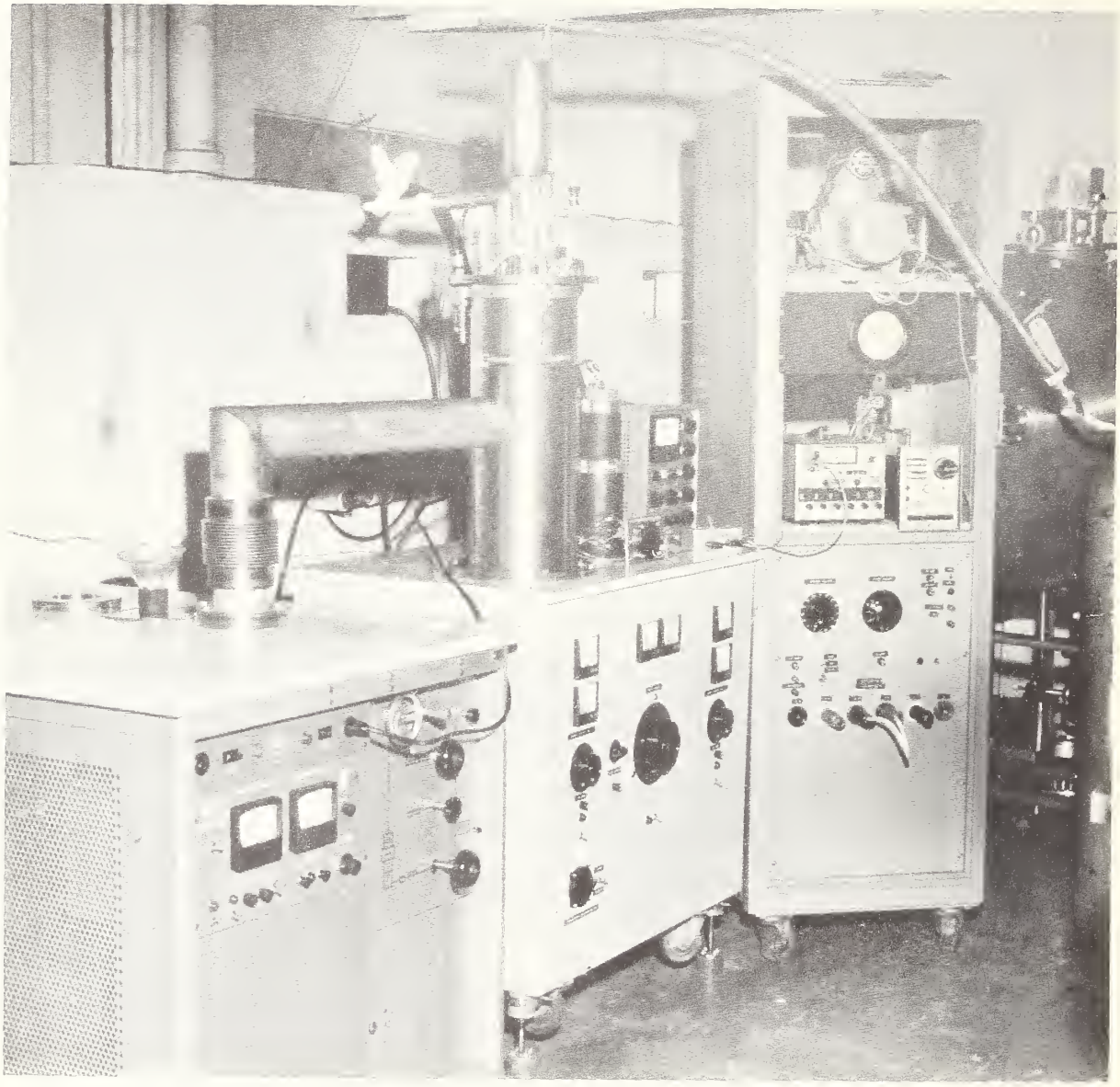

Shown on the right is the main power supply, and on the left the pumping station. The apparatus is mounted on a console containing the auxiliary power supplies and other instrumentation.

Fig. 4. The conductivity apparatus in operation

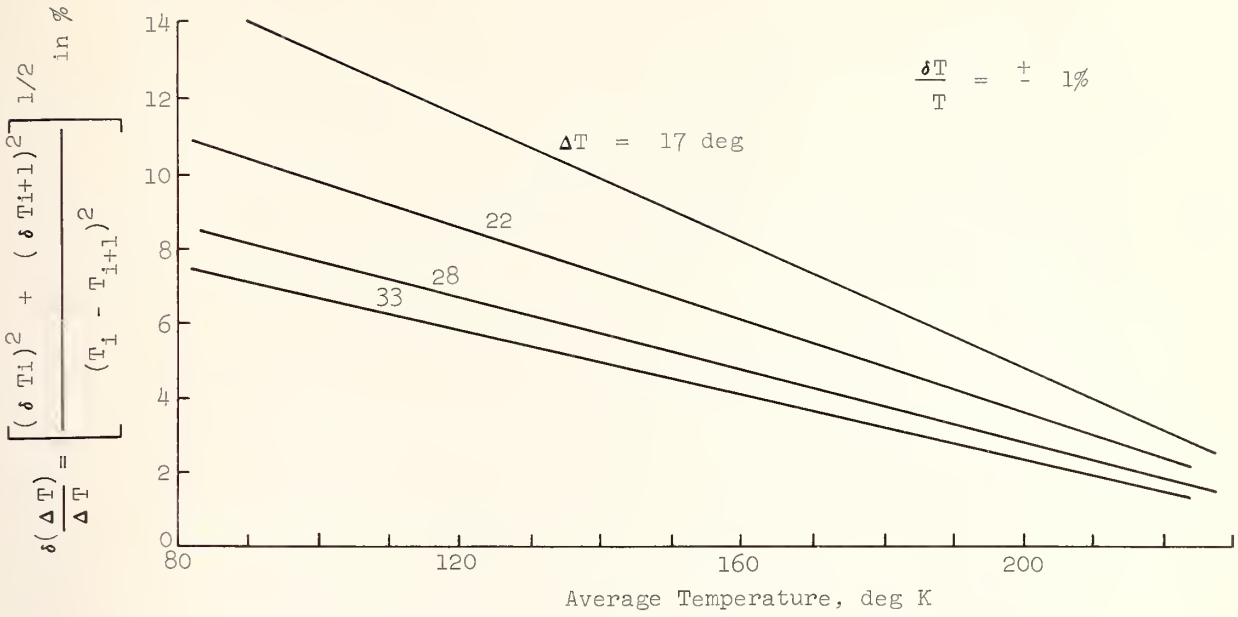

Fig. 5. Differential temperature measurement error

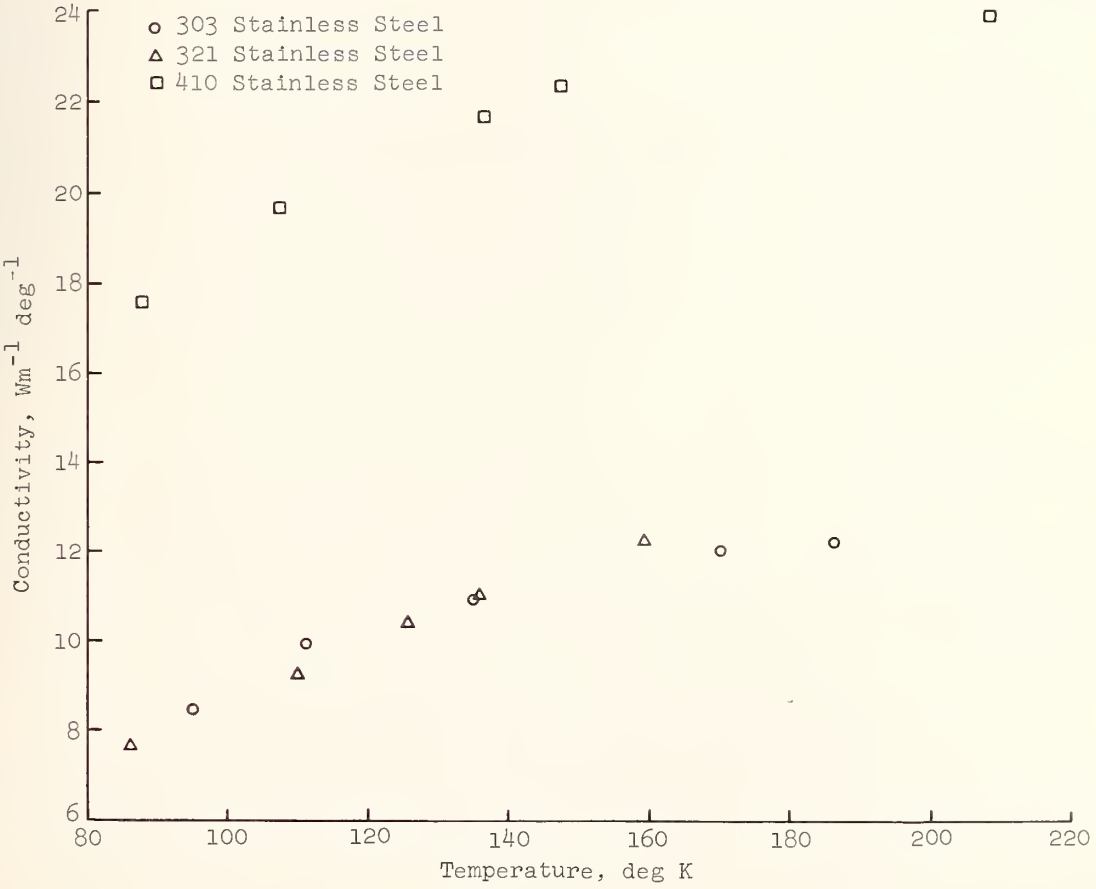

Fig. 6. Thermal conductivity of three stainless steels

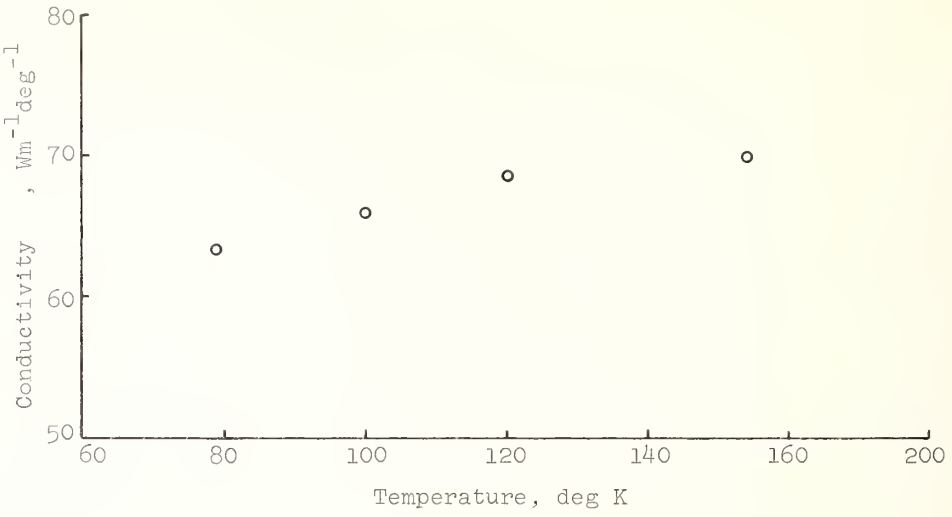

Fig. 7. Thermal conductivity of SAE 1020 steel

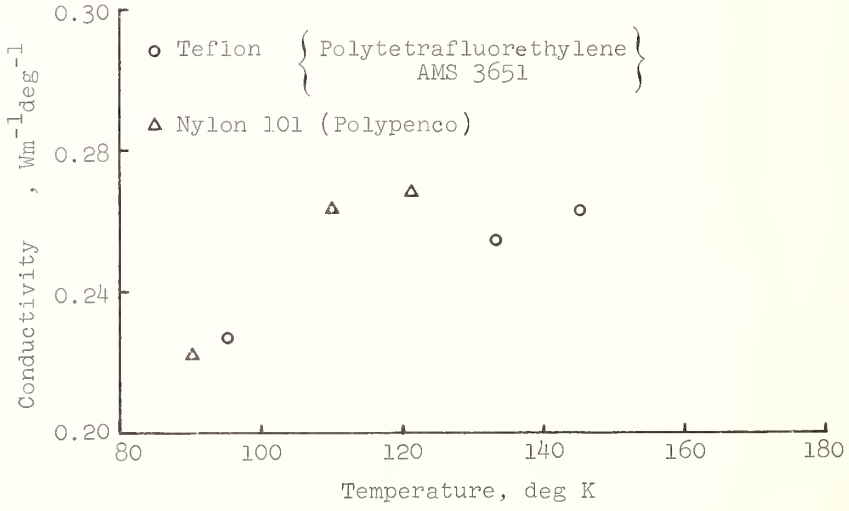

Fig. 8 Thermal conductivity of nylon and teflon

The Thermal Conductivities of Several Metals: An Evaluation Of A Method Employed By The National Bureau of Standards

David R. Williams and Harold A. Blum

SMU Institute of Technology
Dallas, Texas

An absolute method, developed by Watson and Robinson at the National Bureau of Standards, for the determination of thermal conductivity as a function of temperature was tested with four metals whose thermal conductivities ranged from 16 to 120 $W\ m^{-1}\ °C^{-1}$ from 38 to 345°C. In addition, a comparative method and a low heat loss absolute method were also developed with this apparatus. Some remarks about costs and operations are also included.

Key Words: Aluminum, conductivity, iron, metals, steel, thermal.

1. Introduction

An absolute method for determination of thermal conductivity of metals was developed at the National Bureau of Standards by Watson and Robinson [1][1]. We constructed the apparatus and measured the thermal conductivities of four metals, namely AISI 316, AISI 303MA, ARMCO iron, and 2024-T 351.

The advantage of the method is that thermal conductivity can be obtained as a function of temperature within a wide range of temperatures provided two experiments are conducted. In addition to this approach, we tested two other procedures for using this apparatus which also has merit in some cases. One of these is a comparative procedure in which the apparatus is calibrated with Armco iron whose thermal conductivity is well known [2] and in the second case we found it possible to adjust the temperatures of the guard and specimen in such a manner that the heat loss from specimen to guard was negligible. These latter methods only require one experiment in order to obtain the thermal conductivity data. It is the purpose of this paper to report the results of this study and to discuss some of the limitations and possibilities of this system. The complete description of the study has been reported by Williams [3].

2. Description of Methods

Three methods of analysis are applied to the experimental data obtained in tests using the previously described apparatus. These methods are:

1. An absolute method devised by Watson and Robinson [1] which requires the data obtained from a two-run experiment. In one run the temperature of the specimen is higher than the guard while the opposite holds for the second run. A heat balance equation is written for the specimen in each run. The heat input to the specimen is equated to the thermal conductivity and the radial heat loss - both expressed as functions of temperature. The two equations are solved simultaneously to yield the thermal conductivity and heat loss.

2. A comparative method, wherein by a series of experiments, using Armco iron, the apparatus is calibrated for heat transfer between specimen and guard. Thereafter, thermal conductivities for other specimens are obtainable on a relative basis from the results of a one-run experiment.

3. A "no-loss" absolute method for which the temperature differences between specimen and guard are reduced to the extent that heat transfer between the two

[1]Figures in brackets indicate the literature references at the end of this paper.

becomes negligible. On this basis, thermal conductivities are determinable on an absolute basis from the results of a one-run experiment.

3. Results

3.1 The Experiments

In this investigation, the first seven experiments included two runs each. As explained previously, the data obtained from a run (a) and a run (b) are required for the solution of λ values by the absolute method of Watson and Robinson [1].

These seven experiments are the following:

Experiment No.	Specimen Material	Average Specimen Temperatures Span VI	Span I	Remarks
1	AISI 316	72 °C	231 °C	Tested by N.B.S.
2	AISI 303MA	50	137	
3	AISI 303MA	73	234	
4	Armco iron	55	147	
5	Armco iron	77	245	
6	2024-T351	55	144	
7	2024-T351	78	216	

In this tabulation, span VI and span I refer to segments of the specimen near the sink and heater respectively. The average specimen temperature in each span designates the arithmetic average of the temperatures in that span from runs (a) and (b).

Further experiments consisted of nine individual runs using the Armco iron specimen. The object of these nine runs was to calibrate the apparatus for heat transfer between specimen and guard as a basis for determining λ values by a comparative method.

These nine calibration runs were divided into three subsets of three runs each. In each subset, the specimen temperature was maintained essentially constant, and the guard temperature was changed for each of the three runs.

Each subset of three runs provided bonus results in that any two runs of a subset can be paired and analyzed by the Watson and Robinson [2] absolute method. This pairing of runs was, in fact, done to the extent that six additional analyses were made on Armco iron by this absolute method. For consistency with the above table, these six pairs of runs are identified as six additional two-run experiments, numbered 8 through 13 in the continuing tabulation below:

Experiment No.	Specimen Material	Average Specimen Temperatures Span VI	Span I	Calibration Runs
8	Armco iron	48 °C	127 °C	1 and 2
9	Armco iron	48	128	2 and 3
10	Armco iron	67	212	4 and 5
11	Armco iron	67	211	5 and 6
12	Armco iron	87	311	7 and 8
13	Armco iron	86	302	8 and 9

3.2 Thermal Conductivities of AISI 316 Stainless Steel

The particular AISI 316 specimen used in Experiment 1 was earlier tested by the National Bureau of Standards, and the results were reported by Watson and Robinson [4]. These investigators determined thermal conductivities of AISI 316, in the range from 90°C to 840°C, to be:

$$\lambda = 13.33 + 17.27\left[\frac{T}{1000}\right] - 4.3334\left[\frac{T}{1000}\right]^2 + 3.32\left[\frac{T}{1000}\right]^3 \qquad (4\text{-}1)$$

where λ is thermal conductivity, W m^{-1} $°C^{-1}$, and T is temperature, °C.

The data from Experiment 1 performed here were analyzed by the Watson and Robinson [1] method, and the relationship of λ and temperature was found by the least-squares method for a temperature range from 72°C to 231°C to be:

$$\lambda = 13.478 + 9.47 \times 10^{-3}T + 5.60 \times 10^{-5}T^2 \qquad (4\text{-}2)$$

Values of λ, obtained, are presented in Table 1. Comparisons are also made for values of λ computed by the comparative method and the "no-loss" absolute method.

Table 1. Thermal conductivity values of AISI 316 stainless steel.

Span No.	Specimen Mid-Span Temperature (°C)		Thermal Conductivities (W m^{-1} $°C^{-1}$)							
	Run (a)	Run (b)	N.B.S.	W. & R. Method	% Diff.	Comparative Method	% Diff.	"No-Loss" Method	% Diff.
I	231.3	230.7	17.12	18.27	+6.7	17.78	+3.8	17.04	-0.5
II	201.7	201.0	16.65	17.47	+4.9	17.26	+3.6	16.64	-0.1
III	170.9	170.3	16.16	16.57	+2.6	16.78	+3.9	16.61	+2.8
IV	139.1	139.1	15.66	15.71	+0.3	15.41	-1.5	15.83	+1.1
V	105.8	105.5	15.10	14.96	-0.9	14.03	-7.1	14.83	-1.8
VI	71.6	71.7	14.55	14.44	-0.7	13.63	-6.3	14.41	-0.9

3.3 Thermal Conductivities of AISI 303MA Stainless Steel

Experiments 2 and 3 were performed with the AISI 303MA specimen. From the data in Experiment 2, thermal conductivities were determined for a temperature range from 50°C to 137°C; from Experiment 3, λ values were found in the temperature range from 73°C to 234°C.

Application of the Watson and Robinson [1] absolute method to Experiment 2 data yields the following relationship for thermal conductivity:

$$\lambda = 13.257 + 2.46 \times 10^{-2} \quad (50 < T < 137C) \qquad (4\text{-}3)$$

For Experiment 3, the Watson and Robinson absolute method provides the following equation for λ as a function of temperature:

$$\lambda = 14.189 + 1.99 \times 10^{-2}T \quad (73 < T < 234C) \qquad (4\text{-}4)$$

In the overlapping temperature range, the values of λ determined by equations (4-3) and (4-4) agree within approximately three percent.

Published values of thermal conductivity could not be found for this particular stainless steel. The alloying elements and percentages thereof in AISI 303MA and AISI 303 are identical with two exceptions: AISI 303MA contains 0.60% molybdenum, maximum, and 0.50/0.90% aluminum; whereas, AISI 303 does not contain these elements. The influence which these added elements might have on thermal conductivity can only be surmised to be small.

Table 2 includes thermal conductivities for AISI 303 as given by McAdams [3].

In Table 2, values of thermal conductivity of AISI 303MA are presented for the Watson and Robinson method applied to Experiment 2 data; in addition, values are given for the comparative and "no-loss" methods as applied to run (a) of Experiment 2.

Arbitrarily, the values of λ obtained by the "no-loss" method are used as a basis

for comparison of the values derived by the other methods. Comparison is expressed in percent of difference from the "no-loss" value in each span.

Table 2. Thermal conductivities of AISI 303MA stainless steel.

Span No.	Specimen Mid-Span Temperature (°C)		Thermal Conductivities (W m^{-1} $°C^{-1}$)					
	Run (a)	Run (b)	"No-Loss" Method	W. & R. Method	% Diff.	Comparative Method	% Diff.	AISI 303 (Information Only)
I	136.7	137.8	16.62	16.62	0	16.30	-2.0	16.75
II	119.4	120.6	16.24	16.28	+0.1	15.69	-3.4	16.52
III	102.2	103.4	16.42	15.79	-3.8	15.41	-6.1	16.30
IV	85.0	86.0	16.19	15.29	-5.6	14.76	-9.0	16.07
V	67.7	68.3	15.90	14.84	-6.6	14.15	-10.9	15.85
VI	50.0	50.1	15.55	14.58	-6.2	13.80	-11.1	15.60

3.4 Thermal Conductivities of Armco Iron

Equation 4-5 represents the application of the method of least-squares to the values reported by thirteen investigators [2] of Armco iron and is valid over a temperature range from -18°C to 538°C.

$$\lambda = 74.32 - 6.22 \times 10^{-2} T \qquad (4\text{-}5)$$

Consequently, knowing the thermal conductivity for Armco iron permits further evaluation of the apparatus and the method of Watson and Robinson [1]. Also, it provides the basis for the comparative method and a means of evaluating the "no-loss" method.

To this end, eight experiments were performed using the Armco iron specimen. These experiments are numbers 4, 5, 8, 9, 10, 11, 12, and 13. The eight experiments were analyzed by the Watson and Robinson method and by the "no-loss" method. In addition, the comparative method was applied to run (a) of experiment 4 and run (a) of experiment 5.

Thermal conductivities are presented for Experiment 12 in Table 3 and Experiment 4 in Table 4 as typical of the data obtained. The basis for presenting the errors is to assume the Goldsmith [2] data is correct.

The application of the Watson and Robinson [2] absolute method produced poor results for Experiments 4 and 5 [Data in Table 3]. The reason is not known. In another six experiments, however, the Watson and Robinson [2] analysis technique provided overall results within 1.5% of the reference values from equation 4-5.

Validity of the "no-loss" method is seen to be related to the specimen-to-guard temperature difference. For example, in Experiment 9, the specimen temperature is higher than guard temperature by approximately 6°C over the length of the bar. Thus, the cumulative loss of heat from the specimen results in progressively poorer results from span I to span VI for the "no-loss" method.

In experiment 10, where the "no-loss" method affords very favorable values for λ the average radial temperature difference between specimen and guard is approximately 2°C.

Table 3. Thermal conductivity values of Armco iron from experiment 12

Span No.	Specimen Mid-Span Temperature (°C)		Thermal Conductivities ($W\ m^{-1}\ °C^{-1}$)					
	Run (a)	Run (b)	Ref. (2)	W. & R. Method	% Diff.	Comparative Method	% Diff.	"No-Loss" Method	% Diff.
I	315.6	306.0	54.67	55.08	+0.8	Not Used		56.14	+2.7
II	265.6	258.2	57.77	58.30	+0.9			60.20	+4.2
III	218.1	211.7	60.74	61.57	+1.4			64.84	+6.8
IV	172.8	167.8	63.58	65.05	+2.3			68.70	+8.0
V	129.4	125.6	66.26	68.80	+3.8			68.87	+3.9
VI	88.4	86.1	68.82	72.88	+5.9			71.66	+4.1

Table 4. Thermal conductivity values of Armco iron from experiment 4

Span No.	Specimen Mid-Span Temperature (°C)		Thermal Conductivities ($W\ m^{-1}\ °C^{-1}$)						
	Run (a)	Run (b)	Ref. (2)	W. & R. Method	% Diff.	Comparative Method	% Diff.	"No-Loss" Method	% Diff.
I	147.2	146.1	65.17	62.40	-4.3	62.83	-3.9	63.30	-2.9
II	128.3	127.2	66.34	63.68	-4.0	62.43	-5.9	62.94	-5.2
III	109.4	109.0	67.50	63.92	-5.3	64.47	-4.5	65.20	-3.4
IV	91.0	90.5	68.64	63.78	-7.1	64.53	-6.0	65.60	-4.4
V	72.8	72.2	69.77	63.59	-8.9	65.22	-6.5	66.62	-4.5
VI	55.1	55.0	70.88	63.58	-10.4	66.97	-5.5	68.75	-3.0

3.5 Thermal Conductivities of 2024-T351 Aluminum Alloy

Two experiments, numbers 6 and 7, were performed using the 2024-T351 aluminum specimen. The temperature range in each of these experiments overlapped to permit a comparison of λ values in the common temperature range. No reference was found for the thermal conductivity of this particular aluminum.

Table 5 summarizes the results from Experiment 6. The three methods of analysis provide generally comparable values for λ. Values calculated by the "no-loss" method are higher than the mean and are progressively departing therefrom in the successive spans on the specimen. Nominally, a 5°C radial temperature difference existed over all the spans. Therefore, the departure of λ values by the "no-loss" method is reasonable.

In the overlapping temperature range of experiments 6 and 7, the application of the Watson and Robinson method to each experiment gives values of λ which agree within three percent.

Table 5. Thermal conductivity values of 2024-T351 aluminum from experiment 6

Span No.	Specimen Mid-Span Temperature (°C)		Thermal Conductivities ($W\ m^{-1}\ °C^{-1}$)				
	Run (a)	Run (b)	W. & R. Method	Comparative Method	% Diff.	"No-Loss" Method	% Diff.
I	143.9	143.4	138.90	139.63	+0.5	142.40	+2.5
II	127.0	126.7	135.46	133.59	-1.4	137.34	+1.4
III	109.4	109.3	131.96	129.35	-2.0	134.33	+1.8
IV	91.7	91.7	128.54	127.26	-1.0	133.86	+3.8
V	73.8	73.9	125.27	122.29	-2.4	129.43	+3.3
VI	55.4	55.5	122.24	120.08	-1.8	127.90	+4.6

4. Discussion

The method of Watson and Robinson [1] has been tested in a limited range (38-345C) for four metals whose thermal conductivities range from about 16 to 120 watts/M-°C. Agreement within 3% was obtained on one common sample.

Two other procedures were found to be successful in many cases. One method depended upon the calibration of the system with Armco iron while the second method depended on obtaining an average temperature difference between the specimen and guard of less than 2°C. This latter method assumes no radial heat losses and is treated as if it were an absolute method. The advantage of these latter methods, when applicable, is that only one experimental run is required to obtain thermal conductivity as a function of temperature compared with the two runs required for the Watson and Robinson absolute method.

This apparatus does provide the advantage of obtaining thermal conductivity as a function of temperature in one experimental setup and in one or two experimental runs. It requires a relatively large specimen of specific size (about 0.37 meters long and about 0.4 cm. diameter) which can be machined in order to provide a place for the source and for the sink. The experiment takes about one day per run, about a day for machining and only a short time for analysis with a computer program. The safe minimum elapsed time from the receipt of the sample to the reporting of data would be about three days.

There are possibilities for further simplification and greater flexibility with this apparatus.

5. Acknowledgements

We appreciate the help of Daniel R. Flynn of the National Bureau of Standards for furnishing us with the details of the apparatus and a sample for comparison. This study was part of a project supported by the National Aeronautics and Space Administration (NsG 711/004 007 004).

6. References

[1] Watson, T.W. and Robinson, H.E., Thermal conductivity of some commercial iron-nickel alloys, Journal of Heat Transfer, November, 1961.

[2] Goldsmith, A., Waterman, T., Hirschhorn, H., Handbook of thermophysical properties of solid materials, Volume 1 - Elements, revised ed., Armour Research Found., Pergamon Press, 1961.

[3] Williams, David R., Thermal conductivity of some metals, M.S. Thesis, November, 1966, SMU Institute of Technology, Dallas, Tex.

[4] Watson, T.W., and Robinson, H.E., Thermal conductivity of a sample of type 316 stainless steel, NBS Rept. 7818, March 22, 1963.

[5] McAdams, W. H., Heat transmission, Third ed., McGraw-Hill Book Co., 1954.

A Longitudinal Symmetrical Heat Flow Apparatus For The Determination Of The Thermal Conductivity Of Metals And Their Alloys

H. Chang[1] and M. G. Blair[2]

Energy Conversion Division
Nuclear Materials and Equipment Corporation
Leechburg, Pennsylvania 15656

The present paper describes an apparatus used for determining the thermal conductivities of metals and their alloys in the temperature range 50° to 1000°C. The measurements are made on a small-diameter cylindrical rod sample subjected to one-dimensional longitudinal heat transfer. The colorimetric heater, welded into a cavity half-way between the ends of the sample, provides, because of its location and construction, equal and symmetrical heat transfer from the center of the sample to either of the two ends, and allows input heat to be calculated precisely. Because of the presence of the guard, which is radially isothermal with the sample, no heat loss is expected through the heater leads or by radiation from any portion of the sample.

The thermal conductivities of Tophel Special (approximate composition 90% Ni 10% Cr) up to 500°C has been measured in this apparatus and reported. Tophel Special is an excellent metallic thermoelectric material. The precision and accuracy of the apparatus is discussed, and modifications may be easily made to measure the thermal conductivities of high melting point metals and their alloys. The reported data are preliminary, and current measurements on standard materials are designed to confirm the accuracy of the apparatus.

Key Words: Electrical resistivity, figure of merit, nickel-base alloy, Seebeck coefficient, thermal conductivity.

1. Introduction

The electrical power output of a radioisotope thermoelectric generator is directly proportional to the figure of merit, Z, of the thermoelectric materials used to convert thermal energy directly into electrical energy. Z is defined as $S^2/\rho\lambda$, where S, ρ, and λ are respectively the Seebeck Coefficient, electrical resistivity, and thermal conductivity of the material. Thermoelectric materials with high figures of merit are, therefore, excellent candidates for use in thermoelectric generators. In order to compute the figure of merit of a given material, therefore, it is essential to know its thermal conductivity. Although the figure of merit of metallic thermoelectric materials is often an order of magnitude smaller than those of semi-conductors, metallic thermoelectric materials may be preferred for practical reasons. Such is the case for Tophel Special (manufactured by Wilbur B. Driver Company), an alloy of Ni and Cr, the thermal conductivity of which is unknown. The largest Tophel Special samples available for testing, which have the same physical properties as those of the usual fabricated small diameter thermoelectric elements, are cylindrical rods with a diameter of approximately 3.2 mm. A precise and an accurate method for measuring the thermal conductivity of metals and their alloys which are available only in small diameter samples is, therefore, required.

---

[1] Manager, Energy Conversion Physics Department

[2] Physicist

Although the present absolute method of measuring thermal conductivity is reminiscent of those employed by Schofield (1) and R. W. Powell (2), the present method utilizes flexibility of design and temperature control in order to accommodate cylindrical samples of small diameter.

The accuracy of the data depends on the degree to which the thermal response of the sample can be made to approach the ideal conditions assumed in theory and on the magnitude of the errors involved in the various experimental measurements. The unique feature of the apparatus reported in this paper is the heater built into a cavity half-way between the ends of the cylindrical rod sample. This construction minimizes heat loss and allows input heat to be calculated precisely. The apparatus is also capable of measuring materials with high melting points, such as refractory metals, which may not be available in large sizes.

2. Description of the Method

The absolute method for measuring the thermal conductivities of metals and alloys described here utilizes a small heater placed in a cavity midway between the two ends of a long cylindrical sample. Radial radiative heat transfer from the surface of the sample is eliminated by a coaxial tube sample guard which may be heated so that the difference between the sample surface temperature and the guard surface temperature, measured at any location equidistant from the longitudinal center of the sample and guard, is zero.

This arrangement insures bidirectional conductive heat transfer from the center of the sample to either of the two ends. Considering the axis of the cylindrical sample to be coincidental with the y axis of a rectangular coordinate system, with the longitudinal center coincidental with the origin, the one-dimensional steady-state heat transfer equation (assuming the thermal conductivity is independent of temperature) governing heat conduction from the center of the sample to the top end is simply given as

$$Q_1 = - \lambda A \left(\frac{d\theta}{dy}\right)_1 , \tag{1}$$

where Q_1 = heat transferred from the center of the sample to the top end
A = area perpendicular to the direction of heat transfer
$\left(\frac{d\theta}{dy}\right)_1$ = temperature gradient established in the positive y direction

Similarly, the one-dimensional steady-state heat transfer equation governing heat conduction from the center of the sample to the lower end is

$$Q_2 = - \lambda A \left(\frac{d\theta}{dy}\right)_2 , \tag{2}$$

where Q_2 = heat transfer from the center of the sample to lower end
$\left(\frac{d\theta}{dy}\right)_2$ = temperature gradient established in the negative y direction.

The total power input Q_t to the sample heater is the sum

$$Q_t = Q_1 + Q_2 , \tag{3}$$

or

$$Q_t = - \lambda A \left[\left(\frac{d\theta}{dy}\right)_1 + \left(\frac{d\theta}{dy}\right)_2\right] . \tag{4}$$

The thermal conductivity λ is calculated from Eq. (4) to be

$$\lambda = - (Q_t/A) \left[\left(\frac{d\theta}{dy}\right)_1 + \left(\frac{d\theta}{dy}\right)_2 \right]^{-1} \quad (5)$$

Equation (5) is used to calculate λ if $\left(\frac{d\theta}{dy}\right)_1$ and $\left(\frac{d\theta}{dy}\right)_2$ are not equal, which indicates that the heat transfer from the center of the sample to either of the two ends is unequal. However, when the heat transfer from the center of the sample to both of the two ends is made to be equal, $\left(\frac{d\theta}{dy}\right)_1$ equals $\left(\frac{d\theta}{dy}\right)_2$, and Equation (5) reduces to

$$\lambda = - (Q_t/2A) \left[\left(\frac{d\theta}{dy}\right)_1 \right]^{-1} . \quad (6)$$

Either Equation (5) or Equation (6) may be used to calculate the thermal conductivity, λ, the choice depending upon the symmetry of the experimentally measured gradients.

Moreover, in the case where all the heat input is made to flow in only one direction by creating an isotherm at either the top or bottom half of the cylindrical sample, then one of the temperature gradients in (5) is zero. If the heat is made to flow to the top end, then $\left(\frac{d\theta}{dy}\right)_2$ in Equation (5) is made zero, and Equation (5) reduces to

$$\lambda = - (Q_t/A) \left[\left(\frac{d\theta}{dy}\right)_1 \right]^{-1} . \quad (7)$$

Deliberate creation of such an isotherm in one direction provides essentially a second experiment. With its experimental findings, the results of the bidirectional experiment may be correlated, thereby giving a double check on the accuracy of both results.

3. Apparatus

The schematic diagram and the details of the apparatus used to measure the thermal conductivity of Tophel Special (a thermoelectric material, of approximate composition 90% Ni and 10% Cr, supplied by Wilbur B. Driver Company) are shown in Figure 1 and Figure 2 respectively. The high-temperature sample heater (detail A of Figure 2) is made by threading a continuous length of .178 mm (.007") diameter tantalum wire through all of the 7 bores of a multibore alumina tube 2.5 cm in length (Degussa catalog No. 60-077175, outside diameter = 1.75 mm and bore diameter = .20 mm). The two free ends of tantalum wire, which form the power leads to the heater, are at opposite ends of the alumina tube, and are brought out through the sample wall through two alumina-insulated holes discussed below.

The cylindrical sample rod is fabricated from a single 3.18 mm (.1274") diameter 200 mm long Tophel Special rod. To place the heater in a cavity within the sample, located at the longitudinal center of the sample rod, the rod was cut into two pieces of equal length, and flat bottomed 2.38 mm (.0935") holes were bored concentric with the rod in either direction at the break. The cavity holes were bored deep enough to allow for the symmetric spacing of the heater in the sample and to include 1 mm alumina insulators at both ends. A .838 mm diameter hole was drilled radially into the cavity 1.5 mm toward the break from the bottom of each cavity hole for passage of the heater power leads and their alumina insulators. After insertion of the heater and alumina insulators, the sample was rejoined by TIG (Tungsten Inert Gas) welding at the break. To facilitate the welding, the ends at the break were machined to a close-tolerance fit, mating a relief entubulation on one side to a counter bore on the other. This joint was subsequently fused by the weld.

The dual encapsulation of the sample heater within the ceramic and within the sample provides, aside from the necessary electrical insulation, the dual benefit of more uniform heat transfer to the sample and the elimination of heat leakage from the sample, for which accounting would otherwise be difficult. A .127 mm diameter (.005") platinum 10% rhodium wire is tack welded to each of the heater leads at the point of their emergence from the sample to serve as voltage leads. The locations of the voltage leads are so chosen that they effect the most accurate reading of the voltage drop across the sample heater possible. Precise measurement of this voltage and of the current through the heater gives the most accurate possible measurement of the power input.

The two-bore oval cross-section alumina insulator carries each pair of leads radially through the guard, and away from the apparatus, effecting complete electrical insulation from each other and from other parts of the system. When the sample guard, which will be discussed later, is raised to the temperature of the sample at this location, the power lead is in an isothermal environment and no heat loss from the sample through it or the voltage leads is expected. At the top and bottom ends of the sample, holes are drilled to receive alumina rods which extend to serve as centering and insulating supports. Heaters, which are made by threading a length of .178 mm tantalum wire through 23 uniformly spaced, alumina-insulated holes in a copper cylinder 27 mm in diameter and 12.7 mm in height are attached at top and bottom of the sample. A center hole of the proper diameter allows the heaters to be fitted over the sample, and a positive mechanical contact is made by slotting the toroidal heater and drawing the open side together with screws.

The thermal gradient is obtained by taking temperature differences between the seven pairs of Pt-Pt 10% Rh thermocouples strategically located along the length of the sample. The .127 mm (.005") thermocouple wire pairs were flame fused at the end into a small bead, which was spot welded into a small positioning indentation in the sample at the desired location.

One thermocouple is located at the longitudinal mid-point of the sample, which is also the mid-point of the sample heater. The remaining six pairs of thermocouples are symmetrically located with respect to the center pair (See Figure 2):three pairs attached to the sample above the heater and three below. The thermocouples are evenly spaced on both sides of the center, respectively 19.05 mm (.75"), 31.75 mm (1.25") and 44.45 mm (1.75") from the sample center. The two nearest thermocouples to the sample heater are 6.35 mm (.25") from the end of the center sample heater nearest them.

The sample guard is a tube with an inside diameter of 6.35mm(.25")and a wall thickness of .381 mm (.015"). Since the purpose of the guard is to provide an isothermal radial environment for the sample at all points, a guard is required which will have the same thermal gradient as the sample. This condition can be satisfied ideally if the thermal conductivity and the cross-sectional areas of both tube and sample are the same. This wall thickness was chosen to allow the cross-sectional area of the guard perpendicular to the direction of heat flow to equal that of the sample. Due to the fact that the Tophel Special sample material is not available in rods with diameter greater than 3.175 mm in diameter (.125"); Tophel Special with slightly different heat treatment was selected for the guard. The tube is machined from a solid rod 7.97 mm in diameter (.314") which was also supplied by Wilbur B. Driver Company.

Since the total length of the guard tube required was 143 mm (5.625"), it was difficult to machine such a tube and maintain tolerances on walls of .381 mm thickness. The guard tube was, therefore, machined in two shorter pieces, and subsequently E.B. welded together. (See detail A of Figure 2).

Three heaters are attached to the guard in the same fashion as the sample heaters, one in the center and one on each end of the tube. Six pairs of the Pt-10% Rh thermocouples are attached to the surface of the guard in the same manner as those attached to the surface of the sample. They are located at positions radially opposite those attached on the samples when the guard is properly positioned around the sample. (See Figure 2) A .254 mm diameter wire (.010") Pt-Pt-10 Rh thermcouple is attached to each of the five copper heaters. These thermocouples are placed in the slots of the heater and mechanically affixed when the heaters are tightened on the guard and sample.

In the final assembly, the lower alumina sample support rod fits into a hole drilled into the base of the support framework for this purpose. The top alumina centering rod passes through a hole drilled in the center of the top plate of the framework, and is free to move up and down to allow for the thermal expansion of the cylindrical sample. The top and bottom guard heaters are supported by the top and bottom sample heaters through three alumina support rods, which not only center the guard with respect to the sample but also insulate the components electrically and thermally from each other. The entire structure is thermally insulated by three 1 mil titanium radiation shields. The guard and sample heaters are similarly isolated by sets of radiation shields, and the entire system is operated in 1×10^{-6} mm Hg vacuum. Power is supplied to the sample heater by a Sorensen QRC 40-30A DC power supply, and both the

voltage across the heater and the current through it are measured with a Fluke model 895A DC voltmeter, which has a 1 μv sensitivity. The latter measurement is made across a 1Ω (.05% tolerance) 10 watt precision resistor in series with the heater.

The five peripheral copper heaters are all powered in the same manner (Insert AA of Figure 1) by Powerstat bridges indicated schematically, which are connected directly to the output of a Sorensen 2501 AC voltage regulator. The inputs to these heaters are regulated and controllable to within 10 μv as measured by a Fluke 931 PB RMS differential voltmeter.

The thermocouple emfs are measured by a Leeds & Northrup K-5 potentiometer against a zero-degree reference temperature bath. The distance between the thermocouples was measured by a Nikon measuring microscope.

4. Experimental Procedure and Errors

In conducting the bidirectional heat flow experiment, a symmetrical temperature gradient from the center of the sample to either of the two ends of approximately .8 °C/mm (20 °C/inch) is established under steady-state heat transfer conditions. The top and bottom sample heaters were used to set the temperature at which the thermal conductivity was to be measured; and the center sample heater was used to establish the heat flux and thermal gradient. Top and bottom sample heaters were adjusted by reading the seven sample thermocouples to balance the thermal gradients in both direction to the desired degree. Simultaneously, the three guard heaters were adjusted to achieve a steady-state condition in which the temperatures measured by each of the thermocouples on the sample were matched by the temperature readings of the thermocouples radially opposite each of them on the guard. Careful manipulation of the guard heaters could achieve simultaneous matching of the thermocouple pairs to within ± 2.5°C; and in most cases the matching was considerably better.

Thermal gradients established in this experiment were usually 9° - 10°C between the sample thermocouples spaced at 1.29 cm intervals. Since indications were that the thermal conductivity was a slowly varying function of the temperature, the assumption that there is a linear gradient between thermocouple pairs is realistic. The calculated thermal conductivity was, therefore, postulated to be that at the average temperature of the two thermocouples.

When the gradients were matched to within the 2.5°C tolerance mentioned above, the thermal conductivities measured were consistent within 2%. The single largest source of experimental error inherent in the system is the measurement of the length between thermocouples, affecting the gradient calculation. Couples were made from .127 mm diameter wires by flame-fusing a bead at their juncture. This bead formed a sphere with diameter in excess of 0.5 mm, which was then spot-welded to the sample. Determination of the exact distance between contact points was, therefore, indeterminant by at least 0.5 mm; and since the length between couples was 12.7 mm (.50"), the 2% indeterminacy could account for the 2% spread in the data. The precision of the measurements themselves was .1%.

The confirming procedure for the conductivity data, in the form of the unidirectional heat flow experiment, utilizes the ability of the apparatus to control both temperature and thermal gradient in different portions of the apparatus independently. To make this second measurement, the sample heaters at center and one end are set to establish an isotherm, with resultant net zero heat flux in that direction from the center. The remaining sample heater is set at a reduced temperature to produce the desired gradient in that direction. Meanwhile, the guard heaters are manipulated to make the guard temperature conform to the temperature profile of the sample. Experience with the apparatus operating in this mode indicated that the measured thermal conductivity was relatively insensitive to variation between sample and guard temperatures, on the isothermal side, up to approximately 5°C; but that this method was very sensitive to small differences in sample and guard gradients on the heat transfer side. Confirmation of the bidirectional data, however, was within 2.5% for guard-sample gradients matched to less than 1°C on the gradient side, and guard-sample matched isotherms of 5°C or less.

5. Results and Discussion of Results

The thermal conductivity of Tophel Special has been measured in the temperature range between 70° and 500°C. The values obtained have been tabulated in Table 1 and plotted in Figure 3 (Ref. 3 has been consulted in the numerical reduction of the data).

Table 1. Measured Thermal Conductivity of Tophel Special

Test	Mean Temperature T (°C)	Thermal Conductivity $\lambda \times 10^{-2}$ (watt/M°C)	Test	Mean Temperature T (°C)	Thermal Conductivity $\lambda \times 10^{-2}$ (watt/M°C)
1	73.9	.2276	17	340.2	.254
2	73.9	.2258	18	341.0	.251
3	73.9	.2236	19	341.1	.249
4	73.8	.2218	20	341.4	.248
5	73.8	.2224	21 x	335.3	.251
6	73.5	.2254	22 x	336	.256
7	74.0	.2230	23 x	335	.257
8	188.2	.268	24 x	337.5	.240
9	187.0	.267	25 x	337.9	.253
10	186.5	.264	26	506.3	.197
11	188.2	.261	27	506.1	.197
12	188.2	.259	28	506.1	.197
13	187.6	.268	29	506.0	.198
14	338.0	.249	30	505.7	.199
15	337.9	.250	31	505.5	.200
16	339.7	.248	32	505.3	.199

x Indicates unidirectional confirming runs

The measurements have been made by the bidirectional heat transfer method and verified by the unidirectional method at approximately 350°C. The agreement is excellent, as shown in Figure 3. The thermal conductivity of Chromel P (approximate composition Ni plus Co 90%, Chromium 10%) was measured by Shelton (4), and the thermal conductivity of this material, which is closest to Tophel Special in composition, has also been plotted in Figure 3 for comparison. Although the thermal conductivities of Tophel Special and Chromel P are of the same order of magnitude, there appears to be a difference in their behaviors as a function of temperature.

The thermal conductivity of pure nickel (99.999 pure) was most recently measured by Kirichenko (5) in the temperature range 67-647°C, and by Powell and Tye (6) between 50 and 1050°C. The thermal conductivity of nickel, interestingly enough, exhibits a negative temperature coefficient up to the temperature of the magnetic transformation (ranging from 340 to 350°C), beyond which a positive temperature coefficient was observed.

The thermal conductivity of chromium, as measured by Powell and Tye (7) after a variety of heat treatments shows a negative temperature coefficient for heat treatment above 500°C, but positive temperature coefficients for samples treated at lower temperatures. Thermal conductivity of the Tophel Special sample is much the same as that of the low-temperature chromium at relatively low temperatures, for which data is available. The low temperature data of Sochtig (9) corroborates the order of magnitude of the Powell and Tye data, although their sample had been heat treated at 1000°C. The heat-treated sample of Lucks and Deem (8), on the other hand, corroborates the high temperature annealed sample data observed by Powell and Tye.

6. Acknowledgement

The work described in this paper was conducted as part of the Radioisotope Powered Cardiac Pacemaker Program under the terms of the Contract AT(30-1)-3731 with the Atomic Energy Commission in cooperation with the National Heart Institute. Thanks are due to Mr. David L. Purdy and Mr. Thomas F. Hursen of Energy Conversion Division for their encouragement and to Mr. Stanley L. Stein, Mr. Ray G. Burkett, and Mrs. Carol B. Duffman for assembly, drafting and typing respectively.

7. References

(1) F. N. Schofield, "The Thermal and Electrical Conductivities of Some Pure Metals, " Proc. Roy. Soc. London, 107A, 206-227 (1925).

(2) R. W. Powell, "The Thermal and Electrical Conductivities of Metals and Alloys: Part I, Iron from 0° to 800°C," Proc. Phys. Soc., 46, 659-674 (1934).

(3) R. K. Adams, E. K. Davis, "Smooth Thermocouple Tables of Extended Significance," Vol. II, Section 2.1, (Platinum versus Platinum - 10% Rhodium Thermocouple), ORNL 3649.

(4) S. M. Shelton, W. H. Swanger, "Thermal Conductivity of Irons and Steels and Some Other Metals in the Temperature Range 0 to 600°C," Trans. Am. Steel Treating, 21, 1061-78 (1933).

(5) P. I. Kirichenko, V. E. Mikryvkov, "High Temperature," 2 (2), 176-180 (1964).

(6) R. W. Powell, R. P. Tye, M. J. Hockman, Int. J. Heat Mass Transfer, 8 679-88 (1965).

(7) R. W. Powell, R. P. Tye, J. Inst. Metals, 85, 185-95 (1957).

(8) C. F. Lucks, H. W. Deem, WADC TR55-496, 1-65, (1956), (AD97185).

(9) H. Sochtig, Ann Physik, 5, 38, 97-120 (1940).

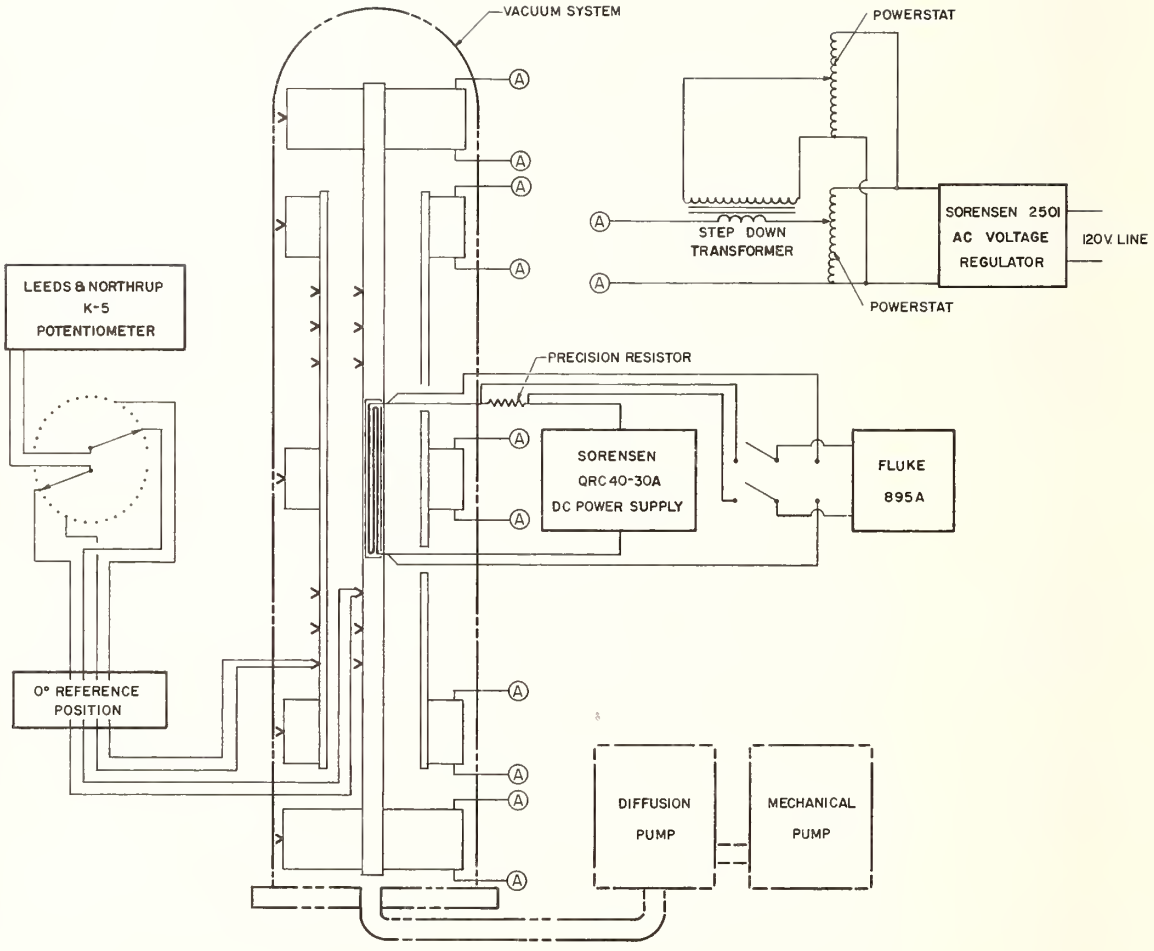

Figure 1 Schematic Diagram of the Apparatus For Measuring Thermal Conductivity of Metals and Alloys

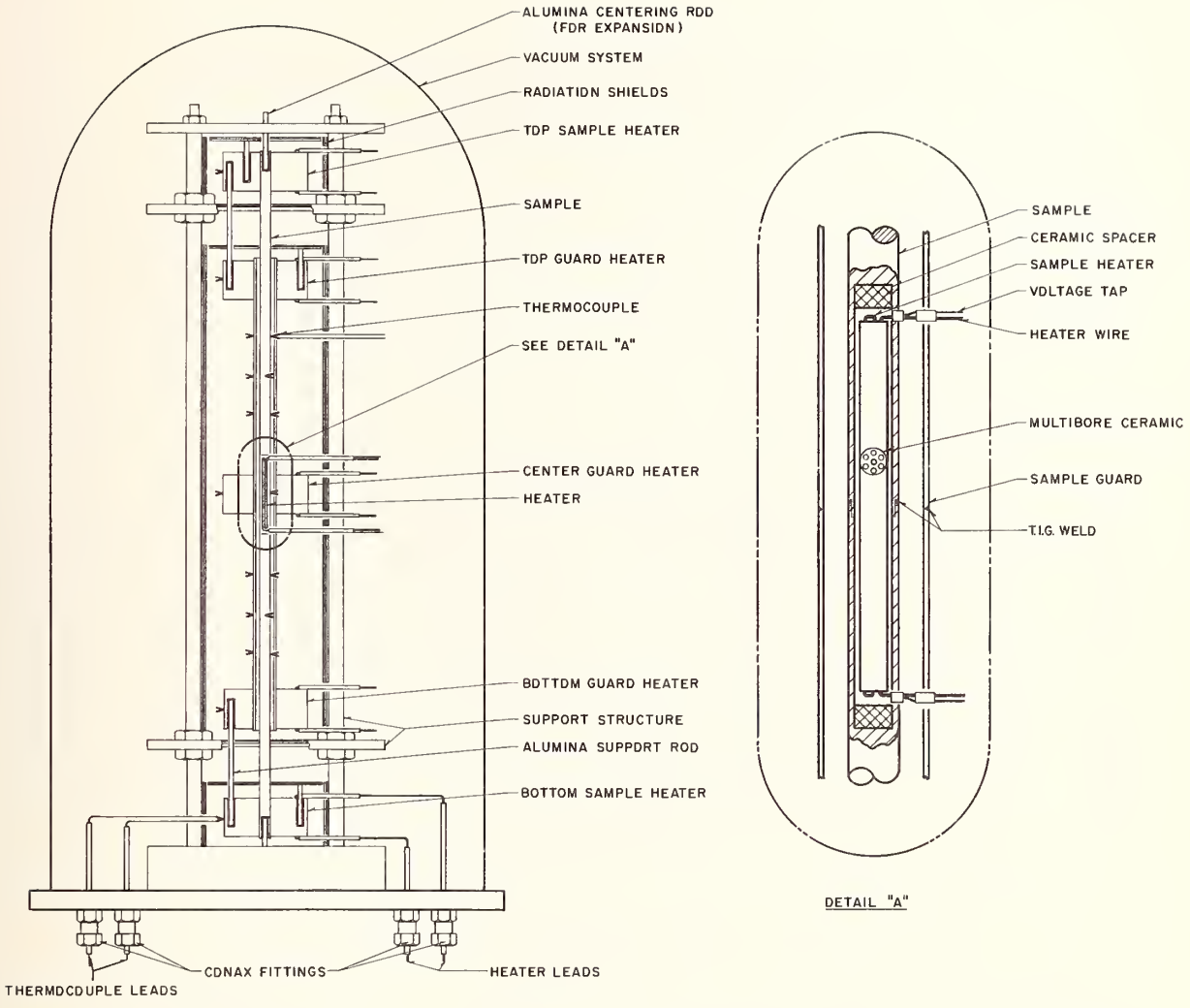

Figure 2 Details of Apparatus For Measuring Thermal Conductivity of Metals and Alloys

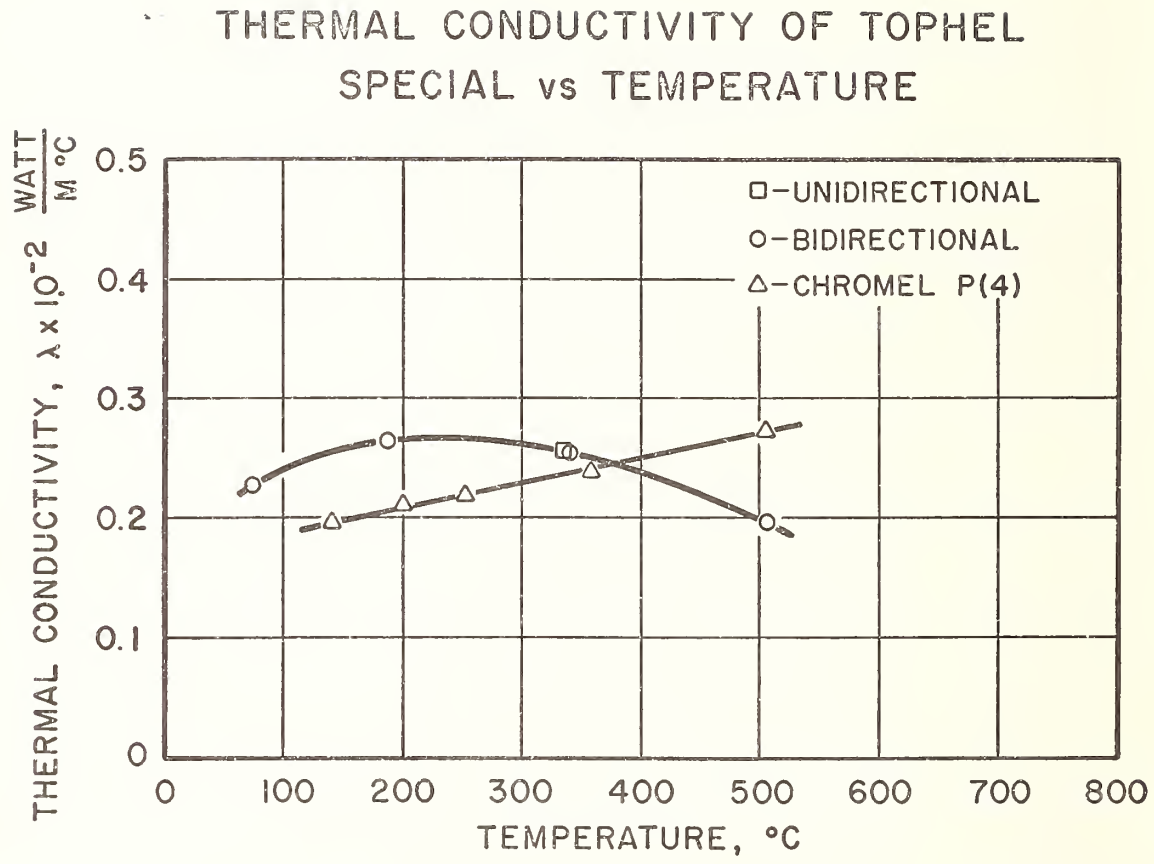

Figure 3 Thermal Conductivity of Tophel Special Vs Temperature

The Intrinsic Electronic Thermal Resistivity of Iron

M. S. R. Chari[1]

National Physical Laboratory of India
New Delhi, India

Starting from Linde's empirical observation that, at temperatures where the electrical resistivity of a (normal, non-transitional) metal has a linear temperature dependence, its electronic thermal resistivity is independent of temperature, Backlund has employed a modified Wiedemann-Franz-Lorenz relation to evaluate the intrinsic component (w_{eg}) of the electronic thermal resistivity of iron. This, in effect, uses a Lorenz parameter smaller than the normal value L_n. Chari has recently obtained values for the w_{eg} of iron, in the temperature region 600 - 1200 °K, from the usual Wiedemann-Franz-Lorenz relation, using the value of the electronic Lorenz parameter L_e, as given by Makinson for a pure monovalent metal having the Debye parameter of iron. Here also, w_{eg} comes out independent of temperature.

In the present paper, a more detailed comparison is made of the two methods. It is shown that, if iron is assumed to contribute one electron per atom to the conduction band, the fractional drops ($\Delta L/L_n$) in the effective electronic Lorenz number, used in these two methods are respectively given by $0.17\theta/1.17T$ and $(b - a)/(1 + b - a)$, where $b = 3\zeta\theta^2/(2\pi^2 DT^2)$ and $a = J_7/(2\pi^2 J_5)$, the symbols ζ, D, J_7 and J_5 having the same meaning as in Makinson's paper. At the Debye temperature θ, the two methods give the same $\Delta L/L_n$. At higher temperatures, the Backlund method gives an effective $\Delta L/L_n$ proportional to $1/T$ while Makinson's method leads to a $1/T^2$ variation and an ideal electronic thermal resistivity w_{eg} which is constant in the temperature range 4θ to 2θ but increases by about 3% in going from 2θ to $3\theta/2$ and by about 6% in going from $3\theta/2$ to θ. At lower temperature, w_{eg} rises rapidly reaching, at $\theta/4$, a value about twice the constant high-temperature value. This rising trend of w_{eg} corresponds to the thermal conductivity minimum at low temperatures ($\approx \theta/5$), which is inherent in the standard theory and is presumably due to an over-estimation of the strength of the electron-phonon interaction.

Key Words: Electronic thermal resistivity, iron, Lorenz number, resistivity, thermal resistivity.

1. Introduction

The component of the electrical resistivity due to the magnetic scattering of free electrons in metals of half-integral spin has been evaluated by Friedal and De Gennes[1][2], using the Born approximation and assuming an exchange interaction between the atomic spin and that of the conduction electron. In the paramagnetic state of such a metal, where it is permissible to consider the electron scattering as elastic, they find that the magnetic contribution (ρ_m) to the electrical resistivity is proportional to $s(s + 1)$, where s is the spin of the magnetic atom.

---

[1]Senior Scientist.

[2]Figures in brackets indicate the literature references at the end of this paper.

Weiss and Marotta[2] have demonstrated this proportionality even in the case of metals having a non-integral spin, using the Van Vleck configuration, replacing $s(s + 1)$ by $\Sigma\, p_i s_i(s_i + 1)$, where p_i is the fraction of atoms in the spin state s_i. They find a surprisingly linear variation of ρ_m with respect to this sum over a wide range of spins, indicating a very narrow range of values for the exchange coupling constant G in the various transitional metals and their alloys.

Assuming the ideal (intrinsic) electrical resistivity ρ_g to be given by the Bloch-Gruneisen expression

$$\rho_g = \frac{AT^5}{\theta^5} \int_0^{\theta/T} \frac{z^5 dz}{(e^z - 1)(1 - e^{-z})} \tag{1}$$

(where θ is the characteristic Debye temperature and A is a constant of the metal), and the magnetic resistivity ρ_m to be proportional to $s(s + 1)$, they analyzed the electrical resistivity data of Pallister [3] on iron. At the temperatures large with respect to T_c and θ, the Bloch-Gruneison term reduces to AT/θ (T_c being the Curie temperature). Since Pallister's ρ - T curve for iron, at such high temperatures, shows the electrical resistivity to have a linear variation with T, they equated the slope of this curve to A/θ and evaluated the ideal electrical resistivity ρ_g. Since the residual electrical resistivity (ρ_o) of iron is negligibly small (compared to ρ_g and ρ_m), subtracting ρ_g from the experimental value of ρ gave ρ_m.

The corresponding components of the thermal resistivity of iron were obtained from Powell's data [4] by Backlund[5], using a modified Wiedemann-Franz relation and, by the present author[6], using the appropriate values of the electronic Lorenz number. A detailed comparison is made here between these two methods.

Recently, careful measurements on the electrical and thermal resistivities of high-purity iron [7, 8, 9] and Armco iron [8, 9] have been reported, which show that the resistivities at the alpha-gamma transition temperature (1180 °K) present a stem-like singularity. It is pointed out in the present paper that these new data may not radically affect the above mentioned discussions (which were based on the old data of Pallister[3] and of Powell[4]).

2. The Lorenz Number

The early theories of metallic conduction were based on a classical concept of the collision process between the conduction electrons and the atomic lattice and predicted a Lorenz number L_n having a universal constancy. The modern Quantum theory of metals, on the other hand, recognizes the inelastic nature of the electron-phonon interaction, requiring an exchange of the phonon energy in the scattering process. Thus, at temperatures T, which are much higher than the Debye temperature θ, where the maximum phonon energy $k\theta$ would be small compared to kT, the electronic Lorenz number L_e has the temperature-independent value L_n. This applies also at low temperatures where elastic impurity scattering is predominant. At intermediate temperatures where the energy of the phonon absorbed or emitted is not negligible compared to kT, the electronic Lorenz parameter falls below the value L_n.

Starting from Wilson's expression[10] for the ideal(intrinsic) electrical resistivity and the ideal electronic thermal resistivity of a metal, Makinson[11] obtained the following expression for L_e of a metal, assuming the lattice waves to be those of an isotropic continuum having an upper frequency limit:

$$\frac{L_e}{L_n} = \frac{\frac{P_o}{4A} + \left(\frac{T}{\theta}\right)^5 J_5}{\frac{P_o}{4A} + X\left(\frac{T}{\theta}, \frac{D}{\zeta}\right)} \tag{2}$$

where

$$X\left(\frac{T}{\theta}, \frac{D}{\zeta}\right) = \left(\frac{T}{\theta}\right)^5 \left[J_5 \left\{1 + \frac{3}{2\pi^2} \frac{\zeta}{D}\left(\frac{\theta}{T}\right)^2\right\} - \frac{1}{2\pi^2} J_7\right], \tag{3}$$

and

$$J_n\left(\frac{\theta}{T}\right) = \int_0^{\theta/T} \frac{z^n dz}{(e^z - 1)(1 - e^z)}. \tag{4}$$

Here the symbols ζ, D, X, J_7 and J_5 have the same meaning as in Makinson's paper: ζ is the Fermi energy, $\zeta/D = (2N_a^2)^{1/3}$, where N_a is the number of conduction electrons per atom, $\rho_o/4A$ is the impurity parameter, ρ_o being the residual electrical resistivity, and A/θ is the slope of the ideal electrical resistivity ρ_g at temperatures $T/\theta > 0.6$.[3] For an ideally pure metal, for which $\rho_o/4A = 0$, eq (1) reduces to

$$\frac{L_e}{L_n} = \left[1 + \frac{3}{2\pi^2}\frac{\zeta}{D}\left(\frac{\theta}{T}\right)^2 - \frac{1}{2\pi^2}\frac{J_7}{J_5}\right] = (1 + b - a) \tag{5}$$

The drop in the value of L_e below the value L_n at the temperature T is given by

$$L = L_n - L_e = (b - a)\, L_n/(1 + b - a) \tag{6}$$

3. The Two Methods for Deriving the Ideal Electronic Thermal Resistivity

3.1. The Bases of the Two Methods

The component w_{eg} of the electronic thermal resistivity of iron, due to phonon scattering has been obtained by two methods, both starting from the value of the corresponding component ρ_g in the electrical resistivity of iron.

One method, due to Backlund[5] is based on the fact that the Block-Gruneison expression (eq 1) leads to a reduced resistivity r (= ρ_T/ρ_θ) of a metal being a universal function of the reduced temperature t (= T/θ). At temperatures above, say $\theta/3$, this function is a straight line given by [12]:

$$r = -0.17 + 1.17t \tag{7}$$

so that $d\rho/dT$ is $1.17\ \rho_\theta/\theta$. Following Linde's observation[13] for normal (non-transitional) metals that w_{eg}, the phonon-scattering component of the electronic thermal resistivity, is independent of temperature as long as the electrical resistivity has a linear temperature dependence, Backlund[5] has evolved a modified Wiedemann-Franz relation

$$w_{eg} = (\rho_g + \bar{\rho}_o)/(L_n T) \tag{8}$$

applicable to transitional metals as well. $\bar{\rho}_o$ is ρ_θ times the intercept, on the negative side of the Y-axis, of the rectilinear ρ_g - T curve and is presumably associated with the zero point energy[14]. In the case of iron at temperatures above about 120 °K, where the ρ_g - T curve is linear, $\rho_g = -\bar{\rho}_o + (1.17\ \rho_\theta T/\theta)$. Backlund thus finds $w_{eg} = 1.17\ \rho_\theta/(L_n\theta) = 0.015$ m deg W^{-1}, independent of temperature.

In the other method[6], w_{eg} is obtained from the relation

$$w_{eg} = \rho_g/(L_g T) \tag{9}$$

where the electronic Lorenz parameter L_g, appropriate to phonon scattering, is read off Makinson's curve (fig. 3 of ref. 11) of L_e/L_n versus T for a typical monovalent metal, having the Debye temperature of iron. The w_{eg} obtained in this manner turns out to be more or less independent of temperature down to 600 °K and has a value ≈ 0.012 m deg W^{-1}. The values of $w_{eg} + w_{es}$ (the subscript s indicating the component due to s - d scattering) obtained in this manner (fig. 1 of ref. 6) join up smoothly to the data of White and Woods[15] on iron at temperatures below 140 °K. In fact, Backlund's data also satisfies this criterion since their w_{es} values are lower by about 0.0035 m deg W^{-1}.

The difference between the constant values 0.015 and 0.012 m deg W^{-1} for w_{eg} are well accounted for by the difference in the values of ρ_g employed in the two methods. Backlund fitted the electrical resistance data of Pallister on iron to an equation of the form $-\ell + mT + nT^3$, whereas we read off values of ρ_g from Weiss and Marottas' ρ_g - T plot, which has a slope about 20% lower.

---

[3] Following Makinson, the slope of the Bloch-Gruneison function is here represented as A/θ, whereas Weiss and Marotta have expressed it as $A/4\theta$.

3.2. The Effective Lorenz Parameter in Iron.

Backlund's modified Wiedemann-Franz relation amounts to using an effective electronic Lorenz number $L_e = \rho L_n/(\rho_g + \bar{\rho}_o)$, so that the fractional drop in the value of L_e at a temperature T is given by $\Delta L/L_n = (L_n - L_e)/L_n = \bar{\rho}_o/(\rho_g + \bar{\rho}_o) = 0.17\theta/1.17T$. In other words, starting from $T \gg \theta^\gamma$, $\Delta L/L_n$ increases linearly with the fall of temperature, taking up the value 0.145 at $T = \theta$. As shown in article 2, Makinson's treatment results in eq (6).

If we assume the impurity parameter $\rho_o/4A = 0$ and that iron contributes one electron per atom to the conduction band, this leads to a $\Delta L/L_n$ having the same value as above (0.145) at the Debye temperature. At higher temperatures, it varies approximately as T^{-2}, while at lower temperatures $T < \theta$, the variation is less rapid, $\Delta L/L_n$ decreasing by a factor of 5 for a decrease of T from θ to $\theta/4$. Taking the impurity parameter into account, (using $\rho_o = 0.001\ \mu\Omega m$) makes no significant difference.

Using eq (2), we have also calculated $\Delta L/L_n$ by Makinson's treatment, using the more realistic value of $N_a = 0.7$ and taking the impurity parameter into account. At temperatures $\theta/4$, $\theta/2$, θ and 2θ, the values of $\Delta L/L_n$ are 0.612, 0.105, 0.049, and 0.028 respectively. In other words, at $T > \theta$, the T^{-2} variation of $\Delta L/L_n$ is maintained, but below θ, the variation is less rapid, as in the case of $N_a = 1$. This latter behaviour is in accordance with the partial filling up, at low N_a, of the theoretically predicted electronic thermal conductivity minimum.

3.3. The Instrinsic Electronic Thermal Resistivity

Backlund's analysis[5] starts with the assumption of a constant value for w_{eg} in the temperature region of a linear ρ - T curve. His modification of the Wiedemann-Franz relation makes sure of this down to about 120 °K for iron.

The value of w_{eg} obtained by us, following Makinson's theoretical evaluation of Lorenz number, is sensibly constant in the temperature region 4θ to 2θ. For $N_a = 1$, w_{eg} increases by about 3% for the temperature drop from 2θ to $3\theta/2$ and by about 6% between $3\theta/2$ and θ. Below θ it rises rapidly, reaching at about $\theta/4$ a value about twice the high temperature value. This rising trend of w_{eg} corresponds to the thermal conductivity minimum at low temperatures ($\approx \theta/5$) which is inherent in the standard theory of Wilson and Makinson and is presumably due to an overestimation of the strength of the electron-phonon interaction. For $N_a = 0.7$, (it is immaterial whether or not the impurity parameter $\rho_o/4A$ is taken into account) the value of w_{eg} at high temperatures is not affected, but now the rise is only about 50% for the temperature drop to $\theta/4$. This again corresponds to the filling up, at small N_a, of the theoretically predicted minimum in the thermal conductivity.

4. The Alpha-Gamma Transformation

More recent measurements on the conductivities of iron[7, 8, 9] show a step-like anomaly at the temperature $T_{\alpha\gamma}$ of the transformation of iron from the magnetically disordered body-centered cubic (b.c.c.) to a face-centered cubic (f.c.c.) structure. The slope of the ρ - T curve above T_c is changing and is different above and below $T_{\alpha\gamma}$. This renders questionable the validity of the original analysis of Weiss and Marotta, who made use of the linear ρ - T curve above T_c.

In this connection, we wish to made the following comments. The slope of the ρ - T curve changes rapidly between the Curie temperature T_c and $T_{\alpha\gamma}$, getting smaller as we approach $T_{\alpha\gamma}$ from T_c. Fulkerson *et al*[8] derive slopes of 3.95, 4.05, and 3.73 X $10^{-10}\Omega m/°K$ for the ORNL Armco iron, ORNL high purity iron and USS high purity iron respectively in the alpha region, and 3.74, 3.69, and 4.00 X $10^{-10}\Omega m/°K$ in the gamma region. Actually, since the temperature interval T_c to $T_{\alpha\gamma}$ is rather small, we have to visualize a true slope somewhat smaller than these values. Since the b.c.c. structure of iron[8] again becomes stable above 1680 °K, Coles[16] has deduced a slope of 3 X $10^{-10}\Omega m/°K$ from the resistivity values just above T_c and those in the δ - iron region. This seems reasonable and agrees with the value obtained by Weiss and Marotta from the old data of Pallister[3], which does not record the resistance drop at $T_{\alpha\gamma}$.

Whereas the use of $d\rho/dT = 3 \times 10^{-10}\Omega m/°K$ results in a $\bar{\rho}_s$ (which is the constant value of magnetic resistivity above T_c) of $0.8\mu\Omega m$, higher values of $d\rho/dT$ of say 4 or 5 X $10^{-10}\Omega m/°K$ would lead to ≈ 0.65 and $0.54\mu\Omega m$ respectively. These latter values for $\bar{\rho}_s$ would be somewhat smaller than the value 0.75 which latter would conform to a linear variation of $\bar{\rho}_s$ with $\Sigma\, p_i s_i (s_i + 1)$. The trend of the rest of the above discussions is not disturbed by such higher values of $d\vartheta/dT$, though the numerical values certainly change. We might add that Koveskiy and Samsonov[17] have given a constant $d\rho/dT$ of 4.79 x $10^{-10}\Omega m/°K$, with no step at $T_{\alpha\gamma}$.

To which component of the electrical resistivity is the step at $T_{\alpha\gamma}$ to be attributed? It was shown by Weiss and Tauer[18] from the specific heat data on iron, that the Debye temperature is about 420 °K in the alpha phase and about 335 °K in the gamma phase. Since we have accepted for $d\rho/dT$, the limiting value, away from the temperatures of transition, it would imply our assuming a value for ρ_s which is the same for the alpha and gamma phases. If this argument is correct and the Debye temperatures of the two phases are taken into account, we can use the Bloch relation $\rho_g \propto RT/N_a\theta^2$ (where R is the Fermi radius) and derive the ratio of the conduction electrons per atom in the two phases as $N_\gamma/N_\alpha = 1.6$. Such an estimation has been indicated by Fulkerson et al who also discuss in detail the step in the thermal conductivity of iron at $T_{\alpha\gamma}$.

5. References

[1] Friedel, J. and De Gennes, P., Anomalies de resistivite dans certains metaux magnetigues, J. Phys. Chem. Solids. 4, 71 (1958).

[2] Weiss, R. J. and Marotta, A. S., Spin-dependence of the resistivity of magnetic metals J. Phys. Chem. Solid. 9, 302 (1959).

[3] Pallister, P. R., The specific heat and resistivity of high purity iron up to 1250 °C. J. Iron Steel Inst. 161, 87 (1949).

[4] Powell, R. W., Further measurements of the thermal and electrical conductivity of iron at high temperatures, Proc. Phys. Soc. (Lond), 51, 407 (1939).

[5] Backlund, N. G., An experimental investigation of the electrical and thermal conductivity of iron and some dilue iron alloys at temperatures above 100 °K, J. Phys. Chem. Solids. 20, 1, (1961).

[6] Chari, M. S. R., The electrical and thermal resistivities of iron. Phys. Stat. Sol. 19, 169 (1967).

[7] Arajs, S. and Colvin, R. V., Electrical resistivity of high purity iron from 300 to 1300 °K. Phys. Stat. Sol. 6, 797 (1964).

[8] Fulkerson, W., Moore, J. P. and McElroy, D. L., Comparison of the thermal conductivity, electrical resistivity, and Seebeck coefficient of a high-purity iron and an Armco iron to 1000 °C., J. Appl. Phys. 37, 2639 (1966).

[9] Laubitz, M. L., Thermal and electrical properties of iron at high temperatures. Can. J. Phys., 38, 887 (1960).

[10] Wilson, A. H., Second-order electrical effects in metals., Proc. Camb. Phil. Soc. 33, 371, (1937).

[11] Makinson, R. E. B., The thermal conductivity of metals., Proc. Camb. Phil. Soc. 34, 474, (1938).

[12] Borelius, G., Temperaturabhangigkeit deswiderstandes ferromagnetischer Metalle. Ann. Phys. LpZ., 8, 261 (1931).

[13] Linde, J. O., An investigation of the validity of the Wiedemann-Franz-Lorenz Law., Ark. Fys. 4, 541 (1952).

[14] Borelius, G., On the connection between electrical resistivity and potential energy in pure metals., Ark. Fys., 11, 291 (1956).

[15] White, G. K. and Woods, S. B., Electrical and thermal resistivity of the transition elements at low temperatures. Phil. Trans. Roy. Soc. (Lond). A251, 273 (1958).

[16] Coles, B. R., Spin-disorder effects in the electrical resistivities of metals and alloys. Adv. Phys. 7, 40 (1958).

[17] Kovenskiy, I. I. and Samsonov, G. V., Electrical resistivity of certain transition metals at high temperatures., Phys. Met. Metallegr., 15, 124 (1963).

[18] Weiss, R. J. and Tauer, K. J., Components of the thermodynamic functions of iron. Phys. Rev. 102, 1490 (1956).

The Thermal Conductivity and Electrical Resistivity of Tungsten-26 Weight Percent Rhenium

A. D. Feith[1]

Nuclear Materials and Propulsion Operation
General Electric Company
Cincinnati, Ohio 45215

Radial heat flow measurements of the thermal conductivity of W-26Re (w/o) have been made over the temperature range from 300 °C to 2200 °C. These data identify a small positive temperature coefficient on conductivity with conductivity values ranging from 56.0 Wm^{-1} deg^{-1} at 300 °C to about 69.0 Wm^{-1} deg^{-1} at 2200 °C.

Electrical resistivity measurements are also reported for both W-26Re and for unalloyed tungsten. This information was employed to calculate the electronic contribution to the thermal conductivity of the W-26Re alloy. At 300 °C the electronic contribution was calculated to be about 65% of the thermal conductivity, whereas at 2200 °C the conductivity is about 90% electronic.

Key Words: Conductivity, electrical resistivity, electronic conduction, phonon conduction, thermal conductivity, tungsten, tungsten-26 rhenium.

1. Introduction

Alloys of tungsten and rhenium have been found to be of considerable interest for potential structural applications at extremely high temperatures. In addition, these alloys have been used extensively as thermocouples with pure tungsten for high temperature measurements. Although much has been reported on the thermal electric output of W-26Re with pure tungsten as a thermocouple, little or no work has been reported on either the thermal conductivity or electrical resistivity of this alloy in the high temperature range (> 1200 °C). The data presented in this report, therefore, fill a vital gap in the knowledge of the thermal properties of this important alloy in the tungsten-rhenium system. They also serve to verify data presented by Jun and Hoch (1)[2] on a similar alloy (W-25Re) but measured by a different method. The general agreement with the predicted values of McElroy (2) suggests that some confidence can be placed in the estimation of fairly reliable conductivity data for an alloy over a broad temperature range when electrical resistivities over this range are known.

2. Description of Specimens

2.1. Thermal Conductivity

The thermal conductivity specimens (W-26Re) and the guard discs (tungsten) were obtained commercially. A powder-metallurgy process was used to fabricate discs which were then machined to the configurations shown in figure 1. The composition of the as-received material is given in table 1. Measured densities were 98.96% of theoretical for the specimen and 98.3% (on the average) of theoretical for the guards.

2.2. Electrical Resistivity

Electrical resistivity specimens were made from the same material used in making the thermal conductivity specimens and also from powder-metallurgy tungsten. For these specimens though, circular rods, 0.32 cm in diameter by 11.43 cm in length were employed. Small holes which were required to accommodate voltage probes were generated by an EDM process.

[1]Principal Engineer
[2]Figures in parentheses indicate the literature references at the end of this paper.

Table 1. Composition of specimens in percent by weight

Tungsten-Rhenium	Tungsten
% rhenium 26.48	
% tungsten 73.39 (by difference)	
% impurities	% impurities
Mo 0.01 - 0.10	Mo 0.01 - 0.10
Fe <0.01	Fe <0.01
Na <0.01	Na <0.01
Ti <0.01	Maximum impurities <0.12%
Ni <0.01	
Maximum impurities <0.13%	

2.3. Microstructures of Specimens

Typical microstructures of the materials used are shown in figure 2. X-ray diffraction studies have shown the alloy material to be a single-phase solid solution with a theoretical density of 19,575 kg/m^3; also, a density of 19,199 kg/m^3 was determined for the unalloyed tungsten.

3. Apparatus

3.1. Thermal Conductivity

Thermal conductivity measurements were obtained in the radial heat flow apparatus which has been described previously (3,4,5). However, one important difference is noteworthy. Because of the high cost of material containing significant amounts of rhenium, some thought was given to the use of lower cost guard materials. In this study the guards were made from tungsten and three guard discs were employed above and below the W-26Re specimen disc. In addition, two discs of tungsten with flanges at the I.D. and O.D. were placed at each interface between the specimen and adjacent guard disc as shown in figure 3. This thermal isolation of the specimen was sufficient to restrict the heat flow to the radial direction in keeping with the boundary conditions of the experiment. In general, this procedure was proven to be satisfactory as indicated by the reproducibility of the data obtained.

Temperatures were measured with a probe-type thermocouple (Pt/Pt + 10Rh) up to 1200 °C and an optical pyrometer from 1000 °C to the maximum temperature of the measurement, 2200 °C. Again, as in the case of the molybdenum measurements (5), the radial thermal gradient was small (3 °C to 20 °C) and great care had to be exercised in the temperature measurement to obtain reasonable precision in the results.

3.2. Electrical Resistivity

Electrical resistivity measurements were made on rod specimens (0.32 cm dia. x 11.43 cm long) by a four-probe method as described previously (5) except that two specimens were placed in series as shown schematically in figure 4. One W-26Re specimen was used in conjunction with an unalloyed tungsten specimen. In this manner, electrical resistivity was measured on the two materials simultaneously. A probe thermocouple was used to determine the temperature of the specimens up to 1200 °C; above this temperature, an optical pyrometer was employed. Voltage probes were of W-26Re for the alloy specimen and tungsten for the unalloyed tungsten specimen. Verification of the temperature level and possible gradient along the specimens was obtained by measuring the thermal e.m.f. between the W and W-Re voltage probes when no external power was supplied to the specimens. Measurements at liquid nitrogen temperature (-196 °C) were also made on as-received and tested specimens.

4. Results

4.1. Thermal Conductivity

The results of the thermal conductivity measurements are shown in figure 5 and in table 2. The initial measurements (series 1, table 2) were made from 300° to 1600 °C. After an interruption of about two months, during which time the specimen and guards were removed from the apparatus, the second series of measurements was made on the same specimen from 1300° to 2350 °C and then down to 1550 °C on final cooling. In both series, reproducibility was demonstrated by repeated measurements over the temperature ranges studied. It can be seen in figure 5 that the conductivity increases with temperature over the entire range although the slope decreases at higher temperatures. The agreement with the values reported by Jun and Hoch (1) is quite good considering the different methods employed. The predicted values of McElroy (2) up to 1500 °C also appear to be verified by these results. McElroy (2)

shows two sets of values in his prediction based on two different assumptions for the lattice component. Both values are shown on the curve to demonstrate the agreement between these predicted values and the experimental results of this study.

Table 2. Thermal conductivity data for W-26Re
Wm^{-1} deg^{-1}

Series 1						Series 2			
Run 1		Run 2		Run 3		Run 1		Run 2	
T, °C	λ	T, °C	λ	T, °C	λ	T, °C	λ	T, °C	λ
308	44.6	551	57.0	1268	67.1	1335	63.5	1685	66.6
404	44.1	578	54.4	1360	58.6	1522	62.2	1708	65.9
507	58.3	781	68.4	1381	57.5	1654	63.5	1779	67.7
673	62.8	848	66.0	1392	61.8	1644↓	63.7	1802	67.8
749	59.1	869	63.6	1566	58.1	1527↓	65.3	1999	62.7
845	61.7	932	65.3	1593	55.5			2008	66.7
759↓	62.3	948	65.8					2040	66.4
728↓	60.4	998	66.0					2021↓	64.0
654↓	58.7	1024	69.0					1910↓	67.4
535↓	55.3	1082	69.7					2008	67.9
413↓	56.0	1147	69.2					2156	70.0
		1148	63.3					2185	69.3
		1210	63.6					2254	68.4
		1146↓	63.4					2349	73.4
		1120↓	55.8					1816↓	68.8
								1657↓	68.6
								1675↓	71.9
								1679↓	66.4
								1542↓	67.4

↓ Indicates measurements during cool down.

Jun and Hoch (1) have reported two distinct values for the thermal conductivity of W-25Re both of which are independent of temperature and which depend upon the method of fabrication; i.e., 62.6 Wm^{-1} deg^{-1} for powder-metallurgy material and 68.0 Wm^{-1} deg^{-1} for arc-cast material in the 1500 °C - 2700 °K range.

4.2. Electrical Resistivity Results

The measured values of the electrical resistivity of W-26Re and unalloyed tungsten are presented in table 3 by individual runs. These data are combined to give the curves in figure 6. Second degree polynomial equations were developed based on these data. The equation for tungsten-rhenium is continuous and fits well within ±1.5% up to about 2370 °K with few exceptions; however, the precision is about ±6% for the few data points above 2370 °K. The equation for the electrical resistivity of W-26Re is:

$$\rho = 1.86430 \times 10^{-7} + 3.37090 \times 10^{-10} T - 1.29457 \times 10^{-14} T^2 \qquad (1)$$

$$\sigma = 2.43036 \times 10^{-9} \ \Omega m$$

where T is in °K, ρ is in Ωm and σ is the standard deviation. Results of this study are somewhat higher than those reported by McElroy (2). This shift is probably due to differences in the materials used in the two experiments. In the ORNL study small diameter tungsten-26 rhenium thermocouple wire (6) was used which may have had a slightly different composition, whereas the material used in this study was a 0.32 cm diameter rod and is characterized by the composition given in table 1.

The values for tungsten were fitted more precisely when two second degree polynomial expressions were used rather than one. This is similar to the method proposed by Moore, et al. (7), and is mainly due to the desire to restrict the expression to a second degree polynomial rather than to suggest a physical change in temperature dependence of resistivity. The equations are:

Table 3. Electrical resistivity of tungsten-26 rhenium and tungsten

T, °C	W-26Re $\Omega m \times 10^8$	W $\Omega m \times 10^8$
30	28.691	5.525
216	34.705	9.893
225	35.023	10.391
680	49.610	23.213
32	28.292	5.302
234	35.297	10.324
573	46.309	19.722
1062	59.982	35.420
30	27.290	5.253
907	56.654	31.282
1308	67.056	43.312
1615	76.598	52.891
31↓	29.019	5.605
28	28.955	5.554
299	37.679	12.002
742	51.378	25.159
752	51.818	25.157
982	58.990	33.111
762↓	52.642	25.845
307↓	37.937	12.235
1213	66.416	40.562
1968	88.356	65.928
1978	88.559	66.608
2196	94.494	69.626
2120↓	91.492	68.276
1955↓	86.360	64.990
1209↓	65.725	40.368
852↓	55.097	28.901
29	28.692	5.539
803	53.616	27.281
1122	63.027	37.562
1503	73.794	49.543
1854	84.312	61.448
2097	90.827	68.551
21		5.327 A.R.
24		5.452 P.T.
25	28.239 A.R.	
25	28.275 P.T.	
-196 LN_2	19.486 A.R.	0.7029 A.R.
-196	19.686 P.T.	0.6276 P.T.

↓ Indicates measurements during cool down.
A.R. - As-received
P.T. - Post-test

$$\rho = 4.33471 \times 10^{-14} T^2 + 2.19691 \times 10^{-10} T - 1.64011 \times 10^{-8} \qquad (300^\circ K < T < 1240^\circ K) \qquad (2)$$

$$\sigma = 3.03318 \times 10^{-9} \ \Omega m$$

and

$$\rho = -4.06012 \times 10^{-14} T^2 + 4.67093 \times 10^{-10} T - 1.97071 \times 10^{-7} \qquad (1240^\circ K < T < 2570^\circ K) \qquad (3)$$

$$\sigma = 1.56328 \times 10^{-8} \ \Omega m$$

where ρ is in Ωm, T is in ^{o}K and σ is the standard deviation.

Numerous resistivity studies have been made on unalloyed tungsten over the past four decades. Moore, et al. (7), have shown that the values of most other investigators are within ±4% of their work; however, each investigator is consistently above or below their results up to 1400°C. The results of this study are within ±1% of the Moore data over the 200 ^{o} to 1400 ^{o}C range.

5. Discussion of Results

5.1. Thermal Conductivity

The increase in thermal conductivity with temperature for refractory alloys has been shown to be typical (2) even though the constituents of the alloy, when considered alone, have a decreasing value with temperature. When separating the total thermal conductivity into two components, phonon conduction (λ_ℓ) and electronic conduction (λ_e), it can be shown by the Wiedemann-Franz-Lorenz law that the flow of heat by electrons is the major component and, therefore, has the greatest influence on the temperature dependence of the thermal conductivity. An equation for total (measured) thermal conductivity is:

$$\lambda_T = \lambda_e + \lambda_\ell = \frac{LT}{\rho} + \frac{1}{A+BT} \qquad (4)$$

where λ_e = thermal conductivity due to electrons
λ_ℓ = thermal conductivity due to phonons
λ_T = total conductivity
L = Lorenz number = constant
= 2.443×10^{-8} V^2/deg^2
T = absolute temperature, ^{o}K
ρ = electrical resistivity in Ωm
and A and B are constants.

Since L is virtually constant within a small range of values, it is generally considered constant for the purpose of discussion. An analysis of the various components of conductivity is shown in table 4 and figure 7. The λ_e curve has about the same characteristic shape as the total conductivity curve while the λ_ℓ curve has an inverse temperature dependence (1/T) similar to the behavior of typical insulators in which the bulk of the conductivity is by phonons.

Table 4. Components of thermal conductivity of W-26Re
Wm^{-1} deg^{-1}

Temp., °C	λ_e	λ_ℓ	λ_T
300	37.3	20.2	57.5
400	40.4	17.6	57.9
500	43.0	15.6	58.6
600	45.3	14.0	59.3
700	47.3	12.7	60.0
800	49.2	11.6	60.8
900	50.8	10.7	61.5
1000	52.3	9.9	62.2
1100	53.7	9.2	62.9
1200	55.0	8.6	63.6
1300	56.1	8.1	64.3
1400	57.2	7.7	64.9
1500	58.3	7.3	65.5
1600	59.2	6.9	66.1
1700	60.2	6.6	66.7
1800	61.0	6.3	67.3
1900	61.9	6.0	67.9
2000	62.7	5.7	68.4
2100	63.5	5.5	69.0
2200	64.2	5.3	69.5
2300	64.9	5.1	70.0

A computer program (see Appendix) was used to fit the data to an equation of the form above. The result obtained is:

$$\lambda_T = \left[2.443 \times 10^{-8} \frac{T}{\rho} + \frac{1}{7.4925 \times 10^{-3} + 7.34269 \times 10^{-5} T} \right] \quad (5)$$

where $\lambda_T = Wm^{-1}\ deg^{-1}$
$T = {}^{o}K$
ρ = electrical resistivity eq (1)
$\sigma = 4.58183\ Wm^{-1}\ deg^{-1}$

5.2. Electrical Resistivity

The electrical resistivity of the W-26Re measured in this program is approximately 8% above the values reported by McElroy (2) at 1400°C. Since McElroy did not report the composition of the material, an explanation for this difference cannot be made. However, the data presented herein have been shown to be reproducible and hence have been used in the section above as an aid in interpreting the thermal conductivity results and to show that the electronic heat conduction is the major portion of the total conductivity.

Resistivity data obtained for unalloyed tungsten in this study fall in a band of values along with those of other investigators as shown in figure 6. The high temperature portion defined by eq (3) is concave downward since the second derivative is negative. This appears to contradict the work reported by Gumenyuk and Lebedev (8) and also that of Worthing, et al. (9). It is not known, at this time whether this is real or whether it is caused by the increased scatter in the high temperature range. R. P. Tye (10) reports resistivity data on pure tungsten to 1450 °C which has a considerably stronger temperature dependence and therefore greater departure from the work of this study and others (8,9).

The work reported by Moore, et al. (7), to 1400°C gives two second degree polynomials with positive second derivatives. Their values are within ±1% of this study in the 200 ° to 1400 °C temperature range. However, Moore corrected his measured values for thermal expansion using an average coefficient of expansion of $5 \times 10^{-6}\ {}^{o}C^{-1}$. This correction amounts to an increase of about 0.7% at 1400 °C which does not alter the relative values significantly. At 2200 °C the increase in resistivity amounts to 1.5% for all three curves shown when correcting for the thermal expansion.

6. Conclusions

The thermal conductivity of tungsten-26 w/o rhenium has been shown to be primarily due to thermal transport by electrons. The lattice or phonon portion of the thermal conductivity varies from approximately 35% at 300 °C to 10% at 2200 °C. Predictions of thermal conductivity by McElroy (2) appear to have been verified.

Electrical resistivity values for W-26Re and tungsten have been shown to be reproducible; comparison of the tungsten values with those of Moore, et al. (7), and others shows good agreement.

7. References

(1) Jun, C. K. and Hoch, M., "Thermal Conductivity of Tantalum, Tungsten, Rhenium, Ta-10W, T-111, T-222, W-25Re in the Temperature Range 1500° - 2800 °K," Third International Symposium on High Temperature Technology, Stanford Research Institute, Sept. 17-20, 1967, to be published.

(2) McElroy, D. L., "High Temperature Materials Program Quarterly Report for Period Ending April 30, 1966," ORNL-TM-1520, Part 1, pp. 53-58.

(3) Feith, A. D., "A Radial Heat Flow Apparatus for High Temperature Thermal Conductivity Measurements," GE-NMPO, GEMP-296, August 1963.

(4) Feith, A. D., "Thermal Conductivity of Several Ceramic Materials to 2500 °C," Advances in Thermal Physical Properties at Extreme Temperatures and Pressures, ASME, 1965

(5) Feith, A. D., "Measurements of the Thermal Conductivity and Electrical Resistivity of Molybdenum," GE-NMPO, GE-TM 65-10-1, October 1965.

(6) Fulkerson, W., private communication, September 15, 1965.

(7) Moore, J. P., Graves, R. S., Fulkerson, W. and McElroy, D. L., "The Physical Properties of Tungsten," 1965 Conference on Thermal Conductivity, Denver, Colorado, October 1965, by permission.

(8) Gumenyuk, V. S. and Lebedev, V. V., "Investigating Heat and Electro-Conduction of Tungsten and Graphite at High Temperatures," Fizika Metallov and Metalovedeniye (2 Jan. 1961), Nr. 1, pp. 29-33, Translation USAEC-NP-TR733.

(9) Worthing, A. G. and Watson, E. M., "Resistance and Radiation of Tungsten as a Function of Temperature," J. Opt. Soc. A., Vol. 24 (114), 1934.

(10) Tye, R. P., "Preliminary Measurements on the Thermal and Electrical Conductivities of Mo, Nb, Ta, and W," from "Niobium, Tantalum, Molybdenum, and Tungsten," A. G. Quarell, Editor, Elsevier Pub. Co., Amsterdam, 1961.

8. Appendix

Procedure used to derive the thermal conductivity equation for W-Re.

1. The desire to fit the thermal conductivity to an equation relating it to the electrical resistivity and to include a term with the proper temperature dependence for phonon conduction required that special data reduction procedures be developed.

2. The fact that the precision in the data appeared to vary as a function of temperature suggested that a method employing weighting functions be used.

3. The electrical resistivity data were treated first for an analysis of variance. This showed the variance to have a temperature dependence which could be correlated with the experiment. The characteristic of the furnace and power controller is that temperatures are maintained very well at high temperatures (> 1000 °C) but relatively poorly at lower temperatures. However, the uncertainties in the measurement of temperature increase at high temperatures. At very high temperatures (> 2000 °C) the voltage drop measurements were not as steady as at lower temperatures. This statistical approach is used to obtain a weighting function which takes into account the experimental confidence in the data.

   In this manner the second degree polynomial for resistivity as a function of temperature was derived.

4. The analysis of variance of the thermal conductivity data showed it to be independent of temperature and, therefore, all data were weighted evenly. This may appear inconsistent with the statement above on electrical resistivity; however, when considering the difference in the magnitude of the error in the measurements in the two properties, ±1.5% for resistivity compared to ±8% to ±10% for conductivity, one can see that the precision in any one property would be sensitive to test conditions whereas the other may not.

   Using the equation for resistivity of W-Re as determined above and starting with the classical Lorenz constant, the constants A and B were determined from the thermal conductivity data. Then L was increased in steps and new values of A and B were obtained. A final analysis to minimize the standard deviation while forcing L back to the classical constant yielded the reported equation.

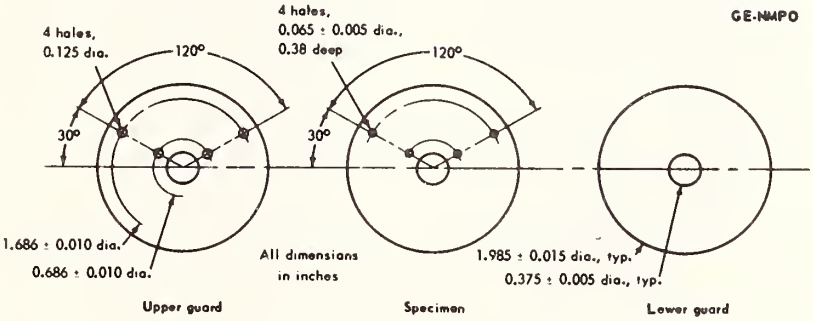

Figure 1. Design of thermal conductivity specimen and guards.

Figure 2. Microstructures of W-26Re and unalloyed tungsten.

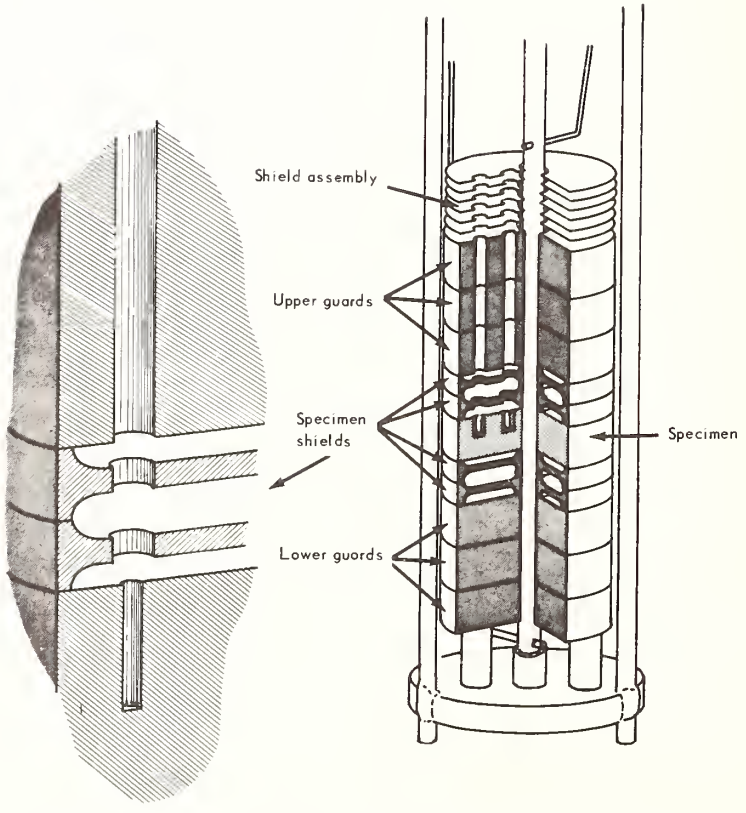

Figure 3. Thermal conductivity specimen and guard assembly.

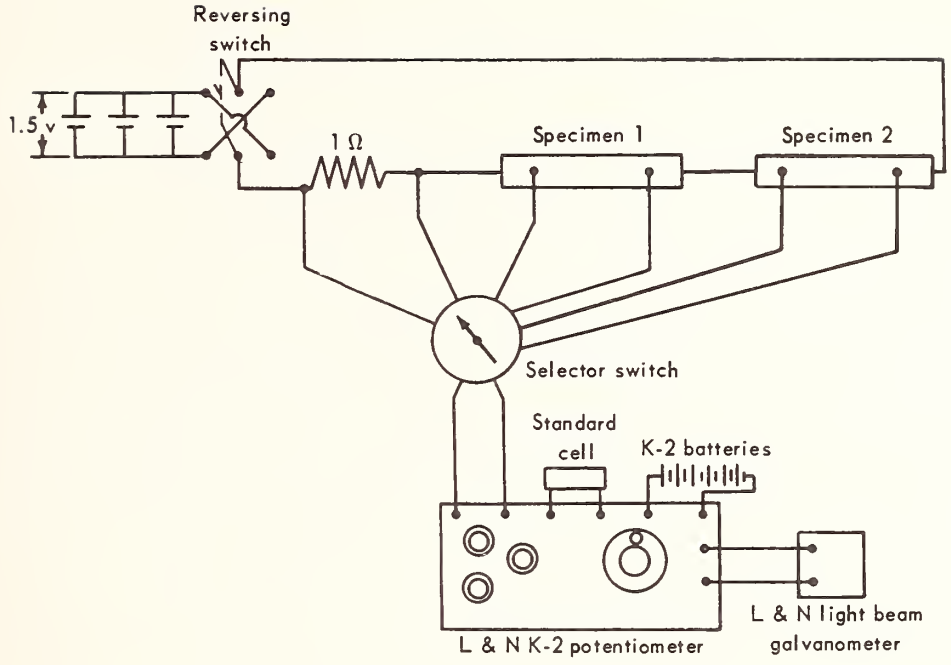

Figure 4. Schematic of electrical resistivity measurement system.

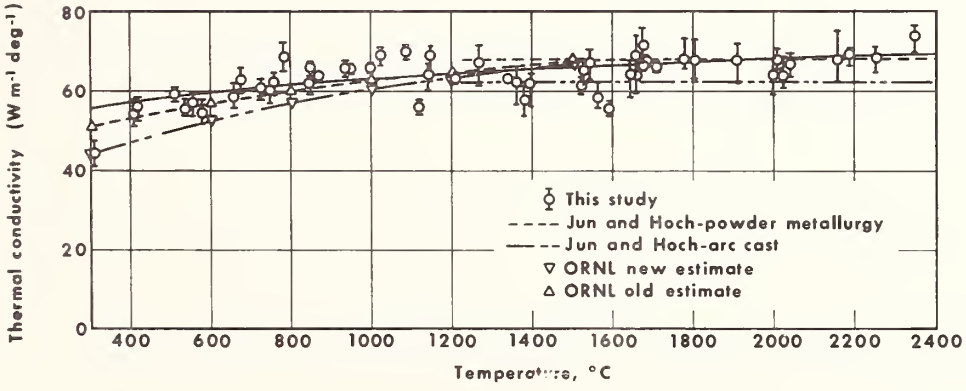

Figure 5. Thermal conductivity versus temperature for W-26Re alloy.

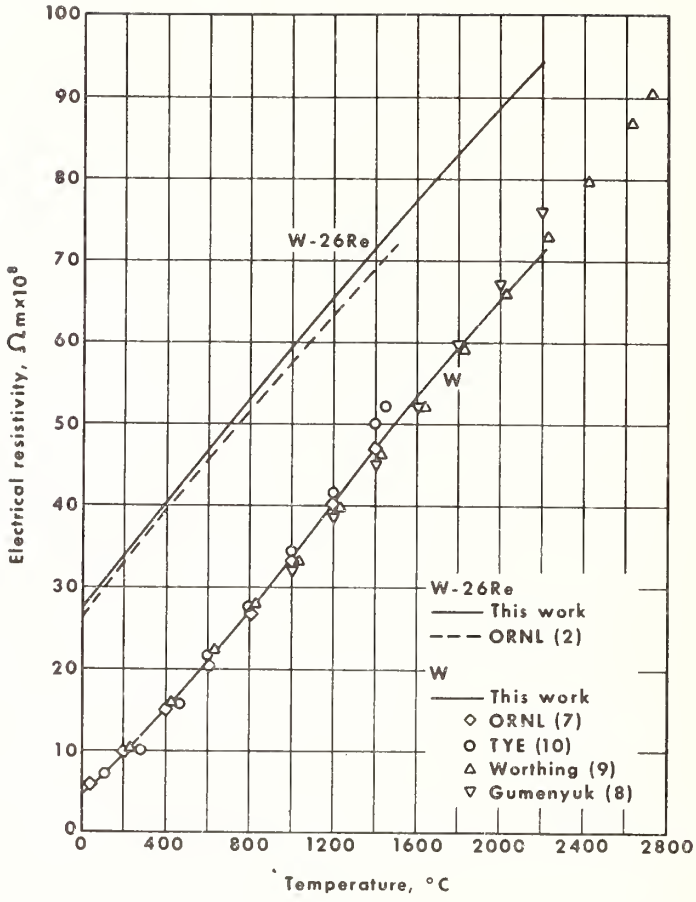

Figure 6. Electrical resistivity versus temperature for W-26Re alloy and unalloyed W.

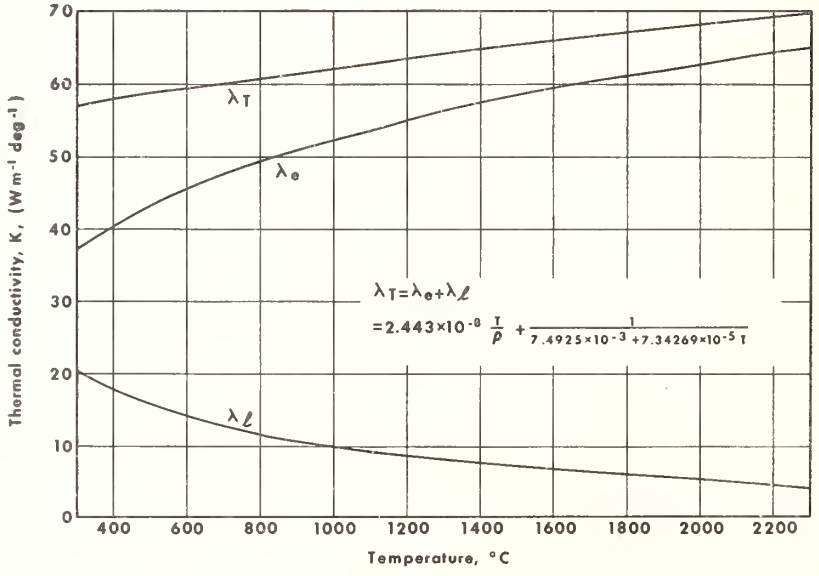

Figure 7. Components of thermal conductivity vs temperature for W-26Re.

Thermal Conductivity of Magnesium Stannide

J. J. Martin, H. R. Shanks and G. C. Danielson

Institute for Atomic Research and Department of Physics
Iowa State University, Ames, Iowa 50010

The thermal conductivity of the semiconductor Mg_2Sn has been determined in the temperature range 80 to 700°K from measurements of the thermal diffusivity. At low temperatures the thermal conduction is entirely lattice conduction, as shown by our earlier measurements from 4 to 300°K. At higher temperatures, however, our results show that bipolar-electronic conduction (diffusion and recombination of electron-hole pairs) becomes important and actually equals the lattice conduction at 700°K. The difference between our measured thermal conductivity and the lattice thermal conductivity is in good quantitative agreement with the calculated bipolar-electronic thermal conductivity, and this agreement gives strong support to the theory of bipolar conduction in semiconductors.

Key Words: Bipolar conductivity, lattice conductivity, magnesium stannide, semiconductor, thermal conductivity, thermal diffusivity.

1. Introduction

Mg_2Sn is a II-IV compound semiconductor with the antifluorite structure and is a member of the Mg_2X family of compounds where X can be Si, Ge, Sn or Pb. Elastic constants and calculated lattice vibration frequencies have been reported by Davis et al. [1][1]. The electrical properties of Mg_2Sn have been reported by Winkler [2] and others [3-5]. Umeda [6] and Crossman [7] report that the electronic structure of Mg_2Sn consists of ellipsoids along the [100] directions. Busch and Schneider [8] have reported thermal conductivity data on Mg_2Sn from 77 to 400°K. Recently, Martin and Danielson [9] measured the thermal conductivity of several Mg_2Sn samples from 4.2 to 300°K. These results indicated that below 300°K lattice conduction is completely dominant in Mg_2Sn; the thermal conductivity is proportional to T^{-1} from 150 to 275°K. Above room temperature Mg_2Sn is completely intrinsic and the lattice conductivity is small (0.075 W/cm-deg at 300°K); hence, the electronic contribution should be a large part of the total thermal conductivity. Therefore, we have extended our measurements by a thermal diffusivity technique to 700°K in order to determine the electronic thermal conductivity of Mg_2Sn.

2. Experimental Procedure

The single crystal sample was grown by a modified Bridgman technique. The sample was grown from 99.999% purity tin and from magnesium distilled under high vacuum in this Laboratory from 99.99% purity starting material. The sample was n-type. Figure 1 shows the electrical resistivity data taken on the diffusivity sample before and after the thermal diffusivity measurements. Figure 1 also shows the Hall coefficient of the sample that was measured prior to the thermal diffusivity measurements. The Hall data indicates that the sample contained approximately 2.5×10^{16} cm^{-3} uncompensated donors before the thermal diffusivity measurements were made. The change in the electrical resistivity data after the diffusivity measurements were completed indicates that the donor concentration increased to about 3×10^{16} cm^{-3}. The sample dimensions were $4.30 \times 4.24 \times 20$mm.

We have developed new instrumentation so that thermal diffusivity data may be taken on short samples by our finite difference method. The new data recording apparatus is similar to our old gear [10] except that Astrodata model 120R amplifiers are used for D. C. amplification and a four trace oscilloscope is used to record the temperature versus time curves. Typical pulse times are 5 sec.

[1] Figures in brackets indicate the literature references at the end of this paper.

The sample was mounted in a sample holder which contained Pt versus Pt-10% Rh and Cu versus constantan thermocouples for temperature measurements above and below room temperature. Three Cu wires were spark welded to the sample at distances of 5, 7.5 and 10mm from the resistance wire heater wound on one end of the sample. A fourth Cu wire was spark welded to the opposite end of the sample for use as a reference lead. The three Cu versus Mg_2Sn versus Cu reference differential thermocouples were used to measure the three temperature versus time curves in the sample. The data were taken in a cryostat-furnace which could cover the temperature range 80 to 700°K.

3. Results

Our thermal diffusivity results are shown in fig. 2. The curve represents the best fit to the data and was used to calculate thermal conductivity values. The thermal conductivity was calculated from the smoothed thermal diffusivity, the x-ray density [11] of 3.592 gm/cm^3 and the specific heat. The specific heat values of Jelinek et al. [12] were used between 80 and 300°K, and the specific heat values of Gschneider [13] were used between 300 and 700°K. The thermal conductivity curve is shown in fig. 3 along with our low temperature thermal conductivity data and the earlier data of Busch and Schneider [8]. Between 80 and 300°K our new data is in good agreement with our old thermal conductivity data and with the data of Busch and Schneider.

4. Discussion

In a semiconductor, heat may be carried by the lattice (phonons) and by the charge carriers (electrons and holes). The total thermal conductivity, K, can be expressed as a sum of the lattice conductivity, K_L, and the electronic thermal conductivity, K_e;

$$K = K_e + K_L. \tag{1}$$

In order to determine K_e we must subtract K_L from the total thermal conductivity. From 150 to 275°K the thermal conductivity of Mg_2Sn goes as T^{-1} which is characteristic of three phonon scattering.

Since the Debye temperature is about 200°K and three phonon scattering processes will continue to dominate the lattice conductivity at higher temperatures, we expect the T^{-1} temperature dependence to continue. Mg_2Sn becomes completely intrinsic near 300°K so we expect the electronic thermal conductivity to become important above 300°K. Figure 4 shows a plot of the thermal resistivity of our sample (K^{-1}) versus T. The line represents the $K^{-1} \sim T$ extrapolation of our data. We will use this line as our high temperature extrapolation of the lattice conductivity.

The electronic thermal conductivity, K_e, was obtained by subtracting the lattice conductivity, K_L, from the total thermal conductivity. At 700°K, $K_e \approx K_L$.

If we assume acoustic mode scattering of both the electrons and holes, the electronic thermal conductivity can be expressed as

$$K_e = \left(\frac{k}{e}\right)^2 \left\{ 2 + \frac{(4 + \Delta E/kT)^2 \, npb}{(bn + p)^2} \right\} \sigma T. \tag{2}$$

In eq(2) k is Boltzmann's constant, e is the electronic charge, ΔE is the energy gap at temperature T, b is the mobility ratio μ_e/μ_n, n and p are the electron and hole concentrations, and σ is the electrical conductivity. The first term expresses the ordinary Wiedemann-Franz law for a non-degenerate material. The second term represents the transport of the recombination energy of the electrons and holes and is called the bipolar contribution to the electronic thermal conductivity. The bipolar term is usually much larger than the Wiedemann-Franz term because $\Delta E/kT >> 1$.

Winkler [2] found an energy gap of $(0.36 - 3 \times 10^{-4} T)$eV for Mg_2Sn. The ratio, b, of the electron mobility to the hole mobility in the intrinsic range was found to be 1.20-1.25 by Lipson and Kahan [14] and 1.23 by Blunt et al. [3]. For the calculation of K_e we shall use b = 1.23. In the intrinsic region (T > 300°K for Mg_2Sn) n=p. The solid line in figure 5 shows the electronic thermal conductivity calculated from eq 2. The electrical conductivity measured on our sample was used in the calculation along with the energy gap of Winkler [2] and b = 1.23. The calculated and measured electronic thermal conductivities agree to within 3mW/cm-deg which is about 5% of the total thermal conductivity.

5. Summary

The thermal conductivity of the semiconductor Mg_2Sn has been determined by thermal diffusivity measurements between 80 and 700°K. The data between 80 and 300°K are in good agreement with our direct thermal conductivity results. From 150-275°K, the thermal conductivity goes as T^{-1} which is characteristic of high temperature lattice conductivity. The electronic thermal conductivity which was determined by subtracting the extrapolated lattice conductivity from the measured thermal conductivity is in good agreement with the calculated electronic thermal conductivity. At 700°K the electronic thermal conductivity was equal to the lattice thermal conductivity.

6. References

[1] Davis, L. C., Whitten, W. B., and Danielson, G. C., J. Phys. Chem. Solids, 28 439 (1967).

[2] Winkler, U., Helv. Phys. Acta. 28 633 (1955).

[3] Blunt, R. F., Frederikse, H. P. R., and Hosler, W. R., Phys. Rev. 100 633 (1955).

[4] Lawson, W. D., Nielsen, S., Putley, E.H., and Roberts, V., J. Electronics 1 203 (1955).

[5] Lichter, B. D., J. Electrochem. Soc. 109 819 (1962).

[6] Umeda, J., J. Phys. Soc. Japan 19 2052 (1964).

[7] Crossman, L. D., Ph.D. thesis, Iowa State University, 1967 (unpublished).

[8] Busch, G. and Schneider, M., Physica, 20 1084 (1959).

[9] Martin, J. J. and Danielson, G. C., Phys. Rev. to be published.

[10] Kennedy, W. L., Sidles, P. H., and Danielson, G. C., Advanced energy conversion Vol. 2, p. 53 (Pergamon Press, Oxford, 1962).

[11] Swanson, H. E., Gilfrich, N. T., and Uriginic, G. M., X-ray diffraction powder patterns. National Bureau of Standards Circular 539, Vol. 5: 41 (1955).

[12] Jelinek, F. J., Shickell, W. D., Gerstein, B. C., J. Phys. Chem. Solids, 28 267 (1967).

[13] Gschneider, K., private communication (1967).

[14] Lipson, H. G. and Kahan, A., Phys. Rev. 133 A800 (1964).

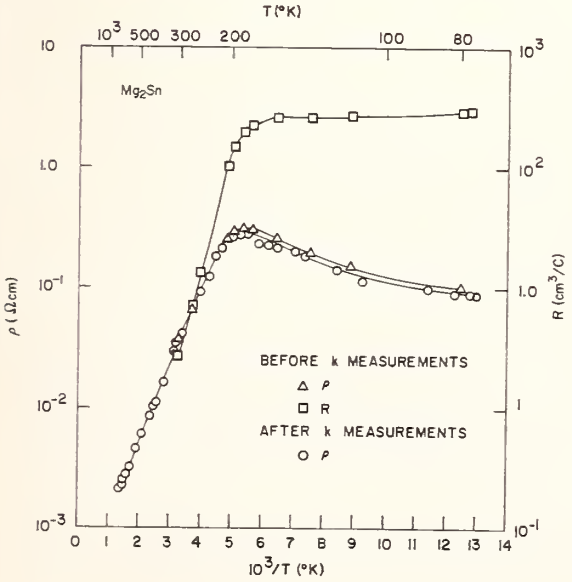

Figure 1. The Hall coefficient and electrical resistivity of our thermal diffusivity sample that were measured before the thermal diffusivity data were taken and the electrical resistivity that was measured after the thermal diffusivity was measured as shown.

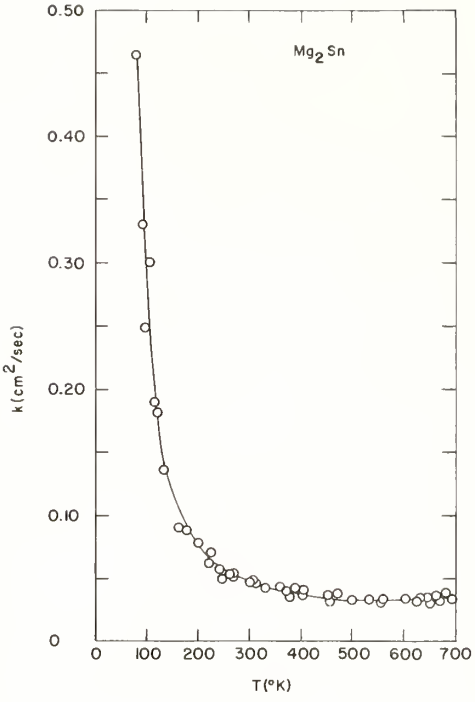

Figure 2. The thermal diffusivity of Mg_2Sn.

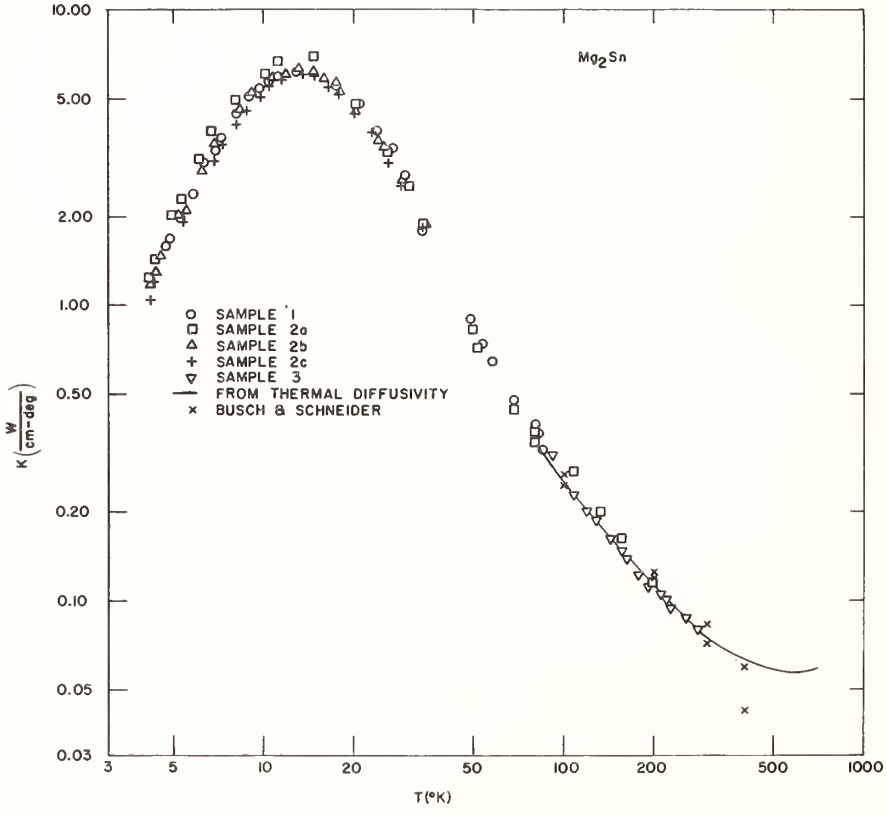

Figure 3. The smoothed thermal conductivity calculated from the thermal diffusivity is shown with the results of our earlier thermal conductivity measurements.

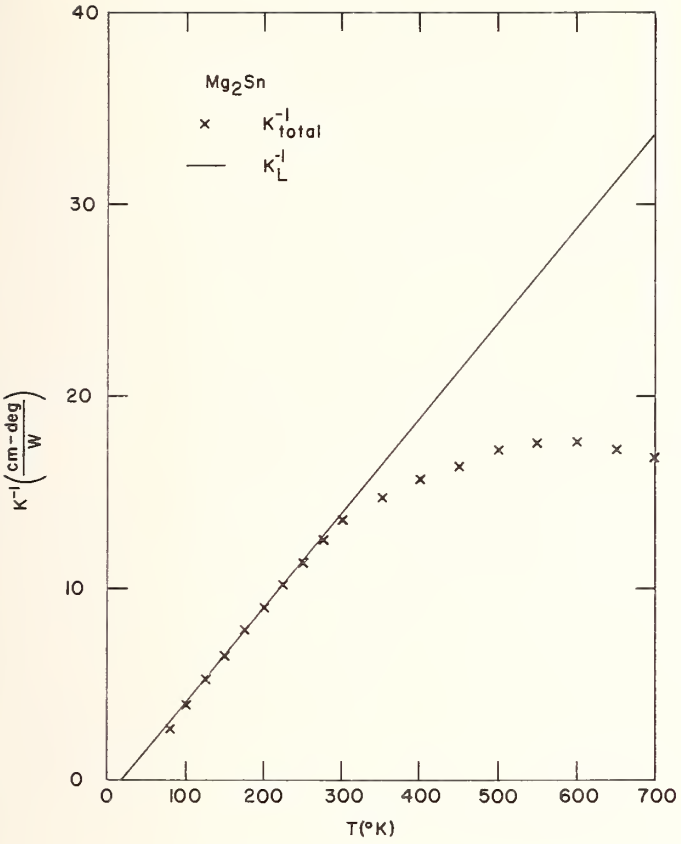

Figure 4. The points show the smoothed thermal resistivity of our sample. The straight line represents our estimate of the lattice conductivity.

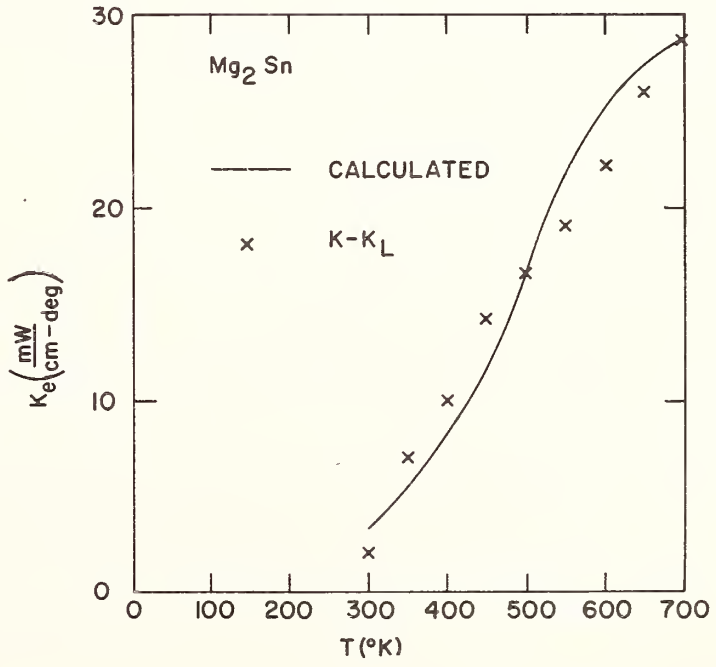

Figure 5. The curve represents the calculated electronic thermal conductivity. The points represent the difference between our total thermal conductivity and the estimated lattice conductivity.

Thermal Properties of SNAP Fuels[1]

C. C. Weeks, M. M. Nakata, and C. A. Smith

Atomics International
A Division of North American Rockwell Corporation
P. O. Box 309
Canoga Park, California

The thermal conductivity of uranium-fueled zirconium hydride was obtained from thermal diffusivity, density, and specific heat over the composition range of H/Zr - 1.58 to 1.81 (atomic ratio). The thermal properties measurements of SNAP fuel materials was complicated by the fact that the hydride decomposes at elevated temperatures and also undergoes phase changes in the temperature range of interest. Uncertainties in the phase diagram of the zirconium hydride system also contributed to the difficulties. Diffusivity was measured by the pulsed laser technique. Enthalpy and specific heat were determined with a high pressure hydrogen drop calorimeter. The calorimeter employs a variable temperature receiver to permit measurements to temperatures above and below the numerous phase boundaries in the Zr-U-H system. The data on the various properties measured were analyzed and plotted with the aid of a computer program and are presented as functions of temperature and composition.

Key Words: Calorimeter, density, diffusivity, SNAP reactor fuel, specific heat, thermal conductivity, thermal diffusivity, thermal properties.

1. Introduction

The thermal properties of zirconium hydride as a function of composition and temperature are of particular interest to the SNAP reactor program since these reactors employ zirconium hydride and uranium as a homogeneous fuel-moderator. Thus, the thermal properties of this material, and in particular the thermal conductivity, are essential to predict the behavior of the moderator during reactor operation. Thermal conductivity is most readily obtained from the relation

$$\lambda = adc_p \quad , \tag{1}$$

where a is the thermal diffusivity, d is the density and c_p is the specific heat.

Since zirconium hydride decomposes at elevated temperatures, studies of this material are complicated by the need to maintain composition during measurements by providing a balancing hydrogen overpressure which is a strong function of temperature. To complicate the matter further, the phase diagram for zirconium hydride is complex and was not well established at atomic ratios of hydrogen to zirconium of 1.6 and greater.

Fig. 1 shows a phase diagram for the zirconium hydride system. The boundaries of the $\delta + \epsilon$ region were not well known at the beginning of the properties program, as indicated by the shaded bands. Data from another program, concurrent with this one, to determine phase boundaries, indicate the δ and ϵ boundaries curve toward each other, joining in the vicinity of 450°C. The δ boundary continues its characteristic curvature to higher H/Zr ratios beyond the intersection. Preliminary results indicate

[1]Work done under AEC Contract AT(04-3)-701

a δto ε boundary near 700°C, for H/Zr = 1.81.

The dashed curves in the upper portion of the figure delineate the equilibrium hydrogen pressures. The required hydrogen overpressure sets a practical limit on the maximum temperature at which the material can be used or studied. In addition to the usual requirements of instrumentation for experimental determination of thermophysical properties, the systems must be capable of operation at hydrogen pressures up to about ten atmospheres.

The samples for specific heat and thermal diffusivity were machined from adjacent cuts of the same fuel rod which, in turn, was from the same extrusion of fuel alloy and contained the reference concentration of modifier. Each sample was fully analyzed before measurements were made. The hydrogen pressure was maintained at equilibrium during temperature changes by following the isochores [1][2] shown in Fig. 2.

Specific heat was measured using a drop calorimeter specifically designed for use with hydride materials. The copper receiver, into which the samples were dropped, can be heated to any predetermined temperature up to 650°C to avoid crossing phase boundaries during sample cooling. Also, hydrogen pressure can be maintained in equilibrium with the sample up to 150 psi. The hydrogen content of each sample was adjusted to a selected H/Zr ratio by maintaining the sample at temperature and equilibrium pressure in the drop calorimeter prior to each series of drops. The method and its limitations are described further in Section 2.

Thermal diffusivity was measured by the flash method using a laser beam as the source of energy. Samples for these measurements were cut from material adjacent to the corresponding specific heat samples. The hydrogen content of each sample was adjusted within the equipment to conform with the same isochores used for specific heat. The flash method is described in more detail in Section 3.

Thermal conductivity can be calculated from specific heat, thermal diffusivity, and density by the relationship

$$\lambda = \alpha d c_p \quad . \tag{2}$$

The experimental program described in this paper yielded specific heat and thermal diffusivity. The thermal conductivity was then computed from these data and from the known density of SNAP fuels as a function of temperature.

2. Specific Heat

2.1 Technique

Drop calorimetry is probably the simplest and most generally applicable method of determining high temperature specific heats. In principle, the method consists of determining the enthalpy change in a material by measuring the heat absorbed in a cool receiver after it receives a heated sample. The specific heat, c_p, of the sample is then obtained from the relation

$$c_p = \frac{dH}{dT} \quad . \tag{3}$$

The most serious limitation of this method is that cooling of the sample may be too rapid to permit phase changes so that the sample is quenched in a non-equilibrium state and evolves less heat than equilibrium conditions would yield. To eliminate this problem, the calorimeter was designed so that the receiver could be maintained up to 650°C, thus eliminating the necessity for dropping through phase boundaries.

In the experimental procedure, the samples were heated to a predetermined temperature, T, in an atmosphere of hydrogen maintained at the equilibrium dissociation pressure. The samples were then dropped (under gravity with electromagnetic braking) into the massive copper receiver maintained at a suitable lower temperature, T_r; the hydrogen overpressure was also re-adjusted to maintain a constant fuel composition. The loss of heat, Q(T), by the sample results in a small temperature increase, δ(T), in the receiver which was measured by a thermopile. The specific enthalpy, H, of the sample at temperature, T, relative to T_r, is then given by

$$H(T) = \frac{Q(T)}{m} = C_r \, \delta(T) \, \frac{M}{m} \quad , \tag{4}$$

---

[2] Figures in brackets indicate the literature references at the end of this paper.

when m is the mass of the sample, C_r is the specific heat of the receiver, and M is the mass of the receiver. By making drops from several sample temperatures, the specific enthalpy was determined as a function of temperature

$$H = a_0 + a_1 T + a_2 T^2 + a_3 T^3 + - - -. \quad (5)$$

The specific heat, c_p, was then determined from the derivative of eq (5) with respect to temperature,

$$c_p = a_1 + 2a_2 T + 3a_3 T^2 + - - -. \quad (6)$$

The values of H and c_p were determined by the use of computer techniques.

2.2 Apparatus

a. System

The drop calorimeter used for obtaining specific heat during this program was designed and constructed by the Dynatech Corporation for Atomics International. Fig. 3 is a cross section of the calorimeter, simplified for clarity. The three basic parts of the apparatus are the furnace, the transition zone, and the receiver.

b. Furnace

The furnace is molybdenum wound with aluminum oxide insulation and molybdenum radiation shields adjacent to the furnace winding. The central portion of the furnace is lined with a thick-walled iron tube to flatten the temperature profile. The temperature is controlled and monitored by Geminol thermocouples, which are relatively insensitive to the hydrogen environment.

c. Transition Zone

The transition zone is heated to reduce heat loss from the receiver along its supporting column. It also contains a pair of movable heat shields to reduce convection losses from the receiver and to prevent furnace radiation from reaching the receiver. These heat shields are actuated by rotary solenoids and are opened and closed quickly during a drop to allow the sample to pass through the transition zone.

d. Receiver

The receiver, which is a copper cylinder weighing about 100 pounds, is vacuum insulated and is thermally shielded by a surrounding copper shell or receiver guard maintained at the receiver temperature. The transition zone heaters and the receiver guard heaters are differentially controlled with reference to the receiver temperature so that they follow it and maintain receiver losses at a very low value. By proper adjustment of the guard and the transition zone temperatures, it is possible to obtain receiver time constants of several hours. The receiver contains a dual-purpose heater. It is used to heat the receiver during electrical calibrations and, when it is desirable, to raise the receiver temperature to avoid dropping through phase boundaries. The temperature rise of the receiver following a sample drop is determined by means of a thermopile consisting of ten chromel-alumel couples.

e. Temperature Control

Temperature sensing for control purposes is provided by chromel-alumel thermocouples throughout the calorimeter except in the furnace. Geminol thermocouples were used in the furnace for control and monitoring because they are relatively insensitive to hydrogen throughout their temperature range.

Furnace control is provided by a null-balance type controller with a controlled rectifier output. The temperature profile in the furnace is controlled manually by adjustment of a secondary heater to correct for end losses.

The control thermocouples for both the transition zone heater and the receiver guard are connected differentially to thermocouples mounted on the receiver. These controllers are also the null-balance type with band width control to minimize temperature overshoot.

f. Drop Mechanism

The drop mechanism permits multiple drops of a sample without opening the furnace. When in place, the sample is supported by a molybdenum wire attached to a magnetic armature which travels inside a nonmagnetic thimble located above the furnace. The armature is supported by a matching set of pole pieces and permanent magnets that fit the outside of the thimble. The magnet assembly is driven up or down the thimble by means of a linear AC motor.

g. Safety

Several safety precautions were taken to minimize the possibility of a hydrogen conflagration. The entire outside vessel was traced with cooling water tubes to maintain the seals near room temperature and to cool any gas which might leak out. A large hood was installed above the calorimeter and exhausted continuously to prevent the chance of hydrogen buildup in the laboratory.

A second exhaust system, vented to the outside of the building, was installed on the calorimeter. During operation, it was continuously purged with argon. Hydrogen from the calorimeter was exhausted through this system. System pressures of one atmosphere and less were pumped into the vent with a mechanical vacuum pump, but gases in the calorimeter at pressures above one atmosphere were exhausted by a quick release mechanism. This mechanism bypasses the vacuum system and consists primarily of a solenoid valve for quick release and a check valve to prevent impurities from backstreaming.

2.3 Calibration

Before the calorimeter could be used, it had to be calibrated to determine the response of the receiver to an addition of heat.

The relationship for the electrical calibration is

$$h = \int EIdt = \int E(e)I(e)\,\frac{dt}{de}\,de \quad , \tag{7}$$

where

h = heat gained by the receiver

E = potential drop across the calibration heater

I = calibration heater current

e = thermopile emf

t = time.

From eq (7) we obtain:

$$\frac{dh}{de} = E(e)I(e)\,\frac{dt}{de} \quad , \tag{8}$$

where dh/de is the receiver characteristic which must be determined to calibrate the receiver since it gives the heat input for an observed change in thermopile emf. To determine dh/de, power is applied continuously to the receiver, and E, I, e, and t are measured at regular intervals over the desired range of receiver temperatures. Values of dh/de are then computed from eq (8) preferably by a computer program. To perform the electrical calibration, power was supplied to the receiver heater from a voltage-regulated, solid-state power supply. The heater current was determined by reading the potential drop across a 0.01% shunt with a precision potentiometer. The voltage across the heater was measured with a potentiometer using probes connected directly to the heater terminations. The receiver response was obtained by a thermopile consisting of ten chromel-alumel thermocouples. The thermopile junctions were imbedded in the outer surface of the receiver so that they would not be in hydrogen. The heater voltage was held constant at 10 volts; current was approximately 4.46 amperes when the receiver was near room temperature. The receiver heating rate was about 10°C per hour. The hydrogen pressure in the receiver was kept at one atmosphere during the calibration.

Originally an electrical calibration was made for the receiver temperature range of room temperature to 350°C, using a single thermocouple on the receiver. These results were compared to a predicted calibration curve obtained by multiplying the mass of the receiver by the specific heat of copper, assuming a linear thermocouple response. The electrical calibration exhibited deviation of about 3%

from the predicted curve. Short runs at various receiver temperatures duplicated the original data quite well, so that it was concluded that the general shape of the experimental curve was real. It showed a direct relationship to deviations from linearity of the thermocouple output as a function of temperature, amounting to about ± 30 microvolts. This effect is, of course, a property of the thermocouple materials and is repeatable.

In addition to deviations caused by the characteristics of the thermocouple materials, there was scattering of data, but to a much lesser degree. It was determined that an error of one microvolt, in a thermocouple reading, resulted in about a 1% change in the value dh/de. Since the potentiometer used to measure the thermocouple output could be read only to one-half microvolt, it was concluded that a single thermocouple was not sensitive enough to maintain the desired accuracy during drop tests at the lower end of the temperature range. In order to increase the receiver thermocouple output to an acceptable value, it was decided to replace the single couple by a ten-element chromel-alumel thermopile.

Because the phase boundaries for the $\delta + \epsilon$ region had not been established, as indicated by the shaded regions in Fig. 1, all drops were made to room temperature. Thus, the ten-element thermopile was calibrated only for a short temperature range of 34° to 50°C.

The dh/de values for the receiver are relatively constant for these short spans and are given as average values in Table 1.

Table 1. Receiver Calibration dh/de (Joules/millivolt)

	Receiver Temperature	Electrical	Copper Drops	Calculated
dh/de	34°-50°C	4.1883	4.2522	4.22

Five calibration drops were made to room temperature values from temperatures between 200° and 600°C, using a 135.6 gm sample of copper. The receiver was at a slightly higher temperature for each successive drop, but remained within the 34° to 50°C range selected for electrical calibration. The average dh/de value for the copper drops is shown in Table 1. The specific heat data for the copper sample was taken from literature values [2].

Calculated values were obtained by multiplying the mass of the receiver by the specific heat of copper, assuming a linear thermocouple response. This was not performed as a precise calibration but to predict the approximate results from the experimental calibration.

2.4 Measurement Technique

Each zirconium hydride sample, before a series of drops, was placed in the calorimeter and the system pumped to a vacuum of approximately 1.3×10^{-3} Nm^{-2} at room temperature. Then, after several purges of ultrapure hydrogen, sample temperatures were raised to values which insured relatively short equilibration periods. The samples were then maintained at the correct temperature and hydrogen pressure for adequate periods of time to insure no more than small fractional percentage deviations from the preselected H/Zr ratios.

Once the sample had been conditioned in the calorimeter, it was subjected to a series of drops from furnace temperatures ranging from about 200°C to 900°C, except for H/Zr 1.81 in which case the upper temperature was restricted by the ten-atmosphere hydrogen pressure limitation placed on the calorimeter.

When the sample was dropped from the furnace, the heat shields in the transition zone were opened long enough to permit passage into the receiver. The emf output from the receiver thermopile was then read with a potentiometer to determine the receiver temperature and the temperature rise. The thermopile emf was recorded at regular increments of time to establish when the sample and receiver reached thermal equilibrium and to check the time constant of the receiver. Normally the system was adjusted to give the receiver a thermal relaxation period of several hours.

In most cases the sample cooled rapidly enough in the receiver following a drop to maintain composition without adjusting the hydrogen pressure. At several of the higher temperatures, the hydrogen pressure was reduced during the sample cooling to maintain composition.

2.5 Data Reduction

To determine specific heat for each composition of zirconium hydride, each series of drops was analyzed to obtain the enthalpy change for each drop. These data were then machine-fitted to a

polynominal expression of enthalpy. The expression for enthalpy was then differentiated to obtain an expression for specific heat.

The enthalpy change for each drop is given by the expression

$$H(T,\theta_2) = \frac{1}{m}\int_{e_1}^{e_2} \frac{dh}{de}\, de = \frac{1}{m}\frac{dh}{de}(e_2 - e_1) \quad , \tag{9}$$

where

$H(T,\theta_2)$ = enthalpy per unit mass from T to θ_2

θ_2 = the receiver temperature after cooling of the sample

e_1 = thermopile emf before the drop

e_2 = thermopile emf after cooling of the sample

Since the initial receiver temperature changes with each drop, a correction must be made to normalize all drops in a particular series to the same receiver temperature, θ_0. A further correction is required due to the molybdenum wire suspension system. The mass of the wire, m_w, is small compared to that of the sample; therefore, its average specific heat, $\bar{C}_w$, may be used to determine its heat contribution over the temperature range T to θ_2. Upon applying these corrections, the expression for the enthalpy change of the sample becomes

$$H(T,\theta_0) = \frac{1}{m}\frac{dh}{de}(e_2 - e_1) - m_w \bar{C}_w (T - \theta_2) + \frac{dH}{d\theta}\Big|_{\theta_0} \frac{d\theta}{de}(e_2 - e_0) \quad , \tag{10}$$

where $dH/d\theta\,|\theta_0$ is the specific heat of the sample at θ_0 and e_0 is the thermopile emf at θ_0.

Since the average initial receiver temperature was approximately 34°C, all data were adjusted to θ_0 = 34°C. The specific heat, $dH/d\theta$, was obtained from earlier work [3] in which pulse heating was used. Since specific heat is the derivative of enthalpy, with respect to temperature, the use of 34°C rather than 0° as the reference temperature does not affect its value.

2.6 Enthalpy and Specific Heat

Enthalpy for each of the four compositions, 1.58, 1.65, 1.70, and 1.81, was determined by a least squares fit of the polynomial expression, eq (5), to the experimental data. The curves for the enthalpy change, with reference to 34°C, are shown in Fig. 4.

The specific heat is the first derivative of the enthalpy; thus, it is expressed as a second degree polynomial. The curves of the specific heat for the four compositions are shown in Fig. 5.

The boundaries between the δ and ε regions had not been well defined before these measurements were made. Therefore, some of the curves may include heat of transformation from one phase to the other. It is believed that any boundary that was crossed in this work had a very small heat of transformation, since it was not apparent from the enthalpy data, and could be neglected in a second degree expression for specific heat.

The enthalpy data were also fitted to a fourth degree polynomial to determine if any subtle effects could be detected as a result of crossing phase boundaries. In comparing the probable error of the coefficients, a midtemperature range effect for the 1.65 and 1.70 samples and a higher temperature range effect for the 1.81 sample were noticed where the probable error became greater than the coefficient. Derivatives of these expressions, giving a third degree equation for specific heat, gave S curve configurations for the specific heat of 1.65 and 1.70. Even though these results are not conclusive, they do have a correlation with preliminary results from the phase study program indicating curvature of the δ to ε phase boundary and, thus, there may be a small effect on the specific heat values determined in this program.

3. Thermal Diffusivity

Thermal diffusivity measurements were made on 1.58, 1.65, and 1.70 H/Zr materials using the pulsed

laser method [4]. In this method, thermal diffusivity is determined from the temperature history of the rear face of a wafer, following a pulse of energy impinging on the front face. For valid results, the following conditions must hold: the energy impulse must be uniformly distributed over the face of the wafer; the duration of the pulse must be negligibly small compared to the characteristic rise time of the specimen; and heat losses must be sufficiently small so that the energy transfer is axially directed through the wafer and the specimen temperature is independent of heat losses for a period long compared to the transient time. When the above conditions are satisfied, thermal diffusivity, a, can be obtained from the simple expression:

$$a = \frac{0.139\ \ell^2}{t_{\frac{1}{2}}} \quad , \tag{11}$$

where ℓ is the specimen thickness and $t_{\frac{1}{2}}$ is the half-time, or the time required to reach half the maximum temperature rise, following the pulse of energy. Where heat losses from the specimen are significant or where the duration of the pulsed energy is not sufficiently short, techniques have been developed [5,6] for applying the necessary corrections to the coefficient given in the above expression.

3.1 Apparatus and Method

The apparatus and method used in determining the thermal diffusivity of hydrides have been reported previously [3,7], so that only a brief description will be given here. Figure 6 is a schematic diagram of the apparatus.

The specimens were in the form of small discs nominally 6.4×10^{-3}m diameter and with thicknesses as shown in Table 2. The specimen was mounted in a stainless steel holder by means of three pins located equidistant around the circumferential edge. Geminol thermocouple wires, 7.6×10^{-4}m diameter (3-mil), were spot-welded to the center of the back face, approximately 1.5×10^{-3}m apart. The specimen holder was then placed within a stainless steel tube furnace, which was designed to contain hydrogen gas atmospheres to pressures in excess of 8×10^5 N/m^2 (6000 torr) at temperatures up to about 1000°C. The system could be evacuated to $< 3 \times 10^{-4}$ N/m^2 ($< 2 \times 10^{-6}$ torr) and back-filled with ultrapure hydrogen gas. Gas pressure was measured with Wallace and Tiernan 0 - 6.7×10^3 N/m^2 (0 - 50 torr) and U. S. Gauge Co. 0 - 8×10^5 N/m^2 (0 - 6000 torr) precision dial gauges.

Table 2. Thermal Diffusivity Specimen Data

H/Zr	Specimen No.	Thickness (m) x 10^{-3}
1.59	1	1.920
	2	1.895
1.65	1	1.869
	2	1.874
	3	2.581
1.70	1	1.816
	2	1.849
	3	1.984

In order to maintain the composition of the material being measured, the specimen was first heated to temperatures greater than 600°C and allowed to equilibrate with the proper hydrogen overpressure in the system. Diffusivity measurements were then made at selected temperature intervals, generally during the cooling cycle. When the specimen temperature was stabilized at a given level, the front face was heated with a short pulse from the laser and the output of the thermocouple was displayed on an oscilloscope and recorded on photographic film.

3.2 Results and Discussion

The data obtained for the three H/Zr compositions were fitted to least squares polynominal equations of the form:

$$a = A_0 + A_1\theta + A_2\theta^2 + A_3\theta^3 + - - -, \tag{12}$$

where a is in cm^2/sec, using a digital computer. In each case, a third degree polynominal was found to fit the data best. Graphs were also obtained by means of the computer, as shown in Fig. 7. The 1.81

H/Zr material was not measured in the present work, since the data obtained previously [3,7] were considered accurate. The 1.81 data, however, are presented here since they were used, along with the specific heat data, in calculating the thermal conductivity of the 1.81 H/Zr material.

Two 1.58 H/Zr specimens were measured. One specimen only, however, was measured over the entire temperature range shown. The second specimen gave values which were in good agreement with those of the first specimen, at the high temperature end, i.e., > 860°C. During the cooling cycle, however, the back face temperature transients were observed to be anomalous. Examination of the specimen after the run indicated the presence of hair-line cracks, which could account for the anomalous behavior. The remaining 1.58 H/Zr specimens available for testing were also found to contain fine cracks, so that no further measurements could be made on the 1.58 H/Zr composition. Since previous examination of the specimens, using gamma graph, showed no apparent flaws, it seems possible that the material is susceptible to structural degradation during storage. The apparent inflection in the curve at about 600°C was not expected, since no phase boundary is known in the temperature range covered. Fine cracks forming at high temperatures might account for the anomaly.

The 1.65 H/Zr curve in Fig. 7 represents measurements made on three specimens in the range of room temperature to 900°C. The individual curves, for each of the three specimens (not shown here) were within a ± 2% band over the entire temperature range. There is an inflection in the curve near 300°C; this would be compatible with a $\delta + \varepsilon \leftrightarrow \delta$ phase boundary at about 300°C for the 1.65 H/Zr composition.

The results of measurements in the room temperature to 870°C range, on three 1.70 H/Zr specimens, are shown in Fig. 7. The curves for each specimen (not shown here) fell within a ± 1.5% band over the entire temperature range. The inflection in the curve at about 500°C suggests a phase change; the $\delta + \varepsilon \leftrightarrow \delta$ boundary at approximately this temperature for the 1.70 H/Zr composition would be in accord with this implication.

The thermal diffusivity of 1.81 H/Zr material, as reported previously [3,7], is included in Fig. 7. The values represent the "best data" from measurements made in a joint program by Atomics International and Battelle Memorial Institute.

3.3 Summary and Conclusions

The 1.65 and 1.70 H/Zr materials gave nearly identical thermal diffusivity values over most of the temperature range covered. The diffusivity versus temperature curve for 1.70 H/Zr, however, deviates from the curve for 1.65 H/Zr at the lower temperatures, the values for 1.70 H/Zr being about 1.5% lower at room temperature. The lower values for 1.70 H/Zr in the lower temperature region is not unexpected since two phases, δ and ε, are presumed to be present, whereas the 1.65 H/Zr is expected to be single-phased down to room temperature.

The diffusivity of the 1.58 H/Zr material is lower than those of the 1.65 and 1.70 H/Zr materials, by approximately 11%, over most of the temperature range covered. Near room temperature, however, the values for 1.70 and 1.58 are nearly equal. The best data for the 1.58 H/Zr material in the region above 700°C would probably be an extrapolation of the curve obtained in the room temperature to 700°C interval.

4. Thermal Conductivity

Since the thermal conductivity, λ, of hydrides cannot be measured directly with meaningful results, it was calculated from the relationship

$$\lambda = adc_p \quad , \tag{13}$$

where a, c_p, and d are the thermal diffusivity, specific heat, and density.

The variation of the densities of SNAP fuel with temperature were determined from earlier thermal expansion measurements [8] obtained on compositions ranging from 1.70 H/Zr to 1.81 H/Zr. Isotropic expansion was assumed since all specimens used in both studies were polycrystalline and were subjected to high temperatures before measurements. Values of the ratio, R, of the density at temperature, θ, to the density at 0°C were obtained from linear expansion measurements on each composition. The ratios obtained (more than 144 values in each case) were fitted to polynomials by a least squares method. The polynomials obtained for the density ratios of 1.70 H/Zr and 1.81 H/Zr were found to be:

$$R_{1.70} = 1 - 1.78 \cdot 10^{-5}\theta - 3.31 \cdot 10^{-8}\theta^2 + 2.3 \cdot 10^{-11}\theta^3 \quad , \tag{14}$$

$$R_{1.81} = 1 - 2.6 \cdot 10^{-5}\theta - 1.64 \cdot 10^{-8}\theta^2 \quad , \tag{15}$$

with standard deviations of 0.00015 and 0.00009, respectively.

The ratio at 900°C for 1.70 H/Zr was found to be only 0.015% more than that of 1.73 H/Zr and 0.7% less than that of zirconium, so that it was considered reasonable to use the 1.70 H/Zr expression for 1.58 H/Zr and 1.65 H/Zr as well. The error introduced into the conductivity values for the two lower compositions will thus be considerably less than 0.7% and probably near 0.02%.

In general, data points of enthalpy and thermal diffusivity were obtained at different temperatures. Therefore, values of specific heat, thermal diffusivity, and density were calculated at 10°C intervals for the required temperature ranges from the polynomial expressions for these quantities. Thermal conductivity was then obtained at each of the temperatures as the product of the three quantities. The resulting values were then subjected to a polynomial least squares treatment which yielded fourth-degree polynomials as the best fit in each case.

The thermal conductivities obtained in this study are given in Fig. 8. The unusual shape of the curve obtained for the 1.58 H/Zr composition, as compared with the curves for the other compositions, is due to two factors. First, the specific heat for 1.58 H/Zr (Fig. 5) appears to be almost a parabolic function of temperature, whereas, the specific heats for the other compositions vary almost linearly with temperature. Secondly, the diffusivity decreases more rapidly in the low temperature region for 1.58 H/Zr fuel than it does for the other compositions.

5. References

[1] H. E. Johnson, "Hydrogen Dissociation Pressures of Modified SNAP Fuels", NAA-SR-9295, March 15, 1964.

[2] Y. S. Touloukian, "Recommended Values of the Thermophysical Properties of Eight Alloys, Major Constituents and Their Oxides", Thermophysical Properties Research Center, Purdue University, February, 1966.

[3] M. M. Nakata, C. J. Ambrose, and R. A. Finch, "Thermophysical Properties of Zirconium-Uranium Hydrides", Proceedings of the 6th Conf. on Thermal Conductivity, Dayton, Ohio, pp. 478-507 (1966).

[4] W. J. Parker, et al., "Flash Method of Determining Thermal Diffusivity, Heat Capacity and Thermal Conductivity", J. Appl. Phys. 32 (9) 1679-84 (1961).

[5] J. A. Cape and G. W. Lehman, "Temperature and Finite Pulse-Time Effects in the Flash Method for Measuring Thermal Diffusivity", J. Appl. Phys. 34 (7) 1909-13 (1963).

[6] R. D. Cowan, "Pulse Method of Measuring Thermal Diffusivity at High Temperatures", J. Appl. Phys. 34 (4) 926-7 (1963).

[7] C. J. Ambrose, R. E. Taylor, and R. A. Finch, "Thermophysical Properties of Zirconium-Uranium Hydride", Symp. of the 4th Conf. on Thermal Conductivity, San Francisco, Calif. (October, 1964).

[8] T. L. Iliff, "SNAP 10A Composition Fuel Alloy for Thermophysical Properties Reference Program", NAA-SR-Memo-11533.

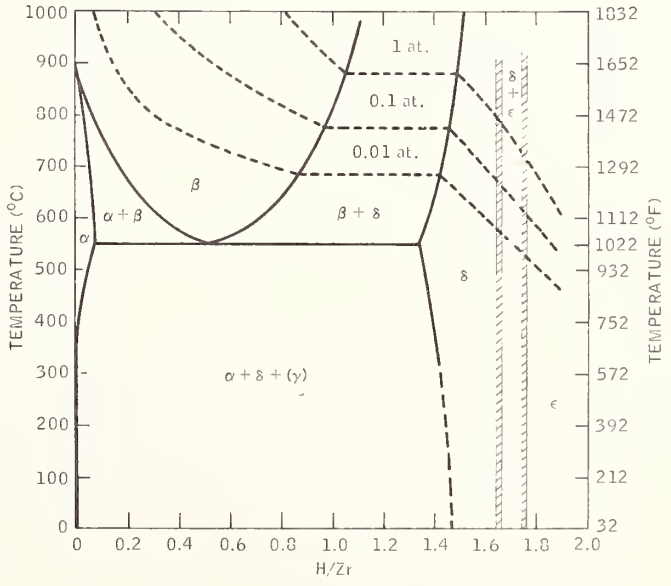

Figure 1. Phase diagram for the zirconium hydride system.

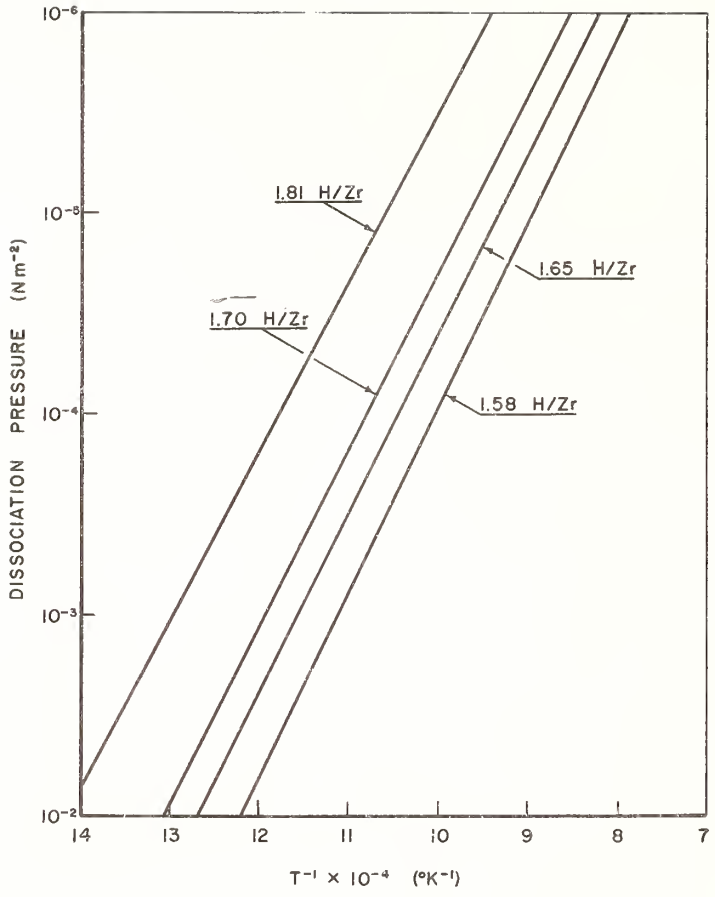

Figure 2. Dissociation pressure of H/Zr fuel.

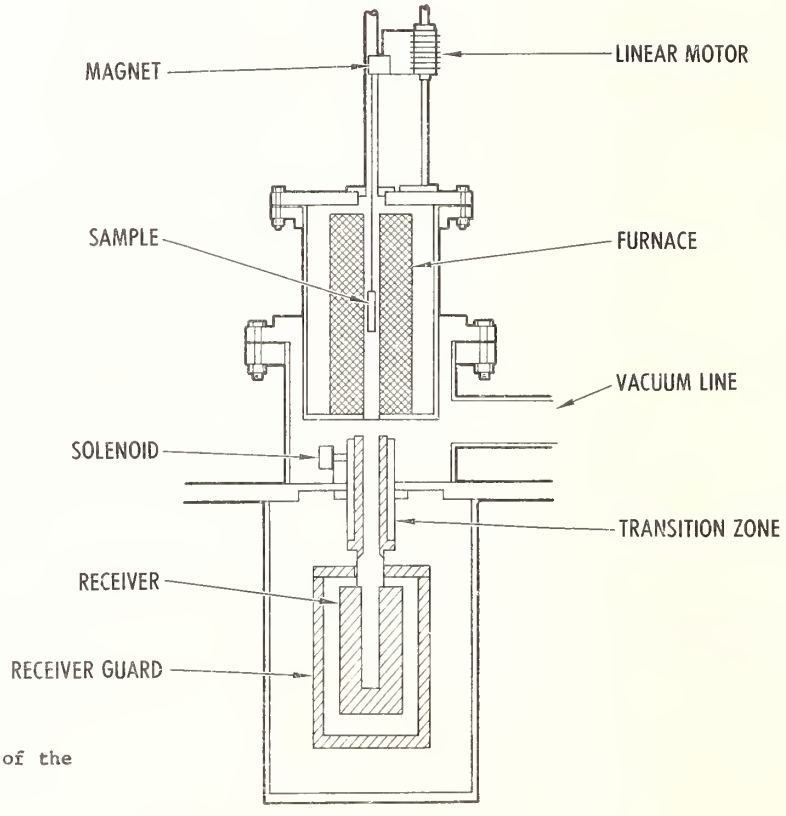

Figure 3. Cross section drawing of the drop calorimeter.

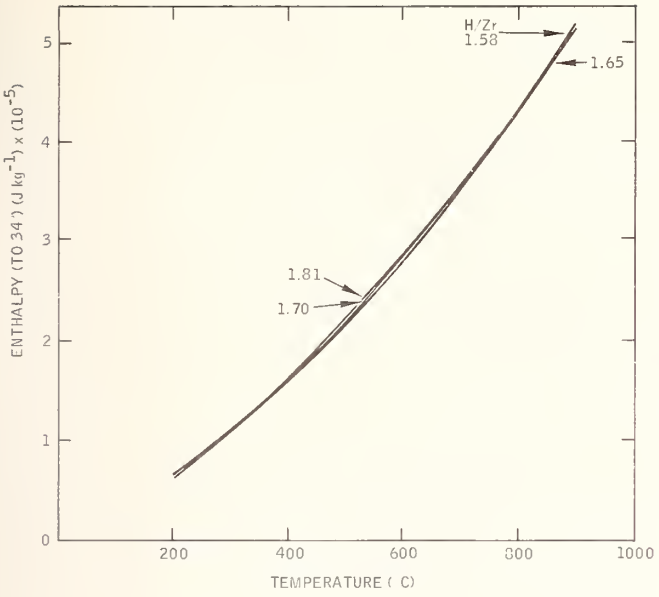

Figure 4. Enthalpy for third degree fit for H/Zr fuel.

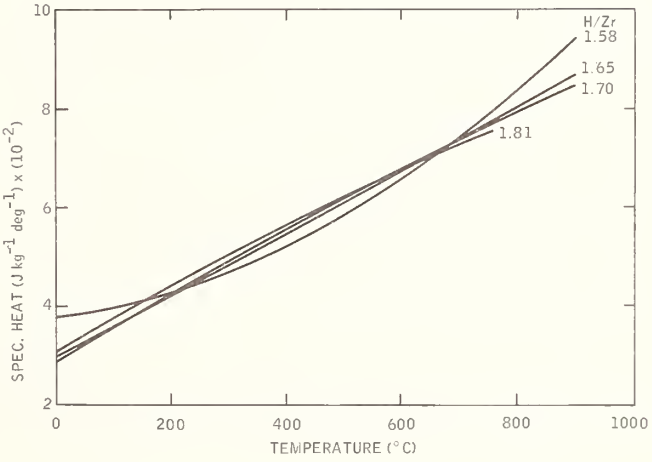

Figure 5. Specific heat for H/Zr fuel from third degree fit of enthalpy.

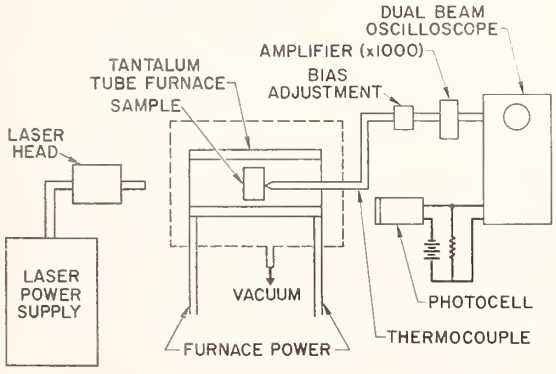

Figure 6. Schematic drawing of system for measuring diffusivity.

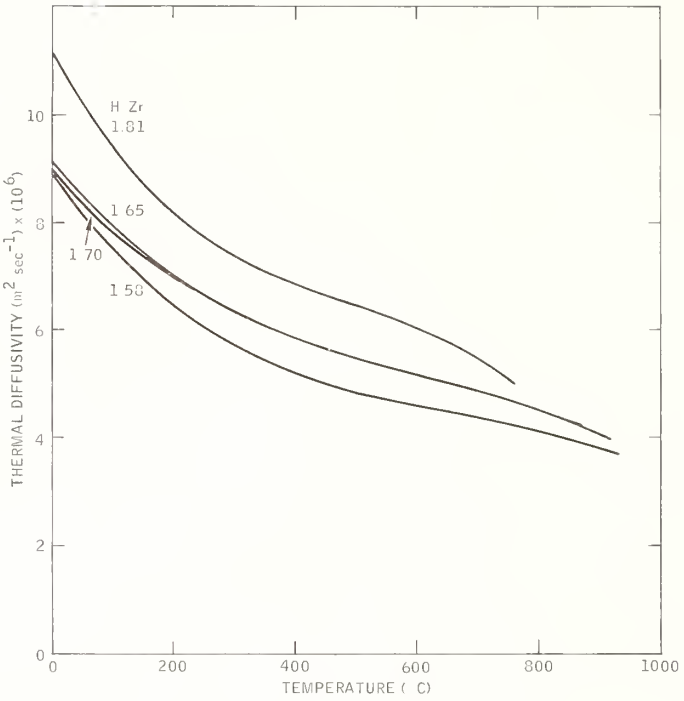

Figure 7. Thermal diffusivity of H/Zr fuel.

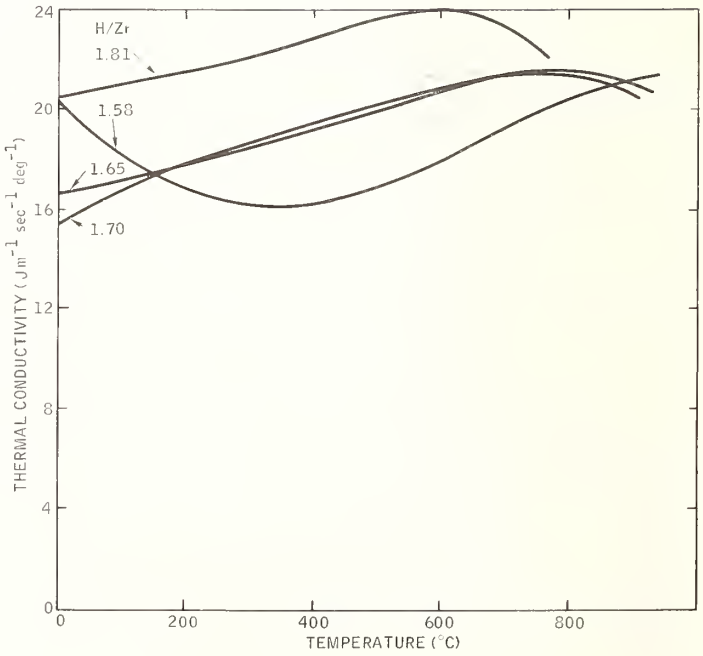

Figure 8. Thermal conductivity of H/Zr fuel.

Thermal Conductivity, Diffusivity, and Specific Heat of Calcium Tungstate from 77° to 300°K

Philipp H. Klein

Materials Branch
NASA Electronics Research Center
Cambridge, Mass. 02139

Thermal conductivity and diffusivity have been measured by a simultaneous method on a single crystal of calcium tungstate containing approximately 0.5 mole per cent of neodymium. These data were used for calculation of c_p throughout the temperature range 80-300°K. Thermal conductivity was found to obey the relationship $\lambda = 822/T$ from 80° to 180°, and remains nearly constant at 4.4 $W\,m^{-1}\,deg^{-1}$ from 180° to 300°. Thermal diffusivity decreases smoothly from 17 X $10^{-6}m^2/s$ at 80° to 2.5 X $10^{-6}m^2/s$ at 200° and 1.4 X $10^{-6}m^2/s$ at 300°. The Debye temperature, estimated from specific heat values below 200°, is approximately 570°K. At 300°K c_p is about 15% greater than c_v, which is consistent with the known large coefficient of thermal expansion of calcium tungstate.

Key Words: Calcium tungstate, conductivity, Debye temperature, diffusivity, heat conductivity, laser material, neodymium, specific heat capacity, thermal conductivity, thermal diffusivity, thermal properties.

1. Introduction

Phase changes and other optical distortions which result from transient thermal phenomena in lasers have been discussed in a number of experimental and analytical studies [1-5][1]. For rigorous treatment of the experimental data, and for predictive use of the analytical results, it is necessary that a detailed temperature distribution within the laser rod be available. Once the thermal diffusivity, a, is known, this distribution can readily be determined, using standard techniques of heat-flow analysis.

Unfortunately, thermal diffusivity has been measured for only a few laser materials. Computation of a ($a = \lambda/c_p d$, where λ is the thermal conductivity, c_p is the specific heat, and d is the density) is also frequently impossible because some of the necessary data are also not available. Computation also involves a risk of error, since measurements of λ, c_p, d have most often been performed on different samples and under differing conditions.

We present here the results of simultaneous measurements of the thermal conductivity and diffusivity of a specimen of neodymium-doped calcium tungstate. From these data, we have calculated the specific heat capacity in the range from 80°K to 300°K, and estimated the Debye temperature. It is hoped that publication of these results will make easier the prediction and analysis of transient phenomena in lasers made from this material.

2. Experimental

2.1 Method and Apparatus

Details of the experimental method have been published [6] and are only summarized here. The apparatus was of the type used for conventional steady-heat-flow measurements of thermal conductivity. A rod-shaped specimen was mounted vertically atop a steel plaque, which was firmly secured to a heavy copper heat sink. A fine-wire heater was wound directly on the sample at its upper end, and two 80-μm

[1] Figures in brackets indicate the leterature references at the end of this paper.

(0.002") copper-constantan thermocouples were cemented along its length. A third thermocouple junction was placed directly within the heat sink, and temperature differences were read with a potentiometer between three different pairs of couples. The absolute heat-sink temperature was determined separately, using a platinum resistance-thermometer.

Radiation errors were kept to a minimum by surrounding the sample with two concentric radiation shields, the inner one of which was mounted directly on the heat sink. The outer shield served also to suspend the heat sink from the top of the calorimeter can, in which the pressure was kept below 0.1 torr. As an additional precaution, power to the sample heater was adjusted to maintain the temperature difference along the specimen at less than one per cent of the absolute temperature of the heat sink.

The steady-state difference in temperature between the points of attachment of the sample thermocouples was determined with constant input to the sample heater. This value was used for calculation of the thermal conductivity. Power was then removed from the heater, and the time required for the temperature difference along the sample to decay to one-half its steady-state value was noted for computation of the thermal diffusivity.[2] For recording the decay of temperature, the output of the thermocouples was amplified and applied to the vertical axis of a strip-chart recorder. Typical half-decay times were about 20 s at 80°K and about 95 s at 300°K. Chart speeds were selected so that the half-decay time represented a deflection of at least 20-25 cm along the time axis.

2.2. Sample

The experimental sample was cut from a single crystal of calcium tungstate, grown by the Czochralski technique from a melt containing 0.5 mole percent each of neodymium and sodium (one atom of each for every 200 calcium atoms). Sylvania Crystal Grade calcium and sodium tungstates were used in preparing the melt, with neodymium oxide and tungstic oxide of purities exceeding 99.99% added in stoichiometric quantities. The crystal was pulled at a rate of approximately 1 cm/h from an iridium crucible in 1 atm of oxygen, then annealed for 24 h at 1200°C in air.

Following annealing, the crystal was oriented by X-ray methods and the sample was cut with its length parallel to the c axis. Final dimensions of the rectangular bar were 2.34 X 2.92 X 23.30 mm.

3. Results and Discussion

3.1. Thermal Conductivity

Figure 1 is a logarithmic plot of the thermal conductivity as a function of temperature. The data are nearly identical to those of Holland [7] for a similar sample.

In the region below 180°K, the equation $\lambda = 822/T$ fits the data quite well. The 1/T dependence of λ in this region indicates that scattering by impurities is the dominant mechanism for scattering of phonons. This is consistent with the fact that our sample contained about 6×10^{25} m^{-3} (6×10^{19} cm^{-3}) neodymium ions and an approximately equal number of sodium ions.

Above 180°K, λ remains almost constant up to 300°K. Ordinarily, the slopes of (log λ)-vs-(log T) curves become more negative at temperatures above the impurity-scattering region. This results from phonon-phonon scattering (Umklapp processes), which yield a dependence of λ proportional to $\exp(\theta_D/\alpha T)$, where θ_D is the Debye temperature and α is a constant. However, the five data points between 180° and 300° in figure 1 represent a total of seven determinations of λ, all within the range 4.26-4.74 $W m^{-1}$ deg^{-1}. There is good evidence that this apparent constancy is real, and not due to experimental error, as we explain below.

Both Holland's [7] and our samples, although prepared and measured entirely independently, showed little change in thermal conductivity between 200°K and 300°K. This fact might be ascribable to increased thermal radiation near room temperature. Our two data points at 297° actually represent results of three determinations, in which the power input to the sample heater was varied by a factor of eight. Despite this, all three measurements yield λ values between 4.42 and 4.45 W m^{-1} deg-1. If radiation from the heated sample had a significant influence at this temperature, greater divergence of the data would be expected.

Accepting as real the invariance of λ in the range 200-300°K does not, however, explain the anomaly. That the phenomenon is a consequence of the presence of impurities is suggested by the single datum of Nassau and Broyer [8], who reported $\lambda = 3.3$ W m^{-1} deg^{-1} at 290°K for an undoped, c-axis-oriented specimen. If plotted in figure 3, this value would lie close to the line $\lambda = 822/T$.

---

[2] The computation involved solution of eqs (6) and (9) of reference [6], which are derived and explained therein.

One might be tempted to relate the apparent constancy of the thermal conductivity to some ordering of the impurity ions. For example, Slack [9] ascribed the temperature-invariant thermal behavior of magnetite to reradiation (scattering) of phonons absorbed in the process of ordering of the octahedral ions. This ordering is a consequence of the proximity of ferrous and ferric ions on neighboring sites, and of the easy exchange of electrons between them. Even if an analogous ordering process could be conceived in our case, it would be extremely unlikely to have an observable effect in our sample. Granting replacement of 1/200 of the calcium ions by neodymium ions, and replacement of another 1/200 by sodium ions, only 1% of the Ca^{++} sites would be affected. With a random distribution of impurities and four molecules of calcium tungstate per tetragonal unit cell, there results a mean distance of at least three lattice spacings between pairs of impurity ions. The distance is far greater than that over which ordering phenomena can be expected, particularly at temperatures as high as 300°K.

3.2. Thermal Diffusivity

Thermal diffusivity results are shown in figure 2, a conventional plot of log a as a function of log T. The uniformity of curvature is notable, in marked contrast with the situation in figure 1. This is a significant point, for it is added evidence for the absence of radiation-induced errors. These results may be compared with estimates [6] of the thermal diffusivity of calcium tungstate containing 0.5 mole per cent neodymium. The estimated values, based on fragmentary and extrapolated data from the literature (and therefore representing, at best, measurements of different specimens) were $a = 20.7 \times 10^{-6}$ m^2/s at 80°K and $a = 1.53 \times 10^{-6}$ m^2/s at 300°K. The corresponding data from figure 2 are each about 10 per cent smaller: 18.0×10^{-6} m^2/s and 1.42×10^{-6} m^2/s, respectively.

3.3. Specific Heat

The data of figures 1 and 2 were used to compute the specific heat capacity at each temperature from the relationship $a = \lambda/c_p d$. No correction was made for the change of density with temperature, a constant value of 6.06×10^3 kg/m^3 (6.06 g/cm^3) [8] being used throughout. The error so introduced is estimated to be of the order of one per cent. Results are shown in figure 3.

Two other room-temperature values of c_p are indicated on figure 3. That shown as a solid square is due to Kopp [10], and was determined more than a century ago. The sample was probably a mineral specimen of scheelite. Kopp found c_p to be invariant from 292°K to 322°K.

The solid circle represents more recent work [11] on a (presumably undoped) sample of high-purity calcium tungstate. Although this point lies remarkably close to the curve calculated from the Debye temperature (see section 3.4), it is impossible to compare its accuracy with that of our data, since no experimental details are given. It is unlikely, however, that our deliberate addition of a total of approximately one mole per cent of impurities is entirely responsible for the difference of 15 per cent between our room-temperature value and this one.

3.4. Debye Temperature

The right-hand ordinate of figure 3 shows the mean heat capacity per gram-atom. This scale was obtained by dividing the molar heat capacity (C_p) by 6, the number of atoms in a molecule of calcium tungstate. Its use in estimating the Debye temperature, θ_D, is described below.

Heat-capacity values read from the righthand ordinate were compared with a graph showing θ_D/T as a function of C_V for a solid conforming to the Debye specific-heat approximation[3]. A value of θ_D/T was read from this curve, and θ_D was obtained by multiplication by the temperature of measurement. A "best" θ_D was then found by trial and error, the criterion being the degree of congruency of the experimental curve and the C_V-vs-T curve of a solid with a Debye temperature of θ_D. The broken curve of figure 3 is a graph of the molar specific heat (at constant volume) of a monatomic solid which obeys the Debye approximation and which has $\theta_D = 570$°K. This curve is seen to be a reasonable fit of the data at all temperatures up to about 190°K ($\theta_D/T = 3$). The divergence of the experimental (C_p) curve from the estimated (C_V) curve above this temperature is to be expected, in view of the approximations made in the estimate. In addition, the relatively large coefficients of thermal expansion (7.9×10^{-6} deg^{-1} in the a direction and 12.7×10^{-6} deg^{-1} in the c direction throughout the temperature range of figure 3 [8] suggest a perceptible difference between C_p and C_V at the higher temperatures.

[3] For this purpose, C_V and C_p were assumed to be equal. The validity of this assumption improves at the lower temperatures.

4. Summary and Conclusions

1. The thermal conductivity of neodymium-doped calcium tungstate, as determined in this study, has been found to agree well with previous measurements [7], although its apparent invariance between 200°K and 300°K remains unexplained.

2. Results for thermal diffusivity, obtained simultaneously with the thermal conductivity, represent the first actual measurements of the property for this material. Published estimates [6], based on composites of data obtained with different samples, are consistently about 10% higher than the measured values.

3. The specific heat capacity at room temperature was found to be about 15% higher than observed by previous authors [11]. At temperatures below 190°K, the heat capacity corresponds to a Debye temperature of 570°K.

4. All results cover the temperature range within which laser oscillators and amplifiers are commonly studied, and are sufficiently accurate to permit refined analyses and predictions [5] of the transient behavior of laser rods made from this material.

5. Acknowledgements

We wish to express our gratitude to Dr. J. D. Childress and Dr. D. H. Ridgley for beneficial discussions, and to Richard Andersson and Donald F. Ellingwood for assistance with portions of the experimental work.

6. References

[1] Cabezas, A. Y., Komai, L. G., and Treat, R. P., Dynamic measurements of phase shifts in laser amplifiers, Appl. Opt. 5, 647 (1966).

[2] Sims, S. D., Stein, A., and Roth, C., Dynamic optical path distortions in laser rods, Appl. Opt. 5., 621 (1966).

[3] Welling, H. and Bickart, C. J., Spatial and temporal variation of the optical path length in flash-pumped laser rods, J. Opt. Sci. Am. 56, 611 (1966).

[4] Blume, A. E. and Tittel, K. F., Thermal effects in laser amplifiers and oscillators, Appl. Opt. 3, 527 (1964).

[5] Quelle, F. W., Jr., Thermal distortion of diffraction-limited optical elements, Appl. Opt. 5, 633 (1966).

[6] Klein, P. H., Thermal conductivity, thermal diffusivity, and specific heat of solids from a single experiment, with application to $Y_{1.98}Nd_{0.02}O_3$, J. Appl. Phys. 38, 1598 (1967).

[7] Holland, M. G., Thermal conductivity of several optical maser materials, J. Appl. Phys. 33, 2910 (1962).

[8] Slack, G. A., Thermal conductivity of MgO, Al_2O_3, $MgAl_2O_4$, and Fe_3O_4 crystals from 3° to 300°K, Phys. Rev. 126, 3427 (1962).

[9] Nassau, K. and Broyer, A. M., Calcium tungstate: Czochralski growth, perfection, and substitution, J. Appl. Phys. 33, 3064 (1962).

[10] Kopp, H., Investigations of the specific heat of solid bodies, Phil. Trans. Roy. Soc. (London) 155, 71 (1965).

[11] Flournoy, P. A. and Brixner, L. H., Laser characteristics of niobium compensated $CaMoO_4$, J. Electrochem. Soc. 112, 779 (1965).

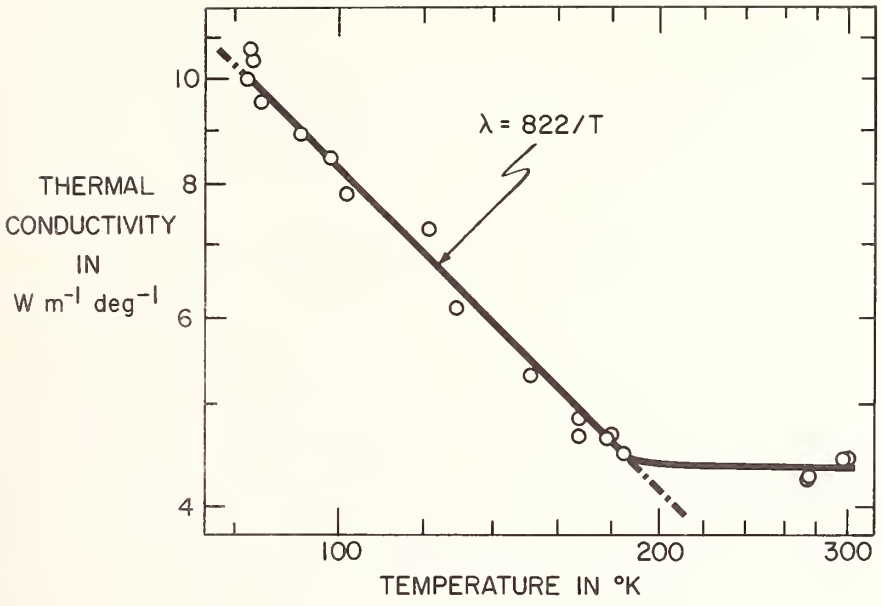

Figure 1. Thermal conductivity of a single crystal of $CaWO_4$: 0.5% Nd^{+3}, measured parallel to the c axis

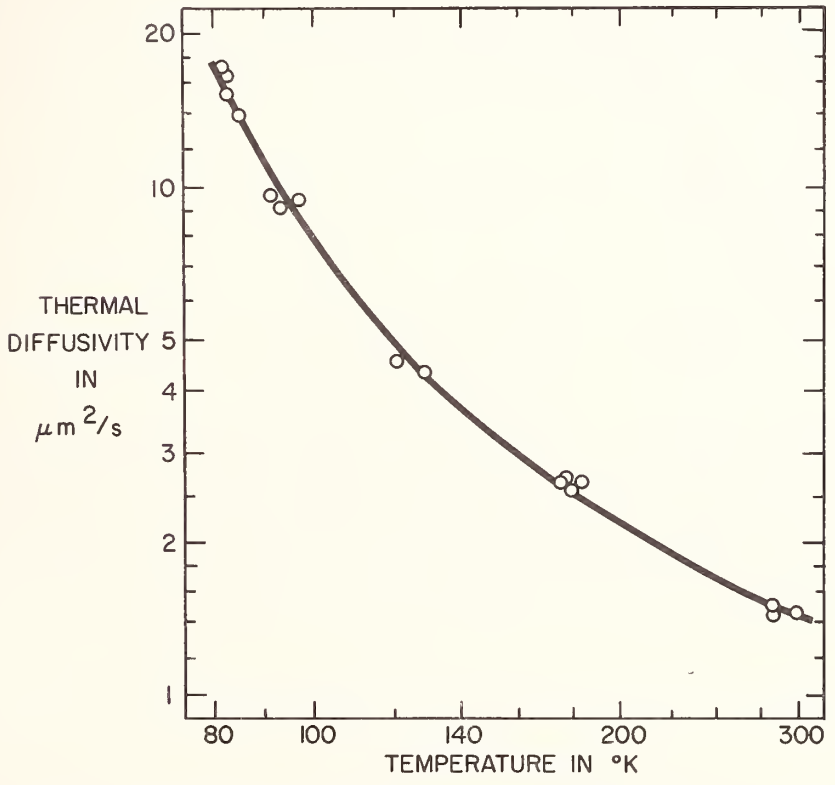

Figure 2. Thermal diffusivity of a single crystal of $CaWO_4$: 0.5% Nd^{+3}.

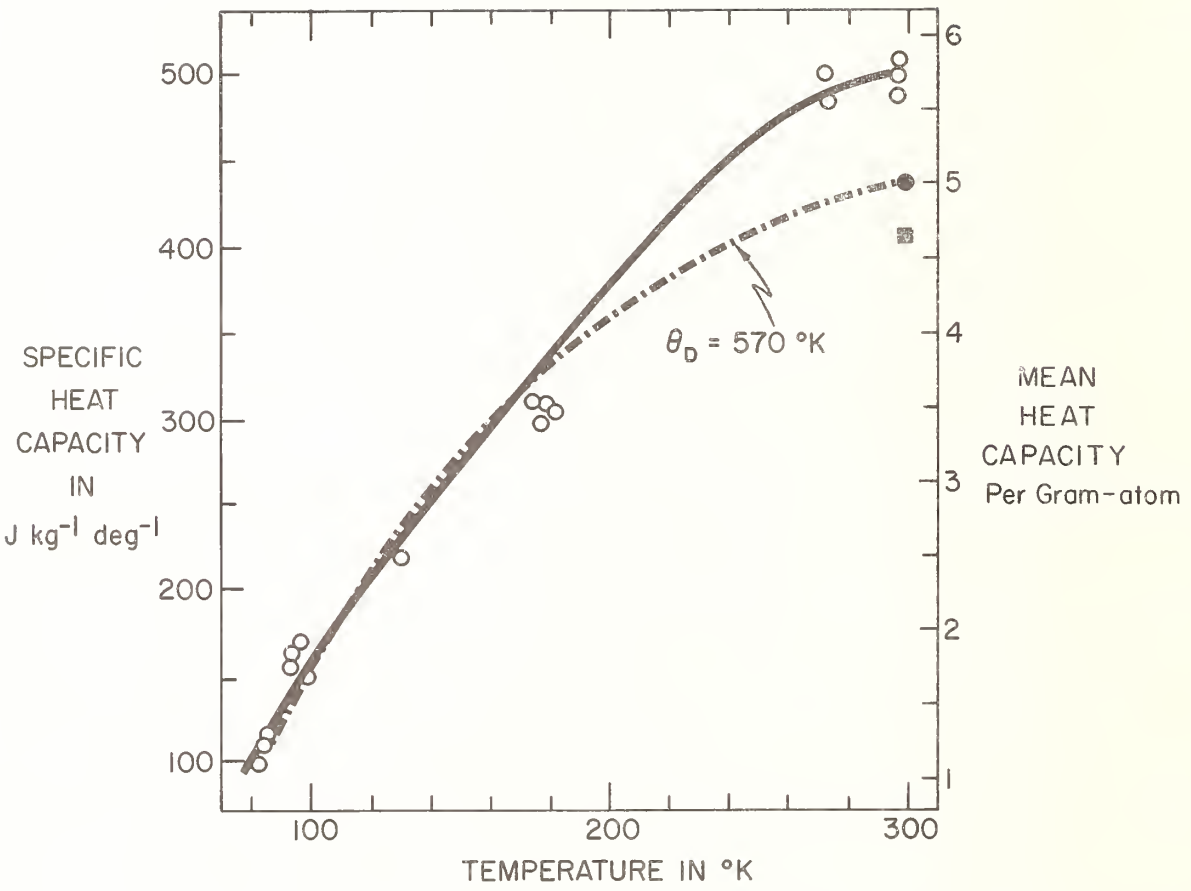

Figure 3. Specific heat capacity, c_p, (lefthand ordinate) and mean heat capacity per gram-atom (= 1/6 molar heat capacity) (righthand ordinate) computed from figures 2 and 3. The solid curve is a fit of the experimental data, which the broken curve is the molar heat capacity, C_v, of a monatomic solid with Θ_D = 570°K. Solid circle: datum from reference 11; solid square: datum from reference 12.

Measurement of the Thermal Conductivity of Self-Supporting Thin Films of Aluminum Oxide and Evaporated Films of Silicon Monoxide[1]

G. A. Shifrin and Robert W. Gammon[2]

Hughes Research Laboratories
Malibu, California 90265

A technique has been developed for measuring the thermal conductivity of self-supporting dielectric thin films for directions in the plane of the film. Two evaporated metal film bolometers on the sample are used both to supply the heat conducted across the narrow gap between them and to measure the temperature difference across the gap. We have applied the technique to anodic aluminum oxide films. The thermal conductivity has been found to be $1.68 \pm .07$ W m^{-1} deg^{-1} (16.8 mW cm^{-1} deg^{-1}) at 37°C for films 325 to 1500 Å thick with no detectable thickness dependence. For comparison bulk polycrystalline aluminum oxide of the same density as the films shows a thermal conductivity of 30.2 W m^{-1} deg^{-1} The lower value of conductivity is believed to be due to amorphous structure in the anodic films. The ± 4% uncertainty given on the value of conductivity represents mainly the geometrical uncertainties of the measurement. The precision on any one sample was much better (± 0.3%). By an extension of the method we have also measured the thermal conductivity of films evaporated onto previously calibrated self-supporting films. To perform this measurement it is necessary to observe the additional conductance due to the evaporated film and to establish its thickness independently. This type of measurement is potentially applicable for studying the thermal conductivity of a great variety of evaporated thin films. We measured the thermal conductivity of evaporated silicon monoxide films to be 0.3 ± 0.1 W m^{-1} deg^{-1} (3 mW cm^{-1} deg^{-1}) for thicknesses from 340 to 560 Å. Since the measurement accuracy was ± 10%, the indicated 33% uncertainty is believed to represent a spread in conductivity values.

Key Words: Aluminum oxide, silicon monoxide, thermal conductivity, thin films.

---

[1] A full report of the experiment and the results will be submitted to the Journal of Applied Physics.

[2] Present address: The Catholic University of America, Washington, D. C. 20017.

Impulse Thermal Breakdown in Silicon Oxide Films[1]

N. Klein and E. Burstein[2]

Dept. of Electrical Engineering
Technion, Israel Institute of Technology
Haifa, Israel

Silicon oxide capacitors with aluminum electrodes were deposited on glass substrates by evaporation in vacuum. The dielectric was about 5000 Å thick and weak spots were eliminated by self-healing breakdowns. On application of voltage pulses, the breakdown voltage was found to increase with pulse duration decreasing from 100 to 10^{-3} s. It was assumed that the breakdown was thermal and caused by Joule heat in the dielectric. The breakdown voltage was calculated by solving the nonlinear equation of conduction of heat with the aid of a digital computer and by approximate analysis. The two solutions agreed with each other and with the experimental results. In principle the thermal conductivity of the substrate can be calculated with the measured breakdown voltages.

Key Words: Electrical breakdown, thermal breakdown, silicon oxide, thermal conductivity, equation of conduction of heat.

1. Introduction

Although the physical process of thermal breakdown in dielectrics has been understood for a long time, difficulties have been encountered in the calculation and observation of thermal breakdown fields, especially when the effect of voltage pulses was considered.

Copple, Hartree, Porter and Tyson[1][3] investigated thermal breakdown of thick dielectrics, which have the form of an infinite slab. They made the simplifying assumption that the electric field is uniform in the dielectric and obtained the thermal breakdown field, F_{pm}, as a function of pulse duration by numerical methods.

Vermeer[2] and O'Dwyer[3] derived relations for F_{pm}, disregarding the effect of heat conduction during the pulse. Hanscomb's[4] observations of thermal breakdown in sodium chloride at 350°C ambient temperature support the validity of O'Dwyer's relation, when the pulses are short, but not when they are of long duration. Vermeer's experimental results of F_{pm} in glass are 10-20% larger than calculated. The discrepancies of calculations and experiment are in both cases ascribed to the influence of heat conduction.

The present work is concerned with impulse thermal breakdown in thin film capacitors of silicon oxide. The temperature of the dielectric of these capacitors is uniform and this circumstance simplifies the analytical treatment considerably relative to the case of thick dielectrics. Account is taken of the effect of conduction of heat and F_{pm} is calculated with the aid of a digital computer and also by approximate analysis. Results of the two methods agree very well, also with the experimental observations for pulses shorter than 0.1 s, for pulses of a few seconds duration the differences of calculated and experimental values is less than 3.5%. It is believed that the relations derived here for F_{pm} are applicable for thicker dielectrics also, when the internal thermal resistance of the dielectric is less than one tenth of the external thermal resistance. The observations of breakdown field as a function of pulse duration make possible in principle the determination of the thermal conductivity of the capacitor substrate.

---

[1]The work reported herein was performed under the sponsorship of the National Bureau of Standards.

[2]The work reported herein forms part of the M.Sc. Thesis of E. Burstein, submitted to the Senate of the Technion in July, 1967.

[3]Figures in brackets indicate the literature references at the end of this paper.

2. The Breakdown Experiments

The capacitors were produced by vapor deposition at 10^{-6} to 10^{-5} Torr pressure on 0.1 cm thick soda glass substrates. The thickness of the silicon oxide dielectric was 3000 to 6000 Å and that of the aluminum electrodes 500 Å. Breakdowns were self-healing and nonshorting, producing a hole through the three layers of the capacitor. The self-healing property of the capacitor made possible hundreds of breakdown experiments on a single sample. Figure 1 shows a sketch of the tested capacitors. Their area was 4×10^{-3} cm^2, where the dielectric was thinnest. The dielectric was reinforced at the capacitor edges adjacent to the electrode contacts, preventing preferential breakdown at these edges.

Prior to the pulse tests the weak spots in the capacitor were eliminated by single hole breakdowns, by applying increasing dc voltages to the capacitor.[5] The remaining capacitor area was quasi-uniform and its electrical conductivity, σ could be fitted well to a relation simple for analysis,

$$\sigma = \sigma_o e^{gV} e^{a(T-T_o)} \tag{1}$$

Here σ_o, a and g are constants, V is the voltage and T and T_o are temperatures of the dielectric and of ambient respectively. The maximum voltage for thermal breakdown, V_{dm}, was observed in the capacitors and this voltage could be calculated to an accuracy better than 1% with the relation derived by Klein and Gafni[5]

$$V_{dm} = \frac{1}{g} \log \frac{\Gamma h}{ea\sigma_o A V_{dm}^2} \tag{2}$$

Here h and A are the dielectric thickness and are respectively, Γ is the thermal conductance of the capacitor and e the natural logarithm base.

The pulse experiments were carried out with step voltages $V_{pm} > V_{dm}$. The pulse rise-time was shorter by at least three orders of magnitude than the time to breakdown τ and the voltage V_{pm} was constant during the pulse to better than 0.1%. On application of a pulse the leakage current i through the dielectric increased first slowly with time t, followed by a very fast increase. This is shown in Fig. 2 by oscillograms obtained on one capacitor for pulse voltages of increasing magnitudes. When the current increased after time τ to a very large magnitude, the capacitor broke down approximately over the whole area by evaporation. This descruction was prevented by diverting the current from the capacitor with a controlled rectifier at a time τ', when the current became 5 to 8 times larger than at t = 0. The time τ' is only a few percent smaller than τ, and τ' is quoted as the measured time to breakdown. The effect of this difference on V_{pm} is negligible because it will be seen that $V_{pm} \propto -\log \tau^{\frac{1}{2}}$. As destructive breakdowns were avoided, a large number of experiments were carried out on a single sample and V_{pm} as a function of pulse duration could be ascertained in the whole range of interest. This is shown for a typical capacitor for the range 0.01 s to nearly 10 s in Fig. 3, where measured values are represented by dots.

The breakdown voltage increases to a maximum for a pulse duration of about 10^{-3}s. The breakdown mechanism radically changes at this voltage, becoming electrical in nature. These breakdowns are not of interest for the present treatment and will be discussed elsewhere.

3. Calculation of the Thermal Breakdown Voltage

The breakdown of the silicon oxide capacitors on dc was found to be thermal. Thus, the nature of the current increase shown in Fig. 2 and the increase of V_{pm} with decreasing τ indicate that the breakdown is thermal for pulses of duration longer than a certain minimum value. This assumption was investigated quantitatively.

The source of heat in the dielectric is Joule heat in the pulse experiments and the power P per unit area of capacitor is, using eq (1)

$$P = \sigma_o V^2 e^{gV} e^{a(T-T_o)}/h = P_o \cdot e^{a(T-T_o)} \tag{3}$$

As the capacitor thickness is three orders of magnitude smaller than its lateral dimensions and the substrate thickness, the capacitor is idealized by the following model: The effect of the capacitor is represented by an infinite plane heat source of power P, situated on an infinite substrate bounded by two parallel planes. Heat is conducted through the substrate only, and the substrate surface opposite the capacitor surface is a ambient temperature. The capacitor temperature is assumed to be uniform. To obtain the times $t = \tau$ as function of applied voltage V_{pm}, when the capacitor temperature

$T \to \infty$ and breakdown arises, the equation of conduction of heat is solved with the appropriate boundary and initial conditions. The coordinates perpendicular to the substrate surfaces is denoted by x and x = H at the capacitor and x = 0 at the opposite surface. The temperature is denoted by T_s

$$\frac{\partial T_s}{\partial t} = k \frac{\partial^2 T_s}{\partial x^2} \quad \text{and} \tag{4}$$

$$K \frac{\partial T_s}{\partial x}\bigg|_{x=H} = P_o e^{a(T-T_o)} \tag{5}$$

with $T_s = T_o$ for $t \leq 0$ and $T_s = T_o$ at x = 0.k is the thermal diffusivity and K the thermal conductivity of the substrate. k is replaced by K /c, c being the specific heat per unit volume of substrate. Normalizing with $\overline{(T_s-T_o)} = a(T_s - T_o)$, $\bar{\tau} = Kt/cH^2$ and $\bar{x} = x/H$, eq (4) and (5) are replaced by

$$\frac{\partial \bar{T}_s}{\partial \bar{t}} = \frac{\partial^2 \bar{T}_s}{\partial \bar{x}^2} \text{ and } \frac{\partial \bar{T}_s}{\partial \bar{x}}\bigg|_{\bar{x}=0} = Be^{\overline{(T-T_o)}} \tag{4a) and (5a}$$

with $\overline{T_s-T_o} = 0$ for $\bar{t} \leq 0$ and for $\bar{x} = 0$; here

$$B = \frac{Ha\sigma_o V_{pm}^2 e^{gV_{pm}}}{hK} \tag{6}$$

The analytical solution of this nonlinear problem of heat conduction does not seem to be known and solution was obtained with the aid of a digital computer. The relevant result, when $\overline{T-T_o} \to \infty$ in the composite is shown in Fig. 4, where B, a function of the breakdown voltage V_{pm}, is plotted against the normalized time to breakdown $K\tau/cH^2$. It should be remarked that the computer handled the problem only for a maximum value of 10 in $\overline{T-T_o}$. The B values in Fig. 4 are therefore consistently smaller than for $\overline{T-T_o} \to \infty$. The difference should be less than 1%.

The pulse breakdown voltage V_{pm} can now be calculated with eq. (6),

$$V_{pm} = \frac{1}{g} \log \frac{hKB(K\tau/cH^2)}{a\sigma_o HV_{pm}^2} \tag{7}$$

with $B = B(K\tau/cH^2)$ obtained from Fig. 3. Equation (7) can be connected with the relation for the dc maximum thermal breakdown voltage V_{dm}, eq (2). For the capacitor model discussed $\Gamma = KA/h$ and

$$V_{pm} = \frac{1}{g} \log \frac{hK}{ea\sigma_o HV_{dm}^2} \tag{2a}$$

hence

$$V_{pm} = V_{dm} + \frac{1}{g} \log[eB(K\tau/cH^2)] - \frac{2}{g} \log(V_{pm}/V_{dm}) \tag{7a}$$

The oscillograms of Fig. 2 show that the leakage current and the power input change relatively little before the current runaway. This property of the formation of the breakdown process leads one to attempt an approximate solution of the heat conduction equation for the case of breakdown, described in the following lines.

A mentioned, the temperature of the thin capacitor is assumed to have a uniform value T. The equation for the capacitor heat balance can then be written simply for unit capacitor area as

$$P\,dt = chdT + K' \frac{dT_s}{dx}\bigg|_{x=H-h} \tag{8}$$

The thermal conductivity and diffusivity are denoted by K' and k' for reasons that will be apparent later. The capacitor top and bottom surfaces are at x = H and x = H - h respectively. The influence of electrodes is disregarded in eq (8), because their thermal resistance is negligible and their heat capacitance is much smaller than that of the dielectric. For c the specific heat of the substrate is taken and this assumption is justified by later results.

An approximate expression is obtained for the conduction term $K' \left.\frac{dT_s}{dx}\right|_{x=H-h}$ by making use of the solution of the heat conduction problem discussed here, when the power is not an exponential function of T, as in eq (3), but constant, $P=P_o$. This solution is denoted by $P_o\varphi(x,t)$ and the assumption is made for the conduction term in eq (8) that

$$K' \left.\frac{dT_s}{dx}\right|_{x=H-h} = K'P_o e^{a(T-T_o)} \left.\frac{\partial\varphi(x,t)}{\partial x}\right|_{x=H-h} \tag{9}$$

As shown in Carslaw and Jaeger[6]

$$P_o\varphi(x,t) = T_s - T_o = \frac{P_o x}{K'} \sum \frac{(1)^n e^{-\frac{k'(2n+1)^2\pi^2 t}{4H^2}} \sin\frac{(2n+1)\pi x}{2H}}{(2n+1)^2} \tag{10}$$

Substituting for $\varphi(x,t)$ in eq (9) and for the derivative in eq (8) and integrating from t = 0 to t and $T = T_o$ to T,

$$\frac{16H^2}{\pi^3 k'h^2}\sigma_o e^{gV}\cdot V^2 \sum_{n=0}^{\infty} \frac{(-1)^n}{(2n+1)^3}\left[e^{-k'(2n+1)^2\pi^2 t/4H^2}\right]\cos\frac{(2n+1)\pi(H-h)}{2H} = \frac{c}{a}\left[e^{-a(T-T_o)} - 1\right] \tag{11}$$

Breakdown arises at the voltage $V = V_{pm}$, when at time $t = \tau$, $T - T_o \to \infty$ and the relation obtained from eq (11) for V_{pm} is

$$V_{pm} = \frac{1}{g}\log\frac{ck'\pi^3 h^2}{16aH^2\sigma_o V_{pm}^2 X(\tau)}$$

with

$$X(\tau) = \sum_{n=0}^{\infty} \frac{(-1)^n}{(2n+1)^3}\left[1 - e^{-k'(2n+1)^2\pi^2 t/4H^2}\right]\cos\frac{(2n+1)\pi(H-h)}{2H} \tag{12}$$

Since $H - h \ll H$, this is approximately

$$X(\tau) = \frac{\pi^3 h}{16H}\left[1 - \frac{8}{\pi^2}\sum_{n=0}^{\infty}\frac{e^{-k'(2n+1)^2\pi^2 t/4H^2}}{(2n+1)^2}\right] \tag{13}$$

with $ck' = K'$

$$V_{pm} = \frac{1}{g}\log\frac{hK'}{a\sigma_o HV_{pm}^2\Psi(\tau)} \tag{12a}$$

with

$$\Psi(K'\tau/cH^2) = 1 - \frac{8}{\pi^2}\sum_{n=0}^{\infty}\frac{e^{-k'(2n+1)^2\pi^2\tau/4H^2}}{(2n+1)^2}$$

Testing the validity of eq (12a) for the limiting case, when $\tau \to \infty$ $V_{pm} = V_{dm}$ and $\Psi(\tau) = 1$, the relation (12a) is found to differ from eq (2a) by the factor e in the denominator of the logarithmic expression. This discrepance can be avoided by replacing K/e for K'. Comparing eq (12a) with the earlier relation (7) for V_{pm} it appears that the condition for equality of results is

$$KB(K\tau/cH^2) = \frac{K'}{\Psi(K'\tau/cH^2)} \tag{14}$$

Replacing in eq (14) numerical values for B and for Ψ as function of the normalized pulse duration, equality of the two sides is found, within 1% accuracy, when

$$K' = K/e \tag{15}$$

The approximate relation for the pulse breakdown is thus

$$V_{pm} = \frac{1}{g} \log \frac{hK}{ea\sigma_o HV_{pm}^2 \Psi(K\tau/ecH)} \tag{12b}$$

with

$$\psi(K\tau/ecH) = 1 - \frac{8}{\pi^2} \sum_{n=0}^{\infty} \frac{e^{-k(2n+1)^2\pi^2\tau/4ecH^2}}{(2n+1)^2}$$

Equations (7) and (12b) were applied to calculate $V_{pm} = f(\tau)$ for the capacitor, the experimental breakdown results of which are presented in Fig. 3. The data of this capacitor and of the substrate were: h = 5000 A, g = p.054 V, c= 2.06 J/cm^3, °C, a = 0.03/°C, $\sigma_o = 1.3\times10^{-12}/\Omega$-cm and H = 0.1 cm. The value of the thermal conductivity was determined by fitting eq (7) to the experimental results for $\tau < 0.1$ s and K = 0.031 W/°C cm was obtained. The results of the calculations with both eq (7) and eq (12b) are represented in Fig. 3 by the curve.

When the approximate calculation of V_{pm} is carried out for the case that the substrate is a semi-infinite solid, the relation for V_{pm} is

$$V_{pm} = \frac{1}{g} \log \frac{h(\pi cK/e)^{\frac{1}{2}}}{2a\sigma_o \tau^{\frac{1}{2}} V_{pm}^2} \tag{16}$$

Breakdown voltages calculated with eq (12b) and (16) agree for $\bar{\tau} < 0.1$.

4. Discussion

Comparison of experimental and calculated results show very good agreement for $\tau < 0.1$ s, and that V_{pm} is practically proportional to $\log 1/\tau^{\frac{1}{2}}$. On the other hand, the experimentally determined thermal conductivity 0.031 W deg^{-1} cm^{-1} is much larger than the highest values found in handbooks for soda glass, 0.012 W deg^{-1} cm^{-1}. The reason seems to be connected with the idealizations of the model. Brestechko[7] showed that heat from the capacitor is conducted not only through the substrate, but also by convection in the ambient air and by conduction through the electrodes to the contact pads (see Fig. 1). The convection accounts for about a 50% increase in thermal conductance. Rough calculations indicate that the difference between the true and the effective value of K is plausibly explained by the influence of the two additional paths of thermal conduction. It is interesting to note that while this influence increases conduction, it does not effect the form of the relations of $V_{pm} = f(\tau)$. It is believed that when the effects of convection and of thermal conduction by the electrodes can be eliminated, the thermal conductivity of the substrate can be determined with short time pulse breakdown measurements.

For pulse durations longer than 0.1 s, measured voltages become higher than calculated and the largest discrepancy is about 3.5% at τ = 2s. These discrepancies are due to further departures from the idealized model, which can effect the functional relationship also. One difference can be ascertained in the side view of Fig. 1: The lateral dimensions of the capacitor are smaller than the substrate thickness. When on pulses of longer duration heat flux penetrates deep into the substrate, the cross section for the flux does not remain constant, as assumed by the model, but increases. This is equivalent to an increase in thermal conductance and in V_{pm}. An opposing effect arises at the bottom surface of the substrate. Measurements shown that the temperature there is not T_o as assumed, but slightly larger, and this decreases the thermal conductance and V_{pm}. The results in Fig. 3 indicate that the first effect is larger than the second one.

It appears that the differences between the idealized model and the test capacitor effect little the validity of the derived relations, and the measure of agreement of observed and calculated breakdown voltages indicate that the breakdowns are thermal.

8. References

[1] Copple, C., Hartree, D. R., Porter, A., and Tyson, H., The evaluation of transient temperature distributions in a dielectric in an alternating field, J. IEE, London, 85, 56, (1939).

[2] Vermeer, J., On the relation between ionic conductivity and breakdown strength of glass, Physica, 22, 1269 (1956).

[3] O'Dwyer, J. J., High temperature dielectric breakdown of alkali halides, Australian J. Phys. 13, 270 (1960).

[4] Hanscomb, J. R., High temperature electrical breakdown in sodium chloride, Australian J. Phys. 15, 504, (1962).

[5] Klein, N. and Gafni, H., The maximum dielectric strength of thin silicon oxide films, IEEE Trans. Electr. Dev. ED-13, 281 (1966).

[6] Carslaw, H. S. and Jaeger, J. C., Conduction of heat in solids, (book) 2nd ed., Ch. III, Oxford Univ. Press, London (1959).

[7] Brestechco, M., DC electrical breakdown in thin silicon oxide films in vacuum, M.Sc. thesis, Technion, Israel Inst. of Techn., (1967).

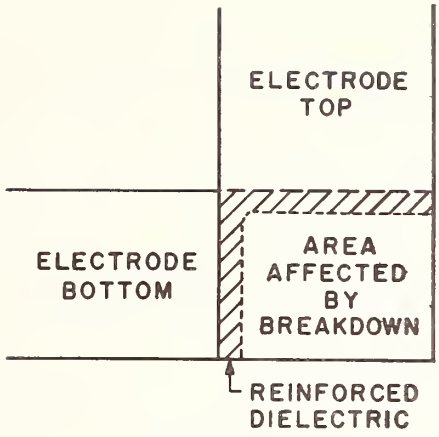

Fig. 1 Sketch of tested capacitor.

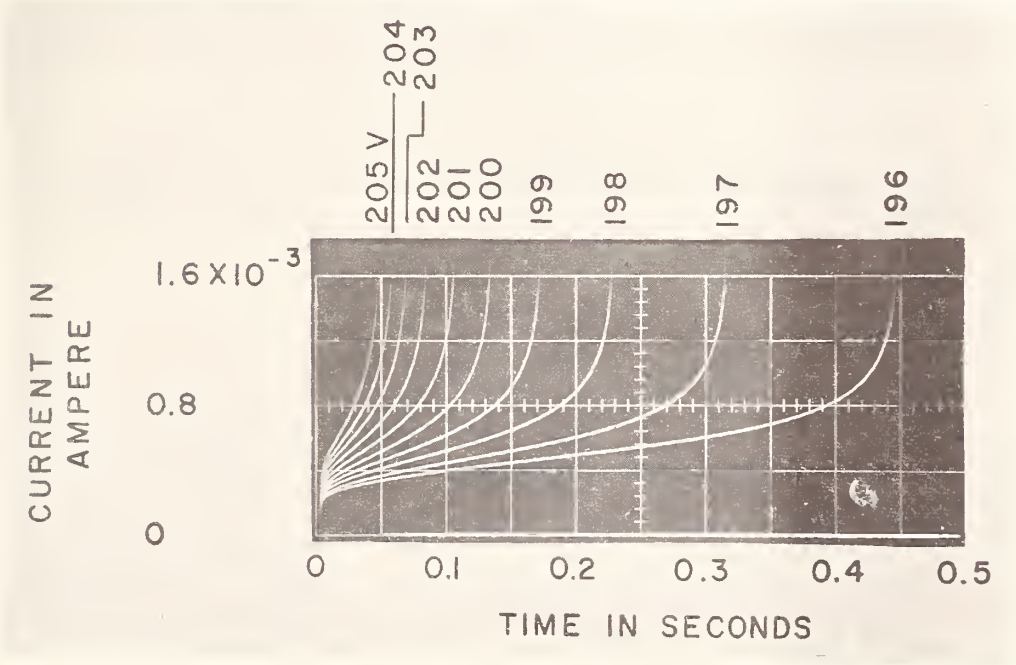

Fig. 2 Oscillogram of thermal breakdown event.

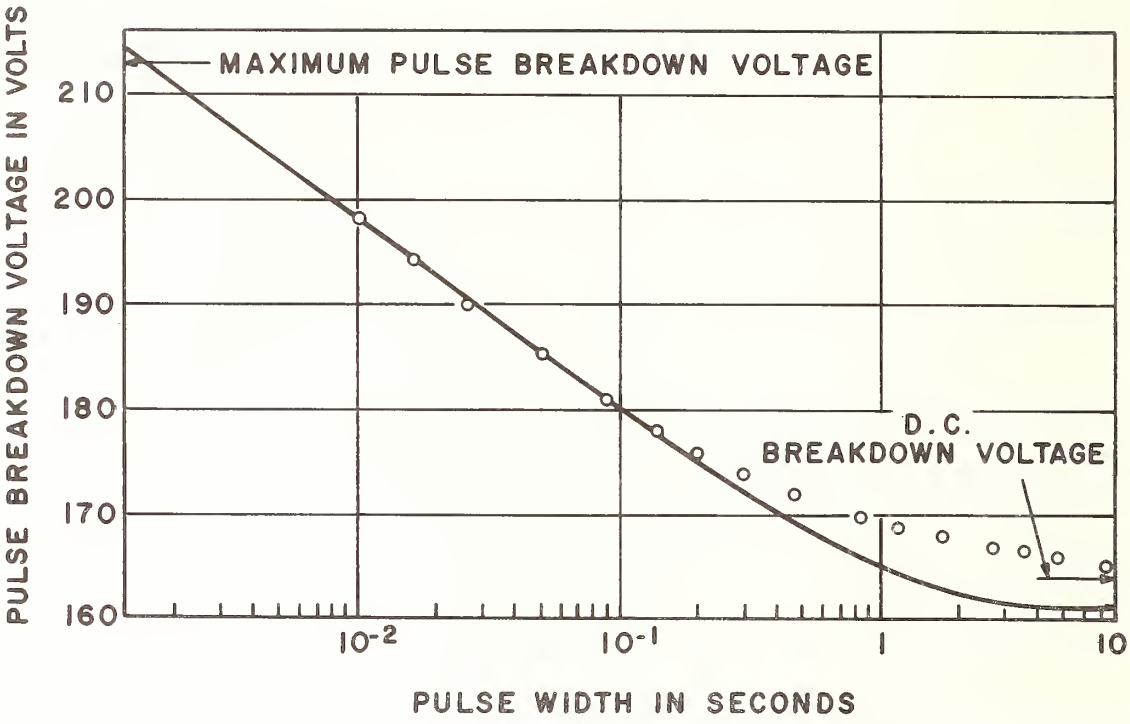

Fig. 3 Pulse breakdown voltage versus pulse duration. Dots measured values, curve calculated.

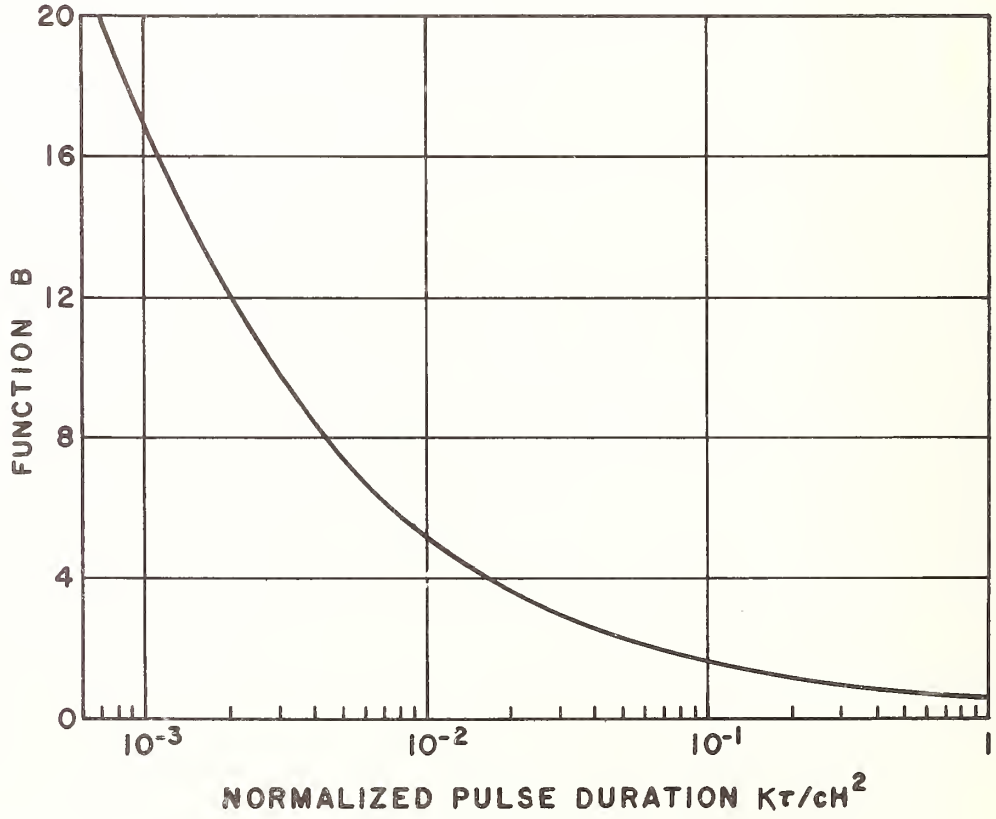

Fig. 4 B as function of normalized time.

High Temperature Radial Heat Flow Measurements

J. P. Brazel

General Electric Company
Re-Entry Systems Department
Philadelphia, Pa. 19101

K. H. Styhr

National Beryllia Corporation
Haskell, New Jersey 07420

Steady state thermal conductivity measurements on three molded graphite structures and one phenolic Refrasil Char composite are presented. Electrical resistivity data and structural characterization of the specimens are included for correlation with other literature values.

Measurements were made in flowing argon at mean specimen temperatures in the range 125°C to 2000°C. Thermal conductivity (λ) of ATJ grade graphite can be reduced almost 50% at 1000°C from about 6 to 3 mW/m°C by a "purification" process of leaching and outgassing. Reduction in λ is less at higher temperatures, about 30% at 1800°C from 2.6 to 1.8 mW/m°C. Specimen hot face temperatures exceeding 2200°C in most cases could not be reached due to the high thermal conductivity of selected specimens and a power supply limitation. A modified apparatus with a larger power supply and equipped for high vacuum as well as inert atmosphere operation is described.

Key words: Apparatus, conductivity, graphites, high temperature, radial heat flow, steady state, thermal conductivity.

1. Introduction

The original intention of presenting a paper at the Seventh Conference on Thermal Conductivity was to compare the thermal conductivity of selected, well-characterized commercial grade graphites as measured in a variety of atmospheres. Unfortunately, a problem developed in the electronic wattmeter of the apparatus equipped with the high vacuum system. Only data acquired in flowing argon were completed in time for the program. Since the basic apparatus has been described in previous conference proceedings (1,2,3)[1], only a brief outline of the equipment is included herein. This stresses the difference between the instruments used in the various atmospheres concerned and specific instrumentation problems arising from the sample materials studied. It is the authors' intention to report complete results and stress interpretation and analysis of the data in a subsequent paper.

[1] Figures in parentheses indicate the literature references at the end of this paper.

2. Specimen Geometry

The specimen stack is cylindrical, 12.7 cm (5") tall and 5 cm (2") in diameter. It contains a 1.9 cm (0.75") concentric axial cavity to accomodate the inner heater which supplies the radial outward temperature gradient. The stack may be composed of a number of thin discs (1.2 cm or greater) or preferably 1 to 3 larger cylinders. In this study all specimen stacks are composed of 3 cylinders, a 5 cm (2") tall specimen and two guard cylinders (upper and lower) of equal height sufficient to total 12.7 cm. A typical specimen, without upper and lower guards, is shown in Figure 1. Since the power dissipated in the 2.54 cm (1") central section of the 12.7 cm (5") tall assembly is separately metered, in addition to metering the total inner heater power, all sensing wells are located within the 2.54 cm central section.

Both radial and axial temperature sensing wells were used in this study. Axial wells have the disadvantage of a finite width in the direction of the temperature gradient; in the examples of Figure 1, 1.57 mm (0.063"). The precise radial location (isotherm) of the average temperature measured by a thermocouple or optical pyrometer is uncertain to some factor dependent upon the temperature gradient across the specific axial well considered. However, since conduction along thermocouple leads in a radial gradient can be significant, axial wells are used exclusively for thermocouple measurements, but only at lower temperatures (below 1500°C) and in situations where the gradient across the well is not large.

Radial sensing wells have the advantage of having a flat bottom plane essentially on an isothermal plane within the specimen. Although this isotherm can be precisely located (± 0.03 mm, 0.001"), temperature measurement by disappearing filament optical pyrometer or automatic optical pyrometer is inherently less precise (± 2°C and 0.5°C), than good thermocouple thermometry (0.01°C). Although it has been determined that black body optical temperature assumptions are valid in most non-isothermal cavities in materials of high emmittance (4), errors increase with decreasing emittance, decreasing L/D cavity ratios, and increasing thermal gradient in the radial cavity. These factors must be considered in each individual case. Thin opaque discs can be used to increase emittance in specimens which are unusually porous or translucent. All specimens in this study were of sufficiently high emittance and contained cavities of sufficiently high L/D ratio and small thermal gradient so that no corrections from these considerations were necessary.

3. Apparatus

The photograph of Figure 2 shows a typical specimen stack assembled on a zirconia pedestal. Although the newer, vacuum-equipped, apparatus is illustrated, specimen assembly, furnace geometry and console are identical to the argon apparatus used except as specifically mentioned here. Both radial sight holes and axial thermocouples are visible. This assembly is inserted into the furnace from underneath as shown in Figure 3. The entire high vacuum system, normally attached to the furnace by four wing bolts, has been lowered about 10 cm and pivoted out of the way to facilitate sample loading. The lower high current (600 amps) inner heater power terminal, consisting of a liquid metal contact assembly contained within the liquid nitrogen cold trap region, is clearly visible in the right foreground. Figure 4 illustrates how the oil diffusion pump system may be readily pivoted back and raised to accomplish the O-ring seal to the furnace. The seven position, self cleaning, radial sight window assembly, as well as a top axial sight window, is also visible in the photograph. Thermocouple wires leading from a multi-contact vacuum feed thru behind the furnace are lead up an external exhaust port behind the vacuum control box to a remote multi-point recorder.

Console controls for inner heater, outer heater, and fail-safe circuits have been previously described (2,3). In Figure 4, the center meter indicates power in watts dissipated from the middle 2.54 cm (1") region of a 13.3 cm (5 1/4") tungsten mesh inner heater. In the vacuum apparatus, a Hall multiplier circuit in a specially designed electronic wattmeter was added to decrease possible AC meter error from ±4% to ±0.5% and to compensate for the small (±1%) power factor correction uncertainty in a VA determination of gauge watts.

A schematic of the furnace interior is shown in Figure 5. It is only slightly different from the previously described arrangement (2). The carbon atmosphere from the samples of this study attacks the tantalum wire voltage probes. A thin (0.13 mm, 0.005") tantalum sheet placed at the I.D. of the specimen within the anti-contamination space serves as a "getter" to retard attack on the probes. Alternately, tungsten may be used for probe wire when the higher impedance electronic wattmeter or a digital voltmeter are employed since I^2R losses in the probe wire are then not significant.

4. Data and Analysis

The formula for calculating λ in a radial geometry has appeared in many papers and texts and is:

$$\lambda = \frac{q \ln \frac{r1}{r2}}{2 \pi l \Delta T}$$

when: q = power in watts, dissipated in the central gauge length
l = central gauge length in meters
ΔT = temperature gradient in ^{o}C between two radial isotherms
r_1, r_2 = radii of the two radial isotherms

then λ is the apparent thermal conductivity in $W/m^{o}C$ directly without need for comparative measurements.

For convenience, a geometric factor may be calculated for any pair of temperature sensing wells. The procedure is illustrated in Figure 1. The form of data accumulation is shown in Table 1 which lists one set of raw data for the As-Received ATJ graphite specimen No. 3. To conserve space, raw data is not presented for all specimens here but may be obtained from the authors. Similarly, calculations of λ from the raw data, using the geometric factors are presented in Table 2. It may be seen from these examples that several types of thermocouples (Chromel-Constantan and Platinum-Rhodium alloys) are used dependent upon the temperature difference to be measured, the temperature range of interest and the reactivity of the specimen or its vapors with the thermoelements. Typical ΔT's for various sensing wells are shown. It is also apparent that the product of "sense volts" (an AC meter reading of the 2.54 cm central gauge section) and total inner heater current was used to calculate gauge watts.

Curves of thermal conductivity vs. temperature in SI units for ATJ graphite both in the As-Received condition and "purified" state are presented in Figure 6. They indicated a marked reduction in thermal conductivity due to the "purification" process of leaching and degassing. Specimens were aligned with the "C" axis parallel to the inner heater. Therefore, the radial outward temperature gradient and measured conductivity is in the AB with-grain plane.

Measurements of electrical resistivity as a function of orientation were made on the lower guard section of each of the graphite samples. These are presented along with density measurements in Table 3. Measurements on the center specimen were not made since this requires cutting the specimen and more conductivity values in other atmospheres are desired. Note that the lower guard of the "purified" ATJ graphite #2 appears to have been cut incorrectly by 90^{o}. Thermal conductivity was to have been measured in the AB plane, and some uncertainty exists now as to whether the AB plane was the radial plane in the specimen. This may account for the converging conductivities at higher temperatures in the two ATJ graphites and will be confirmed by subsequent tests. The value of electrical resistivity measurements, even in the absence of a Wiedemann-Franz law for graphite, is evident.

Measurements were also made on a commercial POCO AXM grade "unpurified" graphite graphitized at a temperature of approximately $4000^{o}F$. Thermal conductivity is plotted as a function of temperature in Figure 7, and is similar both in magnitude and temperature dependence to "purified" ATJ graphite. Density and electrical resistivity data, listed in Table 3, are similar but not precisely in the range listed for the standard

TABLE 1 DATA RECORDED AT STEADY STATE CONDITIONS
As-Received ATJ Graphite

RUN CONDITION	CENTRAL HEATER		RECORDED DATA		THERMOCOUPLES		OUTER HEATER		OPTICAL TEMPERATURES		
			Sense Gauge								
	Volts	Amps	Volts	Watts	TC-1	TC-2	Volts	Amps	T1	T2	T3
R1-1	3.0	300	.290	87	887	883	--	--	--	--	--
R1-2	3.3	315	.330	104	957	952	--	--	--	--	--
R1-3	5.1	395	.610	243	1310	1296	--	--	--	--	--
R1-5	6.4	450	.770	347	--	--	9	80	1295	1280	1258
R1-6	6.9	450	.820	370	--	--	12	135	1788	1769	1753
R2-1	1.2	165	.090	14.9	303.37	302.47*--		--	--	--	--
R2-2	1.8	245	.160	39.2	525.69	524.44*--		--	--	--	--
R3-1	1.2	186	.090	16.7	380.61	380.11*--		--	--	--	--
R3-2	2.0	245	.180	44.1	662.33	660.66*--		--	--	--	--
R3-3	5.0	390	.620	234.0	--	--	--	--	1243	1225	--
R3-4	6.6	450	.790	355.0	--	--	8	100	1714	1670	--

* Thermocouples Chromal-Constantan
Traceable to NBS Calibration

TABLE 2 CALCULATIONS FOR AS-RECEIVED ATJ GRAPHITE

STEADY STATE CONDITION	GAUGE SECTION	MEAN TEMPERATURE	CONSTANT FACTOR	RECORDED DATA		THERMAL CONDUCTIVITY
		°C		Watts	ΔT	mW/m°C
R1-1	TC	885	0.0298	87.00	4	6.50
R1-2	TC	955	0.0298	104.00	5	6.20
R1-3	TC	1300	0.0298	243.00	14	5.17
R1-5	1-2	1668	0.0135	347.00	15	3.12
R1-6	1-2	1780	0.0135	370.00	19	2.63
R2-1	TC	303	0.0283	14.85	0.90	4.669
R2-2	TC	525	0.0283	39.20	1.25	8.875
R3-1	TC	380	0.0283	16.74	0.50	9.46
R3-2	TC	661	0.0283	44.10	1.67	7.50
R3-3	1-2	1241	0.0354	234.00	18	4.60
R3-4	1-2	1700	0.0354	355.00	44	2.79

in the AFML-ADL "Thermal Conductivity Standards Program" (5). This suggests specific specimens will have to be well characterized in order that meaningful, well correlated comparative measurements are possible.

A plot of with-lamina thermal conductivity versus temperature of a commercial phenolic impregnated phenolic Refrasil Char composite is shown in Figure 8. This is included to show that the ablative plastic impregnation causes more than an order of magnitude decrease in thermal conductivity (note the scale change). Moreover, the temperature dependence has changed radically. Top measurement temperature is limited by the temperature stability of the sample and its attack on both furnace components and thermocouples at higher temperatures.

5. Conclusions

The description of apparatus, techniques and specimens and the results of initial tests on selected graphite structures presented here summarizes the first part of a continuing program designed to define more closely the high temperature characteristics of graphite materials. Equipment is available which can determine changes in λ due to materials processing and which is sufficiently sensitive to differentiate between specimens of slightly different microstructure, composition or thermal history. The effects of these differences and of various atmospheres in the "pores" of porous graphite structures is being studied with the hope of presenting additional data at next year's conference.

Table 3. Specimen Characterization. Electrical Resistivity Measurements.

Graphite Material	(direction)	Resistivity (ohm-cm x 10^{-3})
Poco AXM #1	C	1.72
Poco AXM #1	AB	1.69
Purified ATJ #2	C	1.11
Purified ATJ #2	AB	1.83
Purified ATJ #2	AB (90°)	1.15
As Rec'd ATJ #3	C	1.93
As Rec'd ATJ #3	AB	1.12

Density Measurements

Material	Density (g/cc)	Density (lbs/ft^3)
POCO AXM #1	1.73	108.1
Purified ATJ #2	1.67	104.4
As Rec'd ATJ #3	1.72	107.5

8. References

(1) The third conference on Thermal Conductivity, hosted by Oak Ridge National Laboratory, Gatlinburg, Tenn. October 16-18, 1963, Page 428.

(2) The fifth conference on Thermal Conductivity, hosted by The University of Denver, Denver, Colorado, October 20-22, 1965, Page VI-J-1.

(3) The sixth conference on Thermal Conductivity, hosted by AFML, Dayton, Ohio. October 19-21, 1966, Page 405.

(4) E.M. Sparrow "Radiant Emission Characteristics of Nonisothermal Cylindrical Cavities" Applied Optics (4) 1 (1965) Page 41.

(5) A. E. Wechsler and M.L. Minges "Development of High Temperature Thermal Conductivity Standards" The Seventh Conference on Thermal Conductivity, hosted by the National Bureau of Standards, Washington, D.C., November 13-16, 1967.

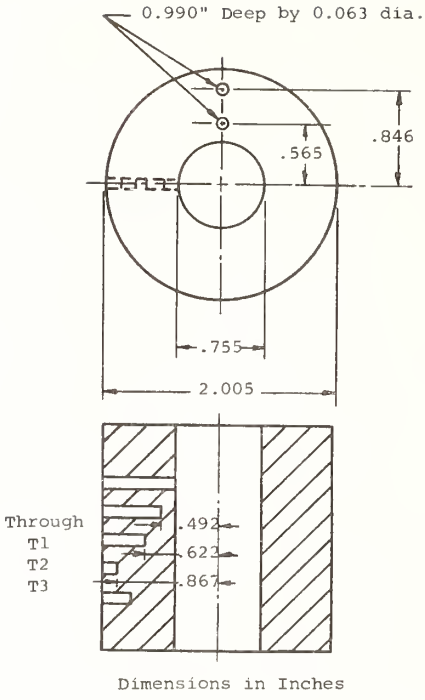

Factor Calculations

$$\text{Factor} = \frac{\ln \frac{r_2}{r_1}}{2\pi l}$$

Where: l=Voltage Probe Separation in cm.
r_1-r_2=Appropriate Radii

1). Thermocouple wells (F_{TC})

$$F_{TC} = \frac{\ln \frac{.622}{.492}}{2\pi\, 2.54} = \frac{\ln 1.498}{15.95} = .0251$$

2). Radial T_1-T_2

$$F_{1-2} = \frac{\ln \frac{.622}{.492}}{2\pi 2.54} = \frac{\ln 1.265}{15.95} = .0146$$

3) Radial T_2-T_3

$$F_{2-3} = \frac{\ln \frac{.867}{.622}}{2\pi\, 2.54} = \frac{\ln 1.333}{15.95} = .0208$$

4). Radial T_1-T_3

$$F_{1-3} = \frac{\ln \frac{.867}{.492}}{2\pi 2.54} = \frac{\ln 1.568}{15.95} = .0355$$

Figure 1 - Specimen Measurements and
Geometric Factor Calculations - Purified ATJ Graphite

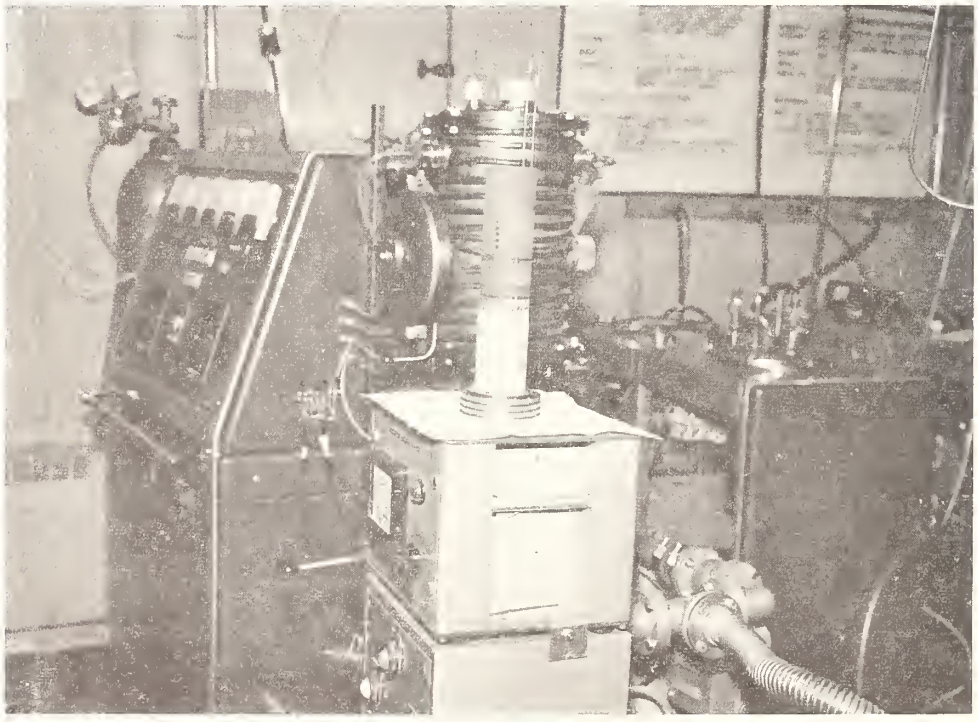

Figure 2. Specimen stack, with thermocouples, assembled on Zirconia Pedestal.

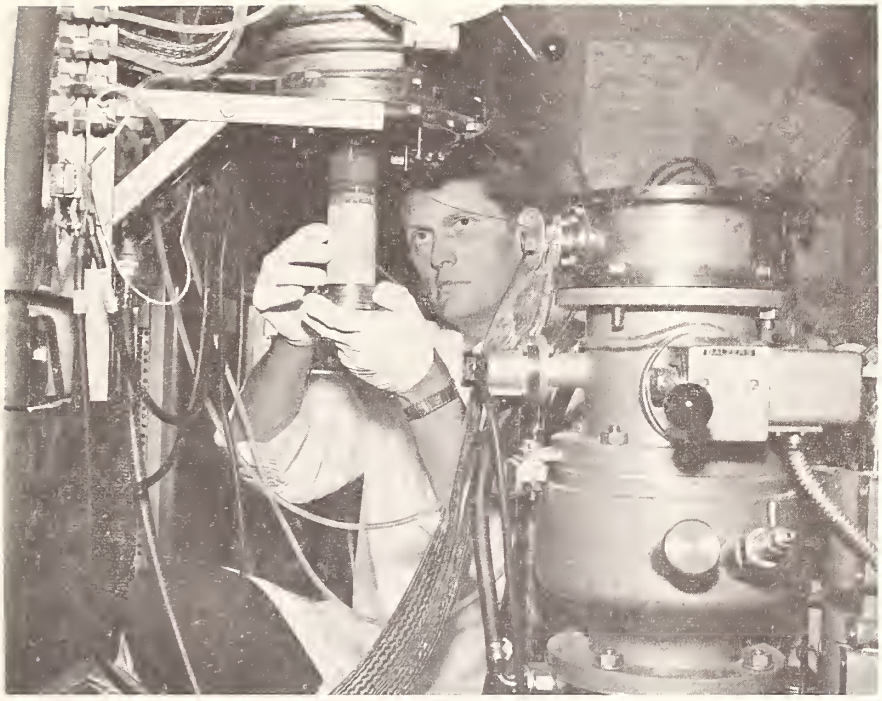

Figure 3. Sample installation into furnace. Lower Vacuum Bell Assembly Pivoted Aside.

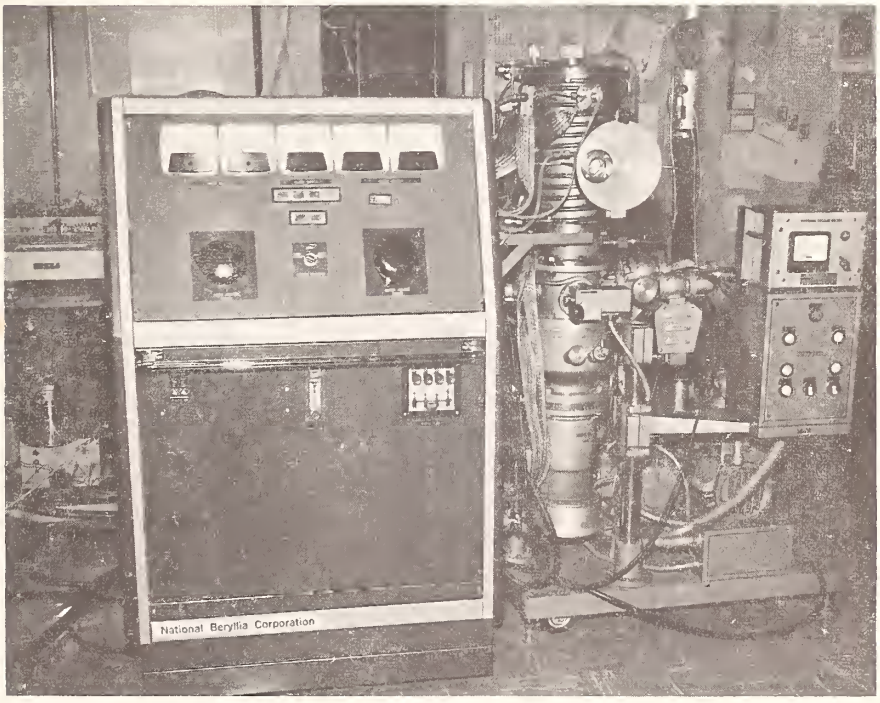

Figure 4. Front View of Apparatus in Operation.

(All photographs courtesy of the General Electric Co.)

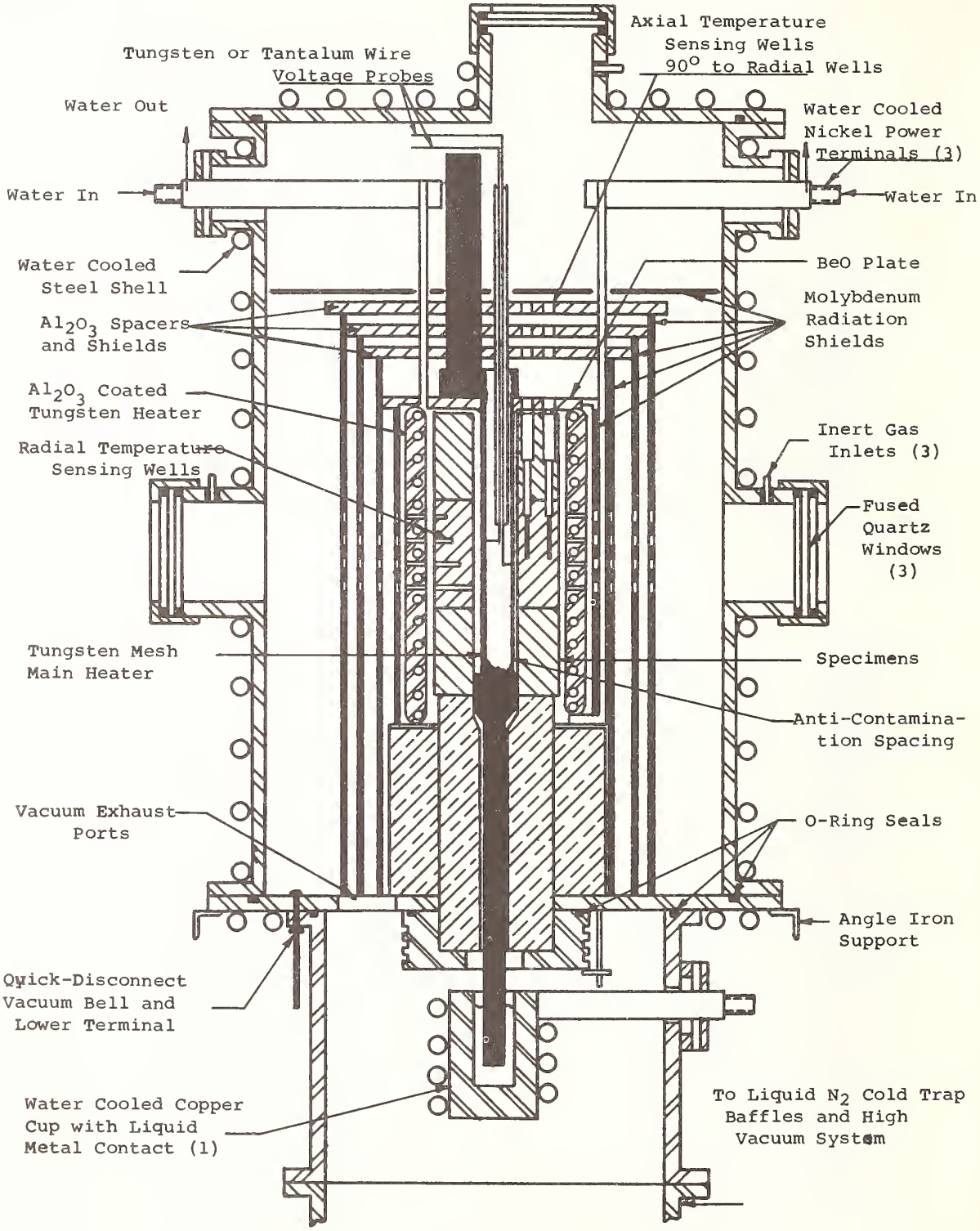
Tungsten or Tantalum Wire Voltage Probes
Axial Temperature Sensing Wells 90° to Radial Wells
Water Out
Water Cooled Nickel Power Terminals (3)
Water In
Water In
Water Cooled Steel Shell
BeO Plate
Molybdenum Radiation Shields
Al_2O_3 Spacers and Shields
Al_2O_3 Coated Tungsten Heater
Radial Temperature Sensing Wells
Inert Gas Inlets (3)
Fused Quartz Windows (3)
Tungsten Mesh Main Heater
Specimens
Anti-Contamination Spacing
Vacuum Exhaust Ports
O-Ring Seals
Angle Iron Support
Quick-Disconnect Vacuum Bell and Lower Terminal
Water Cooled Copper Cup with Liquid Metal Contact (1)
To Liquid N_2 Cold Trap Baffles and High Vacuum System

Figure 5

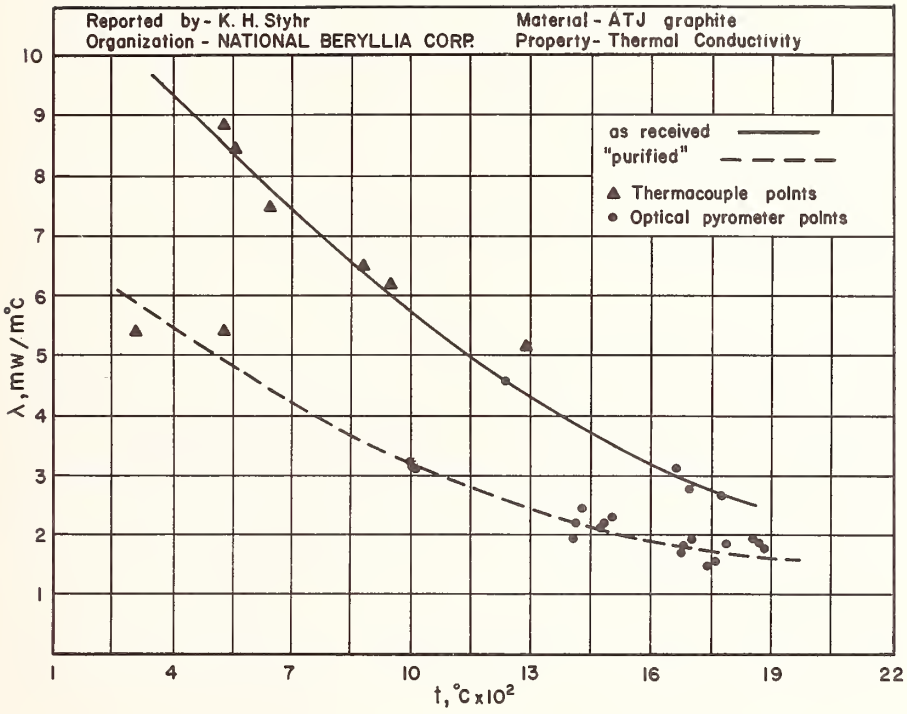

Figure 6

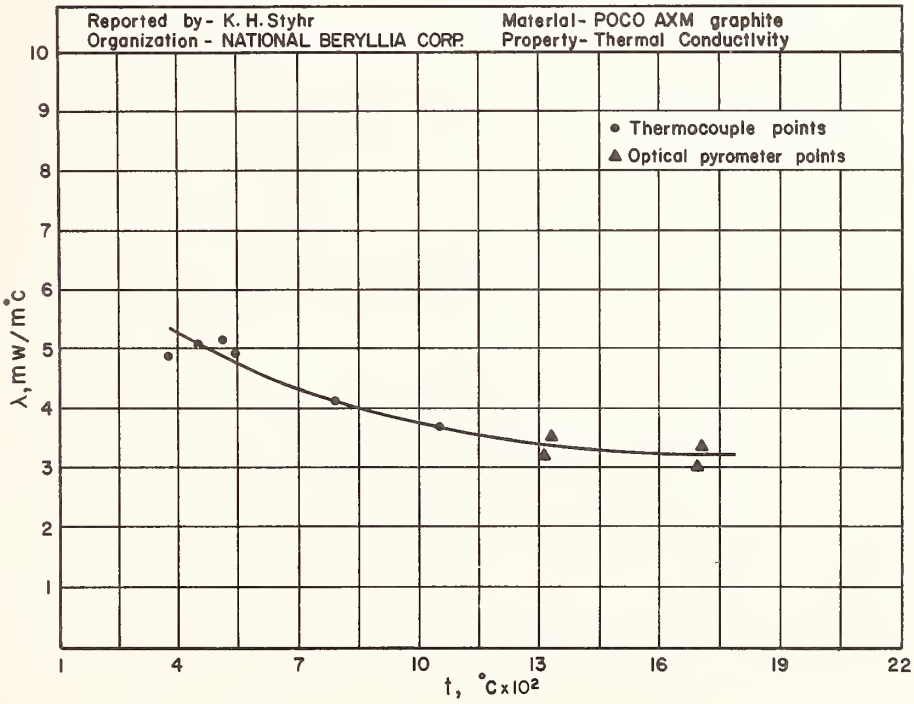

Figure 7

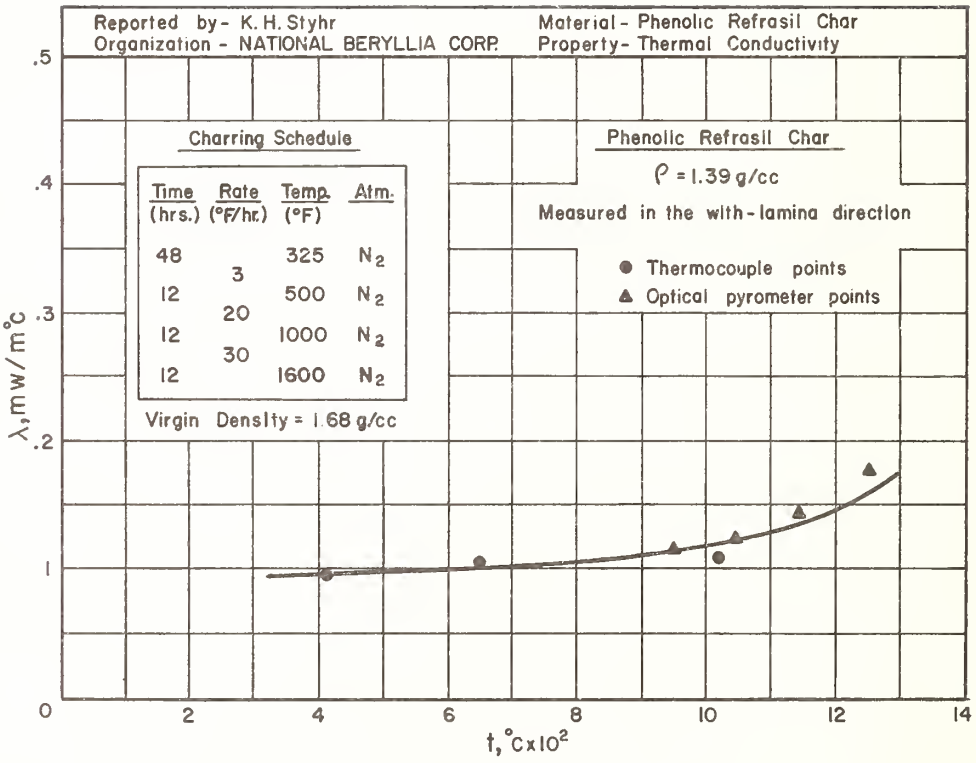
Reported by- K. H. Styhr
Organization - NATIONAL BERYLLIA CORP.
Material - Phenolic Refrasil Char
Property- Thermal Conductivity
Charring Schedule
Time (hrs.) | Rate (°F/hr.) | Temp. (°F) | Atm.
48 | 3 | 325 | N2
12 | | 500 | N2
12 | 20 | 1000 | N2
12 | 30 | 1600 | N2
Virgin Density = 1.68 g/cc
Phenolic Refrasil Char
ρ = 1.39 g/cc
Measured in the with-lamina direction
Thermocouple points
Optical pyrometer points
λ, mw/m°c
t, °C x 10²
0
.1
.2
.3
.4
.5
2
4
6
8
10
12
14

Figure 8

An Investigation of the Mechanisms of Heat Transfer in Low-Density Phenolic-Nylon Chars

E. D. Smyly and C. M. Pyron, Jr.[1]

Southern Research Institute
Birmingham, Alabama 35205

An investigation is being made of the mechanisms of heat transfer during ablation in low-density phenolic-nylon chars. The total objective of the study is to develop a thermal model which can be correlated with characterization studies and property measurements made in the laboratory to analytically extrapolate and predict the overall effective thermal conductivity of the material system under reentry conditions. The objective of the work to date has been to determine the apparent thermal conductivity of the char independent of the act of ablation. Ultimately, the influence of the ablation process will be included.

The chars used in this phase were prepared in an induction plasma torch from three densities of a phenolic-nylon ablative material. The effective thermal conductivities of these chars were measured in vacuum (< 0.01 torr), in nitrogen and in helium between 200°F and 1000°F.

A thermal model was developed from characterization studies of the char structure and correlated with the experimental data to develop an equation which would predict the solid conduction, gas conduction and radiation. Values predicted by this equation agreed closely with the experimental data over the temperature range covered by the measurements, but fell considerably below experimental values obtained on a similar char at elevated temperatures. It was concluded that the conductivity of flight chars is increased at the higher temperatures by an increase in the conductivity of the matrix resulting from graphitization, and by radiant transmission either through voids or through the matrix membranes.

Key Words: Carbon, char, graphite, phenolic-nylon, porous material, thermal conductivity.

1. Introduction

Efforts to describe the mechanisms of heat transfer through ablating materials have met with limited success. The application which concerns us here is the behavior of the char layer on an ablative material during reentry independent of the ablating process. There are several reasons why one desires to be able to predict the response of the char. For earth entry, the actual conditions cannot be duplicated in the laboratory, so that extrapolation is necessary. The heat flux in reentry is partially blocked by the evolution of pyrolysis products through the char. If one attempts to measure the thermal conductivity of a fully degraded char under steady state conditions, this blocking effect is absent and must be accounted for by analysis. On the other hand, if the measurements are made under transient conditions which are less severe than reentry, the data also require analytical corrections. There are arguments pro and con for both steady state and transient techniques. However, in brief, the arguments

[1]Associate Engineer and Head, Thermodynamics Section, respectively.

against the steady state technique are that fairly long times are required for the measurements during which the apparent thermal conductivity of the char may be altered by graphitization. On the other hand, the transient measurements are subject to errors in defining temperature gradients in the degrading material whose properties are changing with depth, while the heat blocking effect, previously mentioned, takes place. It is not the purpose of this paper to argue the merits of test techniques but to propose one approach to analytically predict flight performance from laboratory data. The method used was to produce chars in a plasma jet, and to develop a thermal model for this char which would provide the basis for analytical expressions for the apparent thermal conductivity of this char. These expressions are compared with experimental data obtained on these chars under various gas environments at temperatures ranging from ambient to 1000°F (540°C) and with data obtained in a helium environment at elevated temperatures. In subsequent programs, the ablation process will be injected into the solution.

2. Materials

Chars were made from virgin material of three different densities (19, 30 and 42 lb/ft^3). The virgin material was a low-density phenolic-nylon which consisted of 40 wt% nylon (Du pont Zytel 103), 25 wt% phenolic resin (Union Carbide BRP-5549), 35 wt% phenolic Microballoons (Union Carbide BJO-0930). Densities were varied through variation of the molding pressures. The starting materials were post cured at about 300°F. A more detailed description of composition and processing conditions is presented in Reference [1].[2]

3. Preparation and Characterization of Samples

The specimens were charred in an induction plasma jet consisting of about 70 percent argon-30 percent nitrogen by volume. Cold wall heat flux densities, as measured by a slug calorimeter, averaged about 170 Btu/ft^2-sec at the specimen location about one inch from the end of the quartz tube housing the plasma. Observed front surface temperatures of the specimens, measured with an optical pyrometer, averaged about 4100°F. The charring times were varied between 125 seconds and 180 seconds, depending on the density of the sample, to obtain chars $\frac{1}{2}$ inch thick. The chars were machined into specimens 1 inch diameter x $\frac{1}{2}$ inch thick. Since the chars were quite friable, it was necessary to impregnate them before machining to provide sufficient mechanical strength. The impregnant used was polyalphamethylstyrene, a material which could be completely volatilized by baking the specimens at about 700°F.

Bulk densities were determined from weight and volume calculations. True densities were determined by pulverizing the samples, weighing them, and measuring their volume in a pycnometer. At least 75 percent of the pulverized sample consisted of particles less than two microns in diameter while none of the particles were larger than 12 microns. Porosity was calculated from the relation

$$P = 1 - \frac{\rho_B}{\rho_T} \tag{1}$$

where P, ρ_B, and ρ_T are the porosity, bulk density and true density, respectively. Results are given in Table 1. Note that the bulk densities of the chars ranged from 12 to 20 lb/ft^3, whereas the respective porosities ranged from 88 percent to 79 percent.

Pore size distributions in the chars were obtained by visual observation under the microscope with the aid of a calibrated eye piece which reads in filar units. The specimens used for the photomicrographic evaluations were not impregnated. The specimens were viewed at 100X magnification in a plane parallel to the charring direction. The pore diameter measurements were made in a central zone midway between the front and back surfaces of the sample. Two traverses a few mils apart were made across the char at this location. When grossly irregular pores were encountered, the diameter was approximated. Cracks which ran parallel to the charring direction were not included in the measurements, and only openings which were nearly enclosed were counted as pores. Some areas appeared to represent locations where several pores had been blown out. Since these areas were enclosed by pores on all sides, they were counted as large pores since they probably were created during the charring process. Shown in Figure 1 are photomicrographs of the char produced from the three

[2]Figures in brackets indicate the literature references at the end of this paper.

materials of different virgin densities. Pictures 1(a) and 1(c) are typical, whereas pictures 1(b) and 1(d) are not typical (as many large openings as are shown do not appear in the typical photomicrograph). The porous areas shown in figure 1(b) (away from the large openings) are typical. The samples shown in figures 1 (a), 1(b), and 1(c) were used for the pore size measurements.

Table 1. Results of bulk and true density measurements and porosity calculations for low-density phenolic-nylon chars.

Nominal Density of Virgin Material (gm/cm^3)	Specimen	Bulk Densities of Chars (gm/cm^3)	True Density (gm/cm^3)	Porosity (b)	Average Porosity for Each Virgin Density	Remarks
0.305	19-4	0.196	1.526(a)	0.872		Before run
	19-4	0.188	1.526(a)	0.877	0.876	After run
	19-5	0.186		0.875/0.811		After run
0.481	30-3	0.282		0.813/0.823		Not evaluated
	30-4	0.271	1.501(a)	0.820	0.824	After run
	30-6	0.257		0.829/0.839		After run
0.673	42-3	0.322		0.783/0.786		After run
	42-4	0.319	1.479(a)	0.785	0.786	After run
	42-5	0.315		0.788/0.790		After run

(a) Char was ground using mortar and pestle. Particle sizes of powder used in measurements were:
2 microns or less - 75 percent
3-5 microns or less - 20 percent
6-12 microns or less - 5 percent

(b) A porosity range is given for those samples on which true density measurements were not made. Range is based on the two different true density measurements made on impregnated and unimpregnated chars.

Histograms of the distribution of pore diameters were plotted for each char porosity. The average pore diameters of the materials with porosities of 0.88, 0.82 and 0.79 were 69, 18, and 35 microns, respectively. There was no distinct correlation between the pore diameter distribution and the bulk density of either the virgin material or the char. However, the histograms gave reasonable agreement and indicated the approximate range of pore diameters. A typical histogram is shown in Figure 2. Apparently, the average pore diameter decreases with increasing bulk density up to a point and then increases. Perhaps the porosity of the virgin structure permits outgassing through paths following the existing voids up to a point where the existing voids cannot handle the gas evolution and then larger paths (and pores) are formed to provide gas release.

4. Experimental Apparatus and Procedure

The effective thermal conductivity measurements were made in one direction (the charring direction) in a comparative rod apparatus. Since this type of apparatus is fairly standard and has been described numerous times in the literature, only a brief description is included here.

Basically, this apparatus consisted of a stacked column with the specimen sandwiched between two references of known thermal conductivity. Heat was made to flow through the column, and the thermal conductivity was measured by comparing the temperature drop across the specimen material to the temperature drop through the references. Guard heaters were employed to minimize radial heat losses and axial heat bypass. The guard section was concentric with the specimen column, and the annulus between the column and the guard was filled with diatomaceous earth as an insulation. A schematic of the apparatus is shown in figure 3. A typical temperature profile through the apparatus is given in figure 4.

The apparatus was placed inside a vacuum chamber which was connected to a 15 cfm mechanical pump and a four inch diffusion pump. With this system, it was possible to achieve a vacuum level of

0.002 torr. Pressures were measured with a Hastings thermocouple vacuum gage below 0.1 torr, a McLeod vacuum gage between 0.1 torr and 5 torr, a Dubrovin vacuum gage between 1 torr and 20 torr, and a bourdon tube gage above 20 torr.

The specimens were machined after impregnating the chars with polyalphamethylstyrene to provide sufficient mechanical strength. Machining was performed by first cleaning up the heated surface until it was flat (this usually required the removal of only a small amount of material since this was the best surface), then reducing the thickness a minimum amount until the back (substrate) surface was flat and parallel with the front surface. The specimen was then turned to 1 inch outside diameter, and 0.040 inch thermocouple holes were drilled 0.093 inch from either surface. The gage length between thermocouples generally averaged about 0.25 inch.

After being machined, the specimens were baked at 700°F under a nitrogen purge to remove the impregnant.

The basic uncertainty in the comparative rod apparatus is $\pm$ 5 percent for a normal specimen. The uncertainty was increased for these evaluations because of the shorter specimens, and the low thermal conductivity of the specimens which resulted in a mismatch between the specimen conductivity and the reference conductivity. Two reference materials were available; one was Code 9606 Pyroceram, which has a conductivity of about 50×10^{-5} Btu/sec-ft-°F, and the other was Pyrex, which has a conductivity of about 20×10^{-5} Btu/sec-ft-°F. The Pyrex gave a better match; however, because of the transparency of Pyrex to radiation at temperatures above 500°F, Pyroceram was used for most of the measurements. When a mismatch occurs, it sets up conditions for some of the heat flow through the upper reference to bypass the specimen, thus resulting in the measured value being higher than the true value (if the specimen has a lower conductivity than the reference). Further, analyses by Flynn [2] and Robinson [3] have shown that the error introduced is a function of the conductivity of the insulation material. Based on these analyses errors introduced by the mismatch were estimated to be negligible in vacuum, about $\pm$ 5 percent in nitrogen and about $\pm$ 15 percent in helium. However, the error calculations were based on conditions which did not conform exactly to the experimental conditions and, hence, are subject to considerable uncertainty themselves. For this reason, the corrections were not applied to the data. A consideration of all of the errors led to the conclusion that the random precision in the system was about $\pm$ 10 percent with a possible bias error of +15 percent.

5. Experimental Data

The apparent thermal conductivity was measured on two or more specimens each of chars made from 19, 30, and 42 lb/ft^3 virgin phenolic-nylon. The measurements were made in the charring direction with the temperature gradient maintained in the same direction as it occurred during charring. Measurements were made in vacuum (less than 0.01 torr), in nitrogen and in helium over a temperature range from 400°F to 1000°F. At about 500°F data were obtained at various pressures ranging from less than 0.01 torr to one atmosphere to determine the pressure dependence of the conductivity.

The apparent thermal conductivity versus temperature is plotted in figures 5, 6, and 7 for 19, 30 and 42 lb/ft^3 chars. The low data for specimen 42-4 probably resulted from deterioration of the lower or substrate surface of this specimen during the run. The gage length of specimen 42-3 was only 0.133 inch (about half that of the other specimens) which may have created some additional errors in its evaluation.

A composite plot of the apparent thermal conductivities of the three chars is presented in figure 8. No distinct correlation is seen between the char porosity or density of the virgin material. In vacuum and in nitrogen the conductivity of the 0.79 porosity char fell between that of the 0.82 and 0.88 porosity chars, but was the lowest of the three in helium.

Measurements of the apparent conductivities as a function of ambient gas pressure were made for all three chars in nitrogen and in helium at an average mean temperature of 500°F. A typical plot showing the apparent thermal conductivity of the 0.82 porosity char versus ambient gas pressure in nitrogen is shown in figure 9. The 88 and 79 percent chars behaved similarly and for brevity these plots are not reproduced here, but may be found in Reference [4]. Observe that the apparent thermal conductivity of the char was constant at pressures between about 300 torr and 760 torr. Below 300 torr the conductivity decreased, finally reaching a second plateau at about 1 torr. This behavior can be explained as follows: at higher pressures the mean free path of the gas molecules is shorter than the separation distance, or average pore size, of the char and energy is transferred through the gas almost entirely by intermolecular collisions. As the pressure is reduced, the mean free path becomes on the

order of the separation distance and the gas molecules transfer energy both by intermolecular collisions and by collisions with the cell walls. This range of pressures (or mean free paths) corresponds to the knee of the curve. As the pressure is further reduced, the mean free path becomes longer than the separation distance, and the gas molecules give up energy almost entirely by collisions with the cell walls so that a further reduction in pressure has no effect on the conductivity. Comparing figure 3 with figure 9, it can be seen that the range of measured pore sizes corresponds rather closely with the calculated range of mean free paths over which the apparent thermal conductivity decreases.

It is also important to note that the change in the apparent conductivity of the char as pressure is increased from vacuum to one atmosphere is greater than the thermal conductivity of the gas. This indicates either strong dependence on the gas thermal conductivity or convection effects. Radiation, if it were present, would be a constant component.

Recall from the prior discussion that the theoretical analysis of the bias error introduced because of the conductivity mismatch between the specimens and the references predicted positive errors of 5 and 15 percent in nitrogen and helium, respectively. This is being recalled because there have been several analyses of porous materials which would predict nearly the total gas thermal conductivity as the contribution of the gas to the measured thermal conductivity for this range of porosities, and it is important to determine if this low prediction is probable within the experimental error. The last two columns in table 2 give the maximum possible percentage change in the measured apparent thermal conductivity which can be attributed to the gas and the difference between this value and the measured value, respectively. In the last column, observe that with one exception the difference in the measured increase in conductivity and the increase obtained by adding the thermal conductivity of the gas exceeded the 15 percent bias error in the measurement. This is important in that it indicates that the thermal conductivity of the gas can have more effect on the "apparent" thermal conductivity of the char than its own value. This effect has appeared in the literature before. Young, Hartwig and Norton [5] presented data for firebrick of 0.82 porosity. The apparent thermal conductivity increased in air (nitrogen) from 1.46×10^{-5} Btu/sec-ft-°F at 0.05 torr to 2.52×10^{-5} Btu/sec-ft-°F at 760 torr for a change of 73 percent. By assuming that the air contributed its total conductivity, the change would have been only 40 percent (based on a gas conductivity of 0.48×10^{-5} Btu/sec-ft-°F). One might argue that convection effects are present. Evidence will be presented later which indicates that this effect is small. For the range of porosities which have been evaluated, there is small possibility that the matrix is continuous, especially considering the violent birth of the material. Therefore, delaminations and voids must exist which offer infinite resistance to heat flow at vacuum but which become conducting paths when a continuum gas is introduced.

Table 2. Comparison of the experimental data at approximately 500°F for the three char densities

Specimen Number	Average Bulk Density (gm/cm³)	Average Porosity	Average apparent thermal conductivity in			Absolute change in apparent thermal conductivity going from vacuum to	
			Vacuum in 10^{-5} Btu / sec ft °F	Nitrogen in 10^{-5} Btu / sec ft °F	Helium in 10^{-5} Btu / sec ft °F	Nitrogen in 10^{-5} Btu / sec ft °F	Helium in 10^{-5} Btu / sec ft °F
19-4 and 19-5	0.187	0.88	9.0	12.5	18.8	3.5	9.8
30-4 and 30-6	0.264	0.82	14.5	17.5	22.0	3.0	7.5
42-3 and 42-5	0.318	0.79	13.0	17.5	22.0	4.5	9.0

Specimen Number	Percent Change in Going from Vacuum to (a)		Maximum Possible % Change due to Gas Conduction		Difference between measured % Change and Maximum Possible % Change due to Gas Conduction	
	Nitrogen	Helium	Nitrogen	Helium	Nitrogen	Helium
19-4 and 19-5	38.8	108.8	6.5	39	32.3	69.8
30-4 and 30-6	20.6	51.7	4.1	25	16.5	26.7
42-3 and 42-5	34.6	69.2	4.5	27	30.1	32.2

(a) Percent change - $\frac{\text{Apparent thermal conductivity in gas - apparent thermal conductivity in vacuum}}{\text{Apparent thermal conductivity in vacuum}}$

6. Thermal Analysis

In order to separate the effects of radiation, solid conduction, gas conduction and convection on the apparent thermal conductivity of the char, a thermal analysis was performed. This analysis also allowed the isolation of one of the important intrinsic properties of the char, the thermal conductivity of the matrix.

In the thermal analysis, each of the aforementioned modes of heat transfer was considered. Before proceeding to the thermal model some work by other authors should be discussed.

6.1. Analyses of Porous Materials

Russell [6], Goring and Churchill [7], Euken (presented in Reference [8]), Loeb [9], and many other authors have presented equations for predicting the apparent thermal conductivity of porous materials. In addition, an equation derived by Bruggeman (presented in a paper by Powers [10]) for dispersions may be applied to porous materials. This may be done by treating the pores as the dispersed phase and using the conductivity of the gas within the pores as the conductivity of this phase. The char solid would be treated as the continuous phase. In all of these analyses the authors have assumed that the matrix was continuous (contained no delaminations or irregularities), and most of them give nearly identical results. For completeness, Russell's equation, which has found general acceptance, was applied to the data to ascertain how closely the models for continuous matrices apply. Russell's equation may be written [6]

$$k_a = k_m \frac{k_g P^{2/3} + k_m (1 - P^{2/3})}{k_g P^{2/3} - k_g P + k_m (1 - P^{2/3} + P)} \tag{2}$$

where

k_a = apparent thermal conductivity
k_m = thermal conductivity of matrix
k_g = thermal conductivity of void
P = porosity

Russell's equation was applied to the data by reducing k_m (matrix conductivity) from the vacuum data and then predicting the values for nitrogen and helium. Also, k_m was reduced from the nitrogen data, and the vacuum and helium values were predicted. A temperature of 500°F was assumed for these calculations and radiation was neglected. The vacuum data probably contain the least uncertainty; therefore, for a comparison with the measured data, the predictions based on the vacuum data should be most meaningful. The results of these calculations are shown in table 3. Note that with one exception the values predicted by Russell's equation fell below the measured values by a greater percentage than can be attributed to uncertainty in the measurements (maximum of 25 percent), indicating that a non-continuous model should be assumed for the highly porous chars.

Table 3. Results obtained by applying Russell's equation to experimental data at 500°F

Specimen Number	Apparent Thermal Conductivity Predicted by Russell's Equation Using Value of Matrix Conductivity Reduced from Vacuum Data in 10^{-5} Btu/sec-ft-°F							
	Reduced k_m	In vacuum at 500°F (532°K)	In Nitrogen at 500°F (532°K)			In Helium at 500°F (532°K)		
		Measured	Predicted	Measured	Percent(a) Difference	Predicted	Measured	Percent (a) Difference
19-4	103	9.0	9.5	14.4	51.2	12.3	20.1	64.1
19-5	92	8.1	8.6	11.3	32.4	11.3	16.2	42.8
30-4, 30-6	116	14.8	15.7	17.3	10.2	18.1	21.9	21.7
42-3	88	13.9	14.8	18.5	25.0	17.1	24.3	41.8
42-4	51	8.1	8.6	11.6	35.1	11.3	18.5	63.2
42-5	76	12.0	12.5	16.4	31.4	15.3	18.9	24.2

(a) Percent difference = $\frac{\text{measured conductivity - predicted conductivity}}{\text{predicted conductivity}}$ x 100 percent

6.2. Development of the Thermal Model

a. Physical and Thermal Model

A physical model was assumed which is a first approximation to a noncontinuous matrix. This model is shown in figure 10(a). It was assumed that the material contained cracks which were parallel to the direction of heat flow. These cracks were assumed to occupy some fraction of the total area and extend across the thickness of the material. The char does contain these long cracks but obviously they do not extend through the full thickness; some interconnections exist. However, the number of interconnections appeared to be small. It was also assumed that a large number of one-dimensional heat flow channels existed. Note that a heat flow channel consisted of porous material. Some fraction of the total area, (1-f)F, was assumed to consist of continuous (undelaminated) flow channels and the remaining area, (1-f)(1-F), was assumed to contain delaminations (cracks, breaks, or large voids, normal to the heat flow). That these separations do exist is evident from photomicrographs of the char. Observe in figures 1(b) and 1(d) that voids which separate porous areas are readily visible. The voids shown are perhaps 50 to 100 microns in thickness. Also observe in figure 1(a) that areas exist where the pores are not continuous, and delaminations several pore diameters long are apparent. It is obvious that the char does not consist of well defined delaminated and undelaminated heat flow channels. Further the heat flow will tend to concentrate in the solid areas adjacent to a delamination and thus somewhat bypass the delamination. However, for purposes of this analysis, bypassing effects were neglected, and the heat flow was assumed to be one dimensional.

The thermal conductance network which describes the heat flow through the assumed physical model is shown in Figure 10(b). The separate conductances are outlined below:

K_R = radiant conductance through cracks parallel to the heat flow

K_G = gas conductance through cracks parallel to the heat flow

$K_{m'}$ = solid conductance through undelaminated area

$K_{r'}$ = radiant conductance through undelaminated area

$K_{g'}$ = gas conductance through undelaminated area

K_r = radiant conductance through porous area in the delaminated area

K_m = solid conductance through porous area in the delaminated area

K_g = gas conductance through porous area in the delaminated area

K_{dr} = radiant conductance across delamination

K_{dg} = gas conductance across delamination

Now that the physical model and the thermal conductance network have been defined the equations for the conductances will be explored. Each of the modes of heat transfer, radiation, solid conduction, gas conduction and convection will be discussed under separate headings.

(1). Radiation. There are three radiation components of concern in porous chars. The first is radiation between the walls of the pores; the second is radiation through the cracks which are parallel to the heat flow; and the third is radiation across any delamination (separations normal to the heat flow) In his studies of porous materials (not chars), Russell [6] considered radiation across the pores and used the pore diameter as the effective radiation length. His expression has been modified slightly to account for a radiant length which may be longer than one pore diameter because of the somewhat open pore structure. The radiant conductance obtained in this manner is based on the heat transfer between two parallel plates a finite distance apart. The equation for the radiant conductance through the porous area in a delaminated flow channel may be written

$$K_r = \frac{4\sigma A_r \epsilon T_m^3 x}{(2\rho + \epsilon)x} = \frac{A_r x}{ax} \qquad \left(\begin{array}{l}\text{Radiation through}\\ \text{delaminated flow}\\ \text{channel}\end{array}\right) \tag{3}$$

where

$$a = \frac{2\rho + \epsilon}{4\sigma\epsilon T_m^3}$$

$$A_r = (1-f)(1-F)P^{2/3}A$$

and

σ = Stefan-Boltzmann constant
ϵ = emittance
ρ = reflectance
x = characteristic radiant length
T_m = absolute temperature
f = fraction of total cross-sectional area, normal to the heat flow, occupied by the cracks which are parallel to the heat flow
F = fraction of heat flow channels which are undelaminated
A = total area
P = porosity

Note that the radiation term $\sigma(T_1^4 - T_2^4)$ has been written as $4\sigma T_m^3 \Delta T$. By algebraic manipulation it can be shown that these expressions are equivalent within three percent error if $\Delta T \leq 0.346 T_m$. This will be true for a reasonable heat flux and char thickness. Note in eq 3 that the term x/x has been introduced where x is some characteristic radiation length which is an unknown for phenolic-nylon chars in general. This term was introduced because K_r is a conductance term and in order to obtain an expression for the radiant conductivity from eq 3, a length term is needed, i.e., $k_r = K_r x/A_r$ where k_r is the radiant conductivity. Thus, an expression for the radiant conductivity would contain x in the numerator only. If x is thought of as the spacing between parallel plates, it is obvious that the larger the number of plates (in a given length) the smaller x will be and consequently the radiant conductivity will be less.

The term $(2\rho + \epsilon)$ in eq 3 arises from the use of the graybody shape factor for the heat transfer between the two surfaces with the shape factor being equal to one.

As it is written eq 3 applies to radiation through the porous area in a delaminated flow channel. A similar expression also applies to the radiant conductance of an undelaminated flow channel. This equation may be obtained as follows: Take the reciprocal of the thermal conductance of an element of length x,$(A_r'x/ax)$. This gives the thermal resistance, $ax/A_r'x$, of one element. Then sum all of the resistances over the total length L. In this manner the radiant thermal resistance $aL/A_r'x$ is obtained. Take the reciprocal of the thermal resistance to obtain the thermal conductance

$$K_r' = \frac{A_r'x}{aL} \qquad \left(\begin{array}{l}\text{Radiation through}\\ \text{undelaminated flow channel}\end{array}\right) \tag{4}$$

where

$A_{r'} = (1-f)FP^{2/3}A$
L = thickness across which heat is being transferred

The radiant conductance through the cracks parallel to the heat flow may be written

$$K_R = \frac{4\sigma F_{ir2} L T_m^3 A_R}{L} \qquad \text{(Radiation through cracks)} \tag{5}$$

where

$A_R = fA$

In eq 5, L represents the length of the crack and F_{ir_2} is a reradiation shape factor. Values of the shape factor may be estimated from curves developed by Jakob [11] for radiation through openings. All that is needed for the approximation is the ratio of the minimum crack dimension to the crack length. The term L/L was introduced for use later in summing conductances.

The radiant conductance across the delaminations may be written

$$K_{dr} = \frac{4\sigma A_d \epsilon T_m^3 t}{(2\rho + \epsilon)t} \quad \frac{A_d t}{at} \qquad \text{(Radiation across delaminations)} \tag{6}$$

where

t = delamination thickness
$A_d = (1-f)(1-F)A$

Equations (3) through (6) should adequately describe the radiant heat transfer. The two major unknowns in these equations are (1) the radiant length through the porous area, and (2) the delamination thickness. Transparency of the solid was neglected; this aspect requires further study.

(2) Solid Conduction. Solid conduction through the char accounts for a considerable portion of the heat transfer. The matrix conductance for a delaminated flow channel may be written

$$K_m = \frac{k_m A_m}{x} \quad \begin{pmatrix}\text{Solid conduction through} \\ \text{delaminated flow channel}\end{pmatrix} \tag{7}$$

where

k_m = thermal conductivity of the matrix
$A_m = (1-f)(1-F)(1-P^{2/3})A$

In eq (7) the solid conduction length, x, is taken to be equal to the radiant length. This is of no consequence since any length can be used as long as the summing of lengths is properly performed. The determination of the effective cross-sectional area is most important. Some authors have used $(1-P)A$ as the effective cross-sectional area for isometric pores, where P is the volume pore fraction [8]. Russell [6] and Ribaud (presented in Reference [8]) used $(1-P^{2/3})A$ as the effective conduction cross section. The latter expression appears to best describe the effective cross-sectional area. This relation needs experimental verification for these highly porous chars as it has some bearing on reducing the matrix conductivity from experimental measurements of the "apparent" thermal conductivity.

For an undelaminated flow channel the equation for the solid conductance is

$$K_{m'} = \frac{k_m A_{m'}}{L} \qquad \left(\begin{array}{l}\text{Solid conduction through}\\ \text{undelaminated flow channel}\end{array}\right) \tag{8}$$

where

$A_{m'} = (1-f)F(1-P^{2/3})A$
L = total thickness across which heat is being transferred

(3). Gas Conduction. There are three gas conduction components in the chars: (1) gas conduction through the porous areas, (2) gas conduction through the cracks parallel to the direction of heat flow, and (3) gas conduction across any delaminations. These conductances may be written as follows:

$$K_g = \frac{k_g A_g}{x} \qquad \left(\begin{array}{l}\text{Gas conduction through}\\ \text{delaminated flow channel}\end{array}\right) \tag{9}$$

$$K_{g'} = \frac{k_g A_{g'}}{L} \qquad \left(\begin{array}{l}\text{Gas conduction through}\\ \text{undelaminated flow channel}\end{array}\right) \tag{10}$$

$$K_G = \frac{k_g A_R}{L} \qquad \left(\begin{array}{l}\text{Gas conduction through}\\ \text{cracks}\end{array}\right) \tag{11}$$

$$K_{dg} = \frac{k_g A_d}{t} \qquad \left(\begin{array}{l}\text{Gas conduction across}\\ \text{delamination}\end{array}\right) \tag{12}$$

where

k_g = thermal conductivity of the gas
$A_g = (1-f)(1-F)\,P^{2/3}\,A$
$A_{g'} = (1-f)\,F\,P^{2/3}\,A$
$A_R = fA$
$A_d = (1-f)(1-F)A$
x = characteristic radiant length
L = total thickness across which heat is being transferred
t = delamination thickness

(4). Convection. It was concluded that convection heat transfer was negligible in these experiments. This conclusion was based on the following observations: (1) The structure of the char - the miniscule pore sizes of the chars would tend to retard convection. (2) Experimental conditions - the heat flow was vertically downward through the chars, tending to negate bouyant forces. (3) Experimental observations - heat was induced to flow vertically downward, thus tending to negate bouyant forces. Also, since convection heat transfer is dependent on the temperature difference through the specimens, the apparent thermal conductivity should vary with ΔT if convection were significant. The experimental data showed no dependence on this parameter. (4) Results reported in the literature. Kreith [12] stated that convection in horizontal air spaces, heat from below, does not begin until the Grashof number exceeds 1600. Grashof numbers for the porous chars were much lower. Vershoor and Greebler [13] deduced from measurements on glass wool insulation (having higher porosities and lower apparent conductivities than the porous chars discussed here) that convection accounted for only 16 percent of the total heat transfer. Thus, the evidence seems fairly conclusive that convection effects were negligible in these experiments. However, it would probably be worthwhile to pursue this effect further through experiments designed to induce convection in order to evaluate the effect of this mode on the flight performance.

b. Equation for Apparent Thermal Conductivity of Char

The conductances which are shown in figure 13 and presented in eqs (3) through (12) were combined using the relations for series and parallel electrical conductances to obtain an expression for the apparent conductance, K, of the char. In combining the conductances use was made of the fact that the total thickness of the delaminations in a delaminated flow channel is nt, where n is the total number of

delaminations and t is the average thickness of one delamination. Therefore, the length of the porous area in a delaminated flow channel is (L-nt). The expression for the apparent conductance was reduced to an expression for the apparent thermal conductivity of the char through the relation

$$Q = K\Delta T = \frac{k_a A \Delta T}{L} \tag{13}$$

where

K = apparent conductance
k_a = apparent thermal conductivity
A = total area
L = total length
ΔT = temperature difference

The expression obtained for the apparent thermal conductivity of the char was

$$k_a = \frac{(1-f)(1-F)(t/a + k_g)\left[\frac{x P^{2/3}}{a} + P^{2/3} k_g + (1 - P^{2/3}) k_m\right]}{(1-c)(t/a + k_g) + c\left[\frac{x P^{2/3}}{a} + P^{2/3} k_g + (1-P^{2/3})k_m\right]} \tag{14}$$

$$+ 4 f \sigma F_{ir_2} T_m^3 L + f k_g + (1-f)F\left[P^{2/3} k_g\right.$$

$$\left. + (1-P^{2/3}) k_m + \frac{x P^{2/3}}{a}\right]$$

where

$$c = \frac{nt}{L}$$

The details of the derivation of eq (14) are presented in Reference [4]. The unknowns in eq (14) are F, x, t, c, and k_m.

Continuum values taken from the literature were used for the thermal conductivities of nitrogen and helium at 760 torr.

c. Correlation of Thermal Model with Measurements

The first step taken in order to apply eq (14) to the experimental data was to estimate the radiation terms, $xP^{2/3}/a$, t/a, and $4 f \sigma F_{ir_2} T_m^3 L$. For a radiant length, x, of 508 microns (approximately 10 pore diameters), a reflectance, ρ, of 0.2, an emittance, ϵ, of 0.8, and a reradiation shape factor, F_{ir_2}, of 0.10 (estimated from approximate measurements of the crack size), the radiation terms were negligible at 500°F. Since the radiation terms were small, the value of t had little influence on the results; therefore, this term was ignored in the low temperature calculations. Only the total delamination thickness, nt, was considered in accounting for gas conduction across the delaminations. Therefore, at the 500°F mean temperature only three unknowns remain, namely, c, F, and k_m. The fraction of the total area which was occupied by the cracks, f, was estimated to be 0.1.

The experimental data at 500°F were used with eq (14) to determine the values of c, F, and k_m for each specimen. Experimental data were obtained for three different environmental conditions (vacuum, nitrogen and helium). Thus, the measurements represent the apparent thermal conductivities for three values of k_g (thermal conductivity of gas). One equation in c, F, and k_m was written from eq (14) for each environmental condition. Values taken from the literature were used for the thermal conductivities of nitrogen and helium at 760 torr. In writing these equations the radiation terms were assumed to be zero since calculations had shown that the values of these terms were negligible at 500°F.

Also, the proper values for the char thickness, temperature and porosity, for a given specimen, were substituted into eq (14) along with the values of k_a and k_g for a given environmental condition. Hence, three simultaneous equations were obtained and these equations were solved for c, F, and k_m. Only one set of values for c, F, and k_m was obtained for each specimen at the given temperature level since there were three experimental conditions and three equations were required for a solution.

The results of these calculations are shown in table 4. Also shown in table 4 are the data used in this analysis and the char porosities. The parameter c represents the ratio of the delamination length to the total length; note that the values ranged from 0.6 percent to 7.1 percent of the total length with a mean value of approximately 3 percent. This appears to be a reasonable value and does not represent an excessive amount of cracking. The factor which represented the fraction of the flow channels which were undelaminated, F, ranged from 0.48 to 0.72, which again indicates a reasonable range of values. There was considerable scatter in the matrix conductivity from 127×10^{-5} Btu/sec-ft-°F to 248×10^{-5} Btu/sec-ft-°F. These values are higher than the range of values, 69 to 115×10^{-5} Btu/sec-ft-°F, which is generally accepted for carbon. The data reductions suggest that those specimens having the lowest densities, Specimens 19-4 and 19-5, had the highest matrix conductivity. Note in table 4 that the matrix conductivity was also reduced using P rather than $P^{2/3}$ in eq (14) and yielded lower values which were still higher than the values normally reported for carbon.

Table 4. Results of reducing the parameters c, F, and k_m in eq (14) from the experimental data

Specimen Number	Porosity	Apparent thermal conductivity measured at 500°F(532°K) 10^{-5} Btu/sec-ft-°F		
		Vacuum	Nitrogen	Helium
19-4	0.877	9.02	14.35	20.13
19-5	0.878	8.10	11.34	16.20
30-4, 30-6	0.827	14.81	17.36	21.98
42-3	0.785	13.88	18.51	24.30
42-4	0.785	8.10	11.57	18.51
42-5	0.789	12.03	16.43	18.97

Specimen Number	Porosity	Value of c, F, and k_m in eq (14) obtained by fitting data at 500°F (532°K)			Values obtained for k_m by using P rather than $P^{2/3}$ in eq (14)
		c	F	k_m 10^{-5} Btu / sec ft °F	k_m 10^{-5} Btu / sec ft °F
19-4	0.877	0.022	0.477	248	169
19-5	0.878	0.047	0.545	194	132
30-4,30-6	0.827	0.036	0.710	199	137
42-3	0.785	0.027	0.590	185	125
42-4	0.785	0.071	0.400	155	106
42-5	0.789	0.006	0.720	127	88

Since the range of porosities was small and there was considerable scatter in the parameters, it is hard to evaluate the model for its applicability. The fact that c, F, and k_m varied from specimen to specimen prohibited using one set of values to attempt a correlation of all of the data.

One additional check on the model is to see how the predicted variation in the "apparent" thermal conductivity with temperature agrees with the data. The apparent conductivity was calculated for each specimen over the temperature range from 250°F to 1000°F using the reduced values of c, F, and k_m given in table 4. Typical plots showing a comparison of the measured and calculated apparent conductivities for the 0.79 porosity char, are presented in figure 11. Note that the values predicted at the

higher temperatures usually agreed with the measured values within the experimental uncertainty with the exception of the vacuum data at the higher temperatures for Specimen 42-3. The data for Specimen 42-3 at 500°F in vacuum appear erroneous. There is no reasonable explanation for this large increase of thermal conductivity with temperature. Similar plots for the other two chars may be found in Reference [4].

d. Correlation of Predicted Values with Prior High Temperature Data

In use applications the char layer of an ablator is at temperatures on the order of 5000°F or higher. Thus the critical test of the foregoing analysis is its ability to predict performance at near 5000°F.

Figure 12 shows the apparent conductivity obtained experimentally from measurements on a phenolic-nylon char of the same composition as those reported in this paper. These data were previously reported in Reference [1]. Also plotted are values predicted by eq (14) for various combinations of radiant lengths x and matrix conductivities, k_m. The lowest value of k_m of 231 x 10^{-5} Btu/sec-ft-°F corresponds approximately to the values calculated from eq (14) for the low temperature data. The highest value of k_m corresponds to the conductivity of polycrystalline graphite. The radiant path lengths of 50 and 500 μ correspond to approximately 1 and 10 pore diameters, respectively. Values of c and F were those reduced from eq (14) for an 88 percent porous char. The delamination thickness t of 50μ corresponds to between 2 and 3 delaminations.

There is some uncertainty as to the gas that should be used in the calculations. The experimental measurements were obtained in helium but without evacuating the air beforehand. Thus, pores may have contained nitrogen. The calculations were based on nitrogen. Values predicted for helium would range from 20 to 40 percent higher. From the plots in figure 12 it can be seen that the lowest values of x and k_m give the best agreement with the experimental data at low temperatures, while at high temperatures the reverse is true. Two possible explanations can be offered for this behavior. The first is that the conductivity of the matrix increases due to graphitization. The second is that the thermal model does not adequately account for radiant heat transfer through the char. There is evidence to support both arguments. First, let us inspect the argument that the high apparent conductivity at high temperatures results solely from an increase in the conductivity of the matrix.

In experimental measurements, it has been found that the apparent thermal conductivity of the char is higher on cooling than during heating (see fig. 12). Also, values obtained on reruns of the same specimens are usually higher at low temperatures and converge to about the same values as before at elevated temperatures. This behavior is illustrated in figure 13 which shows data for phenolic-carbon chars. The characters of the curves for chars made at successively higher temperatures led to the proposal, presented in a previous paper [14], that the apparent conductivity of "flight" chars could be represented by the curve drawn through the measured values for the chars at their charring temperatures. These are the "Boxed Values" represented by the heavy curves in figure 13.

Similar effects of temperature on the apparent conductivity of chars have been reported by others. Nagler [15] presented data for a nylon char formed at about 1800°F, which after being heated to about 3800°F during conductivity measurements exhibited a conductivity at about 600°F which was about three times higher than the original value. Similar data (presented in Reference [16]) have been presented by Neubert, Royal and Van Dyken for heat treated pitch coke mixtures.

There are two arguments which suggest additional graphitization with time at temperature exposure and subsequently higher matrix thermal conductivity values. The first is measurements on a plasma char made in this work which indicated that the side of the specimen which was exposed to the highest temperature for the longest period of time had a considerably higher thermal conductivity. The second argument pertains to some experimental data taken by Neubert, Royal and Van Dyken, which is presented in Reference [16]. The material for their experiments consisted of Whiting coke and Barrett No. 30 pitch extruded in long bars and then reimpregnated with pitch. Room temperature measurements were made on heat treated specimens from this material in an axial heat flow apparatus. Separate samples were heated to 2812°F, 4352°F, and 5432°F. The hold times were not specified. The room temperature thermal conductivities of these samples were 485 x 10^{-5}, 1250 x 10^{-5}, and 2330 x 10^{-5} Btu/sec-ft-°F for the heating temperatures of 3812°F, 4352, and 5432°F, respectively. Further, they stated that the lowest conductivity specimen was typical of a product for which the graphitization had barely begun. This statement means little quantitatively, and the applicability of these data to phenolic-nylon char is questionable. However, these results correlate somewhat with the results of the thermal analy-

sis and indicate that "barely begun" graphitization can give high matrix conductivities. If barely begun graphitization means only a slight change in X-ray diffraction patterns from the carbon structure, these results may be significant.

From the foregoing discussion it seems reasonable to conclude that the effective conductivity of the char might increase by a factor of 2 or more during the course of the measurements due to a change in the conductivity of the matrix. This behavior would account for a significant part of the discrepancy between the experimental and theoretical curves in figure 17.

Exactly where in-flight values for the matrix conductivity would fall depends on the effects of time at temperature. An in-flight char would most likely not have as high a thermal conductivity as measured in the steady-state apparatus unless graphitization takes place very rapidly once a given temperature level is reached. Our measurements of the variation of conductivity across a char indicated that this effect may be rapid, occurring over a 120 second time interval. A knowledge of the effect of time at temperature is vital to predictions of the in-flight conductivity. If the time required for graphitization to occur is extremely small, then the thermal conductivity of the char is essentially dependent on the temperature alone. In this event, the thermal conductivity measured in the steady-state apparatus represents the thermal conductivity of the in-flight char.

It was mentioned that the discrepancy might also be due to the failure of the thermal model to account for radiant heat transfer in the char. This might result from the use of too short a radiant length x in the calculations or from transparency of the char matrix. Literature data as well as the glassy appearance of the char structure support this latter possibility. If the radiant energy transmitted through the char is assumed to be the difference between the experimental and theoretical curves in figure 12, (the theoretical curve used was $x = 50$, $k_m = 231$, and it was shifted down to agree with the experimental curve at low temperatures), then a psuedo-transmittance for the char can be computed from the equation

$$K_r = \gamma 4 \sigma T_m^3 L \tag{15}$$

where

K_r = the apparent radiant conductivity
γ = psuedo-transmittance
σ = Stefan-Boltzmann constant
T_m = mean temperature of the char
L = specimen gage length

Values of γ computed in this manner ranged from 0.03 at 1500°F to 0.13 at 5000°F for a radiant length, x, of 50μ. For $x = 500\mu$, γ ranged from 0.02 at 2000°F to 0.07 at 5000°F (table 5). Note that this pseudo transmittance probably is composed of both direct radiation through pores and transparency through the matrix membranes. The character of the portion resulting from transparency can be compared to the behavior of glass, which is practically opaque to radiation of long wave lengths ($> 4.5\mu$) and is fairly transparent to radiation in the wavelength range from 1 to 2.75μ [17]. Thus, following this parallel, the psuedo-transmittance of the char might be expected to increase with increasing temperature not only as direct pore radiation becomes predominant but also as the spectral distribution of radiant energy shifts from longer to shorter wavelengths.

Table 5. Psuedo-transmittance

Temperature °F	Radiant length, x, microns	
	50	500
1000	0.00	0.00
2000	0.05	0.02
3000	0.09	0.04
4000	0.11	0.06
5000	0.13	0.07

One other parameter which might affect the conductivity is time at temperature. The elevated temperature data presented in this paper were obtained in steady-state measurements during runs of several hours. "Flight" chars on the other hand are formed within periods of a few seconds. If the matrix conductivity remains constant during the short flight times, then the effects of temperature observed in the laboratory measurements are inapplicable. Some measurements on chars exposed to varying times at temperature are needed here. Data found here plus that reported by Nagler [15] indicate that soak times of several hours exert much less influence than does temperature in changing the conductivity.

7. Conclusions

At low temperatures heat transfer through phenolic-nylon chars occurs primarily by solid and gas conduction. These two modes are inseparable in that the gas thermally shorts delaminations in the chars and effectively increases the conductive area. At temperatures below 1000°F, the effective conductivity in a nitrogen or helium environment may be twice that in vacuum. The difference in the two values ranges from two to three times the thermal conductivity of the gas. Equation (14) appears to adequately explain the effect of gas conductivity.

At elevated temperatures eq (14) predicts values which are lower than experimental data on laboratory chars by a factor of two or more. This discrepancy is probably due to (1) an increase in the thermal conductivity of the matrix with increasing temperature, (2) difficulty in proper definition of direct radiation transfer, and (3) transparency of the char at higher temperatures. Work on the higher temperature behavior is underway.

Further investigation is needed to determine the effects of time at temperature on the conductivity of the matrix, and the nature of radiant heat transfer mechanisms in the char.

After resolving these problems, methods of accounting for the process of ablation must be incorporated in the mathematical model.

8. Acknowledgement

This work was sponsored by the National Aeronautics and Space Administration, Langley Research Center.

9. References

[1] Engelke W. T., Pyron, C. M., and Pears, C. D., Thermophysical properties of a low-density phenolic-nylon ablation material, NASA CR-809 prepared by Southern Research Institute (1967).

[2] Flynn, D. R., Thermal guarding of cut-bar apparatus, Conference on thermal conductivity methods (1961). (Referenced with permission of author.)

[3] Robinson, H. E., Thermal conductivity reference standards, proceedings of The Second Conference on Thermal Conductivity (1962). (Referenced with permission of the author.)

[4] Smyly, E. D., Pyron, C. M., and Pears, C. D., An investigation of the mechanisms of heat transfer in low-density phenolic-nylon chars, NASA CR-966 prepared by Southern Research Institute (1967).

[5] Young, R. C., Hartwig, F. J., and Norton, C. L., Effect of various atmospheres on thermal conductance of refractories, J. Am. Cer. Soc. 47, No. 5, pp. 205-10 (1964).

[6] Russell, H. W., Principles of heat flow in porous insulations, J. Am. Cer. Soc. 18, No. 1, pp. 1-5 (1935).

[7] Gorring, Robert L., and Churchill, Stuart W., Thermal conductivity of heterogeneous materials, Chem. Engr. Progress, 57, No. 7, pp. 53-9 (1961).

[8] Francl, J., and Kingery, W. D., Thermal conductivity: IX, Experimental investigation of the effect of porosity on thermal conductivity, J. Am. Cer. Soc., 37, No. 2, pp. 99-151 (1954).

[9] Loeb, Arthur L., Thermal conductivity: VIII, A theory of thermal conductivity of porous materials, J. Am. Cer. Soc., 37, No. 2 pp. 96-9 (1954).

[10] Powers, A. E., Conductivity in aggregates, proceedings of the Second Conference on Thermal Conductivity, Ottawa, Ontario, pp. 280-309 (1962).

[11] Jakob, Max, Heat Transfer, John Wiley and Sons, Inc., New York (1957).

[12] Kreith, Frank, Principles of Heat Transfer, International Textbook Co., Scranton, Pa., pp. 318-19 (1962).

[13] Verschoor, J. D. and Greebler, Paul, Heat transfer by gas conduction and radiation in fibrous insulations, Transactions of the ASME, No. 74, pp. 961-68 (1952).

[14] Pears, C. D. and Pyron, C. M., The thermal conductivity of ablative materials by the "boxing" analysis, presented at the Fifth Thermal Conductivity Conference, Denver, Colorado (1965).

[15] Nagler, Robert G., The thermal conduction process in carbonaceous chars, NASA TR 32-1010 prepared by Jet Propulsion Lab., (1967).

[16] Goldsmith, Alexander, Waterman, Thomas E. and Hirschhorn, Harry J., Thermophysical properties of solid material, Vol. I - Elements WADC TR 58-476, pp. I-C-3-c (1960).

[17] Gardon, J. Am. Cer. Soc., 44, No. 7, pp. 305-12 (1961).

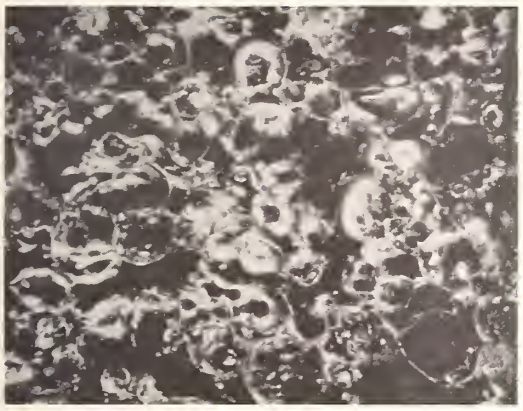

(a) Char of 0.88 porosity
(19 lb/ft³ virgin density)

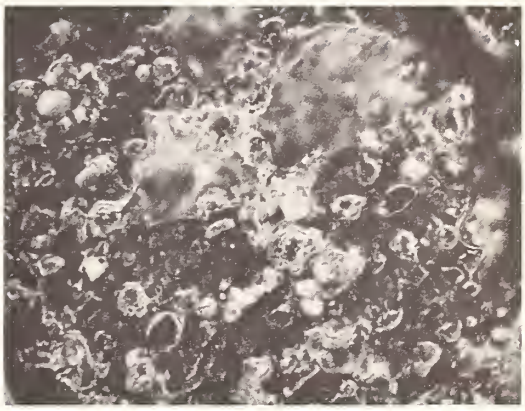

(b) Char of 0.82 porosity
(30 lb/ft³ virgin density)

Charring Direction

(c) Char of 0.79 porosity
(42 lb/ft³ virgin density)

(d) Char of 0.79 porosity
(42 lb/ft³ virgin density)

Figure 1. Photomicrographs at 75X magnification of the three different densities of phenolic-nylon char

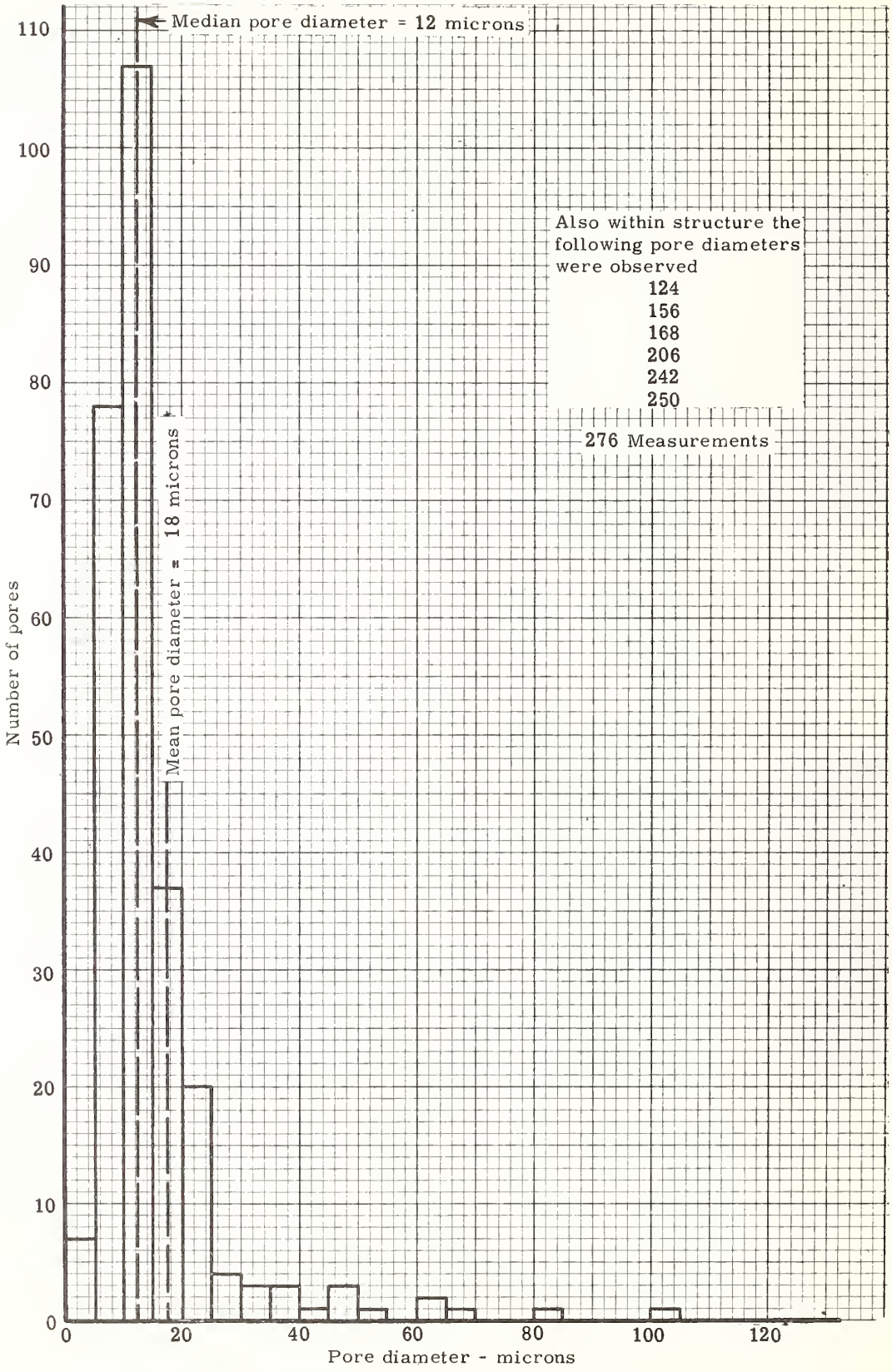

Figure 2. Histogram of pore diameters in the phenolic nylon char of 0.82 porosity (30 lb/ft^3 virgin density)

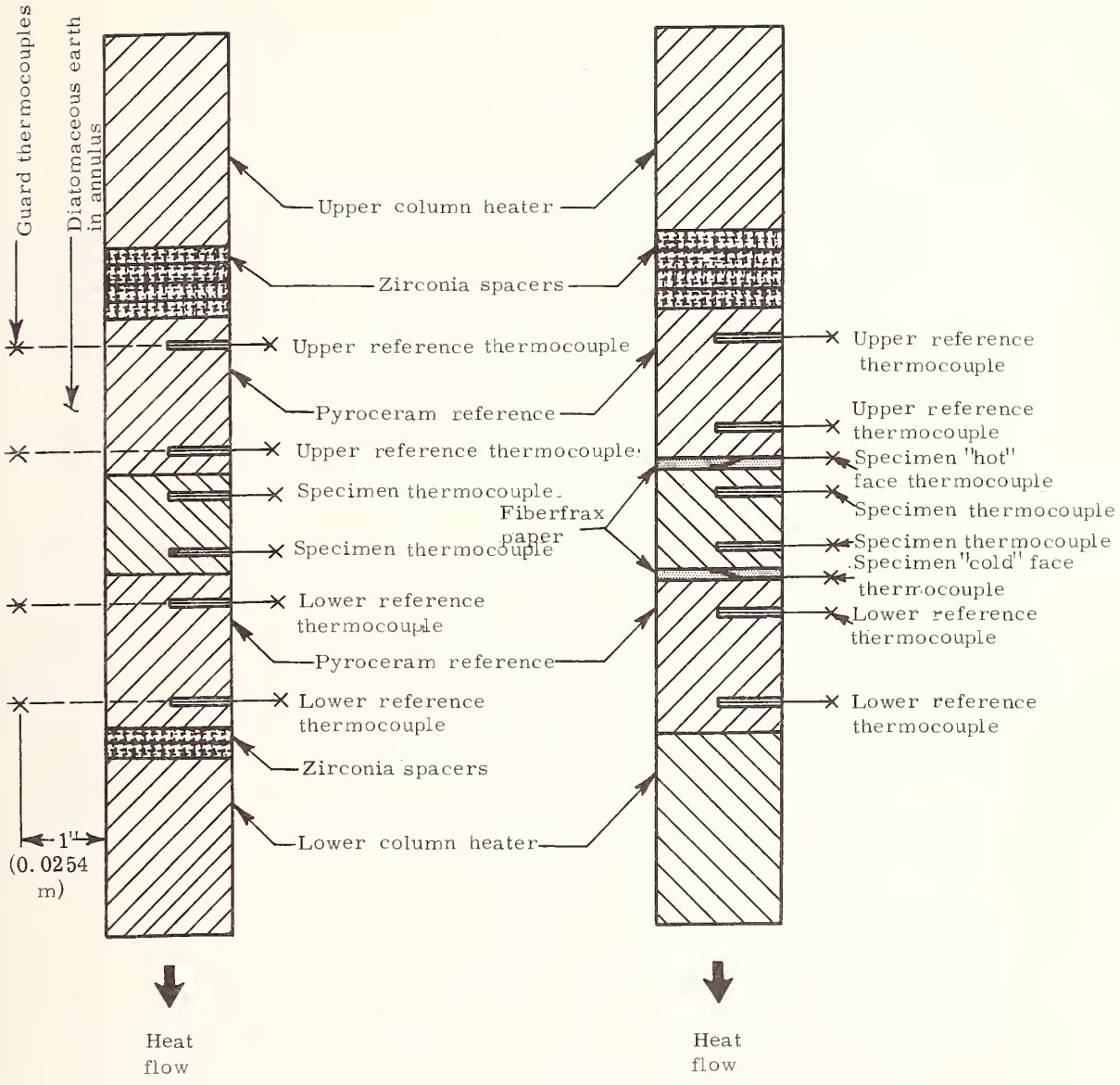

(a) Standard buildup for thermal conductivity evaluations

(b) Buildup for specimen 42-3 (second run) - attempt to measure variation in thermal conductivity across thickness

Figure 3. Schematic diagram of comparative rod apparatus specimen configuration

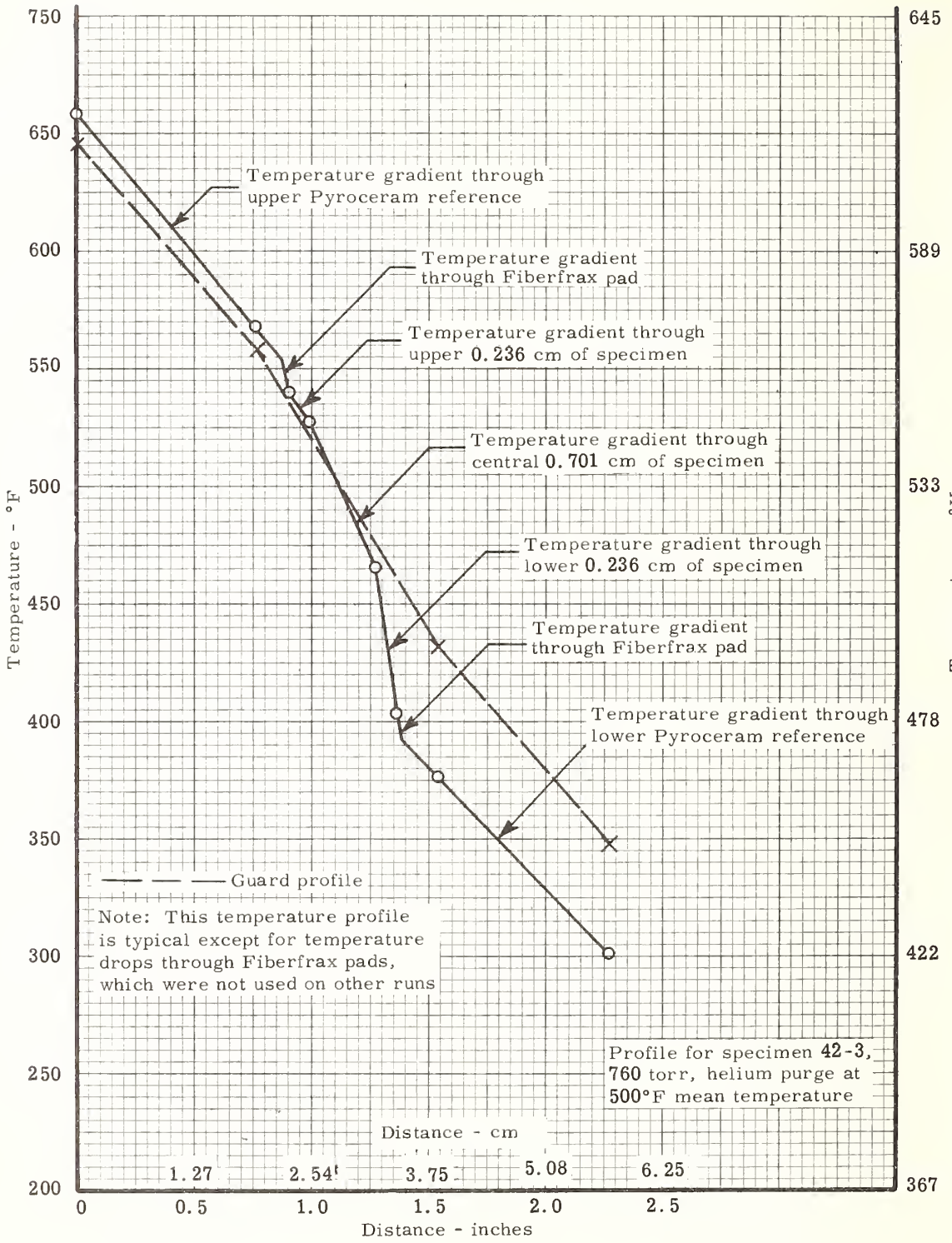

Figure 4. Typical temperature profile for data obtained on comparative rod apparatus using code 9606 pyroceram references

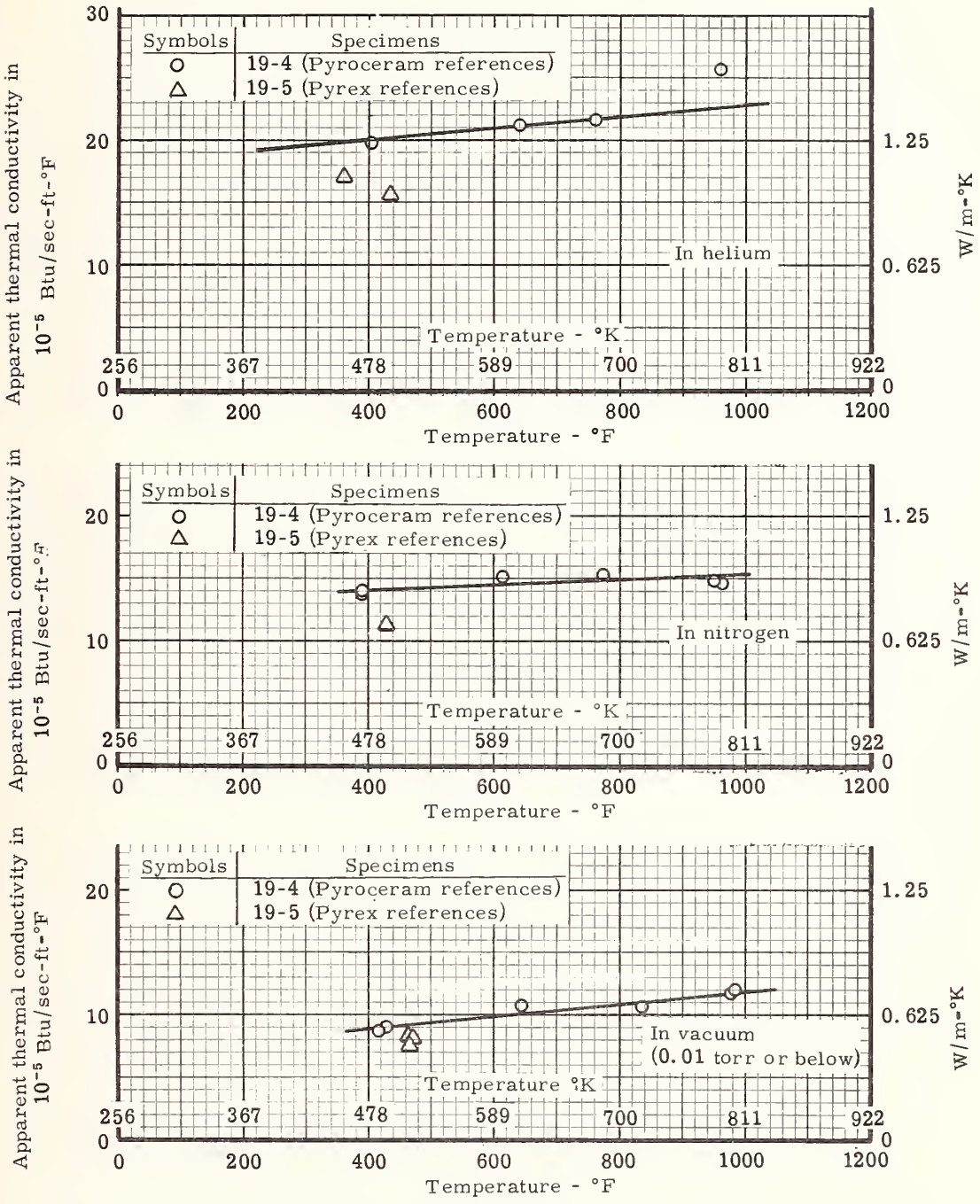

Figure 5. The apparent thermal conductivity of phenolic-nylon char of 0.88 porosity (19 lb/ft^3 virgin density) in vacuum, nitrogen, and helium

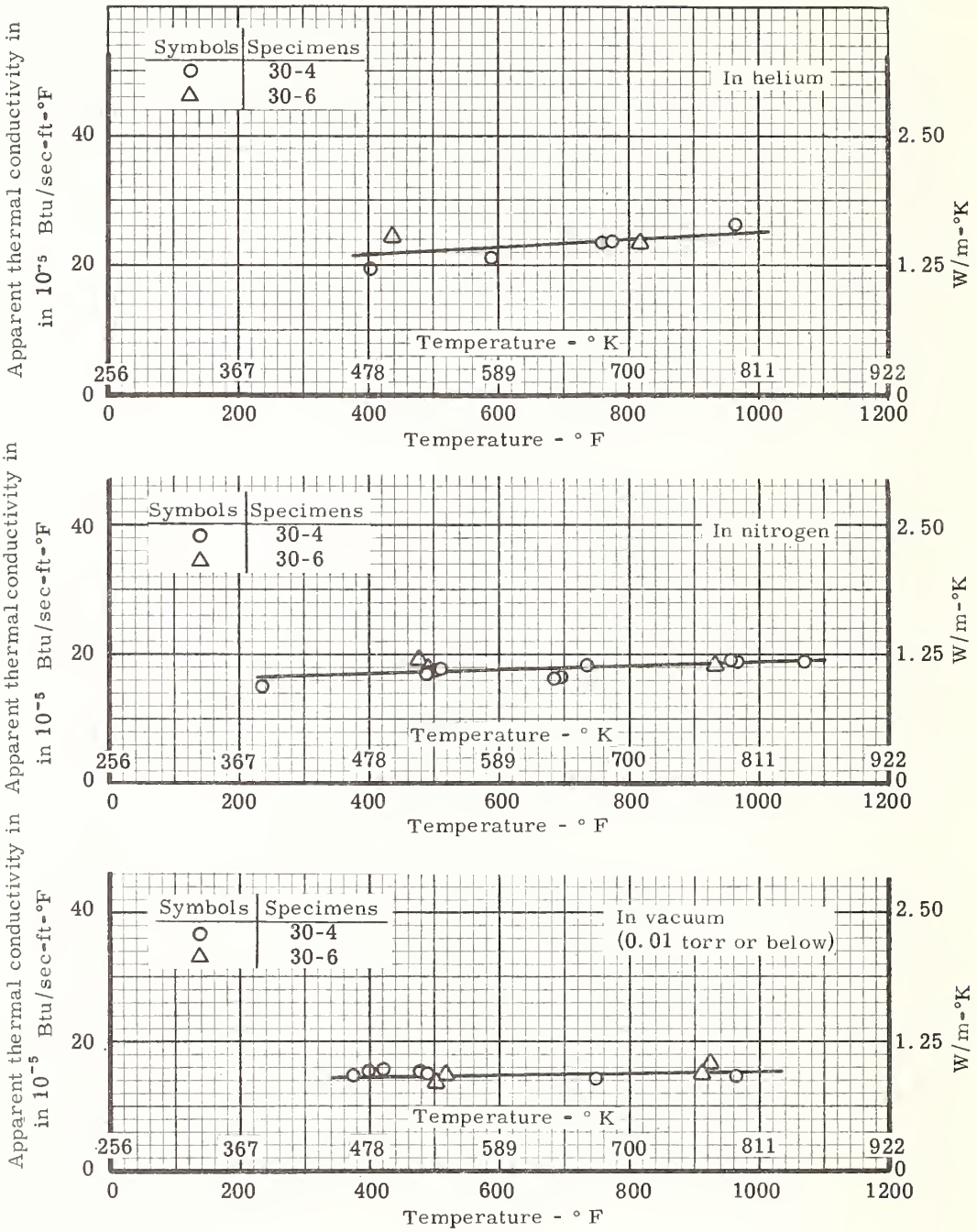

Figure 6. The apparent thermal conductivity of phenolic-nylon char of 0.82 porosity (30 lb/ft^3 virgin density) in vacuum, nitrogen, and helium

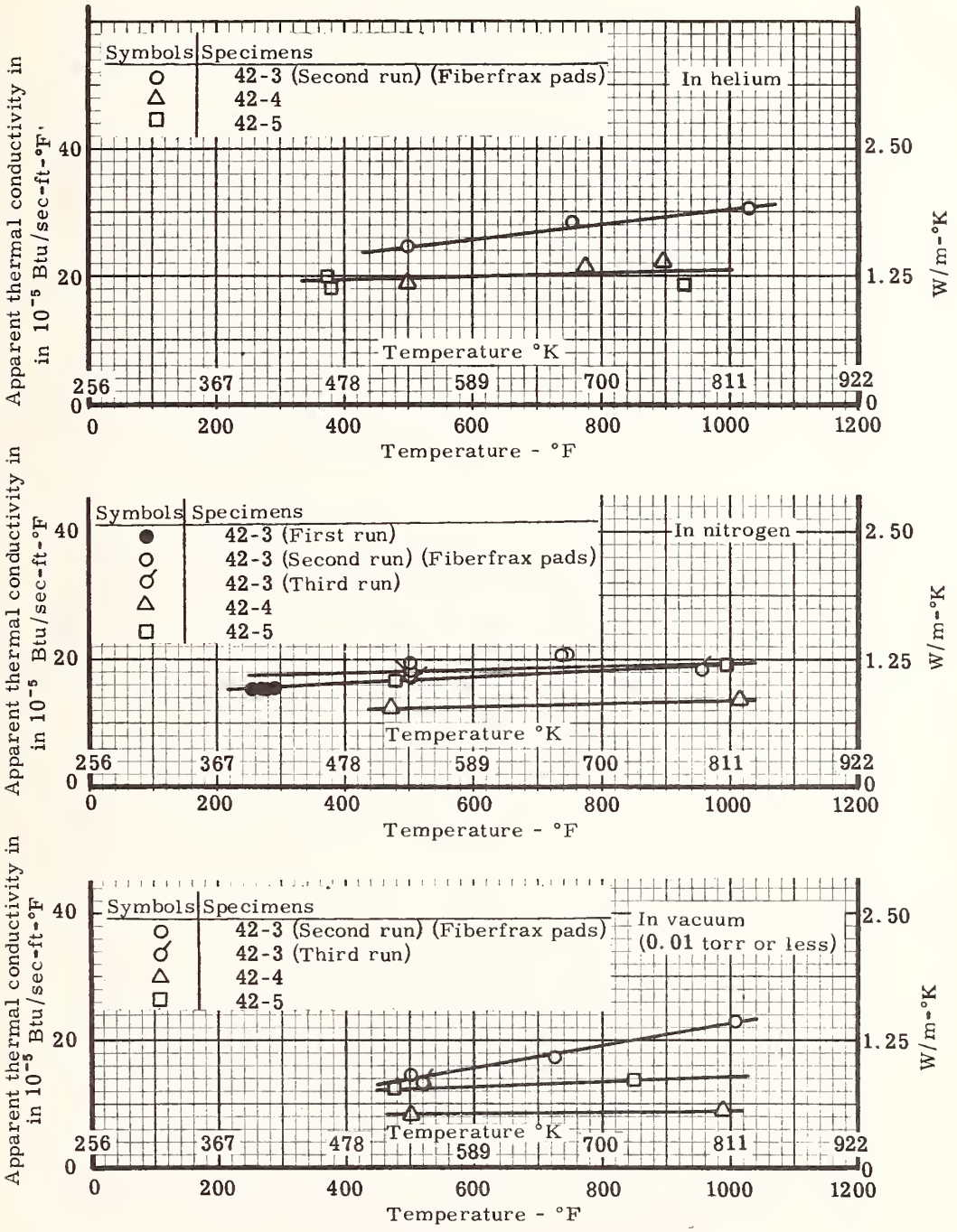

Figure 7. The apparent thermal conductivity of phenolic-nylon char of 0.79 porosity (42 lb/ft^3 virgin density) in vacuum, nitrogen, and helium

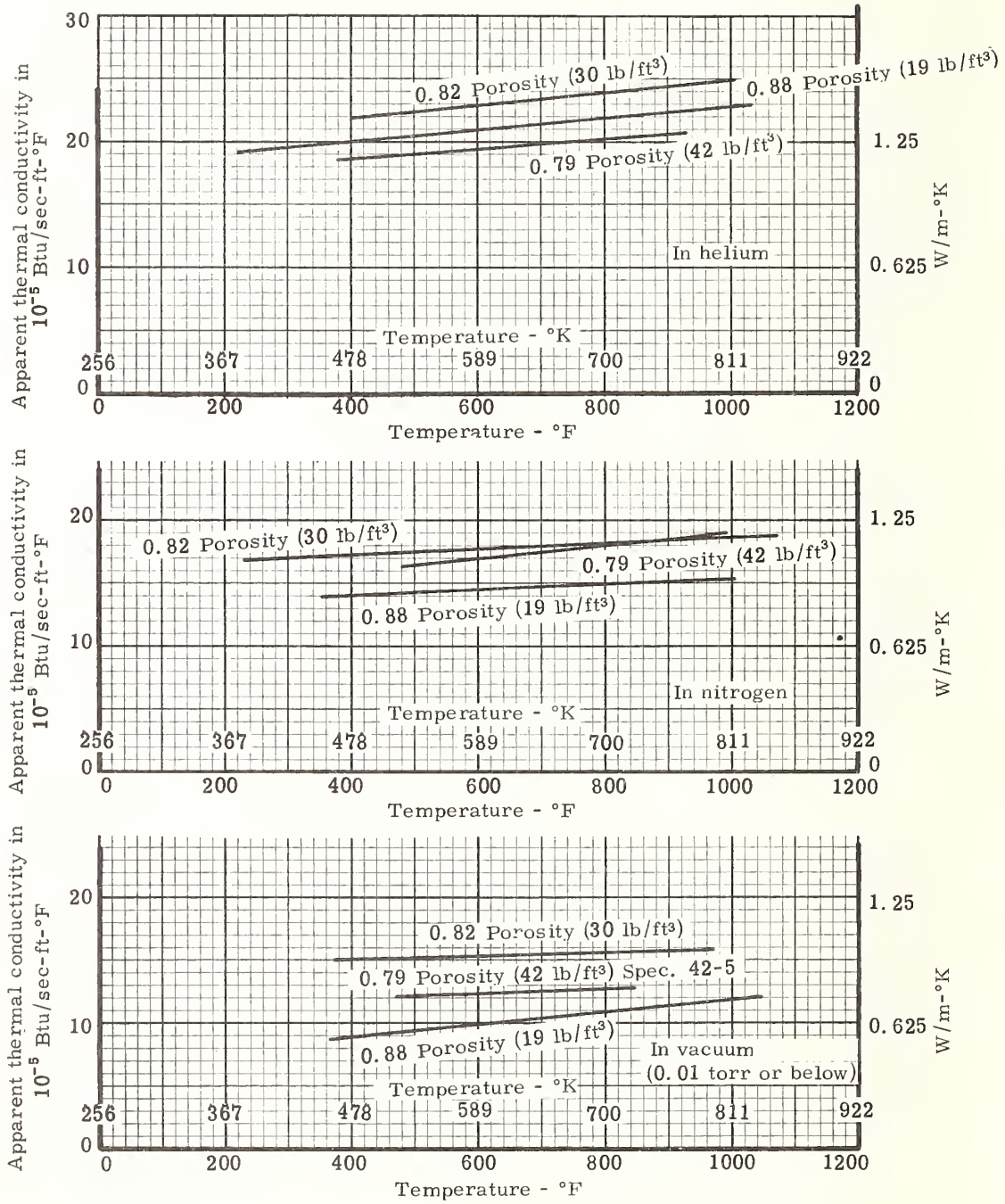

Figure 8. Composite plot of the apparent thermal conductivities of the three phenolic-nylon chars in vacuum, nitrogen, and helium

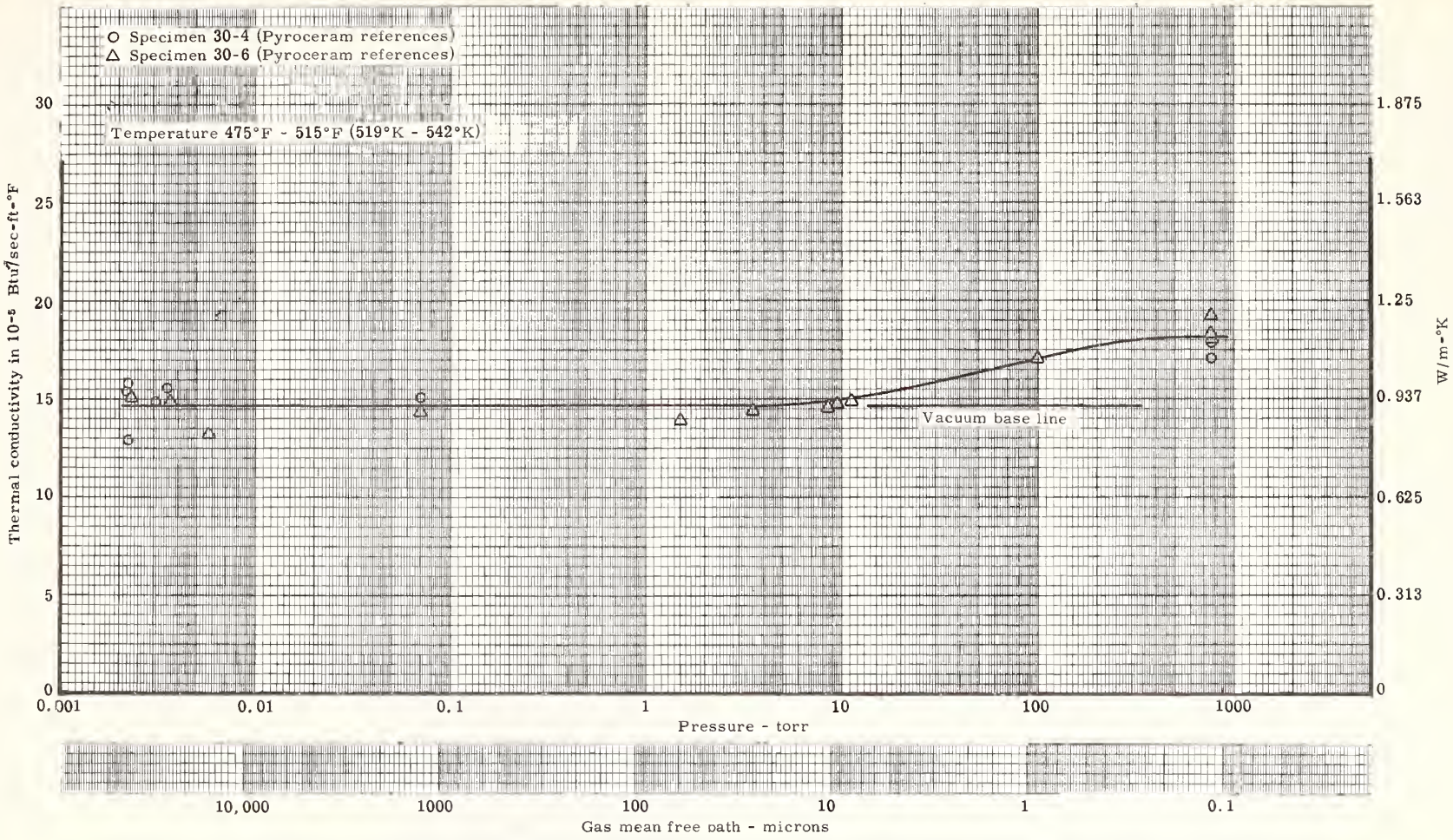

Figure 9. The apparent thermal conductivity of phenolic-nylon char of 0.82 porosity (30 lb/ft^3 virgin density) versus pressure in a nitrogen atmosphere

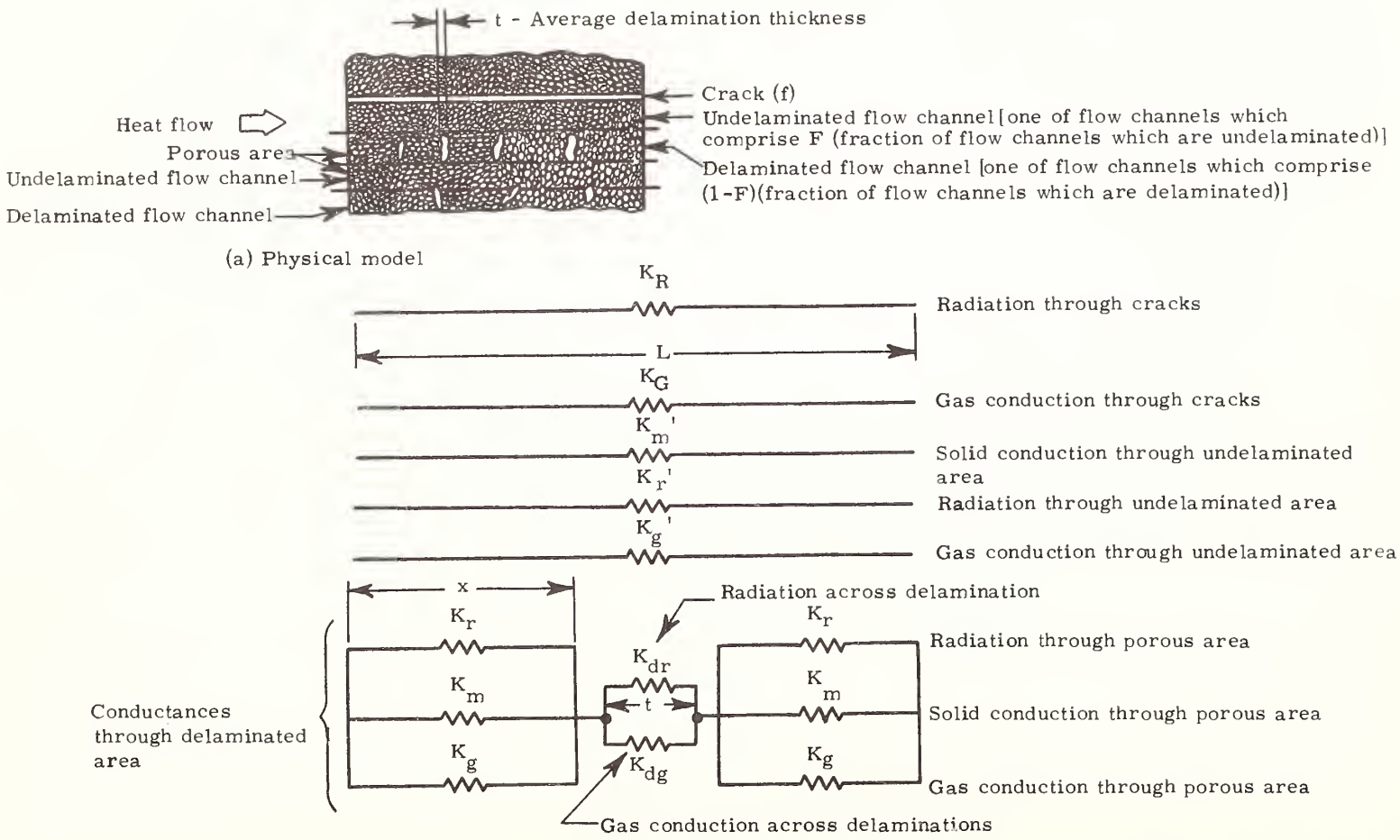

Figure 10. Sketches of physical model and thermal model for porous char

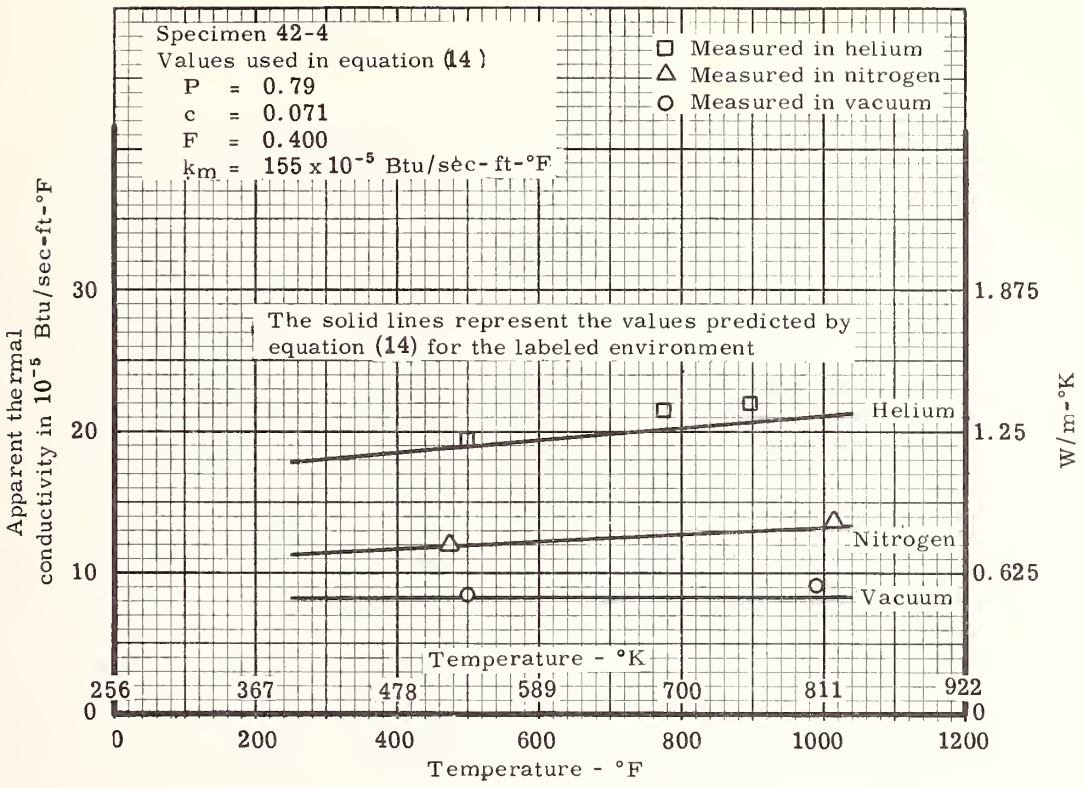

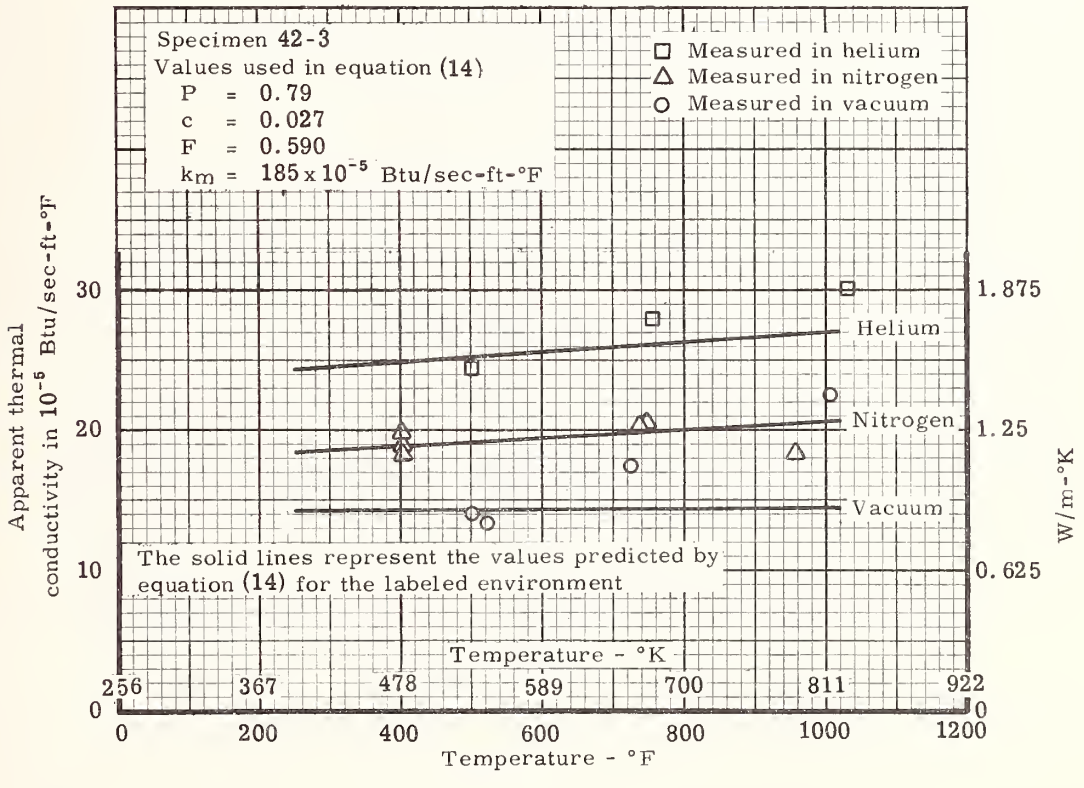

Figure 11. Comparison of the predicted variation in apparent thermal conductivity with temperature with the measured values for specimens 42-3 and 42-4

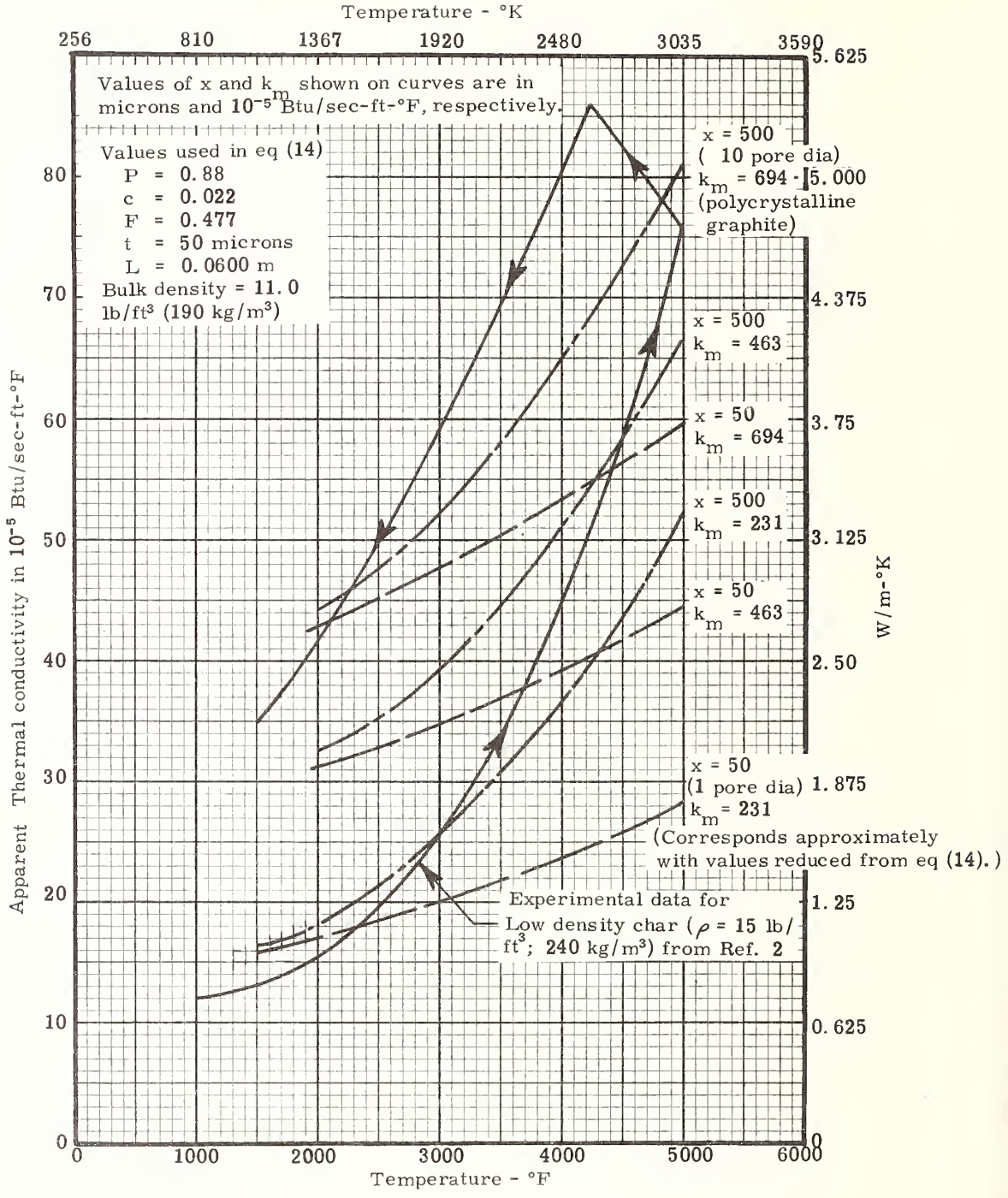

Figure 12. Comparison of the high temperature apparent thermal conductivity predicted by equation (14) for a nitrogen environment with prior data

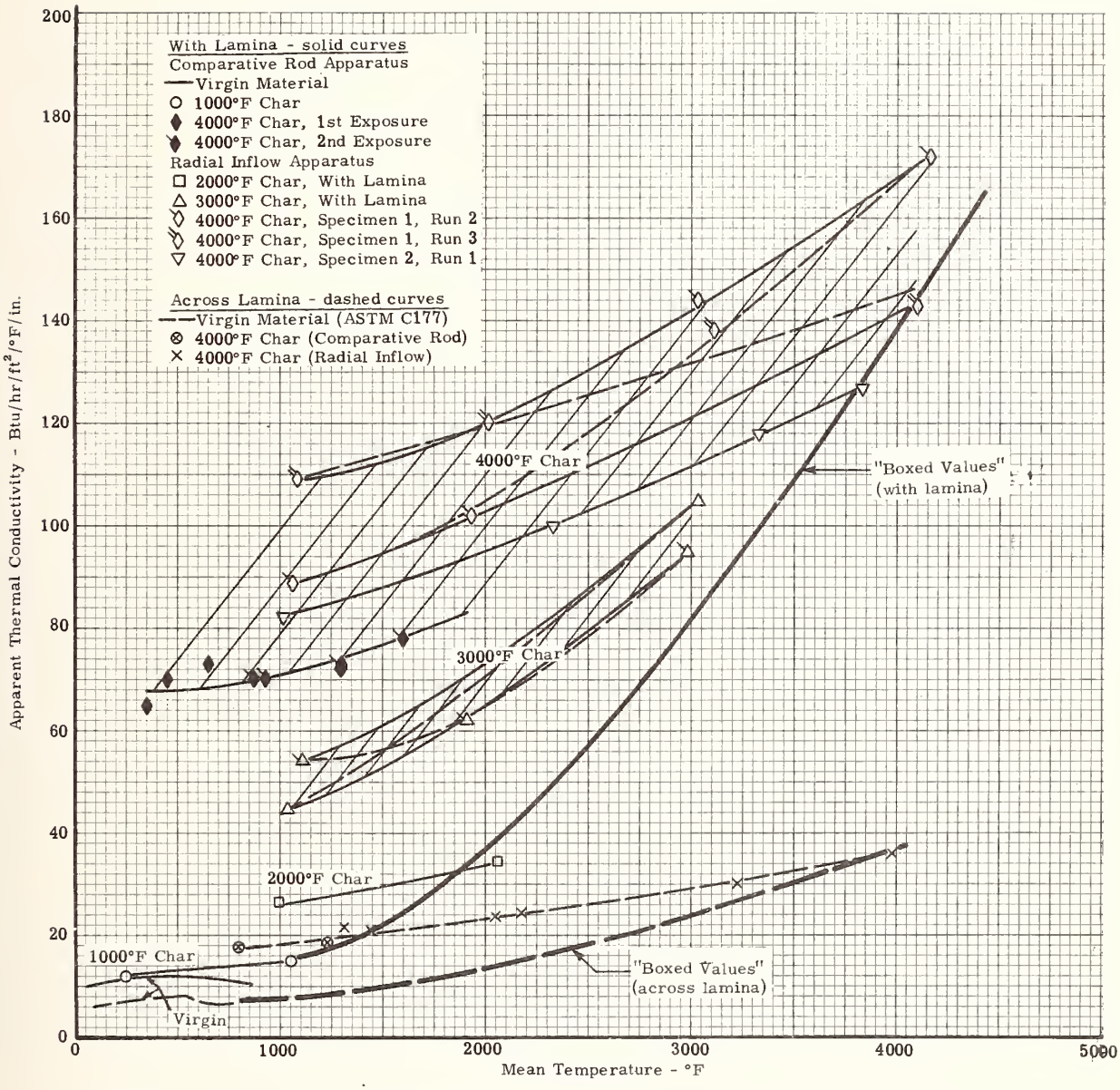

Figure 13. Apparent thermal conductivity of MX4926 (Carbon Filled 30 Phenolic-Carbon Fabric- see AFML-TR-65-133) Precharred at Progressively Higher Temperatures

Biological Specimen Holder for Thermal Diffusivity Determinations

Floyd V. Matthews, Jr.

Agricultural Engineering Department
University of Maryland
College Park, Maryland 20742

and

Carl W. Hall[1]
Agricultural Engineering Department
Michigan State University
East Lansing, Michigan 48823

A specimen holder was designed to hold a cylindrical heat source and a cylindrical potato section in intimate and uniform contact with each other during heat transfer experiments. Appropriate boundary conditions were maintained and thermocouples were placed in desired locations. A finite difference computer program and the recorded temperature history were used to calculate the thermal diffusivity of the potato section.

The heat transfer methods combined with the finite difference method of data analysis had the advantages of speed, simplicity, ease of application to other products, and accuracy. Depending upon test duration, approximately four heat treatments could be completed in an hour. No difficult laboratory preparations or techniques were involved. Other biological products could be adapted to the specimen holder, and large masses were not required. Random errors were cancelled by the finite difference method, but a continuous error of $+1^{\circ}F$ in temperature measurement was found to cause an error of -0.5% or less in the value of thermal diffusivity.

Key Words: Biological specimen holder, computer program, finite difference, potato heat treatment, thermal diffusivity.

1. Introduction

Commercial heat processing of vegetables is usually a transient process during which the physical and thermal properties are changing (3, 7, 11)[2]. If an engineer is to calculate the net energy requirements of the process, he must know the values of the thermal properties over the working range. In the past, he has found it necessary to make vague determinations of the thermal properties and also to assume that these properties remain constant during the processing. With the present development of the science of heat transfer, an engineer should not have to rely on these estimates and assumptions.

Because some biological materials tend to undergo physical and/or chemical changes as heat is applied or removed (4, 9), a determination of the thermal properties should be fast enough to precede such changes. Water is evaporated when heat is applied to most biological materials. If much heat is applied, the final material is not the same as the initial material; the loss of moisture may cause a change in the thermal properties.

Some researchers have used a guarded hot plate, a steady state device, to determine the thermal conductivity of meat (5). Because the guarded hot plate method is of long time duration, at normal processing temperatures a biological product would probably be cooked before the thermal conductivity could be determined. Others have used a modified Cenco-Fitch apparatus, a transient state device, to determine the thermal conductivity of meats, fruits, and vegetables (2, 10). The modified Cenco-Fitch method duplicates the transient process but is subject to errors of approximately 5% (2).

[1] Associate Professor and Professor and Chairman, respectively.

[2] Figures in brackets indicate the literature references at the end of this paper.

Therefore, when the thermal and/or physical properties of a vegetable vary with the heat absorbed, one must use other means to determine them.

2. Biological Specimen Holder

2.1 Description

Beck (1) has developed a method for simultaneously determining the thermal conductivity and specific heat of a material. A heated piece of material with known thermal characteristics is held in uniform contact with material of unknown thermal properties. The temperature histories of the two materials are used to calculate the thermal properties of the unknown material.

Based on the idea above, a biological specimen holder was designed to hold a cylindrical heat source and a cylindrical potato (solanum tuberosum) section in intimate and uniform contact with each other for the duration of an experiment, figure 1. Each half of the specimen holder was made from a 0.076m (3 in.) length of standard 0.1524m (6 in.) diameter steel pipe. The stationary half of the holder was welded to channel iron. A flat base plate and angle iron rails were also welded to the channel iron. V-grooved wheels mated with the angle iron rails maintained accurate alignment in all planes between the movable and stationary halves. The longitudinal displacement of the V-grooved wheels from each other facilitated the rapid installation of the movable half onto the rails. During the experiments a constant pressure was maintained at the heat source-potato section interface by rotating the specimen holder 90^{o} and supporting the holder on the channel iron, figure 2.

A microswitch and its trip lever were fastened to the stationary half and movable half respectively, figure 1. When the halves of the specimen holder were brought together for an experiment, the microswitch completed a circuit for an electric interval timer and for an indexing pen on each recording potentiometer. The microswitch was adjusted to close the circuit when the heat source and potato section made contact.

The insulation for the specimen holder was a polyurethane type with a low thermal conductivity. A 0.1016m (4 in.) length of insulation was machined to a snug fit in the bore of each half of the holder. Mating grooves were machined into the halves of insulation to minimize any air current and convection heat losses. A hole, 0.0246m (31/32 in.) diameter and 0.0254m (1 in.) deep, was machined into the face of the insulation of the movable half of the specimen holder; the potato sections were installed in the hole for the experiments. A hole of the same dimensions was machined into the face of the insulation for the stationary half of the specimen holder; a silicone rubber heat source was installed in the hole for the experiments, figure 1. When an electric heating element was used for the heat source, the temperatures were too high for the stability of the polyurethane insulation; a glass foam insert was made to go between the heating element and the polyurethane insulation, figure 3.

A thermocouple silver soldered to the face of the metal cylinder indicated the temperature at $X = 0$ when the cylinder was used for the heat source. To minimize thermocouple conduction errors, the lead wires were placed across the face of the heat source and wound partially around the circumference of the heat source before entering the insulation of the biological specimen holder. Thermocouples were also located in the body of the specimen at $X = X$ and at the end of the specimen noted as $X =$ infinity in the boundary conditions.

3. Determination of Thermal Diffusivity

3.1 Finite Difference Equation

Considering a body with the following characteristics,

1. λ independent of position and temperature,
2. one dimensional heat flow in the X-direction, and
3. no internal heat generation,

the general heat conduction equation reduces to:

$$a\left(\frac{\partial^2\theta}{\partial X^2}\right) = \frac{\partial\theta}{\partial t} \tag{1}$$

A body subjected to a heat transfer process may be divided into nodal points that are a distance ΔX apart. About any node an energy balance can be written and expressed in finite difference form (8). Temperatures in the body can be expressed with respect to position and time by means of subscripts and superscripts n and t respectively. For one dimensional heat flow in the X-direction in a finite body, nodes are located at $X = 0$, $X = X$, and $X = L$. Temperature boundary conditions may be

specified at X = 0 and at X = L.

In finite difference form, eq (1) becomes:

$$a\left(\frac{\theta_{n-1}^{t+1} - \theta_n^{t+1} + \theta_{n+1}^{t} - \theta_n^{m}}{(\Delta X)^2}\right) = \frac{\theta_n^{t+1} - \theta_n^{t}}{\Delta t} \tag{2}$$

Equation (2) can be solved for the temperature at node n for time t = t+1.

$$\theta_n^{t+1} = \frac{\theta_{n-1}^{m+1} + \theta_{n+1}^{m} + \theta_n^{m}(M-1)}{M+1} \tag{3}$$

where:

$$M = \frac{(\Delta X)^2}{a\Delta t} \quad \text{a dimensionless number} \tag{4}$$

A computer program using finite differences and based on the method of Beck (1) was used to calculate thermal diffusivity from temperature measurements. The basic operations of the program were:

1. The magnitude of ΔX was determined.
2. At the first and last node, a programmed time step was used to calculate temperatures with respect to time:
   t, t+1,...t+i
   where: (t+1) - t = programmed time step
   (t+i) - t = time interval of data
3. The finite difference eq (3) was used with an assumed a to calculate temperatures at each node. Calculations were made in two "passes"; an "odd pass" proceeding from first to last node and an "even pass" proceeding from last to first node.
4. The method of least squares was used to minimize with respect to a the difference between the calculated and measured temperatures.
5. The change in diffusivity was calculated and added to the assumed a to obtain a new value of a.
6. The new value of a was used in an iteration procedure to determine a more accurate value for a.

The above program was based on the following assumptions:

1. Initial and boundary conditions of the body were:
   a. $\theta\ (X,0) = 0$
   b. $\theta\ (0,t) = \theta_1$
   c. $\theta\ (\infty, t) = 0$
2. One dimensional heat transfer.
3. Constant a with respect to time and temperature.
4. The last node was at $X = \infty$.

3.2. Discussion of Results

The biological specimen holder was used to obtain heat transfer data from approximately 150 tests on potato sections. The equipment has also been used to obtain similar data on other agricultural products. The thermal diffusivities of the potatoes, as calculated by the computer program, were within the range of values of other biological materials (6).

Thermal diffusivity data could be obtained during the first 50 seconds of heat treatment; before moisture changes and physical reactions became a problem. This overcomes one of the objections to the guarded hot plate when used at cooking temperatures for biological materials. Because the temperature boundary conditions at X = 0 did not have to be constant, heat loss from the sides of the heat source to the insulation was not critical. Many of the root mean square values of the difference between the actual temperatures and the calculated temperatures were less than 0.28°C(0.5°F). The recording potentiometers had a permissible error of 0.33°C(0.6°F). Random errors were cancelled by the finite difference method, but a continuous error of + 0.55°C (1°F) temperature was found to cause an error of -0.5% or less in the value of the thermal diffusivity. In the literature reviewed, errors of 5% were not uncommon in the determination of thermal properties of biological materials.

The heat transfer methods used in the experiments combined with the finite difference method of data analysis had the advantages of speed, simplicity, ease of application to other products, and accuracy. Depending upon test duration, approximately four heat treatments could be completed in an hour. No difficult laboratory preparations or techniques were involved. Other biological products could be adapted to the specimen holder and large masses were not required.

4. References

(1) Beck, James V., Calculation of thermal diffusivity from temperature measurements. Transactions of the ASME, Journal of Heat Transfer, Series C, 85, 181-182 (1963).

(2) Bennett, A. H., Chace, Jr., W. G. and Cubbedge, R. H., Estimating thermal conductivity of fruit and vegetable components --the Fitch method. ASHRAE Journal, 4, No. 9 80-85 (1962).

(3) Kaczmarzyk, Leonard M., Fennema, O. and Powrie, William D., Changes produced in Wisconsin green snap beans by blanching. Food Technology 17, 943-946 (1963).

(4) Matthews, Floyd V., Jr., Thermal diffusivity by finite differences and correlations with physical properties of heated potato. Thesis for degree of Ph D, Michigan State University, East Lansing (unpublished) (1966).

(5) Miller, Herbert L. and Sunderland, J. Edward, Thermal conductivity of beef. Food Technology 17, 490-492 (1963).

(6) Parker, Rayburn E. and Stout, B. A., Thermal properties of tart cherries. American Society of Agricultural Engineers Paper No. 66-337. Saint Joseph, Michigan. 22 pp. (1966).

(7) Personius, Catherine J. and Sharp, Paul F., Adhesion of potato-tuber cells as influenced by temperature. Food Research 3, 513-524 (1938).

(8) Schneider, P. J., Conduction Heat Transfer. Addison-Wesley, Inc., Reading, Mass. 395 pp. (1955).

(9) Simpson, Jean I. and Halliday, Evelyn G., Chemical and histological studies of the disintegration of cell-membrane materials in vegetables during cooking. Food Research 6, 189-206 (1941).

(10) Walters, Roger E. and May, K. N., Thermal conductivity and density of chicken breast muscle and skin. Food Technology 17, 808-811 (1963).

(11) Weiser, T. Elliot and Stocking, C. Ralph, Histological changes induced in fruits and vegetables by processing. Advances in Food Research 2, 297-342 (1949).

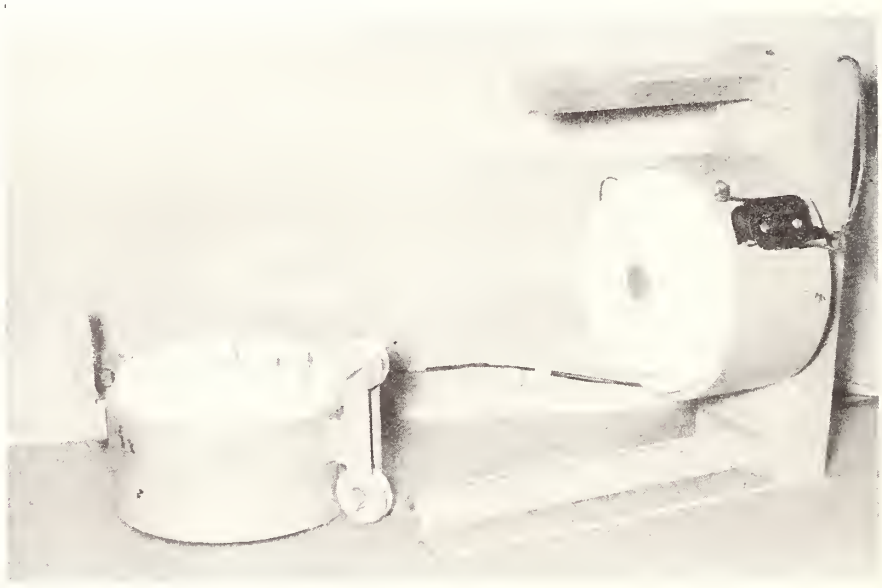

Figure 1. Biological specimen holder with heat source mounted in the center of the white insulation, and with a microswitch mounted on the cylindrical frame.

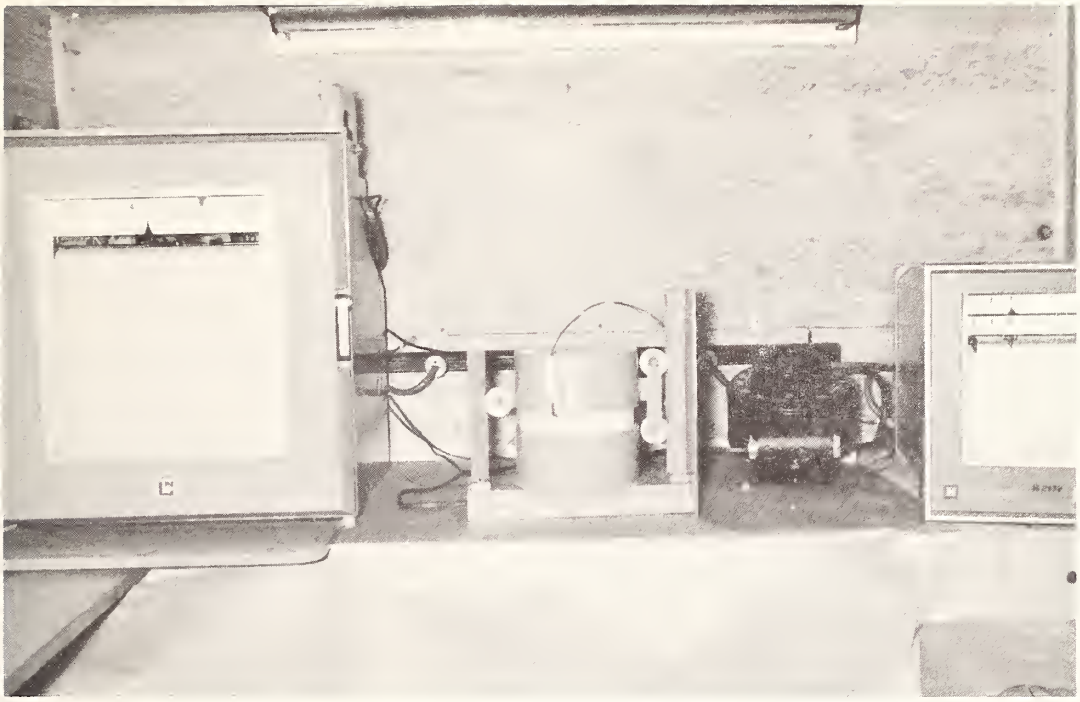

Figure 2. From left to right; recording pen potentiometer, biological specimen holder in testing position, variable transformer, and a recording pen potentiometer.

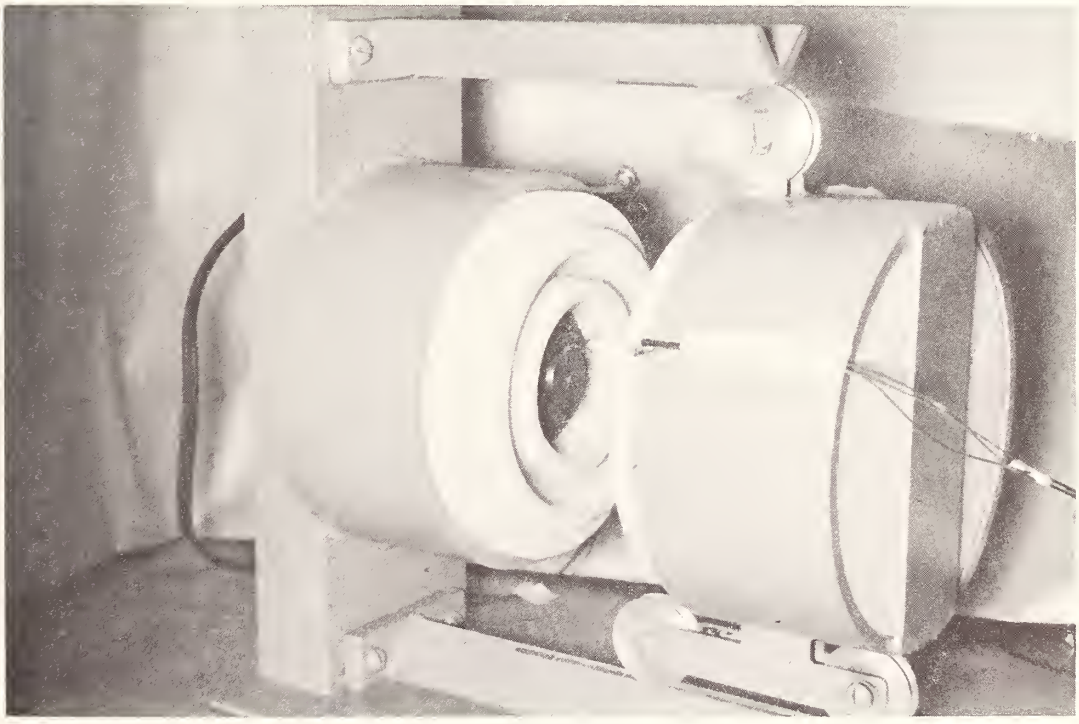

Figure 3. Biological specimen holder just prior to closing for a heat transfer test.

Thermal Diffusivity of Actinide Compounds[1]

J. B. Moser and O. L. Kruger[2]

Argonne National Laboratory
Argonne, Illinois 60439

The thermal diffusivity of the carbides of uranium and plutonium was measured from 500 to 1500°C by means of the USNRDL flash technique. A ruby laser was used as the pulsing source while the disk-shaped specimens were heated in a high vacuum resistance furnace. The rear surface temperature of the specimen was monitored by an optical detector which contained a dual lead sulfide photoconductor in a temperature compensating circuit. The variations in thermal diffusivity as a function of effective carbon content and uranium-plutonium ratio are discussed and compared with results of other investigations.

Key Words: Flash technique, heat conductivity, plutonium carbide, thermal diffusivity, uranium carbide, uranium-plutonium carbide.

1. Introduction

The monocarbides of uranium and plutonium are of considerable interest as fuels for fast reactors, therefore the thermal diffusivity of these materials was measured to high temperatures using the well-known technique developed by Parker and his associates at USNRDL [1][3]. This method was found to be ideally suited for glove box adaptation necessary in plutonium research. In previous work by the authors [2,3] at temperatures from 25 to 700°C, the heat capacity was also measured and the thermal conductivity was calculated. Heat capacity measurements by this technique at high temperatures have not been successful to date, however data for UC and PuC are available [4,5].

The reactor designers are particularly interested in the diffusivity parameter per se at high temperatures, because nuclear fuels are subjected to transient heating in reactor excursions and their thermal performance is then governed by the thermal diffusivity. In order to evaluate the amplitude and phase response of the center temperature to these transient disturbances, computer programs using the diffusivity parameter are useful [6].

The thermal diffusivity of UC of variable density, and PuC, as well as the $(U_{0.8}Pu_{0.2})C$ solid solution was measured. The sintered specimens were of approximately 80% theoretical density and contained small amounts of oxygen and traces of nitrogen. They were prepared by crushing, cold-pressing and sintering arc-cast material. All samples were characterized by chemical analyses, geometrical density measurements and micrographic examinations.

2. Experimental

2.1 Apparatus

The technique and apparatus used in this work have been described adequately [1,7] but a few of the experimental details are given below. A block diagram of the apparatus is shown in figure 1. The specimen was placed in the high temperature vacuum furnace and the front-face was illuminated evenly by the ruby laser mounted on the glove box directly above the furnace. No light from the laser flash was allowed to pass to the infrared detector which was located below the furnace outside the glove box. The water-cooled laser head contained a 1.43 cm ruby rod pumped by a helical flashtube. The system was capable of 30 joules output and was usually fired at 10 to 20 joules with a pulse duration of 500 microseconds. The delay circuit of the oscilloscope was used to trigger the laser after the CRT trace had started. The surface of the disk was coated with colloidal graphite to maintain a uniform emissivity. The lead sulfide detector contained two cells but only one was exposed to the radiation emanating from the specimen. The detection system contained filters which limited its spectral range from 2.0 to 2.6 microns. Collimating lenses made it possible to focus on an area of 0.16 cm diameter on the back of the sample, excluding all radiation coming from other portions of the furnace. Figure 2

[1]Work performed under the auspices of the U. S. Atomic Energy Commission.
[2]Associate Ceramist and Associate Metallurgist, respectively.
[3]Figures in brackets indicate the literature references at the end of this paper.

shows a circuit diagram of the dual cell system. The temperature-compensating circuit kept the cold voltage constant in spite of ambient temperature changes. The output of the circuit was about 10 volts which was bucked with a null circuit and reduced to less than 0.1 volts. Figure 3 shows the calibration curve of the instrument determined from a black-body calibration furnace of standard design. Filters of 75% and 95% absorption extended the low temperature range of the unfiltered unit. The sample temperature was measured by means of a digital voltmeter of 10 megohm impedance to the nearest millivolt. A signal strength of 3 to 5 mV per °C was obtained from the PbS detector which made further amplification unnecessary both for the temperature and the diffusivity measurements. The oscilloscope was used for all diffusivity measurements in the floating differential mode of essentially infinite impedance. The near linear range of the calibration curves was usually used for the diffusivity measurements in order to prevent distortion of the oscilloscope traces. Many measurements were also taken where the output of the ranges of the lead sulfide detector overlapped. Temperatures above 800°C were also measured by means of a disappearing filament optical pyrometer which was sighted on a black-body hole in the sample holder located adjacent to the specimen. The temperatures reported were those of the pyrometer reading above 1000°C and those of the infrared cell below this temperature. When the readings were taken at the same time, the maximum difference between the two devices was 10°C. A standard diffusivity disk taken from an alumina thermal conductivity specimen obtained from Dynatech Inc. was used to calibrate the apparatus. Figure 4 shows the results of these diffusivity determinations compared to the values calculated from the Dynatech thermal conductivity curve. A maximum error of $\pm$ 7-1/2% and an average accuracy of $\pm$ 5% was obtained; a calculation of the experimental precision by summing the errors in the various measurements also yielded $\pm$ 5% error.

2.2 Specimen Characteristics

All the compounds investigated were in the form of disk-shaped specimens 1.83 cm diameter and approximately 0.5 cm thickness which were subsequently lapped down to 0.2 to 0.3 cm thickness for the measurement. The carbides were prepared by fusion of 99.5 wt.% pure metal with spectrographically pure carbon in an arc furnace [8]. The oxygen and nitrogen content of the arc melted material was usually below 0.02 wt.%. The sintered specimens gained in oxygen and nitrogen content during the fabrication process as shown in Table 1.

Table 1. Specimen characteristics.

Material	UC Arc-Cast	UC Sintered 1800°C	$U_{0.8}Pu_{0.2}C$ Sintered 1800°C	PuC Sintered 1400°C
Density % Theoretical	99.0	78.8	74.8	83.8
Carbon wt.%	4.93	4.69	4.66	4.12
Oxygen wt.%	0.0117	0.106	0.202	0.567
Nitrogen wt.%	0.0021	0.0228	0.0206	0.0440
Effective Carbon wt.%	4.94	4.79	4.83	4.58
Effective Carbon at.%	50.8	49.9	50.2	48.9

In addition to carbon, the major impurities of oxygen and nitrogen must be considered since they dissolve in the monocarbide to a considerable extent. A useful quantitative concept here is the equivalent carbon content obtained by summing the oxygen and nitrogen contents as follows:

$$\text{Equivalent wt.\% C} = \text{wt.\% C} + 12/16\ \text{wt.\% O} + 12/14\ \text{wt.\% N}$$

Single phase uranium monocarbide and mixed monocarbide of U/Pu ratio 4:1 can only be obtained if the nonmetal atom content does not exceed 50 at.%; for PuC the upper limit is 46.5 at.%.

The arc-cast uranium carbide had an equivalent carbon content of 4.94 wt.% C (equal to 50.8 at.% C). A small amount of second phase consisting of UC_2 was found in the grains of this specimen (see figure 5). The sintered uranium carbide specimen contained more oxygen but less carbon than the arc-cast material. Whereas the effective carbon content of the arc-cast specimen was only 0.01 wt.% higher than the actual carbon content, this difference in the sintered UC amounted to 0.1 wt.%. Thus an effective carbon content of 4.79 wt.% is obtained on the sintered material which is equivalent to 49.9 at.% C. This results in a formula ratio of $U_{0.50}C_{0.49}O_{0.01}$ if the oxygen is considered separately. A photomicrograph of this sample is shown in figure 6 which gives a good indication of the pore configuration. No second phase was observed which is in good agreement with the calculated composition.

Compounds containing plutonium generally have a greater affinity for oxygen, and the increase in oxygen pick-up with increasing plutonium content is shown in Table 1. The mixed carbide of nominal U/Pu ratio of 4:1 contained 0.2 wt.% oxygen. The calculated effective carbon content of this material was 4.83 wt.% which is considerably greater than the actual carbon content of 4.66 wt.%. The effective

atomic percentage of carbon is 50.2 resulting in stoichiometric $(U_{0.80}Pu_{0.20})C_{1.00}$ or $(U,Pu)_{0.50}C_{0.485}O_{0.015}$ if the oxygen is taken into account separately. The pore configuration of this specimen is shown in figure 7. Since the nonmetal to metal ratio does not exceed one, no significant amounts of second phase would be expected and are in fact not observed in the photomicrograph. Since the plutonium monocarbide was expected to pick up oxygen during specimen fabrication, the carbon content of the arc-melt was purposely kept low. In spite of this precaution, the oxygen pick-up brought the effective carbon above 46.5 at.%. The effective carbon content of this material was 4.58 wt.% which gives an effective atomic percentage of carbon of 48.9 at.%. The atomic ratios are indicated by the formula $Pu_{0.51}C_{0.445}O_{0.045}$. A photomicrograph of this structure seen in figure 8 shows approximately 10% plutonium sesquicarbide (Pu_2C_3) phase.

3. Results and Discussion

All of the present materials except the arc-cast uranium monocarbide, contained enough oxygen and nitrogen to make a calculation of porosity and heat capacity unrealistic, since the lack of stoichiometry and second phase content of the material, would influence both of these properties. For this reason it was decided to analyze the data directly in terms of diffusivity rather than convert them to conductivity as is often done.

The radiation heat loss correction developed by Cowan [9] was applied to all the data. The PuC specimen was first run in vacuum and it was noted that vaporization occured above 1200°C. This specimen was subsequently reduced from an original thickness of 0.31 to 0.26 cm and tested in argon at 1.3 atm pressure up to 1350°C. Even though the thickness and heat loss parameters were now different, the data points fell on the earlier curve.

As has been discussed by the authors before [3] the porosity correction for diffusivity is considerably less than that for thermal conductivity. For the present work, the Maxwell correction was modified to read

$$a_T = \left(\frac{2 + P}{2} \right) a_M$$

where a is diffusivity, P the porosity, and the subscripts T and M denote theoretical and measured values, respectively. This correction was checked for UC where the arc-cast specimen of 99% theoretical density was compared with the sintered one of 79%. At temperatures above 700°C, this correction was found to be in good agreement with the data and the corrected 79% UC values fall on the curve of the arc-cast UC. At lower temperatures this correction did not account for the increase in thermal diffusivity of the arc-cast UC; this is at present thought to be due to the presence of impurities. In the case of the mixed carbide and the PuC the porosity correction would increase the experimental values about 10%. Since the rank of the curves is not changed by these corrections the data shown in figure 9 were not corrected to theoretical density. The order of increase seen here has been found previously by Leary and coworkers [10] who measured the thermal conductivity of UC, $(U_{0.8}Pu_{0.2})C$ and PuC from 200 to 400°C. Considerable work has been done in electrical conductivity measurements [10-12] on well characterized specimens of various purity levels. Comparison of this data shows that the same rank is followed in electrical conductivity as has been observed here in heat transfer. The lower electron transport capability of PuC is probably due to the fact that it is a defect structure, whereas the UC has a much higher electrical conductivity and a higher thermal conductivity as well. PuC could also have a lower lattice component than UC for the same reason.

A comparison in the lower temperature region can be made between the present research and the diffusivity work at the Mound Laboratory [13]. A radial heat flow method was used with the specimen being heated at a constant rate. Some bonding problems were encountered with this method due to the encapsulation of the specimens in tantalum. The UC work was carried out on 96% dense carbide, with a sintering aid consisting of 0.1 wt.% Ni. A carbon analysis of 4.78 wt.% indicated the specimens were stoichiometric; however, the X-ray analysis showed some faint U_2C_3, UO_2 and UC_2 lines. The data agreed quite well with our work on the high density carbide around 400°C, but the thermal diffusivity decreases rapidly to a minimum at 700°C and then rises gradually. The 91% dense $(U_{0.8}Pu_{0.2})C_{0.95}$ values fall on the same curve as our work when the data are corrected to 100% theoretical density. Both the Mound material and our specimen contained about 0.2 wt.% oxygen and both were substoichiometric in carbon so that good agreement was to be expected.

A comparison with thermal conductivity work on arc-cast high-purity material at LASL [10] by a standard axial heat flow method can be made at 400°C, the highest temperature of their research. The UC data is the same as ours but the $(U_{0.8}Pu_{0.2})C$ and the PuC values are much higher than found in our work. The calculated diffusivity of $(U_{0.8}Pu_{0.2})C$ and PuC measured at LASL was 5.3×10^{-6} and $4.3 \times 10^{-6} M^2 sec^{-1}$, respectively. Our diffusivities for these materials were 3.5 for $(U_{0.8}Pu_{0.2})C$ and 2.4 for PuC.

Chemically stoichiometric UC of a carbon content of 4.8 wt.% but with varying impurity contents was investigated by Hayes and DeCrescente [11] who used a radial heat flow method. The results of this work generally fall within the range of our UC data and it covers the temperature span from 1000 to 1500°C. The thermal diffusivity of their highest purity material containing 0.086 wt.% O and 0.052 wt.%

N was 6.5 x $10^{-6}M^2sec^{-1}$ at 1000°C compared to our value of 5.3 x 10^{-6}. At 1175°C their curve went below ours and leveled out at around 1300°C, staying slightly below our results. Above 1250°C there was very little difference between this high purity material and two specimens of combined oxygen and nitrogen content of 0.22 and 0.40 wt.%, respectively.

4. Conclusions

Thermal diffusivity measurements were made over a 1000° temperature range (500 to 1500°C) by means of the same apparatus on materials of similar microstructure and density. The relative magnitudes and trends shown are realistic and have been confirmed in part by other work. The study on the PuC was carried to within 200°C of the melting point.

5. Acknowledgments

Thanks are due to J. W. Thompson, R. E. Mailhiot and L. J. Kocenko for assistance in the various technical aspects of this research. The authors also wish to express their appreciation to H. T. Goodspeed and J. H. Marsh, Jr., of the ANL Chemistry Division, for performing the chemical analyses.

6. References

[1] Parker, W. J., Jenkins, R. J., Butler, C. P., and Abbott, G. L., Flash method of determining thermal diffusivity, heat capacity, and thermal conductivity, J. Appl. Phys. 32, 1679 (1961).

[2] Moser, J. B., and Kruger, O. L., Heat pulse measurements on uranium compounds, J. Nucl. Mat. 17, 153 (1965).

[3] Moser, J. B., and Kruger, O. L., Thermal conductivity and heat capacity of the monocarbide, monophosphide and monosulfide of uranium, J. Appl. Phys. 38, 3215 (1967).

[4] Harrington, L. C., and Rowe, G. H., The enthalpy and heat capacity of uranium monocarbide to 1200°C, PWAC-426, Pratt & Whitney (Jan. 1964).

[5] Kruger, O. L., and Savage, H., Heat capacity of plutonium monocarbide from 400 to 1300°K, J. Chem. Phys. 40, 3324 (1964).

[6] Sanathanan, C. K., Carter, J. C., and Brittan, R. O., Transient temperature distributions in fast reactor fuels with widely varying thermal diffusivity, ANL-7120, Argonne National Laboratory (October, 1965).

[7] Deem, H. W., and Wood, W. D., High temperature thermal diffusivity using a ruby laser as a heat pulse source, Rev. Sci. Instr. 33, 1107 (1962).

[8] Kruger, O. L., Preparation and some properties of arc-cast plutonium monocarbide, J. Nucl. Mat. 7, 142 (1962).

[9] Cowan, R. D., Pulse method of measuring thermal diffusivity at high temperatures, J. Appl. Phys. 34, 926 (1963).

[10] Leary, J. A., Thomas, R. L., Ogard, A. E., and Wonn, G. C., Thermal conductivity and electrical resistivity of UC, (U,Pu)C and PuC, symposium on Carbides in Nuclear Energy, Vol. 1, Macmillan Co., London (1964).

[11] Hayes, B. A., and DeCrescente, M. A., Thermal conductivity and electrical resistivity of uranium monocarbide, PWAC-480, Pratt & Whitney (1965).

[12] Kruger, O. L., and Moser, J. B., Electrical properties and electron-configuration of the monocarbide, monophosphide and monosulfide of plutonium, J. Chem. Phys. 46, 891 (1967).

[13] Wittenberg, L. J., and Grove, G. R., Reactor fuels and materials development plutonium research: 1964 annual report, MLM-1244 (1965).

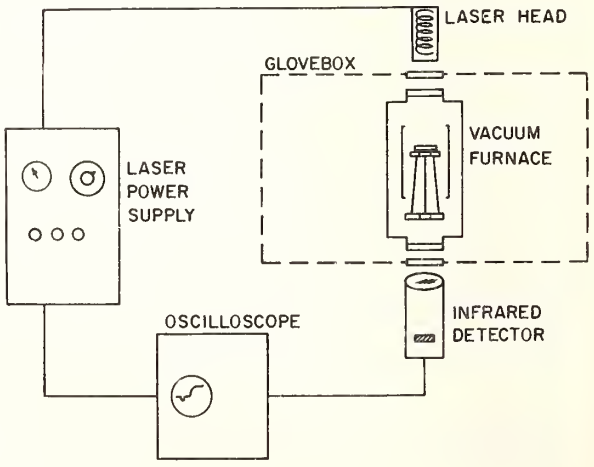

Figure 1. Schematic of thermal diffusivity apparatus.

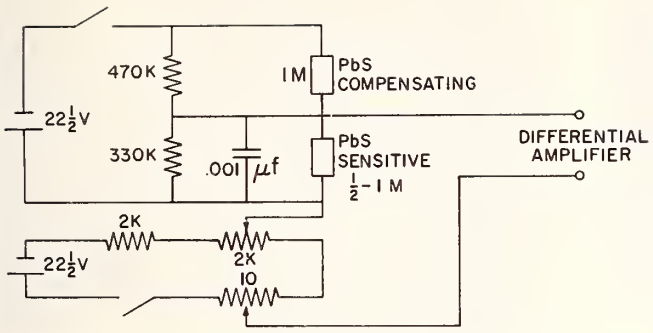

Figure 2. Lead sulfide detector circuit.

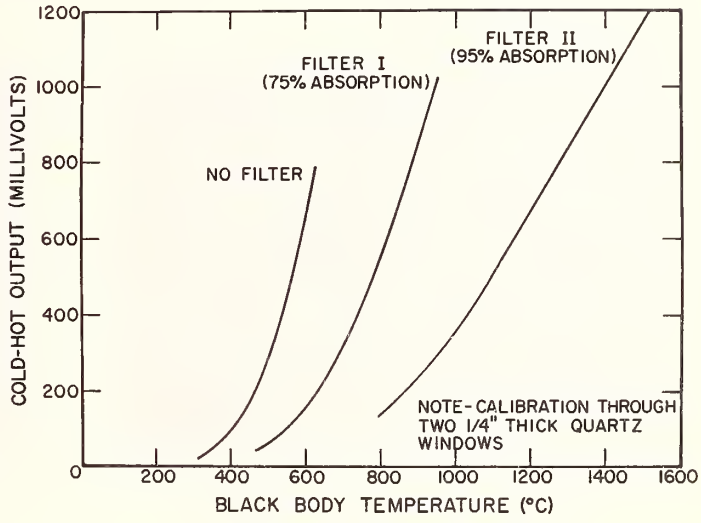

Figure 3. Output of lead sulfide detector as a function of temperature

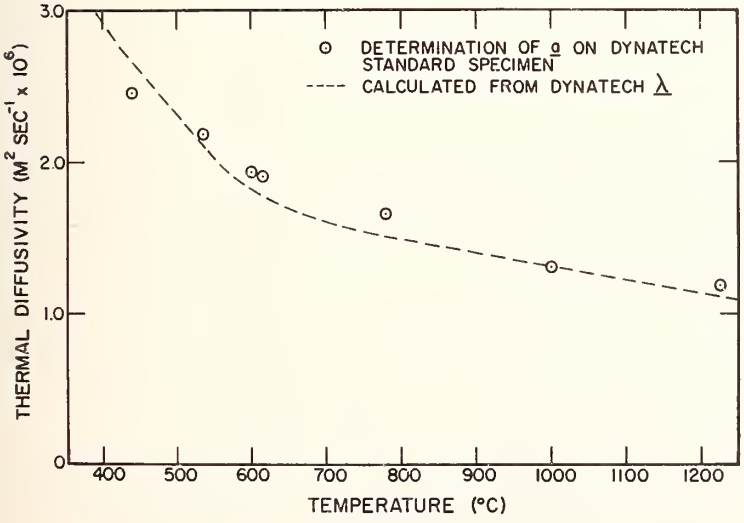

Figure 4. Thermal diffusivity of Al_2O_3 standard.

Figure 5. Microstructure of high purity arc-cast UC. Samll amount of UC_2 - precipitate within grains. (Nitric etch; 56X).

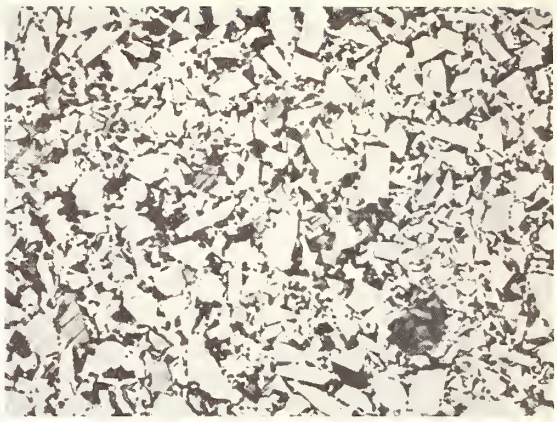

Figure 6. Microstructure of sintered UC showing pore-configuration (150).

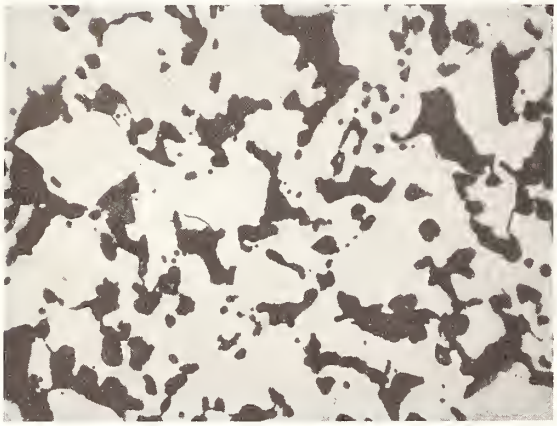

Figure 7. Microstructure of sintered $(U_{0.8}Pu_{0.2})C$ showing pore-configuration (150).

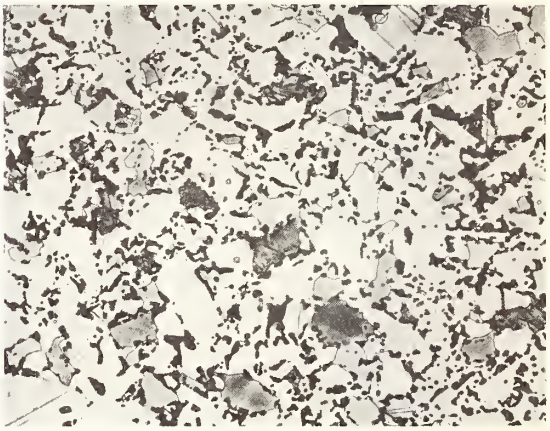

Figure 8. Microstructure of sintered PuC. Shows presence of Pu_2C_3; possibly 10% (150).

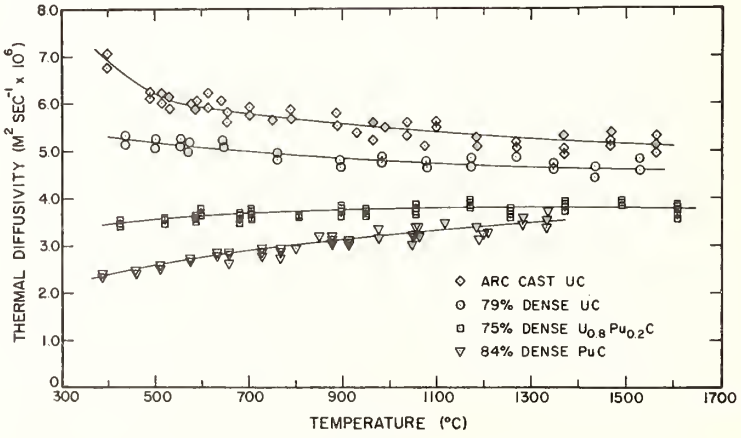

Figure 9. Thermal diffusivity of uranium and plutonium monocarbides.

The Thermal Diffusivity and Thermal Conductivity of Sintered Uranium Dioxide

J.B. Ainscough and M.J. Wheeler[1]

The General Electric Company Limited,
Central Research Laboratories,
Hirst Research Centre,
Wembley, England.

Thermal conductivity values are calculated from 700 thermal diffusivity measurements between 970°K and 2020°K on 25 samples of sintered 2.7% enriched $UO_{2.00}$, 97% of theoretical density. The measurements were made using the modulated electron-beam technique and the thermal conductivities of all the samples, derived by using Moore and Kelley's specific heat values, are represented by

$$k = \frac{1}{0.0227T + 3.38} + 6.6 \times 10^{-13} T^3 \text{ W cm}^{-1} \text{ degK}^{-1} \quad (970\text{-}2020°K)$$

the 95% confidence limits being ± 14½%. This representation of the thermal conductivity is preferred because the values of the constants agree both with the theory and the results of other investigators.

Key Words: Conductivity, diffusivity, heat conductivity, heat diffusivity, modulated electron beam, sintered uranium dioxide, thermal conductivity, thermal diffusivity, uranium dioxide.

This paper will be published in the British Journal of Applied Physics, volume 19, 1968.

[1] Dr. Ainscough is with the U.K.A.E.A., Springfield Works, Salwick, Preston, Lancashire, England.

Suitability of the Flash Method for Measurements of the Thermal Diffusivity of Uranium Dioxide specimens Containing Cracks

D. Shaw, L. A. Goldsmith and A. J. Little

Reactor Development Laboratories, U.K. Atomic Energy Authority,
Windscale Works, Sellafield, Seascale, Cumberland,
England.

The accuracy of thermal diffusivity measurements by the flash-method on reactor fuel specimens containing cracks is discussed. A theoretical treatment for a specimen containing a "model" crack showed that the thermal diffusivity as measured by the flash-method will probably be within 5% of the value derived from a steady-state heat flow method. Measurements on Armco Iron specimens containing restricted heat-flow paths confirmed this conclusion.

Key Words: Armco Iron, cracks, flash-method, model-crack, reactor fuel, steady-state heat flow, thermal diffusivity.

1. Introduction

The flash-method, devised by Parker et al. [1][1] is now an established technique in most laboratories interested in thermal property measurements. In particular, it is of great value in measuring the thermal diffusivities of relatively small specimens on which it would not have been possible to use a steady-state heat flow method. This is especially true of measurements on ceramic or ceramic-based reactor fuel specimens which are rarely manufactured with lengths or diameters in excess of 0.75 in. A possible limitation to the use of the flash-method is in cases where a crack or cracks form across the path of heat-flow, such as may occur in UO_2 pellets during irradiation. The Parker method is, of course, based on heat flow through a continuous medium. It is clearly of interest to determine how well the method applies when used with specimens containing cracks. This note describes a theoretical and an experimental approach to the problem.

2. Thermal Conductivity Measurements on UO_2 Specimens

The flash-method apparatus of Shaw and Goldsmith, which has been described elsewhere [2] was used to carry out a series of measurements at temperatures between 400 and 1000°C on unirradiated and irradiated UO_2 specimens, cut from UO_2 fuel pellets. Measurements were made on each specimen at four temperatures, nominally 400, 600, 800 and 1000°C. At any given temperature, six traces of time versus back-face temperature were taken. Values of $t_{\frac{1}{2}}$ (i.e. the time taken for the temperature of the back face to reach half its maximum rise from the time of delivery of the heat pulse to the opposite face of the specimen) were worked out for each trace and the mean value was used in the formula $\alpha=\omega l^2/(t_{\frac{1}{2}})$ where α is the thermal diffusivity (cm^2/s), ω is a number (see below) and l is the thickness of the specimen (cm). Provided heat losses do not occur, ω has a value of 0.139. At temperatures of about 600°C and higher, significant heat losses occur and it becomes necessary to work out a revised value for ω, using either the method of Cape and Lehmann [3] or of Cowan [4]. Conductivity values were calculated from the product of diffusivity, density and specific heat, using the data of Moore and Kelley [5].

A plot of thermal conductivity values for the unirradiated and the irradiated specimens is shown in figure 1. Irradiation conditions were such i.e. irradiation temperature between 500 and 1000°C and irradiation levels below 10,000 MWD/te, that, according to Clough and Sayers [6] it is most improbable that any of the observed decrease in conductivity was caused by the usual irradiation effects i.e. displaced atoms, defect clusters and porosity. Metallography revealed the presence of cracks (figs. 2 and 3) and it was concluded that the lower values were almost certainly due to the presence of cracks. Clearly, since the accuracy of fuel temperature calculations depends, amongst other things, on the accuracy to which the thermal conductivity is known, it becomes important to assess how accurately the diffusivity (and hence the conductivity) may be measured in a cracked specimen using the flash method.

[1] Figures in brackets indicate the literature references at the end of this paper.

3. Theoretical Treatment

Using an idealised model for the crack, the apparent conductivities for both transient and steady-state heat-flow conditions have been calculated and the results compared with the experimentally determined values.

3.1 Model for the Crack

In devising the model for the crack, the following assumptions were made:

(1) The crack lies on a plane transverse to the direction of the heat flow and has a thickness which is small relative to the specimen thickness.

(2) The temperature distribution in the crack is linear.

(3) Solid contact exists between the two faces of the crack over a fraction of its surface area.

This is demonstrably true, since heat transfer occurred readily through the specimens during tests, in a vacuum of better than 10^{-4} mm Hg and at temperatures where heat transfer by radiation would be negligible. Metallography of several discs showed that all the major cracks were connected to the outer surfaces of the disc so that any helium filler gas originally present in the fuel pin or any of the gases formed during fission would have been pumped away thus eliminating the possibility of heat transfer by gas conduction.

The equation to be solved is the heat conduction equation

$$\alpha \frac{\partial^2 T}{\partial x^2} = \frac{\partial T}{\partial t} \tag{1}$$

α = thermal diffusivity ($m^2/10^4 s$), T=temperature rise (^oC)

The boundary conditions for the transient problem are:

(i) No loss of heat from the back surface,

$$-\left(k\frac{\partial T}{\partial x}\right)_{x=1} = 0 \tag{2}$$

(ii) The heat pulse from the laser beam is of the form

$$-k\frac{\partial T}{\partial x} = H \quad \text{for } 0 < t < \tau, \; x = o$$
$$= o \quad \text{otherwise} \tag{3}$$

(iii) The flow of heat across the crack is continuous

$$\left(-k\frac{\partial T}{\partial x}1\right)_{x=a} = \left(-k\frac{\partial T}{\partial x}2\right)_{x=a} = \left[\frac{T_1 - T_2}{\mu}\right]_{x=a} \tag{4}$$

T_1, T_2 are the temperatures of the material before and after the crack respectively.

a is the distance of the crack from the front surface (cm), 1 is the length of the specimen (cm), k is the thermal conductivity ($kWm^{-1}\,deg^{-1}$), H is the amount of heat absorbed by the specimen from the laser pulse (J), μ is a parameter which is a measure of the effectiveness of the crack and is in effect

$$\mu = \frac{\text{crack thickness}}{\text{conductivity of } UO_2} \times \frac{1}{p} \tag{5}$$

p is the percentage of the crack surface which is in solid contact, (μ can also be interpreted in terms of a crack containing gas), τ is the duration of the pulse.

After working through the mathematics of the problem, a formula was obtained for the temperature on the rear face

$$T_2(1,t) = \frac{H\gamma}{k1} - \frac{2H}{k} \sum_{n=o}^{\infty} f(\lambda_n) e^{-\lambda_n^2 \alpha t} \tag{6}$$

where

$$f(\lambda_n) = \frac{(1 - e^{\lambda_n^2 \alpha \tau})}{\lambda_n^2 \left[1 \cos \lambda_n 1 - k_\mu \lambda_n (b \sin \lambda_n a \cos \lambda_n b + a \sin \lambda_n b \cos \lambda_n a) - k_\mu \sin \lambda_n a \sin \lambda_n b\right]} \tag{7}$$

where $a + b = 1$ and λ_n satisfies

$$\sin \lambda_n 1 = k_\mu \lambda_n \sin \lambda_n a \sin \lambda_n b \tag{8}$$

The first term in the series for T_2 (1, t) is the dominant one and using this fact the following formula is obtained.

$$\log_e \left[\frac{4lf(\lambda_1)}{\alpha\gamma}\right] = \lambda_1^2 \alpha t_{\frac{1}{2}} \tag{9}$$

$t_{\frac{1}{2}}$ is the time taken to reach half the maximum temperature rise.

Parker et al [2] have obtained a similar formula for the diffusivity in terms of $t_{\frac{1}{2}}$

$$\alpha_a = \frac{(.1391)^2}{t_{\frac{1}{2}}} \tag{10}$$

Hence by eliminating $t_{\frac{1}{2}}$ we can obtain a formula relating α_a/α to the other parameters in the problem where α_a is the diffusivity of cracked UO_2 and α is the diffusivity of uncracked UO_2. Assuming that the density and specific heat of the material do not change, the ratios α_a/α and k_a/k will be equivalent.

3.2 Steady State

In the steady state case the ratio of the cracked to uncracked conductivities is given by

$$\frac{k_a}{k} = \frac{1}{(k_\mu + 1)} \tag{11}$$

Comparing this model with actual specimens indicates that typical values for u lie between about 5 and 20. In the case a = b (central crack), the table below lists the values of the ratio of the apparent (measured) conductivity to the actual unirradiated conductivity in both the steady and transient cases.

Table 1

Size of crack (μ)	0	1	5	10	100	∞
Apparent reduction in conductivity (k_a/k) for transient flow	1	.936	.777	.640	.157	0
Apparent reduction in conductivity (k_a/k) for steady flow	1	.958	.820	.699	.188	0

Thus in the cases considered here, the conductivity of cracked UO_2 found by the laser flash method is always somewhat lower than the effective conductivity in the reactor, but not less than 80% of it. The experimentally determined values of conductivity in most of the cracked irradiated specimens (fig. 1) are about 80% of those in uncracked unirradiated specimens. Thus the cracks in the former have about the same effect as an idealised central crack with a value of $\mu = 5$. This suggests that the values of conductivity obtained by the flash method are up to 5% lower than the conductivity of the same specimen under conditions of steady-state heat flow (e.g. in the reactor).

4. Experimental Approach

The object of the work was to compare values of thermal diffusivity obtained by the flash-method on specimens containing artificial discontinuities, simulating cracks, with values obtained by theoretical calculation on the same specimens. To facilitate machining, the specimens were prepared from a bar of Armco iron.

4.1 Specimen Details

Two types of specimens were used. The first, chosen because the steady state thermal conductivity ratios could be calculated to better than 5% were solid cylinders, with annular central grooves of varying size cut into them. The second type, attempting to simulate a cracked specimen, were rectangular slabs with holes of differing size and position drilled through them at right angles to the direction of heat flow. Details of the various specimens are given in Tables 2 and 3.

4.2 Experimental Method

The diffusivity of a solid specimen was first measured at either one of two temperatures, nominally 400 and 600°C. The effective diffusivity of an "inhomogeneous" specimen of similar external dimensions, was next measured at the same temperature, the diffusivity value being calculated using the standard Parker equation as if it were a solid specimen. From these measurements, the ratios of effective diffusivity of the inhomogeneous specimens to that of a solid specimen of similar external dimensions, were obtained. With the specimens machined with central annular grooves, measurements were made with the heat flow in one direction only. With the specimens containing drilled holes, measurements were made with the heat flow in both directions. This reversal had little or no effect on the value of effective conductivity.

4.3 Calculation of the steady-state Values

The steady-state conductivity ratios of the first set of specimens were calculated using a solution derived by Cetinkale [7] for the thermal resistance of two metal surfaces in contact. The thermal resistance of a cylindrical specimen containing a central annular groove with axial heat flow consists of two parts, the simple resistance of the constricted cylinder, and the resistance due to the convergence of the heat flow lines to pass through the restriction. The steady-state resistance, R_T, of the constricted cylinder is,

$$R_T = \frac{l}{\pi R^2 k_s} + \frac{\delta}{\pi r^2 k_s} + \frac{1}{\pi r k_s} \tan^{-1} \frac{R-r}{r} \qquad (12)$$

and equating this to the effective resistance:

$$R_T = \frac{l + \delta}{\pi R^2 k_e} \qquad (13)$$

where R is the radius of the cylinder (cm), r is the radius of the constriction (cm), δ is the length of the contriction (cm), $(\delta + l)$ is the total length of the grooved cylinder (cm), k_s is the thermal conductivity of the solid cylinder ($kWm^{-1}\ deg^{-1}$), and k_e is the effective conductivity of the grooved cylinder ($kWm^{-1}\ deg^{-1}$) gives the ratio ke/ks for these specimens. This analysis assumes that $l \geqslant 2R$ and $l \gg \delta$. This latter condition was not fulfilled, but would probably not introduce an error of more than a few percent. The ratio of solid to 'effective' density was easily calculated, and as the specific heats would be the same, the ratio of 'effective' to solid thermal diffusivity α_e/α_s was found. This latter ratio was in fact virtually independent of δ, the width of the slot, as can be seen in Table 2, below.

Table 2. Thermal diffusivity ratios for the grooved-cylinder specimens

Specimen No.	Specimen size		Groove dimensions		Steady State			Transient Diffusivity Ratio α_{e/α_s}	
	Total Length	Dia. (2R)	Length	Dia. (2r)	Thermal Conductivity ratio k_{e/k_s}	Density ratio ρ_{s/ρ_e}	Diffusivity ratio α_{e/α_s}	($378^{\circ}C$)	($577^{\circ}C$)
1 A	0.750	0.764	0.258	0.536	0.61	1.21	0.74	0.71	0.71
1 B	0.759	0.764	0.156	0.528	0.66	1.12	0.73	0.72	0.69
1 C	0.732	0.760	0.258	0.266	0.20	1.45	0.28	0.27	0.28
1 D	0.759	0.768	0.144	0.256	0.24	1.20	0.29	0.28	0.28

The steady-state conductivity ratios of the second set of specimens were calculated by splitting up the slab into longitudinal sections, as shown in figure 4, calculating the resistance of each section, and summing these resistances, using the resistance in parallel rule, to obtain the total resistance of the slab. The resistance of each elemental constricted slab (R_s) was calculated in a similar manner to that of the first set of specimens, i.e. as the sum of the simple resistance of the constricted slab and the resistance due to the convergences of the heat flow lines. This latter resistance was calculated using the results from reference [7] and converting from cylindrical to linear co-ordinates. The circular holes in the slab were assumed, for ease of calculation, to be rectangular, but of the same cross-sectional area. The whole slab is, clearly made up of a parallel combination of n of these elemental constricted slabs, where n is the number of holes, and the two plain end sections E_1 and E_2, whose resistances are R_1 and R_2 respectively. Thus the reciprocal of the total resistance R_T is:

$$(R_T)^{-1} = n(R_s)^{-1} + (R_1)^{-1} + (R_2)^{-1} \tag{14}$$

$$\text{where } R_s = \frac{1}{x_3 y k_s} + \frac{\delta}{x_4 y k_s} + \frac{4}{\pi y k_s} \operatorname{Cosh}^{-1} \frac{x_3 - x_4}{x_4}, \tag{15}$$

$$R_1 = \frac{(1+\delta)}{x_1 y k_s} \text{ and } R_2 = \frac{(1+\delta)}{x_2 y k_s} \tag{16}$$

(See figure 4 for the meaning of symbols).

Writing the effective resistance of the whole slab:

$$R_T = \frac{1+\delta}{xyk_e} \tag{17}$$

and equating eq (15) to the reciprocal of eq (17), the ratio of the 'steady-state' effective to solid thermal diffusivity is then easily calculated, as in the first set of specimens. Unfortunately the steady-state conductivity values proved to be particularly sensitive both to the shape of the holes and to the specimen dimensions (Table 3). Consequently the steady-state conductivity ratios could not be calculated with an accuracy of better than about 20%.

Table 3. Thermal diffusivity ratios for drilled specimens

Specimen No.	Specimen size		Hole Dimension			Distance of hole centres from upper surface	Steady-state ratios				Transient Method Diffusivity Ratio	
	Length	Dia.	No.	Dia.	Separation		k_e/k_s	ρ_s/ρ_e	α_e/α_s	α_e/α_s MAX	391°C	577°C
2 A	1.039	0.511	7	.079	.034	.112	0.78	1.07	0.83	0.80	0.82	0.79
"	"	"	"	"	"	"	"	"	"	"	0.79	-
"	"	"	"	"	"	.399	"	"	"	"	0.81	0.81
2 B	1.024	0.513	7	.080	.033	.262	0.76	1.07	0.81	0.78	0.70	0.68
"	"	"	"	"	"	"	"	"	"	"	0.70	-
"	"	"	"	"	"	.251	"	"	"	"	0.69	0.69
2 C	1.029	0.514	9	0.052	.025	.258	0.89	1.04	0.92	0.88	0.88	0.84
"	"	"	"	"	"	.256	"	"	"	"	0.85	0.87
2 D	1.036	0.512	7	0.086	0.030	.258	0.75	1.08	0.81	0.74	0.69	0.69
"	"	"	"	"	"	"	"	"	"	"	0.69	-
"	"	"	"	"	"	.254	"	"	"	"	0.69	-
2 E	1.055	0.512	7	0.080	0.034	.142	0.77	1.07	0.82	0.79	0.74	0.73

4.4 Results and Discussion

Details of both sets of specimens, together with a comparison of their 'steady-state' and 'transient' thermal diffusivity ratios are given in Tables 2 and 3.

With the grooved specimens, there is excellent agreement between the 'steady-state' and 'transient' conductivity ratios. The latter values are always less than or nearly equal to the former ones. The drilled-slab specimens show differences between the 'steady-state' and'transient' conductivity ratios of between 2 and 15%. This may, at first sight, appear exceptionally great, but because the 'steady-state' ratio is particularly sensitive to the specimen dimensions this degree of difference is not surprising. For example, a 15% change in the 'steady-state' ratio may be made by assuming the holes to be square instead of rectangular in shape, maintaining the same cross-sectional area, and a difference of only 0.001 in. in hole size and separation gives a 2½% change in this ratio. In addition, practical difficulties made it impossible either to drill the holes accurately orthogonal to the direction of heat flow or parallel to one another. Thus the calculated steady state value could well be in error, and the discrepancies between the steady state and transient ratios are not necessarily due to erroneous diffusivity values. However, the results for these specimens do show that the value of the thermal diffusivity does not markedly depend on the direction of heat flow, as can be seen most clearly for specimen 2A.

5. Conclusion

The theoretical analysis on a specimen containing a "model" crack and the experimental work on specimens containing restricted heat-flow paths, have both shown that the thermal diffusivity of a specimen containing a crack or impediment to heat flow may be obtained to an accuracy of better than about 5% using the flash-method with the equation of Parker et al.

6. References

[1] Parker, W.T. et al. J. Appl. Phys., 32, pp 1979-84 (1961).

[2] Shaw, D. and Goldsmith, L.A. Journ. Sci. Instr., Vol. 43 pp 594-596 (August 1966).

[3] Cape, J. A. and Lehmann, J.W. J. Appl. Phys. 34, No. 7,(July 1963).

[4] Cowan, R.D. J. Appl. Phys. 34, No. 4, Pt. 1 (April 1963).

[5] Moore, G. E. and Kelley, K.K. J. Amer. Ceram. Soc. 69, p2105 (1947).

[6] Clough, D. J. and Sayers, J. B. The measurement of thermal conductivity of UO_2 under irradiation in the temperature range 150 - 1600°C. AERE-R4690. (1964).

[7] Cetinkale, T.N. and Fishenden, M. Thermal conductance of metal surfaces in contact. Am. Soc. Mech. Eng. Proc. General discussion on heat transfer 271-5 (11-13 Sept., 1951).

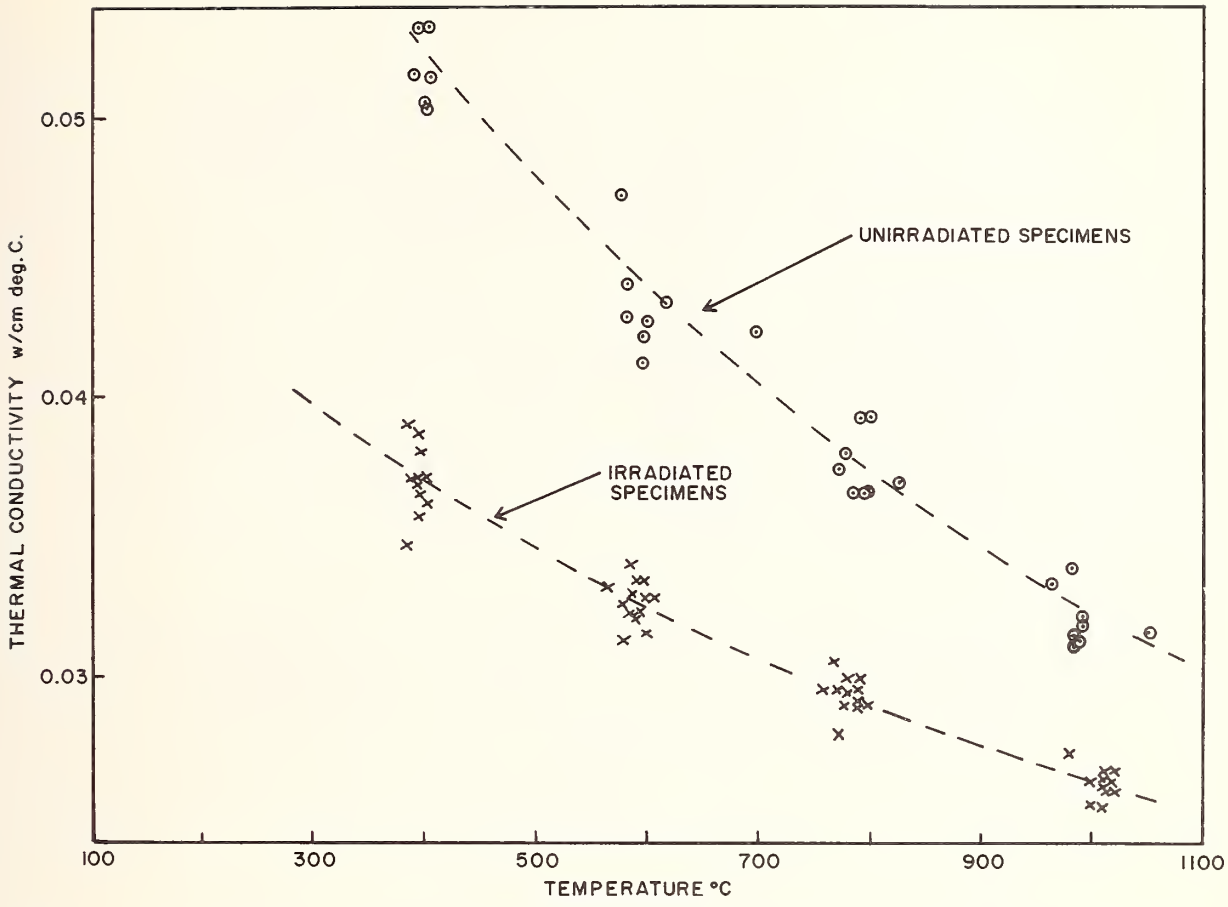

Figure 1. Plot of thermal conductivity versus temperature for unirradiated and irradiated specimens.

Figure 2.

Figure 3.

Sections from irradiated UO_2 pellets showing moderate and severe amounts of cracking respectively.

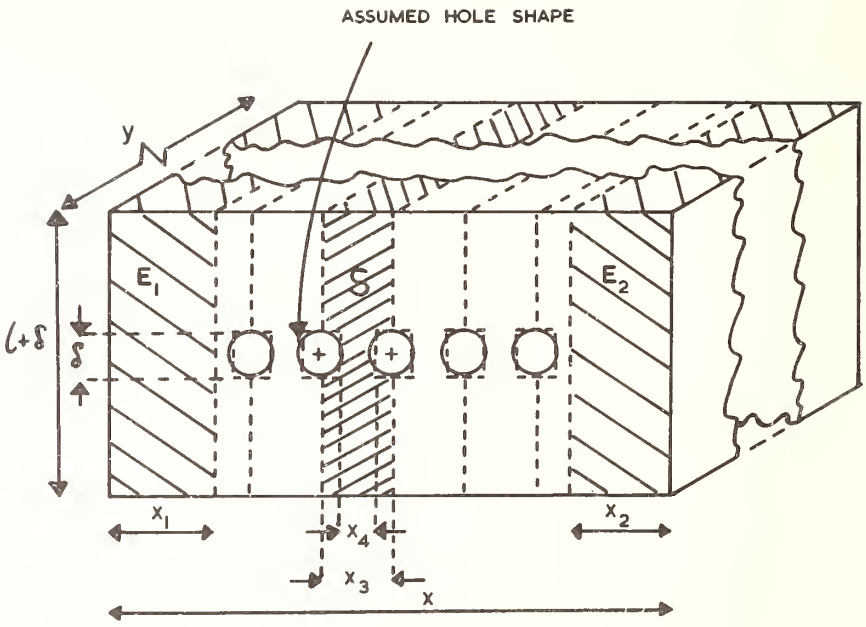

Figure 4. Diagram of drilled-slab specimen showing elemental slab S and end sections E_1 and E_2.

Thermal Conductivity of Uranium Oxycarbides[1]

J. Lambert Bates[2]

Battelle Memorial Institute
Pacific Northwest Laboratory
Richland, Washington 99352

The thermal diffusivity of uranium oxycarbide was measured from 100 to 1500°C as a function of oxygen concentration from 2 to 17 at.% of the anions. The thermal diffusivity (a) of the oxycarbides decreased and the shape of the a-versus-T curve changed as the oxygen content increased. Oxycarbides with the lowest oxygen content showed a decrease in a as the temperature increased, whereas the oxycarbides with the highest oxygen content exhibited a slight increase in a with an increase in temperature. The thermal diffusivities of all specimens approach a common value near 5 x 10^{-6} m^2/s at the higher temperatures.

The calculated thermal conductivities near 1500°C of the uranium oxycarbides are approximately 18 W m^{-1} deg^{-1}, very near the reported values for nearly stoichiometric and slightly hypostoichiometric UC. The thermal conductivities of the oxycarbides can be qualitatively separated into an electronic component, obeying the Wiedemann-Franz-Lorentz law, and a lattice component, varying inversely with temperature. The decrease in thermal conductivity at the lower temperatures with increasing oxygen content results primarily from changes in the lattice component. Small decreases also occur in the electronic component over the entire temperature range due to increases in oxygen content.

Key Words: Armco iron, conductivity, electrical resistivity, pulse method thermal diffusivity, thermal diffusivity, thermal conductivity, uranium carbide, uranium oxycarbide.

1. Introduction

Uranium monocarbide has received considerable attention as a high temperature fuel for nuclear reactors. Unfortunately, it has been difficult to prepare uranium monocarbide entirely free of oxygen, the oxygen often being found in solid solution with the monocarbide structure. The difficulty in producing single-phase specimens has contributed significantly to the wide variation in reported values for thermal conductivity and other high-temperature properties.

Recent extensive investigations have been made of the phase relations in the uranium carbide region of the uranium - carbon - oxygen system [1-4].[3] Single-phase solid-solution uranium oxycarbides can be prepared with oxygen contents approaching 17 atomic percent.

---

[1] This paper is based on work performed under United States Atomic Energy Commission Contract AT(45-1)-1830.

[2] Research Associate, Physical Ceramics Unit, Materials Department, Pacific Northwest Laboratory, operated by Battelle Memorial Institute for the United States Atomic Energy Commission, Richland, Washington.

[3] Figures in brackets indicate the literature references at the end of this paper.

The purpose of this study was to determine the thermal diffusivities of some uranium oxycarbides as a function of oxygen content (to 17 at.%) in the temperature range from 100 to 1500°C, to calculate thermal conductivity values, and to evaluate the data in terms of the electronic and lattice condition processes.

2. Thermal Diffusivity Measurements

The uranium oxycarbide samples were prepared by reaction sintering of calculated quantities of uranium, graphite, and UO_2 powders. The compacts were pulverized and milled to a fine powder in an all-nickel mill under highly purified argon. Pellets were cold pressed and sintered at 1700°C for two hours in an atmosphere of carbon monoxide at or very near the decomposition pressure for each oxycarbide specimen. Details of the fabrication process have been published by Henry et al. [1].

Ceramographic specimens were mounted in resin and rough ground on dry 3/0 and 2/0 emery papers. The specimens were first polished for one hour on a vibratory polisher with 0.3 μm Al_2O_3 in water on Metcloth. A final polish was obtained using 20 μm MgO powder in water on Gamal cloth for 1/2 to 1 hour. The polished surfaces on some specimens were improved by five-second etching followed by hand polishing with MgO in water. This was repeated if necessary to remove final scratch marks. Specimens were etched in 1:1:1 nitric acid, acetic acid, and water at room temperatures.

The compositions and densities of the uranium oxycarbide specimens are shown in table 1. The compositional relationships of each specimen to the reported uranium - carbon - oxygen phase diagram at 1700°C are illustrated in figure 1. UCON-283 ($U_{0.495}C_{0.485}O_{0.02}$) is single phase with minor traces of free uranium and UC_2 (Widmanstätten precipitate) (figure 2). The relative slow cooling rate during the thermal diffusivity measurements resulted in the increase in UC_2 precipitates. The presence of free uranium indicates inhomogeniety on a microscale. Some grain growth appears to have occurred during measurements. UCON-365 ($U_{0.48}C_{0.49}O_{0.03}$) was deliberately made more hyperstoichiometric resulting in a higher Widmanstätten precipitate of UC_2 (figure 3). A precipitate in the grain boundaries in the etched specimen after the thermal diffusivity measurements is probably secondary sesquicarbide (U_2C_3).

Table 1. Description of uranium oxycarbide specimens

Designation	Composition, Atom %			Density $kg/m^3(10^3)$	Microstructure
	U	C	O		
UCON-283	49.5	48.5	2	12.7	Single phase UC_xO_y with trace-free U + UC_2
UCON-288	49.5	35.5	15	12.5	Two-phase UC_xO_y and UO_2 with trace-free U
UCON-289	49.5	33.5	17	12.3	Two-phase UC_xO_y and UO_2 with trace-free U
UCON-365	48.0	49.0	3	13.1	Two-phase UC_xO_y + UC_2 with trace UO_2.

UCON-288 ($U_{0.495}C_{0.355}O_{0.15}$) and UCON-289 ($U_{0.495}C_{0.335}O_{0.17}$) are two phase UC_xO_y and UO_2 with traces of free uranium (figure 4). The UO_2 is the light grey phase and the free uranium is the white phase in the unetched micrographs. UO_2 appears white in the etched specimens.

The as-fabricated cylinders[4] were cut into thin disks (~ 0.100 cm thick and 0.635 cm in diameter) for the thermal diffusivity measurements.

[4] The uranium oxycarbide cylinders for this study were fabricated at the Albany Research Laboratory, United States Bureau of Mines, Albany, Oregon.

The thermal diffusivity of uranium oxycarbide was measured from 100 to 1500°C using a laser-pulse technique [5,6]. The pulse was provided by a 1.27 cm diameter ruby laser with energy output of 3 - 7 joules. The pulse width was 0.54 ms.

The temperature transients on the back surface of the specimens were measured optically using a liquid nitrogen cooled, indium antimonide infrared detector. The signal from the detector was displayed on an oscilloscope and recorded on polaroid film. Corrections were made for heat losses using the method proposed by Cowan [7,8]. No pulse time corrections were required.

The specimen was heated in a vertical tungsten tube furnace which was heated by direct current resistance. The sample was held in a UO_2 holder with small tungsten pins.

Temperatures were measured using Pt versus Pt-13% Rh thermocouples positioned in the holder. This thermocouple was calibrated using another Pt/Pt-13% Rh thermocouple welded to a thin platinum disk set in the sample position. Temperatures were controlled manually.

Measurements were made in a purified argon atmosphere; the inlet argon contained < 1 ppm oxygen and < 5 ppm H_2O. The pressure in the furnace was one atmosphere.

Each specimen was heated initially to 1000°C, and thermal diffusivity measurements made during the increase and decrease in temperature. The samples were removed from the furnace to check for possible reaction with the tungsten or UO_2. The specimen was reinserted in the furnace and thermal diffusivity measurements were made to approximately 1500°C. No reactions between the sample and the UO_2 or W of the holder were detected.

The thermal diffusivity apparatus was calibrated using Armco iron. The thermal diffusivity data (figure 5) for the iron are in satisfactory agreement with the data reported by Cody et al.[9], Godfrey et al.[10], and Shanks et al. [11].

3. Results and Discussion

Thermal diffusivity data for uranium oxycarbide from 100 to 1500°C are shown in figure 6.

The thermal diffusivity (a) of the oxycarbides decreased with increasing oxygen content. This change was most pronounced at the lower temperatures. The diffusivity of the samples containing 15 to 17 at.% oxygen is approximately 60% of that of the samples containing 2 at.% oxygen. This difference decreases as the temperature increases.

The temperature dependence of the oxycarbides varied significantly with oxygen content. The oxycarbides with the lowest oxygen concentration showed a decrease in a as the temperature increased. In contrast, the oxycarbides with the highest oxygen concentration exhibited a very slight increase in a with an increase in temperature. The overall result is that the diffusivities of all the specimens approach a common value near 5×10^{-6} m^2/s at the higher temperatures.

Since there are no reported thermal diffusivity or conductivity data for uranium oxycarbides, comparisons can best be made using data for uranium monocarbides. The magnitude of the thermal diffusivity values at high temperatures above 1100°C fit closely between the thermal diffusivity values of hyper- and hypostoichiometric uranium monocarbide reported by Wheeler [12] (figure 6). However, the temperature dependence of the thermal diffusivities, with the exception of the 51 at.% C reported by Wheeler [12], are somewhat different, with a decrease at lower temperatures. It is more difficult to make a comparison between the thermal conductivities of UC_xO_y and UC because of the wide variations in reported UC thermal conductivity values [12-16].

Thermal conductivities of the uranium oxycarbides were calculated using heat capacity data for uranium monocarbide. Since the preliminary heat content data for UC_xO_y do not differ significantly from that for uranium monocarbide [17], the heat capacity data reported by Godfrey et al. [18] were used for these calculations. These results are shown in figure 7.

The thermal conductivity values for the uranium oxycarbides above 1000°C agree best with nearly stoichiometric UC, (figure 8).

The temperature dependence of the thermal conductivity for UC reported by Dayton and Tipton [13] is most consistent with the temperature dependence of the UC_xO_y data, decreasing with temperature at the lower temperatures. It is also consistent with the decrease in conductivity resulting from an increase in the oxygen content.

The decrease in thermal conductivity due to an increase in oxygen content is attributed to a decrease in both the lattice and electronic components, with the larger decreases at lower temperatures due primarily to changes in lattice conduction. The small decreases in conductivity at the higher temperatures are attributed to decreases in the electronic component of the thermal conductivity. Since uranium carbide and uranium oxycarbide are relatively good electrical conductors in the temperature range of this study, the thermal conductivity will undoubtedly be comprised of an electronic component as well as a lattice component. The electronic component might be expected to obey the Wiedemann-Franz-Lorentz law, and the lattice component will vary inversely with temperature. The following analysis was made to determine qualitatively the changes in λ_ℓ and λ_e which contribute to the decrease in the total thermal conductivity.

The lattice component of the thermal conductivity can be derived by

$$\lambda_\ell = \lambda - \lambda_e \tag{1}$$

where λ_ℓ = lattice conductivity, λ = total conductivity and λ_e = electrical conduction. λ_e can be estimated from the electrical conductivity assuming the validity of the Wiedemann-Franz-Lorentz law

$$\lambda_e = L\ T\ \sigma \tag{2}$$

Data on the electrical properties of uranium oxycarbide are very limited. Ideally, measurements should be made on the same specimens used for thermal diffusivity studies. However, because of the low resistance of the small oxycarbide specimens and the difficulty in fabricating long specimens of high quality, only one reliable data point has been obtained to date. This result indicated that resistivity at room temperature for the oxycarbide was significantly higher than for uranium monocarbide (see figure 9).

Some recent preliminary electrical resistivities for some uranium oxycarbides have been measured by Warren and Lacis [19]. These results show that the electrical resistivity increases with the addition of oxygen, and that the temperature dependence is approximately the same for the oxycarbides as for UC but with higher resistivity values. However, only one set of data could be compared to the specimens used in this study since only electrical resistivity data for oxycarbides with the same stoichiometry ($\sim$50 at.% C) and same oxygen content could be used.

The electrical resistivities for UC ($\sim$50 at.% C) and for stoichiometric uranium oxycarbide with $\sim$15 at.% oxygen used in this analysis are illustrated in figure 9. The electrical resistivity of UC reported by Carneglia [20] is approximately 10% higher than the resistivity reported by Mustacchi et al. [21]. An average of the two sets of data for each temperature was used in this analysis.

The resistivity curve for uranium oxycarbide combines the data of Warren and Lacis [19] for $U_{0.50}C_{0.38}O_{0.15}$ at the higher temperatures with the room temperature data point obtained for $U_{0.495}C_{0.355}O_{0.15}$. The curve is estimated for the intermediate temperatures.

The electrical resistivity curves for the intermediate oxycarbide compositions of 2 and 3 at.% oxygen were estimated from the resistivity curves for UC and $U_{0.495}C_{0.355}O_{0.15}$ (figure 9). It was assumed that the predominant conducting mechanism at 1400°C for UC and the oxycarbides is λ_e and that the differences in the thermal conductivity at 1400°C reflect the differences in the electronic components between specimens.[5] The thermal conductivity data of Dayton and Tipton [13] were used in this analysis since data over the entire temperature range was available. The ratio of the difference between the thermal conductivity of each oxycarbide and UC at 1400°C was the ratio used to estimate the electronic resistivity of the intermediate oxycarbides

[5] Since the thermal conductivity values for $U_{0.495}C_{0.355}O_{0.15}$ and $U_{0.495}C_{0.335}O_{0.17}$ are very close, no attempt was made to separate; only the former is used in the analysis.

($U_{0.495}C_{0.485}O_{0.02}$ and $U_{0.48}C_{0.49}O_{0.03}$) at all temperatures. This assumes that the change in lattice conduction due to oxygen content at 1400°C is negligible.

The electronic component for UC and for the oxycarbides was calculated using eq (2) assuming a theoretical Lorentz number of 2.45×10^{-8} V^2/deg^2 $\left(\frac{\text{watts-ohm}}{(^oK)^2}\right)$ (figure 10). The lattice component was then determined using eq (1) and the measured thermal conductivity values (figure 10). The thermal resistance is also plotted as a function of temperature to determine how closely the lattice component agrees with an inverse temperature relation (figure 11). The linearity of the oxycarbides and UC is relatively good. The thermal conductivity for UC had a lower lattice conductivity than was anticipated. This could have resulted from the inappropriate choice of thermal conductivity data (Dayton and Tipton [13]) since the data relate to 50.3 at.% C in the UC. (It has been demonstrated that the thermal conductivity varies significantly due to stoichiometry.)

The results of this analysis of the thermal and electrical conductivity of UC_xO_y demonstrates qualitatively that both the lattice and electronic conduction of uranium oxycarbide decrease with increasing oxygen content. It also shows that the larger changes occur in the lattice component at the lower temperatures, whereas the thermal conductivity decrease above 1400°C results primarily from changes in the electronic component.

Further study will be necessary to obtain a quantitative understanding of the effects of oxygen composition on the thermal and electrical properties of UC_xO_y.

4. Acknowledgement

The author is indebted to Jack Henry and his associates at the U. S. Bureau of Mines, Albany, Oregon, for providing the specimens for this study.

5. References

[1] Henry, J. L., Paulson, D. L., Blickensdorfer, R. and Kelley, H. J., Phase Relations in the Uranium Monocarbide Region of the System Uranium - Carbon - Oxygen at 1700°C, US Bureau of Mines, No. 6968 (July 1967).

[2] Stoops, R. F. and Hamme, J. V., Phase Relations in the System Uranium - Carbon - Oxygen, J. Am. Cer. Soc. 47 No. 2, 59-62 (1964).

[3] Morlevat, J. P., Contribution a L'Etude du Système Uranium - Carbone - Oxygène, CEA-R-2857 (1965).

[4] Chiotte, P., Robinson, W. C. and Kanno, M., Thermodynamic Properties of Uranium Oxycarbides, J. Less Common Metals 10 273-289 (1966).

[5] Parker, W. J., Jenkins, R. J., Butler, C. P. and Abbott, G. L., Flash Method of Determining Thermal Diffusivity, Heat Capacity, and Thermal Conductivity, J. Appl. Phys. 32 1679-1684 (1961).

[6] Rudkins, R. L., Jenkins, R. J. and Parker, W. J., Thermal Diffusivity Measurements on Metals at High Temperatures, Rev. Sci. Inst. 33 21-24 (1962).

[7] Cowan, R. D., Proposed Method of Measuring Thermal Diffusivity at High Temperatures, J. Appl. Phys. 32 1363-1370 (1961).

[8] Cowan, R. D., Pulse Method of Measuring Thermal Diffusivity at High Temperatures, J. Appl. Phys. 34 976-977 (1963).

[9] Cody, G. D., Abeles, B. and Beers, D. S., Thermal Diffusivity of Armco Iron, Trans. Met. Soc. AIME 221 (2) 25 (1961).

[10] Godfrey, T. G., Fulkerson, W., Kollie, T. G., Moore, J. P. and McElroy, D. L., Thermal Conductivity of Uranium Dioxide and Armco Iron by an Improved Radial Heat Flow Technique, ORNL-3556 (June 1964).

[11] Shanks, H. R., Klein, A. H. and Danielson, G. C., Thermal Properties of Armco Iron, J. Appl. Phys. 38, No. 7, 2885-2892 (1967).

[12] Wheeler, M. J., Thermal Conductivity of Uranium Monocarbide, Carbides in Nuclear Energy V-1 (L. E. Russell, Editor) McMillan and Co., Ltd., London, 358-365 (1964).

[13] Dayton, R. W., and Tipton, C. R., Jr., Progress Relating to Civilian Applications during August 1959, Battelle Memorial Institute, Columbus, Ohio, BMI-1377 102 (1959).

[14] Grossman, L. N., High-Temperature Thermophysical Properties of Uranium Monocarbide, J. Am. Cer. Soc. 46, No. 6, 264-267 (1963).

[15] DeCrescenta and Meller, Uranium Carbide at High Temperatures, Carbides in Nuclear Energy V-1 (L. E. Russell, Editor) McMillan and Co., Ltd., London, 344-349 (1964).

[16] Leary, J. A., Thomas, R. L., Ogard, A. E. and Wonn, G. C., Thermal Conductivity and Electrical Resistivity of UC, (U,Pu)C, and PuC, Carbides in Nuclear Energy V-1 (L. E. Russell, Editor) McMillan and Co., Ltd., London, 365-372 (1964).

[17] Henry, J. L. and Bates. J. L., Private Communication - to be published.

[18] Godfrey, T. G., Wooley, J. A. and Leitnaker, J. M., Thermodynamic Properties of Uranium Carbides, J. Nuclear Materials 21 175-189 (1967).

[19] Warren, I. H. and Lacis, J., University of British Columbia, Vancouver, Canada, Private Communication (1967).

[20] Carneglia, S. C., Single Crystal and Dense Polycrystalline Uranium Carbide: Thermal, Mechanical, and Chemical Properties, Carbides in Nuclear Energy V-1 (L. E. Russell, Editor) McMillan and Co., Ltd., London 407-412 (1964).

[21] Mustacchi, C. and Guiliani, S., Development of Methods for the Determination of the High Temperature Thermal Diffusivity of UC, EUR-337.e (1963).

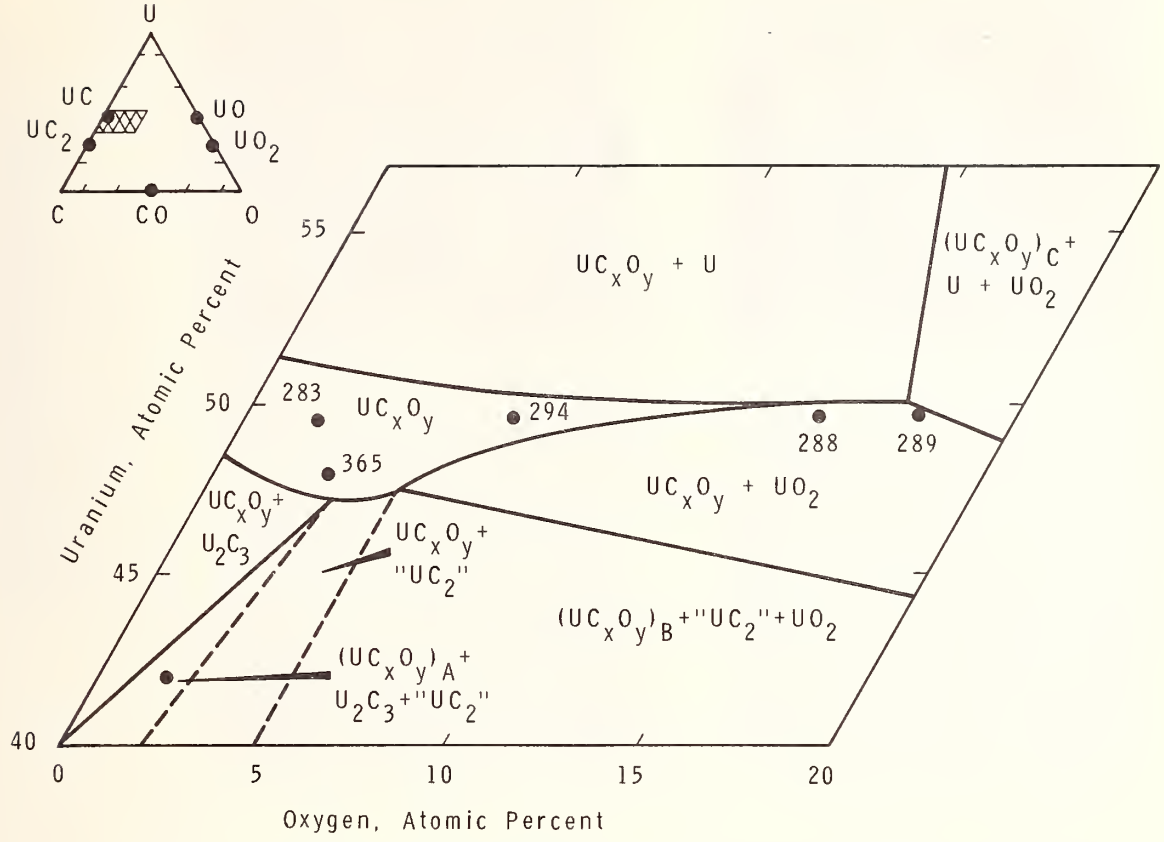

FIGURE 1 Phases and Phase Relations in the U-C-O System at 1700°C Showing Composition of Uranium Oxycarbide Samples [1].

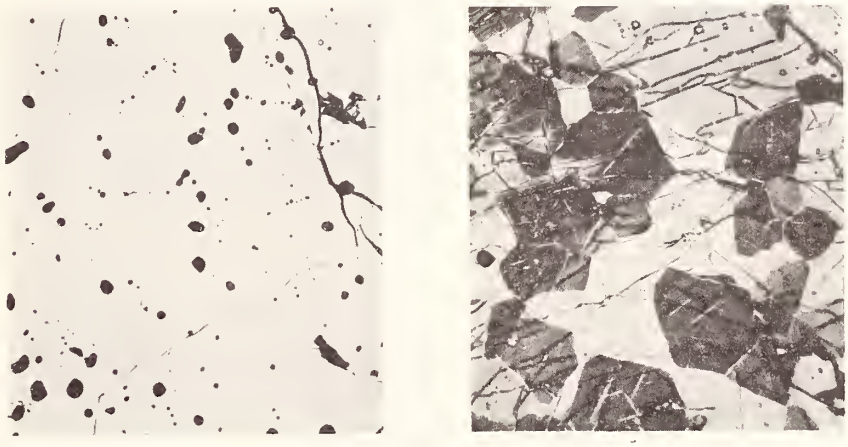

As Polished As Etched

FIGURE 2 Microstructure of $U_{0.495}C_{0.485}O_{0.02}$ (UCON-283) Before and After Thermal Diffusivity Measurements to 1500°C. The Oxycarbide is Single Phase with a Trace of Free Uranium (White Phase). 281X

Before Measurements

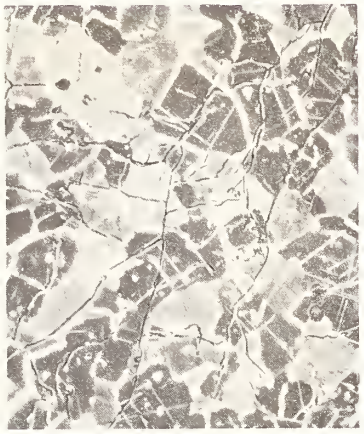

After Measurements

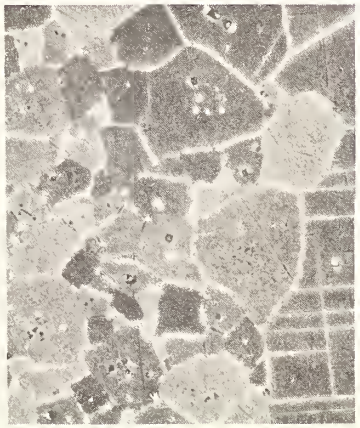

As Polished

As Etched

FIGURE 3 Microstructure of $U_{0.48}C_{0.49}O_{0.03}$ (UCON-365) Before and After Thermal Diffusivity Measurements to 1500°C. The Oxycarbide Contains a Second Phase of U_2C_3 (White Phase at Grain Boundaries) and a Trace of UO_2. 281X

Before Measurements

After Measurements

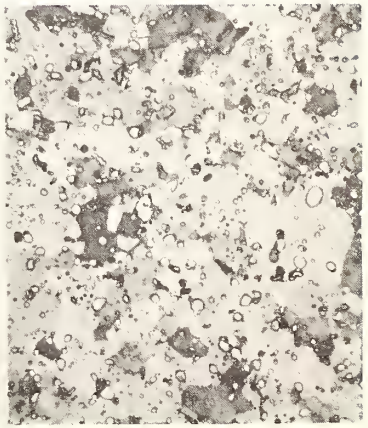

As Polished

As Etched

FIGURE 4 Microstructure of $U_{0.495}C_{0.355}O_{0.15}$ (UCON-288) Before and After Thermal Diffusivity Measurements to 1500°C. The Oxycarbide is two Phase with Minor Phase of UO_2 (Grey Phase in as Polished and White in Etched Surfaces) and a Trace of Free Uranium (a White Phase in as Polished Surface). Black Areas are Pores. 281X

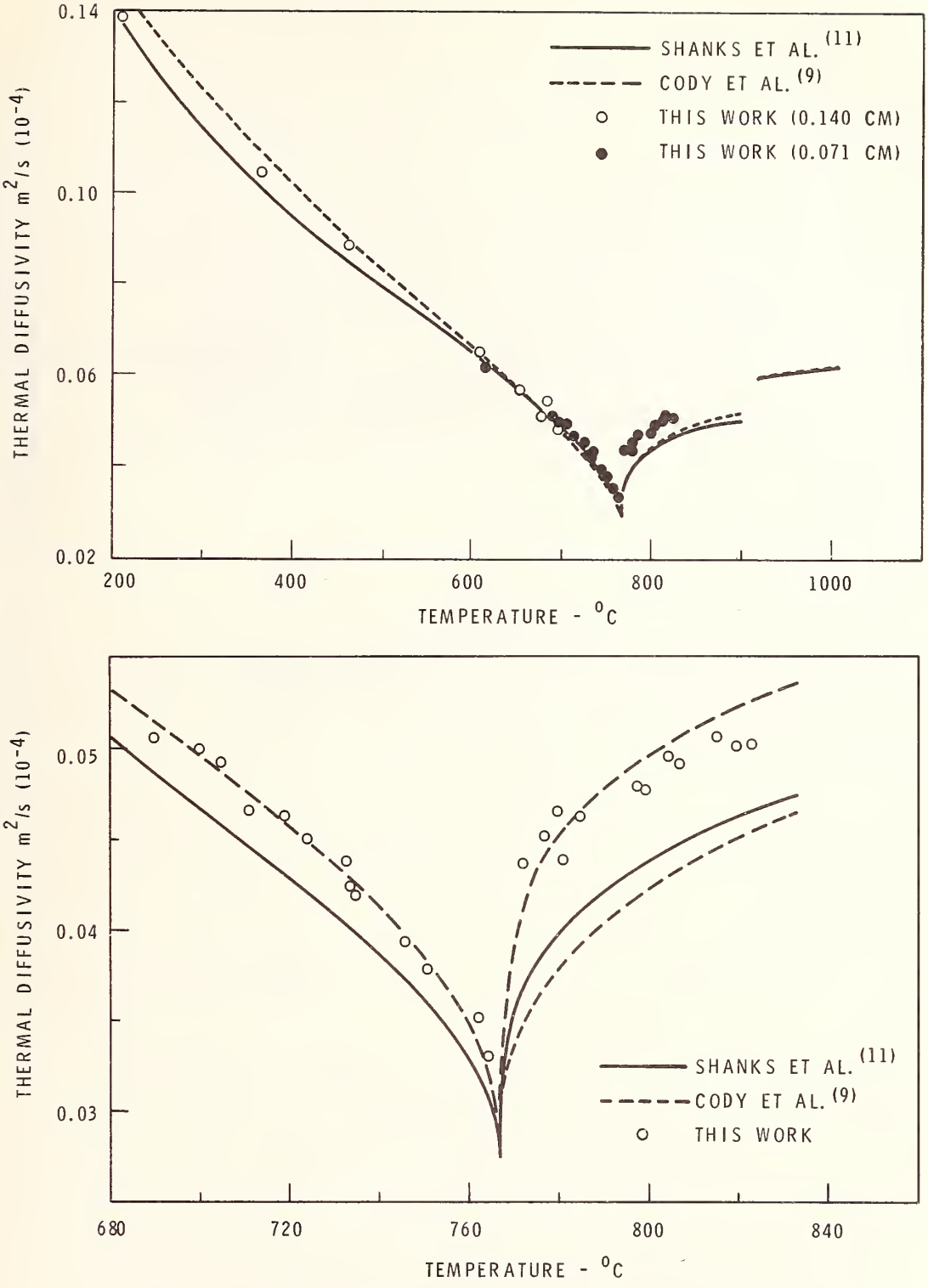

FIGURE 5 Thermal Diffusivity of Armco Iron.

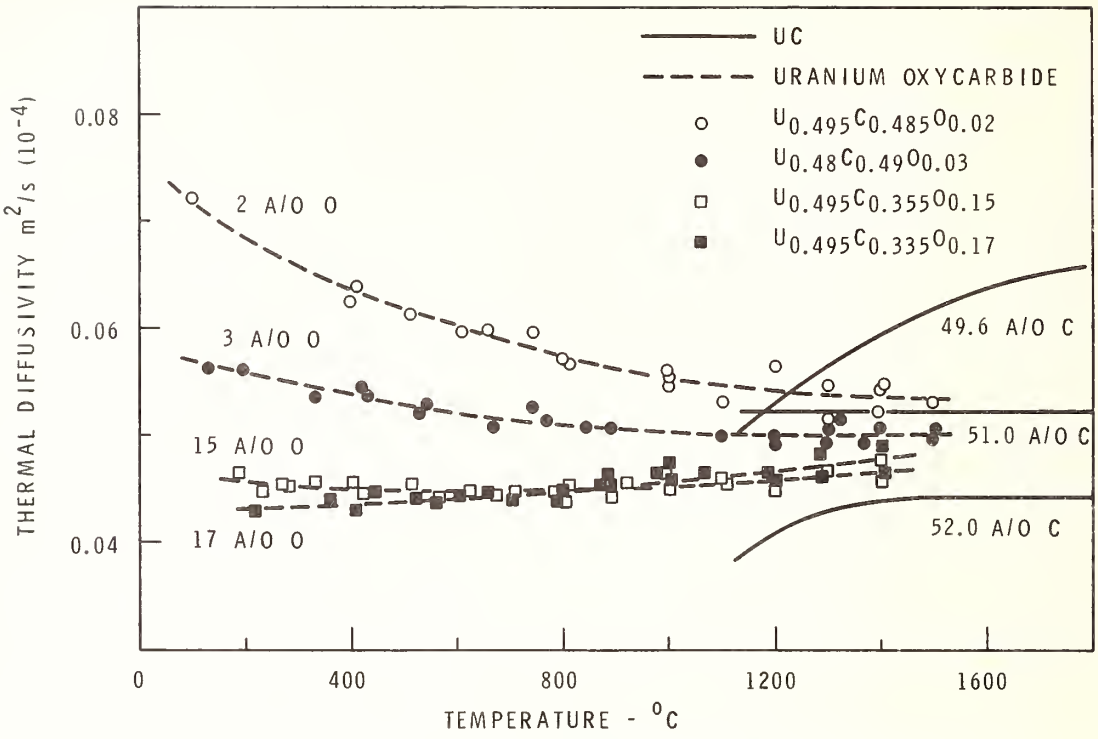

FIGURE 6 Thermal Diffusivity of Uranium Oxycarbide in Relation to the Thermal Diffusivity of Uranium Monocarbide.

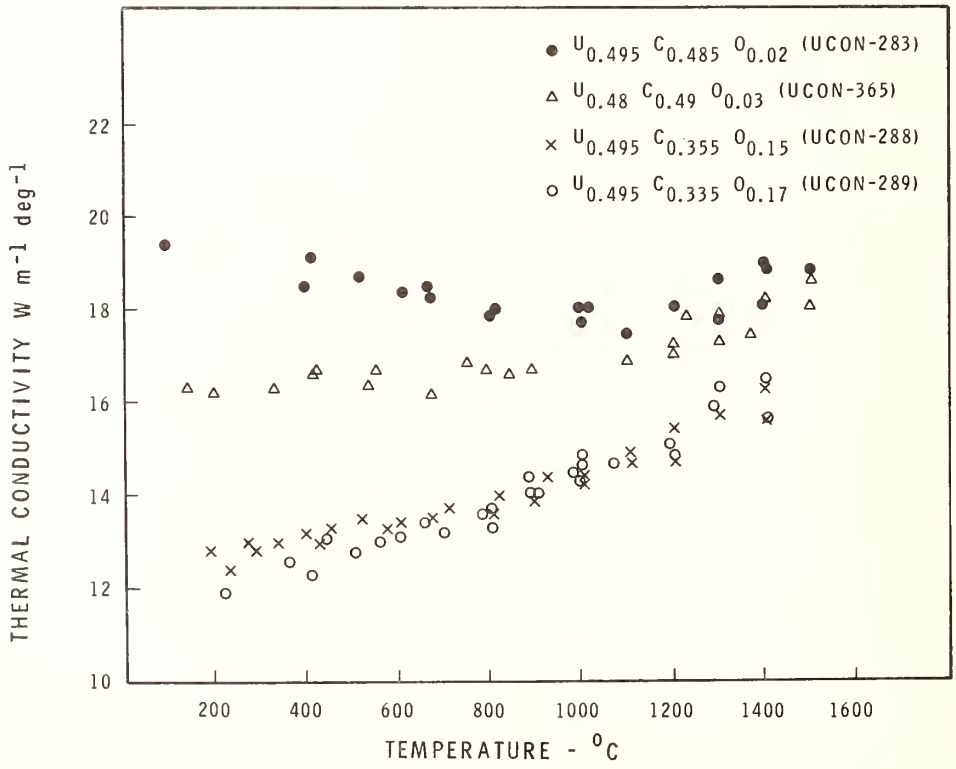

FIGURE 7 Thermal Conductivity of Uranium Oxycarbides. (Not Corrected for Density)

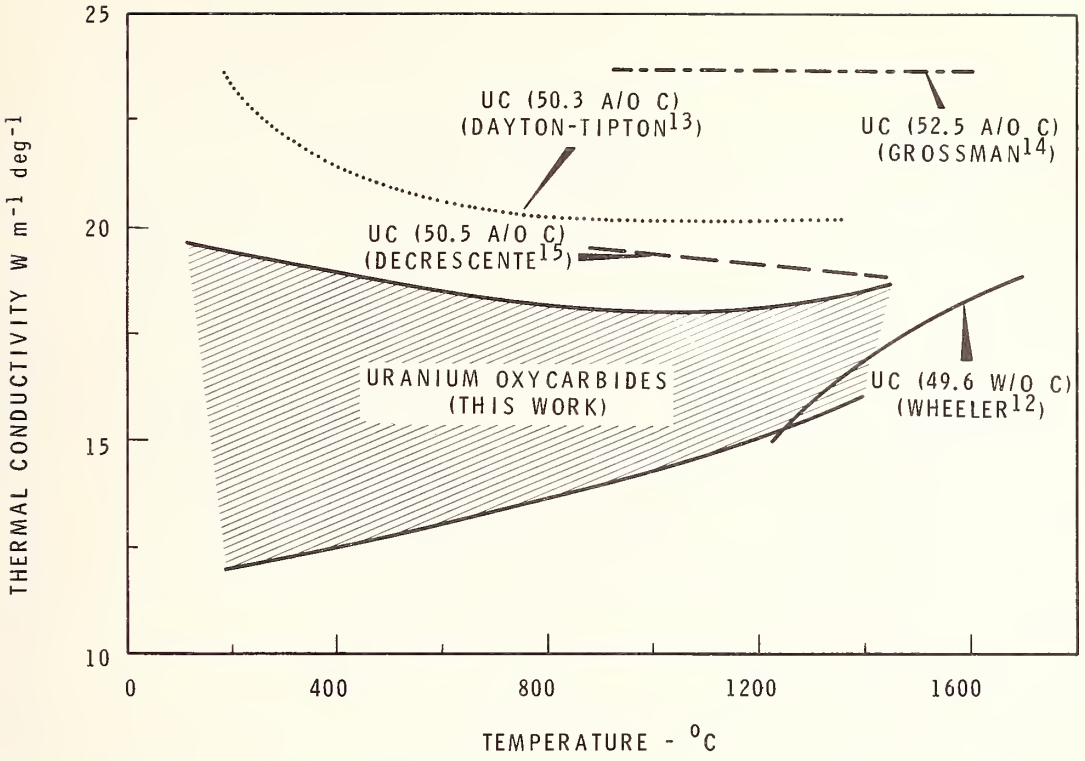

FIGURE 8 Thermal Conductivity of Uranium Oxycarbides in Relation to the Thermal Conductivity of Uranium Monocarbides.

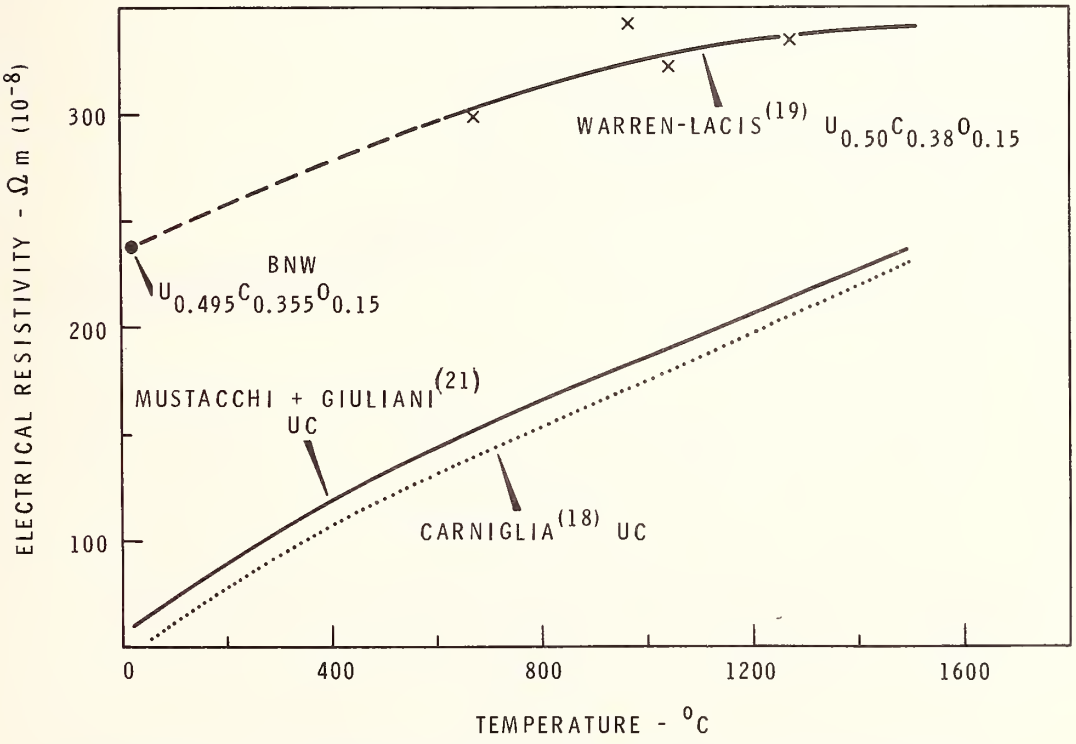

FIGURE 9 The Electrical Resistivity of Uranium Oxycarbide and Uranium Monocarbide.

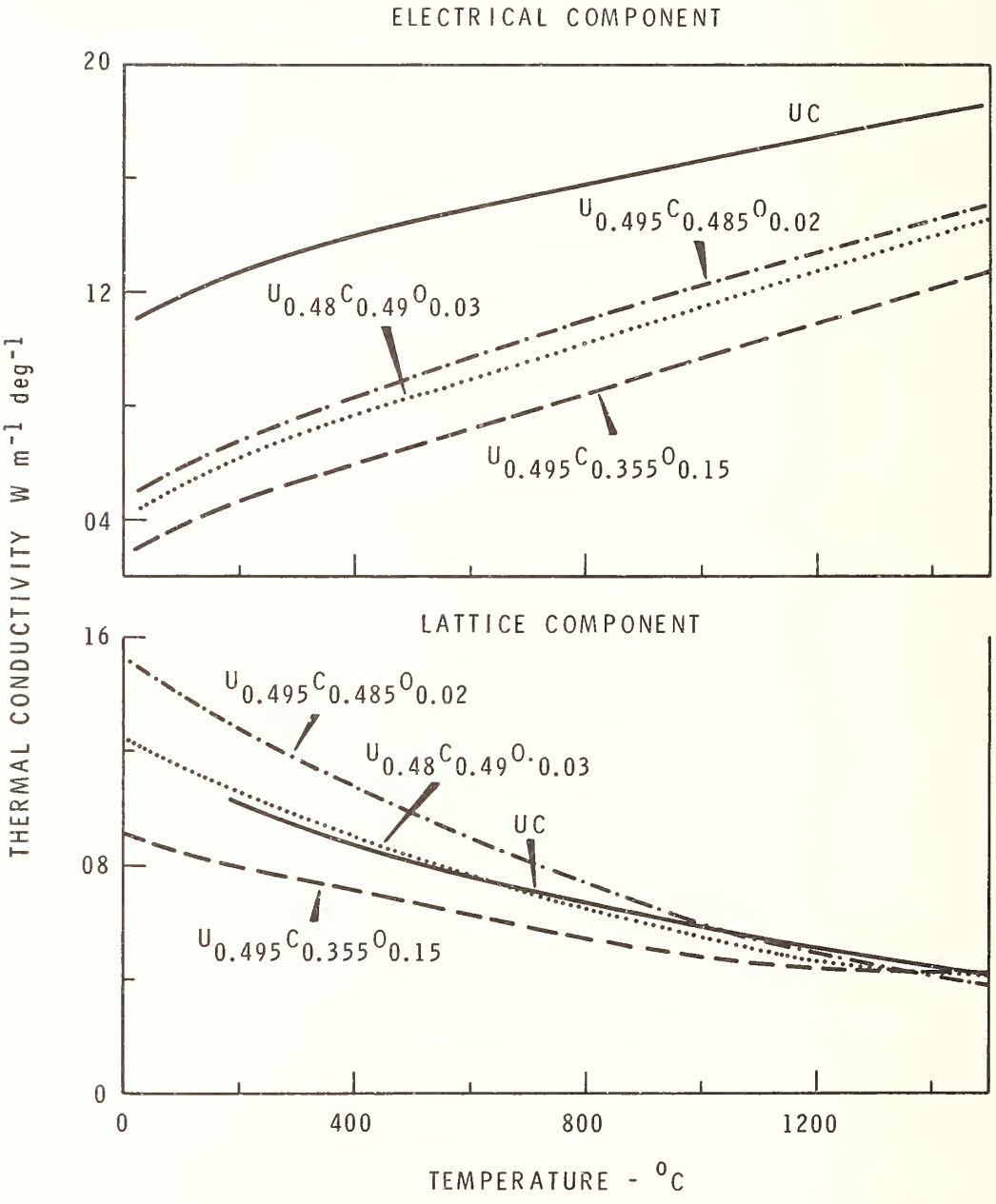

FIGURE 10 The Electronic and Lattice Components of the Thermal Conductivity for Uranium Oxycarbides.

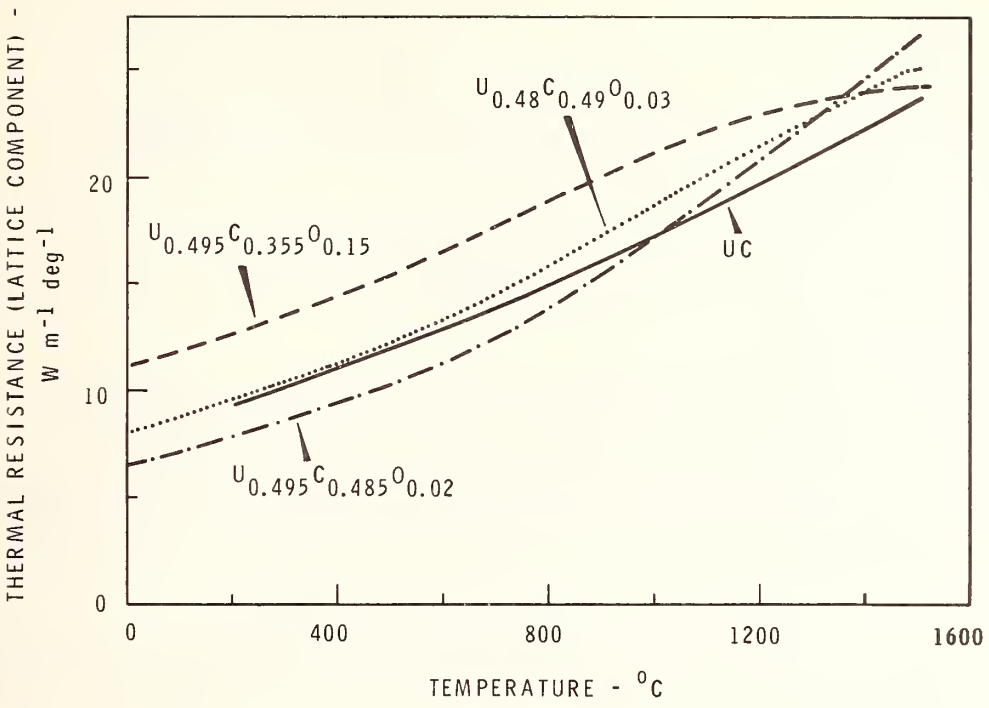

FIGURE 11 The Thermal Resistance of the Lattice Component for Uranium Oxycarbide as a Function of Temperature.

The Effect of Irradiation on the Thermal Conductivity of Some Fissile Ceramics in the Range 150-1600°C Up To a Dose of 10^{21} Fissions cm^{-3}

D. J. Clough

United Kingdom Atomic Energy Authority,
Metallurgy Division, Harwell,
ENGLAND

A study has been made of the effects of irradiation on the thermal conductivity of polycrystalline sintered UO_2 and arc cast and sintered UC.

Measurements have been made continuously during irradiation in a series of experiments, the irradiation capsule being designed to act as a calorimeter. Temperatures have been measured both at the centre of the specimen and its periphery to eliminate the contribution of the specimen/cladding interface to the measured temperature drop.

It has been shown that up to 4×10^{19} fissions cm^{-3} measurable defect damage effects are restricted to continuous irradiation temperatures below 500°C both in UO_2 and UC. Below 500°C in UO_2 reductions of up to 30% in thermal conductivity have been measured up to 4×10^{19} fissions cm^{-3}. The nature of the damage is both dose and temperature dependent as evidenced by anneals performed during irradiation.

Values obtained for UO_2 between 500°C and 1600°C lie close to presently accepted values for the unirradiated material as do those for UC between 500°C and 700°C.

Extension of work to 10^{21} fissions cm^{-3} has shown that the effects of high burn-up on thermal conductivity in both UO_2 and UC irradiated under conditions of high restraint between 500 and 700°C are small (<10%). Low temperature damage phenomena and factors contributing to the possible modification to the thermal conductivity under irradiation to high fission depletions are discussed.

Key Words: Annealing behaviour, arc-cast, conductivity, damage, dose, high burn-up irradiation, restraint, sintered, thermal conductivity, uranium oxide, uranium carbide.

Phase Studies on Fueled Zirconium Hydride[1]

M. M. Nakata, C. A. Smith, and C. C. Weeks

Atomics International
A Division of North American Rockwell Corporation
P. O. Box 309
Canoga Park, California 91304

The phase boundaries of the zirconium-uranium-hydrogen system for atomic ratios from H/Zr - 1.60 to 1.81 were determined by electrical resistivity and thermal expansion measurements. The standard potential drop technique was employed for electrical resistivity measurements and a quartz dilatometer was used for the expansion measurements. Because the hydride dissociates at elevated temperatures, each apparatus was designed to operate with hydrogen gas in the system to maintain the composition of the material. Resistivity measurements were made in the range of 20 to 900°C and with 1.33×10^{-4} to 9.33×10^{5} N/m^2 (10^{-6} to 7×10^{3} torr) of hydrogen gas in the system. Expansion measurements were made between room temperature and 700°C and with 1.33×10^{-4} to 1.87×10^{5} N/m^2 (10^{-6} to 10^{3} torr) of hydrogen. In addition to phase boundary determinations, the thermal expansion coefficients were determined for the various H/Zr ratios. The results of the electrical resistivity and thermal expansion measurements were found to correlate well with data of Moore & Young obtained by x-ray diffraction and hot-stage metallographic techniques.

Key Words: Electrical resistivity, expansion, hydride, phase studies, resistivity, thermal expansion, zirconium hydride, zirconium-uranium-hydrogen system.

(Publication of the complete phase studies work, including the x-ray diffraction and hot-stage metallographic work, in a scientific journal is contemplated; the journal is not identified at this time.)

---

[1] Work done under AEC Contract AT(04-3)-701

On the Development of Methods for Measuring Heat Leakage of Insulated Walls with Internal Convection

G. Lorentzen, E. Brendeng and P. Frivik

Norges Tekniske Høgskole
Trondheim
Norway

The combined effect of conduction and convection has great practical importance in the design of insulated structures. Much more data is needed to permit an exact precalculation of the heat leakage. The ordinary types of apparatus for conductance measurements are inadequate when convection occurs as a result of its influence on the edge compensation and the scale effect.

The performance of insulation with internal natural convection has been studied on full size structures for many years at the refrigeration laboratory of the Norwegian Institute of Technology. An account is given of the methods used and their limitations. Heat flowmeters can give quite accurate data for walls with fibrous or granular insulation with uniform flow resistance, while the convection effect in slab type insulations with slits is much more difficult to measure. A special large "hot box apparatus" has been designed for the testing of such structures. Computer programmes offer the possibility of calculating the convection influence for any wall design with known characteristics and operating conditions. Good agreement of calculated and measured results has been achieved.

Key Words: Computer calculation of internal convection, convection effect, heat flowmeters, hot box apparatus, natural convection, thermal insulation, wall insulation testing.

1. Introduction

It has been found that natural and forced convection can add significantly to the heat leakage of insulated structures (3)[1]. Convection may occur in fibrous or granular materials, which are not completely air tight, as well as in the channel system formed by slits and cracks between insulation slabs, created during erection or as a result of subsequent shrinkage. Data on the effect of convection under actual operating conditions are needed for accurate calculation of heating or cooling loads and for setting up standards of suitable insulation design. This report is concerned with natural convection only.

In a horizontal plate apparatus with the heat flow going downwards no convection can occur, and even with upwards flow the effect will ordinarily be negligible because the level differences are so small. Published conductivity data for insulation materials can therefore usually be taken as valid for convection free conditions. For real structures the convection will depend on their physical dimensions, extension in the vertical direction and the temperature differences, and its effect can only be determined by measurement on life-size samples. A fair number of such investigations have been carried out in our laboratory since 1956 and the programme is still in progress. A record of the methods used will be given in the following.

[1] Figures in parentheses indicate the literature references at the end of this paper.

During the first years the work was mainly concentrated on mineral fibre insulations, using a heat flowmeter technique (1). This method yields accurate results only when the air flow resistance is evenly distributed throughout the insulation material. For cases of non-uniform flow resistance, and particularly for slab type insulations with slits, a special guarded hot box method was developed (2).

2. Heat Flowmeter Method

Extreme care is necessary in using heat flowmeters if reliable results shall be hoped for. Some commonly made errors are illustrated in figure 1 A. The flowmeter adds to the heat resistance of the wall in the area where it is applied, and the heat flow measured is too low. This is particularly so where the meter is placed against a surface with relatively high conductivity, changing the heat flow pattern as schematically indicated by arrows. Another common fault is that the instrument is not sealed completely air tight to the wall. Even very small air currents are sufficient to change the reading drastically. In order to avoid these difficulties the heat flowmeters can be fitted as schematically shown in figure 1 B, giving essentially the same additional insulation over the entire wall surface, unchanged surface film coefficient and complete air seal. A sufficient number of meters must be installed on both sides of the wall to accurately measure the variation of the unit heat flow and check the heat balance (1). If the difference between the measurements of total heat flowing into and out of the wall is too large, this is a clear indication that the method is inadequate.

It is obvious that the heat flowmeter method can only be used when the heat flow varies continuously and fairly evenly over the wall area. This is the case with a homogeneous and uniformly packed mineral fibre insulation, figure 2 A. Even for this case it is necessary to use a fair number of meters to get a sufficiently accurate indication of the heat flow distribution.

When the convection flow is less regular, it is impossible to get a sufficiently accurate record of the flow distribution on the basis of a reasonable number of meter readings. Figure 2 B shows conditions for a wall with slab insulation and 1.7 mm wide slits. The heat flow distribution in a vertical cross section is charted approximately by estimation on the basis of surface temperature measurements and should be taken only as an indication of principle. It is very uneven due to the local flow of air when the slit system emanates to the surface. Heat flowmeters placed for instance as indicated in figure 2 C would give a completely distorted indication and an unreliable average. Measurements on fibre insulations with uneven packing or structural subdivisions can give similar results. In all these cases conditions are complicated by the fact that the air flow follows a three-dimensional pattern extending over the width of the wall, and the areas of the heat flow diagrams in any given section are not necessarily equal.

For this reason the heat flowmeter method has been used mainly for measurements of uniform mineral fibre insulations, and some results will be presented in section 6. The test arrangement is shown schematically in figure 3. The test wall was 2.0 m high and each section 1.1 m wide. Five heat flowmeters, each with 3 separate measuring sections, were used on both sides, giving altogether 30 individual measurements for each wall. The temperature field in the wall and air temperatures at both sides were measured with a total of 70 thermocouples per section. In order to limit the fluctuations of the heat flow measurements the temperatures on either side of the test wall were maintained constant within $\pm$ 1/10°C.

3. Guarded hot Box Method

For measuring the heat leakage of a wall with irregular convection pattern, such as occurs in slab type insulations with slits or various loose fill insulations, a special guarded hot box apparatus was constructed, figure 4. The test wall area is 1.7 x 2.2 m^2 and the standard insulation thickness 200 mm. The required temperature on the cold side is produced by a refrigeration system which is running continuously with constant capacity, and an electric heater with low thermal inertia is used for accurate temperature adjustment. An electronic thermostat with a thermistor bead sensor controls the heater and maintains the temperature with a fluctuation less than $\pm$ 0.15°C.

The electric heat supply to the hot box is taken from a stabilized voltage source and is set constant for each test. It is measured by a precision type wattmeter. The guard box temperature is maintained equal to that of the hot box by a low inertia

electric heater and alcohol cooler, governed by a 230 point thermopile in the separating wall through an electronic null amplifier. This again alternately actuates relays for heating and cooling, and the necessary temperature difference to switch from one to the other is in the order of 0.003°C. The electric circuit diagram is reproduced in figure 5.

The insulation to be tested is fitted between 10 mm panels of chipboard, stiffened on the external side by a framework made from 20 mm thin-wall steel tubing. The guard box is faced on the inside with aluminium sheet in order to limit the radiation heat exchange with the hot box. The entire apparatus is pivoted in a way to permit testing in a horizontal, convection free position or with the wall vertical, or at any intermediate angle.

Temperature differences up to about 70°C can be attained at a mean temperature in the wall of 0°C, depending on the efficiency of the insulation tested. The minimum temperature difference is decided by the fan power dissipation in the hot box and is in the order of 10°C.

3.1. Design of the Edge Area

The most critical design problem of a guarded hot box is the control of heat leakage in the edge area. The best solution necessarily depends on the nature and purpose of the test, and a number of different geometries have been used (2). One of the earlier solutions is schematically shown in figure 6 A, where the test wall extends to the inside perimeter of the hot box and has an area of 2 x 2.5 m^2. A total of 66 small electric heaters along the rim supplied the necessary heat to the part of the wall which was covered by the gasket. The heaters were fed from a constant voltage source and could be regulated by individual rheostats to give isothermal conditions at the wall surface. This could be controlled by means of a number of fine thermocouples in the gasket area. A thin strip of insulation between compensation heaters and wall surface was used to compensate for the film coefficient of the free surface, in order to avoid any temperature difference between air and hot box. In this way all heat leakage through the hot box could be eliminated, and this could also be verified by means of a number of small heat flowmeters installed around the perifery.

This method gave excellent results with regard to accuracy for reasonably convection free materials, but the extensive adjustments were rather time-consuming. When convection occurs right up to the edge region, the situation is different. In this case the adjustment of the compensation heaters to give isothermal surface constitutes a deviation from normal conditions and means that the convection air flow picks up extra heat from this source in the lower part of the test wall. Particularly in testing slab insulations with slits, where the convection current is concentrated right up to the edge, this could induce a sizable error. For such conditions another design was chosen, incorporating a convection free belt, figure 6 B. The complete hot box and rim section of the wall were made in one piece as a monolithic structure of polyurethane foam with glassfibre-polyester covering. The slits in the test wall are displaced from the critical zone, and the width of the belt is chosen sufficiently large to minimize the effect on the temperature field in the actual edge area. The measurements are simplified by the elimination of the compensation heaters, but in all other respects the principle of the heating, cooling and control systems is unchanged. The actual test wall area was reduced to 1.7 x 2.2 m^2 by the new design.

Completely air tight enclosure of the test wall is essential in order to avoid extra heat leakage by air exchange. The hot side is effectively sealed by the plastic foam cast directly against the chipboard panel. The cold side seal is produced by an inflatable tube gasket as shown on the figure. The tightness was checked by pressure test.

It is evident that the effect of convection in slits along the edge of the test section will influence the temperature field in the belt area to some extent, increasing the heat leakage in the lower part and causing a similar decrease in the upper part. The overall influence will be small and can be considered a natural part of the effect to be studied.

The old design had the advantage that all heat produced in the hot box actually passed through the test section. With the new arrangement some of it is lost through the convection free belt and must be deducted from the reading. It was therefore necessary to calibrate the apparatus and find this heat flow as a function of the temperature difference.

3.2. Calibration of Belt Leakage

The calibration was done with the test section carefully insulated with a mineral wool material for which the conductivity was known with great precision from a number of previous measurements. The measured belt heat flow for some values of the temperature difference is indicated by the observation points in figure 7 B.

It is also possible to calculate the temperature field and belt heat flow theoretically by means of an electronic computer. For this purpose a 10 mm square mesh was used, figure 7 A, and the isotherms and heat flow were calculated by iteration on Univac 1107. The necessary heat conductivity data for the polyurethane foam were measured in a normal plate apparatus while the surface temperatures were taken from actual observations on the structure itself. The calibration curve thus calculated is drawn in figure 7 B. It is seen that the deviation of the experimental points is quite small.

The temperature field and heat leakage of the belt is influenced to some extent by the conductivity of the tested material. This effect was calculated on the computer for a wide variation of conductivities, and the result is given by the curve figure 7 C. Within the actual range, covering all common insulation materials, the influence is negligibly small, figure 7 D.

The necessity to correct the measured heat leakage for the belt heat flow obviously means a somewhat reduced accuracy of the absolute value of the apparent conductivity found. However, it does not affect the accuracy of the convection heat flow, which is found as the difference of the figures measured in the vertical and the horizontal position. Any error in the belt heat flow calibration is thus automatically cancelled out.

3.3. Temperature Measurements

The surface temperatures of the test insulation are measured by 20 thermocouples on each side on the inside of the chipboard panels. Each thermocouple is attached to a 20 x 20 mm thin copper plate which is imbedded in the board, flush with the surface. The temperature pattern in the test insulation is measured similarly by means of 80 thermocouples. Another 144 are used to ascertain the temperature distribution in the edge area. All the readings are recorded to an accuracy of 3-4 μV or about 0.1°C by an automatic datalogger system. The output is in the form of punched tape, which can be directly fed into the electronic computer for processing.

4. Computer Calculation of the natural Convection Effect

The measurement of the convection effect on full size samples is very time-consuming and expensive, and it is hardly possible to really test all possible combinations of wall dimensions, insulation materials, slit geometries and temperature differences. It was therefore decided to extend the experimental results by computer calculation.

As a first step a programme was designed for calculating the convection effect in rigid board type insulations with slits (4). It is then necessary to find the air flow pattern and its influence on the temperature distribution in the wall. The heat leakage can subsequently be found from the temperature field. As the mass and heat flow processes are closely interconnected they cannot be calculated separately, and a systematic approach to the correct solution by numerical iteration becomes necessary.

The air flow in the slits is found from pressure and mass balance, figure 8. The coefficient of pressure drop in laminar flow depends on temperature and slit opening. Similarly the temperature distribution is determined by calculation of the heat balance for a large number of points, figure 9, and the accuracy depends on how fine a mesh is used. In this way we get two sets of numerous simultaneous equations, which can be solved on the computer.

The programme thus developed can be used to find the convection effect for any insulation constructed from rigid board material, which is in itself air tight, with a given slit geometry. A similar method for calculation of fibrous or granular insulations with known resistance parameters is being designed, and offers no particular difficulties.

5. Measurements of Air Flow Resistance

The computer calculations outlined require knowledge of resistance data, which can be measured in special tests. As the flow is always laminar, the pressure drop gradient is directly proportional to the velocity or mass flow. For a slit between parallel walls the pressure drop will be

$$\Delta P = 12\ \eta\ v \cdot \frac{L}{a^2} = A \cdot G$$

where η = dynamic viscosity, Ns/m^2
v = mean velocity, m/s
L = length of the slit, m
a = width of the slit, m
A = pressure drop constant, Ns/m^2kg
G = mass flow, kg/s

The results of the measurements can be given directly as pressure drop constants A or in terms of equivalent slit opening a. It was found that the pressure drop in plane-parallel slits between polystyrene foam or "onazote" slabs was about 4% higher than corresponding to the opening measured by mechanical gauging. This is presumably due to the different influence of surface roughness.

For fibrous or granular materials the flow resistance can be characterized by a "hydraulic diameter" D_h. The laminar flow pressure drop is given by the equation

$$dP/dL = \frac{32\ \eta \cdot v}{D_h^2}$$

As an example figure 10 A gives the measured effective hydraulic diameter as function of packing density for two typical mineral wool materials with fibre spectra as shown in figure 10 B.

6. Some Results

Altogether 21 different walls have been measured with the heat flowmeter method, most of them with mineral wool insulation of different density as follows:

A. Loose fill fibreglass: 17.1 - 33.4 - 47.9 - 60.6 - 77.7 - 103.7 kg/m^3
B. Fibreglass bats : 47.0 - 63.7 - 80.0 kg/m^3
C. Rockwool bats : 22.6 - 27.3 - 36.0 - 41.3 - 52.0 - 66.1 - 84.4 kg/m^3

The fibre characteristics of these materials were given in figure 10 B. The insulation thickness was 200 mm and mean temperature about 0°C. Some results in the form of apparent heat conductivities are recorded in figure 11.

So far 8 different walls have been tested in the guarded hot box apparatus, one of them with fibreglass bat insulation of 20.2 kg/m^3 density for calibration purposes, the other with rigid polystyrene or ebonite foam board and different slit openings. Measurements have been made in the horizontal, convection free position and with the wall vertical at temperature differences ranging from 8 to 76°C. A schematic of the typical slit geometry is shown in figure 12, while figure 13 records some of the results. It is obvious that important improvements can be achieved by the simple measure of sealing the surface seams. The actual effect of this operation for two different sealing methods is shown in figure 13 B. Figure 13 D illustrates the very rapid increase of convection for slits larger than 2-3 mm, particularly with high temperature difference. These curves were derived by computation.

7. Conclusion

It is possible by a suitable computer technique to extend the results of laboratory measurements of convection influence to cover all actual wall designs with accurately known characteristics. Work is in progress to provide data in a practical form for a number of commonly used types of construction. Such information will be useful in calculating cooling or heating loads and in setting up quality requirements for insulation materials and workmanship.

8. References

(1) Lorentzen, G. and Brendeng, E., On the influence of free convection in insulated, vertical walls, Proc. X Int. Congr. Refrig. Copenhagen 1959, I p. 254.

(2) Lorentzen, G. and Brendeng, E., The design and performance of a large scale guarded hot box, Bull. Int. Inst. Refrig. Annexe 1962-1, p. 29.

(3) Lorentzen, G., The influence of convection in cold store insulation, The Journal of Refrig., 1965, No. 2, p. 41.

(4) Lorentzen, G. and Nesje, R., Experimental and theoretical investigation of the influence of natural convection in walls with slab type insulation, Bull. Int. Inst. Refrig. Annexe 1966-2, p. 115.

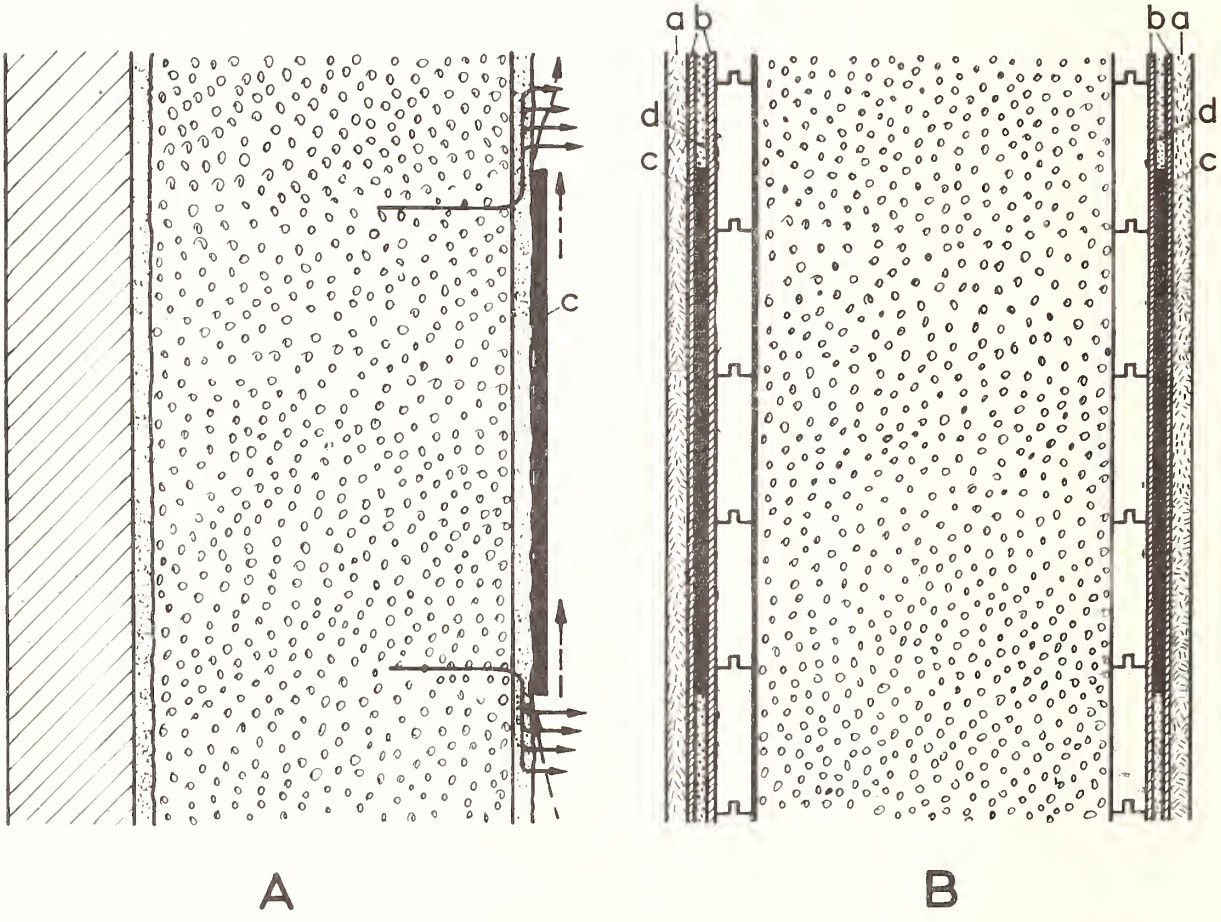

Figure 1.

A: Faulty installation of heat flowmeter may lead to large errors due to conduction in wall surface layer and air leaks, as indicated by arrows.

B: Principle of installation used in the tests.
a: Fibreboard cover plate. b: Soft "porolon" gasket. c: Heat flowmeter.
d: Plate with equal heat resistance.

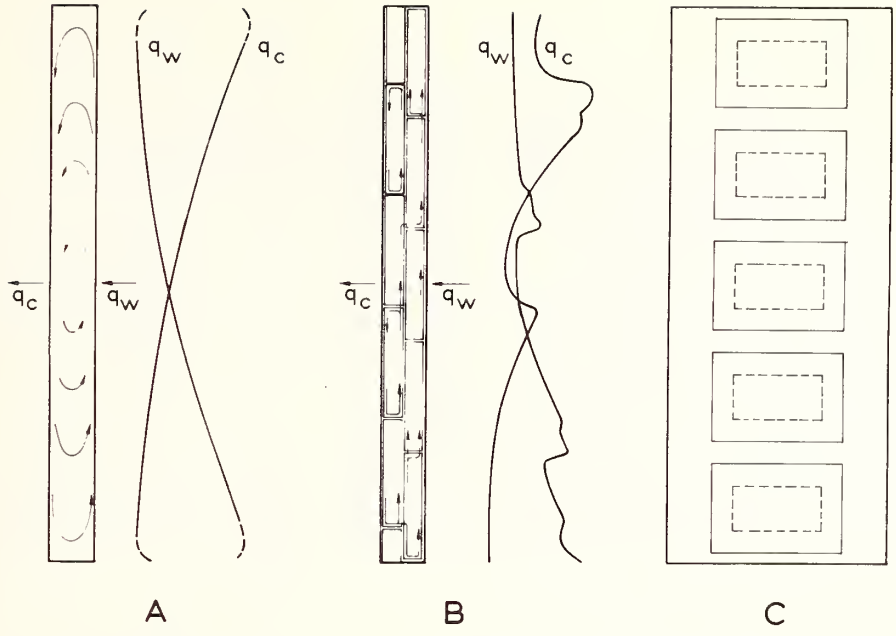

Figure 2.

A: Air flow pattern and heat flow distribution on the warm and cold side of a wall with homogeneous fibre insulation.

B: Similar indication for a wall with rigid board insulation and irregular slits.

C: Typical location of heat flowmeters.

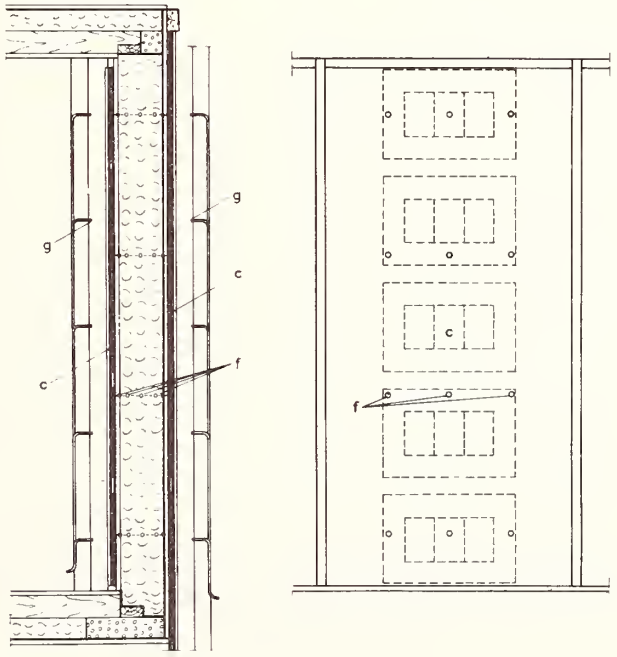

Figure 3.

Arrangement of test wall.

c: Heat flowmeters. f: Wall thermocouples. g: Air thermocouples.

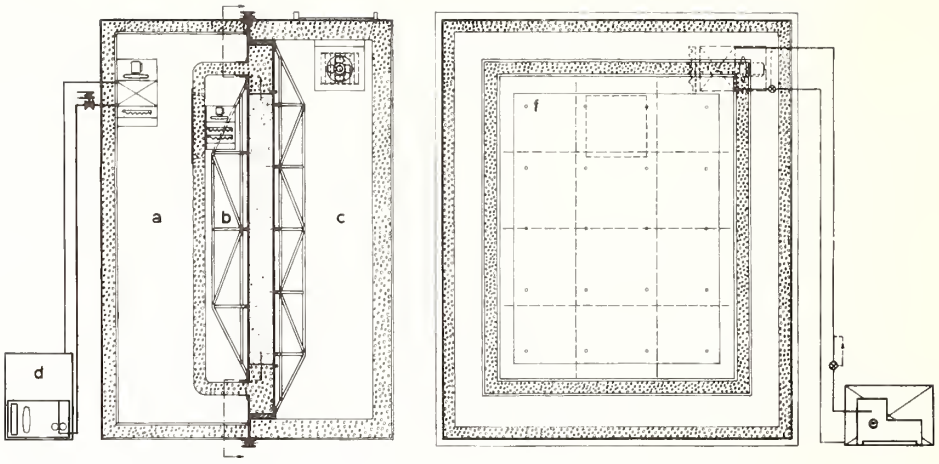

Figure 4.

Design of the "guarded hot box" apparatus in its present form.
a: Guard box. b: Hot box. c: Cold box. d: Alcohol cooling unit.
e: Refrigeration unit. f: Surface thermocouples.

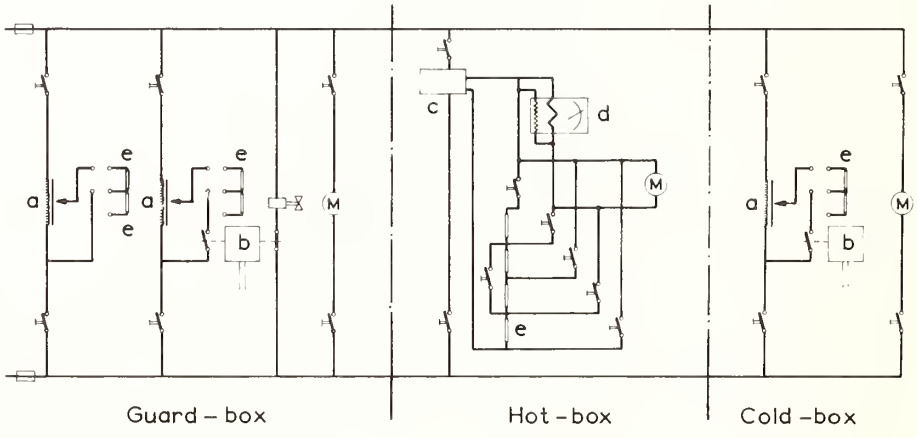

Figure 5.

Electric circuit diagram for the "guarded hot box" apparatus.
a: Voltage regulator. b: Null amplifier/thermostat. c: Voltage stabilizer. d: Precision wattmeter. e: Heater. M: Fan motor.

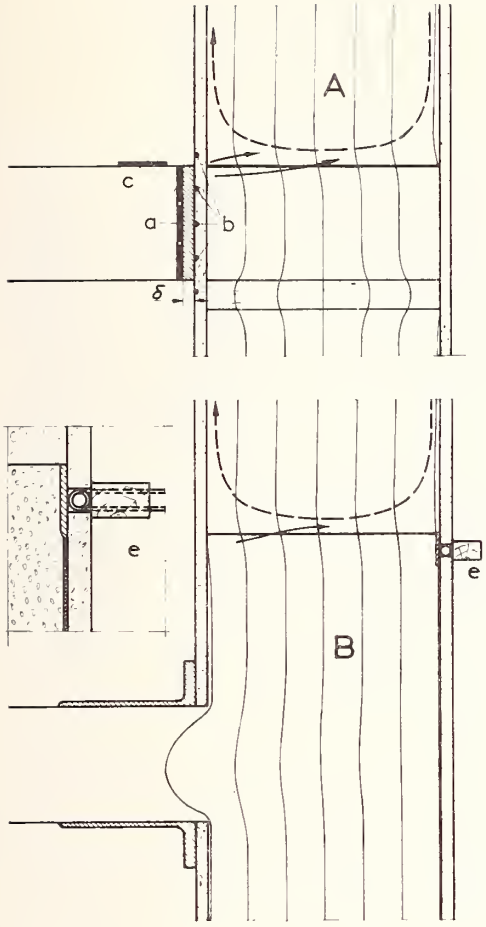

Figure 6.

A: Previous design of edge area and compensation system. a: compensation heaters. b: Thermocouples for control of isothermal conditions. c: Heat flowmeters for leakage control. d: Insulation strip with thickness $\delta = \lambda / \alpha$.
B: New design with "convection free belt." e: Inflatable gasket seal on cold side.

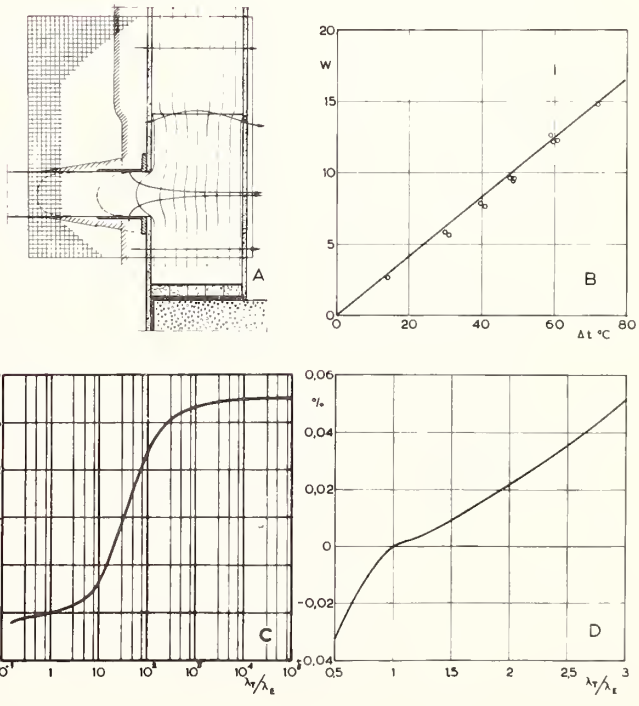

Figure 7.

A: Geometry of edge area with calculated isotherms and heat flow lines.
B: Calculated edge heat leakage as function of temperature difference (curve). Points from calibration tests are indicated.
C: Heat transfer from edge to test area in percent as a function of ratio of heat conductivity.
D: Same correction for the actual range of conductivities.

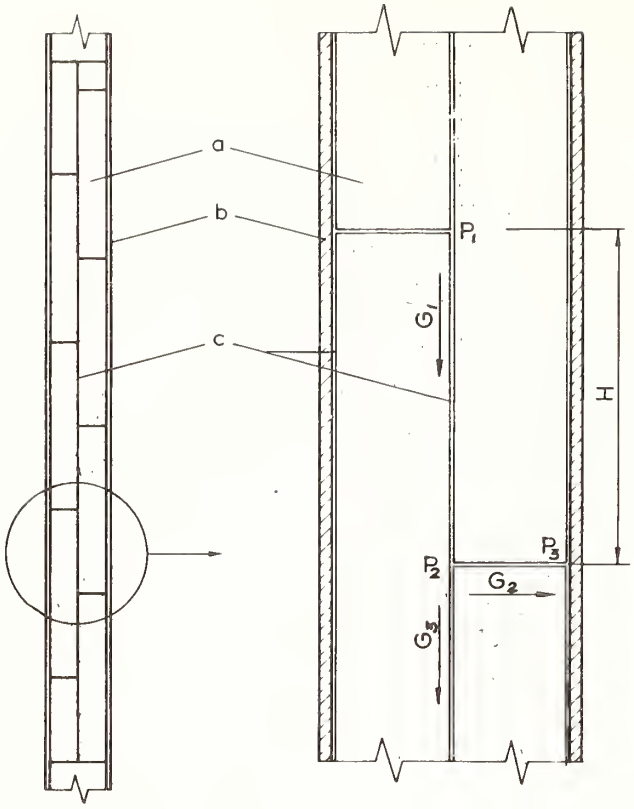

Figure 8. Pressure and mass balance for the convection air flow. a: Insulation slab. b: Paneling. c: Slits between individual slabs of insulation.

P_1, P_2, P_3 .... : Air pressure in the slit junctions.

G_1, G_2, G_3 .... : Mass flow in slits.

A, B, C ..... : Coefficient of pressure drop in laminar flow.

H_1, H_2, H_3 .... : Level difference between slit junctions.

ρ : Density of the air.

Pressure balance: $P_1=P_2-g \cdot \rho \cdot H_1-A\,G_1$

$P_2=P_3+B \cdot G_2$ etc. etc.

Mass balance : $G_1-G_2-G_3=0$ etc. etc.

Similar equations can be written for the whole system and solved on the computer.

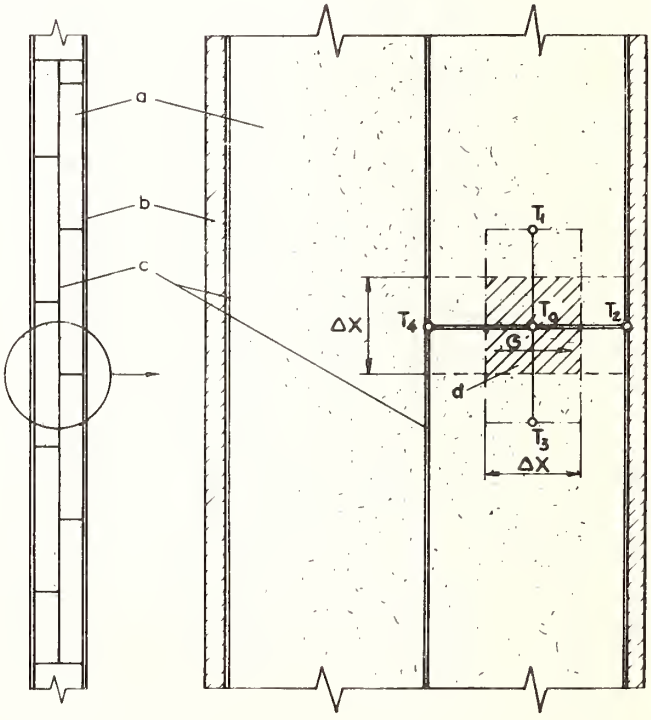

Figure 9. Heat balance for a point in the wall.

T_0, T_1, T_2 .... : Temperature in equidistant points.

G : Air mass flow.

λ : Heat conductivity of insulation material.

Δx : Network modulus.

B : Width of the constant geometry section.

c_p : Spec. heat of air.

Heat balance: $\lambda \cdot B\,(T_1+T_2+T_3+T_4-4T_0)=\frac{1}{2}G \cdot c_p\,(T_2-T_4)$.

For no air flow: $(T_1+T_2+T_3+T_4-4T_0) = 0$.

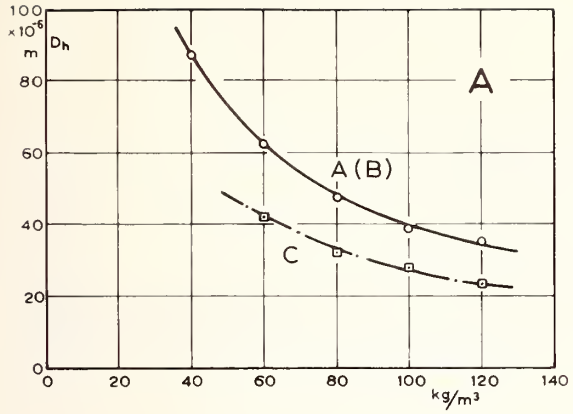

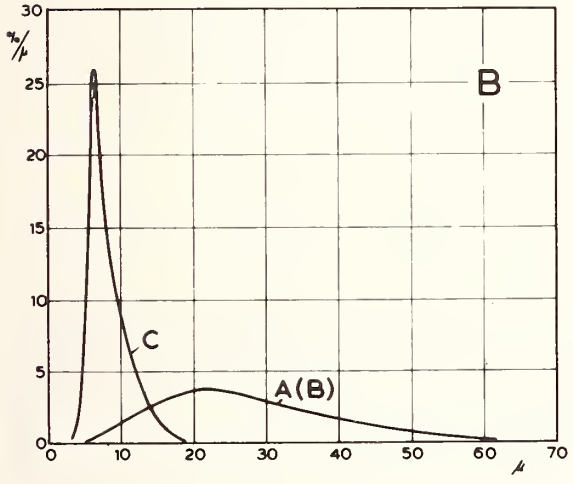

Figure 10.

A: Effective hydraulic diameter for two mineral fibre materials at different density.
B: Fibre diameter distribution for the materials investigated.

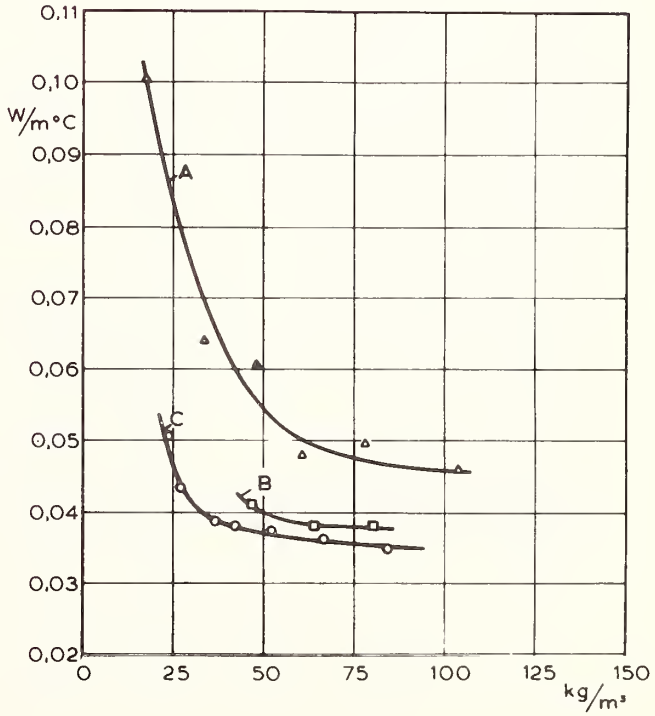

Figure 11. Apparent mean conductivity for walls insulated with different mineral fibre materials with different density.
Curve A: Loose fill insulation, material A.
Curve B: Mat insulation, material A.
Curve C: Bat insulation, material C.

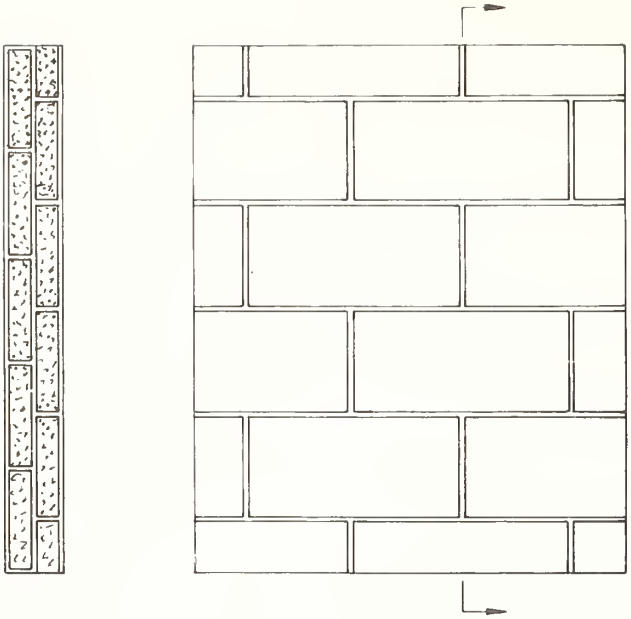

Figure 12. Schematic slab arrangement and slit geometry for test walls with rigid board insulation.

Figure 13.

A: Apparent mean heat conductivity for a polystyrene foam wall insulation with two values of the average slit opening. Results for the same walls in a convection free horizontal position are also shown. The increase due to convection is about 17 percent at $\Delta T = 70\ ^{o}C$ for 2.5 mm slits.

B: Apparent mean heat conductivity for a polystyrene foam wall insulation with 2.5 mm average slits. The improvement by sealing the surface seams on one side is shown.

C: Results for an "onazote" wall insulation.

D: Computer calculated apparent heat conductivity as a function of slit opening for different values of ΔT. The influence of radiation is excluded.

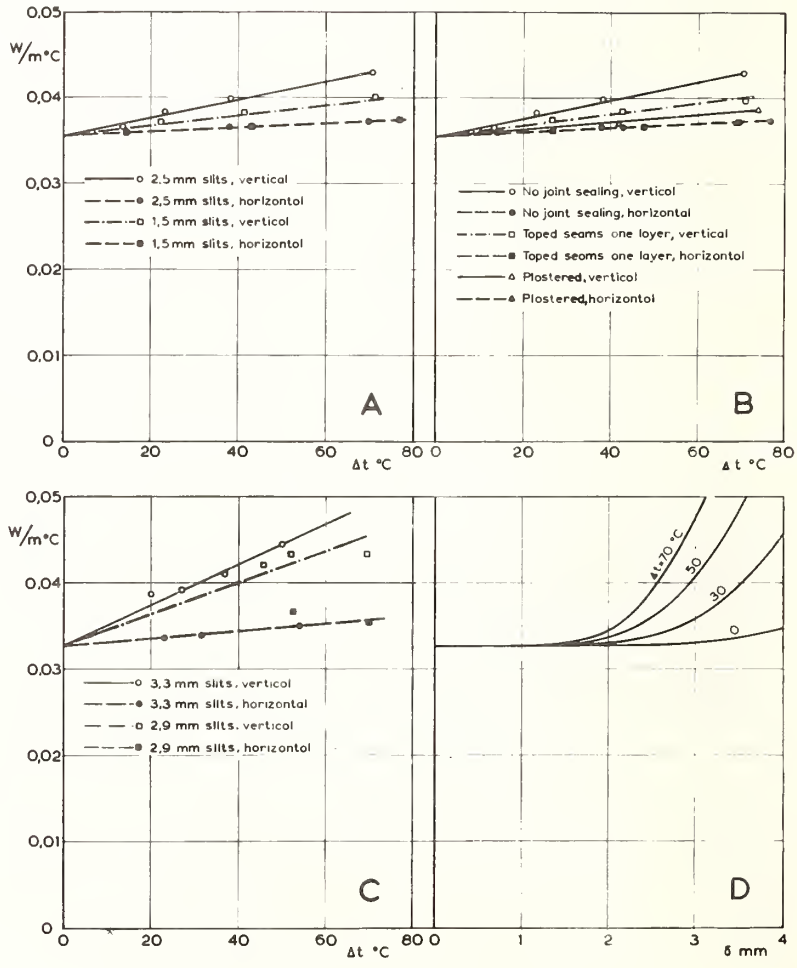

Thermal Diffusivity Measurements from a Step Function Change in Flux Into a Double Layer Infinite Slab

E. K. Halteman and R. W. Gerrish, Jr.[1]
Pittsburgh Corning Corporation
Pittsburgh, Pa. 15239

A step function change of flux into an infinite slab with the output face held at constant temperature was used to determine thermal diffusivity by using a graphical and a time integral method. Samples of gum rubber and foamed polyurethane were used to show deviations from the expected result of the single layer infinite slab theory. Use of a low mass, low heat capacity heater reduced the deviations. A double layer infinite slab analysis was used so as to include the heat capacity of the heater. The error in the diffusivity using the single layer model was determined as a function of the ratio of the heat capacity per unit area of the sample and heater.

Key Words: Double layer infinite slab, heater correction, thermal diffusivity.

1. Introduction

The thermal diffusivity of ceramic and organic insulating materials is most readily obtained from transient linear heat flow through an infinite slab. The relative ease of fabricating the sample in the form of a slab makes this geometry attractive. Plummer, Campbell and Comstock [1] developed a method based on a constant flux into a thick slab of material which was treated as a semi-infinite solid. This method was further refined by Harmathy [2] who also developed a pulse heating scheme. Steere [3] used the constant flux method with samples of plastic assembled from multilayers of thin films. In all cases the finite samples were considered to be infinitely thick during the time when measurements were taken. Also, in each case the heat capacity of the heater was shown to be a small fraction of the heat capacity of the sample and was therefore not included in the analysis.

When the constant flux input method is used with a low density, low specific heat capacity, and low conductivity insulator such as foamed polyurethane, difficulties arise. The conductivities of many solid and foamed insulators are approximately proportional to their densities; hence, their diffusivities are similar. But the heat capacity per unit volume of the sample can vary widely since it depends upon density and specific heat capacity. Thus, for low density organic insulators the heat capacity of the heater may represent an appreciable fraction of the heat capacity of the sample. In such cases it is necessary to treat the heater as a separate layer with its own thermal properties and to determine the diffusivity of the sample from an analysis of a double layer infinite slab model.

2. Theory

The temperature distribution, $\theta(x,t)$, within an infinite slab of thickness, L, is given by the solution of the one dimensional equation of linear heat flow with specified boundary conditions.

$$a\,\theta_{xx}(x,t) = \theta_t(x,t) \text{ for } 0 < x < L \quad . \tag{1}$$

The distance x is measured from the input face and the thermal diffusivity, a, is assumed to be independent of position, time, and temperature. The subscripts denote differentiation with respect to a particular variable.

The boundary condition at the input face, x = 0, will be an input flux, $\Phi = -\lambda\theta_x$, which experiences a step function change at time zero. The temperature of the output face will be held constant. The

[1] Physicists

[2] Figures in brackets indicate the literature references at the end of this paper.

temperature of the output face will be held constant. The temperature of the slab will be uniform and equal to the output face temperature at time zero. These boundary conditions can be written as

$$\begin{aligned} \Phi(0,t) &= -\lambda\theta_x(0,t) = 0, \quad t < 0 \\ \Phi(0,t) &= -\lambda\theta_x(0,t) = \Phi_o, \quad t > 0 \end{aligned} \tag{2}$$

$$\theta(L,t) = 0, \quad t \geq 0 \tag{3}$$

$$\theta(x,t) = 0, \quad t \leq 0 \ . \tag{4}$$

The solution for the homogeneous single layer has been given by Carslaw and Jaeger [4] as

$$\theta(x,t) = \frac{\Phi_o(L - x)}{\lambda} - \frac{8\Phi_o L}{\lambda\pi^2} \sum_0^\infty \frac{\exp(-(2n + 1)^2\pi^2 at/4L^2) \cos(2n + 1)\pi x/2L}{(2n + 1)^2} \ . \tag{5}$$

At the input face, x = 0, and for large values of time the series can be truncated at one term to give

$$\begin{aligned} &\theta(0,t) = \theta_\infty\{1-8\pi^{-2}\exp(-\pi^2 at/4L^2)\} \ , \\ &\text{where } \theta_\infty = \Phi_o L/\lambda \ . \end{aligned} \tag{6}$$

The value of a can be determined from eq (6) or by the use of the time integral which is defined as

$$TI(x) = \int_0^\infty \{1-\theta(x,t)/\theta(x,\infty)\}dt \ . \tag{7}$$

For the input face,

$$TI(0) = L^2/3a$$

at the center of the slab, $TI(L/2) = 1.375(L^2/3a)$ and at the output face $TI(L) = 1.5(L^2/3a)$.

When the heat source for the infinite slab is in physical contact with the slab and has heat capacity itself, the conditions used in deriving eq (5) are not exactly fulfilled as it had been assumed that the heat flux came from a source with no heat capacity. Whenever an electrically energized heat source is used, the power is dissipated in a conducting element which may require a substratum for support. Thin sheets of chromel [1], constantan [2,3], palladium [2], graphite coated asbestos, and Fe-Ni evaporated on plastic have been used as heaters. If the heat capacity of the heater is an appreciable fraction of the heat capacity of the sample, it is necessary to use a double layer infinite slab for a model.

For an infinite slab composed of two layers, each of uniform thickness, an additional pair of boundary conditions are required; namely, the flux and temperature must be continuous at the interface. If the numerical subscripts refer to the sequence of layers from the front face, the boundary conditions may now be expressed as

$$\theta_1(L_1,t) = \theta_2(L_1,t) \tag{8}$$

$$\lambda_1\theta_{1x}(L_1,t) = \lambda_2\theta_{2x}(L_1,t) \tag{9}$$

$$\theta_2((L_1 + L_2),t) = 0, \quad t \geq 0 \tag{10}$$

$$\begin{aligned} &\theta_1(x,t) = 0, \quad t \leq 0, \quad 0 < x < L_1 \\ &\theta_2(x,t) = 0, \quad t \leq 0, \quad L_1 < x < (L_1 + L_2). \end{aligned} \tag{11}$$

This boundary value problem can be solved by the use of the theory of Laplace transforms which converts the partial differential equation in $\theta(x,t)$ to the ordinary differential equation in $U(x,p)$ by the use of the relation

$$U(x,p) = \int_0^\infty \exp(-pt)\,\theta\,(x,t)dt \ .$$

The transformed equations and boundary conditions become

$$U_{1xx}(x,p) - q_1{}^2U_1(x,p) = 0\,, \qquad 0 < x < L \tag{1a}$$

$$U_{2xx}(x,p) - q_2{}^2U\,(x,p) = 0\,, \qquad L_1 < x < (L_1 + L_2) \tag{1b}$$

$$U_{1x}(0,p) = -\Phi_o/\lambda_1 p \tag{2a}$$

$$U_1(L_1,p) = U_2(L_1,p) \tag{8a}$$

$$\lambda_1 U_1\,(L_1,p) = \lambda_2 U_2\,(L_1,p) \tag{9a}$$

$$U_2((L_1 + L_2),p) = 0\,, \tag{10a}$$

where $q_1{}^2 = p/a_1$ and $q_2{}^2 = p/a_2$.

Applying the boundary conditions to the general solution of the transformed equation gives

$$U_1(x,p) = \frac{\Phi_o}{pq_1\lambda_1}\left[\frac{\sigma\ \sinh q_1(L_1 - x)\ \cosh q_2L_2 + \cosh q_1(L_1 - x)\ \sinh q_2L_2}{\cosh q_1L_1\ \cosh q_2L_2 + \sinh q_1L_1\ \sinh q_2L_2}\right],\ 0 < x < L_1$$

$$U_2(x,p) = \frac{\Phi_o}{pq_1\lambda_1}\left[\frac{\sigma\ \sinh q_2((L_1 + L_2) - x)}{\sigma\ \cosh q_1L_1\ \cosh q_2L_2 + \sinh q_1L_1\ \sinh q_2L_2}\right],\quad L_1 < x < (L_1 + L_2)\,,$$

where $\sigma = q_2\lambda_2/q_1\lambda_1 = [\lambda_2d_2C_2/\lambda_1d_1C_1]^{1/2}$. (12)

The solution is given by the inverse transform of eq (12) which may be written as

$$(x,t) = \sum\ (\text{residues of } \exp(pt)\ U(x,p))_{\,p\,=\,p_n}\,, \tag{13}$$

where the summation is taken over all of the singular points p_n of $U(x,p)$. These will be at $p = 0$ and the zeros of the term in brackets of the denominator of eq (12). This term can be zero only if the arguments are imaginary, therefore

$$\sigma = \tan\alpha_{1n}L_1\ \tan\alpha_{2n}L_2 \tag{14}$$

when $q = i\alpha_n$ and it is now necessary to find the n roots of this transcendental equation. Since σ is always positive, a root can appear for only those values of α_1L_1 and α_2L_2 for which the product of the tangents is positive. Rewriting eq (14) as

$$\sigma = \lambda_2L_1A_2/\lambda_1L_2A_1 = \tan A_1\ \tan A_2\ ,$$

roots will occur at the intersections of lines of constant σ and the line with slope of $\lambda_1L_2/\lambda_2L_1$. Using these values of α_n and evaluating the residues of the singularities, the temperature in layer one is obtained as

$$\theta_1(x,t) = \Phi_o\left[\frac{(L_1 - x)}{\lambda_1} + \frac{L_2}{\lambda_2}\right] -$$

$$\frac{2\Phi_o}{\lambda_1}\sum_1^\infty \frac{(\alpha_{2n}\lambda_2 \sin\alpha_{1n}(L_1 - x)\cos\alpha_{2n}L_2 + \alpha_1\lambda_1\cos\alpha_{1n}(L_1 - x)\sin\alpha_{2n}L_2)\exp(-a_1\alpha_{1n}^2 t)}{\alpha_1 D}, \quad 0 < x < L_1$$

and in layer two as (15)

$$\theta_2(x,t) = \frac{\Phi_o[L_1 + L_2 - x]}{\lambda_2} - 2\Phi_o\sum_1^\infty \frac{\sin\alpha_{2n}(L_1 + L_2 - x)\exp(-a_1\alpha_{1n}^2 t)}{D}, L_1 < x < (L_1 + L_2)$$

where $D = [(\alpha_{1n}\alpha_{2n}\lambda_2 L_1 + \alpha_{1n}\alpha_{2n}\lambda_1 L_2)\sin\alpha_{1n}L_1 \cos\alpha_{2n}L_2 + (\alpha_{1n}^2\lambda_1 L_1 + \alpha_{2n}^2\lambda_2 L_2)\cos\alpha_{1n}L_1 \sin\alpha_{2n}L_2]$.

3. Experimental

The experimental arrangement as shown in Figure 1 consisted of a central heater, a pair of identical samples and a pair of constant temperature heat sinks. A high heat capacity heater was fabricated from an asbestos heating paper[2] consisting of a graphite conducting layer between two identical covering sheets of asbestos. The uniformity of the power generation per unit area was sufficient to produce temperature differences of less than 3% under steady state conditions when measured at a dozen points on a square foot sample. Power was supplied to the heater from a regulated AC supply.

A low heat capacity heater was fabricated from a sheet of 0.025 mm polyimide plastic[3] upon which a coating of 0.008 mm iron nickel alloy had been vacuum deposited[4]. A grid of 3.2 mm strips was formed by preferential etching of the Fe-Ni coating.

The high heat capacity samples consisting of 0.305 meter squares with a thickness of 0.0102 meter were cut from a continuous strip of gum rubber. The low heat capacity samples consisted of 0.305 meter square of .0506 m thick foamed polyurethane. A differential thermopile of two junctions of number 30 copper constantan wire was used to measure the temperature. To measure temperatures at interior points in built-up layer samples, the number of couples was increased so that the thermopile outputs were all about equal. Temperatures were recorded with a 12 point recorder at 6 sec. intervals.

The recorded temperatures at the front face of the sample were used to produce a graph of $\ln(\theta_\infty - \theta_t)/(\theta_\infty - \theta_o)$ vs time from which a could be determined from the slope. The time integrals were also determined from the recorder record by the use of numerical integration.

The heat sinks were fabricated from surface ground slabs of .0254 meter aluminum plate and were 0.61 meters square. A labyrinth of 0.00954 meter aluminum with 0.0318 meter channels was bolted to the rear of the heat sink. Thermostated, refrigerated water was circulated through the labyrinth in each sink. The sinks and samples were enclosed with 0.153 meter of foamed polyurethane and placed within an angle iron frame and at a pressure of 300 newtons/square meter applied by means of screw and torque wrench. To shield it from air currents the whole assembly was enclosed within a shroud.

4. Results

Graphical analysis of $\theta(0,t)$ for a sample of gum rubber heated by means of a graphite-asbestos heater confirmed to the expected exponential approach to equilibrium predicted by eq (5). A slight discrepancy was noted between the observed intercept of 0.82 and the expected value of $8/\pi^2 = 0.8105$. Changing to the smaller heat capacity heater of Fe-Ni on plastic lowered the intercept to 0.815 and decreased the time integral from 0.1320 hrs. to 0.1237 hrs. The diffusivity derived from the slope remained essentially the same in the two cases. The reduction in the time integral indicates that less total energy was needed to reach equilibrium as the heat capacity of the heater was reduced.

The graphite-asbestos heater was used with a sample of foamed polyurethane, a light weight insulating material having a thermal conductivity of 0.016 to 0.022 watts $meter^{-1}deg^{-1}$[5] and a density of 25 to 32 kg/m^3[5]. Graphical analysis of this case as shown in Figure 2 indicated an intercept of

[2]Cellotherm, Chemelex, Inc., Mineola, New York

[3]Kapton, Type H, E. I. duPont de Nemours and Company, Wilmington, Delaware

[4]Lashclad X, Lash Laboratories, San Diego, California

0.88 and a diffusivity of 5.71 x 10^{-7} m^2/sec. Upon changing to the Fe-Ni plastic heater, the intercept dropped to 0.83 and the diffusivity increased to 6.77 x 10^{-7} m^2/sec. The time integral was reduced from 0.482 hr. to 0.348 hr. indicating the proportionally higher ratio of the heat capacity of the heater to the sample.

To account for the heat capacity of the heater, it is necessary to consider the experiment as a double layer infinite slab. The flux is assumed to be generated in a plane at x = 0 by Joule heating of an electrical conducting coating having no thickness. The substratum supporting this coating was therefore assumed to be the first layer and to have a thickness of 1/2 of the total thickness of the asbestos-graphite-asbestos heater element. The sample is then assumed to be the second layer. The temperature and, hence, the time integral was measured at the interface between the asbestos and the sample at x = L_1.

In order to use eq (15) to find the value of a_2, it is necessary to know the value of a_1, the diffusivity of the heater substratum. This was done by preparing a sample assembled from a stack of heater elements, thereby, making the properties of layers 1 and 2 identical. The temperatures and time integrals were measured between the first four layers. Eq (15) was simplified by setting $a_1 = a_2 = a$ and, then, this was used to obtain a with the appropriate lengths used for each case. This was accomplished by using a computer program to calculate a time integral for three different values for a, parabolic interpolation to find a new value for a and a new time integral, then using the three closest a's, interpolated to find another new a and then repeating until the fractional change in a was less than 10^{-4}. This usually required 4 or 5 interpolations. A value of 1.28 $\pm$ .03 x 10^{-7} m^2/sec was found for the diffusivity of the graphite-asbestos heater. The thermal conductivity of the heater was determined from a steady state experiment using a heat flow meter.

After determining the necessary thermal properties of the heater, the foamed polyurethane graphite-asbestos heater case was re-examined as a two layer case. By using the experimentally determined time integral of 0.4823 hours and the computer program for evaluating eq (15), a diffusivity of 6.815 x 10^{-7} m^2/sec. was obtained. This result agrees with and is slightly larger than the value obtained by the use of the equation $a = L^2/3(TI)$. The small difference indicates that some error could still be present when using the Fe-Ni plastic heater. Through use of this value for the diffusivity of foamed polyurethane, a value of 1075 Joule $kg^{-1}deg^{-1}$ is obtained for the specific heat; this is in fair agreement with a reported range of 840 to 1045 Joule kg^{-1} deg^{-1} [6].

5. Heater Error Analysis

From examination of the results obtained by graphical and time integral analysis of the transient heat flow in a low heat capacity sample, it has been shown that large errors are introduced when the heat capacity of the heater is ignored. When discussing this type of error, it was found more convenient to use the extensive variables of conductance, λ/L, and heat capacity per unit area, dCL, rather than the intensive variables of conductivity, λ, and diffusivity, a. The conductance ratio, ξ, will be defined as $\lambda_2 L_1/\lambda_1 L_2$ and the ratio of the heat capacities per unit area, ρ, as $d_2C_2L_2/d_1C_1L_1$. From parametric studies of eq (15), it can be shown that at constant conductance ratios, ξ, the heat capacity ratio ρ, is given by $\rho = m[TI_o\lambda_1/d_1C_1L_1^2] + b$ where m and b are functions of ξ and TI_o is the time integral measured at x = 0. As the conductance ratio ξ becomes smaller, the slope approaches 3ξ and the intercept approaches -3. For ξ less than 0.01 the heat capacity ratio approaches $3\xi[TI(0)\lambda_1/d_1C_1L_1^2] - 3$. This can be reduced to $E = 3/\rho$ where E is the error in the time integral due to the presence of the heater; ie., $[TI_o(\text{Heater + Sample}) - TI_o(\text{Sample})]/TI_o(\text{Sample})$. TI_o(Sample) is the time integral of the sample with a massless heater measured at its input face and would be given by $TI_o(\text{Sample}) = L_2^2/3a_2$.

Table 1. Thermal diffusivities determined a step function change in flux units of meter^2/sec.

Sample	Heater	Graphical Method Eq (6)	Time Integral Method Eq (7)	Double Layer Method Eq (15)
Gum Rubber	Graphite, Asbestos	7.97 x 10^{-8}	7.31 x 10^{-8}	
	Fe-Ni, Polyimide	7.97 x 10^{-8}	7.81 x 10^{-8}	
Foamed Polyurethane	Graphite, Asbestos	5.71 x 10^{-7}	4.92 x 10^{-7}	6.815 x 10^{-7}
	Fe-Ni, Polyimide	6.77 x 10^{-7}	6.805 x 10^{-7}	

5. References

[1] Plummer, W. A., Campbell, D. E. and Comstock, Method of measurement of thermal diffusivity to 1000°C, J. Am. Ceram. Soc. 45, 310 (1962).

[2] Harmathy, T. Z., Variable-state methods of measuring the thermal properties of solids, J. Appl. Phys. 35, 1190 (1964).

[3] Steere, R. C., Thermal properties of thin-film polymers by transient heating, J. Appl. Phys. 37, 3338 (1966).

[4] Carslaw, H. S. and Jaeger, J. C., *Conduction of Heat in Solids* (Oxford University Press, Oxford, England, 1959), p.113.

[5] Norton, F. J., Thermal conductivity and life of polymer foams, J. Cell. Plast. 3,23 (1967).

[6] Editors of Modern Plastics, *Plastic in Building* (McGraw-Hill Inc., New York, 1966) p.28.

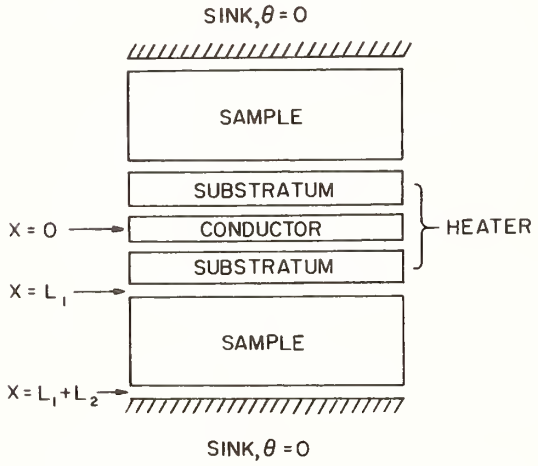

Figure 1. Experiment configuration for double layer infinite slab.

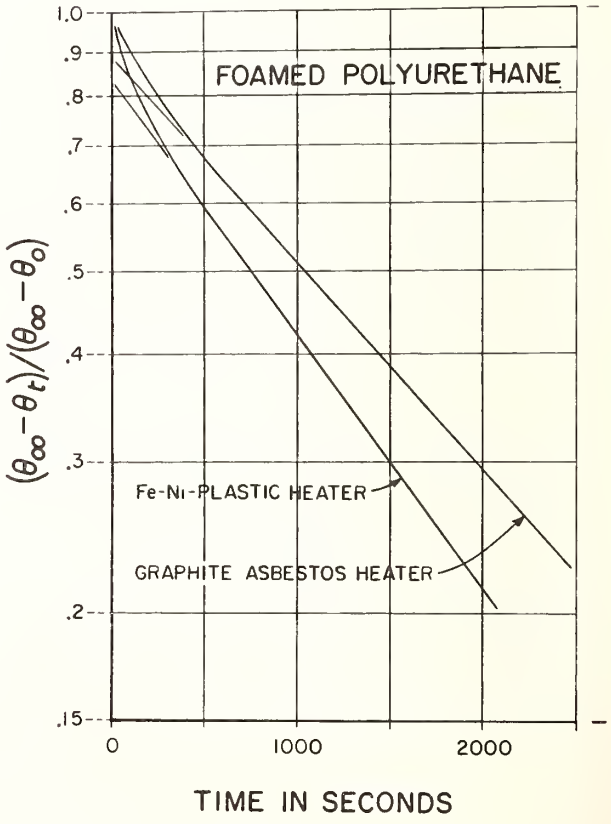

Figure 2. Fractional temperature changes at input face of a foamed ureathane sample.

A Guarded Hot Plate Apparatus for Measuring Thermal Conductivity From -80 + 100 °C

Jean-Claude Rousselle[1]

Laboratoire National d'Essais (L.N.E.)
Paris, France

The described apparatus is used for measuring the thermal conductivity of insulating materials from -80 to + 100 °C. Contrary to the usual methods under which two different types of apparatus are dealt with, the one with guarded hot plate for testings above ambient temperature, the other calorimetric for testings at low temperature, the proposed apparatus can be operated continuously at all temperatures from -80 to +100 °C. It is characterised by a conditioning temperature maintained lower than the lowest temperature prevailing within the sample. This is obtained by means of a controlled gas current obtained, according to the test conditions, either by spraying of liquid nitrogen or hot air circulation. Samples may be placed within plastic air tight bags and maintained in a gaseous medium different from the one used for the thermal conditioning of the surrounding box.

We give a somewhat detailed description of the dimensional and constructive characteristics of the apparatus. For instance, the results of tests performed on a polyurethane sample between -80 and +40 °C are presented. This test has been run with the sample maintained within an air tight envelope enclosing atmospheric air, and with the chamber thermally conditioned by means of liquid nitrogen spraying.

Key Words: Conductivity, guarded hot plate, polyurethane, thermal conductivity.

1. Introduction

For the measurement of the thermal conductivity of insulating materials from -80° to +100° C, the Laboratoire National d'Essais uses, since the beginning of 1967, two identical apparatuses. These apparatuses have been constructed to satisfy the increasing requirement of measurements on refrigeration industry insulating materials above and below the ambient temperature, mainly in the range -80 to +100 °C. In their general arrangement, they are similar to guarded hot plate apparatuses designed for working above ambient temperature. Nevertheless, they include several distinctive features which have been studied to reduce, indeed to remove, the operative difficulties of the standard type arrangement below the ambient temperature. Indeed the guarded hot plate method may even be suitable in case of a surrounding temperature lower than the temperatures prevailing in the samples, and specially the coldest face temperature of these samples. When this condition is realized, the lateral thermal losses appearing on the edges of the sample may be balanced by superheating the guard heater. On the other hand, if the surrounding temperature remains above the sample temperatures (and particularly the hot face temperature) a reheating of the edges takes place and a parasitic thermal flow appears in the central measurement area which, theoretically, implies an adjustment by underheating of the heater edges. This is certainly the reason for which the ASTM Standards recommend two different types of apparatuses on each side of the ambient temperature; that is to say: the guarded hot plate apparatus above this limit (ASTM Standard C 177-63 [1][2]) and the calorimeter making use of the vaporisation latent heat of liquid nitrogen for low temperatures (ASTM Standard C 420-62 T [2]).

---

[1] Engineer Chief of the Thermal Conductivity Department.

[2] Figures in brackets indicate the literature references at the end of this paper.

To make use of two different test set-ups is not always convenient:

a. The setting up and taking down of the specimens on two different apparatuses does not ensure the same thermal contacts on their cold and hot faces.

b. The calorimetric arrangement comprises a guard ring, but as a general rule, there is no balance of the heating element edge heat losses.

c. The guarded hot plate method makes use of two symmetrical specimens while the calorimeter uses only one sample.

d. The heat flow measurement is entirely different: gas flow measurement with the calorimeter, and Joulean-dissipated energy measurement in case of the guarded hot plate.

Laboratories working with the guarded hot plate method recommend particular building arrangements which permit extension of the method to the low temperatures.

The easiest way consists in the use of a large temperature ratio between the two faces of the specimens. In this case, the middle temperature may become higher than the surrounding temperature, and it is then possible to control the superheating. This proceeding is usable only for temperatures close to ambient temperature, and allows only the determination of mean values of thermal conductivity.

Two variations of the following proceeding were also tested:

The stack, including heater, samples and cold plates, is first enclosed within a casing made of high thermal conductivity material such as copper or aluminum. The walls of this casing are in close thermal contact with the cold plates so that their average temperatures are close to the cold plates ones. Obviously, the metal casing and the cold plates are carefully insulated and great care is taken against moisture.

For the second version, the general arrangement is identical with the first one, but the four walls of the metal casing are fitted with a cooling coil. This coil is connected with the cold plates outlet circuit. Both arrangements allow the guarded hot plate method to be used for temperatures as low as -40 °C.

Nevertheless, they constitute a poor improvement since it is impossible to obtain a surrounding temperature lower than the cold plates one. Again, appears the disadvantage of using large temperature variation between the two faces of the specimen.

Because of the disadvantages inherent in these arrangements, the Laboratoire National d'Essais has fitted two of their own apparatuses with the aim of realizing a surrounding temperature always lower than the temperature prevailing within the sample. This result is obtained by means of a thermally insulated external casing controlled in temperature either by a sweeping of gaseous nitrogen resulting from liquid nitrogen evaporation, or by a hot air current.

2. Experimental Equipment

2.1. Specimens

The apparatus is convenient on insulating materials having thermal conductivity values varying from 0.015 to 2 kcal/h m °C. The specimens have to be presented in square shaped panels (500 x 500 mm) of uniform thickness (preferably from 10 to 50 mm). Thickness and surface finish uniformity requirements are those prescribed in ASTM Standard C 177. The specimens are generally enclosed within thin plastic welded bags. As a general rule, the filling fluid is atmospheric air.

2.2. The Apparatus Features

a. Plates Stacking

The stacking constituting the main part of the apparatus is of the conventional type of guarded hot plate set up. It is formed with the following parts, all square shaped (see figure 1):

One electrical heating plate
Two samples on each side of the heater
Two cooling plates in close contact with the cold faces of each sample
Four sheets fitted with thermocouples (these sheets are sandwiched between the metal plates and the samples).

The stacking may be disposed either vertically or horizontally. In horizontal position, in preference, a well known weight loading ensures a good thermal contact between the samples and the heating or cooling plates. A tie-rods and scaled-spring arrangement may also ensure it, particularly in the vertical position. The stacking is placed within a parallelepiped-shaped copper casing, the copper plate ensuring a uniform wall temperature. Thermal insulation between stacking and casing is realized by means of a mineral fibers filling (20 mm thickness) enclosed within air tight envelopes of silicone coated glass cloth.

b. Conditioned Casing (See figures 2 and 3)

The copper casing enclosing the stacking is set up inside a cubic chamber resting on a base-plate. The walls and base-plate are fitted with a steam baked cork insulation 22 cm thick. Sweeping-gas coils (air, nitrogen), liquid coils (oil, methanol, liquid nitrogen) and electrical wiring (heating and measurement) are embedded within the base-plate thermal insulation. Thus it is possible to take down the chamber without disconnecting.

From ambient temperature to -80 °C, the chamber is conditioned by evaporation of liquid nitrogen sprayed by a distributor fitted in the upper part of the chamber. The liquid nitrogen flow is controlled by a solenoid valve and a regulating cock. A platinum probe regulator governs the solenoid valve. A small drain connects the chamber with the atmosphere.

A fan ensures the temperature homogeneity of the chamber. Between ambient temperature and +100 °C the temperature is controlled by an electrical heating resistor coupled with the fan agitating the ambient air. The resistor is controlled by the above mentioned regulator. The chamber is screwed on the base-plate with intercalation of a silicone gasket. The relative pressure inside the chamber does not exceed 100 mm WC.

c. The Features of the Guarded Hot Plate (See figures 4 and 5)

This plate (500 x 500 mm) is realized by inserting a heater between two anodic oxidized matte black painted aluminum plates (5 mm thick).

The central measurement area is 250 x 250 mm square, insulated by an air gap (1.2 mm wide). When fabricating the plates, eight bridges have been kept; they ensure the mechanical bonding of the measurement area with the guard ring (each bridge is about 4 or 5 mm^2 section). The heater constitutes of a wire wound in a double square shaped spiral placed between two asbestos paper sheets (1 mm thick).

The heating wire is 0.8 mm diameter Driver-Harris Nichrome V. The coil pitch is 10 mm. There are two separate coils as far as electric energy is concerned. The first one heats the central area and a bordering part of the guard ring. This arrangement avoids discontinuity of specific heating energy in the air gap zone. The second one (4 whorls) constitutes the guard ring. The Joulean-dissipated energy measurement is performed by means of voltage taps located on a level with the air gap.

Two sheets of silicone coated glass cloth bearing the superheating control thermopiles are tightened between the heater and the two metal plates (0.3 to 0.4 mm thick). These thermopiles are made of 0.2 mm chromel-alumel wire and each comprises 20 pairs of weldings symmetrically disposed 15 mm apart along the margin of the square measurement area of the metal plates (See figure 6).

d. Cooling Plates

The two cooling plates are made of copper plates (5 mm thick each). Two superpositioned coils are thermally bounded with the copper plate by means of Thermon (conductive cement including graphite). The coils are wound in a double, square shaped spiral (copper pipe 10 x 12 mm in diameter, 20 mm pitch). One of the two coils is connected with a methanol circuit controlled by a diaphragm flowmeter. The methanol circulation is provided by a Lauda Cryostat controlled from -80 to +20 °C with ±0.2 to 0.5 °C accuracy. The second coil is connected with a Haake thermostat controlled from +20 to +100 °C with ±0.1 °C accuracy. So we are able to control the temperature of the cold plates between -80 to +100 °C without removing the specimens.

e. Sample Face Temperature Measurement Sheets

Glass cloths (0.2 mm thick) are generally used. The thermocouples wires are insulated with silicone and the junctions remain free. Each sheet bears five 0.2 mm chromel-alumel thermocouples disposed according to the R.I.L.E.M. arrangement [3]. That is to say on each face there is one thermocouple in the middle and four thermocouples in the middle of the half-diagonals. These last four thermocouples are series connected and measure the temperatures difference between the faces of the sample. These sheets are useful with specimens such as mineral wool. For hard materials, rubber plates of known thermal resistance are placed between measurement sheets and specimens.

f. Measurement Equipment (See figure 7)

a. Superheating Control. The two thermopiles of the heating plate are connected separately or in series. A Leeds and Northrup amplifier (type CAT 9835B) and a single channel recorder measure their emf. The guard heater control is manually operated to nearly cancel the unbalance between the central area and the guard ring.

b. Surface specimen temperature measurements. The temperature of each face and the four-times-amplified temperature drop of each specimen are measured. The values are recorded on a multichannel automatic potentiometer. The same apparatus records the temperatures of the copper box and of the chamber. When steady state is reached the surface temperatures of the samples are measured by means of a precision potentiometer (P-12 type A.O.I.P.-1 μV sensitivity).

c. Joulean-dissipated energy measurement in the central area. The heating plate is supplied with direct current. Automatic regulation of the generator is ±0.05% of the fixed value. Standard resistors and the precision potentiometer measure the emf and the current intensity in the measurement area.

3. Tests Run

Presently, tests are being run in the apparatus on polyurethane specimens undergoing different aging treatments. To specify the apparatus working conditions, we describe the test measurements technique and results for a polyurethane specimen.

3.1. Test Description

The test is run on expanded polyurethane having the following characteristics:

Mean density before test:	35.95 kg/m^3
Expansion agent:	freon (exact type not stated)
Aging conditions:	15 months in ambient air and temperature
Specimen sizes:	500 x 502 x 50 mm, 500 x 502 x 50 mm
Total weight of the two samples:	0.905 kg (The two samples are enclosed within air tight bags made of welded plastic film (0.07 mm thick, Manufactured by "La Cellophane" under the name of "Therthene")).
Test in horizontal position	
Loading pressure	0.06 kg/cm^2

Inside the bags, the specimens remain in contact with the atmospheric air initially introduced. During the test no gas sampling has been effected. It may be supposed that during the test an air-freon blend takes place with the temperature changes. Thickness variations of the specimens versus the temperature are measured before starting the test within an insulated glass walled cold chamber. The two specimens remain in their bags and mean temperature and loading conditions are reapplied. Thickness variations are metered with a cathethometer. Before test the specimens have been submitted to a cycling ambient temperature down to -80 °C and back to ambient temperature.

3.2. Test Results

In the test described, the conditioned chamber is always adjusted relative to the cold plates temperature. A small difference between these temperatures is kept for all test points. The measured values during the test are grouped in table 1.

4. Conclusions

These new apparatuses have the following advantages:

A small temperature ratio between the stacking and the surrounding, the surrounding temperature being always below that of the cold plates.

Only a small amount of thermal insulation is required around the stacking (2 cm of fibrous mineral wool).

A very homogenous surrounding temperature, thanks to the copper box. Hence, it follows that:

A small disadjusting of the temperature unbalance between the central area and the guard ring, from one temperature test level to the next. The testing run with a constant central energy, this unbalance needs only a small superheating correction from one point to another.

A much smaller thermal inertia than with a large amount of lateral thermal insulation.

An eminent time benefit. Each point needs, on the average, less than 48 hours instead of a minimum of 72 hours with the previously used procedures.

Adjustments which are as easy at the limits of the temperature range as at ambient temperature.

Testing continuity on either side of the ambient temperature without dismounting the stack. The cooling by evaporation of liquid nitrogen shows ease of utilization and reliability.

5. Acknowledgments

The author wishes to express his appreciation to the management for its acceptance and encouragement concerning the present paper. The author is further indebted to the team of engineers and technicians having performed the fine adjustments of these apparatuses.

6. References

[1] ASTM, C177-63 Thermal Conductivity of Materials by Means of the Grarded Hot Plate.

[2] ASTM, C420-62T. Thermal Conductivity of Insulating Materials at Low Temperatures by Means of the Wilkes Calorimeter.

[3] R.I.L.E.M., Method of Test for Thermal Conductivity of Building Materials by Means of the Guarded Hot Plate. September 1962.

Table 1. Values Obtained for the Thermal Conductivity of the Sample of Polyurethane Foam.

Point N°	Mean Temperature in Samples θ_m °C	Temperature of Hot Face θ_H °C	Temperature of Cold Face θ_c °C	Temperature of Chamber Ambient °C	Unbalance Between Central & Guard Area Δt °C	Temperature Difference $\Delta\theta$ °C	$\frac{\Delta t}{\Delta\theta} \times 100$	R $\frac{cm^2\ °C}{w}$	$k.10^{-2}$ $\frac{w}{cm\ °C}$	Mean Specimen Thickness cm
1	-69.3	-60.3	-78.3	-85	+0.0036	18	0.020	1.740	0.0287	4.99_5
2	-50.2	-41.3_5	-59.1	-66.5	+0.0084	17.8	0.047	1.715	0.0291	4.99_5
3	-31.7	-24.0	-39.4	-46.5	-0.0024	15.4	0.016	1.636	0.0305	4.99_5
4	-18.8	- 9.4	-28.2	-35	-0.0045	18.8	0.024	1.751	0.0285	5.01
5	- 7.0	+ 3.8	-17.8	-24	+0.0018	21.6	0.008	1.959	0.0255	5.01_5
6	$+ 0.9_5$	+11.6	- 9.7	-17.5	-0.0006	21.3_5	0.003	1.932	0.0258	5.01_5
7	$+14.9_5$	+25.9	+ 4.0	- 3.2	0.0	21.8_5		1.997	0.0250	5.02
8	+29.7	$+39.7_5$	+19.6	+12.5	+0.0036	20.1_5	0.018	1.826	0.0273	5.02_5

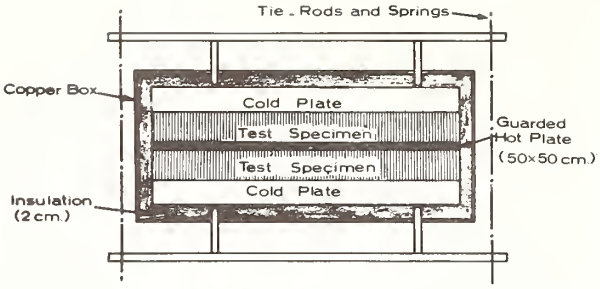

Figure 1. Arrangement of the staking in its copper box.

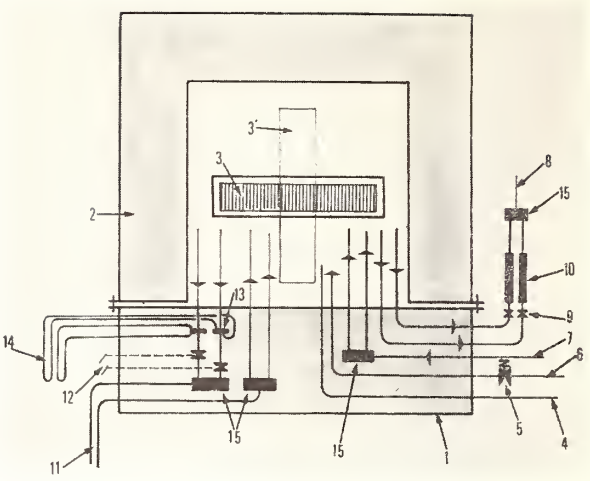

Figure 2. General features of the insulated conditioned chamber.

1 - Insulated base-plate containing the different circuits.
2 - Insulated chamber.
3 - Stacking in his copper box in horizontal position.
3'- The same in vertical position.
4 - Electrical leads and measurements wires.
5 - Solenoid-valve on the liquid nitrogen pipe.
6 - Liquid nitrogen inlet.
7 - Oil inlet.
8 - Oil outlet.
9 - Manuel oil flow control cocks.
10 - Oil float flowmeters.
11 - Methanol circuit.
12 - Methanol flow rate measurement diaphragms.
13 - Manual methanol flow control cocks.
14 - Diaphragms U tubes.
15 - Distributors.

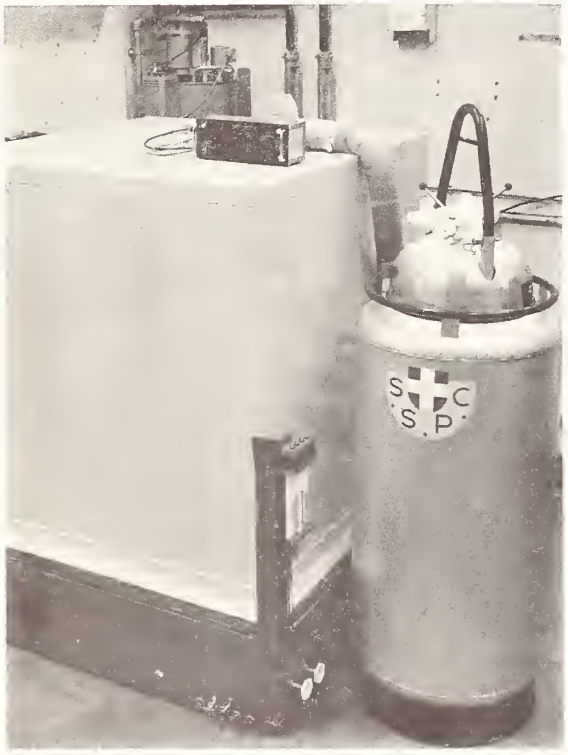

Figure 3. Conditioned chamber with liquid nitrogen tank and oil thermostat in the rear.

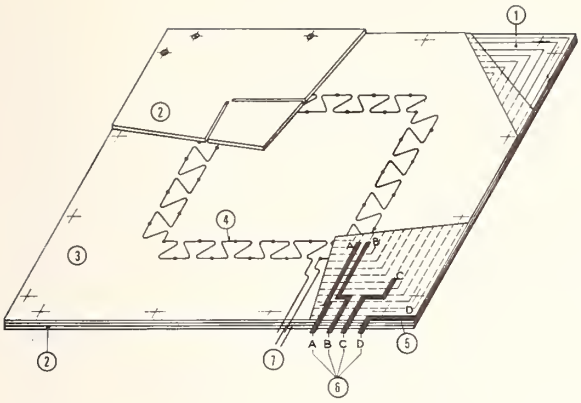

Figure 4. Exploded view of the guarded hot plate.
1 - Heater.
2 - Metal plate.
3 - Thermopile support siliconed glass cloth.
4 - Thermopile.
5-6 - Heating wires connections.
7 - Thermopiles wire connections.

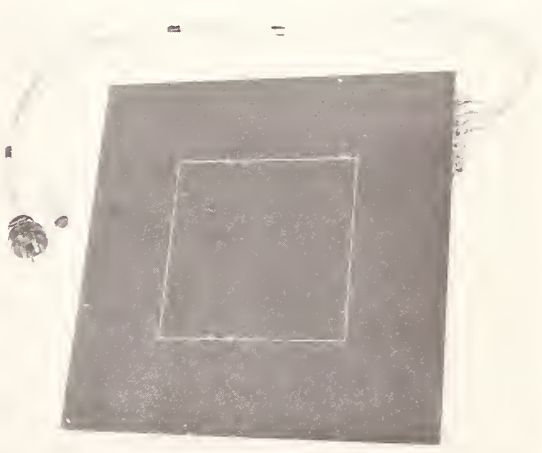

Figure 5. Guarded hot plate.

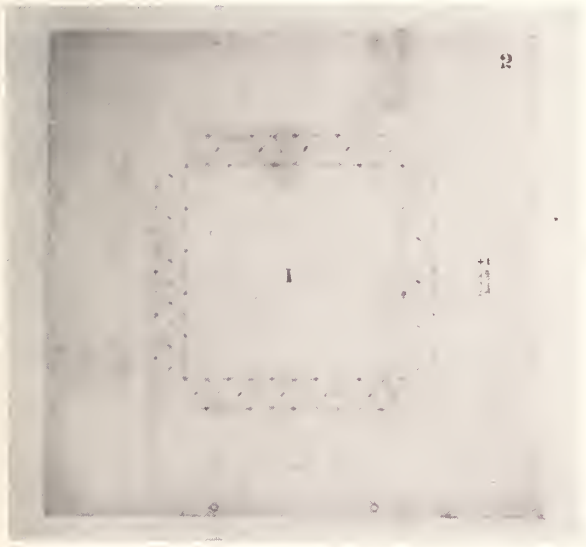

Figure 6. The thermopile and its glass cloth support siliconed both alike.

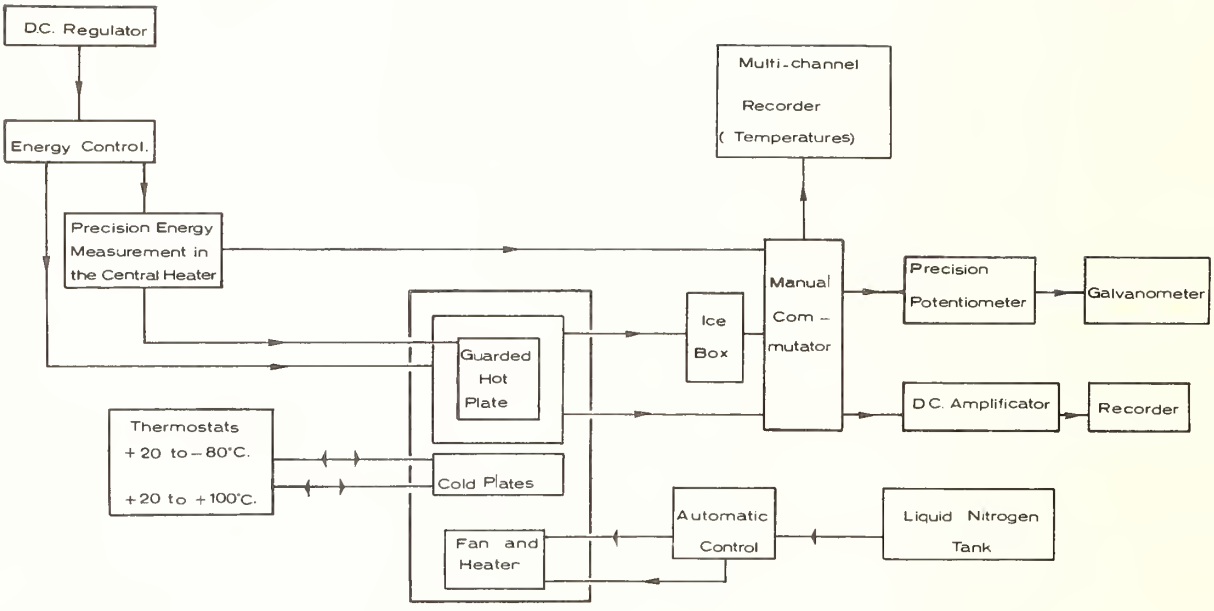

Figure 7. General chart of the guarded hot plate apparatus (range -80 to - 100 °C).

A Study of the Effects of Edge Insulation and Ambient Temperatures On Errors in Guarded Hot-Plate Measurements

H. W. Orr

Division of Building Research,
National Research Council of Canada
Ottawa

The error due to edge effects of the guarded hot-plate apparatus has limited the thickness of specimens that may be tested to approximately one third the dimension of the central section of the heating unit. Samples of known conductivity were tested using various thicknesses of edge insulation and various ambient temperatures. It was found possible to determine the optimum edge conditions so that errors due to edge effects are negligible for very thick specimens.

Key Words: Conductivity, errors, guarded hot-plate, heat conduction, standard test, thermal conductivity, thermal insulation.

1. Introduction

The most widely used and precise method of determining thermal conductivity is with the guarded hot-plate and a standard method using this equipment has been adopted by ASTM (1)[1]. This method of test limits the thickness of specimen to one third the linear dimension of the heating unit. In order to test thick specimens using this method, guarded hot-plates with proportionately large dimensions are required. Another approach is to slice the material and produce a number of thinner specimens that may be tested in a smaller guarded hot-plate. A third approach is to test thick specimens in a small guarded hot-plate apparatus and reduce errors due to edge effects by control of the boundary conditions.

Each of the three methods has its limitations. A large hot-plate is expensive, difficult to build and operate, and not suitable for the majority of specimens. Because of this many laboratories are unlikely to have one. Slicing samples to make specimens thin for testing in smaller guarded hot-plates is not always convenient or desirable and testing thick specimens in small plates can result in large errors due to edge effects. An experimental program was proposed to evaluate the possibility of reducing edge errors so that thick specimens can be tested on small guarded hot-plates.

The guarded hot-plate method for measurement of thermal conductivity is based on the assumption that isotherms in the central area of the test specimens are planes parallel to the hot and cold-plates, i.e., that the heat flow is perpendicular to the faces of the sample. This assumption of one-directional heat flow is valid only for thin specimens unless the edge of the sample has a temperature profile that is nearly the same as that at the centerline of the sample. The normal procedure for the guarded hot-plate is to limit the heat gained or lost from the edge of the sample by using edge insulation, by maintaining the ambient temperature at an appropriate level (2), and by limiting the thickness of the specimen (3) so that errors due to edge effects are negligible.

With thick specimens the isotherms become distorted if heat is allowed to enter and/or leave the edge of the specimens. This may result in an erroneous measurement of thermal conductivity if the edge conditions are not carefully controlled. If the ambient temperature is much above the sample temperature, heat will flow into the edge of the specimen, distorting the isotherms and making the

[1] Figures in brackets indicate the literature references at the end of this paper.

apparent thermal conductivity low. An ambient temperature much below the sample temperature will give the opposite effect. It would appear, therefore, that there is some optimum temperature that will give a minimum error. Since the apparent thermal conductivity is affected by heat entering or leaving the edge of the specimen, edge insulation should help to reduce the flow of heat and consequently reduce the error in the thermal conductivity.

The object of the experimental work reported in this paper was to determine the effectiveness of using edge insulation and of controlling ambient temperature in reducing errors when measuring the thermal conductivity of thick specimens.

2. Experimental

2.1 Equipment

The guarded hot-plate equipment used for the tests was similar to one designed by the National Bureau of Standards in Washington (4). The test area is 10 cm square with a 5-cm-wide guard area that is automatically kept at the same temperature as the test area. The hot-plate was operated in a horizontal position in an insulated box. The temperature in the box was controlled by circulating fluid at a controlled temperature through heat exchanger plates that covered three walls of the box. The air in the box was stirred with a large-diameter, low-speed propeller fan.

2.2 Specimens

Polyurethane foam and silicone rubber were used to make up the samples for test. Thick samples were made by stacking homogeneous material in slices 13 mm to 19 mm thick. The actual thermal conductivity was determined by adding the previously determined resistances of pairs of slices and converting the total resistance to thermal conductivity. The resistance of each pair of slices was determined in two guarded hot-plates, in the plate used for the thick specimens, and in a plate of the same size, similar in design to one developed at the University of Saskatchewan and described by Woodside and Wilson (5). The values obtained with the two guarded hot-plates had a maximum deviation of 0.06 per cent and a mean deviation 0.03 per cent for the polyurethane foam samples and 0.46 per cent and 0.21 per cent respectively for the silicone rubber.

2.3 Method

The first series of tests was carried out to check the effect of varying the thickness of edge insulation. Specimens of polyurethane foam and silicone rubber 85 mm thick were used for these tests. The ambient temperature was controlled close to the mean temperature of the sample 24 C; the temperature difference across the sample was maintained at 22 C. A series of tests was run starting with no edge insulation and applying 13 mm, 25 mm, 51 mm, and 76 mm of edge insulation to the edge of the specimen covering the hot-plate completely and extending 20 mm beyond the faces of the cold-plates. The test was repeated with an ambient temperature of 38 C; all other conditions remained the same. The edge insulation had a thermal conductivity approximately equal to the specimen. The polyurethane samples had edge insulation of polyurethane with a $\lambda = 0.0230$ W $m^{-1}deg^{-1}$ while the silicone rubber samples had neoprene rubber for the edge insulation with a $\lambda = 0.304$. After the completion of these two series an approximate optimum ambient temperature for minimum error was determined by a linear interpolation of the previous results and a third series was run using this ambient temperature. The results of these three tests are given in Table 1 for polyurethane foam and in Table 2 for silicone rubber. The ambient temperature has been converted to a nondimensional temperature index (ATI) by relating it to the temperatures of the hot- and cold-plate, i.e. $ATI = (T_a - T_c) / (T_h - T_c)$. Where T_a is the ambient temperature and T_h and T_c are hot- and cold-plate temperatures respectively.

2.4 Results

The results shown in Tables 1 and 2 have been plotted in figures 1 and 2. The error in thermal conductivity has been plotted against the thickness of edge insulation for corrected ATI. For each thickness of edge insulation the best straightline fit was used to determine the optimum ATI for minimum error and to correct the ATI to 0.5, 1.10, and a value near the optimum for plotting. The values of optimum ATI have been plotted against the thickness of edge insulation in figures 3 and 4.

Table 1 Experimental values of error in thermal conductivity measurements for 85.05 mm polyurethane foam samples

Polyurethane foam samples: $\lambda = 0.230_4$, d = 31.89;

NBS guarded hot-plate, in a horizontal configuration: 203.2 mm x 203.2 mm, test area 101.6 mm x 101.6 mm.

Edge Insulation thickness, mm	Mean Temperature, °C	Temperature Difference, °C	Ambient Temperature Index	Error, per cent
		Series 1		
0	23.89	22.26	0.479	6.4
12.7	24.12	22.86	0.479	3.5
25.4	24.19	22.94	0.476	2.8
50.8	24.28	23.16	0.508	1.7
76.2	24.34	23.21	0.502	1.5
		Series 2		
0	23.91	22.11	1.103	-27.65
12.7	24.25	22.99	1.100	-16.26
25.4	24.13	22.77	1.121	-13.27
50.8	24.39	23.16	1.081	-7.84
76.2	24.18	22.78	1.098	-6.33
		Series 3		
0	24.08	22.56	0.649	-0.6
12.7	24.08	22.61	0.646	-0.7
25.4	24.12	22.28	0.668	-2.2
50.8	24.29	23.14	0.631	0.1
76.2	24.23	23.12	0.626	0.2

The ambient temperature for minimum error is between the mean temperature of the sample and the temperature of the hot-plate. This is the expected result for a guarded hot-plate where the heat is metered at the hot-plate side. If the heat is metered at the cold-plate side the optimum ambient temperature would be between the mean and cold-plate temperatures. When the ATI is not the optimum, edge insulation reduces the error as expected. With thick edge insulations the ambient temperature is not as critical. The optimum ATI appears to be a linear function of the edge insulation thickness. Thicker edge insulation requires a higher optimum ATI. Specimens of high thermal conductivity require higher ATI for minimum error for all thickness of edge insulation.

Using the results of these series of tests an attempt was made to see how thick the specimens could be made and still maintain a reasonable degree of accuracy. The thickness of polyurethane foam specimens was varied from 75 mm to 189 mm while the edge insulation thickness was kept constant at 57 mm and the ATI was near optimum as determined in the first series. As specimen thickness was increased, the measured error was larger than expected when compared with the tests done with 85-mm samples. This would seem to indicate that the optimum ATI is also a function of specimen thickness. The results are shown in Table 3.

3. Conclusion

The error due to the edge effects of the guarded hot-plate may be reduced with edge insulation but only becomes zero when the ambient temperature is at one specific value. The optimum ATI appears

Table 2 Experimental values of error in thermal conductivity measurements for 84.46 mm silicone rubber samples

Silicone rubber samples: $\lambda = 0.246_9$, $d = 1190\ kg/m^3$

Neoprene rubber edge insulation: $\lambda = 0.304$, $d = 1400\ kg/m^3$

NBS guarded hot-plate, in a horizontal configuration: 203.2 mm sq, test area 101.6 mm sq

Edge Insulation thickness, mm	Mean Temperature, °C	Temperature Difference °C	Ambient Temperature Index	Error, per cent
		Series 1		
0	23.87	22.12	0.508	3.62
12.7	23.89	22.10	0.499	3.28
25.4	24.01	22.24	0.502	3.22
50.8	23.94	22.10	0.512	3.31
76.2	23.82	22.08	0.500	3.86
		Series 2		
0	23.82	21.94	1.150	-18.4
12.7	23.75	22.17	1.127	-12.32
25.4	23.99	22.17	1.164	-10.49
50.8	23.93	22.07	1.166	-6.32
76.2	23.84	21.99	1.150	-4.46
		Series 3		
0	24.02	22.52	0.604	0.18
12.7	23.89	22.25	0.603	0.77
25.4	23.92	22.11	0.608	0.97
50.8	23.92	22.05	0.600	2.07
76.2	23.83	22.07	0.610	2.14

Table 3 Experimental values of error in thermal conductivity measurements for polyurethane foam samples tested in an NBS 203.2 mm x 203.2 mm guarded hot-plate using 57 mm of polyurethane foam edge insulation

Sample Thickness, mm	Mean Temperature, °C	Temperature Difference, °C	Ambient Temperature Index	Error, per cent
75.29	23.91	22.25	0.647	-1.0
75.25	23.93	22.26	0.596	-0.6
75.25	23.92	22.21	0.618	-1.4
75.25	23.87	22.12	0.666	-1.9
75.25	23.95	22.25	0.680	-1.8
75.25	23.89	22.14	0.619	-1.4
75.25	23.88	22.13	0.594	-0.9
94.06	23.93	22.28	0.661	-2.4
112.89	23.85	22.14	0.659	-3.5
112.85	23.96	22.26	0.594	-3.0
112.85	23.93	22.24	0.585	-2.3
131.68	23.89	22.24	0.660	-4.0
150.47	23.91	22.28	0.628	-5.0
150.42	23.92	22.26	0.569	0.4
150.42	23.90	22.21	0.564	0.2
150.42	23.89	22.16	0.568	0.3
150.42	23.92	22.22	0.598	-2.1
150.42	23.89	22.17	0.597	-1.9
150.42	23.89	22.17	0.602	-3.1
169.24	23.97	22.40	0.625	-4.1
169.23	23.86	22.16	0.643	-6.7
169.23	23.92	22.25	0.628	-6.4
169.23	23.80	22.01	0.627	-5.4

to be a function of the edge insulation thickness, sample thermal conductivity, and thickness.

In the work reported here the edge insulation had a thermal conductivity the same as the sample. Edge insulation with a thermal conductivity lower than the sample will probably reduce the error due to edge effects, but the optimum ATI will doubtless change.

This paper deals mainly with a sample thickness that is 0.84 times the linear dimension of the central area of the hot-plate. From the values of error obtained with much thicker samples it appears that different values of specimen thickness have different values for the optimum ambient temperature index.

It would appear that samples that are as thick as the width of the central area of the hot-plate may be tested with little additional error provided edge insulation is used and the ambient temperature is maintained at the optimum value. More experience is needed, however, before thick specimens can be tested with assurance that errors due to edge effects have been eliminated. It should be noted that homogeneous samples were used in this study and the results are not necessarily applicable to non-homogeneous specimens.

This is a contribution from the Division of Building Research, National Research Council of Canada, and is published with the approval of the Director of the Division.

4. References

(1) Method of Test for Thermal Conductivity of Materials by Means of the Guarded Hot-Plate (C177 - 63), 1966 Book of ASTM Standards, Part 14, p.17..

(2) Ibid, Paragraph 4(k) p.22.

(3) Ibid, Paragraph 6(a) p.25.

(4) Ibid, Note 1, p.17.

(5) Woodside, W. and Wilson, A.G. Unbalance errors in guarded hot-plate measurements. In Symposium on Thermal Conductivity Measurements and Applications of Thermal Insulations, A.S.T.M. Special Technical Publication No. 217, p.32-46 (1957).

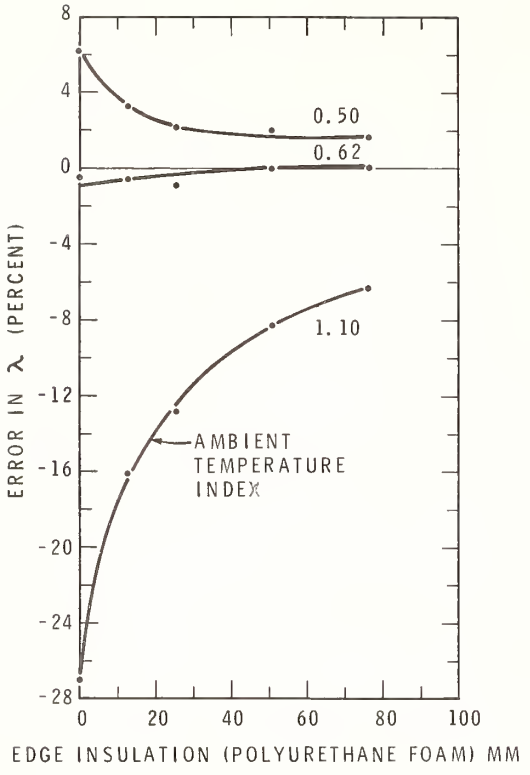

Figure 1. Error in λ vs edge insulation thickness showing effect of ambient temperature indexes for 85 mm samples of polyurethane foam.

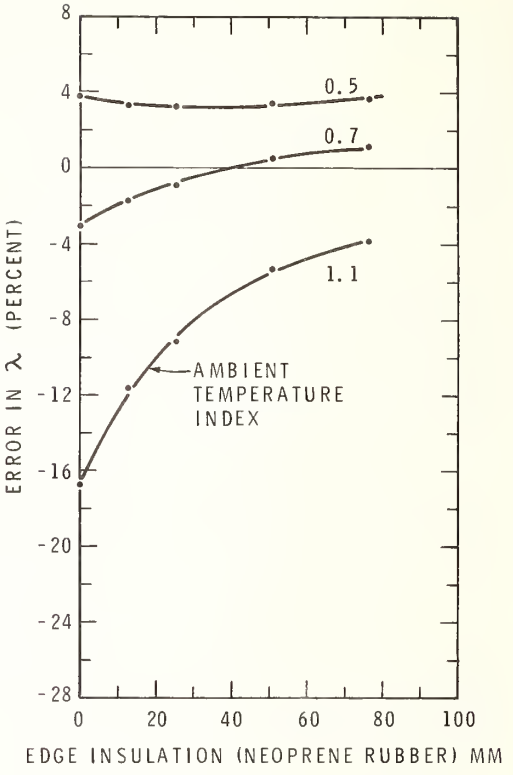

Figure 2. Error in λ vs edge insulation thickness showing effect of ambient temperature indexes for 85 mm samples of silicone rubber.

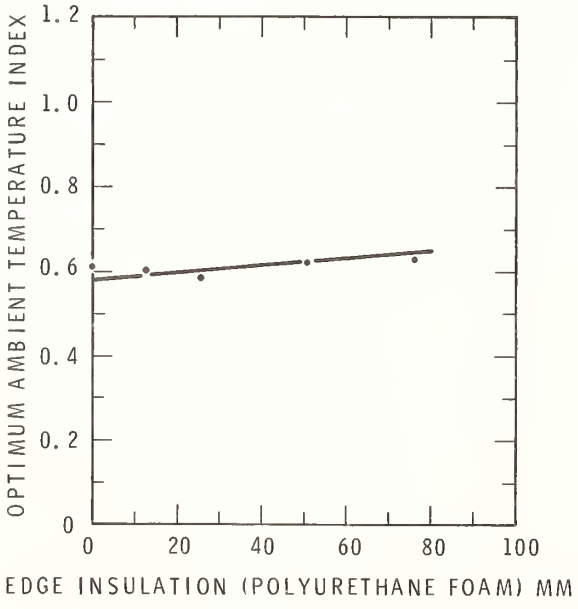

Figure 3. Optimum ambient temperature index vs edge insulation thickness for 85 mm samples of polyurethane foam.

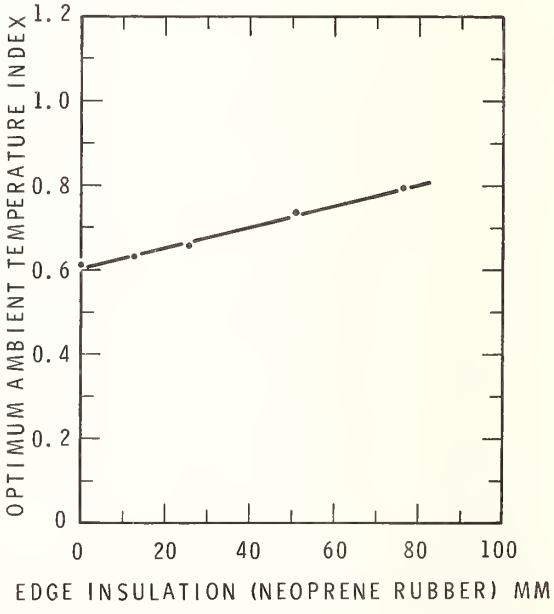

Figure 4. Optimum ambient temperature index vs edge insulation thickness for 85 mm samples of silicone rubber.

Ring Heat Source Probes for Rapid Determination of Thermal Conductivity of Rocks[1]

Wilbur H. Somerton and Mohammad Mossahebi

University of California, Berkeley
National Iranian Oil Company, Tehran, Iran

A ring heat source probe has been developed for the rapid determination of thermal conductivity of rocks. In addition to the short period of time required to run the test (2 - 3 minutes), sample preparation is minimal, requiring only that parallel flats approximately two cm in diameter be cut or ground on opposite sides of the sample. A calibration chart can be provided with each probe so that thermal conductivity can be obtained from simple experimental data without elaborate calculation.

Key Words: Conductivity, diffusivity, probe, ring heat source, rocks, thermal conductivity, thermal properties of rocks.

[1]Paper published in: The Review of Scientific Instruments, Vol. 38, no. 10 (October, 1967)

Thermal Conductivity and Thermal Diffusivity of Green River Oil Shale

S. S. Tihen, H. C. Carpenter, and H. W. Sohns[1]

Laramie Petroleum Research Center
Bureau of Mines, U.S. Department of the Interior
Laramie, Wyoming 82070

Information on the thermal properties of oil shale is necessary for process design of both aboveground and in situ processes. This paper presents data on the thermal conductivities and thermal diffusivities of various grades of oil shale, of retorted shales, and of burned shales which are free of organic matter. The thermal properties are correlated with shale grade, temperature, and bedding plane orientation. Determinations were made both perpendicular and parallel to the bedding planes, and at several different temperature levels. Conductivity values ranged from about .69 W m^{-1} deg^{-1} for 58.6-gallon-per-ton shale to about 1.56 W m^{-1} deg^{-1} for a lean, 8.6-gallon-per-ton shale. Conductivities of the retorted or spent shales from these raw shales ranged from .26 to 1.38 W m^{-1} deg^{-1} and of the burned shales from less than .17 to 1.21 W m^{-1} deg^{-1}. An equation was developed for calculating the thermal conductivity of raw, retorted, and burned Green River oil shales.

Thermal diffusivities were determined experimentally on twelve different grades of raw shale assaying from 8.1 to 59.1 gallons of oil per ton and on the retorted and the burned shales from these raw shales. Thermal diffusivities of raw shales ranged from 2.6 x 10^{-7} to 9.8 x 10^{-7} m^2/sec. Diffusivities of the retorted shales ranged from 1.3 x 10^{-7} to 8.8 x 10^{-7} m^2/sec, and of burned shale from 1.0 x 10^{-7} to 7.2 x 10^{-7} m^2/sec.

Key Words: Burned shale, oil shale, retorted shale, thermal conductivity, thermal diffusivity, transient line source method.

1. Introduction

During the last decade, oil-shale research and development in this country have progressed to the point where oil-shale processing appears to be an emerging industry. A number of aboveground retorting processes have been demonstrated on a pilot or prototype scale, and efforts to develop in place, or in situ, processing methods are currently receiving much attention. The operability of any in situ process is largely dependent on the physical structure and thermal properties of oil shale. Information on the thermal properties of oil shale is necessary for process design of both aboveground and in situ processes.

This paper presents data on the thermal conductivities and thermal diffusivities of oil shales of various grades, of retorted or spent shales, and of burned shales which are free of organic matter. These thermal properties are correlated with shale grade, temperature, and bedding plane orientation.

2. Thermal Conductivity

2.1 Apparatus and Procedure

The apparatus was designed to utilize the transient line source method of measuring thermal conductivity. In this procedure heat is supplied at a constant rate from a line source in the interior of the material being tested and temperature rise at the heat source is measured as a function of time. These data are then used to calculate thermal conductivity. This method, adaptable to a wide variety of materials and conditions, has been used and discussed by a number of investigators (1,2,3).[2] Oil shale

---

[1] Research Chemist, Project Leader, and Project Coordinator, respectively.
[2] Figures in parentheses indicate the literature references at the end of this paper.

is a heterogeneous material which decomposes as it is heated and undergoes changes in physical and chemical properties. Because of these phenomena the transient line source method is particularly suitable for determining thermal conductivity of oil shale.

a. Apparatus

A specially designed oven was used to maintain the oil shale sample at the desired temperature. This oven was designed in such a way that the shale samples could be surrounded by an inert atmosphere, and that inert sweep gas could be used to remove the combustible pyrolysis products during heating.

A direct-current, constant-current power supply was used to heat the line source. An ammeter sensitive to 1 milliampere in the 0 to 1 ampere range was used to measure the current, and a strip recorder with 1-millivolt full-scale sensitivity was used to measure and record temperature.

b. Sample Preparation

The test pieces, 7.5-cm cubes, were prepared from 7.5-cm by 7.5-cm by 18-cm blocks of shale which were carefully chosen for uniformity and absence of fractures. Two 7.5-cm cubes were cut from each block and the remaining material was assayed. These blocks were cut in such a way that the same bedding planes occurred in all three pieces. A face-centered hole was drilled through each of the two cubes to accommodate a slender, multi-hole porcelain tube containing a heating wire and a butt-welded thermocouple. In one cube the hole was parallel to the bedding planes and in the other the hole was perpendicular to the bedding planes. Iron plates were placed on the faces parallel to the bedding planes and bolted together, to restrict separation of the layers during heating (fig. 1). The restraining plates can be seen in position on the blocks of 58.6-gallon-per-ton shale. Subsequent removal of these plates allowed the blocks of rich shale to disintegrate completely. After conductivity determinations had been made on the raw shale, the cubes were retorted in an inert atmosphere at 482° C, and used for retorted shale conductivity determinations. These cubes were then heated in a stream of air to remove all organic matter and subsequently were used for burned shale conductivity determinations. Figure 1 pictures the cubes of burned shale, and clearly shows the disintegration that took place in the shale structure of the richer shales during heating. The lean, 8.6-gallon-per-ton shale developed only tiny cracks during heating. These cannot be seen in the photograph. The 11.4-gallon-per-ton shale developed visible shallow cracks, while the 19.0-gallon-per-ton shale developed larger, deeper cracks.

c. Experimental Procedure

Each pair of shale samples was placed in the oven and the heating wire and thermocouple connections were made, following which the oven was brought to the desired temperature. After the sample had reached constant temperature, current was supplied to the heating wire at constant rate and the temperature rise, with respect to time, was measured.

Five replicates were made on each sample at each of the following ambient temperatures: 38°, 149°, and 260° C. A nitrogen atmosphere was used for the determination at 260° C. Retorted shale determinations were made at 38°, 149°, 260°, 371°, and 482° C, again using a nitrogen atmosphere for temperatures above 149° C. Conductivity determinations on burned shale were made in air at the same temperatures as those on retorted shale, and also at 593° C.

2.2 Calculations and Discussion of Results

The transient line source technique involves calculation of thermal conductivity from power input to the heater wire, the temperature rise of the specimen, and the time. This relationship is expressed by a complex mathematical eq (1) which may be approximated to within less than 1 percent error by the following expression:

$$\theta = -\frac{Q}{4\pi\lambda}\left(\gamma + \ln\frac{R^2}{4at}\right), \qquad (1)$$

if the value of $\frac{R^2}{4at}$ is held equal to or less than 0.0058,

where θ = the temperature rise in °C,
Q = heat supplied per unit length per unit time in J m^{-1} sec^{-1},
λ = thermal conductivity in W m^{-1} deg^{-1},
γ = Euler's constant: 0.5772,
R = distance from the line source in meters,
a = thermal diffusivity in m^2/sec,
and t = time in seconds.

Comparing temperatures at two different times,

$$\theta_2 - \theta_1 = \frac{Q}{4\pi\lambda}\left(\ln\frac{R^2}{4at_1} - \ln\frac{R^2}{4at_2}\right) = \frac{Q}{4\pi\lambda}\ln\frac{t_2}{t_1}. \quad (2)$$

Then

$$\lambda = \frac{Q}{4\pi(\theta_2 - \theta_1)}\ln\frac{t_2}{t_1} \quad (3)$$

Restriction of $\frac{R^2}{4at}$ to 0.0058 is easily met in the laboratory within short periods of time because the values of a for most rocks in the temperature range covered lie between 3.84×10^{-6} to 2.58×10^{-7} m^2/sec and R can be held to values of 3.05×10^{-3} m or less.

Equation (3) requires only the heat input and time-temperature values for calculating thermal conductivity. Temperature rise is plotted as a function of time on semilog paper. After an initial transient period, the values of any two points on straight portion of the curve, along with Q, calculated from the current and resistance per unit length of the heater wire, are used to calculate thermal conductivity.

Because oil shale has a tendency to crack and separate into layers upon heating, only the first portion of the heating curve could be used to determine the slope. Perfect contact between shale and the heating source is not attainable; therefore, the first part of the curve must be corrected for the error which imperfect contact introduces. This can be done by several methods. The one used here consisted of choosing a time, x sec, such that the temperature rise between (8 + x) sec and (32 + x) sec equaled the rise between (32 + x) sec and (128 + x) sec. These points, when plotted against temperature on semilog paper, then fall in a straight line. Therefore, they can be substituted in eq (3) to calculate thermal conductivity.

a. Calculation of the General Equation

Statistical and computer techniques were used to develop exponential, quadratic, and second-order equations from the λ values obtained above for raw shale, retorted shale, and burned shale perpendicular to and parallel to the bedding planes. Statistical examination of these equations showed that the second-order equation gave the lowest standard error of estimate. The following equation, therefore, is the one recommended for calculating the thermal conductivities of Green River oil shales assaying between 8.6 and 58.6 gallons per ton within the temperature ranges of 38° to 260° C for raw shale, 38° to 482° C for retorted shale, and 38° to 593° C for burned shale:

$$\lambda = C_1 + C_2F + C_3T + C_4F^2 + C_5T^2 + C_6FT, \quad (4)$$

where λ is the thermal conductivity of the shale in W m^{-1} deg^{-1},
C_1 through C_6 are constants,
F is the Fischer assay of the original shale in gallons per ton,
and T is the temperature in °C.

Table 1 lists the values of the constants in the above equation for the various conditions under which thermal conductivities were determined, and also the standard error of estimate of λ for each of the conditions. The two curves of figure 2 show the relationship of thermal conductivity at 38° C of raw shale to Fischer assay. The three curves of figure 3 show the thermal conductivities of raw, retorted, and burned shales at 38° C. These figures show that thermal conductivity of Green River oil shale varies inversely as shale grade, and that conductivities of retorted and burned shales are generally lower than those of the raw shales from which they were obtained. The burned shales, in turn, have a lower conductivity than the corresponding retorted shales. This can be accounted for by the fact that the mineral matter is a better conductor of heat than the organic matter and that the organic matter is a better conductor than the voids created by its removal.

3. Thermal Diffusivity

3.1. Apparatus and Procedure

The apparatus used for determining thermal diffusivities of Green River oil shale was essentially the same as that used for the thermal conductivity determinations. However, sample preparation and laboratory procedure differed somewhat.

a. Sample Preparation

The samples were prepared by splitting 7.5-cm cubes of the shale into two equal parts by sawing

TABLE 1. - Constants and standard errors of estimate for the calculation of thermal conductivity of Green River oil shale using the equation:

$$\lambda = C_1 + C_2F + C_3T + C_4F^2 + C_5T^2 + C_6FT$$

	C_1	C_2	C_3	C_4	C_5	C_6	Standard error of estimate
Raw Shale:							
Case A[a]	+1.8081	-3.698×10^{-2}	$+1.980\times10^{-3}$	$+3.056\times10^{-4}$	-5.184×10^{-6}	-1.872×10^{-5}	0.173
Case B[b]	+2.0670	-5.779×10^{-2}	$+1.572\times10^{-3}$	$+5.686\times10^{-4}$	-4.585×10^{-6}	-1.470×10^{-5}	.172
Retorted Shale:							
Case A	+1.8246	-4.4844×10^{-2}	-2.309×10^{-4}	$+3.652\times10^{-4}$	0	$+1.067\times10^{-5}$	.133
Case B	+1.5355	-5.923×10^{-2}	$+3.030\times10^{-5}$	$+6.250\times10^{-4}$	-2.935×10^{-9}	$+2.698\times10^{-6}$	.162
Burned Shale:							
Case A	+1.5583	-4.753×10^{-2}	$+8.724\times10^{-5}$	$+3.651\times10^{-4}$	-8.483×10^{-7}	$+1.142\times10^{-5}$	.157
Case B	+1.2111	-4.927×10^{-2}	$+1.181\times10^{-4}$	$+5.376\times10^{-4}$	-5.009×10^{-7}	$+1.827\times10^{-6}$	.122

[a] Probe perpendicular to shale bedding planes.
[b] Probe parallel to shale bedding planes.

them parallel to the bedding planes. The cut faces were polished to provide good contact when they were placed together. Two small parallel grooves were cut in one of the faces with a scribe mounted in a milling machine. One groove was cut in the center of the block and the other 0.64 cm from it. The heater wire was placed in the center groove and the thermocouple was placed in the outer groove after which the two halves of the block were clamped together securely.

b. Experimental Procedure

The millivolt recorder was adjusted to a 1-millivolt full-scale response and to zero reading. Chart speed was set at 2.54 cm (1 inch) per minute, and as the pens passed one of the time-indicating lines of the chart, current was applied to the heater wire and allowed to flow for 10 minutes. After the block had cooled, the experiment was repeated. Determinations were made at each of five heat input levels on each shale sample.

3.2. Calculations and Discussion of Results

The following eq was used to calculate diffusivities from recorder readings taken at 1-minute intervals:

$$\ln a = \frac{\theta 4\pi\lambda}{Q} + \gamma + \ln\frac{R^2}{4t}, \qquad (5)$$

where the symbols have the same meaning as in eq (1). This eq was obtained by solving eq (1) for ln a. The λ values were from eq (4). Diffusivities which did not vary from the asymptotic value by more than 5×10^{-8} m^2/sec were averaged to obtain the diffusivity for that particular run. The standard deviation of a was about 2.3×10^{-8} m^2/sec for ten runs.

In order to obtain a further indication of the accuracy of the experimentally determined values, they were compared with calculated values obtained by using the following eq:

$$a = \frac{\lambda}{d\ c_p}, \qquad (6)$$

where a = thermal diffusivity in m^2/sec,
λ = thermal conductivity in W m^{-1} deg^{-1},
d = density in kg/m^3,
and c_p = specific heat in J kg^{-1} deg^{-1}.

The values of λ were again obtained from eq (4). Densities and specific heats were obtained from curves which correlated these properties with Fischer assay. Densities of the retorted and of the

burned shales were obtained by assuming that 85 percent of the organic matter was removed by retorting without any change in shale volume, and that burning removed all of the organic matter without any change in volume. The latter densities are in reasonable agreement with those recently reported by Tisot (4).

Table 2 compares the experimentally determined thermal diffusivities with those obtained by use of

TABLE 2. - Thermal diffusivity of Green River oil shale, 10^{-7} m^2/sec

Oil yield	Raw shale		Retorted shale		Burned shale	
gal/ton	Experimental	Calculated	Experimental	Calculated	Experimental	Calculated
8.1	9.0	7.2	4.9	5.7	3.4	4.1
9.7	9.8	7.0	7.2	4.9	6.2	3.9
12.9	8.3	6.2	8.8	4.4	7.2	3.4
13.3	6.7	6.2	3.6	4.4	3.1	3.4
22.6	4.1	4.9	2.3	3.1	1.5	2.1
26.1	3.1	4.4	2.1	2.6	1.5	1.8
28.5	4.1	4.1	-	2.3	2.1	1.5
28.5	4.1	4.1	2.6	2.3	1.8	1.5
48.1	2.6	2.8	1.3	1.5	1.0	.8
50.7	3.4	2.8	2.1	1.5	-	.8
55.0	3.9	3.1	-	2.1	-	1.3
59.1	4.6	3.1	-	2.6	-	1.8

eq (6), which does not require a direct measurement.

The reliabilities of the parameters used in eq (6) are as follows:

λ, $\pm$ 0.10 W m^{-1} deg^{-1},
d, $\pm$ 160 kg/m^3,
and c_p, $\pm$ J kg^{-1} deg^{-1}.

For a 28-gallon-per-ton shale after retorting, the true value of the above parameters could lie anywhere within the following ranges:

λ, 0.47 - 0.67 W m^{-1} deg^{-1},
d, 1730 - 2050 kg/m^3
and c_p, 0.38 - 0.92 J kg^{-1} deg^{-1}.

Substituting the limits of these parameters in eq (6) gives the following limits for a: 2.58×10^{-7} to 4.90×10^{-7} m^2/sec. Considering the heterogeneity of oil shale, this spread is not at all surprising, and the differences between the values calculated by eq (5) and those calculated by eq (6) are well within the limits of accuracy that can be expected.

4. Summary

Thermal conductivities were experimentally determined on several different grades of raw shale and on their respective retorted shales and burned shales. Determinations were made with the heat source both perpendicular and parallel to the bedding planes, and at several different temperatures. Conductivity values ranged from about 0.69 W m^{-1} deg^{-1} for 58.6-gallon-per-ton shale to about 1.6 W m^{-1} deg^{-1} for a lean, 8.6 gallon-per-ton shale. Conductivities of the retorted or spent shales ranged from 0.26 to 1.4 W m^{-1} deg^{-1}, and of the burned shales from less than 0.17 to about 1.2 W m^{-1} deg^{-1}. An eq was developed for calculating the thermal conductivity of raw, retorted, and burned Green River oil shales.

Thermal diffusivities were determined experimentally on twelve different grades of raw shale assaying from 8.1 to 59.1 gallons of oil per ton and on the retorted and the burned shales from these

raw shales. Thermal diffusivities of raw shales ranged from 2.6×10^{-7} to 9.8×10^{-7} m^2/sec. Diffusivities of the retorted shales ranged from 1.3×10^{-7} to 8.8×10^{-7} m^2/sec and of the burned shales from 1.0×10^{-7} to 7.2×10^{-7} m^2/sec.

5. Acknowledgment

The research on which this report is based was done under a cooperative agreement between the Bureau of Mines, U.S. Department of the Interior, and the University of Wyoming.

6. References

(1) Marovelli, R. L. and Veith, K. F. Thermal conductivity of rock: measurement by the transient line source method, BuMines Rept. of Inv. 6604 (1965).

(2) Lentz, C. P. A transient heat flow method of determining thermal conductivity: application to insulating materials, Can. J. of Technol., 30, No. 6, 153-166 (1952).

(3) Underwood, W. M. and McTaggart, R. B. The thermal conductivity of several plastics, measured by an unsteady state method, Chem. Eng. Prog. Symposium Series, Heat Transfer, 56, No. 30, 261-268 (1960).

(4) Tisot, P. R. Alterations in structure and physical properties of Green River oil shales by thermal treatment, J. of Chem. and Eng. Data, 12, No. 3, 405-411 (July 1967).

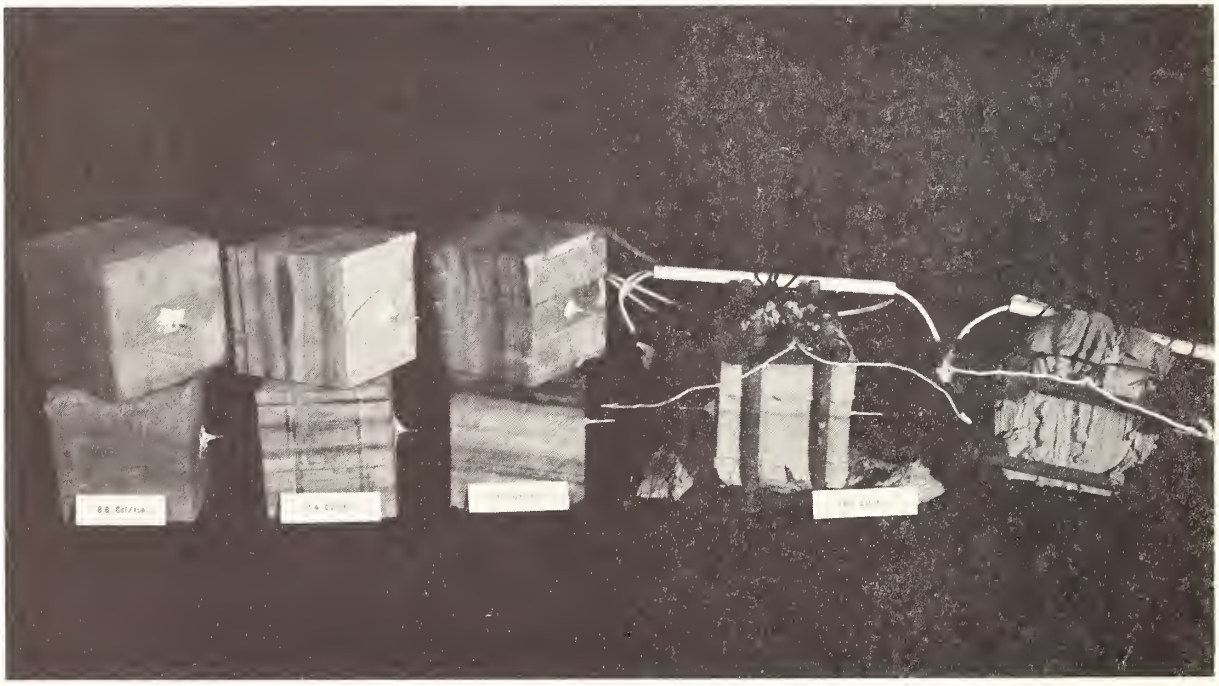

FIGURE 1. - Burned shale test pieces used for thermal conductivity determinations.

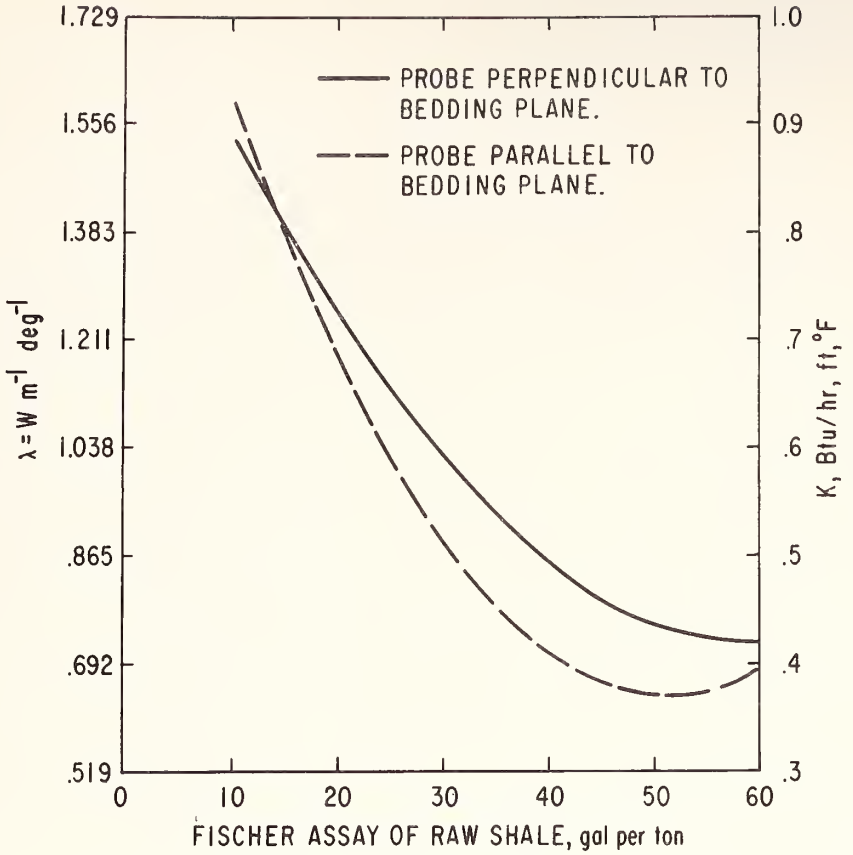

FIGURE 2. - Thermal conductivity of Green River oil shale.

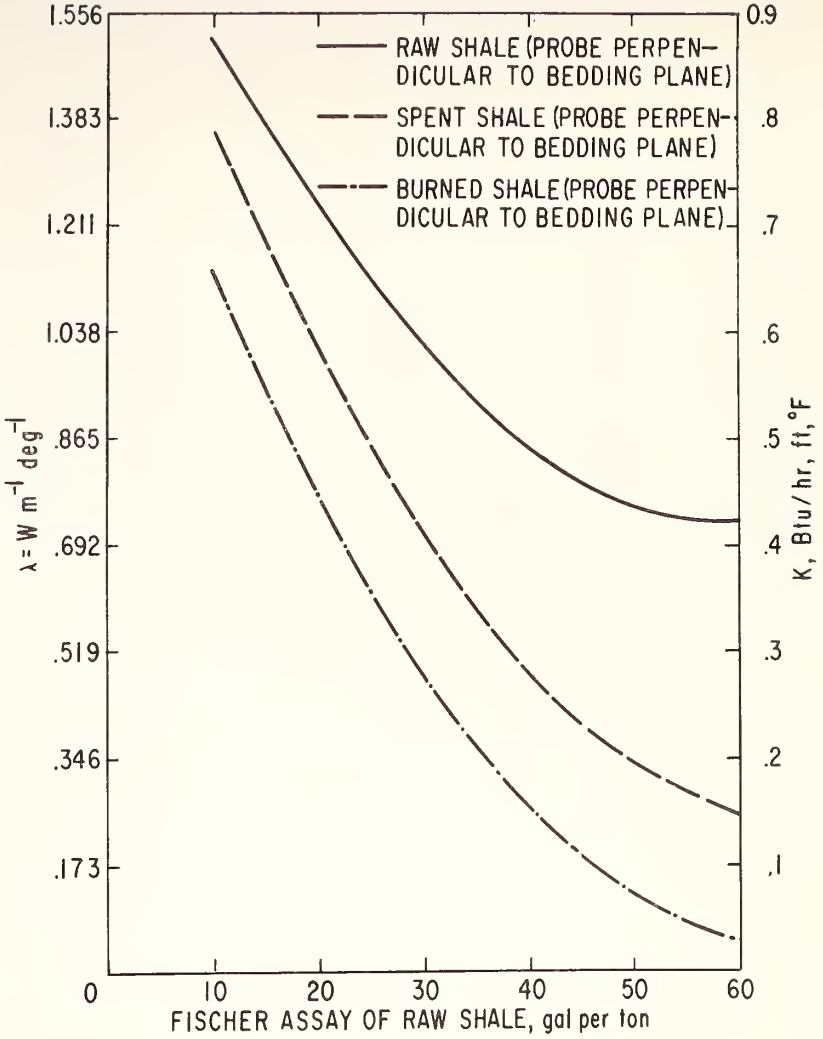

FIGURE 3. - Thermal conductivities of raw, spent, and burned Green River oil shales.

Experimental Study Relating Thermal Conductivity to Thermal Piercing of Rocks[1]

V.V. Mirkovich

Mineral Processing Division, Mines Branch
Department of Energy, Mines and Resources
Ottawa, Canada

Thermal conductivity of 19 selected Canadian rocks was measured to determine the effect of thermal conductivity on thermal piercing of rocks. Rocks with a higher thermal conductivity generally tend to pierce better, but a definite relation could not be established. However, a very good correlation was obtained between the thermal piercing rate and the product of thermal diffusivity and thermal expansion.

Key words: Rocks, thermal conductivity, thermal diffusivity, thermal expansion.

[1]Submitted for publication to Internal Journal of Rock Mechanics and Mining Sciences.

Measurement of Thermal Conductivity of Gases

S. C. Saxena

Thermophysical Properties Research Center
Purdue University
West Lafayette, Indiana

We describe briefly a number of methods which have been used for the measurement of thermal conductivity of gases and gas mixtures. These are: (1) the concentric sphere method, (2) the parallel plate method, (3) the coaxial cylinder method, (4) the hot-wire method, (5) the thermal diffusion column method, (6) the line source flow method, (7) the plasma or arc method, and (8) the shock tube method. Some of the less used methods are also mentioned. It is felt that for a particular set of experimental conditions one technique may be preferable over others. The regions of temperature and pressure where thermal conductivity researches, both experimental and theoretical, will be useful are outlined.

Key Words: Thermal conductivity, gases, conductivity cells.

1. Introduction

In many engineering calculations involving heat transfer, the knowledge of thermal conductivity appears as an important parameter. With increasing efforts in nuclear and space technology the need for such data is felt more and more. Even the fundamental understanding about the nature of polyatomic molecules is facilitated to a large extent if elaborate and accurate data on thermal conductivity are available. Such considerations have given incentive to the development of methods which may be appropriate for an accurate measurement of thermal conductivity under varying conditions of temperature, pressure and composition.

In this article, we briefly discuss those methods which have proved sufficiently accurate and adoptable for measurement over a range of experimental conditions. Both steady and unsteady state methods are considered. In the former category the temperature profile is time invariant, while in the latter the temperature field changes with time. Detailed reviews on the subject are written from time to time. Mention may be made of the two recent ones, Tsederberg [1][1], and Saxena and Gandhi [2]. Westenberg [3] has given a brief description of the major methods used for determining thermal conductivity of gases.

For a quick and approximate estimate of the thermal conductivity, relative methods have been developed. Thus, if a constant heat flux is allowed to pass through two plane parallel layers of two substances, temperature gradients are established which are inversely proportional to the thermal conductivities of the two substances. Again if the conductivity of one substance is known that of the other is determined by measuring the thicknesses of the two layers and temperature drops across them. Similarly, in another arrangement a wheatstone bridge is formed with hot-wire cells in two adjacent arms. In one of the cells a suitable reference gas in enclosed. While in the other successively gases of known thermal conductivity, to obtain a calibration graph of thermal conductivity versus the deflection of the galvanometer showing the imbalance of the bridge. Actual determination of thermal conductivity then involves putting the unknown sample in the cell and noting the galvanometer deflection. The latter is the principle of a commercially available unit for gas analysis by the name katharometer. Accurate determination of thermal conductivity is not possible by such relative methods for here no account is taken of those corrections which are dependent on the nature of gas like accommodation, wall and convection effects etc. In the rest of this article we discuss only the absolute methods where an accurate determination is theoretically possible. Such methods are mostly developed for steady state operation and the ones considered here are: the concentric sphere method, the parallel plate method, the coaxial cylinder method, the hot-wire method, the thermal diffusion column method, and the line source flow method, etc. We also mention the unsteady state methods amongst which the shock tube and arc methods are to be noted for their unique appropriateness at such high temperatures where other methods will fail. In each of the methods, we describe only a representative effort and their general scope and appropriateness for the determination of thermal conductivity of gases.

[1] Figures in brackets indicate the literature references at the end of this paper.

2. The Concentric Sphere Method

In recent years, this method has been developed by Sage and coworkers. A schematic of the apparatus is shown in figure 1 and is after Richter and Sage [4]. It consists of a stainless steel pressure vessel A which is immersed in a constant temperature bath B. The innermost sphere C is fitted with an electric heater D and can thus be heated to any desired temperature. This sphere is surrounded by two carefully machined spherical shells E and F. To determine the temperatures of the internal and external surfaces of shells E and F respectively, thermocouples are installed. Further, these shells are pressure-compensated so that the spacing between them can be determined as a function of pressure and temperature. The shells are spaced by six pins shown at G in the figure. The hemispheres E and F approximate to a spherical surface within a maximum deviation of 0.00125 cm and an average deviation of 0.0005 cm. The effective path length between E and F was determined, by filling the space with mercury, as 0.05 cm at 23° C.

The thermal conductivity is determined by measuring the temperature difference between the two concentric spherical shells which enclose the test material, while a known radial thermal flux passes between them. The energy added to the inner sphere C is determined by conventional calorimetric technique within an uncertainty of 0.05 percent. The heat loss also occurs through pins G, and stem H containing leads J. The pins are constructed of low thermal conductivity steel and at the point of contact are less than 0.025 cm in diameter. The maximum energy loss through these pins is 0.0060 of the energy added to the heater D. The thermal leakage through the stem H is determined by measuring the temperature gradient in the vicinity of the guard heater K, with a differential thermocouple. This loss is less than 0.0001 of the energy added to the heater.

Convection was found to be present in the apparatus [4] even when the product of the Prandtl and Grashof numbers is less than 1000. Consequenty measurements were made at several different temperature gradients and the apparent thermal conductivity was extrapolated to zero temperature difference to obtain a value free from convection effect.

The thermal radiation was determined by taking measurements on the cell evacuated to a pressure less than 1 micron. The combined magnitude of corrections, conduction through pins and radiation, is about 3 and 15 percent at about 4° and 200° C respectively. The results are estimated to be accurate within a probable error of less than 4 percent, [5].

In a later effort [6] the apparatus was slightly modified. The two spherical shells were eliminated from the high pressure region and instead a new inner sphere was placed in the present outer shell. The two spherical surfaces were gold plated to reduce energy transport by radiation.

3. The Parallel Plate Method

This method in its simplest form employs a thin horizontal layer of gas enclosed between two perfectly plane surfaces maintained at two different temperatures. The upper plate is kept at a higher temperature to avoid convection, and guard rings are used to ensure the flow of heat as unidirectional and vertically downward. The radiative heat loss is carefully determined and then the thermal conductivity is calculated from the simple Fourier's relation. The various attempts made so far on an apparatus of this type are already reviewed [1, 2], and here we will briefly mention the elaborate experimental arrangement of Michels, Sengers and Van Der Gulik [7] which could be used successfully even in the critical region [8, 9].

A vertical cross section of the conductivity cell is shown in figure 2. L, U and G made of electrolytic copper are the lower plate, upper plate and guard ring respectively. Q is an insulation cap. The relevant surfaces of the two plates and G are machined flat within a micron so that gas layers as thin as 0.4 mm could be used. These are also highly polished to decrease radiation and coated with 0.1 micron thick layer of silicon oxide to avoid any change in radiation constant with time. Both U and L are fitted with a platinum spiral which can be used both as resistance thermometer as well as heater. The guard ring G contains a heating element. The temperature of the measurement is obtained from L, while the temperature difference between U and L is obtained with a thermocouple of which the junctions 1 and 2 are located close to the surface of the plates. The temperature differences between U and L varied from 0.006° C to 0.4° C. The temperature difference between U and G is controlled by a thermocouple with a sensitivity of 2×10^{-4}° C. The distance between upper and lower plates is adjusted by three small glass spacers S, located between the guard and the lower plate. All possible precautions were taken to reduce the number of sources for convection at the minimum. The accuracy of the thermal conductivity is estimated to be one percent [10].

4. The Coaxial Cylinder Method

In the simplest form, one uses here two coaxial cylinders mounted in a perfectly vertical position with a very small annular gap which is filled with the gas. If the thickness of the gas is small compared to the length of the cylinders, the thermal flow will be fairly radial and Fourier's law will control the heat conducted.

Keyes and Sandell [11] employed two concentric cylinders of silver with an annulus of about 0.6 mm. A schematic of their apparatus is shown in figure 3. The inner cylinder or emitter carries an axial heater wire. The bottom end of the cell is closed with a silver piece adjustable in its distance from the cylinders and this dis-

tance is kept the same as the gap between the cylinders. A small correction due to the additional flow of heat from the corners of the bottom disc of the emitter is applied. At the top end there is a heat guard to intercept the flow of heat from or to the emitter. This is accomplished by maintaining the guard at the same temperature as the emitter. This arrangement also ensures that there is no heat loss or gain from the emitter through the heater and thermocouple leads. The heat lost by radiation from the emitter surface, conducted away by the centering supports etc. are evaluated by taking measurements on the cell while it is under vacuum. Rothman and Bromley [12] further improved the basic design of such a cell to be appropriate for measurements up to 800° C. Glassman and Bonilla [13], in an endeavor to avoid the uncertainty in the measurements because of radiation and its increasing magnitude with increase in temperature, employed a nonabsorbent and nonradiative cylinder of fused silica, and cooling air stream.

5. The Hot-Wire Method

Broadly speaking in this method a metal wire is placed axially in a metal or glass cylinder. The wire acts both as a heater as well as a thermometer. The test gas is filled in the cylinder and the whole assembly is immersed in a thermostat, or a cryostat or furnace as the case may be. For the computation of thermal conductivity all one needs to know is the change in resistance of the axial wire when a certain current is passed, which heats the wire, in the presence of a gas over its value at zero current. In practically all types of hot-wire cells, the undesirable convection, radiation, end conduction and temperature discontinuity effects are present in varying proportions. The temperature discontinuity and convection effects are brought to minimum by careful design and installation of the cell, and operating at a proper pressure. In the thick-wire variety of the hot-wire cell the end conduction is corrected by using a thick wire which is soldered at the two ends in the closing caps of the cell. This provides a well defined boundary condition with the result that an adequate theoretical formulation of the heat flow becomes possible. In the thin wire variant on the other hand two thin potential leads are used and these directly measure the potential drop across a central portion of the wire where the temperature is supposedly uniform. In a third type of arrangement one uses two identical cells differing only in length and these are connected across the two adjacent arms of a bridge. The measurements under these conditions refer to the small central portion of the longer cell whose length is equal to the difference of the lengths of two individual cells. The radiation correction is estimated either theoretically on the basis of Stefan-Boltzmann law or by taking differential measurements with and without gas. A small wall effect correction arising because of the finite thickness of the cell wall is not only small but is also calculable with good accuracy.

The thin-wire conductivity cell of Taylor and Johnston [14] is shown in figure 4 and that of the thick-wire type of Kannuluik and Martin [15] in figure 5. The latter variant has been extensively used in recent years [16, 17].

It may be pointed out that the spherical arrangement was introduced to avoid thermal leakage around the peripheries of plane surfaces or at the ends of the cylindrical section [4]. It is felt that a spherical heater producing uniform heat flux is difficult to fabricate. Furthermore the influence of eccentricity on the accuracy of the measurements is only a function of the eccentricity itself and not of the direction of eccentricity [18]. In the cylindrical arrangement, on the other hand it is possible to tolerate some variation in the thickness of the gas layer at the ends when the axial adjustment is correctly made. This is because the heat-transfer areas at the ends are small compared with that of the annulus. It has also been found [7] that adequate operation is possible in the parallel plate method when a small angle exists between the vertical and temperature gradient. The cylindrical geometry does not permit that. To get around such problems Leidenfrost [18] employed a cell with a vertical cylinder and hemispherical ends within a similar cavity.

6. The Thermal Diffusion Column Method

Blais and Mann [19] introduced a hot-wire type of thermal diffusion column to determine thermal conductivity at relatively higher temperatures. Timrot and Umanskii [20] have also employed this method. Saxena and coworkers have also used this technique and some of their preliminary results are available [21, 22]. In figures 6 and 7 are shown the column designs used by Timrot and Umanskii [20], and Saxena and coworkers [21, 22] respectively. The thermal conductivity is determined from the temperature dependence of the amount of heat transmitted by the gas. The maximum temperature of measurement is limited by the thermal stability of the wire used in the column. The method is remarkably successful and notably simple for conductivity measurements up to about 3000° K.

7. The Line Source Flow Method

This technique introduced and described in detail by Westenberg and deHaas [23] uses a line source of heat stretched across the jet exit of the test gas under laminar flow. The former is obtained by a fine electrically heated wire and the latter by a furnace and a series of precision screens. The passing gas stream gets heated and the temperature at any point down stream rises above its free stream value. By measuring the transverse or axial or both decay temperature profiles down stream the thermal conductivity of the gas can be calculated. The method is an absolute one and is used in the temperature range 300-1200° K. The precision here is not as high as of the other static methods and its accuracy is estimated at 2-3 percent.

8. The Plasma or Arc Method

The thermal conductivity of nitrogen in a well stabilized cylindrical arc of 5 mm diameter and 100 ampere current intensity is determined in the temperature range from 6000 to 13000° K by Burhorn [24]. For such a free burning arc the energy loss by radiation can be neglected in comparison to that by conduction. Further, for such a stationary arc at atmospheric pressure, assuming that the plasma radiation is negligible, the mathematical representation becomes simple. The electrical energy supplied to a volume element is completely withdrawn by conduction. The experimental arrangement is shown in figure 8.

The arc burns between the 4 mm thick tungsten cathode and the water cooled copper anode through a 5 mm diameter cylindrical opening along the axis of a cascade of ten copper plates. The cascade plates have an outer diameter of 5.0 cm and a thickness of 8 mm. The distance between the plates is 1 mm. Each plate is provided with a channel for water cooling, all are insulated from each other. A quartz window, 5 mm in diameter, is provided for observations. The arc is ignited by the application of voltage when the anode and cathode are connected by a thin wire. This arrangement is immersed into a tank which is slowly purged by pure nitrogen.

The light leaving the longitudinal slit in a quartz window is focused by an objective on the spectrograph slit and diffracted by a plane grating of high dispersion. A rotating sector in front of the slit permits quantitative reduction of the light. The absolute intensity of radiation of the arc crater is determined by equalizing the arc and light source. A careful experimentation and analysis enables the determination of the temperature distribution along the arc radius and other necessary quantities. The success of this method can be gauged by the fact that this is the highest temperature where thermal conductivity measurements are made so far.

Wienecke [25] has measured the total thermal conductivity for the plasma of a high-current carbon arc in the temperature range from 4000° to 10,000° K. This is achieved by observing the cooling trend of a currentless plasma. The input of the electrical energy is then absent as also the flow which is coupled with the arc current.

9. The Shock Tube Method

An unsteady state method, useful for the measurement of thermal conductivity at high temperatures, using a shock tube is described by Smiley [26] and since then has been used by a number of other workers [27-30] up to temperatures as high as 8600° K. The principle of operation is simple. When the diaphragm separating the high pressure and low pressure chambers of a shock tube is broken, the high pressure gas drives a shockwave. At the end wall of the tube the shock wave is reflected back through the hot gas. The temperature rise of the end plate, which forms the boundary of the shock tube, is measured as a function of time. This information enables the determination of the constants occurring in the assumed temperature variation of thermal conductivity. The biggest advantage of the technique consists in that no corrections for convection and radiation are needed.

10. Some Other Methods

A mention may be made of some other methods which have been used for the measurement of thermal conductivity of gases. Peterson and Bonilla [31] suggested an unsteady state frequency response technique in which the wire of the hot-wire cell is heated by an alternating current. This results in the generation of the third harmonic of the fundamental heating frequency and whose magnitude depends on the conductivity of the gas. A dilatometric method is developed by Timrot and Totskii [32] for the measurement of thermal conductivity of corrosive gases. In principle, it is similar to the coaxial cylinder method except now the temperature drop in the gaseous layer is measured in terms of the thermal expansion of the walls enclosing the layer and the end effects are eliminated by inserting the heater to various depths.

Methods of somewhat limited applicability have been proposed by Lindsay and Bromley [33]; Robin, Dewasnes and Mabboux [34], and Evans and Kenney [35]. As these cannot be used to determine the absolute values of thermal conductivity over an extended range of variables, we will defer any discussion on them.

Eckert and Irvine [36] determined directly the Prandtl number and hence thermal conductivity by measuring the subsonic temperature recovery factor. This is of course an indirect method.

11. Conclusions

We have mentioned above the various popular methods used so far for measuring thermal conductivity of gases. A critical assessment is possible on this basis and with the knowledge of the opinions of a large number of workers who have used the individual methods. The latter part is not given any space in the present article but with that also in mind we suggest here some general conclusions for the adoption of a technique for a set of measurements. These are:

(a) At temperatures not too far from room and for pressures around one atmosphere many techniques seem to be almost equally good and the choice is more or less a personal preference.

(b) For temperatures up to 1000° C and up to one atmosphere operation, the hot-wire method seems simple, quick and accurate. This recommendation is also valid for low temperatures.

(c) For temperatures beyond 1000° C and up to about 2500° C, the thermal diffusion column method is unique as long as the pressure is below one atmosphere.
(d) For operation at high pressures, the parallel plate and coaxial cylinder methods are the probable choices with a preference for the former.
(e) Shock tube and arc methods will have to be developed for measurements at still higher temperatures.
(f) It is just too unfortunate that only one method will not enable all ranges to be covered.

12. References

[1]. Tsederberg, N.V., Thermal conductivity of gases and liquid (M.I.T. Press, Massachusetts, 1965).

[2]. Saxena, S.C. and Gandhi, J.M., Methods of measuring thermal conductivity of gases, J. Sci. Ind. Res., to be published.

[3]. Westenberg, A.A., A critical survey of the major methods for measuring and calculating dilute gas transport properties, Advances in Heat Transfer, Vol. 3, p. 253 (Academic Press Inc., New York, 1966).

[4]. Richter, G.N. and Sage, B.H., Thermal conductivity of fluids. Nitrogen dioxide in the liquid phase, Ind. Eng. Chem., J. Chem. Eng. Data Ser. 2, 61 (1957).

[5]. Richter, G.N. and Sage, B.H., Thermal conductivity of fluids. Nitric oxide, J. Chem. Eng. Data 4, 36 (1959).

[6]. Richter, G.N. and Sage, B.H., Thermal conductivity of fluids. Nitrous oxide, J. Chem. Eng. Data 8, 221 (1963).

[7]. Michels, A., Sengers, J.V. and Van Der Gulik, P.S., The thermal conductivity of carbon dioxide in the critical region. I. The thermal conductivity apparatus, Physica 28, 1201 (1962).

[8]. Michels, A., Sengers, J.V. and Van Der Gulik, P.S., The thermal conductivity of carbon dioxide in the critical region. II. Measurements and conclusions, Physica 28, 1216 (1962).

[9]. Michels, A. and Sengers, J.V., The thermal conductivity of carbon dioxide in the critical region. III. Verification of the absence of convection, Physica 28, 1238 (1962).

[10]. Sengers, J.V., Bolk, W.T. and Stigter, C.J., The thermal conductivity of neon between 25°C and 75° C at pressures up to 2600 atmospheres, Physica 30, 1018 (1964).

[11]. Keyes, F.G. and Sandell, D.J., New measurements of the heat conductivity of steam and nitrogen, Trans. Am. Soc. Mech. Eng. 72, 767 (1950).

[12]. Rothman, A.J. and Bromley, L.A., High temperature thermal conductivity of gases, Ind. Eng. Chem. 47, 899 (1955).

[13]. Glassman, I. and Bonilla, C.F., Thermal conductivity and Prandtl number of air at high temperatures, Chem. Eng. Prog. Symp. Series 5, 49, 153 (1953).

[14]. Taylor, W.J. and Johnston, H.L., An improved hot wire cell for accurate measurement of thermal conductivities of gases over a wide temperature range: Results with air between 87° and 375° K, J. Chem. Phys. 14, 219 (1946).

[15]. Kannuluik, W.G. and Carman, E.H., The thermal conductivity of rare gases, Proc. Phys. Soc. 65B, 701 (1952).

[16]. Srivastava, B.N. and Saxena, S.C., Thermal conductivity of binary and ternary rare gas mixtures, Proc. Phys. Soc. 70B, 369 (1957).

[17]. Gambhir, R.S. and Saxena, S.C., Thermal conductivity of binary and ternary mixtures of krypton, argon and helium, Mol. Phys. 11, 233 (1966).

[18]. Leidenfrost, W., An attempt to measure the thermal conductivity of liquids, gases, and vapors with a high degree of accuracy over wide ranges of temperature (-180 to 500° C) and pressure (vacuum to 500 atm), Int. J. Heat Mass Transfer 7, 447 (1964).

[19]. Blais, N.C. and Mann, J.B., Thermal conductivity of helium and hydrogen at high temperatures, J. Chem. Phys. 32, 1459 (1960).

[20]. Timrot, D.L. and Umanskii, A.S., Investigation of the thermal conductivity of helium, High Temperature 3, 345 (1965).

[21]. Saksena, M.P. and Saxena, S.C., Measurement of thermal conductivity of gases using thermal diffusion columns, Phys. Fluids 9, 1595 (1966).

[22]. Saxena, V.K., Saksena, M.P. and Saxena, S.C., Measurement of thermal conductivity of gases using thermal diffusion column: neon, Indian J. Phys. 11, 597 (1966).

[23]. Westenberg, A.A. and deHaas, N., Gas thermal conductivity studies at high temperature. Line source technique and results in N_2, CO_2, and N_2-CO_2 mixtures, Phys. Fluids 5, 266 (1962).

[24]. Burhorn, F., Calculation and measurement of the thermal conductivity of nitrogen up to 13,000° K, Z. Physik 155, 42 (1959).

[25]. Wienecke, R., Experimental and theoretical determination of the thermal conductivity of the plasma in a high-current carbon arc, Z. Physik 146, 39 (1956).

[26]. Smiley, E. F., The measurement of the thermal conductivity of gases at high temperatures with a shock tube: Experimental results in argon at temperatures between 1000° K and 3000° K, Ph. D. thesis, The Catholic University of America, Washington, D. C., 1957.

[27]. Lauver, M. R., Shock-tube thermal conductivity, Phys. Fluids 7, 611 (1964).

[28]. Collins, D. J., Greif, R. and Bryson, A. E., Measurements of the thermal conductivity of helium in the temperature range 1600-6700° K, Int. J. Heat Mass Transfer 8, 1209 (1965).

[29]. Collins, D. J. and Menard, W. A., Measurement of the thermal conductivity of noble gases in the temperature range 1500 to 5000° K, Trans. Am. Soc. Mech. Eng. 88, 52 (1966).

[30]. Carey, C. A., Carnevale, E. H. and Marshall, T., Experimental determination of the transport properties of gases. Part II. Heat transfer and ultrasonic measurements, Tech. Rep. AF ML-TR-65-141, Parametrics, Inc., September 1966.

[31]. Peterson, J. R. and Bonilla, C. F., The development of a frequency response analysis technique for thermal conductivity measurement and its application to gases at high temperatures, Third symposium on Thermophysical Properties, Am. Soc. Mech. Eng., 264, March 1965.

[32]. Timrot, D. L. and Totskii, E. F., Dilatometric method for the experimental determination of the thermal conductivity of corrosive gases and vapors at high temperatures, High Temperature 3, 685 (1965).

[33]. Lindsay, A. L. and Bromley, L. A., Use of the unsteady state method for the determination of the thermal conductivity of gases, UCRL Report-1128 (1951).

[34]. Robin, J., Dewasnes, P. and Mabboux, C., Dynamic determination of the thermal conductivity of carbon dioxide at different temperatures, Compt. Rend. 250, 3003 (1960).

[35]. Evans, E. V. and Kenney, C. N., Flow method for determining the thermal conductivity of gas mixtures, Nature 203, 184 (1964).

[36]. Eckert, E. R. G. and Irvine, T. F., New method for measurement of Prandtl number and thermal conductivity of fluids, J. Appl. Mech. 24, 25 (1957).

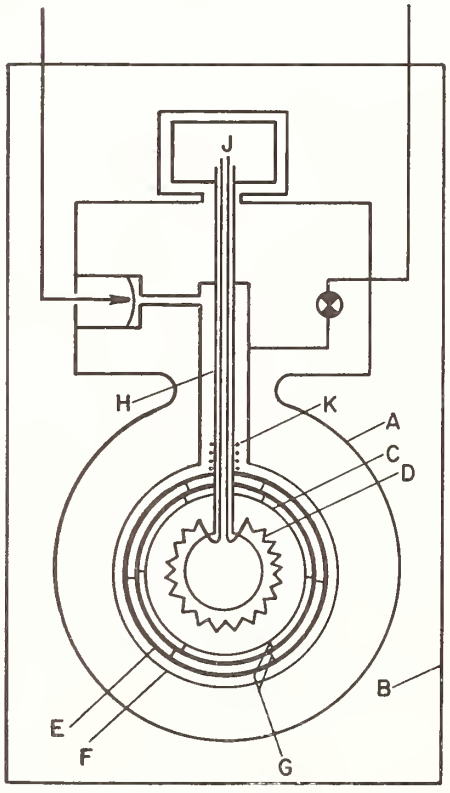

Figure 1. The concentric sphere type conductivity cell, reference [4].

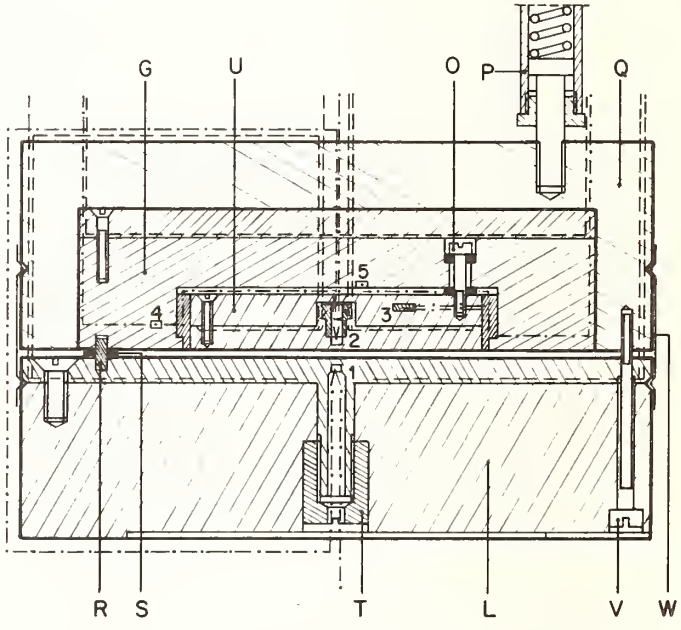

Figure 2. The parallel plate type conductivity cell drawn to scale 1 to 1. - - - leads to the electrical measuring and heating circuit, - · - · - · thermocouples leads, reference [7].

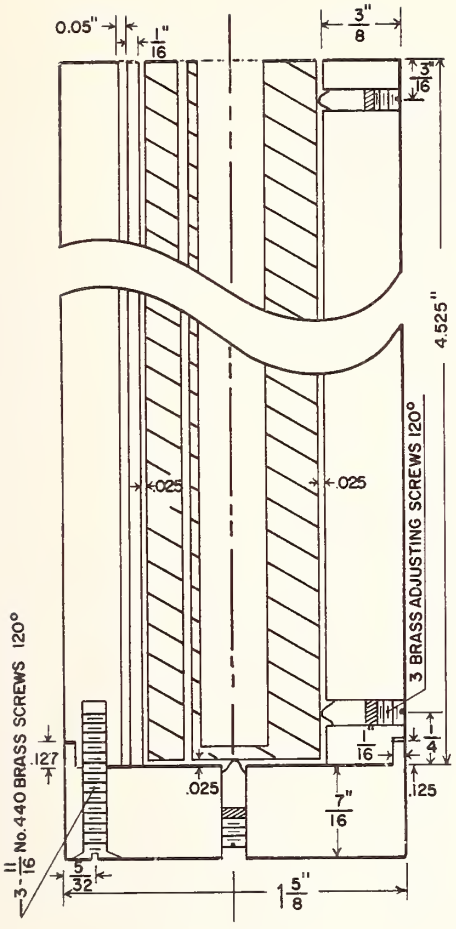

Figure 3. The coaxial cylinder type conductivity cell, reference [11] .

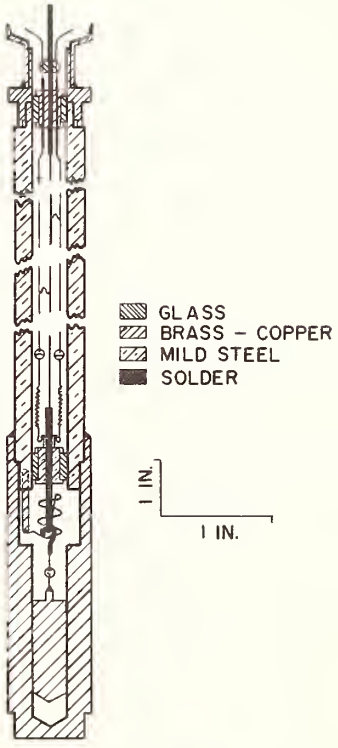

Figure 4. The thin hot-wire conductivity cell, reference [14] .

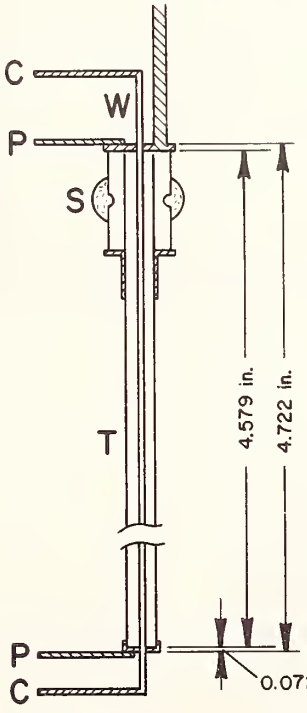

Figure 5. The thick hot-wire conductivity cell. W, platinum wire; T, Pt-Ir tube; C, current lead; P, potential lead; S, seal. Diameter of the wire 0.1465 cm, mean internal diameter of the tube 0.7169 cm, reference [15] .

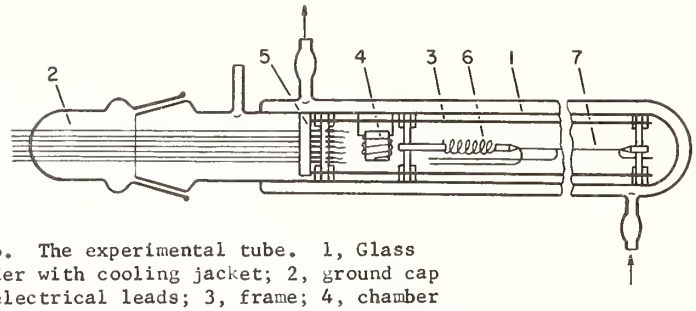

Figure 6. The experimental tube. 1, Glass cylinder with cooling jacket; 2, ground cap with electrical leads; 3, frame; 4, chamber for heating sodium; 5, joint carrying electrical leads; 6, spring for stretching the wire; 7. measuring wire with potential contacts, reference [20] .

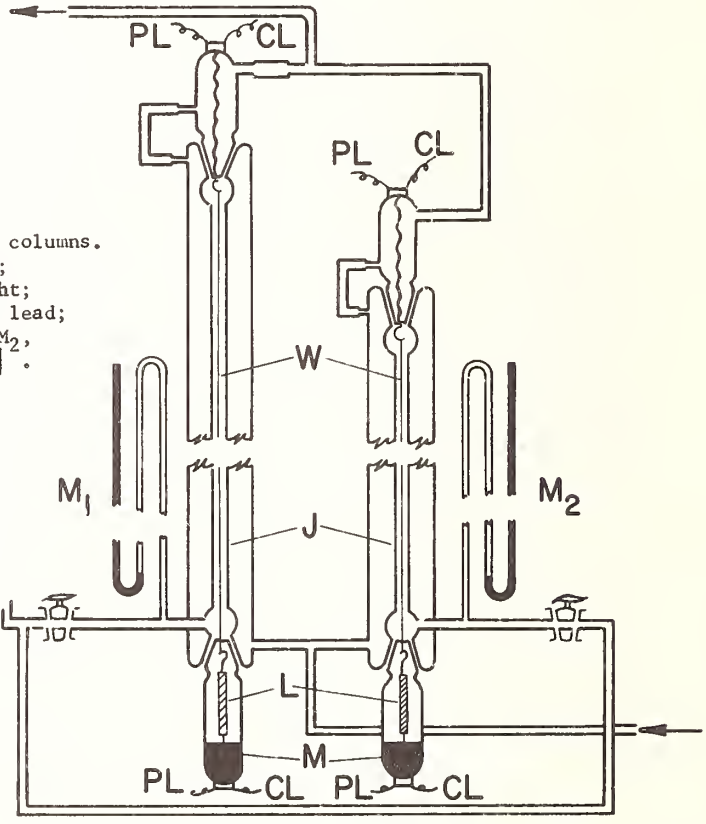

Figure 7. The conductivity columns. J, glass tube with jacket; W, platimun wire; L, weight; M, mercury; PL, potential lead; CL, current lead; M_1 and M_2, manometers, reference [21] .

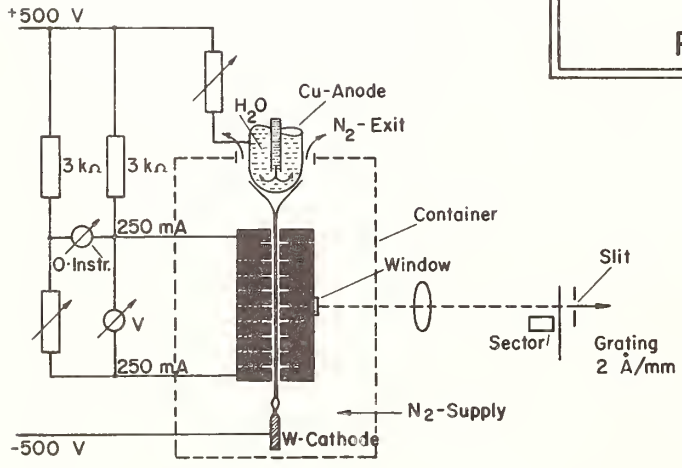

Figure 8. The schematic of the arc method, reference [24] .

Thermal Conductivity of Gases: Hydrocarbons at Normal Pressures

Dipak Roy and George Thodos

Northwestern University
Evanston, Illinois

Thermal conductivity measurements for hydrocarbons, obtained from a comprehensive literature search, were used to produce the product $k^*\lambda$, where $\lambda = M^{1/2} T_c^{1/6}/P_c^{2/3}$. This product represents the composite contribution due to the translation, rotational, and vibrational motions associated with the mechanics of a polyatomic molecule. For monatomic gases, which possess only translational motion, $k^*\lambda$ is identical to $(k^*\lambda)_t$, the translational contribution of these hydrocarbons. This approach permitted the establishment of the composite contribution due to rotation and vibration, $X = (k^*\lambda)_r + (k^*\lambda)_v$ as the difference, $k^*\lambda - (k^*\lambda)_t$.

The ratio $X/X_{T_R} = 1.00$ when plotted against T_R produced a unique relationship for the saturated aliphatic hydrocarbons, except for methane. The olefins, acetylenes, naphthens, and aromatics produced their specific $X/X_{T_R} = 1.00$ versus T_R relationships. Group contributions, developed in this study, permit the establishment of $X_{T_R} = 1.00$ to be used for obtaining X at other temperatures.

When the translational contribution, $(k^*\lambda)_t$ is added to $X = (k^*\lambda)_r + (k^*\lambda)_v$, the product $k^*\lambda$ is obtained for the hydrocarbons. Using this approach, thermal conductivities have been calculated for 27 hydrocarbons of all types and have been compared with experimental measurements to produce an average deviation of 2.1% for 109 points.

The Thermal Conductivity of 46 Gases at Atmospheric Pressure

P. E. Liley

Thermophysical Properties Research Center
Purdue University
2595 Yeager Road
West Lafayette, Indiana 47906

Available information on the thermal conductivity of 46 gases at atmospheric pressure is reviewed and most probable values recommended. Departure plots are given for sixteen substances of wide interest showing the accord between the different information and the recommended values. 255 references are cited. Some brief comments are made on the state of the art and on additional information sources, partly contained in 9 additional references.

Specifically, the substances considered are acetone, acetylene, air, ammonia, argon, benzene, boron trifluoride, bromine, n-butane, carbon dioxide, carbon monoxide, carbon tetrachloride, chlorine, deuterium, ethane, ethyl alcohol, ethyl ether, ethylene, fluorine, Freon-11, Freon-12, Freon-13, Freon-21, Freon-22, Freon-113, helium, heptane, hexane, hydrogen, hydrogen chloride, iso-butane, krypton, methane, methyl alcohol, methyl chloride, neon, nitric oxide, nitrogen, nitrogen peroxide, nitrous oxide, oxygen, pentane, propane, sulfur dioxide, toluene, and xenon.

Key Words: Conductivity, thermal conductivity, gases, atmospheric pressure, recommended values.

Calculation of Total Thermal Conductivity of Ionized Gases

Warren F. Ahtye[1]

Vehicle Environment Division
Ames Research Center, NASA
Moffett Field, California 94035

The suitability of the Boltzmann equation for calculating transport coefficients of partially ionized gases is discussed. Analytical and experimental investigations are cited to show that it can be used as a starting point to calculate the total thermal conductivity. The Chapman-Enskog solution of the Boltzmann equation is used to derive an expression for the total thermal conductivity, composed of three parts - the translational, reactive, and thermal diffusive components. The reactive and thermal diffusive components are explicitly expressed in terms of the multicomponent and thermal diffusion coefficients. Effects of higher order Sonine expansion terms are examined for the various transport coefficients. The first three orders of the Sonine expansion terms are required for the accurate calculation of the translational thermal conductivity, whereas only the first two orders are sufficient for the calculation of the multicomponent and thermal diffusion coefficients. These diffusion coefficients are then used to calculate the reactive and thermal diffusive components of the total thermal conductivity of hydrogen, nitrogen, and argon at conditions where the reactive component is at a maximum. These values of the reactive conductivity are examined to determine the relative importance of multicomponent and thermal diffusion. The predominant mechanism for hydrogen is the binary diffusion of atoms and ions, although the effects of thermal diffusion of electrons is also important. Thermal diffusion becomes more dominant as the molecular weight of the atom increases. In fact, the multicomponent diffusive effects for argon cancel, and the reactive thermal conductivity can be attributed almost entirely to the thermal diffusion of electrons.

Key Words: Boltzmann equation, Chapman-Enskog formulation, ionized gases, multicomponent diffusion, thermal conductivity, thermal diffusion.

1. Introduction

An object traveling through an atmosphere has part of its kinetic energy converted into thermal excitation of the surrounding flow field gas molecules. When the speed is sufficiently high, the gas decomposes into a complex mixture of molecules, atoms, ions, and electrons. The total thermal conductivity of this gas must be known in order to determine the heat flux into the surface of the object. In the calculation of the thermal conductivity of this ionized gas, one would ask the following questions. First, does the presence of charged particles introduce phenomena which affect the thermal conductivity? Second, is the theory which is used for neutral gases sufficiently general to account for these phenomena? This paper will describe some of the analytical and experimental work done in the past few years to resolve these two questions.

The greatest difference between an ionized gas and a neutral gas lies in the range of intermolecular forces. For example, the effective range of the force between two neutral particles or a charged particle and a neutral particle is orders of magnitude smaller than the average intermolecular spacing. These effective ranges are in accord with the basic assumption that particle collisions in the gas are binary - a necessary condition for the validity of the Boltzmann equation governing the transport coefficients of neutral gases. In contrast, the effective range of the intermolecular forces between two charged particles is usually greater than the average intermolecular spacing. At first appearance, this suggests

[1]Research Scientist

that the Boltzmann equation is not valid for gases with an appreciable degree of ionization[2]. This situation prompted Spitzer and his coworkers [1 and 2][3] to derive a theory which describes transport phenomena (specifically electrical and thermal conductivity) of an electron gas where the interactions are attributed to many long-range simultaneous but independent Coulombic interactions. The collision term in the Boltzmann equation was replaced by the Fokker-Planck expression which describes these simultaneous interactions. Recently Gross [3], Grad [4], Koga [5], and others re-examined the mathematical implications of the Boltzmann and Fokker-Planck equations and concluded that the Boltzmann equation was valid for ionized gases after all. Grad stated that

> ". . .The critical point here is that, although the two physical pictures are entirely different, their mathematical descriptions are identical! The net effect of many successive independent small impulses is the same as many simultaneous independent small impulses, provided only that the means and variances of the two impulse distributions are the same (actually, the entire probability distributions were taken to be the same). Thus we conclude, without setting pencil to paper, that the Fokker-Planck equation, which is an immediate consequence of the simultaneous grazing impulse model, must yield results identical with those obtained from the Boltzmann equation, provided that an appropriate grazing collisions approximation is made and the same cut-off is used in the latter computation."

The equivalence between the Boltzmann and Fokker-Planck equation for the case of a fully ionized gas was further demonstrated by the excellent agreement of the two sets of values of transport coefficients based on these equations [2].

A more rigorous theory for fully ionized gases can be derived from Bogolyubov-Born-Green-Kirkwood-Yvon hierarchy of equations [6] which account for simultaneous but dependent interactions (i.e. many particle correlations). An analysis by Sundaresan and Wu [7] has shown that the thermal conductivity from the B-B-G-K-Y approach is almost identical to that for the Fokker-Planck approach.

The accuracy of the Boltzmann equation was demonstrated in two recent experiments by Emmons [8] and Morris [9]. The goal of their experiments was the measurement of the electrical and thermal conductivity of partially ionized gases. Although the thermal conductivity could not be measured accurately at large degrees of ionization because of the masking effects of thermal radiation, the electrical conductivity was measured. In figures 1 and 2 the experimental values of the electrical conductivity are compared with values based on the Boltzmann equation (second-order Chapman-Enskog formulation). It can be seen that the agreement is fairly good over the entire range of temperatures (degree of ionization ranging from 1 percent at 9000°K to 100 percent at 22,000°K). Since the predominant cross section for the electrical conductivity is the well-verified Coulombic cross section, the agreement shown in figures 1 and 2 is a good indication of the validity of the Chapman-Enskog formulation of the Boltzmann equation for all degrees of ionization. Unfortunately, this is no guarantee that the values of the thermal conductivity can be accurately predicted at these high degrees of ionization since the predominant cross sections (e.g. atom-ion elastic and charge-exchange cross sections) are not known accurately, and since there are different types of diffusional effects present in thermal conduction. This means that measurements of thermal conductivity are still necessary.

2. Derivation of Total Thermal Conductivity

The analytical and experimental work described in the previous section indicate that the Boltzmann equation can be used as a starting point to calculate the total thermal conductivity. The approach described in this paper is the same as the Chapman-Enskog formulation applied to the case of neutral monatomic gas mixtures by Hirschfelder, Curtiss, and Bird [10] and will be examined to determine its suitability for a partially ionized gas. Besides the difference in the range of intermolecular forces a partially ionized gas differs from a neutral gas in two other respects. First, a charge separation field arises because of local differences in the ion and electron concentrations, and second, the ratio of the mass of the heaviest particle to that of the lightest particle increases by at least three orders of magnitude due to the presence of free electrons. A great amount of foresight was used in the derivation of the complete Chapman-Enskog formulation, for there exist terms which account for these two differences. In principle the charge separation field can be calculated since a macroscopic force term is included in the Chapman-Enskog formulation. The much larger mass ratio in partially ionized gases is not really a fundamental difference, but it does mean a re-evaluation of certain computational simplifications which were carried over from the calculation of the thermal conductivity of neutral gas mixtures. For example, it has been customary to discard certain Sonine expansion terms in the translational thermal conductivity and the multicomponent diffusion coefficients, and to omit effects of thermal diffusion on the total thermal conductivity [10]. An examination of thermal diffusive effects does show that the effects are small for neutral gas mixtures, but it also shows that the effects become increasingly important as the

[2]The Boltzmann approach is presently the only one available for the calculation of transport coefficient of partially ionized gases, although many competing approaches are available for fully ionized gases.

[3]Figures in brackets indicate the literature references at the end of this paper.

ratio m_{heavy}/m_{light} increases. Consequently, the author [11 and 12] showed that it was necessary to include the discarded Sonine expansion terms and to include thermal diffusive effects. The results of these calculations will be described in the next section.

The calculation of the total thermal conductivity is based on the expression for the heat flux vector

$$\underline{q} = \sum_i n_i h_i \underline{V}_i - \lambda_t \frac{\partial T}{\partial \underline{r}} - nkT \sum_i \frac{1}{n_i m_i} D_i^T \underline{d}_i, \tag{1}$$

where D_i^T is the thermal diffusion coefficient, and h_i is the total enthalpy of a particle of species i. The quantity λ_t is the thermal conductivity of a spatially homogeneous gas mixture without concentration gradients. The diffusion velocity, $\underline{V}_i$, is defined as

$$\underline{V}_i = \frac{n^2}{n_i \rho} \sum_j m_j D_{ij} \underline{d}_j - \frac{1}{n_i m_i T} D_i^T \frac{\partial T}{\partial \underline{r}} \tag{2}$$

where D_{ij} is the multicomponent diffusion coefficient and the "forcing potential" for a partially ionized gas in the absence of pressure gradients is defined as

$$\underline{d}_i = \frac{\partial x_i}{\partial \underline{r}} - \frac{n_i m_i}{p\rho} \left(\frac{\rho}{m_i} \epsilon_i \underline{E}_i - \sum_j n_j \epsilon_j \underline{E}_j \right) \tag{3}$$

where ϵ_i is the charge, $Z_i e$, for a particle of species i, and $\underline{E}_s$ is the electric field generated by a difference in ion and electron concentrations. Equation (3) differs from the expression for $\underline{d}_i$ in [10] in that $Z_i e \underline{E}_s$ describes an internal macroscopic force whereas the corresponding quantity in [10] describes an external macroscopic force. However, the conceptual difference is only apparent as $\underline{E}_s$ always stems from an external energy source (e.g. heating coils). Assume that this energy is imposed on the system such that the average temperature is high enough to ionize the gas, but the temperature gradient is small enough to justify linearization procedures. The temperature gradient induces concentration gradients, $\partial x_i/\partial \underline{r}$, and a charge separation field, $\underline{E}_s$. If it is assumed that both $\partial x_i/\partial \underline{r}$ and $\underline{E}_s$ are proportional to the temperature gradient, it can be seen from eqs (2) and (3) that $\underline{V}_i$ and $\underline{d}_i$ are also proportional to the temperature gradient. The heat flux vector can then be expressed as

$$q = -(\lambda_r + \lambda_t + \lambda_d) \frac{\partial T}{\partial \underline{r}} = -\lambda_{total} \frac{\partial T}{\partial \underline{r}} \tag{4}$$

The reactive component of the thermal conductivity, λ_r, derives its name because of the addition of the reaction energy to the enthalpy of the individual species [13]. This mode of heat transfer can be described in terms of a diffusion cycle. In the higher temperature region the concentration of ions and electrons are larger than in the lower temperature region, forcing the charged particles to diffuse toward the lower temperature region. In this region, the ion recombines with an electron, thereby releasing the ionization energy (i.e. transport of energy). The cycle is completed when the atom is forced by the atomic concentration gradient to diffuse toward the higher temperature region where the ionization process occurs. The translation component, λ_t, is the conductivity of a spatially homogeneous gas mixture without concentration gradients, and is the only component explained by simple kinetic theory [10]. For obvious reasons, the third component of the thermal conductivity, λ_d, is called the thermal diffusive component. Unfortunately, no simple physical picture can describe this mode of heat transport.

The calculation of λ_t is straightforward and is described by Hirschfelder, Curtiss, and Bird [10]. Before numerical values for λ_r and λ_d can be calculated it is necessary to obtain values for the concentration gradient of each species and the charge separation field, all in terms of the temperature gradient. The simplest case which can be examined is that for a gas undergoing the reaction $A \rightarrow I + e$ (i.e. a ternary mixture of atoms, A, ions, I, and electrons, e). The solution of the problem can be expressed in terms of four dependent variables - the concentration gradients for the atom, ion, and electron, and the charge separation field, all expressed in terms of the temperature gradient. However, there are only three independent equations relating these four quantities. Two of these equations are statements of the flux conservation of elemental particles as formulated by Butler and Brokaw [13]. For the ternary mixture the elemental particles are defined as a singly charged ion and an electron. Then flux conservation requires that the diffusion velocities be related as follows[4]:

[4]More explicit forms of (5) and (6), where $\underline{V}_i$ is expressed in terms of $\underline{d}_i$, was used in the calculation of [14].

$$x_A \underline{V}_A + x_I \underline{V}_I = 0, \tag{5}$$

$$x_A \underline{V}_A + x_e \underline{V}_e = 0. \tag{6}$$

The third equation can be derived from the expression for the equilibrium constant,

$$K_p = \prod_{i=1}^{3} (x_i p)^{a_i}, \tag{7}$$

where the a_i's are the stoichiometric coefficients for the reaction ($a_A = -1$, $a_I = 1$, $a_e = 1$). Combination of the gradient of eq (7) with explicit expressions for the charge separation force results in

$$\frac{d \ln K_p}{dT} \cdot \frac{\partial T}{\partial \underline{r}} = -\frac{1}{x_A} \underline{d}_A + \frac{1}{x_I} \underline{d}_I + \frac{1}{x_e} \underline{d}_e. \tag{8}$$

The author [12] discussed the difficulties in solving eqs (5), (6), and (8) for $\partial x_i/\partial \underline{r}$ and $\underline{E}_s$, but could not offer a solution. Subsequently, Meador and Staton [15] circumvented the problem of too many variables by assuming that the concentration gradient of the ion was equal to that for the electron. They justified this assumption by combining concepts from electrostatics and plasma physics with expressions from non-equilibrium thermodynamics, then using order of approximation arguments. The accuracy of this approach will be discussed later. Meador and Staton used the equality of $\partial x_I/\partial \underline{r}$ and $\partial x_e/\partial \underline{r}$ in eqs (5), (6), and (8) to solve for $\partial x_A/\partial \underline{r}$ and $\underline{E}_s$. Their expression for the reactive component of the thermal conductivity is

$$\lambda_r = \frac{n n_e n_A k T^2 D_{AI}}{(n_e + n_A)^2} \left(\frac{\partial \ln K_p}{\partial T} \right)^2 \tag{9}$$

which is identical to the Butler and Brokaw expression for dissociating gases [13] if it is assumed that the multicomponent diffusion coefficient D_{AI} can be approximated by the binary diffusion coefficient $\mathcal{D}_{AI}$. This equation has several implications: (1) The reactive component is completely dominated by the binary diffusion between the ion and atom, (2) The reactive component is independent of the motion of the electron, and (3) The reactive component is not affected by thermal diffusive effects.

In a subsequent paper [14] the author also derived an expression for the total thermal conductivity. In contrast to the Meador and Staton work, it was not necessary in [14] to rely on any subsidiary assumptions, and the derivation was exact within the framework of the Chapman-Enskog formulation. The crux of this approach is not to separate the forcing potential, $\underline{d}_i$, of eq (3) into $\partial x_i/\partial \underline{r}$ and $\underline{E}_s$ components, but to solve for $\underline{d}_i$ directly by making use of the conservation of the net flux for each elemental particle. Physically, this means that regardless of the value of the charge separation field, the concentration gradients will readjust themselves so that the net flux is conserved (eqs (5) and (6)). Therefore, the combined effects of $\partial x_i/\partial \underline{r}$ and $\underline{E}_s$ in the form of $\underline{d}_i$ is a more logical dependent variable than its components. The solution for the various $\underline{d}_i$'s is then obtained from eqs (5), (6), and (8). The determinantal expression for the various $\underline{d}_i$'s is

$$d_i = \frac{\partial T}{\partial \underline{r}} \frac{\begin{vmatrix} a_{11} & a_{12} & a_{13} & -c_1 \\ a_{21} & a_{22} & a_{23} & -c_2 \\ a_{31} & a_{32} & a_{33} & -c_3 \\ \delta_{i1} & \delta_{i2} & \delta_{i3} & 0 \end{vmatrix}}{\begin{vmatrix} a_{11} & a_{12} & a_{13} \\ a_{21} & a_{22} & a_{23} \\ a_{31} & a_{32} & a_{33} \end{vmatrix}} \equiv \delta_i \frac{\partial T}{\partial \underline{r}} \tag{10}$$

where

$$
\begin{aligned}
a_{11} &= (n^2/\rho)m_A D_{IA}, & a_{23} &= (n^2/\rho)m_e D_{Ae},\\
a_{12} &= (n^2/\rho)m_I D_{AI}, & c_2 &= (D_A^T/m_A T) + (D_e^T/m_e T),\\
a_{13} &= (n^2/\rho)m_e D_{Ae} + (n^2/\rho)m_e D_{Ie}, & a_{31} &= -x_A^{-1},\\
c_1 &= (D_A^T/m_A T) + (D_I^T/m_I T), & a_{32} &= x_I^{-1},\\
a_{21} &= (n^2/\rho)m_A D_{eA}, & a_{33} &= x_e^{-1},\\
a_{22} &= (n^2/\rho)m_I D_{AI} + (n^2/\rho)m_I D_{eI}, & c_3 &= d \ln K_p/dT.
\end{aligned}
\tag{11}
$$

A combination of eqs (1), (2), (10), and (11) gives the final expression for the total thermal conductivity:

$$
\lambda_{total} = \lambda_t + \left[-h_I \frac{n^2}{\rho}(m_A D_{IA}\delta_A + m_e D_{Ie}\delta_e) - h_A \frac{n^2}{\rho}(m_I D_{AI}\delta_I + m_e D_{Ae}\delta_e) - h_e \frac{n^2}{\rho}(m_A D_{eA}\delta_A + m_I D_{eI}\delta_I) + \frac{h_A D_A^T}{m_A T} + \frac{h_I D_I^T}{m_I T} + \frac{h_e D_e^T}{m_e T} \right] + \left[nkT\left(\frac{D_A^T \delta_A}{n_A m_A} + \frac{D_I^T \delta_I}{n_I m_I} + \frac{D_e^T \delta_e}{n_e m_e} \right) \right] \tag{12}
$$

where λ_t is the translational thermal conductivity, the sum of all terms containing the various h_i's is the reactive thermal conductivity, and the sum of the remaining terms is the thermal conductivity due to thermal diffusion. Note that the reactive component has two modes. The first is by multicomponent diffusion and the second by thermal diffusion. For a fully ionized gas[5] (i.e. no neutral particles) eq (12) reduces to

$$
\lambda_{total} = \lambda_t - \frac{k}{n D_{eI}} \left(\frac{D_e^T}{\mu} \right)^2 \tag{13}
$$

where μ is the reduced mass of the electron-ion system.

Since the terms in eq (12) are so complex it would be impossible to single out by inspection any one mechanism (e.g. thermal diffusion) as being the chief contributor to λ_r or λ_d. This can be done only by an inspection of the numerical values which are described in the next section. However, it can be seen from eq (12) that there is a definite need for accurate values of the multicomponent and thermal diffusion coefficients since λ_r and λ_d are determined by D_{ij} and D_i^T, and since δ_i (the combined effect of the concentration gradients and the charge separation field) are also determined by D_{ij} and D_i^T (eqs (10) and (11)).

3. Numerical Values of Higher Order Transport Coefficients

The importance of higher order Sonine expansion terms in the expressions for λ_t, D_{ij}, and D_i^T will be described first. The expressions for λ_t, D_{ij}, and D_i^T [10] are the ratio of two determinants. If the first and second Sonine expansion terms are used (second approximation) then both determinants contain four subdeterminants which are designated as the 00, 01, 10, and 11 subdeterminants, where the 0 corresponds to the first Sonine polynomial and the 1 corresponds to the second Sonine polynomial. In the calculation of the thermal conductivity of neutral gases the 00, 01, and 10 subdeterminants are normally discarded (first approximation) with very little loss in accuracy [10]. Unfortunately, this simplification was carried over into the calculation of the thermal conductivity of partially ionized gases. The result of this approximation is shown in figure 3 for partially ionized argon. The second approximation of λ_t [12] is larger than the first approximation by 30 percent at 50-percent ionization and larger by 50 percent at complete ionization. An inspection of the numerical values of the elements in the λ_t subdeterminants [12] show that the increase in λ_t in going from the first to the second approximation can be attributed to the inclusion of additional terms in the 00 subdeterminant arising from interactions between unlike particles (A-I, e-A, and e-I). Subsequent analyses by DeVoto [16 and 17] showed that third order Sonine expansion terms for the translational thermal conductivity were also appreciable. Figure 3 shows that the difference between the third and second approximations for λ_t is roughly the same as the difference between the second and first approximations. DeVoto's calculations, however, show very little difference between the third and fourth approximations. Landshoff's [18] calculations for an electron gas show roughly the same trends in going from the second to the fourth approximation.

[5] The author [12] erroneously identified λ_t with Spitzer's [2] field free thermal conductivity. The error was resolved by the analysis of Meador and Staton.

Multicomponent diffusion coefficients are usually approximated by retaining only the first Sonine expansion terms (i.e. using only the 00 subdeterminant). These first-order coefficients are compared with the second-order coefficients (i.e. both first and second Sonine expansion terms) in figure 4. The second-order coefficients $D_{e\text{-}A}(2)$ and $D_{e\text{-}I}(2)$ are larger than the corresponding first-order coefficients by 25 percent at 50-percent ionization and by 45 percent at complete ionization. An inspection of the numerical values of the elements in the D_{ij} subdeterminants show that the increase in D_{ij} in going from the first to the second approximation can be attributed to the inclusion of terms in the 11 subdeterminant arising from interactions between like particles (A-A, I-I, and e-e). The electron-electron interaction is especially important since a simple hard sphere model shows that D_{ij} is inversely proportional to the product of the collision cross section and the reduced mass. In contrast, the first- and second-order coefficients for diffusion between heavy particles (e.g. $D_{A\text{-}I}$) differ by only a few percent. DeVoto's calculations show that there is little difference between second- and third-order multicomponent and thermal diffusion coefficients.

It is essential that second-order thermal diffusion coefficients be used since these coefficients are identically zero in the first approximation. Typical values of the second-order thermal diffusion coefficients for the argon atom, ion, and electron from [11] are shown in figure 5. In the expression for the total thermal conductivity (eq (12)), D_i^T always occur in combination with the particle mass in the denominator. Although the electron thermal diffusion coefficient, D_e^T, is at most two orders of magnitude smaller than those for the atom and ion, the electron mass is four orders smaller. Consequently, thermal diffusive effects can be attributed almost entirely to the electron term. Another interesting conclusion can be reached by an inspection of figure 5. It can be seen that the atom and ion thermal diffusion coefficients are within 1 percent of each other in magnitude from a few percent ionization up to extremely high degrees of ionization (approximately 95 percent). Beyond this point D_i^T decreases in value, changes sign, then approaches the value of D_e^T near 100-percent ionization. These variations imply that the diffusive motion of both the atom and ion are essentially independent of that for the electron, up to large degrees of ionization. The diffusive motion of the electrons, in turn, is dictated by the ion rather than the atom because of the greater magnitude of the Coulombic forces[6]. These same conclusions were reached from an examination of the second-order multicomponent diffusion coefficients.

The previous discussion of second-order values of D_{ij} and D_i^T leads towards the calculation of λ_r and λ_d from eqs (10), (11), and (12). The author recently made a series of calculations for hydrogen, nitrogen, and argon for a pressure of one atmosphere and temperatures corresponding to 50-percent ionization. The values of λ_r were compared with those based on the expressions derived by Meador and Staton [15]. The values of λ_r from the two sets of calculations agreed within a few percent. However, this is not necessarily a verification of the Meador and Staton approach, as calculations have shown that any non-trivial assumed values of $\partial x_I/\partial \underline{r}$ and $\partial x_e/\partial \underline{r}$ will result in the same values of λ_r and λ_d. The agreement can be explained as follows. The values of λ_r and λ_d are determined not by the separate effects of the concentration gradients and the charge separation field, but by their combined effects. Consequently, if erroneous values of the concentration gradients were initially assumed the constraints of the problem (eqs (5), (6), and (8)) would compensate for this error in the resulting value of the charge separation field.

A more critical comparison could come from the determination of the predominant mechanism for the reactive component of the thermal conductivity. The reactive component from eq (12) can be resolved into two components: (1) the sum of the $h_i n^2 m_j D_{ij} \delta_j/\rho$ terms which shall be called the D_{ij} component for identification, and (2) the sum of the $h_i D_i^T/m_i T$ terms which shall be called the D_i^T component. The results are summarized in the following table.

Table I. Thermal Conductivity Components for Partially Ionized Gases (p = 1 atm, 50% ionization)

Gas	$\lambda_t(2)$	$\lambda_r(2)$ W m^{-1} deg^{-1}		$\lambda_d(2)$
	W m^{-1} deg^{-1}	D_{ij} component	D_i^T component	W m^{-1} deg^{-1}
Hydrogen	1.30	5.77	1.78	-0.20
Nitrogen	1.34	0.87	1.30	-0.25
Argon	1.31	-0.17	1.32	-0.29

[6]As a result, the values of D_e^T calculated for partially ionized argon can be used for other partially ionized gases to a good degree of accuracy.

For hydrogen the largest contribution comes from the D_{ij} component, and the predominant term in this component is the $h_I n m_A D_{IA} \delta_A / \rho$ term as predicted by Meador and Staton. However, the thermal diffusive contribution is not negligible, but comprises 25 percent of the value of λ_r. As the mass of the heavy particle increases, thermal diffusive effects become relatively more important. For example, in nitrogen the D_i^T component of λ_r is larger than the D_{ij} component. In argon the D_{ij} component is almost zero due to the cancellation of the ion term by the atom and electron term. Consequently, the reactive thermal conductivity for argon can be attributed almost entirely to the D_i^T component, and the predominant term in this component is the $h_e D_e^T / m_e T$ term. This result is in direct contradiction to those predicted by Meador and Staton and indicates that one or more of their initial assumptions may be erroneous.

This paper has described the analytical work done in the past few years to clear up some of the uncertainties in the expression for the total thermal conductivity of a partially ionized gas. The author feels that the theoretical basis for this expression is currently on substantial ground. However, there are several deficiencies which must be resolved before accurate values can be calculated. The first of these is the lack of measured or calculated cross sections for collisions between an atom which is chemically unstable at low temperatures (e.g. nitrogen or oxygen) and an electron, ion, or another chemically unstable atom. A second deficiency is the absence of terms in the expressions for the transport coefficients which account for inelastic collisions, and the lack of measured or calculated cross sections for these inelastic collisions. A third deficiency is the absence of any experimental verification of the total thermal conductivity, especially in the region of 50-percent ionization where λ_{total} peaks because of the reactive component. A method which shows some promise is the ultrasonic absorption technique as used by Carnevale et al. [19]. Consequently, large amounts of analytical and experimental effort must still be expended to remedy these deficiencies before accurate values of the total thermal conductivity of a partially ionized gas can be obtained.

4. References

[1] Cohen, Robert S., Spitzer, Lyman, Jr., and Routly, Paul Mc R.: The Electrical Conductivity of an Ionized Gas. Phys. Rev., vol. 80, no. 2, Oct. 15, 1950, pp. 230-238.

[2] Spitzer, Lyman, Jr., and Härm, Richard: Transport Phenomena in a Completely Ionized Gas. Phys. Rev., vol. 89, no. 5, March 1953, pp. 977-981.

[3] Burgers, Johannes, ed.: Statistical Plasma Mechanics. Symposium of Plasma Dynamics, Addison-Wesley Publishing Co., Reading, Mass., 1960, pp. 164-169.

[4] Grad, H.: Modern Kinetic Theory of Plasmas. Proc. Fifth Int. Conf. on Ionization Phenomena in Gases, Vol. II, North-Holland Publ. Co., Amsterdam, 1962, pp. 1630-1649.

[5] Koga, Toyoki: The Generalized Validity of the Boltzmann Equation for Ionized Gases. Proc. Third Int. Symposium on Rarified Gas Dynamics, Vol. I, Academic Press, N. Y., 1963, pp. 75-93.

[6] Wu, Ta-You: Kinetic Equations of Gases and Plasmas. Addison-Wesley Publishing Co., Reading, Mass., 1966.

[7] Sundaresan, M. K., and Wu, Ta-You: Thermal Conductivity of a Fully Ionized Gas. Can. J. Phys., vol. 42, no. 4, April 1964, pp. 794-813.

[8] Emmons, Howard W.: Arc Measurements of High-Temperature Gas Transport Properties. Phys. Fluids, vol. 10, no. 6, June 1967, pp. 1125-1136.

[9] Morris, James: Private Communication

[10] Hirschfelder, Joseph O., Curtiss, Charles F., and Bird, R. Byron: Molecular Theory of Gases and Liquids. John Wiley and Sons, Inc., N. Y., 1954.

[11] Ahtye, Warren F.: A Critical Evaluation of Methods of Calculating Transport Coefficients of a Partially Ionized Gas. Proceedings of the 1964 Heat Transfer and Fluid Mechanics Institute, Stanford Univ. Press, 1964.

[12] Ahtye, Warren F.: A Critical Evaluation of Methods for Calculating Transport Coefficients of Partially and Fully Ionized Gases. NASA TN D-2611, 1965.

[13] Butler, James N., and Brokaw, Richard S.: Thermal Conductivity of Gas Mixtures in Chemical Equilibrium. J. Chem. Phys., vol. 26, no. 6, June 1957, pp. 1636-1643.

[14] Ahtye, Warren F.: Total Thermal Conductivity of Partially and Fully Ionized Gases. Phys. Fluids, vol. 8, no. 10, Oct. 1965, pp. 1918-1919 (Erratum, vol. 9, no. 1, Jan. 1966, pp. 224).

[15] Meador, W. E., Jr., and Staton, L. D.: Electrical and Thermal Properties of Plasmas. Phys. Fluids, vol. 8, no. 9, Sept. 1965, pp. 1694-1703.

[16] DeVoto, R. S.: Transport Properties of Partially Ionized Monatomic Gases. Dept. of Aeronautics and Astronautics, Stanford University Rep. SUDAER No. 207, 1964.

[17] DeVoto, R. S.: Argon Plasma Transport Properties. Dept. of Aeronautics and Astronautics, Stanford University Rep. SUDAER No. 217, 1965.

[18] Landshoff, Rolf: Convergence of the Chapman-Enskog Method for a Completely Ionized Gas. Phys. Rev., vol. 82, no. 3, May 1, 1951, p. 442.

[19] Carnevale, E. H., Lynnworth, L. C., and Larson, G. S.: Ultrasonic Determination of Transport Properties of Monatomic Gases at High Temperatures. J. Chem. Phys., vol. 46, no. 8, April 1967, pp. 3040-3047.

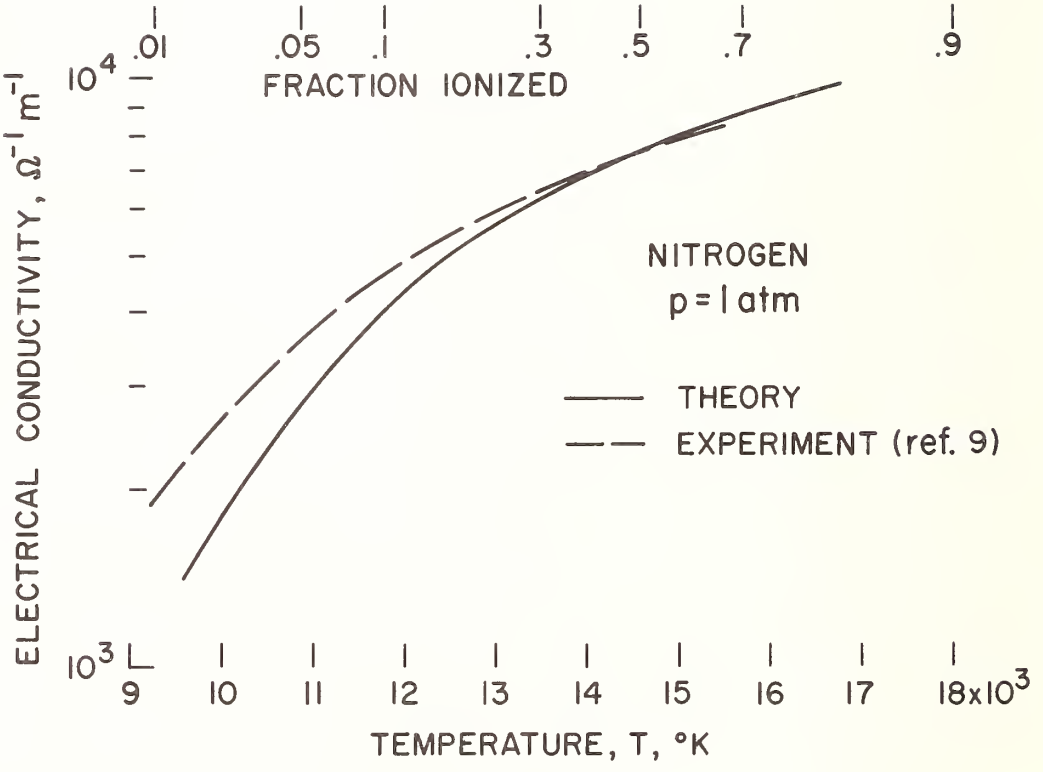

Figure 1.- Comparison of experimental and theoretical electrical conductivity of nitrogen.

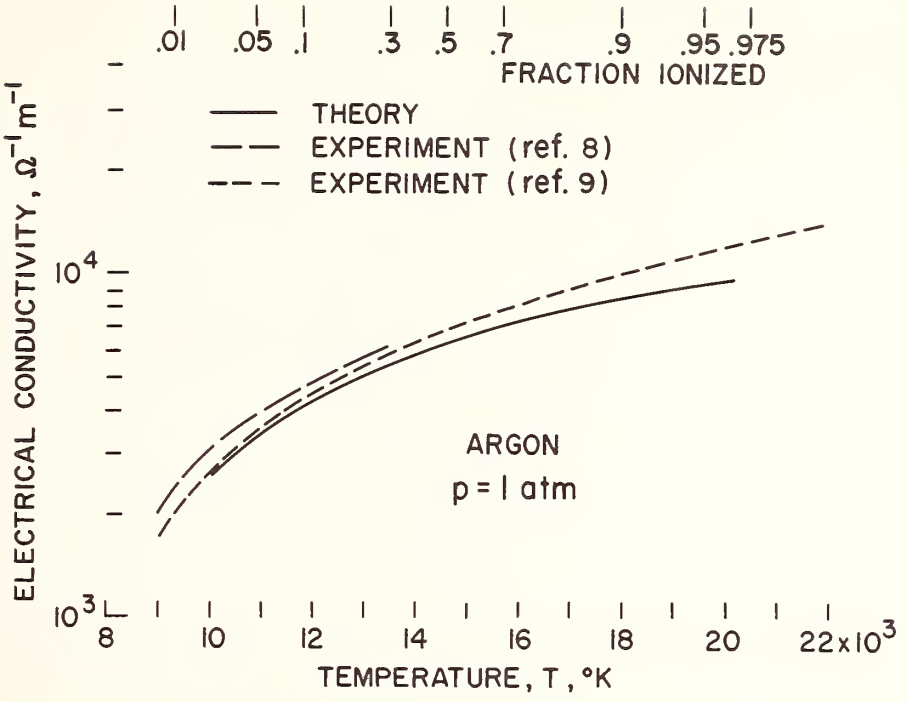

Figure 2.- Comparison of experimental and theoretical electrical conductivity of argon.

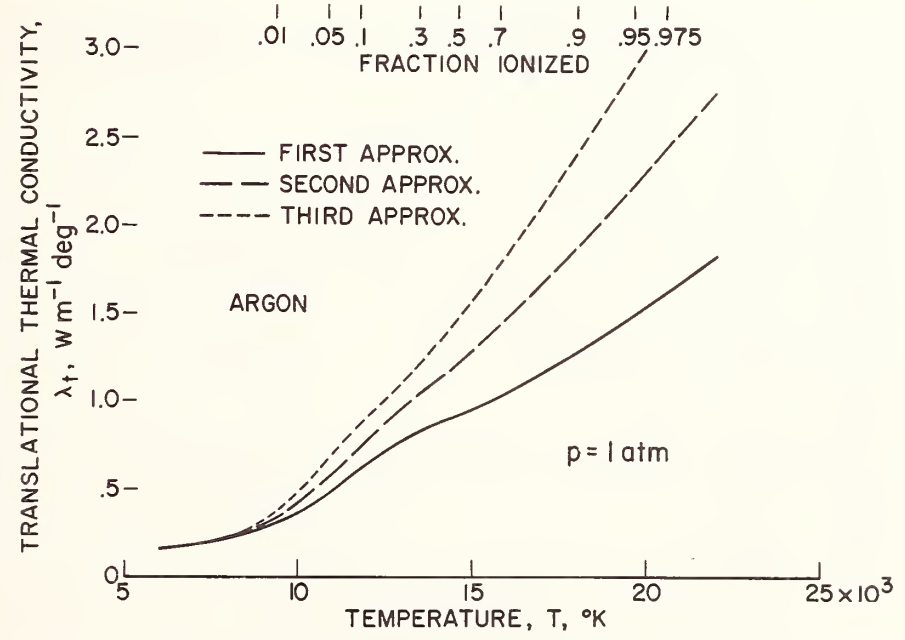

Figure 3.- Comparison of various approximations for calculating the translational thermal conductivity of argon.

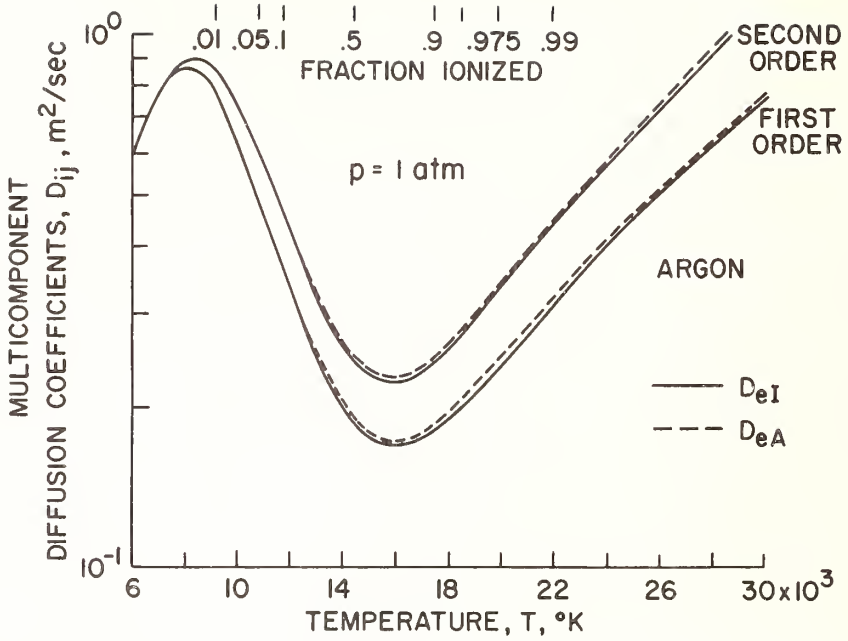

Figure 4.- Comparison of various approximations for calculating multicomponent diffusion coefficients of argon.

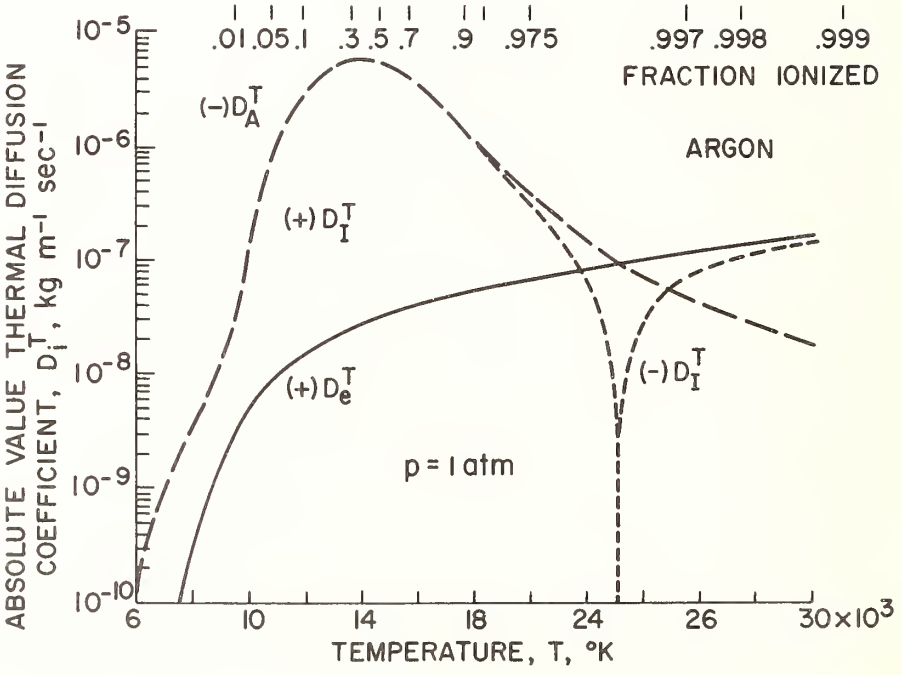

Figure 5.- Thermal diffusion coefficients of argon.

Thermal Conductivity of the Alkali Metal Vapors and Argon

Chai-sung Lee and Charles F. Bonilla

Liquid Metals Research Laboratory,
Department of Chemical Engineering
Columbia University, New York, N.Y. 10027

The frequency response to alternating current of a fine wire surrounded by alkali metal vapor was studied theoretically and experimentally for determining the thermal conductivity of the vapor. Data were obtained for cesium and rubidium vapors at pressures from 0.0829 to 0.214 atm. A new method was employed of correcting for temperature jump and vapor volumetric heat capacity.

In addition, the thermal conductivity of the alkali metal vapors was calculated by gas kinetics theory, including the effects of dimerization and heat of association. Good agreement between experiment and theory was obtained considering the possible errors. The total probable experimental error is estimated at 6.1%, and the uncertainty in the theoretical analysis at about 25%. Reliability of the method is indicated by agreement with literature values for argon up to 1085°C. The standard error of the argon correlation is estimated at 1.6%.

Key Words: Conductivity, heat conductivity, thermal conductivity, argon, lithium vapor, sodium vapor, potassium vapor, rubidium vapor, cesium vapor, hot wire cell.

1. Introduction

Measurement of the thermal conductivity of alkali metal vapors is difficult because of the high temperatures required, involving radiation between the surfaces, and because of the chemical activity of the alkali metals on containers, gases, and other materials which they may contact.

Thus, only preliminary or approximate results are to be found in the literature. Gottlieb and Zollweg (1)[1] measured heat dissipation from tungsten ribbon at a single temperature in cesium, rubidium and potassium vapors at low pressures. On extrapolating to infinite pressure for each vapor they obtained an approximate value of the monomer conductivity. Stefanov et al (2) employed a concentric tube geometry with sodium and potassium vapors, obtaining the temperature difference by differential thermal expansion of the tubes, as originally proposed by Timrot et al (3). Radiation has a large effect in this geometry, and reached 85% of the heat transmitted. Achener (4) is employing laminar flow in a long hot isothermal tube and measuring the average temperature rise. Theoretically the Nusselt number approaches 3.658. The above results all seem somewhat low, or else inconsistent.

In view of considerable interest in the thermal conductivity of the alkali metal vapors, particularly for kinetic theory studies, correlating heat transfer data, and calculating results of hypothetical fast reactor transients, a previously developed transient hot-wire method for measuring the thermal conductivity of gases at high temperatures was adapted to these vapors.

2. Mathematical Model for the Transient Hot-Wire Method

As in previous studies in this laboratory (5,6,7) a concentric wire in a cylindrical shell is employed, the annulus between being filled with the test gas or

[1] Figures in parentheses indicate the literature references at the end of this paper.

vapor. The radius of the wire is r_1 and of the shell r_2, and the wire must have a substantial temperature coefficient of resistance. Pure sinusoidal current of a single frequency $i = \sqrt{2}\, I \sin \omega\theta$ is passed through the wire and the IR drop across it is measured.[2]

The equation governing conduction in the annulus is:

$$\frac{k}{c\rho}\left(\frac{\partial^2 t}{\partial r^2} + \frac{1}{r}\frac{\partial t}{\partial r}\right) = \frac{\partial t}{\partial \theta} \qquad \text{for } r_1 < r < r_2 \tag{1}$$

The outer boundary condition is simply:

$$t = t_2 \text{ at } r = r_2 \tag{2}$$

since the large mass of the shell keeps it isothermal and the low heat velocity makes temperature jump there negligible.

The inner boundary condition is here written as the heat balance:

$$(\sqrt{2}\, I \sin\omega\theta)^2 \bar{R} = \pi r_1^2 c'\rho' L \frac{\partial t}{\partial \theta} - 2\pi r_1 L k \frac{\partial t}{\partial r} + 2\pi r_1 L h (t - t_2) \quad \text{at } r = r_1 \tag{3}$$

The wire is so fine that its average temperature can be taken as t_1, and the temperature variation is small so that the radiant heat transfer coefficient h and the electrical resistance $\bar{R}$ are assumed constant for this purpose.

In the previous studies on permanent gases (7) it was possible to adjust the pressure to high values, maintaining the mean free path and the temperature jump small as well as substantially constant. Accordingly, the thermal conductivity in eq (3) was that of the gas, as in eq (1).

In this work with alkali metals the pressure must be below saturation, and thus is relatively low, and temperature jump is appreciable at the inner wall. An exact statement of this boundary condition can be written that includes the temperature jump as an equivalent series heat transfer coefficient, however it is considerably more complicated and cannot be solved analytically. Therefore a means of correcting the boundary condition for temperature jump in a simpler way was sought. This was accomplished by substituting k^0 for k in the heat balance, where k^0 is sufficiently reduced that the correct heat conduction term is calculated when t_1 is the wire temperature rather than the vapor temperature. The expression for k^0 is obtained from temperature jump theory (8) as:

$$\frac{k^0}{k} = 1 + \frac{1}{r_1 \ln(r_2/r_1)} \frac{2-a}{a} \frac{k}{c_v} \frac{\sqrt{2\pi R T}}{(\gamma+1)} \frac{1}{p} \qquad \text{for } r_1 \ll r_2 \tag{4}$$

The solution of these equations can thus be given in the same form as previously (6,7), but indicating with the superscript the dimensionless ratios in which k^0 appears. The solution is:

$$t_1 = t_2 + \frac{I^2 \bar{R} \ln(DR)}{2\pi k^0 L [RR^0 \ln(DR) + 1]} + \frac{I^2 \bar{R}(AR^0)}{\omega c' \pi r_1^2 \rho' L} \cos(2\omega\theta + \phi^0) \tag{5}$$

Capital initials have been used for readier recognition of the dimensionless ratios. These ratios, and others shortly to be used, are defined as follows:

[2] See section 8. for nomenclature.

AR°	Amplitude Ratio (where g_D° and b_D° are, like AR° itself, complex functions of CR, CDR, DR, RR (or QR), and TJF)	$(CR^\circ/4)\sqrt{g_D^\circ + b_D^\circ}$
CDR	Capacity Density Ratio	$c'\rho'/c\rho$
CR°	Conductivity Ratio	$2\omega c'\rho' r_1^2/k^\circ$
DR	Dimension Ratio	r_2/r_1
RR°	Radiation Ratio	hr_1/k°
QR	Fraction Radiative Heat	q_{rad}/q_{tot}
TJF	Temp. Jump Factor	$\frac{k(2-a)\sqrt{2\pi RT}}{a\, c_v(\gamma+1) r_1 \ln(DR)} \frac{1}{p}$
TJC	Temp. Jump Correction Term	$(AR^\circ - AR)/AR$
RR	Radiation Ratio for TJF=0	$QR/((1-QR)\ln(DR))$

Derivation of the equations for AR° and of ϕ° for the case of zero temperature jump (AR and ϕ) has already been carried out analytically (5), and values have been calculated for various ranges of the other dimensionless ratios (6,7). In this study it was necessary to carry the calculations to still higher values of CDR and lower values of CR, due to the lower values of thermal conductivity and density encountered with the alkali metals. Figure 1 shows the results for the case of zero radiation correction (RR = 0) and for the dimension ratio DR = 1000, a satisfactory value for all of the work here described. The turn-up of the curves for high CDR below CR = 0.1 had not been expected.

Figure 2 gives the temperature jump correction, TJC, with which AR° can be calculated from AR, and vice versa. In the actual interpretation of experimental runs the computer program (9) calculates the value of TJC for each specific run.

The temperature difference $t_1 - t_2$ in eq (5) is obtained from an experiment by observing the departure of the IR drop across the fine wire from the pure sine wave that it would be if R were constant. The IR drop across the fine wire can be shown (9) to be:

$$E = \sqrt{2} I \sin\omega\theta \left[R_2 + \frac{\overline{dR}}{dt}(t_1 - t_2)\right] = \sqrt{2} E_1 \sin\omega\theta - \sqrt{2} E_3 \sin(\omega\theta + \phi) + \sqrt{2} E_3 \sin(3\omega\theta + \phi) \tag{6}$$

where:

$$E_1 = IR_2 + \frac{I^3 \bar{R} \ln(DR) \frac{\overline{dR}}{dt}}{2\pi k^\circ L [RR^\circ \ln(DR) +]} \tag{7}$$

$$E_3 = \frac{I^3 \bar{R} (AR^\circ) \frac{\overline{dR}}{dt}}{2\omega c' m L} \tag{8}$$

E_3, and thence AR°, can be obtained in an experiment, in principle (7) from the phase lag of the third harmonic behind the fundamental (the "phase angle method"), However, the direct measurement of the amplitude of E_3 (the "amplitude method") is more accurate and convenient, and is the method exclusively employed so far.

The value of E_3 can be determined by placing the thermal conductivity cell as one leg of a Wien bridge, as shown in Figure 3. Balancing the bridge with respect to the fundamental frequency f cancels out the first two terms of eq (6), allowing the third harmonic voltage to show up at the bridge output terminals. E_3 is then obtained (7) as follows:

$$E_3 = E_{3R}\left[1 + R_c\left(\frac{1}{R_d} + \frac{1}{R_M}\right)\right] \tag{9}$$

where the wire resistance $R_c = (R_d/R_a)R_b$. The decade capacitors are used to balance out the equivalent reactive impedance of the wire and yield a sharper null point. They would also be read if the phase-shift method were being employed. Operation of the system will be described under Experimental Procedure.

An "absolute" determination of thermal conductivity by the above procedures is impractical for many reasons, and in particular because of the difficulty in obtaining an accurate value of r_1, the wire radius. If a quantity designated by GP is defined by:

$$GP = CR \times k \times 10^5, \tag{10}$$

and experimental curves of AR vs. GP are drawn for two different gases, the ratio of the two GP's corresponding to any single value of AR is the same as the ratio of the thermal conductivities of the two gases. If one gas is a reference gas of known thermal conductivity the thermal conductivity of the test gas can be readily obtained. This is the method employed in this study.

3. Cell Design and Operation

Two types of cell were tested, employing different seals for the insulated lead. Cell No. 1 (fig. 4) consists of a boiler, measurement cell, and seal complex, all machined from SS-310, and connection lines. The seal in contact with the vapor space consisted of frozen alkali metal inside and outside of a fused alumina (Lucalox tube) 1/16 inch OD x 1/64 inch ID. Commercial sintered alumina, though designated impermeable, was found to short-circuit by permeation when used below the freeze-seal. In operation, the cell was thoroughly evacuated cold and then the freeze-seal water and the cell heater both turned on. In due course the freeze-seal was established and the evacuation stopped. This cell yielded the rubidium data.

Cell No. 2 (fig. 5) employed a dry seal consisting of a washer and a disk of Nb-1% Zr sheet brazed to the opposite ends of a Lucalox sleeve, as developed for sodium vapor lamps. This seal was tight, but was more fragile and was limited to some 800°C. The cesium data were obtained with this cell.

To resist corrosion by the alkali metals tungsten wires were employed, rather than platinum, the other metal so far studied. The finest wires available (0.00012 inch in diameter) were used, since they permit higher frequencies to be utilized. With the wire diameter fixed, the temperature jump and radiation corrections can be substantially reduced by employing higher frequencies, and thereby working in a higher range of CR as shown in figure 2. This, however, is in contradiction with the fact that AR vs. CR curves are linear only in the low range of CR (fig. 1). The necessary frequency to obtain a convenient compromised value of CR is given in Table 1, from preliminary estimates.

Table 1. Frequency for a Conductivity Ratio of 0.1

Gas or Vapor	k/k_{Cs} at 750° C	Frequency of Current at Diameter of Tungsten Wire, In. (0.0003)	(0.00012)
He	64.2	57	348
N_2	11.0	10	61
A^2	4.68	7.4	45
Cs	1.00	1	6.1
Rb	1.46	1.5	9.2
K	2.48	2.5	15.3
Na	4.88	4.6	28.1
Li	13.7	13.4	81.8

Although the mathematical model assumes concentricity, this is not important because of the relative method employed and the high ratio DR. Furthermore, no amount of tension could be applied to these fine wires. Accordingly, joints to the nickel leads were made by gently squeezing the lead around the loose tungsten wire with adjustable vice-pliers.

In view of the fine size of the tungsten wire, and its oxidizability, it was necessary to eliminate all possible oxygen from the system. This was done by adding several grams of Ti-Zr chips ("Getterloy") to the cell before charging it with alkali metal, and initially heating the cell slowly under argon pressure to prevent the

vapor from rising. When this is done carefully with fresh metal, each new 0.00012 inch wire will last for a number of runs up to 1000°C or higher.

The cells were mounted in two independent vertical furnaces. The lower one set the liquid alkali metal temperature, and therefore the pressure of the vapor, and the upper one set the vapor temperature or superheat.

4. Experimental Procedure

In general, the sequence of tests in a complete run included:

(a) Insertion of the wire and sealing of the cell.

(b) Charging the cell with alkali metal.

(c) Measuring the electrical resistance of the wire at room temperature with a low current in the Wien bridge at a selected frequency in argon to prevent in-leakage and calculating the length of the wire from the known resistance per unit length.

(d) Measuring the resistance of the wire up to high cell temperatures in argon to determine dR/dt as a function of temperature.

(e) Cool the cell to room temperature and adjust the argon pressure to atmospheric, then carrying out a calibration run with argon over a range of about 5 to 100 cycles per second (CR about 0.05 to 1.0 and CDR about 3,000).

(f) Recheck the room temperature resistance of the wire (if drift occurs it may not invalidate previous data).

(g) Set the hot-wire current up to the operating range and read off the resistance again from the bridge.

(h) Read the effective voltage across the hot wire with the thermocouple voltmeter.

(i) Set the band-pass filter at 3 times the impressed frequency.

(j) Pass the bridge output through the decade amplifier and the filter, and measure it, E_{3R}, on the VTVM.

(k) Turn the switch from test (1) to calibration (2) position and set the oscillator to 3 times fundamental frequency.

(l) Apply about 1 volt, measured by the thermocouple voltmeter, to the calibration circuit.

(m) Adjust the voltage divider until the same output E_{3R} is read on the VTVM. This yields the absolute value of E_{3R}.

(n) From E_{3R} we calculate E_3 by eq (9) and then AR^o by eq (8).

(o) Employing the computer program for TJC, this quantity is computed by iteration, as well as thermal conductivity k, and radiation correction (with a=0.9(13)).

(p) Corrections for a small drift of CDR from 3,000, a value chosen as the reference, and end conduction are also calculated using the formulas developed in the previous work (7).

(q) The corrected amplitude ratio, AR, is now obtained by applying the above correction terms to AR^o. This yields one point of the corrected AR vs. the corresponding GP, as obtained with argon but valid for any gas or vapor.

(r) Repeat the above steps from (f) on at a number of other frequencies to obtain a calibration curve for AR vs. GP.

The alkali metal part of a run takes the following steps using the same wire:

(s) Evacuate the apparatus at least to 3×10^{-5} mm Hg.

(t) Gradually heat the boiler and cell, and attain steady temperatures while keeping the cell temperature at least about 100°C higher than the boiler temperature. The vacuum line is disconnected at the moment when the boiler reaches about 150°C.

(u) Repeat steps from (f) through (r) for five different frequencies, 5 to 50 cps., to obtain the AR vs. GP curve for the alkali vapor. The correction for the large difference between volumetric heat capacity ratio CDR and the reference value is made this time by means of an experimentally determined set of data by a computer program (9). These are low pressure data where CDR is large.

(v) Finally, take the ratio of AR on the above curve to that of the calibration curve at GP = 0.1, and multiply the ratio by the thermal conductivity of argon at the temperature of calibration to obtain the desired thermal conductivity of the alkali vapor.

Since the above ratios were found to be significantly dependent on the value of GP in its high range, the ratio was taken in the low range of GP where it is no longer sensitive to the values of GP. An example of the value of GP in such a range is 0.1.

5. Experimental Results

Experimental results for argon are shown in figure 6. These points were the last and most reliable made, and were all obtained on one wire (No. 12). The pressure was varied from 1 to 10 atmospheres to keep CDR constant, as these pressures have shown no effect on the thermal conductivity of argon. The solid lines represent the first series of consecutive runs., After a recalibration run the dashed lines were obtained. The small change noted between the two calibration runs shows that the properties and dimensions of the wire changed very little during each set. The spacing of the curves at GP = 0.1 yields the following thermal conductivity relative to that at the calibration temperature of 32.6°C.

Table 2. Thermal Conductivity of Argon Relative to 32.6°C.

t, °C	86	160	216	346	459	569	707	855	987	1085
$k_t/k_{32.6}$	1.132	1.351	1.470	1.706	1.889	2.062	2.350	2.558	2.786	2.859

These values agree very closely (9) with those of Nuttall (10) with Liley's correlation (11) and with Peterson's earlier points by this method (7) and are within 2% of Vargaftik and Zimina (12). Applying a cubic equation in t to the above points, making it pass through unity at 32.6°C, and extrapolating to 0°C yielded $k_o/k_{32.6} = 0.91588$. Dividing the equation through by this quantity gives the correlation:

$$(k_t/k_o) = 1 + 2.91287 \times 10^{-3}t - 1.37670 \times 10^{-6}t^2 + 4.8245 \times 10^{-9}t^3 \qquad (11)$$

for °C and cal/sec. cm °C, with a standard deviation of 0.041. The good internal consistency of these results, and their agreement with the others above cited seem to validate the experimental and computational procedures here employed. The effect of temperature on the thermal conductivity of an alkali metal vapor requiring perfect evacuation of the cell and deoxidation of the alkali metal would evidently be somewhat more difficult to measure successfully. However, such a measurement by itself would not be adequate. Successful experimental results with the alkali metals relative to argon were still more difficult to achieve, as they required consecutive successful tests with argon and with the alkali metal on the same wire. Furthermore, at low pressures the temperature jump correction was undesirably high. However, successful runs were carried out with cesium and rubidium in the 0.1 to 0.2 atmosphere range. These runs are shown in figure 6 and the calculated results are listed in Table 3.

Table 3. Thermal Conductivity of Cesium and Rubidium Vapors.

			Impurities, parts/million							
Alkali Metal	% Purity	Source	Li	Na	K	Rb or CS	Temperature, °C.	Pressure, atmos.	Thermal Conductivity, cal./sec. cm °C	Estd. Error %
Cs	99.999	Dow	1	8	8	10	615	0.214	0.1587	4.6
Cs							554	0.0984	0.2060	"
Cs							547	0.0974	0.2120	"
Rb	99.8+	Kawecki	10	70	500	700	772	0.0882	0.2280	5.1
Rb							826	0.0829	0.2158	"

These results are plotted in figures 7 and 8. Internal consistency is seen to be good, under the circumstances. These metals were of highest commercial purity, and analyzed typically as shown in Table 3. A correction on the thermal conductivity may be calculated assuming ideal liquid and vapor mixtures, available vapor pressure data, and the relative thermal conductivities of Table 1. Although the lighter impurities have higher thermal conductivities, they also are less volatile. For the cesium the correction is entirely negligible. For the rubidium it amounts to a total of only 440 parts per million of the thermal conductivity, thus was not subtracted.

Gottlieb and Zollweg's data are at such low pressures (less than 3 torr) that their thermal conductivities, though extrapolated to eliminate temperature jump, can be ascribed to monomer. Their rubidium point is seen in figure 8 to agree fairly well with the present results, but their cesium point is high in figure 7. However, their own conclusion was that their rubidium value was low and their cesium value reasonable. Achener's results on rubidium are for essentially saturated vapor at higher pressures (4). They are seen to be lower than these, but are considered only preliminary and are expected to rise somewhat (14).

6. Calculation of Thermal Conductivity from Kinetic Theory for Associating Vapor

Calculations of the thermal conductivity of alkali metal vapors have been carried out by Davies et al (13) for vapor consisting exclusively of monomer atoms. However, this is not the case, particularly for vapor at or near saturation and at substantial pressures, as of interest in fast breeder reactor coolant studies. Even small concentrations of dimer considerably increase the thermal conductivity due to the heat of change in equilibrium composition with temperature, which adds diffusion of the heat of reaction to the conduction of sensible heat.

The procedure outlined by Vanderslice et al (15) for predicting the transport properties of hydrogen at high temperatures includes the effect of dissociation. It was decided to apply this procedure to the alkali metal vapors. Potential energy functions for the monomer atoms were taken from Davies' table (13). The potential energy functions and collision integrals for monomer-dimer and dimer-dimer interactions were calculated by Vanderslice's perfect pairing procedure (16,17). Next the translational conductivity of the binary mixture was calculated (18), then the internal conductivity of the mixture (19), and then the conductivity due to chemical reaction (19,20). Full details are available elsewhere for the potential energy functions and equilibrium and frozen thermal conductivity results (9), as well as for viscosity and the thermodynamic properties (21).

7. Conclusions and Acknowledgements

Final results are given in Tables 4 through 8 and figures 7 through 10. The trend with temperature of the thermal conductivity of slightly superheated vapor is particularly noteworthy. It is seen that the thermal conductivity shows a minimum value at a temperature several hundred degrees above saturation, increasing dimer contents at lower temperatures substantially increasing the thermal conductivity at all but the highest pressures. With lithium the minima are still higher.

Agreement between the calculated and experimental results for cesium and rubidium is seen to be good. The results of Stefanov et al on sodium and potassium are also seen to be in fair agreement with the calculated results, particularly as to showing a similar trend of increasing thermal conductivity with decreasing temperature. It is concluded that the results calculated by this method closely represent the equilibrium thermal conductivities of the alkali metal vapors.

The authors are happy to acknowledge support by the U.S. Atomic Energy Commission, Division of Research, under Contract AT(30-1)-2660 with Columbia University, and donation of the cesium by the Dow Chemical Company. The AEC serial number of this publication is CU-2660-37.

8. Nomenclature

a	Accommodation coefficient	
c	Specific heat at constant pressure of the test gas	cal/gm ^{o}C
c'	Specific heat of fine wire	"
c_v	Specific heat at constant volume of the test gas	"
f	Frequency of the heating current	cps
k	Thermal conductivity of the test gas	cal/sec.cm. ^{o}C
k^{o}	Thermal conductivity of a fictitious gas	"
m	Fine wire mass per unit length	gm/cm
p	Pressure of the test gas	atm

Table 4 Equilibrium Thermal Conductivity of Cesium Vapor
(cal/sec.cm.°C) x 10^4

T(°K)	Monomer	Pressure, atm 0.02	0.05	0.1	0.2	0.5	1	2	5	10	Saturation
500	0.0810										0.1023
600	0.0920										0.1341
700	0.1026	0.1349									0.1655
800	0.1129	0.1232	0.1375	0.1585	0.1923						0.1922
900	0.1230	0.1270	0.1329	0.1422	0.1590	0.1977					0.2129
1000	0.1328	0.1348	0.1376	0.1421	0.1506	0.1729	0.2013				0.2281
1100	0.1426	0.1436	0.1451	0.1476	0.1523	0.1653	0.1837	0.2112			0.2394
1200	0.1523	0.1529	0.1537	0.1552	0.1580	0.1660	0.1779	0.1976	0.2347		0.2481
1300	0.1619	0.1623	0.1628	0.1637	0.1655	0.1707	0.1787	0.1926	0.2224	0.2494	0.2550
1400	0.1714	0.1717	0.1721	0.1727	0.1739	0.1774	0.1829	0.1930	0.2162	0.2405	0.2610
1500	0.1810	0.1811	0.1814	0.1818	0.1827	0.1852	0.1892	0.1965	0.2146	0.2355	0.2666
1600	0.1905	0.1906	0.1908	0.1911	0.1917	0.1936	0.1965	0.2021	0.2163	0.2338	0.2719
1700	0.2000	0.2001	0.2002	0.2005	0.2009	0.2023	0.2046	0.2088	0.2201	0.2347	0.2772
1800	0.2095	0.2096	0.2097	0.2099	0.2102	0.2113	0.2131	0.2164	0.2255	0.2377	0.2827
1900	0.2190	0.2191	0.2192	0.2193	0.2196	0.2205	0.2219	0.2246	0.2320	0.2422	0.2882
2000	0.2286	0.2287	0.2287	0.2288	0.2291	0.2298	0.2309	0.2331	0.2392	0.2479	0.2940
2100	0.2382	0.2383	0.2383	0.2384	0.2386	0.2391	0.2401	0.2419	0.2470	0.2544	0.3000
2200	0.2478	0.2478	0.2479	0.2480	0.2481	0.2486	0.2494	0.2509	0.2552	0.2615	0.3061
2300	0.2575	0.2575	0.2575	0.2576	0.2577	0.2581	0.2588	0.2601	0.2638	0.2692	0.3125
2400	0.2672	0.2672	0.2673	0.2673	0.2674	0.2677	0.2683	0.2694	0.2726	0.2773	0.3190
2500	0.2769	0.2770	0.2770	0.2770	0.2771	0.2774	0.2779	0.2788	0.2816	0.2857	0.3258
2600	0.2867	0.2867	0.2868	0.2868	0.2869	0.2871	0.2875	0.2884	0.2908	0.2944	0.3327
2700	0.2965	0.2966	0.2966	0.2966	0.2967	0.2969	0.2973	0.2980	0.3001	0.3033	0.3397
2800	0.3064	0.3064	0.3064	0.3065	0.3065	0.3067	0.3070	0.3077	0.3095	0.3124	0.3469
2900	0.3163	0.3163	0.3163	0.3164	0.3164	0.3166	0.3169	0.3174	0.3191	0.3216	0.3543
3000	0.3263	0.3263	0.3263	0.3263	0.3264	0.3265	0.3268	0.3273	0.3287	0.3310	0.3618

Table 5 Equilibrium Thermal Conductivity of Rubidium Vapor
(cal/sec.cm.°C) x 10^4

T(°K)	Monomer	Pressure, atm 0.02	0.05	0.1	0.2	0.5	1	2	5	10	Saturation
500	0.1118										0.1325
600	0.1271										0.1702
700	0.1419	0.1946									0.2105
800	0.1562	0.1725	0.1951	0.2286							0.2485
900	0.1703	0.1765	0.1856	0.1999	0.2259						0.2812
1000	0.1841	0.1869	0.1911	0.1979	0.2109	0.2451	0.2897				0.3081
1100	0.1978	0.1992	0.2014	0.2050	0.2120	0.2315	0.2595	0.3028			0.3297
1200	0.2113	0.2122	0.2134	0.2155	0.2196	0.2313	0.2491	0.2791	0.3388		0.3469
1300	0.2247	0.2253	0.2260	0.2274	0.2299	0.2374	0.2491	0.2698	0.3162	0.3617	0.3610
1400	0.2381	0.2385	0.2390	0.2398	0.2416	0.2466	0.2546	0.2692	0.3045	0.3439	0.3729
1500	0.2514	0.2517	0.2520	0.2526	0.2538	0.2574	0.2630	0.2736	0.3006	0.3334	0.3832
1600	0.2647	0.2649	0.2652	0.2656	0.2665	0.2690	0.2732	0.2811	0.3019	0.3288	0.3926
1700	0.2780	0.2782	0.2784	0.2787	0.2793	0.2813	0.2844	0.2905	0.3067	0.3288	0.4014
1800	0.2913	0.2914	0.2916	0.2918	0.2923	0.2938	0.2963	0.3010	0.3139	0.3321	0.4099
1900	0.3046	0.3047	0.3049	0.3050	0.3054	0.3066	0.3086	0.3123	0.3228	0.3379	0.4183
2000	0.3180	0.3181	0.3181	0.3183	0.3186	0.3196	0.3211	0.3242	0.3328	0.3454	0.4266
2100	0.3313	0.3314	0.3315	0.3316	0.3319	0.3327	0.3339	0.3365	0.3436	0.3542	0.4350
2200	0.3448	0.3448	0.3449	0.3450	0.3452	0.3458	0.3469	0.3490	0.3550	0.3641	0.4436
2300	0.3582	0.3582	0.3583	0.3584	0.3586	0.3591	0.3600	0.3618	0.3669	0.3747	0.4522
2400	0.3717	0.3717	0.3718	0.3719	0.3720	0.3725	0.3732	0.3748	0.3791	0.3859	0.4610
2500	0.3852	0.3854	0.3853	0.3854	0.3855	0.3859	0.3866	0.3879	0.3917	0.3975	0.4700
2600	0.3988	0.3990	0.3989	0.3990	0.3991	0.3994	0.4000	0.4011	0.4044	0.4096	0.4791
2700	0.4125	0.4126	0.4125	0.4126	0.4127	0.4130	0.4135	0.4145	0.4174	0.4219	0.4884
2800	0.4262	0.4262	0.4262	0.4263	0.4263	0.4266	0.4271	0.4279	0.4305	0.4345	0.4979
2900	0.4399	0.4401	0.4400	0.4400	0.4401	0.4403	0.4407	0.4415	0.4438	0.4473	0.5075
3000	0.4537	0.4538	0.4538	0.4538	0.4539	0.4541	0.4544	0.4551	0.4571	0.4603	0.5172

Table 6 Equilibrium Thermal Conductivity of Potassium Vapor
(cal/sec.cm.°C) x 10^4

T(°K)	Monomer	Pressure, atm 0.02	0.05	0.1	0.2	0.5	1	2	5	10	Saturation
500	0.1851										0.1979
600	0.2100										0.2450
700	0.2339										0.3015
800	0.2571	0.3422	0.2931	0.4130							0.3618
900	0.2797	0.3121	0.2929	0.3420	0.3954						0.4197
1000	0.3019	0.3163	0.3077	0.3302	0.3563	0.4241					0.4710
1100	0.3238	0.3311	0.3267	0.3382	0.3521	0.3902	0.4441				0.5142
1200	0.3454	0.3495	0.3471	0.3535	0.3615	0.3840	0.4179	0.4741			0.5497
1300	0.3668	0.3693	0.3678	0.3718	0.3767	0.3908	0.4127	0.4513	0.5362		0.5786
1400	0.3881	0.3898	0.3888	0.3914	0.3945	0.4038	0.4186	0.4455	0.5099	0.5803	0.6025
1500	0.4093	0.4104	0.4098	0.4115	0.4137	0.4201	0.4304	0.4497	0.4984	0.5570	0.6226
1600	0.4304	0.4312	0.4307	0.4320	0.4336	0.4382	0.4456	0.4598	0.4970	0.5449	0.6401
1700	0.4515	0.4521	0.4518	0.4527	0.4538	0.4572	0.4628	0.4735	0.5023	0.5413	0.6558
1800	0.4726	0.4730	0.4728	0.4735	0.4743	0.4769	0.4812	0.4895	0.5121	0.5439	0.6704
1900	0.4936	0.4940	0.4938	0.4943	0.4950	0.4970	0.5004	0.5069	0.5250	0.5512	0.6843
2000	0.5147	0.5150	0.5149	0.5153	0.5158	0.5174	0.5201	0.5253	0.5400	0.5617	0.6978
2100	0.5358	0.5361	0.5359	0.5363	0.5367	0.5380	0.5402	0.5445	0.5566	0.5747	0.7112
2200	0.5570	0.5572	0.5570	0.5573	0.5577	0.5588	0.5606	0.5641	0.5742	0.5895	0.7246
2300	0.5782	0.5784	0.5783	0.5785	0.5788	0.5797	0.5812	0.5842	0.5927	0.6057	0.7381
2400	0.5995	0.5996	0.5997	0.5997	0.6000	0.6007	0.6020	0.6045	0.6118	0.6230	0.7517
2500	0.6208	0.6210	0.6210	0.6210	0.6212	0.6219	0.6230	0.6251	0.6314	0.6411	0.7656
2600	0.6422	0.6423	0.6423	0.6424	0.6426	0.6432	0.6441	0.6459	0.6513	0.6598	0.7797
2700	0.6637	0.6638	0.6639	0.6639	0.6640	0.6645	0.6653	0.6669	0.6716	0.6790	0.7940
2800	0.6853	0.6854	0.6855	0.6854	0.6856	0.6860	0.6867	0.6881	0.6922	0.6987	0.8085
2900	0.7069	0.7070	0.7072	0.7071	0.7072	0.7075	0.7082	0.7094	0.7130	0.7188	0.8233
3000	0.7286	0.7287	0.7288	0.7288	0.7289	0.7292	0.7297	0.7308	0.7341	0.7392	0.8383

Table 7 Equilibrium Thermal Conductivity of Sodium Vapor
(cal/sec.cm.°C) x 10^4

T(°K)	Monomer	Pressure, atm 0.02	0.05	0.1	0.2	0.5	1	2	5	10	Saturation
500	0.3072										0.4909
600	0.3489										0.7525
700	0.3889										1.0384
800	0.4277										1.2891
900	0.4656	0.9611	1.4624								1.4761
1000	0.5027	0.6772	0.9022	1.2008	1.6067						1.5993
1100	0.5393	0.6092	0.7073	0.8547	1.0995	1.5736					1.6719
1200	0.5754	0.6072	0.6535	0.7266	0.8595	1.1729	1.5100				1.7093
1300	0.6111	0.6273	0.6512	0.6898	0.7630	0.9539	1.1985	1.5136			1.7244
1400	0.6466	0.6556	0.6690	0.6908	0.7332	0.8496	1.0141	1.2610	1.6487		1.7264
1500	0.6819	0.6873	0.6954	0.7085	0.7343	0.8076	0.9170	1.0973	1.4398	1.6965	1.7214
1600	0.7171	0.7206	0.7256	0.7341	0.7506	0.7985	0.8724	1.0015	1.2798	1.5369	1.7134
1700	0.7523	0.7547	0.7579	0.7636	0.7747	0.8072	0.8584	0.9513	1.1693	1.4016	1.7047
1800	0.7874	0.7890	0.7913	0.7953	0.8030	0.8258	0.8623	0.9301	1.0989	1.2980	1.6968
1900	0.8225	0.8238	0.8253	0.8282	0.8338	0.8503	0.8770	0.9275	1.0584	1.2244	1.6904
2000	0.8577	0.8588	0.8599	0.8620	0.8661	0.8784	0.8984	0.9367	1.0390	1.1759	1.6859
2100	0.8930	0.8935	0.8947	0.8962	0.8994	0.9088	0.9241	0.9537	1.0345	1.1471	1.6836
2200	0.9284	0.9289	0.9297	0.9310	0.9334	0.9407	0.9526	0.9759	1.0406	1.1334	1.6833
2300	0.9639	0.9643	0.9650	0.9660	0.9679	0.9736	0.9832	1.0018	1.0541	1.1311	1.6850
2400	0.9996	1.0000	1.0005	1.0013	1.0028	1.0074	1.0151	1.0302	1.0731	1.1373	1.6887
2500	1.0355	1.0360	1.0362	1.0368	1.0381	1.0419	1.0482	1.0606	1.0961	1.1501	1.6941
2600	1.0715	1.0717	1.0722	1.0727	1.0737	1.0768	1.0820	1.0924	1.1221	1.1678	1.7011
2700	1.1077	1.1078	1.1084	1.1086	1.1095	1.1122	1.1165	1.1252	1.1503	1.1893	1.7096
2800	1.1441	1.1448	1.1446	1.1450	1.1456	1.1479	1.1516	1.1590	1.1804	1.2138	1.7195
2900	1.1808	1.1815	1.1813	1.1815	1.1821	1.1840	1.1871	1.1935	1.2118	1.2407	1.7305
3000	1.2176	1.2187	1.2180	1.2182	1.2187	1.2204	1.2231	1.2285	1.2444	1.2696	1.7426

Table 8 Equilibrium Thermal Conductivity of Lithium Vapor
(cal/sec.cm.°C) x 10^4

T(°K)	Monomer	Pressure, atm 0.02	0.05	0.1	0.2	0.5	1	2	5	10	Saturation
500	0.5220										0.5421
600	0.5934										0.6713
700	0.6619										0.8695
800	0.7282										1.1479
900	0.7929										1.4953
1000	0.8562										1.8850
1100	0.9185										2.2845
1200	0.9800										2.6653
1300	1.0409	2.0199									3.0075
1400	1.1012	1.5540	2.1472	2.9534							3.3004
1500	1.1613	1.3864	1.7006	2.1690	2.9377						3.5416
1600	1.2211	1.3414	1.5146	1.7852	2.2667	3.3504					3.7335
1700	1.2808	1.3494	1.4498	1.6106	1.9098	2.6568	3.5428				3.8817
1800	1.3404	1.3818	1.4430	1.5423	1.7318	2.2353	2.9023	3.8067			3.9929
1900	1.4001	1.4264	1.4652	1.5290	1.6525	1.9936	2.4782	3.2129			4.0736
2000	1.4599	1.4770	1.5030	1.5454	1.6284	1.8633	2.2127	2.7838	3.8531		4.1299
2100	1.5198	1.5319	1.5493	1.5785	1.6360	1.8012	2.0546	2.4907	3.4032		4.1669
2200	1.5798	1.5881	1.6007	1.6215	1.6623	1.7812	1.9672	2.2992	3.0522	3.8104	4.1890
2300	1.6402	1.6461	1.6554	1.6704	1.7002	1.7875	1.9262	2.1801	2.7913	3.4717	4.1997
2400	1.7008	1.7057	1.7120	1.7232	1.7455	1.8109	1.9159	2.1118	2.6047	3.1970	4.2015
2500	1.7617	1.7658	1.7702	1.7788	1.7957	1.8455	1.9263	2.0791	2.4764	2.9828	4.1966
2600	1.8229	1.8266	1.8295	1.8362	1.8492	1.8879	1.9509	2.0713	2.3927	2.8214	4.1867
2700	1.8845	1.8866	1.8898	1.8949	1.9051	1.9357	1.9855	2.0815	2.3427	2.7040	4.1728
2800	1.9465	1.9494	1.9507	1.9550	1.9629	1.9873	2.0272	2.1045	2.3182	2.6223	4.1559
2900	2.0089	2.0102	2.0128	2.0157	2.0223	2.0419	2.0741	2.1370	2.3130	2.5692	4.1366
3000	2.0717	2.0742	2.0746	2.0771	2.0826	2.0986	2.1250	2.1766	2.3225	2.5388	4.1153

r	Radial distance from the center of the fine wire	cm
r_1	Fine wire radius	"
r_2	Outer shell radius	"
t	Instantaneous temperature	^oC
t_1	Instantaneous temperature of the wire	"
t_2	Outer shell temperature	"
E	IR drop across the fine wire	volts
E_1	Major rms fundamental voltage	"
E_3	Rms third harmonic voltage	"
E_{3R}	Bridge output rms third harmonic voltage	"
I	Rms current passing through the fine wire	amps
L	Length of the fine wire	cm
R	Gas constant, instantaneous electrical resistance	ohms
$\overline{R}$	Average electrical resistance of the fine wire	"
R_M	Thermocouple voltmeter resistance	"
$\frac{\overline{dR}}{dt}$	First derivative of electrical resistance with respect to the average wire temperature	ohms/^oC
T	Absolute temperature	^oK
γ	Ratio of specific heats	
θ	Time	sec
ρ	Density of the test gas	gm/cm^3
ρ'	Density of the fine wire	"
ϕ	Phase shift angle	radians
ω	Angular frequency, $2\pi f$	radians/sec

9. References

(1) Gottlieb, M. and R. J. Zellweg, J. Chem. Phys. 39, 10, 2773-2774(Nov.1963).

(2) Stefanov, V. I., D. L. Timrot, E. E. Totskee and Ch. Venkhao, Thermophysics of High Temperature 4, 141(1966), Academy of Science, USSR.

(3) Timrot, D. L. and E. E. Totskee, Thermophysics of High Temperature, 3, No. 5(1965).

(4) Achener, P. Y., AGN Report No. 8222, Contract AT(04-3)-368, p.7, Aerojet-General Corp., San Ramon, Calif.(May 1967).

(5) Lee, C. S. and Bonilla, C. F., Technical Report No. 1, Contract Nonr 266 (11), Columbia Univ., N.Y.(1952).

(6) Tarmy, B. L., PhD Dissertation, Dept. of Chemical Engineering, Columbia Univ.(1956).

(7) Peterson, J. R., Eng.Sc.D. Dissertation, Dept. of Chemical Engineering, Columbia Univ.(1963); Peterson, J. R. and Bonilla, C. F., Third Symposium on Thermophysical Properties, ASME, pp. 264-276(March 22-25, 1965).

(8) Kennard, E. H., Kinetic Theory of Gases, McGraw-Hill, N.Y. 1938

(9) Lee, C. S., Eng.Sc.D. Dissertation, Dept. of Chemical Engineering, Columbia Univ.(1968). To be available through University Microfilms, Inc., Ann Arbor, Mich.

(10) Nuttall, R. L., Nat'; Bur. Standards Circ. 564, Washington, D.C. (1955).

(11) Liley, P. E., Private communication (Dec.,1966).

(12) Vargaftik, N. B. and Zimina, N. Kh., Teplofizika Vysokikh Temperatur, 2, 5, 716-724(1964).

(13) Davies, R. H., Mason, E. A. and Munn, R. J., Phys. Fluids, 8, 3, 444(1965).

(14) Achener, P. Y., Private communication (Nov.1, 1967).

(15) Vanderslice, J. T., Weissman, S., Mason, E. A. and Fallon, R. J.,Phys. Fluids, 5, 2, 155(1962).

(16) Vanderslice, J. T., Mason, E. A. and Lippincott, E. R.,J. Chem. Phys., 30 129(1959).

(17) Vanderslice, J. T. and Mason, E. A., J. Chem. Phys., 33, 492(1960).

(18) Muckenfass, C. and Curtiss, C. F., J. Chem. Phys., 29, 1273(1958).

(19) Hirschfelder, J. O., J. Chem. Phys., 26, 274(1957).

(20) Butler, J. N. and Brokaw, R. S., J. Chem. Phys., 32, 1005(1960).

(21) Lee, D. I., Eng.Sc.D. Dissertation, Dept. of Chemical Engineering, Columbia Univ.(1967). To be available through University Microfilms, Inc., Ann Arbor, Mich.

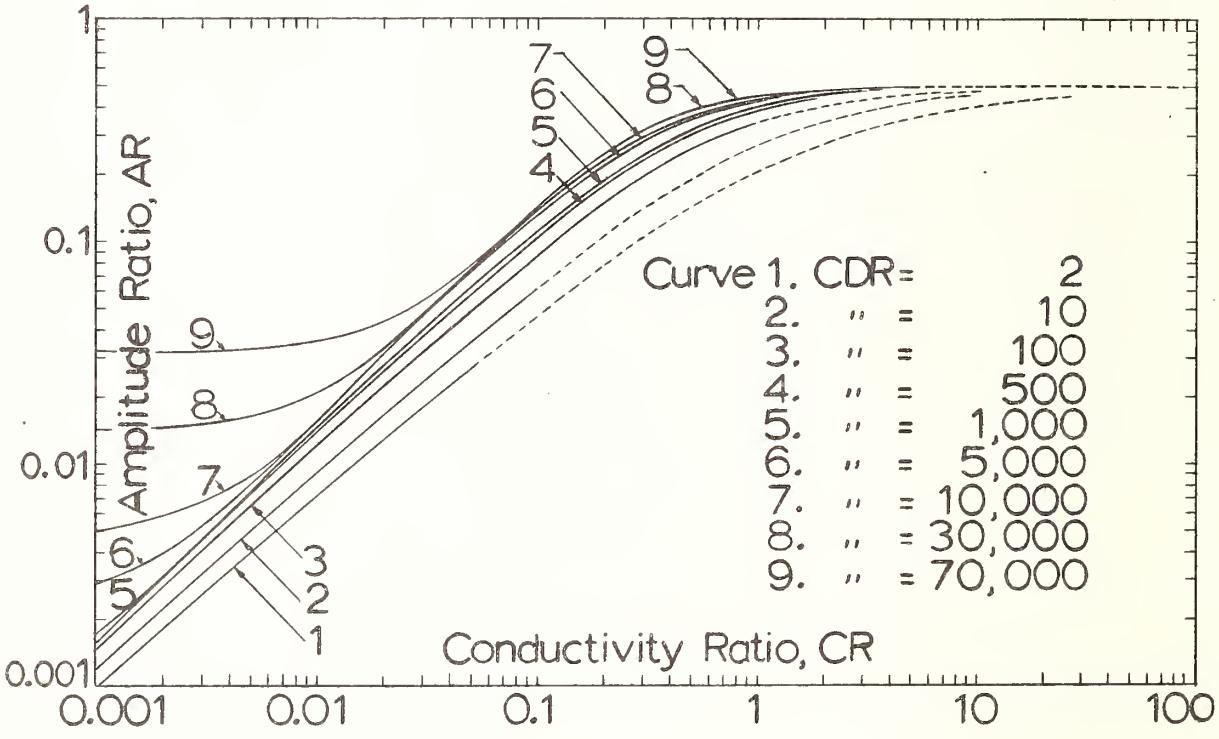

Figure 1. Theoretical Frequency Response Curves for Radius Ratio (DR) of 1000, and Zero Temperature Jump (TJF), and Thermal Radiation (QR).

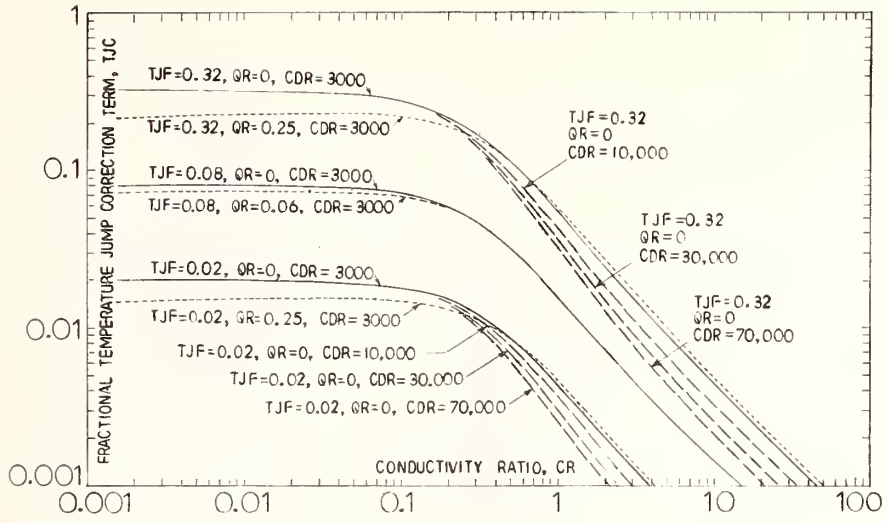

Figure 2. Fractional Temperature Jump Correction Term as a Function of Conductivity Ratio (CR) for Various Values of Temperature Jump Factor (TJF), Thermal Radiation (QR), and Volumetric Heat Capacity Ratio (CDR).

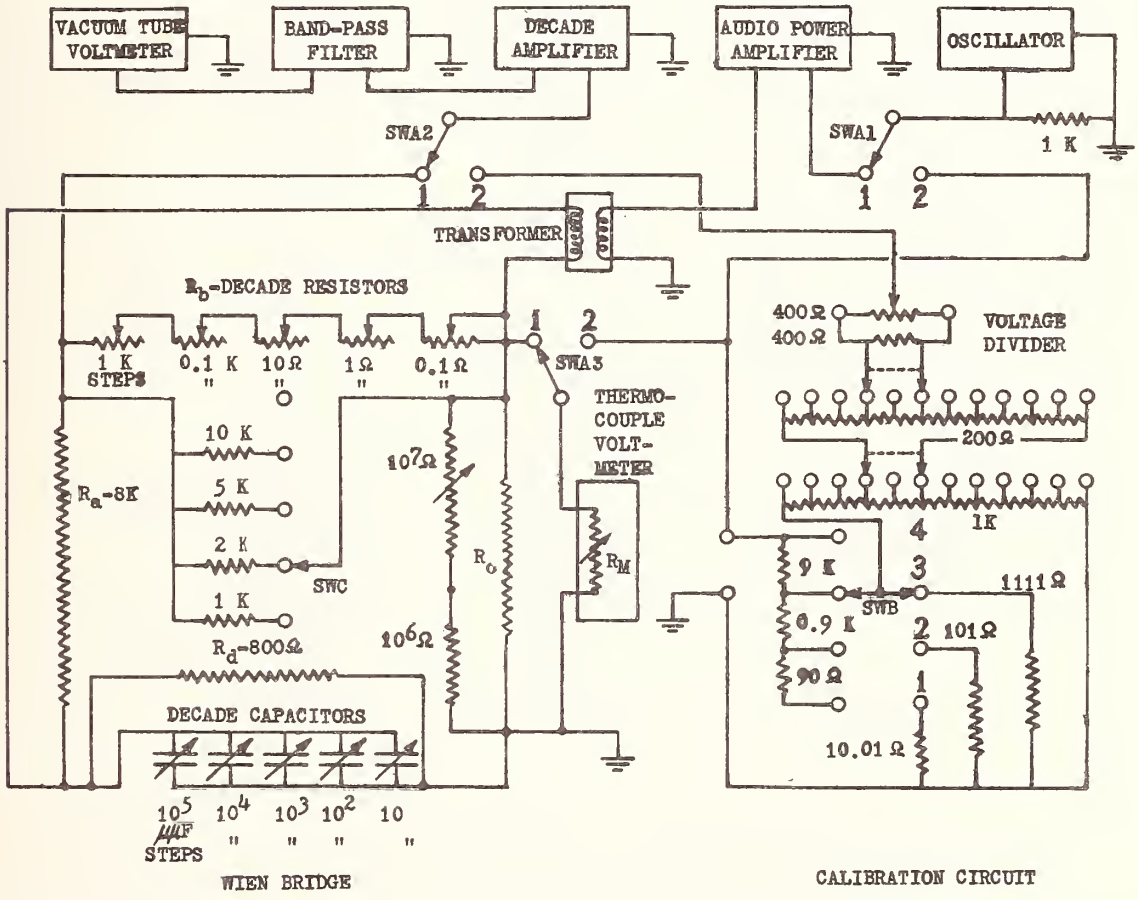

Figure 3. Power, Measurement, and Calibration Circuit of a Hot Wire Transient Thermal Conductivity Cell.

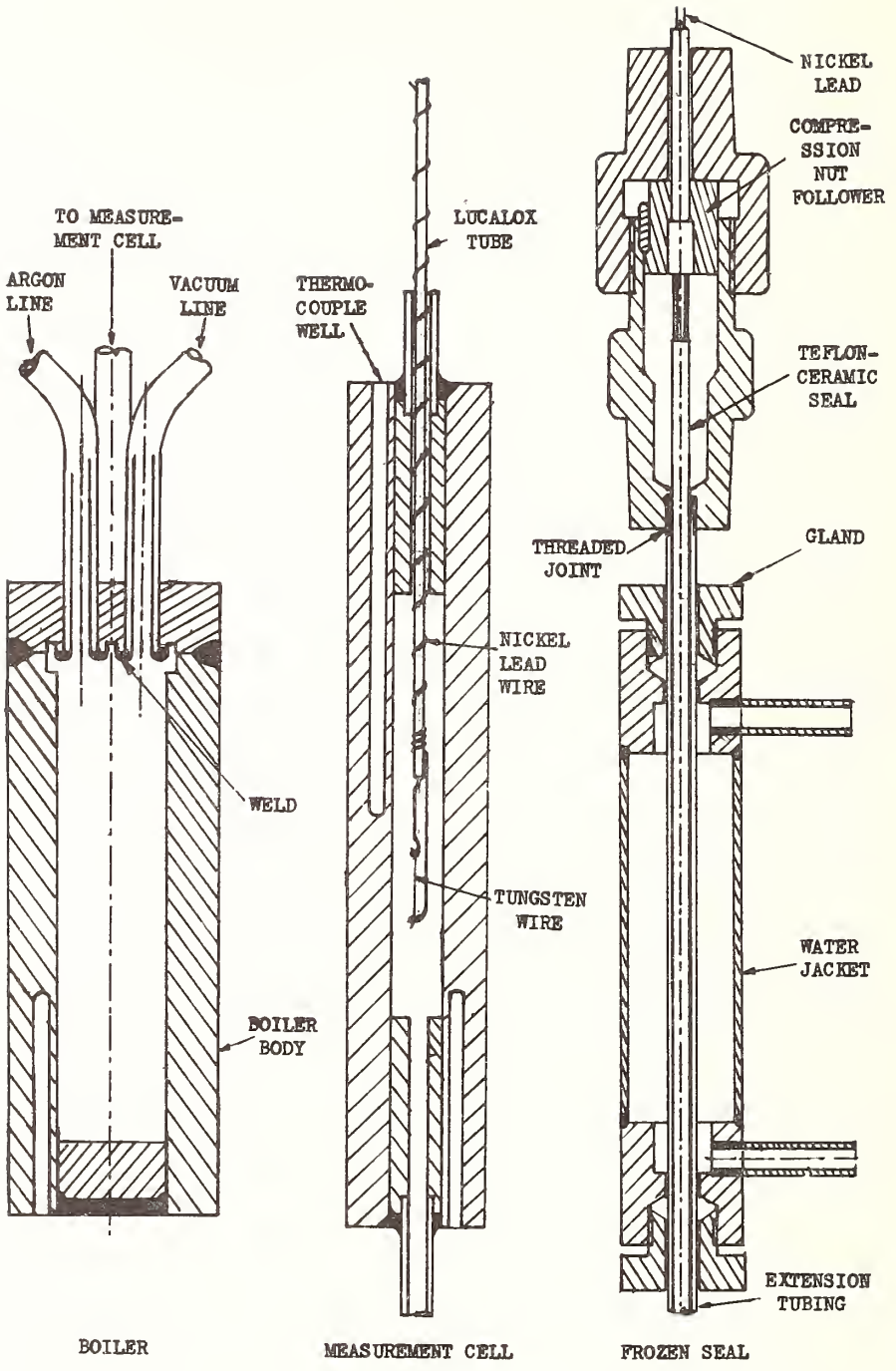

Figure 4. Hot Wire Thermal Conductivity Cell with Frozen Metal Seal.

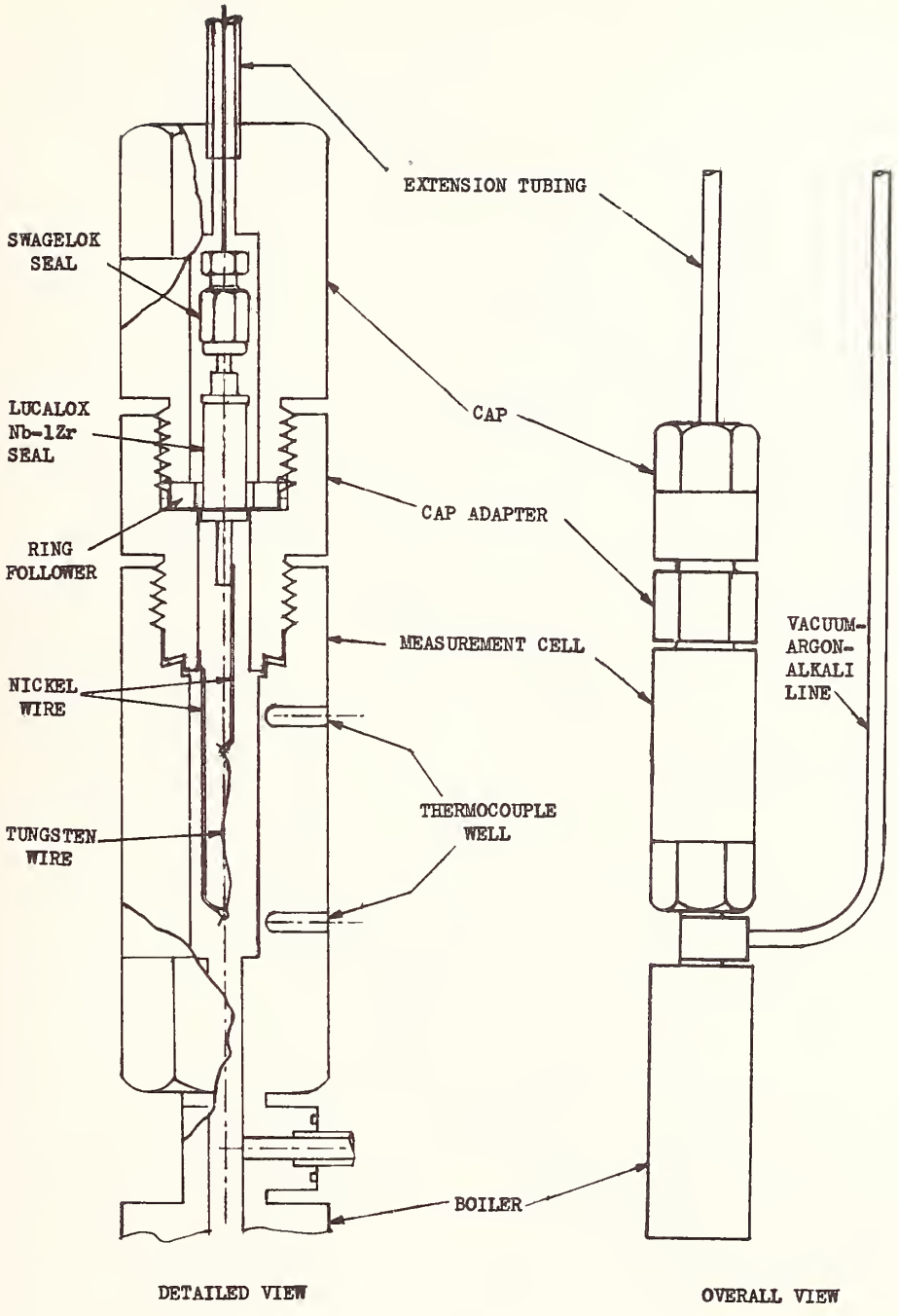

Figure 5. Hot Wire Thermal Conductivity Cell with Brazed Seal.

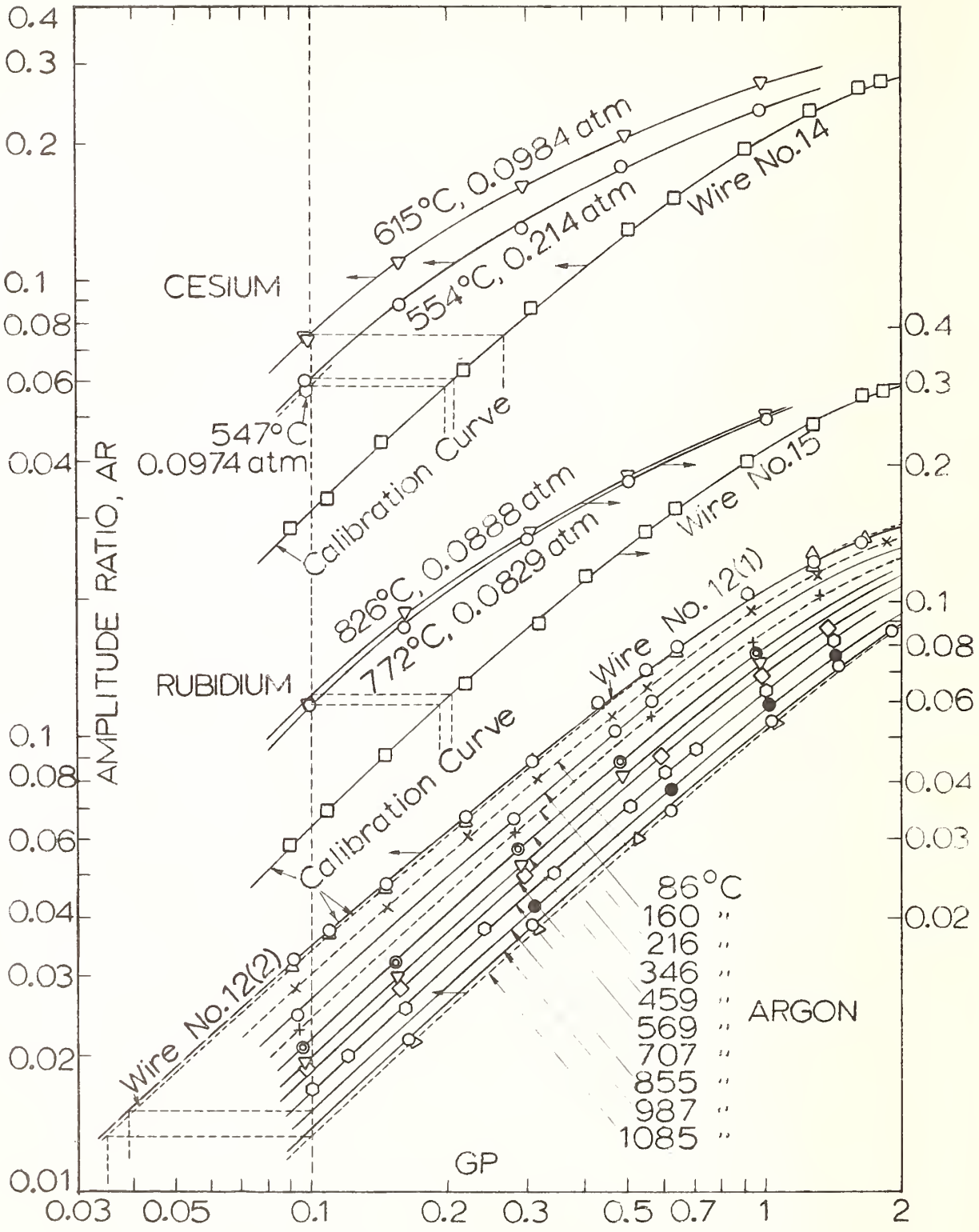

Figure 6. Working Curves for Thermal Conductivity Tests on Argon, Rubidium and Cesium.

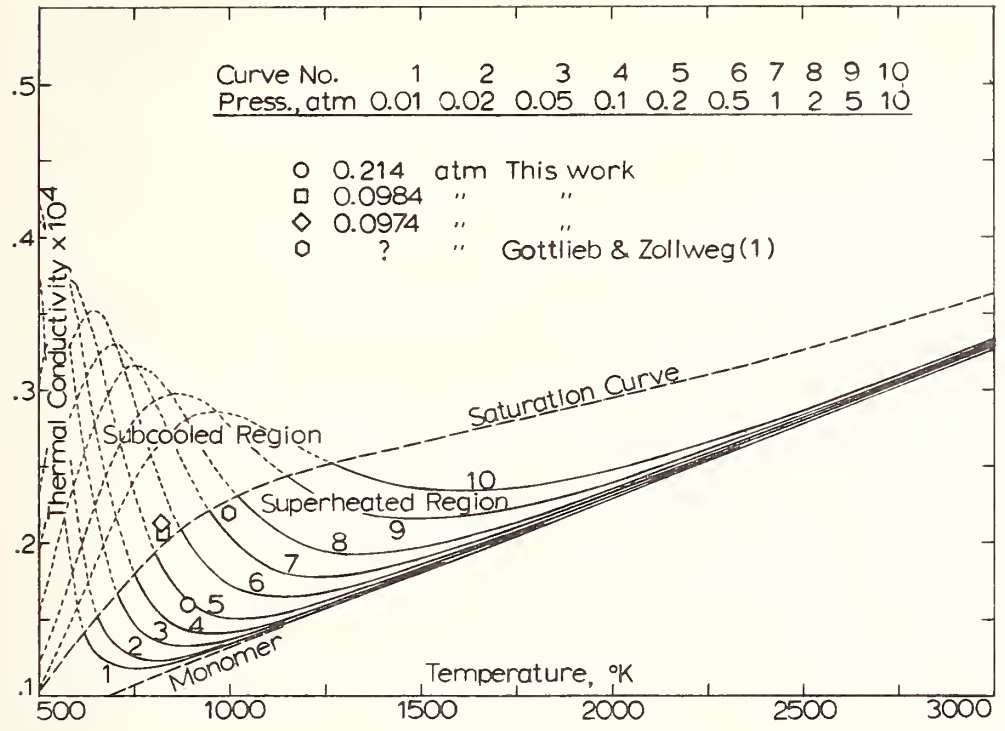

Figure 7. Experimental and Calculated Thermal Conductivity Results for Cesium Vapor.

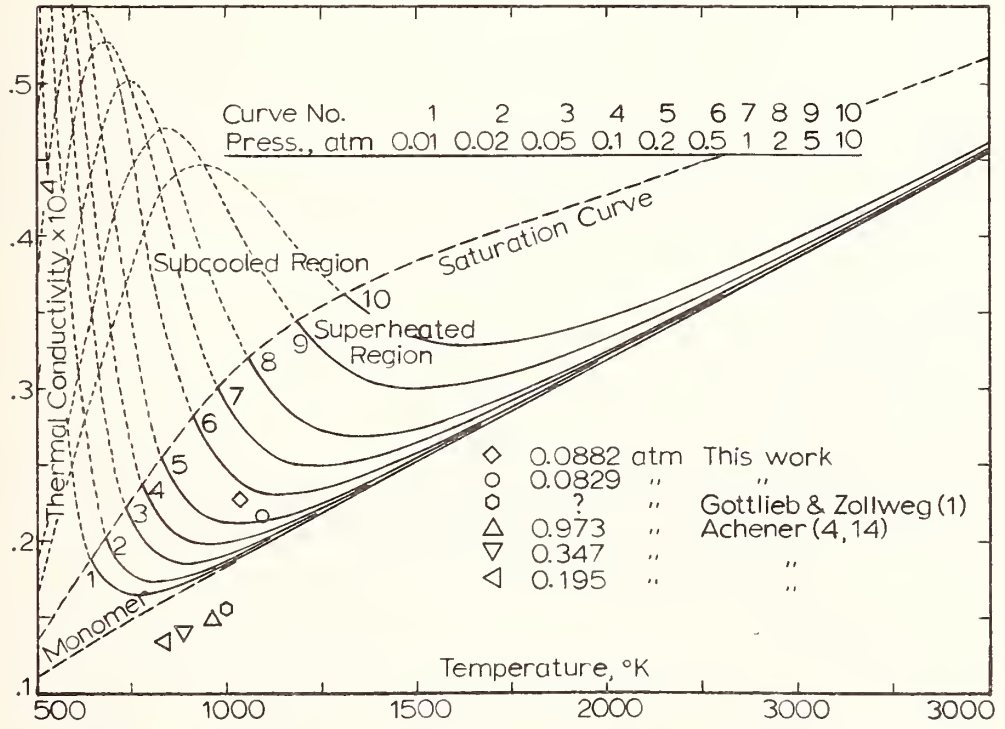

Figure 8. Experimental and Calculated Thermal Conductivity Results for Rubidium Vapor.

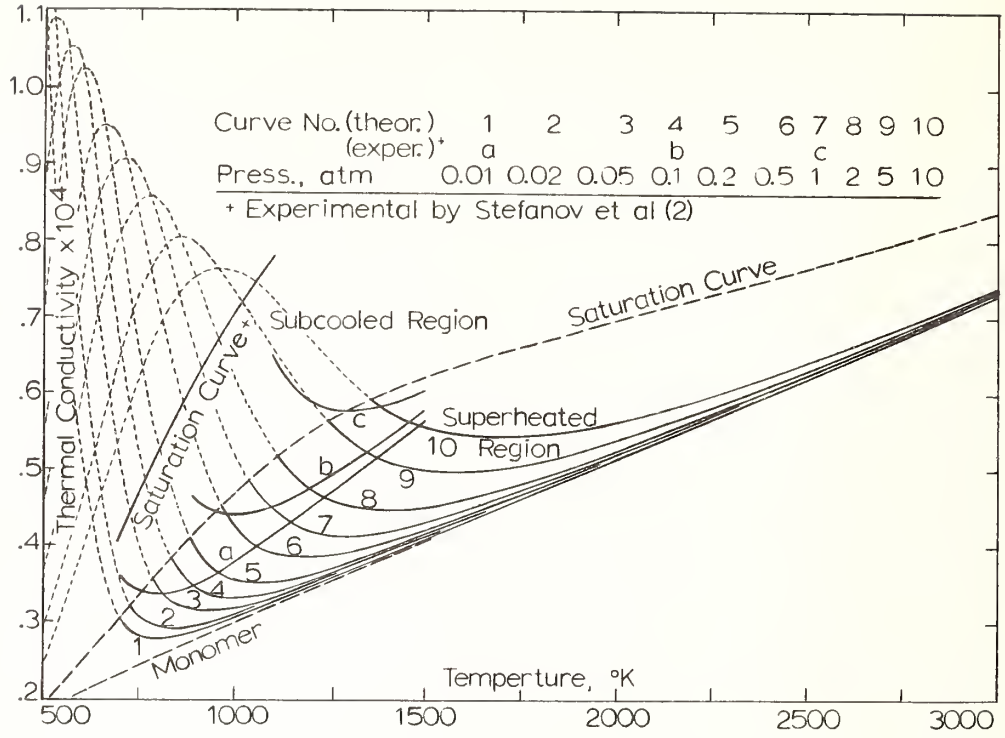

Figure 9. Experimental and Calculated Thermal Conductivity Results for Potassium Vapor.

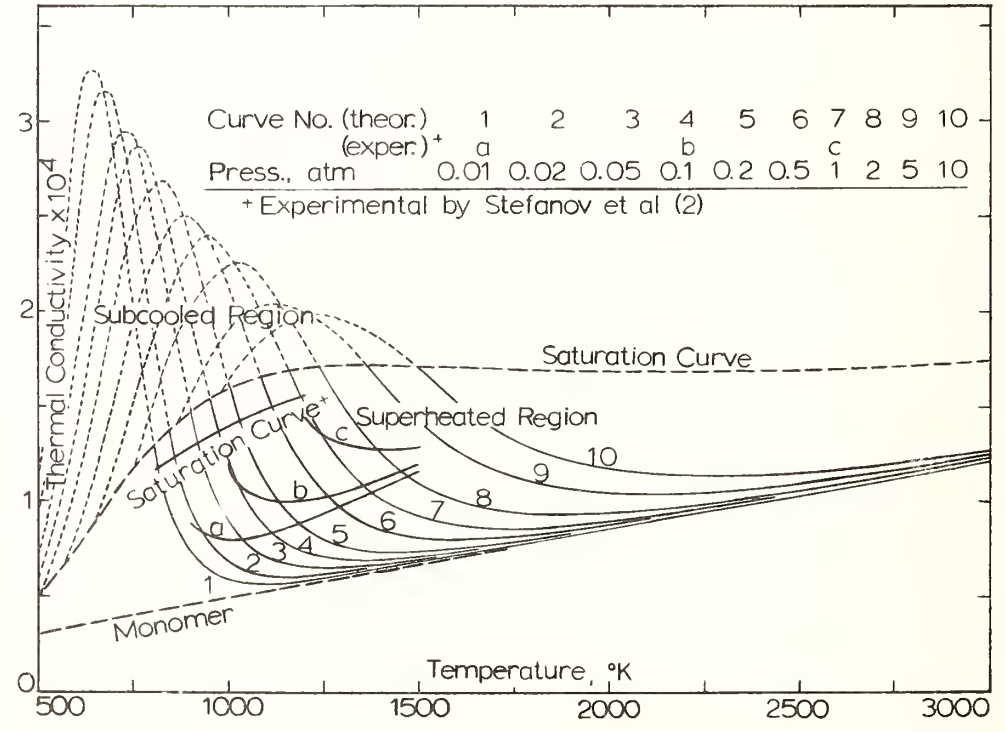

Figure 10. Experimental and Calculated Thermal Conductivity Results for Sodium Vapor.

Recent Developments at Bellevue on Thermal Conductivity Measurements of Compressed Gases

B. Le Neindre, P. Bury, R. Tufeu, P. Johannin, and B. Vodar

Laboratoire des Hautes Pressions - C.N.R.S.
1, Place A. Briand - Bellevue - (France)

In this paper we give a description of an apparatus adapted to the measurement of the thermal conductivity of gases in the temperature range from 25 to 700°C and at pressures up to 120×10^6 N/m^2 (1200 bar).

The concentric cylinder method was used with different gaps (from 0.2 to 0.25 mm) and with a temperature difference from 1 to 4 deg C between cylinders.

Tables giving experimental thermal conductivity values are presented for argon, nitrogen, methane, carbon dioxide near 25°C, and helium near 30°C in the pressure range up to 120×10^6 N/m^2 (1200 bar).

The data are estimated to be accurate within 1.5 per cent; however, in general, the data are consistent within 0.5 per cent.

Key words: Gases, pressure, radial heat flow.

1. Introduction

Over the last decade there has been interest in thermal conductivity coefficients of the dense gaseous and liquid phases. The relevant experimental data were needed for the development of industrial plants working at high pressure and temperature. Therefore, the study of thermal conductivity has been undertaken for water(1)[1], heavy water (2) in the liquid and gaseous phases, helium, and carbon dioxide. On the other hand, in order that the validity of any given theory of the non-equilibrium state might be assessed, there is a need for experimental data of thermal conductivity coefficients of the simplest molecules, i.e. argon, nitrogen and argon-helium mixtures.

2. Description of Method and Details of Apparatus

A vertical concentric cylinder method has been used for these measurements. The experimental method and the design and assembly have been described in several papers (1, 2, 3, 4, 5). Some constructional details and modifications of the apparatus are summarized here.

In this method heat is generated in the inner cylinder (or emitter) and passes outward through a narrow gap (between 0.2 and 0.25 mm) to the outer system, consisting of the outer cylinder and of two centering pieces (fig. 1). The fluid under test is contained within the annulus.

The use of end guards at the inner cylinder has been avoided by judicious location of thermocouples, and by proper nonuniform heating of the inner cylinder to compensate for end effects.

---

[1] Figures in parentheses refer to literature references cited at the end of this paper.

The inner cylinder has been mounted within the outer cylinder by five insulating plugs. From the emitter heat is transferred by conduction, convection and radiation through the fluid and conduction through the insulating plugs, thermocouples and resistance leads. At ambient temperature, and far from the critical point, heat is transferred almost entirely by conduction through the fluids, the leads, and the ceramic supports.

The experiments show that the thermal contact resistance between ceramic supports and silver is not completely negligible. Therefore, it is not possible to calculate the heat losses due to these supports. The thermal resistance of the system has been treated as if it were composed of two thermal conductances in parallel. With insulating plugs of quartz the "parallel" heat transfer by leads and ceramic supports has been found equal to 1.8×10^{-3} W $m^{-1} deg^{-1}$ for a gap of 0.25 mm using the value 17.35×10^{-3} $m^{-1} deg^{-1}$ for the thermal conductivity of argon at 25°C and 0.1×10^{6} N/m^2.

Several experiments have been done with different numbers and kinds of plugs, and different types of gases. These experiments have shown that the "parallel" heat transfer is a constant at 25°C.

The electrical capacitance of the cell measured in air at room temperature determines the goemetrical constant of the cell which enters into the calculation of the thermal conductivity coefficient.

The thermal conductivity cell is placed in a high pressure vessel heated externally by a vertical solid thermostat in copper (fig. 2). The heating unit consists of six electrical heaters, each heater is associated with a hand operated variable transformer and a Pt - Pt 10% Rh thermocouple. Power to each element is hand controlled so that the longitudinal gradient is negligible. Input voltage to the variable transformers is controlled by an automatic temperature regulator. The sensing element of the temperature regulator is a Pt - Pt 10% Rh thermocouple located on the outside of the central heater so as to minimize the time-lag in regulation; temperature stability was better than 0. 1 deg C. The large thermal inertia of the high pressure vessel and the small time-lag in temperature regulation insure a complete absence of detectable temperature fluctuations in the thermal conductivity cell.

The pressure in the high pressure vessel is measured by means of Bourdon type gauges manufactured by Heise Co. (USA). Temperature differences between emitter and receiver are accurately measured by means of eight Pt - Pt 10% Rh thermocouples connected in series. The emf of the thermocouples is measured by means of a Wenner potentiometer (Leeds & Northrup Co.) with a Keithley null detector, the sensitivity of which is better than 0.1 μV.

3. Measurements and Results

Since stabilization of temperature requires a rather long period of time, all measurements have been made at constant temperature and varying pressure. A variation of pressure also produces a slight change in the temperature equilibrium due to the heat of compression and the modification of the temperature distribution in the high pressure vessel. The time necessary to reach equilibrium under these conditions is highly dependent on the thermal conductivity of the gas used in the experiment; it takes about one hour for argon and less for the other gases. Measurements have been made in general at decreasing pressures with some verification points at increasing pressures.

The aim of this work was to provide thermal conductivity coefficients of fluids in large temperature and pressure ranges. Because of difficulties in making measurements under high pressure at constant temperature, an attempt was made to find empirical relations for the variation of thermal conductivity coefficients with pressure. As it will be shown subsequently, the relation

$$\Delta\lambda_{\rho,T} = \lambda_{\rho,T} - \lambda_{o,T} = f(\rho) \qquad (1)$$

is true for a gas in a large temperature and pressure range[2] (where $\lambda_{\rho,T}$ is the thermal conductivity coefficient at density ρ and temperature T, $\lambda_{o,T}$ is the thermal conductivity coefficient at density zero and temperature T.) It is possible to use this relation to interpolate and extrapolate the experimental thermal conductivity coefficient of a gas.

On the other hand, assuming that this relation can be applied to another gas, a measurement of thermal conductivity as a function of temperature up to T°C and another measurement as a function of pressure up to P N/m^2 along an isotherm provide thermal conductivity coefficients in the pressure-temperature range desired.

---

[2]It may be recalled here that for a larger range (1600 bar and 700°C) some deviations from this sample relation were observed for nitrogen (3) (4).

All measurements have been plotted in the (λ,ρ) diagram. The first measurements have been carried out for different gases near 25°C at pressures up to 120×10^6 N/m^2 (1200 bar). The thermal conductivity coefficient has been calculated at 25°C using eq (1) at constant density:

$$\lambda_{\rho,T} - \lambda_{o,T} = \lambda_{\rho,25°C} - \lambda_{o,25°C} \tag{2}$$

$$\lambda_{\rho,T} - \lambda_{\rho,25°C} = \lambda_{o,T} - \lambda_{o,25°C} \tag{3}$$

It is found that the variation of the thermal conductivity coefficient at atmospheric pressure is a linear function of the temperature in a large interval around 25°C:

$$\lambda_{o,T} = \lambda_{o,25°C} + a(T - 25) \tag{4}$$

so that eqs (3) and (4) give

$$\lambda_{\rho,T} - \lambda_{\rho,25°C} = a(T - 25) \tag{5}$$

The accuracy of the data obtained for λ is estimated to be 1.5%.

3.1 The Thermal Conductivity Coefficient of Argon

The gas was commercial argon with a purity of 99.995%. Measurements have been carried out with two gas thicknesses, one of 0.2 and another of 0.25 mm. The results are presented in table I. The density ρ was deduced from the compressibility isotherms (6) (7). The last column of the table gives the thermal conductivity coefficients calculated at 25°C using eq (5) and the value a = 0.044. Thermal conductivity is plotted as a function of density and compared with results obtained by Michels, Sengers and Van der Klundert (8) in figure 3. Our results agree with theirs quite satisfactorily up to 700 kg/m^3 being 1% higher thereafter, which is still within the limits of our accuracy.

Measurements have recently been carried out from 25°C to 700°C and pressures up to 100×10^6 N/m^2 (1000 bar). The accuracy of these data is 1.5% from 25°C to 300°C and 4% from 300 to 700°C. In figure 4, λ versus density is plotted. The marked points have been cross-plotted from isobaric curves of the λ - T diagram made from experimental data.

To a first approximation, as can be seen in this diagram, all the isotherms can be obtained by translation; along the λ axis, and this within the limits of our accuracy, so we think that the relation given by eq (5) is verified.

Our data are always lower than the values of Tsederberg, Popov and Morozova (9) with the deviation being as large as 8%.

3.2 The Thermal Conductivity Coefficient of Nitrogen

The results are presented in table II, where the density ρ was calculated from the compressibility isotherm (10). The last column of the table gives the thermal conductivity coefficient at 25°C calculated using eq (5) and the value a = 0.065. Thermal conductivity is plotted as a function of density and compared (fig. 5) with the results obtained by Michels and Botzen (11), and by Misic and Thodos (12). The deviation of our results from those of these last authors is in general less than 3%.

3.3 The Thermal Conductivity Coefficient of Methane

Methane was obtained from "Air Liquide" in Paris and, as specified by the suppliers, has a purity of 99.99%. The density ρ has been calculated from the equation of state of Benedict, Webb and Rubin with the coefficients proposed by Katz, et al (13).

The agreement between these calculated values of thermal conductivity and the experimental data of Deffet and Ficks (14) is better than 0.5%.

The results are presented in table III, where the thermal conductivity coefficient at 25°C was calculated by using eq (5) with the coefficient a = 0.152.

In figure 6, λ is plotted as a function of density and is compared with the results of Golubey (15) and those of Misic and Thodos (16). The data found in all these experiments show a satisfactory agreement in the low density range. At high density the deviation between our results and the data of Misic and Thodos reaches 12%. Comparison of the 25°C isotherm to upper isotherms shows the distortion in the critical density range.

The data of Stolyarov, Ipatiev and Teodorovice (19) for the thermal conductivity of methane do not exhibit good consistency and hence are not included in our data comparison.

3.4 The Thermal Conductivity Coefficient of Carbon Dioxide

For carbon dioxide and other gases which have high critical points, such as ethane, it is difficult to find a reference isotherm. At 25°C the saturation line is crossed and anomalies can occur near this curve. In the critical region, measurements of the transport coefficients are hampered by the fact that gravity can easily generate convection currents and convective heat flow. The compressed gas has been obtained by vaporization of the liquid of 99.95% purity.

In table IV some data are presented near the 25°C isotherm for densities far from saturation. The density has been deduced from the compressibility data of Michels, et al (18) and Kennedy (19). In the last column the thermal conductivity coefficient at 25°C has been calculated, using eq (5) with a = 0.082.

In figure 7, where λ is plotted as a function of ρ, it can be seen that the differences for constant density between the isotherm at 132°C and the isotherm at 25°C are approximately the same if one stays far from the saturation line. Therefore, eq (5) can be used to calculate the thermal conductivity coefficient at 25°C. The deviations from the data of Michels, Sengers and Van der Gulik (20) are less that the 1.5% accuracy limits claimed by us.

3.5 The Thermal Conductivity Coefficient of Helium

Helium gas was obtained from the Air Products Company (United States) with a specified purity of 99.997%. The results are presented in tables V and VI. The data in table VI were obtained in experiments on thermal conductivity coefficients of argon-helium mixtures and are comparable with the values obtained by Johannin, et al (4) on helium. The thermal conductivity coefficient at 30°C was calculated using eq (5) with a = 0.317, and where the density was deduced from compressibility data (21, 22).

In figure 8, where λ is plotted in terms of density, it can be seen that for densities up to 10 kg/cm^3, the scatter in the experimental points approaches our 1.5% error limit. For higher densities the consistency is better and our results agree satisfactorily with the data of Tsederberg, et al (23).

At densities from 0.15 to 10 kg/m^3 an accommodation effect associated with the condition of the surface was shown. It can be calculated by extrapolation of the thermal conductivity coefficients in terms of the reciprocal of the pressure. At these densities an impurity effect due to outgassing of the metallic walls should also be considered.

3.6 The Thermal Conductivity Coefficient of Argon-Helium Mixtures

Recently, a study of mixtures of noble gases has been carried out. In figure 9 the thermal conductivity coefficient is plotted in terms of pressure and in figure 10 in terms of composition. A good correlation exists between our results and the data of Iwasake and Kestin (24) on the viscosity of argon-helium mixtures.

3.7 The Thermal Conductivity Coefficient of Steam

The thermal conductivity coefficient of steam is of great industrial interest and several studies have been carried out in the world. A first investigation has been made from 100 to 334°C and from 0.1×10^6 N/m^2 (1 bar) up to the saturation pressure in a tight cell, but mechanical stresses caused by thermal expansion have adversely affected the results. A new study has been undertaken over a larger temperature range.

By now, several measurements have been carried out at high temperatures, and the results will be published next year. Agreement of our results with the most reliable existing data is satisfactory. The sensitivity and the reproducibility of the method is high, and the accuracy is great enough for industrial applications but perhaps insufficient for theoretical investigation.

TABLE I

Thermal Conductivity of Argon

$P \times 10^{-6}$ N/m^2	ρ kg/m^3	T °C	ΔT °C	$\lambda \times 10^3$ $Wm^{-1}deg^{-1}$	$\lambda_{25°C} \times 10^3$ $Wm^{-1}deg^{-1}$
0.1	1.61	29.4	2.40	17.5	17.3
0.1	1.62	24.7	3.43	17.4	17.4
2.9	47	28.6	3.78	18.8	18.6
3.5	58	24.2	3.21	18.6	18.7
4.2	69	30.2	3.27	19.4	19.2
5.1	85	28.2	3.62	19.7	19.5
5.3	87	30.2	2.76	19.7	19.4
5.4	88	37.1	2.68	20.1	19.6
5.4	88	37.6	2.69	20.0	19.5
7.1	121	23.7	2.97	20.3	20.4
7.7	127	27.5	3.44	20.8	20.7
8.4	140	29.6	3.00	21.3	21.1
10.8	179	26.6	3.19	22.5	22.4
13.2	228	22.8	2.58	23.5	23.6
14.7	246	28.8	2.65	24.5	24.3
17.4	293	25.7	2.76	26.4	26.3
21.2	350	29.4	3.39	28.6	28.3
21.2	352	29.0	2.94	28.6	28.4
28.3	458	28.8	2.96	33.1	32.9
30.5	484	28.7	2.47	34.4	34.3
33.2	506	34.4	2.98	35.9	35.5
34.3	522	33.9	2.89	36.6	36.2
38.3	580	28.8	2.51	39.4	39.2
40.1	596	29.8	3.38	40.4	40.2
45.2	649	27.9	2.29	43.5	43.4
49.0	684	27.4	2.86	45.3	45.2
50.1	688	29.4	2.98	46.4	46.2
51.2	691	34.6	2.14	46.2	45.8
51.7	705	27.5	2.11	47.4	47.2
51.8	705	27.2	2.09	47.6	47.5
58.8	741	34.5	1.97	50.3	49.9
60.2	763	29.0	2.67	51.9	51.8
69.0	801	36.5	1.79	55.6	55.1
71.0	805	40.4	3.25	56.4	55.7
79.4	853	38.3	3.06	60.1	59.5
80.1	880	28.5	2.27	61.6	61.5
85.7	905	28.3	2.18	64.3	64.2
89.0	897	38.0	2.86	64.5	63.9
90.2	902	37.9	2.84	65.0	64.5
93.9	937	28.0	2.06	68.3	68.2
98.5	936	37.2	2.70	68.6	68.1
99.6	941	37.0	2.68	69.2	68.7
102.0	958	36.7	2.63	70.4	69.9
105.6	982	27.9	1.92	73.5	73.3
117.8	1022	27.7	1.79	78.7	78.6
125.7	1045	27.8	1.74	81.0	80.9

Table II

Thermal Conductivity of Nitrogen

$P \times 10^{-6}$ N/m^2	ρ kg/m^3	T °C	ΔT °C	$\lambda \times 10^3$ $Wm^{-1}deg^{-1}$	$\lambda_{25°C} \times 10^3$ $Wm^{-1}deg^{-1}$
0.1	1.13	27.4	2.89	25.8	25.7
0.1	1.13	28.9	3.55	26.0	25.8
0.2	2.3	31.0	3.29	26.1	25.7
1.9	22	28.7	3.45	26.9	26.6
3.0	34	30.7	3.14	27.5	27.1
3.3	37	27.1	2.74	27.2	27.1
3.5	40	28.3	3.36	27.7	27.5
3.5	40	28.5	3.36	27.6	27.4
5.2	58	30.2	3.15	28.9	28.6
6.0	68	28.0	3.22	29.0	28.8
6.4	72	26.6	2.59	28.9	28.8
9.2	103	29.3	2.82	30.8	30.5
9.2	104	26.2	2.46	30.5	30.4
9.2	104	27.4	3.05	30.8	30.6
10.1	112	30.1	2.91	31.5	31.2
10.6	120	24.2	2.43	31.3	31.4
12.6	141	26.9	2.87	32.9	32.8
14.2	155	29.1	2.59	33.8	33.5
15.3	166	30.6	3.34	34.9	34.5
15.9	175	26.6	2.70	35.0	34.9
18.5	195	31.5	4.29	36.9	36.5
20.8	214	30.6	3.07	38.1	37.8
21.6	227	26.1	2.45	38.8	38.8
22.3	229	28.7	2.26	39.0	38.8
25.1	252	30.6	3.21	41.2	40.9
30.4	295	30.4	2.97	44.8	44.5
31.8	305	29.0	3.61	45.9	45.6
34.5	323	30.3	2.80	47.6	47.2
40.0	357	30.0	2.62	51.1	50.8
40.5	360	29.9	3.25	51.4	51.1
41.3	364	29.9	3.88	52.0	51.7
45.3	385	29.6	2.45	54.6	54.3
48.8	401	29.5	2.36	56.9	56.6
50.7	410	29.5	3.49	58.1	57.8
51.8	416	29.2	2.87	58.5	58.2
59.3	448	29.1	3.21	63.6	63.3
74.2	500	30.3	2.37	72.3	72.0
75.5	505	28.7	2.82	72.9	72.7
78.6	513	30.2	2.29	74.0	73.6
84.2	528	30.1	2.20	77.1	76.8
85.6	534	28.5	2.62	78.1	77.9
90.2	544	30.0	2.11	80.4	80.1
94.6	557	28.2	2.47	83.5	83.3
98.1	563	29.8	2.01	84.8	84.5
102.7	575	28.0	2.36	87.7	87.5
105.2	581	27.8	2.32	89.2	89.0
107.5	584	29.7	1.90	89.7	89.4
108.8	588	27.8	2.27	91.2	91.0
114.1	599	27.6	2.21	94.0	93.8
118.7	608	27.8	2.16	95.9	95.7

TABLE III

Thermal Conductivity of Methane

$P \times 10^{-6}$ N/m^2	ρ kg/m^3	T °C	ΔT °C	$\lambda \times 10^3$ $Wm^{-1}deg^{-1}$	$\lambda_{25°C} \times 10^3$ $Wm^{-1}\ deg^{-1}$
0.1	0.64	34.2	3.98	35.6	34.2
0.14	0.91	25.5	2.54	34.5	34.4
1.0	6.5	31.3	3.98	35.8	34.9
1.0	6.5	25.4	2.50	35.0	34.9
4.4	29.5	30.7	3.69	38.8	37.9
5.0	35.1	25.3	2.29	38.4	38.4
5.8	40.0	33.2	3.51	40.7	39.3
7.3	52.0	29.7	3.43	41.9	41.2
10.1	76.8	25.7	2.54	45.2	45.1
10.5	74.3	31.6	3.08	46.8	45.8
10.5	78.3	28.3	3.12	46.3	45.8
13.7	103.	31.0	2.81	51.3	50.4
14.7	115.	26.2	2.73	53.2	53.0
16.3	125	30.3	2.61	55.7	54.9
18.5	142	29.6	2.45	59.3	58.6
20.4	159	25.6	2.17	62.6	62.5
21.6	164	28.9	2.27	64.3	63.7
22.3	168	30.1	2.24	65.4	64.6
26.9	193	29.6	2.05	71.6	70.9
30.6	215	25.3	1.77	77.0	77.0
32.3	217	29.4	1.87	78.7	78.1
38.6	241	29.2	1.71	86.3	85.7
40.7	250	25.5	1.76	89.0	89.0
45.4	260	29.2	1.58	93.8	93.2
50.9	275	25.6	1.84	99.7	99.6
51.4	274	29.1	1.49	99.9	99.3
58.2	287	28.9	1.40	106.6	106.0
60.9	294	25.5	1.70	108.8	108.7
69.0	304	28.6	1.29	115.9	115.4
71.5	310	25.5	1.70	118.4	118.3
78.5	317	28.5	1.21	123.2	122.7
82.1	323	25.5	1.70	126.8	126.7
87.0	326	28.3	1.15	129.5	129.0
93.9	333	25.4	1.71	134.4	134.3
95.9	335	28.1	1.10	136.4	135.9
101.7	341	25.3	1.80	141.1	141.0
103.6	342	28.0	1.06	141.9	141.4
106.9	344	28.0	1.04	143.5	143.1
116.2		28.2	1.00	150.6	150.1

Table IV

Thermal Conductivity of Carbon Dioxide

$P \times 10^{-6}$ N/m^2	ρ kg/m^3	T °C	ΔT °C	$\lambda \times 10^3$ $Wm^{-1}deg^{-1}$	$\lambda_{25°C} \times 10^3$ $Wm^{-1}deg^{-1}$
0.1	1.72	35.0	3.73	17.1	16.3
0.1	1.72	35.4	3.72	17.2	16.4
0.38	7.1	22.8	3.65	16.5	16.7
0.45	8.3	22.6	3.64	16.5	16.7
0.83	14.8	34.6	3.64	17.6	16.8
2.00	39	30.9	3.24	18.3	17.8
2.34	41	33.8	3.40	19.0	18.2
2.65	56	22.4	3.29	18.5	18.7
5.51	164	22.5	3.43	27.4	
5.58	172	20.5	2.55	29.8	
5.69	174	21.5	2.11	30.0	
13.1	808	32.9	1.66	90.3	
10.7	840	23.6	3.13	96.0	96.2
16.2	842	33.0	1.55	96.1	95.5
18.8	866	33.0	1.49	100.3	99.7
19.5	872	33.0	1.46	101.9	101.2
19.7	875	32.3	2.64	103.9	103.3
21.1	927	23.4	2.69	112.4	112.6
22.9	896	32.2	2.53	108.4	107.8
30.8	976	23.2	2.45	123.6	123.8
32.3	954	30.6	2.21	120.5	120.0
41.2	1015	23.1	2.27	133.8	133.9
42.1	996	30.0	2.04	130.8	130.3
51.0	1043	22.9	2.14	142.1	142.3
53.2	1028	29.4	1.89	140.8	140.4
62.7	1071	22.7	2.01	151.3	151.1
68.8	1062	31.6	1.83	150.9	150.4
74.0	1094	22.5	1.91	159.6	159.8
82.4	1110	22.4	1.84	165.7	165.9
95.0	1131	22.3	1.77	172.4	172.7
104.1	1145	22.1	1.72	177.5	177.8

Table V

$P \times 10^{-6}$ N/m^2	ρ kg/m^3	T °C	ΔT °C	$\lambda_x \times 10^3$ $Wm^{-1}deg^{-1}$	$\lambda_{30°C} \times 10^3$ $Wm^{-1}deg^{-1}$
0.1	0.15	37.8	2.22	153.6	151.1
0.5	0.82	37.6	2.23	154.6	152.2
1.8	2.76	37.5	2.22	155.3	152.9
3.7	5.60	35.5	2.21	156.2	154.5
4.0	6.10	37.3	2.20	157.0	154.7
6.8	10.28	37.1	2.17	158.8	156.6
7.1	10.69	35.2	2.18	158.6	156.9
10.0	14.85	36.9	2.15	160.5	158.3
10.5	15.62	35.0	2.16	160.6	159.1
12.4	18.75	29.3	2.16	160.4	160.6
12.5	18.44	36.7	2.13	161.0	159.8
15.7	22.85	34.7	2.12	163.2	161.8
16.7	24.21	36.5	2.10	164.1	162.0
20.5	29.30	36.2	2.08	165.8	163.8
21.5	30.6	34.6	2.09	165.9	164.5
25.2	35.3	35.9	2.06	167.9	166.0
30.5	42.0	35.5	2.03	170.4	168.7
31.5	41.7	34.2	2.04	170.4	169.0
36.4	49.0	35.2	2.00	173.0	171.4
41.3	54.6	33.9	1.99	174.7	173.5
42.4	55.8	34.8	1.97	175.8	174.3
49.5	63.6	34.5	1.94	178.8	177.4
50.6	65.0	33.6	1.94	178.9	177.8
57.8	72.8	31.2	1.92	181.8	181.4
59.6	74.2	33.2	1.91	182.6	181.5
60.9	75.2	33.9	1.87	184.0	182.8
62.3	77.2	30.9	1.90	183.6	183.3
66.7	81.6	30.8	1.89	185.0	184.8
69.4	84.0	32.9	1.86	187.4	186.5
74.5	88.6	33.4	1.84	189.8	188.7
79.1	93.0	31.7	1.82	191.2	190.3
81.4	94.8	33.0	1.81	192.7	191.7
87.6	100.4	32.3	1.79	195.0	194.3
90.2	102.4	32.6	1.77	197.0	196.2
94.1	106.0	32.1	1.76	197.9	197.2
97.8	108.9	32.0	1.75	199.8	199.2
98.3	109.4	31.8	1.75	200.2	199.7
104.9	114.6	31.6	1.72	203.0	202.6
105.9	115.4	31.5	1.72	203.7	203.2
106.2	115.6	31.8	1.72	203.3	202.8
108.9	117.6	31.5	1.71	205.2	204.7
112.8	120.6	31.6	1.69	206.4	205.9
113.8	121.4	31.6	1.69	207.0	206.6
118.7	125.0	31.5	1.67	209.0	208.5
121.8	127.2	31.4	1.66	209.8	210.2
125.3	129.8	31.4	1.65	211.5	211.1
128.5	132.2	31.4	1.64	212.9	212.4

Table VI

0.1	0.16	31.9	2.52	152.9	152.3
0.79	1.20	31.6	2.48	155.3	155.4
1.76	2.74	31.2	2.47	156.6	156.3
3.48	5.43	30.8	2.46	157.2	157.0
6.90	10.59	30.4	2.44	158.4	158.3
10.44	15.82	29.8	2.42	159.5	159.5
14.55	21.71	29.0	2.39	161.4	161.9
14.55	21.71	29.0	2.40	161.3	161.7

4 References

(1) Le Neindre B., Johannin P., Vodar B. C.R. Acad. Sci. Paris 258, 3277(1964)

(2) Le Neindre B., Johannin P., Vodar B. C.R. Acad. Sci. Paris 260, 67 (1965)

(3) Johannin P. Journal de Recherches C.N.R.S. 43, 116 (1958)

(4) Johannin P., Vodar B., Wilson H. Progress in International Research on Thermodynamic and Transport Properties A.S.M.E. 418, (1962)

(5) Johannin P., Le Neindre B., Vodar B. Experimental methods to study thermal conductivity coefficients of fluids - Sixth Conference on Thermal Conductivity. N.P.L. London July 1964

(6) Michels A., Sengers J.V. and Van der Gulik P.S. Physica 28, 1216 (1962)

(7) Michels A., Wijker Hub and Wijker Hk Physica 15, 627 (1949)

(8) Michels A., Sengers J.V. and Van der Klundert L.J.M. Physica 29, 149 (1963)

(9) Tsederberg N.V., Popov V.N. and Morosova N.A. Teploenergetika, 6, 82 (1960)

(10) Michels A., Lunbeck R.J., and Wolkers G.J. Physica, 17, 801 (1951)

(11) Michels A., Botzen A. Physica, 19, 585 (1953)

(12) Misic D., Thodos G. A.I. Ch. E. Journal, 11, 650 (1965)

(13) Katz D.L. and Others Handbook of Natural Gas Engineering Mc Graw Hill Book Company.N.Y. (1959)

(14) Deffet L., Ficks F. Advances in Thermophysical Properties at Extreme Temperatures and Pressures Purdue. A.S.M.E. (1965)

(15) Golubev I.F. Teploenergetika, 12, 78 (1963)

(16) Misic D., Thodos G. Physica, 32, 885 (1966)

(17) Stolyarov E.A., Ipatiev V.V. and Teodorovich V.P. Zhur Fiz. Khim. 24, 166 (1950)

(18) Michels A., Michels C. Proc. Roy. Soc. (London) 160 A., 348 (1937)

Michels A., Michels C., Wouters H. Proc. Roy. Soc. (London) 153 A., 214 (1935)

Michels A., Blaisse B., Michels C. Proc. Roy. Soc. (London) 160 A., 358 (1937)

(19) Kennedy G.C. American Journal of Sciences 252, 225 (1954)

(20) Michels A., Sengers J.V., and Van der Gulik E.S. Physica, 28, 1201 (1962)

(21) Michels A., Wouters H. Physica, 8, 923, (1941)

(22) Wiebe R., Graddy V.W., Heins C. J. Amer. Chemical Society 53, 1721 (1931)

(23) Tsederberg N.V., Popov V.N., Morozova N.A. Thermo-Physical Properties of Helium. Gosenergoizdat (1961)

(24) Iwasaki H., Kestin J. Physica, 29, 1345 (1963)

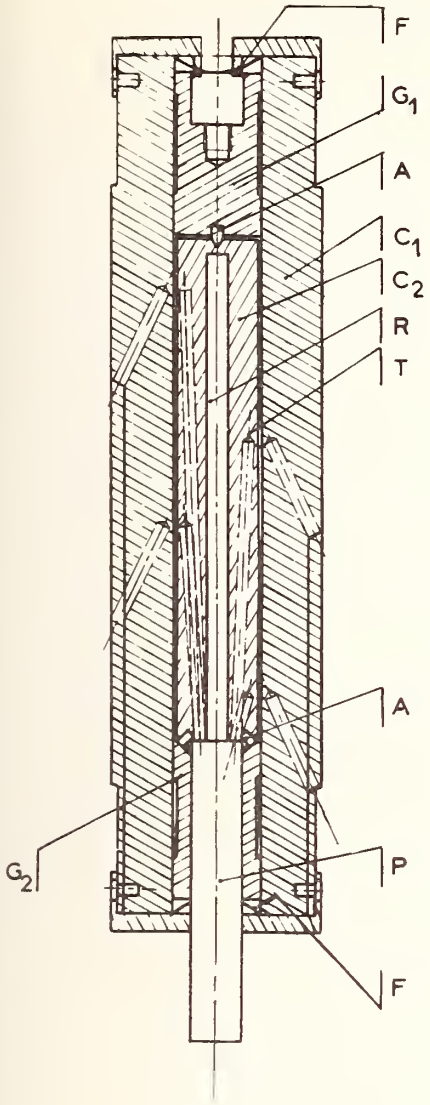

Figure 1. The thermal conductivity cell.
C_1, external cylinder; C_2, internal cylinder; G_1, and G_2, centering pieces; R, heater; T, thermocouple hole; A, isolating plug, P, ceramic piece; F, spring.

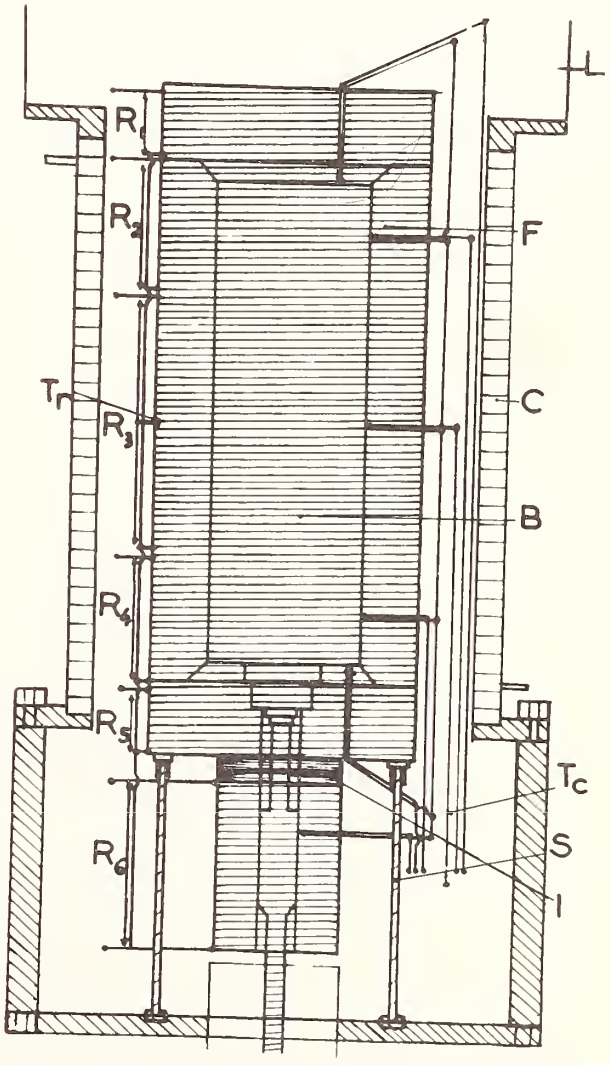

Figure 2. The thermostat and the high pressure vessel.
B, high pressure vessel; F, thermostat; L, rock-wool isolating; C, water jacket; S, isolating support, R_1 R_2 R_3 R_4 R_5 R_6 heaters; Tr, control thermocouples; T_c, measuring thermocouple; I, isolating piece.

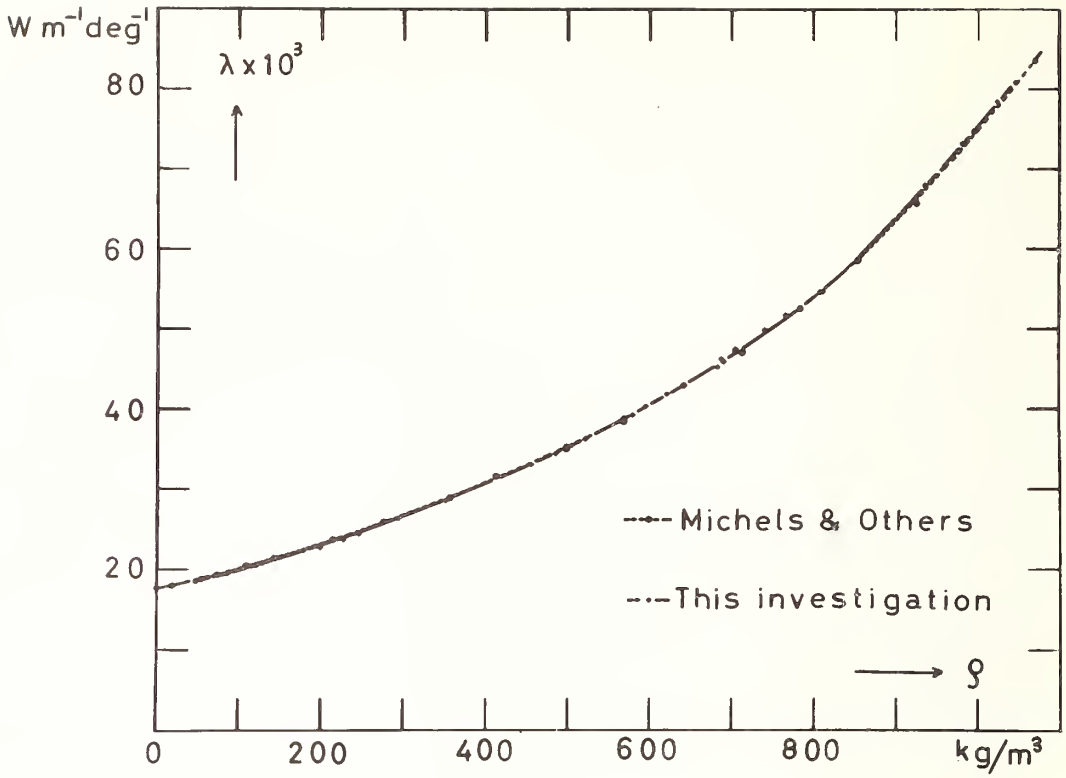

Fig. 3 - The thermal conductivity coefficient of argon at 25°C versus density

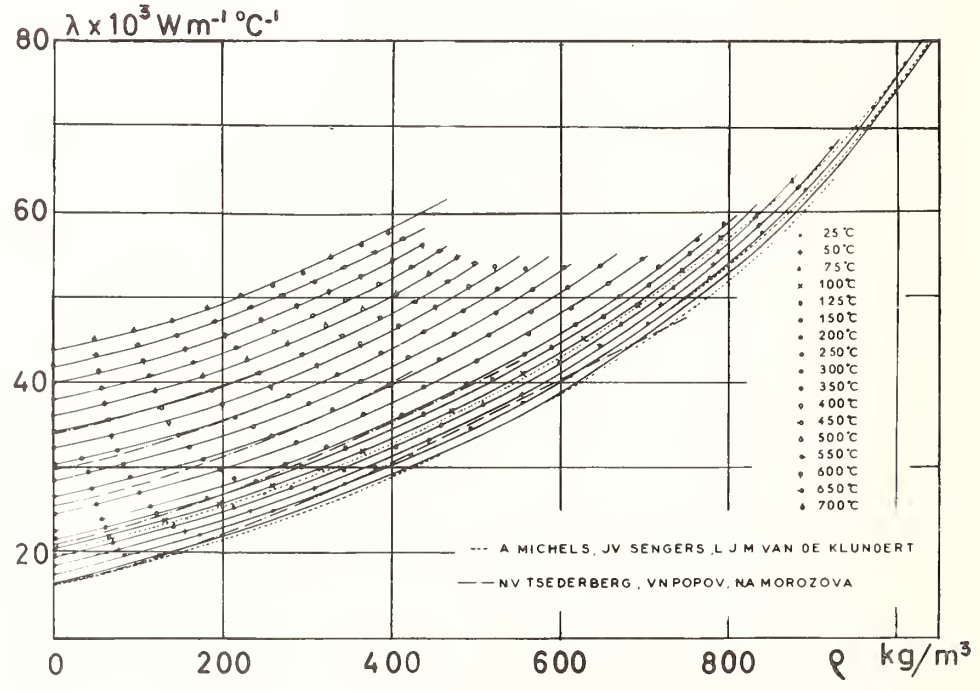

Fig. 4 - Isotherms of thermal conductivity coefficients of argon versus density from 25°C to 700°C

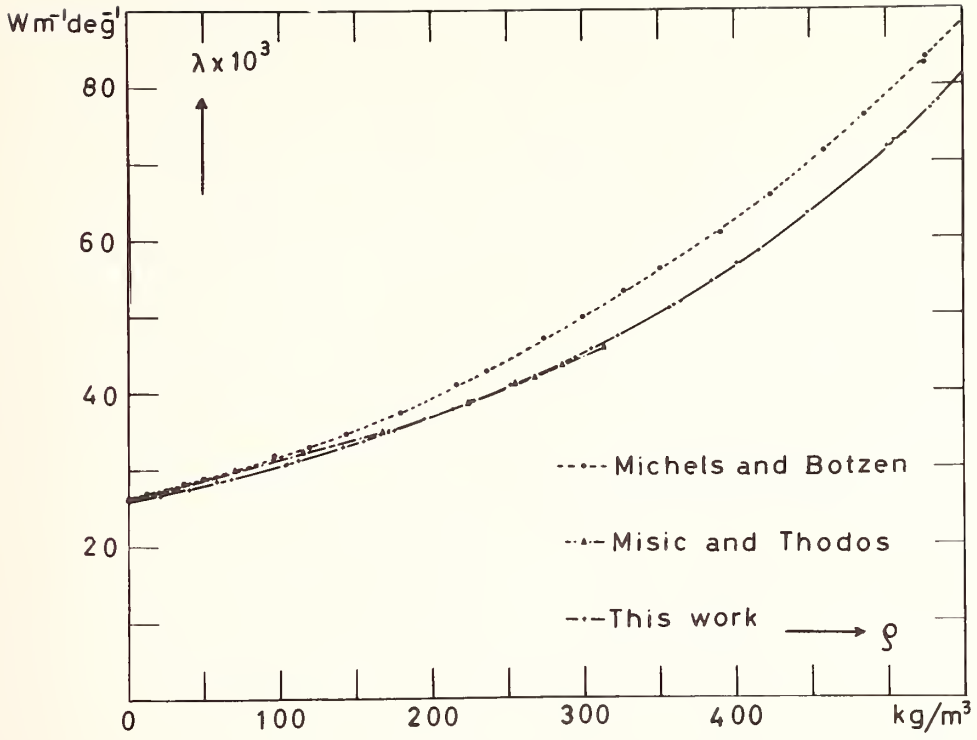

Fig. 5 - The thermal conductivity coefficient of nitrogen at 25°C versus density

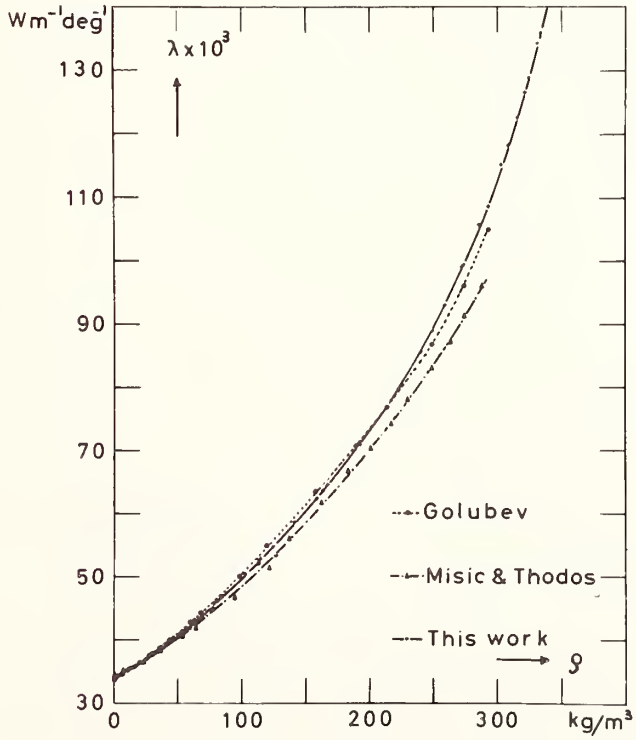

Fig. 6 - The thermal conductivity coefficient of methane at 25°C versus density

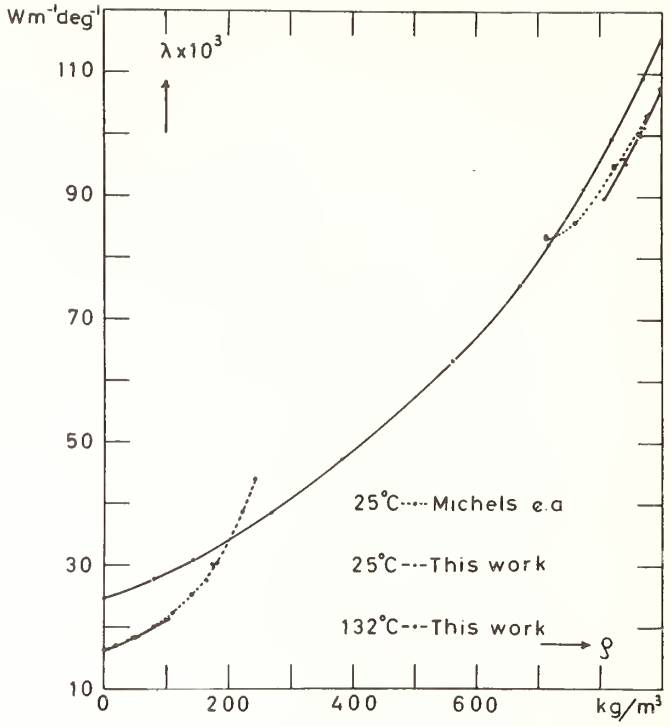

Fig. 7 - The thermal conductivity coefficient of carbon dioxide versus density at 25°C and 132°C

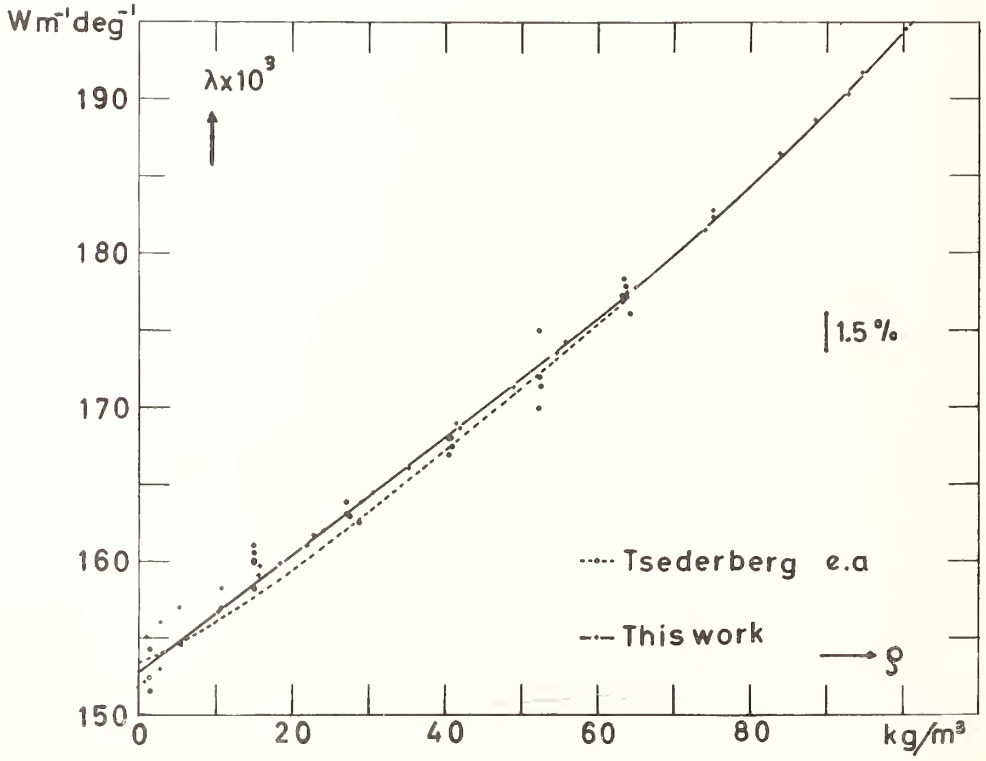

Fig. 8 - The thermal conductivity coefficient of helium at 30°C versus density

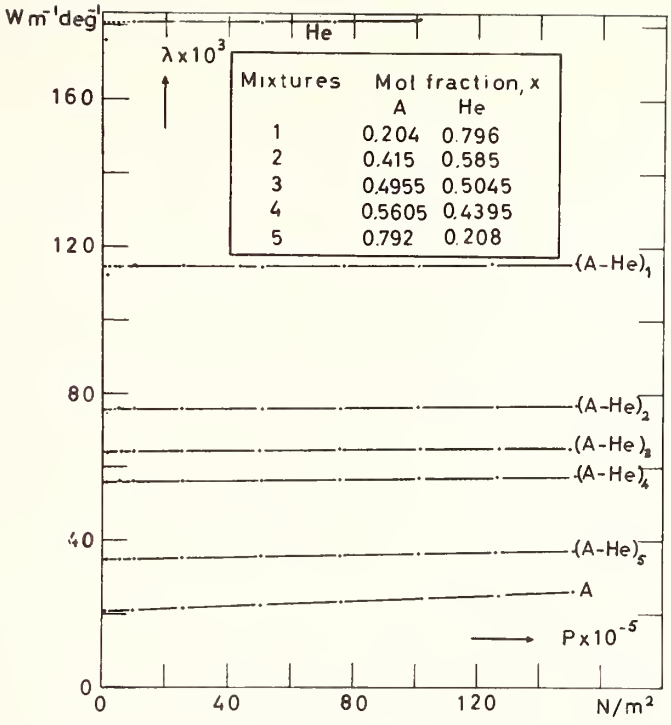

Fig. 9 - The thermal conductivity coefficient of argon helium mixtures in terms of pressure for several compositions at 97°C

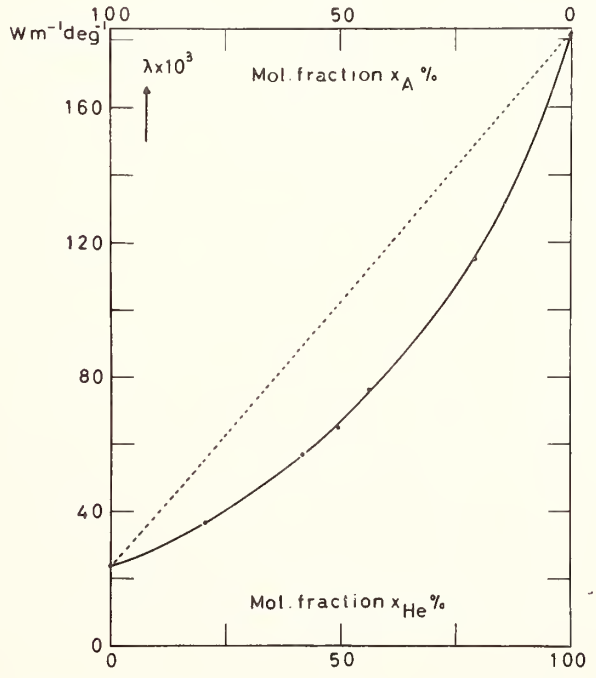

Fig. 10 - The thermal conductivity coefficient of argon helium mixtures in terms of composition at $10x10^6$ N/m^2 (100 bar) and at 97°C

Theoretical Developments on the Density Dependence of the Thermal Conductivity of Compressed Gases

J. V. Sengers

National Bureau of Standards
Washington, D. C.

In contrast to the thermodynamic properties of gases the thermal conductivity as well as other transport properties cannot be represented by a virial expansion in terms of the density. The reason is that the occurrence of multiple collisions leads to dynamical correlations whose characteristic length is associated with the mean free path which itself is a function of the density and becomes infinite at low densities. As a result the transport properties contain terms logarithmic in the density. A summary will be given of theoretical results obtained for a model gas to illustrate these effects. Implications for the interpretation of experimental thermal conductivities of gases will also be discussed.

Discrepancies Between Viscosity Data for Simple Gases[1]

H. J. M. Hanley and G. E. Childs

Cryogenic Data Center
Institute for Materials Research
National Bureau of Standards
Boulder, Colorado

It has been known for some time that Kestin and his co-workers have reported dilute gas viscosity coefficients which differ from the usually accepted values. Recent work from the Los Alamos Scientific Laboratory supplements Kestin's results. We show that there is no evidence for not accepting this different data. We feel that the whole subject of dilute gas viscosity measurements above room temperature should be reexamined both from the experimenter's and correlater's viewpoint. There is evidence that published tables may be incorrect by as much as 10% above 600°K.

Key Words: Argon, correlation, dilute gas, discrepancies, high temperature viscosity, potential function.

1. Introduction

Numerous experimental workers have studied the viscosity of dilute gases. One might indeed assume that the experimental aspects of the viscosity have been sufficiently covered for the common gases and that the viscosity coefficient tables available are satisfactory. This assumption is not valid. We show here that, because of a serious and largely ignored disagreement over experimental values, published tables of the viscosity coefficient above room temperature are likely to be incorrect.

2. Kinetic Theory Expression for the Viscosity Coefficient

Kinetic theory provides rigorous expressions for dilute gas transport coefficients. For the viscosity coefficient, η, we have [1][2]:

$$\eta = \frac{266.93\ (MT)^{\frac{1}{2}}}{\sigma^2\ \Omega^{(2,2)*}\ (T^*)} \times 10^{-8}\ \text{N s m}^{-2}\ . \qquad (1)$$

Here M is the molecular weight, $T(°K)$ the temperature, and $\sigma(Å)$ is a parameter representing the distance between two molecules. The term $\Omega^{(2,2)*}(T^*)$ is called the collision integral: the entity involving the collision dynamics and the intermolecular potential between two molecules. The collision integral is determined as a function of reduced temperature, T^*. The reduced temperature is defined by the relation, $T^* = T/(\epsilon/k)$, where ϵ is the maximum energy of attraction between the molecules, and k is Boltzmann's constant.

Equation (1) can, however, only be applied to experiment if we know the intermolecular potential function. Only then can we compute $\Omega^{(2,2)*}$ and obtain values for σ and ϵ/k. Quantum mechanics has yet to derive a function from first principles so we are required to use a function based on a model. Hence the ability to use eq (1) to correlate and predict experimental data rests on a proper choice of the model function.

---

[1] This article is essentially that of H. J. M. Hanley and G. E. Childs, Science, 159, 1114 (1968), copyright 1968 by the American Association for the Advancement of Science.

[2] Figures in brackets indicate the literature references at the end of this paper.

In the past, one has usually relied on intuition to make this choice. Recently, however, we have clarified the overall relation of model functions, theoretical expressions (such as eq (1)), and experiment [2-4]. Two points from this study are relevant here so we list them:

1. Potential functions have been derived and classified in terms of families. For example we have the m-6 family where m is a family parameter. If U(r) is the interaction potential of two molecules separated by distance r, the functions of the m-6 family are written:

$$U(r) = \epsilon \left[\left(\frac{\sigma}{r}\right)^{m} - \left(\frac{\sigma}{r}\right)^{6} \right] \Big/ \left[\left(\frac{6}{m}\right)^{\frac{6}{m-6}} - \left(\frac{6}{m}\right)^{\frac{m}{m-6}} \right], \qquad (2)$$

where the distance parameter σ is equal to the distance separating the molecules when $U(r) = 0$. The family parameter, m, depicts the repulsive part of the interaction. When $m = 12$, we have the famous 12-6 or Lennard-Jones potential.

The exponential:6 (Exp:6) family is frequently used. The characteristic family parameter here represents the steepness of the repulsive part of the interaction potential and is given the symbol α. Other families of interest are the Kihara and the Morse.

Now we have shown that all families are essentially part of the same large family with respect to their relation to experiment. This means that if we can fit a member of a given family to experimental data via a theoretical expression, we can get the same fit from a member of another family. Alternatively, members of different families can be interchanged without materially altering the fit. There is nothing special about any of the families known at this time. They are equivalent.

2. We can only make a significant selection of a function and its parameters from experiment if we have data outside the reduced range of about

$$2 < T^{*}_{12\text{-}6} < 5 \; . \qquad (3)$$

Here $T^{*}_{12\text{-}6}$ is given by $T^{*}_{12\text{-}6} = T/(\epsilon/k)_{12\text{-}6}$, where $(\epsilon/k)_{12\text{-}6}$ is the well-depth parameter for the gas from the 12-6 function[3]. Any function will fit data in the range of eq (3). We must have data outside this range if we are to find a function suitable for extrapolation purposes. We give an example for the case of argon. Since $(\epsilon/k)_{12\text{-}6}$ for argon is about 120°K, the range of eq (3) is approximately $240 < T°K < 600$. We have found that all the functions of all the families tested can, via eq (1), fit experimental viscosity data in this range. An example has been published as figure 2 of reference [5] (see also [3, 4]). The point we wish to make is that only one member of a family can fit this data and data above 600°K. Furthermore, if we fit data above 600°K with a given function, we will automatically fit data in the range $240 < T°K < 600$.

We mention the above two points because our discussion makes use of fits of kinetic theory expressions to experimental data. We feel that the fits given below are satisfactory and that any conclusions are not influenced by our choice of potential functions.

3. Experimental Discrepancies

There is a disagreement between two sets of experimental viscosity coefficient data for several gases. The disagreement is depicted for the case of argon in figure 1. One set, open circles, represents data points which are generally accepted as correct and which are used to compute the tabulations available. Here we have fitted this set to eq (1) with the 40-6 potential function. The references for these points are given in another publication [5], but data above 500°K are mainly from the work of Trautz and Vasilesco [6]. The other set, closed circles, are points from the work of Kestin and coworkers [7-9] (300 - 570°K) and from recent work by a group at the Los Alamos Scientific Laboratory, which we designate by G. M. W. [10] (1100 - 2100°K). These closed circle points were also fitted to the 40-6 function. It is very obvious that the discrepancy is striking. Up to this point the potential function plays no special role with respect to the discrepancy. The potential function is merely being used to represent data as far as figure 1 is concerned. A similar diagram would be obtained if the average of the open circle data set was used as a reference for figure 1.

---

[3] This deviation is made only for convenience. The factor $(\epsilon/k)_{12\text{-}6}$ is available for most substances. There is nothing special about the 12-6 function here.

The discrepancy between the work of Kestin and the work of others has been known, of course, for some time. Mason also reported several years ago [11] that the high temperature viscosity data of Trautz and Vasilesco could be in error. For tabulation purposes, however, the discrepancy has usually been overlooked, possibly due to the simple fact that Kestin's results are different. In fairness to this negative point of view, it is only recently that high temperature data have become available to supplement Kestin's work. Also much of Kestin's results lie in the temperature range of eq (3). This being the case it is difficult to pin down a correlating function from these data alone (point 2 above) and the discrepancy could have been caused by systematic error. The situation is different when we take Kestin and G. M. W. together. One can show by plotting their data on the same graph that their data are compatible and, furthermore, here we have data which are definitely outside the range of eq (3) and so can make positive statements on the correlating potential function.

Figure 2 shows the fit of Kestin and the G. M. W. data alone. We found that an m of about 12 or 15 was the best. Eventually we used the Exp:6 function with $\alpha = 15$. This is equivalent to an m of about 13. (Remember, point 1 above, there is absolutely no significance in changing from one family to another. We changed to the Exp:6 family only because we did not have available collision integrals for $m = 13$ or 14).

4. Analysis

We now show that there is no justification for omitting the Kestin (and now G. M. W.) work. Indeed, we give substantial evidence that this work is correct.

Part of our analysis is based on the fact that kinetic theory predicts that the thermal conductivity of a dilute monatomic gas, λ, is linearly related to the viscosity by the expression:

$$\lambda = f\, c_v\, \eta \tag{4}$$

where c_v is the specific heat per gram at constant volume and f is a constant. Theory predicts that this constant is very close to 2.50. Explicitly the kinetic theory expression for λ is [1]:

$$\lambda = \frac{8.3264\ (T/M)^{\frac{1}{2}}}{\sigma^2\ \Omega^{(2,2)*}\ (T^*)} \times 10^{-6}\ \text{W m}^{-1}\ \text{deg}^{-1}\ . \tag{5}$$

If one can properly fit experimental viscosity data to eq (1), then one must be able to represent experimental thermal conductivity data by eq (5) without altering the correlation parameters. We thus determined theoretical thermal conductivity coefficients for argon from eq (5) using the function and parameters found suitable for the open circle viscosity data. These values were compared to experimental values taken from references [12-17]. Figure 3 shows the deviation curve. This figure clearly indicates that the correlation of λ is not satisfactory, even allowing for the wide scatter of the thermal conductivity data. There is a systematic trend of the data away from a proper fit. This deviation has been observed before but usually has been attributed to f rather than to errors in η or λ. There is no theoretical evidence that f (i.e., eqs (1) and (5)) can change by an amount necessary to cause the systematic deviation of figure 3.

Let us see what happens when we fit the thermal conductivity to the Exp:6 function with $\alpha = 15$, i.e., "fit" on the basis of the Kestin and G. M. W. data. The result, given as figure 4, shows a substantial improvement over figure 3. (It should be noted that the parameters used could be adjusted so as to balance the deviations of fig. 4 around zero. In particular, this could be done while keeping the fit of the viscosity data to within the experimental precision. We have not done this; our only purpose was to check the thermal conductivity on the basis of a fit to viscosity which was not prejudiced by other considerations. We stress that any adjustment would involve a small change in ϵ/k or σ, not in α or m).

We have another simple, but less exact, procedure which does not involve a potential function. Assuming that the gases obey the principle of corresponding states, a reduced viscosity, η_R, should be a universal function of reduced pressure p/p_c and reduced temperature T/T_c. Here p_c and T_c are the critical pressure and temperature respectively. The reduced viscosity is then given by

$$\eta_R = \eta_{expt}\, M^{-1/2}\, p_c^{-2/3}\, (RT_c)^{(1/6)}\ . \tag{6}$$

We know that the principle of corresponding states is not precisely obeyed for the noble gases and obeyed only approximately for polyatomic gases of simple structure. Nevertheless eq (6), and others like it, provide a simple method to correlate data. Figure 5 shows a plot of the reduced viscosity of argon from Trautz and the workers who agree with him (open circles), and from Kestin and G. M. W. (closed circles). Also included are reduced viscosities of neon (squares) and hydrogen (triangles). These latter viscosities are reduced from measurements taken below 400°K and are assumed not to have the systematic deviation represented by figure 1. Because of the approximate nature of the principle of corresponding states and uncertainties in the values of p_c and T_c (especially for neon) we can only expect to see a trend from figure 5. This is what we get: No points fall on a single line, but it is apparent that the closed circles are closer to such a line than are the open circles.

4.1 Evidence from Elastic Scattering

From figure 3 and, to a much lesser extent, figure 5, the evidence is in favor of the Kestin and G. M. W. data. However, we have found that both the 40-6 and 13 (approx.)-6 functions fit the two sets of viscosity data. Can we decide between the two functions from an independent experiment? We think we can. The repulsive part of the intermolecular potential can be estimated from precise and powerful experiments on the elastic scattering of high energy beams of neutral atoms. Results from these experiments for argon indicate that the repulsive exponent is between 7 and 14 [19]. Hence, if we assume that the 40 and 13 exponents of the 40-6 and 13-6 functions respectively are indicative of the true repulsion, then the conclusion from scattering experiments is that one must favor the 13-6 potential and rule out the 40-6 potential.

5. Conclusion

We have demonstrated that the work of Kestin and G. M. W. cannot be excluded from future estimates of the viscosity coefficient of argon above room temperature. We have based our arguments on argon because a) eqs (1) and (4) are only valid for monatomic gases, b) thermal conductivity data for the other monatomic gases are not available in the required temperature range to allow us to repeat figures 3 and 4, and c) the elastic scattering of the argon-argon system has been particularly well studied.

A further argument in favor of the Kestin and G. M. W. results can be based on the fact that not only are the two experiments independent, but the methods are entirely different. Kestin's measurements were made with an oscillating disc viscometer while the Los Alamos measurements were made with a capillary viscometer. Each of the methods is presumably subject to different systematic errors. The presence of large systematic errors of the same sign and magnitude in both experiments would seem highly improbable.

Our conclusion is not restricted to argon, however. Trautz and his co-workers have had a tremendous influence on high temperature viscosity estimates for many gases. If he (and other authors who agree with him) is incorrect for argon, he is possibly incorrect for the other gases. We mention, in this respect, that Kestin and co-workers report a disagreement between their results and Trautz's and other workers for several gases [9] (e.g., CO_2, N_2, Ne, H_2, He, Kr, air). The Los Alamos group [10], as well, report results for hydrogen, helium and nitrogen which differ from the previously accepted values, but which seem to agree with Kestin's results.

Hence we believe that the dilute gas viscosity coefficients above room temperature for all simple gases (Ar, Ne, Kr, He, H_2, O_2, N_2, etc.) should be reexamined both from the experimenter's and correlater's point of view. Not only are new experiments clearly required, but an analysis of the old experiments, with an eye to discover possible overlooked corrections, is necessary.

6. Acknowledgement

This work was supported by the National Aeronautics and Space Administration's Office of Advanced Research and Technology, Contract number R-06-006-046.

7. References

[1] Hirschfelder, J. O., Curtiss, C. F., and Bird, R. B., Molecular Theory of Gases and Liquids, 2nd edition (Wiley, 1964).

[2] Klein, M., Determination of intermolecular potential functions from macroscopic measurements, J. Res. Nat. Bur. Std. 70A, 259 (1966).

[3] Hanley, H. J. M., and Childs, G. E., The viscosity and thermal conductivity coefficients of dilute neon, krypton, and xenon, Nat. Bur. Std. Technical Note 352 (March 1967).

[4] Hanley, H. J. M., and Klein, M., On the selection of the intermolecular potential function: application of statistical mechanical theory to experiment, Nat. Bur. Std. Technical Note 360 (November 1967).

[5] Hanley, H. J. M., Comparison of the Lennard-Jones, exp-6, and Kihara potential functions from viscosity data of dilute argon, J. Chem. Phys. 44, 4219 (1966).

[6] Trautz, M., and Zink, R., Die reibung wärmeleitung und diffusion in gasmischungen. XII. Gasreibung bei höheren temperaturen (The viscosity, heat conduction and diffusion of gas mixtures. XII. The viscosity of gases at higher temperatures), Ann. Physik 7, 427 (1930); Vasilesco, V., Recherches experimentales sur la viscosite des gaz aux temperatures elevees (Experimental research on the viscosity of gas at high temperatures), Ann. Phys. (Paris) 20, 137 (1945).

[7] Kestin, J., and Leidenfrost, W., An absolute determination of the viscosity of eleven gases over a range of pressures, Physica 25, 1033 (1959).

[8] Kestin, J., and Whitelaw, J. H., A relative determination of the viscosity of several gases by the oscillating disk method, Physica 29, 335 (1963).

[9] DiPippo, R., An absolute determination of the viscosity of seven gases to high temperatures, Ph.D. Thesis, Brown Univ. (June 1966).

[10] Guevara, F. A., McInteer, B. B., and Wageman, W. E., private communication. These authors have made their results on hydrogen, helium, argon, and nitrogen available prior to submitting them for publication. The data may still be subject to minor modifications (± 1%).

[11] Mason, E. A., and Rice, W. E., The intermolecular potentials for some simple nonpolar molecules, J. Chem. Phys. 22, 843 (1954).

[12] Michels, A., Sengers, J. V., and Van de Klundert, L. J. M., The thermal conductivity of argon at elevated densities, Physica 29, 149 (1963).

[13] Eucken, A., Über die temperaturabhängigkeit der Wärmeleitfähigkeit einiger gase (Concerning the temperature dependence of thermal conductivity of several gases), Physik. Z. 12, 1101 (1911).

[14] Keyes, F. G., and Vines, R. G., The thermal conductivity of nitrogen and argon, J. Heat Transfer 87, 177 (1965).

[15] Kannuluik, W. G., and Carman, E. H., The thermal conductivity of rare gases, Proc. Phys. Soc. (London) B65, 701 (1952).

[16] Rothman, A. J., Thermal conductivity of gases at high temperatures, U. S. Atomic Energy Comm. UCRL 2339, (1953).

[17] Vargaftik, N. B., and Zimina, N. Kh., Heat conductivity of argon at high temperatures, High Temperature 2, 645 (1964), translated from Teplofiz. Vysok. Temp. 2, 716 (1964).

[18] Johnston, H. L., and McCloskey, K. E., Viscosities of several common gases between 90°K and room temperature, J. Phys. Chem. 44, 1038 (1940); Buddenburg, J. W., and Wilke, C. R., Viscosities of some mixed gases, J. Phys. Colloid Chem. 55, 1491 (1951); Michels, A., Schipper, A. C. J., and Rintoul, W. H., The viscosity of hydrogen and deuterium at pressures up to 2000 atmospheres, Physica 19, 1011 (1953).

[19] Amdur, I., and Mason, E. A., Scattering of high-velocity neutral particles. III. Argon-argon, J. Chem. Phys. 22, 670 (1954); Amdur, I., and Jordan, J. E., Molecular Beams, Editor, J. Ross (Interscience, 1966).

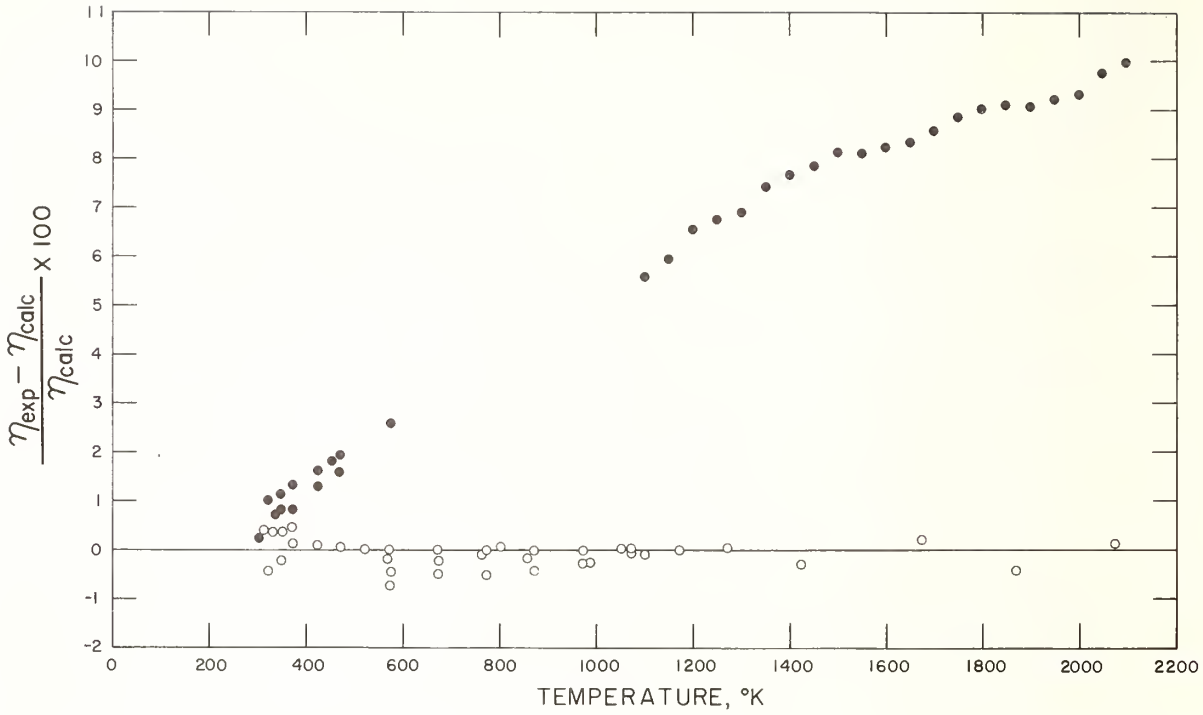

Figure 1. Argon viscosity percent deviation curve. η_{calc} represents the calculated viscosity coefficients from eq(1) using the 40-6 function with σ = 3.15 Å and ϵ/k = 224.1°K. η_{exp} represents the experimental viscosity coefficients. Open circles represent data of Trautz and Vasilesco [6] and other workers [5]. Closed circles represent data of Kestin and co-workers [7-9] and Wageman and co-workers [10].

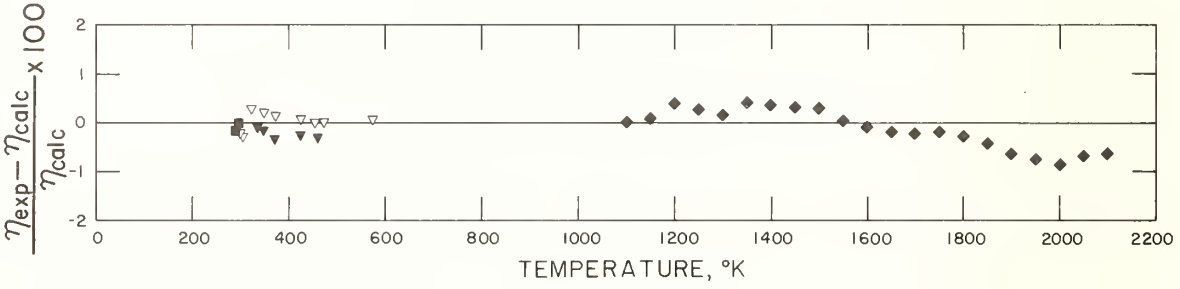

Figure 2. Argon viscosity percent deviation curve. η_{calc} represents the calculated viscosity coefficients from eq(1) using the Exp:6 function with α = 15, σ = 3.68 Å, ϵ/k = 156.5°K. η_{exp} represents Kestin and G. M. W. experimental viscosity data. (This function is very similar to the 13-6 function). Key: ■ [7], ▼ [8], ▽ [9], ◆ [10].

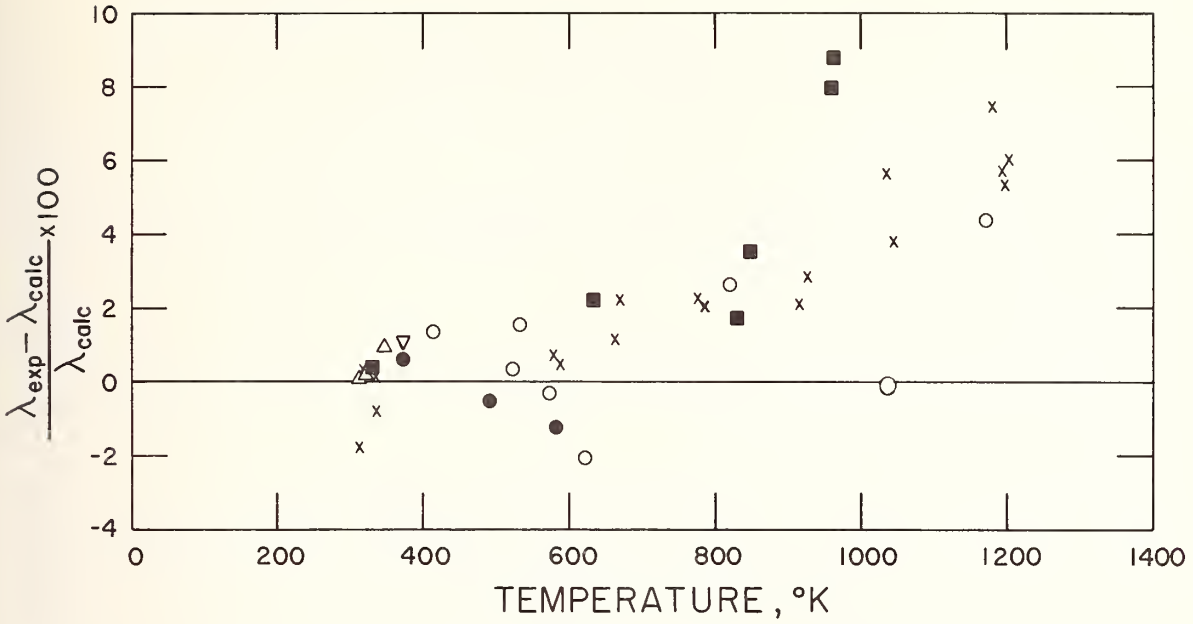

Figure 3. Argon thermal conductivity percent deviation curve. λ_{calc} and λ_{exp} represent the calculated and experimental thermal conductivity coefficients with respective parameters suitable for the viscosity correlation of figure 1. Key: △ [12], ▽ [13], ○ [14], ● [15], □ [16], X [17].

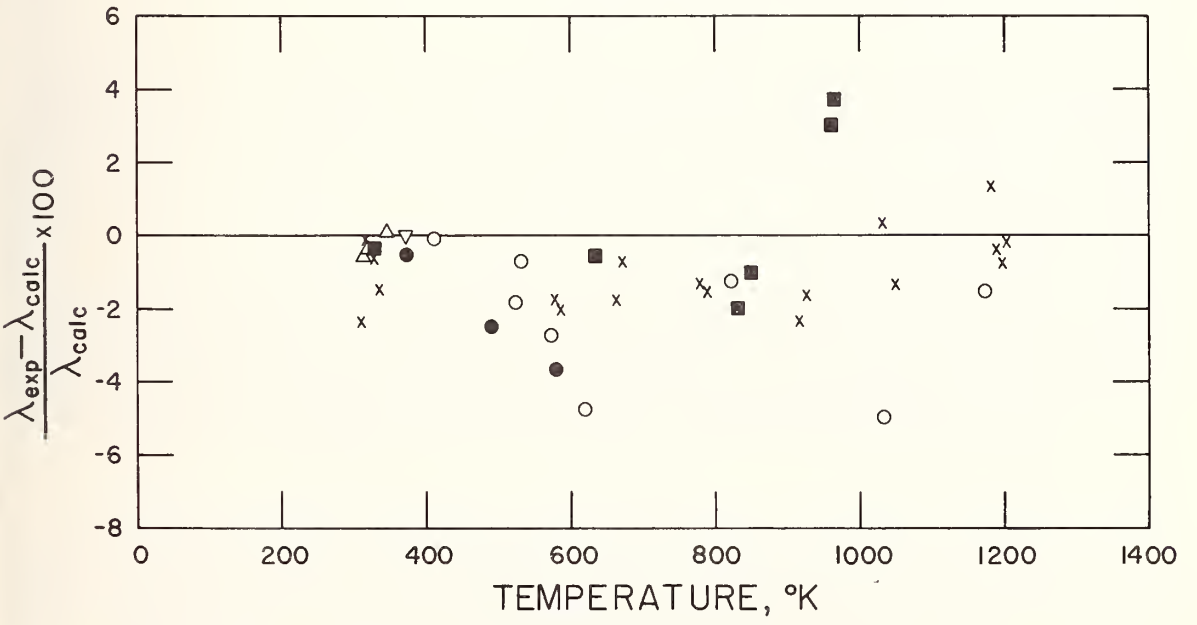

Figure 4. Argon thermal conductivity percent deviation curve λ_{calc} and λ_{exp} represent the calculated and experimental thermal conductivity coefficients with respective parameters suitable for the viscosity correlation of figure 2. Symbols as in figure 3.

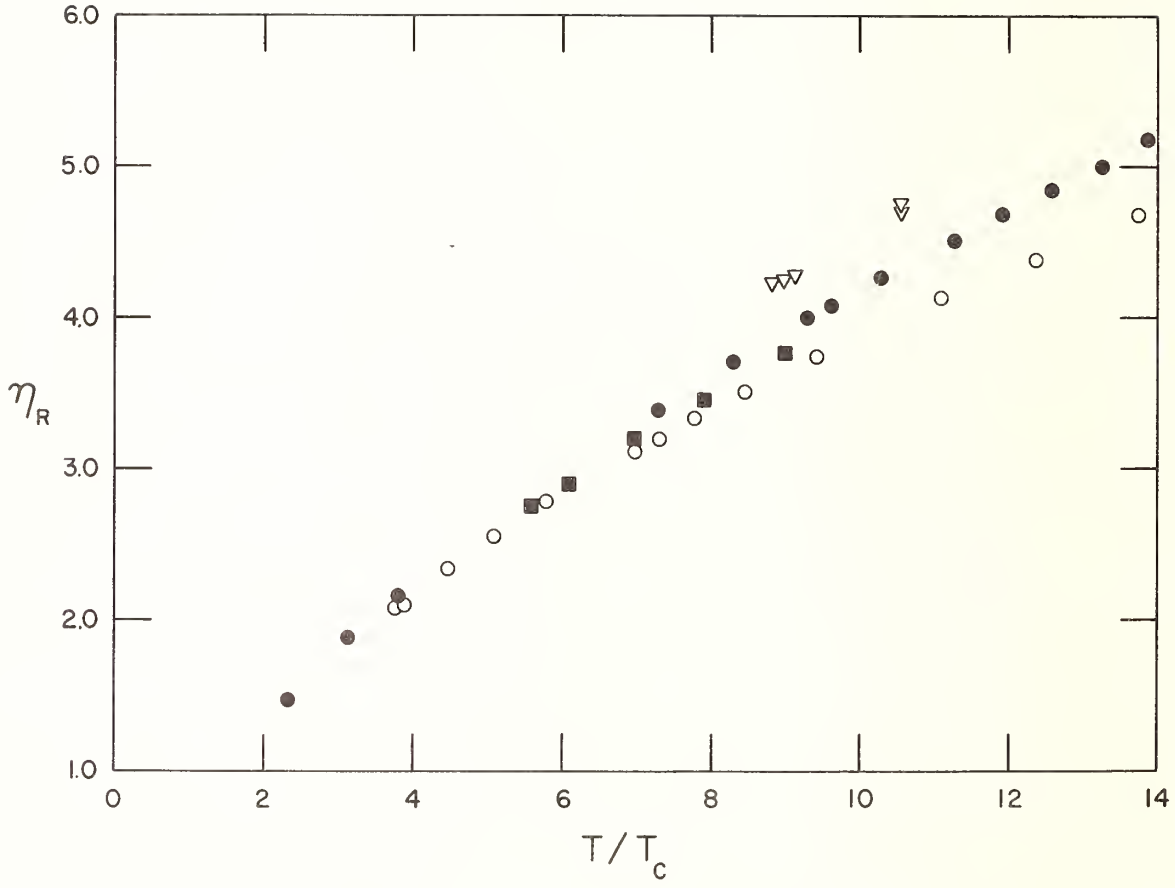

Figure 5. Plot of the viscosity reduced by critical values, eq (6), versus T/T_c where T_c is the critical temperature. The closed circles are reduced argon viscosities from Kestin and G. M. W., open circles are reduced from Trautz and the workers who agree with him. The squares are reduced viscosities of neon taken from reference [3]. The triangles are viscosities for hydrogen [18]. Both the neon and hydrogen data are measurements taken below 400°K.

Thermal Conductivity of Binary, Ternary and Quaternary Mixtures of Polyatomic Gases

S.C. Saxena

Thermophysical Properties Research Center, Purdue University, West Lafayette, Indiana

and

G.P. Gupta

Department of Physics, University of Rajasthan, Jaipur, Rajasthan, India

The thermal conductivity of argon, hydrogen, oxygen, nitrogen, argon-hydrogen, argon-nitrogen, argon-oxygen, argon-hydrogen-nitrogen and argon-hydrogen-nitrogen-oxygen systems are reported at temperatures 40°, 65° and 93° C, and for mixtures at several compositions. The measurements are taken on a thick-wire cell of the hot-wire type. The experimental results are compared with the predictions of rigorous theory as well as with the values obtained on approximate, semitheoretical, and Lindsay-Bromley methods. The competence of some simpler procedures to predict thermal conductivity of multicomponent mixtures is also investigated with conclusions of some practical importance.

Key Words: Gases, kinetic theory, multicomponent mixtures, thermal conductivity, thick-hot-wire cell.

1. Introduction

In the last few years we have been engaged in a program of measurement of thermal conductivities of rare gases and their binary and ternary mixtures [1-3][1], and deuterium and its binary and ternary mixtures with rare gases [4,5]. The method adopted was the thick-wire variant of the hot-wire cell and measurements covered the temperature range 30° to 100° C. The details of the apparatus, theory of the method and various corrections which need to be applied are being reported in a recent paper [6]. The general incentive behind the work has been: (a) to check the rigorous kinetic theories in their appropriateness to explain heat transfer through gases and gas mixtures, (b) to examine and develop new correlation procedures so that reliable estimation may become possible wherever direct data are not available, and (c) to resolve in due course some of the discrepancies observed in the existing data [7-10].

The present paper reports as a continuing effort of this program thermal conductivity data on Ar, H_2, N_2, O_2, Ar-H_2, Ar-N_2, Ar-O_2, Ar-H_2-N_2 and Ar-H_2-N_2-O_2 systems at temperatures of 40°, 65°, and 93° C. These are compared with the values obtained from rigorous kinetic theory, approximate, semitheoretical, Lindsay-Bromley and simpler methods of computing thermal conductivity of mixtures. A critical comparison of the observed and various calculated values enables some interesting conclusions to be drawn regarding the appropriateness of different procedures in correlating or predicting the thermal conductivity of gas mixtures.

2. Apparatus

The principal component of the experimental arrangement is the hot-wire cell. It consists of a precisely bored stainless steel tube having an effective length of 10.44 cm and an internal diameter of 0.6412 cm. The bore is found to be uniform within one part in 600. Along the axis is run a platinum wire 0.05076 cm in diameter as measured by a profile projector having the least count of 0.002 cm. The effective length was determined by measuring the resistance. The top end is closed by silver soldering a brass cap and the bottom end by a kovar cap through a c-40 glass seal. This arrangement provides the necessary electrical insulation between the main metal body of the cell and the axial platinum wire. Current and potential leads are soldered at the two metal end caps, while a side connection enables the cell to be either evacuated or loaded with any desired gas. An efficient high

[1] Figures in brackets indicate the literature references at the end of this paper.

vacuum pumping system evacuates the conductivity cell up to 10^{-6} cm of mercury. A suitably designed gas handling system is used to prepare precise mixtures of different known compositions and also to charge the cell and compress it to any desired value up to an atmosphere. The cell is vertically mounted in a thermostat bath which can be maintained at any temperature from room to 100° C within an accuracy of ± 0.01. This is obtained by efficient stirring, distributed heaters energized by regulated electrical power, a contact thermometer, and a sensitive relay and proportional control system. A Tinsley vernier potentiometer of the type 4363 D, reading directly up to 0.1 microvolt is employed for electrical measurements.

3. Theory and Corrections

The theory of the thick-wire cell is well developed [11-13] and consequently only the necessary working relations are reproduced here. The differential equation for the radial heat flow through the gas is,

$$\pi r_1^2 K \frac{d^2\theta}{dz^2} - 2\pi r_1 h\theta + I^2 \rho_0 (1 + \alpha\theta) = 0 , \qquad (1)$$

where

$$h = \lambda [r_1 \ell n (r_2/r_1)]^{-1} , \qquad (2)$$

K and λ are the thermal conductivity values of the wire material and test gas respectively, r_1 the radius of the wire, r_2 the inner radius of the cell tube, ρ_0 the resistance per unit length of the wire at the bath temperature, θ the temperature excess of the wire over that of the bath at a distance z from the center and α the temperature coefficient of resistance of the wire. Assuming the ends of the wire to be at the bath temperature, the solution of eq (1) is,

$$\left(\frac{1}{\beta\ell}\right)\left[1 - \frac{\tanh \beta\ell}{\beta\ell}\right] = \frac{2\pi r_1^2 K (\bar{R}_\theta - R_0)}{R_0^2 I^2 \alpha \ell} , \qquad (3)$$

where

$$\beta^2 = \frac{2h}{r_1 K} - \frac{I^2 R_0 \alpha}{2\pi r_1^2 K \ell} , \qquad (4)$$

Here $\bar{R}\theta$ is the resistance of the wire when a current I is flowing, R_0 is the resistance at the bath temperature and 2ℓ is the length of the cell wire.

In practice the heat flow lines through the gas are slightly curved at the ends. The exact solution then is given by,

$$\frac{\pi (\bar{R}\theta - R_0)}{2 R_0 \alpha} = C_1 N_{01} - \frac{1}{3} C_3 N_{03} + \frac{1}{5} C_5 N_{05} - - - , \qquad (5)$$

The defining relations for C_i and N_{on} are given in reference [11]. The correction for the nonradial flow of heat is the difference in the two conductivity values as obtained from eq (2) and eq (5) respectively. This correction is negligible for values of λ below 0.04 μW $m^{-1} deg^{-1}$, about 0.7% for λ ranging from 0.04 to 0.08, 1% for λ between 0.08 and 0.12, and 1.2% for λ values above 0.12.

By careful design and installation of the conductivity cell and selection of operating conditions, the convection effect is found to be negligible in our measurements. The temperature jump effect is also likewise reduced. In a note [14] both these corrections are discussed and it is found that the measurements taken at gas pressures varying between 8 and 16 cm of mercury are not contaminated by these uncertainties.

The radiation correction is evaluated experimentally by taking measurements on the highly evacuated cell for different bath temperatures. I, R_0 and $R\theta$ are thus experimentally determined and the corresponding λ_r determined from eqs (2) to (4). For example, the correction at about 100°C is 0.9 and 6% for He and Xe respectively.

The wall effect is negligible for our cell and the correction amounts to only 0.02%. Again the noncentering of the wire has no serious effect on our values. Calculations reveal the correction to be 0.04, 0.98 and 4.06% only for wire displacements from the true center by 0.01, 0.05 and 0.1 cm respectively. We thus claim our measurements to be absolute.

For the gases and gas mixtures examined here the thermal energy absorption is negligible and we have ignored this correction.

4. Results

Spectroscopically pure argon supplied by M/S British Oxygen Co. has been used in these measurements. The resistance of the cell wire with zero current at different bath temperatures R_0, is determined by highly evacuating the cell and measuring resistance as a function of current. R_0 is then obtained by extrapolation of the plots of I^2 against $\bar{R}_\theta^{-1}$ to $I = 0$. α is obtained by measuring the resistance of a specimen of platinum wire at ice, steam and boiling sulphur temperatures and evaluating the constants A and B of the relation,

$$R = R_0 [1 + A(T - 273.16) + B(T - 273.16)^2] . \qquad (6)$$

α is then evaluated at any temperature by

$$\alpha = \frac{1}{R} \frac{dR}{dT} . \qquad (7)$$

T is the temperature in °K.

The thermal conductivity of the platinum wire at 40° C is determined in the same set up by taking measurements on a highly evacuated cell and using eq (3). h is now $h_r = 4e\sigma T^3$, e and σ are the emissivity of the platinum wire and Stefan's constant respectively. At higher temperatures K is obtained on the basis of this value and its temperature dependence from the literature [15].

Now all that remains to be determined for calculating the gas conductivity is the cell wire resistance $\bar{R}_\theta$, when it is heated a couple of degrees above the bath temperature (4 to 6°), by passing a current I in the presence and absence of the gas. This λ value is assigned the average temperature as the arithmetic mean of the wire and wall temperatures. The λ values so obtained, after corrections for the various undesirable but unavoidable side effects are recorded in tables 1 to 4 for pure, binary, ternary and quaternary mixtures, respectively.

Table 1 Comparison of presently measured λ values (μW $m^{-1}deg^{-1}$) with literature and theoretical values.

Temp.°C \ Gas	Ar	H_2	N_2	O_2	
40	0.0185	0.182	0.0268	0.0281	Present
	0.0185	0.185	0.0268	0.0278	Literature
	0.0	+1.6	0.0	-1.1	% dev
	0.0183	0.192	0.0277	0.0280	Theoretical
	-1.1	+5.5	+3.4	-0.4	% dev
65	0.0193	0.194	0.0290	0.0291	Present
	0.0196	0.198	0.0283	0.0296	Literature
	+1.5	+2.1	-2.4	+1.7	% dev
	0.0195	0.202	0.0294	0.0298	Theoretical
	+1.1	+4.1	+1.4	+2.4	% dev
93	0.0210	0.204	0.0312	0.0313	Present
	0.0209	0.209	0.0301	0.0318	Literature
	-0.5	+2.5	-3.5	+1.6	% dev
	0.0208	0.214	0.0312	0.0317	Theoretical
	-1.0	+5.0	0.0	+1.2	% dev

The precision of our measurements is on the average about 1% depending upon the value of thermal conductivity. A detailed error analysis reveals that a gas thermal conductivity value within 2% of the true value at the worst is obtained if no error is made in determining the thermal conductivity of the wire. It also reveals that if the gas is pumped out so that the electrical heat generated can only flow along the wire (neglecting radiation) an uncertainty of nearly 1% at the worst will exist in K. Then the resulting uncertainty in λ could be as much as 4%. However, this represents the most unfavourable case in which all errors are assumed to contribute in the same direction. On the average, a considerable cancellation of such uncertainties will occur so that one can expect λ to be accurate to about 1 to 2%. This can be further reduced by multiple measurements. This estimate does imply that uncertainties arising from convection etc., are negligible. The three diatomic gases as supplied by M/S British Oxygen Co. were used. These were stated to be 99.9% pure and we made no effort to further purify them.

Table 2 Comparison of experimental and various calculated λ values for binary mixtures in μW m^{-1}deg^{-1}. Entries in columns 4 to 7 are percentage deviations.

Gas pair (temp.)	Ar mole fraction	Exptl.	Rigor. eq(10)	Approx. eq(11)	Lindsay-Bromley	Semitheor. eq(13)
H_2-Ar	0.202	0.1245	+4.1	+4.8	+0.6	+1.2
(40°C)	0.388	0.0891	+1.8	+5.4	-0.6	-
	0.614	0.0557	+2.1	+7.5	+0.8	+1.3
(65°C)	0.202	0.1325	+3.5	+4.7	+0.5	+1.0
	0.388	0.0955	+0.5	+4.3	-1.6	-1.1
	0.614	0.0589	+2.2	+7.4	+0.8	+1.2
(93°C)	0.202	0.1395	+4.4	+5.0	+0.8	+1.4
	0.388	0.1026	-0.8	+2.6	-3.3	-2.7
	0.614	0.0640	-0.1	+4.9	-1.7	-1.2
N_2-Ar	0.188	0.0255	+1.3	-2.6	-0.7	-0.8
(40°C)	0.492	0.0227	+0.2	-3.1	+0.1	-
	0.767	0.0207	-1.8	-3.4	-1.0	-1.0
(65°C)	0.188	0.0269	+1.7	-0.7	+1.1	+1.1
	0.492	0.0241	+0.4	-2.7	+0.6	+0.5
	0.767	0.0220	-1.9	-4.4	-1.9	-2.0
(93°C)	0.188	0.0292	-0.5	-1.2	+0.6	+0.5
	0.492	0.0254	+1.1	-0.1	+3.2	+3.1
	0.767	0.0234	-1.8	-2.3	+0.2	+0.2
O_2-Ar	0.249	0.0252	+1.2	-0.4	+2.0	+0.2
(40°C)	0.484	0.0228	-0.9	-0.9	+2.5	-
	0.753	0.0208	-1.2	-2.6	+0.1	-1.9
(65°C)	0.249	0.0272	-0.8	-4.6	-2.3	-4.0
	0.484	0.0245	-0.5	-4.5	-1.2	-3.6
	0.753	0.0221	-1.7	-4.9	-2.3	-4.2
(93°C)	0.249	0.0292	-1.4	-4.1	-1.8	-3.5
	0.484	0.0262	-0.1	-3.1	+0.2	-2.2
	0.753	0.0234	-0.4	-2.1	+0.6	-1.4

Table 3 Comparison of experimental and various calculated λ values for ternary mixtures of Ar-N_2-H_2 in μ W m^{-1} deg^{-1}. In columns 5, 6 and 7 are recorded the percentage deviations.

Temp. °C	mole fraction Ar	mole fraction N_2	Exptl.	Approx. eq(11)	Lindsay-Bromley	Semitheor. eq(13)
40	0.298	0.501	0.0417	+0.3	-2.9	-0.4
	0.103	0.289	0.0918	+4.5	-1.0	+2.8
65	0.298	0.501	0.0439	+1.6	-1.7	+0.9
	0.103	0.289	0.1021	+0.1	-5.1	-1.5
93	0.298	0.501	0.0471	+1.0	-2.3	+0.4
	0.103	0.289	0.1067	+1.1	-4.3	-0.5

Table 4 Comparison of experimental and various calculated λ values for quaternary mixtures of Ar-N_2-O_2-H_2 in μW m^{-1}deg^{-1}. Columns 6, 7 and 8 give the percentage deviations.

Temp. °C	mole fraction Ar	mole fraction O_2	mole fraction N_2	Exptl.	Approx. eq(11)	Lindsay-Bromley	Semitheor. eq(13)
40	0.132	0.364	0.125	0.0615	+4.7	-0.2	+1.0
	0.250	0.244	0.374	0.0360	-0.8	-1.7	-1.2
65	0.132	0.364	0.125	0.0671	+1.4	-3.3	-2.2
	0.250	0.244	0.374	0.0383	-1.3	-2.2	-1.6
93	0.132	0.364	0.125	0.0717	+0.7	-4.0	-2.8
	0.250	0.244	0.374	0.0423	-4.3	-5.2	-4.6

5. Comparison with Theory

In table 1 our results are compared with the smooth values recommended on the basis of available measurements [8,9]. The agreement may be regarded as satisfactory and it seems the estimate of disagreement between different measurements as 2% is reasonable. Considerable careful work will be required to improve this to within 1%.

In table 1 we also record the theoretically computed λ values. For Ar as well as for the frozen part (λ°) we use the expression given by Hirschfelder, Curtiss and Bird [16],

$$\lambda^\circ = \frac{0.083266\sqrt{T/M}}{\sigma^2 \Omega^{(2,2)*}(T^*, \alpha)} f_\lambda^3 (T^*, \alpha) \quad . \tag{8}$$

Here M is the molecular weight of the gas and the reduced omega collision integral is a function of the reduced temperature $T^* = k\,T/\epsilon$. k is the Boltzmann constant, and α, ϵ and σ are the potential parameters. f_λ^3 is a correction factor and its value is determined by T^* and α. We have used the modified Buckingham exp-six potential for which all the necessary collision integrals are tabulated by Mason [17]. The potential parameters are known for the gases of our current interest [18-20] and are reproduced in table 5.

Table 5 Exponential-six potential parameters and Sutherland constants for pure gases.

Gas	α	ϵ/k, °K	r_m, Å	S
H_2	14.0	37.3	3.337	83
N_2	17.0	101.2	4.011	103
O_2	17.0	132	3.726	138
Ar	14.0	123.2	3.866	147

For polyatomic gases we use the expression derived by Hirschfelder [21],

$$\lambda = \lambda^\circ \left[0.115 + \frac{0.354\,\gamma}{\gamma - 1}\right] \quad . \tag{9}$$

γ is the ratio of the specific heat of the gas at constant pressure to that at constant volume. Two more formulations are available [22,23] but for our present work eq (9) is found adequate.

In general, we find that the theoretically predicted values for pure gases, table 1, agree with our measurements within the limits of uncertainty in the data. Further, for polyatomic gases the theoretical estimates are not very precise and the agreement between theory and experiment is worst for hydrogen and the difference is appreciable in magnitude. Unforunately, the refined formulations [22,23] which consider the relaxation of internal-translational energy are also not able to improve upon the disagreement and special consideration is due for this gas. In this paper the deviations are designated as positive or negative whenever the values are greater or smaller than the corresponding measured values respectively.

In table 2, our results for the three binary systems are presented and are compared with the predictions of theory and other procedures for computing λ. The rigorous calculations are based on the expression derived by Hirschfelder [24] as,

$$\lambda_{mix} = \lambda^\circ_{mix} + \sum_{i=1}^{n} (\lambda_i - \lambda_i^\circ)\left[1 + \sum_{\substack{j=1 \\ j \neq i}}^{n} \frac{D_{ii}}{D_{ij}} \frac{x_j}{x_i}\right]^{-1} \quad . \tag{10}$$

Here λ_{mix} refers to the thermal conductivity of the mixture of n components, D to the diffusion coefficient, and x_i to the mole fraction of the i - th component in the mixture. The frozen thermal conductivity of the mixture λ°_{mix} is obtained from the expression derived by Muckenfuss and Curtiss [25] with the modification suggested by Mason and Saxena [26]. D_{ij} are also computed and we use the exp-six potential with parameters reproduced in table 6 and obtained on the basis of combination rules of Mason and Rice [18]. λ and λ° are also computed from eqs (9) and (8) respectively. The calculated λ_{mix} values are not reported but instead their percentage deviations from the experimental values for convenience of evaluation. It is to be noted that this simple theory [24] does quite well in reproducing the experimental results and therefore more complicated theories developed by Monchick, Pereira and Mason [27], and Saxena, Saksena, Gambhir and Gandhi [28] are not considered. The average absolute deviation is

1.4% for 27 mixtures of table 2. A slightly enhanced discrepancy for H_2 - Ar mixtures may also be partly due to translational relaxation, Saksena, Saxena and Mathur [29]. This correction is significant only when the masses involved differ considerably and consequently it is likely to be appreciable only for this system.

Table 6 Exponential-six potential parameters and Sutherland constants for binary gas pairs.

Gas pair	α_{12}	ϵ_{12}/k, °K	$(r_m)_{12}$, Å	S_{12}
H_2-Ar	14.0	69.7	3.574	111
N_2-Ar	15.5	111.8	3.951	123
O_2-Ar	15.5	131.2	3.785	142

Mason and Saxena [30] simplified the expression obtained by Hirschfelder, eq (10), and instead suggested the following simpler but approximate relation:

$$\lambda_{mix} = \sum_{i=1}^{n} \lambda_i \left[1 + \sum_{\substack{j=1 \\ j \neq i}}^{n} \varphi_{ij} \frac{x_j}{x_i}\right]^{-1}, \tag{11}$$

where

$$\varphi_{ij} = \frac{1.065}{2\sqrt{2}} \left(1 + \frac{M_i}{M_j}\right)^{-\frac{1}{2}} \left[1 + \left(\frac{\lambda_i^\circ}{\lambda_j^\circ}\right)^{\frac{1}{2}} \left(\frac{M_i}{M_j}\right)^{\frac{1}{4}}\right]^{-2}. \tag{12}$$

The φ_{ij} for each system were computed at the lowest temperature and the same were used at the two higher temperatures. The φ_{ij} values are reported in table 7 and λ_{mix} values in column 5 of table 2. The agreement between theory and experiment is only fair, the average absolute deviation for all the 27 mixtures is 3.5%.

Table 7 Values of φ_{ij} at 40° C.

Gas pair	Approximate		Lindsay-Bromley		Semitheoretical	
	φ_{12}	φ_{21}	φ_{12}	φ_{21}	φ_{12}	φ_{21}
H_2 -Ar	0.254	1.982	0.561	2.071	0.281	2.190
N_2-Ar	0.995	1.119	0.985	1.010	0.936	1.049
O_2-Ar	0.994	1.134	0.962	1.039	0.977	1.115

Lindsay and Bromley[31] also derived an expression for λ mix of the type given by eq(11), but suggested another relation for φij. The latter at 40° C are reported in table 7 while the values for Sutherland constants S are given tables 5 and 6. S values are taken from Chapman and Cowling [32] and S_{12} are computed as geometric mean of S_1 and S_2. The calculated values reported in column 6 of table 2 agree with the experimental data within an average absolute deviation of only 1.2%.

Mathur and Saxena [33] suggested a semitheoretical method according to which φ_{ij} of eq (11) are determined on the basis of the following relation:

$$\frac{\varphi_{12}}{\varphi_{21}} = \frac{\lambda_1^\circ}{\lambda_2^\circ} = \frac{M_2}{M_1} \frac{\eta_1}{\eta_2}, \tag{13}$$

and one λ_{mix} value. Here η_1 is the coefficient of viscosity of the pure component i. This method is found very sucessful in predicting thermal conductivity of binary and ternary mixtures [33-35]. Calculated values of φ_{ij} at 40° C are reported in table 7 and those of λ_{mix} in column 7 of table 2. The experimental values are reproduced within an average absolute deviation of 1.7%.

Similar calculations and comparison against the directly measured values for ternary and quaternary mixtures are reported in tables 3 and 4 respectively. The approximate, Lindsay-Bromley and semitheoretical proce-

dures predict for the two systems values which agree with the experiments within an average absolute percentage deviations of 1.4, 2.9 and 1.1; and 2.2, 2.8 and 2.2 respectively.

Thus, on the whole the approximate and Lindsay and Bromley methods are of competing accuracy, and the former is slightly more preferable because one needs less initial information and computation is simpler. The semitheoretical method seems to most reliable and should be preferred when one λmix value for all involved binary systems is known. These conclusions are in conformity with earlier more detailed investigations. It may be pointed out that the relation (11) is approximate for polyatomic gas mixtures, by considering a more rigorous theory[28], Saksena and Saxena[35] have derived its alternative form.

Simpler methods, like simple mixing rules, reciprocal mixing rules, a combination of the two, and a quadratic expression, are also used for computing λmix [37]. The values so obtained are designated as λSM, λRM, λC, and λQ respectively and are reporduced in table 8. The quadratic function does not seem to be adequate for reproducing the composition dependence, and the success of the combination method for a quick and approximate estimate is notable. The method reproduces the data for binary, ternary and quaternary mixtures within an average absolute deviation of 4.2, 4.8 and 2.0% respectively.

Table 8 Comparison of experimental and various calculated λ values according to simpler procedures for binary systems. Computed percentage deviations from experimental values are tablulated in columns 3 to 6.

Gas pair (temp.)	Ar mole fraction	λ_{SM}	λ_{RM}	λ_{C}	λ_{Q}
H_2-Ar	0.202	+19.7	-47.5	-13.8	+3.6
(40°C)	0.388	+33.2	-53.8	-10.3	-
	0.614	+46.8	-49.0	- 1.1	-6.2
(65°C)	0.202	+19.7	-48.2	-14.3	+4.0
	0.388	+32.0	-55.0	-12.3	-
	0.614	+47.0	-49.8	- 1.3	-4.8
(93°C)	0.202	+20.0	-46.8	-13.4	+5.2
	0.388	+29.4	-54.6	-12.6	-
	0.614	+42.3	-49.7	- 3.4	-4.1
N_2-Ar	0.188	- 0.8	- 2.8	- 1.8	-0.8
(40°C)	0.492	+ 0.1	- 3.3	- 1.6	-
	0.767	- 1.0	- 3.3	- 2.1	-1.1
(65°C)	0.188	+ 1.1	- 1.4	- 0.1	+0.8
	0.492	+ 0.6	- 3.5	- 1.4	-
	0.767	- 1.9	- 4.8	- 3.3	-2.4
(93°C)	0.188	+ 0.6	- 1.8	- 0.6	-1.1
	0.492	+ 1.5	- 0.7	+ 1.2	-
	0.767	+ 0.2	- 2.5	- 1.1	-2.2
O_2-Ar	0.249	+ 2.2	- 1.0	+ 0.6	+0.3
(40°C)	0.484	+ 2.9	- 1.4	+ 0.7	-
	0.753	+ 0.4	- 2.8	- 1.2	-2.0
(65°C)	0.249	- 2.1	- 5.1	- 3.6	-1.6
	0.484	- 0.9	- 4.9	- 2.9	-
	0.753	- 2.0	- 5.0	- 3.5	-1.4
(93°C)	0.249	- 1.6	- 4.5	- 3.0	-1.9
	0.484	+ 0.5	- 3.3	- 1.4	-
	0.753	+ 0.9	- 2.0	- 0.6	+0.4

Relations for predicting diffusion and viscosity coefficients on the basis of thermal conductivity and other experimental data are known [38-41]. In table 9 we report such indirectly generated D_{ij} and η_{mix} values. The former are compared with the directly measured values as well as with the predictions of rigorous theory [16]. The measured values of η_{mix} for H_2-Ar system agree with the generated values within an average absolute deviation of 1.3%. Thus, we find that such approaches are quite dependable and act as valuable procedures for generating data on other transport properties.

Table 9 Indirectly generated coefficients of diffusion (D_{ij}), (μ m^2/s) and viscosity η_{mix}, (μ Ns/m^2) for binary gas systems.

Gas pair (temp.)	Ar mole fraction	Generated D_{ij}	Mean D_{ij}	Measured D_{ij}	Theoretical D_{ij}	Generated η_{mix}
H_2-Ar	0.202	90.7				1729
(40°C)	0.388	93.1	92	93	87.7	2053
	0.614	90.9				2253
(65°C)	0.202	103.1				1832
	0.388	107.6	105	105	100	2183
	0.614	103.2				2385
(93°C)	0.202	117.6				1942
	0.388	127.6	123	123	115	2309
	0.614	123.0				2505
N_2-Ar	0.188	22.6				1967
(40°C)	0.492	21.7	22.2	21.2	21.0	2140
	0.767	22.4				2262
(65°C)	0.188	23.8				2066
	0.492	24.4	24.7	24.8	24.1	2243
	0.767	25.9				2390
(93°C)	0.188	28.2				2176
	0.492	27.0	27.9	-	27.7	2346
	0.767	28.6				2491
O_2-Ar	0.249	20.2				2169
(40°C)	0.484	20.4	20.7	21.3	21.0	2209
	0.753	21.4				2270
(65°C)	0.249	26.1				2371
	0.484	25.0	25.6	24.4	23.9	2440
	0.753	25.8				2488
(93°C)	0.249	29.9				2490
	0.484	28.3	28.7	-	27.8	2546
	0.753	28.0				2588

6. References

[1] Gambhir, R.S. and Saxena, S.C., Thermal conductivity of binary and ternary mixtures of krypton, argon and helium, Mol. Phys. 11, 233 (1966).

[2] Gandhi, J.M. and Saxena, S.C., Thermal conductivity of binary and ternary mixtures of helium, neon and xenon, Mol. Phys. 12, 57 (1967).

[3] Mathur, S., Tondon, P.K. and Saxena, S.C., Thermal conductivity of binary, ternary and quaternary mixtures of rare gases, Mol. Phys. 12, 569 (1967).

[4] Gambhir, R.S. and Saxena, S.C., Thermal conductivity of the gas mixtures: Ar-D_2, Kr-D_2 and Ar-Kr-D_2, Physica 32, 2037 (1966).

[5] Gandhi, J.M. and Saxena, S.C., Thermal conductivities of the gas mixtures: D_2-He, D_2-Ne and D_2-He-Ne, Brit. J. Appl. Phys. 18, 807 (1967)

[6] Gambhir, R.S., Gandhi, J.M. and Saxena, S.C., Thermal conductivity of rare gases, deuterium and air, Indian J. Pure & Appl. Phys., in press.

[7] Saxena, S.C., Gandhi, J.M., Thermal conductivity of multicomponent mixtures of inert gases, Rev. Mod. Phys. 35, 1022 (1963).

[8] Gandhi, J.M. and Saxena, S.C., Thermal conductivity of monatomic gases and binary gas mixtures, University of Rajasthan Studies (Physics) 1, 7 (1965).

[9] Gambhir, R.S. and Saxena, S.C., Thermal conductivity of common nonpolar polyatomic gases, Suppl. Def. Sci. J. 17, 35 (1967).

[10] Saxena, S.C., Mathur, S. and Gupta, G.P., The thermal conductivity data of some binary gas mixtures involving polyatomic gases, Supp. Def. Sci. J. 16, 99 (1966).

[11] Kannuluik, W.G. and Martin, L.H., The thermal conductivity of some gases at 0° C, Proc. Roy. Soc. A144, 496 (1934).

[12] Kannuluik, W.G. and Carman, E.H., The thermal conductivity of rare gases, Proc. Phys. Soc. B65, 701 (1952).

[13] Srivastava, B.N. and Saxena, S.C., Thermal conductivity of binary and ternary rare gas mixtures, Proc. Phys. Soc. B70, 369 (1957).

[14] Gupta, G.P. and Saxena, S.C., Pressure dependence of thermal conductivity in a hot-wire type of cell, Can. J. Phys. 45, 1418 (1967).

[15] Powell, R.W. and Tye, R.P., The promise of platinum as a high temperature thermal conductivity reference material, Brit. J. Appl. Phys. 14, 662 (1963).

[16] Hirschfelder, J.O., Curtiss, C.F. and Bird, R.B., Molecular theory of gases and liquids (John Wiley & Sons, Inc., New York, 1954).

[17] Mason, E.A., Transport properties of gases obeying a modified Buckingham (exp-six) potential, J. Chem. Phys. 22, 169 (1954).

[18] Mason, E.A. and Rice, W.E., The intermolecular potentials of helium and hydrogen, J. Chem. Phys. 22, 522 (1954).

[19] Mason, E.A. and Rice, W.E., The intermolecular potentials for some simple nonpolar molecules, J. Chem. Phys. 22, 843 (1954).

[20] Vanderslice, J.T., Mason, E.A. and Maisch, W.G., Interactions between oxygen and nitrogen: O-N, O-N_2, and O_2-N_2, J. Chem. Phys. 31, 738 (1959).

[21] Hirschfelder, J.O., Heat conductivity in polyatomic or electronically excited gases. II, J. Chem. Phys. 26, 282 (1957).

[22] Mason, E.A. and Monchick, L., Heat conductivity of polyatomic and polar gases, J. Chem. Phys. 36, 1622 (1962).

[23] Saxena, S.C., Saksena, M.P. and Gambhir, R. S., The thermal conductivity of nonpolar polyatomic gases, Brit. J. Appl. Phys. 15, 843 (1964).

[24] Hirschfelder, J.O., Heat conductivity in polyatomic, electronically excited, or chemically reacting mixtures. III, Sixth International Combustion Symposium, p. 351 (Reinhold Publishing Corporation, New York, 1957).

[25] Muckenfuss, C. and Curtiss, C.F., Thermal conductivity of multicomponent gas mixtures, J. Chem. Phys. 29, 1273 (1958).

[26] Mason, E.A. and Saxena, S.C., Thermal conductivity of multicomponent gas mixtures. II, J. Chem. Phys. 31, 511 (1959).

[27] Monchick, L., Pereira, A.N.G. and Mason, E. A., Heat conductivity of polyatomic and polar gases and gas mixtures, J. Chem. Phys. 42, 3241 (1965).

[28] Saxena, S.C., Saksena, M.P., Gambhir, R.S. and Gandhi, J.M., The thermal conductivity of nonpolar polyatomic gas mixtures, Physica 31, 333 (1965).

[29] Saksena, M.P., Saxena, S.C. and Mathur, S., Thermal conductivity of mixtures of monatomic gases and translational relaxation, Trans. Faraday Soc. 63, 591 (1967).

[30] Mason, E.A. and Saxena, S.C., Approximate formula for the thermal conductivity of gas mixtures, Phys. Fluids 1, 361 (1958).

[31] Lindsay, A.L. and Bromley, L.A., Thermal conductivity of gas mixtures, Ind. Eng. Chem. 42, 1508 (1950).

[32] Chapman, S. and Cowling, T.G., The mathematical theory of nonuniform gases (The University Press, Cambridge, 1953).

[33] Mathur, S. and Saxena, S.C., Methods of calculating thermal conductivity of binary mixtures involving polyatomic gases, Appl. Sci. Res. 17, 155 (1967).

[34] Gupta, G.P. and Saxena, S.C., Calculation of thermal conductivity of polyatomic gas mixtures at high temperatures, Def. Sci. J. 16, 165 (1966).

[35] Mathur, S. and Saxena, S.C., Calculation of thermal conductivity of ternary mixtures of polyatomic gases, Indian J. Pure & Appl. Phys. 5, 114 (1967).

[36] Saksena, M.P. and Saxena, S.C., Thermal conductivity of polyatomic gas mixtures and Wassiljewa form, Appl. Sci. Res. 17, 326 (1967).

[37] Gandhi, J.M. and Saxena, S.C., Thermal conductivity of multicomponent mixtures of inert gases: Part III - some simpler methods of computation, Indian J. Pure & Appl. Phys. 4, 461 (1966).

[38] Gandhi, J.M. and Saxena, S.C., Correlation between thermal conductivity and diffusion of gases and gas mixtures of monatomic gases, Proc. Phys. Soc. 87, 273 (1966).

[39] Mathur, S. and Saxena, S.C., Relations between thermal conductivity and diffusion coefficients of pure and mixed polyatomic gases, Proc. Phys. Soc. 89, 273 (1966).

[40] Gupta, G.P. and Saxena, S.C., Prediction of thermal conductivity of pure gases and mixtures Supp. Def. Sci. J. 17, 21 (1967).

[41] Saxena, S.C. and Agrawal, J.P., Interrelation of thermal conductivity and viscosity of binary gas mixtures, Proc. Phys. Soc. 80, 313 (1962).

Thermal Conductivities of Gaseous Mixtures of Diethyl Ether with Inert Gases

P. Gray, S. Holland and A. O. S. Maczek

School of Chemistry
The University
Leeds 2
U.K.

Thermal conductivities of binary mixtures of diethyl ether with four inert gases, helium, argon, neon and nitrogen have been measured at sub-atmospheric pressure at 50°C and 100°C (ca. 0.5% error). In the composition dependence curves, measured thermal conductivities were always less than molar average values. The difference was most marked for helium and least for nitrogen, and pronounced minima were displayed by $(C_2H_5)_2O$-Ar. At 100°C the $(C_2H_5)_2O$-Ar system showed a point of inflexion. The experimental values have been applied to test the success of Hirschfelder and Eucken's approach to the thermal conductivity of binary mixtures containing polar polyatomic molecules. When empirical estimates of the thermal conductivity of mixing have to be made from properties of pure constituents the most successful form of equation is that due to Wassiljewa (1904). It is capable of accommodating varied behaviour including maxima, minima and points of inflexion. The conditions necessary for these phenomena are investigated briefly. Physically, its success arises from the simple way in which it takes account of processes in mixing of gases. A_{ij} are coefficients giving relative efficiencies in impeding transport of energy. Empirical formulae depend for their success on reliable estimates for A_{ij}. The formulae of Lindsay and Bromley, normally successful, here fail to give good predictions and errors of about 5% in thermal conductivity at equimolar concentrations occur.

Key Words: Binary mixtures, diethyl ether and inert gases, gas phase, Hirschfelder approximation, thermal conductivity, Wassiljewa equation.

1. Introduction

The present paper is concerned with the dependence of thermal conductivity on the composition of binary mixtures of a polar polyatomic gas, diethyl ether, with the non polar gases, helium, neon, argon and nitrogen.

Previous work [1,2,3][1] on this type of mixture has shown a non-linear variation of conductivity with composition which can neither be represented successfully by empirical equations nor be predicted adequately by present kinetic theory. This is in contrast to mixtures of polar gases only or to mixtures of non polar gases only. In these cases conductivity-composition dependence deviates less from molar averages and empirical or theoretical estimations.

The first approximation to the rigorous kinetic theory of gases [4-9] accounts successfully for the thermal conductivities of mixtures of monatomic gases.

For mixtures of diatomic or of polyatomic gases Hirschfelder [10] has assumed that the total thermal conductivity of each consituent is separable into translational and internal (rotational and vibrational) contributions.

$$K = K_{trans} + K_{int} \qquad (1)$$

[1] Figures in brackets indicate the literature references at the end of this paper.

The translational contribution to the thermal conductivity of the mixture is calculated as if the individual gases were all monatomic. Each pure gas is regarded as having a translational thermal conductivity which is related to the viscosity

$$K_{1\ trans}\ \ 2.5\eta_1 C_{v1} = 3.75\ \eta_1 R/m_1 \qquad (2)$$

The first approximation to rigorous theory for a binary mixture then gives

$$K_{trans} = (K_{1\ trans}\frac{x_2}{x_1} + a + b\,K_{2\ trans}\frac{x_1}{x_2})/(\frac{x_2}{x_1} + c + b\frac{x_1}{x_2}) \qquad (3)$$

where the values of the constants a, b, c are well established [4]. The internal contribution to the thermal conductivity of the mixture is calculated from the equation

$$K_{int} = \frac{K_{1\ int}}{1 + \frac{D_{11}x_2}{D_{12}x_1}} + \frac{K_{2\ int}}{1 + \frac{D_{22}x_1}{D_{12}x_2}} \qquad (4)$$

This theory gives satisfactory agreement in a number of cases [10-13] and considerable discrepancies in others [1,10-14]. Subsequent attempts have been made to take into account the interchange at collision between translational and internal energy [14]. For example, allowance has been made for inelastic collisions. The corrections are small and may be in the wrong sense. For strongly polar gases, theory and experiment have been compared only in a few cases [14-16].

Of empirical equations the most successful is due to Wassiljewa [17]

$$K = \sum_i K_i / (1 + \sum_j A_{ij}\, x_j/x_i), \qquad (5)$$

where K and K_i are the thermal conductivities of the mixture and pure component i respectively; x_i is the mole fraction of component i; A_{ij} is one of a set of adjustable parameters.

The A_{ij} have a simple physical significance [18-20]. They are a measure of the ratio of the efficiencies with which molecules j and molecules i impede the transport of heat by molecules i. Equation (5) may be written in an alternative form for a binary mixture as

$$K = \frac{1}{R_1 + \alpha_{12}x_2/x_1} + \frac{1}{R_2 + \alpha_{21}x_1/x_2}, \qquad (6)$$

where $R_1 = 1/K$, $\alpha_{12} = A_{12}/K_1$ and $\alpha_{21} = A_{21}/K_2$. Thus α_{12} is a single resistance expressing the extent to which molecules 2 impede the transport by molecules 1. R_1 expresses the extent to which molecules 1 impede transport by their own kind. Thus if molecules 2 are more efficient than molecules 1 in impeding transport of heat by 1 then α_{12} will be greater than R_1.

This is, however, an oversimplification of the effect of molecular interaction on transport phenomena. It overestimates impedance of transport of one molecule by another and neglects smaller effects such as transfer of transport. For a binary mixture it has been shown [19, 21] that the first approximation to rigorous theory reduces to eq. (5) with A_{ij} slightly dependent on composition. When the molecular weights of the components of the gas mixture are very different, a formula of the Wassiljewa type is theoretically possible [21] but errors are greater.

The Wassiljewa equation is also flexible algebraically. This is not the case for a linear or quadratic expression where the scope is more limited. Thus eq.(5) can represent not only (i) a minimum or (ii) a maximum but also (iii) a point of inflexion and (iv) the intersection of the molar average line by the conductivity-composition curve.

Estimates of A_{ij} for polar gases may be made from the empirical equation of Lindsay and Bromley [22] in terms of viscosity η, Sutherland's constant S, and molecular weight of pure components:

$$A_{ij} = \tfrac{1}{4}\left\{1 + \frac{\eta_i}{\eta_j}\left(\frac{M_j}{M_i}\right)^{\frac{3}{4}}\left(\frac{T + S_i}{T + S_j}\right)^{\frac{1}{2}}\right\}^2 \frac{T + S_{ij}}{T + S_i} \quad , \tag{7}$$

where $S_{ij} = (S_i S_j)^{\frac{1}{2}}$ if i and j are both non polar, and $S_{ij} = 0.733\,(S_i S_j)^{\frac{1}{2}}$ if one of i or j is polar.

Francis [23] suggested an expression

$$A_{ij} = \left(\frac{\sigma_{ij}}{\sigma_{ii}}\right)^2 \left(\frac{2M_j}{M_i + M_j}\right) \left(\frac{\Omega_{ij}^{(2,2)}}{\Omega_{ii}^{(2,2)}}\right) , \tag{8}$$

where σ_{12} is the collision diameter for unlike molecules and $\Omega_{ij}^{(2,2)}$ is a collision integral tabulated [4] as a function of the reduced temperature.

The aims of the paper are a) to provide reliable experimental data for binary polar-nonpolar gas mixtures b) to use these data to estimate resistances to heat transfer c) to test Hirschfelder's approximation and d) to test empirical equations of the Wassiljewa form.

2. Nomenclature

The components of the mixture are identified by the suffixes:

$$1 = (C_2H_5)_2O; \quad 2 = Ar; \quad 3 = He; \quad 4 = Ne; \quad 5 = N_2$$

Thus K_1 is the thermal conductivity of pure diethyl ether, x_2 is the mole fraction of argon. Binary diffusion and Wassiljewa coefficients are identified by a pair of suffixes; A_{ij} is the coefficient of the quotient x_j/x_i and A_{ji} is that of its reciprocal.

3. Experimental Method

3.1. Apparatus

The thermal conductivity cell employed [25] was of the two wire type; a heating wire through which a known current is passed to supply heat to the cell, and a measuring wire which acts as a resistance thermometer indicating the rise in temperature of the gas at a point in the cell as a change in resistance. Both wires were thin tungsten spirals (30 ohm at 20°C) stretched longitudinally down the cell some 2-3 mm apart. Mercury cells of high stability were used to supply current both to the heating circuit and the Wheatstone bridge. The thermostat temperature was kept constant to about 0.02°C.

3.2. Procedure

The difference, Δ, between the resistances of the wire with two different standard heating currents is inversely proportional to the thermal conductivity of the gas in the cell. Δ is reproducible to better than 0.0008 ohm for the pure gases used in this work. This represents, at best, a precision of $\pm 0.2\%$ for diethyl ether at 50°C, and, at worst, a precision of $\pm 1\%$ for helium at 100°C.

3.3. Calibration

Δ was determined at 50°C and 100°C for various gases (He, Ne, Ar, Kr, Xe) whose thermal conductivities are known. The greatest weight was given to the data of Kannuluik and Carman [26] and the 'best' value from reference [27].

The product $K\Delta$ was not constant, but fell smoothly by some 20% between helium and xenon. At each temperature a plot of $K\Delta$ against Δ was constructed.

The absolute accuracy of our measurements depends on the accuracy of the values used for the calibrating gases. In the region of interest in this work, the accuracy of the data of Kannuluik and Carmen [26] is ca. 1%.

4. Results

Δ was measured at 50°C and 100°C for the four binary mixtures of diethyl ether with helium, neon, argon and nitrogen and the thermal conductivities deduced. These are shown in figs. 1-4. Also shown in these figures are the predictions of Hirschfelder and of the Lindsay-Bromley [22] equation. Tables 1 and 2 give a summary of the parameters used in deducing these predictions and table 3 shows their average discrepancies.

Table 1. Pure component properties.

Gas	T (°C)	$K^{(a)}$ (cal $km^{-1}s^{-1}$ $degK^{-1}$)	$\eta^{(b)}$ (g km^{-1} s^{-1})	$D_{ii}^{(c)}$ (1 atm cm^2 s^{-1})	$K_{trans}^{(d)}$ ($cal.km^{-1}s^{-1}deg\ K^{-1}$)	$K_{int}^{(e)}$ ($cal.km^{-1}s^{-1}deg\ K^{-1}$)	$\delta_{ii}^{(f)}$	$\sigma_{ii}^{(g)}$ Å	M (gm)
$(C_2H_5)_2O$	50	4.15_0	8.18	0.0383	-0.8221	3.328	0.08	5.539	74.123
	100	5.31_1	9.31	0.0501	-0.9356	4.375			
Ar	50	4.49_1	23.93	0.2049	-4.491	0	0	3.465	39.948
	100	5.04_2	27.07	0.2682	-5.042	0			
He	50	38.0_0	20.96	1.7959	-38.00	0	0	2.576	4.003
	100	41.6_5	23.23	2.2755	-41.65	0			
Ne	50	12.3_6	33.35	0.5750	-12.36	0	0	2.858	20.183
	100	13.5_7	36.90	0.7331	-13.57	0			
N_2	50	6.58_4	18.80	0.2307	-4.999	1.585	0	3.749	28.014
	100	7.38_3	21.01	0.2982	-5.587	1.796			

(a) Experimental values. (b) Experimental data [41, 27]. (c) Calculated from data in reference [4] and [42]. (d) From eq. 2. (e) From eq. 1. (f) From reference [4] and [33]. (g) From reference [4]

Table 2. Mixture properties.

system (i) + (j)	T (°C)	$D_{ij}=D_{ji}^{(a)}$ (1 atm.cm^2s^{-1})	$A_{ij}^{*(b)}$	$B_{ij}^{*(b)}$	a ($cal.km^{-1}s^{-1}deg\ K^{-1}$) (c)	b (c)	c (c)	$A_{ij\ int}$ (d)	$A_{ji\ int}$ (d)	Mass ratio M_j/M_i
$(C_2H_5)_2O$ + Ar (1) (2)	50	0.0897	1.096	1.137	8.751	3.744	3.979	0.395	0.394	1.85
	100	0.1176	1.094	1.126	9.906	3.734	3.973	2.284	2.281	
$(C_2H_5)_2O$ + He (1) (3)	50	0.4077	1.102	1.091	134.62	143.609	9.066	0.087	0.089	18.52
	100	0.5208	1.103	1.090	19.311	18.610	8.923	4.405	4.369	
$(C_2H_5)_2O$ + Ne (1) (4)	50	0.1667	1.096	1.099	27.579	7.902	5.967	0.212	0.216	3.67
	100	0.2144	1.097	1.093	29.902	7.681	5.902	3.449	3.419	
$(C_2H_5)_2O$ + N_2 (1) (5)	50	0.1022	1.094	1.123	9.208	3.564	3.918	0.346	0.348	2.65
	100	0.1332	1.094	1.112	10.257	3.518	3.895	2.257	2.239	

(a) Calculated from reference [4]. (b) Data from reference [4] and [33]. (c) Parameters of eq. 3 calculated according to reference [7]. (d) $A_{ij\ int} = D_{ii\ int}/D_{ij\ int}$.

Deviations from the molar average are in all cases negative ranging from 1% for $(C_2H_5)_2O$-Ar at 50°C to 43% for $(C_2H_5)_2O$-He at 100°C. $(C_2H_5)_2O$-N_2 shows less deviation from the linear mean than $(C_2H_5)_2O$-Ne but both curves appear fairly symmetrical. $(C_2H_5)_2O$-Ar and $(C_2H_5)_2O$-He are markedly unsymmetrical. $(C_2H_5)_2O$-Ar shows a broad shallow minimum between 50% and 60% diethyl ether at 50°C and a sharper minimum at 15% diethyl ether at 100°C. This curve also shows the unusual phenomenon of an inflexion point occuring between 40% and 60% diethyl ether at 100°C.

Table 3. Average discrepancies from observed thermal conductivity

System (i) + (j)	T (°C)	Wassiljewa + experimental A_{ij} (mean %)	Hirschfelder approximation (mean %)	Wassiljewa + Lindsay-Bromley A_{ij} (mean %)	Wassiljewa + Francis A_{ij} (mean %)
$(C_2H_5)_2O$ + Ar (1) (2)	50	+0.05	+3.01	+4.82	+3.62
	100	+0.01	+2.31	+3.22	+3.11
$(C_2H_5)_2O$ + He (1) (3)	50	-0.73	+4.32	-2.63	+3.69
	100	+0.41	+2.98	-4.81	+2.76
$(C_2H_5)_2O$ + Ne (1) (4)	50	-0.01	+3.15	+4.16	+4.67
	100	-0.08	+2.37	+2.36	+4.34
$(C_2H_5)_2O$ + N_2 (1) (5)	50	+0.12	+2.28	+3.80	+3.14
	100	+0.10	+2.09	+2.63	+3.93

5. Discussion

There are no previous experimental data on the binary mixtures discussed here. For pure components previous experimental data on thermal conductivity of diethyl ether [28, 29] and nitrogen [30-34] agree well.

Binary mixtures of diethyl ether (μ = 1.15 Debye) with other weakly polar molecules, chloroform and diethylamine [2], show an almost linear relationship between thermal conductivity and composition. This is also found to be the case with binary mixtures of diethyl ether and the more strongly polar ammonia (μ = 1.47 Debye) [29]. Mixtures of nonpolar gases (argon and neon) with ammonia give non-linear curves in which the thermal conductivity falls below the molar average [39]. Methanol (μ = 1.7 Debye) and argon mixtures show a maximum in the conductivity-composition curve; in this case the thermal conductivity lies well above the molar average [2]. This is also true in binary mixtures of nitrogen [35] or of air [3] with ammonia.

Minima in conductivity-composition curves have also been found for H_2- He, N_2- Ar, O_2 - Ar [36,37], and are accounted for by relaxation of rotational energy. In each of these cases the thermal conductivities of the pure components lie close to each other. Consequently, a minimum might be expected in the $(C_2H_5)_2O$-Ar system. In the N_2- Ar and O_2- Ar systems [37] the minima occur at a small percentage of the diatomic molecule and their depth increases with increasing temperature. In $(C_2H_5)_2O$-Ar the trend is not so consistent; the position and depth of the minimum is very sensitive to the temperature.

There is an overall similarity between the four conductivity-composition curves studied here. They show a certain amount of resemblance to the non polar binary mixture benzene-argon [2]. Mixtures of n-heptane with inert gases might provide a better comparison since n-heptane and diethyl ether have similar molecular weights, viscosities and molecular structure.

5.1. Hirschfelder Approximation

The parameters for the calculation of thermal conductivity from eqs. (3) and (4) are shown in tables 1 and 2. In determining values of A_{ij}^* and B_{ij}^* tabulations of Hirschfelder [4] were used for the Lennard-Jones potential (δ = 0). In the case of diethyl ether δ = 0.08 and A_{ij}^* and B_{ij}^* tabulations of the Stockmayer potential were used.

Hirschfelder's calculations are based on the assumptions that there is no interchange between translational and internal energy transport and that values adopted for parameters expressing unlike interactions have to be based on combining rules. The combination rules are

$$\sigma_{ij} = (\sigma_{ii} + \sigma_{ij})/2$$

$$\varepsilon_{ij} = (\varepsilon_{ii}\ \varepsilon_{ij})^{\frac{1}{2}} \qquad (10)$$

$$\delta_{ij} = (\delta_{ii}\ \delta_{ij})^{\frac{1}{2}}\ [(\sigma_{ii}\sigma_{jj})^{\frac{1}{2}}/\sigma_{ij}]^3$$

From table 3 it may be seen that Hirschfelder's approximation overestimates thermal conductivity for each binary mixture. This is most for $(C_2H_5)_2O$-He and least for $(C_2H_5)_2O$-N_2 with the greatest deviations occuring at 50°C and in compositions of between 40% and 60% diethyl ether.

5.2. Wassiljewa coefficients

5.2.1. Introduction

"Best" values of A_{ij} have been estimated from the experimental results for the four binary mixtures. If A_{ij} and A_{ji} are both considered freely disposable there exists a large range of pairs of values which give an equally good fit with experimental thermal conductivity. If an independent general relation between the two were available the prediction of the A_{ij} would be easier. Such a relationship [19] is

$$\frac{A_{ij}}{A_{ji}} = \frac{\eta_i}{\eta_j}\left(\frac{M_j}{M_i}\right)^{\nu}. \qquad (12)$$

There is good reason to believe that $\nu = \frac{3}{4}$[19,24] and our "best" A_{ij} are calculated on this assumption.

Values of A_{ij} for experiment, Lindsay-Bromley and Francis are shown in table 4. From tables 3 and

Table 4. Values of A_{ij}.

	Experimental A_{ij}		Lindsay-Bromley A_{ij}		Francis A_{ij}	
	50°C	100°C	50°C	100°C	50°C	100°C
A_{12}	0.504	0.491	0.439	0.446	0.355	0.360
A_{21}	2.340	2.270	2.039	2.064	2.647	2.599
A_{13}	0.254	0.242	0.265	0.274	0.030	0.032
A_{31}	5.810	5.400	6.061	6.091	6.189	6.151
A_{14}	0.352	0.348	0.336	0.326	0.150	0.155
A_{41}	3.810	3.660	2.978	3.426	4.250	4.185
A_{15}	0.474	0.468	0.427	0.437	0.275	0.281
A_{51}	2.260	2.190	2.035	2.045	2.733	2.611

4 it may be seen that "best" A_{ij} fit observed results well and show only small dependence on temperature. They are also consistent with minima and an inflexion for $(C_2H_5)_2O$-Ar system (Appendix).

5.2.2. Empirical estimates

The experimental data permits a test of Lindsay-Bromley A_{ij} (table 3). In all cases except $(C_2H_5)_2O$-He, the thermal conductivities are overestimated by an average of 3%, which is about 1% worse than Hirschfelder's approximation. For $(C_2H_5)_2O$-He the thermal conductivity is underestimated by about 3%. The greatest deviations occur for mixtures between 40% and 60% diethyl ether. For example, the maximum deviation for $(C_2H_5)_2O$-Ar at 50°C is +6.7% at 60% diethyl ether and for $(C_2H_5)_2O$-He it is -7.3% at 60% diethyl ether.

Thus in all cases except $(C_2H_5)_2O$-He the Lindsay-Bromley equation underestimates A_{ij}. The factor 0.733 [38] in the equation

$$S_{ij} = 0.733\,(S_i S_j)^{\frac{1}{2}} \qquad (13)$$

has no rigorous foundation. It was introduced by Lindsay and Bromley in an attempt to reduce the high values of A_{ij} which their formula gave for mixtures of polar and nonpolar gases. In the case of diethyl

ether with neon or argon or nitrogen much improved values of A_{ij} are obtained if diethyl ether is considered to be non polar, ($S_{ij} = 1.0 \times \sqrt{S_i S_j}$). Such an assumption, however, provides even less adequate values of A_{ij} for mixtures of diethyl ether with helium. We conclude that the Lindsay-Bromley equation is very unreliable where there is a very great difference in the masses of the constituents of a binary mixture, and that the combining rule for S_{ij} depends too critically on the decision whether a given gas is polar or not.

The A_{ij} predicted by the Francis equation uniformly overestimate thermal conductivities of our mixtures by between 2% and 4% (tables 3 and 4). It is useful, however, even when the masses of constituents differ greatly.

5.2.3. "Best" Experimental values

As already stated values of A_{ij} may be given a simple interpretation. They are a quotient of efficiencies of impeding transport of heat. In all cases studied here, one of the Wassiljewa coefficients is much greater than one, and the other is much smaller than one. Diethyl ether is more effective in impeding the transport of heat by the inert gas than the inert gas is in impeding the transport of heat by diethyl ether. As most of the heat is transferred by the inert gas this causes the thermal conductivity of diethyl ether-inert gas mixtures to fall below molar averages.

When considering impedance of heat transport, mass ratios and relative sizes must be considered (tables 1 and 2). These two factors cannot be distinguished in the case studied here since they effectively follow similar trends. Thus helium which is small and light is most effectively impeded by the large, heavy diethyl ether. Consequently the thermal conductivity of the mixture can fall by as much as 40% below molar average. The effect of replacing helium by neon, nitrogen and argon reflects the increased masses and collision diameters of these molecules; negative deviations decrease in proportion to the mass ratios. However, even for mixtures of diethyl ether with argon in which the mass ratio (1.85) is not very large, the combined effect of relative mass and size results in diethyl ether being about five times more effective in impeding the transport of heat by the other molecule than is argon.

6. Appendix[2]

As already stated, the Wassiljewa equation is capable of accommodating turning points and inflexions. The conditions for these are derived below.

On introducing $z = x_j/x_i$ and assuming i refers to the component with lower thermal conductivity eq. (5) becomes

$$K = \frac{K_i}{1 + A_{ij}z} + \frac{K_j}{1 + 1/A_{ij}z} \quad . \tag{16}$$

For a turning point $dK/dz = 0$ or $dK/dx = 0$ so that

$$\frac{dK}{dz} = \frac{A_{ij}^2 A_{ji} K_j (1+A_{ij})^2 - A_{ij} K_i (A_{ij}z + A_{ij}A_{ji})^2}{(1 + A_{ij}z)^2 (A_{ij}z + A_{ij}A_{ji})^2} = 0 \tag{17}$$

therefore,

$$A_{ij}z = \frac{\sqrt{A_{ij}A_{ji}K_i/K_j} - 1}{1 - \sqrt{1/A_{ij}A_{ji}} \cdot K_i/K_j} \quad . \tag{18}$$

A_{ij}, A_{ji}, K_i, K_j and z are all positive. If the right hand side of eq.(18) is negative there can be no turning point, since this implies a negative (physically impossible) value of z. There must therefore be a monotonic variation of K with z and

$$K_j/K_i > A_{ij}A_{ji} > K_i/K_j \quad .$$

For a turning point the right hand side of eq. (18) must be positive so

$$A_{ij}A_{ji} < K_i/K_j \quad \text{or} \quad A_{ij}A_{ji} > K_j/K_i$$

2 In collaboration with Dr. J. K. Sutton, N.E.L., East Kilbride, Glasgow, U.K.

To obtain the conditions for a maximum or minimum $dK/dz = 0$ is substituted into the value of d^2K/dz^2 where

$$\frac{1}{2A_{ij}^2} \quad \frac{d^2K}{dz^2} = \frac{K_i}{(A_{ij}z+1)^2} \left\{ \frac{A_{ij}A_{ji}-1}{(A_{ij}z+1)(A_{ij}z+A_{ij}A_{ji})} \right\} . \qquad (19)$$

The sign of the equation is determined by the sign of $(A_{ij}A_{ji} - 1)$.

If $A_{ij}A_{ji} > 1$, a minimum is obtained and
If $A_{ij}A_{ji} < 1$, a maximum is obtained.

For each binary mixture experimental A_{ij} values, K_i/K_j and K_j/K_i are shown in table 5.

Table 5

System (i) + (j)	50°C					100°C				
	$A_{ij}A_{ji}$	K_i/K_j	K_j/K_i	Ø	$ØA_{ij}A_{ji}$	$A_{ij}A_{ji}$	K_i/K_j	K_j/K_i	Ø	$ØA_{ij}A_{ji}$
$(C_2H_5)_2O$-Ar	1.180	0.924	1.082	1.020	1.204	1.115	0.947	1.053	0.993	1.107
$(C_2H_5)_2O$-He	1.476	0.109	9.157	1.902	2.807	1.408	0.127	7.842	1.832	2.579
$(C_2H_5)_2O$-Ne	1.342	0.336	2.978	1.363	1.829	1.274	0.391	2.555	1.306	1.664
$(C_2H_5)_2O$-N_2	1.071	0.630	1.586	1.160	1.242	1.024	0.719	1.390	1.115	1.142

From the table it is clear that the Wassiljewa expression for $(C_2H_5)_2O$-He, $(C_2H_5)_2O$-Ne and $(C_2H_5)_2O$-N_2 predicts a monotonic variation of thermal conductivity with x. The mixtures of $(C_2H_5)_2O$-Ar both at 50°C and 100°C satisfy the conditions for a minimum value in the thermal conductivity-composition curve. These are calculated at 57% and 14% diethyl ether at 50°C and 100°C respectively which are in agreement with experiment (fig.1).

In order to derive the condition for a turning point, eq.(18) is expressed in terms of resistances as explained earlier. Thus if $R_{ii} = 1/K_i$ and $\alpha_{ij} = A_{ij}/K_i$ etc. eq. (18) becomes

$$\alpha_{ij}z = \frac{R_{ii}\alpha_{ij}\alpha_{ji}\,(1-R_{ii}/\sqrt{\alpha_{ij}\alpha_{ji}})}{R_{ii}R_{jj}\,(\sqrt{\alpha_{ij}\alpha_{ji}}\,/\,R_{jj} - 1)} . \qquad (20)$$

Thus a minimum occurs when $\alpha_{ij}\alpha_{ji} > R_{ii}R_{ij}$ or when the product of resistances for unlike interactions is greater than that for like interactions.

A point of inflexion occurs when d^2K/dz^2 or $d^2K/dx^2 = 0$. An inflexion in the K - z plot does not necessarily coincide with the inflexion in the K - x plot, thus

$$\frac{d^2K}{dx^2} = \frac{dz}{dx}\left[2(1+z)\frac{dK}{dz} + (1+z)^2\frac{d^2K}{dz^2}\right], \qquad (21)$$

where d^2K/dz^2 is given by eq.(19) and dK/dz by eq.(17). When $d^2K/dx^2 = 0$.

$$A_{ij}z = \frac{(1-ØA_{ij}A_{ji})}{(Ø - 1)} , \qquad (22)$$

where

$$\phi^3 = \frac{1}{A_{ij}A_{ji}} \cdot \frac{K_i}{K_j} \cdot \frac{(A_{ij} - 1)}{(A_{ij} - A_{ij}A_{ji})} \quad . \qquad (23)$$

The conditions become

$$\phi > 1 > \phi A_{ij}A_{ji} \quad \text{or} \quad \phi < 1 < \phi A_{ij}A_{ji} \quad .$$

From table (5) the only mixture satsifying the condition for an inflexion is $(C_2H_5)_2O$-Ar at 100°C. This is calculated to occur at 55% diethyl ether in agreement with experiment (fig.1).

Symbols

1,2...	subscripts designating chemical species in a mixture.
A^*, B^*	quantities defined by Hirschfelder et al (4).
A_{ij}	coefficients giving relative efficiencies in impeding transport.
a,b,c	quantities expressing results of a first approximation to rigorous theory for a binary mixture.
C_v	thermal capacity of unit mass at constant volume.
D	diffusion coefficient.
K	thermal conductivity.
M	molecular weight.
R	gas constant.
S	Sutherland's constant.
trans, int.	subscripts denoting translational and internal contributions.
$x_1 x_2$	mole fractions.
Δ	experimental quantity inversely proportional to K.
δ	parameter of the Stockmayer potential for polar gases defined by Mason and Monchick [42].
η	viscosity.
σ	collision diameter.
μ	dipole moment.

We thank Drs. J. R. Sutton and P. K. Chakraborti for useful discussion.

7. References

[1] Gray, P. and Wright, P. G. Proc.Roy.Soc.A(267) 408 (1962).

[2] Bennett, L.A. and Vines, R. G. J.Chem.Phys. 23 1587 (1955).

[3] Cheung, H, Bromley, L.A. and Wilke, G. R. Amer. Inst.Chem.Engineers J. 8 221 (1962).

[4] Molecular theory of gases and liquids, Hirschfelder, J.O., Curtiss, C. F. and Bird, R. B., Wiley, New York, (1964).

[5] Euskog, D., Phys.Z. 12 533 (1911).

[6] Chapman, S. Phil.Trans. A(207) 115 (1917).

[7] Mathematical theory of non-uniform gases, Chapman, S. and Cowling, T.G., C.U.P.(1939).

[8] Muckenfuss, C. and Curtiss, C.F., J.Chem.Phys. 29 1273 (1958).

[9] Mason, E.A. and Saxena, S.C., J.Chem.Phys. 31 511(1959).

[10] Sixth symposium on Combustion, Hirschfelder, J.O., (Reinhold 1956).

[11] Mason, E. A. and Saxena, S. C., Phys.Fluids, 1 301 (1958).

[12] Brokaw, R.S., J.Chem.Phys., 29, 391 (1958).

[13] Srivastava, B.N. and Barua, A. K., J.Chem.Phys. 32 427 (1960).

[14] Monchick, L., Pereira, A.N.G. and Mason, E. A., J.Chem.Phys., 42, 3241 (1965).

[15] Baker, B. and Brokaw, R.S. J.Chem.Phys., 40 1523 (1946) and 46 2846 (1967).

[16] Baker, B. and Brokaw, R.S., J.Chem.Phys., 43 3519 (1965).

[17] Wassiljewa, A., Phys.Z. 5 737 (1904).

[18] Cowling, T.G., Proc.Roy.Soc., A(263) 186 (1961).

[19] Wright, P. G. and Gray, P., Trans.Faraday Soc., 58 1 (1962).

[20] Cowling, T. G., Gray, P. and Wright, P.G. Proc. Roy.Soc., A(276) 69 (1963).

[21] Burnett, D., J.Chem.Phys., 42 2533 (1965).

[22] Lindsay, A. L. and Bromley, L. A. Ind.Eng. Chem. 42 1508 (1950).

[23] Francis, W.E. Trans.Faraday Soc., 54 1492 (1958)

[24] Huck, R. J. and Thornton, E., Proc.Phys.Soc. (in press).

[25] Gray, P. and Wright, P. G., Proc.Roy.Soc. A(263) 161 (1961).

[26] Kannuluik, W. G. and Carman, E. H., Proc.Phys. Soc. B(65) 701 (1952).

[27] Thermophysical properties research center data book, Purdue Research Foundation, Lafayette, Indiana, (1966).

[28] Bennett, R. G. and Vines, L. A. J. Chem.Phys., 23 1587 (1955).

[29] Srivastava, B. N. and Das Gupta, A. J. Chem. Phys. 46 3592 (1967).

[30] "Tables of thermal properties of gases" J. Hilsenrath et al., Nat.Bur.Stand.Circular 564, (Washington)(1955).

[31] Pereira, A. N. G. and Raw, C. J.G., Phys. Fluids, 6 1091 (1963).

[32] Westenberg, A. A. and de Haas, N., Phys.Fluids, 5 266 (1962).

[33] Rothman, A. J. and Bromley, L. A. Ind.Eng.Chem., 47 899 (1955).

[34] Keyes, F. G., Trans.Am.Soc.Mech.Eng., 74 1303 (1952).

[35] Gray, P. and Wright, P. G., Progress in international research on thermodynamics and transport properties, A.S.M.E. Conference report, Academic Press (New York) 1962).

[36] Mukhopadhyay, P. and Barua, A. K., Brit.J. Appl.Phys. 18 635 (1967).

[37] Mukhopadhyay, P. and Barua, A. K., Brit.J. Appl.Phys., 18 1307(1967).

[38] Gruss, H., Schmick, H, Wiss Veroffente Siemens-Konzern 7 202 (1928).

[39] Srivastava, B. N. and Das Gupta, A., Brit.J. App.Phys., 18 945 (1967).

[40] Mason, E. A. and Monchick, L. J.Chem.Phys. 30 1622 (1962).

[41] Flynn, G. P., Hanks, R. V., Lemaire, N. A. and Ross, J., J.Chem.Phys. 38 154 (1963).

[42] Monchick, L. and Mason, E. A., J.Chem.Phys. 35 1676 (1961).

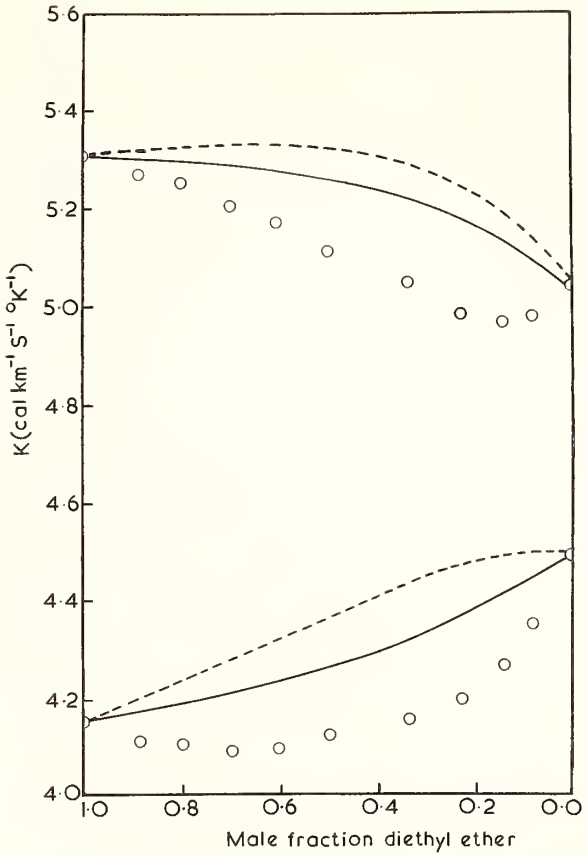

Figure 1. The effect of composition on thermal conductivity for $(C_2H_5)_2O$-Ar. Lower curve, 50 °C, upper curve 100 °C. Broken curve: Wassiljewa equation, A_{ij} from the predictions of Lindsay and Bronley; continuous curve: Hirschfelder approximation; O: our experimental values.

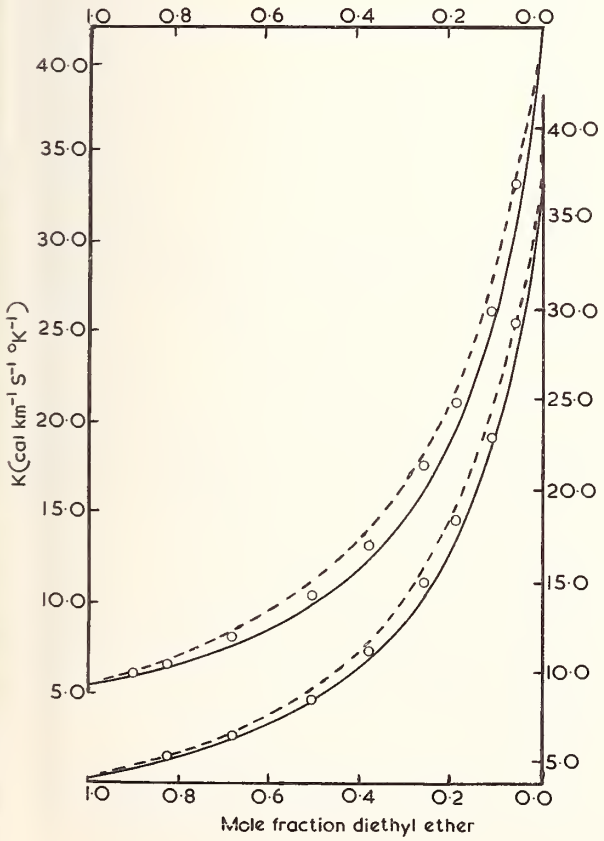

Figure 2. The effect of composition on thermal conductivity for $(C_2H_5)_2O$-He. The legend is the same as figure 1 except broken curve: Hirschfelder approximation, continuous curve: Wassiljewa equation A_{ij} from the predictions of Lindsay and Bromley.

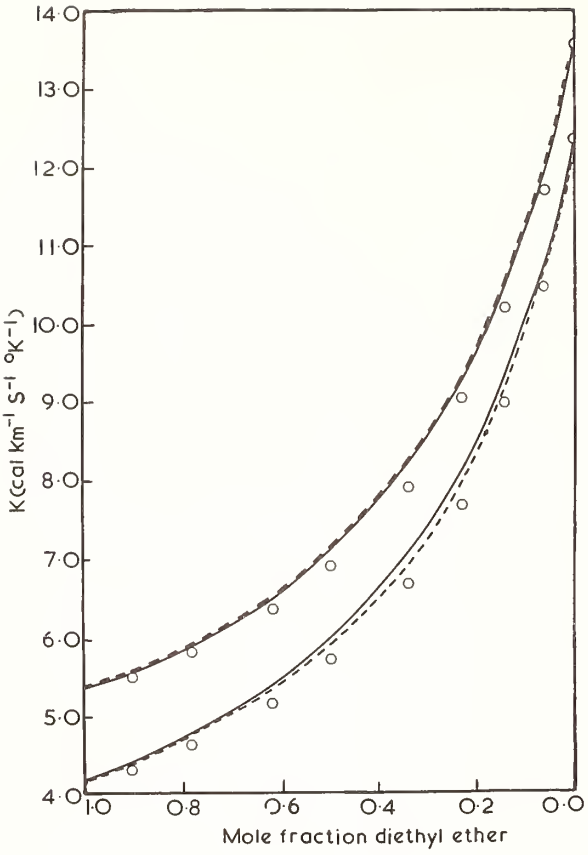

Figure 3. The effect of composition on thermal conductivity for $(C_2H_5)_2O$-Ne. The legend is the same as figure 2.

Figure 4. The effect of composition on thermal conductivity for $(C_2H_5)_2O$-N_2. The legend is the same as figure 2.

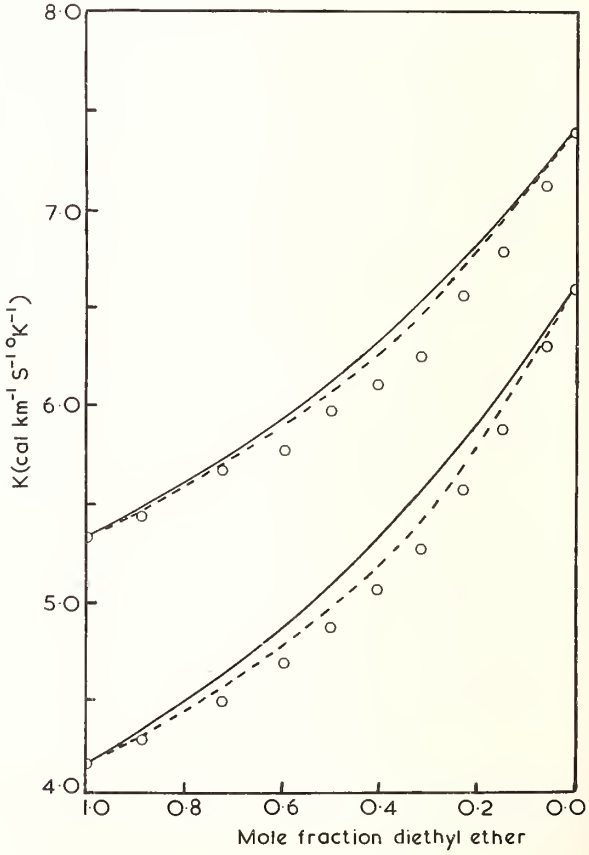

Determination of the Eucken Factor for Parahydrogen at 77°K

Lee B. Harris[1]

Research Laboratories
Xerox Corporation
Rochester, N. Y. 14603

At 77°K the measured change in thermal conductivity of hydrogen caused by a change in the relative proportions of ortho- and parahydrogen can be used to determine the dimensionless parameter δ introduced by Hirschfelder [3][2] in his formula for the "modified Eucken correction" and which is a measure of the contribution of rotational energy to the thermal conductivity of a polyatomic gas. This method, which is very reproducible and is not sensitive to systematic errors in the measurement of absolute thermal conductivity, yields $\delta = 0.75$. An analogous method, using the variation of thermal conductivity at 311°K of a H_2-Ar mixture [14] as the proportion of H_2 is increased, yields $\delta = 0.76$, which is in excellent agreement with values previously obtained by other investigators from absolute measurements of thermal conductivity [14] and Prandtl number [3,17]. Both of these values are significantly lower than those calculated for hydrogen by Hirschfelder [3], and suggest that the diffusion coefficient for rotational energy is lower than that for self-diffusion of hydrogen.

Key Words: Eucken factor, gases, gas mixtures, hydrogen, orthohydrogen, parahydrogen, thermal conductivity.

1. Introduction

For a monatomic gas the thermal conductivity λ is given [1] very closely by

$$\lambda = \frac{15}{4}\frac{R}{M}\eta \tag{1}$$

where R is the gas constant, M the molecular weight, both in molar units, and η is the viscosity. For a polyatomic gas, eq (1) is usually corrected in a manner first suggested by Eucken [2]; Hirschfelder [3] generalized the "Eucken correction" [4] to

$$\lambda' = \lambda\left[1 + (2/5)\,\delta\,(C_r/F)\right] \equiv \lambda f'_H \tag{2}$$

where C_r is the rotational specific heat and λ is the thermal conductivity excluding rotational energy transport; f'_H is called the "modified" Eucken correction and differs from the "Eucken factor", f, generally encountered in the literature [4]. Hirschfelder's [3] expression for δ is

$$\delta_H = (4/5)\Omega^{(2,2)*}/\Omega^{(1,1)*} = (2/3)\rho D/\eta \tag{3}$$

where D is the coefficient of self-diffusion, ρ is the gas density and $\Omega^{(1,1)*}$ and $\Omega^{(2,2)*}$ are collision integrals [5]. Eucken's original equation is a special case of eq (2) obtained by letting $\rho D/\eta = 1$, in which case δ_H takes the value

$$\delta_H = 2/3 \equiv \delta_E \tag{4}$$

---

[1] Scientist

[2] Figures in brackets indicate the literature references at the end of this paper.

Thermal conductivity measurement provides a value of the Eucken factor, f, from which the value of δ may be estimated. However, the accuracy of this estimate is severely affected by the fact that the term involving δ in eq (2) is always a relatively small contribution and is especially small at low temperatures, where the rotational motion is restricted by quantum effects. For hydrogen below 100°K the term involving δ contributes less than 10% so that a 1% error in measuring thermal conductivity becomes a 10% error in determining δ. Low temperature thermal conductivity data for hydrogen [6] shows a spread of about 5%; and the corresponding values of δ differ by a factor of two. Consequently, although the thermal conductivity of hydrogen is used to detect the ortho-to-para conversion [7] it has not been possible for students of that phenomenon to correlate their results with theoretical or experimental results such as those cited above. Such correlation is also hampered by the fact that most of the investigators cited above have not considered orthohydrogen and parahydrogen as separate constituents. In this paper a method is described with which δ may be accurately determined at 77°K from the relative change in thermal conductivity associated with the ortho-to-para conversion. Only an outline of the method, and the results are given here. Details of the apparatus and procedure and further discussion of the results will be published elsewhere.

2. Method

For a binary gas mixture, Hirschfelder's [8] expression for thermal conductivity is

$$\lambda'_{12} = \lambda_{12} + (\lambda'_1 - \lambda_1) \Big/ \left[1 + (x_2/x_1)(D_{11}/D_{12})\right] + (\lambda'_2 - \lambda_2) \Big/ \left[1 + (x_1/x_2)(D_{22}/D_{12})\right] \tag{5}$$

where the subscripts 1, 2 and 12 denote gas #1, gas #2 and the mixture, respectively, and x refers to mole fraction. λ' includes the effects of rotational energy and λ does not. For a mixture of ortho- and parahydrogen, since the difference between these two species is purely rotational, it is approximately true (denoting ortho and para by subscripts o and p respectively) that

$$\lambda_{op} = \lambda_o = \lambda_p \equiv \lambda \tag{6}$$

If it is true that

$$D_{oo} \simeq D_{pp} \simeq D_{op} \tag{7}$$

where the subscripts o and p refer to ortho- and parahydrogen respectively, then substituting (6), (7) and (2) into (5) and using the fact that $x_o + x_p = 1$, one obtains:

$$\lambda'_{op} = \lambda\left\{1 + (2/5R)(C_r)_o \delta_o + x_p b\right\} \tag{8}$$

where

$$b = (2/5R)\left[(C_r)_p \delta_p - (C_r)_o \delta_o\right] \tag{9}$$

The quantity b may therefore be determined experimentally by measuring the relative rate of change $(1/\lambda)(\partial \lambda'_{op}/\partial x_p)$.

Once b has been determined experimentally, eq (9) provides a relationship between δ_o and δ_p. If sufficient additional information regarding either of these is available from other experimental data or from theory, then one may determine their values individually. At 100°K or lower, orthohydrogen behaves almost like a monatomic gas [i.e., $(C_r)_o \simeq 0.01$ cal/mole]. Therefore, at such temperatures (9) yields

$$\delta_p = \left[R/(C_r)_p\right](5/2)b \qquad (T \leq 100°K) \tag{10}$$

Equation (10) is used in determining the results to be reported here.

To measure thermal conductivity, a cylindrically symmetrical hot-wire cell was used, for which it is well-known that, neglecting radiation and end-effects, the rate of heat transfer $\mathring{Q}$ out through the cell is [9]

$$\mathring{Q} = K \int_{T_o}^{T_r} \lambda'_{op}(T)\, dT \qquad (11)$$

$$K = 2\pi L / \ell n(r_o/r)$$

where L is the length of the cell and T_r and T_o are the temperatures at the wire surface (radius r) and at the outer wall (radius r_o), respectively. From eq (11) it can be shown that

$$\lambda'_{op}(T_o) = (1/K) \left\{ \lim_{T_r \longrightarrow T_o} \left[\mathring{Q} / (T_r - T_o) \right] \right\} \qquad (12)$$

To avoid measurement errors that occur at small values of $(T_r - T_o)$ it is best to plot $\mathring{Q} / (T_r - T_o)$ vs. $(T_r - T_o)$ and extrapolate linearly to $(T_r - T_o) = 0$.

At 100°K or lower temperatures it is possible to determine λ from the experimental data. Since at these temperatures the rotational motion of orthohydrogen is "frozen", the thermal conductivity of pure orthohydrogen ($\lambda'_{0.0}$) is equal to λ. Since λ'_{op} is a linear function of x_p [see eq (8)], $\lambda'_{0.0} \simeq \lambda'_{0.25} - \Delta\lambda'$. Therefore,

$$\lambda \simeq \lambda'_{0.25} - \Delta\lambda' . \qquad (13)$$

3. Results

Figure 1 shows a plot of $\frac{\mathring{Q}}{T_r - T_o}$ for one set of experimental data. The lower points and corresponding straight line are for normal hydrogen; the upper points and straight line are for 50.3% parahydrogen. Table 1 shows experimental values of $\lambda'_{0.5}$ and $\lambda'_{0.25}$, [calculated by extrapolating the straight lines to $T_r - T_o = 0$ according to eq (12)]; and λ from eq (13).

Table 1. Values of thermal conductivity and δ obtained from ten experiments at 77°K.

mw./cm. deg. K.					
$\lambda'_{0.5}$	$\lambda'_{0.25}$	λ	λ_{theor}	b	δ_p
.5920	.5796	.567	.506	.0863	.731
.5870	.5750	.563		.0843	.714
.5878	.5754	.563		.0869	.736
.5861	.5730	.560		.0922	.782
.5786	.5661	.553		.0897	.760
.5803	.5678	.555		.0886	.751
.5738	.5617	.550		.0869	.737
.5761	.5631	.550		.0931	.789
.5789	.5664	.553		.0895	.758
.5787	.5669	.555	.506	.0841	.713
					.747
		Mean values and 99.9% confidence limits			±.04

The fourth column shows a theoretical value of λ calculated from kinetic theory [10]. The correspon-

ding values of b and δ_p are given in columns five and six. The value of C_r used in these calculations was obtained by calculating from Farkas's equations [7] the rotational energy of parahydrogen at fifty equally spaced temperatures between 50°K and 100°K. These points were least-square fitted by a fourth degree polynomial which was then differentiated at 77.2°K to obtain C_r = 0.5862 cal/mole. The first line in the table is calculated from the data of Fig. 1. Lines two through ten of Table 1 show the results of nine more runs. All data was taken during a three-month interval in which the equipment was shut down twice, once to replace the platinum wire and once to modify the Baratron connections. The last line in Table 1 shows the mean values and 99.9% confidence limits [11] for the value of δ_p.

4. Discussion

The mean value of δ_p differs significantly from the value $\delta_H \sim 0.88$ calculated by Hirschfelder for $T^* = 2$ (which corresponds to liquid nitrogen temperature for H_2, since $T^* = T/(\epsilon/k)$ and $\epsilon/k \sim 37°$ for H_2, where ϵ is the well-depth parameter of the intermolecular potential and k is Bolzmann's constant). Some values of δ for hydrogen can be calculated using absolute measurements of viscosity and thermal conductivity. From the data of Stolyarov and of Hilsenrath[12], Liley [6] gives values of 2.310 and 2.175 respectively for the Eucken factor, f, at 77°K. The corresponding [4] values of f' are .942 and .910 from which eq (8) yields negative values of δ_p. At 100°K the data of Johnston & Grilly [13] gives f' = 1.03 from which δ_p = 0.4 for a normal mixture of three parts ortho- and one part parahydrogen. The variation among these values of δ_p illustrates the previously mentioned difficulty in using absolute thermal conductivity measurements, which must be extremely accurate to give reliable values of δ, especially at low temperatures. At higher temperatures, Srivastava and Srivastava [14] found δ = 0.76 at 311°K and they calculated that δ = 0.74 according to data of Johnston & Grilly [13] at 300°K. At the same temperature Hirschfelder's [3] calculations give $\delta \simeq 0.89$.

Interestingly, it is possible to use the thermal conductivity of monatomic-diatomic gas mixtures in a manner entirely analogous to that which was described above for mixtures of ortho- and parahydrogen. Calling the monatomic gas #1 and the diatomic gas #2, using eqs (2) and (6), differentiating with respect to x_2 and evaluating the derivative at $x_2 = 0$ (and noting that $x_1 + x_2 = 1$), one obtains

$$\delta_2 = \left[R/(C_r)_2\right] (5/2)b' \tag{16}$$

where

$$b' = (D_{22}/D_{12}) \left(\frac{d\left[(\lambda'_{12} - \lambda_{12})/\lambda_2\right]}{dx_2} \right)_{x_2 = 0} \tag{17}$$

Equations (16) and (17) have the considerable advantage that they are not limited to any particular temperature range or any particular diatomic gas. To use them, however, one must know $(d\lambda_{12}/dx_2)$, which may be found either theoretically [15] or from thermal conductivity measurements at temperatures low enough that $(C_r)_2 \simeq 0$. The value of δ obtained from (16) and (17) depends not on the absolute value of thermal conductivity, but only on its relative variation with mixture ratio. Srivastava and Srivastava [14] measured the thermal conductivity of mixtures of hydrogen and argon at 311°K. From their data, eqs (16) and (17) yield [16] δ_2 = 0.76. The agreement between this value of δ and that determined from the absolute thermal conductivity measurements is excellent.

Hirschfelder [3] pointed out that δ can be calculated from the Prandtl number, and using Keyes's [17] data for hydrogen, he found that δ = 0.64 at 173°K and δ = 0.77 at 273°K.

5. Conclusions

A new method has been devised with which Hirschfelder's [3] parameter δ for rotational heat transfer can be determined from the relative change of thermal conductivity of gas mixtures. This method was used to evaluate δ for parahydrogen at 77°K using mixtures of ortho- and parahydrogen; the value so obtained is $\delta_p(77°K) = 0.75$. This result is not sensitive to systematic errors in the measurement of absolute thermal conductivity and is probably more reliable than any of the values obtained previously from absolute measurements of thermal conductivity. When applied to the thermal conductivity [14] of a mixture of hydrogen and argon at room temperature, the new method yields δ = 0.76 for normal hydrogen. This value is in excellent agreement with the values 0.74 and 0.76 obtained from absolute thermal conductivity measurements [13,14] and the value 0.77 from measurement of Prandtl number [3,17].

6. Acknowledgment

An experimental study of the heterogeneous catalysis of the ortho-to-parahydrogen conversion was

suggested to me by W. Roth of Xerox Corporation.

8. References

[1] Hirschfelder, J.O., C.F. Curtis and R.B. Bird; Molecular Theory of Gases and Liquids (John Wiley & Sons, N.Y., 1964) p. 534.

[2] Eucken, A., Phys. Z., 14, 329 (1913).

[3] Hirschfelder, J.O., J. Chem. Phys. 26, 282 (1957). See Ref. 1, p. 527 for the second equality in equation (3).

[4] Ref. 1, pp. 498ff., 534, 574. Many authors use the well-known "Eucken factor" (designated f), which is defined by the relation $\lambda' = f C_v \eta / M$. I shall follow the practice of Hirschfelder and use the "Eucken correction" defined by the first and last members of eq (2), denoting it by f' instead of f. The relation between the two is $f'/f = (4/15)C_v/R$. For values of C_v, see ref. 7, pp. 19, 26.

[5] Ref. 1, p. 484.

[6] The literature on this subject is surveyed by P.E. Liley in Thermodynamic Transport Properties: Gases, Liquids, Solids papers (Symposium, Lafayette, Indiana, 1959). Other data is compiled by S.C. Saxena and J.P. Agrawal [J. Chem. Phys. 35, 2107 (1961)].

[7] Farkas, A., Orthohydrogen, Parahydrogen and Heavy Hydrogen (Cambridge University Press, 1935).

[8] Hirschfelder, J.O., in Sixth Symposium (International) on Combustion, (Reinhold Publishing Corp., N.Y., 1957),p351.

[9] Zemansky, M.W., Heat and Thermodynamics, 3rd ed., McGraw Hill, 1951, p. 83.

[10] Ref. 1, p. 534.

[11] Confidence limits are obtained using the "Student-t" distribution. See A.M. Mood, Introduction to the Theory of Statistics, 1st ed., McGraw-Hill, 1950, p. 225.

[12] Hilsenrath, et. al., NBS circular 564 (1955); Stolyarov, E.A., Zhur. Fiz. khim., 24, 279 (1950), both quoted by Liley in ref. 10.

[13] Johnston, H.L. and E.R. Grilly, J. Chem. Phys. 14, 233 (1946).

[14] Srivastava, B.N. and R.C. Srivastava, J. Chem. Phys. 30, 1200 (1959).

[15] Ref. 1, Chapter 8.

[16] The cited paper does not quote a value of D_{22}. I used the value 1.285 $cm^2 sec^{-1}$ at 273°K [P. Hartek and H.W. Schmidt, Z. Physik. Chem., 21B, 447 (1933)]. To correct it to 311°K, I used the formula $D = \text{const.} \times \sqrt{T^3/\mu_2}(1,1)^*(T^*)$ [see Ref. 1, p. 527] which gives $D_{22} = 1.61$ $cm^2 sec^{-1}$ at 311°K. C_r was taken equal to R. which is very nearly true for $T \geq 300$°K.

[17] Keyes, F.G., SQUID Technical Report 37, MIT (April 1, 1952); Trans. ASME, 76, 809 (1954) and 77, 1395 (1955).

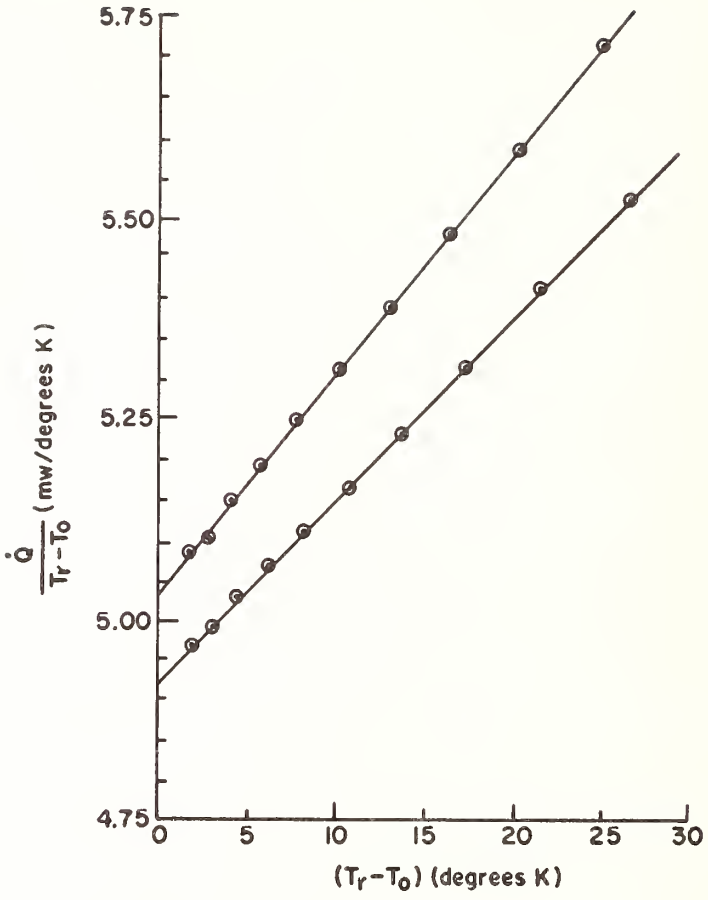

Figure 1. Thermal conductivity data corresponding to the first line of Table 1. Upper points and straight line are for a 50-50 ortho-para mixture. Lower points and line are for normal hydrogen.

Prediction of Minor Heat Losses in a Thermal Conductivity Cell and Other Calorimeter Type Cells

D. R. Tree and W. Leidenfrost

Mechanical Engineering
Purdue University
Lafayette, Indiana 47907

In recent years there has been an increasing number of reported thermal conductivity measurements of liquids, gases and gas mixtures. The major emphasis of these works has been to obtain thermal conductivity values with a high degree of accuracy. Several authors have reported values which they claim have an error of less than 1%. In the present work some of the factors affecting the accuracy of thermal conductivity measurements in a calorimeter type thermal conductivity cell are considered. In this work a calorimeter type cell is defined to be a cell where the inner body is completely surrounded by the outer body and the fluid to be tested is placed within a cavity between these two bodies. The inner body is always at a higher temperature than the outer body.

The steady state heat flow by conduction for such a cell is $q_k = k_L B\Delta T$ where k_L is the thermal conductivity of the fluid, B is a geometrical constant of the cell, and ΔT is the temperature difference between the two bodies.

A method is developed for very accurately measuring the geometrical constant. This method has yielded the geometrical constant with an error of less than 0.01 percent.

A method is also developed that allows the total heat input to the cell to be measured with a high degree of accuracy. Unfortunately, all of the heat input to the inner body is not transferred by conduction through the test layer. There are at least three other ways that heat can be transferred from the inner body to the cold outer body. They are: 1) by free convection in the test fluid; 2) by conduction along the devices used to position the two bodies with respect to each other, by conduction along the wires used to supply power to the hot inner body, and by conduction along the wires used to obtain the temperature of the inner body; and 3) by radiation between the two bodies.

A detailed analysis of each of these methods of heat transfer is made, and a method of predicting or measuring each is obtained. The analysis shows that by proper design of the instrument that heat transfer by free convection is so small that if it is neglected the error in the thermal conductivity is negligible.

This is not true of the other two forms of heat transfer if accuracies of 1% or better are desired. The heat loss along the connecting devices and lead-in wires is shown to produce the largest error and its value is the most difficult to obtain. The neglecting of this method of heat transfer can cause error of more than 1% in the measured thermal conductivity value. It appears that the only way of obtaining accurate predictions of the lead-in loss heat transfer

is by direct measurements.

In the literature there are reported two different methods of obtaining the radiation heat transfer in this type of cell. These two methods give quite different results for certain fluids. These two methods are reviewed and equations for one of the methods are developed.

Experimental data is obtained to support the theoretical equations developed.

Key Words: Convection, geometric constant, lead-in losses, minor heat losses, radiation, thermal conductivity, thermal conductivity cells (hot-wire, parallel plates, concentric cylinders).

1. Introduction

For numerous applications in physics and engineering the exact value of the transport and thermodynamics properties must be known. One of the major problems connected with the precise experimental measurements of these properties has been to determine the minor heat losses from the testing cell. In this paper these losses are determined for a thermal conductivity cell, but the methods can be used for any calorimetric instrument.

In the past, the three most common types of thermal conductivity cells used have been 1) the hot-wire or Scheirmacher's cell, 2) the horizontal parallel plate arrangement and 3) the concentric cylinder cell.

The hot-wire apparatus consists of a fine wire, generally platinum, axially stretched between the ends of a closed cylinder. The area between the wire and the cylinder is filled with the fluid to be tested. The wire serves as the heater and also as a thermometer and the cylinder as a constant temperature heat sink.

The main disadvantages of this method are the difficulties or placing and keeping the wire exactly on the axis of the cylinder, heat losses from the ends of the wire and an inhomogeneous temperature field. The inhomogeneous temperature field can produce free convection currents. The convection currents as well as the heat losses from the end of the wire are greatly influenced by the radial and axial dimensions of the annulus.

The second method uses two horizontal parallel plates with the material to be tested between them. To eliminate free convection the upper plate serves as the heater and the lower plate as the constant temperature heat sink.

One of the main advantages of this type of cell is the fact that the plate separation and the temperature difference can be made large without introducing free convection. This is not true of any other system. Its main disadvantage is the heat loss from the edges of the plate. This effect is increased as both the plate separation and the temperature difference are increased. To reduce this effect most parallel plate cells are built with some type of a guard heater.

While these guard heaters do reduce heat loss from the edges of the plate, it is very difficult to control their temperature, and it has been impossible to keep them at the same temperature as the cell. This results in two major problems. One, the time to reach steady state condition is greatly increased and two, a temperature difference exists along the wires used to supply power to the cell and the wires used to measure temperatures in the cell. These temperature gradients introduce another path for heat flow.

To try to reduce the edge effects of the parallel plate cell, the third system, that of two concentic cylinders, has been used. This system consists of two, generally metallic, cylinders. The larger cylinder has a hole drilled through it that is slightly larger than the outside diameter of the smaller cylinder. The smaller cylinder is placed in this hole and the material to be tested is placed between the two cylinders. The inner cylinder serves as the heater and the outer cylinder as the constant temperature heat sink.

The main disadvantage of this system is to assure perfect alignment of the axes

of the cylinders. Although edge effects are much smaller then in the parallel plate cell, they still exist and guard heaters are still required. Another disadvantage is that the distance between the two cylinders and the temperature difference must be small in order to prevent convective currents.

In order to overcome some of the disadvantages of the above named cells, especially the edge effects and the need for guard heaters, many different types of cells were considered. A few of these cells are listed below.

In 1948, Riedel [1][1] made modifications to the concentric cylinder cell by placing a right circular cone on each end of the cylinder and making a matching cavity in the outer cylinder. This elimated any edge effects but greatly increased the problem of making and assembling the instrument. It also introduced inhomogenities in the temperature field.

Riedel [2], because of the large disagreement between his earlier work and other reported values of the thermal conductivity of several hydrocarbons, also constructed a concentric sphere apparatus. The inner sphere was the heater and the outer sphere served as the constant temperature heat sink. This cell, like his modified circular cylinder arrangement, eliminated any edge effect. Its great disadvantages were in construction, especially making sure that the spheres were truly concentric, and in obtaining isothermal surfaces. In addition the method of supporting the inner sphere greatly increased heat transfer along the supporting members.

In 1953, Schmidt and Leidenfrost [3] reported thermal conductivity values obtained with an arrangement that employed concentric cylinders with hemispherical ends. Like the conventional concentric cylinder cell, this cell used the inner cylinder as the heater and the outer cylinder as a heat sink. It also eliminated any edge effects, and Leidenfrost [4] showed that the main parts of this cell could be very accurately positioned with respect to each other.

Although the last three cells have eliminated any edge effect, they all have introduced a new problem. Each has the inner body as a heater element and each requires that the inner body be held in a fixed position with respect to the outer body. This requires some type of a support and wires running from the outer cold body to the inner hot body. Thus introducing a path for heat flow and a new unknown in determining thermal conductivity.

The purpose of this work is to examine this loss along with the other heat losses due to convection and radiation, and to examine some other factors which affect the accuracy of thermal conductivity measurements.

2. Description of Apparatus

2.1 Basic Unit

Figure 1 shows a schematic drawing of the thermal conductivity cell. The equations given in this paper are for this instrument, but the methods used for calculating the minor heat losses can be applied for any calorimeter type device where the cold body completely surrounds the hot body and where the cold body has a connection to the hot body through a holding rod (or rods) and lead-in wires.

The cell is made from two concentric cylinders with hemispherical ends. The inside or heater element, also called hot body, 1[2], and the outside or cold body, 2, are separated by a gap, nominally 0.05 cm. They are made from pure copper and are gold plated on all parts in contact with the fluid to be tested.

The low strength of copper, especially at high temperatures and pressures, makes it necessary to follow special precautions in order to avoid damage to the cell. Thus the unit, as shown in Figure 1, is placed inside a high pressure vessel which makes it possible to maintain the pressure on the outside of the cold body the same as exists in the gap of the cell. The high pressure vessel is surrounded by a constant temperature bath.

---

1 Figures in brackets indicate the literature references at the end of this paper.
2 Number refers to number on Figure.

3. Basic Equations and Correction Factors

The steady state heat flow by conduction for any configuration with two isothermal surfaces can be written as

$$q_k = k_L B \Delta T \tag{1}$$

where q_k = heat flow by conduction
k_L = thermal conductivity of the fluid between the isothermal surfaces
B = geometric constant
ΔT = temperature difference between isothermal surfaces

The geometric constant in equation 1 is a function of the shape of the isothermal surfaces and the distance between these surfaces. Since for most cases the shape and/or the distance between the surfaces changes with temperature, the geometric constant changes with temperature.

Equation 1 is solved for the thermal conductivity k_L to give

$$k_L = \frac{q_k}{B \Delta T} \tag{2}$$

To determine thermal conductivity, the heat transfer by conduction, the geometric constant and the temperature difference must be measured or determined.

3.1 Geometric Constant

If all heat flow is radial the steady state heat transfer equation by conduction through a fluid layer in the form of a cylindrical annulus with hemispherical ends can be written as

$$q_k = k_L \Delta T \quad 2\pi \left[\frac{h}{\ln \frac{D}{d}} + \frac{D\,d}{D-d}\right] \tag{3}$$

where h = length of cylinder
d = inside diameter
D = outside diameter

Comparing Eq. 3 with Eq. 4, the geometric constant B is

$$B = 2\pi \left[\frac{h}{\ln \frac{D}{d}} + \frac{D\,d}{D-d}\right] \tag{4}$$

Several disadvantages exist in determining the geometric constant in this manner, First, the equation assumes that all heat flow is radial, but in the combined arrangement used here there exists a thermal inhomogeneity in the transition from the cylindrical to the spherical portion of the annulus due to the fact that at this point the temperature profile across the gap changes from a logrithmic to a hyperbolic one. Leidenfrost [4] stated that this effect can be made small by a proper choice of a diameter and gap width, but even with this error made small, direct measurements of the length and diameters prove to be extremely difficult and they are functions at the temperature and pressure.

No matter how careful one is and how sensitive are the instruments used, it is still impossible to determine the geometric constants exactly because it is impossible to account for surface roughness and other inhomogeneties [4].

A better way of determining B is to use an analog between the geometric constant of the heat transfer equation and the geometric constant in the equation of electrical capacitance of the cell assembly. Due to the similarity between the electrical and the thermal fields all non-homogeneties will be included. (See detailed information in reference 4.) Leidenfrost [4] has shown that the geometric constant determined in this manner can be obtained with an error of less than 0.01 percent.

The value of B as determined by the electrical capacitance analog will be the same as the value of B in the heat transfer equation only if the relative position of the hot and cold bodies are exactly the same in both measurements. Thus, there is a need for some device to accurately position these two units (with respect to each other). This is accomplished by the two tubes (numbers 4 and 5) shown in Figure 1.

3.2 Heat Input

Heat is supplied to the unit by an electrical heater inside the heater element. The total heat input to this heater is found by using the electrical circuit shown in Figure 2. R_1, R_2 and R_3 are standard resistors, R is the resistance of the heater and R_L is the resistance of all lead-in wires.

The current I_1 was determined by measuring the voltage drop across R_1 and current I_2 by measuring the voltage drop across R_2. All voltages are measured with a six-dial Rubicon potentiometer.

The current through the heater is

$$I = I_1 - I_2 \tag{5}$$

and the voltage drop across the heater is

$$V = I_2(R_2 + R_3) - IR_L \tag{6}$$

The total heat input becomes

$$q_T = VI \tag{7}$$

or

$$q_T = I^2R \tag{8}$$

If equation 8 is used, the resistance of the heater as a function of temperature is required but if Eq. 7 is used only the change in the lead-in resistance as a function of temperature is needed. Since all parts of the lead-in wire except for a small amount passing through the centering rod are outside the instrument, it can be held at a constant temperature. The lead-in wire inside the instrument is made from constantan wire and the changes in its resistance over the temperature range used are negligibly small. Therefore, by using Eq. 7 the need to know the temperature dependence of any resistance is eliminated.

The constantan wire also serves another purpose. Because of its low thermal conductivity and its high electrical resistance as compared to copper, it serves to reduce heat transfer by conduction along the centering rod and lead-in wires. This effect is discussed later in section 3.4.

Unfortunately, all of the heat input is not transferred by conduction through the test layer. There are at least three other major ways that heat can be transferred from the heater element to the cold body. They are:

1) by free convection in the fluid,
2) by conduction along the centering rod and lead-in wires, and
3) by radiation across the gap.

The total heat input q_T can be written as

$$q_T = q_k + q_r + q_c \pm q_l \pm \cdots \tag{9}$$

where q_k = heat transfer by conduction through the fluid layer
q_c = heat transfer by free convection in the fluid layer
q_l = heat transfer by conduction through centering rod and lead-in wires
q_r = Heat transfer by radiation across the gap

3.3 Heat Transfer by Free Convection

In any arrangement, except a horizontal layer of test fluid uniform heat from above, free convection motion will be present. However, it has been shown that for very slow motion, heat transfer by free convection adds nothing to the total heat transfer. For example, Kraussold [5] showed that free convection heat transfer in a cylindrical liquid layer had no contribution to total heat flow if the product of the Grashof number (Gr) and the Prandl number (Pr) was below 600. Schmidt and Milverton [6] reported a theoretical product of Gr. Pr of 1709 below which the heat transfer by convection of a fluid enclosed between two horizontal plates heated from below

contributed nothing to the total heat flow. They also reported an experimental value of 1770 $\pm$ 140. Schmidt and Leidenfrost [3] established a critical Gr. Pr product for the configuration of the combined arrangement of the present test cell of 1200.

The product of the Grashof number and the Prandtl number is

$$\text{Gr Pr} = \left[\frac{g \beta \Delta T \rho^2 S^3}{\mu^2}\right] \left[\frac{\mu c_p}{k_L}\right] \tag{10}$$

where g = acceleration due to gravity
β = coefficient of volumetric expansion
ρ = density of fluid
S = average thickness of fluid layer
μ = dynamic viscosity
c_p = constant-pressure specific heat

By careful design of the cell and by controlling the temperature difference between the two isothermal surfaces the Grashof-Prandtl product can always be kept below its critical value. Thus, the effect of free convection can be reduced to a point where it is of no importance.

3.4 Lead-In Losses

Figure 3 shows a schematic drawing of a typical device used to hold the hot body in the desired position with respect to the cold body (see Figure 1). In many instances two or more devices are required to assure perfect positioning. Generally, by careful design, the heat transfer by conduction along all but one of the devices can be reduced to an insignificant amount, by making this device (or these devices) from a poor conducting material such as nickel-steel alloys, making the tube (or tubes) thin walled, and drilling many small holes in the tube wall (or walls) to further reduce the heat transfer area.

Quite different is the situation in the case of the top tube (4) in Figure 1. This tube not only serves as a positioning device but also as an enclosure for all lead-in wires.

In this case the centering rod consisted of:

1) a tapered hollow stainless steel tube Stl,
2) two insulated constantan wires carrying current to the heater element. The insulation of these wires is aluminum-oxide and serves as an electrical insulator but has a rather high thermal conductivity (approximately 0.22 watts $cm^{-1}C^{-1}$ at 25°C). The ceramic and heater wires are enclosed and electrically shielded by a stainless steel tube (St2). This unit (constantan wires, insulator and stainless steel tube) is referred to as the "heater lead-in unit."
3. threethermocouples enclosed in insulators. This unit is referred to as "thermocouple unit."

To calculate the heat loss through the centering rod the following assumptions are made:

1) That each of the units considered above (stainless steel tube Stl., heater lead-in unit, and thermocouple unit) is a homogeneous material with constant properties.
2) That the stainless steel tube Stl is not tapered.
3) That each end of the centering rod is held at a constant temperature; the lower end at the temperature of the hot body t_h and the upper end at the temperature of the cold body t_c.

Even with these assumptions it is impossible to calculate the lead-in losses. If two additional assumptions are made it becomes mathematically possible to evaluate these losses.

These assumptions are:

1) That the temperature of any cross section of any one of the three units described above is a constant. This assumption does not imply that the

temperature of all three cross sections are the same.

2) That the heat transfer between each section of each unit and its surrounding can be written as $q = C_{ij} (T_i - T_j)$ where C_{ij} is a constant which depends only on the geometry and the average temperature of the centering rod. T_i and T_j are the temperatures of the cross section and its surrounding respectively.

Figure 4 shows a schematic diagram of a section of the centering rod.

Referring to this figure the following equations result:

$$q_r = C_{1c} (T_i - T_c)\, dZ \tag{11}$$

$$q_{h1} = C_{12} (T_1 - T_2)\, dZ + C_{13} (T_1 - T_3)\, dZ \tag{12}$$

$$q_{h2} = C_{21} (T_2 - T_1)\, dZ + C_{23} (T_2 - T_3)\, dZ \tag{13}$$

$$q_{h3} = C_{31} (T_2 - T_1)\, dZ + C_{32} (T_3 - T_2) \tag{14}$$

$$q_i = -K_i A_i \frac{dTi}{dZ} \tag{15}$$

$$q_i + dq_i = -K_i A_i \frac{dT_\rho}{dZ} + \frac{d}{dZ} \left(-K_i A_i \frac{dT_i}{dZ}\, dZ\right) \tag{16}$$

where i = 1, 2, or 3.

therefore

$$\frac{d^2T_i}{dZ^2} = \frac{C_{1c}}{K_1A_1} (T_1 - T_c) + \frac{C_{12}}{K_1A_1} (T_1 - T_2) + \frac{C_{13}}{K_1A_1} (T_1 - T_3) \qquad (a)$$

$$\frac{d^2T_2}{dZ^2} = \frac{C_{21}}{K_2A_2} (T_2 - T_1) + \frac{C_{23}}{K_2A_2} (T_2 - T_3) \qquad (b)$$

$$\frac{d^2T_3}{dZ^2} + \frac{\dot{q}}{K_3} = \frac{C_{31}}{K_3A_3} (T_3 - T_1) + \frac{C_{32}}{K_3A_3} (T_3 - T_2) \qquad (c)$$

Theoretically equation 16a, b, and c can be solved simultaneously for T_1, T_2 and T_3. Once these temperature distributions are known the heat transfer along the centering rod can be found. The big problem with this approach is the fact that the C_{ij} are not known and they are very difficult if not impossible to determine.

Therefore a simpler approach is needed. This is accomplished by looking at three special cases listed below. It was hoped that by looking at these three cases the lead-in loss could be bracketed.

These three cases are:

1) there is no internal radial heat flow i.e. $q_{h1} = q_{h2} = q_{h3} = 0$. This gives the minimum heat loss.
2) there is no internal resistance to radial flow from the heater lead-in unit, but there is not other internal radial heat flow i.e. $q_{h1} = q_{h2} = 0$ while $q_{h3} = C_{1c}(T - T_c)$. This case should give the maximum loss.
3) the centering rod is regarded as a solid homogeneous, slender rod with uniform heat generation. This is an ideal case.

Case 1

For case 1 the following assumptions are made

(a) The heater wires, ceramic insulators and stainless steel tube St2 (heater lead-in unit) are considered as one material with thermal conductivity k_h and resistance R_h. It is assumed that this unit generates heat uniformly but has

no radial heat flow.
k_h is defined as

$$k_h A_h = k_h \frac{\pi D^2_{St2}}{4} = 2k_{Con}A_{Con} + k_{Cer}A_{Cer} + k_{Stl}A_{Stl}$$

where the subscripts:
Con = constantan
Cer = ceramic
St = stainless steel
and R_h = total resistance of heater lead-in unit

(b) The thermocouples and their insulator are one material with conductivity k_{Tc} (with no radial heat flow, and no heat generation).
k_{Tc} is defined as

$$K_{Tc}A_{Tc} = k_{Tc} \frac{\pi D^2_{Ins}}{4} = 3(k_{Pl}A_{Pl} + k_{Rd}A_{Rd} + k_{Ins}A_{Ins})$$

where
Pl = platinum
Rd = platinum - platinum 10 percent rhodium
Ins = insulation

(c) The stainless steel tube Stl has radial heat flow only to the fluid being tested and none toward the inside of the tube.
The differential equation and boundary conditions for case 1 and assumption a are

$$\frac{d^2t}{dZ^2} + \frac{\dot{q}}{k_h} = 0 \tag{17}$$

where $\dot{q}$ = heat generated in the wires
and $t = t_h$ when $Z = 0$
$t = t_c$ when $Z = L$ (18)

where Z is the distance along the axes of the centering rod. Equation 17 with boundary condition 18 is solved to give

$$t = -\frac{\dot{q}Z^2}{2k_h} + \left(\frac{\dot{q}L}{2k_h} - \frac{t_h - t_c}{L}\right) Z + t_h \tag{19}$$

where L = length of centering rod. Letting $\theta = t - t_c$ and $\Delta t = t_h - t_c$ and noting that

$$\dot{q} = \frac{I^2R_h}{A_hL}$$

where A_h = area of heater lead-in unit
Equation 19 becomes

$$\theta = -\frac{I^2R_h}{2Lk_hA_h} Z^2 + \left(\frac{I^2R_h}{2k_hA_h} - \frac{\Delta t}{L}\right) Z + \Delta t \tag{20}$$

The amount of heat transferred from the heater element is

$$q_{1a} = -k_hA_h \frac{d\theta}{dZ}\Big|_{Z=0} = -k_hA_h \left[\frac{I^2R_h}{2k_hA_h} - \frac{\Delta t}{L}\right] = \frac{k_hA_h}{L}\Delta t - \frac{I^2R_h}{2} \tag{21}$$

The differential equation for case 1 and assumption b is

$$\frac{d^2t}{dZ^2} = 0 \tag{22}$$

with boundary conditions 18.

Equation 22 with boundary conditions 18 is solved to give

$$\theta_{1b} = \frac{-\Delta t}{L} Z + \Delta t \tag{23}$$

and the heat loss from the heater element is

$$q_{1b} = \frac{k_{Tc} A_{Tc}}{L} \Delta t \tag{24}$$

The differential equation for case 1 and assumption c is

$$\frac{d^2 t}{dz^2} = \frac{k_L (t - t_c)}{k_{St1} A_{St1}} \frac{2\pi}{\ln \frac{D_a}{D_i}} \tag{25}$$

where D_a, D_i = diameter of annulus as shown in Figure 3 with $D_i = D_{iave}$ and the boundary condition are given by Eq. 18.

Letting $M^2 = \frac{2\pi k_L}{k_{St1} A_{St1}} \frac{1}{\ln \frac{D_a}{D_i}}$ and $\theta = t - t_c$ the

differential Eq. 25 is

$$\frac{d^2\theta}{dz^2} - M^2\theta = 0 \tag{26}$$

with boundary conditions

$$\begin{aligned} \theta &= \Delta t \text{ at } Z = 0 \text{ (a)} \\ \theta &= 0 \text{ at } Z = L \text{ (b)} \end{aligned} \tag{27}$$

The general solution to 26 is $q_{1c} = c_1 e^{-MZ} + c_2 e^{MZ}$.

Using the boundary conditions of Eq. 27, the above equation is solved and yields

$$q_{1c} = \frac{\Delta t}{1 - e^{2ML}} \left[e^{MZ} - e^{2ML} e^{-MZ} \right]$$

This equation is reduced to give

$$q_{1c} = \frac{\sinh [M(L-Z)]}{\sinh (ML)} \Delta t \tag{28}$$

The heat transfer from the heater element is

$$q_{1c} = M k_{St1} A_{St1} \Delta t \coth (ML) \tag{29}$$

The total heat transfer from the heater element for case 1 is the sum of Eqs. 21, 24, and 29 or

$$q_1 = \left[\frac{k_h A_h}{L} + \frac{k_{Tc} A_{Tc}}{L} + M k_{St1} A_{St1} \coth (ML) \right] \Delta T - \frac{I^2 R_h}{2} \tag{30}$$

If the heat transfer from the heater element by convection and radiation is assumed to be negligibly small, then the total heat input can be written as

$$q_T = I^2R = k_L B\Delta T + q_{1,2,3} \tag{31}$$

where $q_{1,2,3}$ is the heat transfer by conduction along the centering rod and lead-in wires. The subscripts 1, 2, and 3 refer to the three cases considered and only one at a time can be used.

Solving for I^2 from Eq. 31 gives

$$I^2 = \frac{k_L B\Delta T}{R} + \frac{q_{1,2,3}}{R} \tag{32}$$

Substituting Eq. 32 into Eq. 30 and using q_1 gives

$$q_1 = \left[\frac{k_h A_h + k_{Tc} A_{Tc}}{L} + M\, k_{Stl} A_{Stl} \coth (ML) - \frac{k_L B}{2}\frac{R_l}{R}\right]\Delta t \Big/ \left[1 + \frac{R_h}{2R}\right] \tag{33}$$

For the special case where $K_L \to 0$ (This is the case where all energy generated in the hot body is transfered to the cold body by radiation through the gap and by conduction along the centering rod. This condition is experimental, obtainable by drawing a vacuum in the space between the hot and cold bodies.)

q_1 is

$$q_1(0) = \left[\frac{k_h A_h + k_{Tc} A_{Tc} + k_{Stl} A_{Stl}}{L}\right]\Delta t - \frac{I^2 R_h}{2} \tag{34}$$

(See reference 10 for proof of equation 34.)

Case 2

The assumptions made for case 2 are:

a) The heater lead-in unit is defined as in case 1a but is loosing heat from its outer surface at the rate $2\pi k_L (t_2 - t_c)/(\ln \frac{D_a}{D_i})$ where t_2 is the temperature, as defined in assumption 2b below.

b) The remainder of the centering rod is one solid material having thermal conductivity k_2 and temperature t_2 but loosing as much heat at its outer surface as it gains from the heater lead-in unit. k_2 is defined as

$$k_2 A_2 = k_2 \frac{\pi D_{i\ ave}^2}{4} = 3\, k_{Pl} A_{Pl} + 3\, k_{Rd} A_{Rd} + 3\, k_{Ins} A_{Ins} + k_{Stl} A_{Stl}$$

In order to obtain temperature t_2, case 2 and assumption b must be solved first. The differential equation for this case is

$$\frac{d^2 t}{dZ^2} = 0 \tag{35}$$

with the boundary conditions (18), viz

$$t_2 = t_h \quad \text{when } Z = 0$$
$$t_2 = t_c \quad \text{when } Z = L \tag{18}$$

The solution to Eqs. 35 and 18 is

$$t_2 = \frac{-\Delta t\, Z}{L} + t_h \tag{36}$$

and the heat transfer from the heater element is

$$q_{2b} = \frac{k_2 A_2}{L} \Delta t \tag{37}$$

The differential equation for case 2 and assumption a is

$$k_h A_h \frac{d^2 t}{dZ^2} = \frac{2\pi k_L}{\ln \frac{D_a}{D_i}} (t_2 - t_c) - \dot{q} A_h \tag{38}$$

Substituting Eq. 36 into 38 and solving gives

$$t = N \left[-\frac{\Delta t}{6L} Z^3 + \frac{\Delta t}{2} Z^2 \right] - \frac{\dot{q}}{k_h} \frac{Z^2}{2} + C_1 Z + t_h \tag{39}$$

where

$$N = \frac{2\pi k_L}{k_h A_h \ln \frac{D_a}{D_i}}$$

and

$$C_1 = -\frac{\Delta t}{L} + \dot{q} \frac{L}{2k_L} - \frac{N}{3} L^2 \Delta t$$

The heat transfer from the heating element is

$$q_{2a} = -k_h A_h C_1 = k_h A_h \Delta t \left(\frac{1}{L} + \frac{NL}{3}\right) - \dot{q} \frac{LA_h}{2} \tag{40}$$

since $\dot{q} = \frac{I^2 R_h}{A_h L}$ equation 40 becomes

$$q_{2a} = k_h A_h \Delta t \left(\frac{1}{L} + \frac{NL}{3}\right) - \frac{I^2 R_h}{2} \tag{41}$$

The total heat transfer in case 2 is

$$q_2 = q_{2a} + q_{2b} = \frac{(k_h A_h + k_2 A_2}{L} + \frac{NL}{3} k_h A_h) \Delta t - \frac{I^2 R_h}{2} \tag{42}$$

As in case 1, if the heat transfer by convection and radiation are neglected

$$I^2 = \frac{k_L B \Delta T}{R} + \frac{q_2}{R} \tag{43}$$

and equation 42 is

$$q_2 = \left[\frac{k_h A_h + k_2 A_2}{L} + \frac{2\pi L k_L}{3 \ln \frac{D_a}{D_i}} - \frac{k_L B}{2} \frac{R_h}{R}\right] \Delta t / \left[1 + \frac{R_h}{2R}\right]$$

Looking again at the special case where $k_L \to 0$, equation 42 becomes

$$q_2(0) = \left[\frac{k_h A_h + k_2 A_2}{L} \right] \Delta t - \frac{I^2 R_1}{2} \qquad (44)$$

Case 3

Leidenfrost [4] assumed that the entire centering rod is a slender rod with uniform heat generation and arrived at the following equation

$$\theta = \Delta t \frac{\sinh [P (L-Z)]}{\sinh (PL)} - \frac{\dot{q} \cosh [P (\frac{L}{2} - Z)]}{k_s P^2 \cosh (\frac{PL}{2})} + \frac{\dot{q}}{k_s P^2} \qquad (45)$$

where

$$P^2 = \frac{2\pi k_L}{k_s A_s \ln \frac{D_a}{D_i}}$$

A_s = average cross-section area of the rod = $\frac{\pi D_{i\ ave}^2}{4}$

k_s = apparent thermal conductivity of the rod and is defined as follows:

$$k_s A_s = k_{Cer} A_{Cer} + 3k_{Pl} A_{Pl} + 3k_{Rd} A_{Rd} + 2k_{Con} A_{Con} + k_{St1} A_{St1} + k_{St2} A_{St2} + 3k_{Ins} A_{Ins}$$

D_a, D_i are the diameters of the annulus as shown in Figure 3 with $D_i = D_{i\ ave}$.
Using Equation 45, the heat transfer from the heating element for Case 3 is:

$$q_3 = B_1 \sqrt{k_L} \tanh (\frac{PL}{2}) \left[\frac{\coth (PL)}{\tanh (\frac{PL}{2})} \Delta t - \frac{I^2 R_h}{B_2 k_L} \right] \qquad (46)$$

where

$$B_1^2 = \frac{2\pi k_s A_s}{\ln \frac{D_a}{D_i}}$$

$$B_2 = \frac{2\pi L}{\ln \frac{D_a}{D_i}}$$

Neglecting heat transfer by convection and radiation equation 46 may be written as

$$q_3 = \frac{B_1 \sqrt{K_L} \tanh (\frac{PL}{2}) \left[\frac{\coth (PL)}{\tanh (\frac{PL}{2})} - \frac{BR_h}{B_2 R} \right] \Delta T}{1 + \frac{B_1}{B_2} (\frac{R_h}{2}) k_L \tanh (\frac{PL}{2})} \qquad (47)$$

Leidenfrost [4] points out that by correctly designing the thermal conductivity cell Eq. 47 will always be zero. This is accomplished by making PL large enough so that for the lowest value of k_L being tested the coth (PL) and tanh $(\frac{PL}{2})$ approach unity.

Then the ratio $\frac{BR_h}{B_2R}$ can be made unity by proper choice of R_h and R thus making $q_3 = 0$. If k_L is increased PL increases but the value of coth (PL) and tanh $(\frac{PL}{2})$ remain unchanged. This same scheme will not work for cases 1 and 2. It is true that for any given k_L cases q_1 and q_2 can be made zero; but as soon as k_L changes, q_1 and q_2 will no longer be zero.

For the special case where $k_L \rightarrow 0$ Eq. 46 reduces to

$$q_3(0) = \frac{k_s A_s}{L} \Delta t - \frac{I^2 R_l}{L} \tag{48}$$

(See reference 10 for the proof of Eq. 48.)

It would have been convenient to compare the final equations; 32, 42, and 46 with some experimental results to see which equation will give the best results for this instrument. This can be done for the special case $k_L = 0$. For convenience the equations for $k_L = 0$ for cases 1, 2 and 3 are written as

$$q_1(0) = \frac{k_h A_h + k_{Tc} A_{Tc} + k_{Stl} A_{Stl}}{L} \Delta t - \frac{I^2 R_h}{2} \tag{34}$$

$$q_2(0) = \frac{k_h A_h + k_2 A_2}{L} \Delta t - \frac{I^2 R_h}{2} \tag{44}$$

$$q_3(0) = \frac{k_s A_s}{L} \Delta t - \frac{I^2 R_h}{2} \tag{48}$$

Replacing $k_h A_h$, $k_{Tc} A_{Tc}$, $k_2 A_2$ in the above equations by what they are equal to yields

$$q_1(0) = (2k_{Con} A_{Con} + k_{Cer} A_{Cer} + k_{St2} A_{St2} + 3k_{Pl} A_{Pl} + 3k_{Rd} A_{Rd} + 3k_{Ins} A_{Ins} + k_{Stl} A_{Stl}) \frac{\Delta t}{L} - \frac{I^2 R_h}{2}$$

$$q_2(0) = (2k_{Con} A_{Con} + k_{Cer} A_{Cer} + k_{St2} A_{St2} + 3k_{Pl} A_{Pl} + 3k_{Rd} A_{Rd} + 3k_{Ins} A_{Ins} + k_{Stl} A_{Stl}) \frac{\Delta t}{L} - \frac{I^2 R_h}{2}$$

$$q_3(0) = (2k_{Con} A_{Con} + k_{Cer} A_{Cer} + k_{St2} A_{St2} + 3k_{Pl} A_{Pl} + 3k_{Rd} A_{Rd} + 3k_{Ins} A_{Ins} + k_{Stl} A_{Stl}) \frac{\Delta t}{L} - \frac{I^2 R_h}{2}$$

or $q_1(0) = q_2(0) = q_3(0)$ and no help is obtained in determining which equation to use.

The resulting equations from cases 1, 2, and 3 were solved and part of the results are shown in figures 5 and 6. The graphs show the lead-in loss as a function of the resistance of the lead-in heater unit. It is interesting to note that the graph of q_1 and q_2 are parallel and that a resistance of approximately 3 ohms that the graph of q_2 and q_3 intersect. These same results hold ture for a thermal conductivity range from 0.0005 to 0.007 watts/cm-C (The total range checked). The intersection point of q_2 and q_3 increased from approximately 2.7 ohms to 3.2 ohms as the thermal conductivity increased from -.0007 watts/cm-C to 0.0007 watts/cm-C. It should be pointed out that in these graphs q_3 never becomes negative but if R_h were increased to higher values q_3 would also become negative.

If the average of q_1 and q_2 is used as a lead-in loss correction for the thermal conductivity measurements and if it is assumed that the true lead-in loss correction is somewhere between q_1 and q_2 then the uncertainty in the thermal conductivity caused by using this value as a function of the thermal conductivity of the test fluid is

shown in Figure 7. The figure shows that for thermal conductivities as low as 1.5 x 10^{-3} watts/cm-C (approximately that of toluene) that the percent uncertainty can approach 1%.

a. Conclusions

From this work it is obvious that the calculation of the lead-in loss is very difficult. In fact, theoretical calculations appear to be almost impossible. Thus, there appears to be only one way to obtain these losses and that is to experimentally measure them. Yet, these rough estimates of lead-in loss show that the uncertainty in the measured value of the thermal conductivity can be 1% or more if lead-in losses are neglected. Therefore, anyone who reports thermal conductivity value of accuracy greater than 1% must account for the lead-in losses of their instrument.

3.5 Heat Loss By Radiation

Three distinct cases of radiant heat exchange can exist. They are: 1) perfectly opaque fluid, 2) transparent fluid not capable of emitting or absorbing radiation and 3) a transparent fluid capable of emitting and absorbing radiation.

The radiant heat exchange in case 1 is zero.

In the second case, the fluid is transparent and not capable of emitting or absorbing radiation as is the case of most monatomic gases. Due to the small thickness of the gas layer as compared to the hot body radius, the cell is treated as two infinitely large parallel plates. The surfaces are assumed to be isothermal, diffuse emitters and absorbers of thermal radiation. For these conditions the equation for heat transfer by radiation is

$$q_r = \frac{n^2 \sigma A (T_h^4 - T_c^4)}{\frac{1}{\epsilon_1} + \frac{1}{\epsilon_2} - 1} \tag{49}$$

where

n = index of refraction
σ = Stefan-Boltzman constant
A = area = geometric constant time thickness of the fluid gap
T_h = temperature of hot body
T_c = temperature of cold body
ϵ_1 = emissivity of hot surface
ϵ_2 = emissivity of cold surface

Since $\epsilon_1 = \epsilon_2 = \epsilon$ Eq. 49 becomes

$$q_r = \frac{n^2 \sigma BS (T_h^4 - T_c^4)}{\frac{2}{\epsilon} - 1} \tag{50}$$

In the third case the fluid is partly transparent and capable of emitting and absorbing radiation as is the case with most liquids and polyatomic gases. In 1964 Leidenfrost [4] calculated the radiation heat transfer between two infinitely large parallel plates for this situation. The walls of the test cell were assumed to be isothermal, diffuse emitters and abosrbers of thermal radiation and to have constant radiation properties except for variation with wave length. The fluid was supposed to be an isotropic homogeneous gas or liquid which could absorb and emit thermal radiation, and the fluid was at rest. Leidenfrost actually calculated the net heat transfer per unit area from the hot surface. Poltz [7] started out with the same basic equation and assumptions as Leidenfrost but calculated the heat transfer per unit area by radiation across any arbitrary plane in the test fluid, and then took an average of the radiation heat transfer across all arbitrary planes in the test fluid. The conservation of energy equation shows that the radiant heat transfer is not constant over the gap width. Both Leidenfrost and Poltz assumed a linear temperature profile across the gap, but Leidenfrost stated that for calculation of T^4, terms containing $(\Delta T)^3$ and $(\Delta T)^4$ could be neglected while Poltz stated terms of the order of

$(\Delta T)^2$ could be neglected. These two methods of approach led to quite different results at lower values of optical thickness but agree quite well at higher values. The shape of both author's heat transfer by radiation versus optical thickness curves is shown in Figure 8. One disadvantage exists if Poltz's approach is used; the radiation heat transfer does not approach zero as the emissivities of the walls approach zero. The effect of dropping terms of order $(\Delta T)^2$ and higher for the temperature difference of approximately 2.5 degrees was not made clear in either paper. For these reasons the heat transfer by radiation between two infinitely large parallel plates is again calculated. The physical model considered is shown in Figure 9. Making the same assumption as Leidenfrost [4] for the physical system shown in Figure 9, the radiation heat flux coming from surface i and passing through a fluid having a monochromatic absorption coefficient κ_λ and an index of refraction n_λ is given as

$$q_{ri} = 2\int_0^\infty \left[R_{o\lambda}E_3(\tau_{o\lambda}) + \int_0^{\tau_{o\lambda}} n_\lambda^2(\tau_\lambda)E_{b\lambda}(\tau_\lambda)E_2(\tau_\lambda)d\tau_\lambda - \frac{1}{2}R_{i\lambda}\right]d\lambda \qquad (51)$$

where $R_{(i,0)\lambda}$ = radiosity or radiant energy leaving (emitted and reflected) a surface.

n_λ = index of refraction

$E_{b\lambda}$ = emissive power of a black body radiating into a fluid having an idea of n

τ_λ = optical depth; $\tau_\lambda = \int_o^y \kappa_\lambda dy$

$\tau_{\lambda o}$ = optical thickness; $\tau_{\lambda o} = \int_o^s \kappa_\lambda dy$

κ = absorption coefficient

$E_n(X)$ = exponential integral function defined by

$E_n(X)$ = $\int_o^1 \mu^{n-2}\exp(-\frac{x}{\mu})d\mu$

Equation 51 stated in words is

q_{ri} = energy leaving surface 0 times its attenuation + energy emitted by the fluid layer times its attenuation - energy leaving surface i, which is simply the net heat transfer by radiation from the i^{th} surface.

The radiosity at surface i is

$$R_{i\lambda} = \epsilon_{i\lambda}n_\lambda^2(0)E_{b\lambda}(0) + 2(1-\epsilon_{i\lambda})\left[R_{o\lambda}E_3(\tau_{o\lambda}) + \int_o^{\tau_{o\lambda}} n_\lambda^2(\tau_\lambda)E_{b\lambda}(\tau)E_2(\tau_\lambda)\,d\tau_\lambda\right] \qquad (52)$$

where $\epsilon_{i\lambda}$ = emissivity of the surface i.

The first term on the right had side of equation 52 represents the emission of energy by surface i and the second term gives the fraction of the energy incident on i that is reflected from it.

The equation for the energy leaving 0 is similar to equation 52, viz.

$$R_{o\lambda} = \epsilon_{o\lambda}n_\lambda^2(\tau_{o\lambda})E_{b\lambda}(\tau_{o\lambda}) + 2(1-\epsilon_{o\lambda})\left[R_{i\lambda}E_3(\tau_{o\lambda}) + \int_o^{\tau_{o\lambda}} n_\lambda^2(\tau_\lambda)E_{b\lambda}(\tau)E_2(\tau_{o\lambda} - \tau_\lambda)d\tau_\lambda\right] \qquad (53)$$

where $\epsilon_{o\lambda}$ = emissivity of the surface 0.

Equation 52 and 53 could be solved simultaneously and the resulting radiosities introduced into equation 51. However, the evaluation of this equation would be very complex due to the double integration that results.

The assumption is made that ϵ_λ and n_λ can be replaced by an appropriate average value and that an average absorption coefficient is given by Planck's mean value

$$\kappa = \frac{\int_o^\infty \kappa_\lambda E_{b\lambda} d\lambda}{\int_o^\infty E_{b\lambda} d\lambda} = \frac{\int_o^\infty \kappa_\lambda E_{b\lambda} d\lambda}{\sigma T^4} . \tag{54}$$

where λ = wave length
$E_{b\lambda}$ = monochromatic emissive power of a black body.
Then equation 53 becomes

$$R_o = \epsilon_o n^2 E_b(\tau_o) + 2(1-\epsilon_o)\left[R_i E_3(\tau_o) + n^2 \int_o^{\tau_o} E_b(\lambda) E_2(\tau_o - \tau) d\tau\right]$$

$$= \epsilon_o n^2 \sigma T_o^4 + 2(1-\epsilon_o)\left[R_i E_3(\tau_o) + n^2 \sigma \int_o^{\tau_o} T^4(\tau) E_2(\tau_o - \tau) d\tau\right]$$

or
$$R_o = \epsilon_o n^2 \sigma T_o^4 + 2(1-\epsilon_o)\left[R_i E_3(\tau_o) + n^2 \sigma P_o'\right] \tag{55}$$

$$P_o' = \int_o^{\tau_o} T^4(\tau) E_2(\tau_o - \tau) d\tau$$

Equation 52 becomes

$$R_i = \epsilon_i n^2 E_b(0) + 2(1-\epsilon_i)\left[R_o E_3(\tau_o) + n^2 \int_o^{\tau_o} E_b(\tau) E_2(\tau) d\tau\right]$$

$$= \epsilon_i n^2 \sigma T_i^4 + 2(1-\epsilon_i)\left[R_o E_3(\tau) + n^2 \sigma \int_o^{\tau_o} T^4(\tau) E_2(\tau)\, d\tau\right]$$

or
$$R_i = \epsilon_i n^2 \sigma T_i^4 + 2(1-\epsilon_i)\left[R_o E_3(\tau_o) + n^2 \sigma P_i'\right] \tag{56}$$

where

$$P_i' = \int_o^{\tau_o} T^4(\tau) E_2(\tau) d\tau$$

Further, equation 51 becomes

$$q_{ri} = 2\left[R_o E_3(\tau_o) + n^2 \int_o^{\tau_o} E_b(\tau) E_2(\tau) d\tau - \frac{1}{2} R_i\right]$$

$$= 2\left[R_o E_3(\tau_o) + n^2 \sigma \int_o^{\tau_o} T^4(\tau) E_2(\tau) d\tau - \frac{1}{2} R_i\right] \tag{57}$$

$$= 2\left[R_o E_3(\tau_o) + n^2 \sigma P_i' - \frac{1}{2} R_i\right]$$

Introducing the following dimensionless variables,

$$\theta = \frac{T}{T_i}, \quad \varphi = \frac{q_{ri}}{n^2 \sigma T_i^4}, \quad \beta = \frac{R}{n^2 \sigma T_i^4}$$

equation 57 becomes

$$\varphi = \frac{q_{ri}}{n^2\sigma T_i^4} = 2\left[\frac{R_o}{n^2\sigma T_i^4} E_3(\tau_o) + \frac{n^2\sigma P_i'}{n^2\sigma T_i^4} - \frac{1}{2}\frac{R_i}{n^2\sigma T_i^4}\right] =$$

$$2\left[\beta_o E_3(\tau_o) + P_i - \frac{1}{2}\beta_i\right] \tag{58}$$

where

$$P_i = \frac{P_i'}{T_i^4} = \int_o^{\tau_o} \frac{T^4(\tau)}{T_i^4} E_2(\tau)d\tau = \int_o^{\tau_o} \theta^4(\tau) E_2(\tau)d\tau$$

Equation 55 becomes

$$\beta_o = \frac{R_o}{n^2\sigma T_i^4} = \frac{\epsilon_o n^2\sigma T_i^4}{n^2\sigma T_i^4} + 2(1-\epsilon_o)\left[\frac{R_i}{n^2\sigma T_i^4} E_3(\tau_o) + \frac{n^2\sigma P_o'}{n^2\sigma T_i^4}\right]$$

$$= \epsilon_o\theta_o^4 + 2(1-\epsilon_o)\beta_i E_3(\tau) + 2(1-\epsilon_o)P_o \tag{59}$$

where

$$P_o = \frac{P_o'}{T_i^4} = \int_o^{\tau_o} \frac{T^4(\tau)}{T_i^4} E_2(\tau_o - \tau)d\tau = \int_o^{\tau_o} \theta^4(\tau) E_2(\tau_o - \tau)d\tau$$

and

$$\theta_o = \frac{T_o}{T_i}$$

and Eq. 56 becomes

$$\beta_i = \frac{R_i}{n^2\sigma T_i^4} = \frac{\epsilon_i n^2\sigma T_i^4}{n^2\sigma T_i^4} + 2(1-\epsilon_i)\left[\frac{R_o E_3(\tau_o)}{n^2\sigma T_i^4} + \frac{n^2\sigma P_i'}{n^2\sigma T_i^4}\right] \tag{60}$$

$$= \epsilon_i + 2(1-\epsilon_i)P_i$$

Solving for β_o and β_i from Eqs. 59 and 60 gives

$$\beta_o = \frac{\epsilon_o\theta_o^4 + 2\epsilon_i(1-\epsilon_o)E_3(\tau_o) + 4(1-\epsilon_o)(1-\epsilon_i)E_3(\tau_o)P_i + 2(1-\epsilon_o)P_o}{1-4(1-\epsilon_o)(1-\epsilon_1)E_3^2(\tau_o)} \tag{61}$$

Since $\epsilon_o = \epsilon_i = \epsilon$ equation 61 reduces to

$$\beta_o = \frac{\epsilon\theta_o^4 + 2(1-\epsilon)\epsilon E_3(\tau_o) + 4(1-\epsilon)^2 E_3(\tau_o)P_i + 2(1-\epsilon)P_o}{1-4(1-\epsilon)^2 E_3(\tau_o)} \tag{62}$$

$$\beta_i = \frac{\epsilon_i + 2(1-\epsilon_i)E_3(\tau_o)\epsilon_o\theta_o^4 + 4(1-\epsilon_i)(1-\epsilon_o)E_3(\tau_o)P_o + 2(1-\epsilon_i)P_i}{1-4(1-\epsilon_o)(1-\epsilon_i)E_3^2(\tau_o)} \tag{63}$$

and since $\epsilon_i = \epsilon_o = \epsilon$ equation 63 reduces to

$$\beta_i = \frac{\epsilon + 2\epsilon(1-\epsilon)E_3(\tau_o)\theta_o^4 + 4(1-\epsilon)^2E_3(\tau_o)P_o + 2(1-\epsilon)P_i}{1-4(1-\epsilon)^2E_3^2(\tau_o)} \tag{64}$$

Before the values of P_o and P_i can be obtained, the temperature distribution between the plates is needed. In general the temperature can be found by the solution of the conservation of energy equation. This has been done by Viskanta and Grosh [8] and by Viskanta [9]. Viskanta [9] pointed out that if $(K\not{\kappa}/4n^2\sigma T^3)$ were large the temperature distribution was very little affected by the presence of radiation. He showed that as this term approached infinity the heat transfer is only by conduction and for the case where the term is zero heat transfer is only by radiation. Leidenfrost [4] stated that when this term was larger than or equal to 10 the conduction temperature profile can be used. Reference [4] also states that regardless of what $(K\not{\kappa}/4n^2\sigma T^3)$ is, if the temperature difference between the plates is small, the linear temperature profile of conduction can be used.

In this work both the above conditions are met. Thus the temperature profile is given by

$$T = T_i + (T_o - T_i)\frac{Y}{S} \tag{65}$$

or

$$\theta_Y = \frac{T}{T_i} = \frac{T_i}{T_i} + \left(\frac{T_o}{T_i} - \frac{T_i}{T_i}\right)\frac{Y}{S} = 1 + (\theta_o - 1)\frac{Y}{S} = 1 + (\theta_o - 1)\frac{KY}{KS}$$

or

$$\theta(\tau) = 1 + (\theta_o - 1)\frac{\tau}{\tau_o} \tag{66}$$

Introducing equation 66 into the equations for P_i and P_o gives

$$P_i = \frac{1}{2} - E_3(\tau_o) + \frac{4(\theta_o-1)}{\tau_o}\left[\frac{1}{3} - \tau_o E_3(\tau_o) - E_4(\tau_o)\right]$$

$$+ \frac{6(\theta_o-1)^2}{\tau_o^2}\left[\frac{1}{2} - \tau_o^2E_3(\tau_o) - 2\tau_oE_4(\tau_o) - 2E_5(\tau_o)\right]$$

$$+ \frac{4(\theta_o-1)^3}{\tau_o^3}\left[\frac{6}{5} - \tau_o^3E_3(\tau_o) - 3\tau_o^2E_4(\tau_o) - 6\tau_oE_5(\tau_o) - 6E_6(\tau_o)\right]$$

$$+ \frac{(\theta_o-1)^4}{\tau_o^4}\left[4 - \tau_o^4E_3(\tau_o) - 4\tau_o^3E_4(\tau_o) - 12\tau_o^2E_5(\tau_o) - 24\tau_oE_6(\tau_o) + 24E_7(\tau_o)\right] \tag{67}$$

and

$$P_o = \frac{1}{2} - E_3(\tau_o) + \frac{4(\theta_o-1)}{\tau_o}\left[-\frac{1}{3} + \frac{\tau_o}{2}E_4(\tau_o)\right]$$

$$+ \frac{6(\theta_o-1)^2}{\tau_o^2}\left[\frac{1}{2} - \frac{2}{3}\tau_o + \frac{\tau_o^2}{2} - 2E_5(\tau_o)\right]$$

$$+ \frac{4(\theta_o-1)^2}{\tau_o^3}\left[-\frac{6}{5}+\frac{3}{2}\tau_o-\tau_o^2+\frac{\tau_o^3}{2}+6E_6(\tau_o)\right]$$

$$+ \frac{(\theta_o-1)^4}{\tau_o^4}\left[4-\frac{24}{5}\tau_o+3\tau_o^2+\frac{1}{2}\tau_o^4-24\,E_7(\tau_o)\right] \qquad (68)$$

(See Reference 10 for a complete derivation of equations 67 and 68).

The values of $E_n(X)$ are tabulated and are found in such books as Reference 11. Equations 67 and 68 may be substituted into the equations for β_o and β_i and in turn β_i and β_o into the equation for φ.

Considering surface 0 as the hot surface, with the help of a digital computer, the radiation heat transfer was calculated. The results are shown in Figure 10 for values of τ_o from 0.01 to 1 and ϵ from 0.1 to 1. The average temperature across the gap is 25° C and $\Delta T = 2°C$.

To investigate the error introduced in the calculation of the radiant heat transfer by dropping the $(\Delta T)^2$ etc terms from the T^4 calculation, these terms are neglected and the resulting temperature profile used to calculate the radiant heat transfer. The equations of this work are used for all calculations. Two cases are considered: 1. $(\Delta T)^3$ and $(\Delta T)^4$ term are neglected as did Leidenfrost [4], and 2. $(\Delta T)^2$ and higher order terms are neglected as did Poltz [7]. The results of this investigation are shown in Figure 11.

Because little or no data exists for the values of the absorption coefficient, the value of this property is determined in the following manner. The monochromatic absorptivity α_λ of a fluid with thickness S is defined as

$$\alpha_\lambda = (1-\epsilon-\kappa_\lambda S) \qquad (69)$$

where κ_λ = monochromatic absorption coefficient.

Plots of α_λ versus wavelength λ are available for most substances [12]. Unfortunately, these plots were generally for an average temperature of 25°C and a pressure of 1 atm. Figure 12, although not for any substance, shows a characteristic plot of these curves. The following assumptions, although not completely correct, are also made. The monochromatic absorption coefficient is not a function of temperature, pressure or fluid thickness. With these assumptions it is theoretically possible to solve for κ_λ versus λ from α_λ versus λ curve, susbtitute into Eq. 54 and solve κ, but this is not practically possible because of the erratic behavior of the curve. Instead, the curve is divided into sections as shown in Figure 12 and an average α_λ for each section is found. This average is found by dividing the area under the curve of each section (found with a planimeter) by the wave length difference of each section. The dashed line of Figure 12 indicated the average α_λ for each area. By using Eq. 59, κ_λ for each section is found. To find $\int_0^\infty \kappa_\lambda E_{b\lambda} d\lambda$ of equation 54 values of $E_{b\lambda}$ are obtained [13] and multiplied by κ_λ. These results are plotted and a smooth curve drawn through them. The integral is equal to the area under this curve. This area is also determined by a planimeter. Once this integral was found, κ was found by dividing the integral by σT^4. The values of the absorption coefficients found by this method for toluene and carbon tetrachloride are tabulated in Table 1.

Certainly, the values of κ found by the above procedure are not as accurate as one would like, but under the circumstances with no other data available they are the best that can be obtained. As other methods and better data for finding κ become available, the accuracy of the radiation heat transfer can be improved by using these results.

Two other properties, index of refraction and total emissivity, are needed before the radiation heat loss can be determined. The index of refraction for almost all fluids has been determined at 1 atmosphere pressure and 25°C temperature and can be found in several handbooks. Reference 14 contains indices of refraction for many materials.

To check the validity of the many assumptions made in finding the heat losses and to find the value of emissivity of the cell, some experimental check is needed. If a perfect vacuum exists in the cell cavity, the only means of heat transfer from the hot body is by radiation and conduction along the lead-in wires and centering rod, viz.

$$q_t = q_r + q_l$$

In order to obtain this check, data was taken for total heat input versus temperature difference as the pressure was lowered from 1,000μ Hg to 0.2μ Hg, the lowest pressure obtainable with the present equipment. Figure 13 shows the results of these tests. The curve was extrapolated to very low pressures (approximately 0.001μ Hg) and this value of heat transfer was considered to be the absolute vacuum value.

Using Equation 48 for the lead-in heat transfer and equation 50 with n = 1 for the radiation heat transfer in a vacuum, ϵ was found to be 0.135.

A second series of tests are run for total heat transfer (at a pressure of approximately 0.2μ Hg) versus temperature difference for two different average temperatures, 20°C and 60°C (See Figure 14). The results of Figure 13 showed at this pressure a considerable amount (approximately 1/3 of total heat transfer) of free molecular conduction heat transfer takes place.

The heat transfer by free molecular conduction may be written as:

$$q_f \propto N\bar{V}\Delta T \tag{70}$$

where N = number of molecules per unit volume
$\bar{V}$ = average velocity of the molecules
ΔT = temperature difference

For a Boltzman velocity distribution $\bar{V} \propto T^{1/2}$, or $q_f \propto NT^{1/2}\Delta T$
Since N did not change when going from 20°C to 60°C, q_f becomes

$$q_f = CT^{1/2}\Delta T$$

where C = constant.

Using Eqs. 48 and 50 with $\epsilon = .135$, the value of C was obtained from the 20°C data. Using this value of C and equations 48 and 50, the total heat transfer at 60°C was calculated to be 0.0142 watt/C. The value obtained experimentally was 0.0146 watt/C giving a difference of 2.8 percent between the calculated and measured values, thus providing experimental support for all values used and assumptions made.

4. Conclusion

In this work it has been shown that it is possible to estimate or measure the minor heat losses for a calorimeter type cell. The three most important minor losses of convection, radiation and lead-in losses have been treated with the following results.

By careful design and control of temperature differences between the two isothermal surfaces, the effect of convective heat transfer can be made small enough to be neglected.

The radiation heat transfer equations are valid, but the results from these equations can be improved when better data is available for absorption coefficients, indices of refraction, etc.

The exact value of lead-in loss heat transfer can only be obtained experimentally, but the equations given here should bracket this loss. If the centering rod can be constructed as in Case 3, the lead-in loss of heat transfer can be made zero.

5. REFERENCE

[1] Riedel, L., Thermal Conductivity Measurements on Liquids*, Mett. Kaltetech. Inst. u Reichsforschung. Anstalt Lebansmittelfrischalt. Tech. Hochshule Karlysyuhe No. 2, 1948, pp 1-47.

[2] Riedel, L., New Thermal Conductivity Measurements of Organic Liquids, Chem.-Ingr.-Tech., 23, 1951, pp 321-324. English Trans. AEC-TR-1822, May 1962.

[3] Schmidt, E. and Leidenfrost, W., The Influence of Electric Fields on the Heat Transfer in Liquid Electrical Non-Conductors, Forsch. Gebiete Ingenieurw., 19, 1953, pp 65-80.

[4] Leidenfrost, W., An Attempt to Measure the Thermal Conductivity of Liquids, Gases, and Vapors with a High Degree of Accuracy Over a Wide Range of Temperature (-180 to 500 C) and Pressure (vacuum to 500 atm.), Intern. J. Heat Mass Transfer, 7 (4), 1966, pp 447-478.

[5] Kraussold, H., Heat Transfer in Cylindrical Liquid Layer by Free Convection, Forsch. Gebiete Ingenieurw., B5(4), 1934, pp. 186-191.

[6] Schmidt, R. J. and Milverton, S. W., On the Instability of a Fluid when Heated from Below, Proc. Roy. Soc. (London), A152, 1935 pp 586-594.

[7] Poltz, H., The Thermal Conductivity of Liquids II. The Radiation Portion of the Effective Thermal Conductivity. Intern. J. Heat Mass Transfer, 8(4), 1965, pp 515-527.

[8] Viskanta, R. and Grosh , R. J., Heat Transfer by Simultaneous Conduction and Radiation in an Absorbing Medium, Trans. ASME J. Heat Transfer, 84C, 1963, pp 63-72.

[9] Viskanta, R., Heat Transfer in Couette Flow of a Radiating Fluid with Viscous Dissipation, Proceedings of the 8th Midwestern Mechanics, Pergamon Press, April 1-3, 1963.

[10] Tree, D. R., Precise Determination of the Thermal Conductivity of Liquids and Gas Mixtures, Ph.D. Thesis, Purdue University, August, 1966.

[11] Kourganoff, V. and Busbridge, I. W., Basic Methods in Transfer Problems, Oxford University Press, London, 1952.

[12] Infrared Spectral Data, Americal Petroleum Institute Research Project 44.

[13] Pivononsky, M., Tables of Blackbody Radiation Functions, MacMillen Company, 1961.

[14] Handbook of Chemistry and Physics, 45th Edition, Chemical Rubber Publishing Co., 1965.

* Titles of German and Russian papers translated into English.

Table 1

Absorption Coefficient

Temperature in °K	Absorption Coefficient Toluene in cm^{-1}	Absorption Coefficient Carbon Tetrachloride in cm^{-1}
273	20.1	29.7
280	29.9	31.0
300	31.3	40.6
320	32.5	33.3
340	33.3	33.7
360	33.8	34.1
373	36.4	35.1

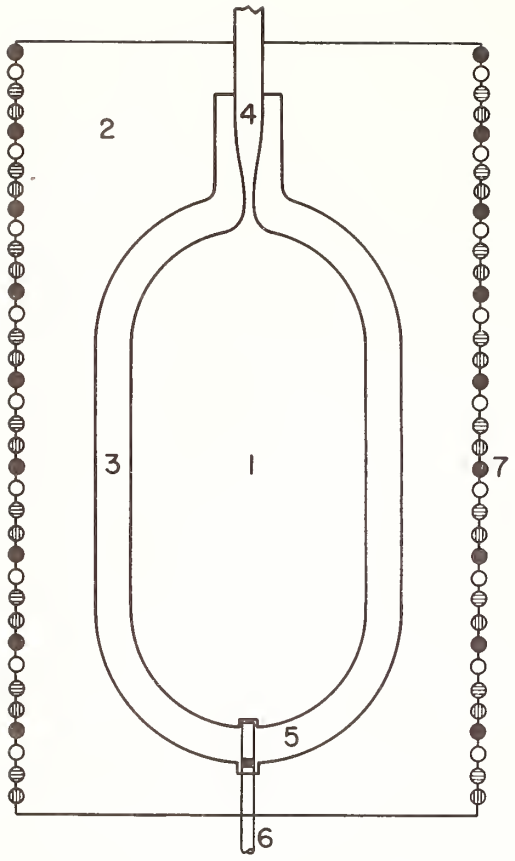

Figure 1. Instrument for measuring thermal conductivity.

Figure 2. Electric circuit for the measurement of power input to the heater element.

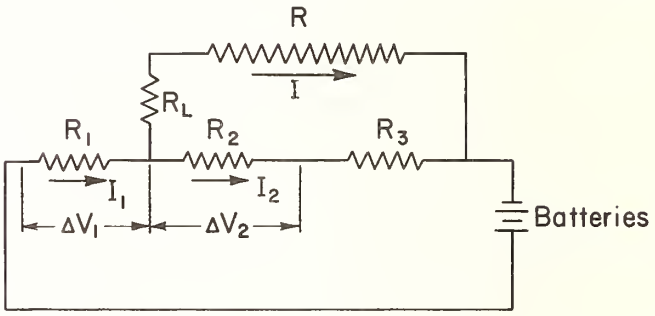

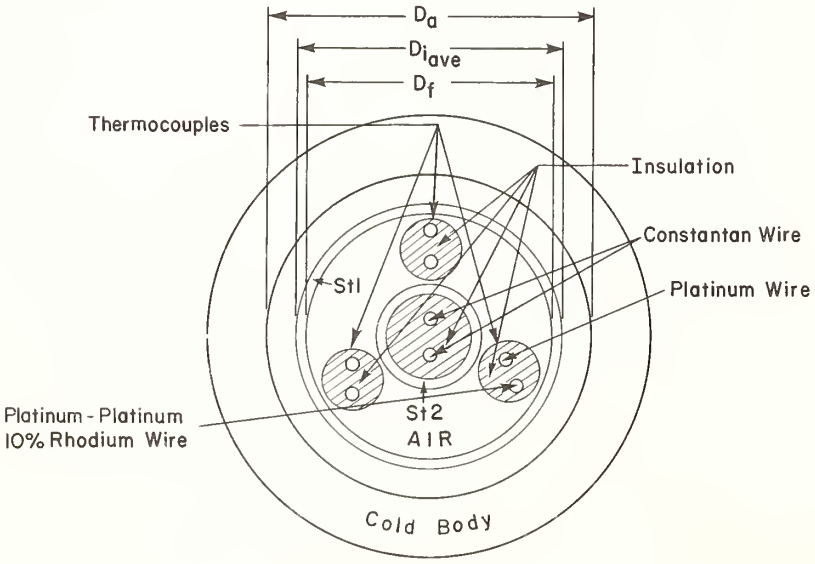

Figure 3. Centering rod of length L.

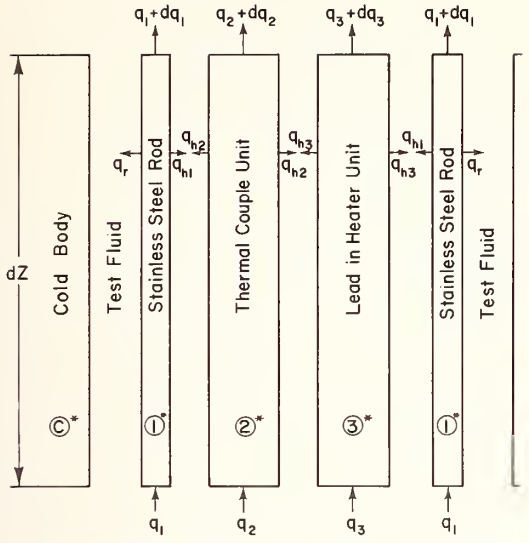

*Number or letter in circle refers to subscript in heat transfer equation.

Figure 4. Schematic drawing of a section of the centering rod.

Figure 5. Lead in loss versus Rh for a thermal conductivity of 0.0007 $\frac{\text{watts}}{\text{cm-c}}$.

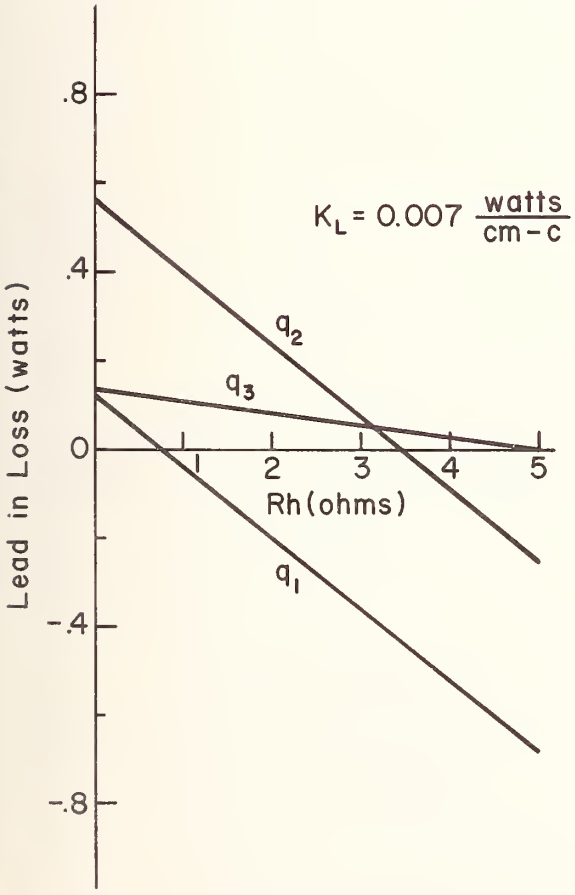

Figure 6. Lead in loss versus Rh for a thermal conductivity of 0.0035 $\frac{\text{watts}}{\text{cm-c}}$.

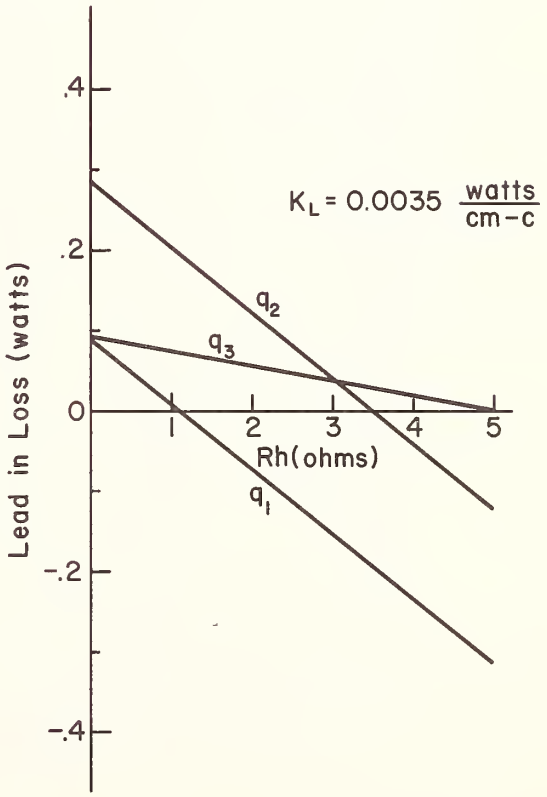

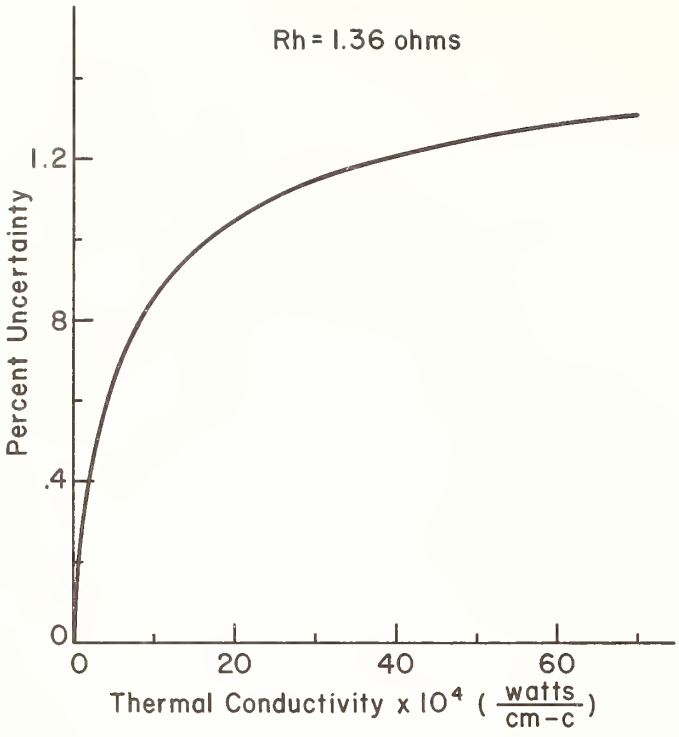

Figure 7. Precent uncertainty versus thermal conductivity.

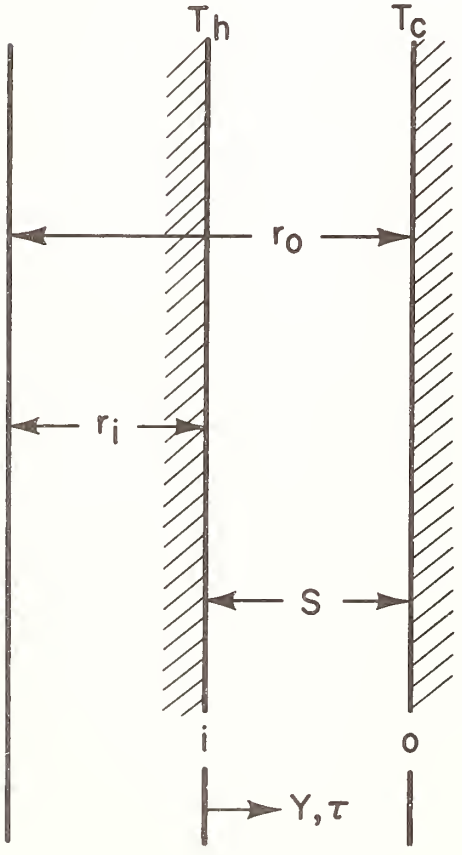

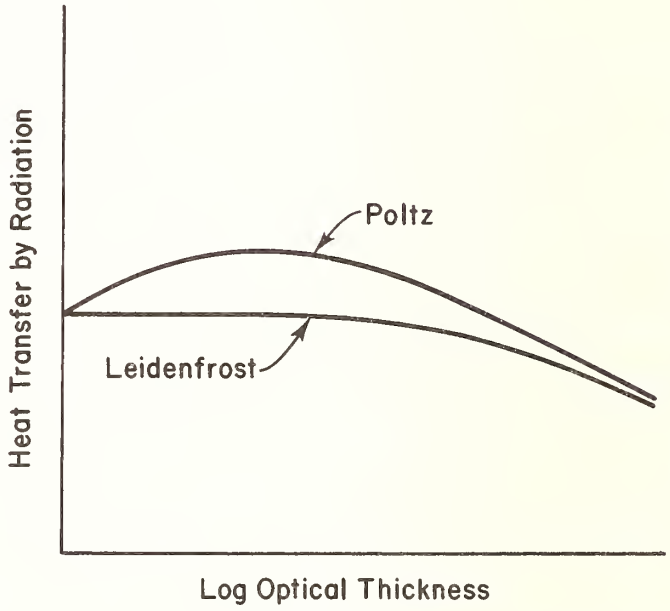

Figure 8. Heat transfer by radiation versus optical thickness.

Figure 9. Physical model considered for radiation heat transfer.

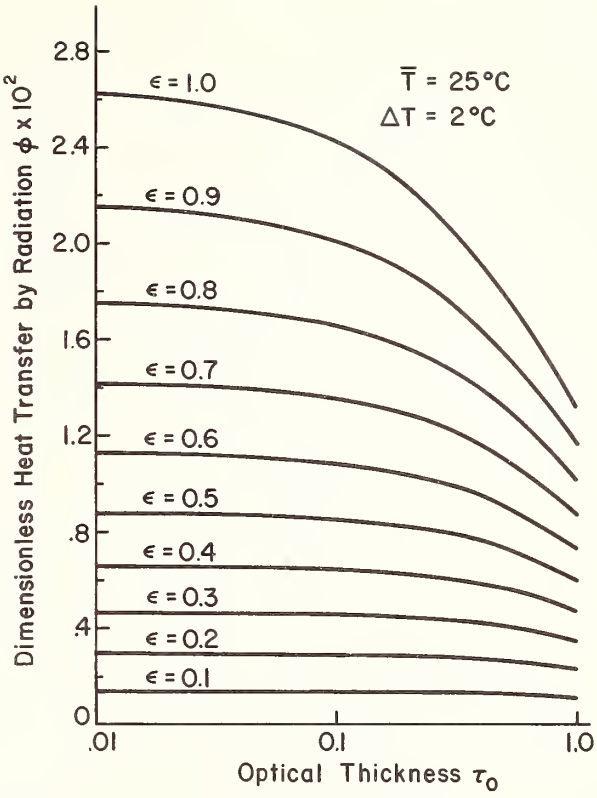

Figure 10. Dimensionless heat transfer by radiation.

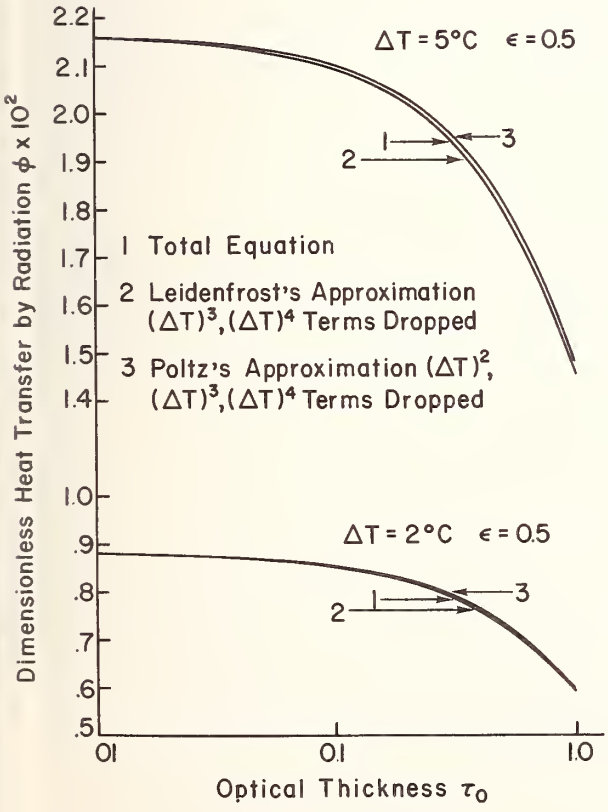

Figure 11. Comparison of radiation heat transfer $\bar{T}$ = 25 °C.

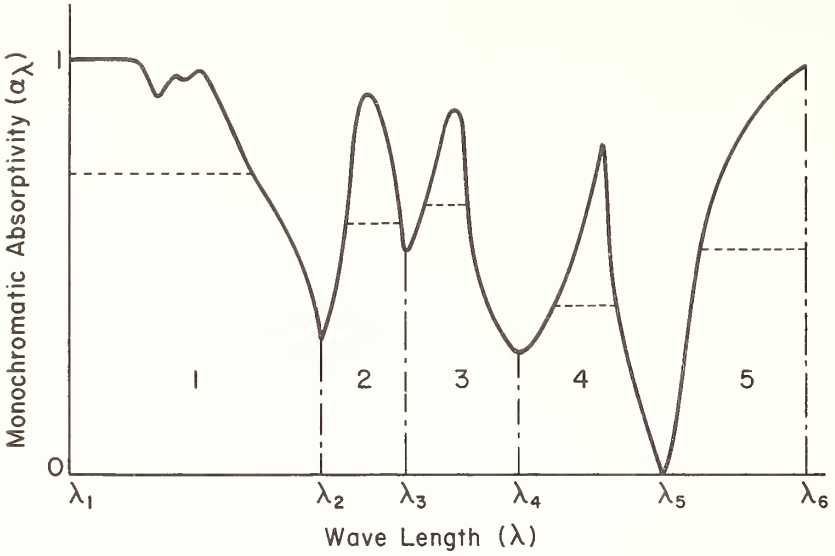

Figure 12. Monochromatic absorptivity versus wavelength.

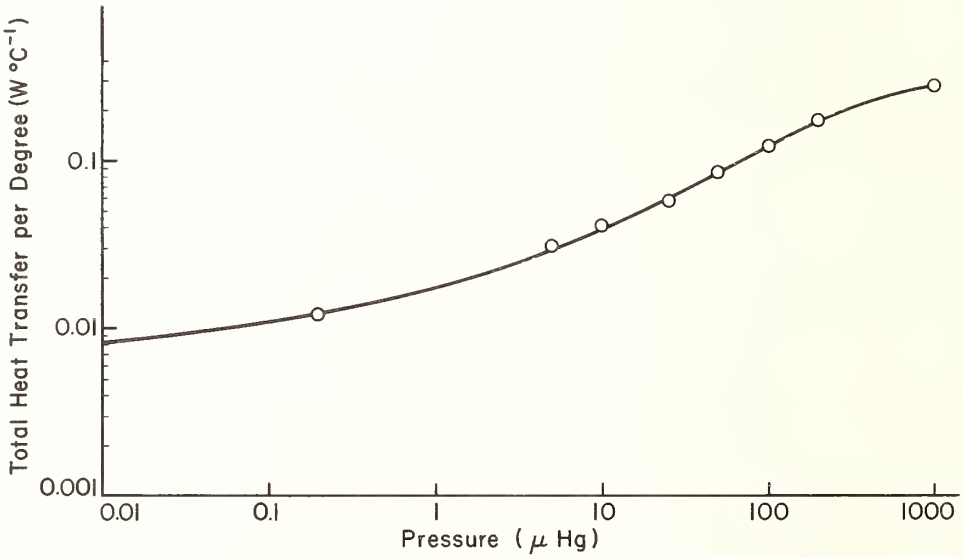

Figure 13. Vacuum heat transfer data.

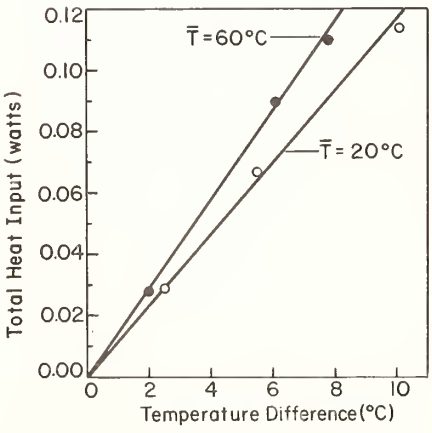

Figure 14. Heat transfer at a pressure of 0.2μ Hg.

The Thermal Conductivity of Pure Organic Liquids[1]

J. E. S. Venart and C. Krishnamurthy[2]

Faculty of Engineering
The University of Calgary
Calgary, Alberta, Canada

Unsteady state absolute measurements are presented for the thermal conductivity, of pure organic liquids in the temperature range 15 to 130°C. The measured results are thought to be accurate to ±0.5%.

Key Words: Conductivity, heat conductivity, liquids, organic liquids, thermal conductivity.

1. Introduction

In recent years there has been a rapid development in the sophisticated analytical and numerical methods used in heat transfer and flow studies. The efficient and economic use of these tools by research and industry implies the availability of accurate values of the thermophysical properties for the fluids involved--density, specific heat, viscosity, thermal conductivity and their variation with temperature and pressure--unfortunately this is not the case except for a few fluids. In addition to the above the physical and theoretical chemist wishes today to extend his knowledge of the structure of liquids; accurate equilibrium and nonequilibrium thermophysical property data can not help but assist in this area. Accurate measurements of density, specific heat, and viscosity can now be attained to a precision of one part in a thousand; with thermal conductivity this is no longer true-- for liquids deviations in reported data can exceed 10% even with reliable apparatus and experienced investigators [1,2].[3]

It is the purpose of the present investigation to provide some data for water and several pure organic liquids.

2. Source and Purity of Materials

With the exception of water, all liquids studied in the present investigation were pure organic liquids of analytic (A.R) quality, meeting the American Chemical Society (A.C.S) specifications. Some of these liquids are of A.R quality supplied under the designation of British Pharmacopoeia (B.P) standards. Details of purity of the various liquids are listed in Table 1. The water employed in the present investigation was triple distilled water containing no dissolved gases.

---

[1]Work performed with the support of the National Research Council of Canada under Grant Number NRC.A.2788.

[2]Department of Mechanical Engineering.

[3]Figures in brackets indicate the literature references at the end of this paper.

Table 1. Source and purity of liquids.

Compound	Purity	Reagent Quality	Manufacturing Pharmaceutical Company	Standard Specifications
Methanol Ethanol 100% N-Butanol Ethylacetate		A.R.*	Fischer	A.C.S.#
Glycol Glycerol N-propanol Aniline		A.R.	B.D.H.	B.P.† Standards
Benzaldehyde		A.R.	Matheson Coleman & Bell Company	A.C.S.
Acetic acid 100%		A.R.	Allied Chemical Company of Canada	A.C.S.

#A.C.S. means American Chemical Society Standard Specification.
†B.P. means British Pharmacopoaia Standards.
*A.R. means analytical reagents with maximum purity.

3. Method and Apparatus

An absolute transient line source method of measuring the thermal conductivity of liquids was utilized in the present investigation. Unlike steady-state methods, the transient method requires only simple apparatus and yields accurate results in a relatively short time.

3.1 Basic Theory

In transient measurements of thermal conductivity, temperature is a time dependent variable. The development of this temperature is obtained by passing a continuous electric current through a thin straight axial wire immersed in the homogeneous medium maintained initially in thermal equilibrium. After a short interval of time the temperature rise at the surface of the wire will be proportional to the logarithm of time. The entire arrangement, to a first approximation, can be treated as an infinite line source with constant heat generation in an extended or infinite medium.

The solution of the one dimensional radial heat conduction equation,

$$\left(\frac{\partial^2 T}{\partial r^2} + \frac{1}{r}\frac{\partial T}{\partial r}\right) = \frac{1}{\alpha}\left(\frac{\partial T}{\partial t}\right) \tag{1}$$

with the boundary conditions

$$t = 0; \quad r \neq 0, \quad T = 0 \tag{1a}$$

$$t > 0; \quad r = \infty, \quad T = 0 \tag{1b}$$

$$t > 0; \quad r \to 0, \quad -2\pi r\lambda\left(\frac{\partial T}{\partial r}\right) = \frac{q}{\ell} = \text{Constant} \tag{1c}$$

yields on solution

$$T_\infty(r,t) = \frac{q}{4\pi\lambda\ell}\,\mathrm{Ei}\left(-\frac{r^2}{4\alpha t}\right) \tag{2}$$

where $T_\infty(r,t)$ is referred to the temperature rise in any radial position r. Here $-Ei\left(\frac{-r^2}{4\alpha t}\right)$ is the exponential integral defined by

$$-Ei\ (-x) = \int_x^\infty \frac{e^{-Z}}{Z}\, dZ = -0.5772 + \ln\left(\frac{1}{x}\right) + \frac{x}{1\ 1!} - \frac{x^2}{2\ 2!} + \ldots\ldots \tag{3}$$

For $x << 1$, the infinite series may be truncated after the first two terms to a reasonable degree of accuracy. The resulting equation thus acquires the form

$$T_\infty(r,t) = \frac{q}{4\Pi\ell\lambda}\left(-0.5772 + \ln\frac{4\alpha t}{r^2}\right) \tag{4}$$

The difference between two temperatures T_1 and T_2 at two times t_1 and t_2 is therefore given by

$$\Delta T = T_\infty(r,t_2) - T_\infty(r,t_1) = \frac{q}{4\Pi\lambda\ell}\ln\left(\frac{t_2}{t_1}\right)$$

or

$$\Delta T = \frac{q}{4\Pi\lambda\ell}\,\Delta\ln t \tag{5}$$

From eq (5) it can be readily seen that a plot of ΔT vs. $\Delta\ln t$ will give a straight line with slope $\frac{q}{4\Pi\lambda\ell}$ thus, knowing the energy liberated per unit length and unit time at the wire, the thermal conductivity of the substance can be obtained from the slope.

With a line source of finite diameter, the inner boundary condition, eq (1c) must be modified to:

$$t > 0,\ r = r_0,\ \frac{q}{\ell} = -2\pi r_0\lambda\left(\frac{\partial T}{\partial r}\right) + \pi {r_0}^2 C_0\rho_0\left(\frac{\partial T}{\partial t}\right) = \text{Constant}$$

since in the theoretical case the medium situated in the region $r < r_0$ will take up a certain amount of energy depending on its heat capacity, which is different than that for the fluid at $r \geq r_0$, the solution of eq (4) will embody a term dependent on the heat capacities of the wire and medium. Assuming a constant amount of heat q generated in a perfectly conducting wire with no contact resistance between the wire and the medium, the solution as given by Carslaw and Jaeger [3] is,

$$T\ (r,t) = \frac{q}{4\pi\lambda\ell}\left[\ln t + \ln\frac{4}{r^2} - \gamma + \frac{r}{2\alpha t} + \frac{(\omega-2)r^2}{2\omega\alpha t}\left(\ln\frac{4\alpha t}{r^2} - \gamma\right) + \ldots\right] \tag{6}$$

where $\gamma = 0.5772$ is Euler's constant and 'ω' is twice the ratio of the heat capacity of an equivalent volume of the medium to that of the wire

$$\omega = 2\,\frac{C_p\rho_m}{C_p\rho_w} \tag{6a}$$

For $\frac{r^2}{2\alpha t} << 1$ the last three terms in eq (6) tend to zero and hence eqs (6) and (4) become identical. However, since convection usually limits the times of measurement to short intervals it is necessary to make this correction.

3.2 Apparatus

The apparatus used was similar to that employed by Horrocks and McLaughlin [4]. Only those items of significant difference will be discussed.

The cell design (fig. 1) used in this work was similar to that of [4], with the exception of the provision for evacuation and filling. In addition the provisions made for a double thermostated bath and cell resistance calibrations were very much as has been described by [4].

The major problem involved in the transient method is the measurement of the unsteady temperature. This time dependent temperature is measured by the variation of the electrical resistance of the heating wire.

For eq (5), $\lambda = \frac{q}{4\pi\ell}\frac{\Delta \ln t}{\Delta T}$, and the small temperature rise (0.5°C) experienced in the present work, the temperature coefficient of the resistance, $\frac{dR}{dT}$ of the wire can be treated effectively as a constant during each measurement. Therefore,

$$\frac{1}{\Delta T} \simeq \frac{1}{\Delta R}\left(\frac{dR}{dT}\right) .$$

Substitution yields $\lambda = \frac{q}{4\pi\ell}\frac{\Delta \ln t}{\Delta R}\frac{dR}{dT}$ as $q = V\,I$, the heat liberated, differentiation of Ohm's law gives

$$\Delta R = \frac{I(\Delta V) - V(\Delta I)}{I^2}$$

resulting in

$$\lambda = \frac{VI}{4\pi\ell}\frac{\Delta \ln t}{\left(\frac{\Delta V}{I} - \frac{V}{I^2}\Delta I\right)}\frac{dR}{dT} , \tag{7}$$

where R is the resistance of the source of length ℓ between the potential leads through which a current I flows under a potential V.

The current is measured in terms of the voltage V_I developed across a standard 25 ohm resistance in series with the cell. Both potentials V and V_I were measured by three dial, 0.03% accurate, potentiometers (Honeywell 2746). The transient voltages, $\Delta V_I = 25\ I$ and ΔV_V, across the standard resistance and wire were determined simultaneously by a two channel strip chart recorder (HP Mosley Model 7100B) with a full scale deflection of 1mV using a chart speed of 1 or 2 inches/sec.

Current was supplied to the dummy resistance, R_B, and wire by a six volt storage battery and adequate current control was maintained by the adjustable resistance R_A. To prevent voltage fluctuations in the electrical circuit on switching, a ballast resistor was used to match the cell resistance. Switching was accomplished by a manually operated fast response relay. The complete circuit arrangement is shown in figure 2.

4. Corrections and Sources of Error

As discussed previously, the major source of error is due to the finite wire diameter which necessitates a correction for the thermal capacity of the heater. Considering the last two terms of the eq (6)

$$C(t) = \left[\frac{r^2}{2\alpha t} + \frac{(\omega-2)\ \alpha^2}{2\omega\alpha t}\ln\left(\frac{4\alpha t}{r^2} - \gamma\right)\right] \tag{8}$$

eq (5) can be written to include this correction term as

$$T_\infty(r,t_2) - T_\infty(r,t_1) = \frac{q}{4\pi\lambda\ell}\left[\Delta \ln t + C(t_2) - C(t_1)\right] \tag{9}$$

or
$$\Delta T = \frac{VI}{4\pi\lambda\ell} \times \frac{\Delta \ln t}{1} \left[1 + \frac{C(t_2)-C(t_1)}{\Delta \ln t}\right] . \quad (10)$$

Subsequent substitutions and reduction allows eq (7) to be written as

$$\lambda = \frac{VI}{4\pi\ell} \frac{\Delta \ln t}{\left(\frac{\Delta V}{I} - \frac{V}{I^2}\Delta I\right)} \frac{dR}{dT} \left[1 + \frac{C(t_2) - C(t_1)}{\Delta \ln t}\right] \quad (11)$$

The specific heat correction for the organic liquids is approximately 3×10^{-3} W m^{-1} deg^{-1}, decreasing with an increase in temperature. The calculated corrections were applied to each liquid test result.

Other sources of possible error can be cited:

(a) distortion of the one dimensional time-dependent temperature field by the finite length of the wire,
(b) effect of an outer boundary,
(c) convection,
(d) radiation.

With careful regard to the physical design of the apparatus all these corrections, with the exception of the radiation error, may be reduced to less than 0.2% [4].

The calculation of the heat transferred by radiation unfortunately poses a more difficult problem; Poltz [5] has dealt with this problem for the steady state situation of parallel flat plates; an extension of his work to the transient radial case has not as yet been made. Therefore for all results considered here the fluids were assumed either transparent or richly absorbent and the resultant correction negligible, therefore for the fluids reported all measurements do not require correction for any effect due to the absorptivity of the fluid within the range of accuracy stated.

In addition to the above the only other major correction necessary is due to the finite time lag of the recorder, that is, the recorded voltage lags of the applied voltage. The lag of the recorder was determined by the utilizing phase relationship between two wave forms of the same frequency and amplitude. Wave forms derived from a function generator and from a tapping on the recorder slide wire were analyzed by means of the lissajous pattern on an oscilloscope. The sine of the phase angle existing between the two being obtained from the maximum horizontal deflection and the projected length on the x axis of the lissajous pattern. For the frequencies of interest the lag was obtained as a linear function of the velocity of the recorder pen.

Taking into account all effects the results presented are believed accurate to ±0.5%.

5. Results

A compilation of measured values of thermal conductivity at the different test temperatures are presented in Table 2. Each determination reported here is a mean of two to three measurements. With the exception of water, the temperature dependence of thermal conductivity data for all liquids was found to be, within the experimental error, a linear relationship of the form

$$\lambda = \lambda_0 + \left(\frac{d\lambda}{dT}\right)T \quad (12)$$

where T is in °C. Here the temperature coefficient of thermal conductivity, $\frac{d\lambda}{dT}$, was negative for all liquids with the exception of ethylene glycol and glycerol. The constants in the above equation, λ_0 and $\frac{d\lambda}{dT}$ were found by means of a linear least squares analysis applied to the experimental values. Values of conductivity, temperature coefficient so found and the applicable range of temperature are listed in Table 3. Water showed an increasing thermal conductivity over a temperature range 0 - 80°C with non-linear temperature dependence. The temperature conductivity data was best fitted by a parabolic curve,

$$\lambda = A_0 + A_1T + A_2T^2 \text{ , W } m^{-1} \text{ } deg^{-1} \quad (13)$$

where the computed coefficients and the corresponding uncertainties are

$$A_0 = 564.8\ (\pm 3.4)10^{-3}$$

$$A_1 = 1.99_7(\pm 0.17_2)10^{-3}$$

$$A_1 = -0.0085_7(\pm 0.0017_5)10^{-3}$$

Table 2. Conductivity Data for Pure Organic Liquids and Water

Temperature °C.	Thermal Conductivity Calculated from Equation (7) (λcal 10^3) W m^{-1} deg^{-1}	Specific Heat Correction Calculated from Last Term of Equation (11) (λcp 10^3) W m^{-1} deg^{-1}	Total Thermal Conductivity (λcal + λcp) = $\lambda_T 10^3$ W m^{-1} deg^{-1}
Water			
13.5	590.0	0.17	590.2
13.5	592.2	0.17	592.4
20.8	596.7	0.18	596.9
19.0	597.8	0.18	600.1
31.0	619.8	0.20	620.0
30.5	619.5	0.20	619.7
32.0	623.0	0.20	623.2
42.0	629.7	0.22	629.9
41.5	629.7	0.22	630.0
62.0	657.5	0.27	657.7
62.0	656.8	0.27	657.1
82.5	670.3	0.33	670.6
82.5	670.3	0.33	670.6
Methanol			
20.0	197.8	2.49	200.3
20.2	198.0	2.50	200.5
25.0	195.3	2.47	197.8
25.0	195.2	2.47	197.7
34.9	193.4	2.47	195.9
34.6	193.4	2.47	195.9
43.5	191.8	2.48	194.3
43.5	191.7	2.48	194.2
52.0	189.6	2.45	192.0
53.2	189.4	2.43	191.9
61.5	186.5	2.43	188.9
61.0	186.4	2.44	188.8
Ethanol			
17.0	163.2	2.62	165.9
17.2	164.8	2.62	167.4
23.5	160.8	2.46	163.3
25.0	160.2	2.45	162.7
36.0	152.9	2.31	155.2
38.0	152.5	2.31	154.8
46.5	146.6	2.14	148.7
46.0	147.0	2.14	149.1
57.0	141.7	1.99	143.7
58.0	141.6	1.99	143.6
68.0	135.9	1.88	137.8
67.5	135.6	1.89	137.5
76.5	131.2	1.80	133.0
N-Propanol			
16.0	151.4	2.47	153.9
15.7	151.3	2.47	153.7
25.0	149.8	2.36	152.2
25.0	150.8	2.36	153.2
38.5	145.1	2.19	147.3
40.0	144.9	2.19	147.1
55.0	141.2	2.00	143.2

Table 2 (continued)

Temperature °C.	Thermal Conductivity Calculated from Equation (7) (λcal 10^3) W m^{-1} deg^{-1}	Specific Heat Correction Calculated from Last Term of Equation (11) (λcp 10^3) W m^{-1} deg^{-1}	Total Thermal Conductivity (λcal + λcp) = $\lambda_T 10^3$ W m^{-1} deg^{-1}
N-Propanol (cont'd)			
55.0	141.0	2.00	143.0
65.5	137.9	1.99	139.9
66.0	137.2	1.99	139.2
N-Butanol			
15.2	151.5	2.52	154.0
15.2	151.5	2.52	154.0
20.5	151.0	2.42	153.4
20.5	151.0	2.42	153.4
34.5	146.5	2.34	148.9
34.0	146.4	2.34	148.8
47.5	144.1	2.22	146.3
64.5	140.9	2.20	143.1
64.5	140.8	2.20	143.0
82.0	138.4	1.87	140.3
101.5	134.6	1.69	136.3
Glycol			
16.0	248.5	1.71	250.3
16.0	248.7	1.72	250.4
31.0	251.0	1.66	252.7
31.0	251.0	1.66	252.7
61.5	256.5	1.54	258.1
61.5	256.0	1.54	257.5
75.0	258.0	1.46	259.4
76.0	258.2	1.46	259.7
91.5	262.1	1.38	262.5
92.0	260.6	1.38	262.0
103.8	262.8	1.35	264.2
103.7	262.8	1.35	264.1
103.0	266.9	1.24	268.1
132.85	266.7	1.24	267.9
Glycerol			
17.4	284.9	1.40	286.3
35.9	286.6	1.26	287.9
58.0	288.7	1.15	289.9
58.0	288.5	1.15	289.6
76.4	289.7	1.03	290.7
76.5	290.0	1.03	291.0
95.5	291.5	0.95	292.4
114.0	293.4	0.86	294.3
113.6	293.2	0.86	294.1
Ethylacetate			
16.0	146.4	2.37	148.8
16.4	146.2	2.35	148.6
26.3	143.0	2.34	145.4
25.2	143.4	2.34	145.7
39.0	138.7	2.34	141.0
39.0	139.1	2.32	141.4
48.2	135.4	2.34	137.7
47.8	135.3	2.35	137.6
56.0	132.6	2.32	134.9
57.0	132.6	2.32	135.0
Benzaldehyde			
16.0	149.5	2.51	152.0
16.0	150.1	2.52	152.6
34.5	142.4	2.52	145.0
34.5	142.3	2.52	144.9
51.6	136.0	2.52	138.5

Table 2 (continued)

Temperature °C.	Thermal Conductivity Calculated from Equation (7) (λcal 10^3) W m^{-1} deg^{-1}	Specific Heat Correction Calculated from Last Term of Equation (11) (λcp 10^3) W m^{-1} deg^{-1}	Total Thermal Conductivity (λcal + λcp) = $\lambda_T 10^3$ W m^{-1} deg^{-1}
Benzaldehyde (cont'd)			
52.0	135.8	2.54	138.4
67.2	132.1	2.56	134.7
67.5	132.0	2.56	134.6
Aniline			
21.5	160.3	2.21	162.5
21.0	160.1	2.21	162.3
41.2	159.8	2.17	161.9
41.2	159.3	2.17	161.5
57.0	158.7	2.14	160.8
57.0	158.3	2.14	160.5
77.5	157.5	2.09	159.6
77.5	157.4	2.09	159.4
93.0	155.9	2.09	157.9
93.0	156.7	2.09	158.8
100% Acetic Acid			
17.5	156.4	2.18	158.6
17.5	156.4	2.18	158.6
30.5	154.9	2.15	157.1
30.5	154.9	2.15	157.1
47.5	151.2	2.11	153.3
47.5	152.2	2.12	154.3
63.0	148.8	2.08	150.9
63.0	148.7	2.07	150.8
79.0	146.5	2.02	148.5

Table 3. Fitted Values of Conductivity and Temperature Coefficients

Name of the Liquid	Thermal Conductivity of Liquid at 0°C. with uncertainty in λ_0 x 10 W m^{-1} deg^{-1}	Temperature Coefficient of Thermal Conductivity with uncertainty in $\frac{d\lambda}{dT} 10^3$ W m^{-1} deg^{-2}	Range of Measurements °C.
Methanol	205.0 (±0.5)	-0.256 (±0.011)	20 - 61
Ethanol	176.4 (±0.5)	-0.573 (±0.009)	17 - 76
N-Propanol	159.2 (±0.5)	-0.295 (±0.011)	16 - 66
N-Butanol	156.9 (±0.4)	-0.208 (±0.007)	15 - 101
Ethylene Glycol	248.1 (±0.2)	+0.153 (±0.002)	16 - 133
Glycerol	285.0 (±0.2)	+0.080 (±0.002)	17 - 113
Ethylacetate	154.4 (±0.2)	-0.344 (±0.005)	16 - 57
Benzaldehyde	157.4 (±0.7)	-0.349 (±0.014)	16 - 67
Aniline	163.9 (±0.3)	-0.568 (±0.004)	21 - 93
Acetic Acid	161.9 (±0.4)	-0.171 (±0.007)	17 - 79

6. Discussion

In order to check the reliability and accuracy of the apparatus, conductivity measurements were made first on water and methanol for which thermal conductivities are well established to at least ±1% over the temperature range 0 - 100°C.

6.1 Water

The usage of water as a thermal conductivity standard was first proposed by Riedel [6]. To assure the validity of the apparatus, conductivity measurements were carried out on water over a temperature

range 0 - 80°C. A comparison of this work with earlier research was limited to seven papers published since 1950.

Figure 3, a deviation plot for eq (13), indicates that at 0°C. the values reported by Riedel [6,7, 8] and the present work are virtually the same. Slightly higher values are reported by LeNeindre and Vodar [9] in 40 - 70°C. range. Excepting the temperature range 0 - 20°C, consistantly higher values are reported by Challoner and Powell [1] . The agreement with Poltz [5] is excellent, and in addition, in very good agreement with the equation recommended by the Sixth International Conference [11] on the properties of steam in the temperature range, which is also shown in Figure 3.

6.2 Methanol

Twelve thermal conductivity determinations were made on Methanol. A comparison of this work with four major investigations is shown in figure 4. The agreement with Poltz [5] and Fritz and Poltz [16] is 0.1 and 0.4 per cent respectively.

6.3 Other Liquids

The above agreement is evidence that the apparatus will yield reproducible and accurate results for most liquids and strongly supports the work of Poltz [10] since the measurements are made with two entirely different apparatus.

7. References

[1] Challoner, A. R., and Powell, R. W., *Pro. Roy. Soc. (London)* A238, 90 (1956).

[2] Riedel, L., *Chem. Ingr. Tech.*, 23 (19), 465-484 (1951).

[3] Carslaw, H. S., and Jaeger, J. C., "Conduction of heat in solids," Oxford University Press (1959).

[4] Horrocks, J. K., and McLaughlin, E., *Pro. Roy. Soc. (London)*, A273, 259 (1963).

[5] Poltz, H., "Die Wärmeleitfähigkeit von Flüssigkeiten III," *Int. J. Heat Mass Transfer*, Vol. 8, 609-620, Pergamon Press (1965).

[6] Riedel, L., *Chem. Ingr. Tech.*, 23, 321 (1951).

[7] Riedel, L., *Forsch Gebiete, Ingenieurw*, 11, 340 (1940).

[8] Riedel, L., *Arch. Tech. Messen.*, 1, 273 (1954).

[9] LeNeindre, B., Johanin, P., and Vodar, B., *C.R. Acad. Sc. Paris*, Vol. 258, 3277 (1964).

[10] Poltz, H., and Jugel, R., "The Thermal Conductivity of Liquids IV," *Int. J. Heat Mass Transfer*, 10, 1075 (1967).

[11] *The Thermal Conductivity Panel of "The 6th International Conference" on the properties of steam, Paris, June 22-24, 1964, Technical Report No. 15.*

[12] Schmidt, E., and Leidenfrost, W., *Chem. Ingr. Tech.*, 26, 35 (1964).

[13] Vargaftik, N. B., and Oleshchuk, O. N., *Teploenerg.*, 6, 70 (1959).

[14] Challoner, A. R., Gundry, H. A., and Powell, R. W., *Proc. Roy. Soc.* A, 245 (1241) 259-261 (1958).

[15] Mason, H. L., *Trans. Amer. Soc. Mech. Engrs.* 76(5), 817-821 (1954).

[16] Fritz, W., and Poltz, H., *Int. J. Heat Mass Transfer*, 5(2), 307 (1962).

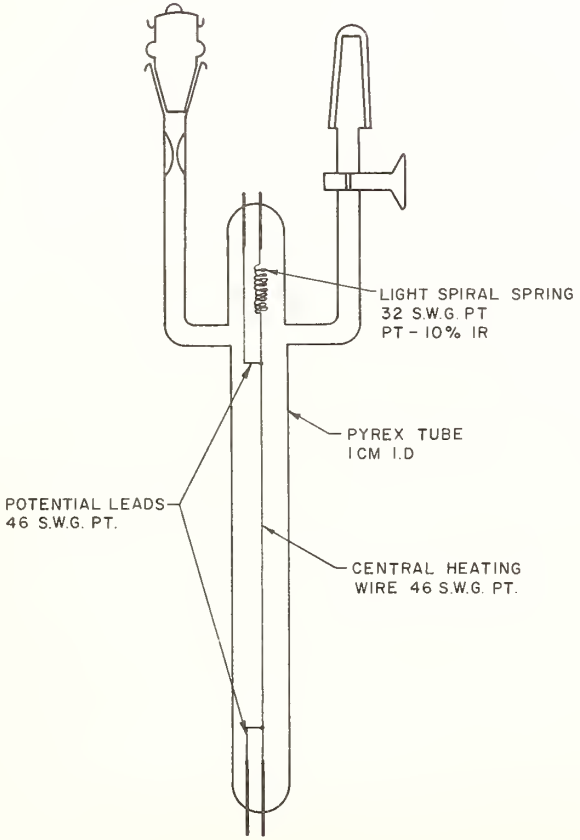

Figure 1. Cell Detail

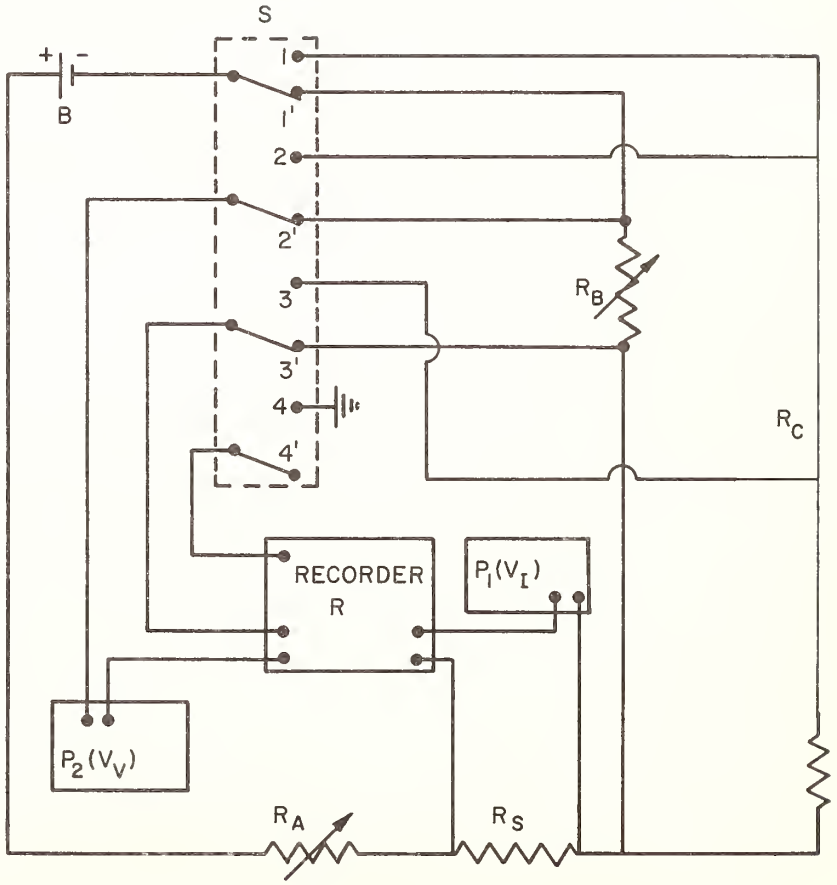

Figure 2. Schematic layout of a typical hot wire cell and the associated electrical circuit

B battery, R_A adjustable resistance, R_B ballast resistance, R_C cell resistance, R_S standard resistance, P_1 & P_2 potentiometers, R recording potentiometer, S relay switch

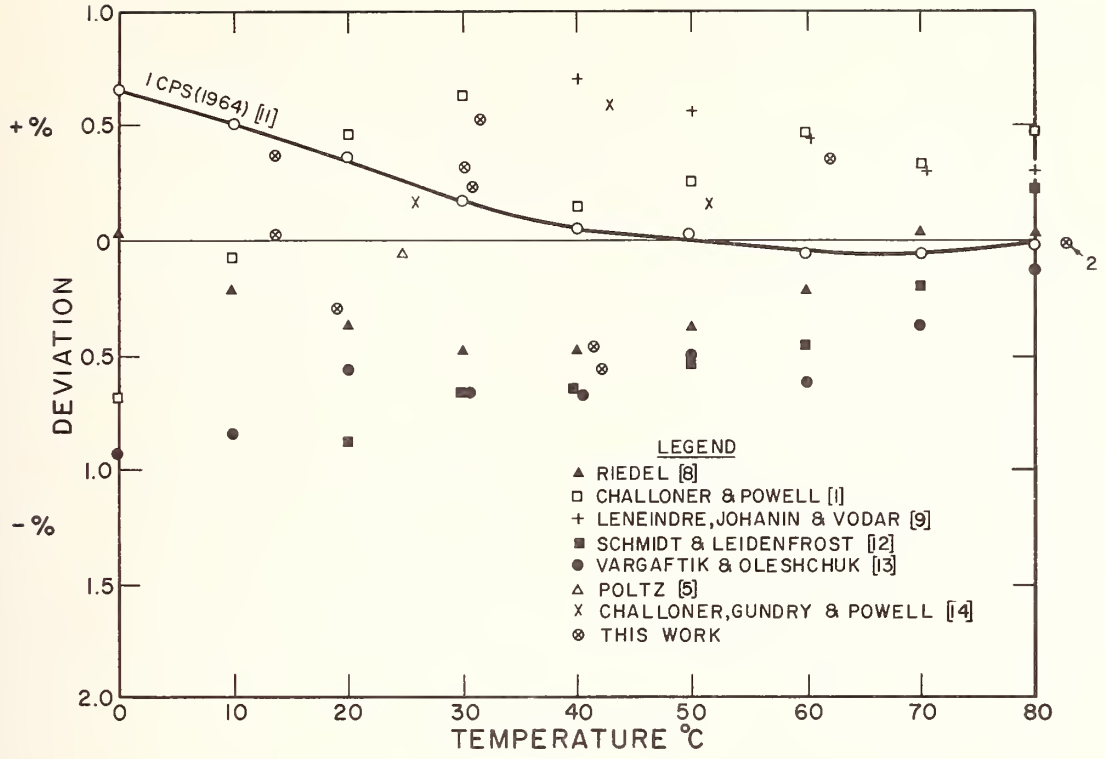

Figure 3. Deviation plot for the thermal conductivity of water against temperature

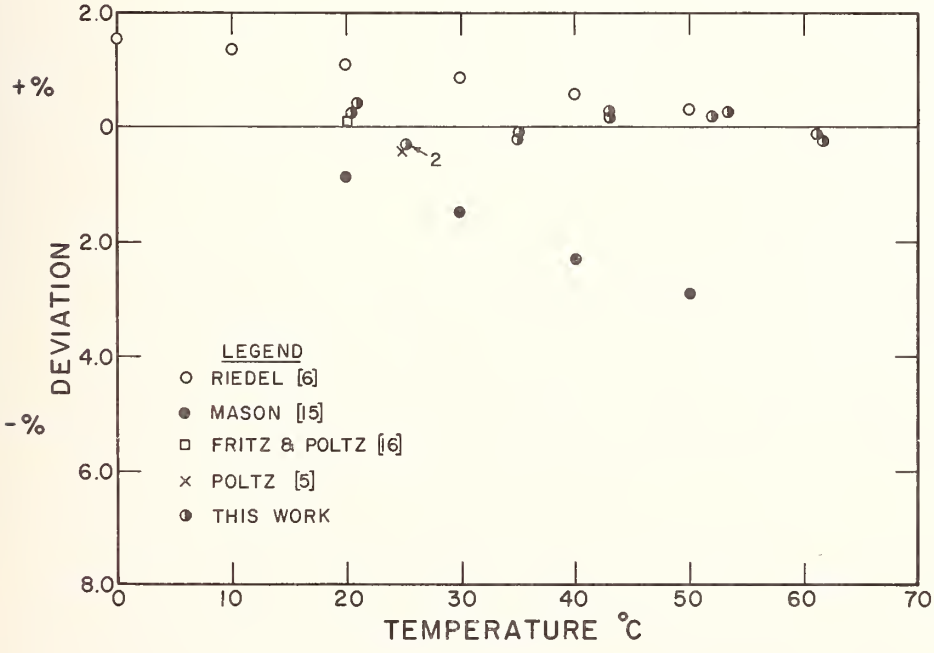

Figure 4. Deviation plot for the thermal conductivity of methanol against temperature

Pressure and Temperature Dependence of the Thermal Conductivity of Liquids

E. McLaughlin[1]

Chemical Engineering Department
Louisiana State University
Baton Rouge, Louisiana

Differences in behaviour between the coefficients of shear viscosity and thermal conductivity of liquids with respect to changes in pressure, temperature and molecular structure are reviewed. A lattice model is used to interpret the behaviour of the coefficient of thermal conductivity and comparisons are made with results based on the Enskog theory.

Keywords: Enskog theory, effect of pressure on thermal conductivity, effect of temperature on thermal conductivity, lattice model, liquids, thermal conductivity.

In the study of the pressure and temperature dependence of viscosity η and thermal conductivity λ of liquids, most attention has been devoted to the effect of temperature, as distinct from pressure, and in addition to viscosity rather than thermal conductivity. This has possibly arisen because of the exponential type dependence of viscosity on temperature at atmospheric pressure.

$$\eta = \eta_o \exp (E_\eta/RT) \tag{1}$$

which invited discussion in terms of the activation energy E_η for viscous flow [1][2]. The coefficient of thermal conductivity on the other hand being approximately linear in temperature at atmospheric pressure

$$\lambda = \lambda_o - AT \tag{2}$$

and more difficult to measure precisely, tended to be neglected.

It is the purpose of the present paper to summarize briefly some of the main differences in behaviour of the coefficients of viscosity and thermal conductivity and attempt to explain these in terms of a simple model which can also be used to determine the factors which control the pressure and temperature dependence of thermal conductivity.

In comparing the experimentally determined behaviour of the two coefficients the main differences are as follows:

1. Firstly, as mentioned above, at atmospheric pressure the temperature dependence of viscosity is much steeper than the temperature dependence of thermal conductivity. For example, comparative figures for benzene show that the viscosity drops by 50% between 20 and 70°C while the thermal conductivity falls by only about 11%.

2. Secondly, the thermal conductivity of a liquid is insensitive in magnitude to changes in molecular structure whereas the viscosity of a liquid is very sensitive to such changes. This can best be illustrated by looking at the magnitude of both coefficents for a series of closely related molecules. Table 1 lists values [2] for such

---

[1] N.S.F. Senior Visiting Foreign Scientist
Permanent address: Department of Chemical Engineering and Chemical Technology, Imperial College, London S.W.7., England

[2] Figures in brackets indicate the literature references at the end of this paper.

a series of aromatic hydrocarbons at the melting point and shows that although all the thermal conductivities lie within a few percent of each other substantial differences occur in the viscosities particularly on going from para - to meta - to ortho - terphenyl where there is a fortyfold increase.

Table 1. Viscosities and Thermal Conductivities of a Series of Liquid Aromatic Hydrocarbons at the Melting Point

	benzene	diphenyl	p-terphenyl	m-terphenyl	o-terphenyl
$\eta \times 10^4$ Kg $m^{-1}sec^{-1}$	8.2	14.3	8.0	53.2	322.0
$\lambda \times 10^2$ W m^{-1} deg^{-1}	14.8	13.8	12.8	13.7	13.2
A	0.032	0.014	0.011	0.0036	0.0069

3. Thirdly, although the thermal conductivities of most organic liquids are roughly the same lying between 8×10^{-2} to 30×10^{-2} W m^{-1} deg^{-1} there are significant differences in the temperature dependence of the coefficient. Again this can be illustrated with the series of aromatic polyphenyl hydrocarbons discussed above for which the coefficient A of eq (2) has been listed in Table 1 on taking λ_o as the conductivity at 0°C. The results show that A is greatest for the simplest molecule of the series, benzene, and decreases with increasing molecular complexity to give the smallest values for ortho - and meta - terphenyl. This again contrasts with the temperature dependence of the coefficient of viscosity which is steepest for the most complex molecules and lowest for the simplest.

4. Finally, although the coefficient of thermal conductivity at atmospheric pressure decreases with increasing temperature for normal liquids, Bridgman [3] showed that for a number of liquids he studied, the temperature dependence reversed sign above about 5000 bars beyond which the coefficient increased with increasing temperature at constant high pressure. Again in contrast, no reversal in the sign of the temperature dependence of viscosity was obtained for the same liquids at high pressures.

To set up a model to use in an attempt to explain these features of the behaviour of the thermal conductivity of a liquid it is necessary to make assumptions about

(i) the structure of the liquid
(ii) the molecular mechanism of transport
(iii) the molecular shape
(iv) the intermolecular forces

In order to keep the model simple, the assumptions will be necessarily crude. Firstly, the liquid is assumed to be a quasi-crystalline assembly. This is not an unreasonable assumption for liquids well away from the critical region in view of the small volume change on fusion which usually occurs, of the order of 10%, and the fact that study of the X-ray patterns of liquids reveal only a small decrease in co-ordination number compared with the solid. For example, for argon [4] decreasing from 12 to 10.4 in the liquid close to the freezing point. In addition, the specific heats of solids and liquids close to the freezing point are not substantially different. This evidence suggests that energy- and volume-wise a solid-like model for the liquid would not be grossly in error. In theories of thermal conduction derived from statistical mechanics the structure of the fluid turns up in terms depending on the radial distribution function $g_o^{(2)}(r)$. In the absence of experimental values of $g_o^{(2)}(r)$ such terms can only be readily determined from experimental data if they are thermodynamic in form such as:

$$\frac{pV}{NKT} = 1 - \frac{N}{6VkT} \int r\, \phi'(r)\, g_o^{(2)}(r)\, d^3r \qquad (3)$$

or for an s, q potential

$$\phi(r) = Ar^{-s} - Br^{-q} \quad (s>q)$$

$$\frac{6VkT}{N\sigma^2}\left[-\frac{sq}{3}\frac{U'}{NkT} + \left(s + q - 1\right)\left(\frac{pV}{NkT} - 1\right)\right] \simeq \int \nabla^2 \phi(r)\, g_o^{(2)}(r)\, d^3r \qquad (4)$$

where U' is the configurational energy of the liquid [5], σ the molecular diameter, and the other symbols have their usual significance.

In the cell model of the liquid adopted, it is natural to assume that the molecules oscillate about fixed sites with a mean frequency ν determined by the properties of the system. In a temperature gradient the excess energy $l\, du/dx$, between molecules in layers a distance l apart, is handed on by 'collisions' with neighbors at the extremity of the vibration. The heat flux J_q can therefore be written [6]

$$J_q = -\lambda \frac{dT}{dx} = -n_A\, 2\, \nu l \frac{du}{dx} = -\sqrt{2}\, \nu\, C_v \frac{1}{a} \frac{dT}{dx} \tag{5}$$

hence

$$\lambda = \sqrt{2}\, \nu\, C_v/a \tag{6}$$

where n_A is the number of molecules per unit area of the liquid, C_v the specific heat at constant volume per molecule, and a the nearest neighbor distance. In eqs (5) and (6) the lattice geometry has been assumed to be f.c.c. so that $a^3 = \sqrt{2}\, v$ where $v = V/N$ is the volume of the system per molecule and $l = a\sqrt{2}/2$.

From eq (6) it is now possible [7] [8] to determine the factors which control the pressure and temperature dependence of thermal conductivity. In the first approximation we will assume C_v is constant, hence on differentiation we obtain the set of equations:

$$\frac{1}{\lambda}\left(\frac{\partial \lambda}{\partial T}\right)_p = -\alpha\left[\frac{1}{3} - \left(\frac{\partial \ln \nu}{\partial \ln v}\right)_p\right] \tag{7}$$

$$\frac{1}{\lambda}\left(\frac{\partial \lambda}{\partial p}\right)_T = \beta_T\left[\frac{1}{3} - \left(\frac{\partial \ln \nu}{\partial \ln v}\right)_T\right] \tag{8}$$

$$\frac{1}{\lambda}\left(\frac{\partial \lambda}{\partial T}\right)_v = \frac{1}{\nu}\left(\frac{\partial \nu}{\partial T}\right)_v \tag{9}$$

where α is the coefficient of thermal expansion and β_T the isothermal compressibility.

The quantity $-(\partial \ln \nu/\partial \ln v)$ is known in solid state theory as Gruneisen's constant and if this is assumed constant $(1/\lambda)(\partial\lambda/\partial T)p$ should be linear in α. As the coefficient of thermal expansion is largest for simple molecules, these have the steepest temperature dependence of thermal conductivity. Conversely as the more complex molecules have lower coefficients of thermal expansion they have a lower temperature dependence of thermal conductivity. Examination of a plot of $(1/\lambda)(\partial\lambda/\partial T)_p$ against α for a series of liquids, however, shows [7] that although the results all lie on a single curve, this curve does not pass through the origin but cuts it at $\alpha \simeq 0.5 \times 10^{-4}$ deg^{-1}. It is to be expected therefore that for liquids with α less than this value the coefficient of thermal conductivity would increase with increasing temperature. This has been shown to be the case with liquids at high pressure [8], where beyond about 5000 bars α values are generally less than 0.5×10^{-4} deg^{-1}. Likewise it has been shown that the pressure dependence of thermal conductivity is substantially controlled by the isothermal compressibility as plots of available data [3] in the form $(1/\lambda)(\partial\lambda/\partial p)_T$ are linear in β_T.

These conclusions therefore provide partial answers to points 3 and 4 raised above. With regard to point 2, calculated vibrational frequencies in liquids are not sensitive to molecular structure. Hence, provided the specific heat term in eq (6) does not include rotational or internal vibrational modes as is suggested by studies of the experimental behaviour of the ratio $m\lambda/k\eta$ [9], and the transport properties of isotopic molecules [10] but is purely a lattice term, then insensitivity to molecular structure in λ is to be expected.

To summarise therefore, as eq (1) indicates, the temperature dependence of viscosity is controlled by energy parameters and hence one would expect sensitivity of this coefficient to changes in pressure, temperature, and molecular structure. Such changes would, in addition, be greatest for the most complex molecules. In contrast, as eq (7) and (8) indicate the pressure and temperature dependences of thermal conductivity are substantially controlled by volume parameters and hence, compared with viscosity, relatively insensitive to changes in pressure and temperature.

In view of the comparative success of the model it is pertinent to examine the relationship of the present results to those obtained from statistical theories. This is possible for hard sphere molecules of diameter σ where the model corresponds to that of a particle in a rectangular cell potential with a frequency ν given by [7]

$$\nu = \sqrt{\frac{8kT}{\pi m}} \qquad \frac{1}{4(a - \sigma)} \tag{10}$$

so that $(\partial \ln \nu / \partial \ln v)_p$ can be evaluated to yield [7]

$$\frac{1}{\lambda}\left(\frac{\partial \lambda}{\partial T}\right)_p = -\alpha\left[\frac{1}{3} - \frac{1}{2T\alpha} + \frac{1}{3}(y + 1)\right] \tag{11}$$

where $y = (pV/RT) - 1 = \sigma/(a-\sigma)$ has been obtained from the free volume theory of a dense fluid of hard spheres [11].

Existing statistical theories of thermal conductivity of hard spheres, in the approximation that only binary collisions are important, all reduce essentially to the form first proposed by Enskog [11]

$$\lambda = \frac{\lambda_o b_o}{V}\left[\left\{\frac{1}{y} + \frac{3}{5}\right\} + \left\{\frac{3}{5}\left(1 + \frac{3}{5}y\right) + 0.3957y\right\}\right] \tag{12}$$

where λ_o is the thermal conductivity of the corresponding dilute gas and b_o the hard sphere second virial coefficient. The first term of eq (13) arises from the diffusive type displacement of molecules which is small for dense fluids ($y \gg 1$). On discarding this term to bring the models on to the same comparative basis it is found on differentiation that

$$\frac{1}{\lambda}\left(\frac{\partial \lambda}{\partial T}\right)_p = -\alpha\left[1 - \frac{1}{2T\alpha} + \frac{1}{3}(y + 1)\, f(y)\right] \tag{13}$$

where $f(y) \to 1$ for $y \ggg 1$. Eqs (12) and (13) are therefore seen to be substantially of the same form. A similar correspondence is found for the case of the pressure dependence of thermal conductivity which on the present model is given by:

$$\frac{1}{\lambda}\left(\frac{\partial \lambda}{\partial p}\right)_T = \beta_T\left[\frac{1}{3} + \frac{1}{3}(y + 1)\right] \tag{14}$$

Broad agreement with experiment and close correspondence in form with the Enskog results therefore suggest the essential correctness of the conclusion that the pressure and temperature dependences of thermal conductivity of liquids are determined by the coefficients of isothermal compressibility and thermal expansion respectively.

Finally, it is well known that for a number of simple fluids when λ is plotted against density for various temperatures the isotherms are either co-incident or very close together. This also is in agreement with results obtainable from the present model as from eq (10)

$$\left(\frac{\partial \lambda}{\partial T}\right)_v = \frac{\lambda}{2T} \tag{15}$$

and if evaluated on the simple harmonic oscillator model for ν [6]

$$\left(\frac{\partial \lambda}{\partial T}\right)_v = 0 \tag{16}$$

The rectangular cell potential can be looked on as the limiting case of anharmonicity and hence $(\partial\lambda/\partial T)_v$ for liquids would be expected to lie within the limits given by eqs (15) and (16) and hence closely spaced together or coincident, which is in agreement with experiment [8].

References

[1] Glasstone, S., Laidler, K. J., and Eyring, "The Theory of Rate Processes", McGraw-Hill,

[2] Horrocks, J. K. and McLaughlin, E. Proc. Roy. Soc. (London), A 273, 259 (1963).

[3] Bridgman, P. W. "The Physics of High Pressure," Bell and Sons, London (1949).

[4] Eisenstein, A. and Gingrich, N. S. Phys. Rev. 62, 261 (1942).

[5] Rowlinson, J. S. "Liquids and Liquid Mixtures," Butterworths, London (1959).

[6] Horrocks, J. K. and McLaughlin, E. Trans. Faraday Soc., 56, 206 (1960).

[7] Horrocks, J. K. and McLaughlin, E. Trans. Faraday Soc., 59, 1709 (1963).

[8] Kamal, I. and McLaughlin, E. Trans. Faraday Soc., 60, 809 (1964).

[9] McLaughlin, E. Chem. Rev., 64, 389 (1964).

[10] Horrocks, J. K., McLaughlin, E., and Ubbelohde, A. R. Trans. Faraday Soc., 59, 1110 (1963).

[11] Hirschfelder, J. O., Curtis, C. F. and Bird, R. B. "Molecular Theory of Gases and Liquids" Wiley, New York (1954).

Thermal Conductivity of Several Dielectric Liquids of Low Boiling Point

R. C. Chu, O. Gupta, J. H. Seely

International Business Machines Corporation
Systems Development Division, Poughkeepsie, New York

This paper presents recent thermal conductivity measurements for three, low-saturation temperature, dielectric liquids: FC-78, Freon C51-12, and Freon 113.

The measurements were made through the mechanism of steady-state, radial heat-flow in a thin annulus. The system was calibrated using air and distilled water.

Emphasis is placed on comparing the results obtained against data of other investigators and the measurement techniques used. An assessment of the accuracy of the measurements and the effect of natural convection and air solubility are also discussed. The experimental apparatus used and the details of instrumentation are illustrated by schematics and photographs.

Key Words: Thermal conductivity, heat transfer, coolant property, measurement technique.

1. Introduction

Developments in electronic components and packaging techniques have created a dual problem in cooling. On one hand, heat fluxes have been increased by orders of magnitude, so that high values of heat transfer coefficients are needed. In addition, when the response times of circuits are measured in nanoseconds or picoseconds, the temperature difference between the components becomes an important consideration.

The above criteria are best satisfied by liquid cooling techniques, particularly subcooled-flow-boiling systems and subcooled-pool or saturated-pool-boiling systems. Intimate contact between liquid and components is often necessary in such systems, so that dielectric properties, chemical inertness, and material compatibility must also be considered. A further restriction exists in electronic cooling; namely, silicon and germanium semiconductor devices must be maintained at relatively low temperatures (100°C or less). In recent years, several manufacturers have developed fluorinated heat-transfer liquids that satisfy most requirements. Because these products have not had a widespread use, some of their physical properties are not well-established. In particular, thermal conductivity, because it is of paramount importance in a thermal system and because it is somewhat difficult to measure, has been of concern to designers of heat transfer systems. For comparing thermal characteristics of these liquids, we decided to perform our own conductivity measurements, primarily intending to obtain accurate results for correlating heat transfer data. After an extensive searching of literature in the field, the "thin annulus" technique which is most compatible with our instrumentation capability was selected.

2. Experimental Techniques

2. 1 Theoretical Considerations

The "thin annulus" technique for measurement of thermal conductivity is based on the following radial heat-flow equations:

$$q = \frac{2\pi\lambda L\,(\Delta T)}{\mathrm{Ln}\ r_2/r_1} = C\lambda\Delta T \tag{1}$$

where:

L = length of annulus, m

r_1, r_2 = inner and outer radius of annulus, m

ΔT = temperature difference across the liquid annulus, ^{o}C

λ = thermal conductivity w m^{-1} deg^{-1}

C = constant of test configuration, m

$$= \frac{2\pi L}{\mathrm{Ln}\ r_2/r_1}$$

Rearranging equation (1), gives

$$\lambda = \frac{q}{C\Delta T} \tag{2}$$

Equation (2) is derived with the assumptions that heat flow takes place purely in the conduction mode. It is obvious that this assumption is somewhat unrealistic, as natural convection always exists in such a configuration. However, if ΔT and annulus thickness are properly selected, it is possible to minimize the natural convection effect to a negligible degree. Indeed, this is the only way one can make the "thin annulus" method work. For our measurements, an annulus thickness of 0. 025 and 0. 080 inch and a 5. 0 inches length was selected. The reason for choosing two different annulus dimensions is to determine the natural convection effect due to annulus thickness.

2. 2 Description of Apparatus

The apparatus, which is made up of a series of concentric cylinders, is shown in figure 1. The innermost cylinder is made of a ceramic material and has four inner passageways, each of which houses a 0. 005 inch diameter nichrome wire. This arrangement ensures a uniform heat flux along the length of the heat source. The ceramic heater is clad with a copper cylinder which serves as the inner surface of the annular test section. The outer surface is formed with another copper cylinder which is positioned by means of two nylon rings. A high degree of concentricity is maintained between the rings and the cylinder to guarantee a uniform annulus. The outer portion of the apparatus forms a water jacket which serves as a heat sink.

Provisions are made for mounting eleven iron-constantan thermocouple junctions. Two sets of diametrically opposed junctions are mounted to record the internal temperature of the copper cylinder cladding around the heater -- one set near the top and one set near the bottom of the apparatus. Another pair of junctions, 180^{o} apart, are located at the center to record the temperature of the inner surface of the test annulus. The five remaining thermocouples are used for monitoring the outer section of the annulus and water temperatures. Arrangements are provided for filling the test section with liquid and for purging the system of air. A schematic of the liquid conductivity experimental testing system is shown in figure 2. The experimental equipment is shown in figure 3.

2. 3 Test Procedure

Liquid is poured into the test section through one of the venting tubes to form a liquid annulus. When the filling operation is completed, the system is turned on, power and temperature readings are taken when thermal equilibrium is established. Various heat-flux levels are used to evaluate the natural convection effect. Two levels of sink temperatures are applied for determining the temperature coefficient of conductivity. Similar tests are repeated for all three liquids.

2. 4 Results

Thermal conductivity measurements obtained on three dielectric liquids, FC-78, (a product of the 3M Company), Freon C-51-12, Freon 113 (products of the duPont Company) are shown in figure 4 as a function of heat flux. Conductivity versus temperature data of the three liquids are compared with data of other investigators (see figure 5).

It is evident that the data obtained from the 0. 080 inch thick annulus test section shows a substantial natural convection effect. However, it is equally evident that the thinner annulus (δ_2 = 0. 025 inch) has virtually eliminated the natural convection heat transfer in the system. These comparative results easily suggest the postulation that the discrepancies of other reported data may very well be caused by this important factor.

3. Discussions

1. One of the reasons that we chose two different annulus thicknesses was to see how this critical dimension affects measurements on various kinds of fluids. The data shown in figure 4 can be used to estimate, quantitatively, the natural convection effect due to wider annulus thickness. Furthermore, if we extend the δ_2 line, shown in figure 4-A, we will see that it intersects with the δ_1 line at about 100 W/M^2 heat flux, which can be interpreted as the maximum heat flux allowable to avoid natural convection for the annulus of δ_2 thickness.

2. One of the most striking characteristics of these dielectric liquids is their relatively high air solubilities (see example in figure 6). Our experience indicates that it is extremely difficult, if not impossible, to maintain a consistency of these liquids in air solubilities, as they are extremely temperature dependent at a given pressure which for our case is atmospheric. Because these liquids all have negative temperature coefficients in air solubilities, this can cause an increase of observed thermal conductivity when liquid temperature is raised to a higher level. This effect seems to be particularly pronounced with wider annulus thickness (see results in figure 4).

3. Since natural convection is affected not only by annulus thickness (δ), but also by ΔT and liquid properties (see Table 1) such as thermal expansion coefficient (β) and kinematic viscosity (γ), it is generally true that with a given δ and ΔT, better accuracy can be expected for liquids with higher kinematic viscosity and lower coefficient of thermal expansion, like water, and will show considerable error for the converse case; that is, lower γ and higher β like air. We did observe these aforementioned results during our system calibration, using water and air.

4. Conclusions and Recommendations

The thermal conductivity values summarized in this paper represent our recent measurements in this area. Based on our instrumentation capability and extremely good repeatibility of data, it is our judgment that these results do have good absolute accuracy. We have found the information to be quite meaningful and useful in making heat transfer correlations of these liquids.

We would like to suggest that these liquids be further evaluated with broader temperature range and various solubilities, to determine the effects of these variables on thermal conductivity.

5. Acknowledgment

The authors wish to thank all members of IBM's Poughkeepsie Heat Transfer Development Department for their encouragements and discussions during the pursuing of this work.

Table 1. Properties of the three dielectric liquids.

Manufacturer	FC-78 3M Co.	Freon-113 DuPont	Freon C51-12 DuPont
Nominal Boiling Point ^{o}F	122	117.5	113.5
Density at $77^{o}F$ - lb/ft^3	106.0	97.7	104.4
Specific Heat at $77^{o}F$ - Btu/lb-^{o}F	.248	.218	.266
Thermal Conductivity at $77^{o}F$ - Btu/hr-ft-^{o}F	See figure 5		
Kinematic Viscosity at $77^{o}F$-c. s.	.44	.42	.61
Heat of Vaporization at the Boiling Point - Btu/lb	41.0	63.1	40.0
Coefficient of Expansion ft^3/ft^3-^{o}F	.009	.00078	.00073
Surface Tension at $77^{o}F$ - dynes/cm	13.0	19.0	11.6
Dielectric Constant at $77^{o}F$ and 1kc	1.81	2.41	1.80
Dielectric Strength at $77^{o}F$ $\frac{volts}{mil}$	430	310	420
Solubility of air in liquid at 1 atm. & $77^{o}F$ mol. %	.50 (estimated)	.12	.15

6. Bibliography

[1] Grimm, T. C., and Kreder, K. R., "Apparatus for Measuring Thermal Conductivity of Liquids From -70°C to +200°C," Proceedings of the Conference on Thermal Conductivity, 1965.

[2] Ingersoll, L. R., Zobel, O. J., and Ingersoll, A. C., "Heat Conduction," McGraw-Hill Book Company, New York, 1954.

[3] Jakob, M., "Heat Transfer," Vol. 1, John Wiley & Sons, Inc., New York, 5th Printing Sept. 1956.

[4] Kern, D. Q., "Process Heat Transfer," McGraw-Hill Book Company, New York, 1950.

[5] Mason, H. L., "Thermal Conductivity of Some Industrial Liquids from °C to 100°C," ASME Transactions, 76, 1954.

[6] Technical Information by the Chemical Division of the 3M Company, "3M Brand Inert Fluorochemical Liquids," 1966.

[7] Technical Bulletin by the Freon Products Division of duPont, "Freon C-51-12 Fluorocarbon," 1967.

[8] Van der Held and Van Drumen, "A Method of Measuring the Thermal Conductivity of Liquids," Physica, 15, 1945.

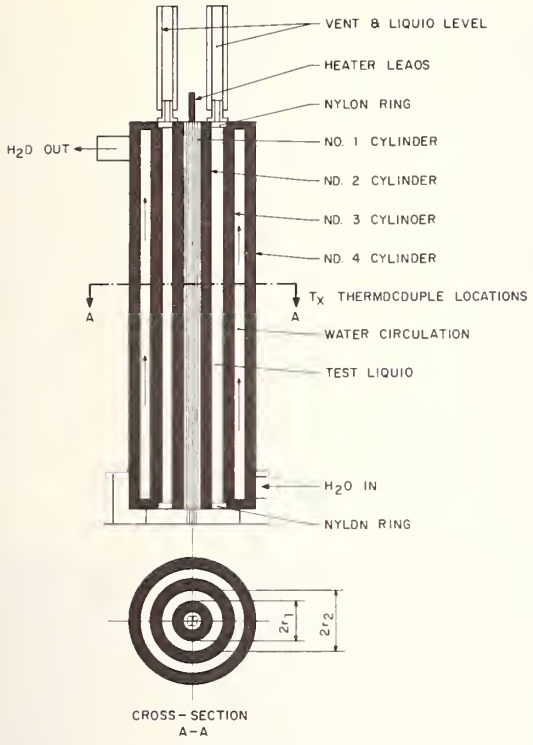

Figure 1. Liquid thermal conductivity apparatus.

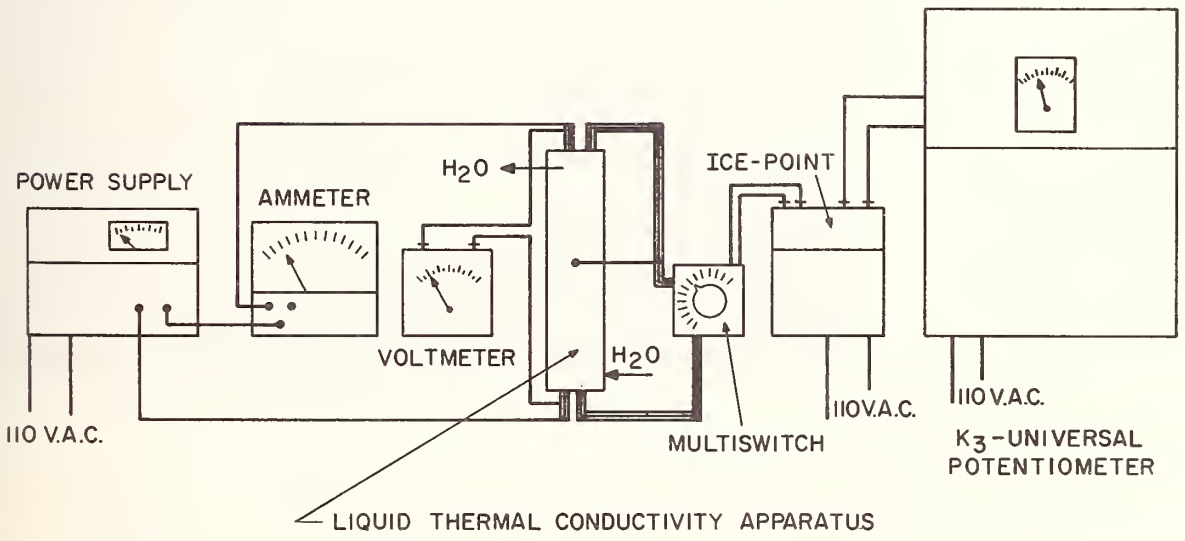

Figure 2. Schematic of the liquid conductivity testing system.

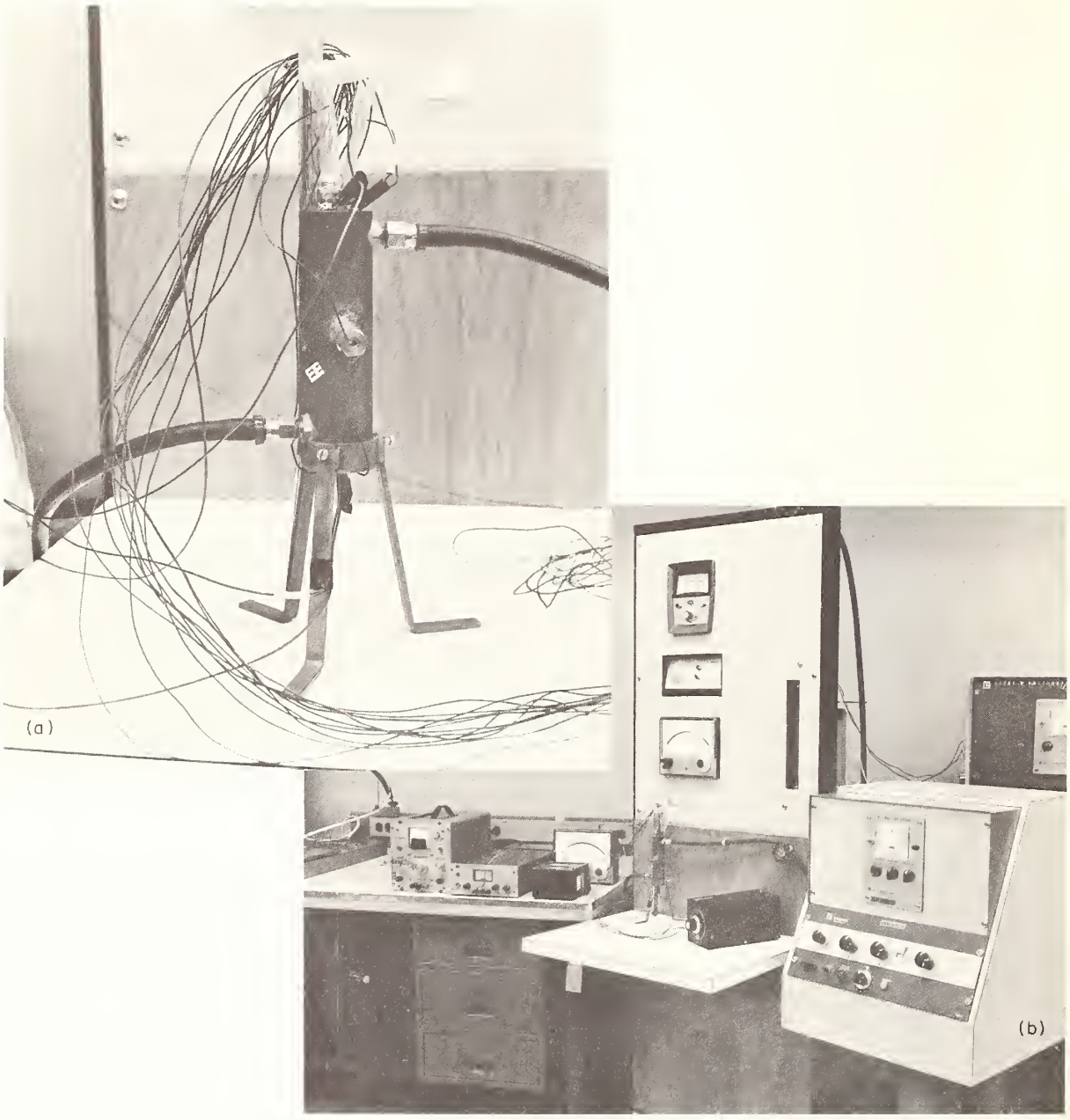

Figure 3. Photograph of the experimental equipment.
A) Test section. B) Experimental system.

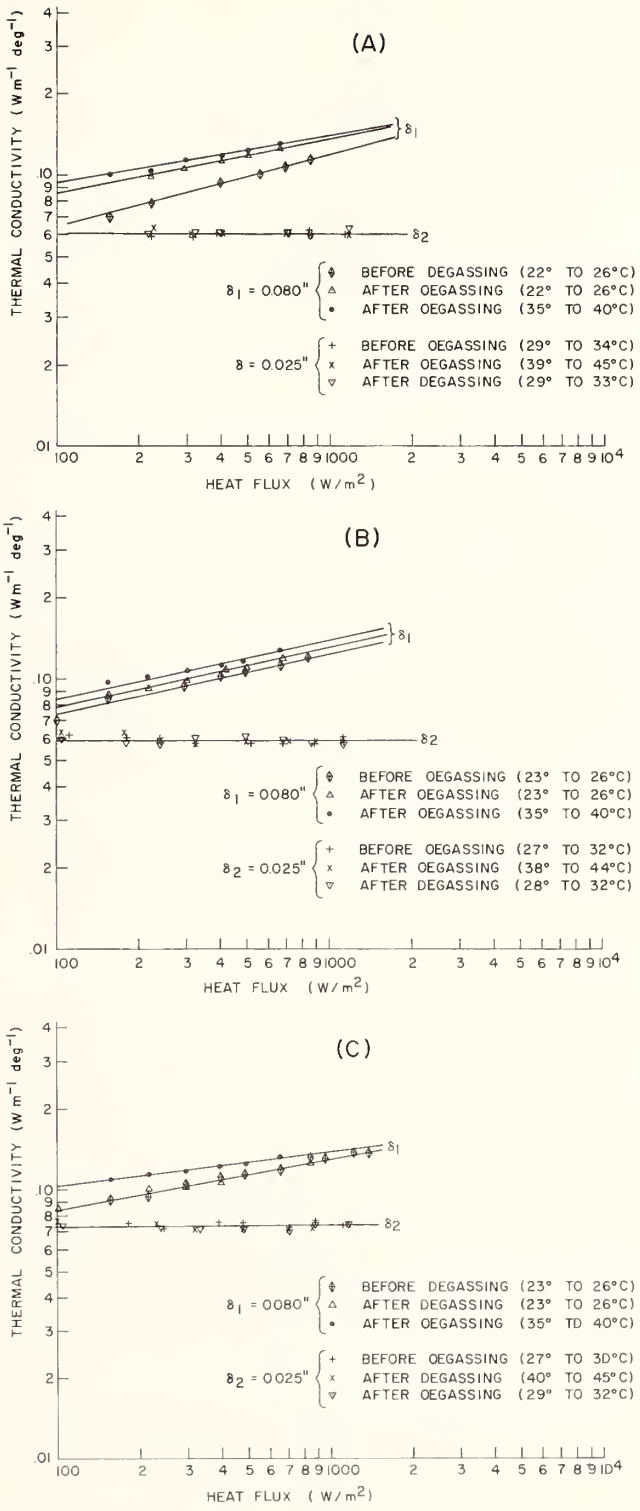

Figure 4. A) Thermal conductivity of FC-78 vs. heat flux.
B) Thermal conductivity of C51-12 vs. heat flux.
C) Thermal conductivity of Freon 113 vs. heat flux.

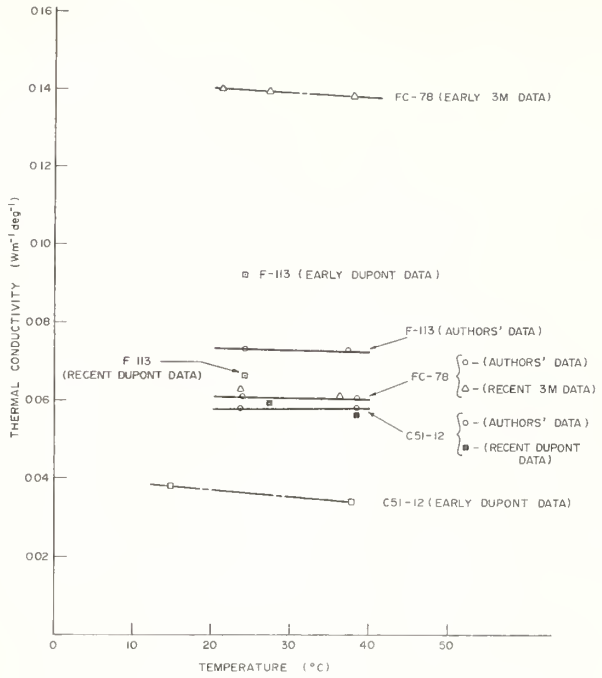

Figure 5. Conductivity vs. temperature of the three liquids compared with data of other investigators.

Figure 6. Air solubility of FC-78.

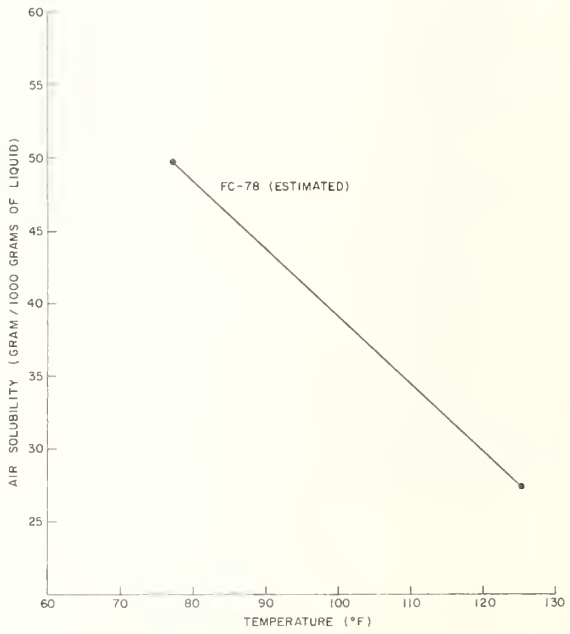

Thermal Conductivity of Two-Phase Systems

Alfred L. Baxley[1], Nicholas C. Nahas[2], and James R. Couper

Department of Chemical Engineering
University of Arkansas
Fayetteville, Arkansas

An experimental-theoretical study was conducted to establish a theoretically sound and numerically accurate technique for predicting two-phase system thermal conductivity. Experimental data were obtained with the aid of newly designed concentric-sphere type apparatus. Thermal conductivities were measured for representative volume fractions of several liquid-solid and liquid-liquid systems.

A digital simulation technique was proposed for the prediction of two-phase thermal conductivities. The model used as a basis a constant density function random placement of the discontinuous phase within a large cubical system. In the design of the model, consideration was given to three-dimensional heat conduction, potential field interaction, the thermal conductivities of both phases, and the volume fraction of the discontinuous phase.

The model was tested along with the models of eight other investigators on data of five investigations, including the authors' data. The authors' model predicted thermal conductivities with a mean error of twenty percent, an error variance of 1.35, and it was biased below the experimental values by an average of eleven percent.

Key Words: Conductivity, thermal conductivity, two-phase, liquid-solid systems, liquid-liquid systems, suspensions, emulsions.

1. Introduction

In the design of heat transfer equipment the evaluation of heat transfer coefficients for heterogeneous two-phase liquid-liquid or liquid-solid systems has been troublesome. In such a design it is necessary to know the thermal conductivity, specific heat, viscosity, density and coefficient of thermal expansion of the heterogeneous system.

During the past eighty years, numerous methods have been proposed for the calculation of thermal conductivity of two-phase systems. These methods [3,4,5,6,8,10,11,13,14,15,16,17,19,20,21,23,24,25,26,28] have most commonly assumed that the effective thermal conductivity of a real two-phase system is the same as for a system of simple geometry having the same volume fraction of the two phases. The effective conductivity of the simplified model is then found from the analytic solution of Fourier's equation with appropriate boundary conditions. In general, most of these techniques have been found to be approximate and unrelated to each other. The assumptions of thermal conductivity not varying with temperature, orderly arrays of well-defined geometric configurations in established distributions, and particle non-interaction are the most important of those which have been used in the development of theoretical models.

The experimental data are meager and the experimental techniques require considerable patience and care. Even under the most desirable conditions, the accuracy of existing correlations cannot be

---

[1]Presently employed at Celanese Chemical Company, Corpus Christi, Texas
[2]Presently employed at Humble Oil and Refining Company, Baytown, Texas

expected to be better than about ± 20%. As a result, the design engineer occasionally uses the thermal conductivity of a liquid phase which is usually the continuous medium and over designs the heat transfer, a costly compromise brought about by the lack of understanding of the existing phenomena and the lack of experimental data.

2. Theoretical Analysis

Thermal conductivity is defined for a homogeneous, isotropic medium by the Fourier equation:

$$\lambda = \frac{-Q/A}{\partial T/\partial X} \qquad (1)$$

where Q is the heat flow rate, A is the area of heat transfer, $\partial T/\partial X$ is the applied temperature gradient, and λ is the thermal conductivity.

According to the Fourier equation, the concept of thermal conductivity dictates that it represent a ratio of heat transfer through a constant area to an applied constant temperature potential. The definition further implies that the material is homogeneous and isotropic. One of the results of the above definition is that the thermal conductivity is a basic intensive property of the material.

As the basic concept of thermal conductivity is applied to a two-phase system, some of the above criteria are immediately violated. Two-phase systems are neither isotropic nor homogeneous, and the resultant thermal conductivity cannot be defined as an intensive property of the material. Although thermal conductivity for two-phase systems does not adhere to some of the original criteria, it is nevertheless a useful concept.

A photomicrograph of a liquid-solid suspension revealed that the suspension was a randomly oriented unsymmetric spatial array of irregularly shaped particles in a continuous medium. Further, some of the particles seemed to be in contact, and there appeared to be no basic repeated structure. Observations such as these have led historically to consideration of the following system variables: liquid and solid thermal conductivity, volume fraction of solids, particle orientation, particle distribution, particle shape, and particle "bridging".

The classical approach has been to combine all or part of the above variables into a predictive type "equation". Such equations have usually been developed considering the basic repeated unit of spatial configuration, for example, a cubic array of cubes. However, the photomicrograph revealed that such a basic unit is not easily defined and the authors believe that an entirely different approach would prove more satisfactory.

A detailed survey and critical review of the literature [7] clearly indicated the need for a numerical-statistical approach for predicting the conductivity of suspensions and emulsions. Deissler and Eian [4] applied a numerical technique to a two-dimensional array of cylinders. The temperature distribution at regular intervals in the model were determined using finite difference techniques and a relaxation procedure. They suggested that their model could be improved by considering a random distribution of solid cubes in a three-dimensional cubical system. Such an approach would be based on the premise that any liquid-solid system can be represented to any degree of approximation by a three-dimensional cubical system composed of small liquid and solid cubes. Effectively, any irregularly shaped particle can be "built" to any degree of approximation by arranging a sufficient number of small solid cubes according to a predetermined format. Further, particles could be placed into the large cubical system according to any specified statistical distribution. Following such a system synthesis would be the application of isothermal and insulation requirements to the proper planes, the application of a temperature potential, the determination of system temperature profiles, and finally, the calculation of heat flows and thermal conductivity.

2.2. Problem Documentation

The first step in the procedure is to establish system dimensions, boundary conditions, and initial system thermal conductivity. The physical system was "built" to the limit of the computing machine capacity and was represented as a three-dimensional matrix. (The computer available was an IBM 7040 with a 16K memory.) The dimensions are shown in figure 1 along with the directional convention.

The front and rear temperatures (TFRONT and TREAR) are isothermal, TFRONT being larger numerically than TREAR. In this particular study, TFRONT = 1.10°C (2°F) and TREAR = 0.55°C (1°F). The planes IK and JK are insulated so that all net heat flows in the K direction. Initially, all positions

in the system are occupied by the conductivity of the continuous phase, making the initial system thermal conductivity equal to that of the pure liquid.

Following this the number of solid cubes was determined and each was randomly placed. The system dimensions were selected to provide the largest conventional three-dimensional matrix which would fit into the computer memory. The dimensions of the matrix were 8 x 8 x 11 resulting in 704 system cubes. Therefore, the number of solid cubes required to build a given volume fraction (f) was 704 times f. Programming features were provided to neglect fractions of solid cubes.

Random coordinates (I, J, K) were produced by a 0-1.0 constant density random number generator. For each solid cube to be placed in the system, three random numbers between 0-1.0 are generated in the subroutine. By manipulation in the simulation program, these three random numbers are converted into I, J, K coordinates. If a random set of coordinates is duplicated, it is discarded and another set selected. When a solid cube is placed into the system, the solid thermal conductivity replaces the liquid thermal conductivity stored previously in that location in the computer program.

Step three is to determine the average working thermal conductivities and assign the initial temperature distribution. The equation for the series model, as given by Jakob [9], is used to compute the average working conductivities between adjacent cubes.

$$\lambda_e = \frac{\lambda_c \lambda_d}{0.5\lambda_c + 0.5\lambda_d} \tag{2}$$

where λ_e is the average thermal conductivity, λ_c is the thermal conductivity of the continuous phase, and λ_d is the thermal conductivity of the discontinuous phase. Next, an initial temperature distribution is assigned to the system cubes, assuming them as the pure liquids. In this particular problem solution, a 0.55°C (1.0°F) ΔT with a 0.055°C (0.1°F) ΔT per k-plane was used. However, any convenient temperature drop could be assumed.

Step four is to compute the actual temperature distribution. As the program is documented, there exists a unique solution for system temperatures. The condition which must be met by every cube temperature for a solution to exist is the Laplace equation

$$\frac{\partial^2 T}{\partial I^2} + \frac{\partial^2 T}{\partial J^2} + \frac{\partial^2 T}{\partial K^2} = 0 \tag{3}$$

Also, each temperature in the system must be bounded by TFRONT and TREAR. In application, Laplace's equation merely requires that the temperature at every cube be constant. This condition is satisfied only when there is no net heat accumulation in each cube. Therefore, a heat conduction balance can be written around every cube in the system, excluding the front and rear K planes. The basic system section around which each heat balance is written is shown in figure 2. Each cube represented by the numbered circles is assumed to be isothermal. Heat flow to the center cube, T7, is regarded as positive. The resulting heat balance is

$$\sum_{i=1}^{i=6} \frac{\lambda_{i7}(T_i - T_7)}{L} A = R_7 \tag{4}$$

where L is the distance between the cube being considered and cube 7. R_7 is the residual heat flow in the relaxation scheme. Application of this balance to all system cubes, except the 128 front and rear cubes, results in a system of 576 simultaneous, linear equations. Since all conductivities are known, each equation contains 7 unknowns, and no two equations contain the same 7 unknowns. A solution to such a large number of linear equations can be accomplished only by a numerical relaxation technique. Further, to program the technique of relaxation requires superimposing on it an iterative scheme. This scheme is described by Varga [27].

In applying Varga's scheme to the solution of the 576 heat balances, the following basic convergence equation results

$$T^{i+1} = T^i + \frac{W}{\sum_{i=1}^{i=6} \lambda_{i7}} \left[\sum_{i=1}^{i=6} \lambda_{i7} (T_i - T_7) \right] \tag{5}$$

Equation 5 states that a better estimate of any cube temperature results from adding a group of terms to an initially specified cube temperature. This group of terms is seen to be a constant divided by the sum of the surrounding working thermal conductivities and multiplied by the thermal residue, R. This is quite logical when it is realized that a negative R results from T_7 being too high. The appropriate action is thus to reduce T_7 by the aforementioned amount. If a positive R occurs, T_7 is too low and should be increased in the same manner. This basic convergence equation is applied to each cube temperature repeatedly until the sum of the absolute values of the residuals is less than or equal to 0.55°C (1°F).

The final step in the program is to determine heat flows and effective system thermal conductivity. The solution for temperature distribution results in the resolution of heat conduction from each cube into three orthogonal vectors. Since for the entire system, all net heat is being conducted in the K direction, this is the quantity of heat on which the system thermal conductivity should be based. Further, with the correct temperature distribution established, it follows that heat conducted through all K-planes is identical. The net K-plane heat flow is easily calculated by summing K-directed heat flows between every cube in adjacent K-planes. With this heat flow determined, effective system thermal conductivity is readily obtainable from a modified Fourier equation:

$$\lambda_e = \frac{11\ Q}{(8)(8)(TFRONT - TREAR)} \qquad (6)$$

Initially, no model was proposed specifically for liquid-liquid systems, for it was believed that the model developed might be satisfactory or could be extended to include liquid-liquid systems with minor modifications.

3. Experimental

3.1 Thermal Conductivity Measurements

A concentric-sphere type of thermal conductivity cell was designed and built by Baxley and Couper [1]. A schematic drawing of the cell is shown in figure 3. The annular space, which was 0.444×10^{-2} m.(0.175 inches) between the inner and outer spheres, contained the systems to be tested. Heat was generated electrically at the cell center by passing direct current through a specially constructed carbon resistance heater. The heat generated passed radially through the cell and the test systems. Thermal conductivity of the experimental systems was calculated from the equation for three-dimensional radial heat conduction in a sphere.

The rate of heat generation was obtained by measuring the current flow through and the voltage drop across the carbon resistance heater in the inner sphere. The meters used were certified as accurate to $\pm$ 0.25% of full-scale reading.

The temperature difference across the test systems, of the order of 0.55°C (1°F), was determined by a Leeds and Northrup K-3 Potentiometer, using copper-constantan thermocouples.

The entire thermal conductivity apparatus was immersed in a constant temperature oil bath during test runs so that the temperature distribution through the cell was uniform. Large excursions in bath temperatures were accomplished using an immersion heater or a refrigeration unit. The bath temperature was controlled in a classical fashion by a laboratory mercurial thermoregulator-relay-light bulb circuit. The resulting bath temperature variation was maintained at less than $\pm$ 0.0055 °C (0.01°F). A recording potentiometer was used to continuously monitor temperatures throughout the systems making possible the observation of transient temperatures and indicating when steady-state had been attained.

The average error expected in the measured thermal conductivity values was 4%. A detailed error analysis and a more thorough description of the test apparatus appears in a previous publication [1].

3.2 Experimental Systems

Each suspension used in this study was observed to experience no appreciable settling at 10°C (50°F) for a one hour period. One hour was sufficient time to make all thermal conductivity measurements for any suspension. The conductivities were experimentally determined for suspensions of polypropylene glycol (PPG), aluminum oxide-PPG and selenium-PPG. The suspensions were prepared by

slowly mixing predetermined weights of the finely divided powders into the liquid. After each suspension was charged to the cell, it was evacuated to 100 microns absolute pressure to remove any trapped air. The volume fraction of solids was varied from 0.1 to 0.5. Data were taken on all three systems between 1.7°C (35°F) and 10°C (50°F).

In the emulsion phase of the work, solutions of hydroxyethyl cellulose were dispersed in polypropylene glycol and in a commercial plasticizer known as Flexol. The volume fraction varied from 0.1 to 0.3 for the dispersed phase. The experimental temperature range was from 4.5°C (40°F) to 60.0°C (140°F).

4.0 Results

4.1 Liquid-Solid Systems

The thermal conductivities obtained from the model were compared with those predicted by eight other models. The eight other models were those developed by Russell [25], Lichtenecker [15], Jefferson [11], Maxwell [17], Rayleigh [23], Bruggeman [3], Meredith and Tobias [19,20,21], and the series model as shown by Jakob [9]. All nine models were tested on liquid-solid data of Lees [14], Jefferson [11], McAlister and Orr [18], Johnson [12], and the authors' data.

From Table 1 it can be seen that experimental values of suspension thermal conductivity are more closely related to liquid thermal conductivity and volume fraction than to thermal conductivity of the solid. For example, compare the results of the aluminum-water system ($\lambda_c = 0.657$, $\lambda_d = 204$, $f = 0.175$) with those for the aluminum-grease system ($\lambda_c = 0.284$, $\lambda_d = 204$, $f = 0.180$). If the same solid is used in almost the same volume fraction, an increase in liquid thermal conductivity by a factor of 2.3 increases the effective conductivity by a factor of 4.0. Further, for the aluminum-water system, a change in f from 0.055 to 0.210 changes the effective conductivity by a factor of 2.3. Now consider the zinc-grease system ($\lambda_c = 0.282$, $\lambda_d = 112$, $f = 0.22$) and the aluminum-grease system ($\lambda_c = 0.284$, $\lambda_d = 204$, $f = 0.24$) and note that an increase in the solid conductivity by a factor of 1.82 causes the effective conductivity to increase from 0.420 $Wm^{-1}deg^{-1}$ to 0.429 $Wm^{-1}deg^{-1}$. This increase is not significant.

TABLE 1

Comparison of Other Investigators' Data
With Authors' Model
Liquid-Solid Systems at 10°C

SYSTEM	λ_c $Wm^{-1}deg^{-1}$	λ_d $Wm^{-1}deg^{-1}$	f	λ_{exp} $Wm^{-1}deg^{-1}$	λ_{Model} $Wm^{-1}deg^{-1}$
Aluminum-Water	0.657	204	0.055	0.761	0.724
			0.115	0.969	0.802
			0.175	1.401	0.976
			0.210	1.730	1.042
Aluminum-Grease	0.284	204	0.070	0.320	0.328
			0.120	0.330	0.354
			0.180	0.349	0.429
			0.240	0.429	0.500
			0.320	0.586	0.972
Zinc-Grease	0.282	112	0.020	0.296	0.290
			0.080	0.322	0.323
			0.160	0.380	0.392
			0.220	0.420	0.498
			0.330	0.557	0.795
Copper-Water	0.657	382	0.055	0.744	0.721
			0.115	0.934	0.820
			0.175	1.141	0.932
			0.210	1.280	1.159
			0.245	1.436	1.273
			0.295	1.826	1.730

For data on other systems and other models see reference [2]

If one compares the thermal conductivities of the aluminum-water (λ_c = 0.657, λ_d = 204) and copper-water (λ_c = 0.657, λ_d = 382) systems, it is seen that the effective conductivity is higher for the system with the lower solid conductivity. This result dramatically emphasizes the influence of system variables other than λ_c, λ_d and f. These variables may include particle description, spatial distribution, and particle-particle contact.

Table 2 is presented to demonstrate the comparison between Baxley's model and experimental data obtained by use of the spherical cell.

TABLE 2

Comparison of Authors' Data with
Authors' Model
Liquid-Solid Data

SYSTEM	λ_d $Wm^{-1}deg^{-1}$	λ_c $Wm^{-1}deg^{-1}$	f	λ_{exp} $Wm^{-1}deg^{-1}$	λ_{Model} $Wm^{-1}deg^{-1}$
Aluminum Oxide-PPG 10°C	38.9	0.140	0.100	0.198	0.166
			0.200	0.429	0.219
			0.300	0.741	0.338
			0.400	1.192	0.635
			0.500	1.840	1.398
Aluminum-PPG 1.7°C	216	0.137	0.100	0.230	0.160
			0.200	0.465	0.228
			0.300	0.879	0.610
			0.400	1.580	1.717
Selenium-PPG 10°C	5.19	0.140	0.100	0.180	0.167
			0.200	0.219	0.208
			0.300	0.315	0.274
			0.400	0.422	0.374
			0.500	0.486	0.512

For data on other systems and other models see reference [2]

On the 51 systems tested, the authors' model gave predicted conductivities with a mean error of 20.5%, an error variance of 1.350 and is biased below the experimental value by an average of 10.95%. Since the predictability of a model improves as the mean error and error variances are reduced, the authors' model is slightly better than the best model of any previous investigation [10,11]. The mean errors of all other models except the series model and Russell's model compare reasonably well with the authors' model. These two models each had a mean error in excess of 32%. It was observed that both of these models have high errors even for systems of low severity, i.e., low values of λ_d/λ_c or low values of f.

It was quite unexpected that Jefferson's model, with limiting assumptions of linear heat flow and a cubical array of spherical particles would predict conductivity as well as the authors' model. It was also unexpected that Jefferson's model was better than Maxwell's model. Prior to this study, it was generally expressed in the literature that Maxwell's model was the best model for all types of systems.

In general, the authors' model was found to experience larger errors as severity parameters λ_d/λ_c and f were increased. In thirty of the 57 cases tested, the authors' model predicted thermal conductivity with a cumulative average error of less than 10%. Extensive information on the liquid-solid suspensions may be found in reference [2].

4.2 Liquid-Liquid Systems

None of the theoretical models predicted the thermal conductivity with consistent accuracy. Predicted results based on all models with the exception of the authors' gave approximately linear functions of temperature. As a typical example of such behavior, see figure 4. For more complete results on the liquid-liquid systems, the reader is directed to reference [22].

The authors' model was tested using the liquid-liquid data obtained. It yielded data with the mean error approximately the same as for liquid-solid systems. However, Jefferson's model [11] gave effective thermal conductivity values at low volume fractions less than 0.3, with an error less than 11.4%. This result might have been expected since Jefferson's model involved the distribution of spherical particles in a cubical section. Research is presently underway to improve the authors' model.

5. Conclusions

A stable, explicit, numerical solution has been developed for the thermal conductivity of three-dimensional, nonhomogeneous media. The model represents a fresh approach to the problem in that it simulates heterogeneous system thermal conductivity. The model is a general numerical solution to potential field problems, and is particularly attractive for heterogeneous systems. The model is therefore not restricted to heat conduction, but can be readily extended without hesitation to any heterogeneous system property for which the Laplace equation is applicable.

The authors' model was found to predict thermal conductivity for all cases with a mean error, error variance, and error bias of 20.5%, 1.35%, and 10.95%, respectively. The model was found to predict thermal conductivity slightly better than the best model of previous development [10,11].

The variance of the predicted thermal conductivities for a suspension of a given volume fraction solids, due to a variety of solid cube placements, was found to be generally quite small. It was less than 0.010 for 69% of the cases tested. Variances larger than 0.010 were found for systems with large values of λ_d/λ_c and f.

6. Acknowledgement

The authors wish to acknowledge the financial support of this project by the National Science Foundation through grants NSF GP-1152 and GK-1151.

7. References

[1] Baxley, A. L. and J. R. Couper, Thermal Conductivity of Two-Phase Systems: Design and Construction of a Thermoconductimetric Apparatus, University of Arkansas Engineering Experiment Station Research Report No. 6, Fayetteville, Arkansas January (1965).

[2] Baxley, A. L. and J. R. Couper, Thermal Conductivity of Two-Phase Systems: Thermal Conductivity of Suspensions, University of Arkansas Engineering Experiment Station Research Report No. 8, Fayetteville, Arkansas, November (1966).

[3] Bruggeman, D. A. G., Dielectric Constant and Conductivity of Mixtures of Isotropic Materials, Ann. Physik, 24, 636-79 (1935).

[4] Deissler, R. G. and C. S. Eian, Investigation of Effective Thermal Conductivity of Powders, NACA RM E52C05 (1952).

[5] Fricke, H., The Electrical Conductivity of Suspensions of Homogeneous Spheroids, Phys. Rev., 24, 575-87 (1924)

[6] Goldsmith, A., et al, Handbook of Thermophysical Properties of Solid Materials, The MacMillan Co., New York (1961).

[7] Griffis, C. L., N. C. Nahas, and J. R. Couper, Thermal Conductivity of Two-Phase Systems: A Survey and Critical Evaluation of the Literature, University of Arkansas Engineering Experiment Station Research Report No. 5, Fayetteville, Arkansas, March (1964).

[8] Hamilton, R. L. and O. K. Crosser, Thermal Conductivity of Heterogeneous Two Component Systems, Ind. Eng. Chem. Fund., 1, 187-90 (1962).

[9] Jakob, M., Heat Transfer, Vol. I, p. 88, John Wiley & Sons, Inc., New York (1950).

[10] Jefferson, T. B. et al, Thermal Conductivity of Graphite-Silicone Oil and Graphite-Water Suspensions, Ind. Eng. Chem., 50, 1589-1592 (1958).

[11] Jefferson, T. B., Thermal Conductivity Determinations for Suspensions of Graphite in Water and Oil, Ph.D. Dissertation, Purdue University (1955).

[12] Johnson, F. A., U. K. Atomic Energy Estab. Lab., Reprint ASEE No. R/R 2578.

[13] Kannuluik, W. G. and L. H. Martin, Conduction of Heat in Powders, Proc. Roy. Soc. (London), A141, 58 (1933).

[14] Lees, C. H., On the Thermal Conductivity of Single and Mixed Solids and Liquids and Their Variation with Temperature, Proc. Roy. Soc.(London), A191, 339-440 (1898).

[15] Lichtenecker, K., The Electrical Conductivity of Periodic and Random Aggregates, Phys. Z., 10 1005-1008 (1909).

[16] Loeb, A. L., The Theory of Thermal Conductivity of Porous Materials, J. Am. Ceram. Soc. 37, 96-9 (1954).

[17] Maxwell, J. C., A Treatise on Electricity and Magnetism, Vol. I, 435-49, Oxford University Press, London (1946).

[18] McAlister, A. and C. Orr, Thermal Conductivity of Aluminum and Zinc Powder Suspensions, J. Chem. and Eng. Data, 9 (1964).

[19] Meredith, R. E. Studies on the Conductivities of Dispersions, Ph.D. Dissertation, University of California, Berkeley (1960).

[20] Meredith, R. E. and C. W. Tobias, Conductivities in Emulsions, J. Electrochem. Soc., 108, 286-90 (1961).

[21] Meredith, R. E. and C. W. Tobias, Resistance to Potential Flow Through a Cubic Array of Spheres, J. Appl. Phys., 31, 1270-1273 (1960).

[22] Nahas, N. C. and J. R. Couper, Thermal Conductivity of Two-Phase Systems: Thermal Conductivity of Emulsions, University of Arkansas Engineering Experiment Station Research Report No. 7, Fayetteville, Arkansas, March (1966).

[23] Rayleigh, R. J. S., On the Influence of Obstacles Arranged in Rectangular Order Upon the Properties of a Medium, Phil. Mag., 34, 481-507 (1892).

[24] Runge, I., On the Electrical Conductivity of Metallic Aggregates, Tech. Physik, 6, 61-8 (1925).

[25] Russell, H. W., Principles of Heat Flow in Porous Insulators, J. Am. Ceram. Soc., 18, 1-5 (1938).

[26] Tsao, G. T., Thermal Conductivity of Two-Phase Materials, Ind. Eng. Chem. 53, 395-7 (1961).

[27] Varga, R. S., Matrix Iterative Analysis, Prentice Hall, Inc., Englewood Cliffs, N. J. (1962).

[28] Von Frey, G. S., The Electrical Conductivity of Binary Aggregates, Zeitschrift fur Electrochemie, 38, 260-74 (1932).

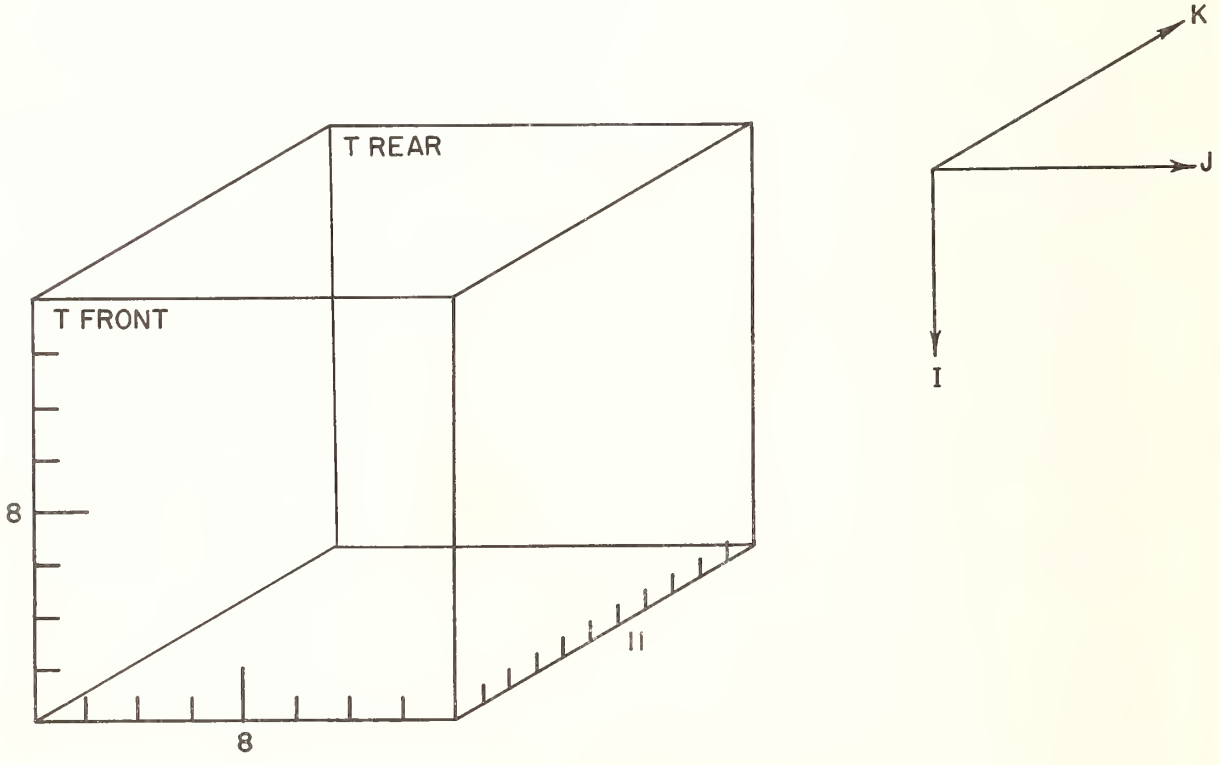

Figure 1 Digital Simulation System Dimensions

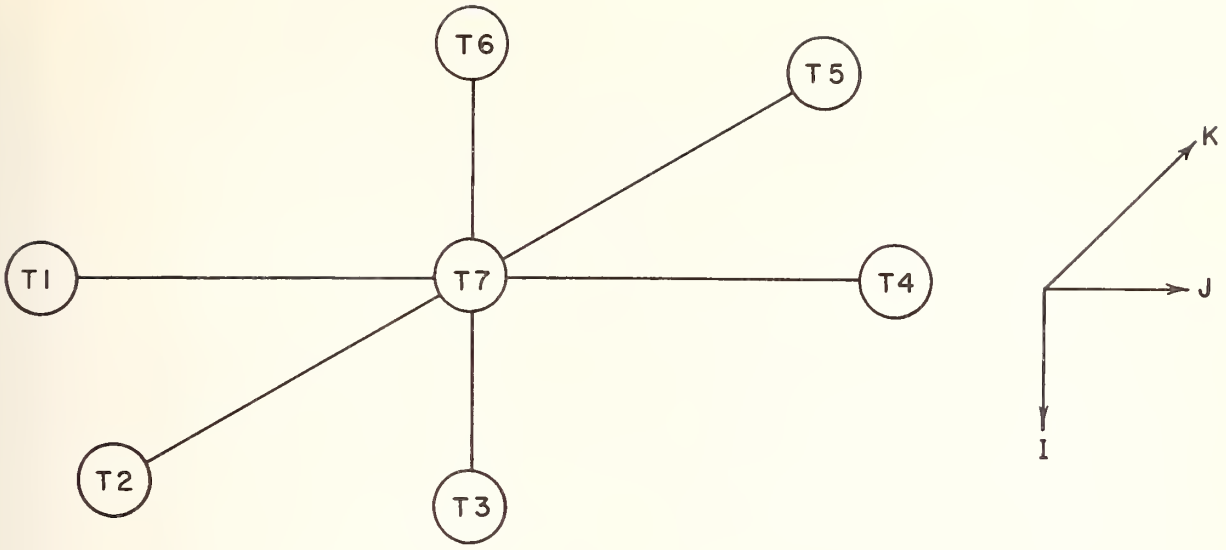

Figure 2 Heat Balance Basic System Section

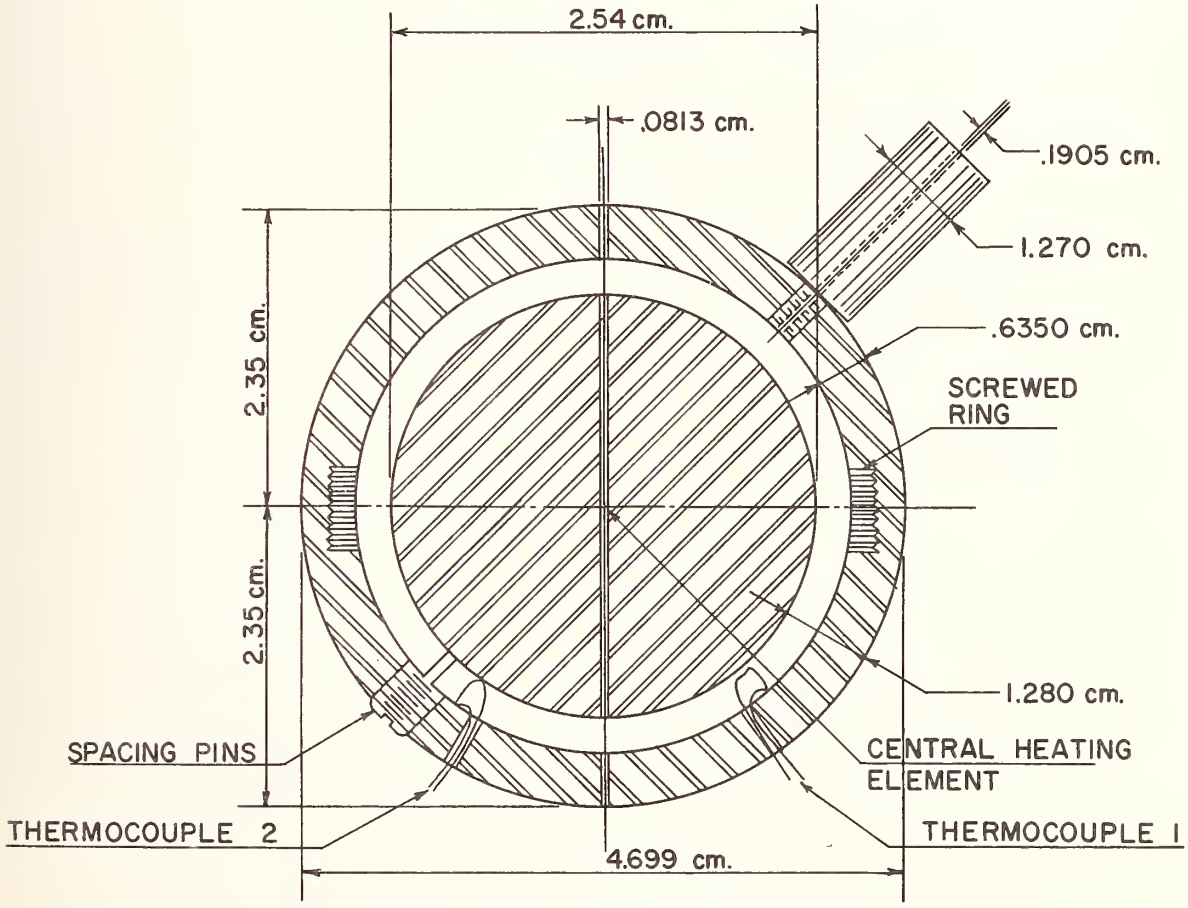

Figure 3 Concentric Sphere Thermal Conductivity Cell II

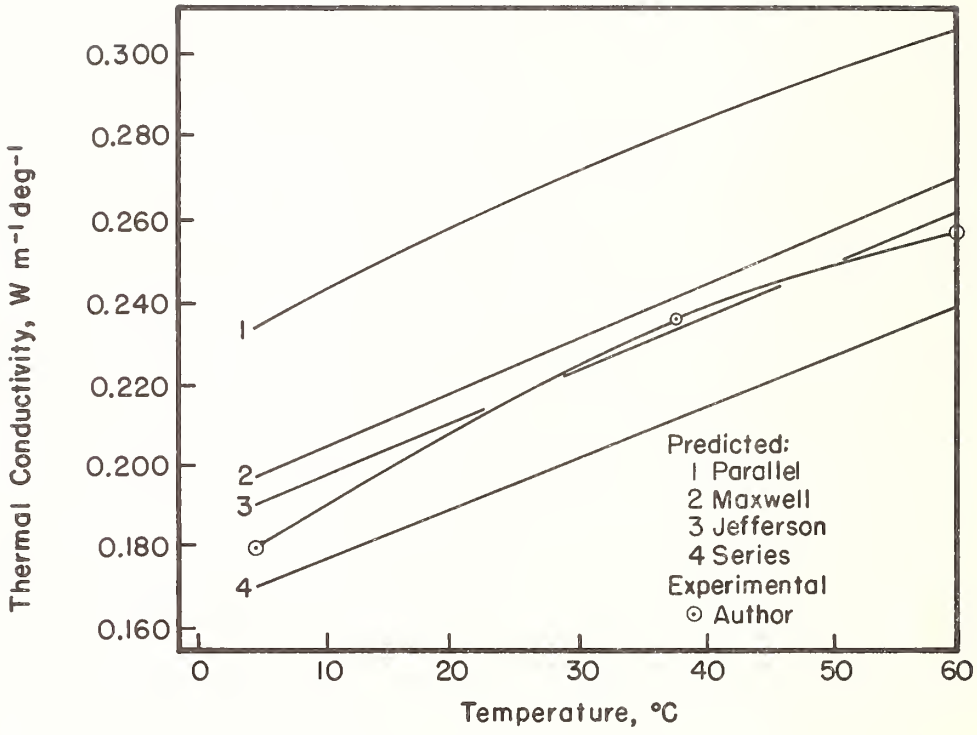

Figure 4 Experimental and Predicted Results for Cellosize in EPO, f = 0.3

Measurements of the Thermal Conductivity of Granular Carbon and The Thermal Contact Resistance at the Container Walls

C. A. Fritsch and P. E. Prettyman[1]

Bell Telephone Laboratories, Incorporated
Whippany, New Jersey

Experimental measurements of the thermal resistance of granular carbon in a brass container under room conditions are presented for both loose and compacted states. The thermal resistance is described as consisting of two parts: the resistance due to the effective thermal conductivity of the "continuum", and a contact resistance due to the interface between a layer of granules and the container walls. Results indicate that the thermal resistance depends on the packing and, to some extent, on the wall geometry relative to the grain size. The contact resistance can be a factor of 2 greater than the continuum resistance across a path corresponding to one grain diameter.

Key Words: Carbon, conductivity, contact conductance coefficient, granular carbon, heat conductivity, particulate medium, thermal conductivity, thermal contact resistance.

1. Introduction

Heat transfer through particulate media, of interest in innumerable applications, is generally characterized by an effective thermal conductivity. The multiphase system is treated as a continuum. However, in those situations where the particles occupy a significant percentage of the transfer path, one might suppose that an additional thermal resistance is experienced at the container walls. A significant reduction in contact area may occur there since the particle arrangement is influenced by the wall. Hence, the region close to the wall may more properly be described in terms of a contact resistance coefficient.

A study of the thermal resistances in particulate systems having large grain sizes should be of interest in such fields as packed-bed heat exchangers, regenerative heat exchangers, and ordnance applications. Another is the standard Bell System telephone transmitter.

Studies at Bell Telephone Laboratories have indicated that the thermal response of the granular carbon microphone to the imposition of a bias current has a direct bearing on the efficiency of the microphone as a transmitter. For an understanding of this problem, detailed knowledge of the thermal resistance of the granular carbon and its container is necessary. To the authors' knowledge, the measurement of a contact type resistance between a wall and a particulate medium had heretofore not been performed. Thus the experimental study presented here was undertaken to measure both the continuum resistance and the wall contact resistance of granular carbon. Both the loose and compacted states for the system were considered at atmospheric pressure and temperatures near room conditions.

---

[1] Member of Technical Staff and Technical Aide, respectively.

2. Apparatus

Radial heat flow through a series of concentric cylinders was first taken as the logical choice for the experimental configuration. (Heat losses were more readily controlled in this arrangement than in an apparatus using axial conduction.) The total thermal resistance for each cylindrical container in terms of the thermal conductivity λ, and the contact conductance coefficient h_c, can be expressed as follows:

$$R = \frac{\ln(D_o/D_i)}{2\pi\lambda L} + \frac{1}{h_c A_o} + \frac{1}{h_c A_i} = \frac{\Delta T}{Q} \tag{1}$$

Where D denotes the cylinder diameter, A the area and L the length. The subscripts o and i denote the outer and inner walls, respectively, of each cavity. To determine the resistance, R, both the radial heat flow, Q, and the temperature difference, ΔT, between adjacent cylinders had to be measured. Hence, a monitored wirewound resistance heater was inserted in the innermost cylinder. Thermocouples in a radial line, positioned on the cylinders, were used to determine the temperature drop.

Measurements for two different cavities were used to obtain two independent equations for the simultaneous solution of λ and h_c. Unfortunately, the process of solving these two equations produced a serious loss in accuracy so that modification of the apparatus was required.

A vertical cross section of the final apparatus is shown in figure 1. The carbon granules were contained in the annular space between the two brass cylinders, and the styrofoam insulator blocks at each end. Two rows of thermocouples were immersed in the granular carbon. The thermal resistance corresponding to the temperature differences of the immersed thermocouples consisted of the continuum resistance only, i.e., from eq (1),

$$R = \frac{\ln(D_o/D_i)}{2\pi\lambda L} \tag{2}$$

Once λ was determined from this measurement the thermal resistance between an immersed thermocouple and one on a wall was used to evaluate h_c. In this case eq (1) became

$$R = \frac{\ln(D_o/D_i)}{2\pi\lambda L} + \frac{1}{h_c A_o} \tag{3}$$

Placed within the inner cylinder was a heater, nichrome wire wrapped on a phenol-fiber tube. Centrally located voltage taps were attached at a spacing of 5.08 cm. A separate guard heater was provided at each end to control the heat losses.

The 2.54 cm outside-diameter brass inner cylinder consisted of a 5.08 cm centrally located test section. A 2.54 cm length of tubing of the same diameter was glued with an epoxy cement to each end. The inner cylinder was made in three electrically isolated pieces to allow differential thermocouple readings. The wall thickness was 0.159 cm (1/16 inch).

The 7.62 cm outside-diameter brass outer cylinder had a wall thickness of 0.159 cm and was 10.80 cm long. The outside surface was painted flat black to maximize the radiative heat transfer from the cylinder.

Chromel-alumel thermocouples were positioned in two vertical planes 90 degrees apart. Most of the thermocouples were in the plane illustrated in figure 1. The principal thermocouple, designated REF, was attached to the center of the test section. A similar row of two thermocouples was placed in the annulus at 90 degrees to the vertical plane containing REF. The actual positions of the resistance measuring thermocouples are listed in Table 1. These positions were measured to within 0.025 cm accuracy.

Table 1. Thermocouple locations.

Thermocouple Designation	Location	Radial Position (cm)	Azimuthal Position w.r.t. REF
REF	Test section	1.27	--
4	Carbon medium	1.70	90°
5	Carbon medium	2.77	90°
6	Carbon medium	1.75	0°
7	Carbon medium	2.81	0°
9	Outer cylinder	3.66	0°

Thermocouples at the extremities of the inner cylinder were used to adjust the guard heaters. An additional couple was placed in the 90 degree plane for tests for variation around the test section. Couples were added at the ends of the outer cylinder to indicate the extent of axial variations.

The REF thermocouple was connected through a Leeds and Northrup ten-position thermocouple switch to an ice junction and differentially to each thermocouple in the system. A Leeds and Northrup K-3 potentiometer and a type-E galvanometer were used to read the EMFs.

The input to the portion of the heater under the test section was measured by two Simpson voltmeters. The current was calculated by measuring the voltage drop across a 10 ohm resistor in series with the heater. The voltage was measured by using the voltage taps on the test section heater.

3. Characterization of Medium

Western Electric Company standard telephone transmitter carbon, sieve size -55 to +70, was used in these studies. Figure 2 is a photomicrograph of the granules with a 25 μm (one-mil) wire as a reference scale. The photograph shows the irregular shapes of the granules. The size and eccentricity of a statistical sampling of the carbon is given in figure 3[2].

First the density of the granular carbon in both loose and totally compacted states was determined in a 50 cm^3 graduated cylinder and with a calibrated balance. The loose state was accomplished by putting carbon in the graduated cylinder and gently tumbling the graduate end-over-end a number of times. The volume was observed and the carbon weighed; a density of 900 kg/m^3 was calculated. The totally compacted state was obtained by tapping the graduate until no further change in volume was observed.[3] The carbon was then weighed and a density of 1000 kg/m^3 was computed.

---

[2] Taken with permission from unpublished work of M. C. Huffstutler, Jr. and Miss B. T. Kerns at Bell Telephone Laboratories. The eccentricity is the ratio of the longest axis to the dimension perpendicular to it, on the same surface.

[3] After the rather mild tapping, no further effect was produced by striking the graduate vigorously.

Then, measurements were made with the carbon granules in various states of compaction from loose to totally compacted. The loose state was attained by carefully filling the annular space between the test section and the outer cylinder, leaving a small space at the top. The apparatus was then gently tumbled to loosen the particles. The partially compacted state was accomplished by pouring the carbon granules freely into the annular space until it was filled - pouring tends to compact the granules. The totally compacted state was achieved by filling the annular space while tapping the outer cylinder, until no more carbon could be added.

The density of the partially and totally compacted states in the test apparatus was determined by computing the volume and weighing the carbon granules. For the totally compacted state the computation gave a density of 1000 kg/m^3 in agreement with the previous determination. The density of the loose state was not determined from the in situ measurements since the size of the small space left to insure a loose state could not be accurately measured.

4. Experimental Results

The experimental results for the states tested are presented in Table 2. The actual temperatures at each thermocouple location can be computed by subtracting the appropriate temperature differences from the temperature of test section, T_{REF}. The different heat inputs listed were chosen so that sufficiently large temperature differences could be measured, yet the temperature of the continuum never exceeded 41 deg C. The temperatures read differentially with T_{REF} were accurate to within 0.05 deg. Consequently, the other temperature differences could be as much as 0.1 deg in error. The power input to the heater was accurate to within 2 percent. All thermocouples and voltmeters were calibrated against laboratory standards.

Table 2. Experimental measurements and results.

	Run						
	1	2	3	4	5	6	7
Density (kg/m^3)	900	900	900	960	960	1000	1000
Heat input, Q (watts)	0.797	0.797	0.440	0.838	0.445	0.445	0.442
T_{REF} (deg C)	38.39	38.39	33.17	40.28	34.72	32.78	33.00
$T_{REF} - T_4$ (deg)	2.81	2.88	1.64	2.62	1.68	1.58	1.51
$T_4 - T_5$ (deg)	5.21	5.22	2.80	4.79	3.06	2.73	2.67
$T_{REF} - T_6$ (deg)	2.73	2.74	1.62	2.71	1.69	1.50	1.56
$T_6 - T_7$ (deg)	4.83	4.94	2.81	4.88	2.94	2.67	2.53
$T_7 - T_9$ (deg)	2.89	2.90	1.67	2.88	1.86	1.55	1.54
$\lambda_{(4-5)}$ ($W\ m^{-1}\ deg^{-1}$)	0.232	0.232	0.241	0.266	0.222	0.247	0.251
$\lambda_{(6-7)}$ ($W\ m^{-1}\ deg^{-1}$)	0.246	0.239	0.234	0.256	0.225	0.247	0.260
$h_{c\ (7-9)}$ ($W\ m^{-2}\ deg^{-1}$)	370	430	230	260	160	390	270

Equations (2) and (3) were used to compute the values of λ and h_c. The λ values were determined using two adjacent thermocouple readings in the continuum, e.g., T_4 and T_5, or T_6 and T_7. (In this determination, the contact resistance terms were omitted since the 30 gauge thermocouple wires - 250 μm in diameter - were about the same size as the carbon granules and hence did not act like a wall.) The average value of λ from each run was used to determine h_c with the temperature difference of T_7 minus T_9 in eq (3).

5. Experimental Error Analysis

The possible sources of experimental errors in radial-flow thermal conductivity apparatus have been carefully described by Flynn [1][4]. Of these sources, some can be shown to be negligible while some contribute only to the absolute uncertainty.

Considering first the question of whether or not steady-state had been reached when the measurements were taken, most of the runs were made at least 5 hours after the heaters were turned on. However, in some cases the apparatus was left operating overnight resulting in essentially no change in the measured parameters.

The length of the test section as determined by the location of the voltage taps was measured to within 2%. This factor affects the absolute uncertainty only since it was constant for all runs. The relative radial location of the inner and outer cylinders was measured to the same accuracy. Hence, an eccentricity of 0.03 was possible. According to Flynn [1] this eccentricity contributes error of less than 0.1%.

In a given run the total power generated was measured to within 2%. The location of the thermocouples was determined so that the logarithm of the ratios of the appropriate diameters varied by less than 3%. The fact that the thermocouples were embedded in the brass cylinders and were not exactly on the surface of the walls could account for less than 0.2% error [1] for the heat flows used here. As mentioned earlier, the temperature differences were accurate to within 0.1 deg which corresponds at most to a 5% error.

Lastly, since the outer cylinder was not guard heated but rather it stood vertically in air one might rightfully ask what were the effects of axial heat flow. The inverse of our situation was solved by Flynn [1] but his results are also applicable here. Using the temperature differences measured by the thermocouples placed on the ends of the outer cylinder the maximum correction for the resistance across the cavity due to axial heat flow was always less than 1%. Since all the λ values were determined from the thermocouples immersed in the granular carbon, the actual error is probably somewhat less than 1%.

Combining the absolute values of all these errors the maximum amount that the λ values could be in absolute error is 13%. The relative error within a given run is 8%. Since the contact resistance was on the order of one tenth of the total thermal resistance measured, the error in measuring h_c would be amplified by a factor of 10.

6. Discussion of Results and Conclusions

The averages of the measured thermal conductivity of granular carbon for the loose state (900 kg/m^3), the partially compacted state (960 kg/m^3) and the totally compacted state (1000 kg/m^3) were 0.237, 0.244 and 0.251 W m^{-1} deg^{-1}, respectively. These values indicate an increase in λ almost in proportion to the increase in density (compaction). Due to the scatter in h_c, no trend in that coefficient could be ascertained. However, the average value is about 300 W m^{-2} deg^{-1}. This value of h_c corresponds to a thermal resistance at the wall, a factor of 2 greater than the continuum resistance across a path corresponding to one grain diameter.

---

[4] Figures in brackets indicate the literature references at the end of this paper.

It is of interest to compare the measurements reported here to some of the analytical models for thermal conductivity of particulate media. Apparently, all of the analytical description had assumed at most point contact between the solid particles immersed in a fluid. The exact solution, such as that by Deissler and Boegli [2], have considered idealized grain shapes and have computed the attendant temperature profiles. The approximate solutions, such as that of Russell [3], have considered the heat to flow in parallel through the discontinuous (solid) and continuous (fluid) phases and then in series through the fluid phase. The heat flow through a continuous aggregate of solid is neglected. Godbee and Ziegler [4] have modified Russell's equation to account for a statistical distribution of particle sizes. They have also taken into account free molecular effects in gases for sufficiently small grain sizes and low pressure.

For the conditions of interest here the free molecular effects can be neglected. A calculation of the Godbee and Ziegler's statistical parameter, α, for the distribution of figure 3 yields, $\alpha = 0.99$, and for values of α near unity the Godbee and Ziegler model reduces to Russell's equation. In addition, for large ratios of solid conductivity to fluid conductivity (here, it is nearly 1600) Russell's equation becomes independent of the solid conductivity yielding,

$$\lambda = \lambda_{air} \left[\frac{1}{1-V_d^{1/3}} \right] \tag{4}$$

where V_d is the volume fraction of solid. Taking the solid density of the carbon grains to be 2240 kg/m^3 one obtains $V_d = 0.4$ for the loose state. Hence, Russell's equation predicts $\lambda = 0.10$ W m^{-1} deg^{-1}. As in other studies, Russell's equation underpredicts λ by a factor of 2.4 for the loose state. It is quite possible that this difference can be attributed to the existence of solid to solid conduction that was neglected in the analytical models.

An interesting aspect of this study comes out of the thermal resistance values between the test section and thermocouples 4 and 6. If one applies the values of $h_{c(7-9)}$ tabulated in Table 2 to eq (3) with A_o replaced by A_i and calculates a value of λ for this region, a value of about 0.34 W m^{-1} deg^{-1} is obtained. (Conversely, if one takes the values of $\lambda_{(4-5)}$ or $\lambda_{(6-7)}$ and tries to compute $h_{c(4)}$ or $h_{c(6)}$ he will find that h_c will be negative.) Apparently the thermal resistance in this apparatus is a function of radial position. Note that the λ value of 0.34 represents a 40% increase over the average value for the loose state. Hence, such a marked change cannot be attributed to experimental error. In addition, this "inconsistency" was present in all of measurements made in this work. Deissler and Boegli [2] made experimental measurements of the temperature as a function of radius and their reported values indicate that λ is independent of radius. However, their ratio of grain size to wall radius was a factor of 20 smaller than the condition considered here.

Since the design of this experiment was not sufficient to assess this effect the answer must come from future studies. A study could center around two precisely instrumented cylindrical apparatus arrangements, one consisting of a row of several thermocouples immersed in the continuum at small and large radii, the other a series of concentric cylinders at the same radial positions as the thermocouples in the first apparatus. The measurements from the first apparatus for the effective thermal conductivity at each radial section could then be used in the second apparatus to determine h_c, as a function of radial position. Because Western Electric standard carbon is precision manufactured and of a narrow distribution, this medium is a good candidate for such future studies.

In summary, the thermal conductivity of granular carbon has been measured and the presence of a thermal contact resistance at a wall has been demonstrated. The wall contact resistance is important only when a single grain occupies a significant portion of the heat transfer path between container walls. A dependence of these coefficients on radius of curvature of the multiphase system seems to exist.

8. References

[1] Flynn, D. R., A radial-flow apparatus for determining the thermal conductivity of loose-fill insulations to high temperatures, J. Research NBS 67C (Eng. and Instr.) 129 (1963).

[2] Deissler, R. G. and Boegli, J. S., An investigation of effective thermal conductivities of powders in various gases, Trans. Am. Soc. Mech. Eng. 80 1417 (1958).

[3] Russell, H. W., Principles of heat flow in porous insulators, J. Am. Ceram. Soc. 18 1 (1935).

[4] Godbee, H. W. and Ziegler, W. T., Thermal conductivities of MgO, Al_2O_3, and ZrO_2 powders to 850° C. II. Theoretical, J. Appl. Phys. 37 56 (1966).

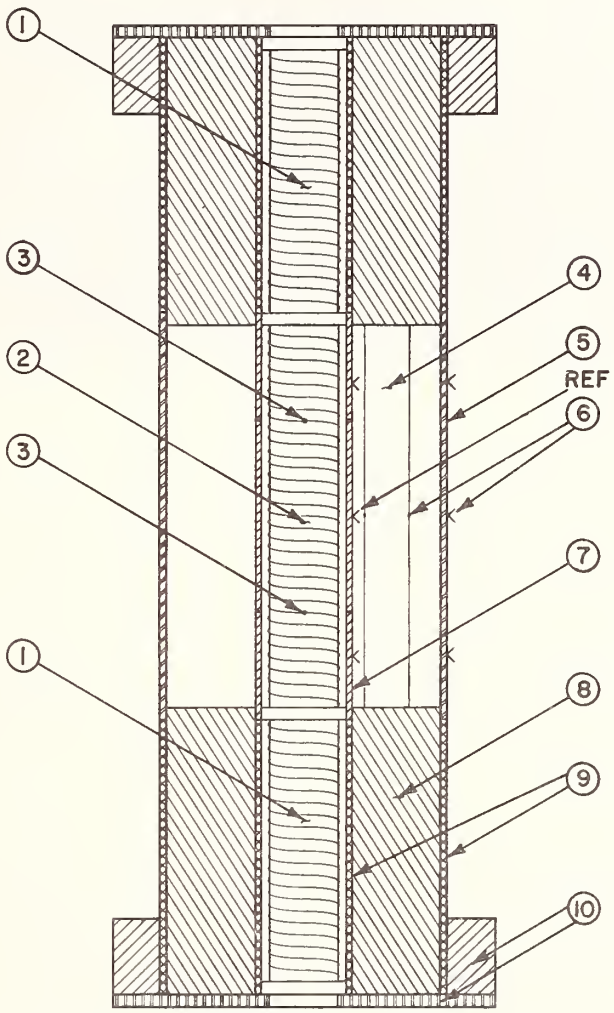

Figure 1. Vertical Cross Section of Experimental Apparatus.

1. Guard heaters. 2. Test section heater. 3. Voltage taps. 4. Annular cavity for granular carbon. 5. Outer brass cylinder. 6. Thermocouples. 7. Inner brass cylinder. 8. Styrofoam insulator. 9. Phenolfiber alignment tubes. 10. Support blocks.

Figure 2. Photomicrograph of Typical Carbon Granules

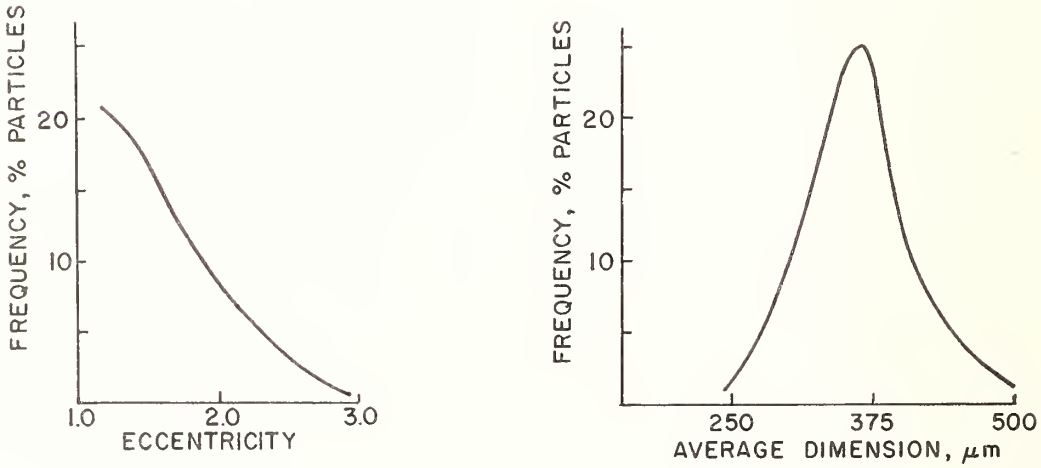

Figure 3. Size and Eccentricity Distribution of Granular Carbon.

The Thermal Conductivity of Thoria Powder From 400° to 1200°C[1] In Various Gases At Atmospheric Pressure

A. D. Feith[2]

Nuclear Materials and Propulsion Operation
General Electric Company
Cincinnati, Ohio 45215

The thermal conductivity of powdered thoria at 75% of theoretical density was measured in a radial heat flow apparatus. Several different types of gas (He, N_2, He + 52% N_2, Ar) were introduced into the powder matrix to study the effect of the conductivity of the gas phase on the conductivity of the compact. The results of this work indicate that the thermal conductivity of the system varies only slightly, if at all, from one gas to another, but considerably lower conductivity values are obtained when the pore phase is evacuated. With a gas present, values of about 1.25 Wm^{-1} deg^{-1} at 400 °C, 1.05 Wm^{-1} deg^{-1} at 1000 °C, and 1.5 Wm^{-1} deg^{-1} at 1200 °C were obtained whereas in vacuum the values were about 0.5 Wm^{-1} deg^{-1} in the 400 ° to 750 °C temperature range. The estimated precision of the data including the effect of the different gases was about ±10%.

Key Words: Conductivity, gaseous atmospheres, radial heat flow, powder, thoria.

1. Introduction

The purpose of this work was to determine the thermal conductivity of thoria powder which was vibra-packed to 75% of theoretical density and to determine the effect of the type of gas present in the voids on the thermal conductivity of the compact. Although the results of this study are to be applied to production engineering problems, they may also contribute to the understanding of heat flow in powder-gas systems at high volume fraction solid. A detailed study by Godbee (1)[3] on MgO, ZrO_2, and Al_2O_3 powders of considerably lower volume fraction solid than used in this study demonstrates that the conductivity of a powder-gas system can be predicted from the conductivity of the solid and the conductivity of the gas. The success of such a prediction is based on the knowledge of several other parameters including particle size, shape, and distribution; contact area and inter-particle spacing. It may be concluded from a discussion by Kennard (2) that in powder-gas systems where the inter-particle spacing is very small the conductivity of the system is not dependent upon the thermal conductivity of the bulk gas but rather on the free molecular conduction. The results of this current study which are described below seem to confirm, qualitatively at least, this latter concept.

2. Equipment

The measurements described in this report were performed in a radial heat flow apparatus which has been previously described in detail (3). The equipment was developed specifically for measuring the thermal conductivity of solid materials in inert or reducing atmospheres. Previous measurements on relatively high density compacts of ZrO_2, UO_2, BeO, and Mo (4,5), have been shown to be reproducible and in good agreement with the work of other laboratories. The estimated precision of the apparatus is about ±6% above 1000 °C. However, the precision is more nearly ±10% below 1000 °C. Due to the nature of the specimen used in this study, some modifications in the usual experimental setup and procedures were necessary; these are described below.

---

[1]This work was performed under U.S.A.E.C. Contract No. AT(07-2)-1.
[2]Principal Engineer
[3]Figures in parentheses indicate the literature references at the end of this paper.

3. Specimen and Container

Property measurements on powdered materials pose many problems which are not associated with solid materials. The major problem is to maintain the geometric requirements of the measuring system. For the radial heat flow system, it is necessary to contain the powder in a cylindrical can with a center hole of a specific size to fit the apparatus. The specimen container used in this study is shown in detail in figure 1. Thermocouple wells were placed at three different radial locations in a plane parallel to the centerline of the can to avoid having them in the same radial plane thereby minimizing the effect of the presence of the tubes on the geometry of the isotherms. One additional tube extended from the top of the can to facilitate the required changes in the atmosphere. Careful measurements of the radial positions of the ends of the thermocouple wells were made prior to filling the can with the powder. These measurements were necessary for the determination of the value $\ln(r_2/r_1)$ which is used in calculating the thermal conductivity (3).

The free volume of the can was determined by weighing it empty and then filled with distilled water, correcting the density of the water for its temperature. The amount of ThO_2 powder required to give an average density of 75% to 80% of theoretical density was determined from the free volume. A vibrational packing system was then used to load the powder in the can. The resulting specimen had a gross density of 75.02% theoretical. Radiographs were made to determine that the thermocouple wells were still located in their original positions.

A Type 304 stainless steel extension tube, sufficiently long to protrude through the top of the furnace, was welded to the can. This tube was then connected to a manifold which had gas and vacuum facilities connected to it. The manifold also had a vent to the atmosphere so that the pressure of the gas in the can would remain close to one atmosphere (see figure 2).

The gases were supplied from individual bottles which could be exchanged while the system was evacuated. Valving in the manifold isolated the gas system from the vacuum system. Flow rates of the gases were adjusted by use of a metering valve in the manifold and a valve in the vent line so that a pressure slightly above one atmosphere (~765 Torr) was maintained in the manifold. A portable mechanical vacuum pump, having a pumping speed of 425 liters/min., was used to exhaust the system to 3.5×10^{-2} Torr when changing from one gas to another. Two or three purges were made each time the gas was changed.

3.1. Thoria Powder

The specimen material used in this work had the particle size distribution listed in table 1. While this is not a fine powder, about 75% of the particles are less than 150 microns in diameter.

Table 1. Particle size distribution of thoria powder (typical)

Sieve Size	Particle Size (mm)	%
-325	0.044	30.5
-200 +325	0.074	17
-100 +200	0.149	27.5
-50 +100	0.297	17.5
-20 +50	0.840	6.5
+20	0.840	1

4. Thermocouples

Calibrated chromel-alumel thermocouples, constructed from 0.0254 cm diameter wire and insulated with alumina, were used to measure the temperature in the thermocouple wells. These thermocouples were constructed in a manner such that the beads entered the small diameter tube at the bottom of the wells. Calibration indicated that the couples were in agreement with each other and within 1 °C of a standard couple up to 800 °C, 2 °C at 800° and 900 °C, and 3 °C at 1000 °C. Above 1000 °C the departure from the standard increased and some variations in the couples occurred. The indicated temperatures during test were corrected by the calibration errors in determining the true temperatures and temperature differences in the specimen.

5. Test Procedure

The specimen was loaded into the furnace and the thermocouple and gas connections were made. Helium was introduced into the furnace volume surrounding the specimen container while the specimen container was being evacuated overnight. The pressure in the can reached 3.5×10^{-2} Torr as a result of this pump down. Helium was then introduced into the specimen container until an equilibrium pressure of about 765 Torr was reached. The system was evacuated again and refilled with helium before bringing the specimen to temperature.

After maintaining the furnace at 700 °C overnight, measurements were made in the 700° to 1050 °C temperature range on heating and in the 600° to 400 °C range on cooling. These values are shown in table 2 and in figure 3.

Measurements were also performed with the specimen evacuated to about 3.5×10^{-2} Torr in the temperature range of 430° to 750 °C in order to establish a value for the conductivity of the powder phase alone and to provide a basis for determining the effect of the different atmospheres. The values obtained in vacuum are also shown in table 2 and figure 3.

Following the vacuum measurements, tests were performed using a gas mixture of He + 52% N_2 (v/o). The mixed gas was changed twice by cycling from vacuum to gas a total of three times before measurements were made. During this time the center heater was energized and qualitative observations were made of the voltage drop and current in the heater, and measurements of the specimen ΔT were made. When the gas was evacuated, the ΔT in the specimen increased and the operating temperature of the center heater rose causing a larger voltage drop due to its higher resistivity at the higher temperature. Re-introducing the gas caused the operating conditions to restore the same values obtained in the previous observation. This exercise provided qualitative evidence that the gas did permeate the powder matrix. Quantitative evidence was given by the conductivity data. Measurements with the mixed gas present were made during heating and cooling between 400° and 1200 °C. These data are shown in table 2 and figure 3.

A second set of measurements was obtained in helium from 400° to 1200 °C. The data below 1000 °C for this run indicate that virtually no change occurred in the conductivity as a result of the prior thermal cycling; however, the data in the 1000° to 1150 °C range were somewhat higher (~20%) than when He + 52% N_2 was present.

5.1. Additional Measurements

After completing the above measurements and observing that the type of gas made little difference, measurements were made using 100% nitrogen and then argon. These gases have much lower thermal conductivities than those previously used, as shown in table 3. The results of the measurements in these two gases are compiled in table 2 and figure 3.

5.2. Discussion of Results

The data in table 2 have been summarized by drawing a smooth curve through each set of data and are tabulated in table 4 at even increments of temperature to show the quantitative effect of the gas.

It will be observed that the conductivity of the compact (with a gas present) varies a maximum of ±10% about a mean value for any temperature regardless of the type of gas present. If this system were sensitive to the conductivity of the gas and obeyed the model proposed by Godbee (1), the conductivity at 500 °C would vary from 1.91 Wm^{-1} deg^{-1} for helium down to 0.37 Wm^{-1} deg^{-1} for argon or a ratio of approximately 6 to 1; this was not experienced in this study.

Close examination of the data in table 2 may cause speculation that the conductivity of the compact was changing with time and temperature cycling since the final measurements in helium (2nd cycle on cooling) are higher by about 25% in the 1000° to 1050 °C range than the initial values in the mixed gas. This is probably due to experimental error rather than densification by sintering. Separate studies on similar systems indicated that sintering does not occur at temperatures below 1500 °C.

A review of the literature describing thermal conductivity studies performed on two-phase (powder-gas) compacts (1) suggests that the effect of the conductivity of the gas may be limited by the distances between the solid particles. It could, in fact, cause the gas to behave in three distinctly different modes as a heat conductor.

1. Where the spacing between the particles is large in relation to the mean free path of the gas, the contribution of the conductivity of the gas would be that of the bulk gas.

2. Where the spacing is very small in relation to the mean free path, i.e., approximately equal to it, especially surrounding the points of contact between the particles, the thermal transport is more closely related to the free-molecular heat conduction which has been shown by Kennard (2) as being related to the specific heat, pressure, and temperature.

Table 3. Thermal conductivity of gases at one atmosphere of pressure (Wm^{-1} deg^{-1})

Temp., °C	Argon[a]	Nitrogen[a]	He + 52% N_2[b]	Helium[a]
400	3.27×10^{-2}	4.80×10^{-2}	10.9×10^{-2}	27.0×10^{-2}
450	3.44	5.05	11.6	28.5
500	3.60	5.28	12.2	29.9
550	3.76	5.52	12.8	31.3
600	3.91	5.75	13.4	32.7
650	4.05	5.97	14.0	34.1
700	4.19	6.19	14.6	35.5
750	4.30	6.40	15.2	36.9
800	4.47	6.61	15.8	38.2
850	4.60	6.82	16.4	39.6
900	4.74	7.02	17.0	40.9
950	4.88	7.22	17.6	42.2
1000	5.01	7.43	18.2	43.6
1050	5.15	7.64	18.8	44.9
1100	5.28	7.85	19.4	46.2
1150	5.41	8.08	20.0	47.5
1200	5.54	8.20	20.6	48.8
1250	5.68	8.54	21.2	50.0
1300	5.81×10^{-2}	8.79×10^{-2}	21.8×10^{-2}	51.4×10^{-2}

(a) Powell, R. W., Ho, C. Y. and Liley, P. E., "Thermal Conductivity of Selected Materials," NSRDS-NBS-8, U.S. Dept. of Commerce, National Bureau of Standards, Nov. 1966.

(b) After Wright, J. M., "Calculated Thermal Conductivities of Pure Gases and Gaseous Mixtures at Elevated Temperatures," AECD-4197, Hanford Works, Richland, Wash., Dec. 1955. Computerized by R. Pugh, GE-NMPO.

Table 4. Thermal conductivity of powdered thoria at 75% theoretical density with various gas atmospheres[a] (Wm^{-1} deg^{-1})

Temp., °C	Helium	He + 52% N_2	Nitrogen	Argon	Vacuum[b]
400	1.28	1.30	1.22	1.07	0.4
500	1.22	1.22	1.18	1.01	0.43
600	1.19	1.16	1.07	1.00	0.47
700	1.18	1.13	1.04	1.05	0.5
800	1.18	1.13	1.03	1.25	
900	1.22	1.17	1.06		
1000	1.28	1.22			
1100	1.37	1.32			
1200	1.50	1.46			

(a) Values from smooth curve through each set of data.

(b) At approximately 3.5×10^{-2} Torr.

3. At intermediate particle spacings there would be conduction by both mechanisms.

When relating the considerations above to the system under study, it is reasonable to consider the structure as having a random distribution of particle spacings ranging from contact to several hundred microns. Extensive measurements and mathematical analyses will be required to determine the statistical distribution of particle spacings and the contact area between the particles to estimate the contribution of the gas conductivity and the solid conduction in this system. However, the results of these measurements would seem to indicate that the mode of heat conduction in the gas is primarily by free molecular heat transport since differences in the conductivities of the system when filled with the various gases are too small to be explained by the bulk conductivities of the gases. Furthermore, the values measured in vacuum are higher than would be expected in a system which would have large inter-particle distances and small contact area.

The recommended values for high density (98% of theoretical) sintered thoria (6) are shown in figure 3 for comparison.

Table 2. Thermal conductivity data for thoria powder in various gases (Wm^{-1} deg^{-1})

Temp., °C	1st Cycle						2nd Cycle[a]					
	Heating			Cooling			Heating			Cooling		
	Max.	Min.	Avg.	Max.	Min.	Avg.	Max.	Min.	Avg.	Max.	Min.	Avg.
Helium												
377				1.39	1.10	1.20						
386							1.34	1.25	1.29			
420										1.42	1.35	1.39
429				1.10	1.36	1.21						
492				1.34	1.07	1.20						
506										1.50	1.45	1.48
529				1.23	1.06	1.14						
571							1.26	1.25	1.24			
708	1.31	1.07	1.18									
711	1.32	1.09	1.22									
750	1.26	1.22	1.24									
772	1.16	1.12	1.14									
797	1.12	1.01	1.06									
828							1.29	1.25	1.28			
989	1.14	1.11	1.13									
1002										1.58	1.33	1.47
1130										1.69	1.39	1.56
1138										1.65	1.40	1.54
1181							1.62	1.25	1.45			
Vacuum												
414				0.663	0.571	0.616						
436	0.450	0.399	0.423									
445	0.445	0.401	0.442									
517	0.444	0.437	0.440									
650	0.423	0.409	0.417									
752	0.610	0.525	0.565									
He + 52% N_2												
394	1.33	1.12	1.12	1.39	1.30	1.35						
446	1.35	1.10	1.21									
449				1.38	1.27	1.32						
556	1.23	1.08	1.15									
614	1.25	1.12	1.18									
637				1.24	1.20	1.22						
654				1.24	1.20	1.22						
731	1.24	1.08	1.15									
788	1.18	1.09	1.14									
823	1.13	1.07	1.10									
874				1.37	1.33	1.35						
930	1.12	1.11	1.11									
971				1.27	1.19	1.25						
1076	1.22	1.18	1.20									
1092	1.25	1.17	1.22									
1147	1.40	1.30	1.35									
1157				1.47	1.44	1.46						
1197	1.63	1.34	1.50									
1201	1.61	1.52	1.57									
Nitrogen												
406	1.25	1.17	1.22									
442	1.20	1.12	1.17									
513	1.17	1.05	1.12									
529	1.14	1.04	1.10									
692	1.13	1.01	1.08									
735	1.06	0.974	1.02									
911	1.07	1.02	1.05									
Argon												
460	1.04	1.03	1.03									
582	0.973	0.946	0.962									
698	0.976	0.971	0.965									
734	1.12	1.09	1.11									
787	1.31	1.28	1.30									

(a) Data obtained after testing with He + 52% N_2.

6. Conclusions and Recommendations

The results of these measurements indicate that the conductivity of the powder-gas compact used in this study will not be greatly affected by a change in composition of the gas as long as the gas pressure does not vary. Stated in another manner, helium with its high conductivity does not significantly increase the conductivity of the powder-gas compact over the values obtained with argon which has a much lower conductivity. Air, which has a conductivity approximating that of nitrogen, would contribute equally as well as helium or any other gas to the conductivity of the compact. This, of course, assumes that the system is dry and that sorbed water vapor and other fluids are kept to a minimum; Godbee (1) points out that such materials would enhance the thermal conductivity of the powders.

Further studies in which gas pressure, particle size, and bulk density are variables may shed new light on the contribution of the gas phase on the conductivity of the two-phase compact.

7. References

(1) Godbee, H. W., "Thermal Conductivity of MgO, Al_2O_3 and ZrO_2 Powders in Air at Atmospheric Pressure from 200°F to 1500°F," Oak Ridge National Laboratory, ORNL-3510, April 1966, and private communication April 12, 1967.

(2) Kennard, E. H., Kinetic Theory of Gases, McGraw-Hill Book Company, Inc., New York, 1938, p. 315.

(3) Feith, A. D., "A Radial Heat Flow Apparatus for High Temperature Thermal Conductivity Measurements," GE-NMPO, GEMP-296, August 1963.

(4) Feith, A. D., "The Thermal Conductivity of Several Ceramic Materials to 2500°C," Advances in Thermophysical Properties at Extreme Temperatures and Pressures, ASME, March 1965.

(5) Feith, A. D., "Measurements of the Thermal Conductivity and Electrical Resistivity of Molybdenum," GE-NMPO, GE-TM 65-10-1, October 1965.

(6) Powell, R. W., Ho, C. Y., and Liley, P. E., "Thermal Conductivities of Selected Materials," NSRDS-NBS-8, U.S. Department of Commerce, National Bureau of Standards, November 1966.

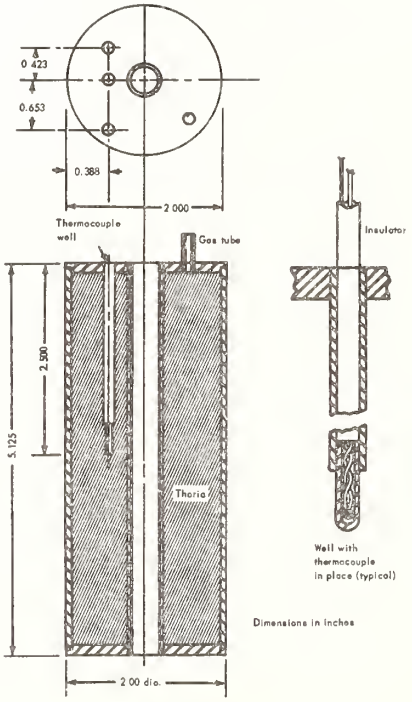

Figure 1. Specimen container used to determine the thermal conductivity of thoria powder.

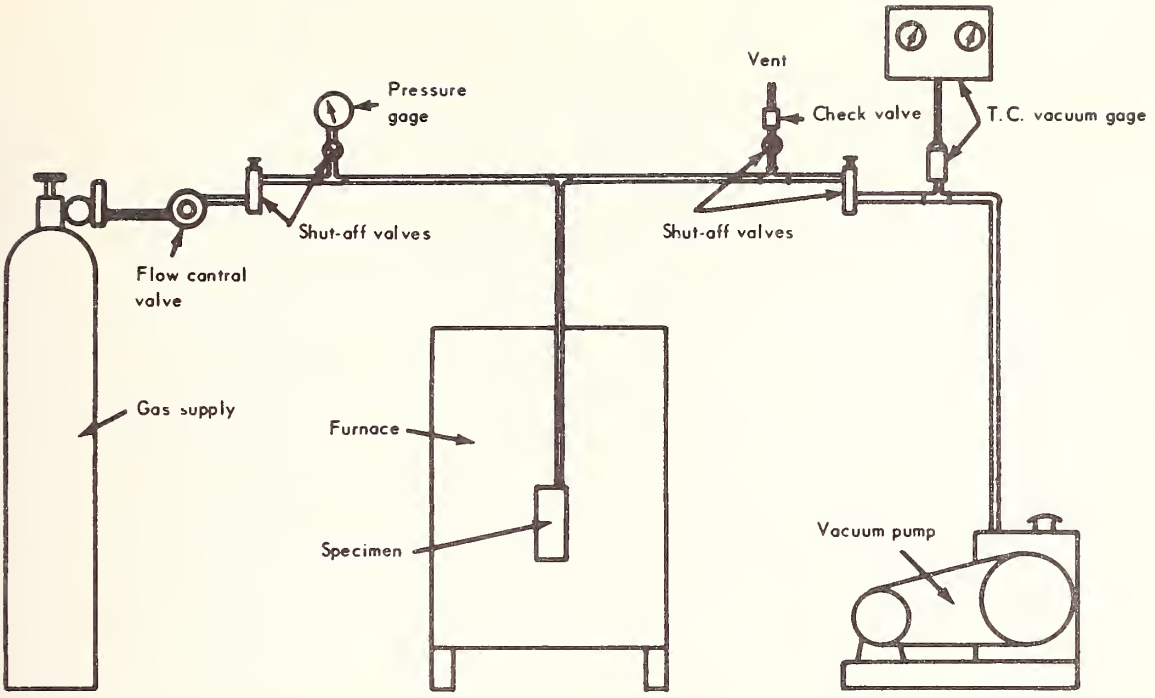

Figure 2. Schematic diagram of gas supply and vacuum system.

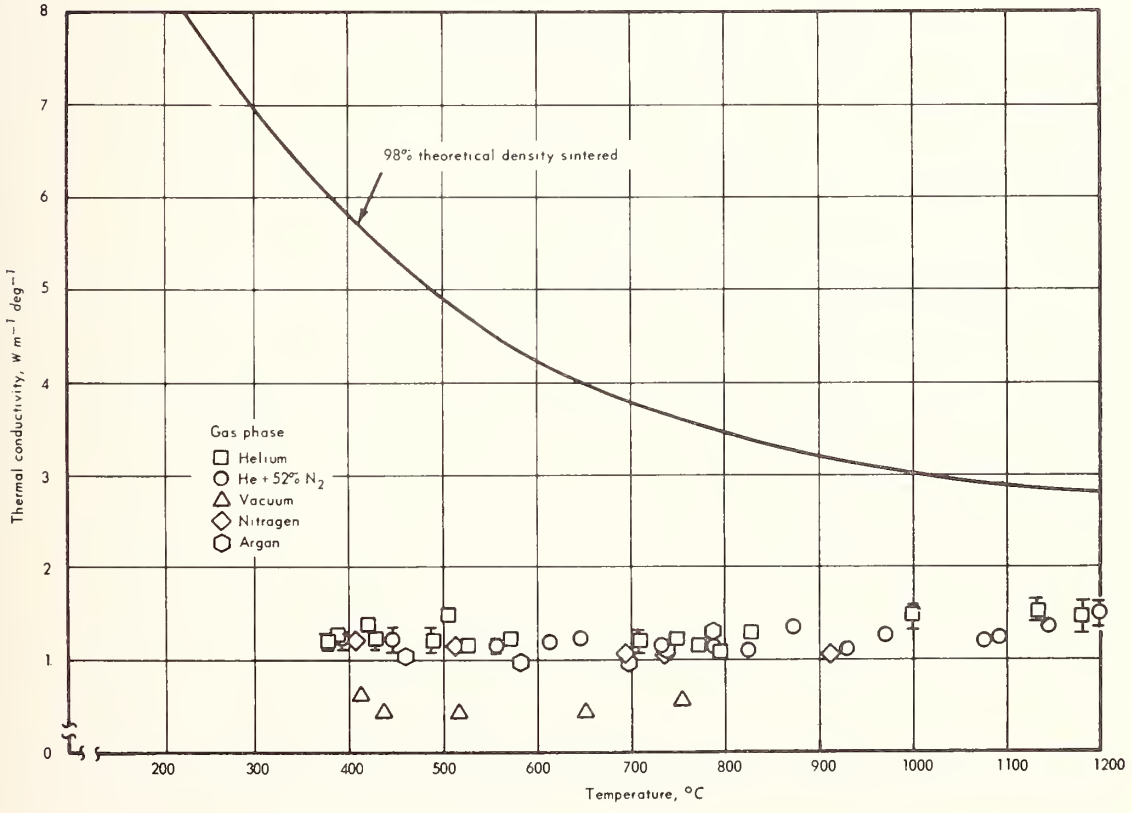

Figure 3. Thermal conductivity versus temperature for powdered thoria at 75% theoretical density in various atmospheres.

Thermal Conductivity of a 58% Dense MgO Powder in Nitrogen[1]

J. P. Moore, D. L. McElroy, and R. S. Graves

Oak Ridge National Laboratory
Oak Ridge, Tennessee

A technique for measuring the thermal conductivity of small quantities ($\approx$ 220 cm^3) of powders from 300 to 1300 °K is described in detail. A thorough analysis is made of the determinate and indeterminate errors of the technique.

Results of measurements on a 58% dense MgO powder in N_2 gas as a function of temperature at 1 atm absolute gas pressure are presented. These results are compared to data obtained by previous investigators for a similar powder. The experimental results and this comparison reflect serious error sources for this radial technique.

Key Words: Magnesium oxide, nitrogen, powders, radial heat flow, two-phase media

[1]Research sponsored by the U. S. Atomic Energy Commission under contract with the Union Carbide Corporation.

Measurements of the Thermal Conductivity of Glass Beads in a Vacuum at Temperatures from 100° to 500°K

R. B. Merrill[1]

Space Sciences Laboratory
The George C. Marshall Space Flight Center
Huntsville, Alabama, 35812

A method of measuring thermal conductivity has been developed that is suitable for measuring evacuated powders. This method gives consistent results, it is fast, and the initial and boundary conditions are easily met. The temperature dispersion during any one measurement is small enough to make measurements as a function of temperature meaningful. The conductivity was measured for glass beads in a vacuum of at least 2×10^{-6}torr ($3 \times 10^{-4} N/m^2$) or better over a temperature range of 100° - 500°K. The particle sizes used were 10μ - 20μ, 38μ - 53μ, and 125μ - 243μ. The conductivity can be represented by an expression of $\lambda = AT^3 + B$ where A and B are constants and T is the absolute temperature. The value of A does not change significantly over the range in powder sizes from 10μ to 243μ.

Key Words: Differentiated Line Heat Source method, evacuated powder, glass beads, Line Heat Source method, radiative transfer, temperature dependence, thermal conductivity.

1. Introduction

The theory of heat transfer through powders in a vacuum considers two modes. One mode involves radiative transfer. Wesselink [1][2], Laubitz [2], Schotte [3], and many others have derived theoretical expressions for this mode. One thing these expressions have in common is that the radiant conductivity is proportional to the temperature raised to the third power. The other mode concerns solid conduction. Halajian et al [4] derived an expression in which the value is nearly independent of temperature. Watson [5] was one of the first to suggest that the conductivity could be represented by the equation

$$\lambda = AT^3 + B, \tag{1}$$

where λ is the thermal conductivity, T is the absolute temperature, and A and B are constants.

The theoretical derived equations state that the conductivity should be temperature dependent. Watson [5] assumed this relationship and measured the effect of changing the porosity and particle size for spherical glass beads, olivine powders, and several other materials. But Bernett et al [6] measured olivine basalt powders and silica powder and found little temperature dependence. Recently Wechsler [7] has shown that there is indeed a temperature dependence. The above conflicting evidence suggests that the thermal conductivity should be measured as a function of temperature, but this is a very difficult thing to do. One reason for the difficulty is that the temperature excursion for one measurement usually is so large as to obscure the temperature that properly should be assigned to the measured conductivity.

[1] Physicist
[2] Figures in the brackets indicate the literature references at the end of this paper.

The goals of this research were: (1) to find a method suitable for measuring the conductivity as a function of temperature, (2) to measure the conductivity, and (3) to compare these measurements with theoretic values and other measurements reported in the literature.

2. Method of Measurement

2.1. Configuration

The method used to make measurements, developed especially for the work, is called the "Differentiated Line Heat Source" method (abbreviated as DLHS). This method has the same geometry as the Line Heat Source (LHS) method, but deviates in that the temperature change is differentiated with respect to time.

The geometry of this method is cylindrical. A long heater wire runs along the axis, and parallel to it is a thermocouple. The construction used to hold these wires and leads is called a heater and thermocouple assembly. The container which holds the powder and which supports the heater and thermocouple assembly is called the sample holder.

The heater and thermocouple assembly is constructed as shown in figure 1. The heater is a constantan wire one-thousandth of an inch in diameter, attached to copper posts on a glass base. The other parallel wire is an iron-constantan thermocouple, also one-thousandth of an inch in diameter. The thermocouple junction is located midway between the two posts. The iron lead is attached to an iron post and the constantan lead to a constantan post. Similar wires run to the exit electrical connector in the vacuum system. The two wires are about 0.06 centimeter apart and about twenty centimeters long.

The supports are made of glass and are bonded together at both ends with a ceramic-type cement. The wire heater and thermocouple assembly are placed in the glass tubes as depicted in figure 2; they open into the vacuum chamber through the base plate. The powder is put into a container inside the vacuum chamber, and the chamber is evacuated. The tube is brought to a temperature of about 500°K by a nichrome heater surrounding the tube. To ensure thorough outgassing, the powder (while still in the vacuum) is poured into the tube from the container over an eight-hour period.

The temperature of the tube is controlled by immersing it in liquid nitrogen or by heat supplied from the nichrome heater. The rate of temperature change is controlled by the radiation shielding of a dewar, evaporating liquid nitrogen, and/or the heater.

A block diagram of the entire measuring system is depicted in figure 3. The voltage applied across the line heater is supplied by a precision d.c. power supply. Constantan has a low thermal coefficient of resistivity so that the power input remains constant during a measurement. The temperature of the powder is measured at the junction through balancing a Leeds and Northrup K-3 universal potentiometer until a null condition is reached. The reference junction is maintained at the triple point by a thermocouple reference system. Amplifiers (1) and (2) are Leeds and Northrup d.c. microvolt amplifiers model 9835. The differentiating circuit differentiates the zero to one-volt output of amplifier (1). Figure 4 is a schematic of the differentiating circuit with the appropriate values of the components marked. The constant rate of change term is initially bucked to a null condition with potentiometer (2), which is constructed from a battery and a variable resistor. Figure 5 is a typical trace of a run by the strip chart recorder, showing all the pertinent data taken.

A series of runs is begun as follows. After the sample has been outgassed, the temperature is changed to some initial temperature. The electronics system is allowed to warm up and stabilize during this time. The scale factors on amplifiers (1) and (2) are set so that they will not overrun during a test. The rate of change is next subtracted from the output of the differentiating circuit by setting potentiometer (2). The temperature is measured by potentiometer (1), and then the run is initiated almost immediately by applying a voltage across the line heater.

2.2. Theory of Measurement

The solution of the heat transport equation is written as

$$v \equiv T - T_0 = g(t) + \int_0^t \frac{F}{4\pi\lambda\,(t-t')} \exp\left[-b^2/4a(t-t')\right] dt' , \qquad (2)$$

where T_0 is the initial temperature, F is the heat flux per unit length of the heater wire, λ is the thermal conductivity, t is the time, b is the separation distance between the heater wire and the thermocouple, and a is the thermal diffusivity. The second term in eq (2) is readily recognized as the solution for the LHS method where uniform initial conditions prevail. The first term is apparent from Green's method of solving the heat transport equations. The dependence of the temperature change due to the initial conditions is completely described by the function g(t). This function can be expanded in a Taylor's series, and if the time interval is small enough, the higher order terms can be neglected. This means that the solution to the heat transfer equation may be written as

$$v = A_0 + A_1 t + \int_0^t \frac{F}{4\pi\lambda(t-t')} \exp\left[-b^2/4a(t-t')\right] dt' , \tag{3}$$

where the time is sufficiently small and where A_0 and A_1 are constants.

The DLHS method considers the derivative of the temperature change; hence,

$$\frac{dv}{dt} = A_1 + \frac{F}{4\pi\lambda t} \exp(-b^2/4at) \tag{4}$$

and

$$\lambda = F \exp(-b^2/4at)/4\pi (dv/dt - A_1)t . \tag{5}$$

The conductivity can be measured with this arrangement while the temperature is changing uniformly. A typical measurement takes only a few minutes.

Three methods are used to calculate the conductivity. The first two are based upon the following considerations. For the case in which the maximum change of temperature with respect to time occurs,

$$\lambda = F/4\pi e(dv/dt - A_1)_m t_m , \tag{6}$$

where $(dv/dt - A_1)_m$ denotes the maximum change of temperature with respect to time and t_m refers to the time at which this occurs. The maximum happens to be fairly broad. A more precise way to calculate the conductivity is to use the time $t_{\frac{1}{2}}$ where $(dv/dt - A_1) = \frac{1}{2} (dv/dt - A_1)_m$. This condition is satisfied when $t_{\frac{1}{2}} = 0.37337 t_m$ and when $t_{\frac{1}{2}}' = 4.316 t_m$. Methods 1 and 2 now may be defined as follows.

Method 1 uses the first halfway point, $t_{\frac{1}{2}}$, so that $\lambda = 0.37337F/4\pi e(dv/dt - A_1)_m t_{\frac{1}{2}}$.

Method 2 uses the second halfway point, $t_{\frac{1}{2}}'$, so that $\lambda = 4.316F/4\pi e(dv/dt - A_1)_m t_{\frac{1}{2}}'$.

Method 3 involves fitting the curve expressed by eq (4) to the strip chart record. Two unknown parameters, x_1 and x_2, (defined as: $x_1 \equiv \lambda$ and $x_2 \equiv b^2/4a$) are found by this method. The minimized function is of the least-squares form, and the minimization is performed by a numerical method called "A Variable Metric Minimization Scheme" [8, 9].

3. Data

The conductivity versus temperature is plotted in figures 6 through 9. The abscissa is the absolute temperature in degrees Kelvin, and the conductivity is expressed along the ordinate in units of 10^{-4} watt m^{-1} $°K^{-1}$. The selection of a semi-log graph presentation allows all of the conductivity data for one particle size to be conveniently located on one graph. Figure 6 is a plot of the conductivity data for the 10μ - 20μ size powder. Method 2 gives the smoothest data. The maximum chart reading for these measurements was reached in a time "t_m" on the order of ten seconds. This means that the uncertainty in this time is large for the usual method 1 data-reduction procedure. The uncertainty explains the scatter in the data. The initial points near t_m were used by method 3.

Figure 7 is a plot of the data for the 38μ - 53μ size powder. The data represented by the half-moons were found in the literature [10]. Table 1 gives the pertinent properties of these measurements.

Table 1. Glass beads, 50μ average particle size

Method	Temperature °K	Gas Pressure torr	Gas Pressure N/m^2	λ ($\times 10^{-3}$) watt $m^{-1}\,°K^{-1}$
LHS	298	8×10^{-5}	1×10^{-2}	2.5
Probe	298	5×10^{-4}	7×10^{-2}	3.2
Guarded cold plate	190	2×10^{-4}	3×10^{-2}	1.7

These values are greater than the other values reported. The relatively high gas pressure may have resulted in an appreciable gas conduction.

The data represented by the squares were also found in the literature [11]. These data are for 44μ - 74μ glass beads at a pressure of less than 2×10^{-6} torr (3×10^{-4} N/m^2) and were gathered by an LHS method. The system was stabilized for at least twenty-four hours.

Figure 8 is a plot of the 125μ - 243μ data (sample number 5) and of data found in the literature for powders in this size range. The data represented by the half-moons have the properties as given in table 2 [10].

Table 2. 150μ average particle size

Method	Temperature °K	Gas Pressure torr	Gas Pressure N/m^2	λ ($\times 10^{-3}$) watt $m^{-1}\,°K^{-1}$
LHS	298	3×10^{-4}	4×10^{-2}	5.0
Probe	298	3×10^{-5}	4×10^{-3}	5.0
Guarded cold plate	190	3×10^{-4}	4×10^{-2}	4.6

The data represented by the squares was also obtained from the literature [11].

Figure 9 is a plot of the remaining 125μ - 243μ data of sample numbers 3 and 4. The solid line in this diagram describes the data of sample number 5.

The conductivity versus temperature data, summarized in figures 6 through 9, are used to determine the constants A and B of eq (1) by the least-squares method. Table 3 is a summary of the values of A and B for the various particle sizes. Some of the conductivity data appears disjointed between 200°K and 300°K. Separate calculations were made for all the data below and above 300°K. The quantity represented by "f" is the sum of the squares of the deviation.

Table 3. Values of the constants A and B found by the least-squares method

Particle Size, μ	Sample No.	Method of Data Reduction	No. of Experiments	B($\times 10^{-3}$) watt $m^{-1}\,°K^{-1}$	A($\times 10^{-10}$) watt $m^{-1}\,°K^{-4}$	f
10-20*	7	2	11	.484	.230	.0155
10-20*	7	3	11	.346	.252	.0556
10-20*	7	1	11	.472	.276	.213
38-53*	6&8	1	24	.454	.327	.0241
38-53**	6&8	1	17	.153	.358	.0143
38-53***	6&8	1	7	.437	.452	.0083
125-243*	5	1	41	.071	.542	.107
125-243**	5	1	28	-.132	.565	.151
125-243***	5	1	13	.0870	.639	.00034
125-243*	3	1	27	.151	.310	.0037
125-243*	2	1	17	-.093	.417	.00522

* All the data points used in computing the values
** All the data points above 300°K used in computing the values
*** All the data points below 300°K used in computing the values

4. Conclusions

Method 3 gives nearly the same results as the numerically simpler methods 1 and 2. Applying the first halfway point as in method 1 is useful because the length of the run is shorter, and hence the uniform rate of change of the temperature, which is initially determined, need hold for a shorter time when compared to method 2. Method 2 becomes more useful, however, when the uncertainty in the first halfway point becomes unacceptable as demonstrated by the conductivity data of the 10μ - 20μ powder.

The percent difference between the measured and the calculated conductivity from eq (1), using the values of A and B as given in table 3, is always within the estimated random error. Therefore, the conductivity can be represented within the experimental error by the expression $\lambda = AT^3 + B$. The value of A does not change significantly over the range of powder sizes from 10μ to 243μ. This means that the value of A is not adequately described for these particle sizes by the theories of Wesselink, Laubitz, and Russell. Laubitz's expression is more descriptive when Watson's data are included.

5. Acknowledgements

The author gratefully acknowledges the advice and encouragement given by Dr. Daniel Decker of Brigham Young University. The author also wishes to acknowledge the support given to him by Mr. G. Heller and Mr. J. Fountain of Space Sciences Laboratory, MSFC.

6. References

[1] Wesselinck, A. J., Astron. Inst. of Netherlands 10, 351 (1948).

[2] Laubitz, M. J., Can. J. Phys. 37, 798 (1959).

[3] Schotte, W., A. I. Ch. E. J. 6, 798 (1959).

[4] Halajian, J. D., Reichman, J., and Karafiath, L. L., Correlation of Mechanical and Thermal Properties of Extraterrestrial Materials, Grumman Research Department Report RE-280, 17 (Jan. 1967).

[5] Watson, K., The Thermal Conductivity of Selected Silicate Powders in Vacuum From 150° - 350°K, Thesis, The California Institute of Technology, Pasadena (1964).

[6] Bernett, E. C., Wood, H. L., Jaffe, L. D., and Marlens, H. E., A.I.A.A.J. 1, 1402 (1963).

[7] Wechsler, A. E., Glass Beads — A Standard for the Low Thermal Conductivity Range?, paper No. 7 in this volume.

[8] Davidson, W. C., Variable Metric Method for Minimization, Argonne National Laboratory, Lemont, Ill. (1959).

[9] Decker, D., Private communication, Brigham Young University, Provo, Utah.

[10] Wechsler, A. E. and Glaser, P. E., ICARUS 4, 335 (1965).

[11] Wechsler, A. E. and Simon, I., Thermal Conductivity and Dielectric Constant of Silicate Materials, Arthur D. Little Co. Report, 91 (1966).

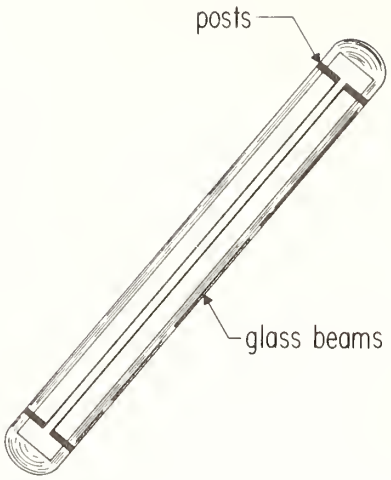

Figure 1. Line Heater and Thermocouple Assembly

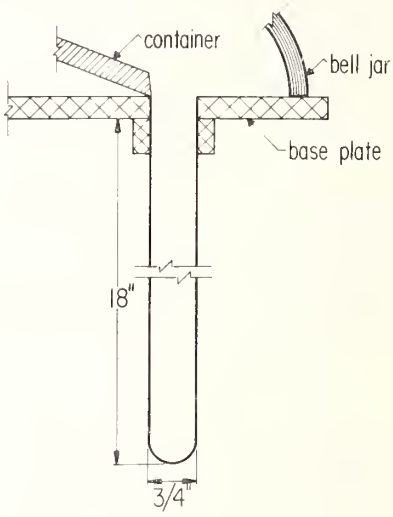

Figure 2. Sample Holder

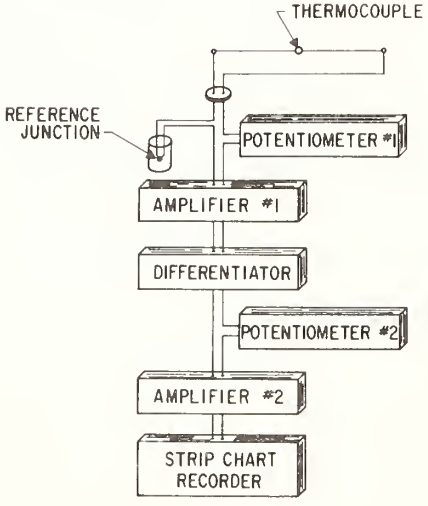

Figure 3. Block Diagram of the Measuring System

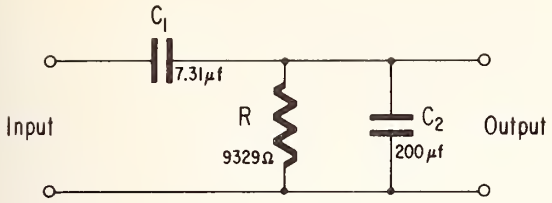

Figure 4. Schematic of the Differentiating Circuit

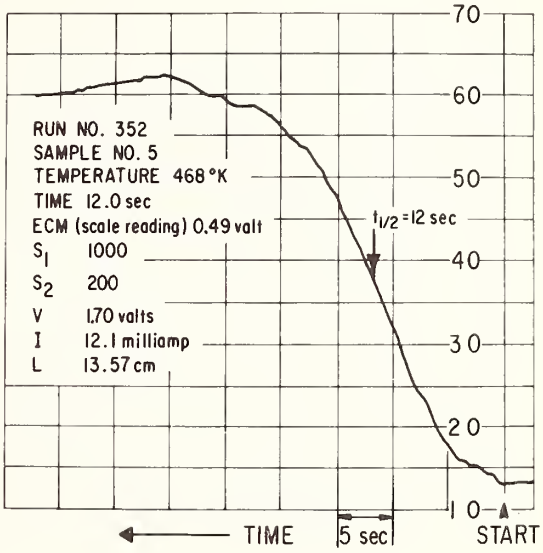

Figure 5. Typical Trace of Run by the Strip Chart Recorder

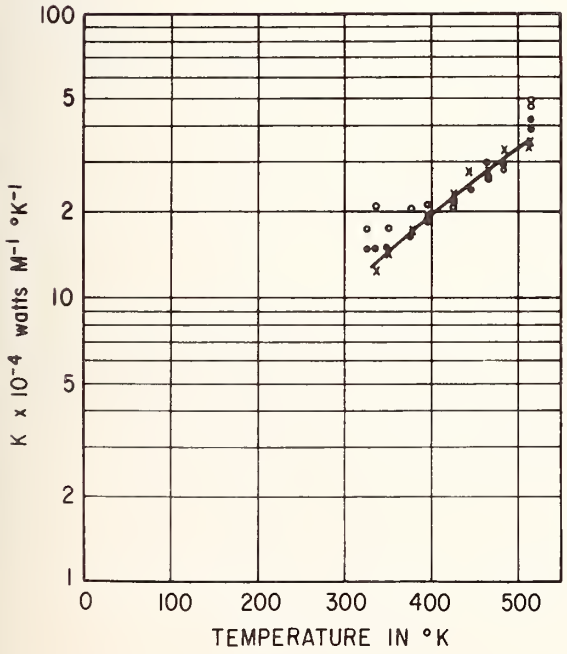

Figure 6. A Plot of the Conductivity for the 10μ - 20μ Size Powder

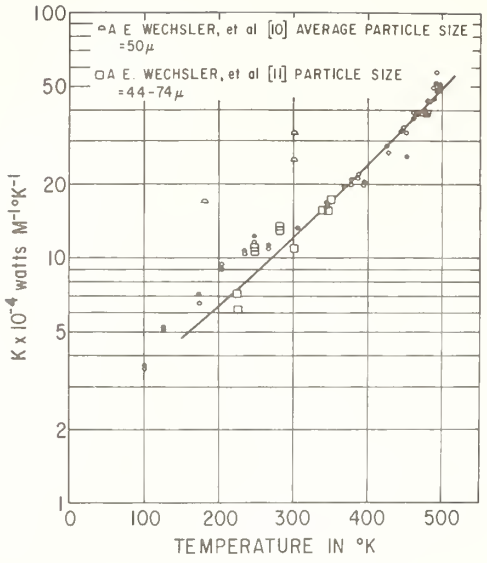

Figure 7. A Plot of the Conductivity for the 38μ - 53μ Size Powder

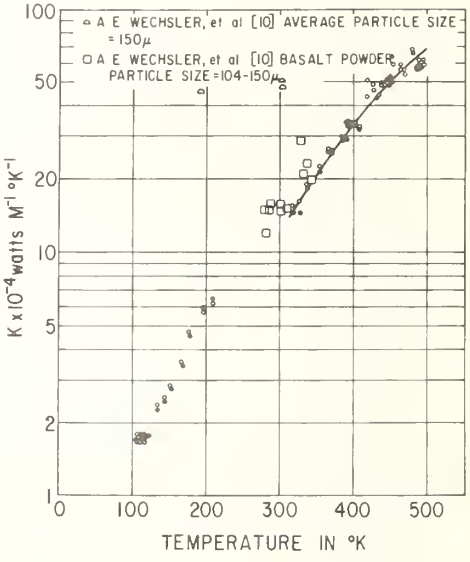

Figure 8. A Plot of the Conductivity for the 125μ - 243μ Size Powder of Sample Number 5

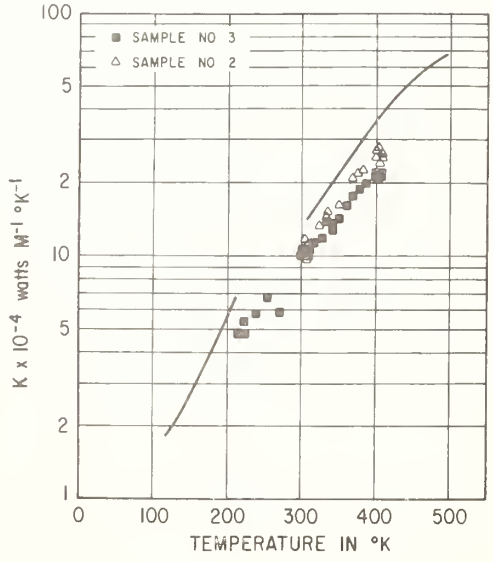

Figure 9. A Plot of the Conductivity for the 125μ - 243μ Size Powder of Samples Number 2 and 3

The Measurement of the Effective Thermal Conductivities of Well-Mixed Porous Beds of Dissimilar Solid Particles by use of The Thermal Conductivity Probe

C. S. Beroes and H. D. Hatters[1]

Chemical and Petroleum Engineering Department
University of Pittsburgh
Pittsburgh, Pennsylvania 15213

The effective thermal conductivities of well-mixed porous beds at various compositions of glass and steel beads were measured using two thermal conductivity probes. The interstitual gases were dry air and carbon dioxide. The gas pressure was varied from 1.25 mm Hg to atmospheric pressure at 26°C. The effects of volume fraction of steel in the steel-glass mixture of beads is determined and explained. A better understanding of the energy transfer mechanism is provided by analyzing the experimental data with respect to the effects of the pure solid thermal conductivities and the differences in particle surface. A technique has been developed to measure the degree of mixedness of porous beds of dissimilar solids.

Key Words: Dissimilar solid particles, glass shot-steel shot, mixed porous beds, thermal conductivity, thermal conductivity probe.

1. Introduction

The measurement of the effective thermal conductivities of porous mixtures of dissimilar solid particles is important because thermal conductivity data is very necessary in many processes where porous solids must be heated or cooled. Furthermore, such data is important in insulation applications. This study was undertaken to establish a reliable technique to provide quick, reproducible measurements of effective thermal conductivities of said porous mixtures.

The purpose of this study described in this paper was three-fold: To determine the suitability of the thermal conductivity probe method as a means of measuring the thermal conductivities of porous mixtures of dissimilar solid particles; to compare a rugged thermal conductivity probe, constructed at the University of Pittsburgh Chemical Engineering Laboratory with a commercially available laboratory-type thermal conductivity probe; and to determine the effective thermal conductivities of beds of well-mixed dissimilar solid particles, and relate these conductivity measurements to the thermal conductivities of the pure materials, and the concentration of each material in the mixture.

---

[1] Associate Professor and MS Candidate, respectively.

2. Experimental Measurements

2.1 Measurement Method

The thermal conductivity probe method was chosen for thermal conductivity measurements because of its quickness, simplicity, the small volume of sample required, and because it is a direct method (i.e. it allows measurement of thermal conductivities directly, thereby, eliminating the necessity for specific heat and density knowledge). The thermal conductivity probe method has been used by many investigators (1,2,3)[2], and the theory (1,4) concerned with its use is well-known.

2.2 Apparatus

A Model CS-48 thermal conductivity probe consisting of an 0.12" o.d. bifilar heater coil of 0.001" constantan wire in an 0.020" o.d. x 0.002" wall x 8.75 long stainless steel sheath was first tested in this service. An 0.0005" x 0.005" Chromel "P" thermocouple located at the midpoint inside the probe allows measurement of the temperature of the probe. This probe was built by Custom Scientific Instruments of Kearney, New Jersey, and is a laboratory type instrument of high accuracy and reproducibility. Current measurements of about 7.65 milliamperes were made at a heater resistance of 1,520 ohms with a flux of approximately 0.09 watt in this probe.

Instrumentation for this probe system consisted of a twelve volt battery as a power supply, a Sanborn Model 296 Recorder with a low level preamplifier Model 350-1500 was used to record time and temperature. A Leeds and Northrup Model 8690 potentiometer was used to set recorder at full scale deflection for an emf. of 0.5 millivolt and a Simpson Model 260 milliammeter was used for the current measurement. A Shallcross resistance box Model 817-B was used to control the current at the proper level.

A more rugged probe (see fig. 1) was constructed at the University of Pittsburgh Chemical Engineering Laboratory by drawing a double length of thirty gauge constantan wire into an 0.072" o.d. x 0.052" i.d. stainless steel sheath 8.75" long. An iron constantan thermocouple was located at the midpoint inside the probe. Current measurements of about 0.25 amperes were made at a heater resistance of 4.10 ohms with a resultant energy flux of approximately 0.25 watt. The instrumentation for this probe was the same as that previously described with the following exceptions: A variable DC power supply was used to replace the twelve volt battery and a Westinghouse ammeter replaced the Simpson milliammeter. In both systems, the heater circuits were arranged as shown in figure 2.

A vacuum system used with the above system allowed measurement of the effective thermal conductivities of the porous mixture in dry air and carbon dioxide at various levels of pressure from atmospheric to 1.25 mm Hg absolute.

[2] Figures in parentheses indicate the literature references at the end of this paper.

3. Samples

The particulate materials selected for use in this study were steel shot and glass shot. These materials were selected because of (a) the difference in the effective thermal conductance of the pure particulate systems, (b) their suitability as typical particulate materials.

Table 1 shows the suppliers and particle sizes. Mixtures of 0, 25, 50, 75, and 100 per cent steel shot (by volume) were made using a laboratory constructed spouted bed mixer. A ten hour mixing time was used for all samples.

4. Experimental Procedure

Initially, the sample material whose thermal conductivity was to be measured was inserted into the sample hold (reaction kettle) and vibrated by hand to insure good contact between the probe and sample material. The probe and sample material were then allowed to equilibrate (thermally) for a minimum of eight hours. (When vacuum runs where made the system pressure was then reduced and controlled at the desired pressure level for one to one and one-half hours prior to the measurement of thermal conductivity.) When the sample temperature changed less than 0.1°F, steady state conditions were assumed to have been reached, and a thermal conductivity measurement was made. The initial temperature of the sample was determined, heater power applied and measured, and the time-temperature response was recorded for ten minutes. Gas pressure and heater current were maintained at constant levels throughout the duration of each run.

5. Experimental Design

As previously stated, one purpose of this study was to experimentally determine the general effect of mixing on the effective thermal conductivities of porous beds of dissimilar solids. Mixtures of glass shot and steel shot were prepared at 0, 25, 50, 75, and 100 per cent concentrations by volume. Each of the above mixtures was blended for ten hours using a spouted bed mixer in an effort to get uniform mixtures. The average effective thermal conductivities of these mixtures were evaluated at ten levels of pressure (from atmospheric to 1.25 mm Hg) in dry air and in carbon dioxide at room temperature. The average effective thermal conductivities were obtained by averaging together the effective thermal conductivities taken at three points in the mixture.

6. Results

Comparison of the thermal conductivity probe made at the Univ. of Pittsburgh Chemical Engineering Laboratory and laboratory-type commercially available probe was carried out prior to conducting the runs on the glass shot-steel shot mixtures. Thermal conductivity values obtained with the two probes were identical, and extremely reproducible. The reproducibility of the more rugged probe is estimated to be approximately 0.2 per cent.

Tables 2 and 3 show the experimental average effective thermal conductivities obtained in this study, and compares the experimental values with values calculated from:

$$k_{eff,\ mixture} = \psi_1 k_{eff,s1} + \psi_2 k_{eff,s2}$$

where,

$k_{eff,\ mixture}$ = effective thermal conductivity of the mixture.

$k_{eff,s1}$ = effective thermal conductivity of solid material 1.

$k_{eff,s2}$ = effective thermal conductivity of solid material 2.

ψ_1, ψ_2 = volume fractions of solid materials 1 and 2 respectively.

It should be noted that this equation allows calculation of the volume fractions of each component in a binary system provided experimental values for $k_{eff,\ mixture}$, $k_{eff,s1}$, and $k_{eff,\ s2}$ are known.

From the experimental data, it is observed that the pressure of the interstitial gas affects the effective thermal conductivity of each of the pure particulate components. There is a range of pressures for which the effective thermal conductivity is very nearly constant. Below this range, the thermal conductivity decreases rapidly as the pressure is reduced toward zero. This breakaway pressure for constant conductivity is different for different gases. For glass and steel in dry air at 26°C, this pressure as shown on figure 3 is approximately 225 mm Hg. On figure 4, for the same conditions except that the interstitial gas is carbon dioxide instead of dry air, the breakaway pressure is about 125 mm Hg.

The observed effects of pressure can be explained by the kinetic theory of gases. For the range where the pressure has no effect on thermal conductivity, the mean free path of the gas molecules is small compared with the distances between the particles which are effective in transferring heat. For the long mean free paths which occur at low pressures, the thermal conductivity varies with pressure. Deissler and Eian (5) have developed equations which indicate that the pressure at which effective thermal conductivity begins to vary with pressure (breakaway pressure) is a function of the Knudsen number, and further, the effective thermal conductivities of powders become nearly independent of pressure at same ratio of mean free path of gas molecules to a characteristic dimension of the powder particles.

7. Conclusion

The thermal conductivity probe method is a highly reproducible and accurate technique for the measurement of the effective thermal conductivity of porous beds of solid particles. The average effective thermal conductivity of a mixture of unconsolidated dissimilar solids is closely approximated by the weighted average effective thermal conductivity calculated using the volume fractions and the effective thermal conductivities of the pure components under the same conditions.

8. Acknowledgment

The work described herein was carried out for the Applied Research Laboratory of the United States Steel Corporation under Research Contract No. 5639.

9. References

(1) Wechsler, A. E. and Kritz, M. A., Development and use of thermal conductivity probes for soils and insulations, Summary report prepared by Arthur D. Little, Inc., for the U.S. Army Cold Regions Research and Engineering Lab under Contract No. D.A-27-021-AMC-25(X), (1965).

(2) D'Eustachio, D and Schreiner, R. E., A study of a transient heat method for measuring thermal conductivity, Trans. of the Amer. Soc. of Heat. and Vent. Engrs., 58, 333-339, (1952).

(3) Woodside, W. and Messmer, J. H., Thermal conductivity of porous, media. I. unconsolidated sands, Jour. of Appl Phys., 32, 1688-1699, (1961).

(4) Carslaw, H. S. and Jaeger, J. O., Conduction of heat in solids. Oxford: Oxford University Press, (1959).

(5) Deissler, R. G. and Eian, C. S., Investigation of effective thermal conductivities of powders, NACA Research Memorandum E52C05, (1952).

Table 1. List of Particulate Materials.

Material	Average Particle Diameter	Manufacturer
Type 405, Glass IV, Microbeads	306 microns	Microbeads, Inc., Jackson, Miss.
Size S-70 Steel Shot	334 microns	Pangborn "Rotoblast", The Pangborn Corp., Hagerstown, Md.

Table 2
Thermal Conductivities of Mixtures
System I: Steel Shot-Glass Shot Mixtures in Dry Air at 26°(±3°)C.

Pressure (mm Hg)	Eff. Thermal Cond. (k_{s1}) of pure steel system shot (BTU/hr (°F/in)ft^2)	% steel in mixture (vol)	Eff. Thermal Cond. (k_{s2}) of pure glass shot system (BTU/hr (°F/in)ft^2)	Eff. Thermal Cond. (k_{eff}) based on vol. fractions in mixture (BTU/hr (°F/in)ft^2)	Average effective thermal conductivity (observed)
		75%		1.78	1.81
730	1.92	50%	1.38	1.65	1.67
		25%		1.51	1.53
		75%		1.78	1.80
350	1.92	50%	1.38	1.65	1.68
		25%		1.51	1.51
		75%		1.78	1.74
225	1.92	50%	1.38	1.65	1.70
		25%		1.51	1.51
		75%		1.64	1.64
150	1.74	50%	1.34	1.54	1.55
		25%		1.44	1.46
		75%		1.52	1.52
75	1.60	50%	1.28	1.44	1.46
		25%		1.36	1.32
		75%		1.39	1.39
50	1.45	50%	1.22	1.33	1.35
		25%		1.28	1.29
		75%		1.15	1.17
25	1.18	50%	1.04	1.11	1.10
		25%		1.08	1.08
		75%		0.865	0.860
10	0.853	50%	0.902	0.877	0.880
		25%		0.889	0.901
		75%		0.478	0.490
3	0.400	50%	0.711	0.555	0.564
		25%		0.633	0.653
		75%		0.357	0.370
1.25	0.285	50%	0.572	0.428	0.450
		25%		0.499	0.556

Table 3

Thermal Conductivities of Mixtures

System II: Steel Shot-Glass Shot Mixtures in Carbon Dioxide at 26°(±3°)C.

Pressure (mm Hg)	Eff. Thermal Cond. (k_{s1}) of pure steel system shot (BTU/hr (°F/in)ft^2)	% steel in mixture (vol)	Eff. Thermal Cond. (k_{s2}) of pure glass shot system (BTU/hr (°F/in)ft^2)	Eff. Thermal Cond. (k_{eff}) based on vol. fractions in mixture (BTU/hr (°F/in)ft^2)	Average effective thermal conductivity (observed)
		75%		1.18	1.18
730	1.24	50%	1.03	1.13	1.16
		25%		1.08	1.07
		75%		1.18	1.32
350	1.24	50%	1.01	1.12	1.14
		25%		1.07	1.06
		75%		1.18	1.20
225	1.24	50%	1.01	1.12	1.13
		25%		1.07	1.04
		75%		1.18	1.19
150	1.24	50%	1.00	1.11	1.23
		25%		1.06	1.10
		75%		1.16	1.15
75	1.23	50%	0.950	1.09	1.10
		25%		1.02	1.02
		75%		1.04	1.06
50	1.09	50%	0.890	0.988	0.990
		25%		0.958	0.961
		75%		0.813	0.810
25	0.837	50%	0.745	0.791	0.816
		25%		0.767	0.774
		75%		0.646	0.665
10	0.653	50%	0.625	0.639	0.633
		25%		0.632	0.627
		75%		0.411	0.403
3	0.355	50%	0.580	0.468	0.475
		25%		0.524	0.517
		75%		0.396	0.385
1.25	0.341	50%	0.560	0.451	0.435
		25%		0.505	0.526

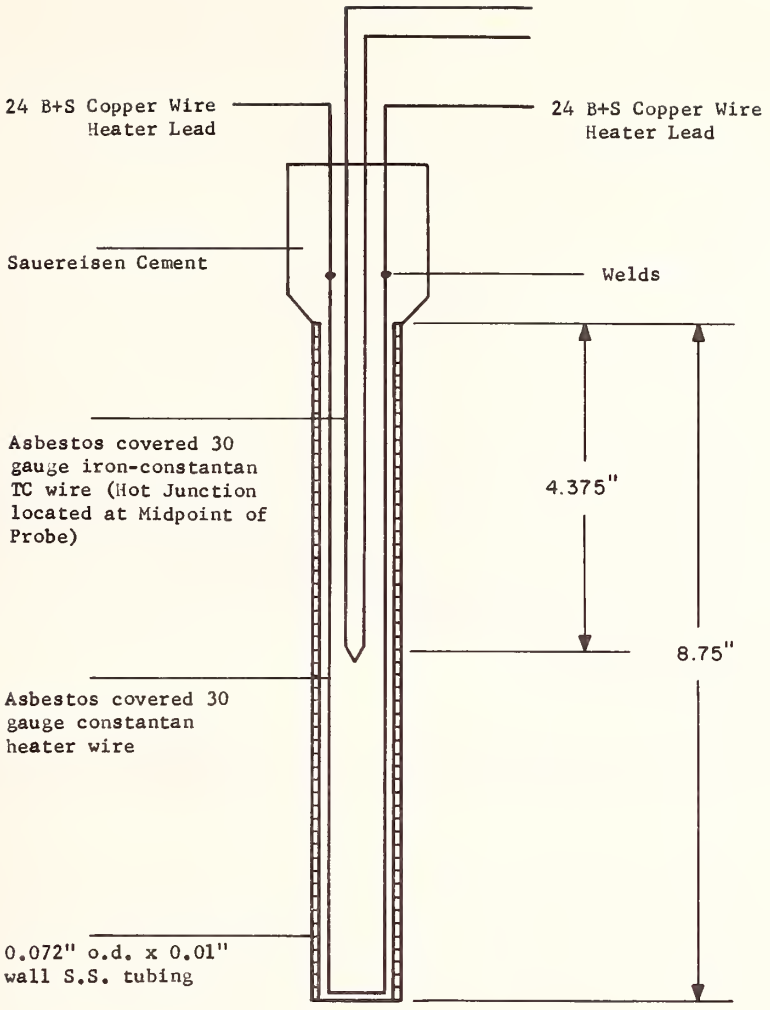

Figure 1. Schematic diagram of thermal conductivity probe constructed at the University of Pittsburgh.

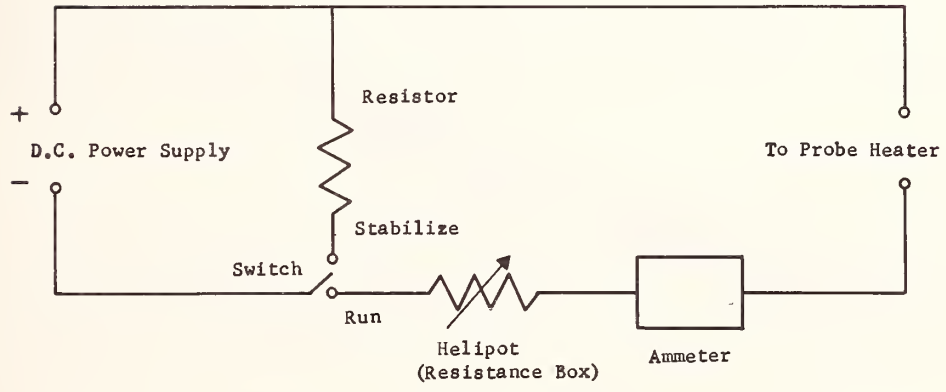

Figure 2. Schematic diagram - probe heater circuit.

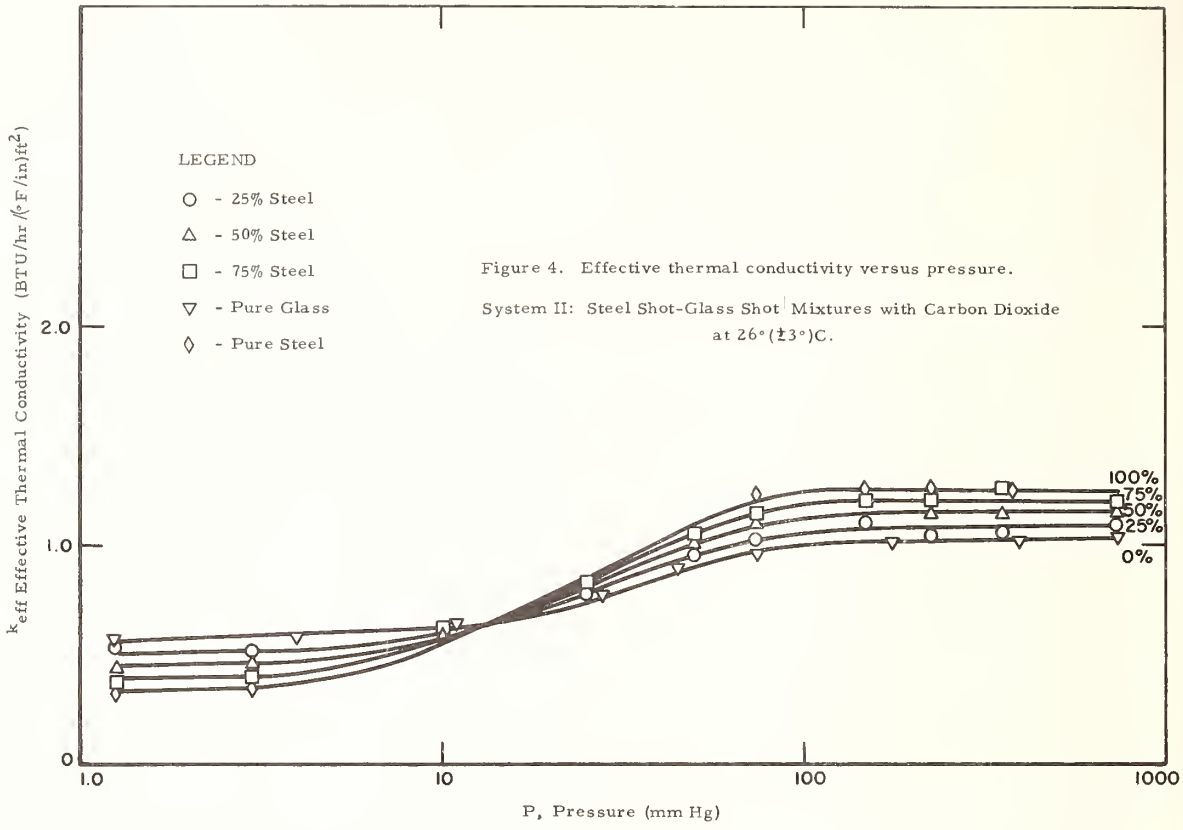

Figure 4. Effective thermal conductivity versus pressure.

System II: Steel Shot-Glass Shot Mixtures with Carbon Dioxide at 26°(±3°)C.

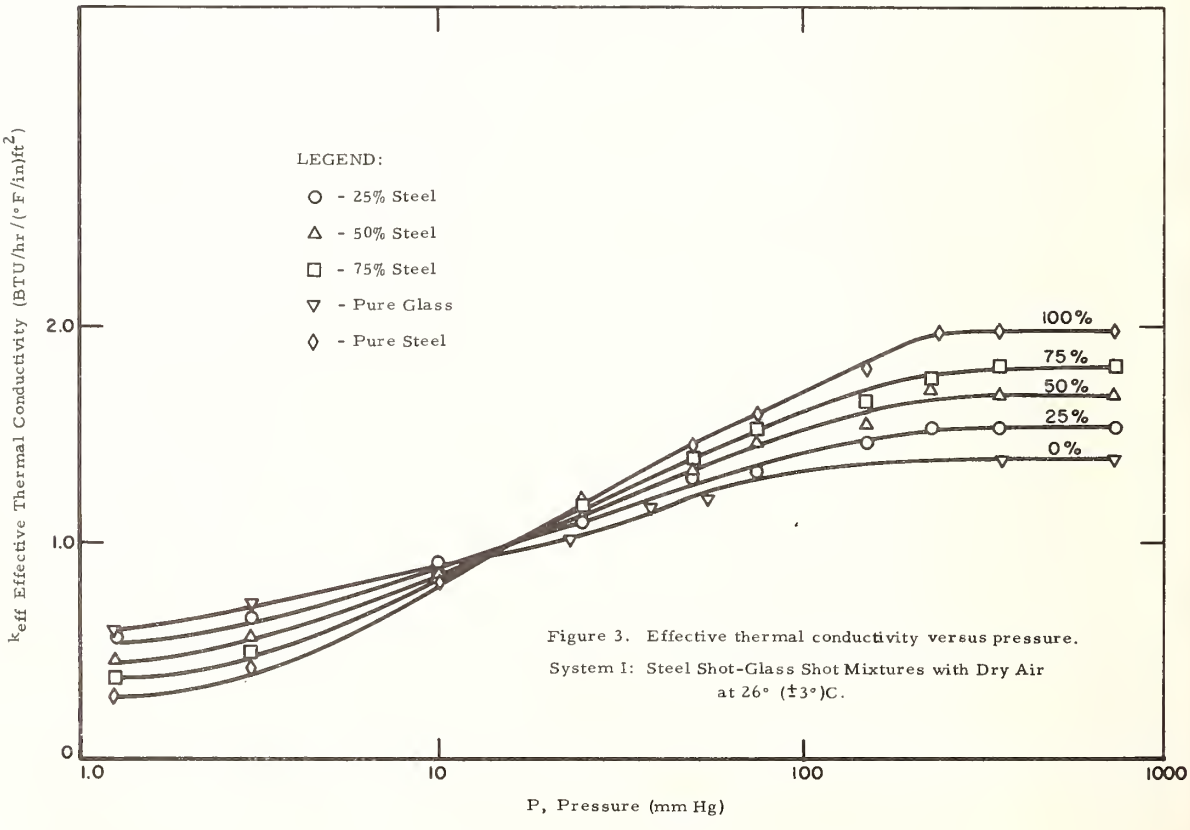

Figure 3. Effective thermal conductivity versus pressure.

System I: Steel Shot-Glass Shot Mixtures with Dry Air at 26° (±3°)C.

Thermal Conductivity Measurements on a Fibrous Insulation Material

R. R. Pettyjohn

General Dynamics Corporation
Convair Division
San Diego, California

Apparent thermal conductivities of a high temperature fibrous insulation were determined as a function of temperature, pressure, and density. These measurements were conducted in an air atmosphere at various pressures from 10^{-2} to 760 mm Hg, and mean temperatures from 400° to 800°K. Specimen densities were varied from 55 to 149 kg/m^3. The data obtained from these measurements were analyzed to determine the various modes of heat transfer. The modes investigated were radiation, gaseous and fiber conduction, convection, and improved conduction between the individual fibers due to the presence of the gaseous medium. The apparent thermal conductivity-density products ($K\rho$) were determined for each density and subsequently compared. The scattering cross-sections per unit volume were also determined as a function of density.

Key Words: Conductivity, fibrous insulation, heat transfer, insulating materials, insulation, scattering cross-sections, thermal conductivity, thermal conductivity-density products, thermal insulation.

1. Introduction

Many of the advanced re-entry and hypersonic cruise vehicles will be exposed to a more severe thermal environment than normally encountered by those of today. Most of these future vehicles will also be required to make multiple missions. Therefore, their thermal protection systems will be required not only to provide higher temperature capabilities, but also to withstand these environments repeatedly. In order for such a system to be developed, a survey was conducted to determine what type of insulation would best meet these requirements. The fibrous insulations were found to offer the greatest potential. Unfortunately, no single insulation provided its best thermal protection capabilities over the entire anticipated temperature range.

In general, the thermal physical properties of insulating materials are sacrificed as the temperature capabilities are increased. For example, if a higher maximum continuous use temperature is desired, an insulating material with a higher conductivity and density is normally required. In order to overcome this penalty, the designer can use a composite insulation system. That is, various types of insulations are selected to meet the thermal environment within the composite system. Consequently, not all insulating materials must withstand the maximum environmental temperature, but each must be capable of being an effective insulator over the temperature range at which it will be exposed. Therefore, a thermal insulating system can be optimized by using the more effective lower temperature insulations in the cooler portions of the composite. The evaluation of these lower temperature or back-up insulations was the main objective of this program.

From an earlier phase of this program, the weight and dimensional stabilities of each insulation was determined over the anticipated temperature range. The most promising back-up insulation, a fibrous silica blanket, was then selected for this phase of the program. In general, the manufacturers provided adequate conductivity data on their insulations in one atmosphere of air. However, they had very little data on their insulations when exposed to various partial vacuums. Normally, it is desirable for the designers of aerospace vehicles to take advantage of the improved thermal conductivities of these insulations in a space environment. Therefore, this phase of the program was to determine the apparent conductivities of the selected insulation at various reduced pressures, mean temperatures, and bulk densities.

The following equations were used to determine the gaseous conduction contribution at all the temperatures and pressures evaluated:

$$\left(\frac{K_p}{K_{P_o}}\right)_T = \frac{1}{1 + \frac{P_o L_{go}}{P\,d}\left(\frac{T}{T_o}\right)^{n+0.5}} = \frac{1}{1 + P'} \tag{1}$$

$$d = \frac{\pi D}{4 f} \tag{2}$$

Where:

$\left(\frac{K_p}{K_{P_o}}\right)_T$ = the ratio of the gaseous conduction at the environmental pressure and temperature to that of the gaseous medium at standard conditions,

P_o = standard pressure, 760 mm Hg.,

P = environmental pressure,

L_{go} = standard mean free path length,

T = standard temperature, 273°K. (492°R.),

T_o = environmental temperature,

n = property constant of gas (air = 0.754),

d = calculated pore size, defined by eq. (2),

D = fiber diameter, 1.3 microns,

f = ratio of bulk density to theoretical density.

The convection and/or improved fiber conduction, as represented by the increment C in figure 5, was also calculated with the aid of these gaseous conduction parameters since both were considered to be proportional to the number of gas molecules present at the various reduced pressures.

Next, the conductivities contributed by the residual gaseous medium, the individual fibers, and radiation were considered. From the above calculations, the residual gas contribution at 0.01 mm Hg. was found to be virtually zero. The fiber conduction was also found to be negligible at these densities Typical conduction values were found to be 0.0002, 0.0003, and 0.0005 W $m^{-1}deg^{-1}$ for densities of 55, 98, and 149 kg/m^3, respectively. The solid conduction of silica was found not to change appreciably over the temperature range investigated (400° to 800°K). Therefore, the radiation contributions can be obtained directly from figures 2, 3 and 4. Total calculated conduction contributions were then compared with the experimental data as shown in figure 6. The primary deviations between the experimental and calculated conductivities occurred at the intermediate pressures (3 to 29 mm Hg. range). This was expected since the greatest rate of change in the apparent conductivity occurred when the pressure at which the mean free path length of the gaseous medium contained within a fibrous insulation equaled the mean interfiber spacing.

From eq (1) and the discussion above, the pore size, the conductivity of the gaseous medium, and the mean free path length of the medium appear to be the primary controlling factors of the gaseous conduction contributions at these intermediate pressures. Therefore, the accuracy at which any one of these factors is determined has a definite influence upon the calculated conductivity. It is fortunate that such a questionable ratio between the mean free path length and the pore size can exist and still produce a reasonably accurate calculated gaseous conduction contribution. The primary reason for this accuracy is that the ratio is contained in the P' portion of eq (1) and, consequently, does not influence the calculation proportionately. The thermal conductivity of the gaseous medium, however, is directly proportional, but fortunately has been verified by several investigators and is assumed to be reasonably accurate.

Another series of curves can be generated by combining the data represented in figures 5 and 6. This series is represented by figure 7. These curves show each conduction contribution as a function of temperature. Figure 7 illustrates how each conduction contribution is related to the mean temperature of the specimen while being exposed to a particular environmental pressure. In this case, the pressure is at one atmosphere. As the pressure is reduced, the gaseous conduction contributions are diminished

2. Experimental Procedure and Equipment

The thermal conductivity measurements were conducted with the aid of a radial heat flow apparatus. Figure 1 shows the basic construction of the unit and one of its four automatic temperature control systems for the guard heaters. The apparatus consists of essentially two concentric ceramic cores that were heated by six wire wound, resistance heating elements. The inner elements on each core were used to provide the temperature gradient across the test specimen, while the remaining four elements were used to minimize any axial heat flow from the central test section.

The basic operation of each guard heater system was as follows: whenever a temperature difference existed between the central and guard heaters, a small D.C. voltage was generated by the series connected differential thermocouples. This voltage was detected by a highly sensitive moving-coil, reflecting-type galvanometer. The voltage applied to the galvanometer caused its suspended mirror to rotate. With the light beam source focused onto this mirror, its rotation was greatly amplified by the deflection of the light beam. When the light beam was deflected onto the light sensitive resistor, the current flow through the resistor was greatly increased. The resulting current flow was fed directly into the D.C. transistor amplifier. The power output of the amplifier was proportional to the resistance change of the light sensitive resistor. This power was fed directly to its corresponding guard heater. Therefore, each system essentially maintained its guard heater at the same temperature as their central heater. Each central heater received its electrical power from a variable direct current power supply that was usually set at a fixed level at the beginning of the test. Temperature gradients of 15°K/cm were normally established through the specimen at each mean temperature. The thickness of the specimen was slightly less than 6 cm. Its length was 28 cm.

The conductivity measurements were conducted in a large test chamber that was sealed and evacuated to the desired pressure level. After each of the desired pressure and temperature equilibriums were reached, the respective thermal conductivities were computed and recorded.

3. Discussion and Results

The results of the apparent thermal conductivity measurements are graphically illustrated in figures 2, 3, and 4. The measurements were conducted in an air atmosphere at various pressures from 10^{-2} to 760 mm Hg., and mean temperatures from 400° to 800°K. The specimen densities were varied from 55 to 149 kg/m^3. Figure 5 represents a reasonable approximation of the various conduction contributions to the apparent conductivities of the fibrous silica blanket at a mean temperature of 778°K (1400°R). Similar curves can also be generated to represent these contributions at each of the mean temperatures and densities evaluated. From this figure, increment D is the major contributor to the total heat transfer. This indicated that the gaseous medium within the highly porous structure of the insulation had a considerable influence upon its apparent conductivity at atmospheric pressure. This was expected because the void volume of all the insulations evaluated exceeded 90 percent.

Normally, pressure has very little influence upon the thermal conductivity of an unconfined gaseous medium, because with any change in pressure, the density of the molecules will change proportionally, while their path length changes inversely, yielding essentially a constant heat transfer. Therefore, a gas contained within a fibrous insulating material reacts very similarly to an unconfined gas near atmospheric pressures, because the fiber spacing (or apparent pore size) is normally much larger than the mean free path of the gas molecules. However, as the pressure of the gaseous medium is reduced, the mean free path length of the molecules will increase until it reaches the average diameter of the pore size. As the pressure is reduced further, intermolecular collisions will occur less, while the molecular to fiber collision will occur more often. At the very low pressures where the mean free path is much larger than the pore size, the number of molecules available to transport heat is once again proportional to any further decrease in pressure. Therefore, as the number of molecules approaches zero, the conductivity due to gaseous medium also approaches zero. Thus, the typical "S" shaped curve is obtained when the apparent thermal conductivity of a fibrous insulating material is measured as a function of pressure. From figure 5, it should also be noted that the thermal conductivity values appear to be asymptotically approaching a minimal value at the lower pressures. This remaining conduction is primarily due to radiation and, to a minor extent, residual gas conduction and solid conduction of the individual fibers. This amount is represented by A. Increment B represents the conductivity contribution of the air medium. This quantity must be corrected to allow for the volume occupied by the glass fibers. It should be noted that the sum of A and B does not equal the apparent conductivity of the insulation at atmospheric pressure. Other investigators have noted this difference, C, and attribute it to convection and/or improved conduction between the individual fibers due to the presence of the environmental gas. At this time, it should be noted that a theoretical approach to analytically develop an "apparent" thermal conductivity requires a simultaneous solution of all the above-mentioned modes, because each mode is dependent upon the temperature gradient which is controlled by the total heat transfer. However, for this study, it was assumed that an analytical expression could be developed for each mode independent of the others, and that the apparent thermal conductivity would be the sum of the conductivities of each mode.

until only the radiation contributions remain. A plot of the radiation contributions shows them to be decreasing as the density of the specimen is increasing (see figure 8). This reduction in radiation was primarily attributed to the increasing scattering characteristics of the denser insulations. The scattering cross sections were calculated from the radiation contribution of the above thermal conductivity measurements. Since the absorption cross section has been shown to be two orders of magnitude less than the scattering cross section, it was omitted from the general equation, leaving the following modified equation for making these calculations:

$$N = \frac{4 \sigma J^2 Tm^3}{K_r}, \qquad (3)$$

Where:

N = scattering cross section per unit volume, m^{-1}

K_r = radiation contribution, W $m^{-1} deg^{-1}$,

J = index of refraction of silica,

σ = Stefan-Boltzmann constant,

Tm = mean temperature, °K.

The results obtained from these calculations are shown in figure 9. The scattering cross sections were found to increase with increasing temperature and density.

Since weight is of primary importance in the design of a flight vehicle, the product of the conductivity and density ($K\rho$) is often used in the aerospace industry to determine the thermal efficiency of an insulation system. These products were determined at the various temperatures, pressures, and densities. With the aid of figures 10 and 11, the density at which the insulation is the most efficient can be selected for the anticipated environmental condition. For example, if the temperature of the environment is approximately 780°K and exists at an altitude where the pressure is below 10 mm Hg., the insulation with a density of 149 kg/m3 has a lower $K\rho$ product than either of the lower density insulations. Therefore, the thermal efficiency of the 149 kg/m^3 insulation at this particular environmental condition exceeds either of the other densities investigated. At pressures down to at least 10 mm Hg., the rate of decline in $K\rho$ of the 149 kg/m^3 insulation exceeded the others. This appears to be due to the rate of reduction in the gaseous conduction contribution, because the rate will increase to a maximum as the mean free path length approaches the pore diameter. However, the lower $K\rho$ values at pressures below 10 mm Hg. appear to be related to the radiation attentuation characteristics and its relationship with the size of the fiber (or the apparent pore size resulting from the small fiber diameter). It is recommended that this characteristic be investigated more thoroughly. This is a very interesting characteristic, because if the thermal efficiencies of two insulations at different densities are almost equal, the one with the greater density should be selected. Normally, it will be easier to install and should provide a more reliable composite insulation system.

4. Conclusions

Gaseous conduction and radiation were found to be the major contributors to the total heat transfer through the fibrous silica insulation in one atmosphere of air at mean temperatures from 400° to 800°K, and bulk densities from 55 to 149 kg/m^3. In a partial vacuum of 10^{-1} mm Hg. or less, radiation became the only major contributor. At the intermediate pressures, 3 to 29 mm Hg., the gaseous conduction contributions were found to be reduced to approximately half of those obtained at one atmosphere. An increase in the specimen density (from 55 to 149 kg/m3) was found to yield a substantial decrease in the total heat transfer through insulating materials of this type. The primary reduction was found to result from the large decrease in the radiation contribution.

The thermal conductivity-density products ($K\rho$) were found to be lower than expected. At the intermediate pressures (14 mm at 780°K), the insulation with a density of 149 kg/m^3 was found to have a higher thermal efficiency (lower $K\rho$) than any of the insulations evaluated. From a practical viewpoint, the higher density insulation would reduce the handling difficulties normally encountered during the assembly of an insulation system. Also, for a vehicle requiring a sizeable insulation system, the bulk volume of the vehicle would be reduced considerably.

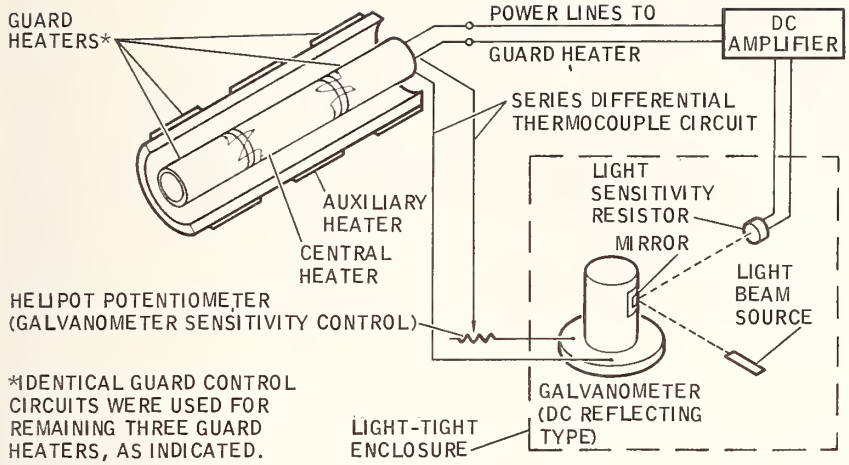

Figure 1. Guard heat control system.

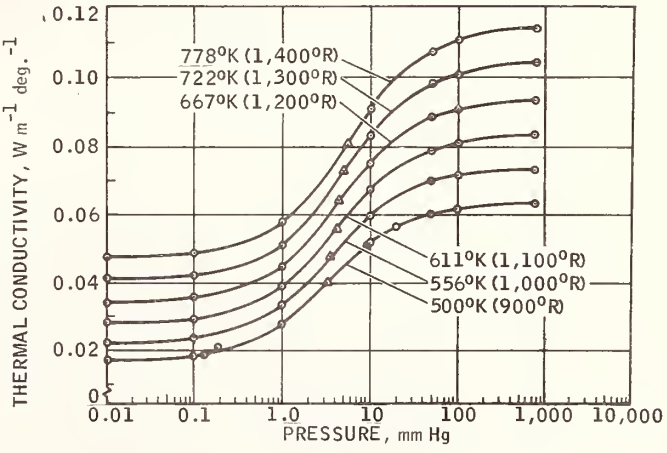

Figure 2. Apparent thermal conductivity of a fibrous silica insulation at various environmental pressures and mean temperatures (density = 55 kg/m^3).

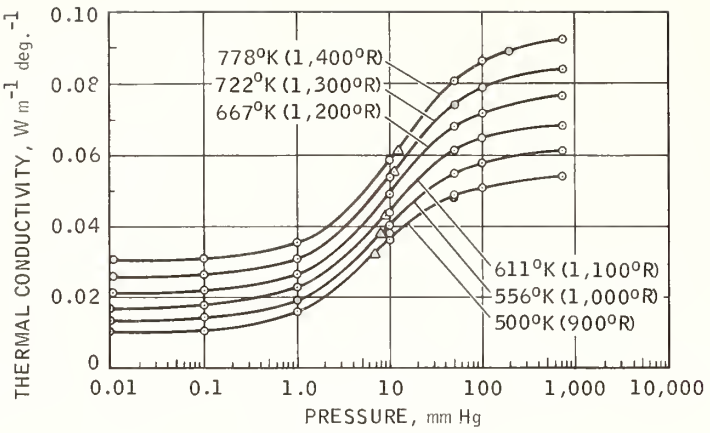

Figure 3. Apparent thermal conductivity of a fibrous silica insulation at various environmental pressures and mean temperatures (density = 98 kg/m^3).

Figure 4. Apparent thermal conductivity of a fibrous silica insulation at various environmental pressures and mean temperatures (density = 149 kg/m^3).

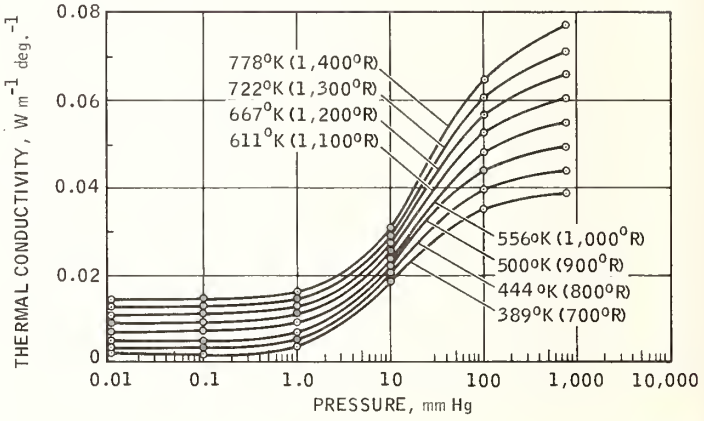

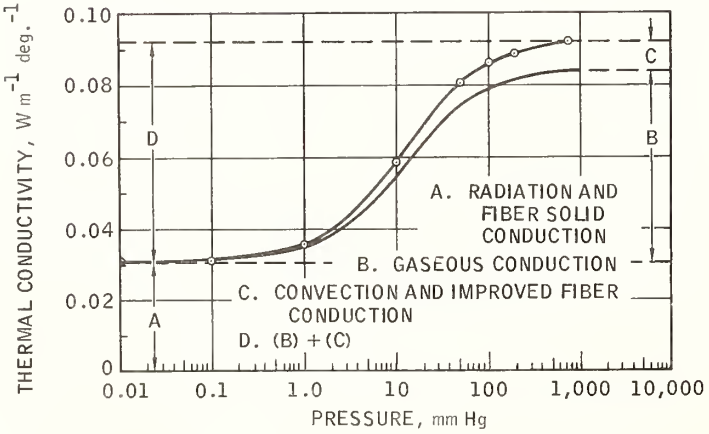

Figure 5. Accumulative conduction contributions to the apparent thermal conductivity of a fibrous silica insulation in an air atmosphere at various environmental pressures. (Mean temperature = 780 °K and density = 98 kg/m^3).

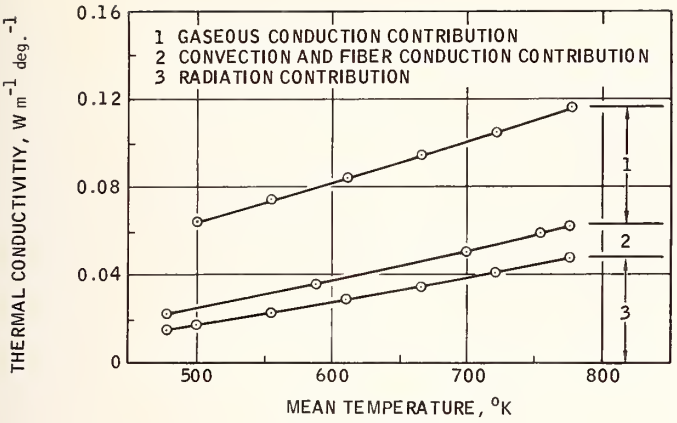

Figure 6. Thermal conductivity of a fibrous silica insulation at various reduced pressures in an air atmosphere, (Density = 55 kg/m^3).

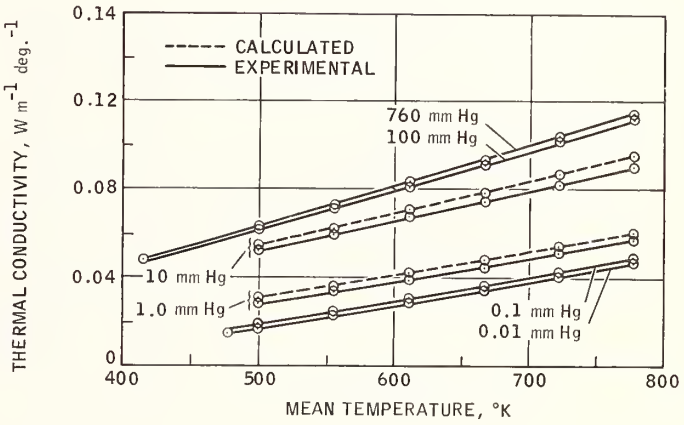

Figure 7. Accumulative conduction contributions to the apparent thermal conductivity of a fibrous silica insulation in one atmosphere of air (density = 55 kg/m^3).

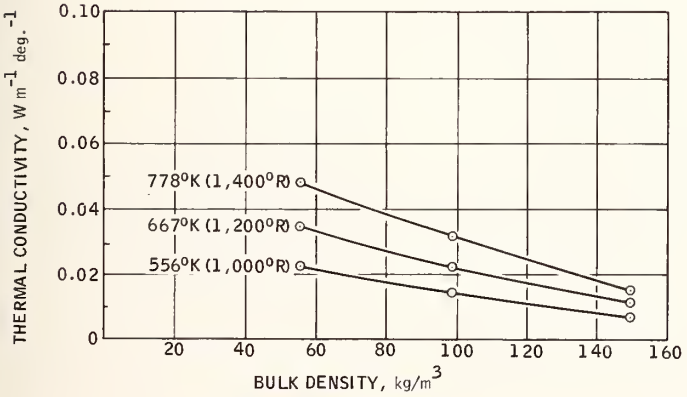

Figure 8. Radiation contributions for various densities of the fibrous silica insulation.

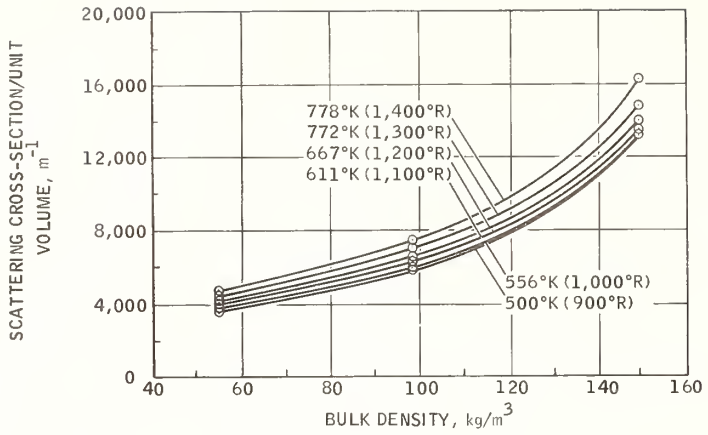

Figure 9. Scattering cross section of the fibrous silica insulation at various densities.

Figure 10. Thermal conductivity-density products of the fibrous silica at various environmental pressures and bulk densities in an air atmosphere (mean temperature = 500 °K).

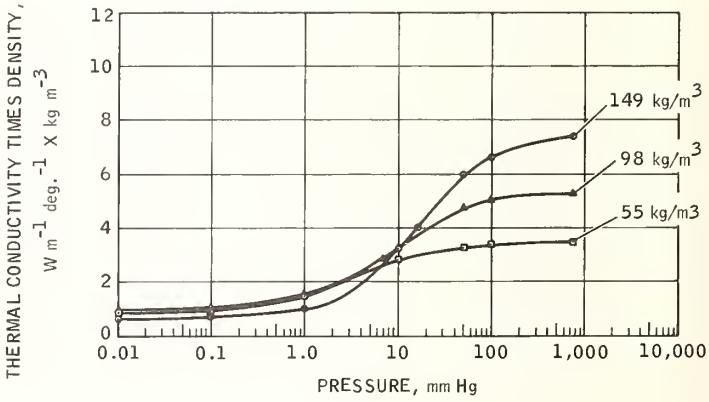

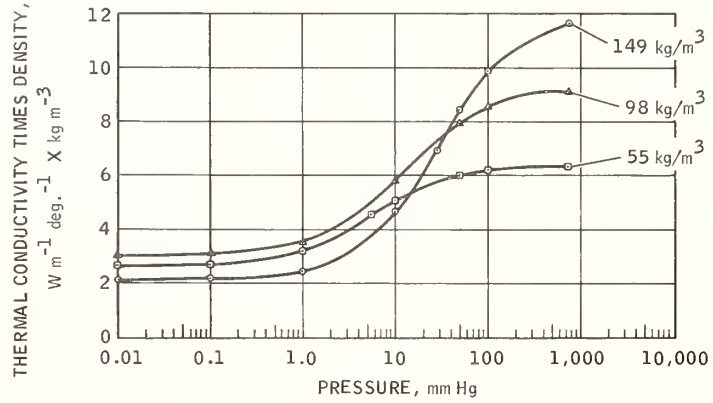

Figure 11. Thermal conductivity-density products of the fibrous silica at various environmental pressures and bulk densities in an air atmosphere (mean temperature = 780 °K).

The Effect of Thickness and Temperature on Heat Transfer through Foamed Polymers

T.T. Jones[1]

Rideal Research Laboratories
Monsanto Chemicals Limited
Corporation Road
Newport, Monmouthshire
Great Britain.

The mode and extent of heat transfer through polymer foams is difficult to define. While it is relatively easy to eliminate convection effects by choosing sufficiently small cell sizes there is still left the apportioning of the heat transferred between the modes of conduction and radiation. This proportion is a function of the temperature of the determination, the thickness of the sample, its density and its cell size.

The apparent thermal conductivity of plane horizontal layers of still air confined between parallel surfaces of varying emissivity is shown to increase with thickness of the air layer, its temperature and the emissivity of the surfaces. This is due to the varying relative effects which the radiated and conducted heat have on the total heat transfer.

Similarly a study of foamed polystyrenes of varying density and cell size at different temperatures and thickness shows similar trends to those observed with air layers. The apparent conductivity increases with thickness and temperature but tends to level off with thickness due to the absorption of the radiated heat by the polymer. The influence of the emissivity of the confining surfaces is also not as important as for air layers due to the polymer cell walls adjacent to the surface acting as emitters and absorbers of radiation.

Using, as a first approximation, a theoretical model for the foam based on a series of parallel alternate polymer and air layers at right angles to the direction of heat flow, it is possible to arrive at an estimate of the distance apart of such hypothetical layers and relate it to density and cell size. Low density and large cell size combine to produce high radiation components and increase in distance apart of the hypothetical layers.

Key Words: Apparent thermal conductivity, cell size, convection, emissivity, foam density, heat transfer, polymer foams, polystyrene foams, thermal conduction, thermal conductivity, thermal radiation.

1. Introduction

It is relatively easy to define and understand what is meant by the thermal conductivity of a simple gas, liquid or solid, and experiments can be devised which give an unambiguous estimate of the quantity desired. In the case of gases in particular considerable precautions have to be taken in order to eliminate or correct for the influence of radiation and convection on the determination.

If, however, we are dealing with a composite material such as discrete gas globules embedded in a solid continuous phase then the question arises as to what exactly determines the mode of transference of heat through such a medium. If the gas is distributed haphazardly in cells of varying shapes and sizes then in certain cases it is quite certain that part of the heat transmitted through such a medium is carried by convection currents. The simplest way to eliminate this effect is to reduce the size of the cells so as to limit the gas circulation.

---

[1] Research Scientist.

It is not so easy however tc eliminate the effect of radiated heat. Moreover, the proportion of heat transmitted by radiation to that by conduction varies with the mean temperature of the determination, the thickness of the sample, its density, its cell size and the nature of the surfaces which are in contact with those of the sample. It follows therefore that if convection is eliminated by reducing the cell size sufficiently then the total heat conducted, namely the apparent conductivity of the material, is also dependent on the above parameters.

It is the purpose of this paper to demonstrate the above effects for a number of foamed polystyrene examples, whose cell size is small enough to eliminate the effect of convection.

2. Apparatus and Materials

2.1. Apparatus

The apparatus used for the measurements consists of a heat flow meter constructed by Technisch Physische Dienst T.N.O. en T.H. Delft and described by J. de Jong and L. Marquenie (1)[2]. This method was originally described by D.L. Lang (2) and has been shown to give results which correlate well with those of the guarded hot plate, e.g. see J.M. Buist, D.J. Doherty and R. Hurd (3).

The heat flow meter of dimensions about 5 cm diameter and 0.32 cm in thickness is placed in the cut-out centre of a 25 cm x 25 cm P.V.C. guard of the same thickness. The test specimen is divided into two 25 cm x 25 cm square specimens of equal thickness which are placed above and below the heat flow meter assembly. The hot source is placed on top of this arrangement and the cold sink below. Both hot source and cold sink consist of plates 22.5 cm in diameter forming part of circulating thermostated water systems respectively controlled to any desired temperature between 5°C and 75°C $\pm$ .05 deg. The thickness of the hot source and cold sink are about 2.5 cms respectively and are encased, except for the working surfaces, in 7.5 cm deep polymer foam lagging. The whole apparatus is enclosed in an air thermostat controlled at the mean temperature of the determination.

The heat flow meter output in milli volts measures the heat flux through the system, the calibration factor being 14.47 $W\,m^{-2}$ per mV at 20°C. This factor decreases by 1% for each 10 deg. increase in temperature above 20°C.

2.2. Materials

Three polystyrene foams were studied in this investigation, namely Samples A, B and C.

Sample A was of average density 20.1 Kg/m^3 and contained cells of widely varying cell size from very fine to very large as is shown in figures 1 and 2. Some cells were over 1 mm in maximum dimension.

Sample B was of average density 15.2 Kg/m^3 and contained a narrower distribution of smaller cell sizes as shown in figure 3.

Sample C was of average density 28.7 Kg/m^3 . . The distribution of cells was rather like sample B, but with slightly smaller cells and thicker cell walls, as shown in figure 4.

3. Heat Transfer through Plane Layers of Air

In order to understand why the apparent conduction of heat through foamed polymers is so dependent on temperature, thickness, density etc. the question of the apparent conductivity of plane layers of still air is first considered.

If a layer of still air is enclosed between two infinite parallel planes 1 and 2 composed of materials of emissivity ϵ_1 and ϵ_2 and reflectivities $(1 - \epsilon_1)$ and $(1 - \epsilon_2)$ at absolute temperatures T_1 and T_2 respectively then it can be shown (e.g. see Poltz (4)) that the flux of radiant heat per square metre, Q_R passing from plane 1 to plane 2, providing the intervening air does not absorb any of this heat, is given by

$$Q_R = \frac{\sigma\,\epsilon_1\epsilon_2}{\epsilon_1 + \epsilon_2 - \epsilon_1\epsilon_2}\left(T_1^4 - T_2^4\right), \qquad (1)$$

where σ is Stefan's constant = 5.67×10^{-8} $W\,m^{-2}\,deg.^{-4}$

If the distance apart of the two planes is x and the mean thermal conductivity of the air in the layer is λ_{mean} i.e. the conductivity at the mean temperature of the layer, then, provided that the difference in temperature $(T_1 - T_2)$ is not more than say 10 to 15 deg. the flux of conducted heat per square metre, Q_C, is given to a very close approximation by

[2]Figures in brackets indicate the literature references at the end of this paper.

$$Q_c = \frac{\lambda_{mean}(T_1 - T_2)}{x} \quad (2)$$

Hence the total heat flux per square metre Q_T is given by

$$Q_T = Q_R + Q_C = \frac{\sigma \epsilon_1 \epsilon_2}{\epsilon_1 + \epsilon_2 - \epsilon_1 \epsilon_2}(T_1^4 - T_2^4) + \frac{\lambda_{mean}(T_1 - T_2)}{x} \quad (3)$$

The apparent thermal conductivity of the air in the layer, app, is given by

$$\lambda_{app} = \frac{Q_T x}{(T_1 - T_2)} = \lambda_{mean} + \frac{\sigma \epsilon (T_1^4 - T_2^4) x}{2 - \epsilon (T_1 - T_2)} \quad (4)$$

when, for the sake of convenience, $\epsilon_1 = \epsilon_2 = \epsilon$ i.e. the materials of the two plane surfaces have the same emissivity.

It is eq. (4) that explains why the apparent conductivity is a function of the temperature as well as the thickness of the layer.

3.1. The Change in Apparent Conductivity of Still Layers of Air with Thickness

It is expected from eq. (4) that the apparent thermal conductivity of still layers of air will increase linearly with the thickness and the plot will have an intercept which is equal to the thermal conductivity of the air at the mean temperature of the experiment.

The slope of the line will be $\frac{\sigma \epsilon}{2 - \epsilon} \frac{(T_1^4 - T_2^4)}{(T_1 - T_2)}$ and so will become greater as the temperature of the determination increases. If the emissivity of the surfaces enclosing the layer of air is very small, e.g. as for polished silver or aluminium surfaces then the slope will also be very small.

Experiments with still cylindrical layers of air were conducted by separating the hot source and cold sink from the heat flow meter at various distances by means of cylindrical spacers made of polystyrene foam of various thicknesses with holes of internal diameter 15 cms. The surfaces of hot source, cold sink and heat flow meter were first covered with aluminium foil of low emissivity and the heat flux at a mean temperature of 37.5°C with $T_1 - T_2 \simeq 15$ deg. was measured at various thicknesses from 1.25 to 7.5 cm. All surfaces were then covered with a 0.005 cm. thick polystyrene foil and experiments repeated at a mean temperature of 40°C with $T_1 - T_2 \simeq 10$°C and thickness varied from 1.25 to 7.2 cm. Figure 5 shows plots of apparent thermal conductivity against layer thickness for the two kinds of foils used, the differing slopes being due to the differing radiation contributions of the foils. Using the expression for the slope and the experimental values of the slopes gives values of 0.047 and 0.66 for the emissivity of the aluminium and polystyrene foils respectively. The figure of 0.66 may appear low for polystyrene but the foil is highly polished.

The intercept of the lines on figure 2 is virtually the same at approximately 2.7×10^{-2} W m^{-1} deg^{-1} which is quite close to that for air at a temperature of about 40° C.

The apparent increase in thermal conductivity with thickness is clearly due to the radiation contribution.

3.2. The Change in Apparent Conductivity of Still Layers of Air with Temperature

If the thickness of the layer, x, is held constant and the mean temperature of the layer varied but keeping the difference in temperatures of planes 1 and 2 constant i.e. $T_1 - T_2$ = constant, then it can be shown from eq. (4) that

$$\lambda_{app} = \lambda_{mean} + \frac{\sigma \epsilon x}{2 - \epsilon}(4T_{mean}^3 + T_{mean} \Delta T^2) \quad (6)$$

where $T_{mean} = (T_1 + T_2)/2$ and $\Delta T = T_1 - T_2$

For T_{mean} in the region 290 $\longrightarrow$ 350°K and $T_1 - T_2$ about 10 deg. it can be shown that $T_{mean} \Delta T^2$ is

negligible compared with $4T^3_{mean}$ hence

$$\lambda_{app} = \lambda_{mean} + \frac{4\sigma\epsilon x\ T^3_{mean}}{2 - \epsilon} \qquad (7)$$

It is expected that the variation of the apparent thermal conductivity with temperature should be approximated by the above expression.

The apparent conductivity of a still layer of air of thickness 1.23 cms was determined at mean temperatures of 35 to 65°C using aluminium foil on the flat surfaces and $\Delta T \simeq 10^{\circ}C$. In another experiment polystyrene foil was used instead of aluminium foil, the thickness increased to 2.4 cms and temperature varied from 20 to 70°C. The results of these experiments are shown on figure 6 where the apparent conductivity is plotted against temperature.

The marked difference between the effect of polystyrene foils and aluminium foils placed on the flat surfaces is again observed both in the magnitude of the apparent conductivity and the way it varies with temperature.

The dotted line on figure 6 is obtained by calculating the value of the constant $\frac{4\sigma\epsilon x}{2 - \epsilon}$ in eq. (7) from a nominal apparent conductivity at 40°C (T_{mean} = 313°K) namely λ_{app} = 0.106 W m^{-1} deg^{-1} and taking a value of λ_{mean} = 0.0271 W m^{-1} deg^{-1} from the literature. The constant is then used in eq. (7) to calculate values of λ_{app} at other temperatures using the appropriate values of λ_{mean} given in the literature.

The dotted line is a plot of these calculated values and shows a reasonable correspondence between experiment and theory.

It is now possible to consider the apparent thermal conductivity of foamed polymers when temperature and thickness are changed.

4. The Apparent Thermal Conductivity of Foamed Polymers

The problem of the apparent thermal conductivity of foamed polymers has already been recognised and Fischer (5) reviewed the situation quite recently and gave examples of the effect of temperature, thickness, density and emissivity of the surfaces confining the sample. The theoretical basis for the interpretation of these effects is given well by Poltz (4) and the present results will be examined in the light of this theory.

For the thickness studies the polymer foams were studied at thicknesses between 1 and 5 cms on each side of the heat flow meter at mean temperatures of 15, 40 and 65°C with aluminium foils covering the hot source, cold sink and heat flow meter surfaces and a temperature difference of 20 deg. across the full thickness.

The foams were cut into 1 cm or 2 cm thick sheets with a hot wire and the slightly fused surface thus produced removed by rubbing lightly on fine garnet paper. Sample A however was too friable for this preparation of its surfaces and they were left alone. The various combinations of sheets taken to construct any desired thickness were chosen at random.

For the temperature study a fixed combination to give a thickness of 3 cms was chosen and adhered to, and studies were conducted at mean temperatures ranging from 15 to 65°C.

4.1. The Change in Apparent Conductivity of the Three Polystyrene Foams with Thickness

The results obtained with the three foams at different total thicknesses and at three temperatures are given in figure 7.

When these plots are compared with those for still air layers between aluminium surfaces there are two main differences. Firstly, there is a more rapid increase in apparent thermal conductivity with thickness for low thicknesses and secondly this rapid increase diminishes as the thickness increases and appears to level off at some constant value at a sufficiently large thickness.

It is likely that the apparent conductivity at small thicknesses will approach that of the composite, but with a slope smaller than the slope observed due to the influence of the aluminium in reducing the radiation contribution. At large thicknesses the influence of the low emissivity of the aluminium surfaces is clearly not felt.

From experience with air layers the steeper the slope of the apparent conductivity versus thickness plot and the greater the absolute value the greater is the radiation contribution. On this basis it is clear that the radiation component for Sample A > Sample B > Sample C.

The reason for the greater radiation component for Sample A over Sample B of lower density must be associated with its greater cell size causing less scattering of radiation. The cell size of sample C is a little smaller than that of sample B also the cell walls are thicker. Both these effects combine to reduce the radiation component in sample C over that in Sample B.

The difference between the total heat transmitted and the heat conducted i.e. the radiated heat must bear a relationship to both the cell size which influences the scattering of radiated heat and the amount of solid polymer which absorbs it.

The theory given by Poltz (4) combines these two effects. Essentially the foam is considered to be composed of a solid scaffolding composed of very thin parallel layers running at right angles to the direction of heat flow. The layers are supported by parallel layers running at right angles. Each thin layer of emissivity ϵ_L is assumed to absorb a small portion of the heat radiation falling normally on it. The radiation is also scattered by reflection, the reflectivity being $1 - \epsilon_L$.

The system is now replaced by a system of very thin radiation impermeable lamellae parallel to the thin layers and replacing a number n_F of them. These lamellae are at a distance S apart and so

$$S_L = n_F S_F$$ where S_F is the distance apart of the original very thin

parallel layers.

This theory leads to a constant apparent conductivity at very large thicknesses in terms of the actual thermal conductivity of the composite medium and a radiation component.

The theory leads to the following expression for the constant apparent conductivity $\lambda_{app(d\to\infty)}$ at very large thicknesses

$$\lambda_{app\ (d\to\infty)} = \lambda + 4\sigma T^3 \quad \frac{\epsilon_L S_L}{2 - \epsilon_L} \tag{8}$$

where λ is the actual thermal conductivity of the composite medium. This is of exactly the same form as for air layers as given by eq. (7) except that S_L is a constant namely the distance apart of the hypothetical radiation impermeable lamellae.

It is this quantity S_L that is a function of both the density and the cell size. The greater the density and so the greater the absorbed heat the smaller is S_L. Again, the smaller the cell size, the greater the scattering of radiated heat and so the smaller is S_L. The effect of emissivity of the cell walls is given by the $\epsilon_L / (2 - \epsilon_L)$ term. The composite term $\frac{\epsilon_L S_L}{2-\epsilon_L}$ is the quantity that determines the extent of heat transferred by radiation at any temperature.

In order to estimate the above quantity Poltz (4) shows that by plotting the reciprocal of the apparent thermal conductivity, λ^{-1}_{app}, against the reciprocal of foam thickness, d^{-1}, and extrapolating to $d^{-1} = 0$ it is possible to arrive at an estimate of $\lambda_{app(d\to\infty)}$. The relevant plots are given on figure 8, and values of the reciprocal of $\lambda_{app(d\to\infty)}$ are obtained by extrapolating to $d^{-1} = 0$. If estimates of λ, the actual thermal conductivity of the composite medium, can be made then the value of the quantity $\frac{\epsilon_L S_L}{2-\epsilon_L}$ may be obtained.

The value of λ for a polymer foam, i.e. the conduction contribution, may be approximated by a well established relationship due to Kerner (6) for the properties of composite systems. The relation for the thermal conductivity of a composite system consisting of largely spherical particles of a component of conductivity λ_2, (namely air), immersed in a continuous phase of a component of conductivity λ_1, (namely polystyrene), is given by

$$\lambda = \frac{\lambda_1 \lambda_2 (2V_2 + 1) + 2\lambda_1(1 - V_2)}{\lambda_2 (1 - V_2) + \lambda_1 (2 + V_2)} \tag{9}$$

where V_2 is the fractional volume of the discrete component. It can be shown in the case of light density foams where $V_2 \simeq 1$ and $(1 - V_2) \simeq 0$ that a rough measure of λ is given by

$$\lambda = \lambda_2 + \frac{2\lambda_1 V_1}{3} \qquad (10)$$

where $V_1 = 1 - V_2$ is the fractional volume of the polystyrene. This implies that for low density foams e.g. $V_1 > 0.05$ the thermal conductivity of the composite is essentially that due to the air + 2/3 that due to the polymer present, the remaining 1/3 of the polymer being effectively absent i.e. the portion of the polymer lying at right angles to the direction of flow of heat.

If the values of λ_1 and λ_2 are taken at the temperature T then a value of λ may be calculated for each foam of known density.

Table 1 lists the values obtained in this way for $\frac{\epsilon_L S_L}{2 - \epsilon_L}$ using the values obtained from figure 8 for $\lambda_{app(d\to\infty)}$ and for λ using Kerner's equation and values of λ_1 and λ_2 taken from the literature, (7) and (8), (9) respectively. Table I also gives the value of S_L assuming a value for $\epsilon_L = 0.66$.

Table 1. Extrapolated estimates of the apparent thermal conductivity of the foam samples at $d \to \infty$ and calculated values of S_L.

T	$\lambda^{-1}_{app(d\to\infty)}$	$\lambda_{app(d\to\infty)}$	λ	$\lambda_{app(d\to\infty)} - \lambda = 4\sigma T^3 \frac{\epsilon_L S_L}{2 - \epsilon_L}$	$\frac{\epsilon_L S_L}{2 - \epsilon_L}$	S_L ($\epsilon_L = 0.66$)
^oK	$W^{-1} m\ deg$	$W\ m^{-1}\ deg^{-1}$	$W\ m^{-1}\ deg^{-1}$	$W\ m^{-1}\ deg^{-1}$	cm	cm
Sample A, Average density 20.1 Kg/m^3						
288	20.7	0.0483	0.0269	0.0214	0.395	0.80
313	19.65	0.0509	0.0289	0.0220	0.32	0.64
338	17.25	0.0580	0.0309	0.0271	0.315	0.63
					mean 0.34	mean 0.69
Sample B, Average density, 15.2 Kg/m^3						
288	23.2	0.0431	0.0265	0.0166	0.305	0.62
313	22.35	0.0447	0.0285	0.0162	0.23	0.47
338	20.5	0.0488	0.0305	0.0183	0.21	0.42
					mean 0.25	mean 0.50
Sample C, Average density, 28.7 Kg/m^3						
288	25.25	0.0396	0.0276	0.0120	0.22	0.45
313	24.80	0.0403	0.0297	0.0106	0.15	0.31
338	23.50	0.0426	0.0317	0.0109	0.12	0.25
					mean 0.16	mean 0.34

It is now seen how S_L changes from one Sample to the other, assuming $\epsilon_L = 0.66$. The hypothetical layers in Sample A are almost 7 mm apart and decrease to 5 and 3.4 mm for Samples B & C respectively. Sample A, in spite of its higher density, has a greater radiation component than Sample B of lower density. This is accounted for by the finer cells of Sample B scattering the radiation. Sample C has a still smaller radiation component than Sample B. This is accounted for both by its greater density and slightly finer cells causing greater absorption of radiation and greater scattering.

If the value for ϵ_L is not correct the relative magnitudes of S_L will still be the same and the above observations are still valid.

4.2. The Change in Apparent Thermal Conductivity of the Three Polystyrene Foams with Temperature

The three foams were studied at temperatures of 15° to 65°C at a constant total thickness of 6 cms. The results are shown on Fig. 9.

The influence of the change in temperature on λ_{app} is seen to be in the order Sample A > Sample B > Sample C which is as expected from the relative values of S_L respectively.

5. Summary and Conclusions

The combined influence of cell size and density on the apparent thermal conductivity of foamed polymers is shown for three examples by its variation with thickness and temperature. This behaviour is attributed to the effect cell size and density have on the heat radiated through the structure.

6. Acknowledgements

I wish to thank the Directors of Monsanto Chemicals Limited for permission to prepare this paper for presentation at the Seventh Conference on Thermal Conductivity.

I also wish to thank Mr. S. Baxter for his continued interest and encouragement during the progress of this work.

Finally, thanks are due to Mr. T.G. Wigmore who carried out the experimental part of the work and some of the calculations and to Mr. F. J. Parker for preparing the micrographs of foam sections.

7. References

(1) de Jong, J. and Marquenie, L., Heat-flowmeters and Their Applications, Instrument Practice, 16(1), 45 (1962).

(2) Lang, D.L., A Quick Thermal Conductivity Test on Insulating Materials. A.S.T.M. Bulletin, Sept. 1956, p.58.

(3) Buist, J.M. Doherty, D.J. and Hurd, R., Urethane Rigid foams; Factors Affecting their Behaviour as Thermal Insulants. Progress in Refrigeration Science and Technology, 1965, p.271.

(4) Poltz, H., Einfluss der Wärmestrahlung auf die Isolierwirkung poröser Dämmschichten. Allg. Wärmetechnik, 11 64 (1962).

(5) Fischer, F., Die Problematik von Wärmeleitfahigkeitsmessungen an Schaumstoffen. Kunststoffe, 56 321 (1966).

(6) Kerner, E.H., The Electrical Conductivity of Composite Media. Proc. Phys. Soc. B69 802, 808 (1956).

(7) Ueberreiter, K. and Nens, S., Spezifische Wärme, spezifisches Volumen, Temperatur-und Wärmeleitfähigkeit von Hochpolymeren Kolloid Zeit, 123, 92 (1951).

(8) Weast, R.C. and Selby, S.M., Handbook of Chemistry and Physics, 1966-1967. The Chemical Rubber Co.
Kaye G.W.C. and Laby T.H., Tables of Physical and Chemical Constants, 1957, Longmans, Green and Co.

(9) McAdams W.H. Heat Transmission, Third Edition McGraw - Hill Book Co. Inc.

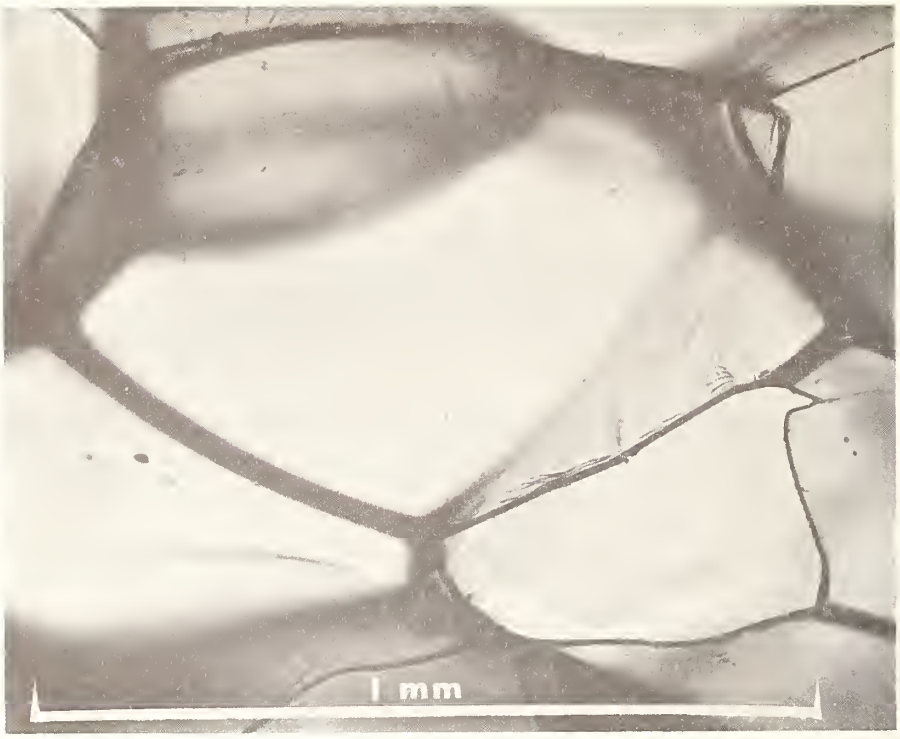

Figure 1. Micrograph of section of Sample A.

Figure 2. Micrograph of section of Sample A.

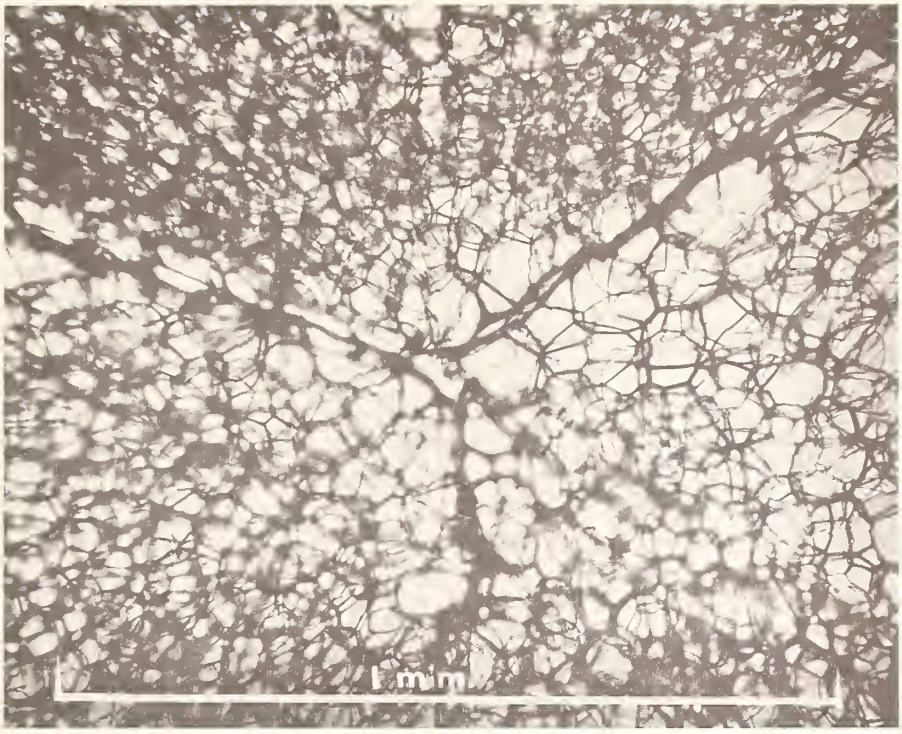

Figure 3 Micrograph of section of Sample B

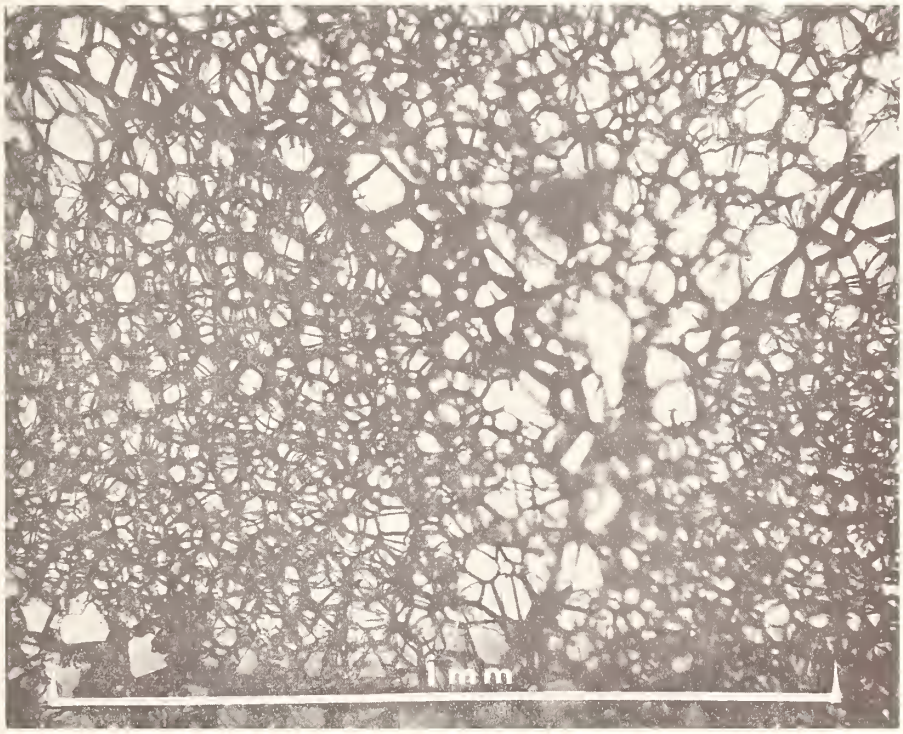

Figure 4 Micrograph of section of Sample C.

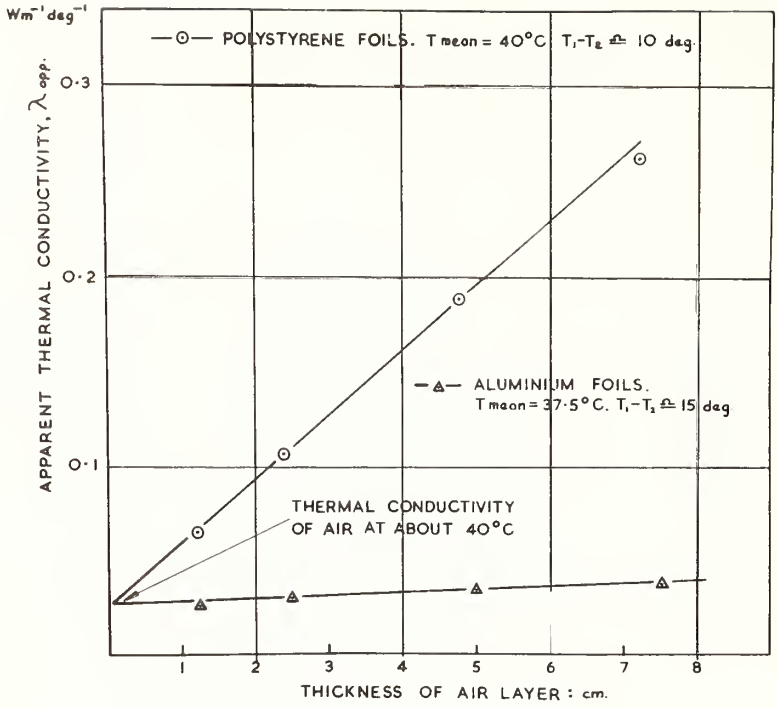

Figure 5. Plot of apparent thermal conductivity of still air layers against thickness showing effect of emissivity of confining surfaces.

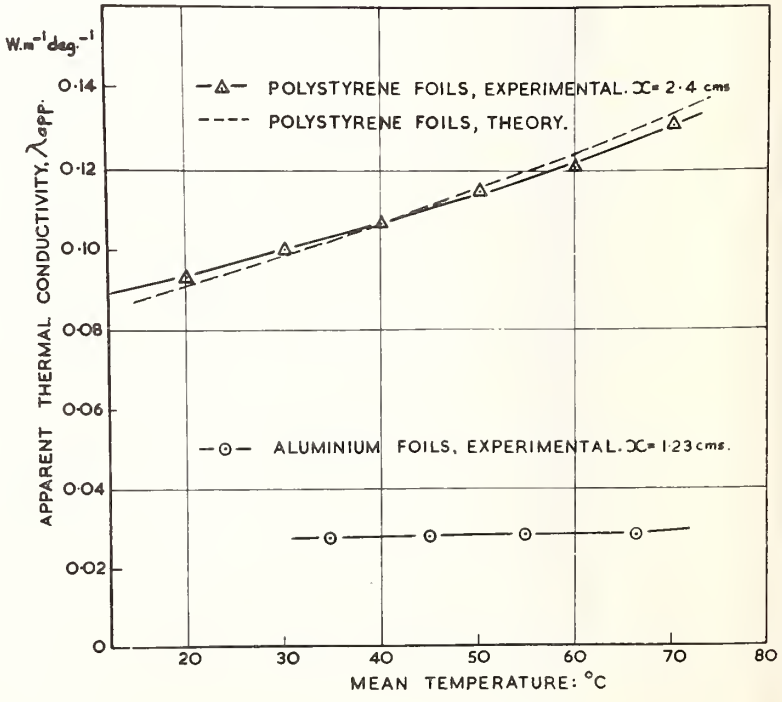

Figure 6. Plot of apparent thermal conductivity of still air layers against temperature showing effect of emissivity of confining surfaces.

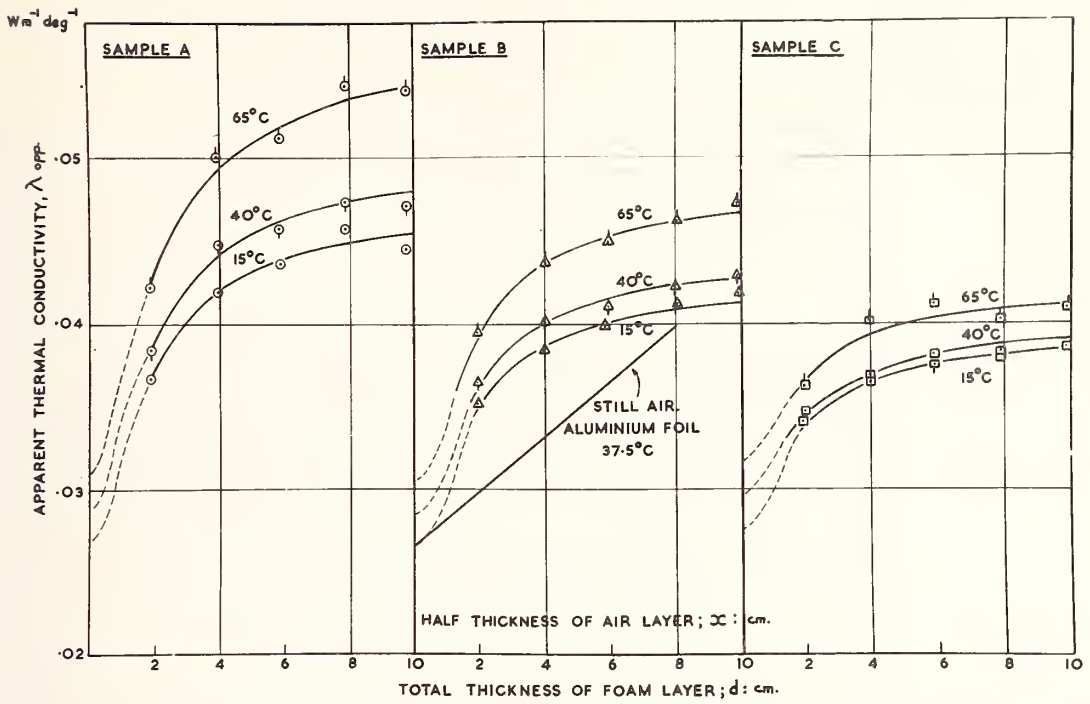

Figure 7 The effect of thickness on the apparent thermal conductivity of three polystyrene foams at three temperatures.

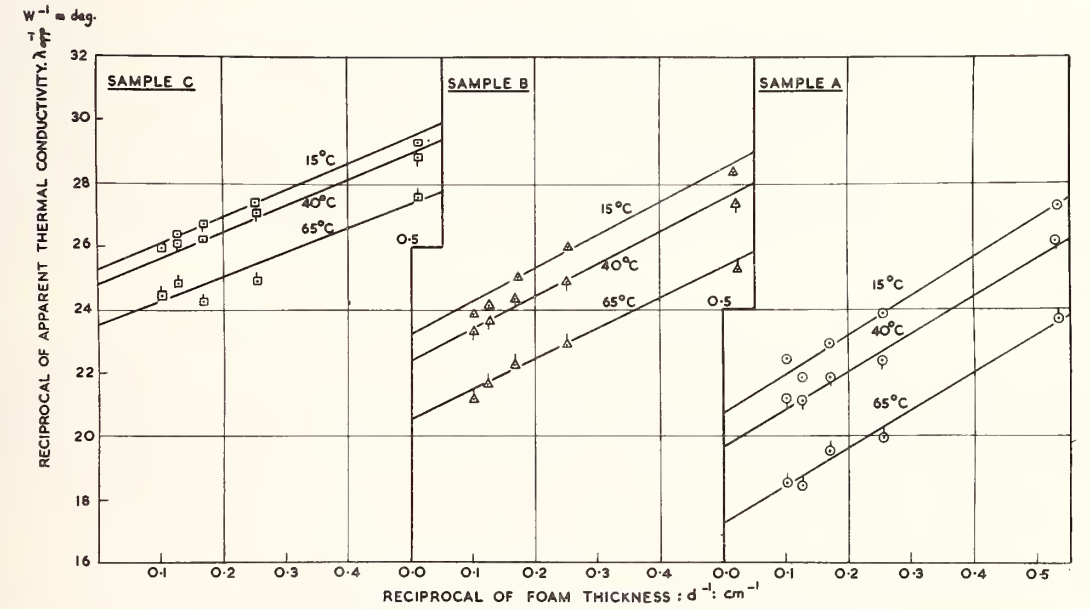

Figure 8 Plot of the reciprocal of apparent thermal conductivity of three polystyrene foams against the reciprocal of the thickness at three temperatures.

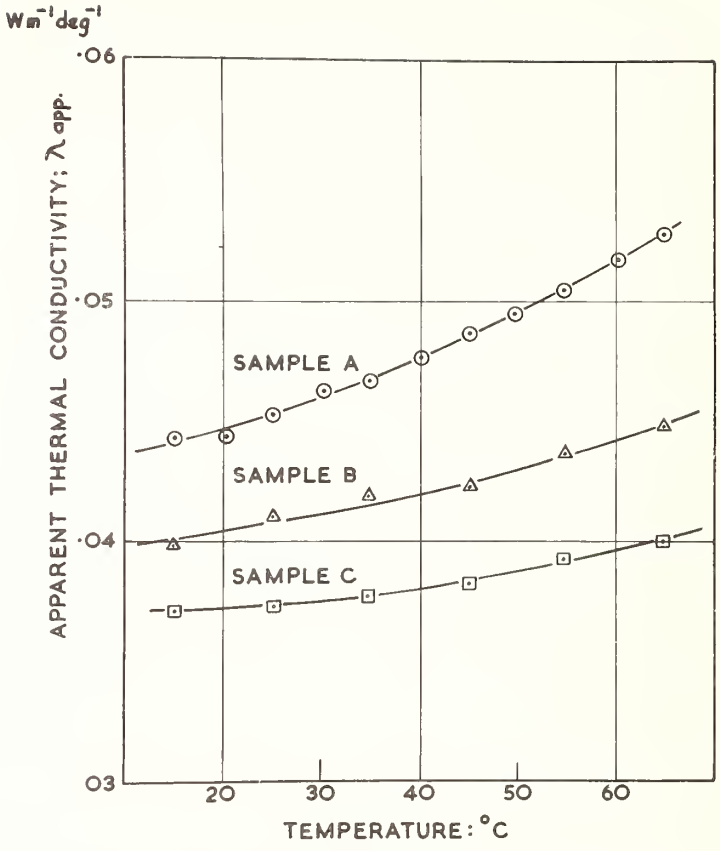

Figure 9. The effect of temperature on the apparent thermal conductivity of three polystyrene foams, at a constant total thickness of 6 cms.

Measurements of In-Vivo Thermal Diffusivity of Cat Brain

G. J. Trezek, D. L. Jewett, and T. E. Cooper[1]

University of California

The thermal diffusivity of living brain tissue was studied immediately after cessation of cerebral blood flow by means of the transient thermal response to a cold line source. In cat brain, by numerical fitting of the observed temperature field to the governing heat conduction equation, diffusivity values in the range of 0.125 to 0.110 mm^2/sec were obtained, these values being close to that of water evaluated at the same temperature. During the succeeding 2 1/2 hours the thermal diffusivity decreased approximately 50%.

Key Words: Brain tissue, central nervous system, living tissue, local cooling, thermal diffusivity.

1. Introduction

Thermal conductivity and diffusivity are important properties which must be known in order that heat transfer equations can be fully applied to a given system. Accurate knowledge of the heat transfer properties of brain tissue has become particularly important with the advent of both neurosurgical techniques utilizing cryoprobes and radio-frequency probes, and other research using localized brain cooling. As an approach to brain heat transfer properties we have chosen to study the transient temperature field generated by a cold line source; this approach differs in principle from the more usual "hot plate" methods used to determine thermal conductivity. Analytical solutions of the governing equations can be generated most easily if the magnitude contribution of each of the terms is known approximately.

The problem is simplified if the convective terms due to blood flow can be neglected. Although these terms are probably an order of magnitude less than the conductive terms [1][2], they can be completely eliminated by cessation of blood flow. The thermal properties immediately upon cessation of the blood flow closely approximate the in-vivo condition since the brain is still viable for a few minutes.

A recent survey by Chato[2] has shown that only a limited amount of thermal conductivity and diffusivity data is available for biological materials and the measurements made on internal organs have been performed only on in-vitro specimens. Comparative information on in-vivo and in-vitro measurements is lacking. Measurements of thermal conductivity in excised dog brain by Ponder [3] showed values close to that for water.

2. Analytical Considerations

A measurement of thermal diffusivity can be made by observing the transient temperature field in a particular media. As a first approximation, we have considered the brain as a homogeneous media even though there is an inter-mixture of white and gray matter. So as not to induce edge effects and other non-symmetrical effects which would ultimately perturb the temperature field and have to be accounted for analytically, a line source cooling probe was selected for the creation of a temperature field in the brain. The heat conduction equation expressed in cylindrical coordinates takes the form:

$$dc\,\frac{\partial T}{\partial t} = \lambda\left(\frac{\partial^2 T}{\partial r^2} + \frac{1}{r}\frac{\partial T}{\partial r} + \frac{1}{r^2}\frac{\partial^2 T}{\partial \theta^2} + \frac{\partial^2 T}{\partial z^2}\right) \qquad (1)$$

---

[1]Assistant Professor of Mechanical Engineering, Thermal Systems, Berkeley; Assistant Professor of Physiology and Neurosurgery, School of Medicine, San Francisco; NIH Trainee, College of Engineering, Berkeley; respectively.

[2]Figures in brackets indicate the literature references at the end of this paper.

where $T = T(r, \theta, z)$ is the temperature at r, θ, and z; t is time, d is density, c is specific heat, λ is thermal conductivity, r is the radial distance from the probe, z is the distance from the surface of the brain, and θ is the angular location. The thermal diffusivity (a) is equal to λ/dc and has the units of mm^2/sec. Note the absence of a convective term for blood flow.

3. Experimental Apparatus

A schematic diagram of the experimental apparatus is shown in figure 1. An anesthetized cat was mounted in a sterotaxic frame. The sterotaxic atlas for cat brain gave a reasonably good indication of where the line source cooling probe should be placed in attempting to avoid such areas as the fluid filled ventricles. A location 6 mm anterior to the ear bars and 8 mm from the mid-line was selected for the experiments so that most measurements would be in white matter. A portion of the skull was removed in this area and the 0.5 mm diameter stainless steel cooling probe was inserted vertically 22 mm into the brain.

A linear array of five 0.2 mm diameter stainless steel shielded chromel-constantan thermocouples were mounted in a rotatable three-dimensional traverse which permitted measurement of the field with respect to r, θ, and z. The first thermocouple in the array was positioned 1 mm from the cooling probe, the next two each 1 mm further away and the last two each 2 mm away, allowing temperature measurements up to 7 mm from the probe. Enough of the skull was removed to permit the thermocouple array to be swung through an angle (θ) of 90 degrees. Thus, for a given position of the thermocouples, five values of the temperature field were obtained along the radial distance (r) from the probe at a particular set of θ and z coordinates. The portion of the exposed brain was covered with absorbent cotton soaked with mineral oil to diminish any vertical gradients due to a convective transfer to the air. Extreme care was exercised in positioning the probe and thermocouples to insure that they were mutually parallel. The thermocouples were calibrated against a mercury thermometer of an accuracy of 0.1°C.

Heptane was circulated through the probe from a constant temperature bath. A flow rate of approximately 80 ml/min at 200 psi through the stainless steel hypodermic tubing resulted in a uniform temperature in the z direction on the surface of the cooling probe to within 0.5°C. A twelve channel multipoint recorder was used to moniter the locations shown in figure 1 with an accuracy of ± 0.25°C. During the transient cooling run the recorder was adjusted to record only the five free thermocouples and a single probe temperature repeatedly thereby allowing a more precise specification of the initial transient field. The recording cycle was 1.2 sec/point in either mode.

4. Data Analysis and Results

Values of the thermal diffusivity (a) were obtained by calculating the value of each of the terms in the transient heat conduction equation and then taking the ratio of the time dependent term to the spacial term. This approach was taken for several reasons, namely, 1) An exact solution of the governing equation is feasible for a one dimensional field. Thus some knowledge of the θ and z variation would be required before simplification to a radial dependence could be made. Even assuming a one dimensional spacial dependence the problem is further complicated by the introduction of a time dependent boundary condition, i.e., the cooling probe requires about 40 seconds to reach its steady state value. 2) In order to acquire an appreciation for the manner in which the temperature field develops, that is, a knowledge of what time in the transient field do the various spacial dependencies dominate would prove extremely helpful in guiding future analytical endeavors.

A typical data analysis proceeded as follows: a point in space was selected and all rates of change of temperature with time and space were evaluated at this point. The evaluation of dT/dt can be obtained directly from the chart record while the spacial dependence of temperature is obtained by cross plotting the data at a given time. Typical sets of radial positions versus temperature curves are shown in figures 2 - 5. The initial state values shown in figures 3, 4, and 5 are decreased due to absence of blood flow as body temperature dropped. A complete set of data was first taken for the live case followed by sets of data for the case immediately after the animal expired, i.e. within 15 minutes of the cessation of blood flow, and at 1 1/2 and 2 1/2 hours after expiration. Comparison of the radial dependence (at the same θ and z) within 60 seconds and after 15 minutes from the cessation of blood flow showed no significant differences.

Using the Newton method, a polynomial was fit to the data around the point of evaluation. Analysis of the data showed the angular dependence to be virtually zero which could partially be expected from the geometrical symmetry. The value of the terms for the data shown in figures 2 - 5, evaluated at a radial distance (r) of 3 mm from the cooling probe and a vertical distance (z) of 9.1 mm (which was the approximate mid-line of the probe from the brain surface), are summarized in Table 1. Also shown in Table 1 are the values of (a) obtained from the second experimental animal.

Table 1. Summary of transient heat conduction terms

Time t sec	$\frac{\partial T}{\partial t}$ $\frac{°C}{sec}$	$\frac{1}{r}\frac{\partial T}{\partial r}$ $\frac{°C}{mm^2}$	$\frac{\partial^2 T}{\partial r^2}$ $\frac{°C}{mm^2}$	$\frac{\partial^2 T}{\partial z^2}$ $\frac{°C}{mm^2}$	1st animal a $\frac{mm^2}{sec}$	2nd animal a $\frac{mm^2}{sec}$
Immediately after animal expires						
5	-0.201	0.267	-2.07	0	0.112	0.118
12.5	-0.243	0.789	-3.24	0.50	0.124	0.126
20	-0.208	1.12	-4.20	1.25	0.113	--
1 1/2 hours after expiration						
5	-0.104	0.25	-1.90	0	0.063	0.064
2 1/2 hours after expiration						
5	-0.0667	0.14	-1.65	0	0.044	0.050

5. Discussion

The results of observations made on two animals gave practically identical results for the nature of the temperature field and values of thermal diffusivity even though r,z location was chosen as the evaluation point in the second animal. Analysis of the values shown in Table 1 indicates that the vertical temperature gradient does not contribute in the early part of the transient. In the latter part of the transient (after about 10 sec) heat transfer from the bulk of tissue below the probe destroys the initial one dimensional cooling pattern. Thus, any one dimensional analytical solution would have to be limited to the early transient. Even though the contribution of the various terms varies with time during the transient, it should be noted that the value for (a) remains nearly constant during the transient.

The change in thermal diffusivity during the hours of the experiment is shown in figure 6 and can be readily observed from figures 3, 4, and 5 as a retardation of the development of a given temperature field. Diffusivity values fairly close to that of water evaluated at body temperature of 35°C were obtained for the tissue immediately after expiration. A drop in diffusivity occurs as the tissue begins to deteriorate. Even though a decrease in body temperature occurred in the dead animal (from 35°C to 24°C) the corresponding thermal diffusivity of water is only slightly decreased; thus implying that the physical properties of the tissue must be changing. Since we lack data on d and c it is difficult to ascertain whether it is the thermal conductivity or the density-specific heat product (or both) that result in a decrease in diffusivity with time.

In-vivo measurements of each quantity (d and c) would actually be required in order to resolve this point. It is interesting to note that the value of thermal conductivity obtained by Ponder [3] in in-vitro experiments yields thermal diffusivity values (calculated by using the density and specific heat of water) slightly above the value of water.

As a first approximation, the brain thermal diffusivity can be considered to be that of water; however, our data indicates that the value is probably different from that of water. Possibly such a difference is due to the microscopic structure of the brain which would invalidate our assumption that it can be treated as a homogeneous medium.

6. Acknowledgements

The experimental portion of this study was supported in part by NINDB Grant #NB 05702.

7. References

[1] Jewett, D. L. and Trezek, G. J., Temperature fields in brain with parallel plane cooling probes, Proceedings 20th Annual Conference on Engineering in Medicine and Biology.

[2] Chato, J. C., A survey of thermal conductivity and diffusivity data on biological materials, ASME, Paper #66-WA/HT-37, 1966.

[3] Ponder, E., The coefficient of thermal conductivity of blood and of various tissues, J. of Gen. Physiolgoy, Vol. 45, 1962.

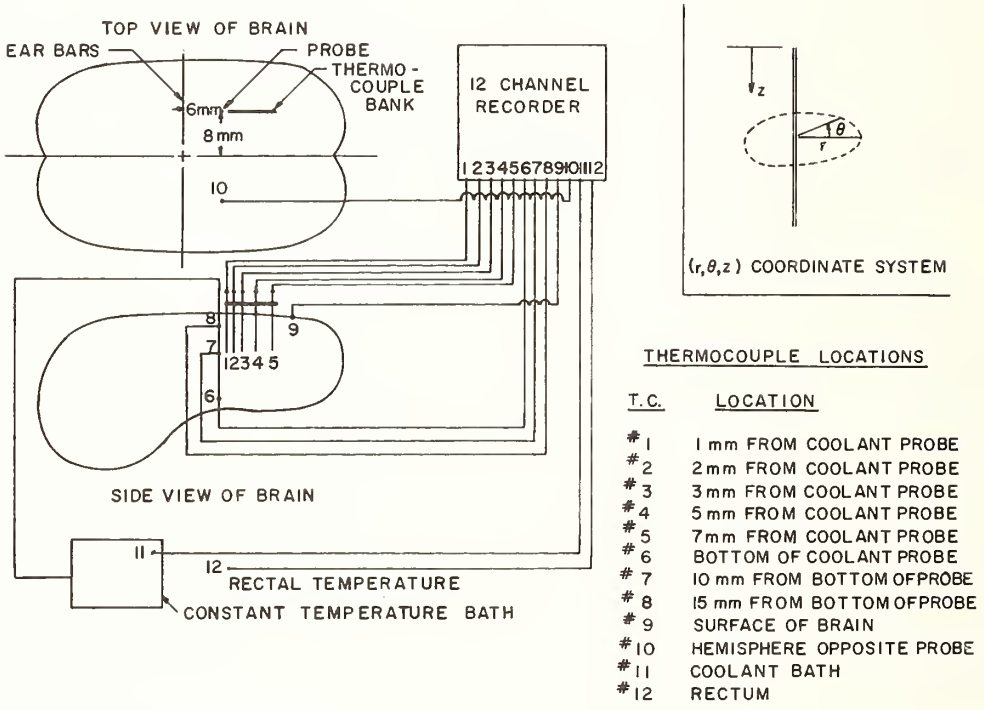

Figure 1. Schematic representation of experimental facility.

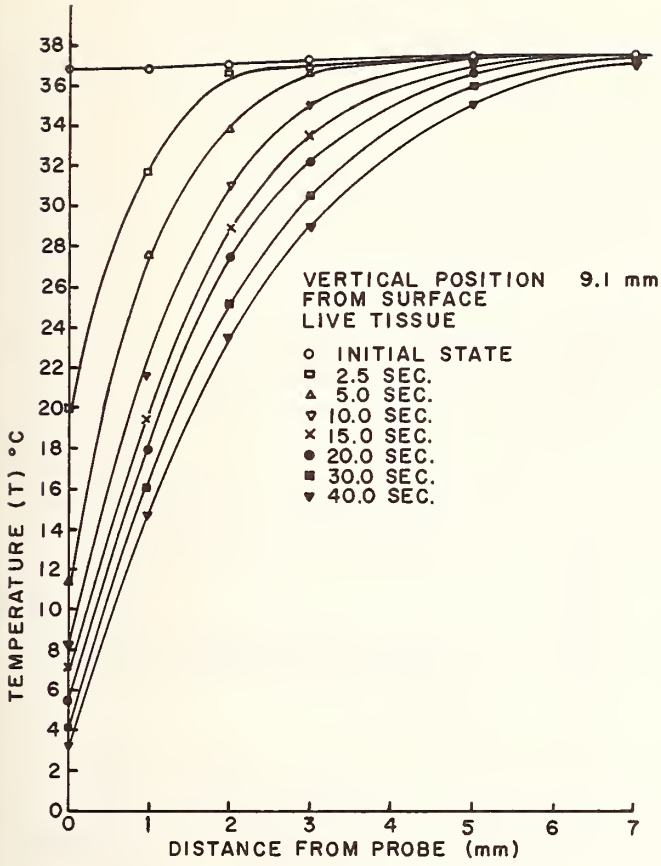

Figure 2. Development of radial temperature field in live tissue.

Figure 3. Development of radial temperature field in tissue immediately after cessation of cerebral blood flow.

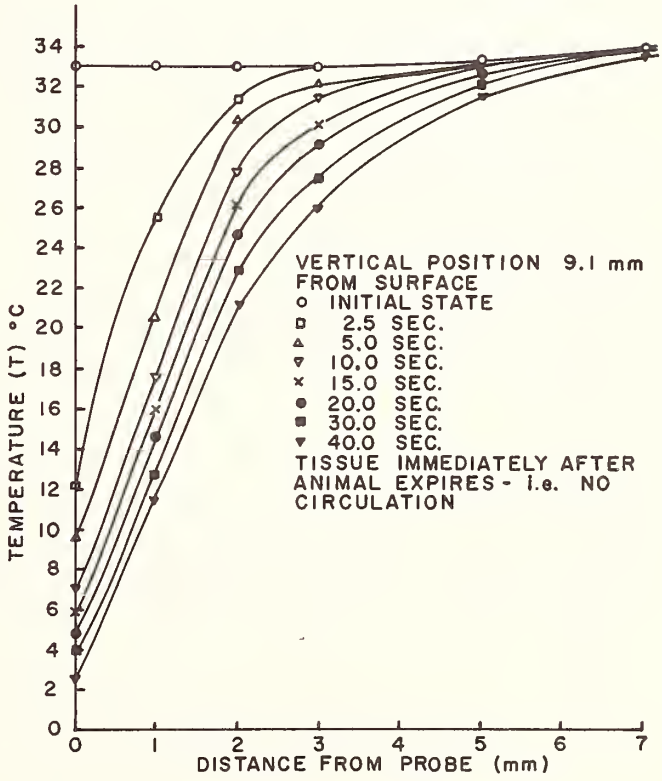

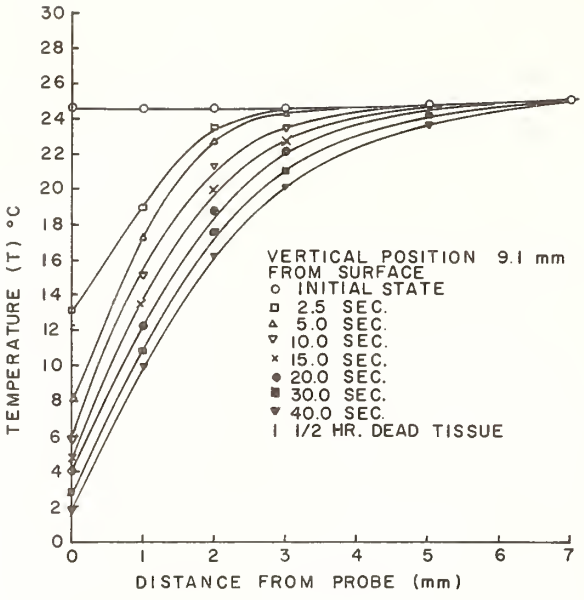

Figure 4. Development of radial temperature field in tissue 1½ hours after cessation of cerebral blood flow.

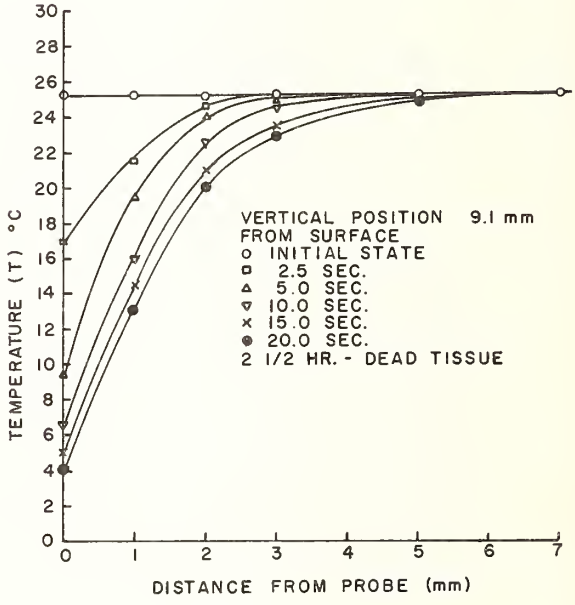

Figure 5. Development of radial temperature field in tissue 2½ hours after cessation of cerebral blood flow.

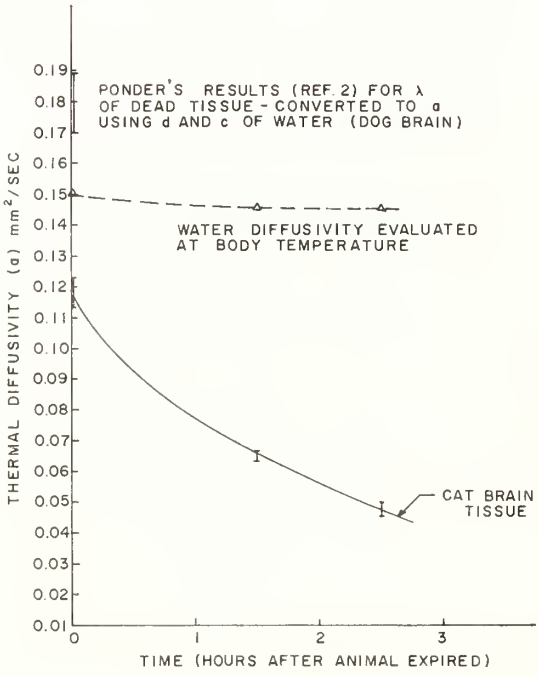

Figure 6. Comparison of thermal diffusivity measurements.

A Correlation for Thermal Contact Conductance of Nominally-Flat Surfaces in a Vacuum

C. L. Tien[1]

University of California
Berkeley, California 94720

A semi-empirical correlation for the thermal conductance of nominally-flat surfaces in a vacuum has been proposed in terms of three dimensionless groups, which characterize, respectively, the thermal contact conductance, the contact pressure, and the surface irregularities. The proposed correlation is shown to be supported quantitatively by previous analytical and experimental investigations.

Key Words: Thermal contact conductance, thermal contact resistance, thermal conductivity, heat conduction, heat transfer.

1. Introduction

The problem of thermal contact conductance has received considerable attention in recent years. Comprehensive surveys of literature on the subject can be found in references [1,2,3,4][2]. In particular, significant progress has been made toward a quantitative analysis of thermal contact conductance in a vacuum environment. Not only is the study of thermal contact conductance in a vacuum of great importance in the thermal design of spacecrafts, but also it serves as a logical starting point for the analysis of the more complex problem involving interstitial fluids. Indeed, impressive analytical groundwork has been laid down by Clausing and Chao [1,5] for macroscopic constriction resistance due to surface waviness or flatness deviations, and by Yovanovich and Fenech [6] and Mikic and Rohsenow [7] for microscopic constriction resistance due to surface roughness of nominally-flat surfaces. Recent analytical attempts also considered the combined effect of surface roughness and waviness upon the overall thermal contact resistance [7,8]. On the other hand, a vast amount of experimental information has become available in recent years. While further analytical and experimental works are needed, the present state of knowledge seems to have reached such a stage that a workable engineering correlation could be constructed for the thermal contact conductance in a vacuum.

The present paper is to establish a correlation for the thermal contact conductance of nominally-flat metallic surfaces in a vacuum environment. Accordingly the effect of surface waviness of flatness deviations is neglected. The correlation, which is based on simple dimensional consideration, consists of three dimensionless groups characterizing respectively the thermal contact conductance, the contact pressure, and the surface irregularities. It is shown that the proposed correlation is in quantitative agreement with previous analytical and experimental results.

2. Dimensional Consideration

Consider two similar metals of nominally-flat, rough surfaces in contact in a vacuum. For dissimilar metals, it is customary to proceed as in the case of similar metals except for the replacement of the metallic physical property by the harmonic mean of those of the dissimilar metals. It is possible, however, to have other complications such as directional effects [9] in the case of dissimilar metals. For this reason, discussions in the present paper will be restricted to the case of similar metals. The rough surfaces under consideration are nominally-flat so that there exists no large-scale waviness

[1] Associate Professor of Mechanical Engineering

[2] Figures in brackets indicate the literature references at the end of this paper.

or flatness deviations. Furthermore, the surface irregularities are assumed to be statistically random and of Gaussian type [10,11]. This is a common assumption for most analyses involving rough surfaces. To describe such a rough surface requires only two statistical parameters, i.e., the rms roughness σ and the autoconvariance length a. These two characteristic lengths are related to the rms slope m by the following relation [11]:

$$2\sigma^2 = a^2m^2 \tag{1}$$

When two statistically-independent rough surfaces are put in contact, the two characteristic lengths are defined by [7]:

$$\sigma^2 = \sigma_1{}^2 + \sigma_2{}^2 \tag{2}$$

and

$$2(\sigma_1{}^2 + \sigma_2{}^2) = a^2(m_1{}^2 + m_2{}^2) \tag{3}$$

It should be noted that, when $\sigma_1 = \sigma_2$ and $m_1 = m_2$, $\sigma = \sqrt{2}\ \sigma_1 = \sqrt{2}\ \sigma_2$ and $m = \sqrt{2}\ m_1 = \sqrt{2}\ m_2$, but still $2\sigma^2 = a^2m^2$.

To perform a dimensional analysis by use of the Pi theorem [12], it requires first the identification of primary physical parameters in the physical problem. It is natural to have thermal contact conductance h and thermal conductivity λ as two of the primary parameters. The two characteristic lengths σ and a for contact surface irregularities must also be included. In addition, the surface deformation as caused by contact pressure P must be taken into account. For the pressure range of practical interest, it has been shown [6] that the deformation is in the plastic range and the characteristic material property is the microhardness H, which may be conveniently represented by three times the tensile yield stress, i.e., $H = 3F_{ty}$.

From the above consideration, it can be stated that the present problem is characterized by the six parameters, h, λ, σ, a, P and H. Indeed they represent the three major phases of the problem, thermal (h, λ), surface (σ , a), and deformation (P,H). A straightforward application of the Pi theorem leads to the conclusion that there exist three dimensionless groups and they can be logically expressed and related as

$$\left(\frac{h\sigma}{\lambda}\right) = b\ \left(\frac{\sigma}{a}\right)^c\ \left(\frac{P}{H}\right)^d \tag{4}$$

where the constants b, c, and d are to be determined from theoretical or experimental results. Based on (1), the above equation may be rearranged as

$$\left(\frac{h\sigma}{\lambda}\right) = fm^g\ \left(\frac{P}{H}\right)^d \tag{5}$$

Indeed, an equation of this type has been obtained by Mikic and Rohsenow [7] through their elaborate analysis of the physical problem. Their relation gives f = 0.9, g = 1, and d = 16/17. It should be realized, however, that their analysis is based on idealized physical models. For actual engineering applications, the validity of the relation (4) or (5), and the values of its constants must be determined by the vast amount of experimental data available in the literature.

3. Correlation of Experimental Data

Most existing experimental data do not contain sufficient information to conclusively determine the suggested correlation. In particular, except for the work of MIT group, information concerning a or m is totally missing. Furthermore, all existing measurements of σ and m are of doubtful nature, since they are based on profilometer readings. Bennett and Porteus [11] have not only demonstrated the deficiency in such readings, but also developed an ingenious optical method for the measurements of σ and m. The lack of information on σ and m, however, does not prevent a check on the suggested functional relationship between $(h\ \sigma/\lambda)$ and (P/H). Summarized in Table 1 are experimental investigations with thermal contact conductance data for nominally-flat surfaces in a vacuum. Surfaces are classified here as nominally flat if the rms roughness is greater than one-tenth of the total flatness deviation. Only data for similar metals and for clean surfaces (without plating or oxide films) are included. Actual data points from various investigations are shown in figures 1 and 2 in terms of $(h\sigma/\lambda\ )$ and (P/H).

In view of the wide range of conditions (pressure, temperature, surface and material) under which data were obtained by various investigators, figures 1 and 2 indicate quite convincingly, if not conclusively, that a power relation does exist as

$$\left(\frac{h\sigma}{\lambda}\right) \propto \left(\frac{P}{H}\right)^d \tag{6}$$

where d = 0.85 approximately. The deviations of experimental data from (6) at low values of (P/H) probably result from the waviness effect, which becomes dominant at low contact pressures. The slight

Table 1 Experiments for thermal contact conductance of nominally-flat surfaces in a vacuum (physical properties given in the table are obtained from reference 13)

series	reference	specimen	size D x L (inch)	minimum vacuum (mm-Hg)	flatness deviation (μm)	rms roughness (μm)	rms slope	contact pressure (KN/m^2)	mean contact temp. ($^\circ$K)	thermal conductivity (Wm^{-1}deg^{-1})	microhardness (10^{4}KN/m^2)
B_A	14	Al 7075-T6	2x1	10^{-5}	15.2	4.67	--	< 7,000	125	0.0080	165
B_S	14	SS 17-4PH	2x1	10^{-5}	10.1	4.07	--	< 7,000	172	0.0015	414
C_A	15	Al 6061-T4	1x1	10^{-5}	1.27	1.59	--	< 700	340	0.0188	33.1
CC_A	5	Al 2024-T4	1/2x2-3/4	10^{-6}	0.38	0.13	--	< 2,200	388	0.0142	104
FA_A	16	Al 6061-T6	2x3	10^{-4}	< 8.9	1.62	--	< 8,300	310	0.0016	725
FA_S	16	SS 304	2x3	10^{-4}	< 2.6	1.56	--	< 8,300	310	0.0015	620
FK_A	17	Al 2024-T4	2x3	10^{-4}	< 8.9	1.63	--	< 8,000	310	0.0121	108
H_S	18	SS 416	1x1-1/2	10^{-6}	(a)	4.30	0.107	< 70,000	420	0.0025	258 (b)
MR_{S1}	7	SS 303	1x1-1/2	10^{-6}	2.03	3.86	0.163	< 8,300	420	0.0017	255 (b)
MR_{S2}	7	SS 303	1x1-1/2	10^{-6}	3.81	4.83	0.150	< 35,000	420	0.0017	255 (b)
MR_{S3}	7	SS 303	1x1-1/2	10^{-6}	3.30	8.64	0.100	< 70,000	420	0.0016	255 (b)
YF_S	6	SS 303	1x1-1/2	10^{-6}	(a)	1.07	0.087	< 28,000	420	0.0017	255 (b)

(a) stated in the reference as nominally flat

(b) value obtained from actual tests indicated in the reference

variation of data trend at large values of (P/H) in some series of data (notably, CC_A and FA_A) could be due to a change of deformation characteristic from plastic to elastic range [6].

From their analysis [7], Mikic and Rohsenow have obtained g = 1 in (5). This power dependence on rms slope m is indeed in good agreement with their experimental data. This functional form may also be checked qualitatively from the data presented in figures 1 and 2. Assuming g = 1 and d = 0.85, it follows that all investigations except for CC_A have surfaces with a rms slope m in the range from 0.01 to 0.13, or in terms of angle, from 1/2 to 10 degrees. This seems to agree qualitatively with other surface characterization studies [19]. The value of m for CC_A data is extremely small (m = 0.0001), and this could be caused by an error in their estimate of σ.

With given values of g and d, the correlation can now be established from the experimental information. It is thus proposed the following correlation for the thermal contact conductance of nominally-flat metallic surface in a vacuum:

$$\left(\frac{h\sigma}{\lambda}\right) = 0.55\ m\ \left(\frac{P}{H}\right)^{0.85} \qquad (7)$$

The above correlation differs slightly from the analytical result of Mikic and Rohsenow [7], but appears to be in better agreement with existing experimental information.

4. Acknowledgment

The author wishes to acknowledge the support of the Miller Institute for Basic Research in Science, University of California (Berkeley), through the appointment of Research Associate Professor during the year of 1967-1968.

5. References

[1] Clausing, A. M. and Chao, B. T., Thermal contact resistance in a vacuum environment, University of Illinois, Eng. Exp. Sta., Report ME-TN-242-1 (August 1963).

[2] Fried, E., Study of interface thermal contact conductance, NASA Document No. 645D652 (May 1964).

[3] Yovanovich, M. M., Thermal contact conductance in a vacuum, Mech. Eng. Thesis, Mass Inst. Tech. (February 1966).

[4] Minges, L. M., Thermal contact resistance, Vol. I-A review of literature, Tech. Report AFML-TR-65-375, Air Force Materials Laboratory, Dayton, Ohio (April 1966).

[5] Clausing, A. M. and Chao, B. T., Thermal contact resistance in a vacuum environment, J. Heat Transfer 87C, 243 (1965).

[6] Yovanovich, M. M. and Fenech, H., Thermal contact conductance of nominally-flat, rough surfaces in a vacuum environment, Thermophysics and Temperature Control of Spacecraft and Entry Vehicles (Ed. G. B. Heller), Academic Press, New York (1966).

[7] Mikic, M. M. and Rohsenow, W. M., Thermal contact resistance, Tech. Rept. No. 4542-41, Dept. of Mech. Eng., Mass. Inst. Tech. (September 1966).

[8] Mikic, M. M., Yovanovich, M. M. and Rohsenow, W. M., The effect of surface roughness and waviness upon the overall thermal contact resistance, Tech. Rept. No. 76361-43, Dept. of Mech. Eng., Mass. Inst. Tech. (October 1966).

[9] Clausing, A. M., Heat transfer at the interface of dissimilar metals--the influence of thermal strain, Int. J. Heat Mass Transfer 9, 691 (1966).

[10] Laning, J. H., Jr. and Battin, R. J., Random Processes in Automatic Control, McGraw-Hill, New York (1956).

[11] Bennett, H. E. and Porteus, J. O., Relation between surface roughness and specular reflectance at normal incidence, J. Opt. Soc. Am. 51, 123 (1961).

[12] Kline, S. J., Similitude and Approximation Theory, McGraw-Hill, New York (1965).

[13] Weiss, V. and Gessler, J. G. (Eds.), Aerospace Structural Metals Handbook, Syracuse Univ. Press, Syracuse, New York (1963).

[14] Bloom, M. F., Thermal contact conductance in a vacuum environment, Missle and Space Systems Division, Douglas Aircraft Company Report SM-47700 (December 1964).

[15] Cunnington, G. R., Jr., Thermal conductance of filled aluminum and magnesium joints in a vacuum environment, ASME Paper No. WA/HT-40 (1964).

[16] Fried, E. and Atkins, H., Interface thermal conductance in a vacuum, J. Spacecraft and Rockets 2, 591 (1965).

[17] Fried, E. and Kelley, M. J., Thermal conductance of metallic contacts in a vacuum, Thermophysics and Temperature Control of Spacecraft and Entry Vehicles (Ed. G. B. Heller), Academic Press, New York (1966).

[18] Henry, J. J., Thermal contact resistance, Sc.D. Thesis, Mass. Inst. Tech. (August, 1964).

[19] Funai, A. and Rolling, R. E., Inspection techniques for characterization of smooth, rough and oxidized surfaces, AIAA Paper No. 67-318, to appear in Thermophysics of Spacecraft and Planetary Bodies (Ed. G. B. Heller), Academic Press, New York (1967).

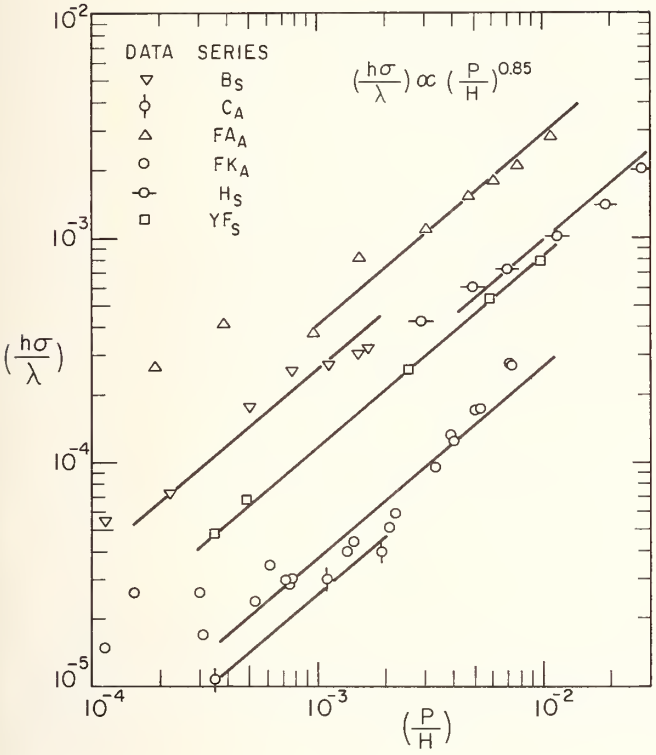

Figure 1. Thermal contact conductance for nominally-flat surfaces in a vacuum (data group 1).

Figure 2. Thermal contact conductance for nominally-flat surfaces in a vacuum (data group 2).

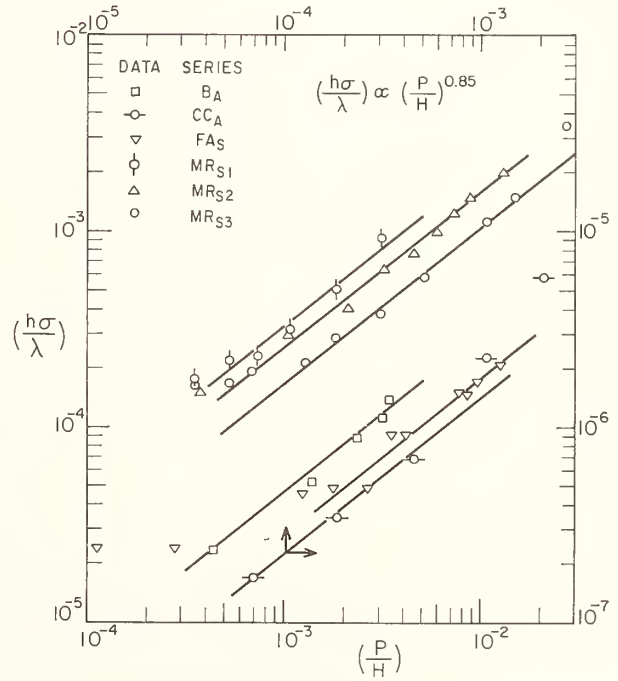

Thermal Conductance of Imperfect Contacts

Evan Charles Brown, Jr. and Vernon Emerson Holt

North Carolina State University
Raleigh, North Carolina

A quantum model of the thermal conductance of imperfect contacts with continuum boundary conditions is presented. The case of a junction with finite roughness and with adsorbed gases at the interface is considered. It is shown that a number of parameters such as surface roughness, flatness, oxide layer thickness, adsorbed gas layer thickness, and contact pressure can be represented by a single variable namely the thickness of a compressible layer between adjoining contact materials. Specific solutions obtained with the aid of a computer for representative materials and layer thicknesses are in good agreement with experiment near and above room temperatures.

Key Words: Conductance, thermal conductance, thermal resistivity, contact resistance, interface resistance.

1. Introduction

The resistance to the flow of heat at the interface of two materials placed together is a well-known and observable phenomena. It is a problem encountered in many applications. Much of the published work in this field has been of an experimental nature. General correlation of data by empirical or analytical models has been a difficult challenge due to a considerable number and variation of variables. A few of the important variables include the relative flatness of the surfaces of the two materials at the interface, kind of material, contact pressure, type and degree of roughness, chemical condition of the surfaces, interface temperature and gradient, and interstitial material.

The available experimental observations are highly specialized and information on important test variables is incomplete because of the complex nature of the thermal contact problem. Rather than fight these variables in the accepted manner one at a time, perhaps it might prove fruitful in this case to join the variables into one parameter and attempt to determine the functional dependence of this parameter in a self-consistent general model. The purpose here is to present a general model for thermal contacts, and to evaluate the model and a few characteristics of the thermal contact problem. Evaluation is made on the basis of some of the recent literature, although a survey or critical evaluation of the literature is not attempted here by any means. Before developing a model for an imperfect contact with interstitial gas or oxide, the classical model for a single perfect interface is reviewed.

2. Perfect Interface

Consider the thermal resistance imposed by two semi-infinite isotropic similar or dissimilar materials placed together as in figure 1 when a heat flux is maintained across a perfect interface. It is assumed here that the energy transport across the interface is due to phonons having discrete energy of $\hbar\omega$ rather than electrons. This assumption has some justification in the subsequent considerations of imperfect contacts.

The transmitted energy from media 1 to media 2 per element of area and time is

$$q_{1-2} = \int_S \varepsilon I_1 dS \tag{1}$$

where ε is the directional transmission coefficient, and I_1 is the energy intensity of the phonons in media 1 striking the interface per elemental solid angle. The integration is over the solid angle S. The energy intensity striking the interface per elemental solid angle in media 1 is

$$I_1 = E_1 c_1 \frac{\cos\theta}{4\pi} \tag{2}$$

where E_1 is the energy density in media 1 and the factor $c\cos\theta/4\pi$ gives the fraction of phonons striking the interface per elemental solid angle, time and unit area of interface. Only the longitudinal phonon model with velocity c_1 is indicated here. The elemental solid angle can be expressed as

$$dS = \sin\theta d\theta d\phi. \tag{3}$$

Substituting eqs. (2) and (3), eq. (1) becomes

$$q_{1-2} = \int_0^{2\pi} \int_0^{\pi/2} \varepsilon \frac{E_1 c_1}{4\pi} \cos\theta\sin\theta d\theta d\phi. \tag{4}$$

Equation (4) may be rewritten as

$$q_{1-2} = \frac{E_1 c_1}{2} \Gamma(\varepsilon) \tag{5}$$

where

$$\Gamma(\varepsilon) = \int_0^{\theta max} \varepsilon \cos\theta \sin\theta \, d\theta \tag{6}$$

is the integrated transmission coefficient for the case of the perfect interface as considered by Little [1][1] with θ_{max} determined by $\sin\theta_1 = c_1/c_2$ for $c_1<c_2$ and by $\theta_{max} = \pi/2$ for $c_1>c_2$. As indicated in figure 1, the directional transmission coefficient is

$$\varepsilon = \frac{4 z_1 z_2}{(z_1+z_2)^2}$$

$$z_1 = \frac{\rho_1 c_1}{\cos\theta_1} \qquad \text{etc.}$$

where ρ_1 is the density of media 1.

The energy density E_1 of phonons in media 1 as derived in texts such as Kittel [2] for Bose-Einstein energy distribution is

$$E_1 = \frac{k^4 T_1^4}{\hbar^3 c_1^3 2\pi^2} \int_0^{x\,max} \frac{x^3}{(\exp x - 1)} dx \tag{7}$$

where

$$x = \frac{\hbar\omega}{kT}, \quad x_{max} = \frac{\hbar\omega_{max}}{kT}$$

and the maximum frequency ω_{max} is assumed to be determined by the periodic spacing of the structure of the material if known, or by the Debye temperature of the material. The symbol $\hbar$ denotes Planck's constant divided by 2π and k is the Boltzmann constant.

[1] Figures in brackets indicate the literature references at the end of this paper.

The derivation of the corresponding equations for each of the two transverse modes is similar to the preceding except that the transverse velocities c_{1t} and c_{2t} are substituted for the longitudinal velocities c_1 and c_2 in all of the above expressions.

As indicated by Little [1], the above description of quantized energy density seems to be quite accurate within the material but does not describe contact conductances very well. Observed contact conductances are much less than suggested by the single perfect interface model. In order to better represent actual imperfect contacts, a plane layer with two interfaces will be incorporated into the model next. This plane layer will represent interstitial gases or oxides and their effect will be subsequently evaluated.

3. Imperfect Contact Represented by a Layer with Two Interfaces

Next, consider the resistance caused by two planes with another plane layer of material between them when a heat flux is maintained across both interfaces as indicated in Figure 2. The transmitted energy from media 1 per element of area and time is

$$q_{1-3} = \int_S \alpha \, I_1 dS \tag{8}$$

where α is the overall transmission coefficient for a layer with two interfaces and I_1 and S are as defined for the single interface case. Hence, using eqs. (2), (3), and (7) in eq. (8) we have

$$q_{1-3} = \int_0^{2\pi} \int_0^{\theta_1 max} \alpha \frac{E_1 c_1}{4\pi} \cos\theta_1 \sin\theta_1 d\theta_1 d\phi. \tag{9}$$

For plane waves and a plane isotropic non-dissipative layer, the transmission coefficient α according to Holt [3] is

$$\alpha = \frac{8Z_1 Z_2^2 Z_3}{(Z_1^2+Z_2^2)(Z_2^2+Z_3^2) + 4Z_1 Z_2^2 Z_3 + (Z_1^2-Z_2^2)(Z_2^2-Z_3^2)\cos(4\pi \frac{d\omega}{c} \cos\theta_2)} \tag{10}$$

where ω is the frequency, $\dot{c}$ is the characteristic or acoustic velocity, d is the thickness of the layer, and Z is as defined before. The limitation on θ is taken as

$$\sin\theta_1 \leq 1 \quad \text{for } c_1 > c_3$$

$$\sin\theta_1 \leq c_1/c_3 \quad \text{for } c_1 < c_3.$$

Equation (9) may be written as

$$q_{1-3} = \frac{E_1 c_1}{2} \Gamma(\alpha) \tag{11}$$

$$\Gamma(\alpha) = \frac{1}{E_1} \int_0^{\omega max} \int_0^{\theta_1 max} \alpha(\omega,\theta) E_1(\omega) \cos\theta_1 \sin\theta_1 d\theta_1 d\omega \tag{12}$$

where $\Gamma(\alpha)$ is the integrated transmission coefficient for this case. The functional dependence has been indicated in parentheses. Since E_1 appears in both the numerator and denominator of eq. (11), the E_1 coefficient in eqs. (11) and (12) may be evaluated using an infinite upper limit in eq. (7) giving

$$E_1(\infty) = \frac{(kT_1)^4 \pi^2}{30\hbar^3 c_1^3}. \tag{13}$$

Substituting eq. (13) into eqs. (11) and (12)

$$q_{1-3} = \frac{(kT_1)^4 \pi^2}{60\hbar^3 c_1^2} \Gamma(\alpha) \tag{14}$$

$$\Gamma(\alpha) = \frac{30\hbar^3 c_1^3}{\pi^2 (kT_1)^4} \int_0^{\omega_{max}} \int_0^{\theta_1 max} \alpha \frac{\hbar\omega^3}{c_1^3 2\pi^2} \left[\frac{1}{e^{\hbar\omega/kT_1} - 1}\right] \cos\theta_1 \sin\theta_1 d\theta_1 d\omega \tag{15}$$

where α is given by (10). The transmission coefficient for the two transverse modes is found by substituting the transverse velocity of propagation in place of the longitudinal velocity. Equation (15) was integrated with the aid of a computer program for several materials with layer thickness as a parameter. In evaluating the impedances Z_1, Z_2 and Z_3, the relationships between the angles of incidence and refraction were expressed as

$$\theta_2 = \sin^{-1}\left(\frac{c_2}{c_1} \sin\theta_1\right)$$

$$\theta_3 = \sin^{-1}\left(\frac{c_3}{c_2} \sin \sin^{-1}\left(\frac{c_2}{c_1} \sin\theta_1\right)\right).$$

Once the transmission coefficient $\Gamma(\alpha)$ is known, the net heat flow q" can be determined as done by Little [1] and Kittel [2] using eq. (14) to obtain

$$(q_{1-3} - q_{3-1}) \quad \text{or}$$

$$q'' = \frac{k^4 \pi^2 \Gamma(\alpha)}{60\hbar^3 c_1^2} [T_1^4 - T_2^4] \tag{16}$$

$$= 5.0 \times 10^9 \frac{\Gamma(\alpha)}{c_1^2} [T_1^4 - T_2^4] \quad W/m^2. \tag{17}$$

Expressions for the transverse modes are the same except for the velocity term.

In the development of this plane layer model of an imperfect contact, local quantum theory has been applied in evaluating the thermal energy density within the contacting materials, and non-local or "global" continuum boundary conditions have been applied in evaluating the thermal energy transport across the contact interface. It is assumed that phonons are the dominant mode of transport across interstitial gas or oxide. Subsequent comparison with experiment supports this assumption.

4. Comparison with Experiment

The value of the transmission coefficient as defined by eq. (17) is tabulated in table 1 for representative experimental data reported by Barzelay et. al. [4] [5] and Ozisik and Hughes [6]. The contact pressure is indicated. Data presented by Fenech and Rohsenow [7] [8], Rogers[9] and Fried[10] was considered in a study of the relation of layer thickness in the model to the experimental variables.

Table 1. Experimental transmission coefficient. The thickness d of an air layer required for agreement of computed values with experimental values of the transmission coefficient is indicated.

Case	T_1 ^oK	Finish Microns CLA	p psi	Γ_{exp}	d m
Steel-Air-Steel	441	~ 3	20	7.93×10^{-8} [6]	9.8×10^{-8}
Al-Air-Al	369	~ .75	7	2.32×10^{-7} [4]	8.30×10^{-8}
SS-Air-SS	369	~ .9	7	6.91×10^{-8} [4]	9.9×10^{-8}

Case	T_1 °K	Finish Microns CLA	p psi	Γ_{exp}	d m
SS-Air-Al	375	~ 1	90	8.41×10^{-8} [5]	5.0×10^{-10}
Al-Air-SS	368	~ 1	90	1.85×10^{-7} [5]	6.0×10^{-10}

The thickness d of an air layer required to make computed values of the transmission coefficient agree with experimental values is also tabulated in table 1. This required layer thickness was obtained by plotting computed values of the total transmission coefficient $\Gamma(\alpha)$ as a function of d for each set of materials as illustrated in figure 3, and then the required value of d can be found corresponding to the experimental $\Gamma(\alpha)$ that satisfied eq. (17). A computed value of the total transmission coefficient $\Gamma(\alpha)$ including both longitudinal and transverse modes that could be compared with experimental determinations was obtained from

$$\Gamma(\alpha) = [\Gamma_l + 2\Gamma_t \, c_l^2/c_t^2]. \tag{18}$$

This is the transmission coefficient plotted in figure 3. Note that $\Gamma(\alpha)$ is a function of d for a particular material arrangement. This layer thickness d may in turn be a function of surface flatness, roughness, interstitial gas or oxide, pressure, temperature, temperature gradient, and other variables. Thus, most of the variables affecting thermal conductance as studied by others have been incorporated into one parameter, d. Dr. P. H. McDonald first suggested this approach to us.

The physical properties of the materials were obtained from the Handbook of Chemistry and Physics 1966 ed. and from the American Institute of Physics Handbook 1963 ed. Values of longitudinal and transverse phonon velocities of propagation were obtained from tabulations of acoustic velocities.

The results of comparisons such as those in table 1 and figure 3 are surprising in several respects. First, the required air layer thickness appears reasonable and consistent with some mean void that would be physically inherent in contacts pressed together normally. Second, the reduction in conductance observed by Barzelay [5] and Rogers [9] from stainless steel to aluminum compared to the conductance from aluminum to stainless steel (with other variables held essentially the same) is predicted remarkably well by the model! As one evidence, note the nearly constant value of d obtained for the last two reciprocal cases in table 1. This effect would not occur if there was no air or oxide layer.

Also, the effect of contact pressure is predicted with some success by treating the layer as compressible with thickness d inversely proportional to pressure. This has some basis, particularly in the elastic region of behavior of the materials. Relative elastic strengths of dissimilar contacting materials are undoubtedly a significant factor in some instances. In cases such as the specific example in figure 3, the effect of pressure usually appears to be less than it is for smoother surfaces with a smaller "d" where a "compressible layer model" suggests $\Gamma(\alpha)$ or conductance roughly proportional to applied pressure over a somewhat steeper portion of the curve in figure 3 in qualitative agreement with a number of observations. The observation of conductance increasing exponentially with pressure by Weills and Ryder [11] for smooth aluminum and bronze appears consistent with the compressible layer model since d and a steep slope on a curve such as Figure 3 is consistent with their results.

Even for thermal contacts in vacuum, some oxide or adsorbed gas will undoubtedly be present at the interface. The "mismatch" of an oxide layer is much less than for the air layer considered above, and calculated conductances are much greater. No such marked increase has been reported for smooth flat surfaces in vacuum by Fried [10]. Adsorbed gases are inherent even in vacuum, and to a phonon with characteristic wavelength less than 100 Angstroms even optically flat surfaces do not look flat.

More detailed comparisons and evaluations are being made, particularly for the role of surface roughness on the equivalent layer thickness for the model described here. However, experimental data is not abundant and often is by necessity incomplete or insufficient to establish a definite pattern that either qualifies or disqualifies a theory. The effect of relative surface flatness is a particularly distressing variable. If the layer thicknesses on the order of 100 Angstroms indicated by the model developed here are indeed representative of actual contacts, relative flatness may be an important variable as pointed out by Ozisik and Hughes [6] even for "optically flat" surfaces considered by Fried [10] who noted that optically polished contacts are the least reproducible, particularly in a vacuum. This is to be expected according to the case considered in figure 3 where the thinner the layer, the more sensitive the transmission coefficient is to layer thickness. Conversely, for a thicker effective layer such as sawtooth milled surfaces might provide, observations should be more reproducible because the transmission coefficient would be less sensitive to changes in effective layer thickness brought about by changes in contact pressure. This would correspond to the region for $d > 10^{-7}$ m in figure 3.

This does not necessarily mean that investigation of this reproducible region will provide greater understanding of contact heat transfer phonomena. The non-reproducible region may reveal more.

The model presented here can be more easily applied to specific cases with some approximation by evaluating $\Gamma(\alpha)$ in eq. (17) for normal incidence ($\theta_1 = 0$) and taking an infinite upper limit for ω_{max} so that $E_1(\omega)$ becomes $E_1(\infty)$ as defined by eq. (13).

5. Summary and Conclusions

A general model for thermal contact conductance is presented in terms of one parameter, an equivalent effective gas or oxide layer thickness that is a function of the several variables. Local quantum concepts have been applied in determining the thermal energy or phonon density within the material and non-local continuum boundary conditions have been superimposed to evaluate the energy transport across the contact interface. It is shown that some of the wide variation in observations is to be expected due to a marked increase in energy transmission with decreasing effective layer thickness, with transmission very sensitive to small changes in the effective layer thickness for the thin layers associated with smooth flat surfaces. The data considered that have a strong dependence on contact pressure fall in this sensitive region and the observed behavior is consistent with treating the layer as being compressible. The effective layer thicknesses required to make the model agree with experiment are roughly on the order of 10^{-8} m (100 Angstroms) so optically flat surfaces may be far from being thermally flat since variations of 10^{-8} m may affect conductance appreciably. The difference reported for the net conductance from aluminum to stainless steel compared to the reciprocal arrangement of stainless steel to aluminum is predicted by the model. A determination of the functional dependence of the effective layer on the several variables has not been attempted, even so the model presented here should be useful in evaluating experiments and in determining how to best change some of the important variables in order to increase or decrease thermal conductances reproducibly.

6. References

[1] Little, W. A., The transport of heat between dissimilar solids at low temperatures. Canadian Journal of Physics, Vol. 37, pp. 334-349. (1959).

[2] Kittel, C., Introduction to Solid State Physics, 2nd Ed. John Wiley and Sons, Inc., New York (1956). Also 3rd ed.

[3] Holt, V. E., Energy transport across interfaces at low temperature, Proceedings 4th annual S.E.S. (October 31, 1966).

[4] Barzelay, M. E., Tong, K. N. and Holloway, G. F., Thermal conductance of contacts in aircraft joints. National Advisory Committee for Aeronautics, Technical Note 3167, Washington, D. C. (1954).

[5] Barzelay, M. E., Tong, K. N. and Holloway, G. F., Effect of pressure on thermal conductance of contact joints. National Advisory Committee for Aeronautics, Technical Note 3295, Washington, D. C. (1955).

[6] Ozisik, M. N. and Hughes, Daniel, Thermal contact conductance of smooth-to-rough contact joints. Paper presented at 1966 Winter Annual Meeting of ASME, N. Y., N. Y., 66WA/HT-54 (1966). Also unpublished data.

[7] Fenech, H. and Rohsenow, W. M. 1959. The thermal conductance of metallic surfaces in contact. Atomic Energy Commission, New York Office, Report 2136. Office of Technical Service, Department of Commerce, Washington, D. C.

[8] Fenech, H. and Rohsenow, W. M. 1963. Prediction of thermal conductance of metallic surfaces in contact. Journal of Heat Transfer, Vol. 85, February, pp. 15-24.

[9] Rogers, G. F. C., Heat transfer at the interface of dissimilar metals. Int. Journal Heat and Mass Transfer, Vol. 2, pp. 150-154 (1961).

[10] Fried, E., Study of Interface Thermal Contact Conductance, Contract NAS 8-11247, No. 66SD44 71 (July, 1966). Also No. 65SD4395 (June 1965).

[11] Weills, N. D. and Ryder, E. A., Thermal resistance measurements of joints formed between stationary metal surfaces. Transactions ASME, Vol. 71, No. 3, pp. 259-267 (1949).

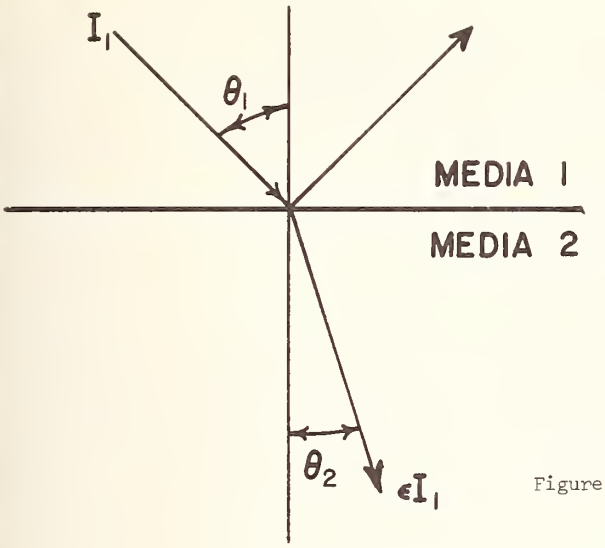

$$\epsilon = \epsilon_{1-2} = \epsilon_{2-1} = \frac{4 Z_1 Z_2}{(Z_1 + Z_2)}$$

$$Z_i = \frac{\rho_i c_i}{\cos \theta_i} \qquad i = 1,2$$

Figure 1. Model for the transmission of phonons across a perfect interface between two isotropic materials.

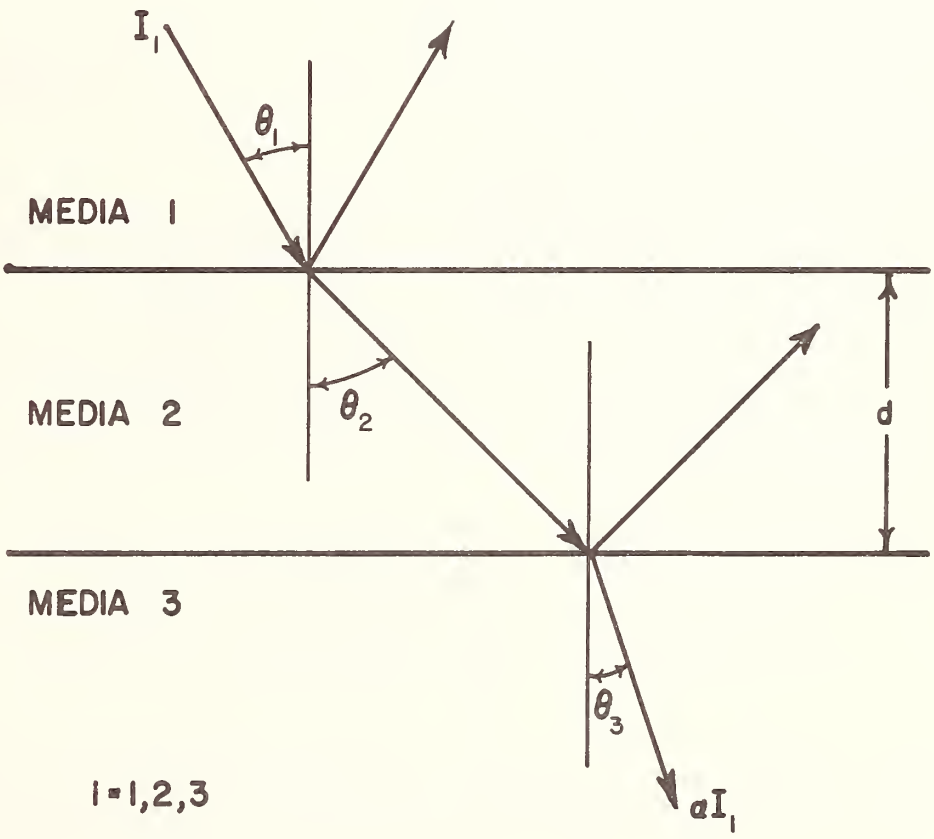

$$Z_i = \frac{\rho_i c_i}{\cos \theta_i} \qquad i = 1,2,3$$

$$\frac{\text{SIN } \theta_i}{\text{SIN } \theta_{i+1}} = \frac{c_i}{c_{i+1}} \qquad i = 1,2$$

Figure 2. Model for the transmission of phonons across a layer representing an imperfect contact.

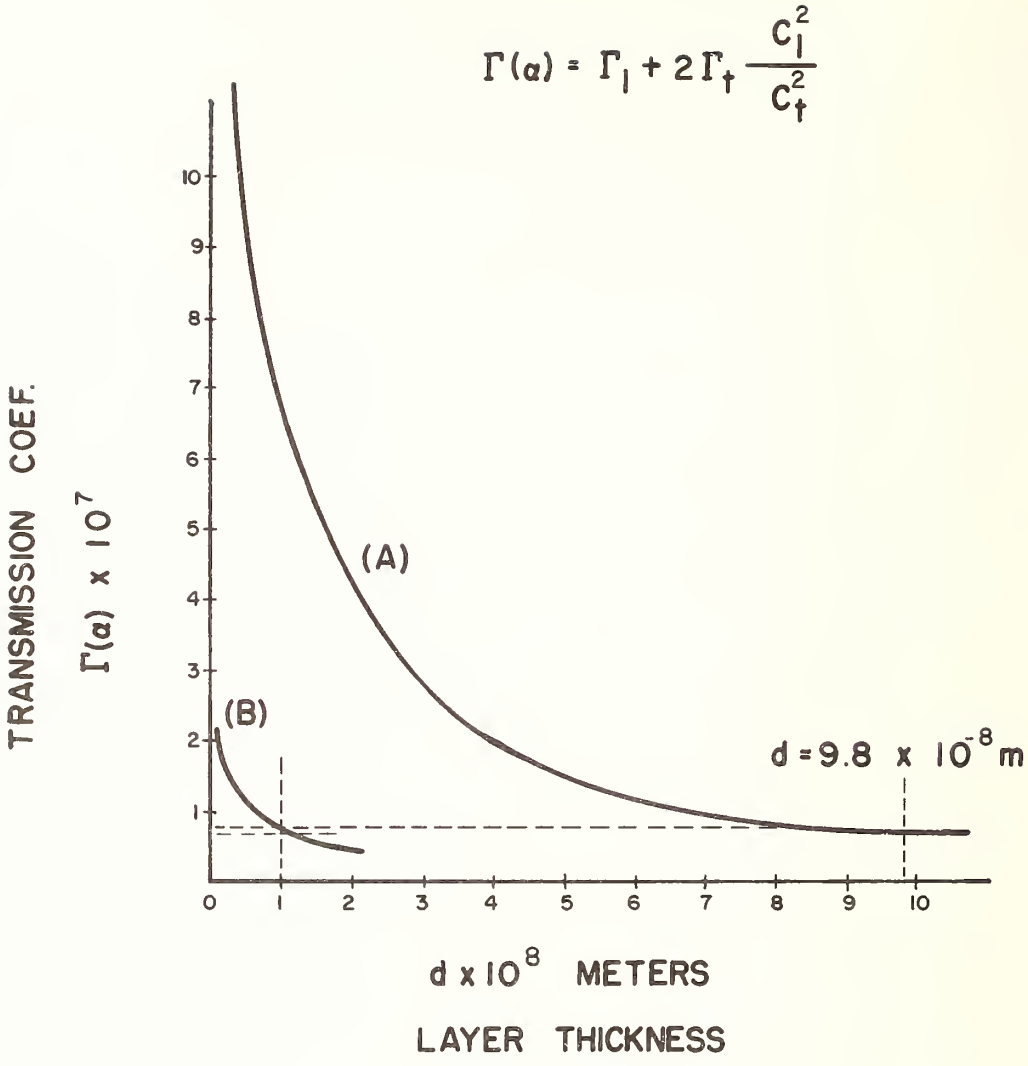

Figure 3. Illustration of procedure for determining the equivalent layer thickness d required to make the theory agree with experiment. (A) Steel-Air-Steel ground surface, $d = 9.8 \times 10^{-8}$ m, $\Gamma = 7.93 \times 10^{-8}$. (B) Stainless Steel-Air-Stainless Steel ground surface, $d = 9.9 \times 10^{-9}$ m, $\Gamma = 6.91 \times 10^{-8}$. (Cases 1 and 3 in table 1).

Ultrasonic Measurement of the Thermal Conductance of Joints in Vacuum[1]

Ludwig Wolf Jr. and Constantine Kostenko[2]

IIT Research Institute
Chicago, Illinois

This paper presents the results of a preliminary study of the feasibility of employing ultrasonics for the determination of the thermal conductance of mechanical interfaces in vacuum. Simultaneous measurements of the ultrasonic transmission and thermal conductance of two test interfaces were performed. The correlation between ultrasonic transmission and thermal conductance is presented for each interface and a method for generalizing these correlations is discussed. It is shown that ultrasonic transmission of an interface is a sensitive indicator of its thermal conductance in vacuum and that it may be possible to correlate the equivalent interfacial thickness with measurements of surface topography.

Key Words: Conductivity, interface resistance, interfacial conductance, thermal conductivity, ultrasonic transmission, ultrasonics

1. Introduction

In vacuum at ordinary temperature levels the conduction of heat through a small portion of the nominal contact area where two mated members are in actual physical contact alone determines the thermal conductance of a mechanical interface.

Because of the complexity of the topography of real surfaces, there seems to be no reliable way to predict actual contact area, or the variation of contact area with applied pressure, from measurements of the surface topography of mated members and of material properties. Since actual contact area is the most important single factor affecting the thermal conductance of an interface, little success can be seen for theoretical studies of thermal contact conductance. It is suggested, therefore, that an empirical-experimental approach which in some ways takes into account the actual physical contact area of an interface between mated members will meet with greater success.

2. Theory

The thermal contact conductance (h_j) of a joint is defined as

$$h_j = \frac{Q}{A\Delta T} \tag{1}$$

where Q is the total rate of heat transferred across the joint, A is its nominal contact area and ΔT is the temperature difference across the joint (which is usually determined by extrapolating the temperature distribution in each of the mated members to the nominal location of the interface). An expression for the heat transferred across the interface, similar in form to the one-dimensional heat flow equation, may be written as

---

[1] This work was supported by the IIT Research Institute

[2] Associate Engineers, Heat and Mass Transfer Section, IITRI

$$Q = k\, A_a \frac{\Delta T}{\Delta X} \tag{2}$$

where k is the thermal conductivity of the mated members (for the present discussion taken to be identical materials), A_a is the actual contact area between the mated members and ΔX is the equivalent interfacial thickness over which the temperature difference ΔT occurs. The above equation is in fact the defining equation for ΔX.

By eliminating $Q/\Delta T$ between Eqs. 1 and 2 the following dimensionless relation is obtained:

$$\frac{h_j \Delta X}{k} = \frac{A_a}{A} \tag{3}$$

This expression relates the thermal conductance to the fraction of the area in actual contact (A_a/A), and the equivalent interfacial thickness (ΔX). Both of these parameters (A_a/A and ΔX) are, in general, functions of the topography of the mated surfaces, the nominal pressure applied to the joint, and the physical properties (yield strength, modulus of elasticity, etc.) of the mated materials. Since it is clear from Eq. 3 that the thermal conductance of an interface is linearly dependent on the thermal conductivity of the material, and since it is reasonable to suppose that ΔX and A_a/A are not functions of thermal conductivity, the role of thermal conductivity on the interface conductance (at least for identical mated materials) need not be discussed further.

If a beam of ultrasonic waves is projected normal to a mechanical interface, a portion of the beam will be reflected by the interface and the remaining portion will be transmitted across the interface. Past experience with ultrasonics tends to support the contention that the fraction of the incident ultrasonic energy that is transmitted across the interface depends only on the fraction of the nominal joint area which is in actual physical contact. If this be the case, it is quite likely that for any particular interface, the percent transmission of ultrasonic energy across the interface will bear a definite relationship to the thermal conductance of the interface.

One could determine experimentally the relationship between the ultrasonic transmission and the thermal conductance by measuring both for a particular interface, and these measurements could be repeated for varying degrees of contact pressure. In this way curves of interfacial thermal conductance and ultrasonic transmission as functions of contact pressure could be generated for a particular interface. These curves could then be cross-plotted to yield a curve of thermal conductance as a function of ultrasonic transmission. (This procedure will be illustrated later).

In general, the relationship between the thermal conductance of a joint and its ultrasonic transmission will be different for different surface finishes even though the actual contact area might be the same. This is seen from Eq. 3. There is a characteristic length dimension (ΔX) associated with each interface. The relationship between the thermal conductance of an interface and its ultrasonic transmission could be determined experimentally (as described above) for a variety of joints with different surface topographies. In this way it would be possible to generate a set of "Correlation Curves" relating the thermal conductance to ultrasonic transmission for mechanical interfaces over a range of typical surface topographies. The existence of such correlation curves would allow the determination of the thermal conductance of a particular interface from a simple, fast, inexpensive measurement of ultrasonic transmission and a knowledge of the surface topography. No knowledge of the contact pressure is required. Hopefully, the correlation curves would not be greatly dependent on surface topography so that interpolation between correlation curves could be made without introducing significant error.

It may be possible to generalize the ultrasonic transmission technique further, thereby making it an even more powerful tool. If the transmission of ultrasonic energy across a mechanical interface is indeed a function only of the fraction of the nominal area actually in contact, then Eq. 3 can be written as

$$\frac{h_j \Delta X}{k} = \frac{A_a}{A} = F(T) \tag{4}$$

where F is a universal function of T, the ultrasonic transmission. If a correlations between the equivalent interfacial thickness (ΔX) and easily measurable properties of surface topograph (i.e. waviness, roughness, etc.) could be obtained and if the variation of ΔX with percent contact area (or with ultrasonic transmission) could be determined, it would be possible to experimentally determine the function F. Thus, the set of correlation curves discussed above could be replaced by a single universal relationship between interface thermal conductance and ultrasonic transmission ($h_j \Delta X/k$ versus T).

It is of interest to discuss a method by which the required correlation between the equivalent interfacial thickness ΔX and surface topograph, and the dependence of ΔX on T (or A_a/A) might be determined. If the ultrasonic transmission is indeed a function only of actual contact area, then according to Eq. 3, any difference in the thermal conductance of two interfaces with the same actual contact area (same ultrasonic transmission) is due to differences in the equivalent interfacial thicknesses, ΔX. If the subscripts 1 and 2 represent two joints with different surface topography, then from Eq. 3

$$h_{j1} = \left(\frac{A_a}{A}\right)_1 \frac{k_1}{(\Delta X)_1}$$

and $$h_{j2} = \left(\frac{A_a}{A}\right)_2 \frac{k_2}{(\Delta X)_2}$$

For identical materials ($k_1 = k_2$) and for equal percent contact area $(A_a/A)_1 = (A_a/A)_2$ or $(T_1 = T_2)$, it is clear that

$$\frac{(\Delta X)_2}{(\Delta X)_1} = \frac{h_{j1}}{h_{j2}} \tag{5}$$

This ratio of equivalent interfacial thicknesses can be determined for any two interfaces by a point to point division of the experimentally generated curves of thermal conductance versus ultrasonic transmission. This procedure will result in a curve of $(\Delta X)_2 / (\Delta X)_1$ versus transmission coefficient, T. At this point it should be noted that this procedure will only allow determination of the ratio of two equivalent interfacial lengths as a function of ultrasonic transmission. It is not possible to determine only ΔX as a function T. This, however, presents no problem since Eq. 4 may be written as

$$\frac{h_j \Delta X_r}{k} \cdot \frac{\Delta X}{\Delta X_r} = F(T) \tag{4a}$$

where ΔX_r is associated with an arbitrarily chosen interface to which all others are compared.

It is reasonable to suppose that by comparing the experimentally-determined ratio of equivalent interfacial thicknesses to parameters describing the surface topology (such as root-mean-square roughness, waviness amplitude, etc.) it may be possible to relate the equivalent interfacial thickness, ΔX, of an interface to an easily measurable parameter describing the surface topography of the mated members.

3. Experimental Program

With the preceding theory as background, a program was undertaken with the following objectives:

(1) To construct an apparatus capable of simultaneously obtaining measurements of thermal conductance and ultrasonic transmission of test interfaces in a vacuum environment.

(2) To establish the existence of the relationship between interface thermal conductance and ultrasonic transmission for a number of interfaces having different surface topographies.

No direct attempt was to be made to investigate the feasibility of generalizing the ultrasonic technique to all surface topographies and material properties. However, as will be seen below, the results of the present program are useful to this end.

A detailed description of the experimental apparatus (both thermal and ultrasonic) and of the experimental procedure are presented in the Appendix. The study was limited to interfaces in which the mated members were constructed of the same material (Armco Iron) and each member of a pair has the same nominal surface topography. Two interfaces were tested; one with turned surfaces, the other with ground surfaces. A profilometer measurement of the surface topography of each of the mated members was obtained. Both the thermal conductance and ultrasonic transmission were measured for each interface over a wide range of nominal contact pressures (0 - 3500 psi).

In figure 1 are shown both the thermal conductance and ultrasonic transmission as functions of the nominal contact pressure for interface No. 1 (turned surfaces). The corresponding data for interface No. 2 (ground surfaces) are given in figure 2. The ultrasonic energy transmitted across the interface is shown as a fraction of the energy transmitted at the highest contact pressure, and thus it varies between 0 and 1. The data of figures 1 and 2 have been cross-plotted in figure 3 to show the relationship between thermal conductance and ultrasonic transmission for each of the two joints. These relationships indicate that ultrasonic transmission is a sensitive indicator of joint thermal conductance.

The profilometer measurements indicated that the mated members of interface No. 1 had a waviness amplitude of about 150 micro-inches and a roughness amplitude of about 150 micro-inches. Interface No. 2 had a considerably smaller waviness amplitude, about 25 micro-inches, and a roughness amplitude of about 100 micro-inches.

The ratio of equivalent interfacial lengths $(\Delta X)_2/(\Delta X)_1$ as given by Eq. 5 is shown in figure 4. This curve was obtained by point-to-point division of the two relationships between the thermal conductance and ultrasonic transmission shown in figure 3. This ratio remains fairly constant over the entire range of ultrasonic transmission (percent contact area).

While these preliminary data do illustrate the techniques involved in the determination of ΔX as a function of T, they do not provide enough information to draw concrete conclusions. Many more experiments of this nature are required. It is difficult with only a single set of data to speculate about the relation between the ratio of equivalent interfacial lengths and the surface topography. For the present tests $(\Delta X)_2/(\Delta X)_1$ had a value of about 0.6. The ratio of waviness amplitudes for the two interfaces was about 0.17 and the ratio of roughness amplitudes was about 0.67. This tends to confirm intuition that the equivalent interfacial length ΔX is strongly dependent on the roughness amplitude, and only weakly related to waviness amplitude. However, much more data must be gathered before any definite statements can be made as to the exact relationship between surface topography and equivalent interfacial length.

In summary, the experimental program has yielded two significant results. These are:

1. Ultrasonic transmission of an interface is a sensitive indicator of its thermal conductance in vacuum.

2. Preliminary investigations indicate that it may be possible to generalize the ultrasonic evaluation of thermal conductance of joints by correlating the equivalent interfacial length with measurements of surface topography.

4. Acknowledgement

The authors wish to thank Messrs. H. Karplus, A. Goldsmith, W. J. Christian, and W. Laurie of IITRI who contributed materially to this work.

5. Appendix

The technique employed to measure the thermal conductance of an interface consisted of passing heat axially along a pair of mated cylinders (1-1/16" diameter, 2-1/2" long). The steady-state temperature distribution in each cylinder was obtained with a precision potentiometer and 36-gage copper-Constantan thermocouples at three axial positions of each cylinder. Since the mated members were of a standard material (Armco Iron), the heat flow through the interface was determined from the constant temperature

gradient in the mated members and their known thermal conductivity. The temperature drop across the interface was obtained by extrapolating the temperature distribution in each member to the nominal location of the interface. An electrical heater (with a PVC insulator) and a water cooled sink (both copper) were provided at the top and bottom of the stack, respectively. All tests were performed near room temperature.

A sketch of the stack arrangement is shown in figure 5. The ultrasonic transducers, which were gold-plated quartz crystals 3/8" in diameter and approximately 1/16" thick, were positioned centrally on the back faces of the mated members. Since an ultrasonic beam does not diverge, only the central 3/8" diameter of the test interfaces (12% of the interface area) was surveyed by the ultrasonics whereas the thermal measurements correspond to the entire interface area. The surfaces were sufficiently uniform that this difference had no significant effect. The transducers were held firmly in place by a spring-loaded insulator and electrical contact plate.

The entire stack was enclosed in a vacuum container equipped with provisions for entry and exit of thermocouple and heater wires, water lines, and a bellows arrangement on the container cover for transmitting an externally applied load to the interface. The vacuum was maintained by a system consisting of a cold trap, diffusion pump, and fore pump. The vacuum was measured with a Pirani gauge (2000μ to 1μ) and an ionization gauge (10^{-3} torr to 10^{-8} torr). The vacuum served two functions; one, to remove the air in the test interface, and two, to prevent convective heat loss from the stack. The tests were conducted at a pressure of approximately 4×10^{-4} torr. No detectable heat loss from the stack could be measured at that vacuum level.

The contact pressure on the interface was varied by applying a force on the stack through a bellows in the top of the vacuum container. The force was applied through a ball joint by a pneumatic cylinder actuated by a commercial nitrogen bottle. The entire assembly was supported within a yoke. The nominal contact pressure of the interface was calculated from the nominal surface area of the joint, the pneumatic cylinder bore, and the gas pressure indicated by the pressure regulator on the nitrogen bottle. There is also a small contact pressure due to atmospheric pressure acting on the bellows. The contact pressure could be varied from near zero to well over 3500 psi.

The ultrasonic transmission through the interface was determined by placing ultrasonic transducers at each end of the mated co-axial cylinders. A short pulse of ultrasonic energy was directed at the interface from one transducer. The energy transmitted through the interface was received by the other transducer and this signal was displayed on an oscilloscope. By means of a switching arrangement it was also possible to obtain a measurement of the energy reflected from the interface. In this arrangement a single transducer serves as both the transmitter and receiver. The ultrasonic transducers were X-cut quartz crystals with a thickness resonant frequency of about 7 megahertz. The crystals were held against the specimen by springs, and a small amount of petroleum jelly was applied to the transducers to assure complete mechanical contact. The pulse to be transmitted was generated by an Arenberg PG 650C pulse generator with a pulse tuned to the resonant frequency of the crystal and the pulse duration set to about 5 micro-seconds, which is about the minimum obtainable with this oscillator. This duration permitted recovery of the WA600 amplifier before the reflected pulse appeared from its round trip to the interface. The time delay of the reflected pulse was approximately 22 micro-seconds. To minimize the adverse effects of drift in the pulse generator and amplifier, the amplitudes of the reflected and transmitted pulse were measured immediately before and immediately after the contact pressure on the interface was changed.

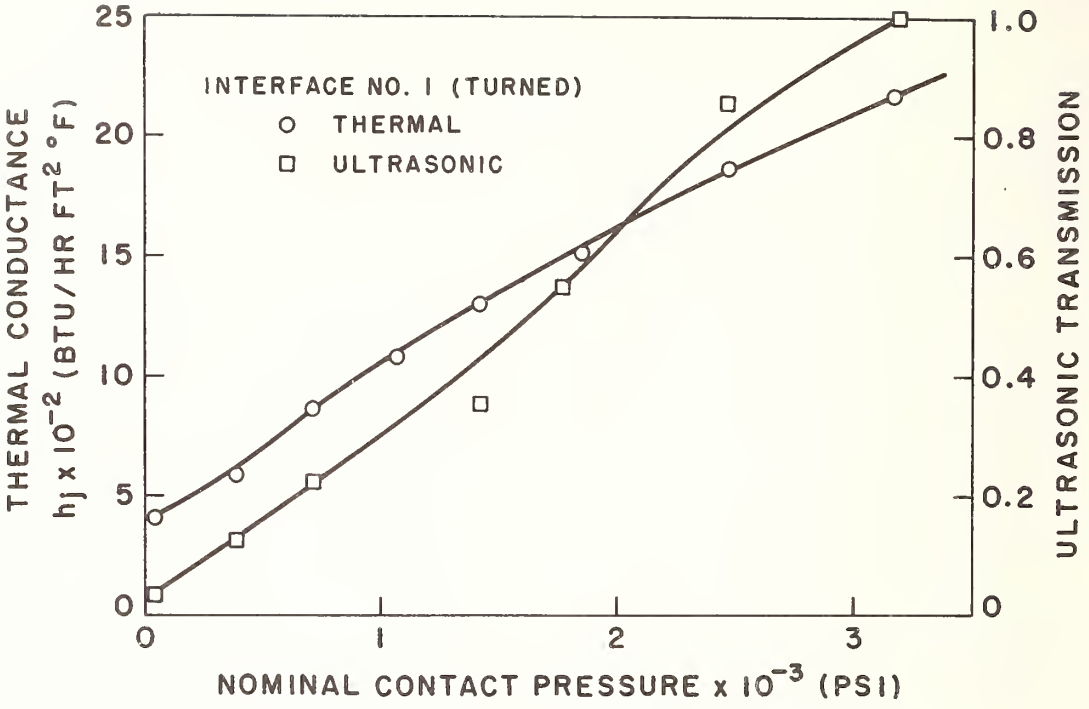

FIG. 1 THERMAL CONDUCTANCE AND ULTRASONIC TRANSMISSION VERSUS CONTACT PRESSURE, INTERFACE NO. 1

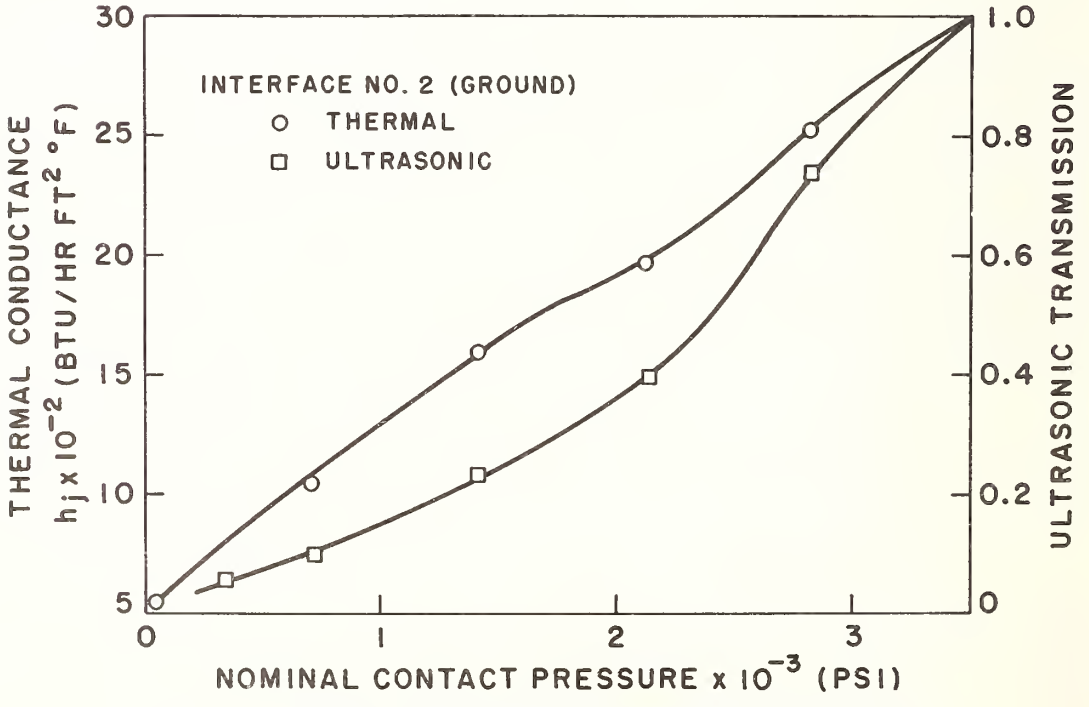

FIG. 2 THERMAL CONDUCTANCE AND ULTRASONIC TRANSMISSION VERSUS CONTACT PRESSURE, INTERFACE NO. 2

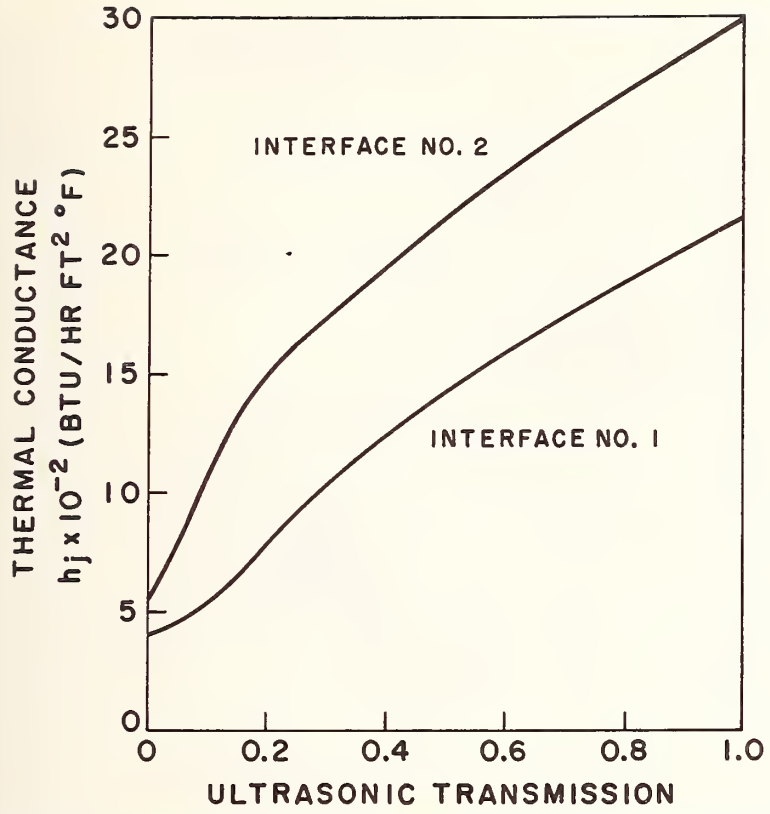

FIG. 3 THERMAL CONDUCTANCE VERSUS ULTRASONIC TRANSMISSION

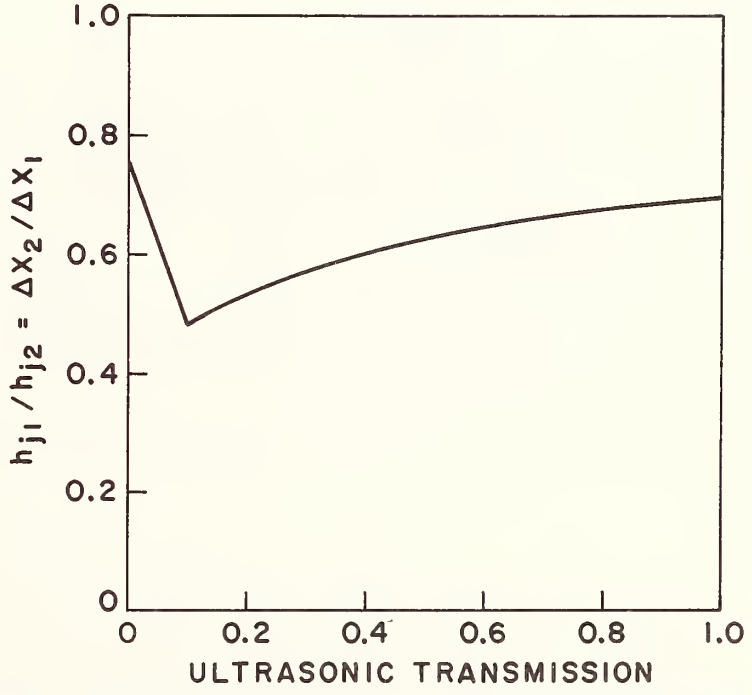

FIG. 4 RATIO OF EQUIVALENT INTERFACIAL LENGTHS VERSUS ULTRASONIC TRANSMISSION

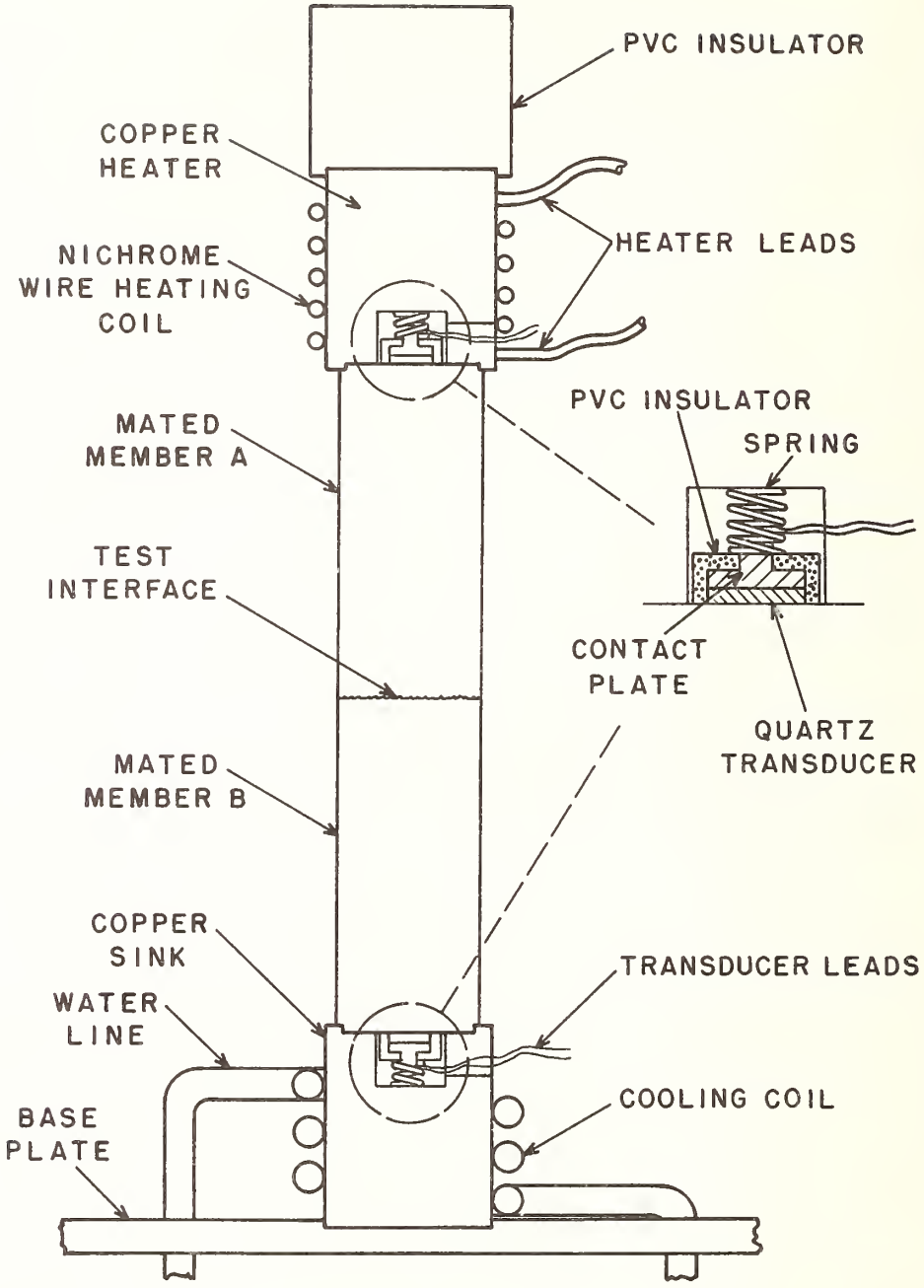

FIG. 5 SKETCH OF STACK ARRANGEMENT

Thermal Resistance of Sapphire-Sapphire Contact

Y. Baer

Laboratorium für Festkörperphysik
ETH, Zürich, Switzerland

The transport of heat between smooth sapphire surfaces has been measured in ultra-high vacuum in the temperature range from 15 to 300°K. The contact consists of a sphere pressed against a plane with a variable load up to 5 kp. The thermal resistance can be separated into two terms: the well known constriction resistance which is mainly determined by the bulk resistivity and the boundary resistance. A theoretical model has been developed to describe the last term. Two parameters must be introduced to take into account the state of real surfaces. The experimental results as a function of load and temperature are in very good agreement with such a model and the influence of different surface treatments is well explained. Further experiments are devoted to contacts between rough surfaces.

Key Words: Thermal contact resistance, sapphire (α-Al_2O_3), thermal conductivity, phonon scattering, mechanical contact, surface physics.

1. Introduction

Interest in the thermal contact problem has increased in the last years and many publications are devoted to the thermal conductivity of porous media and powders. Whereas measurements are rather easy, the theoretical aspects are not quite clear as a result of the complexity of the heat transfer mechanisms and the difficulty of giving a realistic description of the geometrical situation. It appears necessary to search for simple experiments which are concerned with only one mechanism and to investigate what theoretical model is appropriate to give an account of these experimental results. This work is devoted to the study of the phonon flow through a contact with a well defined geometrical shape. An apparatus has been constructed to measure in ultra-high vacuum the thermal resistance of a contact consisting of a sphere pressed against a plane with a variable load. The temperature can be varied from 15 to 300°K. Sapphire (α-Al_2O_3) shows the features of low temperature thermal conductivity in the most characteristic way and its mechanical properties give the possibility of making very well defined surfaces of contact. A theoretical model will be developed to describe the thermal resistance of contacts between insulators. It shows that one term is strongly connected with the structure of the surfaces and the absorbed layers. This prediction is very well confirmed by the experimental results so that such measurements appear as a new tool in surface physics.

2. Apparatus and Measurement Method

Figure 1 shows a schematic diagram of the thermal contact conductance apparatus. The samples are two circular cylinders of 3 mm diameter and 2.5 mm length, the contacting surfaces are highly polished, the one plane , the other spherical. One sample is fastened on the massive copper block A and in good thermal contact with it. The temperature T_3 is kept constant with a sensitive temperature regulator. On the second sapphire a thin tungsten wire is wound so that this sample can be heated with the power $\dot{Q}$. The third sapphire rod acts as a holder only; it is attached to the copper part B, which can

rotate around the pivot P. The load on the contact is produced by the spring elongation. This linear motion is transmitted under vacuum with a Varian Feedthrough. In such a way the error in load is estimated to be less than ± 5 gr. For a given power $\dot{Q}$, two temperature differences are present: $\Delta T_r = T_1 - T_2$ and $\Delta T_m = T_1 - T_3$. ΔT_r is kept small and constant with the help of a temperature regulator which controls the power in the heater H. This regulator has been developed in our laboratories by Fröhlich [1][1], it has an input sensitivity of 10 nV and a zero stability better than 50 nV in the time required for a measurement. The potential difference corresponding to ΔT_m is amplified with a calibrated Keithley 148 Nanovoltmeter and measured with a Leeds and Northrup K-3 Potentiometer. The transfer of heat by radiation can be fully neglected so that the power $\dot{Q}$ corresponds to the heat flow through the contact for a temperature difference ΔT_m. At any temperature T_3 this measurement has been repeated for three different powers in order to eliminate errors due to non vanishing ΔT_r. The error affecting the measurement of λ, the heat flow per degree, has been estimated to be less than ± 2%.

The whole system is enclosed in an ultra-high vacuum vessel and baked at 300-400°C for two days. Following bakeout, a simple cryostat is mounted around the vacuum vessel, which works with nitrogen, hydrogen or helium as cooling liquid.

3. Theory

3.1. The Constriction Resistance

The contact members will always be regarded as isotropic in all their properties. In the case of a plane and a sphere, the contact surface is circular and, if the radius of curvature of the sphere is not too small, such a contact is in fact symmetrical. We consider at first an ideal contact. This means that the resistance is solely determined by the shape of the contact. This well known problem is exhaustively discussed by Holm [2], and has the following solution:

$$\frac{1}{\lambda_p} = R_p = \frac{\rho}{2a} \quad , \tag{1}$$

ρ : thermal resistivity of the contact members a : contact radius

The most striking aspect of the resistance R_p, called constriction resistance, is that the thermal gradient is in fact located in a small sphere of radius 4a around the contact. The validity of (1) is based on the assumption that the definition of ρ has meaning in the gradient region. This is always true as long as $a \gg \Lambda$, where Λ is the phonon mean free path, but as soon as $a \ll \Lambda$, the resistance has a different origin and an independent analysis is required. This size effect will be investigated later.

3.2. The Surface Resistance

A real surface exhibits a serious perturbation of the superficial structure. It is absolutely impossible to give a detailed description, but different kinds of perturbations can be enumerated:

a) Polycrystalline or amorphous films resulting from mechanical polishing or chemical treatment.

b) Stoichiometric deficiency.

c) Foreign atoms adsorbed on the surface.

The two surfaces in contact will only be characterized by a disturbed film of thickness 2d, of unspecified nature. The single condition which must be satisfied is $2d \ll a$, so that this thickness can be neglected in macroscopic considerations. In a Debye model the flow of phonons incident on a surface element dS with frequency ω in the interval ω , $\omega + d\omega$ and polarization γ is given by

$$N(\omega, \gamma, \varphi, T)\, d\omega\, d\varphi\, dS = \frac{\omega_\gamma^2}{(2\pi)^2 c^2} \frac{1}{e^{\hbar\omega/kT} - 1} \cos\varphi \sin\varphi\, d\varphi\, d\omega\, dS \tag{2}$$

[1] Figures in brackets indicate the literature references at the end of this paper.

These phonons have the velocity c and their wave vector $\vec{q}$ is pointing in the solid angle $d\Omega = 2\pi \sin\varphi \, d\varphi$, where φ is the angle between the normal to dS and $\vec{q}$. Only the fraction of the energy due to these phonons

$$N(\omega, \gamma, \varphi, T)\hbar\omega D'(\omega, \gamma, \varphi) \, d\omega \, d\varphi \, dS \tag{3}$$

will be transmitted through the film. In this expression $D'(\omega, \gamma, \varphi)$ is the transmission coefficient. For a temperature gap $\Delta T = 1$ deg, the net flow of heat across the film will be

$$F(\gamma, T) \, dS = \frac{dS}{2(2\pi)^2 c^2 \hbar^2 k T^2} \int_0^{\omega_D} \frac{(\hbar\omega)^4 e^{\hbar\omega/kT}}{(e^{\hbar\omega/kT}-1)^2} D(\omega, \gamma) \, d\omega \tag{4}$$

ω_D : Debye frequency

$D(\omega, \gamma)$ is now a directional average of $D'(\omega, \gamma, \varphi)$. The expression (4) is very similar to that of the specific heat of a phonon gas whose spectrum is multiplied with $D(\omega, \gamma)$. It is well known that the specific heat is very insensitive to the detailed shape of the phonon spectrum so that we can describe the transmission coefficient by the simple relation:

$$\begin{aligned} D(\omega, \gamma) &= H \leq 3 \qquad \omega \leq \omega_c \\ D(\omega, \gamma) &= 0 \qquad\quad \omega > \omega_c \\ \omega_c &\leq \omega_D \end{aligned} \tag{5}$$

ω_c appears as the maximum vibrational frequency transmitted through the film and H as a mean transmission coefficient for $\omega \leq \omega_c$. With these definitions, the conductance λ_s may be written in the convenient form

$$\lambda_s = \frac{1}{R_s} = A H \theta_c^3 C\left(\frac{\theta_c}{T}\right) \pi a^2 \tag{6}$$

$$\text{with } A = \frac{k^4}{6(2\pi)^2 \hbar^3 c^2}, \quad \theta_c = \frac{\hbar\omega_c}{k}$$

$$C\left(\frac{\theta}{T}\right) = 3\left(\frac{T}{\theta}\right)^3 \int_0^{\theta/T} \frac{z^4 e^z}{(e^z-1)^2} \, dz$$

In the low temperature limit we obtain with the usual approximation for the specific heat:

$$\lambda_s = \frac{2 k^4}{(2\pi)^2 \hbar^3 c^2} H \frac{\pi^4}{15} T^3 \pi a^2 \tag{7}$$

This formula, except for the definition of H, is identical to those obtained by Little [3] and Jones and Pennebaker [4]. It is interesting to notice that the expression (7) no longer depends on the parameter θ_c. For practical purposes we define a temperature dependent transmission coefficient:

$$D(T) = \frac{H\theta_c^3 C\left(\frac{\theta_c}{T}\right)}{3\theta_D^3 C\left(\frac{\theta_D}{T}\right)} \tag{8}$$

which is H/3 at low temperatures and decreases to reach the value of $\left(\frac{\theta_c}{\theta_D}\right)^3$ H/3 at very high temperatures. Using this definition, the following expression for the conductance may be obtained:

$$\lambda_s = \frac{1}{4} c C_v D(T) \pi a^2 \tag{9}$$

where C_v is the specific heat per volume unit. If one writes the bulk thermal conductivity in the form $\sigma = 1/3\ c\ C_v \Lambda$, the final result is

$$\frac{1}{R_s} = \lambda_s = \frac{3\sigma}{4\Lambda} D(T)\ \pi\ a^2 \tag{10}$$

3.3. The Total Resistance

The two resistances R_s and R_p have been described separately and the problem is now to determine how to express the total contact resistance. This question requires a detailed discussion which will appear elsewhere [5]. The result is that the total resistance is given simply by the following sum:

$$R = R_p + R_s \tag{11}$$

This formula is a good approximation except when $R_p \approx R_s$. In that short range the total error will be still less than 15%. The combination of equations (1) and (10) gives a useful relation for studying the behaviour of the total contact resistance:

$$\frac{R_s}{R_p} = \frac{8}{3\pi} \frac{K}{D(T)} \tag{12}$$

It can be used to define different ranges as a function of the two parameters K and D(T), as shown in figure 2. An ideal contact is characterized by $D(T) \equiv 1$ so that to any variation of T or a, corresponds a motion along a vertical line. This case has been calculated by Wexler [6] which confirms the approximate validity of the relation (11). At high temperatures (ohmic régime) the constriction resistance is dominant while at low temperatures (Knudsen régime) a new term appears which is absolutely independent of Λ. This resistance is a size effect related to the geometrical shape of a contact and the measurement of the transition range could be used as a direct determination of the mean free path. In the case of a real contact ($D(T) < 1$), the variation of T for a constant radius of contact a, determines now a curve which is no longer vertical and the transition form R_p to R_s occurs in the ohmic range.

4. Models of the Transmission Coefficient

4.1. Disturbed Film Model

It is impossible to give a detailed description of the phonon scattering in the disturbed film. One way to get around this difficulty is to relate the actual disordered structure of the film to statistical parameters. Such a theory has been developed by Ziman [7] who calculated the mean free path Λ_p in irregular materials. He describes the disturbed structure with two parameters: the variance of the sound velocity $\overline{(\delta c)^2}$ and the correlation length L which determines the scale of the irregularities. In the long wave limit the result of Ziman can be used to calculate the transmission coefficient:

$$D \approx 1 - 4\pi^{7/2} \frac{\overline{(\delta c)^2}}{c^2} \alpha \left(\frac{2d}{\lambda}\right)^2 \tag{13}$$

with $\lambda \gg 2d$, $L = \alpha\ 2d$, $\alpha \lesssim 1$.

This expression has only a qualitative validity but it shows clearly that the phonons are scattered only slightly. As the frequency increases the transmission coefficient will become appreciably smaller than one. That means that the phonons have a non-vanishing probability to be scattered more than once, and the definition of $D(\omega, \gamma)$ no longer has meaning. In this case the film resistance can be very simply described by the following expression:

$$\frac{1}{R_f} = \lambda_f = 1/3 \; c \; C_v \frac{\overline{\Lambda_p}}{2d} \pi a^2 = \sigma_f \frac{\pi a^2}{2d} \tag{14}$$

$\overline{\Lambda_p}$ is the mean free path of the dominant phonon mode. It must be noticed that this formula can be formally identified with (9) if one puts

$$D(T) = \frac{4}{3} \frac{\overline{\Lambda_p}}{2d} \tag{15}$$

In ignorance of the numerical factors in (13) it is very difficult to give a criterion for the transition from R_s to R_f but it seems correct to assume that this occurs at about θ_c.

4.2. Interface Resistance

The model of a disturbed film does not take explicitly into account the presence of an interface nor does it suppose that its influence is predominant. The potential between two flat surfaces has probably the form of a Lennard-Jones potential and depends only on the mean separation of these surfaces so that the motion of the atoms parallel to the interface will practically not be coupled. Accordingly, one third of the incident energy only has some probability to be transmitted through the interface and the parameter H will not be greater than one. Little [3] has pointed out a geometrical argument based on the roughness of the surfaces, which shows that the effective transmitting area for a contact between hard crystals is a decreasing function of the frequency. This means in the formalism of this work that, for a constant apparent area of contact, the transmission coefficient is a decreasing function of the frequency. It is a very complex problem to know exactly the scattering at the interface and it would require a detailed description of the force constants that is practically impossible. Ludwig and Pick [8] have calculated the scattering of phonons at defect planes in the simple cubic lattice and an examination of this work shows clearly that the general tendency in all cases is that the high frequencies are more effectively scattered than the low frequencies. It is very difficult to decide at low temperatures what mechanism is the most important because they all are consistent with the definition (5). An observation of pressure dependence of θ_c and H could lead to a conclusion because the disturbed film resistance alone is certainly independent of the mechanical pressure.

5. Analysis Method of the Experimental Results

All the expressions established previously depend on the contact radius a, which is related to the load, for an elastic deformation, by the classic theory of Hertz (see Holm [2]). A direct measurement of the contact radius as a function of load has been carried out under a microscope. The results, as shown in figure 3, are in good agreement with the formula of Hertz and confirm a strictly elastic deformation.

The thermal properties of sapphire are well known [9], [10] but it is of interest in connection with this problem to remember the very great variation of the mean free path as a function of temperature. The total contact resistance can be expressed as the following sum

$$R(a,T) = \frac{1}{2a\sigma(T)} + \frac{1}{\pi a^2 A \; H \; \theta_c^3 \; C(\theta_c/T)} \tag{16}$$

Some remarks are required concerning the validity of this formula:

a) The simple addition of the two terms may cause a maximal error of 15% in the range where $R_p \approx R_s$.

b) The thermal properties have been considered as independent of the mechanical deformation.

c) The parameters θ_c and H are possibly dependent on the load.

d) If the film resistance model is valid, R_f (14) must be substituted for R_s (6) in the high temperature range.

6. Experimental Results and Discussion

6.1. Polycrystalline Surfaces

The surfaces of these samples (S_1) have been submitted to an intensive mechanical polishing which produces a nearly perfect geometrical shape but disturbs strongly the structure to a depth of about 0.5 μm [11]. Fig. 4 shows the temperature dependence of the contact conductance for different contact radii. It is quite clear in this case that R_f must be used in formula (11) to analyze these results, but σ_f is an unknown function. Therefore the constriction term has been substracted from the total resistance and the resistance per area unit has been calculated, as shown in figure 5. This dependence is characteristic of a highly polycrystalline or nearly amorphous structure. If $2\hat{a} \approx 1\,\mu m$ the conductivity of this material is $6 \cdot 10^{-1}$ W $m^{-1} deg^{-1}$ at 300°K which is a typical value for glasses. It appears that mechanically polished surfaces are not convenient to study the surface resistance and that other treatments must be investigated in order to produce better surfaces.

6.2. Treated Surfaces

Two different methods have been used to obtain flat surfaces without perturbing the superficial structure too much. In the first case (samples G) the mechanically polished crystals have been annealed for two hours at 1300°C. Dinichert [11] has shown that this thermal treatment is sufficient to recrystallize the disturbed region. The other samples (B_{11}) have been etched for 2 minutes in orthophosphoric acid at 450°C. In such a way a 3 μm thick film is removed from the surface, which remains perfectly flat and smooth. These two kinds of samples yield the same results which proves that the surface state is no longer influenced by the mechanical polishing. As indicated in figure 6 the temperature dependence of λ is more pronounced and the maxima occur at lower temperatures. An analysis of these results is now possible with the surface resistance model. The low temperature range has been carefully measured and the experimental values fitted to the theoretical expression (6) as shown in figure 7. The characteristic temperature θ_c is small, $\theta_c = \theta_D/5$, this means that an interface acts really as a high frequency phonon filter. The parameter H is independent of the contact radius and its value is consistent with the theoretical prediction. The whole temperature range can be described now by the sum of the two resistances as shown in figure 8. The resistance R_s has been used up to 300°K which is not necessary correct but the possible induced error is small and the agreement is fairly good. The dependence on the contact radius has been measured at high and low temperatures where only one resistance in dominant (see fig. 9 and 10) and the behaviour predicted by equation (16) is fully satisfied. As indicated in figure 10, the points labelled A correspond to a contact closed with a maximal load at room temperature while the points B correspond to a contact opened for 2 minutes at 35°K. The most satisfactory explanation of this effect is that the adsorbed molecules are driven back out of the contact at high temperatures whereas they are strongly bound to the surface at low temperatures. The run A is reproducible so that such adsorption effects have been systematically eliminated.

Contacts between rough surfaces have also been investigated. The results, which will appear elsewhere [5], also give a very nice confirmation of the surface resistance model.

7. Conclusion

The thermal contact resistance under well defined conditions has been interpreted with a two-resistance model. A satisfactory description of the phonon diffraction is given by the parameters θ_c and H which have a simple physical meaning. It is very difficult to decide exactly what mechanism is the most effective, therefore, it seems desirable to vary as much as possible the surface quality and to observe the influence on the transmission coefficient. Unfortunately a comparison with the low temperature measurements of Berman and Mate [12] on sapphire-sapphire contact is very difficult because the effective contact area is not known. A deviation from the T^3-law is not surprising if one realizes that θ_c may be as small as θ_D /5.

The advantage of measuring the thermal resistance with this geometrical shape is that it allows one to study the diffraction on an isolated obstacle independently of any other bulk diffraction. This separation may be used now in varied situations so that it seems permissible to think that this technique will have a scope in the study of many surface properties.

I am very grateful to Prof. G. Busch for helping with the choice of problem and for his continuing encouragement of the work. I would like to thank C. Fröhlich for many helpful discussions and contribution in instrumentation. The author is also indebted to the Schweizerischer Arbeitsbeschaffungskredit for financial support.

8. References

[1] Fröhlich, C., Private Communication.

[2] Holm, R., Electric Contacts Handbook, Springer (1958).

[3] Little, W.A., Canad.J.Phys. 37, 334 (1959).

[4] Jones, R.E. and Pennebaker, W.B., Cryogenics 3, 215, (1963).

[5] Baer, Y., to appear in Phys.Kondens. Materie.

[6] Wexler, G., Proc.Phys.Soc. 89, 927, (1966).

[7] Ziman, J.M., Electrons and Phonons, Oxford (1962).

[8] Ludwig, W. and Pick, H., Phys.Status Solidi 19, 313 (1967).

[9] Slack, G.A., Phys.Rev. 126, 427 (1962).

[10] Holland, M.G., J.Appl.Phys. 33,2910, (1962).

[11] Dinichert, M.P., Bull. de la Société Suisse de Chronométrie (1964).

[12] Berman, R. and Mate C.F., Nature 182, 1662 (1958).

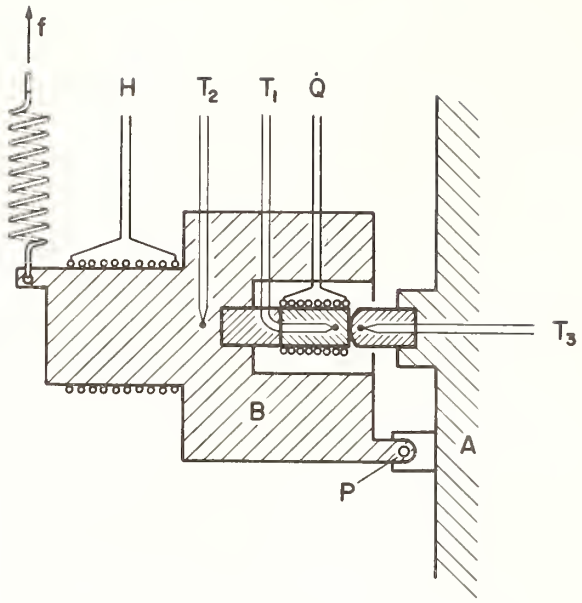

Figure 1. Schematic diagram of the experimental arrangement.

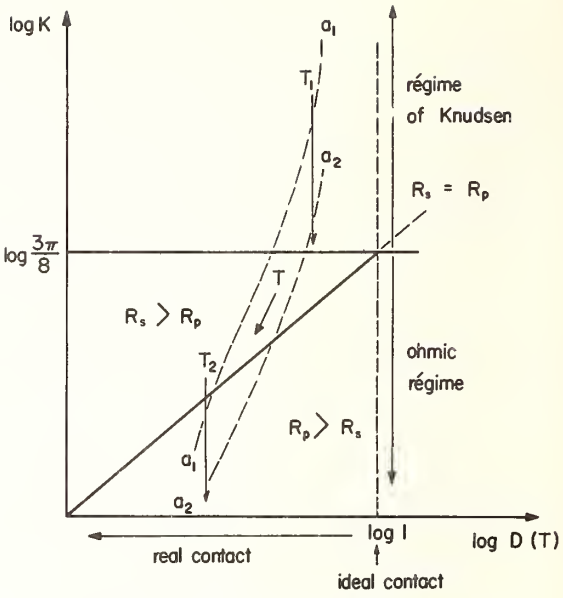

Figure 2. Diagram illustrating the different conduction régimes.

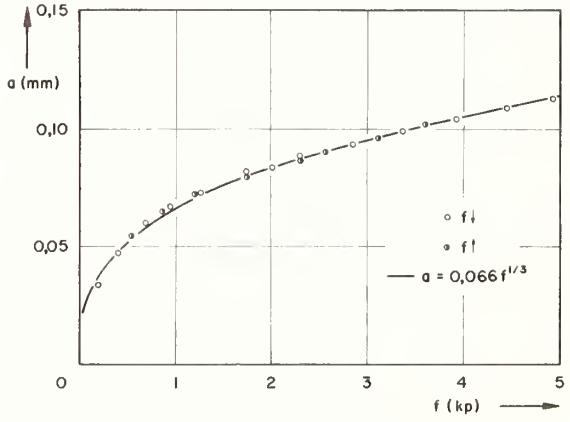

Figure 3. Contact radius versus load.

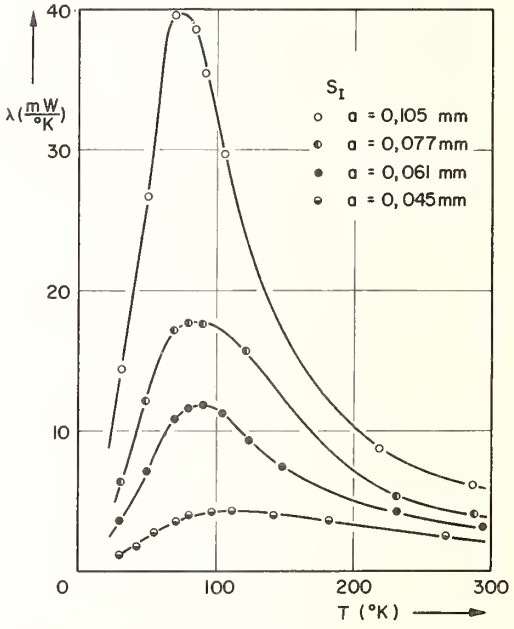

Figure 4. Temperature dependence of thermal conductance for different contact radii (polycrystalline surfaces).

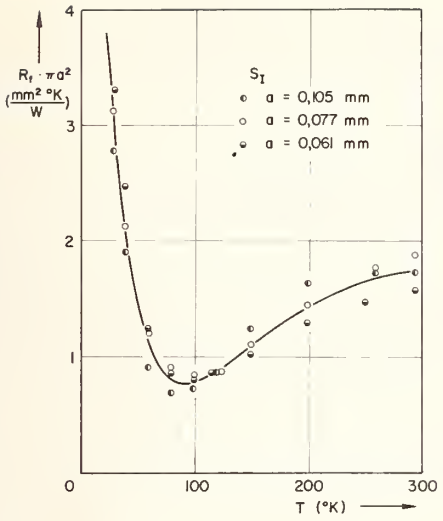

Figure 5. Thermal resistivity of the polycrystalline film as a function of temperature.

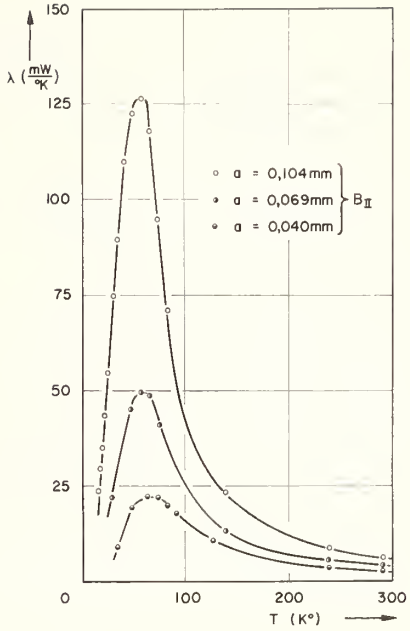

Figure 6. Temperature dependence of thermal conductance for different contact radii (treated surfaces).

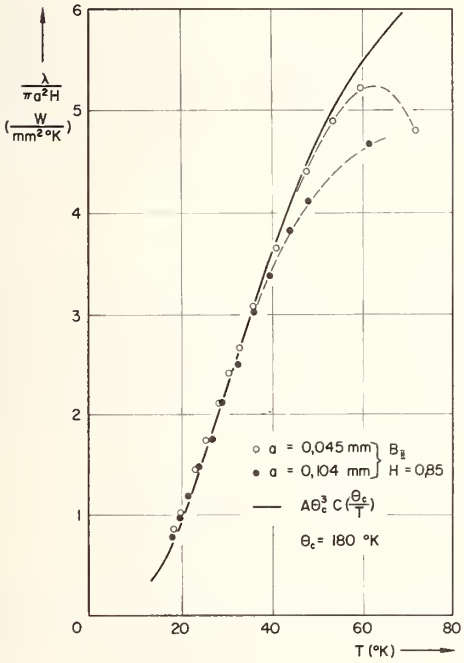

Figure 7. Fit of low temperature results to the formula for the surface resistance model.

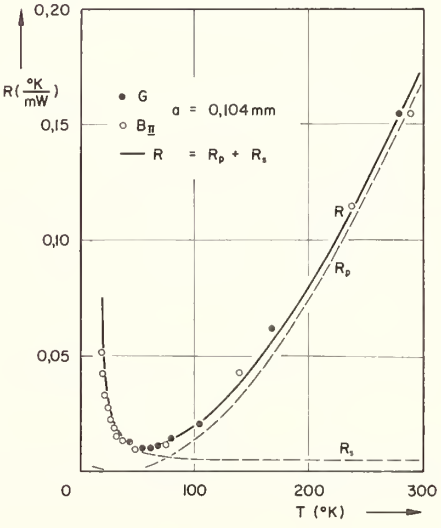

Figure 8. Comparison of experimental values of thermal resistance with theoretical model.

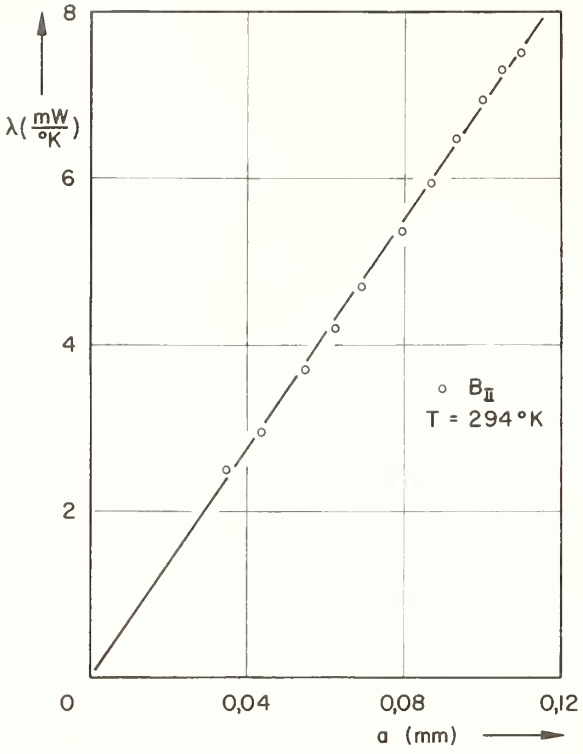

Figure 9. Thermal conductance versus contact radius.

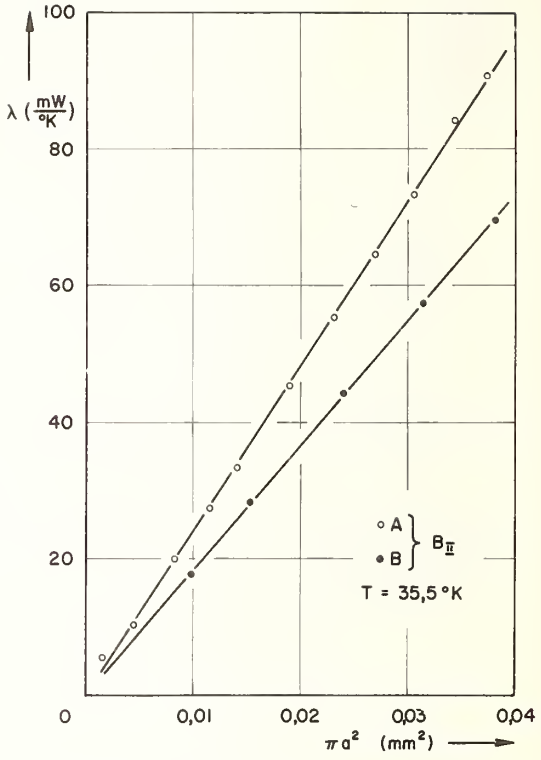

Figure 10. Thermal conductance versus contact area.

Heat Transfer Across Surfaces In Contact: Effects of Thermal Transients on One-Dimensional Composite Slabs

C. J. Moore, Jr.[1]
North Carolina State University
Raleigh, North Carolina

H. A. Blum[2]
Southern Methodist University
Dallas, Texas

Solutions are derived for the time-dependent temperature distribution in a two-layer, composite slab with contact resistance at the interface and contact or convective resistance on the outer boundaries. The applicability of these solutions for the prediction of the transient behavior of real composite systems is evaluated by comparison with experimental results. Experimental data are presented for the transient thermal response of several composite metal systems when subjected to thermal transients in which an attempt was made to approximate the boundary conditions of the theoretical solutions. Comparisons with the experimental data indicate that the theoretical solutions can be used to predict the transient thermal response of systems to which they are applicable to an accuracy sufficient for most engineering purposes.

Key Words: Composite slabs, contact conductance, contact resistance, heat conduction, thermal contact conductance, thermal transients, transient heat conduction.

1. Introduction

In recent years there has been increased interest in studies of thermal contact resistance. Most of these studies have been aimed at understanding the mechanism of heat transfer across a solid interface. This paper presents some of the results of an investigation into the effects of thermal contact resistance on the transient temperature fields in composite solids separated by interfaces which have thermal contact resistance. This study consisted of both theoretical and experimental work, the results of which are given below.

2. Solution of the Boundary Value Problem

The boundary value problem of interest here is that of obtaining the space time temperature distribution in a composite solid medium consisting of two regions separated by an interface which has a resistance to heat flow. Figure 1 depicts the geometry employed and some of the necessary nomenclature. Both regions are assumed one-dimensional and homogeneous within themselves, a discontinuity in thermal properties across the interface is allowed which requires separate solutions for the two distributions. Both solutions must obey the one-dimensional Fourier equation, thus,

$$\frac{\partial^2 t_1}{\partial x^2} = \frac{1}{\alpha_1}\frac{\partial t_1}{\partial \theta} \qquad (0 \le x \le a) \quad , \quad \frac{\partial^2 t_2}{\partial x^2} = \frac{1}{\alpha_2}\frac{\partial t_2}{\partial \theta} \qquad (a \le x \le L) \tag{1}$$

The interface contact conductance coefficient is given the symbol, h_c (w/m^2-deg). There are also heat transfer resistances at the outer boundaries characterized by the conductance coefficients h_1 and h_2.

Initially both regions are at a uniform temperature t_i. At time $\theta = 0$ the temperature at the $x = 0$ boundary is exposed to a medium at temperature t_o and the $x = L$ boundary is kept in contact with a medium

---

[1] Assistant Professor, Mechanical and Aerospace Engineering.

[2] Professor, Mechanical Engineering.

at temperature t_i. All conductance coefficients are assumed to remain constant. It is noted that even though these solutions were developed for the purpose of comparison with experimental results with solid contact conductances at all these boundaries (x = 0, a and L), they are equally applicable to the case of convective fluid heat transfer at the outer boundaries and solid contact resistance in the interface.

In symbolic form the boundary conditions are

$$T_1(x,0) = 0 \qquad 0 \le x \le a \tag{2}$$

$$T_2(x,0) = 0 \qquad a \le x \le L \tag{3}$$

$$k_1\left(\frac{\partial T_1}{\partial x}\right) = h_1(T_1 - 1) \qquad x = 0,\ \theta > 0 \tag{4}$$

$$k_2\left(\frac{\partial T_2}{\partial x}\right) = h_2(T_2 - 0) \qquad x = L,\ \theta > 0 \tag{5}$$

$$k_1\left(\frac{\partial T_1}{\partial x}\right) = k_2\left(\frac{\partial T_2}{\partial x}\right) \qquad x = a,\ \theta > 0 \tag{6}$$

$$k_1\left(\frac{\partial T_1}{\partial x}\right) = h_c(T_2 - T_1) \qquad x = a,\ \theta > 0 \tag{7}$$

Where the normalized temperature T (x, θ) has been used,

$$T_1(x,\theta) = \frac{t_1(x,\theta) - t_i}{t_o - t_i}, \qquad T_2(x,\theta) = \frac{t_2(x,\theta) - t_i}{t_o - t_i} \tag{8}$$

The solutions obtained from eqs (1) by the standard technique of separation of variables in product form are well known. With the proper choice of sign on the separation constants the solutions for the two regions are:

Region (I)

$$T_1(x,\theta) = K_1(x) + \sum_n B_n\left[C_n \cos\gamma_n x + \sin\gamma_n x\right] e^{-\gamma_n^2 \alpha_1 \theta}$$

Region (II)

$$T_2(x,\theta) = K_2(x) + \sum_n B_n\left[F_n \sin\delta_n x + G_n \cos\delta_n x\right] e^{-\delta_n^2 \alpha_2 \theta} \tag{9}$$

These solutions have been written as the sum of steady and time-dependent parts. For the latter, summations have been indicated in anticipation of having to expand the initial condition in a series. The steady state solutions are given by

$$K_1(x) = 1 - S\left(\frac{1}{h_1} + \frac{x}{k_1}\right), \qquad K_2(x) = S\left(\frac{L-x}{k_2} + \frac{1}{h_2}\right) \tag{10}$$

wherein

$$S = \frac{1}{\frac{1}{h_1} + \frac{a}{k_1} + \frac{1}{h_c} + \frac{b}{k_2} + \frac{1}{h_2}} \tag{11}$$

Application of eq (4) gives

$$C_n = \frac{k_1 \gamma_n}{h_1} \tag{12}$$

Next, eq (5) is applied and results in

$$G_n = F_n\left[\frac{N_n + \tan \delta_n L}{N_n \tan \delta_n L - 1}\right] \tag{13}$$

in which

$$N_n = \frac{k_2 \delta_n}{h_2}$$

It is assumed that no heat storage occurs in the infinitesimally thin interface. This is equivalent to saying that the time derivative of both sides of eq (6) are equal, or

$$\gamma_n^2 \alpha_1 = \delta_n^2 \alpha_2 \tag{14}$$

Application of eq (6), together with eqs (13) and (14) yields

$$F_n = -\frac{k_1}{k_2}\sqrt{\frac{\alpha_2}{\alpha_1}}\left[\frac{(C_n \sin \gamma_n a - \cos \gamma_n a)(N_n \sin \delta_n L - \cos \delta_n L)}{N_n \sin \delta_n b - \cos \delta_n b}\right] \tag{15}$$

The eigenvalue equation results from the application of eq (7). After elimination of the derived constants the region I eigenvalue equation becomes

$$\gamma_n = \frac{h_c}{k_1}\left[\frac{C_n + \tan \gamma_n a}{C_n \tan \gamma_n a - 1}\right] + \frac{h_c}{k_2}\sqrt{\frac{\alpha_2}{\alpha_1}}\left[\frac{N_n + \tan\left(\gamma_n b\sqrt{\frac{\alpha_1}{\alpha_2}}\right)}{N_n \tan\left(\gamma_n b\sqrt{\frac{\alpha_1}{\alpha_2}}\right) - 1}\right] \tag{16}$$

From eq (14) the region II eigenvalues are then determined.

Only the series coefficients B_n are needed to complete the solution. As usual these coefficients are obtained by matching the initial condition in a series expansion. Ordinary techniques fail in this case due to the nonorthogonality of the solution eigenfunctions over the full x-interval (0,L) with respect to the usual weighing factor of unity. However, employing the work of Tittle (1)[3] the B_n can be found by evaluating the following integral relation.

$$B_n = \frac{-\int_0^a K_1(x)\left[C_n \cos \gamma_n x + \sin \gamma_n x\right]dx + C^2\int_a^L K_2(x)\left[F_n \sin \delta_n x + G_n \cos \delta_n x\right]dx}{\int_0^a \left[C_n \cos \gamma_n x + \sin \gamma_n x\right]^2 dx + C^2\int_a^L \left[F_n \sin \delta_n x + G_n \cos \delta_n x\right]^2 dx} \tag{17}$$

In this equation the constant, C, called "orthogonality factor" by Tittle is given by

$$C = \left(\frac{\alpha_1 k_2}{\alpha_2 k_1}\right)^{\frac{1}{2}} \tag{18}$$

Proof of the validity of eq (17) is given by Tittle. However, from eq (17) it can be seen that, alternatively, C^2 could be thought of as a discontinuous weighting function, having a value of unity in (o<x<a) and that given by eq (18) in (a<x<L). In a later and more general (unpublished) paper (2) Tittle has given this interpretation.

The integration and simplification of eq (17) is an involved algebraic exercise, thus only the results are given here. The form of B_n makes it simpler to define a new term by

$$B_n = \frac{-2}{E_n} \tag{19}$$

Wherein, E_n is given by

$$E_n = (C_n^2 + 1)\gamma_n a + (C_n^2 - 1)\sin \gamma_n a \cos \gamma_n a + 2C_n \sin^2 \gamma_n a$$
$$+ \frac{k_1}{k_2}\sqrt{\frac{\alpha_2}{\alpha_1}}\left[\frac{\cos \gamma_n a - C_n \sin \gamma_n a}{\cos \delta_n b - N_n \sin \delta_n b}\right]^2\left[(N_n^2+1)\delta_n b + (N_n^2 - 1)\sin \delta_n b \cos \delta_n b + 2N_n \sin^2 \delta_n b\right] \tag{20}$$

[3] Numbers in parentheses indicate the literature reference at the end of this paper.

The final solution can then be written as

Region I

$$T_1(x,\theta) = K_1(x) - \sum_{n=1}^{\infty} \frac{2}{E_n} \left[C_n \cos\gamma_n x + \sin\gamma_n x \right] e^{-\gamma_n^2 \alpha_1 \theta} \tag{21}$$

Region II

$$T_2(x,\theta) = K_2(x) - \sum_{n=1}^{\infty} \frac{2}{E_n} \left[F_n \sin\delta_n x + G_n \cos\delta_n x \right] e^{-\delta_n^2 \alpha_2 \theta}$$

In an earlier paper (3) the solution of a similar problem but with temperature boundary conditions at X = 0 and X = L was given. For that case several plots of dimensionless variables were presented for an arbitrarily defined time to reach steady state. The present solution contains several additional parameters, which makes the production of a similar set of curves more difficult. Work in this area is presently underway. However, emphasis in this paper is placed on the comparison of the above solution with experimental results. These solutions were programmed for use on a digital computer and verified for a range of variables by comparison with a fine-network numerical program.

3. Experimental Program

An experimental program was carried out in which an apparatus was designed, built and operated to provide test data on the transient response of one-dimensional, two-layer metallic systems with contact resistance. The primary purpose of the test data was to check the validity of the theoretical solution for real composite systems. To this end an attempt was made to create experimental conditions which approached, as closely as possible, the theoretical boundary conditions. Only a brief outline of the experimental program will be presented here, details are given in reference (4).

Basically the experimental program consisted of measuring the temperature distribution as a function of time in two metallic cylinders in contact while they were undergoing thermal transients. Figure 2 is a sectional drawing of the test section portion of the experimental apparatus. The other primary quantities measured were the axial force pressing the two cylinders together and the temperatures of the heat source and sink blocks. The entire test apparatus was enclosed in a vacuum bell jar so that lower values of contact conductance could be obtained.

3.1 Test Specimens

The metals used in the experiments were 2024-T351 aluminum, Armco iron and type 303-MA stainless steel. All specimens were made of 2.54 cm bar stock and had nominal lengths of 2.54 or 5.08 cm. Specimen details are given in Appendix A. Each specimen contained five thermocouples to obtain the transient temperature profiles. These thermocouples were chromel-constantan type (26 gage wire) with butt-welded measuring junctions. They were installed in shallow slots in the surface of the specimens. This procedure was employed rather than using drilled holes because: (a) it minimizes the location error of the measuring junction, (b) it gives more intimate contact, and (c) it provides a smaller interruption of the specimen cross section. Both of the latter also insure a better transient response.

In these transient experiments direct measurements of the heat flow are practically impossible. Therefore, calculations of contact conductance were made by evaluating the local heat flux from the thermal conductivity of the materials and the measured slopes of the temperature profiles. Since the conductance values thus depend directly on the thermal conductivity it was necessary to have experimental data for this property. These data were provided by D. R. Williams (5) over the temperature range of interest in these experiments. The values of thermal diffusivity were estimated from data available on similar alloys. Due to lack of information these values were assumed constant.

3.2 Temperature Measurement

The requirement of simultaneous, transient temperature measurements precludes the use of a balancing potentiometer for taking test data, thus all data were recorded on an oscillograph. Thermocouples used in this way have a small electrical current flowing at all times. Thermocouple reference tables are based on a balanced voltage reading and could not be used in this application. It was thus necessary to calibrate all the thermocouples of each specimen set over the range of temperatures to be incurred in the test. This was accomplished by using a portable calibration bath which could be set up adjacent to the test fixture and thus allow all the thermocouple circuits to be in the configuration

used during the tests. Since there was an electrical current flow in this application the temperature versus oscillograph deflection curves were slightly non-linear. The calibration readings were processed by a computer program to fit a least-squares second order polynomial through the calibration data of each thermocouple. These polynomials were used by the test data reduction program to calculate temperatures from the test data deflection readings.

3.3 Source and Sink Blocks

During the experiments the test specimens were held between the source and sink blocks as shown in figure 2. These blocks were constructed of OFHC copper and were hollow with inlet and outlet ports. The sink block temperature was held constant during the experiments by flowing room temperature water from a large tank. Steam from the building heating system was used to maintain the source temperature constant; the temperature was adjustable over the range of 143-153 ^{o}C by means of controlling the pressure using a throttling valve. During the experiments source temperatures of 149-151 ^{o}C were used.

3.4 Test Fixture and Loading System

The basic test fixture is shown schematically in figure 2. The two parallel plates were used to mount the sample holding and loading components, and were adjustable by means of the three threaded connecting rods to accommodate different total specimen lengths. The source block was held by an adapter and thermally insulated to reduce heat loss to the test fixture. As shown in figure 2, this adapter transmitted the applied force through a spherical joint to the upper plate, to which it was connected by three small helical springs. This arrangement was used to insure that any small misalignment in the test column would not cause the contact surfaces to be loaded unevenly. A second, similar adapter was used to hold the sink block. This adapter rested on the load cell (Lockheed Electronics Model WR75-025 Load Washer) which in turn rested on the loading rod of the hydraulic cylinder. This test fixture assembly rested on the base plate of the vacuum chamber.

The force control system is basically a closed-loop electro-hydraulic servomechanism. A double ended hydraulic cylinder applied the force to the test specimens. The cylinder was supplied with a constant pressure, constant flow stream of hydraulic oil by a pump and flow regulator. A proportional type servovalve controlled the pressure differential across the piston of the hydraulic cylinder and thus controlled the force applied to the test samples.

As shown in figure 2, the applied force was transmitted through the force cell. The output voltage of the force cell was used as a feedback signal. By means of a potentiometer an input signal was supplied at a polarity opposite to the feedback signal. The difference between these two voltages is the error signal which was amplified and used to drive the servovalve. In addition to providing a feedback signal for the controller the force cell signal was also used in recording the force on the samples during the experiments.

3.4 Experimental Procedure

The following is a brief outline of the procedures used in operating the test apparatus.

After the thermocouple circuits had been calibrated each end of both specimens was cleaned with acetone and absolute ethyl alcohol. The outside ends of both samples were coated with a thin film of Dow Corning silicone grease to reduce the contact resistance between the specimens and the source and sink block surfaces. Then the specimens were placed in the test apparatus. The samples were pressed together between the source and sink blocks with a pressure of about 10 psi. By a valving arrangement cooling water was circulated through both blocks for about 10 minutes to bring the samples to a uniform temperature. Next, the samples and sink block were lowered by the force system so that the upper (hot side) specimen no longer made contact with the source block. The vacuum bell jar was then lowered and test chamber evacuation started. While the system was pumping down the cooling water was kept flowing through the sink block but was shut off from the source block. Normally it required about 20 minutes to pump the test chamber down to the range of 1-5 microns hg. This pressure range was used because it was low enough to make the interstitial gas conduction small, and because it was easily obtainable with a mechanical pump. When the desired test chamber pressure was reached the oscillograph was started and the steam to the source block was turned on. About 20 seconds was required to bring the source block up to the desired temperature. Finally, an input signal to the force controller raised the sink block and test specimens, bringing the upper specimen into contact with the hot source block. All data were continuously recorded on the oscillograph record throughout the tests.

3.5 Data Reduction Procedure

As mentioned above, all data were recorded continuously on an oscillograph. The trace deflections of each measured quantity were manually read from the oscillograph records with a scale. The time intervals at which data were read varied with the specimens being tested. During the early portion of each experiment smaller time intervals were used because changes were more rapid. As the rate of change became slower the "data times" were more widely spaced. The deflections were read for each data time and were punched onto cards to be read into the data reduction computer program.

Of all the quantities measured and calculated the final results that were compared with the theoretical values consisted mainly of contact conductance results. These values were obtained by making least-squares curve fits through the temperature profiles for each data time and extrapolating these to the boundaries to calculate the contact surface temperatures. Then the contact heat flux was calculated from the local slope of the temperature profiles and the thermal conductivity. Finally, the contact temperature drops were calculated from the extrapolated profiles, and the contact conductance was determined from these temperature drops and the heat flux. The most critical quantities in assessing the accuracy of the results are the temperature measurements. These measurements are believed to be such that the probable accuracy of the calculated temperature drops is about $\pm$ 0.6°C. This made it impossible to calculate conductance values for small contact temperature drops. However, for those values reported here, it is believed that the contact conductance values fall within a range of $\pm$ 10% to $\pm$ 20%, depending on the level, with the lower values being, in general, more accurate.

4. Experimental Results

In the course of analyzing the experimental results it was found that the calculated conductance values appeared to vary sharply during the early portions of each experiment and then approach a steady state value. Although the details will not be given here it was concluded that this variation was only apparent and was the result of the poor accuracy inherent in making calculations with very small temperature drops and sharp slope changes which are present during the early part of the transients. Consequently, the comparisons made below are made using the conductance values calculated after steady state had been reached.

4.1 Comparison of Results

The primary purpose of the present study was to determine whether the constant-property theoretical solutions obtained above could be used to predict, with sufficient accuracy, the transient behavior of a real two-layer solid with contact resistance. For the purposes of comparison two parameters were chosen. The first of these is the time required to approach steady state. This is believed to be a parameter which is characteristic of transient behavior, as well as a practical one. For use in these comparisons the time to approach steady state was defined to be the time at which the temperature drop across the slowest reacting portion of the system was within one "time constant" of its steady state value, i.e., to within e^{-1}, thus the fraction is $1-e^{-1} = .632$. It was necessary to go to a lower value than the 0.99 fraction used in the previous theoretical work (3) to reduce the sensitivity to experimental error. The 99% criterion is more meaningful from a practical standpoint, but in this regime the rate of change of temperature drop with time is very low and small errors in temperature measurement would result in large time errors from experimental data.

The results of the comparisons are presented as plots of time to approach steady state versus interface contact conductance. The actual experimental values are tabulated in Appendix B. Those values shown in the plots reflect slight adjustments in the times made as follows. For each run of a given series, i.e., set of specimens, the contact conductances on the ends of the specimens (the outer boundaries) were different due to the different contact pressures on each run. It was desired to show the data in a form that could be compared to a single theoretical curve for each series, rather than a point-for-point comparison which could not be meaningfully plotted. The test data were plotted on a "map" of theoretical data which consisted of a plot of time to approach steady versus interface contact conductance for various values of the end conductance. From this plot it was found that the experimental data exhibited very nearly the same slopes as the theoretical for dependence on the end conductances. Thus the experimental times to reach steady state were adjusted by adding or subtracting a small amount. This amount is the difference in time found from the theoretical curves, at the experimental value of interface conductance, in going from the end conductance measured in each experiment to a value which was the approximate average for the complete series. In this way experimental values of steady-state time versus interface conductance for the same end conductance could be determined for each test series and compared with theory. It is emphasized that, as can be seen in Appendix B, the adjustments were usually small and should not affect the validity of the comparison. This is indicative of the fact that when the end conductances, h_1 and h_2 are large compared to the interface conductance, h_c, they do not exert as large an influence on the time. This was the case in most of the present data.

The resulting comparisons made are shown in figures 3 through 7 for the six sets of samples tested. In these figures the solid lines represent the theoretical predictions made using the theoretical solution. A constant thermal conductivity calculated from the experimental data at the average specimen mid-point temperatures used in the theoretical solution. The experimental data points are plotted with symbols. It can be seen that the agreement between theory and experiment is better for some test series than for others. The worst comparison is for the first series, shown in figure 3. The agreement for the second series is somewhat better, as seen in figure 4. Figure 5 shows the comparison is still better for the third and fourth series, both on a straight difference and percentage difference basis. The best agreement was found for the fifth and sixth series, as shown in figures 6 and 7. It is obvious that the agreement is better for the slower reacting systems. It is believed that this can be explained by the failure of an experimental boundary condition to match the theoretical boundary condition - specifically, the step rise in the source temperature. It was observed that during the experiments the temperature of the copper source block would "dip" slightly when the upper specimen is brought into contact with it because of the finite capacity of the source block. The dip amounted to about 3-4°C at the maximum and required approximately 10-30 seconds to vanish completely, depending on the system. In other words the overall driving force (total ΔT) was low for the early part of each experiment. As can be seen in figures 3 through 7, and as would be expected, the error thus produced is largest for the systems with the lowest total resistance, which would also have the lowest time to reach steady state. This point is illustrated by comparing figures 6 and 4, the former is for a 5.08 cm Armco Iron specimen above a 5.08 cm aluminum specimen (series 5), where as the latter is for two 5.08 cm aluminum samples (series 2). The Armco Iron sample being a poorer conductor than aluminum does not cause as much of a dip in the source temperature. The dip also does not last as long and this time represents a smaller portion of the time to reach steady state. Thus the error produced is much smaller. Similar arguments explain why the agreement was better for two 5.08 cm aluminum specimens, figure 4, than for a 2.54 cm above 5.08 cm aluminum set, figure 3; as well as why the Armco Iron-aluminum specimens, figure 6, compared better than the reversed aluminum-Armco Iron specimens, figure 5. For the 5.04 cm aluminum above 5.04 cm stainless steel series, figure 7, the dip was about the same as for the first series, but the time represented a much smaller part of the steady state time, which resulted in better agreement. The result of this argument is that the agreement between theory and experiment is good for those experiments which more closely matched the theoretical boundary conditions.

It should be emphasized here that figure 5 contains the results of two test series, (3 and 4). These series used the same specimens except that the surface of the Armco Iron specimen was reground to produce a different surface roughness (see Appendix A). Also, as indicated in figure 5, two of the runs for the third series were made in air. This provided two additional means of varying the interface contact conductance, h_c, and thus furnished a further check on the validity of h_c as a correlating parameter. No effect due to surface finish or the presence of air was noted.

For the second comparison between theory and experiment the overshoot in the interface contact temperature drop was used. As explained in an earlier paper (3), under the condition that

$$\tau = \frac{b}{a}\sqrt{\frac{\alpha_1}{\alpha_2}} > 1 \qquad (22)$$

the temperature drop across the interface contact (ΔT_c) exceeds or overshoots its steady state value for a while during the transient period. The quantity used for comparison in this phenomenon is the time required for the transient ΔT_c to reach its maximum value. In the theoretical work it was found that this time depended on h_c. The experimental values of this parameter are also shown in Appendix B. Small adjustments were also made to this parameter, in the manner discussed above, to provide a set of experimental data for a single value of the end conductance, h_1 and h_2, for each series. The results are plotted in figures 8 through 10, in which the theoretical curves are drawn as solid lines and the experimental points are plotted as symbols. It can be seen that the agreement follows about the same pattern as in the time to approach steady state comparison. Note that the error is such (as in the previous case) that the experimental observations appear to be somewhat slower than the theoretical. That is, the experimental time of maximum overshoot occurs later than the theoretical time. This also seems to support the above argument in that a temporary dip in driving potential should have a delaying effect on the time to reach maximum overshoot. As in figure 5, figure 9 represents tests with two surface roughness combinations and tests in air and vacuum. Again no effects due to these quantities were noted.

As further evidence in the comparison it is pointed out that only four of the six series produced an overshoot in ΔT_c. For the two series (2 and 4) in which $\tau < 1$ no overshoot was found to occur, which agrees with the theoretical work.

In view of the above comparisons the agreement between theory and experiment appears to be good.

5. Summary and Conclusions

Solutions have been derived for the time-dependent temperature distribution in a two layer slab with contact resistance at the interface and contact or convective resistance on the outer boundaries. Experiments have been conducted in which a series of test samples were subjected to thermal transients which closely approximated the boundary conditions used in the theoretical solution. Comparisons made on the basis of time to approach steady state and time of occurrence of maximum overshoot in interface temperature drop show good agreement between theoretical and experimental values. For those cases in which a noted discrepancy in the experimental boundary condition was believed to have only a small effect the agreement was within at least 10%.

On the basis of the above comparisons it is concluded that the theoretical solutions presented could be used to predict the transient response of systems to which they are applicable to an accuracy sufficient for most engineering purposes. That is, with these solutions properly programmed on a digital computer, a knowledge of the required thermal properties and an estimate of the contact conductance from the existing literature, a design engineer could predict the transient response of a given system. Thus used an accuracy at least as good as his knowledge of the contact conductance could be expected. The work reported here is part of a project carried out under grant NsG-711 for the National Aeronautics and Space Administration whose sponsorship is gratefully acknowledged.

6. References

[1] Tittle, C. W., Boundary value problems in composite media: Quasi-orthogonal functions, J. Appl. Physics, 38, pp. 486-488, April 1965.

[2] Tittle, C. W., Personal communication, April 17, 1965.

[3] Blum, H. A., and Moore, C. J., Jr., Transient phenomena in heat transfer across surfaces in contact, ASME Paper No. 65-HT-59, August 1965.

[4] Moore, C. J., Jr., Heat transfer across surfaces in contact: Studies of transients in one-dimensional composite systems, Ph.D. thesis, Southern Methodist University, Dallas, Texas, March 1967. Also NASA Contractor Report CR-84868.

[5] Williams, D. R., The thermal conductivity of several metals: An evaluation of a method employed by the National Bureau of Standards, Southern Methodist University, Master's Thesis, November 1966.

7. Appendix A

Test Specimen Data

Specimen No.	Material	Length	Avg. Surface Roughness of Interface End
3	2024-T351	2.525	1.78×10^{-6} m (rms)
4	2024-T351	5.067	1.91×10^{-6} m (rms)
5	303-MA	5.055	0.076×10^{-6} m (rms)
7	Armco Iron	5.123	0.076×10^{-6} m (rms)
7A	Armco Iron	5.123	0.762×10^{-6} m (rms)
9	2024-T351	5.080	0.508×10^{-6} m (rms)

Material Properties

Material	Therm. Diffusivity (m^2/sec)	Thermal Conductivity (w/m-deg), t in ^{o}C
Armco Iron	200	78.35-0.0757 t
2024-T351 Alum.	670	111.43 + 0.189 t
303-MA St. Stl.	37	14.19 + 0.0199 t

8. Appendix B

Tabulated Data

Series No.	Specimen No's. hot side/cold side	Run No.	p_c	h_c	h_1	h_2	θ_{ss}	θ_{mo}	θ'_{ss}	θ'_{mo}	$h_{ad.}$
1	3/4	5	241	3620	20000	19300	26.1	23.3	26.6	24.7	17000
		6	76	1130	6810	10400	49.4	49.4	44.5	39.7	
		7	138	2200	11200	18300	36.4	33.9	35.3	31.0	
		8	345	6300	26000	27800	20.8	13.6	21.7	16.0	
5	4/5	1	221	516	*	19800	167.5	70.7	164.5	65.8	28400
		2	90	165	4810	4840	245.0	155.0	224.0	95.8	
		3	138	278	*	35700	181.0	101.7	182.0	105.5	
		4	331	499	9680	54500	148.1	72.6	136.5	67.8	
3	4/7	1	221	726	9490	12800	82.8	114.3	77.4	103.5	17000
		2	324	857	10000	19100	79.9	106.5	77.7	101.5	
		3	442	999	12500	28600	75.0	77.5	77.1	79.3	
		4	538	1630	14800	24200	64.9	73.6	66.3	75.5	
		5	152	692	6200	35200	99.7	135.5	101.0	129.0	
		6	200	3830	12000	17700	59.1	53.2	58.1	51.1	
		7	35	2460	4960	28100	74.7	67.8	69.5	52.3	
3	4/7A	1	97	908	8180	7860	83.2	111.3	73.6	93.8	17000
		2	207	1250	10400	13500	74.5	92.9	71.4	85.1	
		3	365	1950	*	32300	66.8	67.8	66.8	72.5	
		4	524	2870	13400	36200	59.1	60.0	62.1	62.9	
4	7A/4	3	152	579	5400	6030	126.7	None	105.5	None	14200
		4	248	664	6720	6400	122.0	None	104.5	None	
		5	379	1110	8270	17000	98.7	None	95.3	None	
		6	1330	5670	17600	29600	70.2	None	74.5	None	
		7	490	1660	9710	19400	89.0	None	89.1	None	
2	9/4	1	131	817	5750	7980	72.1	None	62.8	None	14200
		2	214	1430	8050	13600	58.1	None	54.8	None	
		3	317	1940	9540	20500	54.2	None	53.4	None	
		4	435	1130	12000	15700	52.3	None	53.2	None	
		5	765	2620	14500	24500	43.6	None	46.5	None	

p_c = contact pressure (kN/m^2)
h_c = interface conductance (kw/m^2-deg)
h_1 = hot end conductance "
h_2 = cold end conductance "

θ_{ss} = time to reach steady state (sec)
θ_{mo} = time of maximum overshoot "
Primes indicate adjusted times for $h_1=h_2=h_{ad.}$

*No value.

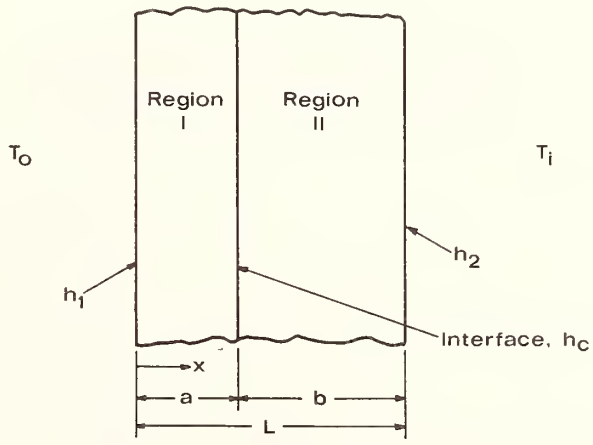

Figure 1. Boundary value problem geometry.

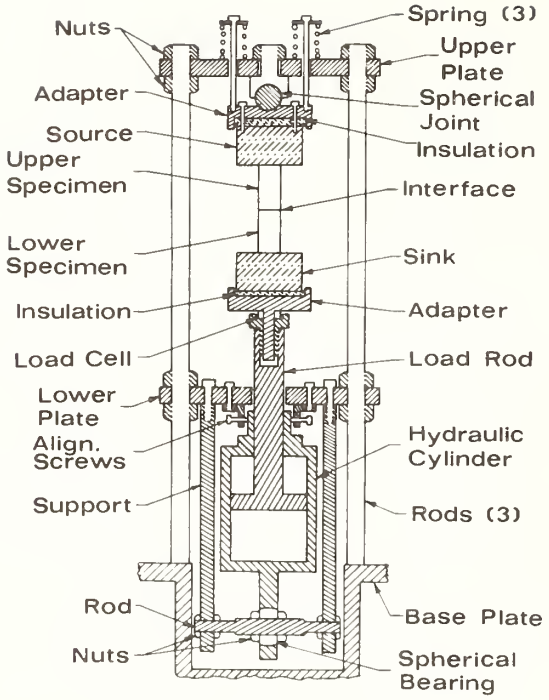

Figure 2. Test apparatus sectional drawing.

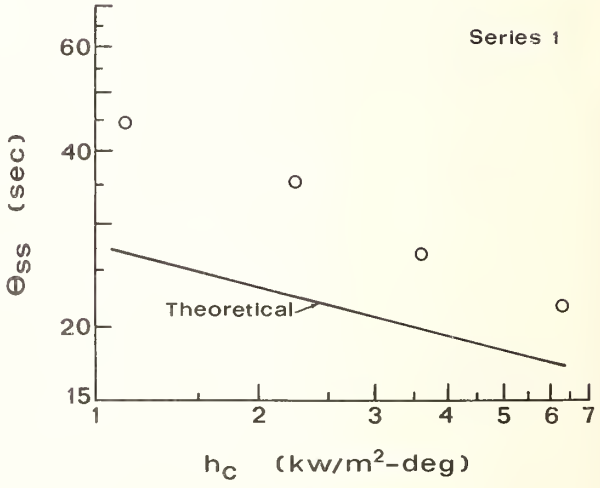

Figure 3. Time to approach steady state versus interface contact conductance for series 1, with h_1 h_2 17,000 kw/m^2-deg.

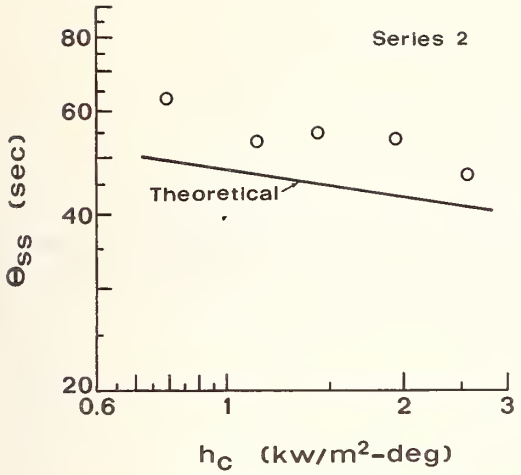

Figure 4. Time to approach steady state versus interface contace conductance for series 2, with h_1 h_2 14,200 kw/m^2-deg.

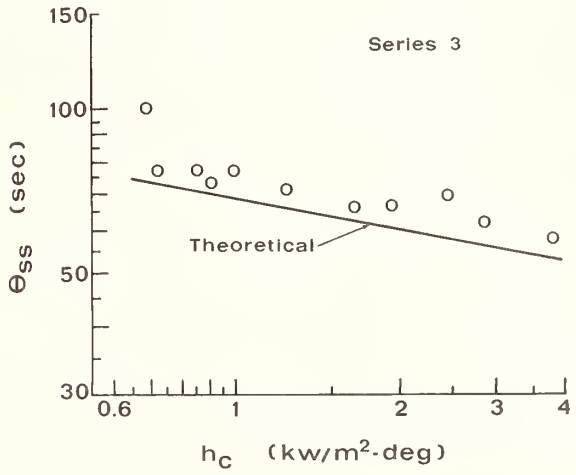

Figure 5. Time to approach steady state versus interface contact conductance for series 3, with h_1 h_2 17,000 kw/m^2-deg.

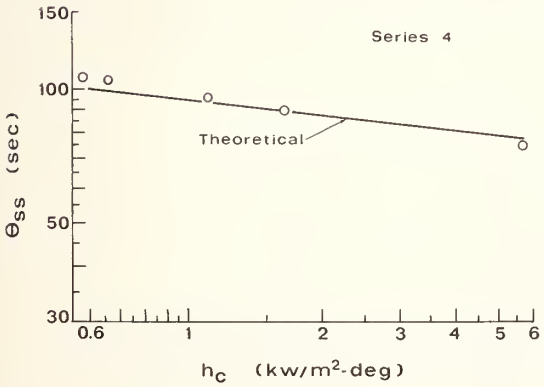

Figure 6. Time to approach steady state versus interface contact conductance for series 4, with h_1 h_2 14,200 kw/m^2-deg.

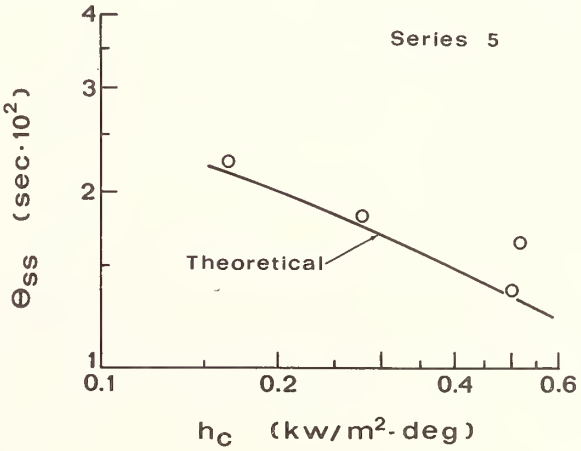

Figure 7. Time to approach steady state versus interface contact conductance for series 5, with h_1 h_2 28,400 kw/m^2-deg.

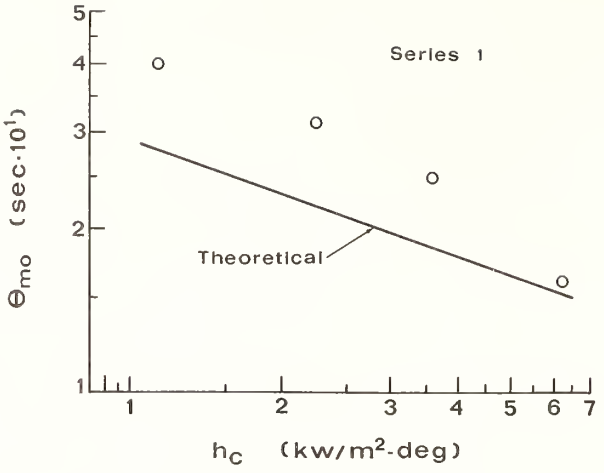

Figure 8. Time of maximum overshoot in interface contact temperature drop versus interface contact conductance for series 3, with h_1 h_2 17,000 kw/m^2-deg.

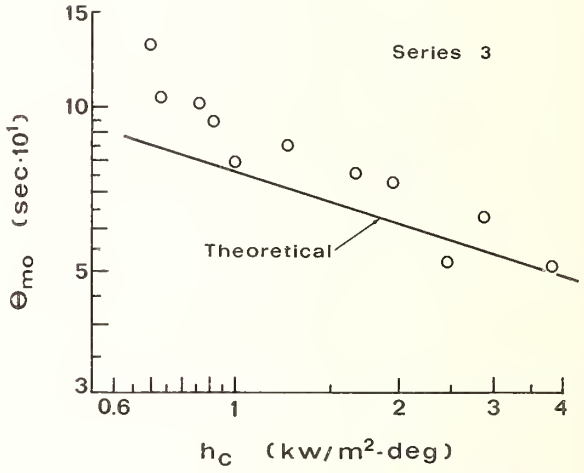

Figure 9. Time of maximum overshoot in interface contact temperature drop versus interface contact conductance for series 3, with h_1 h_2 17,000 kw/m^2-deg.

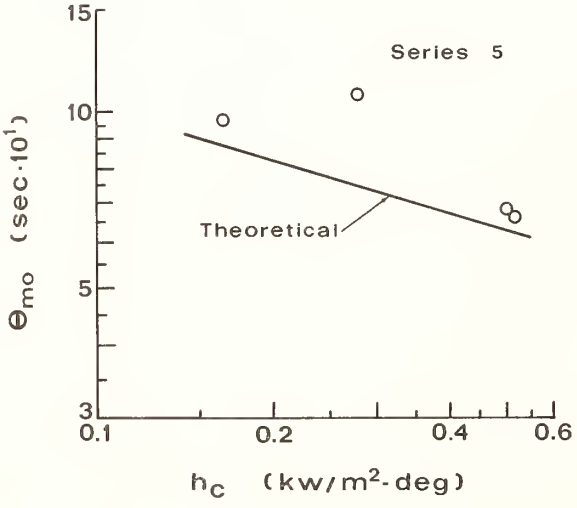

Figure 10. Time of maximum overshoot in interface contact temperature drop versus interface contact conductance for series 5, with h_1 h_2 28,400 kw/m^2-deg.

AUTHOR INDEX

NATIONAL BUREAU OF STANDARDS

The National Bureau of Standards[1] was established by an act of Congress March 3, 1901. Today, in addition to serving as the Nation's central measurement laboratory, the Bureau is a principal focal point in the Federal Government for assuring maximum application of the physical and engineering sciences to the advancement of technology in industry and commerce. To this end the Bureau conducts research and provides central national services in three broad program areas and provides central national services in a fourth. These are: (1) basic measurements and standards, (2) materials measurements and standards, (3) technological measurements and standards, and (4) transfer of technology.

The Bureau comprises the Institute for Basic Standards, the Institute for Materials Research, the Institute for Applied Technology, and the Center for Radiation Research.

THE INSTITUTE FOR BASIC STANDARDS provides the central basis within the United States of a complete and consistent system of physical measurement, coordinates that system with the measurement systems of other nations, and furnishes essential services leading to accurate and uniform physical measurements throughout the Nation's scientific community, industry, and commerce. The Institute consists of an Office of Standard Reference Data and a group of divisions organized by the following areas of science and engineering:

Applied Mathematics—Electricity—Metrology—Mechanics—Heat—Atomic Physics—Cryogenics[2]—Radio Physics[2]—Radio Engineering[2]—Astrophysics[2]—Time and Frequency.[2]

THE INSTITUTE FOR MATERIALS RESEARCH conducts materials research leading to methods, standards of measurement, and data needed by industry, commerce, educational institutions, and government. The Institute also provides advisory and research services to other government agencies. The Institute consists of an Office of Standard Reference Materials and a group of divisions organized by the following areas of materials research:

Analytical Chemistry—Polymers—Metallurgy — Inorganic Materials — Physical Chemistry.

THE INSTITUTE FOR APPLIED TECHNOLOGY provides for the creation of appropriate opportunities for the use and application of technology within the Federal Government and within the civilian sector of American industry. The primary functions of the Institute may be broadly classified as programs relating to technological measurements and standards and techniques for the transfer of technology. The Institute consists of a Clearinghouse for Scientific and Technical Information,[3] a Center for Computer Sciences and Technology, and a group of technical divisions and offices organized by the following fields of technology:

Building Research—Electronic Instrumentation — Technical Analysis — Product Evaluation—Invention and Innovation— Weights and Measures — Engineering Standards—Vehicle Systems Research.

THE CENTER FOR RADIATION RESEARCH engages in research, measurement, and application of radiation to the solution of Bureau mission problems and the problems of other agencies and institutions. The Center for Radiation Research consists of the following divisions:

Reactor Radiation—Linac Radiation—Applied Radiation—Nuclear Radiation.

---

[1] Headquarters and Laboratories at Gaithersburg, Maryland, unless otherwise noted; mailing address Washington, D. C. 20234.
[2] Located at Boulder, Colorado 80302.
[3] Located at 5285 Port Royal Road, Springfield, Virginia 22151.

NBS TECHNICAL PUBLICATIONS

PERIODICALS

JOURNAL OF RESEARCH reports National Bureau of Standards research and development in physics, mathematics, chemistry, and engineering. Comprehensive scientific papers give complete details of the work, including laboratory data, experimental procedures, and theoretical and mathematical analyses. Illustrated with photographs, drawings, and charts.

Published in three sections, available separately:

• Physics and Chemistry

Papers of interest primarily to scientists working in these fields. This section covers a broad range of physical and chemical research, with major emphasis on standards of physical measurement, fundamental constants, and properties of matter. Issued six times a year. Annual subscription: Domestic, $5.00; foreign, $6.00*.

• Mathematical Sciences

Studies and compilations designed mainly for the mathematician and theoretical physicist. Topics in mathematical statistics, theory of experiment design, numerical analysis, theoretical physics and chemistry, logical design and programming of computers and computer systems. Short numerical tables. Issued quarterly. Annual subscription: Domestic, $2.25; foreign, $2.75*.

• Engineering and Instrumentation

Reporting results of interest chiefly to the engineer and the applied scientist. This section includes many of the new developments in instrumentation resulting from the Bureau's work in physical measurement, data processing, and development of test methods. It will also cover some of the work in acoustics, applied mechanics, building research, and cryogenic engineering. Issued quarterly. Annual subscription: Domestic, $2.75; foreign, $3.50*.

TECHNICAL NEWS BULLETIN

The best single source of information concerning the Bureau's research, developmental, cooperative and publication activities, this monthly publication is designed for the industry-oriented individual whose daily work involves intimate contact with science and technology—*for engineers, chemists, physicists, research managers, product-development managers, and company executives.* Annual subscription: Domestic, $1.50; foreign, $2.25*.

*Difference in price is due to extra cost of foreign mailing.

NONPERIODICALS

Applied Mathematics Series. Mathematical tables, manuals, and studies.

Building Science Series. Research results, test methods, and performance criteria of building materials, components, systems, and structures.

Handbooks. Recommended codes of engineering and industrial practice (including safety codes) developed in cooperation with interested industries, professional organizations, and regulatory bodies.

Special Publications. Proceedings of NBS conferences, bibliographies, annual reports, wall charts, pamphlets, etc.

Monographs. Major contributions to the technical literature on various subjects related to the Bureau's scientific and technical activities.

National Standard Reference Data Series. NSRDS provides quantitative data on the physical and chemical properties of materials, compiled from the world's literature and critically evaluated.

Product Standards. Provide requirements for sizes, types, quality and methods for testing various industrial products. These standards are developed cooperatively with interested Government and industry groups and provide the basis for common understanding of product characteristics for both buyers and sellers. Their use is voluntary.

Technical Notes. This series consists of communications and reports (covering both other agency and NBS-sponsored work) of limited or transitory interest.

CLEARINGHOUSE

The Clearinghouse for Federal Scientific and Technical Information, operated by NBS, supplies unclassified information related to Government-generated science and technology in defense, space, atomic energy, and other national programs. For further information on Clearinghouse services, write:

Clearinghouse
U.S. Department of Commerce
Springfield, Virginia 22151

Order NBS publications from:
Superintendent of Documents
Government Printing Office
Washington, D.C. 20402

☆ U.S. GOVERNMENT PRINTING OFFICE : 1968 O—313-361